

**Radical Strategies for (Hetero)benzylic C(sp³)-H Functionalization
and Cross Coupling**

By

Dung (Kristine) L. Golden

A dissertation submitted in partial fulfillment
of the requirements for the degree of

Doctor of Philosophy
(Chemistry)

at the

University of Wisconsin – Madison

2023

Date of Final Oral Examination: 05/03/2023

The dissertation is approved by the following members of the Final Oral Committee:

Shannon S. Stahl, Professor, Chemistry

Tehshik P. Yoon, Professor, Chemistry

Helen E. Blackwell, Professor, Chemistry

Zachary K. Wickens, Assistant Professor, Chemistry

Radical Strategies for (Hetero)benzylic C(sp³)-H Functionalization and Cross Coupling

Dung (Kristine) L. Golden

Under the supervision of Professor Shannon S. Stahl

At the University of Wisconsin-Madison

Abstract

C-H functionalization reactions are among the most useful and synthetically applicable approaches to access structurally complex organic molecules, including pharmaceuticals and agrochemicals. While methods promoting functionalization and cross coupling of C(sp²)-H bonds have found broad applications, a growing number of reactions have focused on functionalizing C(sp³)-H bonds to incorporate three-dimensionality and expand the chemical space. Radical C-H functionalization reactions initiated by hydrogen-atom transfer and proceeding via radical intermediates introduce strategic opportunities to functionalize C(sp³)-H bonds. In addition to the commonly seen radical-chain and biomimetic radical-rebound mechanisms, radical-relay reactions provide the basis for versatile C-H cross-coupling methods with diverse partners. This thesis discloses our recent development of radical-relay and radical-chain (hetero)benzylic C(sp³)-H functionalization and their synthetic utility in accessing three-dimensional chemical space.

Chapter 2 discussed our recent development of a copper-catalyzed benzylic C-H esterification reaction enabled by a "photochemical redox buffering" strategy using *tert*-butyl peroxybenzoate as the oxidant. Copper(I)/peroxide (or Kharasch-Sosnovsky-typed) reactions historically require excess of C-H substrates and forcing reaction conditions, leading to poor synthetic applicability. Copper(I) catalysts interact rapidly with peroxide-based oxidants, resulting in a pool of inactive

copper(II) species, which are incapable of activating oxidants. Our recent efforts in copper/NFSI-catalyzed radical relay functionalization and cross coupling of benzylic C(sp³)–H bonds revealed a "redox buffering" strategy enabling the controlled regeneration of copper(I). For copper/NFSI systems, we have identified that certain nucleophiles (i.e. cyanides and arylboronic acids) can promote the reduction of Cu^{II} to Cu^I, whereas nucleophiles like alcohols and azoles requires additional chemical reductants (i.e. dialkylphosphites) to promote "redox buffering." To address the issues with copper/peroxide system, we have developed a 2,2'-biquinoline/copper-catalyzed reaction under photoirradiation to promote benzylic esterification using limiting C–H substrates. Mechanistic interrogation revealed that light promoted carboxylate-to-copper charge transfer enables the regeneration of copper(I) catalyst, similar to the aforementioned "redox buffering" approach.

Chapter 3 disclosed our recently developed chlorination/ diversification sequence of heterobenzylic C(sp³)–H bonds in 3-alkylpyridines via radical chain. Alkylpyridines are important and prevalent classes of substrates in medicinal chemistry with the (hetero)benzylic C–H bonds having similar bond dissociation energies to alkylarenes. However, copper/NFSI-catalyzed reactions are unsuccessful in accessing these C–H bonds due to the deleterious reactivity between the pyridyl nitrogen atom and NFSI. While chlorination of 2- and 4-alkylpyridines can be achieved using a polar activation strategy, heterobenzylic C–H bonds of 3-alkylpyridines are more amenable to radical-based chlorination. Experimental and density functional theory identified an *N*-chlorosulfonamide reagent for selective chlorination at the heterobenzylic C–H site. Subsequent diversification of heterobenzyl chlorides with a broad scope of nucleophiles enabled facile access to complex cross-coupled products. This method should find broad application for building block modification and library synthesis in drug discovery.

Chapter 4 detailed our investigation in copper/NFSI-catalyzed fluorination of benzylic C–H bonds followed by diversification with various nucleophiles. Redox buffering promoted by addition of boron-based reductants enabled successful fluorination with limiting C–H substrates. Benzyl fluorides were subsequently subjected to nucleophilic displacement catalyzed by Lewis acidic additives, affording C–O, C–N, and C–C bond formations. This method inspired later developments of other radical halogenation/diversification methods to functionalize (hetero)benzylic C–H bonds.

Chapter 5 disclosed our development of a copper/NFSI-catalyzed cross couplings of benzylic C(sp³)–H bonds and azoles enabled by redox buffering. In addition to excellent benzylic selectivity, *N*-site selectivity of azoles was achieved by modifying the reaction conditions. Diverse N-H heterocycles were compatible coupling partners, including pyrazoles, purines, and sultams. The ability to access both regioisomers of azoles via a cross coupling array validated the synthetic utility of this method in pharmaceutical research.

Collectively, radical (hetero)benzylic C(sp³)–H functionalization contributed to a growing number of methods in accessing more three-dimensional chemical space. Mechanistic insights from these reactions will enable further development of more synthetically useful methodologies. Additionally, the synthetic applications should allow chemists to assemble compound libraries with higher complexity and expand the accessible chemical space.

Acknowledgements

I have had such an incredible journey of learning and growth in chemistry for the past 10 years. However, I would not have been able to achieve all my goals without the individuals who have contributed significantly to my experience. I would like to thank Dr. Julia Baker, my undergraduate advisor, who inspired me to pursue a graduate degree and research experience in chemistry. Under her supervision, I learned about the experimental skills and mindset of conducting research as well as how to work independently as a researcher. This experience helped me prepare for the challenges that I would later face in my graduate study. I also would like to thank Dr. John Zubizarreta for being incredibly supportive throughout my undergraduate experience. His passion for seeing students succeed encouraged me to be more confident in tackling newer and bigger things.

My chemistry journey in the Stahl group at UW-Madison has been exciting and inspiring. My advisor, Prof. Shannon Stahl, has been exceptional in shaping who I am today as a scientist. Thank you, Shannon, for taking a chance on me knowing that I had little knowledge or experience in organic chemistry and organometallic catalysis. I was able to learn from Shannon how to think strategically, design experiments, write a manuscript, and present my research. Thank you to Dr. Si-Jie Chen, Dr. Aristidis Vasilopoulos, Prof. Sung-Eun Suh, and Prof. Josh Buss for teaching me the ropes when I was a young graduate student. Thank you to Marco Antonio Lopez for all the scientific discussions on top of being an awesome subgroup mate, office mate, and lab mate. Thank you to my mentee Kaitlyn Flynn for giving me the opportunity to learn chemistry from a different perspective. Thank you to my external collaborators Dr. Shane Krska, Dr. Dipannita Kalyani, Dr. Shishi Lin, Dr. Santeri Aikonen, and Prof. Rob Paton for their hard work. I am also thankful for my committee, Prof. Tehshik Yoon and Prof. Helen Blackwell, for their guidance and support

throughout my graduate journey. I also appreciate everyone in the Department of Chemistry who makes the department a lively and collaborative environment.

I owe all my success and achievements to my mother and father. They have given me unconditional love and opportunities to pursue my goals. I would like to thank my sister for being there for my parents in my absence. I did not have many opportunities to visit my family in Vietnam in these past years, but I am looking forward to making more memories. Thank you to my aunts and uncles who have always been there for me and cheering me on from afar. I would like to thank my in-laws for all their love, support, and guidance. I truly feel like I can always come to them for advice and good banter. Finally, I would like to thank my ever-loving husband and partner in crime Brent Golden. He has always been my rock and willing to stand beside me on all my decisions in life. Words cannot describe how grateful I am to have him by my side and how much his love and support mean to me.

I dedicate this thesis to my family.

Table of Contents

Radical Strategies for (Hetero)benzylic C(sp³)-H Functionalization and Cross Coupling

Abstract	i
Acknowledgements	iv
Table of Contents	vi
List of Figures	xi
List of Tables	xxii
Abbreviations and Acronyms	xxiv
Chapter 1. Radical C(sp³)-H Functionalization and Cross Coupling	1
1.1. Abstract	2
1.2. Introduction	2
1.3. Radical-Chain and Radical-Rebound Reactions	7
1.3.1. RadicalChain	7
1.3.2. Radical Rebound	11
1.4. Radical Relay	12
1.4.1. Radical-Relay Reactions Involving Direct Coupling with a Trapping Reagent or Substrate Partner	12
1.4.2. Kharasch-Sosnovsky Reactions.....	18
1.4.3. Cu/NFSI-Catalyzed C(sp ³)-H Functionalization and Cross-Coupling Methods	22
1.4.4. Radical-Relay Reactions with Catalysts other than Copper.....	30
1.4.5. Photoredox C(sp ³)-H Functionalization and Cross-Coupling Methods	32
1.4.6. Electrochemical Radical-Relay Reactions	41
1.5. Conclusion.....	44
1.6. Thesis Scope.....	44
1.7. Author Contributions.....	45

1.8. Reference.....	46
Chapter 2. Benzylic C–H Esterification with Limiting C–H Substrate Enabled by Photochemical Redox Buffering of the Cu Catalyst	60
2.1. Abstract	61
2.2. Introduction	62
2.3. Results and Discussion	64
2.4. Conclusion.....	71
2.5. Acknowledgements	72
2.6. Author Contributions.....	72
2.7. References	73
Chapter 3. Site Selective Chlorination of Heterobenzylic C(sp³)–H Bonds Enabling High-Throughput Chlorination/Diversification with Oxidatively Sensitive Nucleophiles	77
3.1. Abstract	78
3.2. Introduction	78
3.3. Results and Discussion	80
3.4. Conclusion.....	90
3.5. Acknowledgements	91
3.6. Author Contributions.....	91
3.7. References	991
Chapter 4. Copper-Catalyzed C–H Fluorination/Functionalization Sequence Enabling Benzylic C–H Cross Coupling with Diverse Nucleophiles	94
4.1. Abstract	95
4.2. Introduction	9595
4.3. Results and Discussion	9797
4.4. Conclusion.....	101101
4.5. Acknowledgements	10101

4.6. Author Contributions.....	10202
4.7. References	102
Chapter 5. Site-Selective Copper-Catalyzed Cross-Coupling of Benzylic C–H Bonds and Azoles with Controlled <i>N</i>-Site Selectivity	105
5.1. Abstract	106
5.2. Introduction	106
5.3. Results and Discussion.....	108
5.4. Conclusion.....	115
5.5. Acknowledgements	116
5.6. Author Contributions.....	116
5.7. References	116
Appendix A: Supporting Information Chapter 2	121
2A.I. General Considerations	121
2A.II. Experimental Procedures for Preparations of Compounds.....	122
2A.III. Optimization of the Reaction Conditions	123
2A.IV. Additional Experiments with [Cu(MeCN) ₄]PF ₆ , 2,2'-biquinoline, and TBPB	127
2A.V. UV-visible Experiments with Various Ancillary Ligands	131
2A.VI. Unsuccessful Benzylic C–H Substrates	133
2A.VII. Crystallization and Crystallographic Data for C ₂₅ H ₁₇ CuF ₆ N ₂ O ₂ P (Cu ^{II} -OBz)...	134
2A.VIII. Additional Experiments and Observations	138
2A.IX. Characterization of Compounds.....	143
2A.X. References	150
2A.XI. NMR Spectra.....	152
Appendix B: Supporting Information Chapter 3	190
3B.I. General Considerations	190
3B.II. Experimental Procedures for Preparations of Compounds	191

3B.III. Starting Material Syntheses	196
3B.IV. Reaction Optimization.....	200
3B.V. Computational Methods for Bond Dissociation Free Energy Analysis.....	202
3B.VI. Additional Screening Data with Benzylic C–H Substrates and Azoles	206
3B.VII. Additional Experiments and Observations.....	217
3B.VIII. Characterization of Compounds	219
3B. XIII. Reference	245
3B.XIV. NMR Spectroscopic Data	247
Appendix C: Supporting Information Chapter 4	292
4C.I. General Considerations	292
4C.II. General Procedure for Benzylic C–H Fluorination and NMR Quantitation	292
4C.III. General Procedure for Catalyzed Benzyl Fluoride Displacement	294
4C.IV. Procedure for 3 mmol Scale Fluorination/Functionalization Sequence to Prepare 46	295
4C.V. Screening Tables.....	297
4C.VI. Additional Experiments and Observations.....	300
4C.VII. Quantitative ¹ H and ¹⁹ F NMR Spectra for Benzyl Fluoride Products	304
4C.VIII. Characterization Data for Isolated Cross Coupling Products	329
4C.X. Reference	342
4C.X. ¹ H NMR and ¹³ C NMR Spectra of Isolated Compounds.....	344
Appendix D: Supporting Information Chapter 5	370
5D.I. General Considerations	370
5D.II. Experimental Procedures for Cross-Coupling Reactions	371
5D.III. Optimization of the Reaction Conditions.....	372
5D.IV. Displacement of Benzylic Bromide with 2a	375
5D.V. Additional Screening Data with Benzylic C–H Substrates and Azoles	375

5D.VI. Characterization of Regioselectivity	378
5D.VII. Crystallization and Crystallographic Data for $[(C_6H_5)N(CH_3)_3]_2[CuBr_4]$ and 2a.....	379
5D.VIII. Characterization of Compounds	384
5D.IX. References	417
5D.X. NMR Spectroscopic Data	418

List of Figures

- Figure 1.1. Mechanisms and components of radical-chain, radical-rebound, and radical-relay reactions.** (Aa) General mechanism of radical-chain reaction. (Ab) Representative initiators/reagents for radical-chain reactions. (Ba) General catalytic cycle of radical-rebound reaction. (Bb) Representative iron and manganese catalysts for radical-rebound reactions. (Ca) Generic mechanism of radical-relay reactions involving radical trapping reagents. (Cb) Generic mechanism of catalytic radical-relay reactions. (Cc) Representative oxidants and HAT reagents for radical-relay reactions. (Cd) Representative radical trapping reagents. (Ce) Representative catalytic radical-relay coupling partners. 6
- Figure 1.2. Late-stage C(sp³)-H functionalization reactions via radical chain and radical rebound.** (Aa) General mechanism for radical-chain reaction with a N-X reagent. (Ab) Fluorination reactions of C(sp³)-H bonds. (Ac) Site-selective aliphatic C-H halogenation and xanthylation reactions with N-X reagents. (Ad) Benzylic C(sp³)-H hydroxylation reaction. (B) Iron-catalyzed C-H oxidation reaction. (Ca) Manganese-non-heme catalyzed chiral desymmetrization of cyclohexane. (Cb) Manganese-catalyzed benzylic amination reaction. (Cc) Manganese-porphyrin or -salen catalyzed C-H functionalization reactions. 11
- Figure 1.3. Radical relay involving radical addition to trapping reagents.** (Aa) Oxygenation with Co/NHPI cocatalysts. (Ab) Oxygenation with decatungstate photocatalysts. (Ba/b) PINOylation methods. (Ca) Azidation/cyanation via radical trapping with sulfonyl-X reagents (X = N₃, CN). (Cb) Thiol coupling via radical trapping with sulfonylthiolates. (Da) Amination of heterobenzylic C(sp³)-H bonds with DEAD. (Db) Amination initiated by LMCT with Ce^{IV} reagents. (Ea) Giese-type alkylation with decatungstate photocatalysts. (Eb) Polarity reversal HAT/Giese-type alkylation. (Fa) Minisci reaction with decatungstate photocatalyst. (Fb) Photochemical Minisci-type pyridylation. (G) Photochemical borylation. 16
- Figure 1.4.** Timeline of representative Kharasch-Sosnovsky reactions. 21
- Figure 1.5.** Summary of Cu/NFSI-catalyzed radical-relay functionalization, functionalization/diversification, and cross-coupling reactions of benzylic C(sp³)-H bonds. 29
- Figure 1.6. Catalytic cycle and radical functionalization mechanisms for Cu/NFSI-catalyzed radical-relay reactions.** (a) Inner sphere radical coupling via reductive elimination. (b) Radical-polar crossover pathway. (c) Radical addition to Cu-bound ligand. 30
- Figure 1.7.** Radical-relay C-H functionalization and cross-coupling reactions with catalysts other than copper. 32
- Figure 1.8. Photoredox C(sp³)-H functionalization/cross coupling via radical relay.** (a) Four pathways for photoredox-promoted C-H functionalization/cross coupling. (b) The photoredox toolbox includes HAT reagents, photocatalysts, and metal-/iodine-based catalysts utilized for representative methodologies. 34

Figure 1.9. Different methods for radical-relay C(sp³)-H functionalization and cross coupling using carbon-centered radicals access via photoredox methods. (a) Photoredox-promoted C-H functionalization/cross-coupling reactions involving single electron transfer. (b) Photoredox-promoted C-H functionalization/cross-coupling reactions involving copper catalysts. (c) Photoredox-promoted C-H functionalization/cross-coupling reactions involving nickel catalysts. (d) Photoredox-promoted C-H functionalization/cross-coupling reactions involving iodine-based catalysts..... 36

Figure 1.10. Nickel-catalyzed arylation of C(sp³)-H bonds of inexpensive (co)solvents enabled by *in situ* generation of HAT reagents. (Aa) Energy transfer pathway for arylation of C(sp³)-H bonds. (Ab) Single electron transfer pathway for arylation of C(sp³)-H bonds. (Ba) Examples of arylated products involving energy transfer. (Bb) Examples of arylated product involving single electron transfer. (Bc) Enantioselective arylation of benzylic C(sp³)-H bonds with a chiral bis-imidazoline ligand..... 40

Figure 1.11. Radical-relay reactions involving electrochemistry. (Aa) General mechanism for NHPI-mediated electrochemical oxygenation reaction of C(sp³)-H bonds. (Ab) Oxygenation of allylic C-H bonds. (Ac) Oxygenation of heterobenzylic C(sp³)-H bonds. (Ad) Quinuclidine-mediated oxygenation of C(sp³)-H bonds. (Ae) *N*-alkyl ammonium ylides as a new class of HAT-mediators. (Af) NHPI-mediated iodination followed by pyridination of alkylarenes. (Ba) Oxygenation reactions involving metal-oxo complexes. (Bb) Oxygenation of secondary benzylic C(sp³)-H bonds using Fe-TAML complex. (Bc) Hydroxylation of C(sp³)-H bonds in amine derivatives using a ruthenium-based catalyst. (C) Azidation of C(sp³)-H bonds using Mn^{III} catalyst. (D) Photoelectrochemical azidation reaction of C(sp³)-H bonds. 43

Figure 2.1. Benzylic esterification enabled by photochemical redox buffering. 61

Figure 2.2. (A) Kharasch-Sosnovsky (K-S) allylic C-H esterification. (B) Proposed catalytic mechanism for the K-S reaction and estimated activation barriers for individual steps. (C) Focus of this study is to develop a K-S-type benzylic esterification, capable of using the C-H substrate as a limiting reagent. 63

Figure 2.3. Reactions of diverse 2° benzylic C-H substrates. 66

Figure 2.4. (A) Reactivity of 3° benzylic substrates and assessment of benzylic site-selectivity under the conditions defined in Figure 2.3, and (B) sequential esterification/deprotection of benzylic C-H substrates. 67

Figure 2.5. (A) UV-visible absorption spectra for oxidation of Cu^I complexes with phen (r.t.), bpy (r.t.), and biq (40 °C) ligands without irradiation. (B) TBPB titration experiment with 2:1 biq/Cu^I and 1:1 biq/Cu^I with 30s mixing after every addition. (C) UV-visible absorption spectrum for oxidation of biq/Cu^I under irradiation. (D) UV-visible absorption spectrum of photochemical reduction of biq/Cu^{II}. Reaction of 1:1 biq/Cu^I with TBPB to afford [(biq)Cu^{II}(OBz)]PF₆. For clarity, hydrogen atoms are not shown

in the X-ray structure. (E) Photochemical reactivity of $\text{Cu}^{\text{II}}\text{-OBz}$ in absence of a C–H substrate. (F) Catalytic reactivity of $\text{Cu}^{\text{II}}\text{-OBz}$ under standard reaction condition... 69

- Figure 2.6. Redox buffering pathway for Cu-catalyzed C–H functionalization reactions.** Cu^{II} reduction can be promoted by light (A), coupling partners (B), or sacrificial reagents (C)..... 70
- Figure 3.1.** Chlorination/diversification sequence of 3-alkylpyridines..... 78
- Figure 3.2.** (A) Bioactive molecules with 3-alkylpyridine fragments (B) Chlorination strategies for benzylic and heterobenzylic $\text{C}(\text{sp}^3)\text{-H}$ bonds (C) Sequential chlorination/diversification of 3-alkylpyridines enabled by photochemical radical chain reaction..... 79
- Figure 3.3.** Applications of various C–H chlorination methods on ethylbenzene, 2-ethylpyridine, 3-ethylpyridine, and 3-isobutylpyridine 81
- Figure 3.4.** Analysis of radical chain propagation steps with various NCl-reagents. 84
- Figure 3.5.** Assessment of 3-alkylpyridine C–H substrates 85
- Figure 3.6.** *t*-SNE analysis and HTE 96-well plate assessment of nucleophilic coupling partners with **3** 87
- Figure 3.7.** Sequential chlorination/ nucleophilic displacement of two C–H substrates. 89
- Figure 4.1.** Benzylic C–H fluorination/functionalization sequence to access diverse cross-coupled products..... 95
- Figure 4.2.** C–H cross coupling via benzyl fluorides..... 96
- Figure 4.3.** Cu/NFSI fluorination of benzylic C–H bonds..... 98
- Figure 4.4.** Benzylic C–H cross coupling to C–O, C–N, and C–C bonds via a benzyl fluoride 100
- Figure 5.1.** Cu-catalyzed cross coupling of benzylic C–H bonds and azoles with N-site selectivity 106
- Figure 5.2.** (A) Importance of benzylic N-azoles in drug discovery. (B) Impact of regioselectivity of heterocyclic compounds in medicinal chemistry. (C) Copper-catalyzed regioselective cross couplings of benzylic C–H bonds and N–H heterocycles enabled by various additives. 107
- Figure 5.3.** Evaluation of effects of various solvents and additives on the regioselectivity. (A) Effects of solvents on benzylic C–N cross coupling reaction. (B) Regioselectivity switch observed in cross coupling of **1a** and **2a** with different additives. Conditions

- identical to those shown in part A, using 10 mol% additive instead of TBABr, 10 mol % CuBr₂ instead of CuCl, and DCM:HFIP (7:3) solvent..... 109
- Figure 5.4.** Mechanistic origin of pyrazole regioselectivity. (A) N¹/N²-isomerization test, implicating the the N¹. (B) Proposed mechanism rationalizing the influence of TMSOTf (and other Lewis acids) on the N²/N¹ regioselectivity..... 110
- Figure 5.5.** Assessment of various benzylic C–H substrates in cross coupling reactions with N–H heterocycles with (A) TBACl as the additive for N² regioselectivity and (B) with TMSOTf as the additive for N¹ regioselectivity. Regioisomers >5% were isolated and reported 112
- Figure 5.6.** Assessment of various N–H heterocycles in cross coupling reactions. Substrate scope with diverse N–H heterocycles and indane under kinetically controlled TBACl conditions (A) and in the presence of BF₃•OEt₂ as a Lewis acid cocatalyst (B). Exploration of cross-coupling reactions of diverse N–H heterocycles and (hetero)benzylic C–H scaffolds (C) under the TBACl conditions of Figure 5.6A, unless noted otherwise. Regioisomers formed in >5% yield were isolated 114
- Figure 2A.1.** Homemade LED photoreactor 121
- Figure 2A.2.** Effect of ligand loading on reactivity 126
- Figure 2A.3.** Reaction time course..... 126
- Figure 2A.4.** UV-visible data for biq/Cu^IPF₆ titration experiment 127
- Figure 2A.5.** UV-visible data of [(biq)₂Cu^I]PF₆ and a sample with a 1-to-1 mixture of [(biq)₂Cu^I]PF₆+ [(biq)Cu^{II}(OBz)]PF₆ 131
- Figure 2A.6.** UV-visible absorption spectra of phen/Cu^{II} and bpy/Cu^{II} under 450 nm irradiation. UV-visible absorption spectrum of biq/Cu^{II} under 450 nm irradiation was included in Figure 2.5D. 132
- Figure 2A.7.** Screening data with additional benzylic C–H substrates..... 133
- Figure 2A.8.** A molecular drawing of C₂₅H₁₇CuF₆N₂O₂P shown with 50% probability ellipsoids. All H atoms and minor disorder components are omitted..... 135
- Figure 2A.9.** A molecular drawing of C₂₅H₁₇CuF₆N₂O₂P shown with 30% probability ellipsoids. Note the possible dimeric nature of the complex. The Cu...O separation is 2.6720(15) Å. All H atoms and minor disorder components are omitted. 136
- Figure 2A.10.** ¹H NMR spectrum for irradiation of C₂₅H₁₇CuF₆N₂O₂P under blue LED irradiation..... 138
- Figure 2A.11.** ¹H NMR analysis for irradiation of [(biq)Cu^{II}(OBz)]PF₆ under blue LED irradiation in presence of substrate..... 139

Figure 2A.12. Taped Schlenk Tube.....	140
Figure 2A.13. Absorption spectrum of the ferrioxalate solution	140
Figure 2A.14. Absorption spectrum of the [(biq)Cu ^{II} (OBz)]PF ₆ solution.....	141
Figure 3B.1. Photochemical Setup for Normal Scale Reaction (Left) and Scale-Up Reaction (Right).....	195
Figure 3B.2. The individual HAT and XAT steps, and the overall reaction used to calculate the Δ BDFE and Δ G, respectively.	203
Figure 3B.3. Nitrogen-based nucleophiles in Figure 3.6.	207
Figure 3B.4. Alcohol nucleophiles in Figure 3.6.	208
Figure 3B.5. Carboxylic acid nucleophiles in Figure 3.6.	209
Figure 3B.6. 96-Well Plate Display of Selected Amines for High-Throughput Experiments not included in Figure 3.6.	210
Figure 3B.7. 96-Well Plate Display of Selected Amines for High-Throughput Experiments not included in Figure 3.6.	211
Figure 3B.8. 96-Well Plate Display of Selected Amines for High-Throughput Experiments not included in Figure 3.6.	212
Figure 3B.9. 96-Well Plate Display of Selected Alcohols for High-Throughput Experiments not included in Figure 3.6.	213
Figure 3B.10. 96-Well Plate Display of Selected Alcohols for High-Throughput Experiments not included in Figure 3.6.	214
Figure 3B.11. 96-Well Plate Display of Selected Carboxylic Acids for High-Throughput Experiments not included in Figure 3.6.....	215
Figure 3B.12. 96-Well Plate Display of Selected Carboxylic Acids for High-Throughput Experiments not included in Figure 3.6.....	216
Figure 3B.13. Screening data with additional benzylic C–H substrates. Conv., conversion.....	217
Figure 3B.14. Screening data with additional benzylic C–H substrates. Conv., conversion.....	217
Figure 3B.15. Byproducts detected in UPLC analysis.....	218
Figure 3B.16. Crude ¹ H NMR Spectrum (CDCl ₃ , 400 MHz, 25 °C) of the reaction mixture for 1a following the addition of 0.5 mmol (70 μ L) of mesitylene as an external standard (6.78 ppm). The resolved benzylic protons for 3a is labeled and integrated.....	219

- Figure 3B.17.** Crude ^1H NMR Spectrum (CDCl_3 , 400 MHz, 25 $^\circ\text{C}$) of the reaction mixture for **1t** following the addition of 0.5 mmol (70 μL) of mesitylene as an external standard (6.78 ppm). The resolved benzylic protons for **3t** is labeled and integrated..... 230
- Figure 3B.18.** Crude ^1H NMR Spectrum (CDCl_3 , 400 MHz, 25 $^\circ\text{C}$) of the reaction mixture for **1v** following the addition of 0.2 mmol (7 μL) of mesitylene as an external standard (6.78 ppm). The resolved benzylic protons for **3v** is labeled and integrated..... 232
- Figure 3B.19.** Crude ^1H NMR Spectrum (CDCl_3 , 400 MHz, 25 $^\circ\text{C}$) of the reaction mixture for **1ab** following the addition of 0.05 mmol (7 μL) of mesitylene as an external standard (6.78 ppm). The resolved benzylic protons for **3ab** are labeled and integrated. 235
- Figure 3B.20.** Crude ^1H NMR Spectrum (CDCl_3 , 400 MHz, 25 $^\circ\text{C}$) of the reaction mixture for **1ac** following the addition of 0.05 mmol (7 μL) of mesitylene as an external standard (6.78 ppm). The resolved benzylic protons for **3ac** are labeled and integrated..... 236
- Figure 3B.21.** Crude ^1H NMR Spectrum (CDCl_3 , 400 MHz, 25 $^\circ\text{C}$) of the reaction mixture for **1ad** following the addition of 0.05 mmol (7 μL) of mesitylene as an external standard (6.78 ppm). The resolved benzylic protons for **3ad** are labeled and integrated. 237
- Figure 4C.1.** Competition experiment for 1 $^\circ$ vs. 2 $^\circ$ benzylic C–H bond functionalization reactivity.
..... 304
- Figure 4C.2.** Competition experiment for 2 $^\circ$ vs. 3 $^\circ$ benzylic C–H bond functionalization reactivity.
..... 304
- Figure 4C.3.** Crude ^1H NMR Spectrum (CDCl_3 , 400 MHz, 25 $^\circ\text{C}$) of the reaction mixture following the addition of 0.3 mmol (21 μL) of CH_2Br_2 as an internal standard (4.93 ppm). The resolved product and starting material benzylic protons are labeled and integrated. 305
- Figure 4C.4.** Crude $^{19}\text{F}\{^1\text{H}\}$ NMR Spectrum (CDCl_3 , 377 MHz, 25 $^\circ\text{C}$) of the reaction mixture following the addition of 0.3 mmol (37 μL) of PhCF_3 as an internal standard (-62.73 ppm). The mono-fluoride (-173.76 ppm) is labeled and integrated; the inset shows an enlargement of the proton-coupled mono-fluoride..... 305
- Figure 4C.5.** Crude ^1H NMR Spectrum (CDCl_3 , 400 MHz, 25 $^\circ\text{C}$) of the reaction mixture following the addition of 0.3 mmol (21 μL) of CH_2Br_2 as an internal standard (4.93 ppm). The resolved product and starting material benzylic protons are labeled and integrated. 306
- Figure 4C.6.** Crude $^{19}\text{F}\{^1\text{H}\}$ NMR Spectrum (CDCl_3 , 377 MHz, 25 $^\circ\text{C}$) of the reaction mixture following the addition of 0.3 mmol (37 μL) of PhCF_3 as an internal standard (-62.73 ppm). The mono-fluoride (-173.76 ppm) is labeled and integrated; the inset shows an enlargement of the proton-coupled mono-fluoride..... 306
- Figure 4C.7.** Crude ^1H NMR Spectrum (CDCl_3 , 400 MHz, 25 $^\circ\text{C}$) of the reaction mixture following the addition of 0.3 mmol (21 μL) of CH_2Br_2 as an internal standard (4.92

- ppm). The resolved product benzylic and methyl protons are labeled and integrated.
 307
- Figure 4C.8.** Crude $^{19}\text{F}\{^1\text{H}\}$ NMR Spectrum (CDCl_3 , 377 MHz, 25 °C) of the reaction mixture following the addition of 0.3 mmol (37 μL) of PhCF_3 as an internal standard (-62.73 ppm). The mono- and di-fluoride (-167.02 and -87.62 ppm, respectively) are labeled and integrated. The inset shows an enlargement of the proton-coupled mono-fluoride.
 307
- Figure 4C.9.** Crude ^1H NMR Spectrum (CDCl_3 , 400 MHz, 25 °C) of the reaction mixture following the addition of 0.3 mmol (21 μL) of CH_2Br_2 as an internal standard (4.84 ppm). The resolved product benzylic and methyl protons are labeled and integrated.
 308
- Figure 4C.10.** Crude $^{19}\text{F}\{^1\text{H}\}$ NMR Spectrum (CDCl_3 , 377 MHz, 25 °C) of the reaction mixture following the addition of 0.3 mmol (37 μL) of PhCF_3 as an internal standard (-62.70 ppm). The mono- and di-fluoride (-168.89 and -87.79 ppm, respectively) are labeled and integrated..... 308
- Figure 4C.11.** Crude ^1H NMR Spectrum (CDCl_3 , 400 MHz, 25 °C) of the reaction mixture following the addition of 0.3 mmol (21 μL) of CH_2Br_2 as an internal standard (4.96 ppm). The resolved product benzylic and methyl protons are labeled and integrated. The residual starting material benzylic protons are likewise labeled and integrated.
 309
- Figure 4C.12.** Crude $^{19}\text{F}\{^1\text{H}\}$ NMR Spectrum (CDCl_3 , 377 MHz, 25 °C) of the reaction mixture. The mono- and di-fluoride (-172.67 and -89.32 ppm, respectively) are labeled and integrated. 309
- Figure 4C.13.** Crude ^1H NMR Spectrum (CDCl_3 , 400 MHz, 25 °C) of the reaction mixture following the addition of 0.3 mmol (21 μL) of CH_2Br_2 as an internal standard (4.92 ppm). The resolved product benzylic and methyl protons are labeled and integrated.
 310
- Figure 4C.14.** Crude $^{19}\text{F}\{^1\text{H}\}$ NMR Spectrum (CDCl_3 , 377 MHz, 25 °C) of the reaction mixture following the addition of 0.3 mmol (37 μL) of PhCF_3 as an internal standard (-62.69 ppm). The mono- and di-fluoride (-166.40 and -87.11 ppm, respectively) are labeled and integrated..... 310
- Figure 4C.15.** Crude ^1H NMR Spectrum (CDCl_3 , 400 MHz, 25 °C) of the reaction mixture following the addition of 0.3 mmol (21 μL) of CH_2Br_2 as an internal standard (4.93 ppm). The resolved product and starting material benzylic protons are labeled and integrated. 311
- Figure 4C.16.** Crude $^{19}\text{F}\{^1\text{H}\}$ NMR Spectrum (CDCl_3 , 377 MHz, 25 °C) of the reaction mixture following the addition of 0.3 mmol (37 μL) of PhCF_3 as an internal standard (-62.73 ppm). The mono- and di-fluoride (-179.43 and -95.91 ppm, respectively) are labeled

- and integrated. The inset shows an enlargement of the proton-coupled mono-fluoride.
 311
- Figure 4C.17.** Crude ^1H NMR Spectrum (CDCl_3 , 400 MHz, 25 °C) of the reaction mixture following the addition of 0.3 mmol (21 μL) of CH_2Br_2 as an internal standard (4.93 ppm). The resolved product and starting material benzylic protons are labeled and integrated. 312
- Figure 4C.18.** Crude ^{19}F NMR Spectrum (CDCl_3 , 377 MHz, 25 °C) of the reaction mixture following the addition of 0.3 mmol (37 μL) of PhCF_3 as an internal standard (-62.73 ppm). The mono-fluoride (-179.33) is labeled and integrated. The inset shows an enlargement of the proton-coupled mono-fluoride..... 312
- Figure 4C.19.** Crude ^1H NMR Spectrum (CDCl_3 , 400 MHz, 25 °C) of the reaction mixture following the addition of 0.3 mmol (21 μL) of CH_2Br_2 as an internal standard (4.92 ppm). The resolved product benzylic protons are labeled and integrated. 313
- Figure 4C.20.** Crude $^{19}\text{F}\{^1\text{H}\}$ NMR Spectrum (CDCl_3 , 377 MHz, 25 °C) of the reaction mixture following the addition of 0.3 mmol (37 μL) of PhCF_3 as an internal standard (-62.72 ppm). The mono- and di-fluoride (-173.16 and -92.36 ppm, respectively) are labeled and integrated. The inset shows an enlargement of the proton-coupled mono-fluoride.
 313
- Figure 4C.21.** Crude ^1H NMR Spectrum (CDCl_3 , 400 MHz, 25 °C) of the reaction mixture following the addition of 0.3 mmol (21 μL) of CH_2Br_2 as an internal standard (4.92 ppm). The resolved product and starting material benzylic protons are labeled and integrated. 314
- Figure 4C.22.** Crude $^{19}\text{F}\{^1\text{H}\}$ NMR Spectrum (CDCl_3 , 377 MHz, 25 °C) of the reaction mixture following the addition of 0.3 mmol (37 μL) of PhCF_3 as an internal standard (-62.70 ppm). The mono-fluoride (-166.73) is labeled and integrated. The inset shows an enlargement of the proton-coupled mono-fluoride..... 314
- Figure 4C.23.** Crude ^1H NMR Spectrum (CDCl_3 , 400 MHz, 25 °C) of the reaction mixture following the addition of 0.3 mmol (21 μL) of CH_2Br_2 as an internal standard (4.93 ppm). The resolved product benzylic and methyl protons are labeled and integrated.
 315
- Figure 4C.24.** Crude $^{19}\text{F}\{^1\text{H}\}$ NMR Spectrum (CDCl_3 , 377 MHz, 25 °C) of the reaction mixture following the addition of 0.3 mmol (37 μL) of PhCF_3 as an internal standard (-62.73 ppm). The mono- and di-fluoride (-174.31 and -93.27 ppm, respectively) are labeled and integrated. The inset shows an enlargement of the proton-coupled mono-fluoride.
 315
- Figure 4C.25.** Crude ^1H NMR Spectrum (CDCl_3 , 400 MHz, 25 °C) of the reaction mixture following the addition of 0.3 mmol (21 μL) of CH_2Br_2 as an internal standard (4.93 ppm). The resolved product and starting material benzylic protons are labeled and integrated. 316

- Figure 4C.26.** Crude $^{19}\text{F}\{^1\text{H}\}$ NMR Spectrum (CDCl_3 , 377 MHz, 25 °C) of the reaction mixture following the addition of 0.3 mmol (37 μL) of PhCF_3 as an internal standard (-62.73 ppm). The mono- and di-fluoride (-177.40 and -94.79 ppm, respectively) are labeled and integrated. The inset shows an enlargement of the proton-coupled mono-fluoride. 316
- Figure 4C.27.** Crude ^1H NMR Spectrum (CDCl_3 , 400 MHz, 25 °C) of the reaction mixture following the addition of 0.3 mmol (21 μL) of CH_2Br_2 as an internal standard (4.87 ppm). The resolved product and starting material benzylic protons are labeled and integrated. 317
- Figure 4C.28.** Crude $^{19}\text{F}\{^1\text{H}\}$ NMR Spectrum (CDCl_3 , 377 MHz, 25 °C) of the reaction mixture. The mono-fluoride (-184.35) is labeled and integrated. 317
- Figure 4C.29.** Crude ^1H NMR Spectrum (CDCl_3 , 400 MHz, 25 °C) of the reaction mixture following the addition of 0.3 mmol (21 μL) of CH_2Br_2 as an internal standard (4.93 ppm). The resolved product and starting material benzylic protons are labeled and integrated. 318
- Figure 4C.30.** Crude $^{19}\text{F}\{^1\text{H}\}$ NMR Spectrum (CDCl_3 , 377 MHz, 25 °C) of the reaction mixture following the addition of 0.3 mmol (37 μL) of PhCF_3 as an internal standard (-62.73 ppm). The benzylic fluoride (-183.75 ppm) and CF_3 groups (starting material and product) are labeled and integrated; the inset shows an enlargement of the proton-coupled mono-fluoride..... 318
- Figure 4C.31.** Crude ^1H NMR Spectrum (CDCl_3 , 400 MHz, 25 °C) of the reaction mixture following the addition of 0.3 mmol (21 μL) of CH_2Br_2 as an internal standard (4.91 ppm). The resolved product benzylic proton is labeled and integrated. 319
- Figure 4C.32.** Crude $^{19}\text{F}\{^1\text{H}\}$ NMR Spectrum (CDCl_3 , 377 MHz, 25 °C) of the reaction mixture following the addition of 0.3 mmol (37 μL) of PhCF_3 as an internal standard (-62.68 ppm). The mono-fluoride (-159.91) is labeled and integrated. The inset shows an enlargement of the proton-coupled mono-fluoride..... 319
- Figure 4C.33.** Crude ^1H NMR Spectrum (CDCl_3 , 400 MHz, 25 °C) of the reaction mixture following the addition of 0.3 mmol (21 μL) of CH_2Br_2 as an internal standard (4.91 ppm). The resolved product benzylic proton is labeled and integrated. 320
- Figure 4C.34.** Crude $^{19}\text{F}\{^1\text{H}\}$ NMR Spectrum (CDCl_3 , 377 MHz, 25 °C) of the reaction mixture following the addition of 0.3 mmol (37 μL) of PhCF_3 as an internal standard (-62.68 ppm). The mono-fluoride (-155.88) is labeled and integrated. The inset shows an enlargement of the proton-coupled mono-fluoride..... 320
- Figure 4C.35.** Crude ^1H NMR Spectrum (CDCl_3 , 400 MHz, 25 °C) of the reaction mixture following the addition of 0.3 mmol (21 μL) of CH_2Br_2 as an internal standard (4.92 ppm). The resolved product benzylic proton is labeled and integrated. 321

- Figure 4C.36.** Crude $^{19}\text{F}\{^1\text{H}\}$ NMR Spectrum (CDCl_3 , 377 MHz, 25 °C) of the reaction mixture following the addition of 0.3 mmol (37 μL) of PhCF_3 as an internal standard (-62.70 ppm). The mono-fluoride (-178.75) is labeled and integrated. The inset shows an enlargement of the proton-coupled mono-fluoride..... 321
- Figure 4C.37.** Crude ^1H NMR Spectrum (CDCl_3 , 400 MHz, 25 °C) of the reaction mixture following the addition of 0.3 mmol (21 μL) of CH_2Br_2 as an internal standard (4.92 ppm). The resolved product benzylic proton is labeled and integrated. 322
- Figure 4C.38.** Crude $^{19}\text{F}\{^1\text{H}\}$ NMR Spectrum (CDCl_3 , 377 MHz, 25 °C) of the reaction mixture following the addition of 0.3 mmol (37 μL) of PhCF_3 as an internal standard (-62.70 ppm). The mono-fluoride (-158.62) is labeled and integrated. The inset shows an enlargement of the proton-coupled mono-fluoride..... 322
- Figure 4C.39.** Crude ^1H NMR Spectrum (CDCl_3 , 400 MHz, 25 °C) of the reaction mixture following the addition of 0.3 mmol (21 μL) of CH_2Br_2 as an internal standard (4.94 ppm). The resolved product benzylic proton is labeled and integrated. 323
- Figure 4C.40.** Crude $^{19}\text{F}\{^1\text{H}\}$ NMR Spectrum (CDCl_3 , 377 MHz, 25 °C) of the reaction mixture following the addition of 0.3 mmol (37 μL) of PhCF_3 as an internal standard (-62.74 ppm). The mono-fluoride (-170.59) is labeled and integrated. The inset shows an enlargement of the proton-coupled mono-fluoride..... 323
- Figure 4C.41.** Crude ^1H NMR Spectrum (CDCl_3 , 400 MHz, 25 °C) of the reaction mixture following the addition of 0.3 mmol (21 μL) of CH_2Br_2 as an internal standard (4.91 ppm). The resolved product and starting material benzylic protons are labeled and integrated. 324
- Figure 4C.42.** Crude $^{19}\text{F}\{^1\text{H}\}$ NMR Spectrum (CDCl_3 , 377 MHz, 25 °C) of the reaction mixture following the addition of 0.3 mmol (37 μL) of PhCF_3 as an internal standard (-62.68 ppm). The mono-fluoride (-153.79) is labeled and integrated. The inset shows an enlargement of the proton-coupled mono-fluoride..... 324
- Figure 4C.43.** Crude ^1H NMR Spectrum (CDCl_3 , 400 MHz, 25 °C) of the reaction mixture following the addition of 0.3 mmol (21 μL) of CH_2Br_2 as an internal standard (4.91 ppm). The resolved product and starting material benzylic protons are labeled and integrated. 325
- Figure 4C.44.** Crude $^{19}\text{F}\{^1\text{H}\}$ NMR Spectrum (CDCl_3 , 377 MHz, 25 °C) of the reaction mixture following the addition of 0.3 mmol (37 μL) of PhCF_3 as an internal standard (-62.67 ppm). The mono-fluoride (-206.64 ppm) and di-fluoride (-110.52 ppm) are labeled and integrated. The insets show enlargements of the proton-coupled resonances. 325
- Figure 4C.45.** Crude ^1H NMR Spectrum (CDCl_3 , 400 MHz, 25 °C) of the reaction mixture following the addition of 0.3 mmol (21 μL) of CH_2Br_2 as an internal standard (4.91 ppm). The resolved product and starting material benzylic protons are labeled and integrated. 326

- Figure 4C.46.** Crude $^{19}\text{F}\{^1\text{H}\}$ NMR Spectrum (CDCl_3 , 377 MHz, 25 °C) of the reaction mixture following the addition of 0.3 mmol (37 μL) of PhCF_3 as an internal standard (-62.69 ppm). The mono-fluoride (-208.09 ppm) and the di-fluoride (-111.05 ppm) are labeled and integrated. The insets show enlargements of the proton-coupled resonances. . 326
- Figure 4C.47.** Crude ^1H NMR Spectrum (CDCl_3 , 400 MHz, 25 °C) of the reaction mixture following the addition of 0.3 mmol (21 μL) of CH_2Br_2 as an internal standard (4.91 ppm). The resolved product aromatic and methyl protons are labeled and integrated. 327
- Figure 4C.48.** Crude $^{19}\text{F}\{^1\text{H}\}$ NMR Spectrum (CDCl_3 , 377 MHz, 25 °C) of the reaction mixture following the addition of 0.3 mmol (37 μL) of PhCF_3 as an internal standard (-62.69 ppm). The benzyl-fluoride (-137.39) is labeled and integrated. The inset shows an enlargement of the proton-coupled fluorine resonance. 327
- Figure 4C.49.** Crude ^1H NMR Spectrum (CDCl_3 , 400 MHz, 25 °C) of the reaction mixture following the addition of 0.3 mmol (21 μL) of CH_2Br_2 as an internal standard (4.91 ppm). The resolved product aromatic and methyl protons are labeled and integrated. 328
- Figure 4C.50.** Crude $^{19}\text{F}\{^1\text{H}\}$ NMR Spectrum (CDCl_3 , 377 MHz, 25 °C) of the reaction mixture following the addition of 0.3 mmol (37 μL) of PhCF_3 as an internal standard (-62.69 ppm). The aryl-fluoride (-112.96) and benzyl-fluoride (-135.16) are labeled and integrated. The inset shows an enlargement of the proton-coupled fluorine resonances. 328
- Figure 5D.1.** Screening data with additional benzylic C–H substrates and azoles..... 376
- Figure 5D.2.** Further analyses of reaction outcomes of cross couplings of benzylic C–H bonds and azoles. 377
- Figure 5D.3.** Evidence for regioisomer assignment of benzylic C–H cross coupling products with **2a** 378
- Figure 5D.4.** Proof of regioisomer assignment for benzylic C–H cross coupling products with other ambidentate azoles..... 378
- Figure 5D.5.** A molecular drawing of $[(\text{C}_6\text{H}_5)\text{N}(\text{CH}_3)_3]_2[\text{CuBr}_4]$ 380
- Figure 5D.6.** A molecular drawing of **2a** shown with 50% probability ellipsoids for non-hydrogen atoms. 383

List of Tables

Table 2.1. Reaction optimization for photo-promoted benzylic esterification	65
Table 2A.1. Benzylic Esterification under Thermal Condition ^a	123
Table 2A.2. Benzylic Esterification under Photochemical Condition ^a	124
Table 2A.3. Assessment of Ancillary Ligands ^a	124
Table 2A.4. Copper Salt Screen ^a	125
Table 2A.5. Solvent Screen ^a	125
Table 2A.6. UV-visible Data for Ligand Titration of biq/Cu ^I PF ₆	127
Table 2A.7. Conversion of TBPB with Different Loading of 2,2'-Biquinoline	128
Table 2A.8. UV-visible Data for Oxidation of (biq)Cu ^I by TBPB	129
Table 2A.9. UV-visible Data for Oxidation of (biq) ₂ Cu ^I by TBPB	129
Table 2A.10. UV-visible Data for Reactivity of biq/Cu ^I (1.5:1) / TBPB under Blue LED Irradiation	130
Table 2A.11. Crystal Data and Structure Refinement for C ₂₅ H ₁₇ CuF ₆ N ₂ O ₂ P	137
Table 3B.1. Solvent Screen ^a	20000
Table 3B.2. Additive Screen ^a	20000
Table 3B.3. Chlorination of 3-Isobutylpyridine with Various N-Chloro Reagents ^a	20101
Table 3B.4. Loading of <i>N</i> -(<i>tert</i> -butyl)- <i>N</i> -chloro-3,5-bis(trifluoromethyl)benzenesulfonamide (2) ^a	201
Table 3B.5. BDFE (kcal·mol ⁻¹) values for substrate 1a and N-Cl reagents	20303
Table 3B.6. Reaction Free Energies (kcal·mol ⁻¹) for Individual HAT/XAT Steps and for Overall Chlorination Reaction	20404
Table 3B.7. Absolute Energies (a.u.) for Compound 1a	20404
Table 3B.8. Absolute Energies (a.u.) for the N-Cl Reagents	20505
Table 3B.9. Chlorination data of 3-methylpyridine and derivatives	21818
Table 4C.1. Control Experiments Table	297

Table 4C.2. Solvent Screening Table.....	297
Table 4C.3. Cu Salt Screening Table.....	298
Table 4C.4. Ligand Screening Table	298
Table 4C.5. Base Screening Table.....	299
Table 4C.6. Reductant Screening Table.....	299
Table 4C.7. Reaction Stoichiometry Screening Table.....	300
Table 4C.8. HFIP Loading Screening Table.....	300
Table 4C.9. Benzylic C–H Fluorination Results for Substrates not Included in Figure 4.3.....	301
Table 4C.10. Comparison between Ineffective and Effective Conditions for Forming Desired Product.....	302
Table 4C.11. Benzylic C–F Displacement Results for Less Effective C–H Substrate/Nucleophile Pairs	303
Table 5D.1. Assessment of Ancillary Ligands.....	372
Table 5D.2. Ligand Comparison with Selected Nucleophiles	372
Table 5D.3. Effect of Different Additives in Controlling the Regioselectivity ^a	373
Table 5D.4. Optimization of the Reaction Conditions with Various Solvents, Cu Salts and Temperature ^a	374
Table 5D.5. Investigation of Various Reductants with Ethylbenzene as the Substrate	374
Table 5D.6. Crystal Data and Structure Refinement for [(C ₆ H ₅)N(CH ₃) ₃] ₂ [CuBr ₄].....	38181
Table 5D.7. Crystal Data and Structure Refinement for 2a	383

Abbreviations and Acronyms

HAT	hydrogen atom transfer
[O]	$O_2/2e^-$, H_2O_2 , or other O-atom transfer reagent
NFSI	<i>N</i> -fluorobenzenesulfonimide
TMP	5,10,15,20-tetramesitylporphyrin
TPFPP	5,10,15,20-tetrakis(pentafluorophenyl)porphyrin
ET	electron transfer
TBPB	<i>tert</i> -butyl peroxybenzoate
DTBP	di- <i>tert</i> -butyl peroxide
NHPI	<i>N</i> -hydroxyphthalimide
B ₂ cat ₂	bis(catecholato)diboron
HFIP	1,1,1,3,3,3-hexafluoroisopropanol
PDP	<i>N,N'</i> -bis(2-pyridylmethyl)-2,2'-bipyrrolidine
TIPS _{mcp}	<i>N,N'</i> -dimethyl- <i>N,N'</i> -bis(2-(5-triisopropylsilylpyridyl)methyl)-1,2-trans diaminocyclohexane
Pc	phthalocyanine
TMS	trimethylsilyl (cation)
DEAD	diethyl azodicarboxylate
LMCT	ligand-to-metal charge transfer
TFA	trifluoroacetic acid
(TRIPS) ₂	bis(2,4,6-triisopropylphenyl) disulfide
PFBI-OH	hydroxyl perfluorobenziodoxole
CIB(cat)	B-chlorocatecholborane
DT	decatungstate
TBS	<i>tert</i> -butyldimethylsilyl
BPhen	bathophenanthroline
N~N	β -diketimate ligand: 2,4-bis-(2,6-dichlorophenylimino)pentyl
Ad	1-adamantyl

Phen	phenanthroline
phd	1,10-phenanthroline-5,6-dione
1-Np	1-naphthalene
F-TEDA-PF ₆	1-chloromethyl-4-fluoro-1,4-diazoniabicyclo[2.2.2]octane bis(hexafluorophosphate)
•NSI	benzenesulfonimidyl radical
TBACl	tetrabutylammonium chloride
TMSOTf	trimethylsilyl triflate
BisOx	bisoxazoline ligand
dppb	1,4-bis(diphenylphosphino)butane
L _n	ligands
DCP	dicumyl peroxide
SET	single electron transfer
BI-OH	hydroxyl benziodoxole
PIDA	phenyliodonium diacetate
TBADT	tetra- <i>n</i> -butylammonium decatungstate
4CzIPN	2,4,5,6-tetra(carbazole-9-yl)isophthalonitrile
[Acr ⁺ Mes]	9-mesityl-1,3,6,8-tetramethoxy-10-phenylacridin-10-ium tetrafluoroborate
bpy	2,2'-bipyridine
PhI(<i>p</i> BBA) ₂	bis(4-bromobenzoyloxy)iodobenzene
<i>p</i> -F-ppy	5-fluoro-2-(2-pyridyl-κN)phenyl-κC
dtbbpy	4,4'-di- <i>tert</i> -butyl-2,2'-bipyridyl
5,5'-dmbpy	5,5'-dimethyl-2,2'-bipyridyl
NaDT	sodium decatungstate
Ketone-1	4-methoxy-4'-trifluoromethylbenzophenone
Ketone-2	4,4'-dichlorobenzophenone
EnT	energy transfer
R.E.	reductive elimination

BiIM	biimidazoline
DMBP	4,4'-dimethoxybenzophenone
Cl ₄ NHPI	tetrachloro- <i>N</i> -hydroxyphthalimide
RVC	reticulated vitreous carbon
TBAP	tetrabutylammonium perchlorate
TAML	tetraamido macrocyclic ligand
DDQ	2,3-dichloro-5,6-dicyano- <i>p</i> -benzoquinone
HTE	high-throughput experimentation
DCM	dichloromethane
DFT	density functional theory
Boc	<i>tert</i> -butyloxycarbonyl
TBA	tetrabutylammonium
Conv.	percent conversion of the C–H substrate
ee	enantiomeric excess
d.r.	diastereomeric ratio
r.r.	regioisomeric ratio
ACN	acetonitrile
THF	tetrahydrofuran
DMF	<i>N,N</i> -dimethylformamide
DMAP	4-(dimethylamino)pyridine
BDFE	Bond dissociation free energies

Chapter 1.

Radical C(sp³)-H Functionalization and Cross Coupling

Reproduced with permission from: **Dung L. Golden**, Sung-Eun Suh, Shannon S. Stahl. Radical C(sp³)-H Functionalization and Cross-Coupling Reactions. *Nat. Rev. Chem.* **2022**, *6*, 405–427.
Copyright 2022, Springer Nature Limited

1.1. Abstract

C–H functionalization reactions are playing an increasing role in the preparation and modification of complex organic molecules, including pharmaceuticals, agrochemicals, and polymer precursors. In recent years there have been many reports of radical C–H functionalization reactions initiated by hydrogen-atom transfer (HAT) and proceeding via open-shell radical intermediates. These methods introduce strategic opportunities to functionalize C(sp³)–H bonds. Examples include synthetically useful advances in radical-chain reactivity and biomimetic radical-rebound reactions. A growing number of reactions, however, have been found to proceed via radical relay whereby HAT generates a diffusible radical that is functionalized by a separate reagent or catalyst. The latter methods provide the basis for versatile C–H cross-coupling methods with diverse partners. This chapter highlights recent examples of radical-chain and radical-rebound methods to provide context for a survey of emerging radical-relay methods, which greatly expand the scope and utility of intermolecular C(sp³)–H functionalization and cross coupling.

1.2. Introduction

The efficient synthesis of organic molecules is crucial to drug discovery and development, materials synthesis, and many other domains. C–H functionalization methods provide a means to streamline synthetic routes by avoiding the need for substrate pre-activation. They thus provide access to target molecules in fewer steps and provide efficient strategies to diversify existing chemical structures, including modification of their physicochemical properties and three-dimensional structures. Multiple mechanistic pathways are available for C(sp³)–H functionalization, including those initiated by organometallic C–H activation;^{1–4} atom-transfer methods,^{5–7} such as carbene and nitrene C–H insertion; and those initiated by hydrogen-atom

transfer (HAT) to generate radical intermediates.^{4,8–10} The synthetic utility of radical C–H functionalization reactions was historically viewed with skepticism,¹¹ owing to the challenges in controlling reaction selectivity; however, recent advances have changed this perception. Radical pathways feature in a growing number of synthetically useful methods that enable site-selective functionalization of C(sp³)–H bonds. C–H functionalization reactions that feature a one-for-one replacement of a hydrogen atom with another functional group, such as a halogen, pseudohalogen, or oxygen atom, have been complemented by C–H cross-coupling reactions that permit efficient access to dozens, if not hundreds, of derivatives via reaction of the C–H substrate with broad classes of reaction partners, such as aryl halides, boronic acids, alcohols, and amine derivatives. The latter reactions represent an important class of reactions for pharmaceutical and agrochemical discovery efforts. They enable the rapid elaboration of simple building blocks, of core structures of moderate complexity, and of late-stage structures and bioactive compounds.

Multiple mechanisms are available for radical C–H functionalization reactions. Radical-chain mechanisms (Figure 1.1Aa) are involved in a number of large-scale industrial processes, including chlorination of methane and autoxidation of hydrocarbons, such as cyclohexane and cumene.^{12,13} These reactions feature three general steps: initiation, propagation, and termination. The initiation step generates new radical species, typically by thermal or photochemical cleavage of a weak bond in dihalogens (e.g. Cl₂ and Br₂), peroxides, or specialized reagents, such as AIBN (2,2'-azobis(2-methylpropionitrile)). Propagation steps account for net transformation of the starting material into the reaction product(s). These steps regenerate the radical carrier without net consumption of radical species. The chain process ends in termination steps that consume radicals, such as the direct coupling of two radicals. Recent advances have highlighted the utility of radical-chain reactions for selective functionalization of more complex molecules, benefiting from the

development of new reagents that lead to improved site selectivity in the HAT propagation step.¹⁴⁻¹⁷

The radical-rebound mechanism (Figure 1.1Ba) is closely associated with iron-containing heme enzymes such as cytochrome P450 (CYP) and related non-heme iron enzymes in biology.¹⁸ This collection of biological and synthetic reactions involves high-valent metal-oxo species generated via reaction of a reduced metal complex with oxygen-atom donors, including O₂, H₂O₂, alkyl or acyl hydroperoxides, and PhI=O. HAT from a C(sp³)-H bond to the reactive metal-oxo is followed by rapid recombination (that is, rebound) of the resulting carbon-centred radical with the incipient metal-hydroxide to afford the oxygenated product. Variations of this reaction pathway can lead to other products if the organic radical recombines with a different ligand within the metal coordination sphere. For example, C-H halogenation products can arise from HAT by a metal oxo, followed by reaction of the organic radical with a halide ligand rather than the hydroxide ligand. Analogous C-H amination reactivity is possible with metal-nitrene intermediates derived from the reaction of a reduced metal complex with nitrogen-atom donors, including organic azides¹⁹ and PhI=NR reagents.²⁰ Recent advances include the discovery of new catalysts that promote radical-rebound reactions with complex molecules.¹⁸

Radical-relay reactions (Figure 1.1C) complement radical-chain and radical-rebound reactions and significantly expand the scope of accessible synthetic transformations. An HAT step generates a diffusible organic radical, which is then functionalized by a second reagent or catalyst. In some cases, the radical undergoes direct coupling with a substrate partner or radical trapping reagent (Figure 1.1Ca). In other cases, the radical undergoes metal-catalyzed coupling, reacting by one of several possible mechanisms (Figure 1.1Cb). It can undergo radical-polar crossover, in which electron-transfer (ET) generates a carbocation that reacts readily with diverse nucleophiles.

Alternatively, the carbon-centered radical can react by one of two possible pathways with a transition-metal catalyst containing Ni^{II}, Cu^{II}, or another metal ion: (a) direct addition of the radical to a coordinated ligand on the transition-metal complex, or (b) radical addition to the metal centre and subsequent reductive elimination with the coordinated coupling partner. Each of these pathways supports C–H cross-coupling reactions that generate new carbon–carbon and carbon–heteroatom bonds via reaction with a variety of reaction partners. Recent advances have introduced new methods to access HAT reagents from chemical oxidants and photoactive reagents, in addition to new catalyst systems that support diverse product formation.

The intermolecular C(sp³)–H functionalization and cross-coupling methods represented by these reaction classes provide valuable strategies to diversify organic molecules ranging from simple building blocks to complex molecules.^{21–23} Intramolecular reactions, such as Hoffmann–Loeffler–Freitag and related reactions^{24–26} feature closely related mechanisms but are not covered in this chapter. The content herein begins with a survey of new radical-chain and radical-rebound reactions, followed by a presentation of radical-relay reactions that use C–H bonds as latent nucleophiles in carbon–carbon and carbon–heteroatom bond-forming reactions. Cross-coupling methods include those that feature direct C–H cross coupling, in addition to those that proceed via stepwise C–H functionalization/diversification sequences. Mechanistic features of these reactions are presented, emphasizing those with implications for the synthetic scope of the reactions.

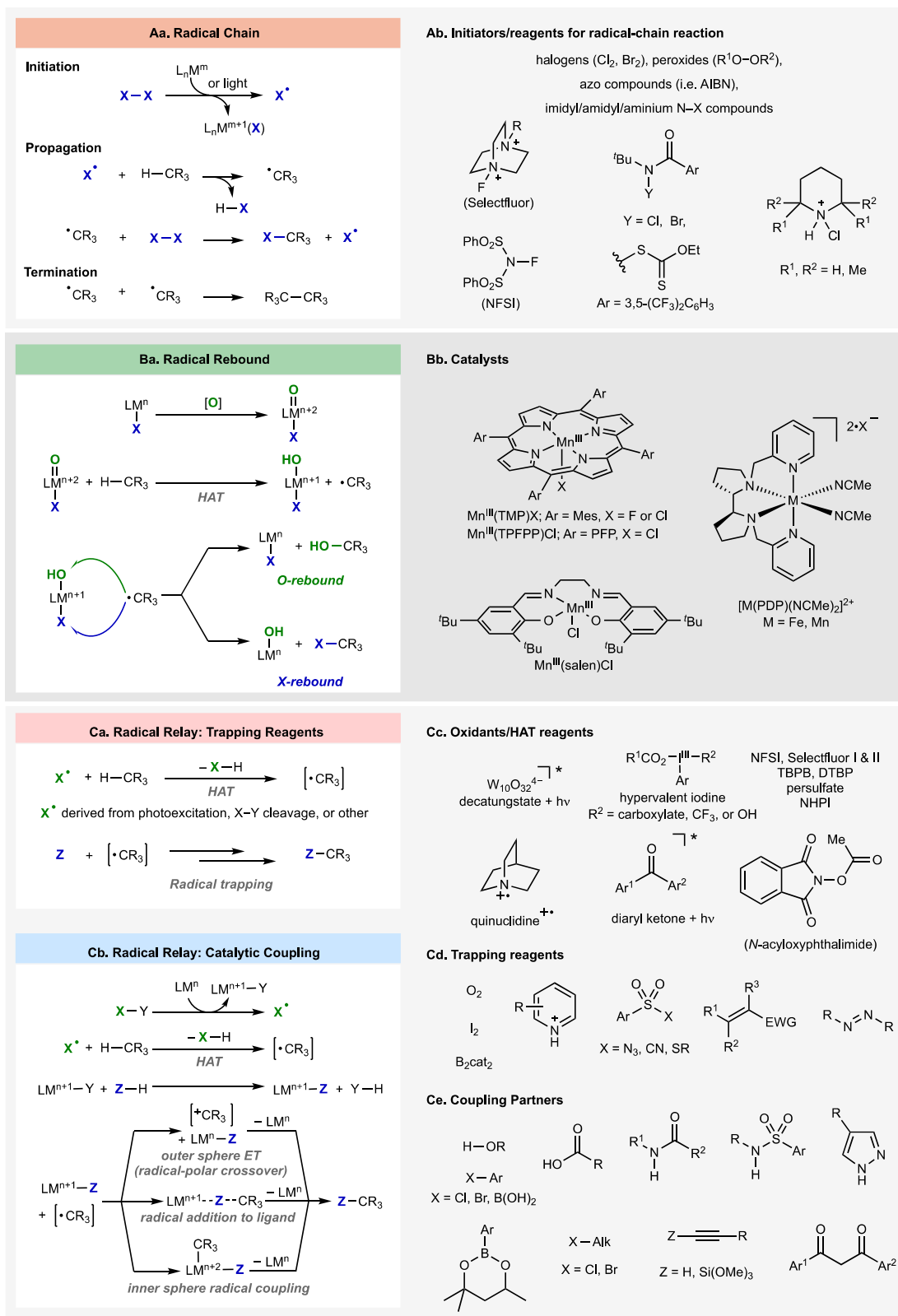


Figure 1.1. Mechanisms and components of radical-chain, radical-rebound, and radical-relay reactions. (Aa) General mechanism of radical-chain reaction. (Ab) Representative

initiators/reagents for radical-chain reactions. (Ba) General catalytic cycle of radical-rebound reaction. (Bb) Representative iron and manganese catalysts for radical-rebound reactions. (Ca) Generic mechanism of radical-relay reactions involving radical trapping reagents. (Cb) Generic mechanism of catalytic radical-relay reactions. (Cc) Representative oxidants and HAT reagents for radical-relay reactions. (Cd) Representative radical trapping reagents. (Ce) Representative catalytic radical-relay coupling partners. Selectfluor I (R = CH₃), 1-chloromethyl-4-fluoro-1,4-diazoniabicyclo[2.2.2]octane bis(tetrafluoroborate); Selectfluor II (R = CH₂Cl), 1-fluoro-4-methyl-1,4-diazoniabicyclo[2.2.2]octane bis(tetrafluoroborate).

1.3. Radical-Chain and Radical-Rebound Reactions

1.3.1. Radical Chain

Conventional radical-chain reactions involving Cl₂ and Br₂ often lack the selectivity required to support synthetically useful, site-selective C–H functionalization of complex molecules. Over the past decade, however, a number of N–X (X = F, Cl) reagents have been shown to promote radical-chain C–H fluorination and chlorination with improved yields and selectivity (Figure 1.2Aa). *N*-Fluorobenzenesulfonimide (NSFI) and Selectfluor reagents are featured in a number of C(sp³)–H fluorination methods, and they have been paired with various initiators, including azobisisobutyronitrile (AIBN),²⁷ BEt₃/O₂,²⁸ and copper(I)²⁹ (Figure 1.2Ab, condition 1). Reactions using Fe(acac)₂/Selectfluor³⁰ (acac = acetylacetonate) and CuOAc/NFSI³¹ support selective fluorination of benzylic C–H bonds and the reactivity is consistent with a radical-chain pathway. A multicomponent Cu(bis-imine)/Selectfluor/*N*-hydroxyphthalimide (NHPI) catalyst system with KB(C₆F₅)₄ as an anionic phase-transfer catalyst supports fluorination of stronger aliphatic C–H bonds.³² N–F reagents have also been paired with photocatalysts, including diarylketone³³ and tetrabutylammonium decatungstate (TBADT).^{27,34} These reagents are capable of promoting HAT from C–H substrates (Figure 1.2Ab, condition 2 and 3), and the resulting carbon-centered radicals can react with fluorinating reagents to afford the desired C–F bonds. It is possible that HAT could proceed via both radical-chain and photocatalyst-promoted steps in these

reactions. Fluorination of benzylic C(sp³)–H bonds has been achieved using 1,2,4,5-tetracyanobenzene, although this photocatalyst is proposed to initiate an electron transfer pathway.³⁵ Collectively, these methods provide effective routes to monofluorinated benzylic and aliphatic C(sp³)–H products. The reactions show good selectivity for benzylic C–H bonds in the photocatalyzed (i.e., diaryl ketone, TBADT) and metal-initiated radical chains. Difluorination can be achieved under more forcing condition and by employing additional Selectfluor and diaryl ketone as photocatalyst.³³

Complementary reagents have been developed to support selective radical-chain chlorination. A sterically encumbered *N*-chloroamide reagent supports chlorination of aliphatic C(sp³)–H substrates under visible-light irradiation, taking advantage of difference in electronics and sterics of various C–H bonds to achieve improved selectivity relative to conventional chlorination methods (Figure 1.2Ac, X = Cl).¹⁴ Steric modulation of aryl ring of the *N*-chloroamide reagent, by shifting two trifluoromethyl groups from meta to ortho positions with respect to the carbonyl group, alters regioselectivity in the chlorination of aliphatic C–H bonds.³⁶ A sterically hindered, 2,2,6,6-tetramethylpiperidinium N–Cl reagent (cf. Figure 1.1Ab) is an effective chlorinating reagent and chain carrier for photoinitiated C–H chlorination.³⁷ The electrophilicity and steric hindrance of the aminium radical confers excellent selectivity in reactions with less sterically hindered methylene C–H sites and with weaker tertiary C(sp³)–H bonds. Radical-chain chlorination of primary or secondary benzylic C–H bonds with *N*-chlorosuccinimide (NCS) has been initiated by reductive activation of NCS with an acridinium-based photocatalyst to generate a nitrogen-centered radical.³⁸ In addition to N–Cl reagents, *tert*-butyl hypochlorite (*t*BuOCl) has been used with a phenanthroline (phen)-ligated silver catalyst to chlorinate C(sp³)–H bonds.³⁹ The reaction has been proposed to proceed via silver-mediated C–Cl bond formation; however, a

radical-chain pathway could also account for the observed reactivity. In the latter pathway, a carbon-centered radical generated by HAT could react via chain propagation with t BuOCl.

Radical-chain reactions have been developed for selective conversion of $C(sp^3)$ -H bonds into C-Br, C-S, and C-O bonds. Variants of the *N*-chloroamide reagent in Figure 1.2Ac in which N-Cl is replaced with N-Br or N-xanthyl (xanthyl = $-S(C=S)OEt$) supports C-H bromination¹⁵ and xanthylation,¹⁶ respectively. Xanthylated products are versatile intermediates in two-step C-H functionalization/diversification reactions in which the xanthyl group may be displaced in a second step by other groups, including allyl, vinyl, CF_3 , D, NR_2 , N_3 , OH, and SR (Figure 1.2Ac).^{16,40} Bis(methanesulfonyl) peroxide supports radical-chain C-H oxygenation of benzylic $C(sp^3)$ -H bonds in the presence of a copper(I) initiator, and the resulting benzyl mesylates undergo facile displacement by water in the presence of hexafluoroisopropanol (HFIP) to afford benzyl alcohols (Figure 1.2Ad).¹⁷

Collectively, these synthetic methods and reagents highlight the emergence of numerous synthetically useful radical-chain reactions. Sterically and electronically tailored N-X and O-X reagents (X = heteroatom substituent) have begun to overcome historical limitations of radical-chain reactions involving simple Cl_2 , Br_2 , and related reagents. Moreover, recent applications of radical-chain reactivity have demonstrated the ability to employ C-H substrates as the limiting reagent and exhibit good site selectivity and compatibility with functional groups that are sensitive to polar reagents.

1.3.2. Radical Rebound

Radical-rebound $C(sp^3)$ -H functionalization takes inspiration from heme and non-heme iron oxygenase enzymes.^{18, 41} Early studies of model complexes for non-heme iron enzymes

investigated reactions with hydrogen peroxide as the oxidant and provided clear evidence for generation of high-valent iron-oxo species.^{42–46} For example, stereospecificity observed in the hydroxylation of alkanes supports rapid rebound of the organic radical with an intermediate Fe–OH species generated via HAT (cf. Figure 1.1Ba).^{46–48} These and related studies established a foundation for more recent synthetic applications of this reactivity using similar catalyst systems. Nitrogen-ligated iron catalysts have been developed for stereo- and site-selective oxidation of aliphatic C–H bonds in molecules containing multiple secondary and tertiary C–H bonds.⁴⁹ The C–H substrate is used as the limiting reagent in these reactions, distinguishing these reactions from the earlier studies, which used excess hydrocarbon substrate with limiting oxidant. Electronic, steric, and stereoelectronic factors contribute to site selectivity,⁵⁰ with reactivity favored at electron-rich and less hindered sites, in addition to sites that relieve strain in the HAT step.^{51,52} These catalyst systems have been implemented for hydroxylation of structurally complex molecules,^{49,52–54} and modification of the ligand structure allows for enhanced and/or altered site-selectivity (Figure 1.2B). Manganese catalysts analogous to the Fe-based catalyst systems have also been employed in synthetically important radical-rebound oxygenation reactions.^{55–57} Enantioselective oxidation of methylene C–H bonds has been achieved by using a chiral tetradentate nitrogen ligand to support enantioselective HAT (Figure 1.2Ca).⁵⁸ Carboxylic acid additives contribute significantly to the reaction outcome by promoting O–O bond cleavage of the hydroperoxide intermediate to afford the reactive metal-oxo species and by replacing a metal-bound hydroxide with a carboxylate ligand that influences both site-selectivity and enantioselectivity in C–H oxidation reactions.^{49,51–54,58–61}

Various manganese-based catalysts show that the radical-rebound pathway can provide the basis for aliphatic C(sp³)–H functionalization beyond oxygenation (Figure 1.2Cb). Mn-porphyrin

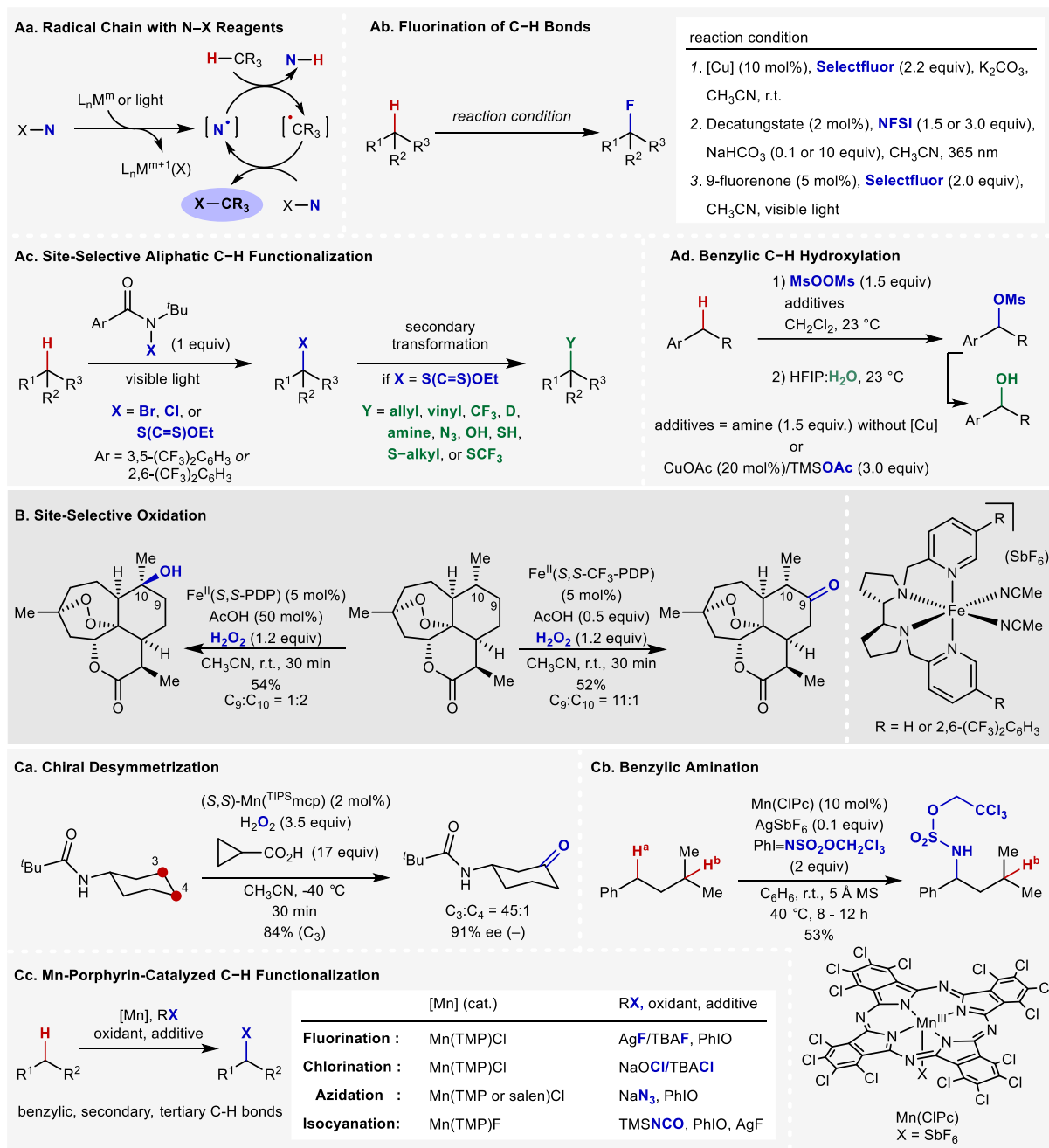


Figure 1.2. Late-stage C(sp³)–H functionalization reactions via radical chain and radical rebound. (Aa) General mechanism for radical-chain reaction with a N–X reagent. (Ab) Fluorination reactions of C(sp³)–H bonds. (Ac) Site-selective aliphatic C–H halogenation and xanthylation reactions with N–X reagents. (Ad) Benzylic C(sp³)–H hydroxylation reaction. (B) Iron-catalyzed C–H oxidation reaction. (Ca) Manganese-non-heme catalyzed chiral desymmetrization of cyclohexane. (Cb) Manganese-catalyzed benzylic amination reaction. (Cc) Manganese-porphyrin or -salen catalyzed C–H functionalization reactions.

and Mn-salen complexes support chemoselective halogenation (fluorination, chlorination)^{62–65} and

pseudohalogenation, with azide⁶⁶ and isocyanate⁶⁷ sources. Most of these reactions employ iodosylbenzene (PhIO) as the oxidant. The radical-rebound mechanism is not limited to oxygen-centered HAT species. A Mn-phthalocyanine catalyst supports sulfonamidation of benzylic C(sp³)-H bonds using a trichloroethoxysulfonamide-derived hypervalent iodine reagent (PhI=NTces) (Figure 1.2Cc).²⁰ The reaction is highly selective for benzylic sites in the presence of other aliphatic C-H bonds and exhibits good functional group tolerance. These efforts showcase synthetically useful applications of the radical-rebound mechanism to achieve site-selective carbon-heteroatom bond forming reactions.

1.4. Radical Relay

The development of radical-relay reactions in recent years has significantly expanded the scope of C(sp³)-H functionalization. The term ‘radical relay’ is used here to describe non-chain radical C-H functionalization reactions in which the HAT species does not incorporate the group or reagent that undergoes coupling with the intermediate organic radical (Figure 1.1)

1.4.1. Radical-Relay Reactions Involving Direct Coupling with a Trapping Reagent or Substrate Partner

The first class of radical-relay reactions, summarized in this section, features the direct addition of an organic radical to a trapping reagent or coupling partner. The HAT species used to generate the organic radical may itself be generated in several different ways: redox processes leading to an oxyl radical (for example, via oxidation of an O-H bond or reductive cleavage of an N-O bond); photochemical excitation of decatungstate anion or aryl ketones; photon-induced ligand-to-metal charge transfer of a transition metal reagent (resulting in homolytic cleavage of a M-OR or M-Cl bond); reductive activation of N-F reagents (such as NFSI or Selectfluor reagents); among other

ways.

Radical-relay C–H oxygenation reactions may be achieved by combining an HAT reagent with O₂ or another oxygen-atom source as the radical trap.^{4,68,69} These methods often exhibit improved selectivity relative to conventional autoxidation methods. A prominent example of this concept features the use of *N*-hydroxyphthalimide (NHPI), which generates the HAT species phthalimido-*N*-oxyl (PINO) in the presence of O₂ and a cobalt catalyst (Figure 1.3Aa).^{70,71} PINO-mediated HAT from weak C(sp³)–H bonds generates a carbon-centered radical that reacts rapidly with O₂, ultimately affording ketones, carboxylic acids, or other oxygenation products. This reactivity was initially demonstrated with simple hydrocarbons,⁷⁰ but it has recently been applied to oxygenation of heterobenzylic C–H bonds in pharmaceutically relevant building blocks.⁷¹ The scope of alkylated heterocycles was extended by the development of an iron, rather than cobalt, cocatalyst.⁷² The oxygenation of methylarenes under Co/NHPI/O₂ conditions typically generates benzoic acid derivatives; however, the use of an HFIP solvent system enables selective formation of benzaldehydes. Hydrogen bonding from HFIP is proposed to polarize the carbonyl group of the aldehyde to prevent further oxidation to benzoic acid.⁷³ Decatungstate (DT) photocatalysts serve as an effective HAT reagent upon near-ultraviolet irradiation, and they support reactivity at C(sp³)–H bonds stronger than those typically reactive with PINO. The excited-state DT species is an electrophilic HAT reagent, and protonated amines undergo reaction at C–H bonds remote from the electron-withdrawing ammonium group, forming ketones in the presence of H₂O₂ (Figure 1.3Ab).⁷⁴ TBADT has been used as an HAT photocatalyst to support the oxygenation of (hetero)benzylic and aliphatic C–H bonds in the presence of O₂ under batch⁷⁵ and continuous flow⁷⁶ conditions.

PINO is a meta-stable radical, and, in addition to serving as an HAT reagent, it can trap carbon-

centered radicals to afford PINOylated products (Figure 1.3B). This reactivity has been achieved by combining catalytic copper(I) chloride, (diacetoxyiodo)benzene ($\text{PhI}(\text{OAc})_2$), and NHPI with the C–H substrate (Figure 1.3Ba).⁷⁷ Similar reactivity has been achieved with a reaction system comprising catalytic copper(II) acetate, Selectfluor, and NHPI (Figure 1.3Bb).⁷⁸ The mechanism of these reactions is not well understood, but reactive HAT species could be generated by oxidation of NHPI or reductive activation of the stoichiometric oxidant, and the Cu catalyst could contribute to each of these processes. Ultimately, the PINOylation product may be formed by coupling of the carbon-centered radical derived from HAT with PINO.

Sulfonyl–X reagents ($X = \text{N}_3, \text{CN}, \text{SR}, \text{SCF}_3, \text{SePh}, \text{Cl}, \text{CH}=\text{CHSO}_2\text{Ph}, \text{and } \text{C}\equiv\text{CAr}$) react with carbon-centered radicals to afford C–X bonds, and they are employed in a number of radical-relay $\text{C}(\text{sp}^3)\text{–H}$ functionalization reactions. Various methods may be used to generate the radical via HAT from a $\text{C}(\text{sp}^3)\text{–H}$ bond. Azidation of aliphatic C–H bonds can proceed under metal-free conditions, using potassium persulfate as the HAT precursor with an arylsulfonyl azide trapping reagent (Figure 1.3Ca).⁷⁹ Photoexcited decatungstate has been used to promote HAT in the presence of tosyl cyanide to support C–H cyanation (Figure 1.3Ca, bottom).⁸⁰ DT-mediated HAT has also been used in combination with other radical traps, including sulfur dioxide,⁸¹ (trifluoromethylthio)phthalimide,⁸² and other sulfonyl–X reagents (for example, methanesulfonyl alkynes⁸³) to achieve C–H functionalization. Reductive activation of the N–F reagent *N*-(*tert*-butyl)-*N*-fluoro-3,5-bis(trifluoromethyl)benzenesulfonamide by copper(I) has been used to generate a nitrogen-centered radical capable of promoting HAT in the presence of $\text{PhSO}_2\text{–X}$ reagents ($X = \text{SCF}_3, \text{SePh}, \text{C}\equiv\text{CPh}, \text{CN}, \text{N}_3, \text{Cl}, \text{CH}=\text{CHSO}_2\text{Ph}$). This reactivity was most extensively demonstrated for the thiolation of $\text{C}(\text{sp}^3)\text{–H}$ bonds (Figure 1.3Cb).⁸⁴ This chemistry is closely related to Cu/NFSI-based C–H functionalization methods elaborated below, with the

distinction that the carbon-centred radical intermediate directly adds to the sulfonyl–X reagent rather than undergoing Cu-catalysed functionalization (see Figure 1.1Ca/b and content below for additional context).

Dialkyl azodicarboxylate reagents react as radical traps to support the amination of C(sp³)–H bonds. A copper(II)/organic HAT catalyst system using diethyl azodicarboxylate (DEAD) has been used to achieve site-selective amination of heterobenzylic C(sp³)–H bonds (Figure 1.3Da).⁸⁵ Copper(II) acts as a Lewis acid catalyst to enhance the reactivity of heterobenzylic positions, leading to high selectivity in the presence of weaker benzylic C–H bonds. Photoinduced ligand-to-metal charge transfer (LMCT) in cerium(IV)–X reagents has been used to generate reactive heteroatom-based radicals that promote HAT from C(sp³)–H bonds. The initial reports proposed the formation of an oxygen-centered radical via LMCT within a cerium(IV)-alkoxide complex;^{86,87} however, a subsequent study implicated the formation of chlorine radical via LMCT involving a Ce^{IV}–Cl fragment.⁸⁸ In both proposed mechanisms, the heteroatom radical promotes HAT, and the resulting carbon-centered radical adds to the dialkyl azodicarboxylate reagent to form a C–N bond. This step leads to the formation of an adjacent nitrogen-centered radical that is proposed to be reduced by cerium(III) and undergo protonation to afford the final product (Figure 1.3Db).⁸⁷ The N–N bond is subjected to hydrogenolysis over Raney Ni to afford the primary amine derivative. DT photocatalysis has also been used to support HAT from C–H bonds in the presence of dialkyl azodicarboxylate to afford the C–N coupling products.^{89,90} A photoreactor equipped with a high intensity LED light has been used to achieve this reactivity under flow conditions.⁹¹

Electron-deficient alkenes can serve as radical traps that provide the basis for C(sp³)–H alkylation. The addition of carbon-centered radicals to alkenes ("Giese reactions"^{92–94}) generates

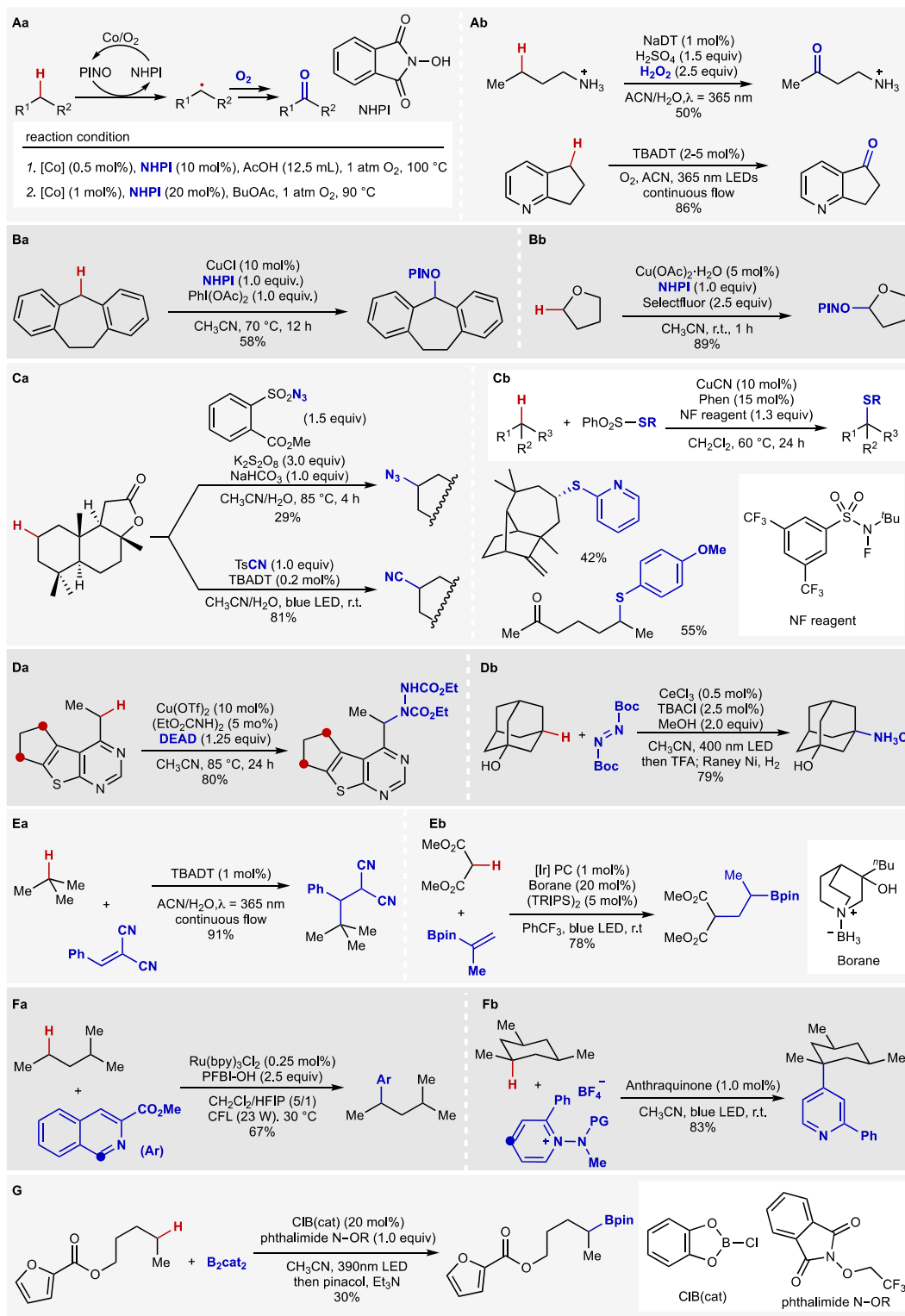


Figure 1.3. Radical relay involving radical addition to trapping reagents. (Aa) Oxygenation with Co/NHPI cocatalysts. (Ab) Oxygenation with decatungstate photocatalysts. (Ba/b) PINOylation methods. (Ca) Azidation/cyanation via radical trapping with sulfonyl-X reagents (X = N₃, CN). (Cb) Thiol coupling via radical trapping with sulfonylthiolates. (Da) Amination of

heterobenzylic C(sp³)–H bonds with DEAD. (Db) Amination initiated by LMCT with Ce^{IV} reagents. (Ea) Giese-type alkylation with decatungstate photocatalysts. (Eb) Polarity reversal HAT/Giese-type alkylation. (Fa) Minisci reaction with decatungstate photocatalyst. (Fb) Photochemical Minisci-type pyridylation. (G) Photochemical borylation.

a new carbon-centered radical that can react with a hydrogen-atom donor (for example, a thiol or other reagent) or undergo one-electron reduction and protonation to afford the alkylated product. Light-promoted LMCT from copper(II),⁹⁵ cerium(IV),^{86,87} and iron(III)⁹⁶ reagents and DT photocatalysts^{97–100} have been used to generate reactive species that support HAT from the C–H substrate. A DT-catalysed Giese-type radical addition reaction was implemented in continuous flow to forge new C(sp³)–C(sp³) bonds between light alkanes, including methane, ethane, propane, isobutane, and electron-deficient alkenes (Figure 1.3Ea).¹⁰¹ HAT reagents typically consist of electrophilic radicals that favour reaction at electron-rich C–H bonds (for example, 3° aliphatic and benzylic C–H bonds); however, polarity-reversed HAT¹⁰² from acidic C–H bonds adjacent to electron-withdrawing groups was enabled by using an amine-borane catalyst under photochemical conditions (Figure 1.3Eb).¹⁰³ Subsequent addition of the organic radical to an unactivated alkene followed by hydrogen abstraction from a thiol-based H-atom donor affords the C(sp³)–C(sp³) coupling product.

Electron-deficient arenes and heterocycles, such as pyridinium compounds, also react readily with nucleophilic radicals ("Minisci reactions"^{104,105}). This reactivity may be used to support (hetero)arylation of C(sp³)–H bonds by generating carbon-centred radicals via HAT. Representative HAT reagents that have been used in Minisci-type coupling reactions include oxygen- and nitrogen-centred radicals derived from peroxides/alcohols and amides,^{106–109} DT photocatalysts,^{110–113} azide radical,¹¹⁴ and hypervalent iodine.¹¹⁵ For example, a ruthenium photoredox catalyst can undergo SET with hydroxyl perfluorobenziodoxole (PFBI–OH) to generate an oxygen-centered radical.¹¹⁵ HAT generates a carbon-centred radical that adds to a

protonated *N*-heteroarene, and subsequent loss of an electron and proton from the adduct affords the Minisci coupling product (Figure 1.3Fa). In another example, anthraquinone proved superior to TBADT and to benzoquinone as a photocatalyst/HAT reagent in the direct coupling of alkanes with *N*-aminopyridinium salts.¹¹⁶ The radical adds to the electron-deficient heterocycle, similar to Minisci reactions, with C4 selectivity (Figure 1.3Fb). The reaction employs 5 equiv of alkane, aldehyde, and other coupling partners (for example, P–H, Si–H substrates).

A primary-selective C–H borylation reaction is initiated by photoinduced electron transfer upon irradiating *N*-(trifluoroethoxy)phthalimide in the presence of bis(catecholato)diboron (B₂cat₂), 10 equiv of the C–H substrate, and 20 mol% *B*-chlorocatecholborane [ClB(cat)] (Figure 1.3G).¹¹⁷ Mesolytic cleavage of the N–O bond affords a trifluoroethoxy radical that is proposed to react with ClB(cat) to generate the reactive HAT species. Because there is no photoredox catalyst, it seems likely to be occurring through a radical rather than radical-polar crossover pathway. Carbon–boron bond formation arises from the reaction of the intermediate organic radical with B₂cat₂. High primary C–H selectivity, even in the presence of weaker secondary and tertiary C–H bonds, is rationalized by the involvement of a chlorine radical–boron 'ate' complex that selectively cleaves sterically unhindered C–H bonds.

1.4.2. Kharasch-Sosnovsky Reactions

The Kharasch–Sosnovsky (K–S) allylic oxidation reaction, first reported in 1958, represents a seminal precedent for catalytic radical-relay reactivity (Figure 1.1Cb).^{118, 119} The original transformation used copper(I) bromide and *tert*-butyl peroxybenzoate (TBPB) to achieve allylic oxidation of cyclohexene, 1-hexene, and 1-octene, affording the allylic benzoate derivatives (Figure 1.4a). The proposed mechanism involves Cu^I-mediated activation of the peroxide, allylic HAT by ^tBuO• and coupling of the allylic radical with Cu^{II}-benzoate (Figure 1.4b).¹²⁰ Asymmetric

C–O coupling, which was initially achieved by using a catalytic amount of L-proline as a chiral ligand (40% yield, 30% ee),¹²¹ implicates inner-sphere coupling of the C–O bond via radical addition to Cu^{II} and C–O reductive elimination (Figure 1.4c). Improved enantioselectivity was achieved by using chiral bis- or trisoxazoline ligands (Figure 1.4e).^{122–125} Most K–S reactions use excess C–H substrate relative to the peroxide reagent. Low temperatures (for example, –20 °C) are needed to enhance enantioselectivity, but these conditions often result in multiple-day reaction times. K–S oxidation methods have been used in synthetic chemistry, for example, to access triterpene natural products (Figure 1.4d).^{126,127} These reactions (and later the oxidation of the sesquiterpene valencene^{128,129}) are among the few examples of K–S reactions that use the C–H substrate as the limiting reagent (Figure 1.4j). Adaptation of K–S-type reactivity has led to oxidation of aliphatic C–H bonds. For example, di-*tert*-butyl peroxide (DTBP) has been used as an oxidant in combination with nitrogen-ligated Cu complexes to achieve *tert*-butyletherification of cyclohexane¹³⁰ and dehydrogenative coupling of carboxylic acids with cyclohexane.¹³¹ These reactions use a large excess of the C–H substrate (≥ 10 equiv).

K–S-type reactions may be used to achieve C–N bond formation, for example, with amide, sulfonamide, and imide coupling partners (Figure 1.4g-i).^{119,132–137} The reactions commonly use *tert*-butyl acylperoxides (i.e., derivatives of TBPB) or DTBP as the oxidant. For example, TBPB derivatives with electron-withdrawing groups on the benzoyl group (3-Cl, 3-CF₃) achieve C–N coupling between primary and secondary sulfonamides and simple methylarenes (25 equiv relative to the nitrogen nucleophile) (Figure 1.4h).¹³⁴ A well-defined diketiminate-ligated Cu complex was used in combination with DTBP to support the amination of a small number of aliphatic C–H substrates (indane, ethylbenzene, cyclohexane) with 1-adamantylamine and other aliphatic amines (Figure 1.4g).¹³⁵ The amine ligand undergoes exchange with a [Cu]–O^tBu intermediate to form a

copper(II)-amido complex, and mechanistic studies indicate that this species can promote direct HAT from the C–H substrate. This reactivity differs from most K–S-type reactions, which feature HAT by an alkoxyl radical. Amination of cyclic and acyclic aliphatic C–H bonds proceeds with various amides, sulfonamides, and phthalimide using a 4,7-dimethoxyphenanthroline/Cu^I catalyst with DTBP as the oxidant (Figure 1.4i).¹³⁶ A variant of the conventional K–S mechanism was proposed, in which a Cu^I-amidate activates the peroxide to generate the *t*BuO•, which promotes HAT from the C–H substrate.¹³⁶ The resulting alkyl radical reacts with a Cu^{II}-amidate species to afford the C–N bond. A photochemical copper(II)-catalyzed method initiates O–O bond homolysis of DTBP at room temperature, supporting C–N coupling of alkanes with various nitrogen nucleophiles under mild conditions.¹³⁷ As with the other K–S-type reactions involving aliphatic substrates, a large excess of the C–H substrate (≥ 10 equiv) is used in these reactions.

K–S reactivity may be used to support C–C coupling reactions with various carbon nucleophiles, including 1,3-dicarbonyl compounds, arylboronic esters, and fluorinated arenes. In the reaction of benzylic C–H substrates with TBPB as the oxidant, C–C coupling with 1,3-dicarbonyl compounds proceeds via sequential formation of a benzylic benzoate, followed by nucleophilic displacement of the benzoate (Figure 1.4f).¹³⁸ Redox-neutral alkenylation of C–H bonds adjacent to oxygen in THF (and related cyclic ether solvents) exhibits features reminiscent of K–S reactions, employing terminal alkynes as coupling partners together with *t*BuOOH and catalytic Cu^ICl under blue LED irradiation.¹³⁹ Arylation of benzylic C–H bonds with arylboronic esters proceeds with DTBP as the oxidant (Figure 1.4k).¹⁴⁰ The reaction is proposed to involve transmetalation between the arylboronic ester and a Cu^{II}–O^{*t*}Bu intermediate to afford an

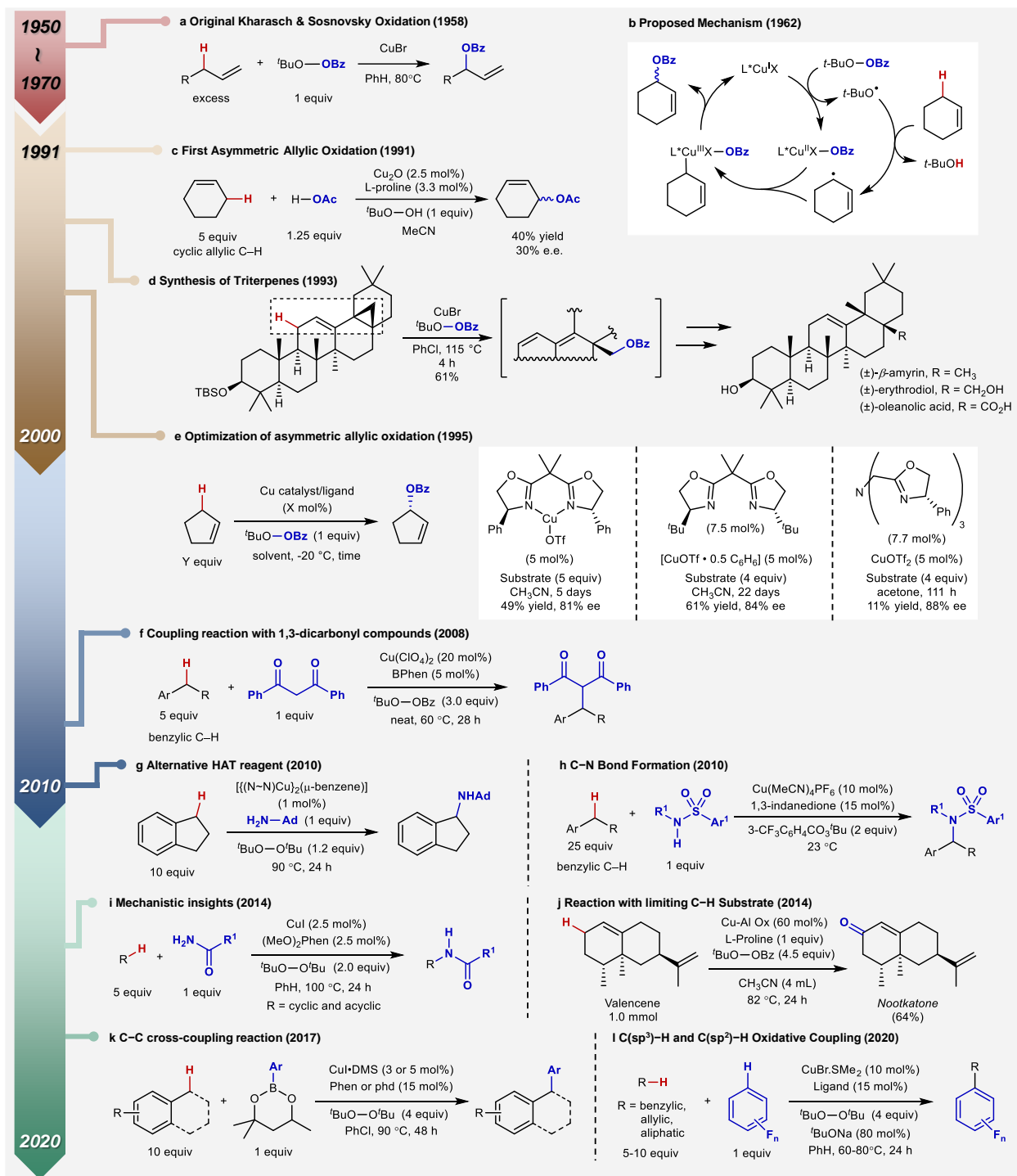


Figure 1.4. Timeline of representative Kharasch-Sosnovsky reactions.

arylcopper(II) intermediate, which undergoes coupling with a benzylic radical generated by HAT from $t\text{-BuO}\cdot$. This reaction affords a variety of diarylmethane and diarylalkane products. β -Diketiminato copper catalysts support direct C-H/C-H coupling of polyfluoroarenes and allylic,

benzylic, and aliphatic C–H substrates using DTBP as the oxidant (Figure 1.4l).¹⁴¹ Each of these reactions employs the C(sp³)–H substrate in excess (for example, 10 equiv) relative to the coupling partner; however, they have synthetic appeal beyond the related C–O and C–N coupling reactions because the more valuable coupling partner (alkyne, arylboronic acid, fluoroarene) is used as the limiting reagent. Thus, inexpensive cyclic ethers and alkylarenes may be used to support the alkylation of valuable coupling partners.

1.4.3. Cu/NFSI-Catalyzed C(sp³)–H Functionalization and Cross-Coupling Methods

The need for excess C–H substrate restricts the synthetic utility of K–S and related oxidative coupling reactions; however, this limitation has been overcome by using NFSI, rather than peroxide-based oxidants, in combination with copper catalysts. These methods show very high selectivity for benzylic C(sp³)–H bonds relative to other positions (for example, 3° C–H bonds), and they are among the most versatile methods for site-selective C–H functionalization and cross-coupling, leading to the formation of new C–X (X = halide, pseudohalide), C–N, C–O, C–S, and C–C bonds (Figure 1.5).

The first Cu/NFSI benzylic C–H functionalization method led to sulfonimidation of benzylic C–H bonds, using NFSI as the HAT reagent and as the coupling partner (Figure 1.5a).¹⁴² This method, which is compatible with primary and secondary benzylic C–H bonds, highlighted the use of the benzylic C–H substrates as the limiting reagent. The first demonstration of Cu/NFSI reactivity for oxidative coupling of C–H substrates with separate nucleophilic reaction partners featured cyanation of benzylic C–H bonds with TMSCN (TMS = trimethylsilyl) (Figure 1.5b).¹⁴³ These reactions employ a chiral bisoxazoline ligand and achieve high enantioselectivity (many with >90% ee), good functional group compatibility, and very high site selectivity for less hindered

secondary benzylic C–H bonds. Density functional theory (DFT) calculations suggest enantioselective C–C bond formation arises from reversible radical addition to a chiral $\text{Cu}^{\text{II}}\text{-CN}$ species followed by selectivity determining reductive elimination (Figure 1.6a, inner sphere radical coupling).

Benzylic C–H trifluoromethylation was demonstrated using a copper(I) source, NFSI or Selectfluor II as the oxidant, and $(\text{bpy})\text{Zn}(\text{CF}_3)_2$ as the trifluoromethyl nucleophile (Figure 1.5c).¹⁴⁴ NFSI is generally the most effective oxidant for primary benzylic substrates, but Selectfluor II, which generates a more reactive nitrogen-centered radical, exhibits improved reactivity with electron-deficient substrates. Improved outcomes were observed with secondary benzylic substrates when using $\text{Zn}(\text{OTf})_2$ and $\text{Zn}(\text{OAc})_2$ additives, an effect attributed to more efficient transmetalation of the trifluoromethyl anion to copper(II), resulting in higher concentrations of $\text{Cu}^{\text{II}}\text{-CF}_3$ species.

Cu/NFSI -catalyzed C–H azidation is achieved by using trimethylsilyl azide (TMSN_3) as the nucleophilic coupling partner (Figure 1.5d).¹⁴⁵ The reaction exhibits very high site-selectivity for secondary benzylic C–H bonds over tertiary aliphatic and benzylic C–H bonds. This selectivity, which exceeds that observed with other radical azidation methods,^{66,146,147} is rationalized by the steric and electronic properties of the sulfonimidyl *N*-centered radical that promotes HAT. Azide is an effective ammonia surrogate, in addition to serving as a precursor to various heterocycles (Figure 1.5d). Complementary Cu/NFSI methods have been developed for coupling with other ammonia surrogates, including carbamates,¹⁴⁸ sulfonamides, and primary carboxamides (Figure 1.5e)¹⁴⁹. These and several other Cu/NFSI -catalyzed oxidative coupling reactions afford racemic products, even when using chiral bisoxazoline ligands similar to those in the cyanation reaction¹⁴⁵. Experimental and computational data indicate the azidation reaction proceeds via a radical-polar

crossover mechanism in which the benzylic radical is oxidized to a cation prior to reaction with an azide nucleophile. The different stereochemical outcomes of these reactions are likely correlated with the influence of different nucleophiles as ligands that modulate the redox properties of the Cu^{II} species, altering the fate of the radical intermediate.

TMSNCS and TMSNCO are additional effective pseudohalide coupling partners, affording benzylic thiocyanate and isocyanate derivatives (Figure 1.5f and 1.5g).^{150, 151} Inter- and intramolecular competition studies in the thiocyanation reaction indicate that HAT from benzylic C–H bonds favours $3^\circ > 2^\circ > 1^\circ$ positions, and thus differs from the azidation reaction, which favors 2° sites. These observations suggest the identity of the HAT reagent may not be identical in all reactions. Both thiocyanate and isocyanate product classes represent versatile precursors to other valuable products. The benzylic thiocyanate products may be converted in two- or three-step sequences and without isolation of the intermediates, into other products, including isothiocyanates, thioureas, trifluoromethylthio, difluoromethylthio, 5-S-benzbromarone-linked tetrazole, and disulfide derivatives. This concept was expanded to enable the synthesis of benzylic isocyanates by developing a benzylic isocyanation/amine coupling sequence. This sequence was shown to be suited to implementation in a high-throughput format, enabling efficient access to large numbers of benzylic ureas with drug-like physiochemical properties.¹⁵¹

The C–H functionalization/diversification strategy illustrated for azides, thiocyanates, and isocyanates in Figures 1.5d, 1.5f, and 1.5g is even more versatile with C–H halogenation methods. C–H fluorination was demonstrated by variation of the original Cu/NFSI conditions, which led to C–H sulfonimidation (Figure 1.5h).^{31, 152} The use of a Brønsted base (Li_2CO_3) and $\text{MeB}(\text{OH})_2$ as an in situ reductant for the copper catalyst (that is, a "redox buffer"; see mechanistic discussion below) induce a switch in selectivity³¹ via initiation of a Cu^{I} -promoted radical-chain pathway

involving NFSI (see *Radical Chain* section above for further discussion and additional references). From a synthetic perspective, benzyl fluorides are not inert like many other alkyl fluorides but are quite labile. This feature may be exploited to support nucleophilic displacement of the fluoride, promoted by the presence of a hydrogen-bond donor, such as hexafluoroisopropanol (HFIP), or a Lewis acid, such as boron trifluoride diethyl etherate ($\text{BF}_3 \cdot \text{Et}_2\text{O}$).^{153–156} The resulting fluorination–substitution sequence enables the replacement of benzylic C–H bonds with a wide range of oxygen-, nitrogen-, and carbon-based groups.¹⁵² Similar concepts have been demonstrated with a Cu/NFSI-catalyzed chlorination method (Figure 1.4i), in which chlorination–substitution facilitates access to products that might be difficult to obtain under the acidic conditions required for fluoride substitution.¹⁵⁷ For example, reactions of phenols with benzyl fluorides promoted by HFIP leads to C–C bond formation, with phenol reacting at the ortho position while reactions with benzyl chlorides under basic conditions leads to C–O bond formation, with phenol reacting at the oxygen atom. These two-step functionalization/diversification methods, initiated by fluorination and chlorination, enable net C–H functionalization with oxidatively sensitive nucleophiles that would not be compatible with a one-step oxidative coupling method using NFSI as the oxidant. This reactivity complements an independent Cu-catalyzed chlorination approach using a dichloramine-T as the oxidant that selectively functionalizes $\text{C}(\text{sp}^3)\text{–H}$ bonds in ketones, enones, and alkylbenzenes.^{158,159} This study also demonstrated nucleophilic displacement of secondary benzyl chlorides with *N*-Boc-piperazine, a further example of functionalization/diversification.

Variants of NFSI have been developed in which one phenylsulfonyl group in NFSI is replaced with a tertiary-alkyl group, and the other is replaced with an electron-deficient arylsulfonyl (for example, 4- CF_3 -phenyl or 3,5- $(\text{CF}_3)_2$ -phenyl). These reagents have been used to achieve complementary radical-relay C–H functionalization, including regio- and enantioselective

cyanation of allylic C(sp³)-H bonds with TMSCN (with limiting C-H substrate),¹⁶⁰ and thiolation of C-H bonds with *S*-aryl benzenethiosulfonates (3 equiv C-H substrate) (see Figure 1.3Cb).⁸⁴ In the former study, DFT calculations implicate a Cu^{II}-bound nitrogen-centered radical as the reactive HAT species, which was proposed to account for modulation of site selectivity. This proposal aligns with the observations above that the specific HAT species could be modified under different conditions. Selectfluor is a related N-F reagent that generates an amine radical-cation — a stronger HAT reagent than the *N*-centered radical derived from NFSI. In the presence of copper catalysts, Selectfluor enables HAT with aliphatic C-H substrates, used in excess (3 equiv to solvent level) relative to the coupling partner.¹⁶¹ Esterification was achieved with various carboxylic acids as coupling partners in the presence of pentanenitrile as additive¹⁶¹. An attempt to couple triflate (from triflic acid) instead resulted in a Ritter-type amidation product derived from pentanenitrile.

Cross-coupling methods that combine reagents from diverse pools of substrates are especially important in synthetic chemistry. Several examples of such C-H cross couplings have been achieved by using Cu/NFSI catalysis. The coupling of benzylic C-H substrates and alcohols enables access to a diverse range of benzyl ethers (Figure 1.5j).¹⁶² Medicinally relevant benzylic C-H substrates undergo cross coupling with sterically and electronically diverse aliphatic alcohols. Mechanistic studies indicate that this reactivity proceeds by a radical-polar crossover mechanism (Figure 1.6b). The reactions were successful only when a dialkyl phosphite was added as a sacrificial reductant to regenerate the reduced catalyst (see mechanistic discussion below). Azoles have also been used as reaction partners in Cu/NFSI-catalyzed benzylic C-H cross-coupling reactions. Pyrazoles exhibit controlled regioselectivity, with differing N-site coupling observed when the reaction was conducted in the presence of either a tetrabutylammonium halide (TBAX) or a silyl triflate additive (Figure 1.5k).¹⁶³ The kinetically favored N₂ site selectivity with TBACl

as the additive contrasts the N1 site selectivity more commonly observed, for example, in substitution reactions with pyrazolide reagents.^{164, 165} Various azoles and other nitrogen heterocycles are effective coupling partners.

Cu/NFSI-catalyzed methods enable carbon-carbon bond formation via benzylic C–H cross coupling with aryl and alkynyl nucleophiles. While K–S-type oxidative coupling of benzylic substrates and aryl boronic acids with DTBP as the oxidant uses excess C–H substrate,¹⁴⁰ the use of NFSI as the oxidant enables reactions to proceed with limiting C–H substrate.¹⁶⁶ The latter reactions are effective with electron-deficient arylboronic acids and proceed at ambient temperature, rather than the high temperatures (90 °C) required for K–S-type reaction. Use of a chiral bisoxazoline ligand supports enantioselective arylation of benzylic C–H bonds of alkylnaphthalenes and related derivatives (Figure 1.5i).¹⁶⁷ Enantioselective coupling of benzylic C–H bonds and alkynyl silane derivatives is also possible, again using chiral bisoxazoline ligands (Figure 1.5m).¹⁶⁸ A modified N–F reagent, in which the two phenyl groups of NFSI were replaced with a 4-fluorophenyl and a 1-naphthyl substituent aryl, led to improvements in the yield and enantioselectivity. The alkylarene is used as the limiting reagent in combination with simple alkynyl trimethoxysilane derivatives.

The catalytic cycle for these Cu/NFSI reactions is believed to follow a mechanism similar to that proposed for K–S reactions (Figure 1.6).¹⁴³ Reductive activation of NFSI by copper(I) initiates the reaction, generating a Cu^{II}–F intermediate and a nitrogen-centered radical (\bullet NSI). The latter species promotes HAT from the C–H bond to generate a diffusible benzylic radical. Studies of a closely related allylic cyanation reaction, which employed modified N–F reagents, provided evidence for an adduct between Cu^{II} and the *N*-centered radical as the HAT reagent.¹⁶⁰ Modification of the nitrogen-centered radical in this manner could account for some variations in

site selectivity that have been observed in different Cu/NFSI described above.

Functionalization of the organic radical can proceed by several different pathways. In some reactions, the nucleophilic coupling partner (for example, TMS-CN) exchanges with fluoride to generate a $\text{Cu}^{\text{II}}\text{-Nuc}$ species. Subsequent addition of the benzylic radical to the Cu^{II} center affords a $\text{Cu}^{\text{III}}(\text{benzyl})(\text{Nuc})$ intermediate that can undergo reductive elimination to afford the desired coupling product via an inner-sphere mechanism (Figure 1.6a). This pathway rationalizes the enantioselective outcomes of certain coupling reactions, including benzylic cyanation, arylation, and alkynylation. Computational studies of the cyanation reaction suggest radical addition to Cu^{II} is reversible, and stereoselectivity is determined in the reductive elimination step.¹⁴³ Alternatively, radical functionalization can proceed via a radical-polar crossover pathway (Figure 1.6b, radical-polar crossover), involving outer-sphere electron transfer from the radical to Cu^{II} . The resulting benzyl cation is then trapped by a nucleophile to afford the observed product. The formation of racemic products in many of the reactions in Figure 1.4, such as etherification,¹⁶² provide support for this mechanism which has also been analyzed by DFT computational studies. DFT analysis of the azidation reaction indicated that radical addition to the distal nitrogen of a coordinated azide ligand (Figure 1.6c) is energetically similar to the radical-polar crossover mechanism.¹⁴⁵ The electron-donating properties of different nucleophiles are expected to influence the $\text{Cu}^{\text{III/I}}$ redox potential and influence whether a benzyl radical adds to Cu^{II} to generate a Cu^{III} intermediate (and thus leading to possible enantioselective bond formation), or whether it undergoes outer-sphere electron transfer, which must result in racemic product formation.

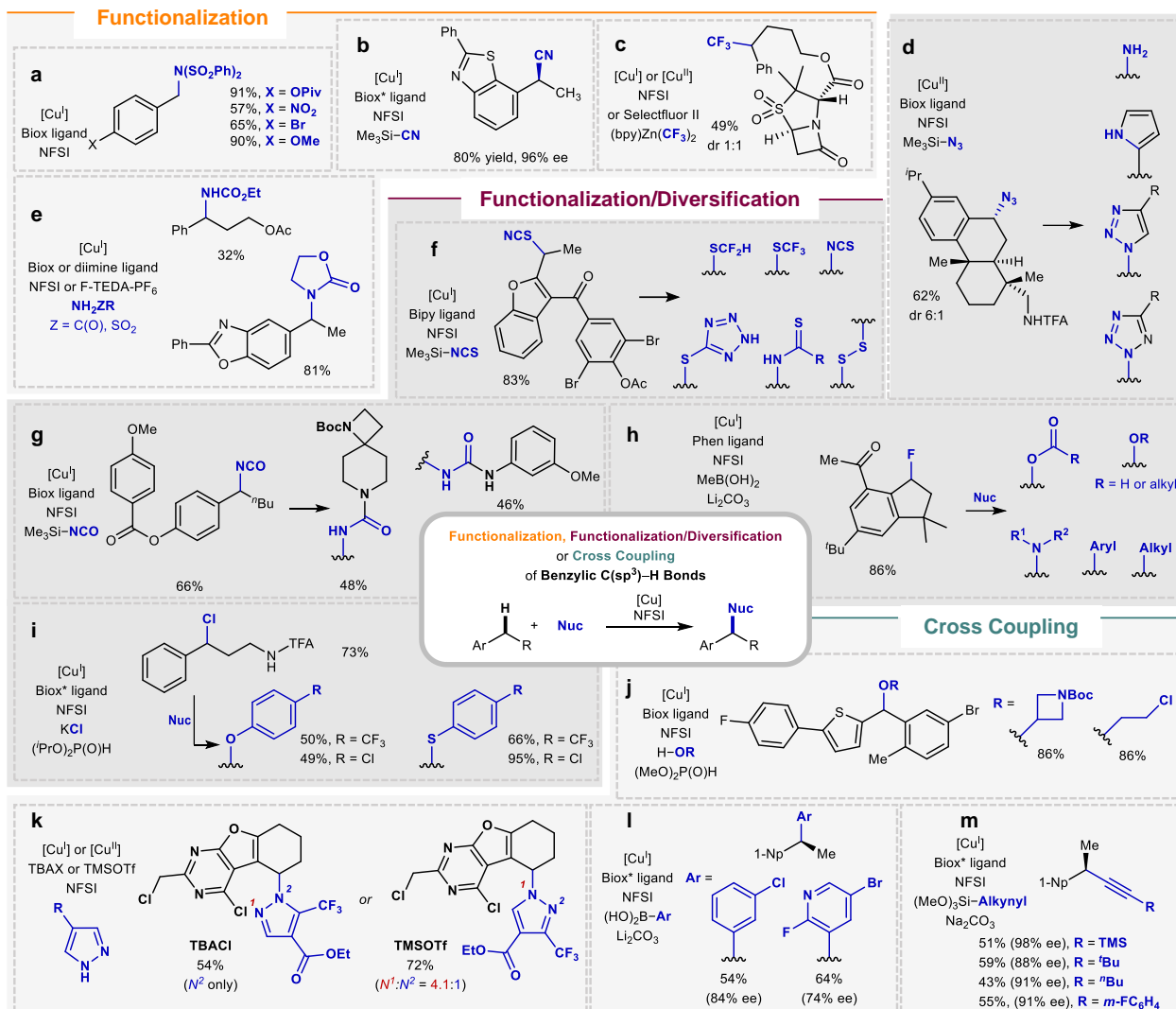


Figure 1.5. Summary of Cu/NFSI-catalyzed radical-relay functionalization, functionalization/diversification, and cross-coupling reactions of benzylic C(sp³)-H bonds.

The •NSI species generated by reductive activation of NFSI by Cu^I can oxidize a second equivalent of Cu^I to generate a Cu^{II}-NSI species, rather than promoting HAT from the C-H substrate (Figure 1.6, bottom cycle). This undesired side reaction leads to unproductive consumption of the NFSI oxidant and Cu^I species, stalling the reaction. This problem was first identified in the study of benzylic etherification.¹⁶² It was overcome by identifying dialkylphosphite as a mild reductant that slowly reduces Cu^{II} to Cu^I during the reaction without directly reacting with NFSI. This "redox buffer" concept has been employed in several Cu/NFSI

radical-relay reactions, including etherification,¹⁶² isocyanation,¹⁵¹ fluorination,³¹ chlorination,¹⁵⁷ and azole coupling.¹⁶³ Reagents that have been used as redox buffers include dialkylphosphites,^{145,151,157,162} MeB(OH)_2 , and B_2pin_2 .^{31,152} Not all Cu/NFSI radical-relay reactions require a redox buffer. If the coupling partner, such as TMSCN or ArB(OH)_2 in the cyanation and arylation reactions, can mediate background reduction of Cu^{II} , for example, through homocoupling to generate cyanogen or biaryls, then no redox buffer is required.

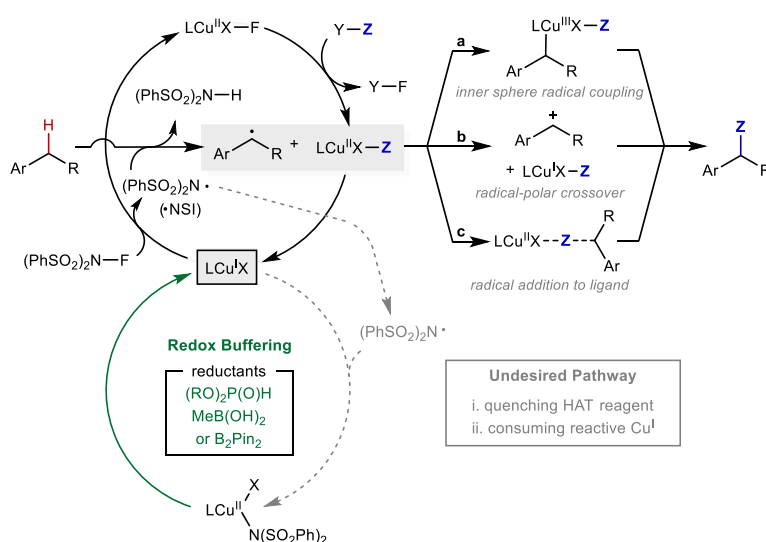


Figure 1.6. Catalytic cycle and radical functionalization mechanisms for Cu/NFSI-catalyzed radical-relay reactions. (a) Inner sphere radical coupling via reductive elimination. (b) Radical-polar crossover pathway. (c) Radical addition to Cu-bound ligand.

1.4.4. Radical-Relay Reactions with Catalysts other than Copper

Various metals other than copper have been used to support synthetically useful oxidative coupling reactions that proceed via radical intermediates (Figure 1.7). Iron(II) chloride and DTBP support the cross coupling of benzylic C–H bonds and 1,3-dicarbonyl compounds¹⁶⁹ and imidazoles¹⁷⁰ (Figure 1.7, Fe), and iron(III) chloride and DTBP was used to achieve coupling of 2-benzylbenzoxazoles and anilines.¹⁷¹ Iron(II) acetate with nitrogen donor ligands catalyses azidation of various $\text{C}(\text{sp}^3)\text{-H}$ bonds with a hypervalent azidoiodine(III) reagent,¹⁴⁶ often favoring

tertiary C–H functionalization. This reactivity was applied to the late-stage functionalization of various complex molecules.¹⁷² Cobalt(II) bromide catalysts support cross coupling of benzylic C–H bonds with amides and sulfonamides and with DTBP as oxidant (Figure 1.7, Co).¹⁷³ Two equivalents of the C–H substrate were used in these reactions. A radical-polar crossover pathway involving a benzylic cation was proposed.

Nickel catalysts have been paired with peroxide oxidants to support oxidative alkylation, arylation, and methylation of C(sp³)–H bonds. A Ni/Cu/Ag-cocatalyst system promotes oxidative C(sp³)–H alkylation of unactivated alkanes (as a cosolvent), using terminal alkynes as the limiting reagent (Figure 1.7, Ni).¹⁷⁴ Ni/triphenylphosphine catalyst systems promote arylation of aliphatic C(sp³)–H bonds with arylboronic acids coupling partners as the limiting reagent.^{175,176} Effective C–H substrates include tetrahydrofuran (THF), 1,4-dioxane, and cyclohexane, which are used as the solvent in the reactions. Methylation of C(sp³)–H bonds with limiting C–H substrates is enabled by photosensitization of peroxides and nickel-mediated radical coupling (Figure 1.7, Ni).¹⁷⁷ Homolysis of tertiary alkyl peroxides generates alkoxy radicals that further react either through HAT with C–H substrates or decompose through β -methyl scission to produce methyl radicals. Various reaction parameters, including temperature, concentration, solvent, and peroxide structure, may be tuned to balance the relative rates of these two reactions. Protonation of C–H substrates containing basic amines deactivates C(sp³)–H sites adjacent to nitrogen to enable methylation at the benzylic positions. This methylation method creates opportunities to explore "magic methyl" effects on medicinally relevant building blocks and drug molecules.¹⁷⁸

Silver catalysts have also been used in radical reactions (Figure 1.7, Ag)¹⁷⁹. A silver-promoted oxidative benzylic C–H trifluoromethoxylation with C–H substrate as the limiting reagent uses potassium persulfate as oxidant.¹⁸⁰ The reaction favors functionalization at secondary > primary >

tertiary benzylic C–H site and can be modified to introduce a fluorine atom and a trifluoromethoxy group at the same site.

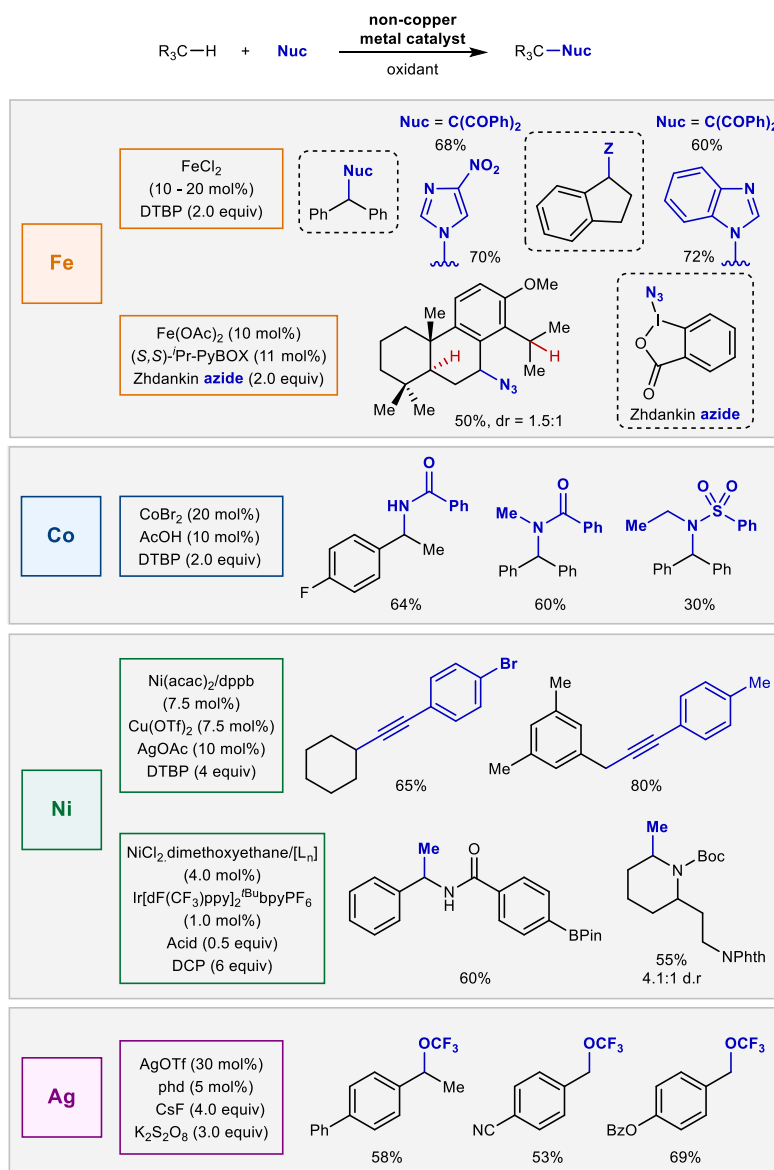


Figure 1.7. Radical-relay C–H functionalization and cross-coupling reactions with catalysts other than copper.

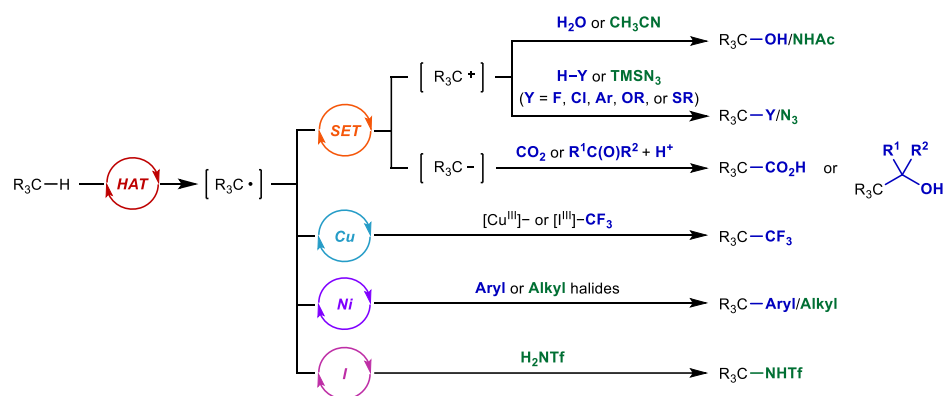
1.4.5. Photoredox C(sp³)–H Functionalization and Cross-Coupling Methods

Photochemical and visible-light photoredox methods provide a versatile strategy to generate organic radicals from a C(sp³)–H substrate and promote radical-relay coupling with diverse

functional groups.^{181–187} The reactions are initiated by abstraction of a hydrogen atom from the C–H substrate. The HAT reagent is generated by photocatalyst-mediated activation of an oxidant, such as a hypervalent iodine reagent, *N*-acyloxyphthalimide, or persulfate, or by direct photoactivation of a reagent, such as decatungstate or benzophenone (Figure 1.8).¹⁸⁸ The introduction of functional groups, including hydroxyl groups, primary amine surrogates, trifluoromethyl, alkyl, and aryl groups, can occur by various mechanisms, similar to the methods outlined above (cf. Figure 1.1Cb and Figure 1.6). Radical-polar crossover reactions, which generate the corresponding cation or anion (Figure 1.8a, SET), are used to support subsequent coupling reactions with nucleophiles and electrophiles, respectively. Transition-metal reagents and cocatalysts can promote coupling via radical-polar crossover or inner-sphere coupling pathways (Figure 1.8a, Cu, Ni). Iodine has been used to trap and support further functionalization of the alkyl radicals (Figure 1.8a, I). Examples of these photochemical radical-relay reactions will be surveyed below, divided into C(sp³)–H functionalization (one-for-one replacement of a C–H bond with another functional group) and cross-coupling reactions (reaction of a C–H bond with a group of similar reagents).

Photoredox-promoted radical-relay methods have been used to support functionalization of C(sp³)–H bonds with halogens, pseudohalogens, acetate, ammonia surrogates, or trifluoromethyl groups. Nucleophilic fluorination of C(sp³)–H bonds has been achieved in two complementary studies using Ir-based photoredox catalysts. In one case, single electron transfer (SET) from the excited state photocatalyst promotes reductive activation of *N*-acetoxyphthalimide.¹⁸⁹ N–O cleavage and decarboxylation of the acetoxy radical generates a methyl radical that promotes HAT from a benzylic or allylic C–H bond. The stabilized carbon-centered radical then undergoes

a General Scheme for Photoredox-Induced C–H Functionalization/Cross-Coupling Reactions



b Catalysts and Reagents used in Photoredox Radical Relay Reactions

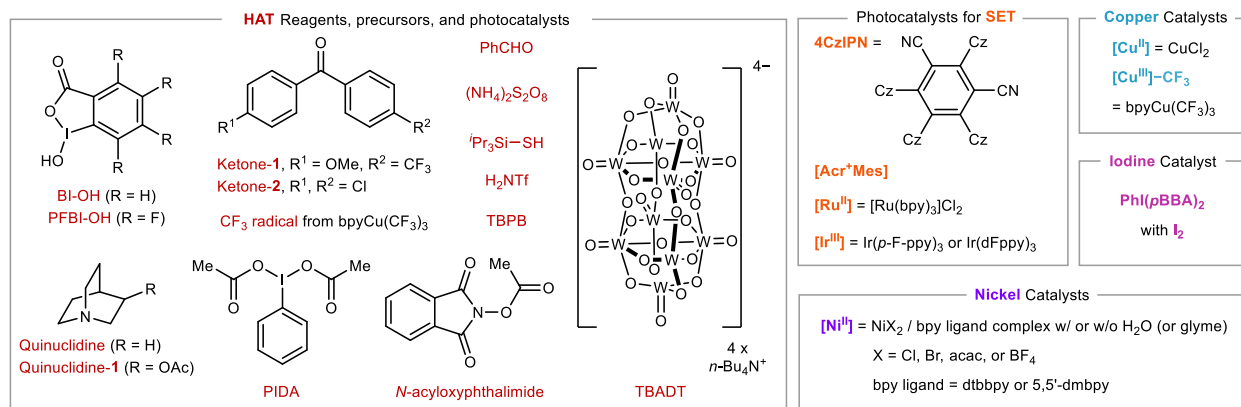


Figure 1.8. Photoredox C(sp³)-H functionalization/cross coupling via radical relay. (a) Four pathways for photoredox-promoted C–H functionalization/cross coupling. (b) The photoredox toolbox includes HAT reagents, photocatalysts, and metal-/iodine-based catalysts utilized for representative methodologies.

SET oxidation by the Ir^{IV} photocatalyst to generate a carbocation that can react with Et₃N•HF.

A related study employed a peroxide-based oxidant (TBPB) with an Ir photocatalyst, resulting in the generation of *tert*-butoxyl radical, which promotes HAT from secondary/tertiary benzylic C–H bonds.¹⁹⁰ A similar radical-polar crossover step, involving SET oxidation of the radical by Ir^{IV}, generates a carbocation that reacts with Et₃N•HF. Both studies prioritized fluorination; however, other nucleophiles were shown to trap the carbocation under the reaction conditions, including chloride, azide, alcohols, thiols, and 1,3,5-trimethoxybenzene (Figure 1.9a, SET).

C(sp³)-H oxygenation and amidation has been achieved by pairing photoredox catalysts with hypervalent iodine oxidants. [Ru(bpy)₃]Cl₂ mediates photochemical reduction of benziodoxole (BI-OH) and its perfluorinated analogue (PFBI-OH) to generate species that promote HAT from tertiary aliphatic and benzylic C(sp³)-H bonds. The Ru^{III} state of the photocatalyst then promotes SET oxidation of the organic radical to generate a carbocation, which can react with H₂O to afford the hydroxylation product.¹⁹¹ The inclusion of CH₃CN or PhCN in the reaction mixtures enables access to the corresponding acetamide or benzamide products via a Ritter-type mechanism (Figure 1.9a, SET).^{192,193} Acetoxylation of primary and secondary benzylic C-H bonds proceeds with an acridinium-based photocatalyst and phenyliodonium diacetate (PIDA) as both the oxidant and source of acetate.¹⁹⁴ Photoredox-based reductive activation of PIDA is proposed to generate a methyl radical, which undergoes HAT with the C-H substrate. The oxidized photocatalyst can then oxidize the organic radical to a carbocation intermediate, and subsequent reaction of acetate with the carbocation affords the acetoxyated product.

An alternative approach to functionalization of organic radicals involves SET reduction to carbanions, followed by reaction with different electrophiles (Figure 1.9a, SET).^{195,196} This approach has been used to convert alkylarenes to aryl acetic acids and related products via C-H coupling with CO₂,¹⁹⁵ and to homobenzylic secondary and tertiary alcohols via C-H coupling with aldehydes and ketones, respectively.¹⁹⁶ These reactions use carbazole- or diarylamine-substituted dicyanoarene photocatalysts. The excited-state photocatalyst oxidizes the thiolate of iPr₃SiSH to generate a thiyl radical, which promotes HAT from the activated C-H bond. The reduced photocatalyst then promotes SET reduction of the carbon-centred radical to afford a carbanion that can react with an electrophile (CO₂ or a ketone) to form a C-C bond.

Light-assisted iodine-catalysed intramolecular C(sp³)-H amination has been the focus of

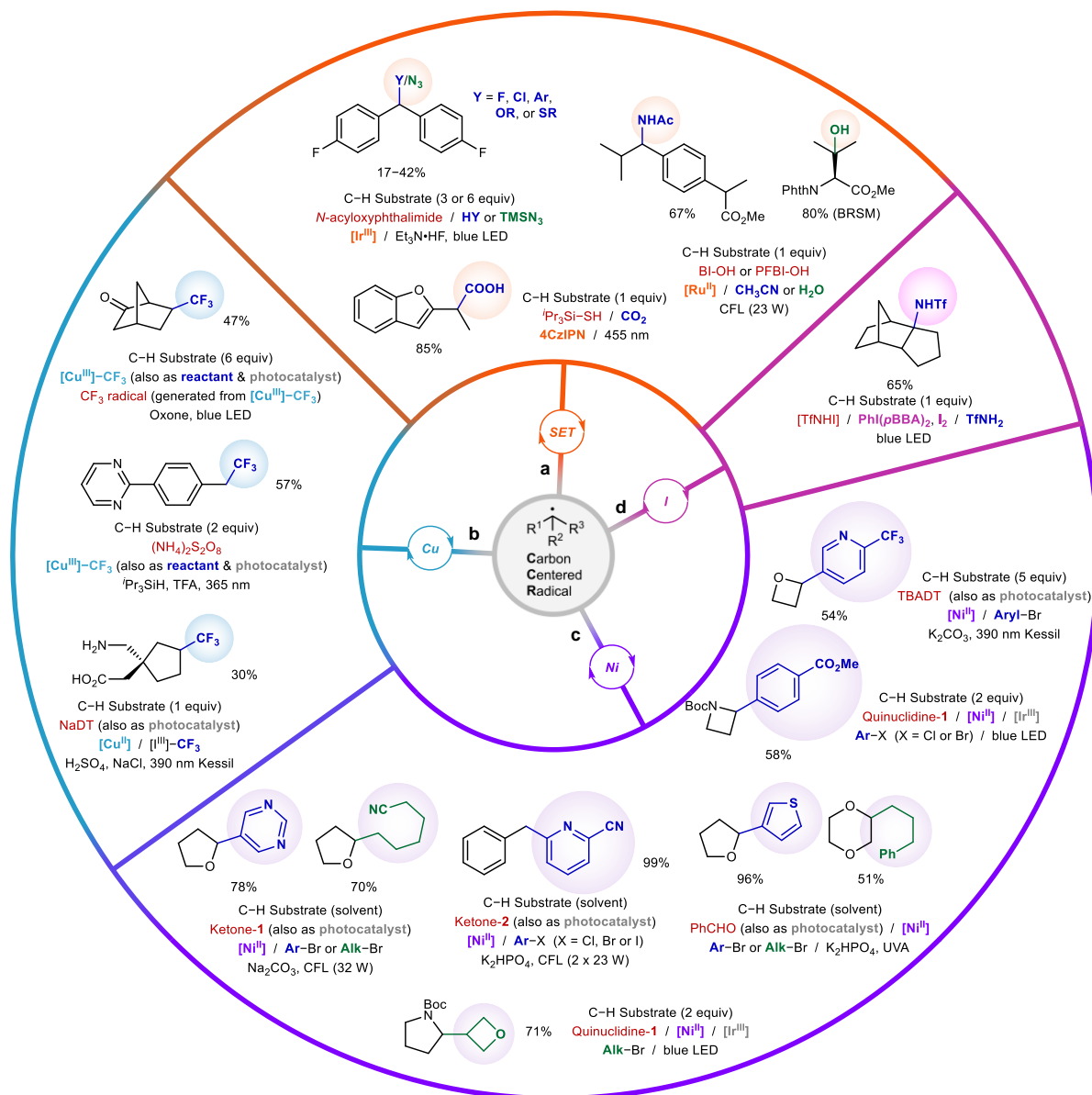


Figure 1.9. Different methods for radical-relay C(sp³)-H functionalization and cross coupling using carbon-centered radicals access via photoredox methods. (a) Photoredox-promoted C-H functionalization/cross-coupling reactions involving single electron transfer. (b) Photoredox-promoted C-H functionalization/cross-coupling reactions involving copper catalysts. (c) Photoredox-promoted C-H functionalization/cross-coupling reactions involving nickel catalysts. (d) Photoredox-promoted C-H functionalization/cross-coupling reactions involving iodine-based catalysts.

considerable development.²⁵ Intermolecular amination of C(sp³)-H bonds has been achieved using bis(4-bromobenzoyloxy)iodobenzene as oxidant and trifluoromethanesulfonamide (H₂NTf) as an HAT reagent and ammonia surrogate (Figure 1.9d, I).¹⁹⁷ In situ reaction of H₂NTf and the

hypervalent iodine reagent generates *N*-iodo triflamide (I–NHTf), which can undergo light-induced homolysis of the N–I bond to afford a sulfonamidyl radical. This step is followed by HAT from the C(sp³)–H substrate, carbon–iodine bond formation, and nucleophilic substitution of the iodide to form the C–N product.

Installation of trifluoromethyl group has also been achieved via a photoredox radical-relay approach with cooperative copper catalysis (Figure 1.9, Cu). The CF₃ group was introduced to the benzylic sites by irradiating a reaction mixture of ammonium persulfate and a bench-stable bpyCu(CF₃)₃ complex¹⁹⁸ in mixed organic/aqueous media (acetone/H₂O 1:1) (Figure 1.9b, Cu).¹⁹⁹ This strategy was also applied to trifluoromethylation of unactivated C(sp³)–H bonds.²⁰⁰ HAT from C–H substrates can be promoted by sulfate radical anion or trifluoromethyl-based radical, via light-induced homolysis of persulfate or bpyCu(CF₃)₃, respectively. The organic radical then reacts with an equivalent of the Cu–CF₃ species to afford a trifluoromethylated product. C(sp³)–H trifluoromethylation has also been achieved using bpyCu(CF₃)₃ and oxone.²⁰¹ In this case, the mechanism is proposed to involve HAT from the C–H substrate by a trifluoromethyl radical, oxidation of the carbon-centred radical to a carbocation by oxone, and reaction of an anionic trifluoromethyl source with the carbocation. In yet another approach, sodium decatungstate has been used in combination with a copper catalyst (CuCl₂) and a trifluoromethyl hypervalent iodine-based oxidant to convert C(sp³)–H bonds to the corresponding C(sp³)–CF₃ products (Figure 1.9b, Cu).²⁰² The photoexcited decatungstate promotes HAT to form a carbon-centred radical, and a Cu^{II}–CF₃ species, generated in situ from CuCl₂ and the CF₃ source, is proposed to react with the organic radical to afford the trifluoromethylated products.

Photoredox methods enable cross coupling of benzylic and aliphatic C–H substrates with diverse aryl or alkyl halide reaction partners. Three general strategies have been employed to

support HAT in these reactions: (a) combining a photocatalyst with a tertiary amine to generate an amine radical cation, (b) use of a reagent that is capable of promoting HAT from its photoexcited state, and (c) photochemical activation of a nickel halide to generate a halogen radical.

The first example of this reactivity used 3-acetoxyquinuclidine combined with an Ir-based photocatalyst and nickel(II) bromide to support cross coupling of activated C(sp³)-H bonds (such as those adjacent to nitrogen in pyrrolidines) with aryl bromides/chlorides (Figure 1.9c, Ni).²⁰³ SET oxidation of 3-acetoxyquinuclidine by the excited-state Ir^{III} photocatalyst generates a quinuclidine radical cation that promotes HAT from the C(sp³)-H bond. This radical generation process is paired with a Ni-based radical functionalization cycle. The nickel cocatalyst reacts with the organic halide species to afford an organonickel(II) species, which promotes C-C coupling by reaction with the radical derived from the C-H substrate. Cross coupling of activated C(sp³)-H and alkyl halides employing quinuclidine, an Ir-based photoredox catalyst, and nickel(II) bromide has been achieved via a similar mechanistic pathway.²⁰⁴ Quinuclidine also promotes HAT from aldehyde²⁰⁵ and the α -C-H bonds of alcohols²⁰⁶ to enable direct arylation and alkylation via Ni-catalysed cross coupling. Nitrogen-centred radicals from sulfonamides have been shown to abstract hydrogen atoms from C-H bonds adjacent to heteroatoms, generating radicals that undergo Ni-catalysed cross coupling with alkyl halides to afford alkylated products.²⁰⁷ Photoexcited 4CzIPN (1,2,3,5-tetrakis(carbazol-9-yl)-4,6-dicyanobenzene) is proposed to oxidize sulfonamide anion to the nitrogen-centred radical, which is responsible for HAT.

TBADT serves as a combined photocatalyst/HAT reagent and supports the arylation of strong aliphatic C-H bonds with aryl bromides.²⁰⁸ Disproportionation of the singly-reduced decatungstate species leads to the regeneration of the active HAT photocatalyst and the doubly-reduced decatungstate species. This second species can then reduce the nickel cocatalyst as is

required for activation of the aryl bromide coupling partner. Benzophenone derivatives are similar to TBADT in their ability to promote HAT from their photoexcited triplet state.^{209,210} This feature has been exploited in combination with nickel catalysis for cross coupling of activated C(sp³)-H bonds with aryl and alkyl halides (Figure 1.9c, Ni).²¹¹ 4,4'-Dichlorobenzophenone (Figure 1.8b, Ketone-2) has been used as a photocatalyst to achieve arylation of primary benzylic C(sp³)-H bonds.²¹² Aryl halides, including chlorides, bromides, and iodides, can be utilized as coupling partners. Benzaldehyde has also been used as a photocatalyst for arylation and alkylation of activated C(sp³)-H bonds (Figure 1.9c, Ni).^{213,214}

Arylation of activated C(sp³)-H bonds has been achieved by combining an Ir-based photoredox catalyst and Ni cocatalyst, in the absence of an HAT reagent (Figure 1.10Ba). In the coupling of aryl bromides with THF (and other solvents with activated C-H bonds), the excited-state photocatalyst Ir^{III*} is proposed to undergo triplet-triplet energy transfer with an ArNi^{II}-Br species to generate a triplet Ni^{II*} species. (Figure 1.10Aa). HAT from the C(sp³)-H bond may involve a bromine radical or proceed via a concerted four-membered transition state involving the Ni-Br bond. The resulting carbon-centred radical can react at Ni to afford the C(sp³)-C(sp²) bond.²¹⁵ A complementary study, involving the coupling of aryl chlorides with THF and related solvents (Figure 1.10Bb),²¹⁶ proposes that the Ir^{III} photocatalyst serves as a SET reagent. Oxidation of an ArNi^{II}-Cl intermediate by the excited state photocatalyst Ir^{III*} generates a Ni^{III} species. Subsequent loss of a chlorine atom leads to HAT from the activated C(sp³)-H bond of the solvent to afford an organic radical that can undergo coupling with the arylnickel(II) species

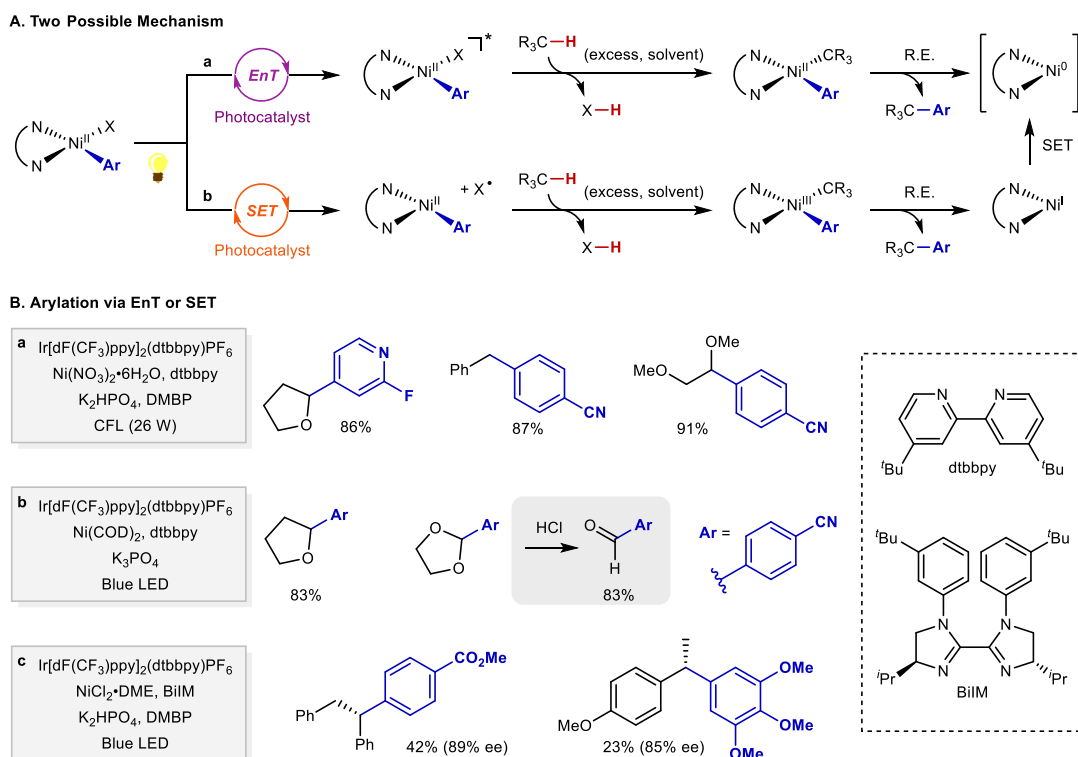


Figure 1.10. Nickel-catalyzed arylation of C(sp³)-H bonds of inexpensive (co)solvents enabled by *in situ* generation of HAT reagents. (Aa) Energy transfer pathway for arylation of C(sp³)-H bonds. (Ab) Single electron transfer pathway for arylation of C(sp³)-H bonds. (Ba) Examples of arylated products involving energy transfer. (Bb) Examples of arylated product involving single electron transfer. (Bc) Enantioselective arylation of benzylic C(sp³)-H bonds with a chiral bis-imidazoline ligand.

(Figure 1.10Ab). The synthetic utility of the latter reaction was demonstrated in a separate report in the cross coupling of (hetero)aryl chlorides with 1,3-dioxolane as the solvent.²¹⁷ The resulting cross-coupled products are readily converted to (hetero)aryl aldehydes following a mild acidic workup at room temperature. An enantioselective benzylic C-H arylation has been achieved with an Ir-based photocatalyst, nickel(II), and a chiral bis-imidazoline ligand (Figure 1.10Bc).²¹⁸ Aryl bromide coupling partners generate ArNi^{II}-Br, which is proposed to generate bromine radical as the HAT reagent upon irradiation in the presence of a photocatalyst. An enantioselective benzylic C(sp³)-H alkenylation reaction has also been achieved with alkenyl bromides as the coupling partners in the presence of an Ir-photoredox catalyst, nickel(II), and a chiral bis-

imidazoline-based ligand.²¹⁹ Complementary nickel/photoredox dual catalysis enables acylation²²⁰ and arylation²²¹ reactions of α -amino C(sp³)–H bonds. In these cases, *N*-arylpiperidine substrates are proposed to generate stabilized α -amino radicals via a more conventional process involving SET oxidation of the substrate.

1.4.6. Electrochemical Radical-Relay Reactions

Electrochemical methods provide additional strategies to achieve C(sp³)–H functionalization via radical relay.^{222, 223} *N*-hydroxyphthalimide (NHPI) was first demonstrated as an electrochemical mediator for C(sp³)–H oxygenation in the 1980s.^{224–226} NHPI undergoes proton-coupled oxidation to phthalimide *N*-oxyl (PINO) at the electrode, and PINO-mediated HAT then generates an organic radical that can react with O₂ or other oxidants, resulting in C–H functionalization (Figure 1.11Aa).²²⁷ These methods complement transition-metal/NHPI cocatalyst systems for C–H oxygenation with O₂.^{68,71,72} Modified NHPI derivatives can lead to improved performance, evident from the use of tetrachloro-*N*-hydroxyphthalimide (Cl₄NHPI) as the HAT mediator in the electrochemical oxidation of allylic C(sp³)–H bonds (Figure 1.11Ab),²²⁸ and an electrochemical NHPI/O₂ system proved effective for C–H oxygenation of alkyl-substituted heterocycles that exhibit poor reactivity with a chemical Co/NHPI/O₂ catalyst system (Figure 1.11Ac).⁷¹ Flow conditions have been developed for the latter process.²²⁹

Different mediators provide a means to expand reactivity beyond activated C–H bonds. Electrochemical oxidation of quinuclidine generates an amine radical cation that promotes HAT and oxygenation of diverse C(sp³)–H bonds under aerobic conditions (Figure 1.11Ad).²³⁰ *N*-alkyl ammonium ylides have been developed as a new class of electrochemical mediators for C(sp³)–H oxygenation through the support of computational method (Figure 1.11Ae).²³¹ These reagents show modified chemo- and site-selectivity relative to previous chemical and electrochemical

methods for C(sp³)-H oxygenation.

NHPI has been paired with iodine, rather than O₂, to enable the iodination of methyl arenes.²³² The resulting benzyl iodide may be employed in subsequent S_N2-base derivatization reactions to access new C-C, C-O, and C-N bonds or undergo *in situ* substitution, for example, by pyridine (Figure 1.11Af). This mediated HAT strategy enables electrochemical C-H functionalization to proceed at electrode potentials 0.7–1.3 V lower than those required by conventional SET-initiated electrochemical benzylic C-H functionalization methods.^{233,234}

Metal-oxo complexes capable of promoting C-H oxygenation have been generated via electrochemical proton-coupled oxidation of metal-aquo complexes (Figure 1.11Ba). Electrochemical oxidation of [(TAML)Fe^{III}(OH)₂]Na (TAML = tetra-amido macrocyclic ligand) generates Fe^{IV} and Fe^V oxo species. The Fe^V-oxo is more reactive and oxidizes secondary benzylic C-H bonds to ketones using water as oxygen-atom source (FIG. 11Bb)²³⁵. Ruthenium-based oxo species derived from *cis*-bis(4,4'-di-*tert*-butylpyridine)ruthenium complex effects electrochemical hydroxylation of C(sp³)-H bonds (Figure 1.11Bc).²³⁶ Basic amines are tolerated, owing to the use of acidic reaction conditions that protect the amines as ammonium salts.

Two complementary electrochemical methods have been developed for C(sp³)-H azidation. Manganese(III) porphyrin or salen complexes and sodium azide promote azidation of C(sp³)-H bonds (Figure 1.11C).²³⁷ The reaction is proposed to proceed via oxidation of Mn^{III} to a Mn^{IV}-diazide species, which promotes HAT from the substrate to generate an organic radical that affords an azide product via coupling with another Mn^{IV}-diazide complex. An electrophotochemical azidation protocol uses MnF₂ in combination with a ketone-based photocatalyst [for example, 9-fluorenone, 2,3-dichloro-5,6-dicyano-*p*-benzoquinone (DDQ), bis(4-methoxyphenyl)methanone]

and sodium azide (Figure 1.11D).²³⁸ The excited-state photocatalyst promotes HAT, and an electrochemically generated Mn^{III} -azide is proposed to react with the carbon-centered radical.

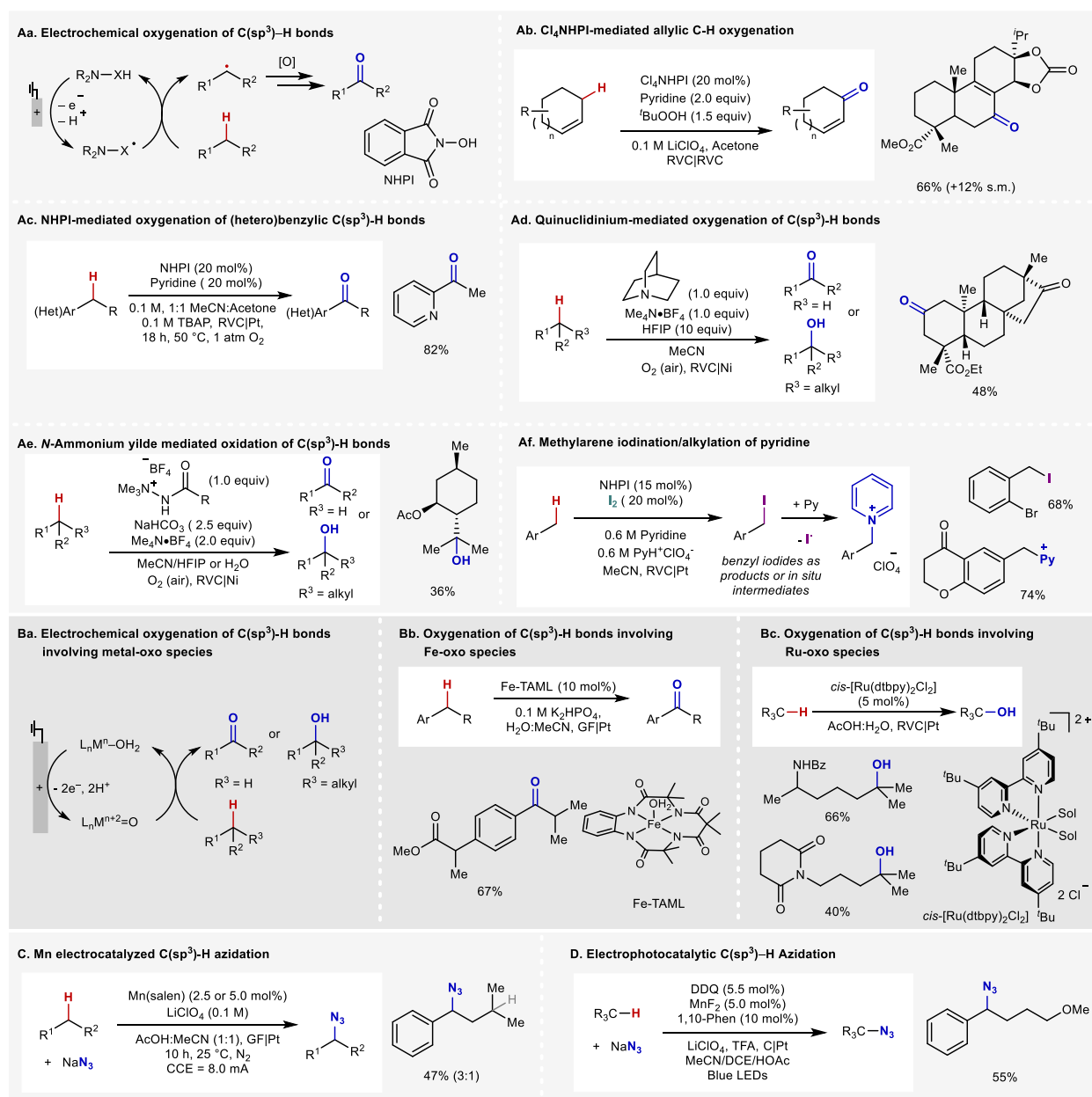


Figure 1.11. Radical-relay reactions involving electrochemistry. (Aa) General mechanism for NHPI-mediated electrochemical oxygenation reaction of $\text{C}(\text{sp}^3)\text{-H}$ bonds. (Ab) Oxygenation of allylic C-H bonds. (Ac) Oxygenation of heterobenzylic $\text{C}(\text{sp}^3)\text{-H}$ bonds. (Ad) Quinuclidine-mediated oxygenation of $\text{C}(\text{sp}^3)\text{-H}$ bonds. (Ae) *N*-alkyl ammonium ylides as a new class of HAT-mediators. (Af) NHPI-mediated iodination followed by pyridination of alkylarenes. (Ba) Oxygenation reactions involving metal-oxo complexes. (Bb) Oxygenation of secondary benzylic $\text{C}(\text{sp}^3)\text{-H}$ bonds using Fe-TAML complex. (Bc) Hydroxylation of $\text{C}(\text{sp}^3)\text{-H}$ bonds in amine

derivatives using a ruthenium-based catalyst. (C) Azidation of C(sp³)-H bonds using Mn^{III} catalyst. (D) Photoelectrochemical azidation reaction of C(sp³)-H bonds.

1.5. Conclusion

Radical reaction pathways offer some of the most versatile methods available for C(sp³)-H functionalization and cross coupling, accessing synthetic scope and utility that is unmatched by other reaction pathways. Major advances have been made in each of the different radical reaction classes, including radical chain, radical rebound, and radical relay. Many of these reactions are able to use the C-H substrate as the limiting reagent, addressing one of the long-standing limitations of this field and supporting application to late-stage functionalization. Radical-relay methods are particularly versatile. These reactions not only enable installation of specific functional groups, including -CN, -CF₃, -N₃, -OH, -SCN, -F, -Cl, -NCO, but also provide the basis for sequential functionalization/diversification methods and direct cross-coupling methods that leverage substrates derived from large pools of reaction partners, such as alcohols, amines/amides, arylboronic acids, and aryl halides. The latter feature greatly expands the scope of accessible products relative to those obtained from typical C-H "functionalization" methods and has profound implications for drug discovery and medicinal chemistry, where access to diverse structures is crucial to the success of the endeavors.

1.6. Thesis Scope

The enclosed thesis research describes a Cu-catalyzed radical relay benzylic C-H esterification reaction, a radical chain heterobenzylic C-H chlorination, a Cu-catalyzed benzylic C-H fluorination/diversification sequence, and a Cu-catalyzed benzylic C-H and azole coupling reaction. The benzylic C-H esterification reaction overcomes the major limitation of the traditional Kharasch-Sosnovsky reaction, which often requires the use of excess C-H substrates relative to

the peroxide (Chapter 2). A "photochemical redox buffering" strategy enables the reduction of resting-state Cu^{II} species to Cu^{I} via light-promoted carboxylate-to-copper charge transfer. This study introduces a unique approach to re-engage inactive Cu catalysts in radical-relay reactions, supporting catalysis under mild conditions with limiting C–H substrates. The second reaction details the development of a radical-chain chlorination reaction targeting heterobenzylic C–H bonds, which are incompatible with Cu-catalyzed radical-relay reactions (Chapter 3). Heterobenzyl chlorides are then subjected to $\text{S}_{\text{N}}2$ displacement to access cross-coupled products with a diverse pool of oxidatively sensitive nucleophiles. The chlorination/diversification strategy was inspired by the success of a Cu-catalyzed radical-relay fluorination reaction. In that study, benzyl fluorides were used as intermediate for nucleophilic displacement in presence of a Lewis acid cocatalyst (Chapter 4). The final chapter (Chapter 5) describes the development of a Cu-catalyzed benzylic C–H cross coupling with *N*-azoles, where *N*-site selectivity can be modified using different additives. Overall, the above studies demonstrate the importance of radical chemistry in functionalizing $\text{C}(\text{sp}^3)\text{--H}$ bonds to access more three-dimensional structures.

1.7. Author Contributions

D.L.G. and S.-E.S. contributed equally to all aspects of the review. D.L.G., S.-E.S., and S.S.S wrote, edited, and reviewed the manuscript.

1.8. Reference

- 1 He, J., Wasa, M., Chan, K. S. L., Shao, Q. & Yu, J.-Q. Palladium-catalyzed transformations of alkyl C–H bonds. *Chem. Rev.* **117**, 8754–8786 (2017).
- 2 Jazzar, R., Hitce, J., Renaudat, A., Sofack-Kreutzer, J. & Baudoin, O. Functionalization of organic molecules by transition-metal-catalyzed C(sp³)–H activation. *Chem. Eur. J.* **16**, 2654–2672 (2010).
- 3 Saint-Denis, T. G., Zhu, R.-Y., Chen, G., Wu, Q.-F. & Yu, J.-Q. Enantioselective C(sp³)–H bond activation by chiral transition metal catalysts. *Science* **359**, eaao4798 (2018).
- 4 Gupta, A., Kumar, J., Rahaman, A., Singh, A. K. & Bhadra, S. Functionalization of C(sp³)–H bonds adjacent to heterocycles catalyzed by earth abundant transition metals. *Tetrahedron* **95**, 132415 (2021).
- 5 Davies, H. M. L. & Manning, J. R. Catalytic C–H functionalization by metal carbenoid and nitrenoid insertion. *Nature* **451**, 417–424 (2008).
- 6 Doyle, M. P., Duffy, R., Ratnikov, M. & Zhou, L. Catalytic carbene insertion into C–H bonds. *Chem. Rev.* **110**, 704–724 (2010).
- 7 Roizen, J., Harvey, M. E. & Du Bois, J. Metal-catalyzed nitrogen-atom transfer methods for the oxidant of aliphatic C–H bonds. *Acc. Chem. Res.* **45**, 911–922 (2012).
- 8 Yi, H. et al. Recent advances in radical C–H activation/radical cross-coupling. *Chem. Rev.* **117**, 9016–9085 (2017).
- 9 Zhang, C., Li, Z.-L., Gu, Q.-S. & Liu, X.-Y. Catalytic enantioselective C(sp³)–H functionalization involving radical intermediates. *Nat. Commun.* **12**, 475 (2021).
- 10 Studer, A. & Curran, D. P. Catalysis of radical reactions: A radical chemistry perspective. *Angew. Chem. Int. Ed.* **55**, 58–102 (2016).
- 11 Labinger, J. A. & Bercaw, J. E. Understanding and exploiting C–H bond activation. *Nature* **417**, 507–514 (2002).
- 12 Sheldon, R. A. & Kochi, J. K. in *Metal-catalyzed oxidations of organic compounds: Mechanistic principles and synthetic methodology including biochemical processes* (Academic Press, Inc., New York, 1981).
- 13 Hermans, I., Spier, E. S., Neuenschwander, U., Turrà, N. & Baiker, A. Selective oxidation catalysis: Opportunities and challenges. *Top. Catal.* **52**, 1162–1174 (2009).
- 14 Quinn, R. K. et al. Site-selective aliphatic C–H chlorination using *N*-chloroamides enables a synthesis of chlorolissoclimide. *J. Am. Chem. Soc.* **138**, 696–702 (2016).
- 15 Schmidt, V. A., Quinn, R. K., Brusoe, A. T. & Alexanian, E. J. Site-selective aliphatic C–H bromination using *N*-bromoamides and visible light. *J. Am. Chem. Soc.* **136**, 14389–14392 (2014).
- 16 Czaplyski, W. L., Na, C. G. & Alexanian, E. J. C–H Xanthylation: A synthetic platform for alkane functionalization. *J. Am. Chem. Soc.* **138**, 13854–13857 (2016).
- 17 Tanwar, L., Börgel, J. & Ritter, T. Synthesis of benzylic alcohols by C–H oxidation. *J. Am.*

- Chem. Soc.* **141**, 17983–17988 (2019).
- 18 Huang, X. & Groves, J. T. Beyond ferryl-mediated hydroxylation: 40 years of rebound mechanism and C–H activation. *J. Biol. Inorg. Chem.* **22**, 185–207 (2017).
 - 19 Huang, X. & Groves, J. T. Taming azide radicals for catalytic C–H azidation. *ACS Catal.* **6**, 751–759 (2016).
 - 20 Clark, J. R., Feng, K., Sookezian, A. & White, M. C. Manganese-catalysed benzylic C(sp³)–H amination for late-stage functionalization. *Nat. Chem.* **10**, 583–591 (2018).
 - 21 Lovering, F., Bikker, J. & Humblet, C. Escape from flatland: Increasing saturation as an approach to improving clinical success. *J. Med. Chem.* **52**, 6752–6756 (2009).
 - 22 Blakemore, D. C. et al. Organic synthesis provides opportunities to transform drug discovery. *Nature Chem.* **10**, 383–394 (2018).
 - 23 Guillemard, L., Kaplaneris, N., Ackermann, L. & Johansson, M. J. Late-stage C–H functionalization offers new opportunities in drug discovery. *Nat. Rev. Chem.* **5**, 522–545(2021).
 - 24 Wolff, M. E. Cyclization of N-halogenated amines (the Hofmann-Löffler reaction). *Chem. Rev.* **63**, 55–64 (1963).
 - 25 Statement, L. M., Nakafuku, K. M. & Nagib, D. A. Remote C–H functionalization via selective hydrogen atom transfer. *Synthesis* **50**, 1569–1586 (2018).
 - 26 Sarkar, S. Cheung, K. P. S. & Gevorgyan V. C–H functionalization reactions enabled by hydrogen atom transfer to carbon-centred radicals. *Chem. Sci.* **11**, 12974–12993 (2020).
 - 27 Nodwell, M. B. et al. Direct photocatalytic fluorination of benzylic C–H bonds with *N*-fluorobenzenesulfonimide. *Chem. Commun.* **51**, 11783–11786 (2015).
 - 28 Pitts, C. R., Ling, B., Woltornist, R., Liu, R. & Lectka, T. Triethylborane-initiated radical chain fluorination: A synthetic method derived from mechanistic insight. *J. Org. Chem.* **79**, 8895–8899 (2014).
 - 29 Pitts, C. R. et al. Direct, catalytic monofluorination of sp³ C–H bonds: A radical-based mechanism with ionic selectivity. *J. Am. Chem. Soc.* **136**, 9780–9791 (2014).
 - 30 Bloom, S. et al. Iron(II)-catalyzed benzylic fluorination. *Org. Lett.* **15**, 1722–1724 (2013).
 - 31 Buss, J. A., Vasilopoulos, A., Golden, D. L. & Stahl, S. S. Copper-catalyzed functionalization of benzylic C–H bonds with *N*-fluorobenzenesulfonimide (NFSI): Switch from C–N to C–F bond formation promoted by a redox buffer and Brønsted base. *Org. Lett.* **22**, 5749–5752 (2020).
 - 32 Bloom, S. et al. A polycomponent metal-catalyzed aliphatic, allylic, and benzylic fluorination. *Angew. Chem. Int. Ed.* **51**, 10580–10583 (2012).
 - 33 Xia, J.-B., Zhu, C. & Chen, C. Visible light-promoted metal-free C–H activation: Diarylketone-catalyzed selective benzylic mono- and difluorination. *J. Am. Chem. Soc.* **135**, 17494–17500 (2013).
 - 34 Halperin, S. D., Fan, H., Chang, S., Martin, R. E. & Britton, R. A convenient photocatalytic fluorination of unactivated C–H bonds. *Angew. Chem. Int. Ed.* **53**, 4690–4693 (2014).
 - 35 Bloom, S., McCann, M. & Lectka, T. Photocatalyzed benzylic fluorination: Shedding “light”

- on the involvement of electron transfer. *Org. Lett.* **16**, 6338–6341 (2014).
- 36 Carestia, A. M., Ravelli, D. & Alexanian, E. J. Reagent-dictated site selectivity in intermolecular aliphatic C–H functionalizations using nitrogen-centred radicals. *Chem. Sci.* **9**, 5360–5365 (2018).
- 37 MacMillan, A. J. et al. Practical and selective sp³ C–H bond chlorination via aminium radicals. *Angew. Chem. Int. Ed.* **60**, 7132–7139 (2021).
- 38 Xiang, M. et al. Visible light-catalyzed benzylic C–H bond chlorination by a combination of organic dye (Acr⁺-Mes) and *N*-chlorosuccinimide. *J. Org. Chem.* **85**, 9080–9087 (2020).
- 39 Ozawa, J. & Kanai, M. Silver-catalyzed C(sp³)–H chlorination. *Org. Lett.* **19**, 1430–1433 (2017).
- 40 Quiclet-Sire, B. & Zard, S. Z. The xanthate route to amines, anilines, and other nitrogen compounds. A brief account. *Synlett.* **27**, 680–701 (2016).
- 41 Huang, X. & Groves, J. T. Oxygen activation and radical transformations in heme proteins and metallophorphyrins. *Chem. Rev.* **118**, 2491–2553 (2018).
- 42 Leising, R. A., Norman, R. E. & Que, L., Jr. Alkane functionalization by non-porphyrin iron complexes: Mechanistic insights. *Inorg. Chem.* **29**, 2553–2555 (1990).
- 43 Chen, K., Costas, M. & Que, L., Jr. Spin state tuning of non-heme iron-catalyzed hydrocarbon oxidations: Participation of Fe^{III}–OOH and Fe^V=O intermediates. *J. Chem. Soc., Dalton Trans.* 672–679 (2002).
- 44 Kim, J., Kim, C., Harrison, R. G., Wilkinson, E. C. & Que, L., Jr. Fe(TPA)-catalyzed alkane hydroxylation can be a metal-based oxidation. *J. Mol. Catal. A: Chem.* **117**, 83–89 (1997).
- 45 Chen, K. & Que, L., Jr. Stereospecific alkane hydroxylation by non-heme iron catalysts: Mechanistic evidence for an Fe^V=O active species. *J. Am. Chem. Soc.* **123**, 6327–6337 (2001).
- 46 Costas, M., Tipton, A. K., Chen, K., Jo, D.-H. & Que, L., Jr. Modeling Rieske dioxygenases: The first example of iron-catalyzed asymmetric *cis*-dihydroxylation of olefins. *J. Am. Chem. Soc.* **123**, 6722–6723 (2001).
- 47 Kim, C., Chen, K., Kim, J. & Que, L., Jr. Stereospecific alkane hydroxylation with H₂O₂ catalyzed by an iron(II)–tris(2-pyridylmethyl)amine complex. *J. Am. Chem. Soc.* **119**, 5964–5965 (1997).
- 48 Costas, M. & Que, L., Jr. Ligand topology tuning of iron-catalyzed hydrocarbon oxidations. *Angew. Chem. Int. Ed.* **41**, 2179–2181 (2002).
- 49 Chen, M. S. & White, M. C. A predictably selective aliphatic C–H oxidation reaction for complex molecule synthesis. *Science.* **318**, 783–787 (2007).
- 50 St John, P., Guan, Y., Kim, Y., Kim, S., Paton, R. S. Prediction of homolytic bond dissociation enthalpies for organic molecules at near chemical accuracy with sub-second computational cost. *Nat. Commun.* **11**, 2328, (2020).
- 51 Chen, M. S. & White, M. C. Combined effects on selectivity in Fe-catalyzed methylene oxidation. *Science.* **327**, 566–571 (2010).
- 52 Gormisky, P. E. & White, M. C. Catalyst-controlled aliphatic C–H oxidations with a predictive model for site-selectivity. *J. Am. Chem. Soc.* **135**, 14052–14055 (2013).

- 53 Howell, J. M., Feng, K., Clark, J. R., Trzepakowski, L. J. & White, M. C. Remote oxidation of aliphatic C–H bonds in nitrogen-containing molecules. *J. Am. Chem. Soc.* **137**, 14590–14593 (2015).
- 54 Osberger, T. J., Rogness, D. C., Kohrt, J. T., Stepan, A. F. & White, M. C. Oxidative diversification of amino acids and peptides by small-molecule iron catalysis. *Nature* **537**, 214–219 (2016).
- 55 Dantignana, V. et al. Chemoselective aliphatic C–H bond oxidation enabled by polarity reversal. *ACS Cent. Sci.* **3**, 1350–1358 (2017).
- 56 Borrell, M., Gil-Caballero, S., Bietti, M. & Costas, M. Site-selective and product chemoselective aliphatic C–H bond hydroxylation of polyhydroxylated substrates. *ACS Catal.* **10**, 4702–4709 (2020).
- 57 Zhao, J., Nanjo, T., de Luca, E. C. & White, M. C. Chemoselective methylene oxidation in aromatic molecules. *Nature Chem.* **11**, 213–221 (2019).
- 58 Milan, M., Bietti, M. & Costas, M. Highly enantioselective oxidation of nonactivated aliphatic C–H bonds with hydrogen peroxide catalyzed by manganese complexes. *ACS Cent. Sci.* **3**, 196–204 (2017).
- 59 White, M. C., Doyle, A. G. & Jacobsen, E. N. A synthetically useful, self-assembling MMO mimic system for catalytic alkene epoxidation with aqueous H₂O₂. *J. Am. Chem. Soc.* **123**, 7194–7195 (2001).
- 60 Oloo, W. N. & Que, L., Jr. Bioinspired nonheme iron catalysts for C–H and C=C bond oxidation: Insights into the nature of the metal-based oxidants. *Acc. Chem. Res.* **48**, 2612–2621 (2015).
- 61 Kal, S., Xu, S. & Que, L., Jr. Bio-inspired nonheme iron oxidation catalysis: Involvement of oxoiron(V) oxidants in cleaving strong C–H bonds. *Angew. Chem. Int. Ed.* **59**, 7332–7349 (2020).
- 62 Liu, W. & Groves, J. T. Manganese catalyzed C–H halogenation. *Acc. Chem Res.* **48**, 1727–1735 (2015).
- 63 Liu, W. et al. Oxidative aliphatic C–H fluorination with fluoride ion catalyzed by a manganese porphyrin. *Science*. **337**, 1322–1325 (2012).
- 64 Li, G., Dilger, A. K., Cheng, P. T., Ewing, W. R. and Groves, J. T. Selective C–H halogenation with a highly fluorinated manganese porphyrin. *Angew. Chem. Int. Ed.* **57**, 1251–1255 (2018).
- 65 Liu, W. et al. Site-selective ¹⁸F fluorination of unactivated C–H bonds mediated by a manganese porphyrin. *Chem. Sci.* **9**, 1168–1172 (2018).
- 66 Huang, X., Bergsten, T. M. & Groves, J. T. Manganese-catalyzed late-stage aliphatic C–H azidation. *J. Am. Chem. Soc.* **137**, 5300–5303 (2015).
- 67 Huang, X. et al. Alkyl isocyanates via manganese-catalyzed C–H activation for the preparation of substituted ureas. *J. Am. Chem. Soc.* **139**, 15407–15413 (2017).
- 68 Ishii, Y., Sakaguchi, S. & Iwahama, T. Innovation of hydrocarbon oxidation with molecular oxygen and related reactions. *Adv. Synth. Catal.* **343**, 393–427 (2001).
- 69 Sterckx, H., Morel, B. & Maes, B. U. W. Catalytic aerobic oxidation of C(sp³)–H bonds.

- Angew. Chem. Int. Ed.* **58**, 7946–7970 (2019).
- 70 Ishii, Y.; Iwahama, T.; Sakaguchi, S.; Nakayama, K. & Nishiyama, Y. Alkane oxidation with molecular oxygen using a new efficient catalytic system: *N*-hydroxyphthalimide (NHPI) combined with $\text{Co}(\text{acac})_n$ ($n = 2$ or 3). *J. Org. Chem.* **61**, 4520–4526 (1996).
- 71 Hruszkewycz, D. P., Miles, K. C., Thiel, O. R. & Stahl, S. S. Co/NHPI-mediated oxygenation of benzylic C–H bonds in pharmaceutically relevant molecules. *Chem. Sci.* **8**, 1282–1287 (2017).
- 72 Cooper, J. C., Luo, C., Kameyama, R. & Van Humbeck, J. F. Combined iron/hydroxytriazole dual catalytic system for site selective oxidation adjacent to azaheterocycles. *J. Am. Chem. Soc.* **140**, 1243–1246 (2018).
- 73 Gaster, E., Kozuch, S. & Pappo, D. Selective aerobic oxidation of methylarenes to benzaldehydes catalyzed by *N*-hydroxyphthalimide and cobalt(II) acetate in hexafluoropropan-2-ol. *Angew. Chem. Int. Ed.* **56**, 5912–5915 (2017).
- 74 Schultz, D. M. et al. Oxyfunctionalization of the remote C–H bonds of aliphatic amines by decatungstate photocatalysis. *Angew. Chem. Int. Ed.* **56**, 15274–15278 (2017).
- 75 Wu, W. et al. $(n\text{Bu}_4\text{N})\text{W}_{10}\text{O}_{32}$ -catalyzed selective oxygenation of cyclohexane by molecular oxygen under visible light irradiation. *Appl. Catal. B: Environ.* **164**, 113–119 (2015).
- 76 Laudadio, G. et al. Selective $\text{C}(\text{sp}^3)\text{--H}$ aerobic oxidation enabled by decatungstate photocatalysis in flow. *Angew. Chem. Int. Ed.* **57**, 4078–4082 (2018).
- 77 Lee, J. M., Park, J., Cho, S. H. & Chang, S. Cu-facilitated C–O bond formation using *N*-hydroxyphthalimide: Efficient and selective functionalization of benzyl and allylic C–H bonds. *J. Am. Chem. Soc.* **130**, 7824–7825 (2008).
- 78 Guo, Z., Jin, C., Zhou, J. & Su, W. Copper(II)-catalyzed cross dehydrogenative coupling reaction of *N*-hydroxyphthalimide with alkanes and ethers via unactivated $\text{C}(\text{sp}^3)\text{--H}$ activation at room temperature. *RSC Adv.* **6**, 79016–79019 (2016).
- 79 Zhang, X., Yang, H. & Tang, P. Transition-metal-free oxidative aliphatic C–H azidation. *Org. Lett.* **17**, 5828–5831 (2015).
- 80 Kim, K., Lee, S. & Hong, S. H. Direct $\text{C}(\text{sp}^3)\text{--H}$ cyanation enabled by highly active decatungstate photocatalyst. *Org. Lett.* **23**, 5501–5505 (2021).
- 81 Sarver, P. J., Bissonnette, N. B. & MacMillan, D. W. C. Decatungstate-catalyzed $\text{C}(\text{sp}^3)\text{--H}$ sulfonylation: Rapid access to diverse organosulfure functionality. *J. Am. Chem. Soc.* **143**, 9737–9743 (2021).
- 82 Schirmer, T. E., Rolka, A. B., Karl, T. A., Holzhausen, F. & König, B. Photocatalytic C–H trifluoromethylthiolation by the decatungstate anion. *Org. Lett.* **23**, 5729–5733 (2021).
- 83 Capaldo, L. & Ravelli, D. Decatungstate as direct hydrogen atom transfer photocatalyst for SOMOphilic alkynylation. *Org. Lett.* **23**, 2243–2247 (2021).
- 84 Mao, R.; Bera, S.; Turla, A. C. & Hu, X. Copper-catalyzed intermolecular functionalization of unactivated $\text{C}(\text{sp}^3)\text{--H}$ bonds and aliphatic carboxylic acids. *J. Am. Chem. Soc.* **143**, 14667–14675 (2021).
- 85 Bentley, K. W., Dummit, K. A. & Van Humbeck, J. F. A highly site-selective radical sp^3 C–H

- amination of azaheterocycles. *Chem. Sci.* **9**, 6440–6445 (2018).
- 86 Hu, A., Guo, J.-J., Pan, H. & Zuo, Z. Selective functionalization of methane, ethane, and higher alkanes by cerium photocatalysis. *Science* **361**, 668–672 (2018).
- 87 An, Q. et al. Cerium-catalyzed C–H functionalizations of alkanes utilizing alcohols as hydrogen atom transfer agents. *J. Am. Chem. Soc.* **142**, 6216–6226 (2020).
- 88 Yang, Q. et al. Photocatalytic C–H activation and the subtle role of chlorine radical complexation in reactivity. *Science* **372**, 847–852 (2021).
- 89 Ryu, I. et al. Efficient C–H/C–N and C–H/C–CO–N conversion via decatungstate-photoinduced alkylation of diisopropyl azodicarboxylate. *Org. Lett.* **15**, 2554–2557 (2013).
- 90 Bonassi, F., Ravelli, D., Protti, S. & Fagnoni, M. Decatungstate photocatalyzed acylations and alkylations in flow via hydrogen atom transfer. *Adv. Synth. Catal.* **357**, 3687–3695 (2015).
- 91 Wan, T. et al. Accelerated and scalable C(sp³)–H amination via decatungstate photocatalysis using a flow photoreactor equipped with high-intensity LEDs. *ACS Cent. Sci.* Accepted Article (2021) <https://doi.org/10.1021/acscentsci.1c01109>.
- 92 Giese, B. Formation of CC bonds by addition of free radicals to alkenes. *Angew. Chem. Int. Ed. Engl.* **22**, 753–764 (1983).
- 93 Crespi, S. & Fagnoni, M. Generation of alkyl radicals: From the tyranny of tin to the photon democracy. *Chem. Rev.* **120**, 9790–9833 (2020).
- 94 Kanegusuku, A. L. G. & Roizen, J. L. Recent advances in photoredox-mediated radical conjugate addition reactions: An expanding toolkit for the Giese reaction. *Angew. Chem. Int. Ed.* **60**, 2–36 (2021).
- 95 Treacy, S. M. & Rovis, T. Copper-catalyzed C(sp³)–H bond alkylation via photoinduced ligand-to-metal charge transfer. *J. Am. Chem. Soc.* **143**, 2729–2735 (2021).
- 96 Kang, Y. C., Treacy, S. M. & Rovis, T. Iron-catalyzed photoinduced LMCT: A 1^o C–H abstraction enables skeletal rearrangements and C(sp³)–H alkylation. *ACS. Catal.* **11**, 7442–7449 (2021).
- 97 Angioni, S. et al. Tetrabutylammonium decatungstate (chemo)selective photocatalyzed, radical C–H functionalization in amides. *Adv. Synth. Catal.* **350**, 2209–2214 (2008).
- 98 Yamada, K. et al. Photocatalyzed site-selective C–H to C–C conversion of aliphatic nitriles. *Org. Lett.* **17**, 1292–1295 (2015).
- 99 Fukuyama, T. et al. Photocatalyzed site-selective C(sp³)–H functionalization of alkylpyridines at non-benzylic positions. *Org. Lett.* **19**, 6436–6439 (2017).
- 100 Fukuyama, T., Nishikawa, T. & Ryu, I. Site-selective C(sp³)–H functionalization of fluorinated alkanes driven by polar effects using a tungstate photocatalyst. *Eur. J. Org. Chem.* 1424–1428 (2020).
- 101 Laudadio, G. et al. C(sp³)–H functionalizations of light hydrocarbon using decatungstate photocatalysis in flow. *Science* **369**, 92–96 (2020).
- 102 Roberts, B. P. Polarity-reversal catalysis of hydrogen-atom abstraction reactions: Concepts and applications in organic chemistry. *Chem. Soc. Rev.* **28**, 25–35 (1999).
- 103 Lei, G., Xu, M., Chang, R., Funes-Ardoiz, I. & Ye, J. Hydroalkylation of unactivated olefins

- via visible-light-driven dual hydrogen atom transfer catalysis. *J. Am. Chem. Soc.* **143**, 11251–11261 (2021).
- 104 Minisci, F., Bernardi, R., Bertini, F., Galli, R., Perchinummo, M. Nucleophilic character of alkyl radicals—VI: A new convenient selective alkylation of heteroaromatic bases. *Tetrahedron* **27**, 3575–3579 (1971).
- 105 Proctor, R. S. J. & Phipps, R. J. Recent advances in Minisci-type reactions. *Angew. Chem. Int. Ed.* **58**, 13666–13699 (2019).
- 106 Leonov, D. & Elad, D. Ultraviolet- and γ -ray-induced reactions of nucleic acid constituents. Reactions of purines with ethers and dioxolane. *J. Org. Chem.* **39**, 1470–1473 (1974).
- 107 Deng, G., Ueda, K., Yanagisawa, S., Itami, K. & Li, C.-J. Coupling of nitrogen heteroaromatics and alkanes without transition metals: A new oxidative cross-coupling at C–H/C–H bonds. *Chem. Eur. J.* **15**, 333–337 (2009).
- 108 Xia, R., Niu, H.-Y., Qu, G.-R. & Guo, H.-M. CuI controlled C–C and C–N bond formation of heteroaromatics through C(sp³)–H activation. *Org. Lett.* **14**, 5546–5549 (2012).
- 109 Shao, X., Wu, X., Wu, S. & Zhu, C. Metal-free radical-mediated C(sp³)–H heteroarylation of alkanes. *Org. Lett.* **22**, 7450–7454 (2020).
- 110 Tzirakis, M. D., Lykakis, I. N. & Orfanopoulos, M. Decatungstate as an efficient photocatalyst in organic chemistry. *Chem. Soc. Rev.* **38**, 2609–2621 (2009).
- 111 Quattrini, M. C. et al. Versatile cross-dehydrogenative coupling of heteroaromatics and hydrogen donors *via* decatungstate photocatalysis. *Chem. Commun.* **53**, 2335–2338 (2017).
- 112 De Waele, V., Poizat, O., Fagnoni, M., Bagno, A. & Ravelli, D. Unraveling the key features of the reactive state of decatungstate anion in hydrogen atom transfer (HAT) photocatalysis. *ACS Catal.* **6**, 7174–7182 (2016).
- 113 Ravelli, D., Fagnoni, M., Fukuyama, T., Nishikawa, T. & Ryu, I. Site-selective C–H functionalization by decatungstate anion photocatalysis: Synergistic control by polar and steric effects expands the reaction scope. *ACS Catal.* **8**, 701–703 (2018).
- 114 Li, G.-X., Hu, X., He, G. & Chen, G. Photoredox-mediated Minisci-type alkylation of *N*-heteroarenes with alkanes with high methylene selectivity. *ACS Catal.* **8**, 11847–11853 (2018).
- 115 Li, G.-X., Hu, X., He, G. & Chen, G. Photoredox-mediated Minisci-type alkylation of *N*-heteroarenes with alkanes with high methylene selectivity. *ACS Catal.* **8**, 11847–11853 (2018).
- 116 Lee, W., Jung, S., Kim, M. & Hong, S. Site-selective direct C–H pyridylation of unactivated alkanes by triplet excited anthraquinone. *J. Am. Chem. Soc.* **143**, 3003–3012 (2021).
- 117 Shu, C., Noble, A. & Aggarwal, V. K. Metal-free photoinduced C(sp³)–H borylation of alkanes. *Nature* **586**, 714–719 (2020).
- 118 Kharasch, M. S. & Sosnovsky, G. The reactions of *t*-butyl perbenzoate and olefins – a stereospecific reaction. *J. Am. Chem. Soc.* **80**, 756 (1958).
- 119 Kharasch, M. & Fono, A. Radical substitution reactions. *J. Org. Chem.* **23**, 325–326 (1958).
- 120 Kochi, J. K. Copper salt-catalyzed reaction of butenes with preesters. *J. Am. Chem. Soc.* **84**,

- 774–784 (1962).
- 121 Muzart, J. Enantioselective copper-catalyzed allylic acetoxylation of cyclohexene. *J. Mol. Catal.* **64**, 381–384 (1991).
- 122 Andrus, M. B., Argade, A. B., Chen, X. & Pamment, M. G. The asymmetric Kharasch reaction. Catalytic enantioselective allylic acyloxylation of olefins with chiral copper(I) complexes and *tert*-butyl perbenzoate. *Tetrahedron Lett.* **36**, 2945–2948 (1995).
- 123 Gokhale, A. S., Minidis, A. B. E. & Pfaltz, A. Enantioselective allylic oxidation catalyzed by chiral bisoxazoline-copper complexes. *Tetrahedron Lett.* **36**, 1831–1834 (1995).
- 124 Kawasaki, K., Tsumura, S. & Katsuki, T. Enantioselective allylic oxidation using biomimetic tris(oxazolines)-copper(II) complex. *Synlett.* 1245–1246 (1995).
- 125 Andrus, M. B. & Zhou, Z. Highly enantioselective copper–bisoxazoline-catalyzed allylic oxidation of cyclic olefins with *tert*-butyl *p*-nitroperbenzoate. *J. Am. Chem. Soc.* **124**, 8806–8807 (2002).
- 126 Corey, E. J. & Lee, J. Enantioselective total synthesis of oleanolic acid, erythrodiol, β -amyrin, and other pentacyclic triterpenes from a common intermediate. *J. Am. Chem. Soc.* **115**, 8873–8874 (1993).
- 127 Neukirch, H. et al. Improved anti-inflammatory activity of three new terpenoids derived, by systematic chemical modifications, from the abundant triterpenes of the flowery plant *calendula officinalis*. *Chem. Biodiversity.* **2**, 657–671 (2005).
- 128 García-Cabeza, A. L. et al. Allylic oxidation of alkenes catalyzed by a copper–aluminum mixed oxide. *Org. Lett.* **16**, 1598–1601 (2014).
- 129 García-Cabeza, A. L. et al. Optimization by response surface methodology (RSM) of the Kharasch–Sosnovsky oxidation of valencene. *Org. Process Res. Dev.* **19**, 1662–1666 (2015).
- 130 Gephart, R. T. et al. Reaction of CuI with dialkyl peroxides: Cu^{II}-alkoxides, alkoxy radicals, and catalytic C–H etherification. *J. Am. Chem. Soc.* **134**, 17350–17353 (2012).
- 131 Tran, B. L., Driess, M. & Hartwig, J. F. Copper-catalyzed oxidative dehydrogenative carboxylation of unactivated alkanes to allylic esters via alkenes. *J. Am. Chem. Soc.* **136**, 17292–17301 (2014).
- 132 Kohmura, Y., Kawasaki, K. & Katsuki, T. Benzylic and allylic amination. *Synlett.* **12**, 1456–1458 (1997).
- 133 Pelletier, G. & Powell, D. A. Copper-catalyzed amidation of allylic and benzylic C–H bonds. *Org. Lett.* **8**, 6031–6034 (2006).
- 134 Powell, D. A. & Fan, H. Copper-catalyzed amination of primary benzylic C–H bonds with primary and secondary sulfonamides. *J. Org. Chem.* **75**, 2726–2729 (2010).
- 135 Wiese, S. et al. Catalytic C–H amination with unactivated amines through copper(II) amides. *Angew. Chem. Int. Ed.* **49**, 8850–8855 (2010).
- 136 Tran, B. L., Li, B., Driess, M. & Hartwig, J. F. Copper-catalyzed intermolecular amidation and imidation of unactivated alkanes. *J. Am. Chem. Soc.* **136**, 2555–2563 (2014).
- 137 Zheng, Y.-W., Narobe, R., Donabauer, K., Yabukov, S. & König, B. Copper(II)-photocatalyzed N–H alkylation with alkanes. *ACS. Catal.* **10**, 8582–8589 (2020).

- 138 Borduas, N. & Powell, D. A. Copper-catalyzed oxidative coupling of benzylic C–H bonds with 1,3-dicarbonyl compounds. *J. Org. Chem.* **73**, 7822–7825 (2008).
- 139 Song, Z.-Q. et al. Photoredox oxo-C(sp³)–H bond functionalization via in situ Cu(I)-acetylide catalysis. *Org. Lett.* **22**, 832–836 (2020).
- 140 Vasilopoulos, A., Zultanski, S. L. & Stahl, S. S. Feedstocks to pharmacophores: Cu-catalyzed oxidative arylation of inexpensive alkylarenes enabling direct access to diarylalkanes. *J. Am. Chem. Soc.* **139**, 7705–7708 (2017).
- 141 Xie, W., Heo, J., Kim, D. & Chang, S. Copper-catalyzed direct C–H alkylation of polyfluoroarenes by using hydrocarbons as an alkylating source. *J. Am. Chem. Soc.* **142**, 7487–7496 (2020).
- 142 Ni, Z. et al. Highly regioselective copper-catalyzed benzylic C–H amination by *N*-fluorobenzenesulfonimide. *Angew. Chem. Int. Ed.* **51**, 1244–1247 (2012).
- 143 Zhang, W. et al. Enantioselective cyanation of benzylic C–H bonds via copper-catalyzed radical relay. *Science*, **353**, 1014–1018 (2016).
- 144 Xiao, H. et al. Copper-catalyzed late-stage benzylic C(sp³)–H trifluoromethylation. *Chem.* **5**, 940–949 (2019).
- 145 Suh, S.-E. et al. Site-selective copper-catalyzed azidation of benzylic C–H bonds. *J. Am. Chem. Soc.* **142**, 11388–11393 (2020).
- 146 Sharma, A. & Hartwig, J. F. Metal-catalyzed azidation of tertiary C–H bonds suitable for late-stage functionalization. *Nature* **517**, 600–604 (2015).
- 147 Margrey, K. A., Czaplyski, W. L., Nicewicz, D. A. & Alexanian, E. J. A general strategy for aliphatic C–H functionalization enabled by organic photoredox catalysis. *J. Am. Chem. Soc.* **140**, 4213–4217 (2018).
- 148 Liu, S. et al. Copper-catalyzed oxidative benzylic C(sp³)–H amination: Direct synthesis of benzylic carbamates. *Chem. Commun.* **56**, 13013–13016 (2020).
- 149 Wang, A., DeOliveira, C. C. & Emmert, M. Non-directed, copper catalyzed benzylic C–H amination avoiding substrate excess. *ChemRxiv*. Preprint at <https://doi.org/10.26434/chemrxiv.8792243.v2> (2019).
- 150 Jiang, C., Chen, P. & Liu, G. Copper-catalyzed benzylic C–H bond thiocyanation: Enabling late-stage diversifications. *CCS Chem.* **2**, 1884–1893 (2020).
- 151 Suh, S.-E., Nkulu, L. E., Lin, S., Krska, S. W. & Stahl, S. S. Benzylic C–H isocyanation/amine coupling sequence enabling high-throughput synthesis of pharmaceutically relevant ureas. *Chem. Sci.* **12**, 10380–10387 (2021).
- 152 Vasilopoulos, A., Golden, D. L., Buss, J. A. & Stahl, S. S. Copper-catalyzed C–H fluorination/functionalization sequence enabling benzylic C–H cross coupling with diverse nucleophiles. *Org. Lett.* **22**, 5753–5757 (2020).
- 153 Champagne, P. A. et al. Enabling nucleophilic substitution reactions of activated alkyl fluorides through hydrogen bonding. *Org. Lett.* **15**, 2210–2213 (2013).
- 154 Champagne, P. A., Benhassine, Y., Desroches, J. & Paquin, J.-P. Friedel–Crafts reaction of benzyl fluorides: Selective activation of C–F bonds as enabled by hydrogen bonding. *Angew.*

- Chem. Int. Ed.* **53**, 13835–13839 (2014).
- 155 Hemelaere, R., Champagne, P. A., Desroches, J. & Paquin, J.-F. Faster initiation in the Friedel–Crafts reaction of benzyl fluorides using trifluoroacetic acid as activator. *J. Fluorine Chem.* **190**, 1–6 (2016).
- 156 Hamel, J.-D. & Paquin, J.-F. Activation of C–F bonds α to C–C multiple bonds. *Chem. Commun.* **54**, 10224–10239 (2018).
- 157 Lopez, M. A., Buss, J. A. & Stahl, S. S. Site-selective chlorination of benzylic C–H bonds by Cu-catalysis. *Org. Lett.* **24**, (2022), in press, DOI: 10.1021/acs.orglett.1c04038.
- 158 Jin, J. et al. Copper(I)-catalyzed site-selective C(sp³)–H bond chlorination of ketones, (*E*)-enones and alkylbenzenes by dichloramine-T. *Nat. Commun.* **12**, 4065 (2021).
- 159 Fawcett, A., Keller, M. J., Herrera, Z. & Hartwig, J. F. Site selective chlorination of C(sp³)–H bonds suitable for late-stage functionalization. *Angew. Chem. Int. Ed.* **60**, 8276–8283 (2021).
- 160 Li, J. et al. Site-specific allylic C–H bond functionalization with a copper-bound N-centered radical. *Nature* **574**, 516–521 (2019).
- 161 Zhou, J., Jin, C., Li, X. & Su, W. Copper-catalyzed oxidative esterification of unactivated C(sp³)–H bonds with carboxylic acids via cross dehydrogenative coupling. *RCS Adv.* **5**, 7232–7236 (2015).
- 162 Hu, H. et al. Copper-catalyzed benzylic C–H coupling with alcohols via radical relay enabled by redox buffering. *Nat. Catal.* **3**, 358–367 (2020).
- 163 Chen, S.-J., Golden, D. L., Krska, S. W. & Stahl, S.S. Copper-catalyzed cross-coupling of benzylic C–H bonds and azoles with controlled *N*-site selectivity. *J. Am. Chem. Soc.* **143**, 14438–14444 (2021).
- 164 Ivanova, A. E. et al. Ambident polyfluoroalkyl-substituted pyrazoles in the methylation reactions. *J. Fluor. Chem.* **195**, 47–56 (2017).
- 165 Huang, A. et al. Regioselective synthesis, NMR, and crystallographic analysis of N1-substituted pyrazoles. *J. Org. Chem.* **82**, 8864–8872 (2017).
- 166 Zhang, W., Chen, P. & Liu, G. Copper-catalyzed arylation of benzylic C–H bonds with alkylarenes as the limiting reagents. *J. Am. Chem. Soc.* **139**, 7709–7712 (2017).
- 167 Zhang, W., Wu, L., Chen, P. & Liu, G. Enantioselective arylation of benzylic C–H bonds by copper-catalyzed radical relay. *Angew. Chem. Int. Ed.* **58**, 6425–6429 (2019).
- 168 Fu, L., Zhang, Z., Chen, P., Lin, Z. & Liu, G. Enantioselective copper-catalyzed alkynylation of benzylic C–H bonds via radical relay. *J. Am. Chem. Soc.* **142**, 12493–12500 (2020).
- 169 Li, Z., Cao, L. & Li, C.-J. FeCl₂-catalyzed selective C–C bond formation by oxidative activation of a benzylic C–H bond. *Angew. Chem. Int. Ed.* **46**, 6505–6507 (2007).
- 170 Xia, Q., Chen, W. & Qiu, H. Direct C–N coupling of imidazoles and benzylic compounds via iron-catalyzed oxidative activation of C–H bonds. *J. Org. Chem.* **76**, 7577–7582 (2011).
- 171 Kumar, J., Suresh, E. & Bhadra, S. Catalytic direct α -amination of arylacetic acid synthons with anilines. *J. Org. Chem.* **85**, 13363–13374 (2020).
- 172 Karimov, R. R., Sharma, A. & Hartwig, J. F. Late Stage Azidation of Complex Molecules.

- ACS Cent. Sci.* **2**, 715–724 (2016).
- 173 Ye, Y.-H., Zhang, J., Wang, G., Chen, S.-Y. & Yu, X.-Q. Cobalt-catalyzed benzylic C–H amination via dehydrogenative-coupling reaction. *Tetrahedron* **67**, 4649–4654 (2011).
- 174 Tang, S., Wang, P., Li, H. & Lei, A. Multimetallic catalysed radical oxidative C(sp³)–H /C(sp)–H cross-coupling between unactivated alkanes and terminal alkynes. *Nat. Commun.* **7**, 11676 (2016).
- 175 Liu, D., Liu, C., Li, H. & Lei, A. Direct functionalization of tetrahydrofuran and 1,4-dioxane: Nickel-catalyzed oxidative C(sp³)–H arylation. *Angew. Chem. Int. Ed.* **52**, 4453–4456 (2013).
- 176 Liu, D. et al. Nickel-catalyzed oxidative radical cross-coupling: An effective strategy for inert Csp³–H functionalization. *Org. Lett.* **17**, 998–1001 (2015).
- 177 Vasilopoulos, A., Krska, S. W. & Stahl, S. S. C(sp³)–H methylation enabled by peroxide photosensitization and Ni-mediated radical coupling. *Science* **372**, 398–403 (2021).
- 178 Schönherr, H. & Cernak, T. Profound methyl effects in drug discovery and a call for new C–H methylation reactions. *Angew. Chem. Int. Ed.* **52**, 12256–12267 (2013).
- 179 Xu, P., Guo, S., Wang, L. & Tang, P. Silver-catalyzed oxidative activation of benzylic C–H bonds for the synthesis of difluoromethylated arenes. *Angew. Chem. Int. Ed.* **126**, 6065–6068 (2014).
- 180 Yang, H. et al. Silver-promoted oxidative benzylic C–H trifluoromethoxylation. *Angew. Chem. Int. Ed.* **57**, 13266–13270 (2018).
- 181 Skubi, K. L., Blum, T. R. & Yoon, T. P. Dual catalysis strategies in photochemical synthesis. *Chem. Soc. Rev.* **116**, 10035–10074 (2016).
- 182 Twilton, J. et al. The merger of transition metal and photocatalysis. *Nat. Rev. Chem.* **1**, 0052 (2017).
- 183 Shaw, M. H., Twilton, J. & MacMillan, D. W. C. Photoredox catalysis in organic chemistry. *J. Org. Chem.* **81**, 6898–6926 (2016).
- 184 Levin, M. D., Kim, S. & Toste, F. D. Photoredox catalysis unlocks single-electron elementary steps in transition metal catalyzed cross-coupling. *ACS Cent. Sci.* **2**, 293–301 (2016).
- 185 Matsui, J. K., Lang, S. B., Heitz, D. R. & Molander, G. A. Photoredox-mediated routes to radicals: The value of catalytic radical generation in synthetic methods development. *ACS Catal.* **7**, 2563–2575 (2017).
- 186 McAtee, R. C., McClain, E. J. & Stephenson, C. R. J. Illuminating Photoredox Catalysis. *Trends Chem.* **1**, 111–125 (2019).
- 187 Chan, A. Y. et al. Metallaphotoredox: The merger of photoredox and transition metal catalysis. *Chem. Rev.* Accepted Article (2021) <https://doi.org/10.1021/acs.chemrev.1c00383>.
- 188 Capaldo, L.; Ravelli, D. & Fagnoni, M. Direct photocatalyzed hydrogen atom transfer (HAT) for aliphatic C–H bonds elaboration. *Chem. Rev.* Accepted Article (2021) <https://doi.org/10.1021/acs.chemrev.1c00263>.
- 189 Leibler, I. N.-M., Tekle-Smith, M. A. & Doyle, A. A general strategy for C(sp³)–H functionalization with nucleophiles using methyl radical as a hydrogen atom abstractor. *Nat.*

- Commun.* **12**, 6950 (2021).
- 190 Zhang, Y. et al. A photoredox-catalyzed approach for formal hydride abstraction to enable a general Csp^3-H fluorination with HF. Preprint at *ChemRxiv* <https://doi.org/10.26434/chemrxiv.14109797.v1> (2021).
- 191 Li, G.-X. et al. A unified photoredox-catalysis strategy for $C(sp^3)-H$ hydroxylation and amidation using hypervalent iodine. *Chem. Sci.* **8**, 7180–7185 (2017).
- 192 Michaudel, Q., Thevenet, D. & Baran, P. S. Intermolecular Ritter-type C–H amination of unactivated sp^3 carbons. *J. Am. Chem. Soc.* **134**, 2547–2550 (2012).
- 193 Kiyokawa, K., Takemoto, K. & Minakata, S. Ritter-type amination of C–H bonds at tertiary carbon centers using iodic acid as an oxidant. *Chem. Commun.* **52**, 13082–13085 (2016).
- 194 Maeda, B., Sakakibara, Y., Murakami, K. & Itami, K. Photoredox-catalyzed benzylic esterification via radical-polar crossover. *Org. Lett.* **23**, 5113–5117 (2021).
- 195 Meng, Q.-Y., Schirmer, T. E., Berger, A. L., Donabauer, K. & König, B. Photocarboxylation of benzylic C–H bonds. *J. Am. Chem. Soc.* **141**, 11393–11397 (2019).
- 196 Berger, A. L., Donabauer, K. & König, B. Photocatalytic carbanion generation from C–H bonds – reductant free Barbier/Grignard-type reactions. *Chem. Sci.* **10**, 10991–10996 (2019).
- 197 Bosnidou, A. E. & Muñoz, K. Intermolecular radical $C(sp^3)-H$ amination under iodine catalysis. *Angew. Chem. Int. Ed.* **58**, 7485–7489 (2019).
- 198 Romine, A. M. et al. Easy access to the copper(III) anion $[Cu(CF_3)_4]^-$. *Angew. Chem. Int. Ed.* **54**, 2745–2749 (2015).
- 199 Guo, S., AbuSalim, D. I. & Cook, S. P. Aqueous benzylic C–H trifluoromethylation for late-stage functionalization. *J. Am. Chem. Soc.* **140**, 12378–12382 (2018).
- 200 He, J., Nguyen, T. N., Guo, S. & Cook, S. P. Csp^3-H trifluoromethylation of unactivated aliphatic systems. *Org. Lett.* **23**, 702–705 (2021).
- 201 Choi, G., Lee, G. S., Park, B., Kim, D. & Hong, S. H. Direct $C(sp^3)-H$ trifluoromethylation of unactivated alkanes enabled by multifunctional trifluoromethyl copper complexes. *Angew. Chem. Int. Ed.* **60**, 5467–5474 (2021).
- 202 Sarver, P. J. et al. The merger of decatungstate and copper catalysis to enable aliphatic $C(sp^3)-H$ trifluoromethylation. *Nat. Chem.* **12**, 459–467 (2020).
- 203 Shaw, M. H., Shurtleff, V. W., Terrett, J. A., Cuthbertson, J. D. & MacMillan, D. W.C. Native functionality in triple catalytic cross-coupling: sp^3 C–H bonds as latent nucleophiles. *Science* **352**, 1304–1308 (2016).
- 204 Le, C., Liang, Y., Evans, R. W., Li, X. & MacMillan, D. W. C. Selective sp^3 C–H alkylation via polarity-match-based cross-coupling. *Nature* **547**, 79–83 (2017).
- 205 Zhang, X. & MacMillan, D. W. C. Direct aldehyde C–H arylation and alkylation via the combination of nickel, hydrogen atom transfer, and photoredox catalysis. *J. Am. Chem. Soc.* **139**, 11353–11356 (2017).
- 206 Twilton, J. et al. Selective hydrogen atom abstraction through induced bond polarization: Direct α -arylation of alcohols through photoredox, HAT, and nickel catalysis. *Angew. Chem. Int. Ed.* **57**, 5369–5373 (2018).

- 207 Ma, Z.-Y. et al. Sulfonamide as photoinduced hydrogen-atom transfer catalyst for regioselective alkylation of C(sp³)-H bonds adjacent to heteroatoms. *Org. Lett.* **23**, 474–479 (2021).
- 208 Perry, I. B. et al. Direct arylation of strong aliphatic C–H bonds. *Nature* **560**, 70–75 (2018).
- 209 Berger, M., Goldblatt, I. L. & Steel, C. Photochemistry of benzaldehyde. *J. Am. Chem. Soc.* **95**, 1717–1725 (1973).
- 210 Dóрман, G., Nakamura, H. Pulsipher, A. & Prestwich, G. D. The life of pi star: Exploring the exciting and forbidden worlds of the benzophenone photophore. *Chem. Rev.* **116**, 15284–15398 (2016).
- 211 Shen, Y., Gu, Y. & Martin, R. *sp*³ C–H arylation and alkylation enabled by the synergy of triplet excited ketones and nickel catalysts. *J. Am. Chem. Soc.* **140**, 12200–12209 (2018).
- 212 Dewanji, A., Krach, P. E. & Rueping, M. The dual role of benzophenone in visible-light/nickel photoredox-catalyzed C–H arylations: Hydrogen-atom transfer and energy transfer. *Angew. Chem. Int. Ed.* **58**, 3566–3570 (2019).
- 213 Zhang, L. et al. The combination of benzaldehyde and nickel-catalyzed photoredox C(sp³)-H alkylation/arylation. *Angew. Chem. Int. Ed.* **58**, 1823–1827 (2019).
- 214 Si, X., Zhang, L. & Hashmi, S. K. Benzaldehyde- and nickel-catalyzed photoredox C(sp³)-H alkylation/arylation with amides and thioethers. *Org. Lett.* **21**, 6329–6332 (2019).
- 215 Heitz, D. R., Tellis, J. C. & Molander, G. A. Photochemical nickel-catalyzed C–H arylation: Synthetic scope and mechanistic investigations. *J. Am. Chem. Soc.* **138**, 12715–12718 (2016).
- 216 Shields, B. J. & Doyle, A. G. Direct C(sp³)-H cross-coupling enabled by catalytic generation of chlorine radicals. *J. Am. Chem. Soc.* **138**, 12719–12722 (2016).
- 217 Nielsen, M. K. et al. Mild, redox-neutral formylation of aryl chlorides through the photocatalytic generation of chlorine radicals. *Angew. Chem. Int. Ed.* **56**, 7191–7194 (2017).
- 218 Chang, X., Lu, H. & Lu, Z. Enantioselective benzylic C–H arylation via photoredox and nickel dual catalysis. *Nat. Commun.* **10**, 3549 (2019).
- 219 Cheng, X.; Li, T.; Liu, Y. & Lu, Z. Stereo- and enantioselective benzylic C–H alkenylation via photoredox/nickel dual catalysis. *ACS Catal.* **11**, 11059–11065 (2021).
- 220 Joe, C. L. & Doyle, A. G. Direct acylation of C(sp³)-H bonds enabled by nickel and photoredox catalysis. *Angew. Chem. Int. Ed.* **55**, 4040–4043 (2016).
- 221 Ahneman, D. T. & Doyle, A. G. C–H functionalization of amines with aryl halides by nickel-photoredox catalysis. *Chem Sci.* **7**, 7002–7006 (2016).
- 222 Novaes, L. F. et al. Electrocatalysis as an enabling technology for organic synthesis. *Chem. Soc. Rev.* **50**, 7941–8002 (2021).
- 223 Chen, N. & Xu, H.-C. Electrochemical generation of nitrogen-centered radicals for organic synthesis. *Green Synth. Catal.* **2**, 165–178 (2021).
- 224 Masui, M., Hara, S., Ueshima, T., Kawagushi, T. & Ozaki, S. Anodic oxidation of compounds having benzylic or allylic carbon and α -carbon to hetero atom using *N*-hydroxyphthalimide as a mediator. *Chem Pharm. Bull.* **31**, 4209–4211 (1983).
- 225 Masui, M., Hosomi, K., Tsuchida, K. & Ozaki, S. Electrochemical oxidation of olefins using

- N*-hydroxyphthalimide as a mediator. *Chem. Pharm. Bull.* **33**, 4798–4802 (1985).
- 226 Masui, M., Hara, S. & Ozaki, S. Anodic oxidation of amides and lactams using *N*-hydroxyphthalimide as a mediator. *Chem. Pharm. Bull.* **34**, 975–979 (1986).
- 227 Nutting, J. E., Rafiee, M. R. & Stahl, S. S. Tetramethylpiperidine *N*-oxyl (TEMPO), phthalimide *N*-oxyl (PINO), and related *N*-Oxyl species: Electrochemical properties and their use in electrocatalytic reactions. *Chem. Rev.* **118**, 4834–4885 (2018).
- 228 Horn, E. J. et al. Scalable and sustainable electrochemical allylic C–H oxidation. *Nature* **533**, 77–81 (2016).
- 229 Mo, Y. & Jensen, K. F. Continuous *N*-hydroxyphthalimide (NHPI)-mediated electrochemical aerobic oxidation of benzylic C–H bonds. *Chem. Eur. J.* **24**, 10260–10265 (2018).
- 230 Kawamata, Y. et al. Scalable, electrochemical oxidation of unactivated C–H bonds. *J. Am. Chem. Soc.* **139**, 7448–7451 (2017).
- 231 Saito, M. et al. *N*-ammonium ylide mediators for electrochemical C–H oxidation. *J. Am. Chem. Soc.* **143**, 7859–7867 (2021).
- 232 Rafiee, M., Wang, F., Hruszkewycz, D. P. & Stahl, S. S. *N*-hydroxyphthalimide-mediated electrochemical iodination of methylarenes and comparison to electron-transfer-initiated C–H functionalization. *J. Am. Chem. Soc.* **140**, 22–25 (2018).
- 233 Hayashi, R., Shimizu, A. & Yoshida, J. The stabilized cation pool method: Metal- and oxidant-free benzylic C–H/aromatic C–H cross-coupling. *J. Am. Chem. Soc.* **138**, 8400–8403 (2016).
- 234 Zhu, Y. et al. A promising electro-oxidation of methyl-substituted aromatic compounds to aldehydes in aqueous imidazole ionic liquid solutions. *J. Electroanal. Chem.* **751**, 105–110 (2015).
- 235 Das, A.; Nutting, J. E. & Stahl, S. S. Electrochemical C–H oxygenation and alcohol dehydrogenation involving Fe-oxo species using water as the oxygen source. *Chem. Sci.* **10**, 7542–7548 (2019).
- 236 Robinson, S. G., Mack, J. B. C., Alektiar, S. N., Du Bois, J. & Sigman, M. S. Electrochemical ruthenium-catalyzed C–H hydroxylation of amine derivatives in aqueous acid. *Org. Lett.* **22**, 7060–7063 (2020).
- 237 Meyer, T. H., Samanta, R. C., Del Vecchio, A. & Ackermann, L. Manganese(III/IV)electrocatalyzed C(sp³)–H azidation. *Chem. Sci.* **12**, 2890–2897 (2021).
- 238 Niu, L. et al. Manganese-catalyzed oxidative azidation of C(sp³)–H bonds under electrophotocatalytic conditions. *J. Am. Chem. Soc.* **142**, 17693–17702 (2020).

Chapter 2.

Benzylic C–H Esterification with Limiting C–H Substrate Enabled by Photochemical Redox Buffering of the Cu Catalyst

Reproduced with permission from: **Dung L. Golden**, Chaofeng Zhang, Si-Jie Chen, Aristidis Vasilopoulos, Ilia A. Guzei, Shannon S. Stahl. Benzylic C–H Esterification with Limiting C–H Substrate Enabled by Photochemical Redox Buffering of the Cu Catalyst. *J. Am. Chem. Soc.* **2023**, *10.1021/jacs.3c01662*. Copyright 2023 American Chemical Society.

2.1. Abstract

Copper-catalyzed radical-relay reactions, originating with the Kharasch-Sosnovsky (K-S) reaction, provide a versatile strategy for selective C–H functionalization. The synthetic utility of reactions with Cu catalysts and peroxide-based oxidants is constrained by the common requirement for excess C–H substrate relative to the peroxide. Here we report a photochemical strategy to overcome this limitation by using a homogeneous Cu catalyst with 2,2'-biquinoline as an ancillary ligand, enabling esterification of benzylic C–H bonds with limiting C–H substrate. Mechanistic studies suggest that blue-light irradiation promotes carboxylate-to-copper charge transfer, reducing the resting-state Cu^{II} species to Cu^{I} , which can activate the peroxide to generate the alkoxy radical hydrogen-atom transfer species. This "photochemical redox buffering" strategy introduces a unique approach to re-engage inactive Cu catalysts in radical-relay reactions, supporting catalysis under mild conditions with limiting C–H substrate.

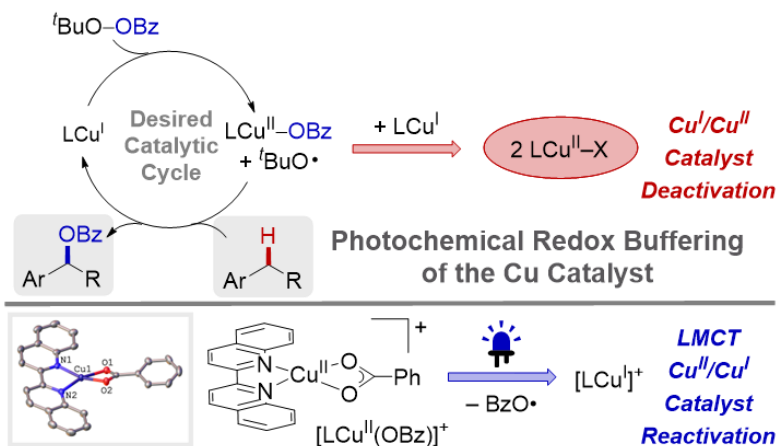


Figure 2.1. Benzylic esterification enabled by photochemical redox buffering.

2.2. Introduction

The Kharasch-Sosnovsky (K-S) reaction was first reported in 1958 and uses a copper catalyst and peroxyester oxidant to convert alkenes to allylic esters (Figure 2.2A).^{1,2} This seminal reaction is a prototype for contemporary radical-relay C(sp³)–H functionalization methods.^{3,4} The proposed mechanism for K-S reactions begins with activation of *tert*-butyl peroxybenzoate (TBPB) by Cu^I to generate a *tert*-butoxyl radical and Cu^{II}-benzoate (Figure 2.2B). The *tert*-butoxyl radical promotes hydrogen-atom transfer (HAT) from the allylic C–H bond, and the resulting allylic radical reacts with a Cu^{II}-benzoate species to form the C–O bond via a putative allyl-Cu^{III} intermediate. While reviewing previous fundamental studies,^{5–7} it became apparent that this simplified mechanism cannot account for key experimental observations. For example, the reported activation barriers for steps 1–3 (Figure 2.2B) suggest the reaction should proceed within seconds at room temperature; however, K-S reactions and later variations that form C–O,⁸ C–N⁹ and C–C¹⁰ bonds often require elevated temperatures (80–120 °C) and/or long (sometimes multi-day) reaction times. From a synthetic perspective, K-S reactions are limited by their typical use of a significant excess of the C–H substrate (3–10 equiv) relative to the peroxide as the limiting reagent. This chapter presents mechanistic hypotheses that could explain these observations and provide the foundation for development of Cu-catalyzed benzylic esterification reactions compatible with use of the C–H substrate as the limiting reagent (Figure 2.2C).

Studies of other radical-relay C–H oxidation reactions^{10b,11} have contributed to rationalize the unexplained features of K-S reactions. Cu^I often reacts rapidly with the peroxide in a 2:1 stoichiometry, converting all Cu^I to Cu^{II}. Warren and coworkers characterized this reactivity between a diketiminate-Cu^I complex and *t*-BuOO*t*-Bu (DTBP),^{8b} and we have observed similar behavior in reactions of Cu^I with *N*-fluorobenzenesulfonimide (NFSI),¹¹ another common

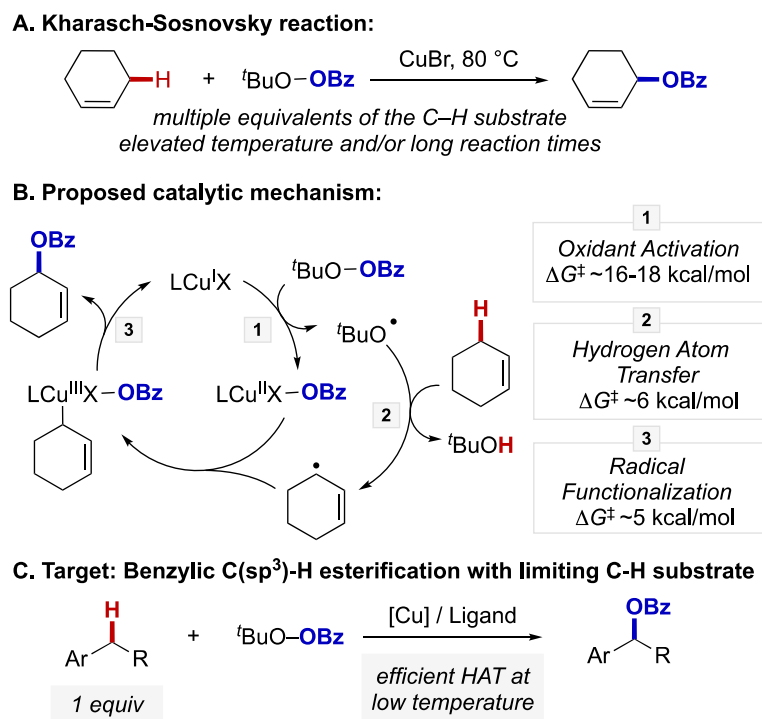


Figure 2.2. (A) Kharasch-Sosnovsky (K-S) allylic C–H esterification. (B) Proposed catalytic mechanism for the K-S reaction and estimated activation barriers for individual steps. (C) Focus of this study is to develop a K-S-type benzylic esterification, capable of using the C–H substrate as a limiting reagent.

oxidant in radical-relay reactions. Since Cu^{II} does not react with peroxides under these conditions, radical generation relies on thermal O–O bond homolysis when Cu^I is depleted, resulting in a need for elevated temperature to initiate the reaction. At high temperature, however, *tert*-butoxyl radical decomposes via β -methyl scission, producing methyl radical and acetone.¹² Use of excess C–H substrate provide a means for the bimolecular HAT step to compete favorably with unimolecular decomposition of *tert*-butoxyl radical under the reaction conditions, but this approach reduces the synthetic utility of the reaction. Recognizing that HAT gains a competitive advantage over β -scission at lower temperature,^{6a,12b} we recently used photochemistry to support O–O cleavage under ambient conditions, leveraging triplet energy-transfer (EnT) with an Ir-based photocatalyst, [Ir{dF(CF₃)ppy}₂(dtbpy)]PF₆ [Ir-F; dF(CF₃)ppy = 2-(2,4-difluorophenyl)-(5-trifluoromethyl)pyridine].¹³ This strategy proved more effective than direct photolysis of the

peroxide,^{14–16} in C–H methylation reactions with di-*tert*-butylperoxide.¹⁷ The present study was initiated with the goal of developing a K-S-type benzylic esterification using a similar photocatalytic EnT concept; however, we instead discovered a photoactive Cu/2,2'-biquinoline (biq) catalyst system that operates in the absence of a photocatalyst. The synthetic and mechanistic results outlined below demonstrate a new "photochemical redox-buffering" mechanism that supports Cu-catalyzed radical-relay C–H functionalization.

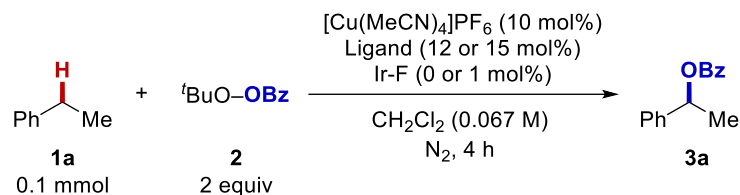
2.3. Results and Discussion

This study was initiated by probing the reaction of ethylbenzene (**1a**) with TBPB (**2**), using **1a** as the limiting reagent. Thermal K-S conditions with [Cu(MeCN)₄]PF₆ and a bidentate nitrogen ligand as the catalyst, including 1,10-phenanthroline (phen), 2,2'-bipyridine (bpy) and biq, led to negligible or low yields of the esterification product **3a** at 40°C and 80 °C (Table 2.1, entries 1–6). The reactions were reassessed in the presence of the Ir-F photocatalyst while irradiating with 450 nm LEDs. A 20% yield of **3a** was observed with the biq-Cu catalyst (Table 2.1, entry 9). Control experiments with this catalyst, in which the reaction solution was irradiated in the absence of Ir-F, led to an even better yield (39% **3a**). Optimized conditions afforded a 74% yield of **3a** (Table 2.1, entry 11) (see Appendix A for full screening data). Eighteen different ligands were evaluated under similar conditions, but only biq led to significant formation of **3a** (see Table 2A.3).

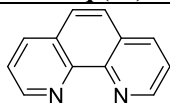
The optimized conditions were then tested with an array of other substrates. Secondary benzylic C–H bonds proved to be particularly effective (Figure 2.3). Ethyl- and *n*-alkylbenzene derivatives, including those with electron-rich and -deficient aromatic substituents and 1° alkyl halides, proceeded in good yield (59–79%, **3b–3n**). The reaction was also effective with a substituted diarylmethane derivative (**3s**),¹⁸ heterobenzylic benzofuran and thiophene substrates

(**3p**, **3r**).¹⁹ The pyridine-containing substrate **2q** exhibited high conversion, but did not afford the

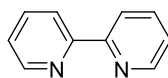
Table 2.1. Reaction optimization for photo-promoted benzylic esterification



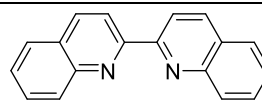
Entry	Ligand (mol%)	Ir-F ^a (mol%)	Temp (°C)	Conv. of 1a ^b (%)	Yield of 3a ^b (%)
<i>Thermal: 40 or 80 °C</i>					
1	phen (12)	0	40	0	0
2	bpy (12)	0	40	0	0
3	biq (12)	0	40	0	0
4 ^c	phen (12)	0	80	3	3
5 ^c	bpy (12)	0	80	6	0
6 ^c	biq (12)	0	80	13	13
<i>Photochemical: 450 nm LED irradiation at 40 °C</i>					
7	phen (12)	1	40	11	0
8	bpy (12)	1	40	4	0
9	biq (12)	1	40	33	20
10	biq (12)	0	40	57	39
11^d	biq (15)	0	40	99	74



phen



bpy



biq

^aIr-F = $[\text{Ir}\{\text{dF}(\text{CF}_3)\text{ppy}\}_2(\text{dtbpy})]\text{PF}_6$. ^b¹H NMR spectroscopy; yield determined using mesitylene as ext. std. ^c1,2-dichloroethane used as the solvent. ^dReaction run for 8 h with 5 equiv of TBPB (**2**).

desired product **3q** (see Figure 2A.7 in the Appendix A for additional examples of unsuccessful substrates). More complex substrates also proved effective, including celestolide (85%, **3t**), ibuprofen methyl ester (58%, **3u**); and benzbromarone methyl ether (55%, **3v**), a derivative of a xanthine oxidase inhibitor.²⁰

and/or weaker C–H bonds.²² Collectively, the reactions in Figures 2.3 and 2.4 provide a means to access benzylic alcohols via benzylic C–H oxygenation, without over-oxidation to the corresponding ketones. This outcome may be realized via C–H esterification, followed by hydrolysis, without isolation of the intermediate ester, as demonstrated in the preparation of **4r**–**4ae** (Figure 2.4B).

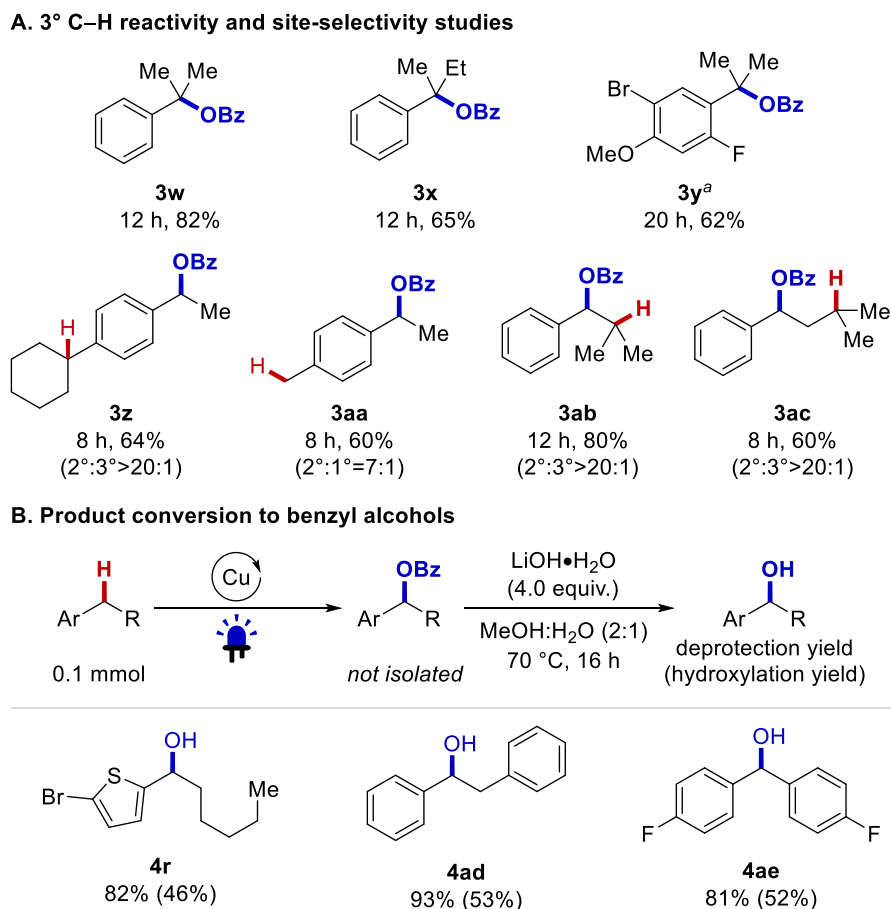


Figure 2.4. Reactivity of 3° benzylic substrates and assessment of benzylic site-selectivity under the conditions defined in Figure 2.3, and (B) sequential esterification/deprotection of benzylic C–H substrates.

Subsequent efforts focused on probing how this biq/Cu^I catalyst system differs from more conventional Cu catalyst systems, such as those bearing phen and bpy ligands. The reaction of TBPB with [Cu(MeCN)₄]PF₆ in the presence of 1.5 equiv of phen, bpy, and biq ligands was monitored by UV-visible spectroscopy (Figure 2.5A). The data show that the phen- and bpy-ligated

Cu^{I} complexes react rapidly with TBPB, undergoing full oxidation of Cu^{I} within seconds after mixing (Figures 2.5A-1 and 2.5A-2). The reaction of TBPB with $\text{biq}/\text{Cu}^{\text{I}}$ is more complex, with rapid partial reaction of Cu^{I} observed immediately after mixing, followed by very slow oxidation of the remaining Cu^{I} over several days (Figure 2.5A-3). Biq is known to form tetrahedral $[(\text{biq})_2\text{Cu}^{\text{I}}]^+$ complexes,^{23,24} and this species is the source of the absorption feature centered at 549 nm. Ligand titration studies, however, revealed that the $[(\text{biq})_2\text{Cu}^{\text{I}}]^+$ species does not begin to appear until nearly a full equivalent of biq is present (see Figure 2A.4). Therefore, the optimized catalyst system, with a biq/Cu ratio of 1.5:1, will have both mono- and bis-ligated $\text{biq}/\text{Cu}^{\text{I}}$ complexes in the reaction mixture. Further studies showed that a 1:1 mixture of $\text{biq}/[\text{Cu}(\text{MeCN})_4]\text{PF}_6$ reacts very rapidly with TBPB, while a 2:1 mixture of $\text{biq}/[\text{Cu}(\text{MeCN})_4]\text{PF}_6$ shows negligible reactivity (Table 2A.7). TBPB titration experiments further show that the rapid oxidation of Cu^{I} proceeds to completion with only 0.5 equiv of TBPB (Figure 2.5B). In summary, these data show that $\text{phen}/\text{Cu}^{\text{I}}$ and $\text{bpy}/\text{Cu}^{\text{I}}$ and 1:1 $\text{biq}/\text{Cu}^{\text{I}}$ undergo very rapid oxidation by TBPB, while the 2:1 $\text{biq}/\text{Cu}^{\text{I}}$ species is nearly inert under analogous conditions.

We then probed the reactivity of $\text{biq}/\text{Cu}^{\text{I}}$ (1.5:1) with TBPB during blue LED irradiation. Analysis of this reaction by UV-vis spectroscopy showed partial disappearance of the $[(\text{biq})_2\text{Cu}^{\text{I}}]^+$ species over the first 5-6 min, consistent with oxidation of Cu^{I} by TBPB; however, the $[(\text{biq})_2\text{Cu}^{\text{I}}]^+$ species reappeared almost fully over the next 6 min (Figure 2.5C). The initial phase of this reactivity suggests that irradiation enhances the rate of $[(\text{biq})_2\text{Cu}^{\text{I}}]^+$ oxidation by TBPB, albeit with a rate much slower than reaction of TBPB with the 1:1 $\text{biq}/\text{Cu}^{\text{I}}$ species. The more notable result is reappearance of $[(\text{biq})_2\text{Cu}^{\text{I}}]^+$ during irradiation, implicating light-promoted reduction of a $\text{biq}/\text{Cu}^{\text{II}}$ species.

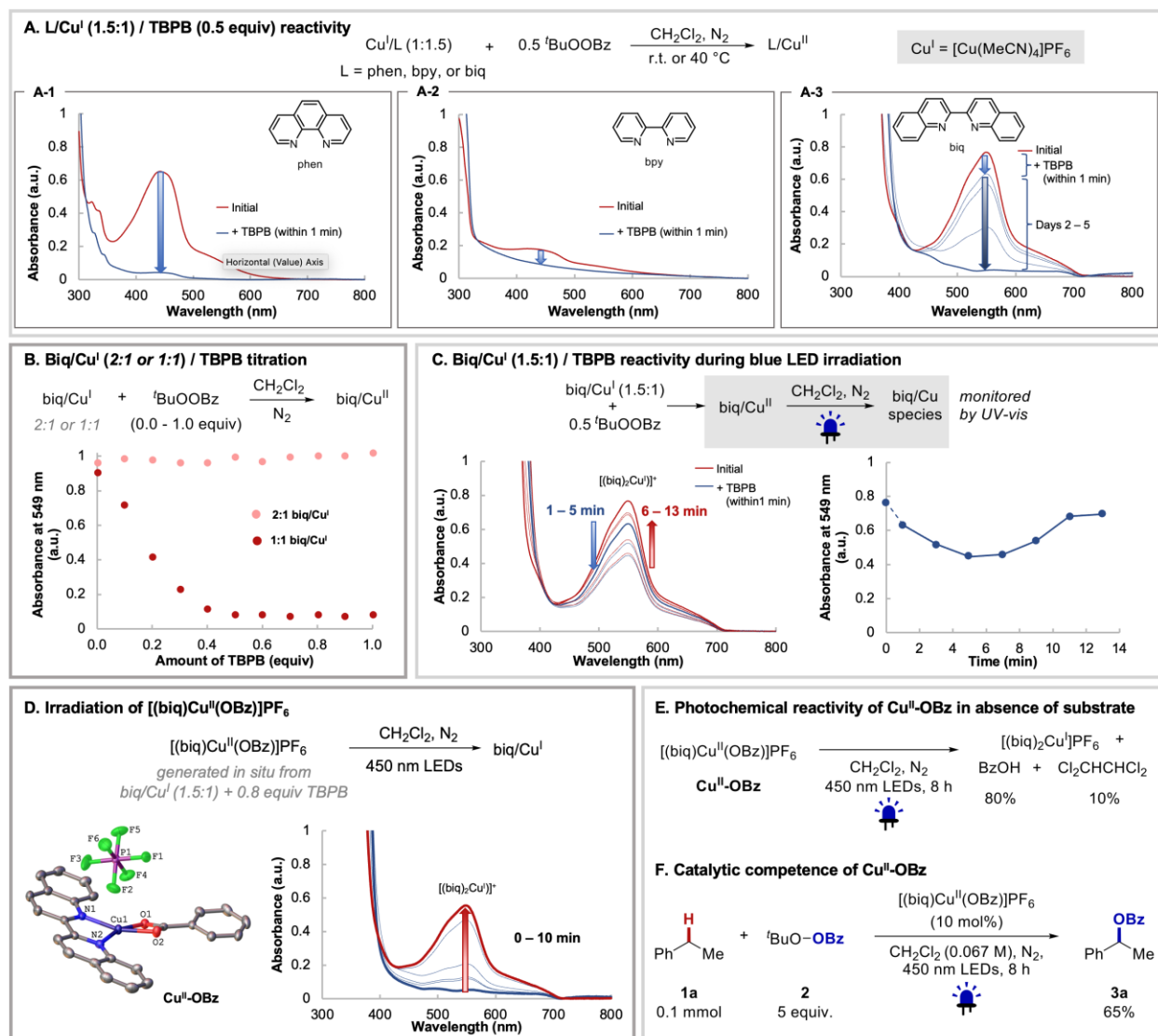


Figure 2.5. (A) UV-visible absorption spectra for oxidation of Cu^{I} complexes with phen (r.t.), bpy (r.t.), and biq (40°C) ligands without irradiation. (B) TBPB titration experiment with 2:1 $\text{biq}/\text{Cu}^{\text{I}}$ and 1:1 $\text{biq}/\text{Cu}^{\text{I}}$ with 30s mixing after every addition. (C) UV-visible absorption spectrum for oxidation of $\text{biq}/\text{Cu}^{\text{I}}$ under irradiation. (D) UV-visible absorption spectrum of photochemical reduction of $\text{biq}/\text{Cu}^{\text{II}}$. Reaction of 1:1 $\text{biq}/\text{Cu}^{\text{I}}$ with TBPB to afford $[(\text{biq})\text{Cu}^{\text{II}}(\text{OBz})]\text{PF}_6$. For clarity, hydrogen atoms are not shown in the X-ray structure. (E) Photochemical reactivity of $\text{Cu}^{\text{II}}\text{-OBz}$ in absence of a C–H substrate. (F) Catalytic reactivity of $\text{Cu}^{\text{II}}\text{-OBz}$ under standard reaction condition.

Reaction of 0.5 equiv of TBPB with $\text{biq}/\text{Cu}^{\text{I}}$ (cf. Figure 2.5B) is expected to form $\text{Cu}^{\text{II}}\text{-OBz}$ and $\text{Cu}^{\text{II}}\text{-O}^t\text{Bu}$ species.^{8b} While the latter species are thermally unstable,^{9b,25} X-ray quality crystals of $[(\text{biq})\text{Cu}^{\text{II}}(\text{OBz})]\text{PF}_6$ ($\text{Cu}^{\text{II}}\text{-OBz}$) were obtained from the reaction (Figure 2.5D, left). A

catalytically relevant mixture of 1.5:1 biq/Cu^I was then fully oxidized by TBPB. Irradiation of this mixture with blue LEDs led to photoinduced reduction of Cu^{II} and the appearance of [(biq)₂Cu^I]⁺ (Figure 2.5D, right). When biq was replaced by phen or bpy in the same experimental sequence, no photoreduction of Cu^{II} was observed (Figure 2A.6). To probe the photoreduction of biq/Cu^{II} further, a solution of **Cu^{II}-OBz** in CH₂Cl₂ was irradiated in the absence of substrate. Analysis of the organic products by ¹H NMR spectroscopy revealed the presence of PhCO₂H and 1,1,2,2-tetrachloroethane (TCE) in 80% and 10% yields with respect to the initial **Cu^{II}-OBz** (Figure 4E).

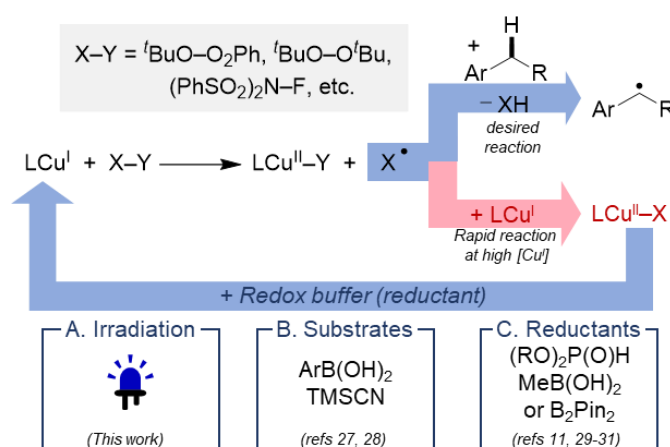


Figure 2.6. Redox buffering pathway for Cu-catalyzed C–H functionalization reactions. Cu^{II} reduction can be promoted by light (A), coupling partners (B), or sacrificial reagents (C).

These products are consistent with photoinduced ligand-to-metal charge transfer (LMCT) in **Cu^{II}-OBz** and release of a benzoyloxy radical, resembling reactivity reported in a number of other recent reports.²⁶ Benzoyloxy radical-promoted HAT from CH₂Cl₂ solvent accounts for TCE formation (Figure 2.5E).²⁷ A separate control experiment confirmed that **Cu^{II}-OBz** is a competent catalyst precursor (Figure 2.5F), indicating that this species can undergo in situ activation by blue LED irradiation under the reaction conditions without requiring addition of a Cu^I source.

The above insights are rationalized by the following mechanistic proposal. The [(biq)Cu^I]⁺ species reacts rapidly with TBPB to generate a [(biq)Cu^{II}(OBz)]⁺ species and a *tert*-butoxyl radical. Ideally, the *tert*-butoxyl radical promotes HAT from the C–H substrate (Figure 2.6, blue arrow),

but it can be quenched by a second equivalent of Cu^{I} when relatively high concentrations of $[(\text{biq})\text{Cu}^{\text{I}}]^+$ are present (Figure 2.6, red arrow).²⁸ The accumulation of Cu^{II} species generated by this reaction accounts for the negligible product formation in the absence of blue LED irradiation (cf. Table 2.1, entries 3 and 6) because Cu^{II} does not activate TBPB under these mild conditions. Blue LED irradiation provides a means to regenerate Cu^{I} , which can promote reductive activation of TBPB to generate a *tert*-butoxyl radical. The mild reaction temperature and negligible Cu^{I} present during the steady-state reaction conditions means that *tert*-butoxyl radical can promote HAT from the C–H substrate with minimal competition from β -methyl scission and/or quenching by Cu^{I} .

These results introduce "photochemical redox-buffering" as a new strategy to support Cu-catalyzed radical-relay C–H oxidation reactions (Figure 5A). This process, in which irradiation of the reaction mixture generates Cu^{I} from resting-state Cu^{II} species, resembles the chemical redox buffering pathways first established for Cu-catalyzed C–H oxidation with NFSI as the oxidant.^{11a} The latter reactions resemble the present reactions, proceeding under mild conditions and using the C–H substrate as the limiting reagent. Mechanistic studies showed that Cu^{I} rapidly reacts with NFSI to generate Cu^{II} species that cannot support catalysis unless a sacrificial reductant is present to regenerate Cu^{I} .^{11a} In some cases, a coupling partner can serve as the reductant (Figure 5B; e.g., TMS-CN and $\text{ArB}(\text{OH})_2$ reduce Cu^{II} via homocoupling to cyanogen or biaryl),^{29,30} while other cases in which the coupling partner is not an effective reductant for Cu^{II} require a separate reagent (Figure 5C).^{11,31–33}

2.4. Conclusion

The observations outlined herein provide an important starting point for further development of Kharasch-Sosnovsky and other Cu-catalyzed radical-relay reactions. Reactions of this type

require both Cu^{I} and Cu^{II} to support formation and functionalization of the organic radical, respectively; however, oxidants such as peroxides and NFSI rapidly convert all of the Cu^{I} to Cu^{II} , deactivating the catalyst and quenching the HAT species. The present study shows that visible light irradiation may be used as an alternative to chemical reagents to buffer the redox state of the Cu catalyst and support catalytic turnover under mild reaction conditions and with the C–H substrate as the limiting reagent. Efforts have been initiated to elaborate on these concepts in an effort to explore new substrate classes and catalyst systems, including variations with chiral ligands, that will expand the synthetic utility of this reactivity.

2.5. Acknowledgements

The authors thank Dr. Scott McCann for helpful discussions related to the Kharasch-Sosnovsky mechanism and Alec Hegg for experimental support during early stages of this project. This work was supported by funding from the NIH (R35 GM134929). Salary funding for C.Z. was provided by the Dalian National Laboratory for Clean Energy. Spectroscopic instrumentation was supported by a gift from Paul. J. Bender, the NSF (CHE-1048642), and the NIH (S10 OD020022). The X-ray diffractometer was partially funded by the NSF (CHE-1919350, to the UW–Madison Department of Chemistry).

2.6. Author Contributions

D.L.G. and C.Z. performed the experimental work and led the data interpretation and analysis. I.A.G. performed X-ray crystallography analysis. All authors contributed to the preparation of the manuscript.

2.7. References

- 1 Kharasch, M. S. & Sosnovsky, G. The Reactions of *t*-Butyl Perbenzoate and Olefins – A Stereospecific Reaction. *J. Am. Chem. Soc.* **1958**, *80*, 756.
- 2 Kharasch, M. & Fono, A. Radical Substitution Reactions. *J. Org. Chem.* **1958**, *23*, 325–326.
- 3 Zhang, Z.; Chen, P.; Liu, G. Copper-Catalyzed Radical Relay in C(sp³)-H Functionalization. *Chem. Soc. Rev.* **2022**, *51*, 1640–1658.
- 4 Golden, D. L.; Suh, S.-E.; Stahl, S. S. Radical C(sp³)-H Functionalization and Cross-Coupling Reactions. *Nat. Rev. Chem.* **2022**, *6*, 405–427.
- 5 (a) Kochi, J. K. The Decomposition of Peroxides Catalyzed by Copper Compounds and the Oxidation of Alkyl Radicals by Cupric Salts. *J. Am. Chem. Soc.* **1963**, *85*, 1958–1968. (b) Kochi, J. K.; Bemis, A. Catalytic Reactions of Peroxides Direct Initiation by Cuprous Species. *Tetrahedron* **1968**, *24*, 5099–5113.
- 6 (a) Small, R. D.; Scaiano, J. C. Absolute Rates of Hydrogen Abstraction by *tert*-Butoxy Radicals. *J. Am. Chem. Soc.* **1978**, *100*, 296–298. (b) Paul, H. Small, R. D.; Scaiano, J. C. Hydrogen Abstraction by *tert*-Butoxy Radicals. A Laser Photolysis and Electron Spin Resonance Study. *J. Am. Chem. Soc.* **1978**, *100*, 4520–4527. (c) Wong, S. K. Direct Measurement of Absolute Rates of Hydrogen Abstraction by *tert*-Butoxy Radicals. A Flash Photolysis Electron Spin Resonance Study. *J. Am. Chem. Soc.* **1979**, *101*, 1235–1239.
- 7 (a) Kochi, J. K.; Subramanian, R. V. Kinetics of Electron-Transfer Oxidation of Alkyl Radicals by Copper(II) Complexes. *J. Am. Chem. Soc.* **1965**, *87*, 4855–4866. (b) Kochi, J. K.; Bemis, A.; Jenkins, C. L. Mechanism of Electron Transfer Oxidation of Alkyl Radicals by Copper(II) Complexes. *J. Am. Chem. Soc.* **1968**, *90*, 4616–4625. (c) Jenkins, C. L.; Kochi, J. K. Solvolytic Routes via Alkylcopper Intermediates in the Electron-Transfer Oxidation of Alkyl Radicals. *J. Am. Chem. Soc.* **1971**, *94*, 843–855. (d) Jenkins, C. L.; Kochi, J. K. "Ligand Transfer of Halides (Cl, Br, I) and Pseudohalides (SCN, N₃, CN) from Copper(II) to Alkyl Radicals. *J. Org. Chem.* **1971**, *36*, 3095–3102. (e) Jenkins, C. L.; Kochi, J. K. Homolytic and Ionic Mechanisms in the Ligand-Transfer Oxidation of Alkyl Radicals by Copper (II) Halides and Pseudohalides. *J. Am. Chem. Soc.* **1972**, *94*, 856–865.
- 8 For representative examples of C–O coupling reactions, see: (a) Andrus, M. B.; Zhou, Z. Highly Enantioselective Copper–Bisoxazoline-Catalyzed Allylic Oxidation of Cyclic Olefins with *tert*-Butyl *p*-nitroperbenzoate. *J. Am. Chem. Soc.* **2002**, *124*, 8806–8807. (b) Gephart, R. T.; McMullin, C. L.; Sapiezynski, N. G.; Jang, E. S.; Aguila, M. J. B.; Cundari, T. R.; Warren, T. H. Reaction of Cu^I with Dialkyl Peroxides: Cu^{II}-Alkoxides, Alkoxy Radicals, and Catalytic C–H Etherification. *J. Am. Chem. Soc.* **2012**, *134*, 17350–17353. (c) Tran, B. L.; Driess, M.; Hartwig, J. F. Copper-Catalyzed Oxidative Dehydrogenative Carboxylation of Unactivated Alkanes to Allylic Esters via Alkenes. *J. Am. Chem. Soc.* **2014**, *136*, 17292–17301. (d) Andrus, M. B.; Chen, X. Catalytic Enantioselective Allylic Oxidation of Olefins with Copper(I) Catalysts and New Perester Oxidants. *Tetrahedron* **1997**, *53*, 16229–16240. (e) DattaGupta, A.; Singh, V. K. Catalytic Enantioselective Allylic Oxidation of Olefins with Copper Complexes of Chiral Nonracemic Bis(oxazolonyl)pyridine Type Ligands. *Tetrahedron Lett.* **1996**, *37*, 2633–2636. (f) Andrus, M. B.; Lashley, J. C. Copper Catalyzed Allylic Oxidation with Peresters. *Tetrahedron* **2002**, *58*, 845–866.

- 9 For representative examples of C–N coupling reactions, see: (a) Powell, D. A.; Fan, H. Copper-Catalyzed Amination of Primary Benzylic CH Bonds with Primary and Secondary Sulfonamides. *J. Org. Chem.* **2010**, *75*, 2726–2729. (b) Wiese, S.; Badeiei, Y. M.; Gephart, R. T.; Mossin, S.; Varonka, M. S.; Melzer, M. M.; Meyer, K.; Cundari, T. R.; Warren, T. H. Catalytic C–H Amination with Unactivated Amines through Copper(II) Amides. *Angew. Chem. Int. Ed.* **2010**, *49*, 8850–8855. (c) Tran, B. L.; Li, B.; Driess, M.; Hartwig, J. F. Copper-Catalyzed Intermolecular Amidation and Imidation of Unactivated Alkanes. *J. Am. Chem. Soc.* **2014**, *136*, 2555–2563. (d) Zeng, H.-T.; Huang, J.-M. Copper-Catalyzed Ligand-Free Amidation of Benzylic Hydrocarbons and Inactive Aliphatic Alkanes. *Org. Lett.* **2015**, *17*, 4276–4279. (e) Kohmura, Y.; Kawasaki, K.; Katsuki, T. Benzylic and Allylic Amination. *Synlett* **1997**, *12*, 1456–1458.
- 10 For representative examples of C–C coupling reactions, see: (a) Borduas, N.; Powell, D. A. Copper-Catalyzed Oxidative Coupling of Benzylic C–H Bonds with 1,3-Dicarbonyl Compounds. *J. Org. Chem.* **2008**, *73*, 7822–7825. (b) Vasilopoulos, A.; Zultanski, S. L.; Stahl, S. S. Feedstocks to Pharmacophores: Cu-Catalyzed Oxidative Arylation of Inexpensive Alkylarenes Enabling Direct Access to Diarylalkanes. *J. Am. Chem. Soc.* **2017**, *139*, 7705–7708. (c) Xie, W.; Heo, J.; Kim, D.; Chang, S. Copper-Catalyzed Direct C–H Alkylation of Polyfluoroarenes by Using Hydrocarbons as an Alkylating Source. *J. Am. Chem. Soc.* **2020**, *142*, 7487–7496.
- 11 (a) Hu, H.; Chen, S.-J.; Mandal, M.; Pratik, S. M.; Buss, J. A.; Krska, S. W.; Cramer, C. J.; Stahl, S. S. Copper-Catalyzed Benzylic C–H Coupling with Alcohols via Radical Relay Enabled by Redox Buffering. *Nat. Catal.* **2020**, *3*, 358–367. (b) Buss, J. A.; Vasilopoulos, A.; Golden, D. L.; Stahl, S. S. Copper-Catalyzed Functionalization of Benzylic C–H Bonds with N-Fluorobenzenesulfonimide: Switch from C–N to C–F Bond Formation Promoted by a Redox Buffer and Brønsted Base. *Org. Lett.* **2020**, *22*, 5749–5752.
- 12 (a) Walling, C.; Wagner, P. Effect of Solvents on Transition States in the Reactions of *t*-Butoxy Radicals. *J. Am. Chem. Soc.* **1963**, *85*, 2333–2334. (b) Wagner, P.; Walling, C. Positive Halogen Compounds. XII. Relative Reactivities of Hydrocarbons toward Alkoxy Radicals Determined by Direct and Indirect Methods. *J. Am. Chem. Soc.* **1965**, *87*, 5179–5185.
- 13 Vasilopoulos, A.; Krska, S. W.; Stahl, S. S. C(sp³)–H Methylation Enabled by Peroxide Photosensitization and Ni-Mediated Radical Coupling. *Science* **2021**, *372*, 398–403.
- 14 Ogata, Y.; Tomizawa, K.; Furuta, K. Photochemistry and Radiation Chemistry of Peroxides. In *Peroxide*; John Wiley & Sons Ltd.; 1983, <https://doi.org/10.1002/9780470771730.ch21>.
- 15 For fundamental studies of peroxide photolysis, see: (a) Sheldon, R. A.; Kochi, J. K. Photolysis of Peresters. Reactions of Alkoxy-Alkyl Radical Pairs in Solution. *J. Am. Chem. Soc.* **1970**, *92*, 5175–5186. (b) McMillan, G.; Wijnen, M. H. Reactions of Alkoxy Radicals. V: Photolysis of Di-*t*-Butyl Peroxide. *Can. J. Chem.* **1958**, *36*, 1227–1232.
- 16 Zheng, Y.-W.; Narobe, R.; Donabauer, K.; Yakubov, S.; König, B. Copper(II)-Photocatalyzed N–H Alkylation with Alkanes. *ACS Catal.* **2020**, *10*, 8582–8589.
- 17 For a recent application of the same concept to Cu-catalyzed C–N coupling, see: Chen, C.; Lian, Z.; Kramer, S. Enantioselective Intermolecular Radical Amidation and Amination of Benzylic C–H Bonds via Dual Copper and Photocatalysis. *Angew. Chem. Int. Ed.* **2023**, e202217638.

- 18 Diarylmethane derivatives are susceptible to over-oxidation to the ketone: Tanwar, L.; Börgel, J.; Ritter, T. Synthesis of Benzylic Alcohols by C–H Oxidation. *J. Am. Chem. Soc.* **2019**, *141*, 17983–17988.
- 19 (a) Zhi, L.; Grote, M.; Reddy, R. K.; Li, W.; Craig, W. Glucagon Receptor Antagonists. Worldwide patent WO2018035172A1, Feb 22, 2018. (b) Hoffman, T. J.; Stierli, D.; Pitterna, T.; Rajan, R. Microbiocidal Oxadiazole Derivatives. Worldwide patent WO2018158365A1, Sept 7, 2018.
- 20 Schepers, G. Benzbromarone Therapy in Hyperuricaemia; Comparison with Allopurinol and Probenecid. *J. Int. Med. Res.* **1981**, *9*, 511–515.
- 21 "Deactivation" refers to the lower reactivity with acidic C–H bonds with electrophilic radicals, such as *tert*-butoxyl radical. Doyle and co-workers have shown preferential reactivity at the tertiary site of ibuprofen ethyl ester under conditions postulated to involve methyl radical as the HAT reagent. The lack of tertiary reactivity in the present reaction suggests *b*-methyl scission from a *tert*-butoxyl radical and HAT by the resulting methyl radical does not contribute significantly. See the following for context: Leibler, I. N M., Tekle-Smith, M. A.; Doyle, A. G. A General Strategy for C(sp³)–H Functionalization with Nucleophiles using Methyl Radical as a Hydrogen Atom Abstractor. *Nat. Commun.* **2021**, *12*, 6950.
- 22 Xue, X.-S.; Ji, P.; Zhou, B.; Cheng, J.-P. The Essential Role of Bond Energies in C–H Activation/Functionalization. *Chem. Rev.* **2017**, *117*, 8622–8648.
- 23 Bpy/Cu and phen/Cu complexes: (a) Holloway, C. E.; Melnik, M. Copper(I) Compounds: Classification and Analysis of Crystallographic and Structural Data. *Rev. Inorg. Chem.* **1995**, *15*, 147–386. (b) Munakata, M.; Kitagawa, S.; Asahara, A.; Masuda, H. Crystal Structure of Bis(2,2'-bipyridine)copper(I) Perchlorate. *Bull. Chem. Soc. Jpn.* **1987**, *60*, 1927–1929. (c) Barilon, J. L.; Tůma, J.; Brochard, S.; Babková, K.; Krupička, M. Design of Bis(1,10-phenanthroline) Copper(I)-Based Mechanochromic Indicators. *ACS Omega* **2022**, *7*, 6510–6517.
- 24 Biq/Cu complexes: (a) Lockhart, T. P. Mechanistic Investigation of the Copper-Catalyzed Reactions of Diphenyliodonium Salts. *J. Am. Chem. Soc.* **1983**, *105*, 1940–1946. (b) Ali, Basem F.; Al-Sou'od, Khaldoun; Al-Ja'ar, Nayef; Nassar, Ahmad; Zaghal, Mukarram H.; Judeh, Zaher; Al-Far, Rawhi; Al-Refai, Mahmoud; Ibrahim, Mohamad; Mansi, Kamal; Al-Obaidi, K. H. Interconversion of Copper(II) to Copper(I): Synthesis, Characterization of Copper(II) and Copper(I) 2,2'-Biquinoline Complexes and Their Microbiological Activity. *J. Coord. Chem.* **2006**, *59*, 229–241.
- 25 Yi, H.; Zhang, G.; Xin, J.; Deng, Y.; Miller, J. T.; Kropf, A. J.; Bunel, E. E.; Qi, X.; Lan, Y.; Lee, J. -F.; Lei, A. Homolytic Cleavage of the O–Cu(II) Bond: XFAS and EPR Spectroscopy Evidence for One Electron Reduction of Cu(II) to Cu(I). *Chem. Commun.* **2016**, *52*, 6914–6917.
- 26 For recent examples of photoinduced LMCT from Cu complexes to generate radicals in synthetic methods, see: (a) Treacy, S. M.; Rovis, T. Copper-Catalyzed C(sp³)–H Bond Alkylation via Photoinduced Ligand-to-Metal Charge Transfer. *J. Am. Chem. Soc.* **2021**, *143*, 2729–2735. (b) Xu, P.; López-Rojas, P.; Ritter, T. Radical Decarboxylative Carbometalation of Benzoic Acids: A Solution to Aromatic Decarboxylative Fluorination. *J. Am. Chem. Soc.* **2021**, *143*, 5349–5354. (c) Chen, T. Q.; Dow, N. W.; Fayad, R.; Hauke, C. E.; Rosko, M. C.; Danilov, E. O.; Blakemore, D. C.; Dechert-Schmitt, A.-M.; Knauber, T.; Castellano, F. N.; MacMillan,

- D. W. C. A Unified Approach to Decarboxylative Halogenation of (Hetero)aryl Carboxylic Acids. *J. Am. Chem. Soc.* **2021**, *144*, 8296–8305. (d) Dow, N. W.; Pedersen, S.; Chen, T. Q.; Blakemore, D. C.; Dechert-Schmitt, A.-M.; Knauber, T.; MacMillan, D. W. C. Decarboxylative Borylation and Cross-Coupling of (Hetero)aryl Acids Enabled by Copper Charge Transfer Catalysis. *J. Am. Chem. Soc.* **2022**, *144*, 6163–6172. (e) Li, Q. Y.; Gockel, S. M.; Lutovsky, G. A.; DeGlopper, K. S. Baldwin, N. J.; Bundesmann, M. W.; Tucker, J. W.; Bagley, S. W.; Yoon, T. P. Decarboxylative Cross-Nucleophile Coupling via Ligand-to-Metal Charge Transfer Photoexcitation of Cu(II) Carboxylates. *Nat. Chem.* **2022**, *14*, 94–99. (f) Su, W.; Xu, P.; Ritter, T. Decarboxylative Hydroxylation of Benzoic Acids. *Angew. Chem. Int. Ed.* **2021**, *60*, 24012–24017. (g) Xu, P.; Su, W.; Ritter, T. Decarboxylative Sulfoximation of Benzoic Acids Enabled by Photoinduced Ligand-to-Copper Charge Transfer. *Chem. Sci.* **2022**, *13*, 13611–13616. (h) Juliá, F. Ligand-to-Metal Charge Transfer (LMCT) Photochemistry at 3d-Metal Complexes: An Emerging Tool for Sustainable Organic Synthesis. *ChemCatChem* **2022**, *14*, e202200916.
- 27 Inclusion of ethylbenzene and 4-ethylanisole in the reaction shown in Figure 2.5E led to only minor conversion of the benzylic substrate (0% and 13%, respectively). This observation suggests most benzylic reactivity under catalytic conditions originates from reaction with tert-butoxyl radical. See Section 2A.VIII, Experiment 2A.11 in Appendix A for details.
- 28 We note that the bis-ligated $[(\text{biq})_2\text{Cu}^{\text{I}}]^+$ species appears largely inert under the reaction conditions; however, it could serve as a reservoir for additional Cu^{I} via ligand exchange. For example, we find that addition of $[(\text{biq})\text{Cu}^{\text{II}}(\text{OBz})]^+$ to a solution of $[(\text{biq})_2\text{Cu}^{\text{I}}]^+$ results in a decrease in the absorbance of the latter species, implicating dissociation of one of the biq ligands from this species. See Figure 2A.6 and associated experimental description in the Appendix A.
- 29 (a) Zhang, W.; Chen, P.; Liu, G. Copper-Catalyzed Arylation of C–H Bonds with Alkylarenes as the Limiting Reagents. *J. Am. Chem. Soc.* **2017**, *139*, 7709–7712. (b) Zhang, W.; Wu, L.; Chen, P.; Liu, G. Enantioselective Arylation of Benzylic C–H Bonds by Copper-Catalyzed Radical Relay. *Angew. Chem. Int. Ed.* **2019**, *58*, 6425–6429.
- 30 Zhang, W.; Wang, F.; McCann, S. D.; Wang, D.; Chen, P.; Stahl, S. S.; Liu, G. Enantioselective Cyanation of Benzylic C–H Bonds via Copper-Catalyzed Radical Relay. *Science* **2016**, *353*, 1014–1018.
- 31 Suh, S.-E.; Nkulu, L. E.; Krska, S. W.; Stahl, S. S. Benzylic C–H Isocyanation/Amine Coupling Sequence Enabling High-Throughput Synthesis of Pharmaceutically Relevant Ureas. *Chem. Sci.* **2021**, *12*, 10380–10387.
- 32 Chen, S.-J.; Golden, D. L.; Krska, S. W.; Stahl, S. S. Copper-Catalyzed Cross-Coupling of Benzylic C–H Bonds and Azoles with Controlled N-Site Selectivity. *J. Am. Chem. Soc.* **2021**, *143*, 14438–14444.
- 33 Lopez, M. A.; Buss, J. A.; Stahl, S. S. Cu-Catalyzed Site-Selective Benzylic Chlorination Enabling Net C–H Coupling with Oxidatively Sensitive Nucleophiles. *Org. Lett.* **2021**, *24*, 597–601.

Chapter 3.

Site Selective Chlorination of Heterobenzylic C(sp³)-H Bonds Enabling High-Throughput Chlorination/Diversification with Oxidatively Sensitive Nucleophiles

3.1. Abstract

Site-selective functionalization of the heterobenzyl C(sp³)-H bonds of pyridines and related heteroaromatic scaffolds remains challenging owing to the differences in reactivities based on locations of the alkyl substituents. While 2- and 4-chloroalkylpyridines can be accessed via acidification/deprotonation of the heterobenzyl C-H bonds, functionalization of 3-alkylpyridines remains challenging. Here we report a photochemical strategy to selectively chlorinate the heterobenzyl C-H sites of 3-alkylpyridines. Computational density function theory calculation guides the design of the chlorinating reagent, which enhances both the reactivity and selectivity for the chlorination of heterobenzyl C-H bonds of 3-alkyl pyridines. The operationally simple chlorination protocol enables the use of the resulting heterobenzyl chlorides as intermediates for rapid diversification with oxidatively sensitive nucleophiles using high-throughput experimentation.

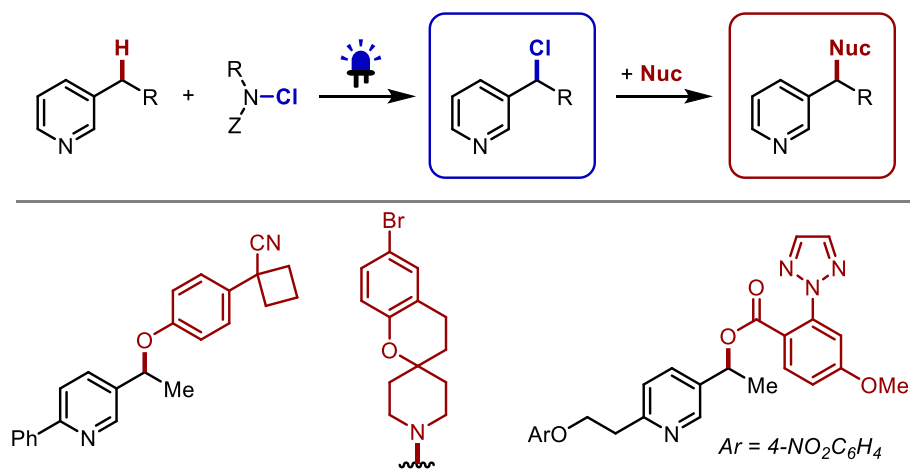
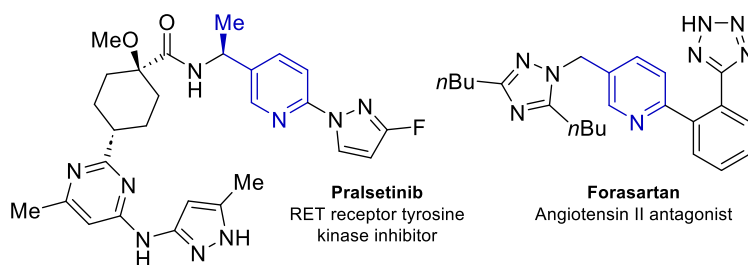


Figure 3.1. Chlorination/diversification sequence of 3-alkylpyridines.

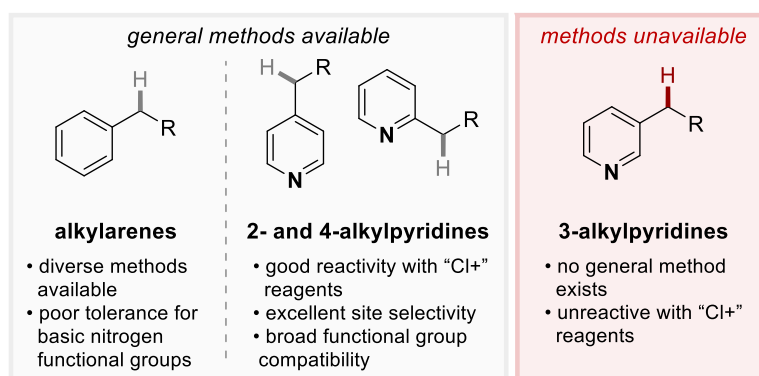
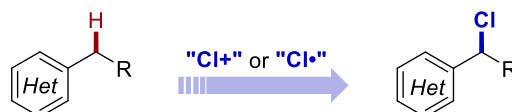
3.2. Introduction

Functionalization of C(sp³)-H bonds has been viewed as an effective strategy to achieve various bond formations, enabling facile access to molecules with increasing three-dimensionality

A. Bioactive molecules containing 3-alkylpyridine fragment



B. (Hetero)benzylic C(sp³)–H functionalization



C. Chlorination/diversification via radical-chain chlorination (*this work*)

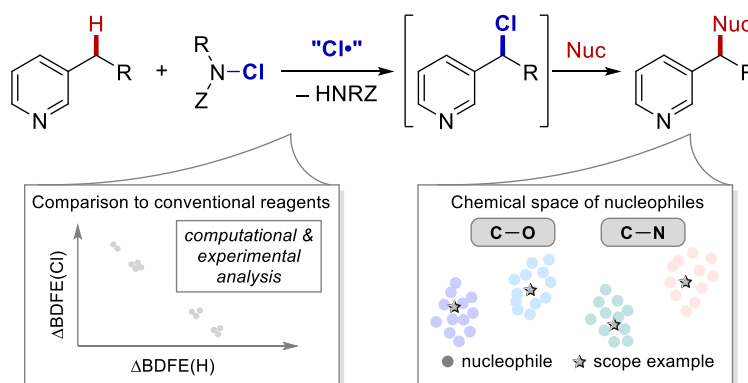


Figure 3.2. (A) Bioactive molecules with 3-alkylpyridine fragments (B) Chlorination strategies for benzylic and heterobenzylic C(sp³)–H bonds (C) Sequential chlorination/diversification of 3-alkylpyridines enabled by photochemical radical chain reaction.

and structural diversity.^{1,2} Benzylic C(sp³)–H bonds C–H sites represent appealing targets for functionalization because of their relatively low bond strength and therefore higher intrinsic reactivity.^{3–45} Additionally, benzylic sites are metabolic hot spots in pharmaceuticals, and products

of benzylic C–H functionalization have important biological implications.⁶ Recent efforts from our lab have shown that a copper/*N*-fluorobenzenesulfonimide (NFSI) catalyzed system enables the installation of various coupling partners onto the benzylic C–H sites, including cyanide,⁷ alcohols,⁸ azide,⁹ fluoride,¹⁰ azoles,¹¹ isocyanate,¹² and chloride¹³. While these reactions are effective for benzylic C–H functionalization, heterobenzylic C–H bonds, such as those in alkylpyridines, showed suboptimal reactivity, resulting in the limited access to medicinally relevant and important heteroaromatic scaffolds (Figure 3.2A).¹⁴ The poor reactivity of Cu/NFSI-catalyzed reactions derives from the incompatibility between NFSI and basic nitrogen atom in alkylpyridines, resulting in an *N*-sulfonylated alkylpyridine substrate with concomitant deactivation of the heterobenzylic C–H site.¹⁵ Our group has recently exploited this *N*-sulfonylation to enable a chlorination/diversification sequence of 2- and 4-alkylpyridines via "polar activation" of heterobenzylic C–H bonds (Figure 3.2B).¹⁶ However, 3-alkylpyridines remain inaccessible via this "polar activation" pathway due to its unfavorable resonance structure formed after deprotonation at the heterobenzylic C–H site.^{16,17} Herein we report a site-selective radical chain chlorination reaction to enable facile access to heterobenzyl chloride of 3-alkylpyridines for subsequent nucleophilic displacement (Figure 3.2C).

3.3. Results and Discussion

We initiated our study by exploring the applicability of other established C–H chlorination methods for functionalizing 3-alkylpyridines' heterobenzylic C–H sites (Figure 3.3). The different methods included: (a) Cu/NFSI,¹³ (b) TCCA/TfCl for chlorination of 2-alkylpyridines,¹⁶ (c) NCS/NH, in which a protonated piperidine radical cation is the hydrogen atom transfer (HAT) agent,¹⁸ (d) NCS/Acr with light-promoted generation of nitrogen-centered radical for HAT by

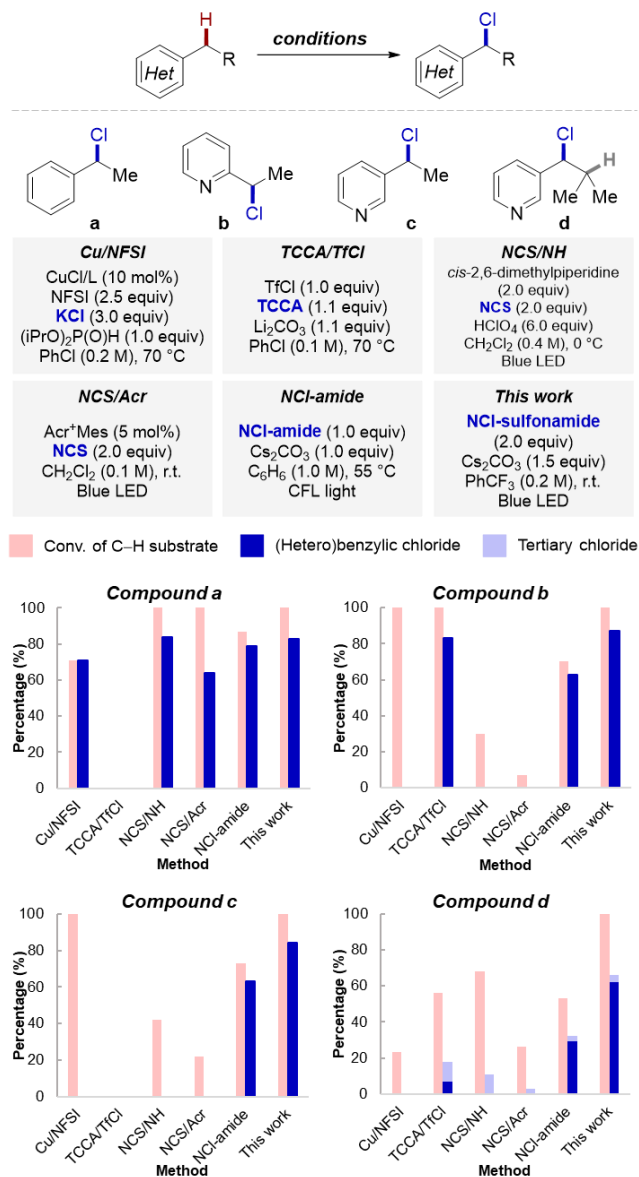


Figure 3.3. Applications of various C–H chlorination methods on ethylbenzene, 2-ethylpyridine, 3-ethylpyridine, and 3-isobutylpyridine. Yields determined by ¹H NMR spectroscopy (external std. = mesitylene).

excited state acridinium photocatalyst,¹⁹ and (e) light-promoted radical chain chlorination with NCl-amide (*N*-(*tert*-butyl)-*N*-chloro-3,5-bis(trifluoromethyl)benzamide).²⁰ Initially, ethylbenzene was used to benchmark the efficiency of these methods for chlorinating benzylic C–H bonds (Figure 3.3, Compound a). As predicted, most of these methods, with the exception of TCCA/TfCl for chlorination of 2-alkylpyridines, were effective in delivering the benzylic chlorides in moderate

to good yields. In stark contrast, when 2-ethylpyridine was used as C–H substrate, Cu/NFSI method showed high conversion with no product formation due to side reactivity between NFSI with the basic nitrogen atom (Figure 3.3, Compound b). Both TCCA/TfCl, and the light-promoted radical chain process using NCl-amide was successful in mediating the chlorination of 2-ethylpyridine in moderate yield (63%). However, as expected from a polar activation pathway, the reaction of 3-ethylpyridine with TCCA/TfCl did not yield the desired chlorinated product (Figure 3.3, Compound c). Similar heterobenzylic chlorination yield to that of 2-ethylpyridine was observed under NCl-amide condition, indicating that 3-alkylpyridines could be functionalized via a photo-initiated radical chain process. Site selectivity between heterobenzylic and tertiary C–H bonds was probed with 3-isobutylpyridine (Figure 3.3, Compound d). Radical-based chlorination reactions should show selectivity for the heterobenzylic position as a result of lower bond dissociation energy of the parent C–H bond.²¹ As predicted, NCl-amide reaction favored the heterobenzylic C–H site functionalization (benzylic:tertiary (B:T) = 6:1); however, poor total chloride yield of 32% was observed. Inspired by the promising results of light-promoted NCl-amide radical chain method, we hypothesized that modification of the carbonyl fragment in NCl-amide to a sulfonyl fragment would increase site selectivity for benzylic site due to the lower intrinsic N–H BDE (7 kcal/mol) of N–Cl sulfonamide.²² A series of NCl-sulfonamides with varying electronics and sterics were synthesized and examined with 3-isobutylpyridine (See Table 3B.3 in Appendix B). The optimal NCl-sulfonamide was identified as *N*-(*tert*-butyl)-*N*-chloro-3,5-bis(trifluoromethyl)benzenesulfonamide (NCl-sulfonamide, **2**), which showed competent reactivity for ethylbenzene (82%), 2-ethylpyridine (87%), and 3-ethylpyridine (**1a**, 84%) with good yields for the chlorinated products. Site selectivity for the benzylic position was also enhanced (B:T = 16:1) with improved overall reactivity when 3-isobutylpyridine was used as the

C–H substrate (see Section 3B.IV in Appendix B for details of reaction optimization).

Once optimal reaction conditions were identified, we next probed the reasons for the varying effectiveness of multiple NCl-reagents in promoting the chlorination reaction (Figure 3.4). Specifically, this study involved careful analysis of the two propagation steps in the radical chain mechanism, namely the hydrogen atom transfer and the chlorine atom transfer. The hydrogen atom transfer step consists of the nitrogen-centered radical abstracting a hydrogen atom from the C–H substrate, resulting in a carbon-centered radical and N–H. The chlorine atom transfer step accounts for the reaction between the carbon-centered radical and another equivalent of NCl-reagent to afford the C–Cl product and a nitrogen-centered radical. Density functional theory (DFT) calculations were used to obtain the bond dissociation free energies (BDFEs) of the C–H and N–H as well as C–Cl and N–Cl bonds using 3-ethylpyridine as the C–H substrate. The examined NCl-reagents included *N*-chlorophthalimide (**1**), *N*-chlorosuccinimide (**2**), trichloroisocyanuric acid (**3**), *N*-chlorosaccharin (**4**), *N*-chloro-*N*-(phenylsulfonyl)benzenesulfonamide (**5**), NCl-amide (**6**), and NCl-sulfonamide (**7**). Correlations were made between differences in BDFEs for the hydrogen atom transfer step ($\Delta\text{BDFE}(\text{H})$), the chlorine atom transfer step ($\Delta\text{BDFE}(\text{Cl})$), and the experimental chlorination yields for 3-ethylpyridine (Figure 3.4, Computed Bond Energies). The analysis revealed that all NCl-reagents have a favorable hydrogen atom transfer step ($\Delta\text{BDFE}(\text{H}) < 0$ kcal/mol) confirming the thermodynamic feasibility for H-atom abstraction from 3-ethylpyridine by the nitrogen-centered radical. However, the radical chain reactions with **1** and **2** have an unfavorable chlorine atom transfer step ($\Delta\text{BDFE}(\text{Cl}) > 0$ kcal/mol), indicating that these NCl-reagents are more energetically stable than the chlorinated product of 3-ethylpyridine. This computational result was consistent with the observed experimental data of no starting material conversion with **1** and **2**. Computationally, the remaining NCl-reagents have favorable chlorine

atom transfer step ($\Delta\text{BDFE}(\text{Cl}) < 0$ kcal/mol). While reaction with **3** is energetically favorable for

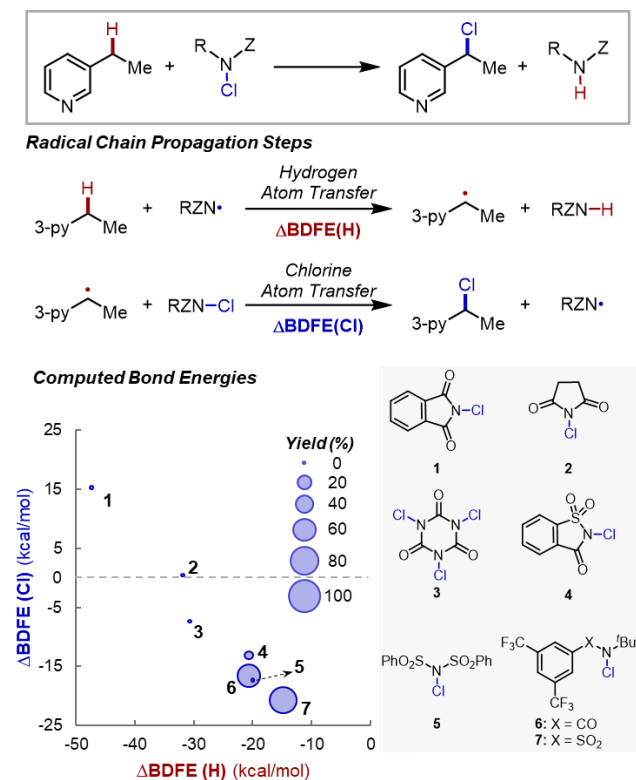


Figure 3.4. Analysis of radical chain propagation steps with various NCl-reagents.

the chlorine atom transfer step ($\Delta\text{BDFE}(\text{Cl}) < -7.3$ kcal/mol), no chlorinated product was observed. *N*-chlorosaccharin (**4**) was successful in chlorinating **3a** with low yield (8%), indicating that there is an energetic threshold for chlorine atom transfer ($\Delta\text{BDFE}(\text{Cl}) \leq -13.1$ kcal/mol). However, **5** exhibited poor reactivity due to the deleterious reaction between sulfonyl groups and basic nitrogen atom similarly to NFSI. While **6** showed moderate product yield, **7** enhanced the reaction yield. Additionally, a less negative $\Delta\text{BDFE}(\text{H})$ value of **7** could explain the improved selectivity for benzylic C–H bond observed with 3-isobutylpyridine (cf. Figure 3.3, Compound d). In general, the examined NCl-reagents promote favorable HAT; however, ones with a $\Delta\text{BDFE}(\text{Cl}) < -13$ kcal/mol are likely to be optimal for radical chain chlorination.

The results in Figure 3 highlight the enhanced heterobenzylic reactivity and selectivity of NCl-

sulfonamide **7** for radical chain chlorination of 3-alkylpyridines and provide a starting point for

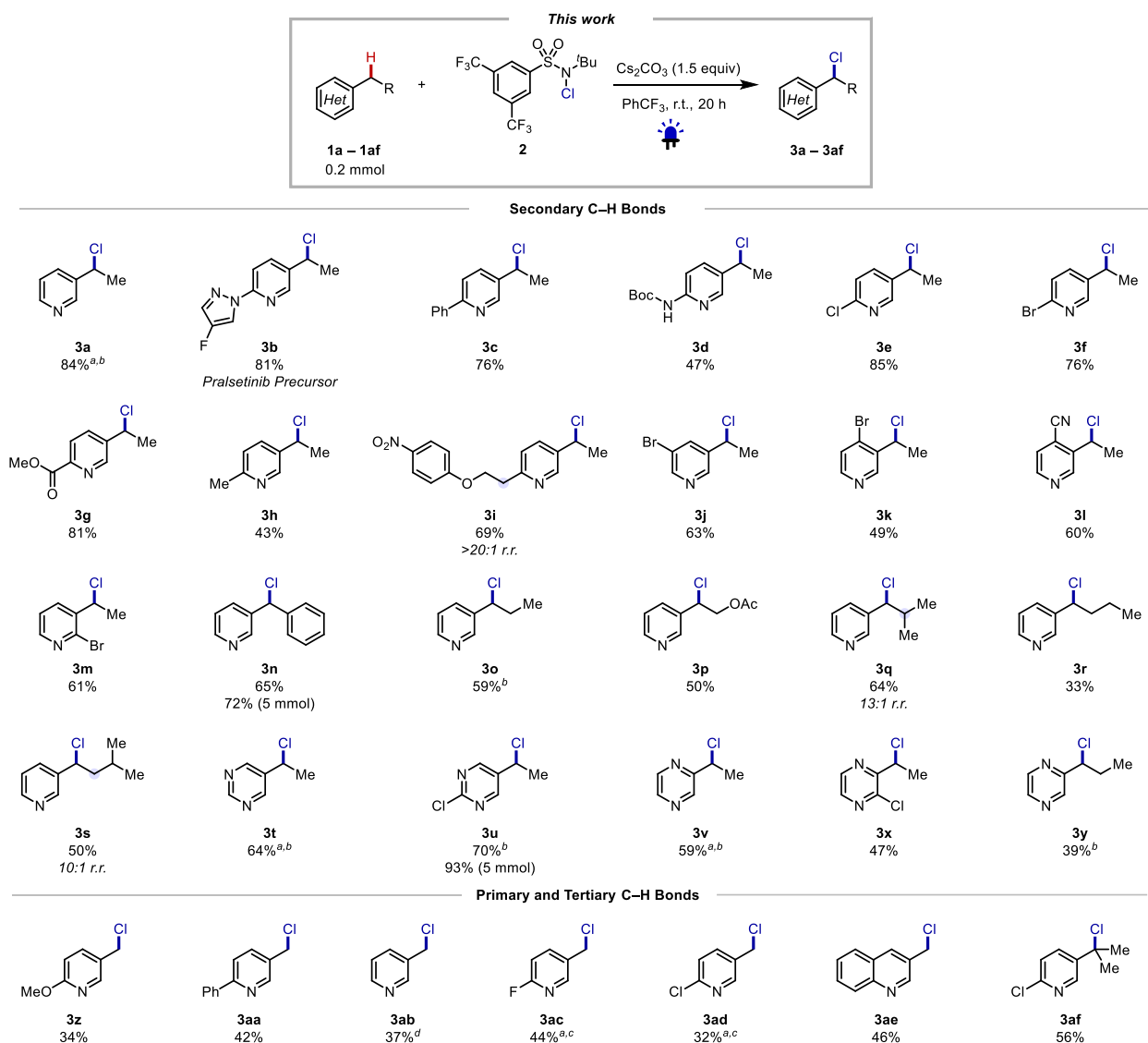


Figure 3.5. Assessment of 3-alkylpyridine C–H substrates. ^aReported as ¹H NMR Yield; ^b0.5 mmol scale; ^c0.05 mmol scale. ^dReaction time 8 h.

chlorination in good-to-excellent yields (**3b – 3g**, 47 – 81%) with broad functional group tolerance, including azole, amide, halides, and ketone. Exclusive site selectivity for the functionalization 3-alkylpyridine was observed over the 2-alkylpyridine position (**3h & 3i**). Electron-poor substituents around the pyridine ring, such as bromo and cyano, are also well tolerated to afford moderate yields of the corresponding heterobenzyl chlorides (**3j – 3m**, 49 – 63%). 3-ethylpyridine with an acetate substituent at the terminal position leads to heterobenzyl

chlorination product in moderate yield (**3p**, 50%), providing versatile bifunctional electrophilic building blocks. 3-alkylpyridines with longer alkyl chains are compatible substrates under the reaction conditions. Specifically, 3-isopentylpyridine shows selectivity for heterobenzylic position; however, the competing C–H bond is the less sterically hindered secondary aliphatic bond instead of the more electron-rich tertiary position (**3s**). This observation suggests that steric effect may override electronics in this reaction in terms of site selectivity. 5-ethylpyrimidine and its chloro-substituted derivative show moderate reactivity (**3t** – **3u**, 64 – 70%). Excellent chlorination reactions of **3n** (72%) and **3u** (93%) were achieved at 5 mmol reaction scale, indicating that chlorination is scalable. 2-ethylpyrazine and derivatives thereof (**3v** – **3y**) are also effective C–H substrates under the optimal reaction conditions. Primary 3-alkylpyridines were also examined, albeit lower reactivity (**3z** – **3ae**) was observed as a result of low conversion of C–H substrate. Longer reaction time did not improve reaction yields while other byproducts were detected (see Table 3B.9 in Appendix B for more details). Tertiary C–H bond (**3af**) was also functionalized in moderate yield (56%). The results in Figure 4 exemplify the generality of the chlorination reaction in accessing diverse heterobenzyl chlorides, which are strategic synthons for subsequent displacement protocol with a broad scope of nucleophilic coupling partners.

Akin to previous reports on benzylic functionalization, we envisioned that heterobenzyl chlorides accessed via the chlorination of 3-alkylpyridines are ideal intermediates for S_N2 chemistry to afford cross-coupled products with nucleophiles, including amines, phenols, and aliphatic alcohols. The chlorinated product of 3-ethylpyridine (**3a**) was used as the model heterobenzyl chloride to evaluate a broad scope of nucleophiles. Three classes of nucleophiles, including amines, carboxylic acids, and alcohols, were examined. To each nucleophile class, we initiated the selection process by employing various filtering parameters, including molecular

weight, incompatible functional groups, and numbers of hydrogen bond donors (see Appendix B for details). Cheminformatic *t*-SNE (t-Distributed Stochastic Neighbor Embedding) clustering

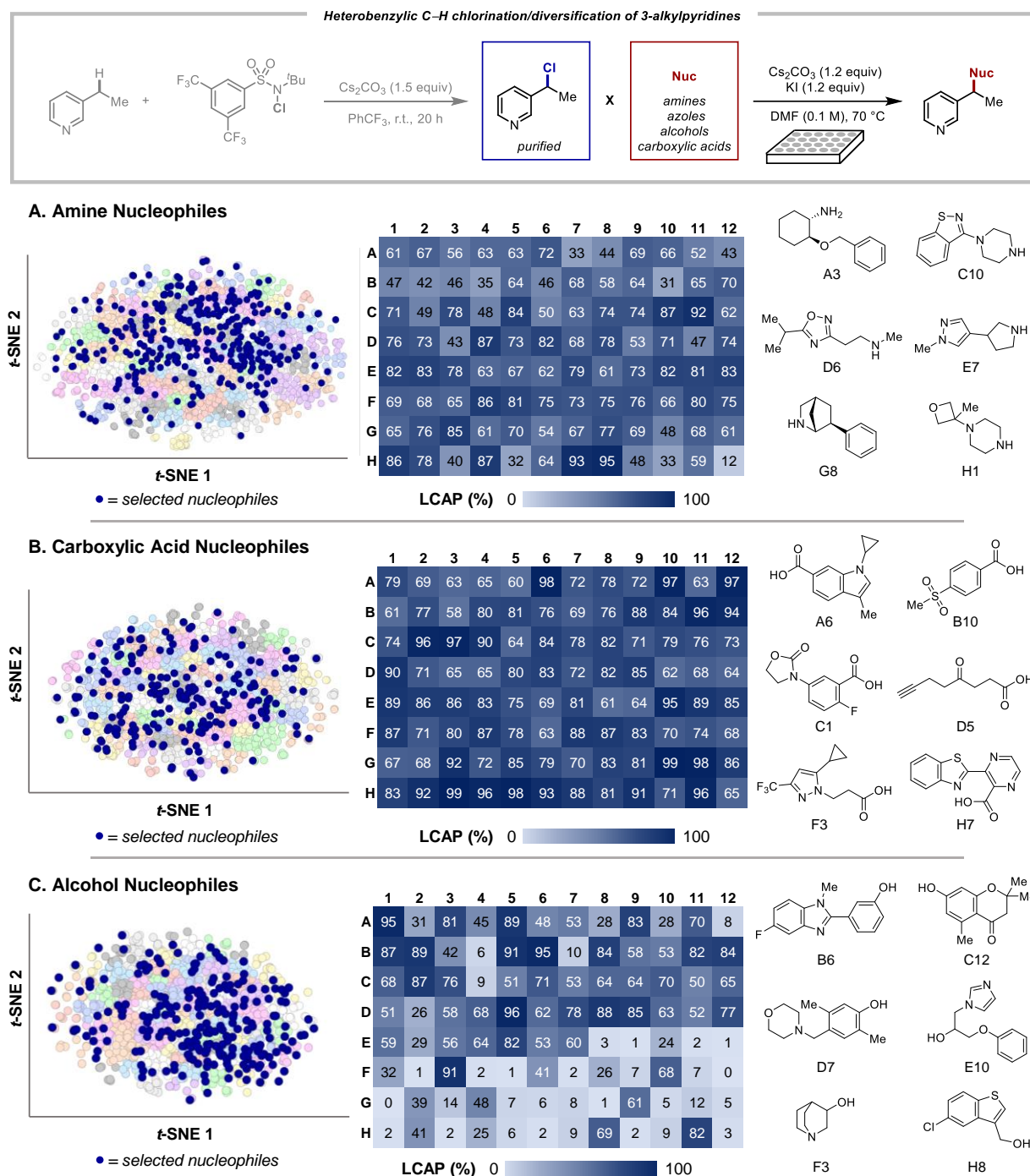


Figure 3.6. *t*-SNE analysis and HTE 96-well plate assessment of nucleophilic coupling partners with **3**. LCAP yield was reported.

algorithm was then applied to visualize the chemical space covered by the selected

nucleophiles. The displacement of **3a** was performed using high-throughput experimentation (HTE) in a 96-wellplate format at 10- μ mol scale of the C–H substrate. The product formation was analyzed by ultra-performance liquid chromatography mass spectrometry (UPLC-MS) to determine the liquid chromatography area percent (LCAP) of the desired products. As shown in Figure 3.6, diverse amine nucleophiles are generally well tolerated under heterobenzyl chloride displacement conditions. Both primary and secondary aliphatic amines, including ones with additional five-membered heterocycles, showed promising reactivity (Figure 3.6, amine, A3 & D6). Better reactivity was observed with cyclic amines regardless of its ring size (Figure 3.6, amine, E7 & G8) or attached functional groups with more structural complexity, such as benzoisothiazole or oxetane (Figure 3.6, amine, C10 & H1). Additionally, azoles are compatible nucleophiles (see Figure 3B.7 in Appendix B). Carboxylic acids are excellent nucleophilic coupling partners for the displacement protocol since both aliphatic and aromatic carboxylic acids resulted in products with > 60 LCAPs. Functional groups, which are sensitive to radical-based chemistry, including cyclopropanes and alkynes, were incorporated into carboxylic acid structures (Figure 3.6, carboxylic acid, A6, D5, F3). Stark contrast in reactivity was observed between aromatic alcohols, or phenols, and aliphatic alcohols. Phenols with various substituents on arenes were well tolerated under displacement reaction condition (Figure 3.6, alcohol, B6, C12, D7). 2-hydroxypyridine, which contains the hydroxyl group adjacent to the nitrogen, delivered two isomers: (1) the desired C–O product; and the (2) C–N product derived from tautomerization of the phenol to 2-pyridone. However, aliphatic alcohols, including both primary and secondary, demonstrated poor reactivity to form the nucleophilic displaced product. The elimination product of **3a** was primarily observed, indicating that the alkoxides formed after deprotonation were promoting an E2 reaction. However, a few electron-rich aliphatic alcohols led to moderate yields

of the desired benzylic ethers (Figure 3.6, alcohol, E10, F3, H8). The *t*-SNE analysis and HTE displacement showed that libraries of cross-coupled products can be generated rapidly to cover a broad chemical space using heterobenzyl chlorides as intermediates.

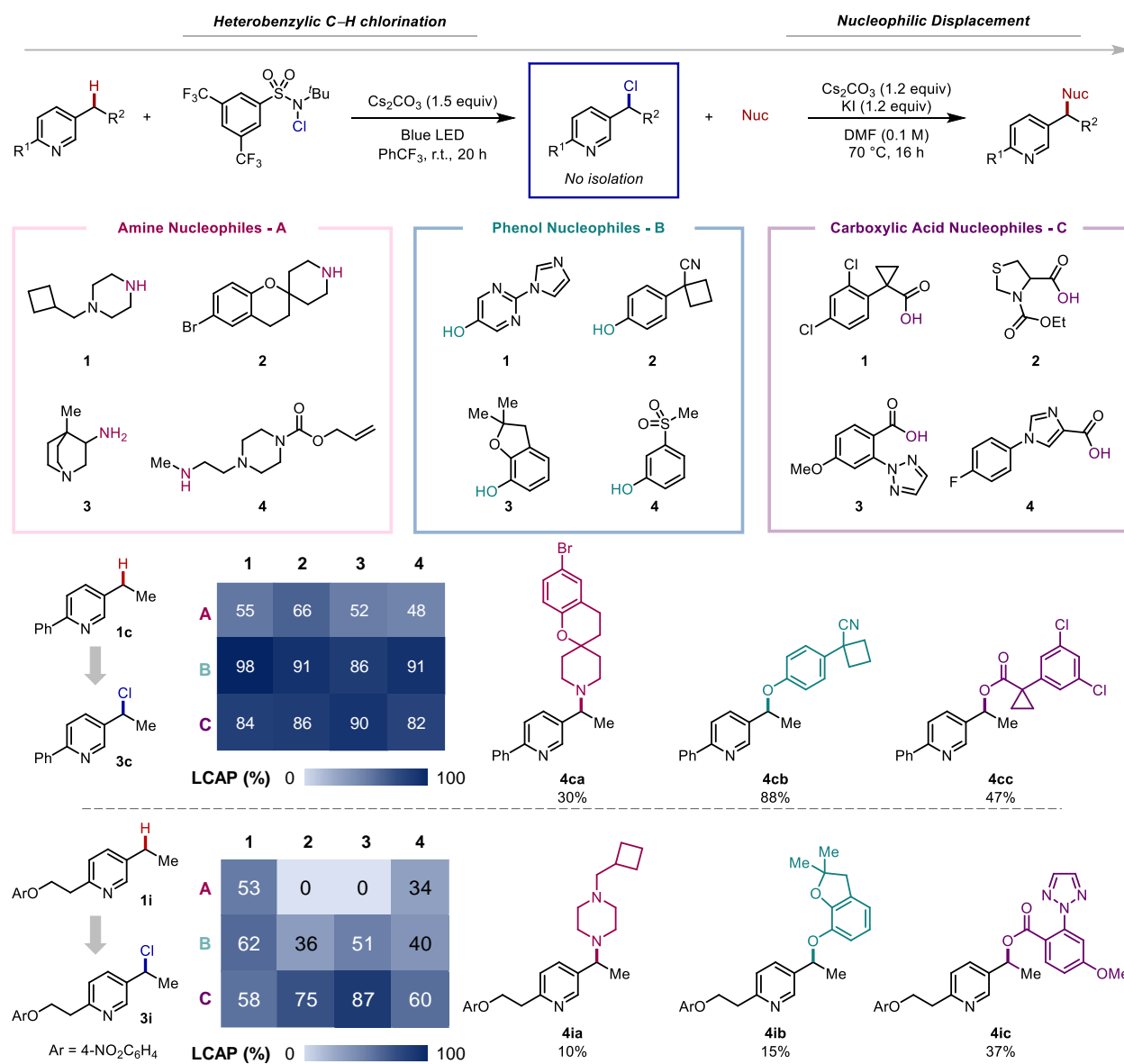


Figure 3.7. Sequential chlorination/ nucleophilic displacement of two C–H substrates.

Given the robust reactivity of **3a** with diverse nucleophiles, we next explored a telescoped process involving sequential heterobenzyl chloride formation followed by nucleophilic displacement. Incorporation of complex nucleophilic coupling partners in an operationally simple

chlorination/diversification sequence without purification of chloride intermediates was demonstrated using two different C–H substrates **1c** and **1i** (Figure 3.7). A collection of 12 nucleophiles from three classes examined in Figure 5 was selected to diversify the 3-alkylpyridine position. Each C–H substrate chlorination reaction was scaled up to 0.5 mmol scale to afford the heterobenzyl chloride stock solution in DMF (See General Procedure (VII) in Appendix B for details), which was subsequently dispensed into separate vials containing KI, Cs₂CO₃, and nucleophile. The product formation was analyzed by UPLC-MS of the crude reaction mixtures. 4-Spiropiperidine and piperazine were tolerated under reaction condition to afford moderate yields of products (Figure 3.7, **4ca** & **4ia**). Structurally diverse phenols and carboxylic acids, including ones with cyclopropane, cyclobutene, and triazole functional groups, showed promising reactivity with both C–H substrates (Figure 3.7, **4cb–cc** & **4ib–ic**, 15–88%). The chlorination/diversification sequence without isolation of chloride intermediates emphasizes the amenability of this method for library synthesis of heterobenzyl amines, ethers and esters in the context of medicinal chemistry applications.

3.4. Conclusion

In summary, we have developed a site-selective and practical light-promoted radical chain chlorination reaction for 3-alkylpyridines. The NCl-sulfonamide shows good selectivity for benzylic position in the presence of other C(sp³)–H sites. Computational DFT calculations provide a predictable model for selections of NCl-reagents to enhance both reactivity and selectivity. Additionally, heterobenzyl chlorides are ideal intermediates for diversification via nucleophilic displacement to introduce structurally complex, oxidatively sensitive, and radical-based incompatible nucleophiles onto the heterobenzyl C–H sites. We anticipate that the

chlorination/diversification sequence described herein will have widespread applications in library synthesis and chemical space exploration in drug discovery and medicinal chemistry.

3.5. Acknowledgements

This work was supported by funding from the NIH (R35 GM134929). Spectroscopic instrumentation was supported by a gift from Paul. J. Bender, the NSF (CHE-1048642), and the NIH (S10 OD020022). The authors thank Christopher Hanneman and Marco Antonio Lopez for helpful discussions.

3.6. Author Contributions

Golden, D. L.: leading experimental work and manuscript preparation

Flynn, K. M.: experimental work and manuscript preparation

Aikonen, S.: computational calculations for bond energies

Kalyani, D.: computational clustering of nucleophiles

3.7. References

- 1 Cernak, T.; Dykstra, K. D.; Tyagarajan, S.; Vachal, P.; Krska, S. W. The Medicinal Chemist's Toolbox for Late Stage Functionalization of Drug-like Molecules. *Chem. Soc. Rev.* **2016**, *45*, 546–576.
- 2 Lovering, F.; Bikker, J.; Humblet, C. Escape from Flatland: Increasing Saturation as an Approach to Improving Clinical Success. *J. Med. Chem.* **2009**, *52*, 6752–6756.
- 3 Xue, X.-S.; Ji, P.; Zhou, B.; Cheng, J.-P. The Essential Role of Bond Energetics in C–H Activation/Functionalization. *Chem. Rev.* **2017**, *117*, 8622–8648.
- 4 Wang, F.; Chen, P.; Liu, G. Copper-Catalyzed Radical Relay for Asymmetric Radical Transformations. *Acc. Chem. Res.* **2018**, *51*, 2036–2046.
- 5 Golden, D. L.; Suh, S.-E.; Stahl, S. S. Radical C(sp³)–H Functionalization and Cross-Coupling Reactions. *Nat. Rev. Chem.* **2022**, *6*, 405–427.
- 6 Thompson, T. N. Optimization of Metabolic Stability as a Goal of Modern Drug Design. *Med.*

- Res. Rev.* **2001**, *21*, 412–449.
- 7 Zhang, W.; Wang, F.; McCann, S. D.; Wang, D.; Chen, P.; Stahl, S. S.; Liu, G. Enantioselective Cyanation of Benzylic C–H Bonds via Copper-Catalyzed Radical Relay. *Science* **2016**, *353*, 1014–1018.
- 8 Hu, H.; Chen, S.-J.; Mandal, M.; Pratik, S. M.; Buss, J. A.; Krska, S. W.; Cramer, C. J.; Stahl, S. S. Copper-Catalyzed Benzylic C–H Coupling with Alcohols via Radical Relay Enabled by Redox Buffering. *Nat. Catal.* **2020**, *3*, 358–367.
- 9 Suh, S.-E.; Chen, S.-J.; Mandal, M.; Guzei, I. A.; Cramer, C. J.; Stahl, S. S. Site-Selective Copper-Catalyzed Azidation of Benzylic C–H Bonds. *J. Am. Chem. Soc.* **2020**, *142*, 11388–11393.
- 10 (a) Buss, J. A.; Vasilopoulos, A.; Golden, D. L.; Stahl, S. S. Copper-Catalyzed Functionalization of Benzylic C–H Bonds with N-Fluorobenzenesulfonimide: Switch from C–N to C–F Bond Formation Promoted by a Redox Buffer and Brønsted Base. *Org. Lett.* **2020**, *22*, 5749–5752. (b) Vasilopoulos, A.; Golden, D. L.; Buss, J. A.; Stahl, S. S. Copper-Catalyzed C–H Fluorination/Functionalization Sequence Enabling Benzylic C–H Cross Coupling with Diverse Nucleophiles. *Org. Lett.* **2020**, *22*, 5753–5757.
- 11 Chen, S.-J.; Golden, D. L.; Krska, S. W.; Stahl, S. S. Copper-Catalyzed Cross-Coupling of Benzylic C–H Bonds and Azoles with Controlled N-Site Selectivity. *J. Am. Chem. Soc.* **2021**, *143*, 14438–14444.
- 12 Suh, S.-E.; Nkulu, L. E.; Krska, S. W.; Stahl, S. S. Benzylic C–H Isocyanation/Amine Coupling Sequence Enabling High-Throughput Synthesis of Pharmaceutically Relevant Ureas. *Chem. Sci.* **2021**, *12*, 10380–10387.
- 13 Lopez, M. A.; Buss, J. A.; Stahl, S. S. Cu-Catalyzed Site-Selective Benzylic Chlorination Enabling Net C–H Coupling with Oxidatively Sensitive Nucleophiles. *Org. Lett.* **2021**, *24*, 597–601.
- 14 (a) Gibson, S.; McGuire, R.; Rees, D. C. Principal Components Describing Biological Activities and Molecular Diversity of Heterocyclic Aromatic Ring Fragments. *J. Med. Chem.* **1996**, *39*, 4065–4072. (b) Ertl, P.; Jelfs, S.; Mühlbacher, J.; Schuffenhauer, A.; Selzer, P. Quest for the Rings. In Silico Exploration of Ring Universe to Identify Novel Bioactive Heteroaromatic Scaffolds. *J. Med. Chem.* **2006**, *49*, 4568–4573. (c) Ritchie, T. J.; Macdonald, S. J. F.; Peace, S.; Pickett, S. D. The Developability of Heteroaromatic and Heteroaliphatic Rings – Do Some Have a Better Pedigree as Potential Drug Molecules than others. *Med. Chem. Commun.* **2012**, *3*, 1062–1069. (d) Taylor, R. D.; MacCoss, M.; Lawson, A. D. G. Rings in Drugs. *J. Med. Chem.* **2014**, *57*, 5845–5869. (e) Ertl, P. Magic Rings: Navigation in the Ring Chemical Space Guided by the Bioactive Rings. *J. Chem. Inf. Model.* **2022**, *62*, 2164–2170.
- 15 Meanwell, M.; Adluri, B. S.; Yuan, Z.; Newton, J.; Prevost, P.; Nodwell, M. B.; Friesen, C. M.; Schaffer, P.; Martin, R. E.; Britton, R. Direct Heterobenzylic Fluorination, Difluorination, and Trifluoromethylthiolation with Dibenzene-sulfonamide Derivatives. *Chem. Sci.* **2018**, *9*, 5608–5613.
- 16 Maity, S.; Lopez, M. A.; Lin, S.; Krska, S. W.; Stahl, S. S. Benzylic C(sp³)–H Diversification of Azaheterocycles Enabled by Substrate Guided Site-Selective C–H Chlorination. *Manuscript in Preparation*.

- 17 Kaur, M.; Van Humbeck, J. F. Recent Trends in Catalytic sp^3 C–H Functionalization of Heterocycles. *Org. Biomol. Chem.* **2020**, *18*, 606–617.
- 18 McMillan, A. J.; Siénkowska, M.; Lorenzo, P. D.; Gransbury, G. K.; Chilton, N. F.; Salamone, M.; Ruffino, A.; Bietti, M.; Leonori, D. Practical and Selective sp^3 C–H Bond Chlorination via Aminium Radicals. *Angew. Chem. Int. Ed.* **2021**, *60*, 7132–7139.
- 19 Xiang, M.; Zhou, C.; Yang, X.-L.; Chen, B.; Tung, C.-H.; Wu, L. Z. Visible Light-Catalyzed Benzylic C–H Bond Chlorination by a Combination of Organic Dye (Acr^+ -Mes) and N-Chlorosuccinimide. *J. Org. Chem.* **2020**, *85*, 9080–9087.
- 20 Quinn, R. K.; Könst, Z. A.; Michalak, S. E.; Schmidt, Y.; Szklarski, A. R.; Flores, A. R.; Nam, S.; Horne, D. A.; Vanderwal, C. D.; Alexanian, E. J. Site-Selective Aliphatic C–H Chlorination Using N-Chloroamides Enables a Synthesis of Chlorolissoclimide. *J. Am. Chem. Soc.* **2016**, *138*, 696–702.
- 21 Xue, X.-S.; Ji, P.; Zhou, B.; Cheng, J.-P. The Essential Role of Bond Energies in C–H Activation/Functionalization. *Chem. Rev.* **2017**, *117*, 8622–8648.
- 22 Tierney, M. M.; Crespi, S.; Ravelli, D.; Alexanian, E. J. Identifying Amidyl Radicals for Intermolecular C–H Functionalizations. *J. Org. Chem.* **2019**, *84*, 12983–12991.

Chapter 4.

Copper-Catalyzed C–H Fluorination/Functionalization Sequence Enabling Benzylic C–H Cross Coupling with Diverse Nucleophiles

Reproduced with permission from: Aristidis Vasilopoulos, **Dung L. Golden**, Joshua A. Buss, Shannon S. Stahl. Copper-Catalyzed C–H Fluorination/Functionalization Sequence Enabling Benzylic C–H Cross Coupling with Diverse Nucleophiles. *Org. Lett.* **2020**, 22, 5753–5757.
Copyright 2020 American Chemical Society.

4.1. Abstract

Site-selective transformation of benzylic C–H bonds into diverse functional groups is achieved via Cu-catalyzed C–H fluorination with *N*-fluorobenzenesulfonimide (NFSI), followed by substitution of the resulting fluoride with various nucleophiles. The benzyl fluorides generated in these reactions are reactive electrophiles in the presence of hydrogen-bond donors or Lewis acids, allowing them to be used without isolation in C–O, C–N, and C–C coupling reactions.

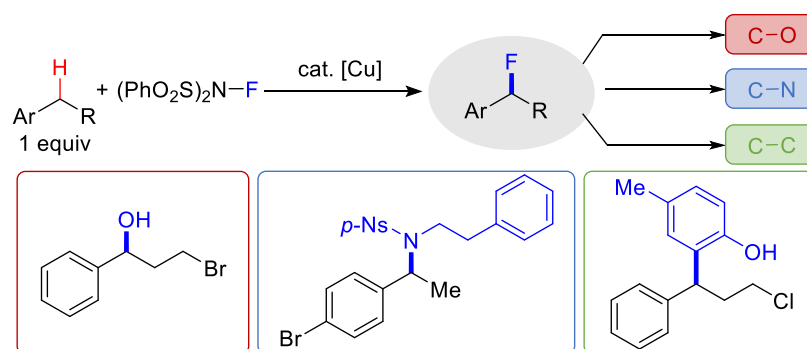


Figure 4.1. Benzylic C–H fluorination/functionalization sequence to access diverse cross-coupled products.

4.2. Introduction

Medicinal chemistry and drug discovery efforts greatly benefit from synthetic coupling reactions that facilitate access to analogs of pharmaceutical building blocks and core structures. Functional groups that participate in efficient coupling, such as carboxylic acids, aryl halides, and boronic acids, provide the foundation for these methods.¹ Expansion of latent functionalities that participate in coupling could greatly increase the scope of synthetic diversity.² Benzylic C–H bonds are an appealing target in this context as they are prevalent in drug-like molecules and are susceptible to site-selective activation owing to their enhanced reactivity (e.g., reduced bond

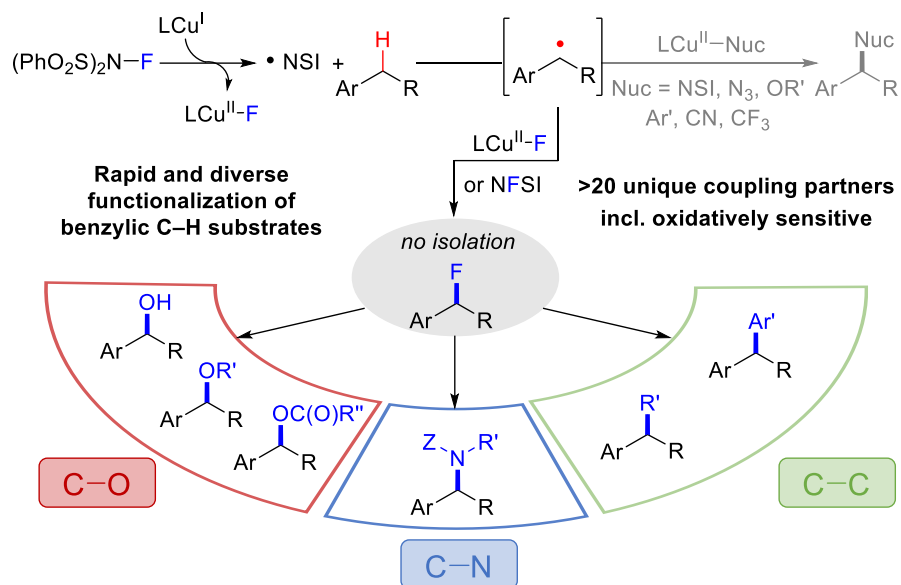


Figure 4.2. C–H cross coupling via benzyl fluorides.

strength, higher acidity). Recent studies demonstrate that benzylic C–H substrates may be used as the limiting reagent in cross-coupling reactions with a number of different reaction partners, including alcohols,³ amides,⁴ and arylboronic acids.⁵ Cu catalysts in combination with *N*-fluorobenzenesulfonimide (NFSI) are particularly effective in these reactions as they exhibit unique selectivity for benzylic C–H bonds and promote a radical relay mechanism that enables coupling with diverse reaction partners (Figure 4.2).^{3a,4b,5a,6} We recently discovered that a Cu/NFSI-based catalyst system switches selectivity, from C–N to C–F bond formation, when the reaction is conducted with MeB(OH)₂ as a redox buffer and Li₂CO₃ as a Brønsted base.⁷ These observations provide the foundation for the present study in which we demonstrate a C–H fluorination/substitution sequence that enables benzylic C–H cross-coupling with diverse oxygen, nitrogen, and carbon nucleophiles (Figure 4.2). This strategy, which takes advantage of the intrinsic lability of benzyl monofluorides,^{8,9} contrasts the many C–H fluorination efforts motivated by the inertness of the C–F bond.^{10,11} This approach allows for successful benzylic C–H cross coupling with reaction partners that are oxidatively sensitive or otherwise incompatible with direct

Cu/NFSI-catalyzed methods, thereby greatly expanding the synthetic scope and versatility of benzylic C–H cross coupling.

4.3. Results and Discussion

The present study began by testing the previously optimized fluorination conditions⁷ with a variety of benzylic C–H substrates (Figure 4.3). *para*-Bromoethylbenzene proceeds effectively in 81% to the corresponding benzylic fluoride product **1** (Figure 4.3). Use of *ortho*-bromoethylbenzene resulted in low conversion of the starting material (<20%), presumably reflecting the deleterious steric or σ -electron withdrawing effect of the *o*-halogen on HAT. Empirical modification of the conditions, including use of 4 equiv of NFSI, replacement of MeB(OH)₂ with B₂pin₂ as the reductant, and operating at 75 °C, led to a 50% yield of the desired product **2**. The modified conditions, either at 55 °C or 75 °C, also proved effective with other electron-deficient substrates (**2**, **4**, **5**, **6**, **9**, **13**, **17**, **19**), while the original conditions were favored for more reactive substrates (**3**, **7**, **8**, **10**, **11**, **12**, **14**). The latter group also includes celestolide, which underwent fluorination in 86% yield (**18**), and substrates with tertiary C–H bonds, leading to **23** and **24** in 92% and 84% yields. Overoxidation to ketone or styrene-derived side products, was observed with more activated C–H substrates, necessitating the identification of milder conditions (35 °C, 0.5 equiv MeB(OH)₂). These conditions allowed several benzylic fluorides to be obtained in good yield (**15**, **16**, **20**), including a bromochroman derivative. Methylarenes appear to favor C–H sulfonimidation rather than fluorination, as observed by the formation of **21** and **22**. A collection of other less successful substrates is provided in Table 4D.9 of Appendix D, but, overall, these results show that the catalytic conditions may be tuned to access good fluorination reactivity for a broad range of benzylic C–H substrates.¹²

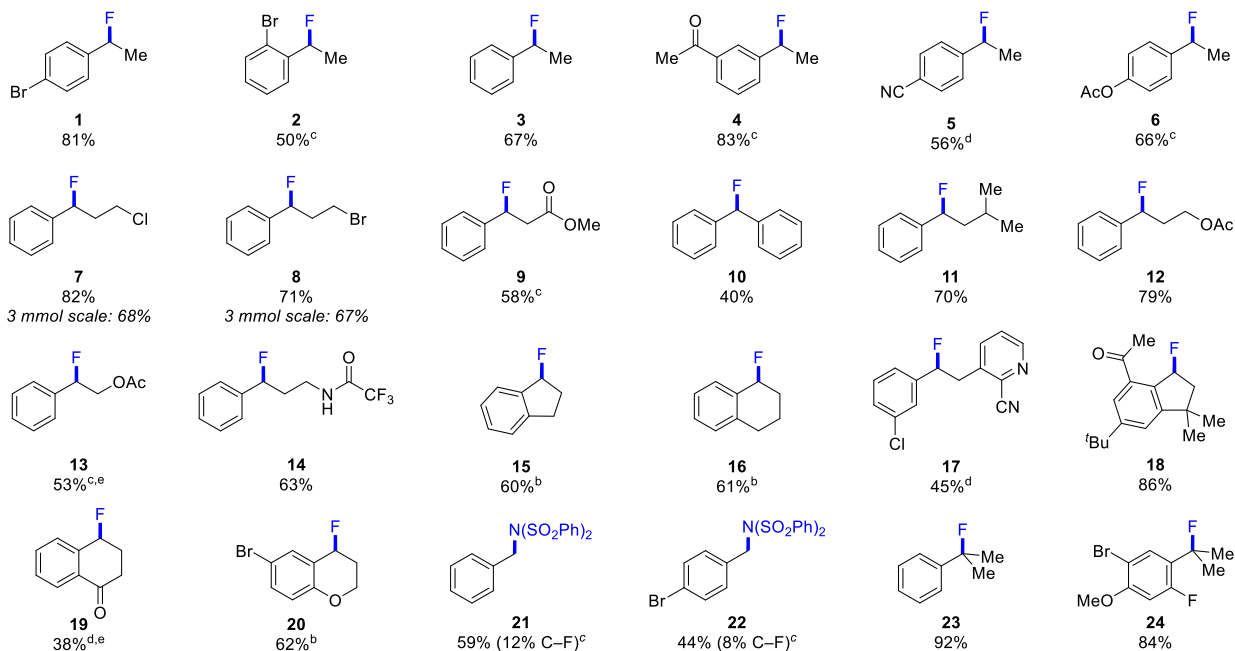
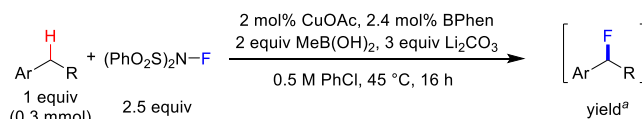


Figure 4.3. Cu/NFSI fluorination of benzylic C–H bonds. ^a¹H NMR yields; CH₂Br₂ or PhCF₃ as int. stds. ^b35 °C, 0.5 equiv MeB(OH)₂. ^c55 °C, 1 mol% Cu/1.2 mol% BPhen, 4 equiv NFSI, 1 equiv B₂pin₂ instead of MeB(OH)₂. ^d75 °C 1 mol% Cu/1.2 mol% BPhen, 4 equiv NFSI, 1 equiv B₂pin₂ instead of MeB(OH)₂. ^eAcetone solvent.

Complications were encountered during product isolation. Many of the products decomposed in the presence of silica gel, and even when stored in glass vessels. These observations belie the frequent incorporation of fluorine in organic molecules to inhibit reactivity at specific sites, for example, to slow drug metabolism.¹⁰ Separately, benzylic monofluorides have been shown to undergo nucleophilic substitution in the presence of acids or hydrogen-bond donors.^{8,9} These insights suggest that monofluorination of benzylic C–H bonds is not a compelling end-goal for many substrates. On the other hand, they suggest that benzyl fluorides could serve as strategic intermediates in a sequential approach to benzylic C–H functionalization.

Efforts to explore sequential C–H fluorination/functionalization were initiated by testing hexafluoroisopropanol (HFIP, 10 equiv) as a hydrogen bond donor to activate the benzyl fluoride

(Figure 4.4).^{9f} Initial results demonstrated conversion of benzyl fluorides to benzyl alcohols by including water as a nucleophile in the reaction mixture (**25–27**). Formation of **25** shows that hydrogen-bond activation supports displacement of the fluoride, even in the presence of a primary alkyl bromide. This fluorination/water-substitution sequence to access benzylic alcohols is noteworthy because C–H oxygenation strategies will typically proceed directly to ketones, reflecting the higher reactivity of alcohols relative to C–H bonds.¹³

Analogous efforts were effective for the formation of benzylic ethers and esters (**28–36**). For less nucleophilic alcohols, like *tert*-butyl alcohol, more forcing conditions were needed to form the product, using $\text{BF}_3 \cdot \text{OEt}_2$ as a Lewis acid catalyst (**28** and **33**).⁹ⁱ This approach also enabled reactivity with alcohols bearing Boc-pyrrolidine or pyridine substituents (**31** and **32**). These results expand the scope of accessible products relative to the recently reported method for direct Cu/NFSI-catalyzed benzylic etherification,^{3a} which shows limited compatibility with basic heterocycles, such as pyridines, and Boc-protected pyrrolidines. Carboxylic acids were also effective coupling partners (**34–36**). These substrates have innate acidity, but the reactions were more effective with HFIP or BF_3 additives. The presence of allylic and benzylic C–H bonds in the carboxylic acids used to prepare **34** and **36** would likely complicate direct C–H carboxylation methods with these partners.

We then targeted C–N coupling reactions. Direct C–H amidation reactions typically feature primary sulfonamides or other stabilized ammonia surrogates capable of generating nitrenoid intermediates.¹⁴ Few precedents exist for oxidative coupling of C–H bonds with carbamates or secondary sulfonamides.^{4b,15} *tert*-Butyl carbamate itself proved to be an effective coupling partner when using $\text{BF}_3 \cdot \text{Et}_2\text{O}$ to activate the benzyl fluoride (**37**). Then a range of secondary sulfonamides were shown to undergo effective displacement of the benzyl fluoride, with $\text{BF}_3 \cdot \text{Et}_2\text{O}$ as an

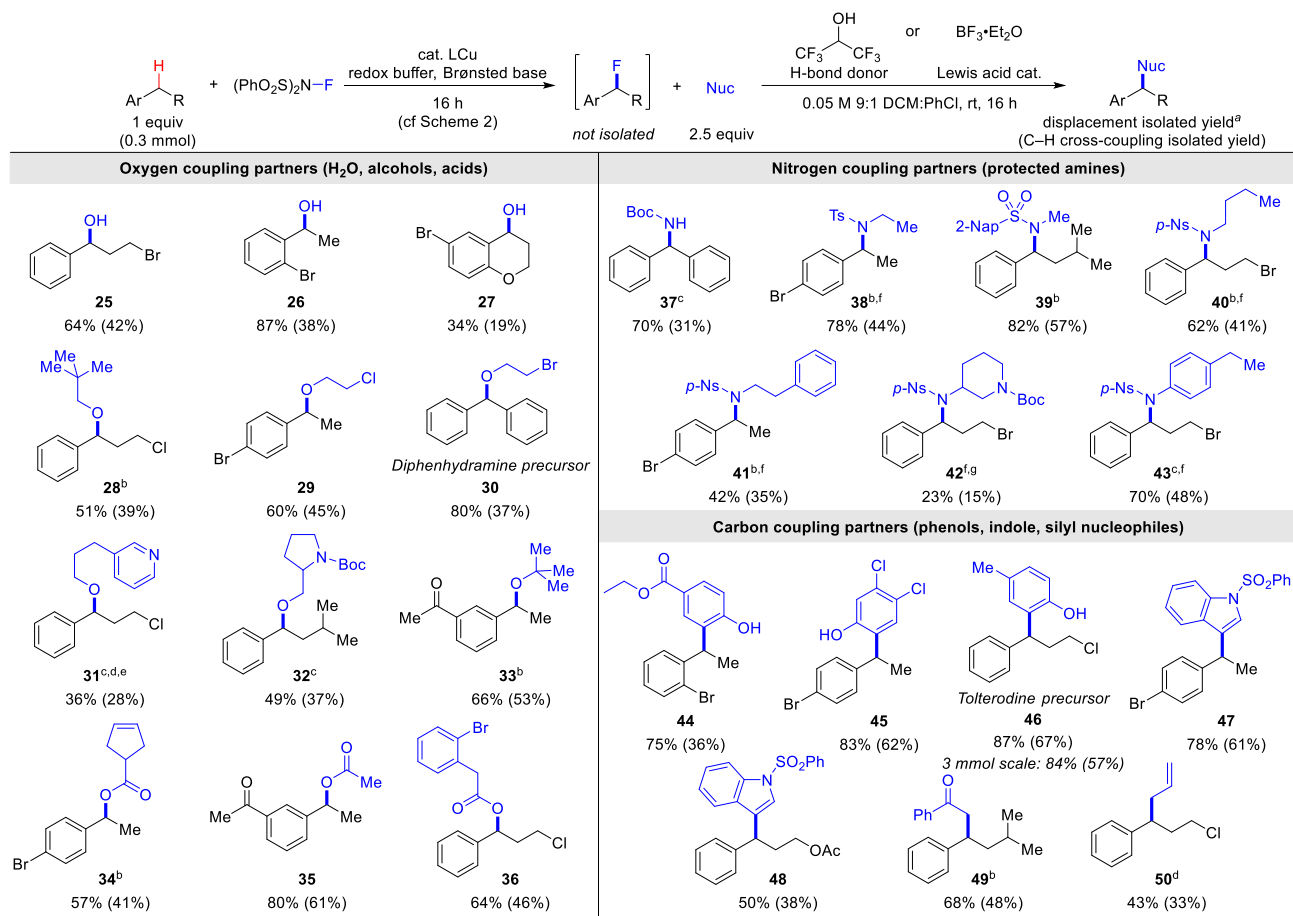


Figure 4.4. Benzylic C–H cross coupling to C–O, C–N, and C–C bonds via a benzyl fluoride. ^aReaction uses 10 equiv HFIP as a H-bond donor. Isolated yields calculated with respect to the ¹H NMR yield of the benzyl fluoride (or the C–H substrate, in parentheses). ^b10 mol% BF₃•Et₂O used instead of HFIP. ^c50 mol% BF₃•Et₂O used instead of HFIP ^dBoth HFIP and BF₃•Et₂O used. ^e2.5 equiv MsOH added to the nucleophile. ^fUsed dichloromethane as the fluorination reaction solvent. ^g1.5 equiv BF₃•Et₂O used instead of HFIP. Isolated as the amine.

activator (**38–43**). The good reactivity with less nucleophilic, but more readily deprotected, nosylamides is noteworthy. Competitive Friedel-Crafts reactivity with chlorobenzene was observed in some of these reactions, but this complication was resolved by using dichloromethane as the solvent for the fluorination step (**40–43**).

The observation of Friedel-Crafts reactivity highlights opportunities for coupling with electron-rich arenes and other carbon nucleophiles that would not be compatible with a direct Cu/NFSI-catalyzed C–H coupling reaction. Such reactivity was demonstrated with phenols (**44–**

46), *N*-sulfonyl indole (47–48), and a silyl enol ether and allyl silane (49–50).

Each of the reactions highlighted above proceeds via a straightforward two-step protocol, without isolation of the benzyl fluoride intermediate. Following the fluorination step, sodium dithionite is added to quench any unreacted NFSI. The slurry is then diluted with dichloromethane and filtered. Subsequent addition of the nucleophile and HFIP/BF₃ promoter initiates the displacement reaction. As conveyed in several instances above, this two-step C–H cross-coupling sequence greatly expands the scope of useful reaction partners. Many of the electron-rich substrates and nucleophiles bearing oxidatively sensitive substituents would decompose or undergo deleterious side reactions with NFSI in a direct oxidative coupling reaction.^{11c,16}

4.4. Conclusion

In summary, the results described above introduce a new strategy to achieve selective benzylic C–H cross-coupling with diverse reaction partners. The use of Cu/NFSI conditions that may be tuned to accommodate different substrate electronic properties allowed formation of benzyl fluorides that may be used without isolation as coupling partners to access products with new C(sp³)–O, –N, and –C bonds. This method joins a number of emerging strategies for C(sp³)–H cross-coupling that involve formation of strategic intermediates, such as xanthate esters, isocyanates, lactones, alkylboronates,¹⁷ that allow rapid access to diversified products.

4.5. Acknowledgements

This work was supported by the NIH (R01 GM126832, R35 GM134929), including a Ruth L. Kirschstein NRSA fellowship (F32 GM129909, to JAB). Spectroscopic instrumentation was partially supported by the NIH (1S10 OD020022-1) and the NSF (CHE-1048642).

4.6. Author Contributions

Vasilopoulos, A.: manuscript preparation and leading experimental work

Golden, D. L.: benzyl fluoride displacement experimental work and manuscript preparation

Buss, J. A.: fluorination experimental work and manuscript preparation

4.7. References

- 1 Brown, D.G.; Boström, J. Analysis of Past and Present Synthetic Methodologies on Medicinal Chemistry: Where Have All the New Reactions Gone? *J. Med. Chem.* **2016**, *59*, 4443-4458.
- 2 (a) Cernak, T.; Dykstra, K. D.; Tyagarajan, S.; Vachal, P.; Krska, S. W. The Medicinal Chemist's Toolbox for Late Stage Functionalization of Drug-Like Molecules. *Chem. Soc. Rev.* **2016**, *45*, 546-576. (b) Blakemore, D. C.; Castro, L.; Churcher, I.; Rees, D. C.; Thomas, A. W.; Wilson, D. M.; Wood, A. Organic Synthesis Provides Opportunities to Transform Drug Discovery. *Nat. Chem.* **2018**, *10*, 383-394.
- 3 (a) Hu, H.; Chen, S.-J.; Mandal, M.; Pratik, S. M.; Buss, J. A.; Krska, S. W.; Cramer, C. J.; Stahl, S. S. Copper-Catalyzed Benzylic C–H Coupling with Alcohols via Radical Relay Enabled by Redox Buffering. *Nat. Catal.* **2020**, *3*, 358-367. (b) Lee, B. J.; DeGlopper, K. S.; Yoon, T. P. Site-Selective Alkoxylation of Benzylic C–H Bonds by Photoredox Catalysis. *Angew. Chem. Int. Ed.* **2020**, *59*, 197-202.
- 4 (a) Zhang, Y.; Dong, J.; Liu, L.; Liu, L.; Zhou, Y.; Yin, S.-F. Manganese(III) Acetate Catalyzed Oxidative Amination of Benzylic C(sp³)–H Bonds with Nitriles. *Org. Biomol. Chem.* **2017**, *15*, 2897-2901. (b) Wang, A.; DeOliveira, C. C.; Emmert, M. Non-Directed, Copper Catalyzed Benzylic C–H Amination Avoiding Substrate Excess. *ChemRxiv* **2019**, <https://doi.org/10.26434/chemrxiv.8792243>.
- 5 (a) Zhang, W.; Chen, P.; Liu, G. Copper-Catalyzed Arylation of Benzylic C–H Bonds with Alkylarenes as the Limiting Reagents. *J. Am. Chem. Soc.* **2017**, *139*, 7709-7712. (b) Yazaki, R.; Ohshima, T. Recent Strategic Advances for the Activation of Benzylic C–H Bonds for the Formation of C–C Bonds. *Tet. Lett.* **2019**, *60*, 151225.
- 6 (a) Ni, Z.; Zhang, Q.; Xiong, T.; Zheng, Y.; Li, Y.; Zhang, H.; Zhang, J.; Liu, Q. Highly Regioselective Copper-Catalyzed Benzylic C–H Amination by *N*-Fluorobenzenesulfonimide. *Angew. Chem. Int. Ed.* **2012**, *51*, 1244-1247. (b) Zhang, W.; Wang, F.; McCann, S. D.; Wang, D.; Chen, P.; Stahl, S. S.; Liu, G. Enantioselective Cyanation of Benzylic C–H Bonds via Copper-Catalyzed Radical Relay. *Science* **2016**, *353*, 1014-1018. (c) Xiao, H.; Liu, Z.; Shen, H.; Zhang, B.; Zhu, L.; Li, C. Copper-Catalyzed Late-Stage Benzylic C(sp³)–H Trifluoromethylation. *Chem* **2019**, *5*, 940-949. (d) Suh, S.-E. Chen, S.-J. Mandal, M.; Guzei, I. A.; Cramer, C. J.; Stahl, S. S. Site-Selective Copper-Catalyzed Azidation of Benzylic C–H Bonds. *J. Am. Chem. Soc.* **2020**, *142*, 11388-11393.

- 7 Buss, J. A.; Vasilopoulos, A.; Golden, D. L.; Stahl, S. S. Copper/NFSI-Catalyzed C–H Fluorination: Switch from C–N to C–F Bond Formation Promoted by a Redox Buffer and Brønsted Base. *Org. Lett.* **2020**, *22*, 5749-5752.
- 8 (a) Amii, H.; Uneyama, K. C–F Bond Activation in Organic Synthesis. *Chem. Rev.* **2009**, *109*, 2119-2183. (b) Hamel, J.-D.; Paquin, J.-F. Activation of C–F Bonds α to C–C Multiple Bonds. *Chem. Commun.* **2018**, *54*, 10224-10239.
- 9 For leading primary references, see: (a) Bernstein, J.; Roth, J. S.; Miller Jr., W. T. The Preparation and Properties of Some Substituted Benzyl Fluorides. *J. Am. Chem. Soc.* **1948**, *70*, 2310-2314. (b) Swain, C. G.; Spalding, R. E. T. III. Mechanism of Acid Catalysis of the Hydrolysis of Benzyl Fluoride. *J. Am. Chem. Soc.* **1960**, *82*, 6104-6107. (c) Toteva, M. M.; Richard, J. P. Hydrogen Bonding and Catalysis of Solvolysis of 4-Methoxybenzyl Fluoride. *J. Am. Chem. Soc.* **2002**, *124*, 9798-9805. (d) Blessley, G.; Holden, P.; Walker, M.; Brown, J. M.; Gouverneur, V. Palladium-Catalyzed Substitution and Cross-Coupling of Benzylic Fluorides. *Org. Lett.* **2012**, *14*, 2754-2757. (e) Champagne, P. A.; Pomarole, J.; Thérien, M.-E.; Benhassine, Y.; Beaulieu, S.; Legault, C. Y.; Paquin, J.-F. Enabling Nucleophilic Substitution Reactions of Activated Alkyl Fluorides Through Hydrogen Bonding. *Org. Lett.* **2013**, *15*, 2210-2213. (f) Champagne, P. A.; Benhassine, Y.; Desroches, J.; Paquin, J.-F. Friedel-Crafts Reaction of Benzyl Fluorides: Selective Activation of C–F Bonds as Enabled by Hydrogen Bonding. *Angew. Chem. Int. Ed.* **2014**, *53*, 13835-13839. (g) Pryyma, A.; Bu, Y. J.; Wai, Y.; Patrick, B. O.; Perrin, D. M. Synthesis and Activation of Bench-Stable 3a-Fluoropyrroloindolines as Latent Electrophiles for the Synthesis of C-2-Thiol-Substituted Tryptophans and C-3a-Substituted Pyrroloindolines. *Org. Lett.* **2019**, *21*, 8234-8238. (h) Zhu, J.; Pérez, M.; Stephan, D. W. C–C Coupling of Benzyl Fluorides Catalyzed by an Electrophilic Phosphonium Cation. *Angew. Chem. Int. Ed.* **2016**, *55*, 8448-8451. (i) Zhou, X.; Ding, H.; Chen, P.; Liu, L.; Sun, Q.; Wang, X.; Wang, P.; Lv, Z.; Li, M. Radical Dehydroxymethylative Fluorination of Carbohydrates and Divergent Transformations of the Resulting Reverse Glycosyl Fluorides. *Angew. Chem. Int. Ed.* **2020**, *59*, 4138-4144.
- 10 Szpera, R.; Moseley, D. F. J.; Smith, L. B.; Sterling, A. J.; Gouverneur, V. The Fluorination of C–H Bonds: Developments and Perspectives. *Angew. Chem. Int. Ed.* **2019**, *58*, 14824-14848.
- 11 For selected primary references directed toward benzylic fluorination, see: (a) Xia, J.-B.; Zhu, C.; Chen, C. Visible Light-Promoted Metal-Free C–H Activation: Diarylketone-Catalyzed Selective Benzylic Mono- and Difluorination. *J. Am. Chem. Soc.* **2013**, *135*, 17494-17500. (b) Bloom, S.; Pitts, C. R.; Woltornist, R.; Griswold, A.; Holl, M. G.; Lectka, T. Iron(II)-Catalyzed Benzylic Fluorination. *Org. Lett.* **2013**, *15*, 1722-1724. (c) Nodwell, M. B.; Bagai, A.; Halperin, S. D.; Martin, R. E.; Knust, H.; Britton, R. Direct Photocatalytic Fluorination of Benzylic C–H Bonds with *N*-Fluorobenzenesulfonimide. *Chem. Commun.* **2015**, *51*, 11783-11786. (d) Meanwell, M.; Nodwell, M. B.; Martin, R. E.; Britton, R. A Convenient Late-Stage Fluorination of Pyridylic C–H Bonds with *N*-Fluorobenzenesulfonimide. *Angew. Chem. Int. Ed.* **2016**, *55*, 13244-13248.
- 12 For previous studies of benzylic fluorination, see refs. 7, 10, 11 and references cited therein.
- 13 For important alternative strategies to convert 2° C–H bonds to alcohols, see: (a) Li, G.-X.; Morales-Rivera, C. A.; Gao, F.; Wang, Y.; He, G.; Liu, P.; Chen, G. A Unified Photoredox-Catalysis Strategy for C(sp³)–H Hydroxylation and Amidation using Hypervalent Iodine. *Chem. Sci.* **2017**, *8*, 7180-7185. (b) Dantignana, V.; Milan, M.; Cussó, O.; Company, A.; Bietti, M.; Costas, M. Chemoselective Aliphatic C–H Bond Oxidation Enabled by Polarity Reversal.

- ACS Cent. Sci.* **2017**, *3*, 1350-1358. (c) Tanwar, L.; Börgel, J.; Ritter, T. Synthesis of Benzylic Alcohols by C–H Oxidation. *J. Am. Chem. Soc.* **2019**, *141*, 17983-17988.
- 14 (a) Clark, J. R.; Feng, K.; Sookezian, A.; White, M. C. Manganese-Catalysed Benzylic C(sp³)–H Amination for Late-Stage Functionalization. *Nat. Chem.* **2018**, *10*, 583-591. (b) Chiappini, N. D.; Mack, J. B. C.; Du Bois, J. Intermolecular C(sp³)–H Amination of Complex Molecules. *Angew. Chem. Int. Ed.* **2018**, *57*, 4956-4959. (c) Nasrallah, A.; Boquet, V.; Hecker, A.; Retailleau, P.; Darses, B.; Dauban, P. Catalytic Enantioselective Intermolecular Benzylic C(sp³)–H Amination. *Angew. Chem. Int. Ed.* **2019**, *58*, 8192-8196. (d) Bakhoda, A.; Jian, Q.; Badieli, Y. M.; Bertke, J. A.; Cundari, T. R.; Warren, T. H. Copper Catalyzed sp³ C–H Amidation: Sterically Driven Primary and Secondary C–H Site-Selectivity. *Angew. Chem. Int. Ed.* **2019**, *58*, 3421-3425.
- 15 Each of the following has an example of a secondary (sulfon)amide as a coupling partner: (a) Pelletier, G.; Powell, D. A. Copper-Catalyzed Amidation of Allylic and Benzylic C–H Bonds. *Org. Lett.* **2006**, *8*, 6031-6034. (b) Ye, Y.-H.; Zhang, J.; Wang, G.; Chen, S.-Y.; Yu, X.-Q. Cobalt-Catalyzed Benzylic C–H Amination via Dehydrogenative-Coupling Reaction. *Tetrahedron* **2011**, *67*, 4649-4654. (c) Bosnidou, A. E.; Muñiz, K. Intermolecular Radical C(sp³)–H Amination under Iodine Catalysis. *Angew. Chem. Int. Ed.* **2019**, *58*, 7485-7489.
- 16 (a) Jing, L.; Yu, X.; Guan, M.; Wu, X.; Wang, Q.; Wu, X. An Efficient Method for Sulfonylation of Amines, Alcohols, and Phenols with *N*-Fluorobenzenesulfonimide Under Mild Conditions. *Chem. Res. Chin. Univ.* **2018**, *34*, 191-196. (b) Rozatian, N.; Ashworth, I. W.; Sandford, G.; Hodgson, D. R. W. A Quantitative Reactivity Scale for Electrophilic Fluorinating Reagents. *Chem. Sci.* **2018**, *9*, 8692-8702.
- 17 For examples of C(sp³)–H functionalization sequences, see: (a) Czaplyski, W. L.; Na, C. G.; Alexanian, E. J. C–H Xanthylation: A Synthetic Platform for Alkane Functionalization. *J. Am. Chem. Soc.* **2016**, *138*, 13854-13857. (b) Huang, X.; Zhuang, T.; Kates, P. A.; Gao, H.; Chen, X.; Groves, J. T. Alkyl Isocyanates via Manganese-Catalyzed C–H Activation for the Preparation of Substituted Ureas. *J. Am. Chem. Soc.* **2017**, *139*, 15407-15413. (c) Zhuang, Z.; Yu, J.-Q. Lactonization as a General Route to β-C(sp³)–H Functionalization. *Nature* **2020**, *577*, 656-659. (d) Oeschger, R.; Su, B.; Yu, I.; Ehinger, C.; Romero, E.; He, S.; Hartwig, J. Diverse Functionalization of Strong Alkyl C–H Bonds by Undirected Borylation. *Science* **2020**, *368*, 736-741.

Chapter 5.

Site-Selective Copper-Catalyzed Cross-Coupling of Benzylic C–H Bonds and Azoles with Controlled *N*-Site Selectivity

Reproduced with permission from: Si-Jie Chen, **Dung L. Golden**, Shane W. Krska, and Shannon S. Stahl. Site-Selective Copper-Catalyzed Cross-Coupling of Benzylic C–H Bonds and Azoles with Controlled *N*-Site Selectivity. *J. Am. Chem. Soc.* **2021**, *143*, 14438-14444. Copyright 2021 American Chemical Society.

5.1. Abstract

Azoles are important motifs in medicinal chemistry, and elaboration of their structures via direct N–H/C–H coupling could have broad utility in drug discovery. The ambident reactivity of many azoles, however, presents significant selectivity challenges. Here, we report a copper-catalyzed method that achieves site-selective cross-coupling of pyrazoles and other N–H heterocycles with substrates bearing (hetero)benzylic C–H bonds. Excellent *N*-site selectivity is achieved, with the preferred site controlled by the identity of co-catalytic additives. This cross-coupling strategy features broad scope for both the N–H heterocycle and benzylic C–H coupling partners, enabling application of this method to complex molecule synthesis and medicinal chemistry.

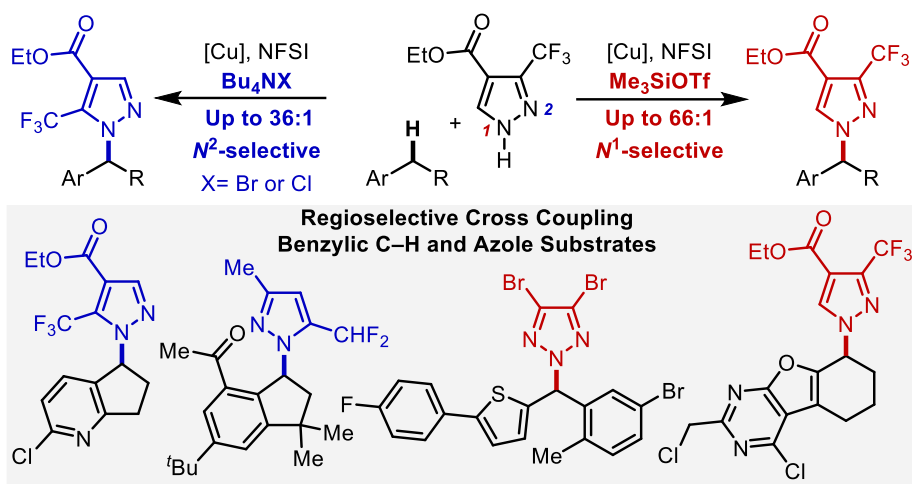


Figure 5.1. Cu-catalyzed cross coupling of benzylic C–H bonds and azoles with *N*-site selectivity

5.2. Introduction

Pd¹ and Cu-catalyzed² C(*sp*²)–N cross coupling reactions are some of the most widely used methods for pharmaceutical synthesis.³ Recent efforts have begun prioritizing complementary methods for C(*sp*³)–N coupling⁴ as a means to expand the topological diversity and

physiochemical properties of the resulting molecules.^{3,5} C–N coupling methods that directly functionalize C(*sp*³)–H bonds bypass the need for pre-functionalized alkyl

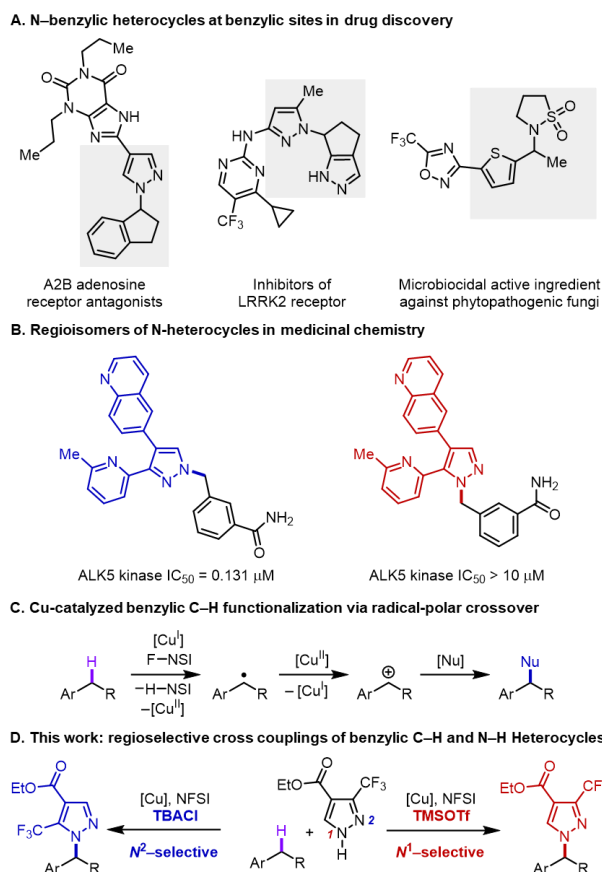


Figure 5.2. (A) Importance of benzylic N-azoles in drug discovery. (B) Impact of regioselectivity of heterocyclic compounds in medicinal chemistry. (C) Copper-catalyzed regioselective cross couplings of benzylic C–H bonds and N–H heterocycles enabled by various additives.

electrophiles and represent important targets for medicinal chemistry.⁶ Significant progress has been made in C(*sp*³)–H amination reactions that install ammonia surrogates via nitrene transfer⁷ or azidation,⁸ while C–H/N–H cross-coupling reactions, for example, with secondary amines/amides or N–H heterocycles, are more limited⁹ and often require excess C–H substrate.¹⁰ Here, we report a copper-catalyzed method for selective cross-coupling of azoles with (hetero)benzylic C–H substrates as the limiting reagent, affording *N*-benzylic heterocycles featured in pharmaceutical and agrochemical compounds (Figure 5.2A).^{11–14} In addition to the

challenge of C–H site selectivity, these reactions feature a second selectivity challenge arising from azoles that incorporate two (or more) nucleophilic nitrogen atoms.¹⁵ This issue has important implications for medicinal chemistry because regioisomeric *N*-substituted azoles can have very different properties and/or bioactivity (Figure 5.2B).¹⁶ The method described herein achieves excellent C–H site selectivity via hydrogen-atom transfer (HAT) from (hetero)benzylic C–H bonds (Figure 5.2C). Reaction with the azole coupling partners via Cu^{II}-mediated radical-polar crossover exhibits excellent *N*¹/*N*² site-selectivity (e.g., with pyrazoles), and variation of the reaction conditions lead to selective formation of either regioisomeric *N*-benzyl product with many coupling partners (Figure 5.2D).

5.3. Results and Discussion

Investigation of oxidative cross coupling of benzylic C–H substrates and N–H azoles started with ethylbenzene (**1a**) and ethyl 3-(trifluoromethyl)-1H-pyrazole-4-carboxylate (**2a**), a pyrazole featured in previous drug discovery efforts.¹⁷ Potential reaction conditions were inspired by recent studies involving the use of copper catalysts in combination with *N*-fluorobenzenesulfonimide (NFSI) as the oxidant. Diverse nucleophilic coupling partners have been used in these reactions, including pseudohalides (cyanide,¹⁸ azide,^{8d} isocyanate¹⁹), alcohols,²⁰ carbamates,²¹ and carbon-based nucleophiles (Zn(CF₃)₂,²² ArB(OH)₂,²³ alkynes²⁴).^{25,26} Cu^I-mediated activation of NFSI generates an *N*-centered radical that promotes selective HAT from benzylic C–H bonds, and subsequent coupling with heteroatom nucleophiles appears to favor a radical-polar crossover pathway involving formation of a benzylic cation intermediate.^{8d,19,20} Complementary studies have shown that mild reductants, such as dialkylphosphites, can promote these reactions by buffering the redox state of the Cu catalyst and ensuring that both Cu^I and Cu^{II} are present in the reaction.

The above mechanistic considerations guided a survey of reaction conditions. Initial screening

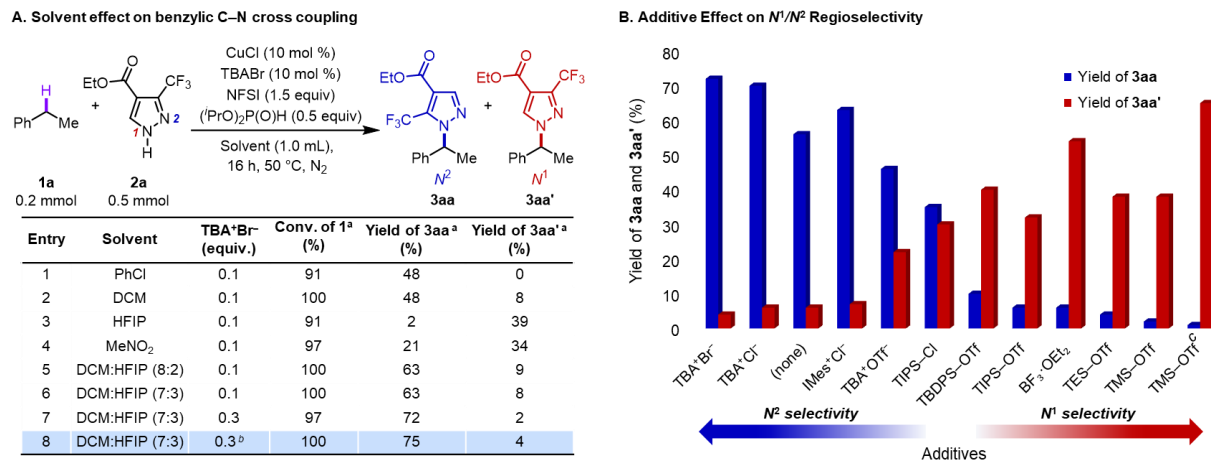


Figure 5.3. Evaluation of effects of various solvents and additives on the regioselectivity. (A) Effects of solvents on benzylic C–N cross coupling reaction. (B) Regioselectivity switch observed in cross coupling of **1a** and **2a** with different additives. Conditions identical to those shown in part A, using 10 mol% additive instead of TBABr, 10 mol % CuBr₂ instead of CuCl, and DCM:HFIP (7:3) solvent. ^aMonitored by ¹H NMR spectroscopy, yield determined using 0.2 mmol mesitylene as internal standard. TBA, tetrabutylammonium; DCM, dichloromethane; HFIP, hexafluoroisopropanol. ^bReaction run with TBA⁺Cl⁻ instead of TBA⁺Br⁻. ^cReaction run at 60 °C.

data showed that Cu/NFSI-catalyzed oxidative coupling of **1a** and **2a** favors the N^2 isomeric product **3aa** when the reaction is conducted in chlorinated solvents PhCl and dichloromethane (DCM) (Figure 5.3A, entries 1-2; see Appendix D for full screening details). Use of more polar solvents [hexafluoroisopropanol (HFIP) and MeNO₂] led to a switch in selectivity, favoring the N^1 isomer **3aa'** (entries 3-4). Tetrabutylammonium (TBA) bromide helped to solubilize the Cu catalyst and improved the reactivity and selectivity. Conventional ancillary ligands, such as phenanthroline or bioxazolines, led to lower yields (see Table 5D.1 and 5D.2 for detailed information). A mixture of DCM:HFIP (7:3) enhanced the conversion of **1a** and improved the product yield to 71% (**3aa** + **3aa'**, entry 5). Increasing the loading of TBABr to 0.3 equiv further improved the reaction yield and increased the $N^2:N^1$ selectivity to 36:1 (entry 6). Optimal results were obtained upon replacing TBABr with TBACl, affording **3aa** in 75% yield (entry 7). Further screening experiments revealed that the N^2/N^1 regioselectivity could be switched to favor the N^1

product **3aa'** with certain additives (Figure 5.3B, see Table 5D.2 for additional data). The initial entries in Figure 5.3B show that additives with halide anions favor formation of the N^2 regioisomer **3aa**. In contrast, additives with triflate anion or Lewis acids, such as silyl triflates or $\text{BF}_3 \cdot \text{OEt}_2$, favor formation of the N^1 regioisomer **3aa'**. Optimal results for the formation of **3aa'** were achieved with trimethylsilyl triflate (TMSOTf) as the additive at 60 °C (67% yield; $N^2:N^1 = 1:66$).

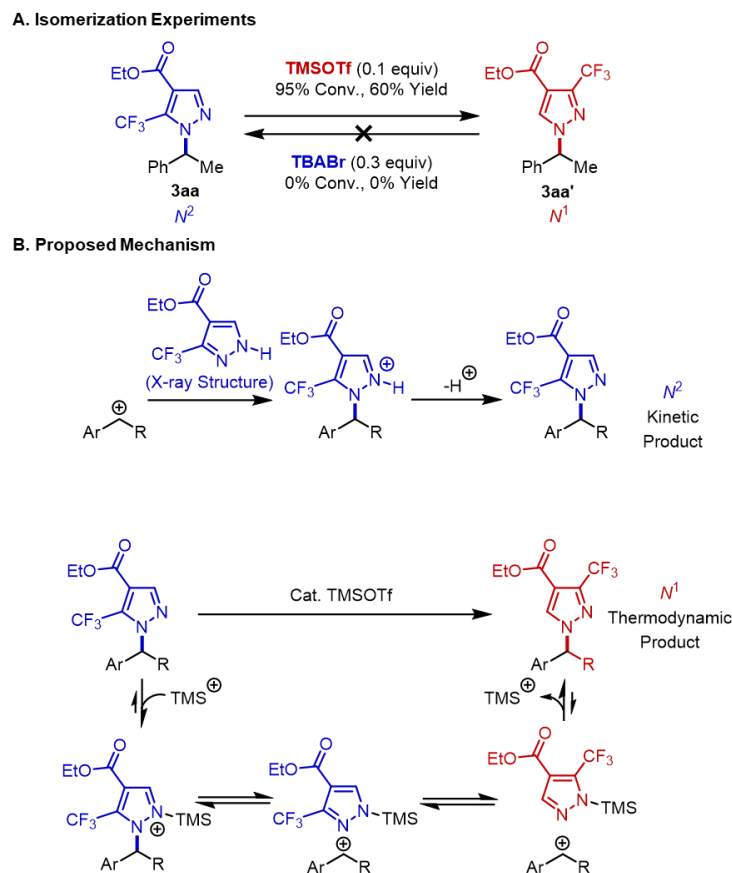


Figure 5.4. Mechanistic origin of pyrazole regioselectivity. (A) N^1/N^2 -isomerization test, implicating the the N^1 . (B) Proposed mechanism rationalizing the influence of TMSOTf (and other Lewis acids) on the N^2/N^1 regioselectivity.

The pyrazole reagent **2a** has an N–H bond at the N^1 position, as revealed by X-ray crystallography and depicted in Figure 5.3A (see Section 5D.VII in Appendix D for details). This structure is consistent with previous reports for other electron-deficient, 3-substituted pyrazoles.²⁸ We postulated that the switch in pyrazole regioselectivity could arise from kinetic versus thermodynamic control over the C–N bond-forming step. Experimental data supported this

hypothesis: addition of addition of TMSOTf to **3aa** induced isomerization of **3aa'**, whereas no isomerization of **3aa'** was observed in the presence of TBABr. These results suggest **3aa** is the kinetic product, and they are rationalized by the non-basic reaction conditions. The observed reactivity with the pyrazole N^2 lone pair (Figure 5.4B, top), contrasts previously reported reactivity with deprotonated pyrazolide reagents which react preferentially at the N^1 site.^{28b, 29} The isomerization data in Figure 3A suggests that strong Lewis acids, such as trimethylsilyl (TMS) cation, can promote isomerization via the benzylic cation and N^2 -TMS species, to the thermodynamically favored N^1 product.^{28b, 30} The data in Figure 5.3A, entries 1-4 suggest that solvents capable of stabilizing charged intermediates also favor the thermodynamic product.

Access to both isomeric pyrazole coupling products is noteworthy because most coupling reactions with pyrazoles employ a base and access only the thermodynamic products.^{29,31} For example, reaction of (1-bromoethyl)benzene with pyrazole **2a** affords exclusively the N^1 isomer **3aa'** (see Section 5D.IV in Appendix D for details). To explore the scope of this reactivity, we evaluated numerous other C–H/N–H cross-coupling reactions with (hetero)benzylic and azole coupling partners (Figures 5.5 and 5.6). Reactions with (hetero)benzylic C–H substrates were initially tested using the TBACl conditions, which tend to be more robust and promote formation of the unique N^2 -pyrazolyl product (Figure 3.5A). Ethylbenzene derivatives with different *p*-substituents are well tolerated (70–86%, **3aa–3da**). While the N^2 product is typically observed under these conditions, only the N^1 product **3ba'** is observed with *p*-MeO-ethylbenzene (**1b**). This result is rationalized by the stability of the benzylic carbocation, which facilitates isomerization to the thermodynamic product (cf. Figure 5.4). The lack of C–N coupling at tertiary C–H sites in reactions with isobutyl- and isopentylbenzene (**3ea**, **3fa**) highlights the exquisite site-selectivity of the HAT steps with the NFSI-derived imidyl radical.^{Error! Bookmark not defined.}^{d,20} The strongly e

electron-withdrawing nitro group in the indane substrate **1g** reduces the product yield (33%, **3ga**).

Benzhydryl *N*-azoles, a

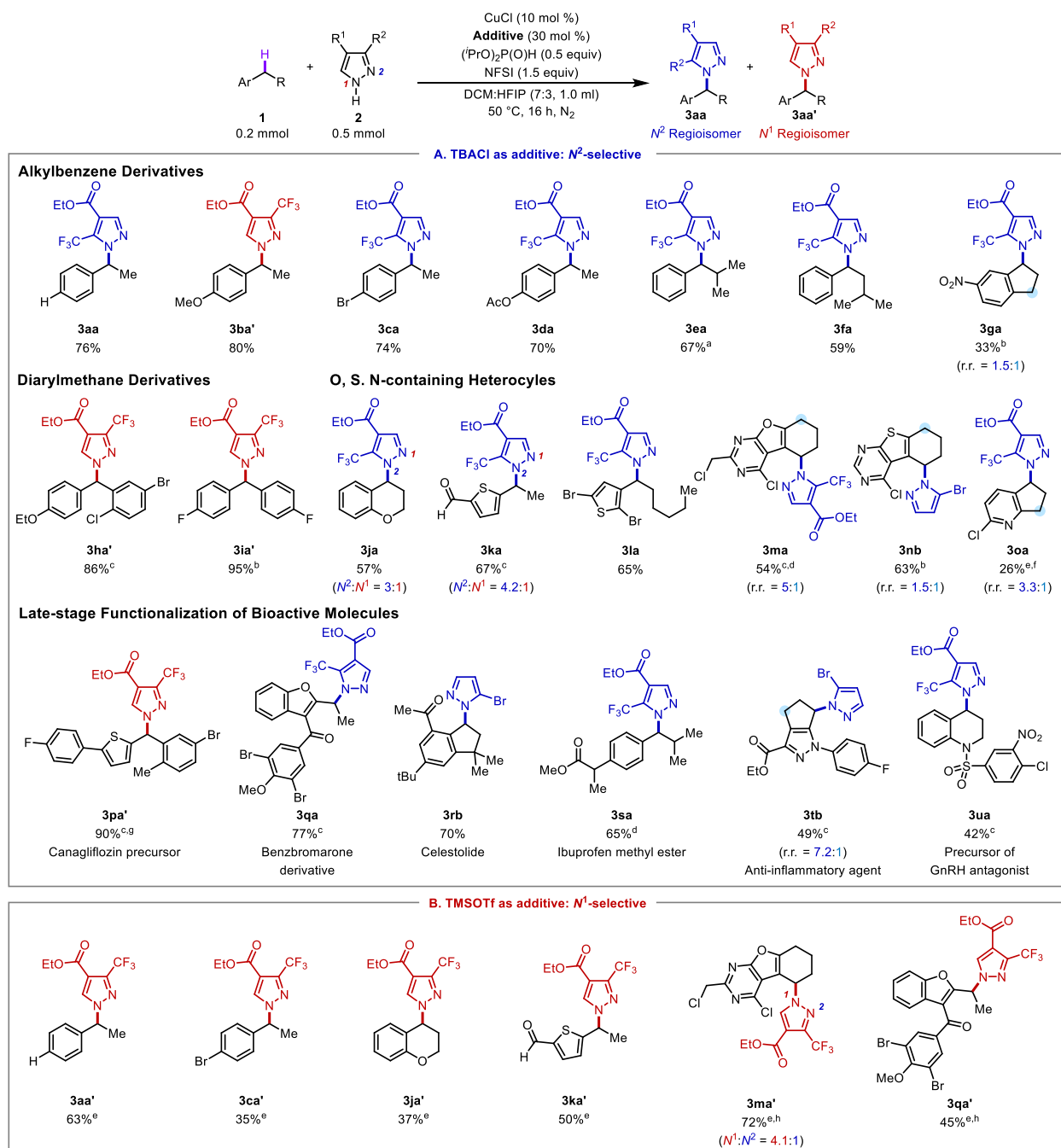


Figure 5.5. Assessment of various benzylic C–H substrates in cross coupling reactions with *N*–H heterocycles with (A) TBACl as the additive for *N*² regioselectivity and (B) with TMSOTf as the additive for *N*¹ regioselectivity. Regioisomers >5% were isolated and reported. ^aConducted in 0.5 mL DCM:HFIP (7:3). ^bConducted with 10 mol % CuBr₂ and 30 mol % TBABr. ^cConducted with

10 mol % TBACl. ^dConducted at 40 °C. ^eConducted at 60 °C. ^fConducted in DCM. ^gConducted at 30 °C. ^hConducted with 10 mol % BF₃•OEt₂.

class of compounds that exhibit aromatase inhibitory activity,³² exhibit good reactivity (86%, **3ha**; 95%, **3ia**) and form only the *N*¹ regioisomers, again rationalized by the benzylic cation stability.

Benzylic pyrazoles of chromans,³³ thiophene,^{14,34} and other substrates bearing oxygen-, sulfur- and nitrogen-containing heterocycles react successfully (**1j–1u**). These reactions demonstrate a tolerance for a formyl group (**3ka**), heteroaryl bromides (**3la**), and pyrimidines (**3ma**, **3nb**).³⁵ The pyridine substrate **1o** reacts in lower yield (26%, **3oa**). Substrates with two possible (hetero)benzylic sites (**1g**, **1m**, **1n**, and **1o**) generate a mixture of products, with moderate to good regioisomeric ratios (r.r.).

Pyrazoles **2a** and 3-bromopyrazole (**2b**) undergo successful late-stage reactivity with bioactive molecules. Examples include an antidiabetic intermediate **1p**, which affords only the *N*¹ coupling product (90%, **3pa'**); benzbromarone methyl ether (77%, **3qa**), a derivative of a xanthine oxidase inhibitor;³⁶ celestolide (70%, **3rb**); ibuprofen methyl ester (65%, **3sa**); an anti-inflammatory anti-allergy agent³⁷ (49%, **3tb**, r.r. = 7.2:1) and a precursor to a GnRH antagonist³⁸ (42%, **3ua**). These results were complemented with a focused assessment of the Lewis acid co-catalytic conditions (Figure 3.5B). These reactions lead to exclusive or high *N*¹ pyrazole site-selectivity in the C–N coupling reactions.

Different pyrazoles and other azole coupling partners were then tested in reactions with indane, motivated by the relevance of *N*-indanyl azoles in medicinal chemistry (Figure 5.6A).³⁹ Symmetrical 4-substituted pyrazoles, bearing fluoro, chloro, iodo, formyl, trifluoromethyl and nitro substituents, undergo coupling in good-to-excellent yields (60–82%, **3vc–3vh**). Other di- and trisubstituted pyrazoles with di- and trifluoromethyl (**2i**, **2j**)^{17a} and sulfonyl chloride (**2k**)

substituents react effectively (52-55% yields, **3vi-3vk**). Successful reactivity, but lower yields are observed with indazole coupling partners **2l** and **2m** (32%, **3vl**; 30%, **3vm**).^{40,41} The dichloropurine derivative **2n** generates both N^9 and N^7 regioisomeric products (58% yield, $N^7:N^9 = 1:1.5$, **3vn**). Triazoles, including 1,2,4- and 1,2,3-isomers **2o** and **2p** and a tetrazole **2q** undergo successful reactivity (77%, **3vo**; 45%, **3vp**; 68%, **3vq**). The reaction with **2p** favors formation of the less common N^1 regioisomer ($N^1:N^2 = 4.6:1$),⁴² consistent with the mechanistic rationale above.

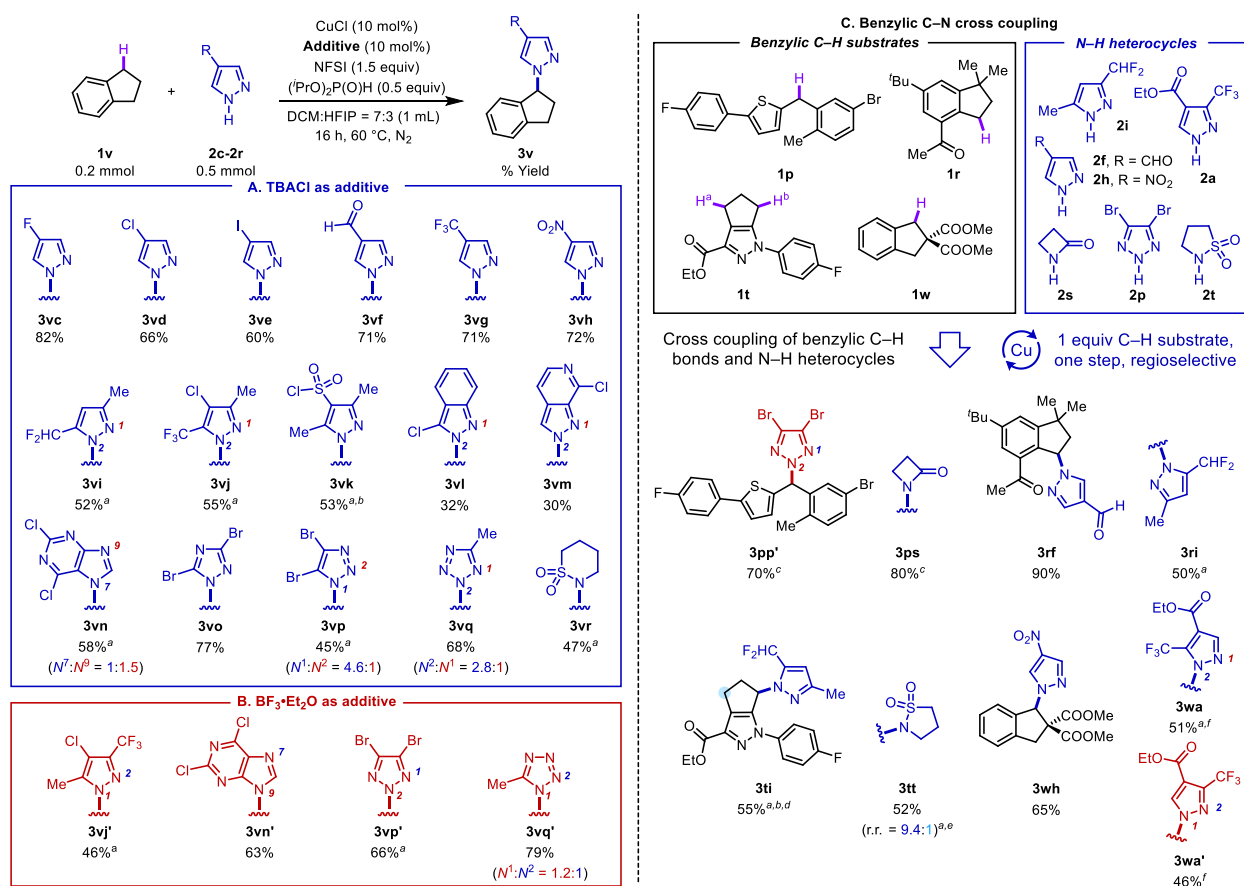


Figure 5.6. Assessment of various N-H heterocycles in cross coupling reactions. Substrate scope with diverse N-H heterocycles and indane under kinetically controlled TBACl conditions (A) and in the presence of $\text{BF}_3 \cdot \text{OEt}_2$ as a Lewis acid cocatalyst (B). Exploration of cross-coupling reactions of diverse N-H heterocycles and (hetero)benzylic C-H scaffolds (C) under the TBACl conditions of Figure 5.6A, unless noted otherwise. Regioisomers formed in >5% yield were isolated. ^aConducted in DCM. ^bConducted at 50 °C. ^cConducted at 30 °C. ^dTrace amount of the other benzylic regioisomer was observed. ^eConducted at 40 °C. ^fConducted with 10 mol % $\text{BF}_3 \cdot \text{OEt}_2$.

Inclusion of $\text{BF}_3 \cdot \text{OEt}_2$ in these reactions enabled modulation of theazole regioselectivity

(results with $\text{BF}_3\cdot\text{OEt}_2$ were slightly better than with TMSOTf). In each of the four cases shown in Figure 5.6B, the favored regioisomer is different from that observed in the TBACl conditions. For example, the reaction with **2j** completely switches from N^2 to N^1 selectivity (46%, **3vj'**). In other cases, use of $\text{BF}_3\cdot\text{OEt}_2$ ensures only a single isomer is formed (63%, **3vn'**; 66%, **3vp'**). In a final assessment of the method, we explored C–N cross coupling reaction with different (hetero)benzylic and *N*-heterocyclic partners (Figure 5.6C). These reactions proceed in moderate-to-excellent yields. The reaction conditions show promise for heterocyclic coupling partners beyond azoles, including the beta-lactam **2s** (80%, **3ps**) and sultams **2r** and **2t** (47%, **3vr**, Figure 5A; 52%, **3tt**, Figure 5.6C). Reactions of the azoles **2a**, **2i**, and **2p** react with the regioselectivity expected from the observation elaborated above. For example, **1p** affords the thermodynamically favored coupling product upon reaction with **2p**, reflecting the stability of benzylic cation. On the other hand, the reaction of **1w** and **2a** afforded the kinetically favored the N^2 regioisomer even with $\text{BF}_3\cdot\text{OEt}_2$ as a cocatalyst (51%, **3wa**). The combined effect of $\text{BF}_3\cdot\text{OEt}_2$ cocatalyst and HFIP as a cosolvent, however, supported a switch in the observed regioselectivity (46%, **3wa'**). The reaction of **1t** and **2i** affords only one of the four possible C–N coupling products (55%, **3ti**), demonstrating both C–H and N-nucleophile selectivity.

5.4. Conclusion

In summary, the results outlined herein introduce a unique synthetic method for direct C(sp³)–H/N–H coupling of (hetero)benzylic substrates and azoles. Multiple features contribute to the potential impact of these methods. Perhaps the most notable feature is the ability to control the azole *N*-site selectivity, often enabling access to either regioisomeric product. Other highlights include the high-to-exclusive (hetero)benzylic C–H site selectivity, use of the C–H substrate as the

limiting reagent, excellent scope for both coupling partners, and broad functional group compatibility. Overall, these C(sp³)-N coupling methods provide efficient access to complex, pharmaceutically relevant structures, and they should find widespread utility for library synthesis and exploration of chemical space in medicinal chemistry and related disciplines.⁴³

5.5. Acknowledgements

The authors thank Iliia A. Guzei and Amelia M. Wheaton for assistance with the X-ray crystallographic characterization of **2a** and [PhN(CH₃)₃]₂[CuBr₄]. This work was supported by funding from the NIH (R35 GM134929). Spectroscopic instrumentation was supported by a gift from Paul. J. Bender, the NSF (CHE-1048642), and the NIH (S10 OD020022).

5.6. Author Contributions

Chen, S.-J.: leading experimental work and manuscript preparation

Golden, D. L: experimental work and manuscript preparation

5.7. References

- 1 Ruiz-Castillo, P.; Buchwald, S. L. Applications of Palladium-Catalyzed C–N Cross-Coupling Reactions. *Chem. Rev.* **2016**, *116*, 12564–12649.
- 2 (a) West, M. J.; Fyfe, J. W. B.; Vantourout, J. C.; Watson, A. J. B. Mechanistic Development and Recent Applications of the Chan–Lam Amination. *Chem. Rev.* **2019**, *119*, 12491–12523. (b) Qiao, J. X.; Lam, P. Y. S. Copper-Promoted Carbon–Heteroatom Bond Cross-Coupling with Boronic Acids and Derivatives. *Synthesis* **2011**, *6*, 829-856.
- 3 Brown, D. G.; Boström, J. Analysis of Past and Present Synthetic Methodologies on Medicinal Chemistry: Where Have All the New Reactions Gone? *J. Med. Chem.* **2016**, *59*, 4443–4458.
- 4 Trowbridge, A.; Walton, S. M.; Gaunt, M. J. New Strategies for the Transition-Metal Catalyzed Synthesis of Aliphatic Amines. *Chem. Rev.* **2020**, *120*, 2613–2692.
- 5 (a) Lovering, F.; Bikker, J.; Humblet, C. Escape from Flatland: Increasing Saturation as an Approach to Improving Clinical Success. *J. Med. Chem.* **2009**, *52*, 6752–6756. (b) Morley, A.

- D.; Pugliese, A.; Birchall, K.; Bower, J.; Brennan, P.; Brown, N.; Chapman, T.; Drysdale, M.; Gilbert, I. H.; Hoelder, S.; Jordan, A.; Ley, S. V.; Merritt, A.; Miller, D.; Swarbrick, M. E.; Wyatt, P. G. Fragment-based hit identification: thinking in 3D. *Drug Discov. Today* **2013**, *18*, 1221–1227.
- 6 Cernak, T.; Dykstra, K. D.; Tyagarajan, S.; Vachal, P.; Krska, S. W. The medicinal chemist's toolbox for late stage functionalization of drug-like molecules. *Chem. Soc. Rev.* **2016**, *45*, 546–576.
- 7 (a) Clark, J. R.; Feng, K.; Sookezian, A.; White, M. C. Manganese-Catalysed Benzylic C(sp³)-H Amination for Late-Stage Functionalization. *Nat. Chem.* **2018**, *10*, 583–591. (b) Chiappini, N. D.; Mack, J. B. C.; Du Bois, J. Intermolecular C(sp³)-H Amination of Complex Molecules. *Angew. Chem. Int. Ed.* **2018**, *57*, 4956–4959.
- 8) (a) Sharma, A.; Hartwig, J. F. Metal-Catalysed Azidation of Tertiary C-H Bonds Suitable for Late-Stage Functionalization. *Nature* **2015**, *517*, 600–604. (b) Huang, X.; Bergsten, T. M.; Groves, J. T. Manganese-Catalyzed Late-Stage Aliphatic C-H Azidation. *J. Am. Chem. Soc.* **2015**, *137*, 5300–5303. (c) Margrey, K. A.; Czaplowski, W. L.; Nicewicz, D. A.; Alexanian, E. J. A General Strategy for Aliphatic C-H Functionalization Enabled by Organic Photoredox Catalysis. *J. Am. Chem. Soc.* **2018**, *140*, 4213–4217. (d) Suh, S.-E.; Chen, S.-J.; Mandal, M.; Guzei, I. A.; Cramer, C. J.; Stahl, S. S. Site-Selective Copper-Catalyzed Azidation of Benzylic C-H Bonds. *J. Am. Chem. Soc.* **2020**, *142*, 11388–11393. (e) Niu, L.; Jiang, C.; Liang, Y.; Liu, D.; Bu, F.; Shi, R.; Chen, H.; Chowdhury, A. D.; Lei, A. Manganese-Catalyzed Oxidative Azidation of C(sp³)-H Bonds under Electrophotocatalytic Conditions. *J. Am. Chem. Soc.* **2020**, *142*, 17693–17702.
- 9 (a) Pandey, G.; Laha, R.; Singh, D. Benzylic C(sp³)-H Functionalization for C-N and C-O Bond Formation via Visible Light Photoredox Catalysis. *J. Org. Chem.* **2016**, *81*, 7161–7171. (b) Yang, Y.-Z.; Song, R.-J.; Li, J.-H. Intermolecular Anodic Oxidative Cross-Dehydrogenative C(sp³)-N Bond-Coupling Reactions of Xanthenes with Azoles. *Org. Lett.* **2019**, *21*, 3228–3231. (c) Hou, Z.-W.; Liu, D.-J.; Xiong, P.; Lai, X.-L.; Song, J.; Xu, H.-C. Site-Selective Electrochemical Benzylic C-H Amination. *Angew. Chem. Int. Ed.* **2020**, *60*, 2943–2947. (d) Hou, Z.-W.; Li, L.; Wang, L. Organocatalytic Electrochemical Amination of Benzylic C-H Bonds. *Org. Chem. Front.* **2021**, *8*, 4700–4705.
- 10 (a) Song, C.; Dong, X.; Yi, H.; Chiang, C.-W.; Lei, A. DDQ-Catalyzed Direct C(sp³)-H Amination of Alkylheteroarenes: Synthesis of Biheteroarenes under Aerobic and Metal-Free Conditions. *ACS Catal.* **2018**, *8*, 2195–2199. (b) Ruan, Z.; Huang, Z.; Xu, Z.; Zeng, S.; Feng, P.; Sun, P.-H. Late-stage azolation of benzylic C-H bonds enabled by electrooxidation. *Sci. China. Chem.* **2021**, *64*, 800–807.
- 11 Eight of top 50 best-selling drugs contain N-benzylic heterocycles: Baumann, M.; Baxendale, I. R.; Ley, S. V.; Nikbin, N. *Beilstein J. Org. Chem.* **2011**, *7*, 442–495.
- 12 Taylor, R. D.; MacCoss, M.; Lawson, A. D. G. Rings in Drugs. *J. Med. Chem.* **2014**, *57*, 5845–5859.
- 13 Estrada, A. A.; Feng, J. A.; Lyssikatos, J. P.; Sweeney, Z. K. Compounds, compositions, and methods. Worldwide patent, WO2017087905 A1, May 26, 2017.
- 14 Hoffman, T. J.; Stierli, D.; Pitterna, T.; Rajan, R. Microbiocidal oxadiazole derivatives. Worldwide patent 2018158365 A1, September 07, 2018.

- 15 Blakemore, D. C.; Castro, L.; Churcher, I.; Rees, D. C.; Thomas, A. W.; Wilson, D. M.; Wood, A. Organic synthesis provides opportunities to transform drug discovery. *Nat. Chem.* **2018**, *10*, 383–394.
- 16 Adams, N. D.; Adams, J. L.; Burgess, J. L.; Chaudhari, A. M.; Copeland, R. A.; Donatelli, C. A.; Drewry, D. H.; Fisher, K. E.; Hamajima, T.; Hardwicke, M. A.; Huffman, W. F.; Koretke-Brown, K. K.; Lai, Z. V.; McDonald, O. B.; Nakamura, H.; Newlander, K. A.; Oleykowski, C. A.; Parrish, C. A.; Patrick, D. R.; Plant, R.; Sarpong, M. A.; Sasaki, K.; Schmidt, S. J.; Silva, D. J.; Sutton, D.; Tang, J.; Thompson, C. S.; Tummino, P. J.; Wang, J. C.; Xiang, H.; Yang, J.; Dhanak, D. Discovery of GSK1070916, a Potent and Selective Inhibitor of Aurora B/C Kinase. *J. Med. Chem.* **2010**, *53*, 3973–4001.
- 17 (a) Mykhailiuk, P. K. Fluorinated Pyrazoles: From Synthesis to Applications. *Chem. Rev.* **2021**, *121*, 1670–1715. (b) Davie, R. L.; Edwards, H. J.; Evans, D. M.; Hodgson, S. T.; Miller, I.; Novak, A. R.; Smith, A. J.; Stocks, M. J. Heterocyclic derivatives. Worldwide Patent 2014188211 A1, November 27, 2014.
- 18 Zhang, W.; Wang, F.; McCann, S. D.; Wang, D.; Chen, P.; Stahl, S. S.; Liu, G. Enantioselective Cyanation of Benzylic C–H Bonds via Copper-Catalyzed Radical Relay. *Science* **2016**, *353*, 1014–1018.
- 19 Suh, S.-E.; Nkulu, L. E.; Lin, S.; Krska, S.; Stahl, S. S. Benzylic C–H Isocyanation/Amine Coupling Sequence Enabling High-Throughput Synthesis of Pharmaceutically Relevant Ureas. *Chem. Sci.* **2021**, *12*, 10380–10387.
- 20 Hu, H.; Chen, S.-J.; Mandal, M.; Pratik, S. M.; Buss, J. A.; Krska, S. W.; Cramer, C. J.; Stahl, S. S. Copper-catalysed benzylic C–H coupling with alcohols via radical relay enabled by redox buffering. *Nat. Catal.* **2020**, *3*, 358–367.
- 21 Liu, S.; Achou, R.; Boulanger, C.; Pawar, G.; Kumar, N.; Lusseau, J.; Robert, F.; Landais, Y. Copper-catalyzed oxidative benzylic C(sp³)–H amination: Direct synthesis of benzylic carbamates. *Chem. Commun.* **2020**, *56*, 13013–13016.
- 22 Xiao, H.; Liu, Z.; Shen, H.; Zhang, B.; Zhu, L.; Li, C. Copper-Catalyzed Late-Stage Benzylic C(sp³)–H Trifluoromethylation. *Chem* **2019**, *5*, 940–949.
- 23 (a) Zhang, W.; Chen, P.; Liu, G. Copper-Catalyzed Arylation of Benzylic C–H bonds with Alkylarenes as the Limiting Reagents. *J. Am. Chem. Soc.* **2017**, *139*, 7709–7712. (b) Zhang, W.; Wu, L.; Chen, P.; Liu, G. Enantioselective Arylation of Benzylic C–H Bonds by Copper-Catalyzed Radical Relay. *Angew. Chem. Int. Ed.* **2019**, *58*, 6425–6429.
- 24 Fu, L.; Zhang, Z.; Chen, P.; Lin, Z.; Liu, G. Enantioselective Copper-Catalyzed Alkynylation of Benzylic C–H Bonds via Radical Relay. *J. Am. Chem. Soc.* **2020**, *142*, 12493–12500.
- 25 Wang, F.; Chen, P.; Liu, G. Copper-Catalyzed Radical Relay for Asymmetric Radical Transformation. *Acc. Chem. Res.* **2018**, *51*, 2036–2046.
- 26 For a survey of other examples of radical C–H functionalization reactions, see: Zhang, C.; Li, Z.-L.; Gu, Q.-S.; Liu, X.-Y. Catalytic Enantioselective C(sp³)–H Functionalization Involving Radical Intermediates. *Nat. Commun.* **2021**, *12*, 475.
- 27 (a) Vasilopoulos, A.; Golden, D. L.; Buss, J. A.; Stahl, S. S. Copper-Catalyzed C–H Fluorination/Functionalization Sequence Enabling Benzylic C–H Cross Coupling with Diverse Nucleophiles. *Org. Lett.* **2020**, *22*, 5753–5757. (b) Buss, J. A.; Vasilopoulos, A.; Golden, D. L.; Stahl, S. S. Copper-Catalyzed Functionalization of Benzylic C–H Bonds with *N*-

Fluorobenzenesulfonimide: Switch from C–N to C–F Bond Formation Promoted by a Redox Buffer and Brønsted Base. *Org. Lett.* **2020**, *22*, 5749–5752.

- 28 (a) Stanovnik, B.; Svete, J. Product Class 1: Pyrazoles. *Science of Synthesis*; Neier, R.; Bellus, D., Eds.; Thieme: Stuttgart, 2002; Vol. 12, pp 15–225. (b) Ivanova, A. E.; Burgart, Y. V.; Saloutin, V. I.; Slepukhin, P. A.; Borisevich, S. S.; Khursan, S. L. Ambident polyfluoroalkyl-substituted pyrazoles in the methylation reactions. *J. Fluor. Chem.* **2017**, *195*, 47–56. (c) Jaćimović, Željko. K.; Novaković, S. B.; Bogdanović, G. A.; Kosović, M.; Libowitzky, E.; Giester, G. Crystal Structure of Ethyl 3-(Trifluoromethyl)-1*H*-Pyrazole-4-Carboxylate, C7H7F3N2O2. *Z. Kristallogr.-New Cryst. Struct.* **2020**, *235*, 1189–1190.
29. Huang, A.; Wo, K.; Lee, S. Y. C.; Kneitschel, N.; Chang, J.; Zhu, K.; Mello, T.; Bancroft, L.; Norman, N. J.; Zheng, S.-L. Regioselective Synthesis, NMR, and Crystallographic Analysis of N1-Substituted Pyrazoles. *J. Org. Chem.* **2017**, *82*, 8864–8872.
30. For selected examples where cations have been used to influence *N*-regioselectivity, see: (a) Goikhman, R.; Jacques, T. L.; Sames, D. C-H Bonds as Ubiquitous Functionality: A General Approach to Complex Arylated Pyrazoles via Sequential Regioselective *C*-Arylation and *N*-Alkylation Enabled by SEM-Group Transposition. *J. Am. Chem. Soc.* **2009**, *131*, 3042–3048. (b) Wang, X.; Wang, Q.; Xue, Y.; Sun, K.; Wu, L.; Zhang, B. An organoselenium-catalyzed N1- and N2-selective aza-Wacker reaction of alkenes with benzotriazoles. *Chem. Commun.* **2020**, *56*, 4436–4439.
31. Hilpert, L. J.; Sieger, S. V.; Haydl, A. M.; Breit, B. Palladium- and Rhodium-Catalyzed Dynamic Kinetic Resolution of Racemic Internal Allenes Towards Chiral Pyrazoles. *Angew. Chem. Int. Ed.* **2019**, *58*, 3378–3381.
32. Jones, C. D.; Winter, M. A.; Hirsch, K. S.; Stamm, N.; Taylor, H. M.; Holden, H. E.; Davenport, J. D.; Krumkalns, E. V.; Suhr, R. G. Estrogen Synthetase Inhibitors. 2. Comparison of the in Vitro Aromatase Inhibitory Activity for a Variety of Nitrogen Heterocycles Substituted with Diarylmethane or Diarylmethanol Groups. *J. Med. Chem.* **1990**, *33*, 416–429.
33. Wang, L.; Doherty, G.; Wang, X.; Tao, Z.-F.; Brunko, M.; Kunzer, A. R.; Wendt, M. D.; Song, X.; Frey, R.; Hansen, T. M.; Sullivan, G. M.; Judd, A.; Souers, A. Apoptosis-inducing agents for the treatment of cancer and immune and autoimmune diseases. Worldwide patent 2013055895 A1, April 18, 2013.
34. (a) Zhi, L.; Grote, M.; Reddy, R. K.; Li, W.; Craig, W. Glucagon Receptor Antagonists. Worldwide patent 2018035172 A1, February 22, 2018.
35. (a) Gangjee, A. Tricyclic Compounds Having Antimitotic and/or Antitumor Activity and Method of Use Thereof. Worldwide patent 2010006032A1, January 14, 2010. (b) Aponte, J. C.; Vaisberg, A. J.; Castillo, D.; Gonzalez, G.; Estevez, Y.; Arevalo, J.; Quiliano, M.; Zimic, M.; Verástegui, M.; Málaga, E.; Gilman, R. H.; Bustamante, J. M.; Tarleton, R. L.; Wang, Y.; Franzblau, S. G.; Pauli, G. F.; Sauvain, M.; Hammond, G. B. Trypanoside, anti-tuberculosis, leishmanicidal, and cytotoxic activities of tetrahydrobenzothienopyrimidines. *Bioorg. & Med. Chem.* **2010**, *18*, 2880–2886.
36. Schepers, G. Benzbromarone therapy in hyperuricaemia; comparison with allopurinol and probenecid. *J. Int. Med. Res.* **1981**, *9*, 511–515.
37. Smith, H. W. Cyclopentapyrazole and tetrahydroindazole compounds. Worldwide patent 8607357, December 18, 1986.

38. Fushimi, N.; Yonekubo, S.; Ohno, K.; Miyagi, T. Nitrogen-containing fused ring derivatives, pharmaceutical compositions containing them and their pharmaceutical use. Japan patent 5308342B2, October 9, 2013.
39. Shu, S.; Cai, X.; Li, J.; Feng, Y.; Dai, A.; Wang, J.; Yang, D.; Wang, M.-W.; Liu, H. Design, synthesis, structure–activity relationships, and docking studies of pyrazole-containing derivatives as a novel series of potent glucagon receptor antagonists. *Bioorg. & Med. Chem.* **2016**, *24*, 2852–2863.
40. Indazoles tend to exist as 1*H*-tautomers: Minkin, V. I.; Garnovskii, A. D.; Elguero, J.; Katritzky, A. R.; Denisko, O. V. The Tautomerism of Heterocycles: Five-Membered Rings with Two or More Heteroatoms. In *Advances in Heterocyclic Chemistry*; Elsevier, 2000; Vol. 76, pp 157–323.
41. Selected methods that achieved indazole *N*2-alkylations: (a) Cheung, M.; Bloor, A.; Stafford, J. A. Efficient and Regioselective Synthesis of 2-Alkyl-2*H*-indazoles. *J. Org. Chem.* **2003**, *68*, 4093–4095. (b) Luo, G.; Chen, L.; Dubowchik, G. Regioselective Protection at *N*-2 and Derivatization at *C*-3 of Indazoles. *J. Org. Chem.* **2006**, *71*, 5392–5395. (c) Slade, D. J.; Pelz, N. F.; Bodnar, W.; Lampe, J. W.; Watson, P. S. Indazoles: Regioselective Protection and Subsequent Amine Coupling Reactions. *J. Org. Chem.* **2009**, *74*, 6331–6334.
42. Wang, X.; Zhang, L.; Krishnamurthy, D.; Senanayake, C. H.; Wipf, P. General Solution to the Synthesis of *N*-2-Substituted 1,2,3-Triazoles *Org. Lett.* **2010**, *12*, 4632–4635.
43. (a) Gordon, E. M.; Barrett, R. W.; Dower, W. J.; Fodor, S. P. A.; Gallop, M. A. Applications of Combinatorial Technologies to Drug Discovery. 2. Combinatorial Organic Synthesis, Library Screening Strategies, and Future Directions. *J. Med. Chem.* **1994**, *37*, 1385–1401. (b) Thompson, L. A.; Ellman, J. A. Synthesis and Applications of Small Molecule Libraries. *Chem. Rev.* **1996**, *96*, 555–600.

Appendix A: Supporting Information Chapter 2

2A.I. General Considerations

Reagents. All reagents were purchased and used as received unless otherwise noted. Tetrakis(acetonitrile)copper(I) hexafluorophosphate, 2,2'-biquinoline, and tert-butyl peroxybenzoate (TBPB) were purchased from Aldrich. Benzylic C–H substrates were purchased from Alfa Aesar, Ambeed, Ark Pharm, AstaTech, Chem-Impex, Combi-Blocks, Enamine, Matrix Chemicals, Millipore Sigma, Oakwood Chemicals and TCI America. HPLC grade dichloromethane was purchased from Sigma Aldrich, was degassed via three freeze-pump-thaw cycles, then was stored with 4Å molecular sieves in the glovebox under N₂ atmosphere. Other solvents were purchased from Fisher Scientific or Aldrich and sparged with N₂ for 30 minutes prior to use. All the reagents were used without further purification. Substrate 1ag was prepared with the procedure reported in literature.¹

Homemade LEDs photoreactors. Photocatalytic reactions were carried out with homemade 6W 450 nm LEDs photoreactors. To ensemble the photoreactor, a 450 nm LED chip (LEDSupply, Part No: CREEXTE-ROY-X) is fixed at the center of black heat sink (LEDSupply, Part No: 102-1489) with a screw and connected with a power transformer (LEDSupply, Part No: APV-12-12), which is surrounded by an aluminum tube (thickness of 2.0 mm, diameter of 5.5 cm, and height of 7.0 cm). The aluminum tube was also connected with the heat sink with screws. The reaction vial is propped up by two paper clips to maintain a 1.5 cm distance between the LED chip and the vial. The reaction vial is cooled by an electric fan (Amazon, ASIN: B012BKZC86) 2 cm above the aluminum tube to maintain the reaction temperature at < 40 °C.

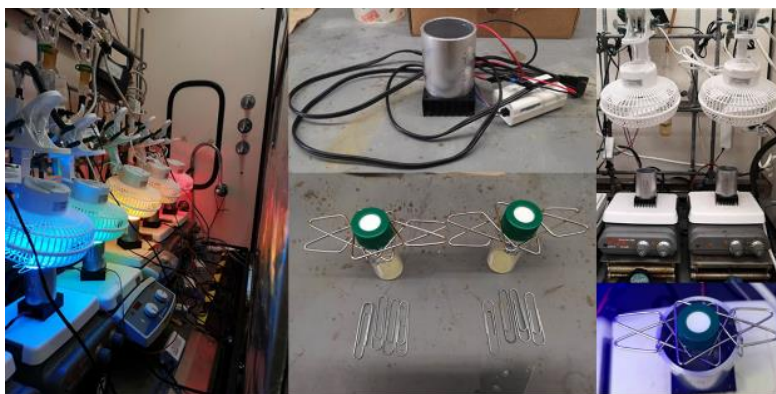


Figure 2A.1. Homemade LED photoreactor

Characterization. ¹H, ¹³C, ¹⁹F and all the 2D NMR spectra were recorded on Bruker 400 MHz or Bruker 500 MHz spectrometers and chemical shifts are reported in parts per million (ppm). ¹H NMR spectra were referenced to tetramethylsilane at 0.00 ppm and ¹³C NMR spectra were referenced to CDCl₃ at 77.16 ppm. Column chromatography was performed using a Biotage Isolera One® with reusable 25 g SNAP Ultra® cartridges, 25 g Sfär® cartridges or standard silica cartridges. Further purification of impure samples was conducted using preparative thin-layer chromatography with Analtech® Glass-Backed Silica G UNIPLATES®. High-resolution mass spectra were obtained using a Thermo Q Exactive™ Plus (ESI or ASAP-MS) by the mass

spectrometry facility at the University of Wisconsin. UV-Vis experiments were performed with a Cary 60 UV-Vis Spectrometer from Agilent in quartz cuvettes.

2A.II. Experimental Procedures for Preparations of Compounds

General Procedure (I) for Photo-promoted Esterification Benzylic C–H Substrates

Tetrakis(acetonitrile)copper(I) hexafluorophosphate (3.7 mg, 0.010 mmol, 10 mol%), 2,2'-biquinoline (3.8 mg, 0.015 mmol, 15 mol%), and benzylic substrate (if solid, 0.10 mmol, 1.0 equiv) were added to a 24 mL glass vial under air with a stir bar. The vial was then moved to a purging glove box under N₂ atmosphere. Dichloromethane (1.5 mL), benzylic substrate (if liquid, 0.10 mmol, 1.0 equiv) and TBPB were added to the reaction vial. The vial was sealed in the glove box and taken out to the homemade LED photoreactor. The reaction was carried out under blue LED (~ 450 nm) irradiation with stirring for the indicated amount of time. When the reaction finished, the mixture was cooled down to room temperature. The crude reaction mixture was filtered through a silica plug using dichloromethane. Mesitylene (14 μL, 0.10 mmol) was added as internal standard. An aliquot (50 μL) from the now homogenous solution was withdrawn for ¹H NMR analysis to detect formation of product and consumption of starting material. After ¹H NMR analysis, the mixture was evaporated under vacuum and the crude mixture was purified by column chromatography or preparative thin layer chromatography (prepTLC).

General Procedure (II) for Deprotection of Benzylic Esters to Alcohols

When the esterification reaction finished, the mixture was cooled down to room temperature and filtered through a silica plug with dichloromethane. The esterification crude mixture was then washed with 2.0 mL of 2.0 M aqueous NaOH solution. The organic phase was collected, and the solvent was evaporated under vacuum. Lithium hydroxide monohydrate (16.8 mg, 0.40 mmol, 4.0 equiv) and 750 μL of methanol:water (2:1) were added to the reaction vial under air. The reaction was carried out with stirring at 70 °C overnight. When the reaction finished, the mixture was extracted with ethyl acetate and water. Then the organic solvent was evaporated under vacuum and the crude mixture was purified by column chromatography.

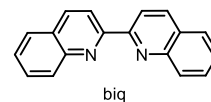
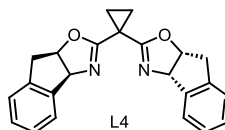
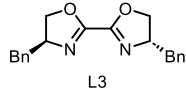
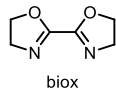
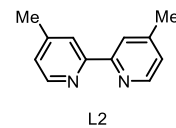
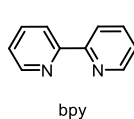
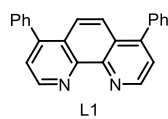
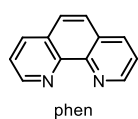
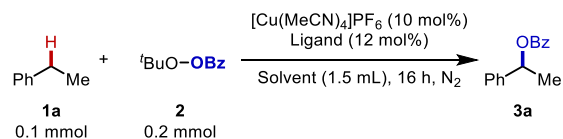
General Procedure (III) for Esterification Benzylic C–H Substrates under Thermal Condition

Tetrakis(acetonitrile)copper(I) hexafluorophosphate (3.7 mg, 0.010 mmol, 10 mol%), 2,2'-biquinoline (3.8 mg, 0.015 mmol, 15 mol%), and ethylbenzene 1a (12.3 μL, 0.1 mmol, 1.0 equiv) were added to a 24 mL glass vial under air. The vial was then moved to a purging glove box under N₂ atmosphere. Dichloromethane or dichloroethane (1.5 mL) and TBPB 2 (38.0 μL, 0.20 mmol, 2.0 equiv) were added to the reaction vial. The vial was sealed in the glove box and taken out to a hot plate. The reaction was heated to 40 °C (dichloromethane as solvent) or 80 °C (dichloroethane as solvent) for 16 hours. When the reaction finished, the mixture was cooled down to room temperature and filtered through a silica plug with dichloromethane. Mesitylene (14 μL, 0.10 mmol) was added as internal standard for ¹H NMR analysis.

2A.III. Optimization of the Reaction Conditions

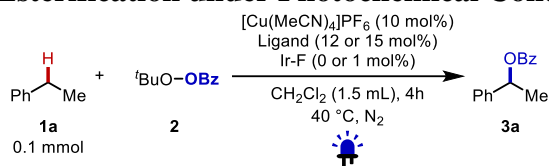
Optimization of reaction conditions were conducted according to general procedure (I) or (III), with variations specified in each table. Reaction yields were monitored by ^1H NMR spectroscopy with 0.1 mmol mesitylene as the internal standard.

Table 2A.1. Benzylic Esterification under Thermal Condition^a



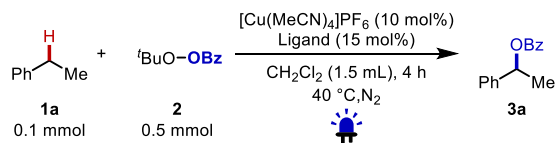
Entry	Solvent	Temperature (°C)	Ligand	Conv. of 1a (%)	Yield of 3a (%)
1	DCE	80	phen	3	3
2	DCE	80	L1	8	0
3	DCE	80	bpy	6	0
4	DCE	80	L2	0	0
5	DCE	80	biox	6	1
6	DCE	80	L3	9	7
7	DCE	80	L4	0	0
8	DCE	80	biq	13	13
9	DCM	40	phen	0	0
10	DCM	40	bpy	0	0
11	DCM	40	biox	0	0
12	DCM	40	biq	0	0

^aConv., conversion.

Table 2A.2. Benzylic Esterification under Photochemical Condition^a

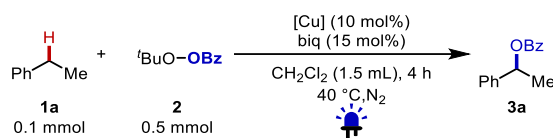
Entry	Ir-F (mol%)	Ligand (mol%)	2 (equiv)	Conv. of 1a (%)	Yield of 3a (%)
1	1	phen (12)	2	11	0
2	1	bpy (12)	2	4	0
3	1	biox (12)	2	16	0
4	1	biq (12)	2	33	20
5	0	biq (12)	2	57	39
6	0	biq (12)	5	73	45
7	0	biq (15)	5	78	58
8 ^b	0	biq (15)	5	99	74

^aConv., conversion. ^bReaction run for 8 h.

Table 2A.3. Assessment of Ancillary Ligands^a

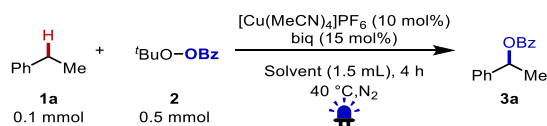
0% Yield 0% Conv.	0% Yield 10% Conv.	0% Yield 5% Conv.	0% Yield 2% Conv.	0% Yield 25% Conv.	0% Yield 4% Conv.
0% Yield 10% Conv.	0% Yield 0% Conv.	52% Yield 73% Conv.	2% Yield 15% Conv.	0% Yield 2% Conv.	0% Yield 4% Conv.
0% Yield 5% Conv.	0% Yield 0% Conv.	20% Yield 99% Conv.	0% Yield 0% Conv.	0% Yield 0% Conv.	Trace 4% Conv.

^aConv., conversion.

Table 2A.4. Copper Salt Screen^a

Entry	Cu salt	Conv. of 1a (%)	Yield of 3a (%)
1	Cu(MeCN) ₄ PF ₆	73	52
2	Cu(MeCN) ₄ BF ₄	26	15
3	Cu(MeCN) ₄ OTf	12	6
4	CuCl	<5	0
5	CuBr	<5	0
6	CuI	<5	0
7	CuOAc	<5	0
8	CuCN	<5	0
9	CuCl ₂	<8	0
10	CuBr ₂	<8	0
11	Cu(OAc) ₂	<8	0
12	Cu(OTf) ₂	35	16
13	Cu(ClO ₄) ₂ ·6H ₂ O	49	24

^aConv., conversion.

Table 2A.5. Solvent Screen^a

Entry	Solvent	Conv. of 1a (%)	Yield of 3a (%)
1	DCM	73	52
2	PhNO ₂	48	26
3	MeNO ₂	40	22
4	C ₆ H ₆	24	12
5	PhCl	57	22
6	PhCF ₃	28	16
7	DCE	47	34
8	DMF	5	0
9	MeCN	24	14
10	Acetone	25	10
11	MeOH	3	0
12	^t BuOH	17	8
13	HFIP	4	4

^aConv., conversion. DCE, 1,2-dichloroethane; DCM, dichloromethane; DMF, dimethylformamide; HFIP, hexafluoroisopropanol

Figure 2A.2. Effect of ligand loading on reactivity

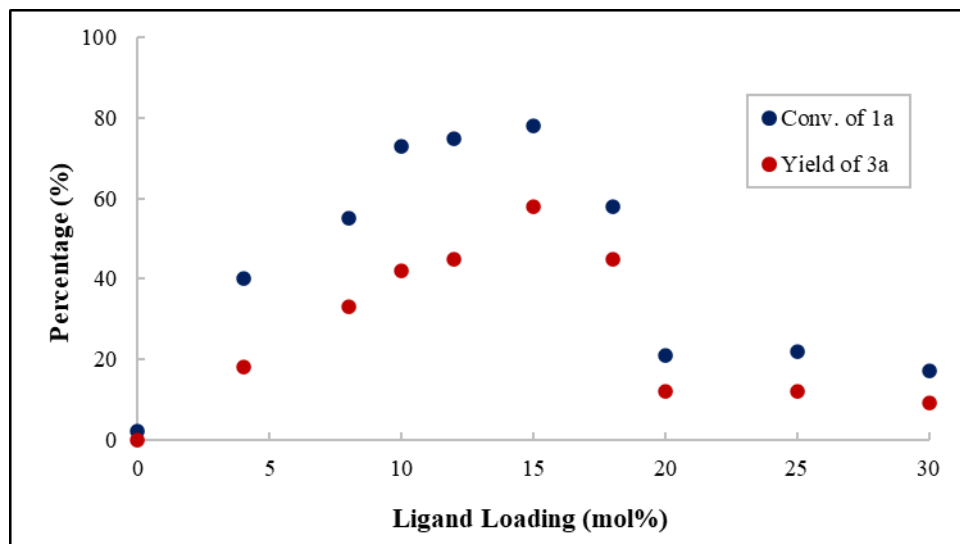
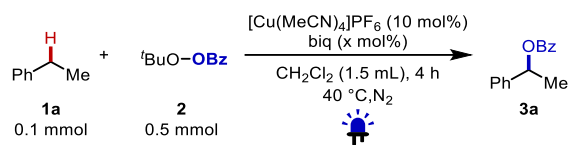
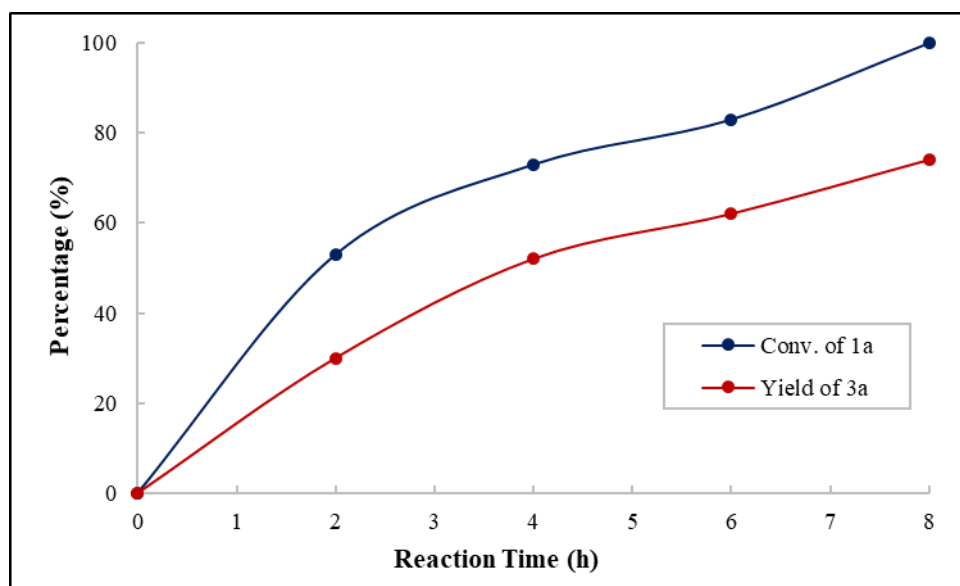
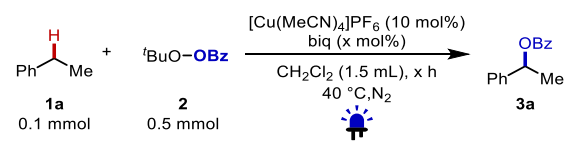


Figure 2A.3. Reaction time course



2A.IV. Additional Experiments with $[\text{Cu}(\text{MeCN})_4]\text{PF}_6$, 2,2'-biquinoline, and TBPB

Experiment 2A.1. UV-visible Experiment with Different Loading of 2,2'-Biquinoline

Tetrakis(acetonitrile)copper(I) hexafluorophosphate (3.7 mg, 0.010 mmol, 1.0 equiv) and 2,2'-biquinoline (biq, 0.0 – 5.1 mg, 0.000 – 0.020 mmol, 0.0 – 2.0 equiv) were added to a 4 mL glass vial under air. The vial was then moved to a purging glove box under N_2 atmosphere. Dichloromethane (1.5 mL) was added to the reaction vial. The vial was sealed in the glove box and stirred overnight. Then, 112.5 μL of the Cu solution was pipetted to a 5 mL volumetric flask and diluted to volume with dichloromethane, affording a stock solution with a total $[\text{Cu}^I]$ of 0.15 mM. The sample for UV-vis measurement was prepared by transferring 2 mL of the 0.15 mM Cu solution to a cuvette.

Table 2A.6. UV-visible Data for Ligand Titration of biq/ Cu^IPF_6

biq conc. (equiv)	Abs @ 549 nm (a.u.)	biq conc. (equiv)	Abs @ 549 nm (a.u.)
0.00	0.0385	1.75	0.7262
0.25	0.0100	2.00	0.8568
0.50	0.0461	2.25	1.0029
0.75	0.0487	2.50	0.9742
1.00	0.1714	2.75	0.9713
1.25	0.3589	3.00	0.9957
1.50	0.5916		

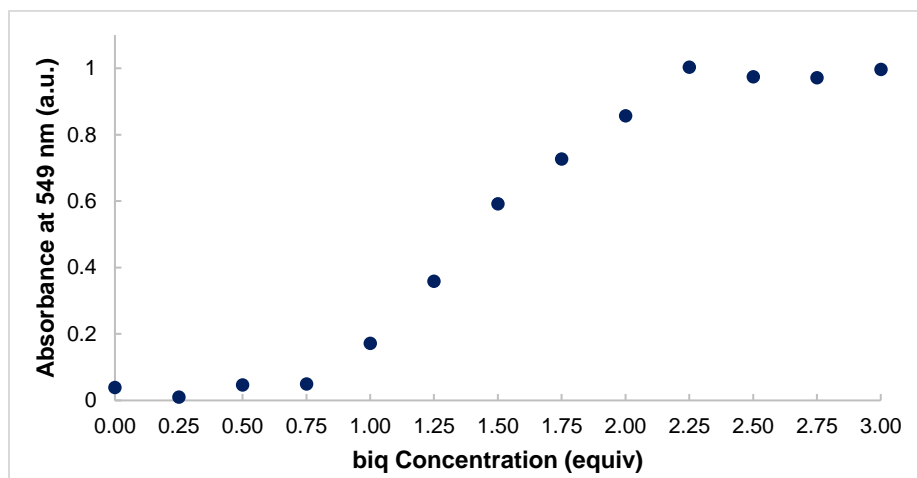


Figure 2A.4. UV-visible data for biq/ Cu^IPF_6 titration experiment

Experiment 2A.2. TBPB Conversion Experiment with Different Loading of 2,2'-Biquinoline

Tetrakis(acetonitrile)copper(I) hexafluorophosphate (37.1 mg, 0.10 mmol, 1.0 equiv) and 2,2'-biquinoline (biq, 25.6 or 51.3 mg, 0.10 or 0.20 mmol, 1.0 or 2.0 equiv) were added to a 4 mL glass vial under air. A 24 mL glass vial was used for photochemical reactions. The vial was then moved to a purging glove box under N₂ atmosphere. Dichloromethane (1.5 mL) and TBPB (9.5 μL, 0.050 mmol, 0.5 equiv) were added to the reaction vial. The vial was sealed in the glove box and brought out to an aluminum heating block. The reaction was carried out with stirring at 40 °C for the indicated amount of time. When the reaction finished, the mixture was filtered through silica with dichloromethane. Mesitylene (14 μL, 0.10 mmol) was added as internal standard. An aliquot (50 μL) from reaction was withdrawn for ¹H NMR analysis to detect consumption of TBPB.

Table 2A.7. Conversion of TBPB with Different Loading of 2,2'-Biquinoline

$$[\text{Cu}(\text{MeCN})_4]\text{PF}_6 + \text{biq} + \text{}^t\text{BuO}-\text{OBz} \xrightarrow[40\text{ }^\circ\text{C, N}_2]{\text{CH}_2\text{Cl}_2 (1.5\text{ mL})} \text{Conversion of } \text{}^t\text{BuO}-\text{OBz}$$

1.0 equiv
0.10 mmol
2

Entry	biq (equiv)	^t BuOOBz (equiv)	Irradiation	Conv. of 2 (equiv)	Remaining 2 (equiv)
1 ^b	1.0	0.5	×	0.5	0.0
2 ^c	2.0	0.5	×	0.02	0.48

^aConv., conversion. ^bReaction run for 10 minutes. ^cReaction run for 30 minutes

Experiment 2A.3. TBPB Titration Experiment with [(biq)Cu^I]⁺ (cf. Figure 2.5B)

Tetrakis(acetonitrile)copper(I) hexafluorophosphate (3.7 mg, 0.010 mmol, 1.0 equiv) and 2,2'-biquinoline (biq, 2.6, 0.010 mmol, 1.0 equiv) were added to a 4 mL glass vial under air. The vial was then moved to a purging glove box under N₂ atmosphere. Dichloromethane (1.5 mL) was added to the reaction vial. The vial was sealed in the glove box and stirred until the reaction mixture was completely soluble. Then, 225 μL of the stock solution was pipetted to a 5 mL volumetric flask and diluted to volume with dichloromethane, affording a stock solution with a total [Cu^I] of 0.30 mM.

A 10 mM stock solution of 2,2'-biquinoline was prepared by adding 5.2 mg of 2,2'-biquinoline to a 4-mL glass vial under air. The vial was then moved to a purging glove box under N₂ atmosphere. Dichloromethane (2.0 mL) was added to the reaction vial. A 10 mM stock solution of TBPB was prepared by adding 9.5 μL of TBPB (0.05 mmol) to a 5 mL volumetric flask and diluted to volume with dichloromethane in the glovebox. Every 3 μL addition of TBPB stock was 0.1 equiv of TBPB with respect to the final [Cu^I] concentration. The sample for UV-visible measurement was prepared by adding 1 mL of the stock solution to the cuvette followed by addition of 850 μL of dichloromethane and TBPB stock. The cuvette was capped and shaken for 30 sec in the glovebox. Then 150 μL of 2,2'-biquinoline (0.75 mM) was added to the cuvette to quench any remaining unreacted Cu^I affording a solution with [Cu] of 0.15 mM.

Table 2A.8. UV-visible Data for Oxidation of (biq)Cu^I by TBPB

Amount of TBPB (equiv)	Abs @ 549 nm (a.u.)	biq conc. (equiv)	Abs @ 549 nm (a.u.)
0.00	0.9062	0.60	0.0805
0.10	0.7144	0.70	0.0699
0.20	0.4123	0.80	0.0763
0.30	0.2286	0.90	0.0748
0.40	0.1129	1.00	0.0776
0.50	0.0791		

Experiment 2A.4. TBPB Titration Experiment with [(biq)₂Cu^I]⁺ (cf. Figure 2.5B)

Tetrakis(acetonitrile)copper(I) hexafluorophosphate (3.7 mg, 0.010 mmol, 1.0 equiv) and 2,2'-biquinoline (biq, 5.6, 0.022 mmol, 2.2 equiv) were added to a 4 mL glass vial under air. The vial was then moved to a purging glove box under N₂ atmosphere. Dichloromethane (1.5 mL) was added to the reaction vial. The vial was sealed in the glove box and stirred until the reaction mixture was completely soluble. Then, 225 μL of the stock solution was pipetted to a 5 mL volumetric flask and diluted to volume with dichloromethane, affording a stock solution with a total [Cu^I] of 0.30 mM. A 10 mM stock solution of TBPB was prepared by adding 9.5 μL of TBPB (0.05 mmol) to a 5 mL volumetric flask and diluted to volume with dichloromethane in the glovebox. Every 3 μL addition of TBPB stock was 0.1 equiv of TBPB with respect to the final [Cu^I] concentration. The sample for UV-visible measurement was prepared by adding 1 mL of the stock solution to the cuvette followed by addition of 1 mL of dichloromethane and TBPB stock. The cuvette was capped and shaken for 30 sec in the glovebox. The final solution for UV-vis analysis had a [Cu] of 0.15 mM.

Table 2A.9. UV-visible Data for Oxidation of (biq)₂Cu^I by TBPB

Amount of TBPB (equiv)	Abs @ 549 nm (a.u.)	biq conc. (equiv)	Abs @ 549 nm (a.u.)
0.00	0.9624	0.60	0.9703
0.10	0.9841	0.70	0.9895
0.20	0.9769	0.80	0.9989
0.30	0.9603	0.90	1.0036
0.40	0.9600	1.00	1.0180
0.50	0.9896		

Experiment 2A.5. Reactivity of biq/Cu^I (1.5:1) / TBPB under blue LED irradiation (cf. Figure 4C)

Tetrakis(acetonitrile)copper(I) hexafluorophosphate (3.7 mg, 0.010 mmol, 1.0 equiv) and 2,2'-biquinoline (biq, 3.8, 0.015 mmol, 1.5 equiv) were added to a 4 mL glass vial under air. The vial was then moved to a purging glove box under N₂ atmosphere. Dichloromethane (1.5 mL) was added to the reaction vial. The vial was sealed in the glove box and stirred until the reaction mixture

was completely soluble. Then, 225 μL of the stock solution was pipetted to a 5-mL volumetric flask and diluted to volume with dichloromethane, affording a stock solution with a total $[\text{Cu}^{\text{I}}]$ of 0.30 mM. The sample for UV-vis measurement was prepared by adding 1 mL of the stock solution to the cuvette followed by addition of 1 mL of dichloromethane ($[\text{Cu}^{\text{II}}] = 0.15 \text{ mM}$). The cuvette was sealed with a PTFE-lined cap in the glovebox. An initial spectrum of the solution was taken without irradiation. A 10 mM stock solution of TBPB was prepared by adding 9.5 μL of TBPB (0.05 mmol) to a 5 mL volumetric flask and diluted to volume with dichloromethane in the glovebox. This solution was then transferred to an 4 mL glass vial and capped with a PTFE-lined septum under N_2 atmosphere.

An initial UV-visible spectrum of the $[\text{Cu}^{\text{I}}]$ solution (0.15 mM) was recorded. Then, a 15 μL aliquot of the TBPB stock solution was injected (0.5 equiv with respect to $[\text{Cu}^{\text{I}}]$) into the cuvette. The vessel was shaken rigorously for 1 min to ensure reactivity between TBPB and Cu^{I} . An UV-visible spectrum was recorded after TBPB addition. The cuvette was then placed under blue LED irradiation. A spectrum was recorded every 2 minutes of blue LED irradiation, ranging from 1 – 13 minutes.

Table 2A.10. UV-visible Data for Reactivity of $\text{biq}/\text{Cu}^{\text{I}}$ (1.5:1) / TBPB under Blue LED Irradiation

Time (min)	Abs @ 549 nm (a.u.)	Time (min)	Abs @ 549 nm (a.u.)
1	0.6325	9	0.5391
3	0.5184	11	0.6842
5	0.4459	13	0.6965
7	0.4586		

Experiment 2A.6. UV-Visible Experiment with $[(\text{biq})_2\text{Cu}^{\text{I}}]\text{PF}_6$ and $[(\text{biq})\text{Cu}^{\text{II}}(\text{OBz})]\text{PF}_6$

$[(\text{biq})_2\text{Cu}^{\text{I}}]\text{PF}_6$ Stock Solution: Tetrakis(acetonitrile)copper(I) hexafluorophosphate (3.7 mg, 0.010 mmol, 1.0 equiv) and 2,2'-biquinoline (biq, 5.1 mg, 0.020 mmol, 2.0 equiv) were added to a 4 mL glass vial under air. The vial was then moved to a purging glove box under N_2 atmosphere. Dichloromethane (1.5 mL) was added to the reaction vial. The vial was sealed in the glove box and stirred until the reaction mixture was completely soluble, affording a stock solution with a total $[\text{Cu}^{\text{I}}]$ of 6.67 mM.

$[(\text{biq})\text{Cu}^{\text{II}}(\text{OBz})]\text{PF}_6$ Stock Solution: Tetrakis(acetonitrile)copper(I) hexafluorophosphate (3.7 mg, 0.010 mmol, 1.0 equiv) and 2,2'-biquinoline (biq, 2.3 mg, 0.009 mmol, 0.9 equiv) were added to a 4 mL glass vial under air. The vial was then moved to a purging glove box under N_2 atmosphere. Dichloromethane (1.5 mL) and TBPB (0.95 μL , 0.005 mmol, 0.5 equiv) were added to the reaction vial. The vial was sealed in the glove box and stirred until the reaction mixture turned green, indicating the oxidation of Cu^{I} to Cu^{II} . This preparation provided a stock solution with a total $[\text{Cu}^{\text{II}}]$ of 6.67 mM.

UV-Visible Sample:

- **$[(\text{biq})_2\text{Cu}^{\text{I}}]\text{PF}_6$ Sample:** 225 μL of the $[(\text{biq})_2\text{Cu}]\text{PF}_6$ stock solution was pipetted to a 5 mL volumetric flask and diluted to volume with dichloromethane, affording a stock solution with

a total $[\text{Cu}^{\text{I}}]$ of 0.30 mM. The sample for UV-visible measurement was prepared by adding 1 mL of the stock solution to the cuvette followed by addition of 1 mL of dichloromethane. The cuvette was sealed with a PTFE-lined cap in the glovebox.

- **$[(\text{biq})_2\text{Cu}^{\text{I}}]\text{PF}_6 + [(\text{biq})\text{Cu}^{\text{II}}(\text{OBz})]\text{PF}_6$ Sample:** 112.5 μL of each stock solution was pipetted to a 5 mL volumetric flask and diluted to volume with dichloromethane, affording a solution with a total $[\text{Cu}]$ of 0.30 mM. The sample for UV-visible measurement was prepared by adding 1 mL of the stock solution to the cuvette followed by addition of 1 mL of dichloromethane. The cuvette was sealed with a PTFE-lined cap in the glovebox.

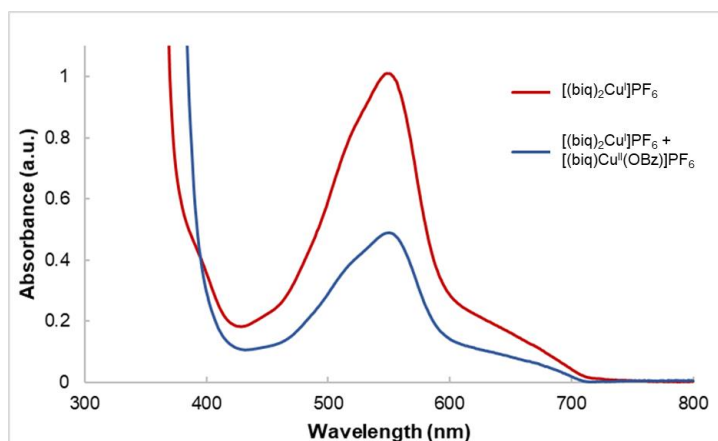


Figure 2A.5. UV-visible data of $[(\text{biq})_2\text{Cu}^{\text{I}}]\text{PF}_6$ and a sample with a 1-to-1 mixture of $[(\text{biq})_2\text{Cu}^{\text{I}}]\text{PF}_6 + [(\text{biq})\text{Cu}^{\text{II}}(\text{OBz})]\text{PF}_6$

2A.V. UV-visible Experiments with Various Ancillary Ligands

Experiment 2A.7. UV-visible Experiment with in-situ oxidation of LCu^{I} (cf. Figure 2.5A)

Tetrakis(acetonitrile)copper(I) hexafluorophosphate (3.7 mg, 0.010 mmol, 1 equiv) and 1,10-phenanthroline (phen, 2.7 mg, 0.015 mmol, 1.5 equiv) were added to a 4 mL glass vial under air. The vial was then moved to a purging glove box under N_2 atmosphere. Dichloromethane (1.5 mL) was added to the reaction vial. The vial was sealed in the glove box and stirred until the reaction mixture was completely soluble. Then, 225 μL of the stock solution was pipetted to a 5 mL volumetric flask and diluted to volume with dichloromethane, affording a stock solution with a total $[\text{Cu}^{\text{I}}]$ of 0.30 mM. The sample for UV-visible measurement was prepared by adding 1 mL of the stock solution to the cuvette followed by addition of 1 mL of dichloromethane. The cuvette was sealed with a PTFE-lined cap in the glovebox. The preparation was repeated for 2,2'-bipyridine (bpy, 2.3 mg, 0.015 mmol, 1.5 equiv) and 2,2'-biquinoline (biq, 3.8 mg, 0.015 mmol, 1.5 equiv) as the ancillary ligands. A 10 mM stock solution of TBPB was prepared by adding 19.1 μL of TBPB (0.1 mmol) to a 10-mL volumetric flask and diluted to volume with dichloromethane in the glovebox. This solution was then transferred to an 8 mL glass vial and capped with a PTFE-lined septum under N_2 atmosphere.

An initial UV-visible spectrum of each $[\text{Cu}^{\text{I}}]$ solution (0.15 mM) was recorded prior to addition of TBPB. A 15 μL aliquot of the TBPB stock solution was injected (0.5 equiv with respect to $[\text{Cu}^{\text{I}}]$)

into the cuvette. The vessel was shaken rigorously for 1 min to ensure even reactivity between TBPB and Cu^{I} . Spectra were collected after 1 minute for reactions with phen and bpy. UV-visible spectra were collected for reaction with biq were collected after 1 minute of mixing then 2, 4, and 5 days with heating at 40 °C.

Experiment 2A.8. UV-visible Experiment with $\text{LCu}^{\text{II}}\text{X}$ under blue LED irradiation (cf. Figure 2.5D)

Tetrakis(acetonitrile)copper(I) hexafluorophosphate (3.7 mg, 0.010 mmol, 1 equiv) and 1,10-phenanthroline (phen, 2.7 mg, 0.015 mmol, 1.5 equiv) were added to a 4 mL glass vial under air. The vial was then moved to a purging glovebox under N_2 atmosphere. Dichloromethane (1.5 mL) and TBPB (1.5 μL , 0.008 mmol, 0.8 equiv) were added to the reaction vial. The vial was sealed by a PTFE-lined septum and removed from the glovebox. The reactions were set to stir at 35 °C on a stir plate at 450 rpm for 16 h. The preparation was repeated twice with 2,2'-bipyridine (bpy, 2.3 mg, 0.015 mmol, 1.5 equiv) and 2,2'-biquinoline (biq, 3.8 mg, 0.015 mmol, 1.5 equiv) as the ancillary ligands.

At the end of the reaction, the mixture with phen and bpy became blue while the mixture with biq became green. The reaction vials were allowed to cool to room temperature and moved to a purging glovebox under N_2 atmosphere. Then, 225 μL of the reaction mixture was pipetted to a 5 mL volumetric flask and diluted to volume with dichloromethane, affording a stock solution with a total $[\text{Cu}^{\text{II}}]$ of 0.30 mM. The sample for UV-visible measurement was prepared by adding 1 mL of the stock solution to the cuvette followed by addition of 1 mL of dichloromethane ($[\text{Cu}^{\text{II}}] = 0.15 \text{ mM}$). The cuvette was sealed with a PTFE-lined cap in the glovebox. An initial spectrum of the solution was taken without irradiation. Subsequently, a spectrum was recorded every 2 minutes of blue LED irradiation, ranging from 2 – 10 minutes.

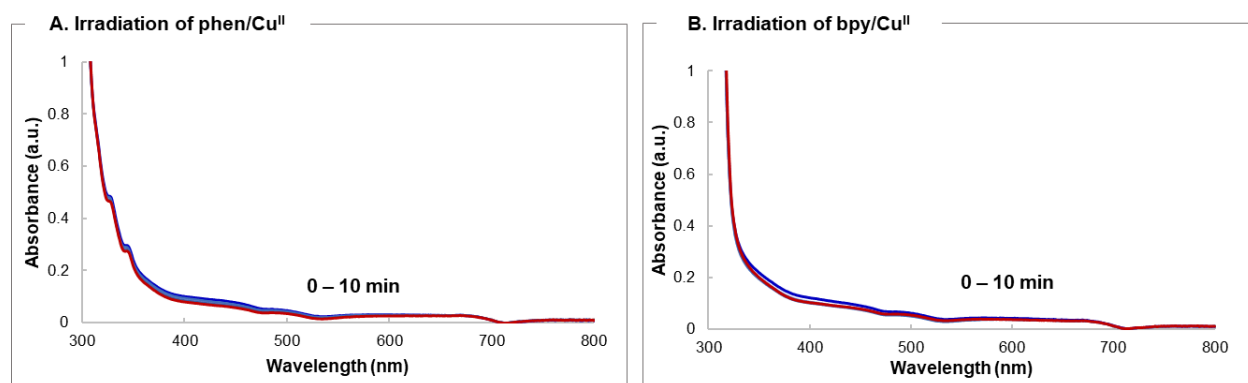


Figure 2A.6. UV-visible absorption spectra of phen/ Cu^{II} and bpy/ Cu^{II} under 450 nm irradiation. UV-visible absorption spectrum of biq/ Cu^{II} under 450 nm irradiation was included in Figure 2.5D.

2A.VI. Unsuccessful Benzylic C–H Substrates

Not all substrates tested afforded good reactivity in the esterification reaction, and a survey of suboptimal results are provided in Figure 2A.7.

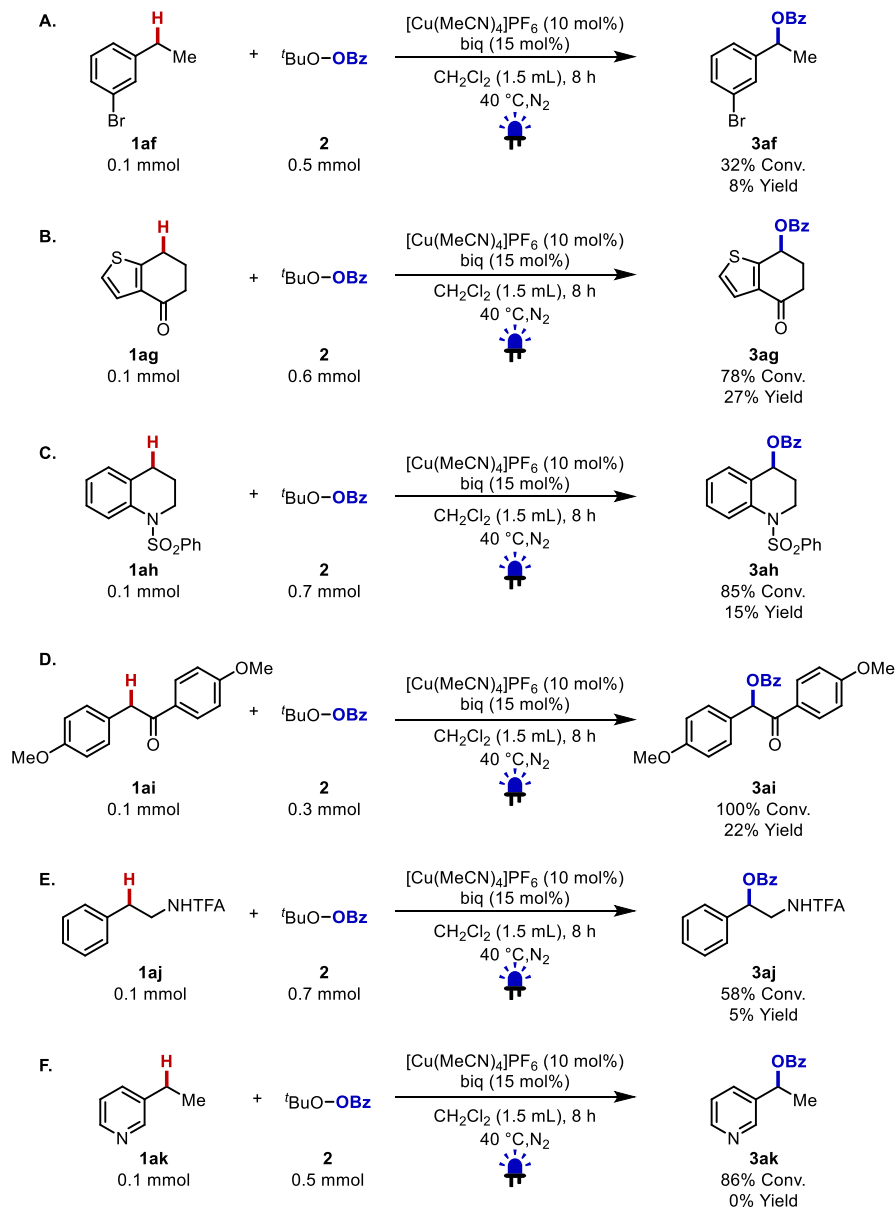


Figure 2A.7. Screening data with additional benzylic C–H substrates.

2A.VII. Crystallization and Crystallographic Data for $C_{25}H_{17}CuF_6N_2O_2P$ (Cu^{II} -OBz)

Preparation

Tetrakis(acetonitrile)copper(I) hexafluorophosphate (372.7 mg, 1.0 mmol, 1.0 equiv.) and 2,2'-biquinoline (256.3 mg, 1.0 mmol, 1.0 equiv.) were weighed into a 100 mL round-bottom flask covered in electrical tape to avoid light exposure. The flask was transferred into a glove box under nitrogen atmosphere. Dichloromethane (30 mL) and *tert*-butyl peroxybenzoate (190.2 μ L, 1.0 mmol, 1.0 equiv.) were then added into the flask. The flask was then sealed with a septum and removed from the glove box. The reaction mixture was then stirred for 16 h. The solvent was removed under vacuum to obtain some green crystals. A small amount of green crystals was transferred into a 4 mL glass vial and dissolved in dichloromethane in a glove box nitrogen atmosphere. The 4 mL glass vial was placed inside a 24 mL glass vial containing pentane. The 24 mL glass vial was then sealed with a 15 mL Teflon cap and transferred into a freezer in the glove box to allow vapor diffusion. A green crystal $C_{25}H_{17}CuF_6N_2O_2P$ was found in the glass vial.

Crystallographic Data for $C_{25}H_{17}CuF_6N_2O_2P$ (Cu^{II} -OBz)

Data Collection

A green crystal with approximate dimensions $0.116 \times 0.078 \times 0.038$ mm³ was selected under oil under ambient conditions and attached to the tip of a MiTeGen MicroMount[®]. The crystal was mounted in a stream of cold nitrogen at 100(1) K and centered in the X-ray beam by using a video camera.

The crystal evaluation and data collection were performed on a Bruker D8 VENTURE PhotonIII four-circle diffractometer with Cu K α ($\lambda = 1.54178$ Å) radiation and the detector to crystal distance of 4.0 cm.²

The initial cell constants were obtained from a 180° ϕ scan conducted at a $2\theta = 50^\circ$ angle with the exposure time of 1 second per frame. The reflections were successfully indexed by an automated indexing routine built in the APEX3 program. The final cell constants were calculated from a set of 9732 strong reflections from the actual data collection.

The data were collected by using the full sphere data collection routine to survey the reciprocal space to the extent of a full sphere to a resolution of 0.77 Å. A total of 57564 data were harvested by collecting 24 sets of frames with 1° scans in ω and ϕ with an exposure time 1–4 sec per frame. These highly redundant datasets were corrected for Lorentz and polarization effects. The absorption correction was based on fitting a function to the empirical transmission surface as sampled by multiple equivalent measurements.³

Structure Solution and Refinement

The systematic absences in the diffraction data were uniquely consistent for the space group $P2_1/n$ that yielded chemically reasonable and computationally stable results of refinement.^{4–9}

A successful solution by intrinsic phasing provided most non-hydrogen atoms from the *E*-map. The remaining non-hydrogen atoms were located in an alternating series of least-squares cycles and difference Fourier maps. All non-hydrogen atoms except those in the minor disorder components were refined with anisotropic displacement coefficients. All hydrogen atoms were included in the structure factor calculation at idealized positions and were allowed to ride on the neighboring atoms with relative isotropic displacement coefficients.

The PF_6^- anion is disordered over three positions in a 81.1(3):10.0(3):8.9(3) ratio. The minor disorder components were refined isotropically with geometry restraints and atomic displacement parameter constraint.¹⁰

The final least-squares refinement of 380 parameters against 4881 data resulted in residuals R (based on F^2 for $I \geq 2\sigma$) and wR (based on F^2 for all data) of 0.0378 and 0.0903, respectively. The final difference Fourier map was featureless.

Summary

Crystal Data for $C_{25}H_{17}CuF_6N_2O_2P$ ($M = 585.91$ g/mol): monoclinic, space group $P2_1/n$ (no. 14), $a = 10.1444(8)$ Å, $b = 13.8188(9)$ Å, $c = 16.6587(14)$ Å, $\beta = 104.893(6)^\circ$, $V = 2256.8(3)$ Å³, $Z = 4$, $T = 100.00$ K, $\mu(\text{CuK}\alpha) = 2.756$ mm⁻¹, $D_{\text{calc}} = 1.724$ g/cm³, 57564 reflections measured ($8.432^\circ \leq 2\Theta \leq 158.992^\circ$), 4881 unique ($R_{\text{int}} = 0.0439$, $R_{\text{sigma}} = 0.0186$) which were used in all calculations. The final R_1 was 0.0378 ($I > 2\sigma(I)$) and wR_2 was 0.0903 (all data).

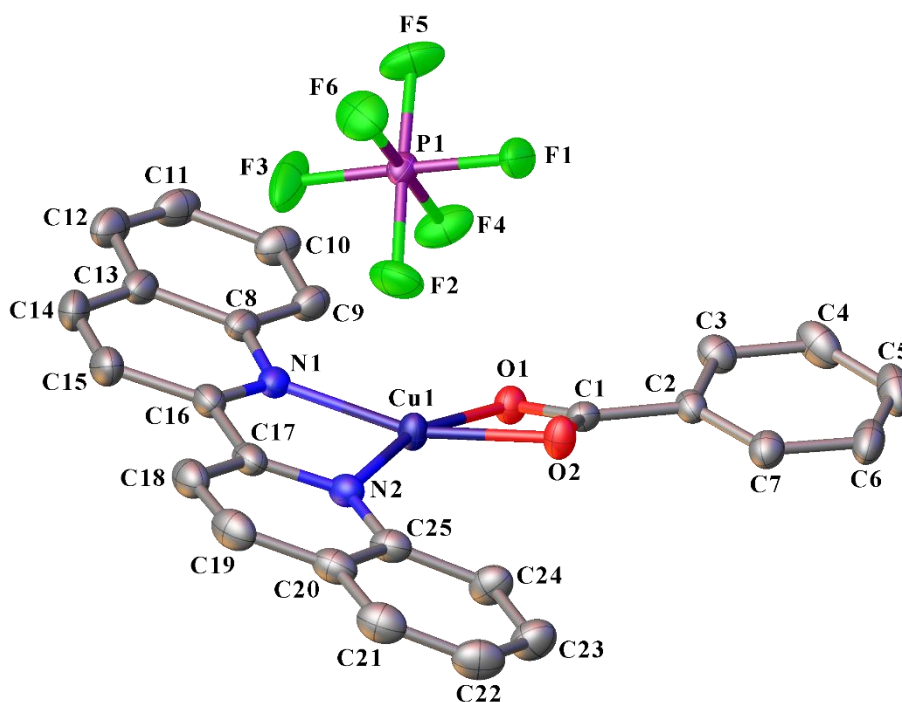


Figure 2A.8. A molecular drawing of $C_{25}H_{17}CuF_6N_2O_2P$ shown with 50% probability ellipsoids. All H atoms and minor disorder components are omitted.

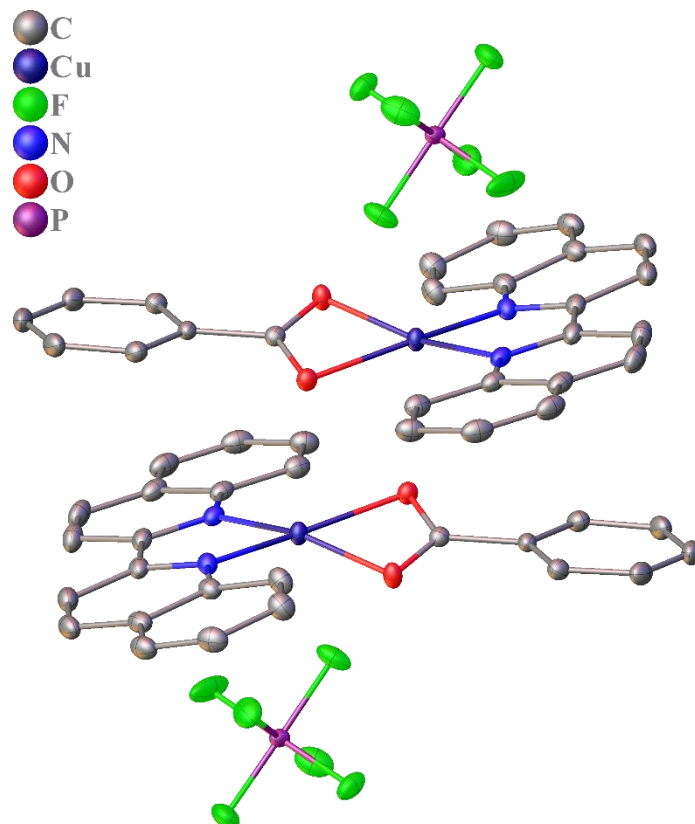


Figure 2A.9. A molecular drawing of C₂₅H₁₇CuF₆N₂O₂P shown with 30% probability ellipsoids. Note the possible dimeric nature of the complex. The Cu...O separation is 2.6720(15) Å. All H atoms and minor disorder components are omitted.

Table 2A.11. Crystal Data and Structure Refinement for C₂₅H₁₇CuF₆N₂O₂P

Empirical formula	[C ₂₅ H ₁₇ CuN ₂ O ₂][PF ₆]
Formula weight	585.91
Temperature/K	100.00
Crystal system	monoclinic
Space group	P2 ₁ /n
a/Å	10.1444(8)
b/Å	13.8188(9)
c/Å	16.6587(14)
α/°	90
β/°	104.893(6)
γ/°	90
Volume/Å ³	2256.8(3)
Z	4
ρ _{calc} /cm ³	1.724
μ/mm ⁻¹	2.756
F(000)	1180.0
Crystal size/mm ³	0.116 × 0.078 × 0.038
Radiation	CuKα (λ = 1.54178)
2θ range for data collection/°	8.432 to 158.992
Index ranges	-12 ≤ h ≤ 12, -17 ≤ k ≤ 17, -21 ≤ l ≤ 21
Reflections collected	57564
Independent reflections	4881 [R _{int} = 0.0439, R _{sigma} = 0.0186]
Data/restraints/parameters	4881/37/380
Goodness-of-fit on F ²	1.130
Final R indexes [I ≥ 2σ (I)]	R ₁ = 0.0378, wR ₂ = 0.0891
Final R indexes [all data]	R ₁ = 0.0404, wR ₂ = 0.0903
Largest diff. peak/hole / e Å ⁻³	0.47/-0.36

2A.VIII. Additional Experiments and Observations

Experiment 2A.9. Irradiation of $\text{Cu}^{\text{II}}\text{-OBz}$ under Blue LED (cf. Figure 2.5E)

$[(\text{biq})\text{Cu}^{\text{II}}(\text{OBz})]\text{PF}_6$ (58.5 mg, 0.10 mmol) was added into a 24 mL glass vial under air. The vial was then moved to a glove box under N_2 atmosphere. Dichloromethane (2.5 mL) was added into vial. The vial was sealed in the glove box and taken out to the homemade LED photoreactor. The reaction was carried out under blue LED irradiation with stirring for 8 hours. When the reaction finished, the mixture was cooled down to room temperature and filtered through a silica plug with dichloromethane. Mesitylene (14 μL , 0.10 mmol) was added as internal standard for ^1H NMR analysis.

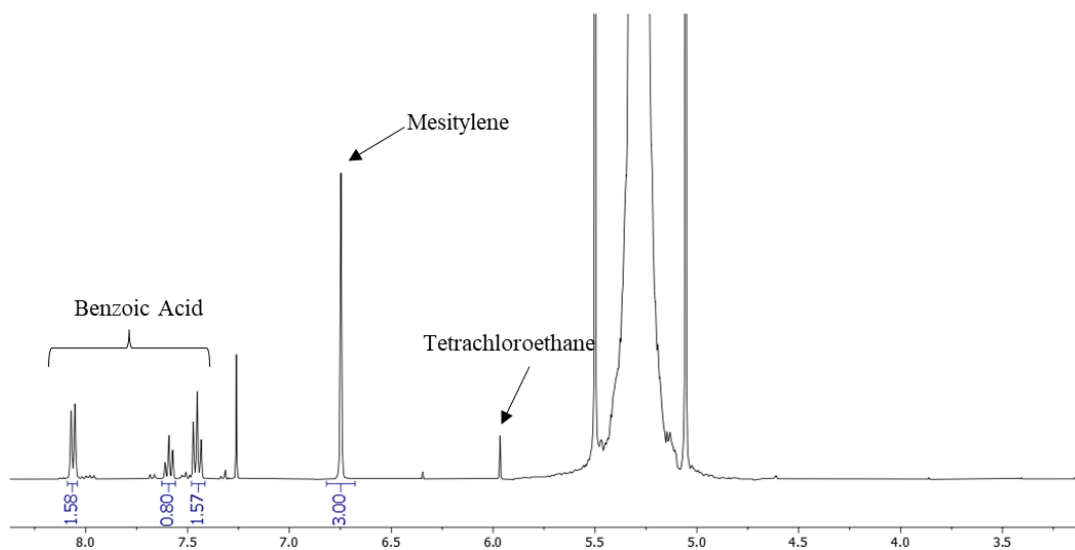


Figure 2A.10. ^1H NMR spectrum for irradiation of $\text{C}_{25}\text{H}_{17}\text{CuF}_6\text{N}_2\text{O}_2\text{P}$ under blue LED irradiation.

Experiment 2A.10. Coupling of **1a** and **2** using $\text{Cu}^{\text{II}}\text{-OBz}$ as Catalyst (cf. Figure 2.5F)

$[(\text{biq})\text{Cu}^{\text{II}}(\text{OBz})]\text{PF}_6$ (5.9 mg, 0.01 mmol, 10 mol%) was added to a 24 mL glass vial under air. The vial was then moved to a glove box under N_2 atmosphere. Dichloromethane (1.5 mL), ethylbenzene **1a** (12.3 μL , 0.1 mmol, 1.0 equiv) and TBPB **2** (95.1 μL , 0.5 mmol, 5 equiv) were added to the reaction vial. The vial was sealed in the glove box and taken out to the homemade LED photoreactor. The reaction was carried out under blue LED (~ 450 nm) irradiation with stirring for 8 hours. When the reaction finished, the mixture was cooled down to room temperature and filtered through a silica plug with dichloromethane. Mesitylene (14 μL , 0.10 mmol) was added as internal standard for ^1H NMR analysis.

Experiment 2A.11. Irradiation of $\text{Cu}^{\text{II}}\text{-OBz}$ in presence of C–H substrate under Blue LED

$[(\text{biq})\text{Cu}^{\text{II}}(\text{OBz})]\text{PF}_6$ (29.3 mg, 0.05 mmol) was added into a 24 mL glass vial under air. The vial was then moved to a glove box under N_2 atmosphere. Dichloromethane (1.25 mL) was added into the vial. Ethylbenzene (6.2 μL , 0.05 mmol, 1 equiv) or 4-ethylanisole (6.6 μL , 0.05 mmol, 1 equiv) was added into the vial. The vial was sealed in the glove box and taken out to the homemade LED photoreactor. The reaction was carried out under blue LED irradiation with stirring for 8 hours.

When the reaction finished, the mixture was cooled down to room temperature. 2,2'-Biquinoline (12.8 mg, 0.05 mmol, 1 equiv) was added to the vial to quench any mono-ligated (biq)Cu^I. The reaction vial was allowed to stir for 30 minutes to allow for complexation. The reaction was filtered through a silica plug with dichloromethane. Mesitylene (7 μ L, 0.05 mmol) was added as internal standard for ¹H NMR analysis.

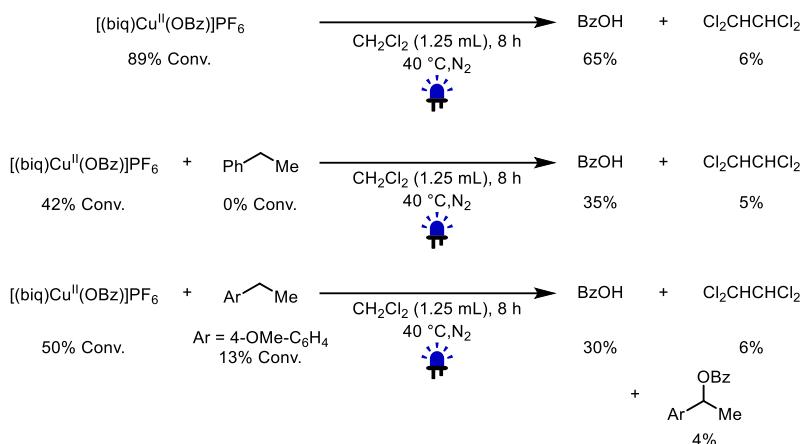


Figure 2A.11. ¹H NMR analysis for irradiation of $[(\text{biq})\text{Cu}^{\text{II}}(\text{OBz})]\text{PF}_6$ under blue LED irradiation in presence of substrate. Conv., conversion.

Experiment 2A.12. Quantum Yield Determination

Determination of the light intensity at 458 nm: The intensity of the 458 nm blue LED light source used in this study was determined following previously reported procedures.^{11,12} A 0.15 M solution of potassium ferrioxalate was prepared by dissolving 2.21 g of potassium ferrioxalate hydrate in 30 mL H₂SO₄ (0.05 M). A buffered solution of phenanthroline was prepared by dissolving 50.0 mg of phenanthroline and 11.25 g of sodium acetate in 50 mL H₂SO₄ (0.5 M). Both solutions were wrapped with aluminum foil and stored in the dark. Next, a Schlenk tube was completely covered in black tape except for a small hole at the bottom (see Figure S11). The prepared tube was charged with 5 mL of the ferrioxalate solution and irradiated for 10 seconds. This solution was then treated with 0.875 mL buffered phenanthroline solution and stirred for 1 h in dark to allow the ferrous ions to completely coordinate to the phenanthroline. The absorbance of the resulting solution was measured at 510 nm. A non-irradiated sample was also prepared, and the absorbance was measured at 510 nm. Finally, the conversion of ferrioxalate was calculated as below:

$$\text{mol Fe}^{2+} = V \cdot \Delta A / (l \cdot \epsilon) = 0.00587 \text{ L} \cdot (2.72 - 0.0805) / (1 \cdot 11,100) = 1.40 \times 10^{-6} \text{ mol}$$

where V is the total volume (0.005875 L) of the solution after addition of phenanthroline, ΔA is the difference in absorbance at 510 nm between the irradiated and non-irradiated solutions, l is the path length (1.000 cm), and ϵ is the molar absorptivity at 510 nm (11,100 L mol⁻¹ cm⁻¹).¹³



Figure 2A.12. Taped Schlenk Tube.

The photon flux was calculated as follows:

$$\text{photon flux} = \text{mol Fe}^{2+} / (\Phi \cdot t \cdot f) = 1.40 \times 10^{-6} / (0.845 \cdot 10 \cdot 0.998) = 1.66 \times 10^{-7} \text{ einstein s}^{-1}$$

where Φ is the quantum yield for the ferrioxalate actinometer (0.845 for a 0.15 M solution),^{14,15} t is the irradiation time (10 s), and f is the fraction of light absorbed at $\lambda = 458 \text{ nm}$ of the ferrioxalate solution (see below for details).

Determination of fraction of light absorbed at 458 nm for the ferrioxalate solution: The absorbance of the irradiated ferrioxalate solution at 458 nm was measured to be 2.625. The fraction of light absorbed (f) by this solution was calculated as below:

$$f = 1 - 10^{-A} = 1 - 10^{-2.625} = 0.998$$

where A is the measured absorbance of the ferrioxalate solution at 458 nm.

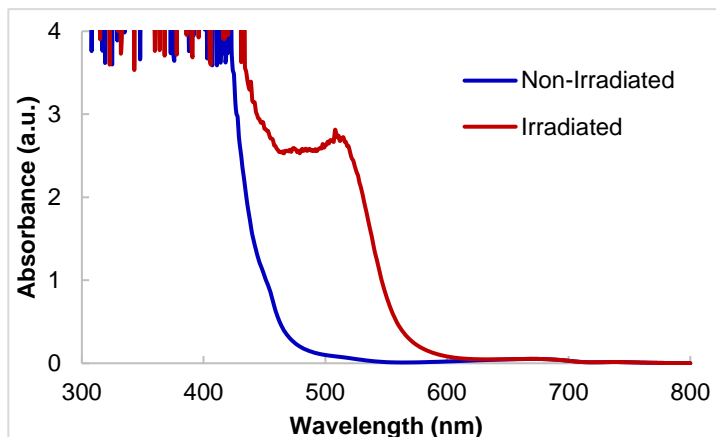


Figure 2A.13. Absorption spectrum of the ferrioxalate solution.

Determination of fraction of light absorbed at 458 nm for the $[(\text{biq})\text{Cu}^{\text{II}}(\text{OBz})]\text{PF}_6$ solution: We performed the quantum yield determination for two different $[(\text{biq})\text{Cu}^{\text{II}}(\text{OBz})]\text{PF}_6$ concentrations, including 5 and 10 mol% at 0.1 mmol scale in 1.5 mL of CH_2Cl_2 .

5 mol% [(biq)Cu^{II}(OBz)]PF₆ solution: The absorbance of [(biq)Cu^{II}(OBz)]PF₆ in CH₂Cl₂ was measured at the reaction concentration of 3.3×10^{-3} M. The measured solution was prepared by dissolving 2.9 mg of [(biq)Cu^{II}(OBz)]PF₆ (C₂₅H₁₇CuF₆N₂O₂P) in 1.5 mL of CH₂Cl₂ in the glovebox. The absorbance of the 5 mol% [(biq)Cu^{II}(OBz)]PF₆ solution at 458 nm was measured to be 0.0984. The fraction of light absorbed (f) by this solution was calculated as below:

$$f = 1 - 10^{-A} = 1 - 10^{-0.0984} = 0.202$$

where A is the measured absorbance of the 5 mol% [(biq)Cu^{II}(OBz)]PF₆ solution at 458 nm.

10 mol% [(biq)Cu^{II}(OBz)]PF₆ solution: The absorbance of [(biq)Cu^{II}(OBz)]PF₆ in CH₂Cl₂ was measured at the reaction concentration of 6.7×10^{-3} M. The measured solution was prepared by dissolving 5.9 mg of [(biq)Cu^{II}(OBz)]PF₆ (C₂₅H₁₇CuF₆N₂O₂P) in 1.5 mL of CH₂Cl₂ in the glovebox. The absorbance of the 10 mol% [(biq)Cu^{II}(OBz)]PF₆ solution at 458 nm was measured to be 0.154. The fraction of light absorbed (f) by this solution was calculated as below:

$$f = 1 - 10^{-A} = 1 - 10^{-0.154} = 0.299$$

where A is the measured absorbance of the 10 mol% [(biq)Cu^{II}(OBz)]PF₆ solution at 458 nm.

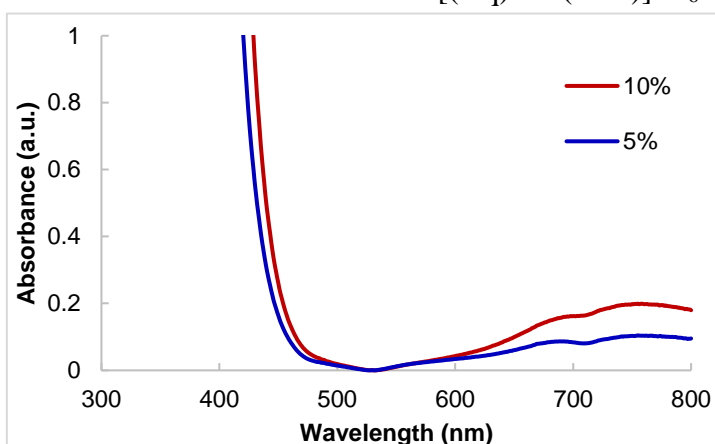


Figure 2A.14. Absorption spectrum of the [(biq)Cu^{II}(OBz)]PF₆ solution.

Determination of quantum yield: The parent reaction was conducted in the same taped Schlenk tube at the optimal conditions in 0.1 mmol scale. After irradiation for 8 h, the yield of product was determined by ¹H NMR (1% yield). The quantum yield was determined as below:

$$\Phi = \text{mol product}/(\text{flux} \cdot t \cdot f)$$

Where Φ is the quantum yield for the reaction, t is the reaction time (28800 s), and f is the fraction of light absorbed at 458 nm for the [(biq)Cu^{II}(OBz)]PF₆ solution.

5 mol% [(biq)Cu^{II}(OBz)]PF₆ solution:

$$\Phi = \text{mol product}/(\text{flux} \cdot t \cdot f) = (1\% \cdot 0.1 \cdot 10^{-3}) / (1.66 \times 10^{-7} \cdot 28800 \cdot 0.202) = 0.103 \text{ (10.3\%)}$$

10 mol% [(biq)Cu^{II}(OBz)]PF₆ solution:

$$\Phi = \text{mol product}/(\text{flux} \cdot t \cdot f) = (1\% \cdot 0.1 \cdot 10^{-3}) / (1.66 \times 10^{-7} \cdot 28800 \cdot 0.299) = 0.0700 \text{ (7.0\%)}$$

Experiment 2A.13. UV-visible Experiment of Reaction Mixture

Tetrakis(acetonitrile)copper(I) hexafluorophosphate (3.7 mg, 0.010 mmol, 10 mol%) and 2,2'-biquinoline (3.8 mg, 0.015 mmol, 15 mol%) were added to a 24 mL glass vial under air with a stir bar. The vial was then moved to a purging glove box under N₂ atmosphere. The vial was then moved to a glove box under N₂ atmosphere. Dichloromethane (1.5 mL), ethylbenzene **1a** (12.3 μL, 0.1 mmol, 1.0 equiv) and TBPB **2** (95.1 μL, 0.5 mmol, 5 equiv) were added to the reaction vial with stirring. Then, 225 μL of the reaction mixture was pipetted to a 5 mL volumetric flask and diluted to volume with dichloromethane, affording a stock solution with a total [Cu^{II}] of 0.30 mM. The sample for UV-visible measurement was prepared by adding 1 mL of the stock solution to the cuvette followed by addition of 1 mL of dichloromethane ([Cu^{II}] = 0.15 mM). The cuvette was sealed with a PTFE-lined cap in the glovebox. An initial UV-visible spectrum was taken.

Another reaction vial was prepared similarly and removed from the glovebox to stir for 8 hours without irradiation. After 8 hours, the reaction vial was moved to the glovebox under N₂ atmosphere. A UV-vis sample was prepared as described above to obtain a final spectrum.

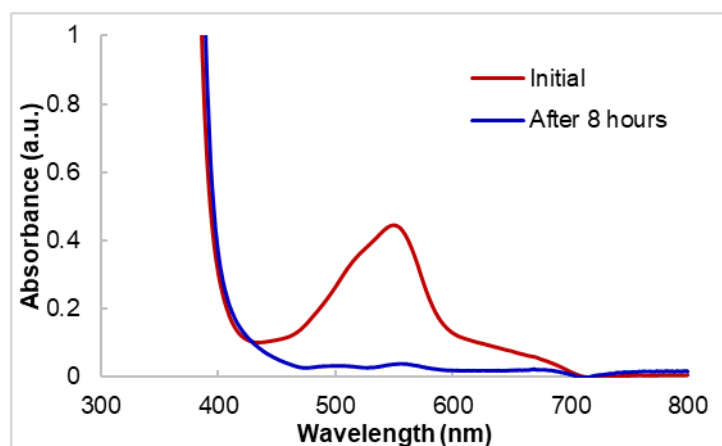
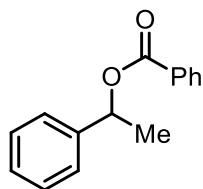


Figure 2A.15. Absorption spectrum of the reaction mixture before and after 8 hours

2A.IX. Characterization of Compounds



1-phenylethyl benzoate, **3a**

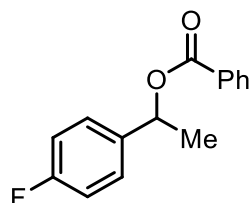
Reaction run using ethylbenzene **1a** (12.3 μ L, 0.1 mmol, 1.0 equiv) and TBPB **2** (95.1 μ L, 0.5 mmol, 5 equiv) following the general procedure I for 8 hours. Yield = 15.6 mg (69%) of clear colorless oil.

Purification: normal phase silica gel column chromatography with 10:1 pentane:ethyl acetate

Spectral data available in the literature: Yes¹⁶

¹H NMR (CDCl₃, 500 MHz): 8.08 (d, J =10.5 Hz, 2H), 7.52 (td, J = 7.5, 1.5 Hz, 1H), 7.45 – 7.40 (m, 4H), 7.35 (t, J =7.5 Hz, 2H), 7.28 (td, J = 7.5, 2.0 Hz, 1H), 6.13 (q, J = 6.5 Hz, 1H), 1.66 (d, J = 6.5 Hz, 3H) ppm.

¹³C NMR (CDCl₃, 126 MHz): 165.77, 141.79, 132.89, 130.55, 129.63, 128.54, 128.32, 127.87, 126.04, 72.89, 22.39 ppm.



1-(4-fluorophenyl)ethyl benzoate, **3b**

Reaction run using 1-fluoro-4-ethylbenzene **1b** (12.4 mg, 0.1 mmol, 1.0 equiv) and TBPB **2** (95.1 μ L, 0.5 mmol, 5 equiv) following the general procedure I for 8 hours. Yield = 19.3 mg (79%) of yellow liquid.

Purification: normal phase silica gel column chromatography with 15:1 pentane:ethyl acetate

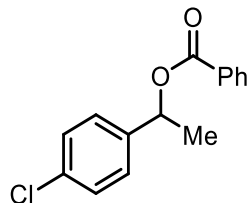
Spectral data available in the literature: No

¹H NMR (CDCl₃, 500 MHz): 8.06 (dd, J = 8.0, 2.0 Hz, 2H), 7.55 (td, J = 7.5, 1.5 Hz, 1H), 7.45 – 7.40 (4H), 7.04 (td, J = 8.5, 2.5 Hz, 2H), 6.11 (q, J = 6.5 Hz, 1H), 1.65 (d, J = 6.5 Hz, 3H) ppm.

¹³C NMR (CDCl₃, 126 MHz): 165.76, 162.36 (d, J = 123.5 Hz), 137.61, 137.58, 133.00, 130.41, 129.63, 128.37, 127.92, 127.85 (d, J = 8.8 Hz), 115.51, 115.34, 72.26, 22.36 ppm.

¹⁹F NMR (CDCl₃, 377 MHz): -114.36 ppm.

HRMS m/z: [M+Na]⁺ calculated for C₁₅H₁₃FO₂ 267.0792, Found: 267.0787.



1-(4-chlorophenyl)ethyl benzoate, **3c**

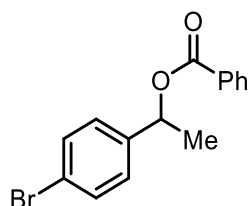
Reaction run using 1-chloro-4-ethylbenzene **1c** (13.5 μ L, 0.1 mmol, 1.0 equiv) and TBPB **2** (95.1 μ L, 0.5 mmol, 5 equiv) following the general procedure I for 8 hours. Yield = 18.5 mg (71%) of clear colorless oil.

Purification: prepTLC with 3:1 pentane:DCM

Spectral data available in the literature: Yes¹⁷

¹H NMR (CDCl₃, 500 MHz): 8.06 (dd, J = 8.0, 1.0 Hz, 2H), 7.56 (tt, J = 7.5, 1.5 Hz, 1H), 7.44 (t, J = 7.5 Hz, 2H), 7.39 – 7.31 (m, 4H), 6.09 (q, J = 6.5 Hz, 1H), 1.65 (d, J = 6.5 Hz, 3H) ppm.

¹³C NMR (CDCl₃, 126 MHz): 165.72, 140.32, 133.67, 133.05, 130.31, 129.63, 128.75, 128.39, 127.49, 72.20, 22.31 ppm.



1-(4-bromophenyl)ethyl benzoate, **3d**

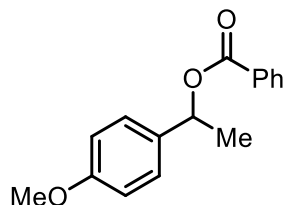
Reaction run using 1-bromo-4-ethylbenzene **1d** (18.5 mg, 0.1 mmol, 1.0 equiv) and TBPB **2** (95.1 μ L, 0.5 mmol, 6 equiv) following the general procedure I for 12 hours. Yield = 19.8 mg (65%) of yellow semisolid.

Purification: prepTLC with 3:1 pentane:DCM

Spectral data available in the literature: Yes¹⁸

¹H NMR (CDCl₃, 500 MHz): 8.06 (d, J = 7.5 Hz, 2H), 7.56 (t, J = 7.5 Hz, 1H), 7.48 (d, J = 7.5 Hz, 2H), 7.44 (t, J = 7.5 Hz, 3H), 7.32 (d, J = 7.5 Hz, 2H), 6.07 (q, J = 6.5 Hz, 1H), 1.65 (d, J = 6.5 Hz, 3H) ppm.

¹³C NMR (CDCl₃, 126 MHz): 165.70, 140.85, 133.06, 131.71, 130.28, 129.63, 128.39, 127.81, 121.79, 72.23, 22.28 ppm.



1-(4-methoxyphenyl)ethyl benzoate, **3e**

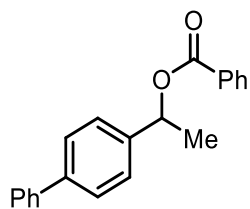
Reaction run using 1-methoxy-4-ethylbenzene **1e** (27.5 μ L, 0.1 mmol, 1.0 equiv) and TBPB **2** (114.1 μ L, 0.6 mmol, 6 equiv) following the general procedure I for 12 hours. Yield = 15.1 mg (59%) of clear colorless liquid.

Purification: normal phase silica gel column chromatography with 15:1 pentane:ethyl acetate

Spectral data available in the literature: Yes¹⁹

¹H NMR (CDCl₃, 500 MHz): 8.06 (dd, J = 8.0, 1.0 Hz, 2H), 7.54(tt, J = 7.5, 1.0 Hz, 2H), 7.44 – 7.37(m, 4H), 6.89 (d, J = 9.0 Hz, 2H), 6.10 (q, J = 6.5 Hz, 1H), 3.80 (s, 3H), 1.65 (d, J = 7.0 Hz, 3H) ppm.

¹³C NMR (CDCl₃, 126 MHz): 165.88, 159.30, 133.86, 132.80, 130.66, 129.63, 128.25, 127.57, 113.88, 72.66, 55.35, 22.21 ppm.



1-([1,1'-biphenyl]-4-yl)ethyl benzoate, **3f**

Reaction run using 4-ethylbiphenyl **1f** (18.2 mg, 0.1 mmol, 1.0 equiv) and TBPB **2** (114.1 μ L, 0.6 mmol, 6 equiv) following the general procedure I for 10 hours. Yield = 23.0 mg (76%) of yellow semisolid.

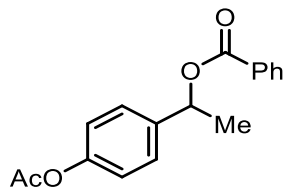
Purification: prepTLC with 3:1 pentane:DCM

Spectral data available in the literature: No

¹H NMR (CDCl₃, 500 MHz): 8.10 (dd, J = 8.0, 1.0 Hz, 2H), 7.60 – 7.51(m, 7H), 7.43 (q, J = 8.0 Hz, 4H), 7.33(tt, J = 7.5, 1.0 Hz, 1H), 6.18 (q, J = 6.5 Hz, 1H), 1.71 (d, J = 6.5 Hz, 3H) ppm.

¹³C NMR (CDCl₃, 126 MHz): 165.85, 140.89, 140.79, 132.94, 130.53, 129.67, 128.77, 128.35, 127.34, 127.12, 126.52, 72.71, 22.36 ppm.

HRMS m/z: [M+Na]⁺ calculated for C₂₁H₁₈O₂ 325.1199, Found: 325.1193.



1-(4-acetoxyphenyl)ethyl benzoate, **3g**

Reaction run using 4-ethylphenyl acetate **1g** (15.9 μ L, 0.1 mmol, 1.0 equiv) and TBPB **2** (114.1 μ L, 0.6 mmol, 6 equiv) following the general procedure I for 12 hours. Yield = 21.3 mg (75%) of clear colorless liquid.

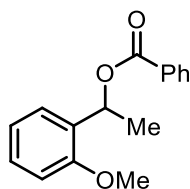
Purification: normal phase silica gel column chromatography with 15:1 pentane:ethyl acetate

Spectral data available in the literature: No

^1H NMR (CDCl_3 , 400 MHz): 8.10 – 8.04 (m, 2H), 7.57 – 7.53 (m, 1H), 7.49 – 7.40 (m, 4H), 7.11 – 7.07 (m, 2H), 6.14 (q, $J = 6.6$ Hz, 1H), 2.29 (s, 3H), 1.66 (d, $J = 6.6$ Hz, 3H) ppm.

^{13}C NMR (CDCl_3 , 126 MHz): 187.47, 165.23, 159.46, 158.10, 153.96, 136.42, 133.85, 133.23, 129.79, 129.52, 128.34, 125.85, 125.78, 124.22, 121.47, 118.65, 117.17, 111.79, 65.30, 60.82, 18.74 ppm.

HRMS m/z : $[\text{M}+\text{Na}]^+$ calculated for $\text{C}_{17}\text{H}_{16}\text{O}_4$ 307.0941, Found: 307.0935.



1-(2-methoxyphenyl)ethyl benzoate, **3h**

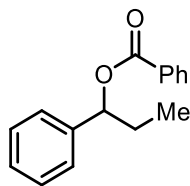
Reaction run using 2-ethylanisole **1h** (14.2 μ L, 0.1 mmol, 1.0 equiv) and TBPB **2** (114.1 μ L, 0.6 mmol, 6 equiv) following the general procedure I for 20 hours. Yield = 18.5 mg (72%) of clear colorless semisolid. Purification: reverse phase silica gel column chromatography with a gradient of 35% \rightarrow 75% MeOH in H_2O

Spectral data available in the literature: No

^1H NMR (CDCl_3 , 500 MHz): 8.15 – 7.98 (m, 2H), 7.58 – 7.51 (m, 1H), 7.50 – 7.35 (m, 3H), 7.29 – 7.21 (m, 1H), 6.97 (td, $J = 7.5, 1.1$ Hz, 1H), 6.89 (dd, $J = 8.3, 1.1$ Hz, 1H), 6.49 (q, $J = 6.5$ Hz, 1H), 3.86 (s, 3H), 1.62 (d, $J = 6.5$ Hz, 3H) ppm.

^{13}C NMR (CDCl_3 , 126 MHz): 165.70, 156.02, 132.79, 130.79, 130.60, 129.64, 128.62, 128.31, 125.79, 120.66, 110.59, 67.93, 55.48, 21.39 ppm.

HRMS m/z : $[\text{M}+\text{Na}]^+$ calculated for $\text{C}_{16}\text{H}_{16}\text{O}_3$ 279.0992, Found: 279.0989.



1-phenylpropyl benzoate, **3i**

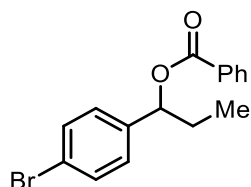
Reaction run using propylbenzene **1i** (13.9 μ L, 0.1 mmol, 1.0 equiv) and TBPB **2** (114.1 μ L, 0.6 mmol, 6 equiv) following the general procedure I for 12 hours. Yield = 17.3 mg (72%) of yellow semisolid.

Purification: normal phase silica gel column chromatography with 15:1 pentane:ethyl acetate

Spectral data available in the literature: Yes²⁰

¹H NMR (CDCl₃, 500 MHz): 8.09 (d, *J* = 8.0 Hz, 2H), 7.55 (t, *J* = 7.5 Hz, 1H), 7.46 – 7.41 (m, 4H), 7.35 (t, *J* = 7.5 Hz, 2H), 7.28 (t, *J* = 7.0 Hz, 1H), 5.92 (t, *J* = 7.0 Hz, 1H), 2.12 – 2.03 (m, 1H), 2.00 – 1.91 (m, 1H), 0.97 (t, *J* = 7.5 Hz, 3H) ppm.

¹³C NMR (CDCl₃, 126 MHz): 165.90, 140.68, 132.89, 130.57, 129.64, 128.43, 128.35, 127.83, 126.49, 77.90, 29.57, 9.96 ppm.



1-(4-bromophenyl)propyl benzoate, **3j**

Reaction run using 1-bromo-4-propylbenzene **1j** (15.5 μ L, 0.1 mmol, 1.0 equiv) and TBPB **2** (114.1 μ L, 0.6 mmol, 6 equiv) following the general procedure I for 12 hours. Yield = 22.0 mg (69%) of clear colorless semisolid.

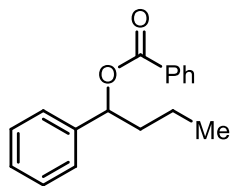
Purification: normal phase silica gel column chromatography with 15:1 pentane:ethyl acetate

Spectral data available in the literature: No

¹H NMR (CDCl₃, 500 MHz): 8.07 (dd, *J* = 8.0, 1.0 Hz, 2H), 7.56 (t, *J* = 7.5 Hz, 1H), 7.48 – 7.43 (m, 4H), 7.28 (d, *J* = 8.0 Hz, 2H), 5.86 (t, *J* = 7.0 Hz, 1H), 2.09 – 1.88 (m, 2H), 0.96 (t, *J* = 7.5 Hz, 3H) ppm.

¹³C NMR (CDCl₃, 126 MHz): 165.81, 139.70, 133.05, 131.61, 130.30, 129.63, 128.41, 128.22, 121.75, 77.22, 29.42, 9.87 ppm.

HRMS *m/z*: [M+Na]⁺ calculated for C₁₆H₁₆BrO₂ 341.0148, Found: 341.0144.



1-phenylbutyl benzoate, **3k**

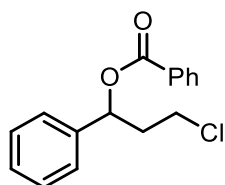
Reaction run using butylbenzene **1k** (15.6 μ L, 0.1 mmol, 1.0 equiv) and TBPB **2** (114.1 μ L, 0.6 mmol, 6 equiv) following the general procedure I for 12 hours. Yield = 16.8 mg (66%) of yellow semisolid.

Purification: normal phase silica gel column chromatography with 20:1 pentane:ethyl acetate

Spectral data available in the literature: Yes¹⁸

¹H NMR (CDCl₃, 500 MHz): 8.08 (d, *J* = 7.5 Hz, 2H), 7.55 (t, *J* = 7.5 Hz, 1H), 7.45 – 7.41 (m, 4H), 7.34 (t, *J* = 8.0 Hz, 2H), 7.28 (t, *J* = 7.5 Hz, 1H), 6.00 (t, *J* = 7.0 Hz, 1H), 2.09 – 2.02 (m, 1H), 1.91 – 1.84 (m, 1H), 1.48 – 1.33 (m, 2H), 0.95 (t, *J* = 7.5 Hz, 3H) ppm.

¹³C NMR (CDCl₃, 126 MHz): 165.88, 140.96, 132.88, 130.57, 129.64, 128.45, 128.34, 127.82, 126.44, 76.49, 38.70, 18.84, 13.85 ppm.



3-chloro-1-phenylpropyl benzoate, **3l**

Reaction run using 1-chloro-3-phenylpropane **1l** (14.3 μ L, 0.1 mmol, 1.0 equiv) and TBPB **2** (190.2 μ L, 1.0 mmol, 10 equiv) following the general procedure I for 24 hours. Yield = 13.7 mg (50%) of clear colorless semisolid.

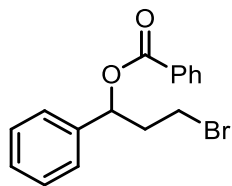
Purification: prepTLC with 25:1 pentane:DCM

Spectral data available in the literature: No

¹H NMR (CDCl₃, 500 MHz): 8.10 – 8.05 (m, 2H), 7.61 – 7.54 (m, 1H), 7.48 – 7.40 (m, 4H), 7.38 – 7.35 (m, 2H), 7.34 – 7.27 (m, 1H), 6.19 (dd, *J* = 8.2, 5.4 Hz, 1H), 3.64 (dt, *J* = 11.0, 6.9 Hz, 1H), 3.53 (dt, *J* = 11.0, 6.5 Hz, 1H), 2.56 (ddt, *J* = 14.5, 8.2, 6.4 Hz, 1H), 2.34 (dtd, *J* = 14.2, 7.0, 5.4 Hz, 1H) ppm.

¹³C NMR (CDCl₃, 126 MHz): 165.52, 139.56, 133.15, 130.08, 129.68, 128.73, 128.44, 128.32, 126.33, 73.80, 40.69, 39.37 ppm.

HRMS *m/z*: [M+Na]⁺ calculated for C₁₆H₁₅ClO₂ 297.0653, Found: 297.0650.



3-bromo-1-phenylpropyl benzoate, **3m**

Reaction run using 1-bromo-3-phenylpropane **1m** (15.2 μ L, 0.1 mmol, 1.0 equiv) and TBPB **2** (190.2 μ L, 1.0 mmol, 10 equiv) following the general procedure I for 24 hours. Yield = 15.0 mg (47%) of white semisolid.

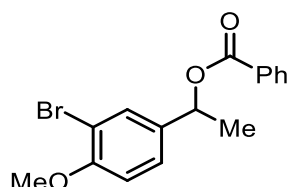
Purification: prepTLC with 25:1 pentane:DCM

Spectral data available in the literature: No

$^1\text{H NMR}$ (CDCl_3 , 500 MHz): 8.10 – 8.05 (m, 2H), 7.59 – 7.55 (m, 1H), 7.48 – 7.42 (m, 4H), 7.39 – 7.34 (m, 2H), 7.33 – 7.28 (m, 1H), 6.16 (dd, $J = 8.1, 5.4$ Hz, 1H), 3.48 (dt, $J = 10.2, 7.1$ Hz, 1H), 3.37 (ddd, $J = 10.3, 7.2, 6.2$ Hz, 1H), 2.65 (ddt, $J = 14.7, 8.2, 6.6$ Hz, 1H), 2.43 (dtd, $J = 14.5, 7.2, 5.4$ Hz, 1H) ppm.

$^{13}\text{C NMR}$ (CDCl_3 , 126 MHz): 165.55, 139.45, 133.17, 130.06, 129.68, 128.74, 128.44, 128.35, 74.71, 39.54, 28.49 ppm.

HRMS m/z: $[\text{M}+\text{Na}]^+$ calculated for $\text{C}_{16}\text{H}_{15}\text{BrO}_2$ 341.0148, Found: 341.0144.



1-(3-bromo-4-methoxyphenyl)ethyl benzoate, **3n**

Reaction run using 2-bromo-4-ethylanisole **1n** (21.5 mg, 0.1 mmol, 1.0 equiv) and TBPB **2** (133.2 μ L, 0.7 mmol, 7 equiv) following the general procedure I for 12 hours. Yield = 26.5 mg (79%) of yellow semisolid.

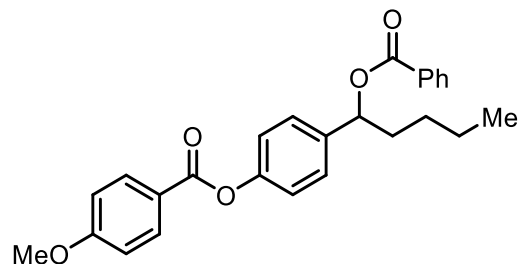
Purification: normal phase silica gel column chromatography with 10:1 pentane:ether

Spectral data available in the literature: No

$^1\text{H NMR}$ (CDCl_3 , 500 MHz): 8.08 – 8.00 (m, 2H), 7.64 (d, $J = 2.2$ Hz, 1H), 7.59 – 7.52 (m, 1H), 7.44 (t, $J = 7.7$ Hz, 2H), 7.36 (dd, $J = 8.5, 2.2$ Hz, 1H), 6.88 (d, $J = 8.5$ Hz, 1H), 6.05 (q, $J = 6.6$ Hz, 1H), 3.89 (s, 3H), 1.65 (d, $J = 6.6$ Hz, 3H) ppm.

$^{13}\text{C NMR}$ (CDCl_3 , 126 MHz): 165.76, 155.58, 135.39, 133.01, 131.24, 130.38, 129.65, 128.38, 126.68, 111.97, 71.98, 56.22, 22.16. ppm.

HRMS m/z: $[\text{M}+\text{Na}]^+$ calculated for $\text{C}_{16}\text{H}_{15}\text{BrO}_3$ 357.0097, Found: 357.0092.



4-(1-(benzoyloxy)pentyl)phenyl 4-methoxybenzoate, **3o**

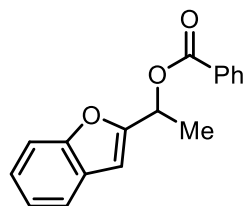
Reaction run using 4-pentylphenyl-4-methoxybenzoate **1o** (29.8 mg, 0.1 mmol, 1.0 equiv) and TBPB **2** (114.1 μ L, 0.6 mmol, 6 equiv) following the general procedure I for 12 hours. Yield = 29.9 mg (72%) of brown semisolid.

Purification: reverse phase silica gel column chromatography with a gradient of 35% \rightarrow 90% MeOH in H₂O Spectral data available in the literature: No

¹H NMR (CDCl₃, 500 MHz): 8.16 – 8.12 (m, 2H), 8.10 – 8.06 (m, 2H), 7.58 – 7.53 (m, 1H), 7.49 – 7.43 (m, 4H), 7.23 – 7.16 (m, 2H), 7.02 – 6.94 (m, 2H), 6.01 (dd, *J* = 7.7, 6.1 Hz, 1H), 3.89 (s, 3H), 2.17 – 2.02 (m, 1H), 1.98 – 1.84 (m, 1H), 1.46 – 1.29 (m, 4H), 0.90 (t, *J* = 7.0 Hz, 3H) ppm.

¹³C NMR (CDCl₃, 126 MHz): 165.86, 164.82, 163.94, 150.59, 138.36, 132.94, 132.31, 130.49, 129.66, 128.37, 127.66, 76.19, 55.53, 36.24, 27.68, 22.47, 13.95 ppm.

HRMS *m/z*: [M+Na]⁺ calculated for C₂₆H₂₆O₅ 441.1673, Found: 441.1666.



1-(benzofuran-2-yl)ethyl benzoate, **3p**

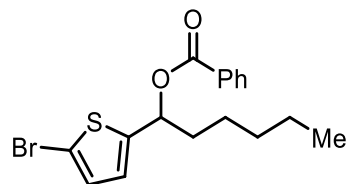
Reaction run using 2-ethylbenzofuran **1p** (14.6 mg, 0.1 mmol, 1.0 equiv) and TBPB **2** (95.1 μ L, 0.5 mmol, 5 equiv) following the general procedure I for 8 hours. Yield = 14.9 mg (56%) of clear colorless liquid.

Purification: normal phase silica gel column chromatography with 20:1 pentane:ethyl acetate Spectral data available in the literature: No

¹H NMR (CDCl₃, 500 MHz): 8.04 – 7.98 (m, 2H), 7.51 – 7.45 (m, 2H), 7.43 – 7.32 (m, 3H), 7.27 – 7.11 (m, 2H), 6.69 (s, 1H), 6.27 (q, *J* = 6.7 Hz, 1H), 1.73 (d, *J* = 6.7 Hz, 3H) ppm.

¹³C NMR (CDCl₃, 126 MHz): 165.71, 156.09, 154.91, 133.12, 130.11, 129.80, 128.38, 127.91, 124.55, 122.87, 121.25, 111.41, 110.00, 104.32, 66.15, 18.58 ppm.

HRMS *m/z*: [M+Na]⁺ calculated for C₁₇H₁₄O₃ 289.0835, Found: 289.0832.



1-(5-bromothiophen-2-yl)hexyl benzoate, **3r**

Reaction run using 5-bromo-2-hexylthiophene **1r** (20.1 μ L, 0.1 mmol, 1.0 equiv) and TBPB **2** (95.1 μ L, 0.5 mmol, 5 equiv) following the general procedure I for 8 hours. Yield = 22.8 mg (62%) of yellow liquid.

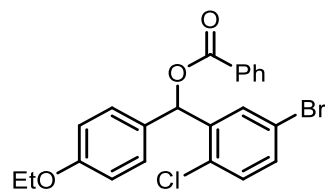
Purification: prepTLC with 3:1 pentane:DCM

Spectral data available in the literature: No

¹H NMR (CDCl₃, 500 MHz): 8.04 (d, J = 7.5 Hz, 2H), 7.55 (t, J = 7.0 Hz, 1H), 7.43 (t, J = 8.0 Hz, 2H), 6.91 (d, J = 4.0 Hz, 1H), 6.87 (d, J = 4.0 Hz, 1H), 6.16 (t, J = 7.0 Hz, 1H), 2.13 – 2.05 (m, 1H), 1.99 – 1.92 (m, 1H), 1.47 – 1.28 (m, 6H), 0.87 (t, J = 7.0 Hz, 3H) ppm.

¹³C NMR (CDCl₃, 126 MHz): 165.69, 145.32, 133.12, 130.06, 129.69, 129.33, 128.40, 126.23, 112.17, 71.91, 36.16, 31.35, 25.19, 22.44, 13.96 ppm.

HRMS m/z: [M+Na]⁺ calculated for C₁₇H₁₉BrO₂S 389.0181, Found: 389.0177.



(5-bromo-2-chlorophenyl)(4-ethoxyphenyl)methyl benzoate, **3s**

Reaction run using 4-bromo-1-chloro-2-(4-ethoxybenzyl)benzene **1s** (32.6 mg, 0.1 mmol, 1.0 equiv) and TBPB **2** (95.1 μ L, 0.5 mmol, 5 equiv) following the general procedure I for 8 hours. Yield = 22.5 mg (50%) of clear colorless oil.

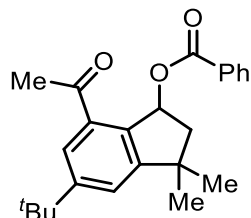
Purification: reverse phase silica gel column chromatography with a gradient of 35% → 90% MeOH in H₂O

Spectral data available in the literature: No

¹H NMR (CDCl₃, 500 MHz): 8.07 – 8.01 (m, 2H), 7.65 (d, J = 2.4 Hz, 1H), 7.52 (ddt, J = 8.8, 7.0, 1.3 Hz, 1H), 7.40 (ddt, J = 7.9, 6.6, 1.1 Hz, 2H), 7.32 – 7.24 (m, 4H), 7.18 (d, J = 8.5 Hz, 1H), 6.82 – 6.78 (m, 2H), 3.95 (q, J = 7.0 Hz, 2H), 1.33 (t, J = 7.0 Hz, 3H) ppm.

¹³C NMR (CDCl₃, 126 MHz): 165.23, 159.05, 140.26, 133.34, 132.06, 131.79, 131.32, 130.64, 129.85, 129.84, 129.82, 129.05, 128.53, 120.83, 114.56, 73.66, 63.48, 14.80 ppm.

HRMS m/z: [M-OBz]⁺ calculated for C₂₂H₁₈BrClO₃ 311.1076, Found: 311.1072.



7-acetyl-5-(*tert*-butyl)-3,3-dimethyl-2,3-dihydro-1*H*-inden-1-yl benzoate, **3t**

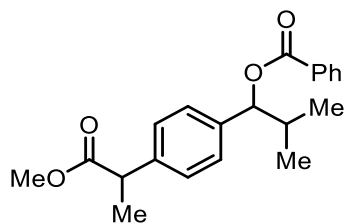
Reaction run using celestolide **1t** (24.4 mg, 0.1 mmol, 1.0 equiv) and TBPB **2** (95.1 μ L, 0.5 mmol, 5 equiv) following the general procedure I for 12 hours. Yield = 31.1 mg (85%) of brown semisolid. Purification: reverse phase silica gel column chromatography with a gradient of 35% \rightarrow 90% MeOH in H₂O

Spectral data available in the literature: No

¹H NMR (CDCl₃, 500 MHz): 7.97 (dd, J = 8.2, 1.4 Hz, 2H), 7.74 (d, J = 1.8 Hz, 1H), 7.54 – 7.47 (m, 1H), 7.45 (d, J = 1.8 Hz, 1H), 7.37 (t, J = 7.8 Hz, 2H), 6.79 (dd, J = 7.0, 2.4 Hz, 1H), 2.54 (s, 3H), 2.47 (dd, J = 14.2, 7.0 Hz, 1H), 2.14 (dd, J = 14.2, 2.4 Hz, 1H), 1.40 (s, 9H), 1.38 (s, 3H), 1.36 (s, 3H) ppm.

¹³C NMR (CDCl₃, 126 MHz): 199.41, 166.07, 155.62, 153.38, 135.70, 135.13, 132.65, 130.64, 129.67, 128.23, 125.40, 123.27, 76.16, 48.62, 42.82, 35.08, 31.45, 31.23, 29.23, 28.32 ppm.

HRMS m/z: [M+H]⁺ calculated for C₂₄H₂₈O₃ 365.2111, Found: 365.2105.



1-(4-(1-methoxy-1-oxopropan-2-yl)phenyl)-2-methylpropyl benzoate, **3u**

Reaction run using ibuprofen methyl ester **1u** (22.0 mg, 0.1 mmol, 1.0 equiv) and TBPB **2** (114.1 μ L, 0.6 mmol, 6 equiv) following the general procedure I for 12 hours. Yield = 19.6 mg (58%) of yellow semisolid.

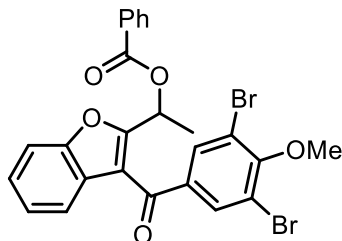
Purification: normal phase silica gel column chromatography with 10:1 pentane:ether

Spectral data available in the literature: No

¹H NMR (CDCl₃, 500 MHz): 8.12 – 8.06 (m, 2H), 7.59 – 7.52 (m, 1H), 7.45 (dd, J = 8.4, 7.1 Hz, 2H), 7.35 – 7.29 (m, 2H), 7.28 – 7.23 (m, 2H), 5.71 (d, J = 7.2 Hz, 1H), 3.70 (q, J = 7.2 Hz, 1H), 3.65 (d, J = 1.2 Hz, 3H), 2.29 – 2.18 (m, J = 6.8 Hz, 1H), 1.47 (dd, J = 7.2, 2.2 Hz, 3H), 1.05 (d, J = 6.7 Hz, 3H), 0.90 (d, J = 6.8 Hz, 3H) ppm.

¹³C NMR (CDCl₃, 126 MHz): 174.96, 174.92, 165.81, 139.88, 138.64, 132.92, 130.56, 129.62, 128.39, 127.33, 127.22, 81.18, 52.02, 45.12, 33.83, 18.91, 18.57, 18.55, 18.43 ppm.

HRMS m/z: [M+NH₄]⁺ calculated for C₂₁H₂₄O₄ 358.2013, Found: 358.2010.



1-(3-(3,5-dibromo-4-methoxybenzoyl)benzofuran-2-yl)ethyl benzoate, **3v**

Reaction run using benzbromarone methyl ether **1v** (43.8 mg, 0.1 mmol, 1.0 equiv) and dibenzoyl peroxide (48.4 mg, 0.2 mmol, 2 equiv) following the general procedure I for 20 hours. Yield = 30.7 mg (55%) of yellow semisolid.

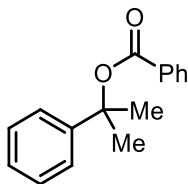
Purification: prepTLC with 20:1 pentane:ethyl acetate

Spectral data available in the literature: No

$^1\text{H NMR}$ (CDCl_3 , 500 MHz): 8.07 – 7.93 (m, 4H), 7.60 – 7.51 (m, 2H), 7.45 – 7.35 (m, 4H), 7.28 (t, $J = 7.6$ Hz, 1H), 6.31 (q, $J = 6.7$ Hz, 1H), 3.96 (s, 3H), 1.84 (d, $J = 6.7$ Hz, 3H) ppm.

$^{13}\text{C NMR}$ (CDCl_3 , 126 MHz): 187.47, 165.23, 159.46, 158.10, 153.96, 136.42, 133.85, 133.23, 129.79, 129.52, 128.34, 125.85, 125.78, 124.22, 121.47, 118.65, 117.17, 111.79, 65.30, 60.82, 18.74 ppm.

HRMS m/z: $[\text{M}+\text{Na}]^+$ calculated for $\text{C}_{25}\text{H}_{18}\text{Br}_2\text{O}_5$ 578.9413, Found: 578.9409.



2-phenylpropan-2-yl benzoate, **3w**

Reaction run using cumene **1w** (13.9 μL , 0.1 mmol, 1.0 equiv) and TBPB **2** (133.2 μL , 0.7 mmol, 7 equiv) following the general procedure I for 12 hours. Yield = 19.6 mg (82%) of clear colorless oil.

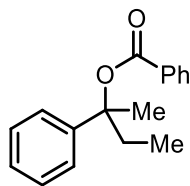
Purification: normal phase silica gel column chromatography with 10:1 pentane:ether

Spectral data available in the literature: No

$^1\text{H NMR}$ (CDCl_3 , 500 MHz): 8.06 – 8.02 (m, 2H), 7.57 – 7.51 (m, 1H), 7.46 – 7.40 (m, 4H), 7.33 (dd, $J = 8.5, 6.9$ Hz, 2H), 7.25 (tt, $J = 7.6, 1.3$ Hz, 1H), 1.92 (s, 6H) ppm.

$^{13}\text{C NMR}$ (CDCl_3 , 126 MHz): 165.15, 145.86, 132.68, 131.57, 129.57, 128.37, 128.32, 127.07, 124.32, 82.23, 28.79 ppm.

HRMS m/z: $[\text{M}+\text{Na}]^+$ calculated for $\text{C}_{16}\text{H}_{16}\text{O}_2$ 263.1043, Found: 263.1041.



2-phenylbutan-2-yl benzoate, **3x**

Reaction run using *sec*-butylbenzene **1x** (15.5 μ L, 0.1 mmol, 1.0 equiv) and TBPB **2** (133.2 μ L, 0.7 mmol, 7 equiv) following the general procedure I for 12 hours. Yield = 16.5 mg (65%) of clear colorless oil.

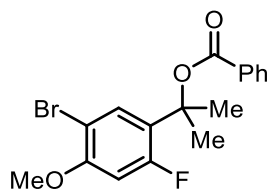
Purification: normal phase silica gel column chromatography with 10:1 pentane:ether

Spectral data available in the literature: No

¹H NMR (CDCl₃, 500 MHz): 8.10 – 8.04 (m, 2H), 7.59 – 7.52 (m, 1H), 7.45 (t, J = 7.7 Hz, 2H), 7.41 – 7.36 (m, 2H), 7.35 – 7.30 (m, 2H), 7.25 – 7.20 (m, 1H), 2.18 (q, J = 7.4 Hz, 2H), 1.96 (s, 3H), 0.90 (t, J = 7.4 Hz, 3H) ppm.

¹³C NMR (CDCl₃, 126 MHz): 165.05, 144.86, 132.68, 131.61, 129.56, 128.33, 128.22, 126.89, 124.71, 84.99, 35.56, 24.52, 8.29 ppm.

HRMS m/z: [M+H]⁺ calculated for C₁₇H₁₈O₂ 259.0884, Found: 259.0881.



2-(5-bromo-2-fluoro-4-methoxyphenyl)propan-2-yl benzoate, **3y**

Reaction run using 1-bromo-4-fluoro-5-isopropyl-2-methoxybenzene **1y** (24.7 mg, 0.1 mmol, 1.0 equiv) and TBPB **2** (190.2 μ L, 1.0 mmol, 10 equiv) following the general procedure I for 20 hours. Yield = 21.7 mg (62%) of yellow semisolid.

Purification: reverse phase silica gel column chromatography with a gradient of 35%→90% MeOH in H₂O

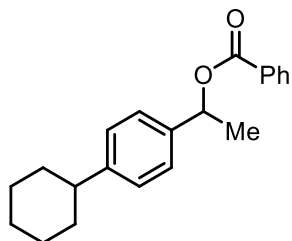
Spectral data available in the literature: No

¹H NMR (CDCl₃, 500 MHz): 8.06 – 7.99 (m, 2H), 7.60 – 7.51 (m, 2H), 7.46 – 7.39 (m, 2H), 6.58 (d, J = 13.2 Hz, 1H), 3.84 (s, 3H), 1.92 (d, J = 1.0 Hz, 6H) ppm.

¹³C NMR (CDCl₃, 126 MHz): 165.20, 159.53 (d, J = 249.8 Hz), 155.96 (d, J = 10.6 Hz), 132.76, 131.14, 130.96 (d, J = 5.8 Hz), 129.59, 128.29, 125.24 (d, J = 12.3 Hz), 105.68 (d, J = 3.5 Hz), 101.29 (d, J = 28.9 Hz), 79.93 (d, J = 2.5 Hz), 56.45, 27.85 (d, J = 2.5 Hz) ppm.

¹⁹F NMR (CDCl₃, 377 MHz): -110.63 ppm.

HRMS m/z: [M-OBz]⁺ calculated for C₁₇H₁₆BrFO₂ 244.9972, Found: 244.9969.



1-(4-cyclohexylphenyl)ethyl benzoate, **3z**

Reaction run using 1-cyclohexyl-4-ethylbenzene **1z** (18.8 mg, 0.1 mmol, 1.0 equiv) and TBPB **2** (95.1 μ L, 0.5 mmol, 5 equiv) following the general procedure I for 8 hours. Yield = 19.7 mg (64%) of yellow semisolid.

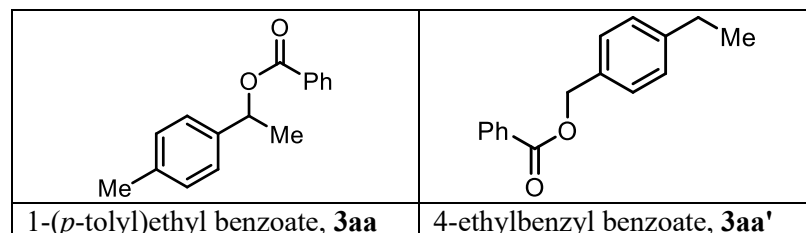
Purification: normal phase silica gel column chromatography with 15:1 pentane:ethyl acetate

Spectral data available in the literature: No

^1H NMR (CDCl_3 , 500 MHz): 8.07 (dd, $J = 8.0, 1.0$ Hz, 2H), 7.54 (t, $J = 7.5$ Hz, 1H), 7.42 (t, $J = 7.5$ Hz, 2H), 7.36 (d, $J = 8.0$ Hz, 2H), 7.20 (d, $J = 8.0$ Hz, 2H), 6.12 (q, $J = 6.5$ Hz, 1H), 2.49 (m, 1H), 1.87 – 1.82 (m, 4H), 1.66 (d, $J = 6.5$ Hz, 3H), 1.45 – 1.35 (m, 4H), 1.28 – 1.22 (m, 2H) ppm.

^{13}C NMR (CDCl_3 , 126 MHz): 165.85, 147.73, 139.06, 132.75, 130.62, 129.65, 128.29, 126.96, 126.11, 72.78, 44.35, 34.31, 26.81, 26.15, 22.23 ppm.

HRMS m/z : $[\text{M}+\text{Na}]^+$ calculated for $\text{C}_{21}\text{H}_{24}\text{O}_2$ 331.1669, Found: 331.1663.



Reaction run using 4-methylethylbenzene **1aa** (12.0 mg, 0.1 mmol, 1.0 equiv) and TBPB **2** (95.1 μ L, 0.5 mmol, 5 equiv) following the general procedure I for 8 hours. Yield = 14.4 mg (60%) of clear colorless semisolid as a mixture of **3aa** (53%) and **3aa'** (7%).

Purification: normal phase silica gel column chromatography with 15:1 pentane:ethyl acetate

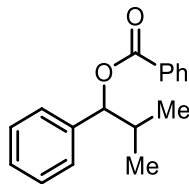
Spectral data available in the literature: No

NMR spectroscopic data for **3aa**

^1H NMR (CDCl_3 , 500 MHz): 8.07 (dd, $J = 8.2, 1.5$ Hz, 2H), 7.58 – 7.51 (m, 1H), 7.43 (t, $J = 7.7$ Hz, 2H), 7.34 (d, $J = 8.0$ Hz, 2H), 7.17 (d, $J = 7.8$ Hz, 2H), 6.10 (q, $J = 6.6$ Hz, 1H), 2.34 (s, 3H), 1.66 (d, $J = 6.6$ Hz, 3H) ppm.

^{13}C NMR (CDCl_3 , 126 MHz): 165.85, 138.84, 137.65, 132.85, 130.64, 129.65, 129.22, 128.31, 126.09, 72.86, 22.33, 21.15 ppm.

HRMS m/z : $[\text{M}+\text{Na}]^+$ calculated for $\text{C}_{16}\text{H}_{16}\text{O}_2$: 263.1043, Found: 263.1039.



2-methyl-1-phenylpropyl benzoate, **3ab**

Reaction run using isobutylbenzene **1ab** (15.7 μ L, 0.1 mmol, 1.0 equiv) and TBPB **2** (114.1 μ L, 0.6 mmol, 6 equiv) following the general procedure I for 12 hours. Yield = 20.2 mg (80%) of yellow semisolid.

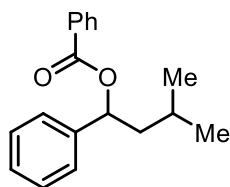
Purification: normal phase silica gel column chromatography with 10:1 pentane:ether

Spectral data available in the literature: No

$^1\text{H NMR}$ (CDCl_3 , 500 MHz): 8.09 (dd, $J = 8.3, 1.4$ Hz, 2H), 7.55 (td, $J = 7.3, 1.4$ Hz, 1H), 7.48 – 7.41 (m, 2H), 7.40 – 7.36 (m, 2H), 7.33 (td, $J = 6.8, 1.2$ Hz, 2H), 7.29 – 7.21 (m, 1H), 5.73 (d, $J = 7.2$ Hz, 1H), 2.32 – 2.19 (m, 1H), 1.05 (d, $J = 6.7$ Hz, 3H), 0.90 (d, $J = 6.8$ Hz, 3H) ppm.

$^{13}\text{C NMR}$ (CDCl_3 , 126 MHz): 165.82, 139.78, 132.90, 130.62, 129.64, 128.39, 128.23, 127.73, 126.95, 81.47, 33.89, 18.88, 18.46 ppm.

HRMS m/z: $[\text{M}+\text{H}]^+$ calculated for $\text{C}_{17}\text{H}_{18}\text{O}_2$ 255.1380, Found: 255.1375.



3-methyl-1-phenylbutyl benzoate, **3ac**

Reaction run using isopentylbenzene **1ac** (17.4 μ L, 0.1 mmol, 1.0 equiv) and TBPB **2** (95.1 μ L, 0.5 mmol, 5 equiv) following the general procedure I for 8 hours. Yield = 16.1 mg (60%) of yellow semisolid.

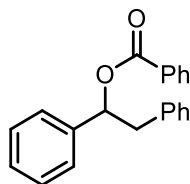
Purification: normal phase silica gel column chromatography with 10:1 pentane:ether

Spectral data available in the literature: No

$^1\text{H NMR}$ (CDCl_3 , 500 MHz): 8.09 – 8.05 (m, 2H), 7.57 – 7.52 (m, 1H), 7.46 – 7.40 (m, 4H), 7.38 – 7.32 (m, 2H), 7.29 – 7.24 (m, 1H), 6.07 (dd, $J = 8.8, 5.1$ Hz, 1H), 2.08 – 1.98 (m, 1H), 1.75 – 1.64 (m, 2H), 1.00 – 0.96 (m, 6H) ppm.

$^{13}\text{C NMR}$ (CDCl_3 , 126 MHz): 165.86, 141.24, 132.87, 130.55, 129.63, 128.48, 128.34, 127.85, 126.44, 75.22, 45.73, 24.86, 22.92, 22.38 ppm.

HRMS m/z: $[\text{M}+\text{Na}]^+$ calculated for $\text{C}_{18}\text{H}_{20}\text{O}_2$ 291.1356, Found: 291.1351.



1,2-diphenylethyl benzoate, **3ad**

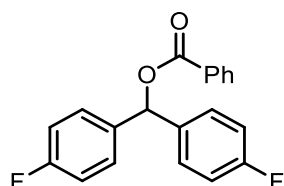
Reaction run using bibenzyl **1ad** (18.2 mg, 0.1 mmol, 1.0 equiv) and TBPB **2** (114.1 μ L, 0.6 mmol, 6 equiv) following the general procedure I for 12 hours. Yield = 19.7 mg (65%) of clear colorless liquid.

Purification: normal phase silica gel column chromatography with 20:1 pentane:ethyl acetate

Spectral data available in the literature: Yes²¹

¹H NMR (CDCl₃, 500 MHz): 8.04 (dd, J = 8.2, 1.4 Hz, 2H), 7.57 – 7.51 (m, 1H), 7.43 (t, J = 7.7 Hz, 2H), 7.36 – 7.11 (m, 10H), 6.18 (dd, J = 7.6, 6.0 Hz, 1H), 3.35 (dd, J = 13.8, 7.7 Hz, 1H), 3.19 (dd, J = 13.8, 6.0 Hz, 1H).

¹³C NMR (CDCl₃, 126 MHz): 165.62, 140.10, 136.92, 132.94, 130.38, 129.62, 129.61, 128.39, 128.35, 128.26, 127.98, 126.58, 126.54, 43.20 ppm.



bis(4-fluorophenyl)methyl benzoate, **3ae**

Reaction run using 4,4'-difluorodiphenylmethane **1ae** (20.4 mg, 0.1 mmol, 1.0 equiv) and TBPB **2** (76.1 μ L, 0.4 mmol, 4 equiv) following the general procedure I for 8 hours. Yield = 23.7 mg (73%) of yellow semisolid

Purification: reverse phase silica gel column chromatography with a gradient of 50% \rightarrow 90% MeOH in H₂O

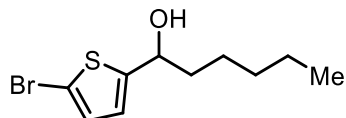
Spectral data available in the literature: No

¹H NMR (CDCl₃, 500 MHz): 8.16 – 8.08 (m, 2H), 7.59 (ddt, J = 7.8, 7.0, 1.3 Hz, 1H), 7.50 – 7.43 (m, 2H), 7.38 (dddd, J = 8.2, 5.2, 2.6, 1.5 Hz, 4H), 7.11 – 7.01 (m, 5H) ppm.

¹³C NMR (CDCl₃, 126 MHz): 164.45 (d, J = 253.4 Hz), 161.47, 135.92 (d, J = 3.3 Hz), 133.34, 129.95, 129.76, 128.92 (d, J = 8.3 Hz), 128.53, 115.59 (d, J = 21.7 Hz), 76.10 ppm.

¹⁹F NMR (CDCl₃, 377 MHz): -113.86 ppm.

HRMS m/z : [M-OBz]⁺ calculated for C₂₀H₁₄F₂O₂ 203.0667, Found: 203.0665.



1-(5-bromothiophen-2-yl)hexan-1-ol, **4r**

Reaction run using 5-bromo-2-hexylthiophene **1r** (20.1 μ L, 0.1 mmol, 1.0 equiv) and TBPB **2** (95.1 μ L, 0.5 mmol, 5 equiv) following the general procedure I for 8 hours. The crude reaction mixture was worked up and carried to the next step following the general procedure II. Yield from Benzylic Ester = 12.0 mg (82%) of yellow oil.

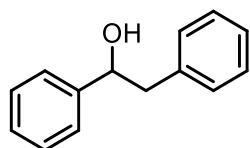
Purification: reverse phase silica gel column chromatography with a gradient of 35% \rightarrow 90% MeOH in H₂O

Spectral data available in the literature: No

¹H NMR (CDCl₃, 500 MHz): 6.90 (d, J = 3.7 Hz, 1H), 6.71 (dd, J = 3.7, 0.8 Hz, 1H), 4.83 (t, J = 6.8 Hz, 1H), 1.93 (s, 1H), 1.88 – 1.71 (m, 2H), 1.43 (tq, J = 8.4, 4.6 Hz, 1H), 1.34 – 1.29 (m, 8H), 0.88 (td, J = 5.7, 1.8 Hz, 3H) ppm.

¹³C NMR (CDCl₃, 126 MHz): 150.64, 129.32, 123.94, 111.32, 70.62, 39.07, 31.53, 25.30, 22.54, 14.00 ppm.

HRMS m/z : [M-H]⁺ calculated for C₁₀H₁₅BrOS 260.9943, Found: 260.9939.



1,2-diphenylethan-1-ol, **4ad**

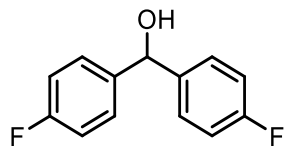
Reaction run using bibenzyl **1ad** (18.2 mg, 0.1 mmol, 1.0 equiv) and TBPB **2** (114.1 μ L, 0.6 mmol, 6 equiv) following the general procedure I for 12 hours. The crude reaction mixture was worked up and carried to the next step following the general procedure II. Yield from Benzylic Ester = 10.4 mg (93%) of yellow semisolid.

Purification: reverse phase silica gel column chromatography with a gradient of 35% \rightarrow 90% MeOH in H₂O

Spectral data available in the literature: Yes²²

¹H NMR (CDCl₃, 500 MHz): 7.39 – 7.33 (m, 4H), 7.30 (tdt, J = 8.0, 6.2, 1.7 Hz, 3H), 7.26 – 7.22 (m, 1H), 7.22 – 7.17 (m, 2H), 4.91 (ddd, J = 8.2, 4.8, 2.9 Hz, 1H), 3.09 – 2.95 (m, 2H), 1.94 (d, J = 2.9 Hz, 1H) ppm.

¹³C NMR (CDCl₃, 126 MHz): 143.82, 138.04, 129.52, 128.53, 128.44, 127.64, 126.65, 125.91, 75.37, 46.12 ppm.



bis(4-fluorophenyl)methanol, **4ae**

Reaction run using 4,4'-difluorodiphenylmethane **1ae** (20.4 mg, 0.1 mmol, 1.0 equiv) and TBPB **2** (76.1 μ L, 0.4 mmol, 5 equiv) following the general procedure I for 8 hours. The crude reaction mixture was worked up and carried to the next step following the general procedure II. Yield from Benzylic Ester = 11.5 mg (81%) of clear colorless semisolid.

Purification: normal phase silica gel column chromatography with 9:1 pentane:ether

Spectral data available in the literature: Yes²³

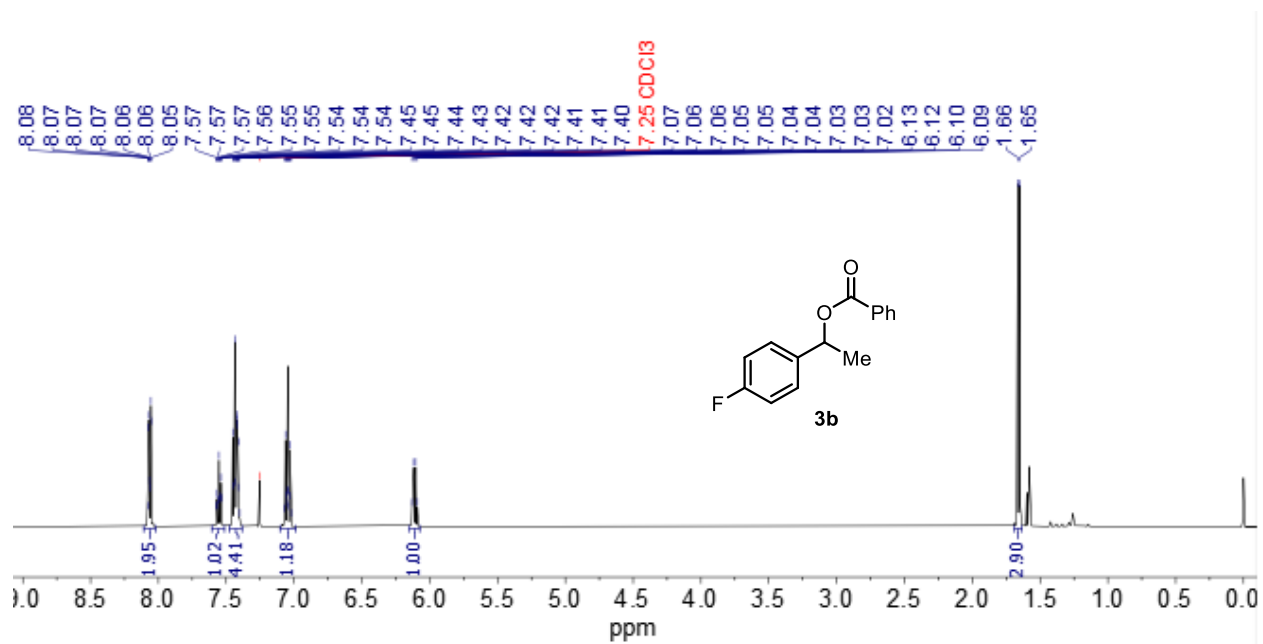
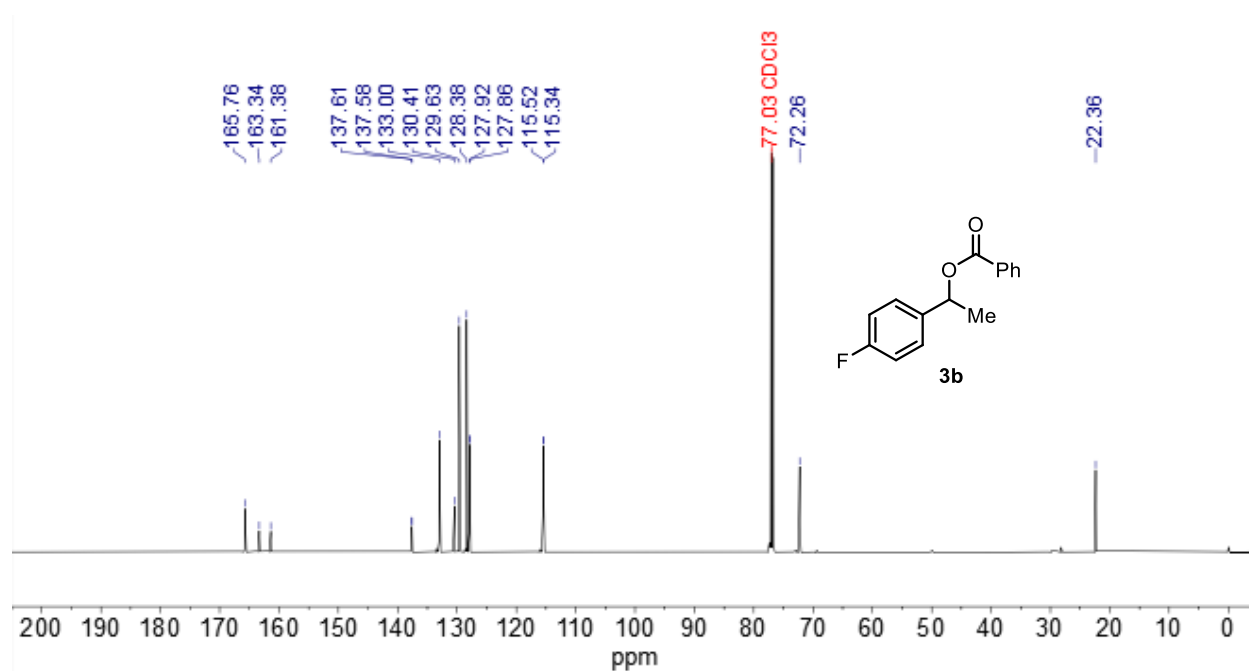
¹H NMR (CDCl₃, 500 MHz): 7.36 – 7.28 (m, 4H), 7.06 – 6.98 (m, 4H), 5.81 (s, 1H), 2.46 (s, 1H) ppm.

¹³C NMR (CDCl₃, 126 MHz): 162.23 (d, *J* = 246.1 Hz), 139.52 (d, *J* = 3.1 Hz), 128.19 (d, *J* = 8.1 Hz), 115.38 (d, *J* = 21.5 Hz), 74.92 ppm.

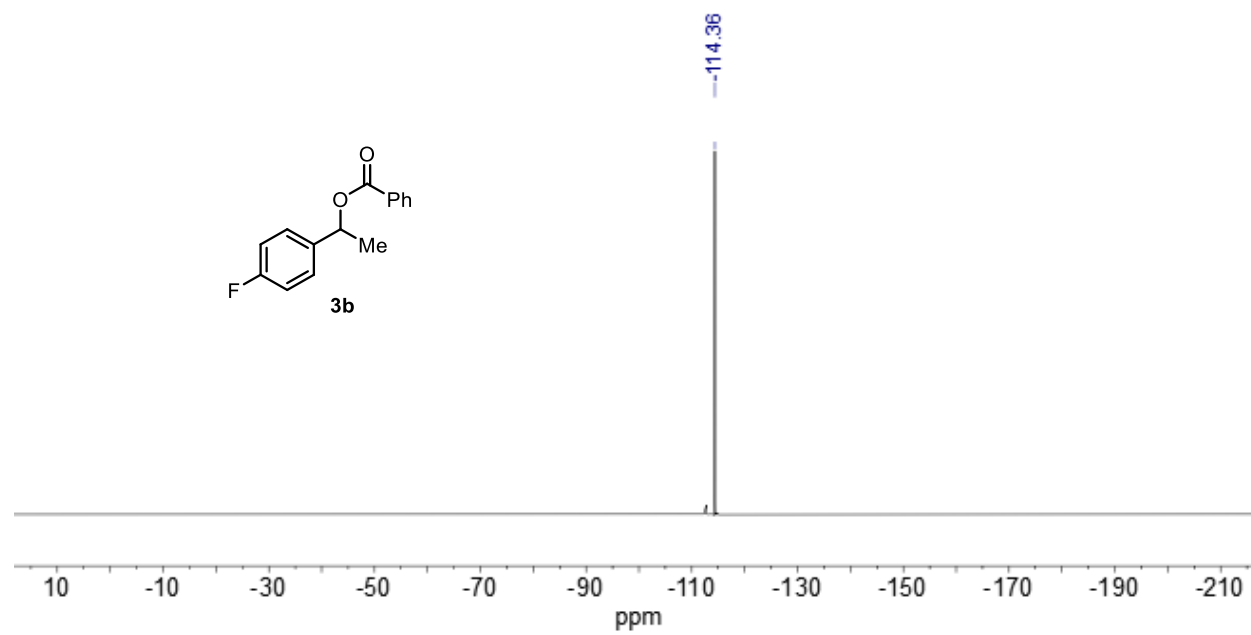
2A.X. References

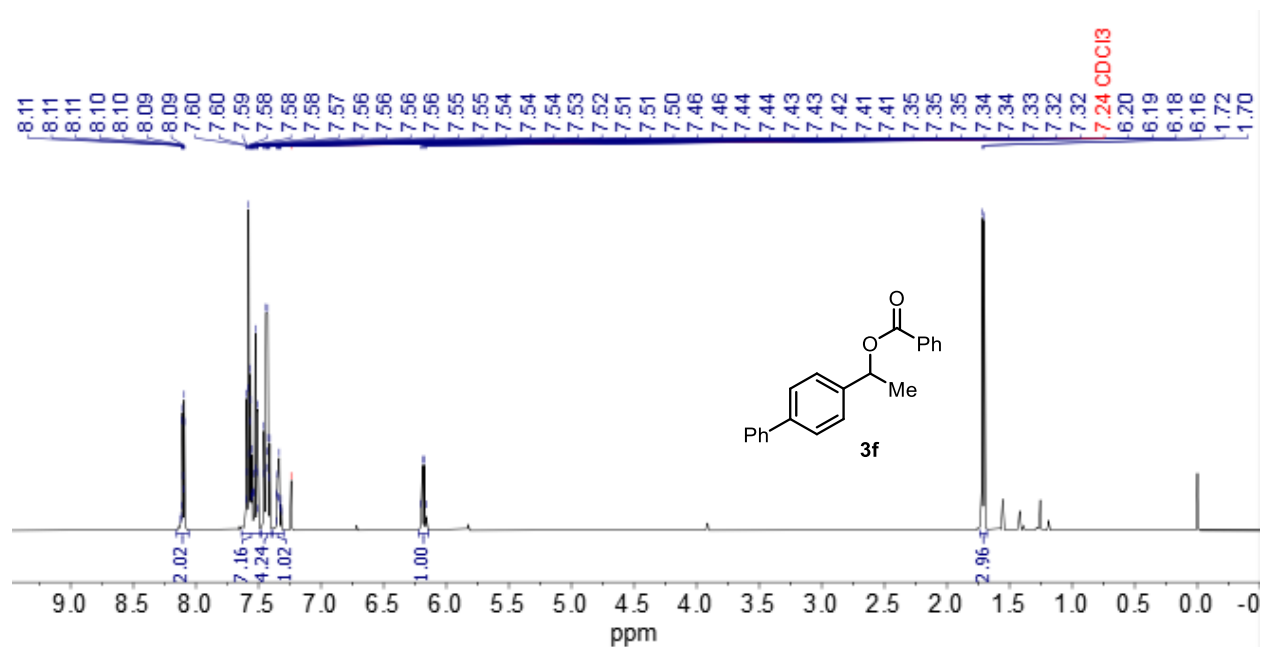
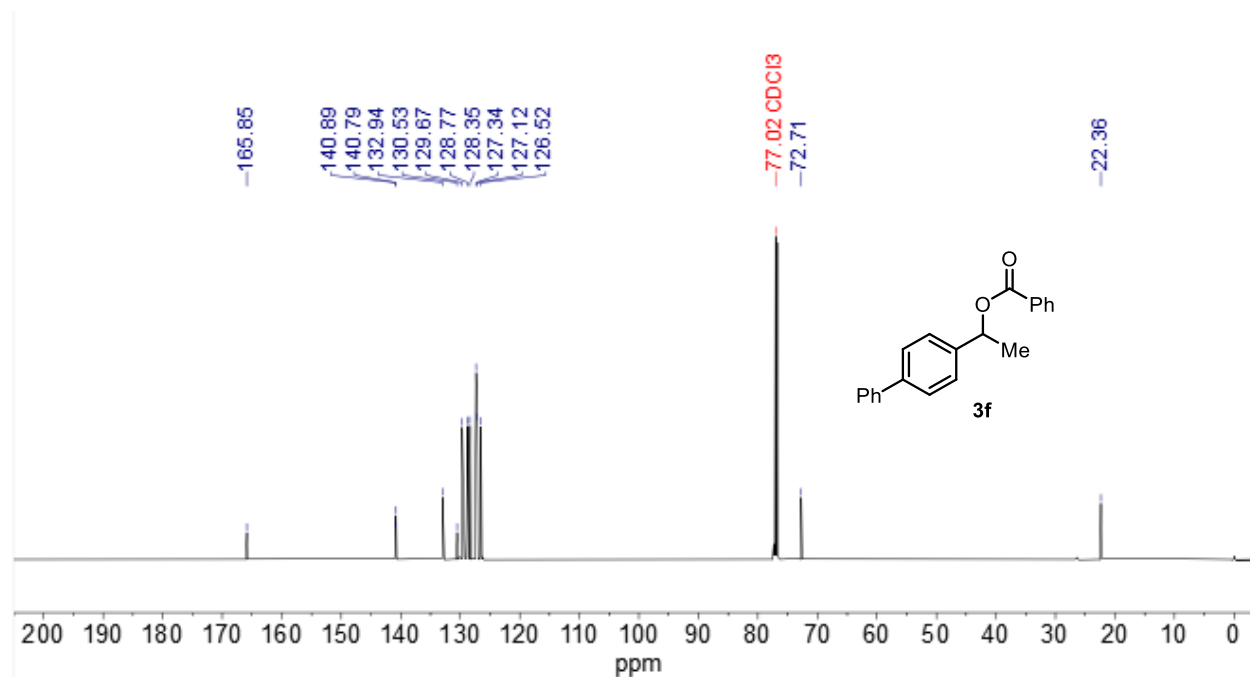
- 1 Hu, H.; Chen, S.-J.; Mandal, M.; Pratik, S. M.; Buss, J. A.; Krska, S. W.; Cramer, C. J.; Stahl, S. S. Copper-Catalysed Benzylic C–H Coupling with Alcohols via Radical Relay Enabled by Redox Buffering. *Nat. Catal.* **2020**, *3*, 358–367.
- 2 Bruker-AXS (2019). *APEX3*. Version 2019.11-0. Madison, Wisconsin, USA.
- 3 Krause, L., Herbst-Irmer, R., Sheldrick, G. M. & Stalke, D. Comparison of Silver and Molybdenum Microfocus X-Ray Sources for Single-Crystal Structure Determination. *J. Appl. Cryst.* **2015**, *48*, 3–10.
- 4 Sheldrick, G. M. (2013b). *XPREP*. Version 2013/1. Georg-August-Universität Göttingen, Göttingen, Germany.
- 5 Sheldrick, G. M. (2013a). The *SHELX* homepage, <http://shelx.uni-ac.gwdg.de/SHELX/>.
- 6 Sheldrick, G. M. SHELXT-Integrated Space-Group and Crystal-Structure Determination. *Acta Cryst.* **2015**, *A71*, 3–8.
- 7 Sheldrick, G. M. Crystal Structure Refinement with *SHELX*. *Acta Cryst.* **2015**, *C71*, 3–8.
- 8 Dolomanov, O. V.; Bourhis, L. J.; Gildea, R. J.; Howard, J. A. K.; Puschmann, H. OLEX2: A Complete Structure Solution, Refinement and Analysis Program. *J. Appl. Cryst.* **2009**, *42*, 339–341.
- 9 Guzei, I. A. (2007-2013). *Programs Gn*. University of Wisconsin-Madison, Madison, Wisconsin, USA.
- 10 Guzei, I. A. An Idealized Molecular Geometry Library for Refinement of Poorly Behaved Molecular Fragments with Constraints. *J. Appl. Cryst.* **2014**, *47*, 806–809.
- 11 Cismesia, M. A.; Yoon, T. P. Characterizing Chain Processes in Visible Light Photoredox Catalysis. *Chem. Sci.* **2015**, *6*, 5426–5434.
- 12 Zheng, J.; Swords, W. B.; Jung, H.; Skubi, K. L.; Kidd, J. B.; Meyer, G. J.; Baik, M. – H.; Yoon, T. P. Enantioselective Intermolecular Excited-State Photoreactions Using a Chiral Ir Triplet Sensitizer: Separating Association from Energy Transfer in Asymmetric Photocatalysis. *J. Am. Chem. Soc.* **2019**, *252*, 13625–13634.
- 13 Hatchard, C. G.; Parker, C. A. A New Sensitive Chemical Actinometer - II. Potassium Ferrioxalate as a Standard Chemical Actinometer. *Proc. Roy. Soc. (London)* **1956**, *A235*, 518–536.
- 14 Demas, J. N.; Bowman, W. D.; Zalewski, E. F.; Velapoldi. Determination of the Quantum Yield of the Ferrioxalate Actinometer with Electrically Calibrated Radiometers. *J. Phys. Chem.* **1981**, *85*, 2766–2771.
- 15 Rabani, J.; Mamane, H.; Pousty, D.; Bolton, J. R. Practical Chemical Actinometry - A Review. *Photochem Photobiol.* **2021**, *97*, 873–902.
- 16 Mayr, S.; Marin-Luna, M.; Zipse, H. Size-Driven Inversion of Selectivity in Esterification Reactions: Secondary Beat Primary Alcohols. *Org. Lett.* **2021**, *86*, 3456–3489.
- 17 Li, C.; Deng, H.; Jin, T.; Li, C.; Jia, X.; Li, J. NHPI- and TBAI-Co-Catalyzed Synthesis of Allylic Esters from Toluene Derivatives and Alkenes. *Synlett* **2018**, *29*, 840–844.

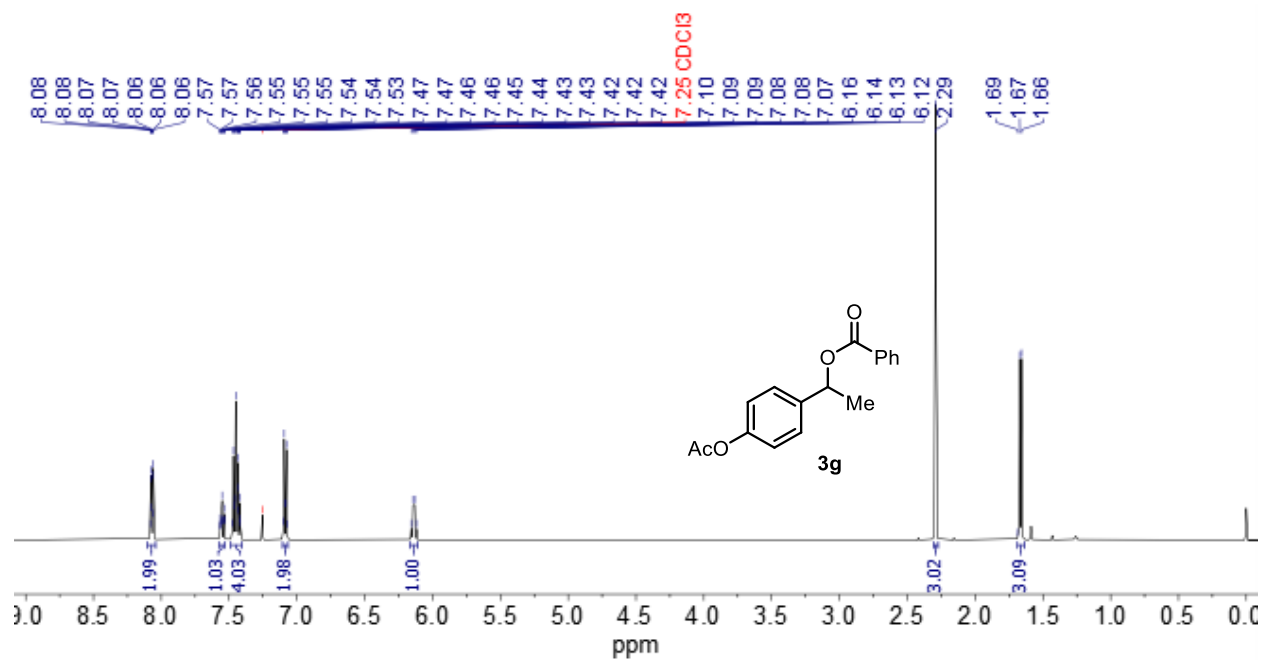
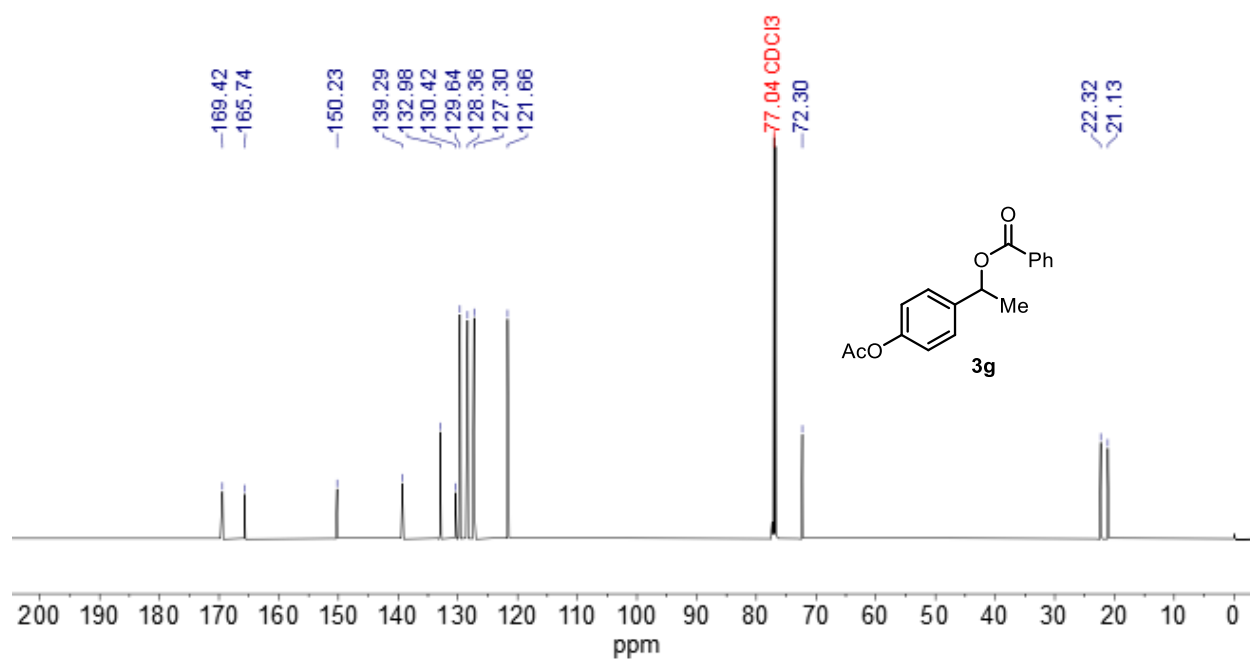
- 18 Baba, H.; Moriyama, K.; Togo, H. Benzylic-Acetoxylation of Alkylbenzenes with $\text{PhI}(\text{OAc})_2$ in the Presence of Catalytic Amounts of TsNH_2 and I_2 . *Tetrahedron Lett.* **2011**, *52*, 4303–4307.
- 19 Lee, B. J.; DeGlopper, K. S.; Yoon, T. P. Site-Selective Alkoxylation of Benzylic C–H Bonds by Photoredox Catalysis. *Angew. Chem. Int. Ed.* **2020**, *59*, 197–202.
- 20 Mayr, S.; Zipse, H. Size-Induced Inversion of Selectivity in the Acylation of 1,2-Diols. *Chem. Eur. J.* **2021**, *27*, 18084–18092.
- 21 Trzepizur, D.; Brodzka, A.; Koszelewski, D.; Wilk, M.; Ostaszewski, R. Selective Palladium-Catalyzed α,β -Homodiarylation of Vinyl Esters in Aqueous Medium. *Eur. J. Org. Chem.* **2021**, *2021*, 6028–6036.
- 22 Weidmann, N.; Harenberg, J. H.; Knochel, P. Continuous Flow Preparation of (Hetero)benzylic Lithiums via Iodine–Lithium Exchange Reaction under Barbier Conditions. *Org. Lett.* **2020**, *22*, 5895–5899.
- 23 Tanwar, L.; Börgel, J.; Ritter, T. Synthesis of Benzylic Alcohols by C–H Oxidation. *J. Am. Chem. Soc.* **2019**, *141*, 17983–17988.

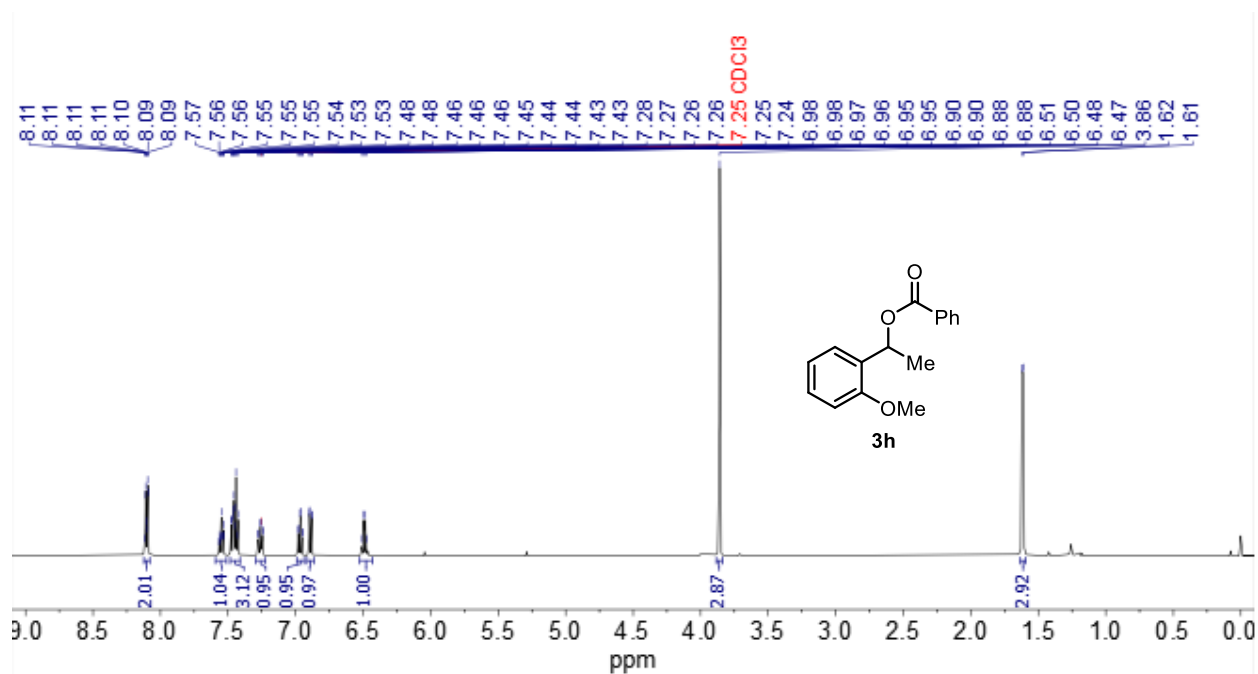
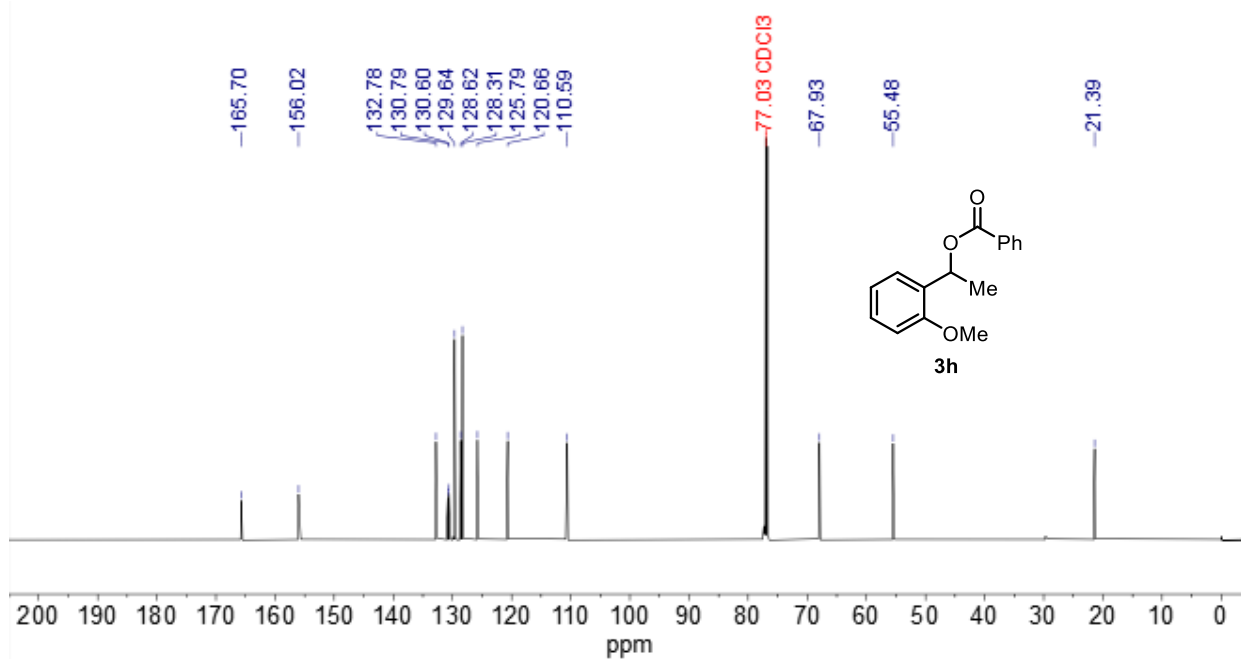
2A.XI. NMR Spectra**¹H NMR (500 MHz, CDCl₃) of 3b****¹³C NMR (126 MHz, CDCl₃) of 3b**

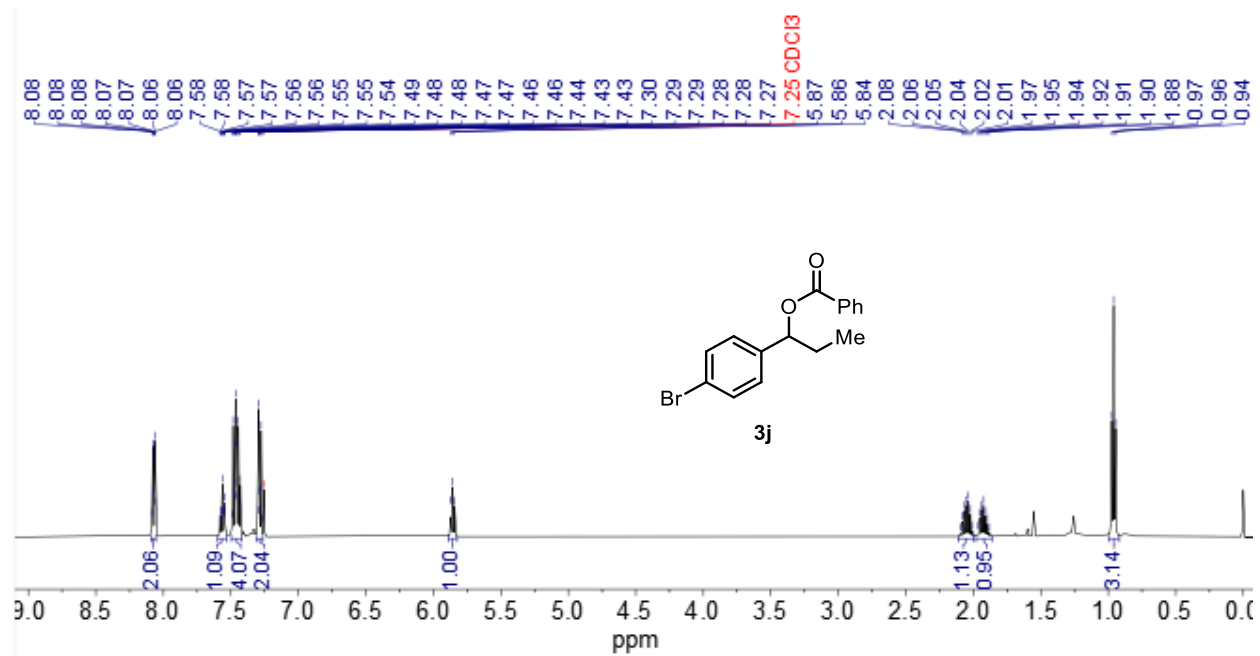
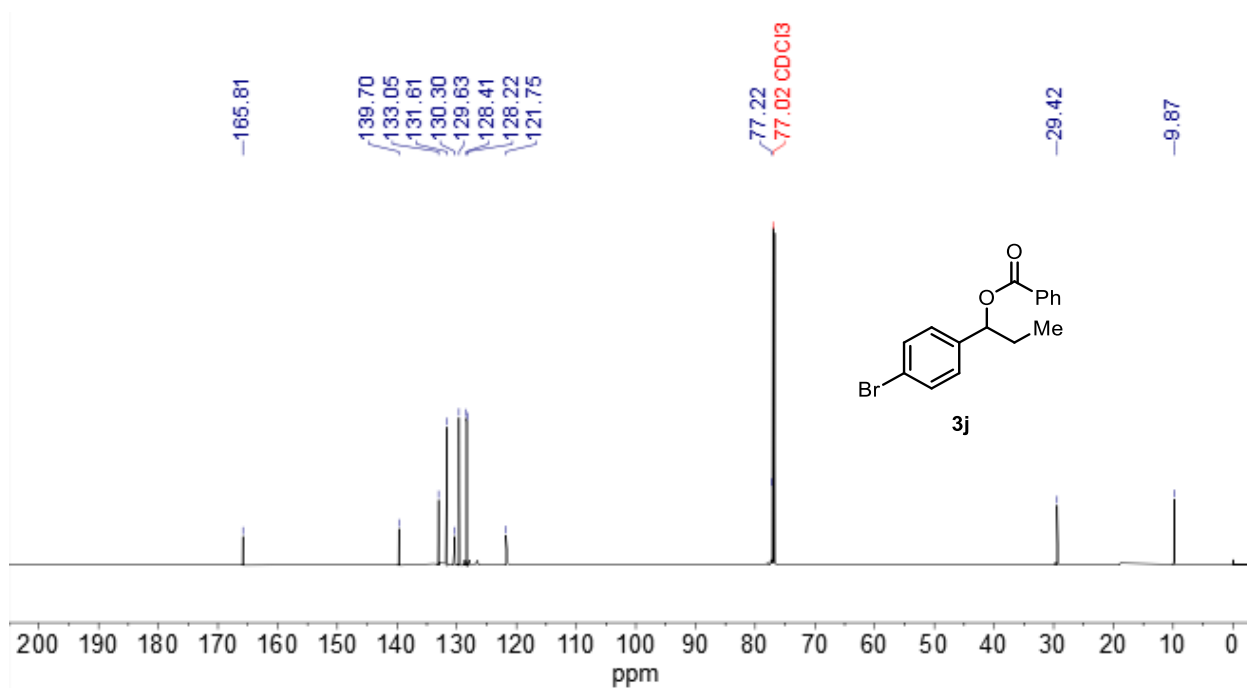
^{19}F NMR (377 MHz, CDCl_3) of **3b**

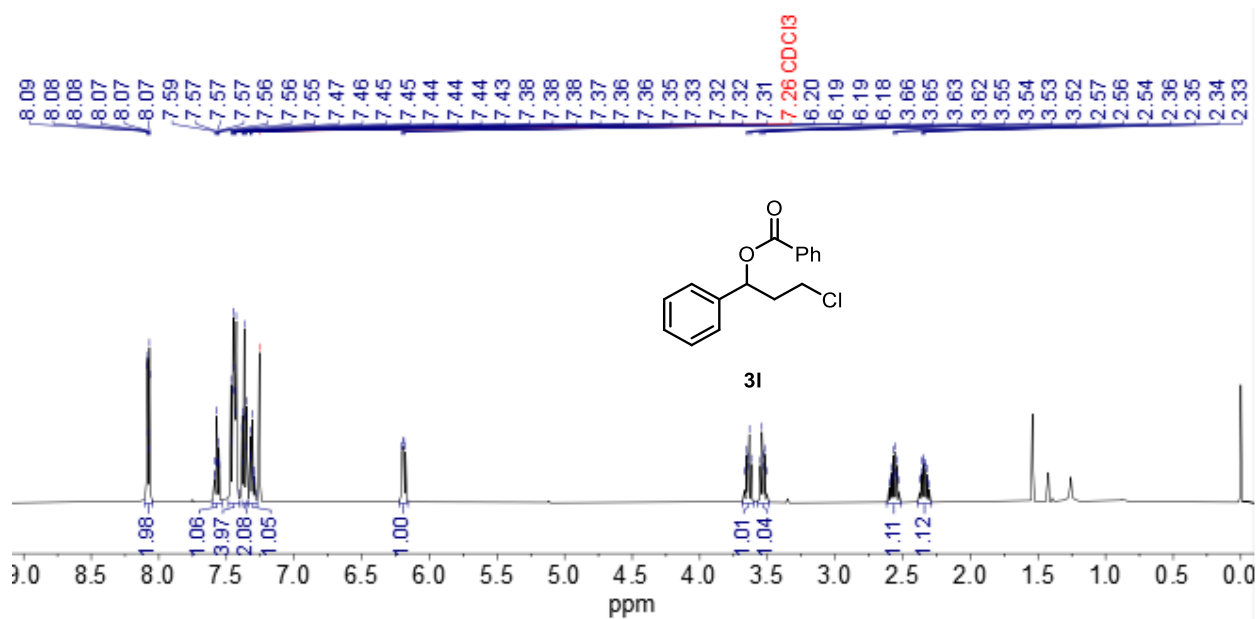
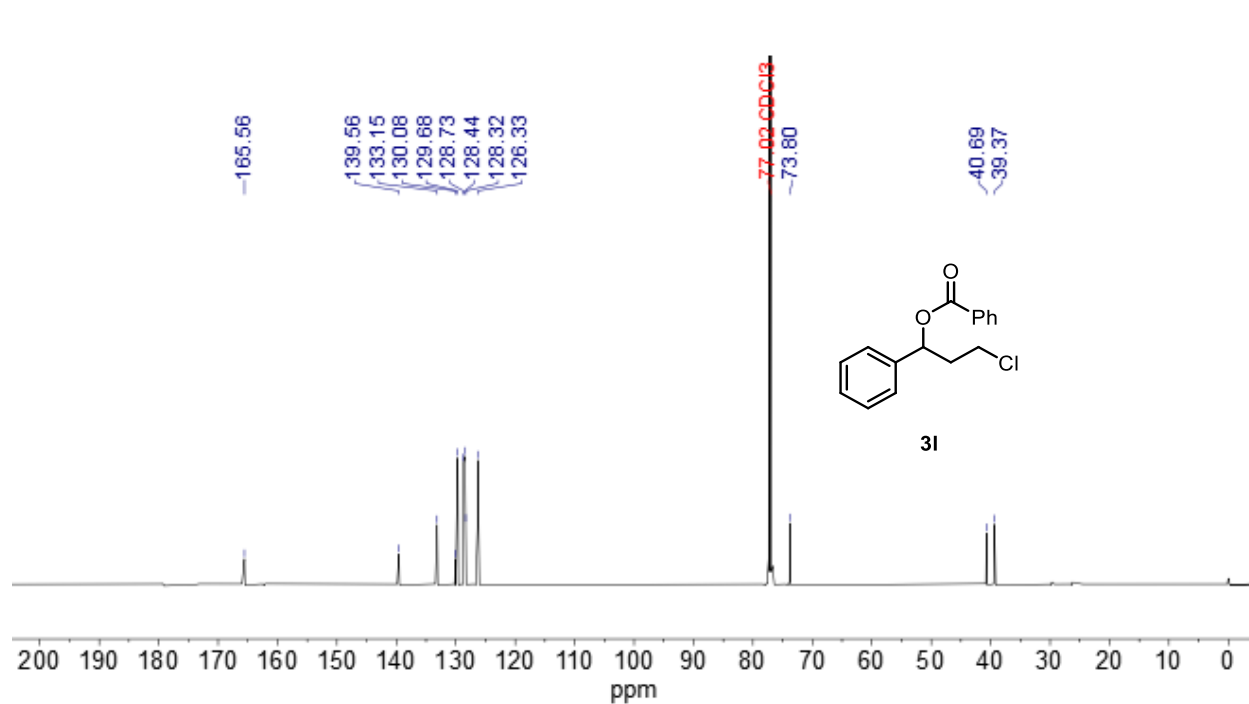


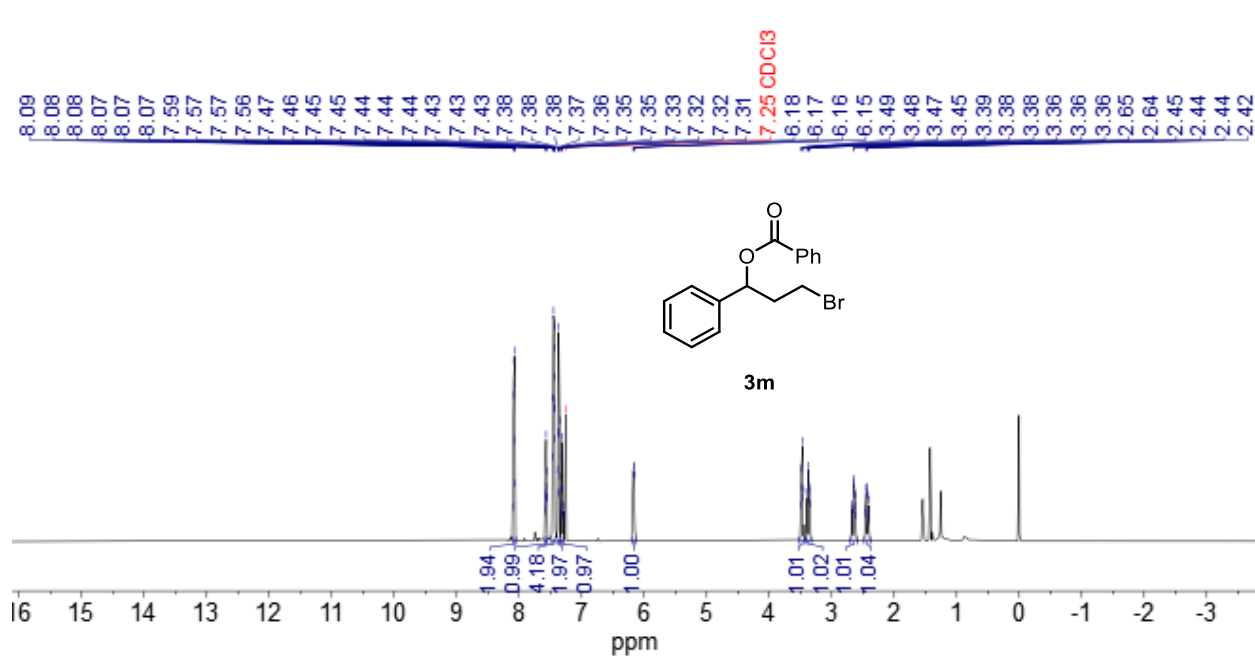
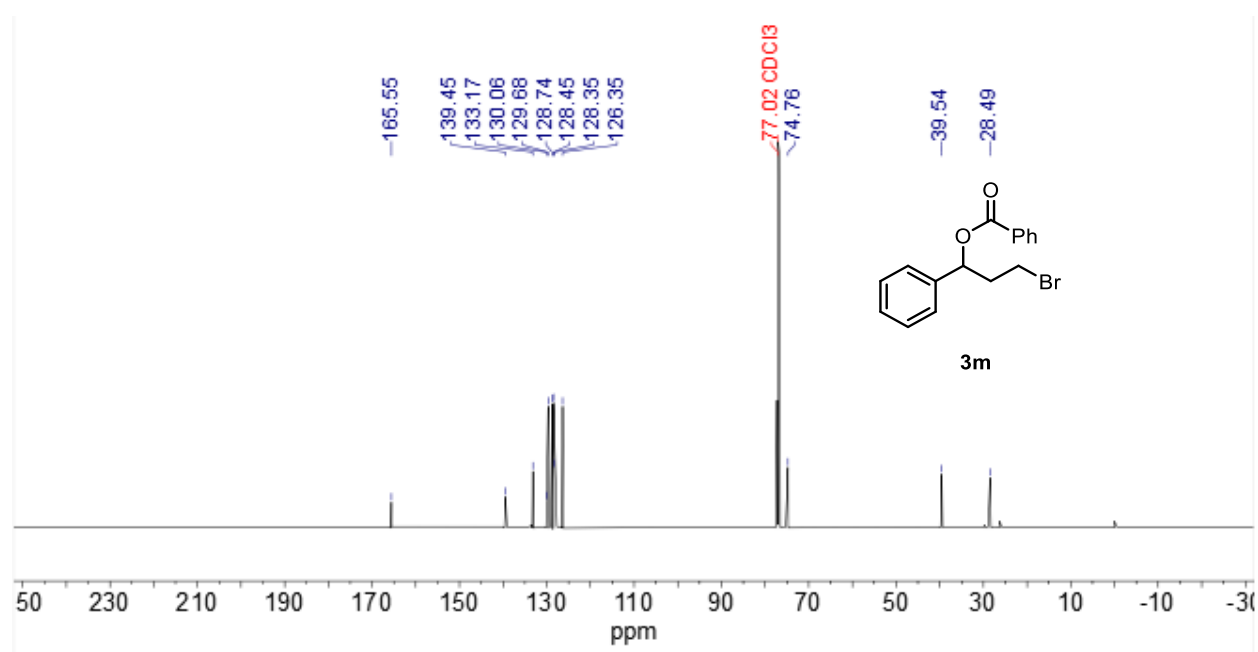
^1H NMR (500 MHz, CDCl_3) of **3f** ^{13}C NMR (126 MHz, CDCl_3) of **3f**

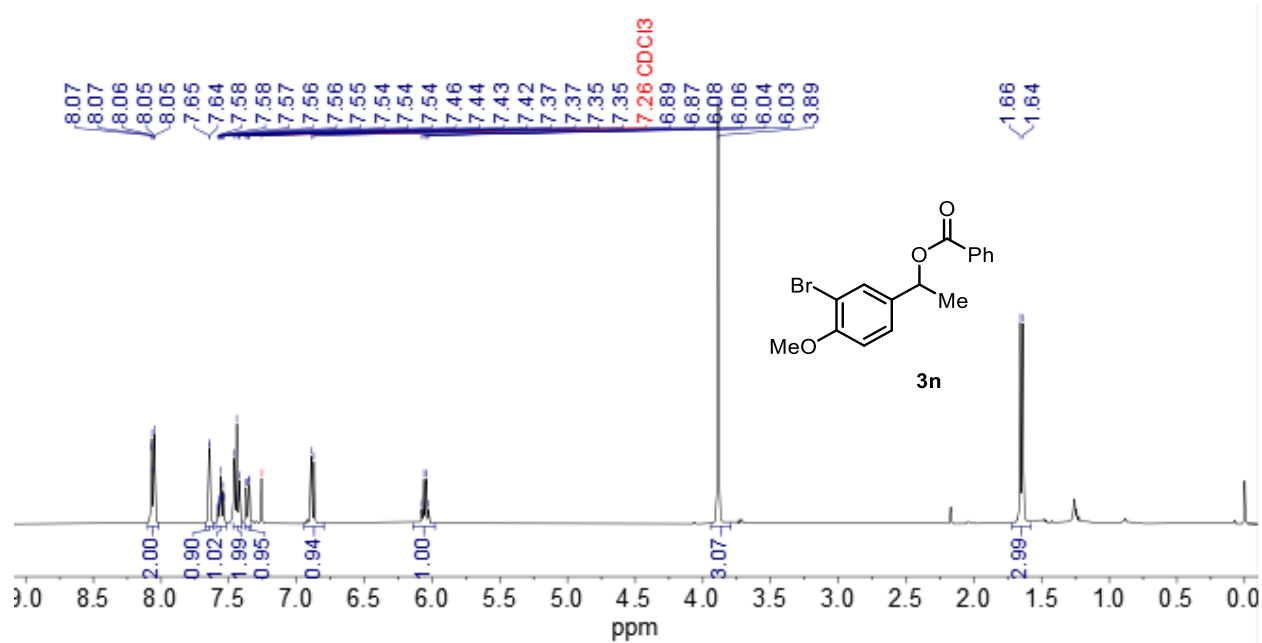
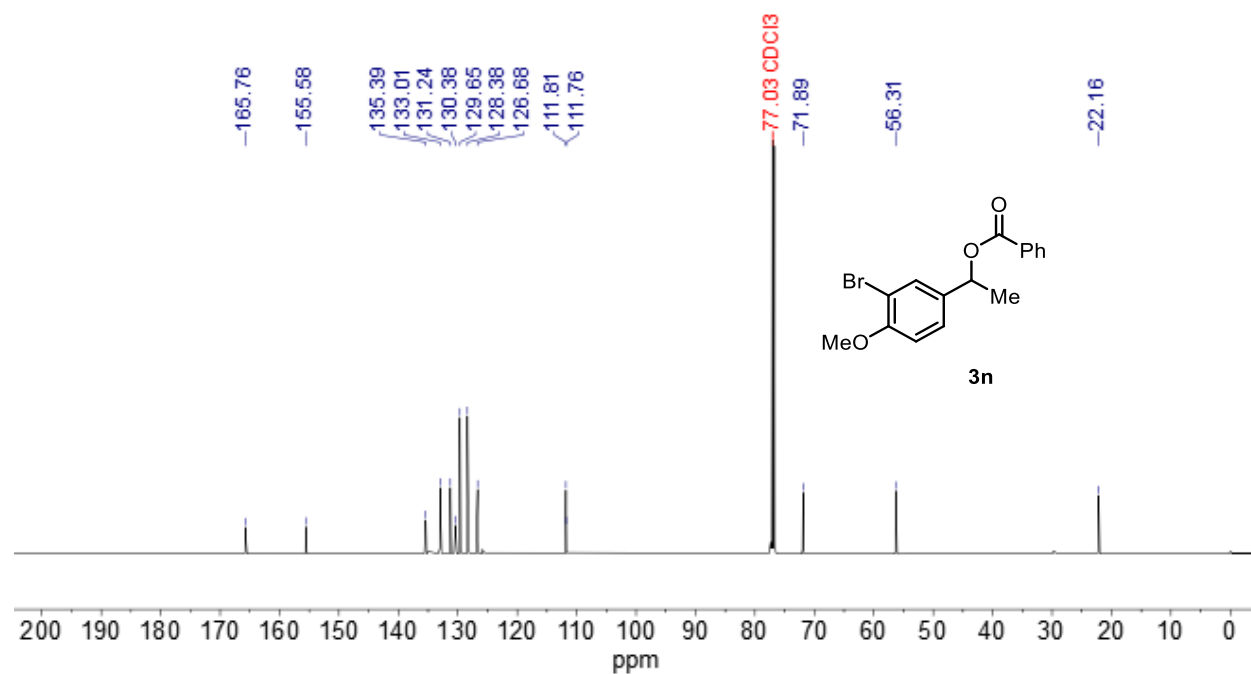
^1H NMR (500 MHz, CDCl_3) of **3g** ^{13}C NMR (126 MHz, CDCl_3) of **3g**

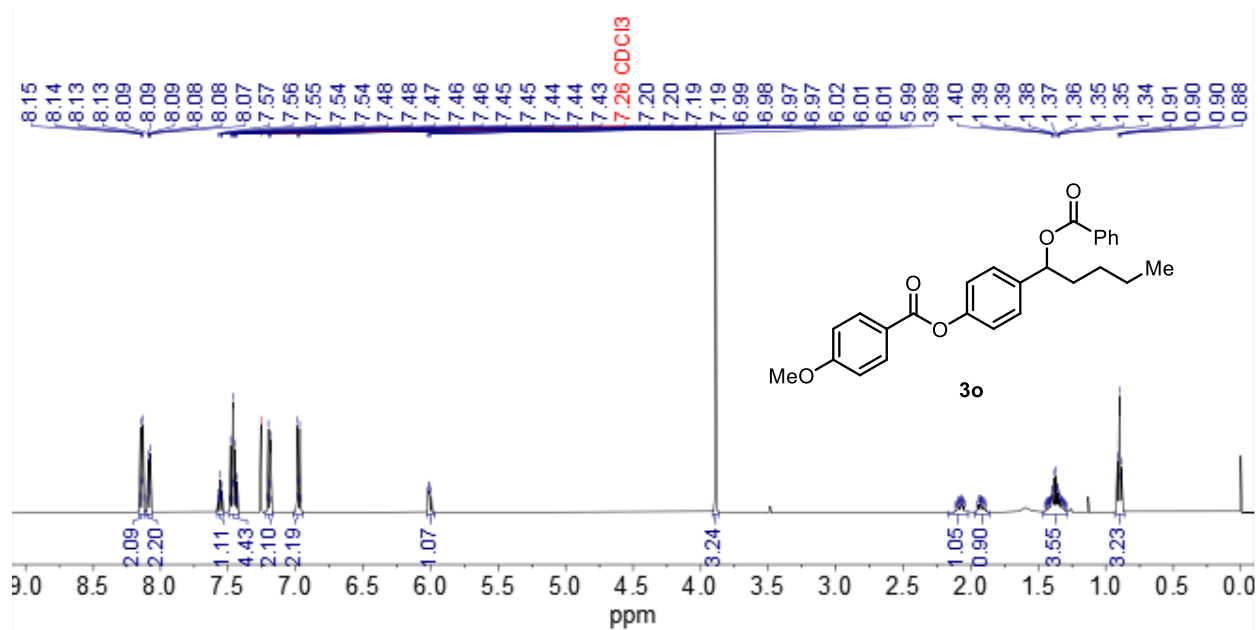
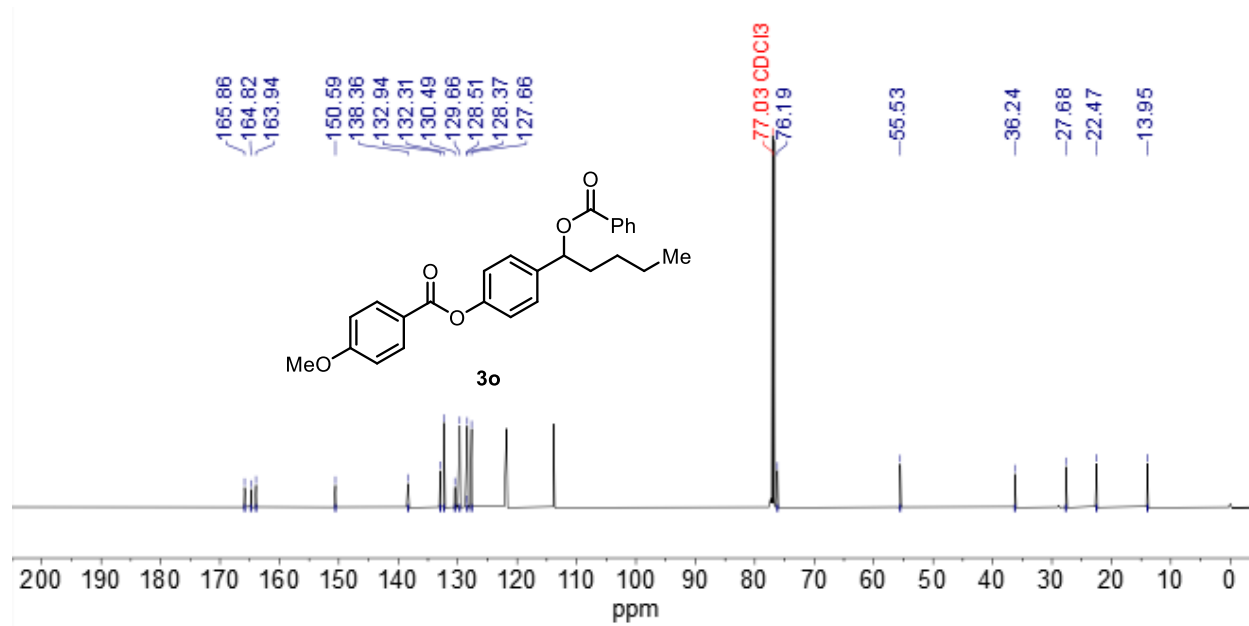
^1H NMR (500 MHz, CDCl_3) of **3h** ^{13}C NMR (126 MHz, CDCl_3) of **3h**

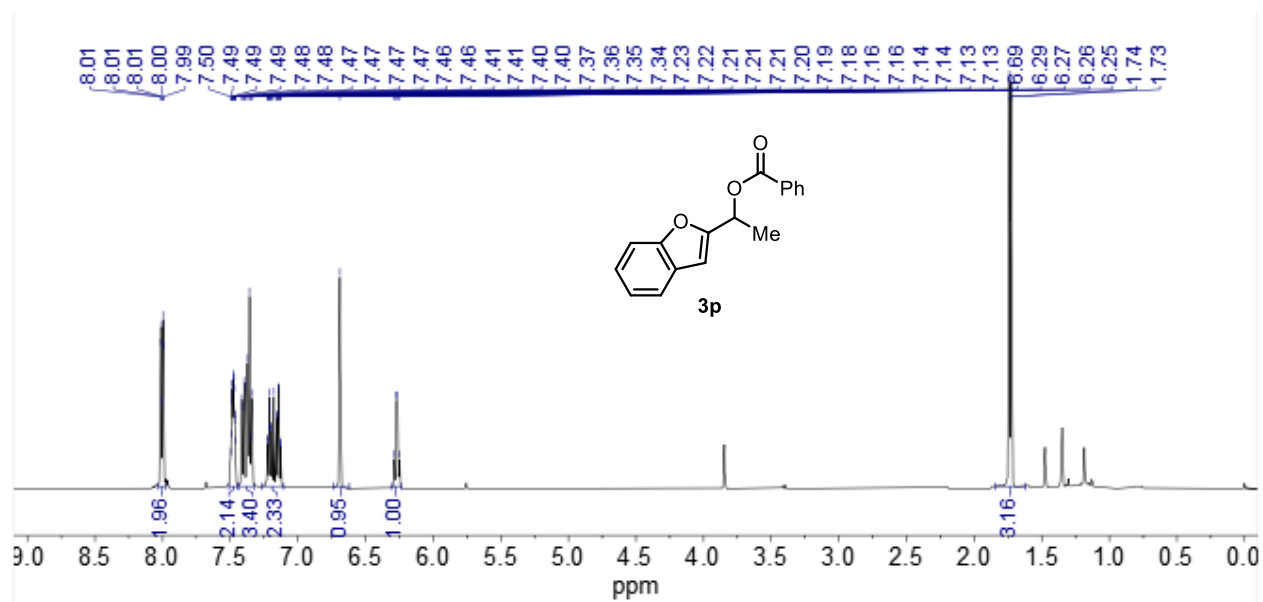
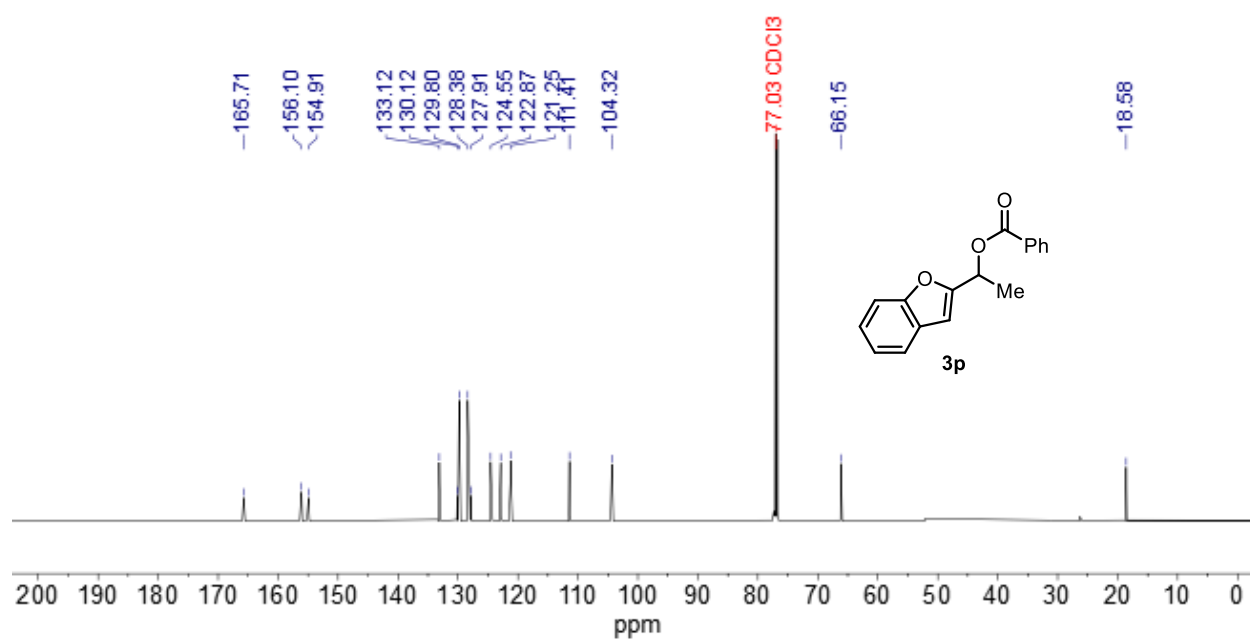
^1H NMR (500 MHz, CDCl_3) of **3j** **^{13}C NMR (126 MHz, CDCl_3) of **3j****

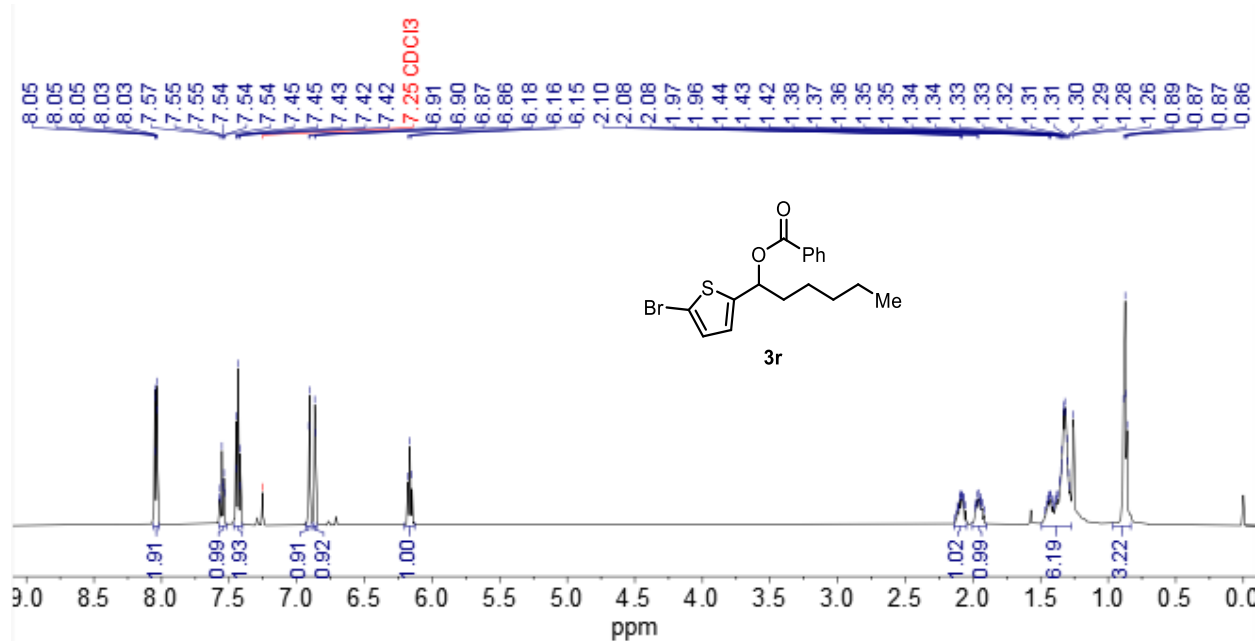
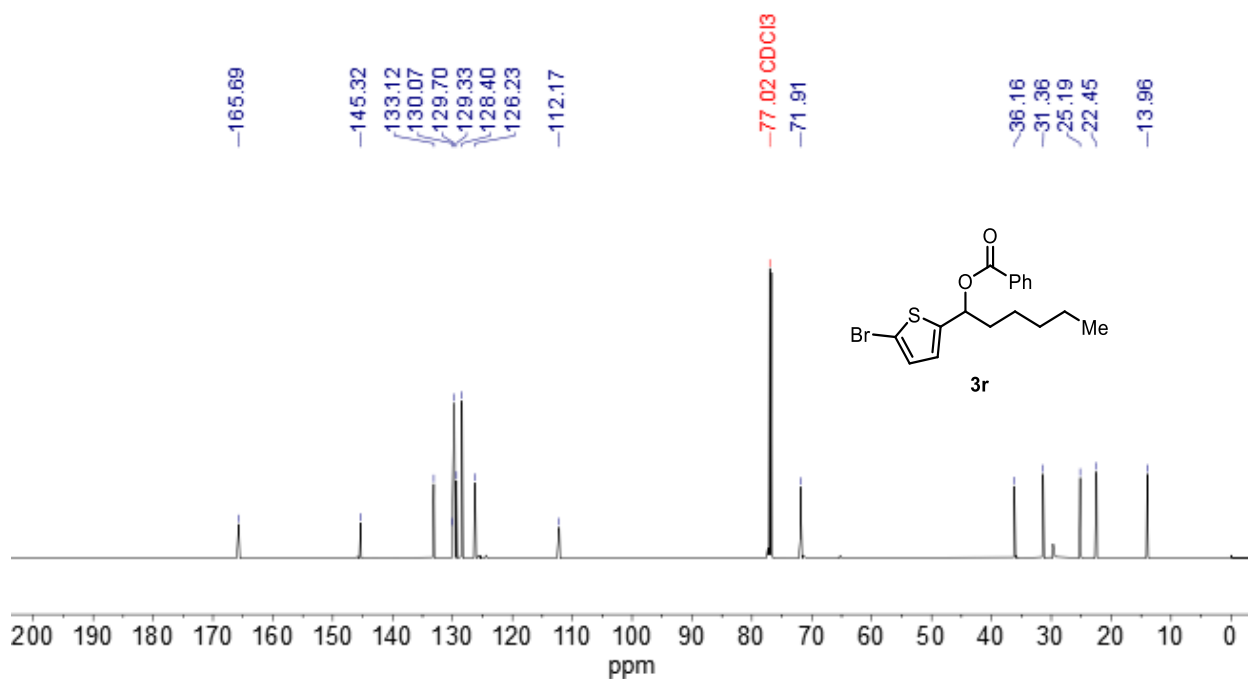
¹H NMR (500 MHz, CDCl₃) of 31**¹³C NMR (126 MHz, CDCl₃) of 31**

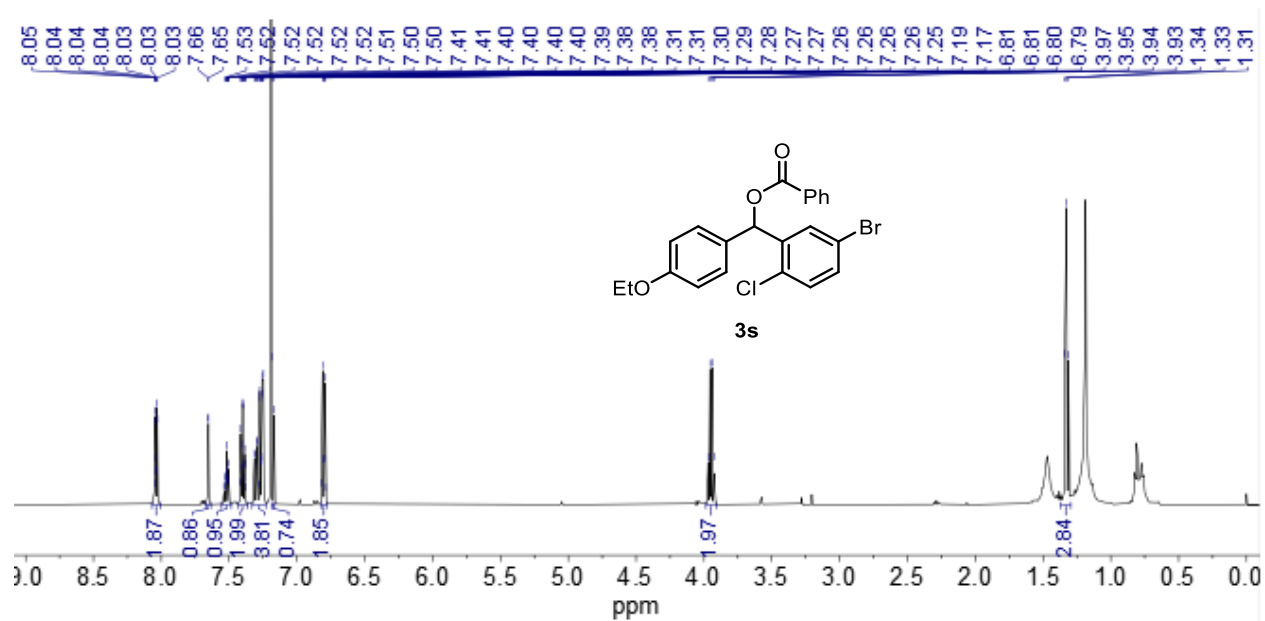
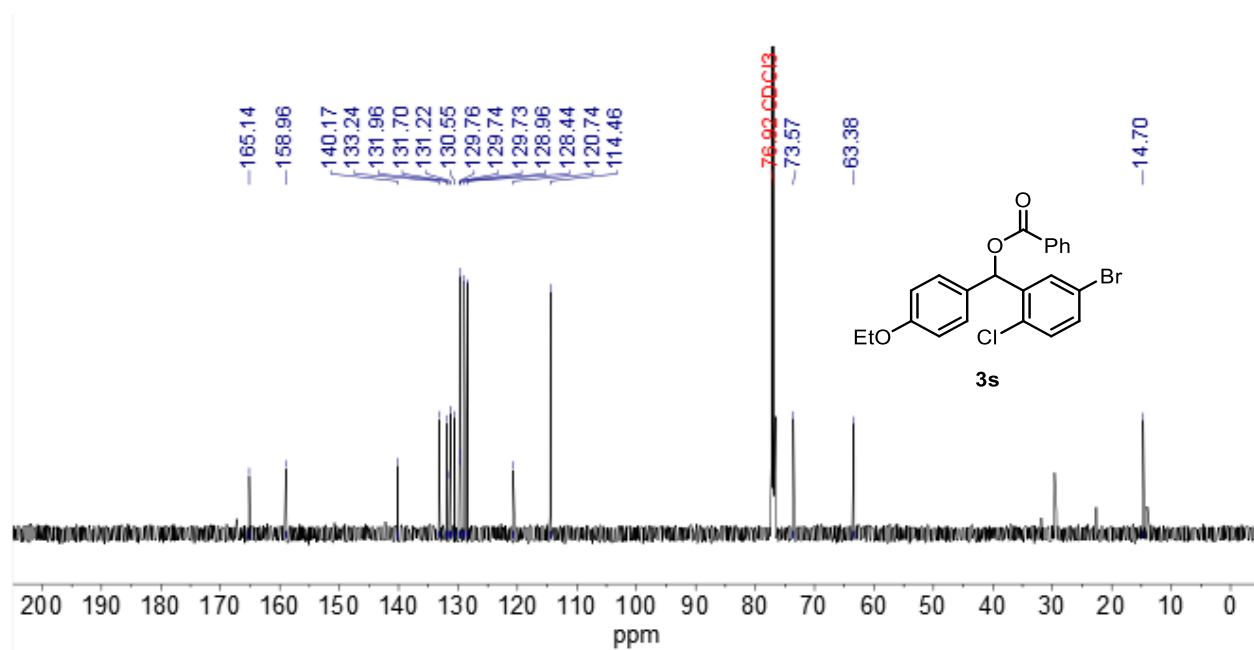
^1H NMR (500 MHz, CDCl_3) of **3m** ^{13}C NMR (126 MHz, CDCl_3) of **3m**

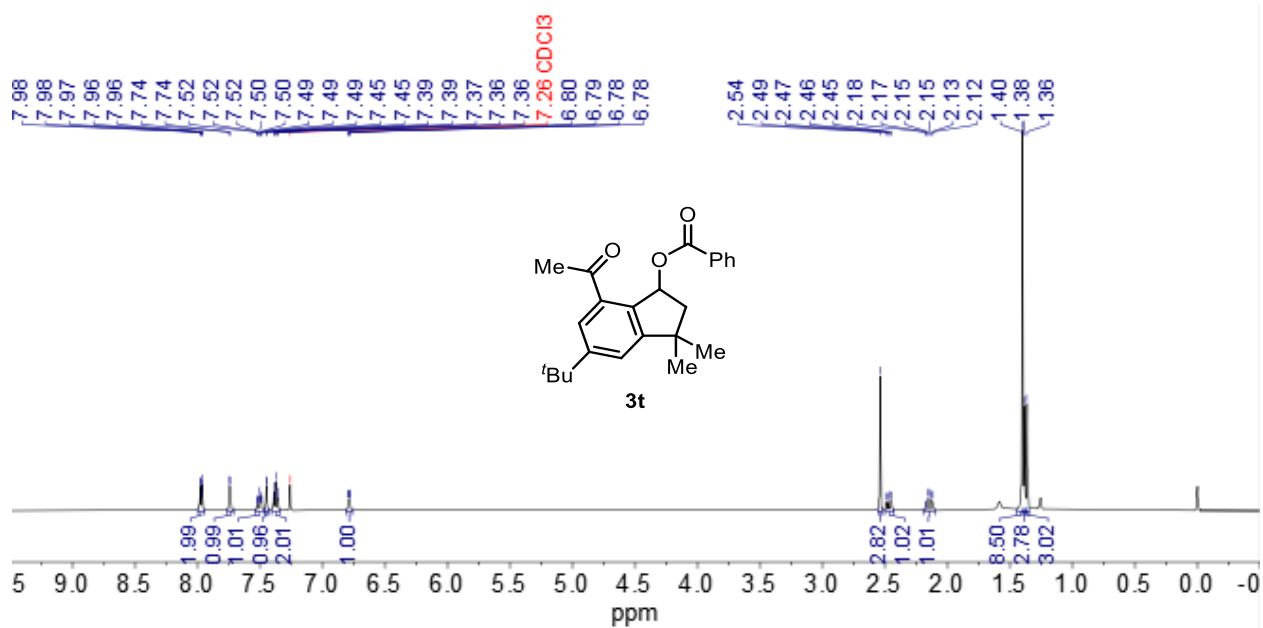
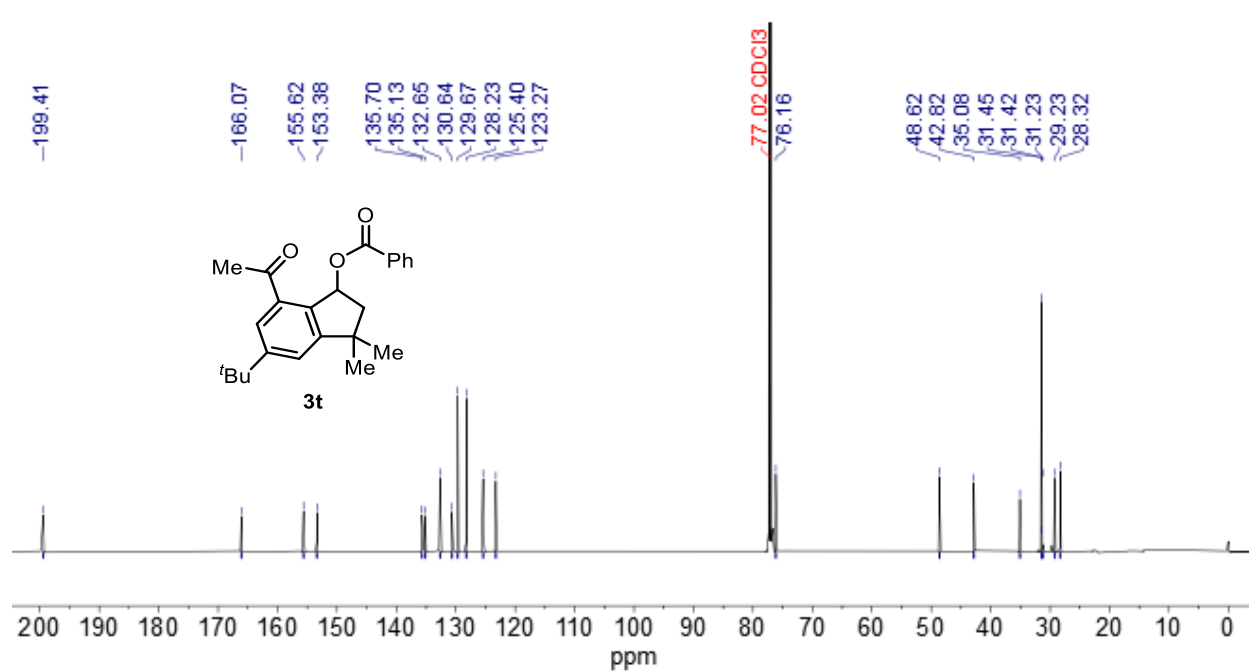
^1H NMR (500 MHz, CDCl_3) of **3n** **^{13}C NMR (126 MHz, CDCl_3) of **3n****

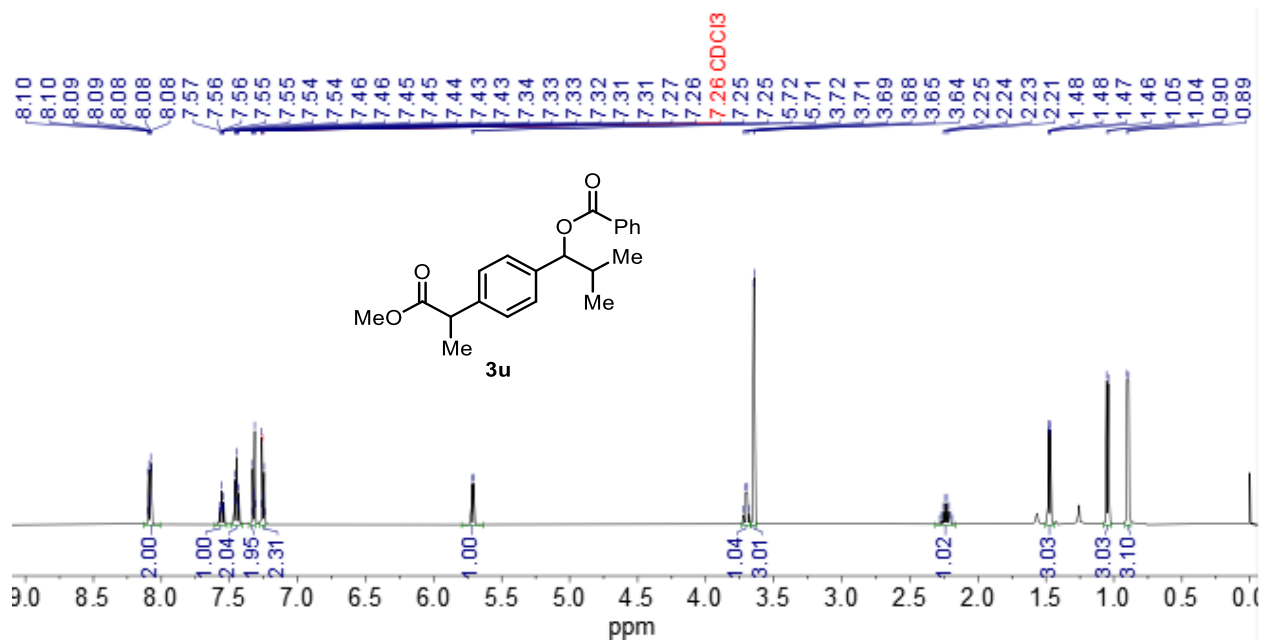
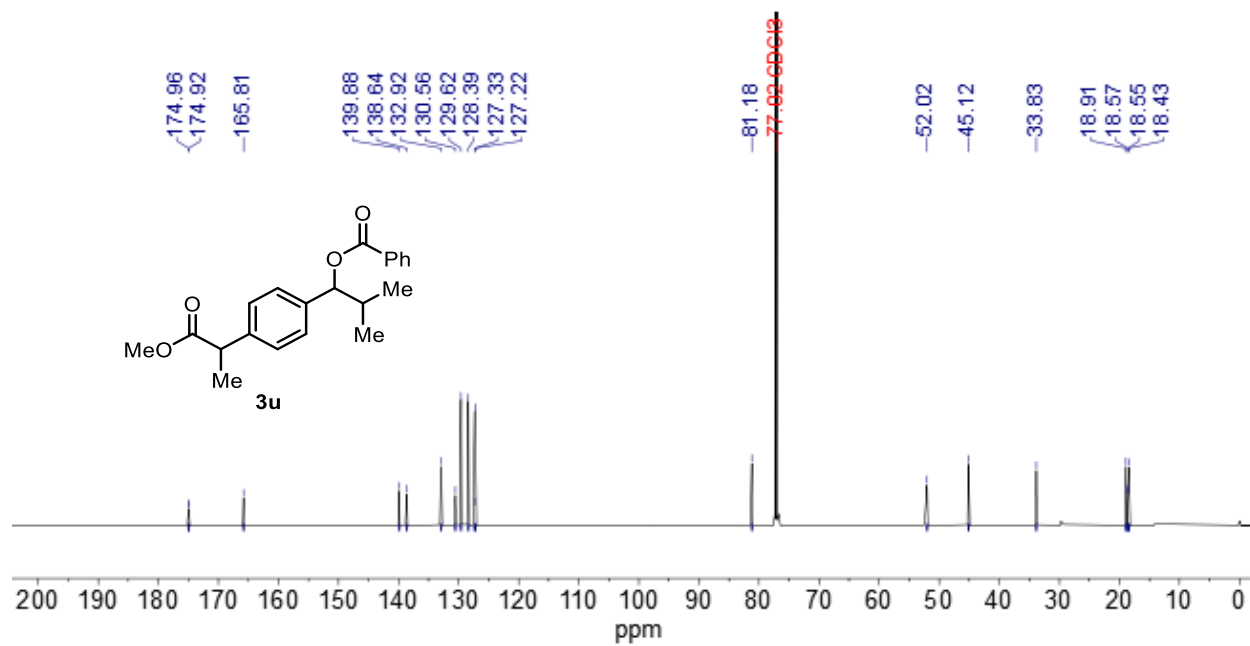
¹H NMR (500 MHz, CDCl₃) of 3o**¹³C NMR (126 MHz, CDCl₃) of 3o**

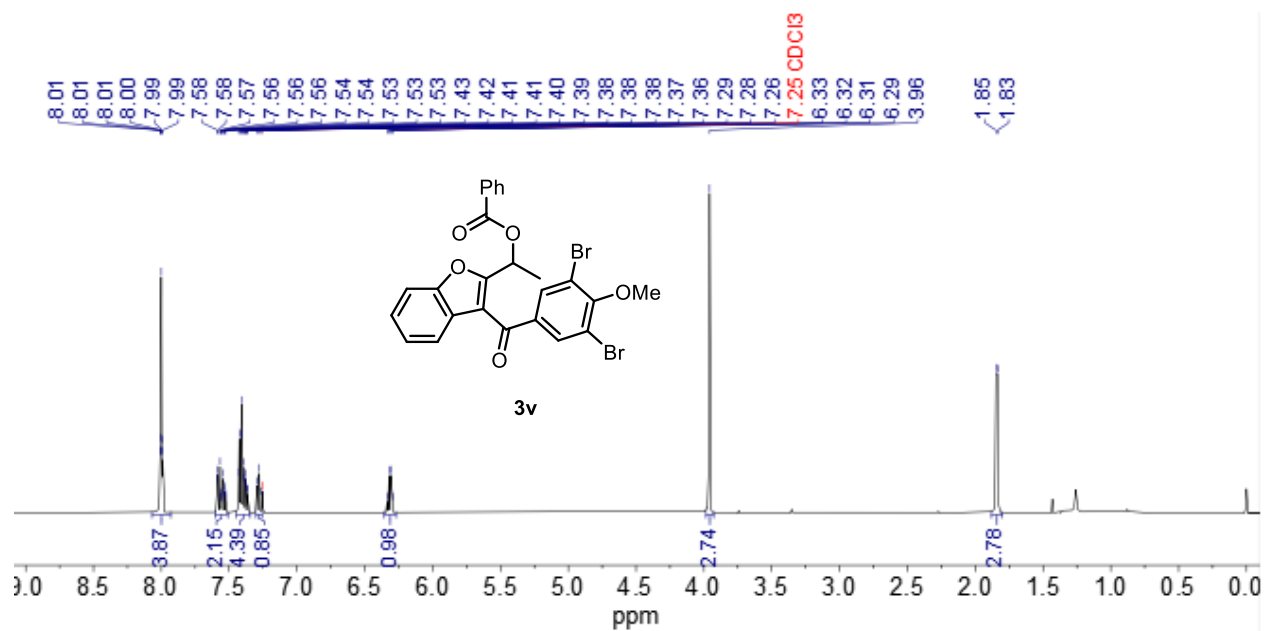
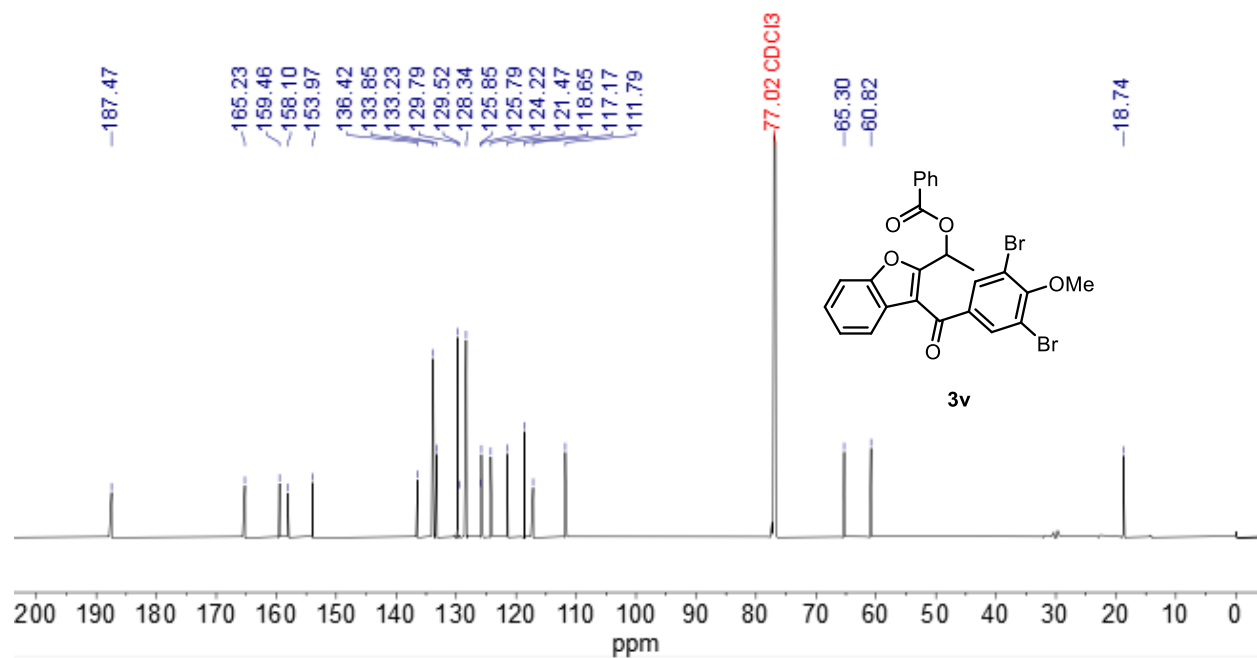
¹H NMR (500 MHz, CDCl₃) of 3p**¹³C NMR (126 MHz, CDCl₃) of 3p**

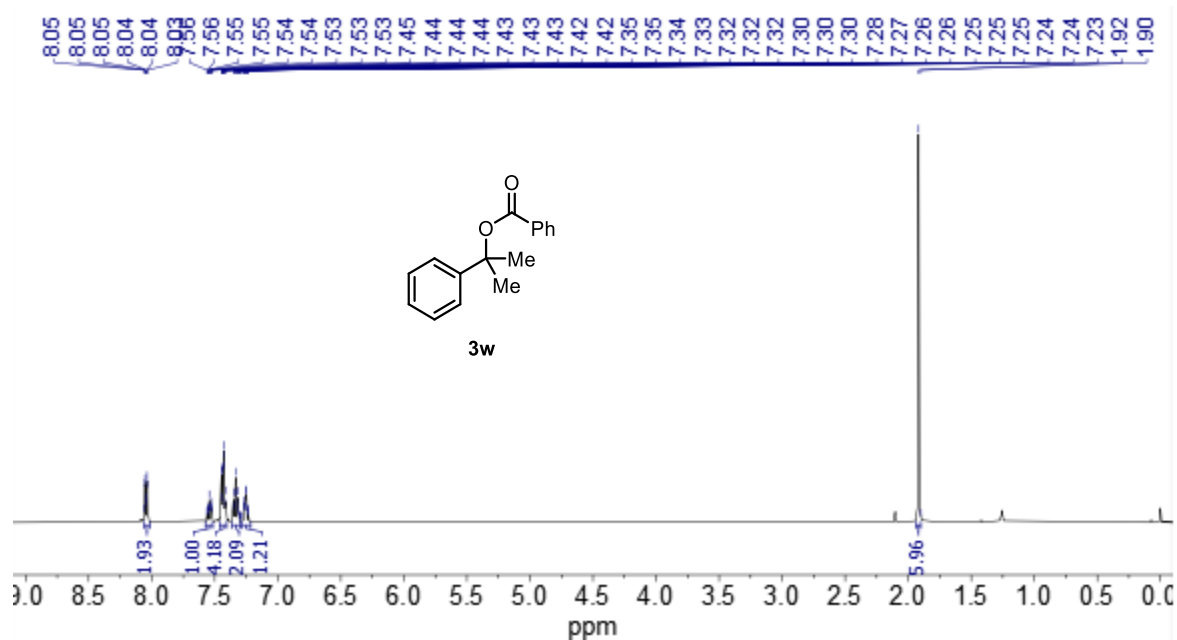
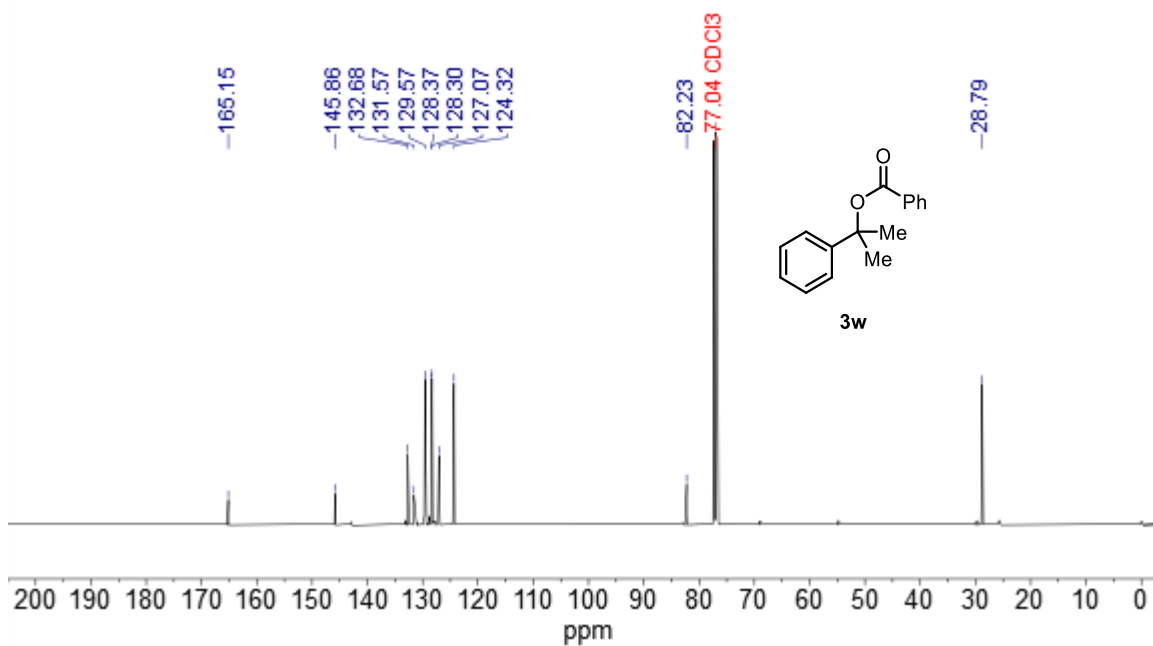
¹H NMR (500 MHz, CDCl₃) of 3r**¹³C NMR (126 MHz, CDCl₃) of 3r**

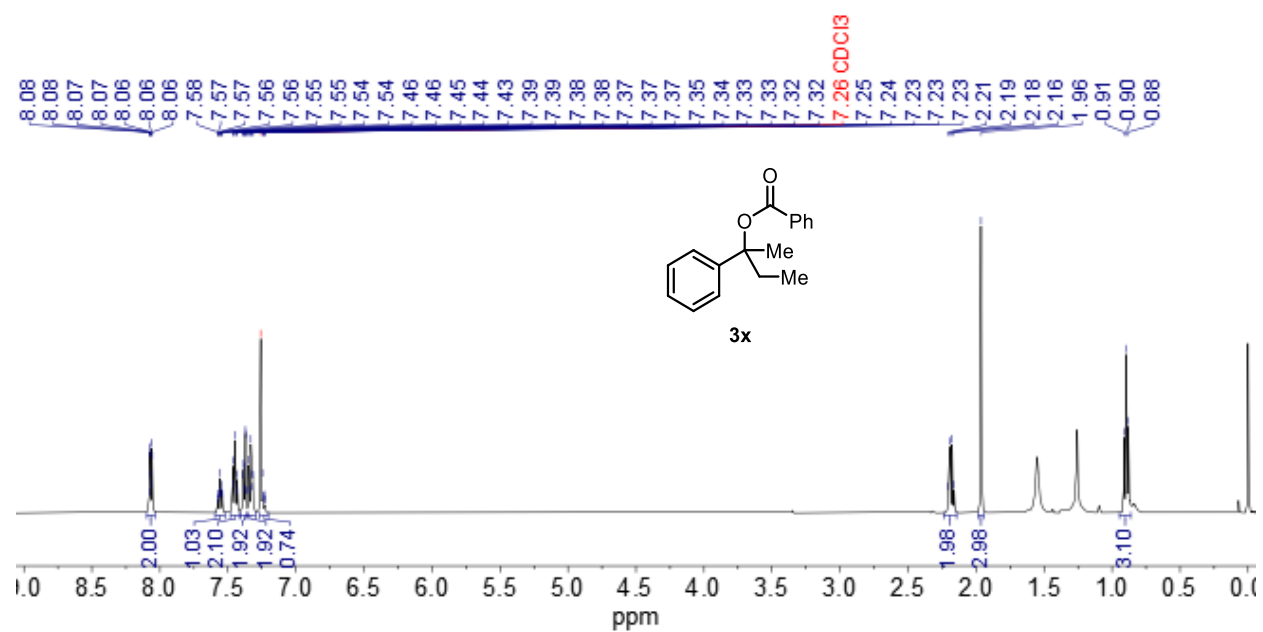
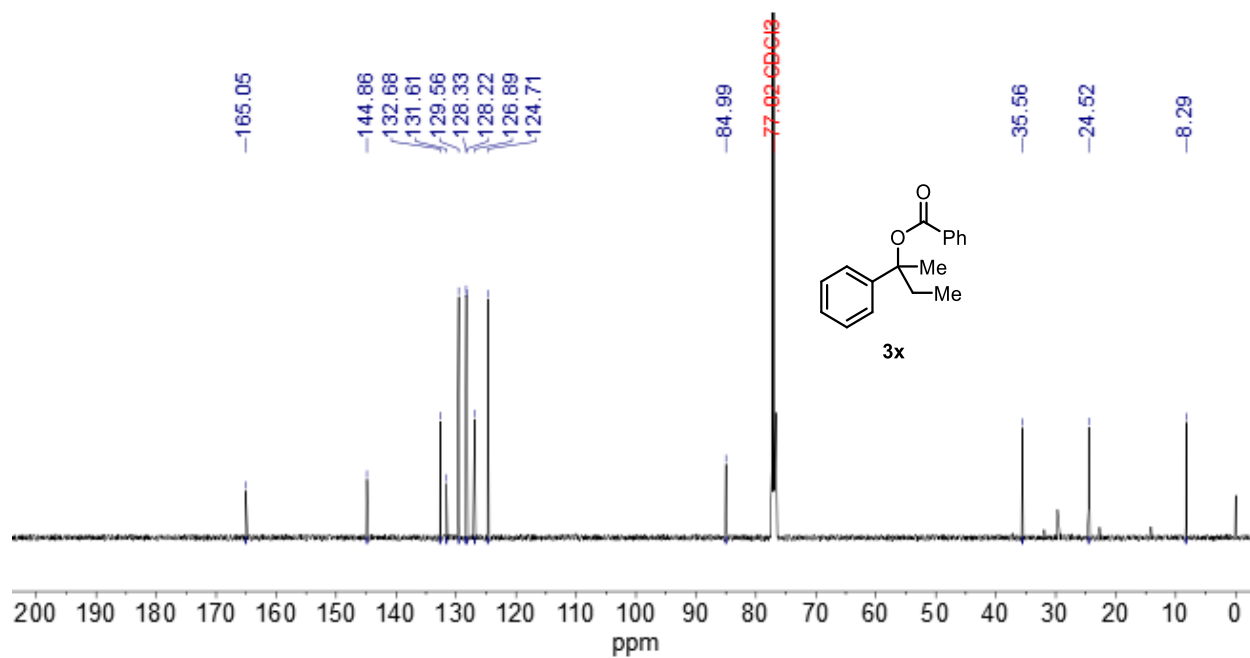
^1H NMR (500 MHz, CDCl_3) of **3s** **^{13}C NMR (126 MHz, CDCl_3) of **3s****

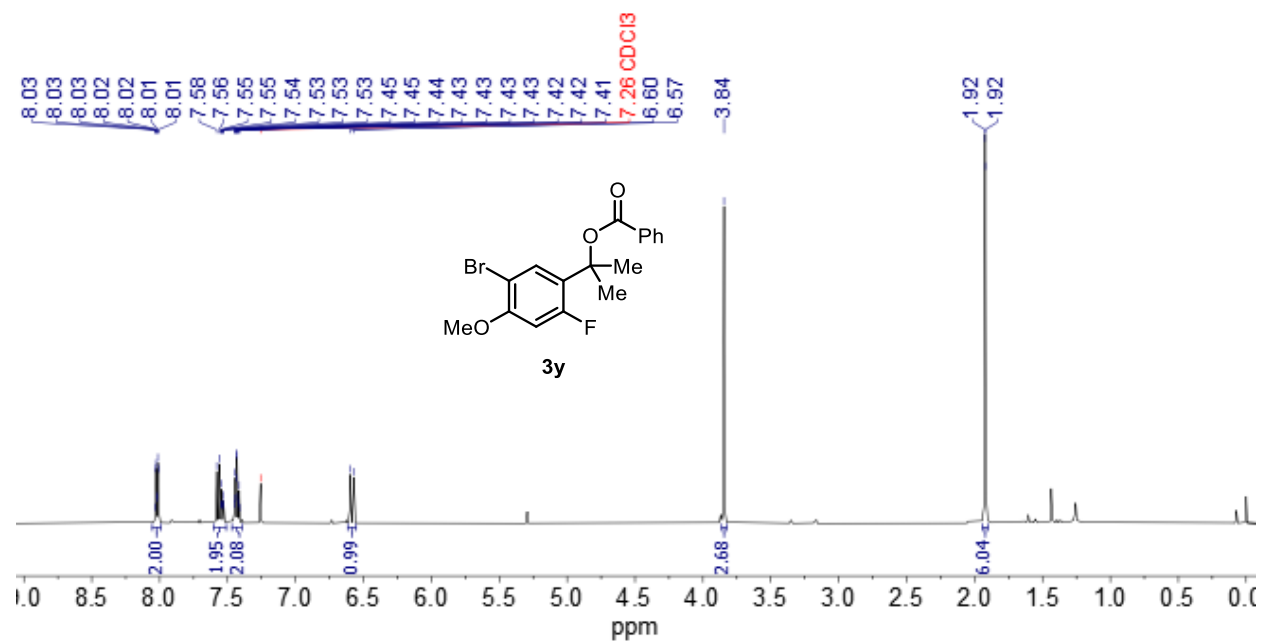
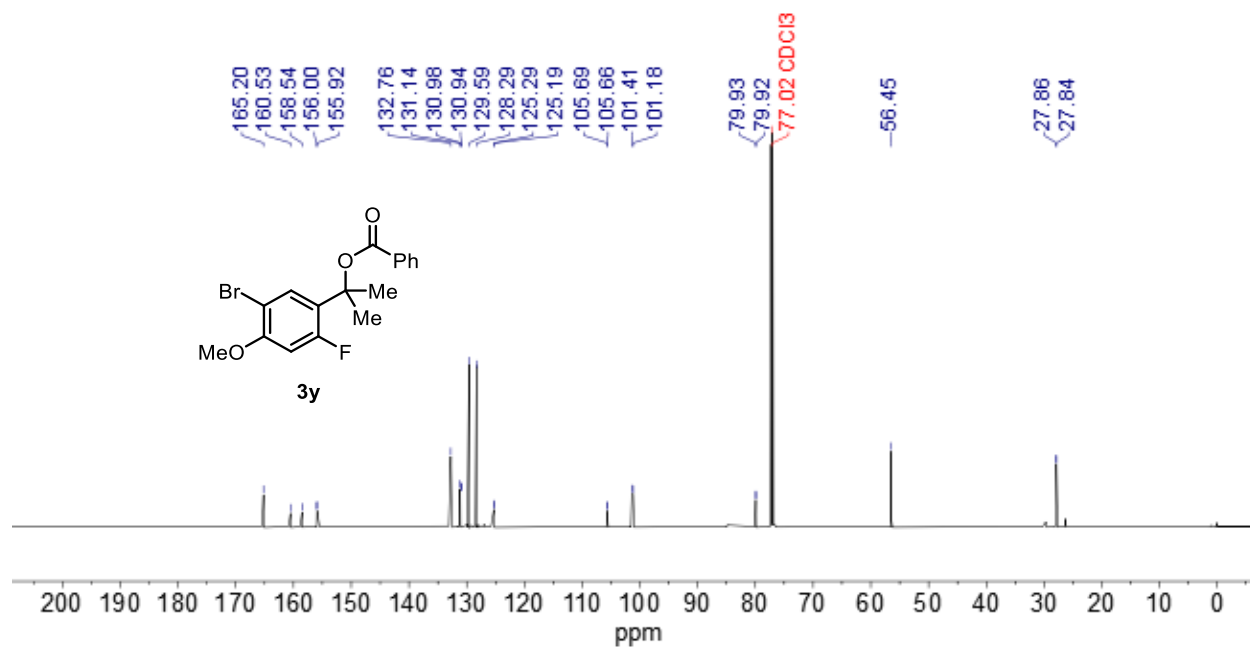
^1H NMR (500 MHz, CDCl_3) of **3t** **^{13}C NMR (126 MHz, CDCl_3) of **3t****

^1H NMR (500 MHz, CDCl_3) of **3u** ^{13}C NMR (126 MHz, CDCl_3) of **3u**

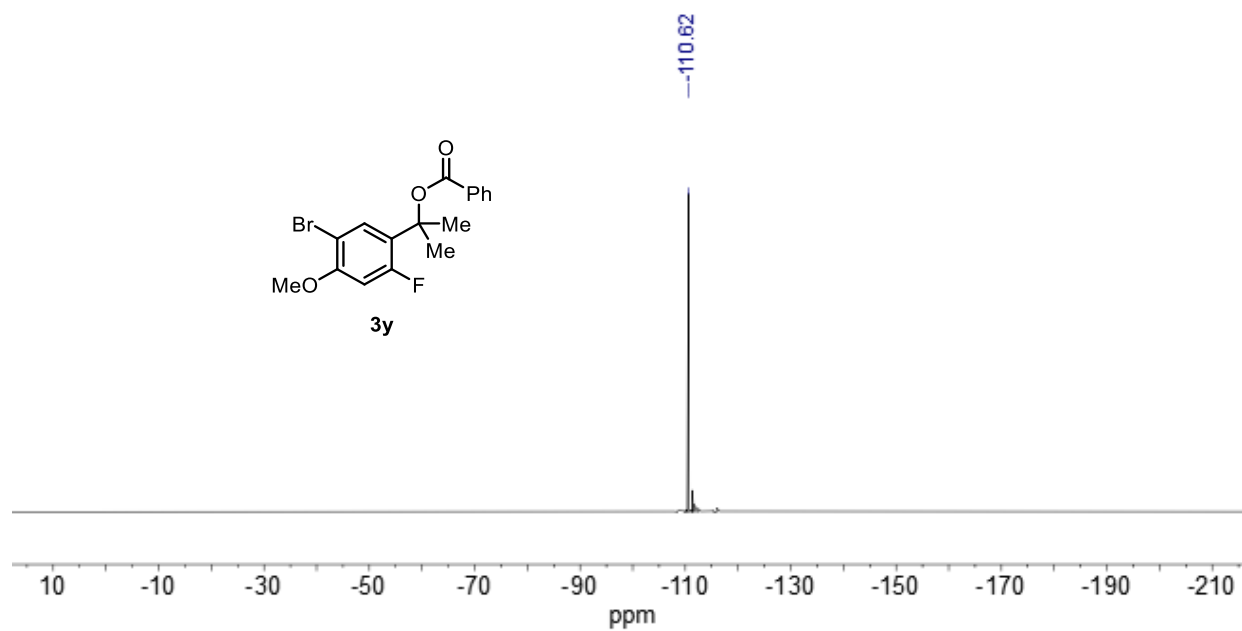
¹H NMR (500 MHz, CDCl₃) of **3v****¹³C NMR** (126 MHz, CDCl₃) of **3v**

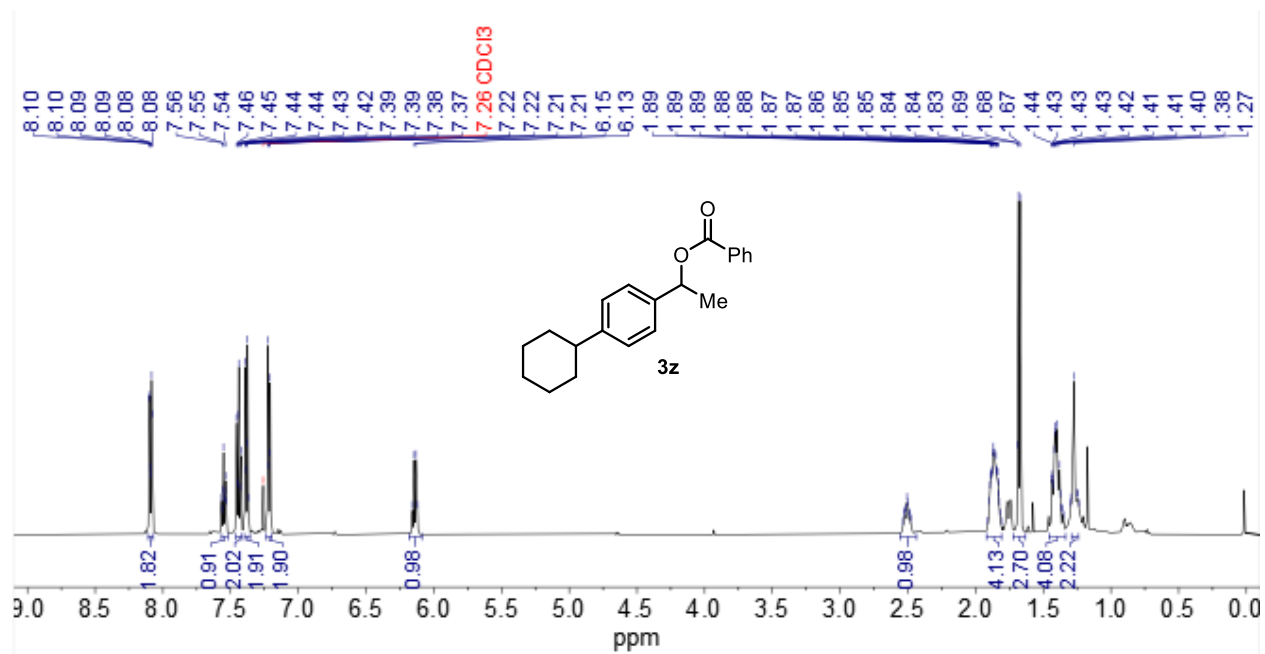
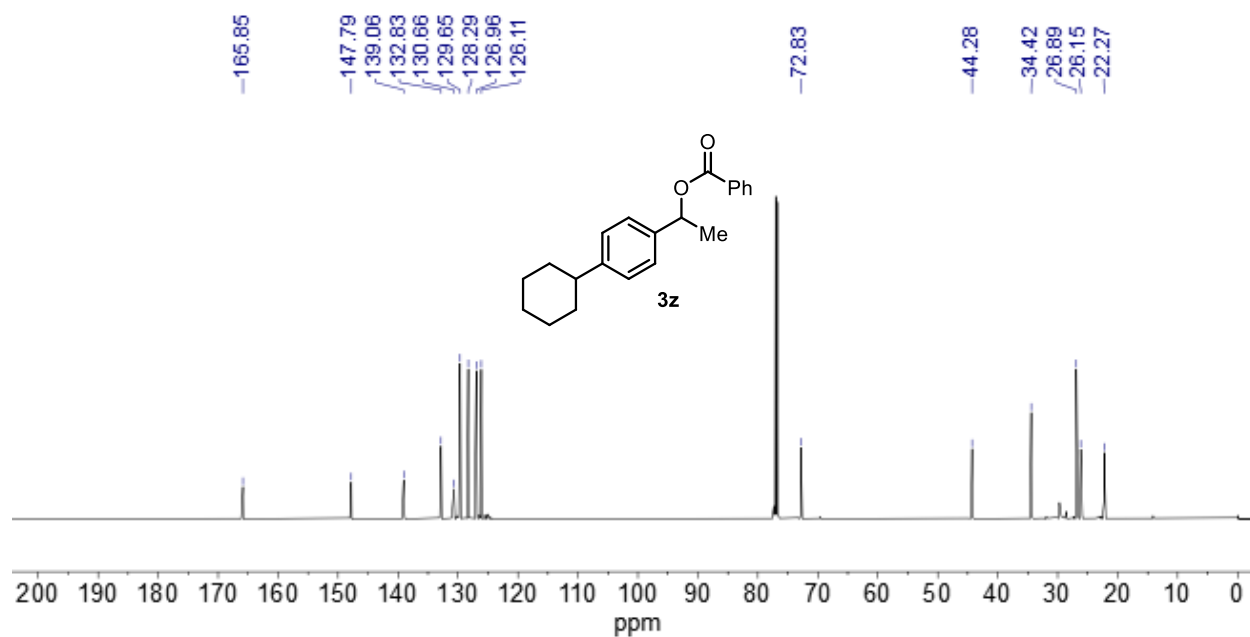
^1H NMR (500 MHz, CDCl_3) of **3w** ^{13}C NMR (126 MHz, CDCl_3) of **3w**

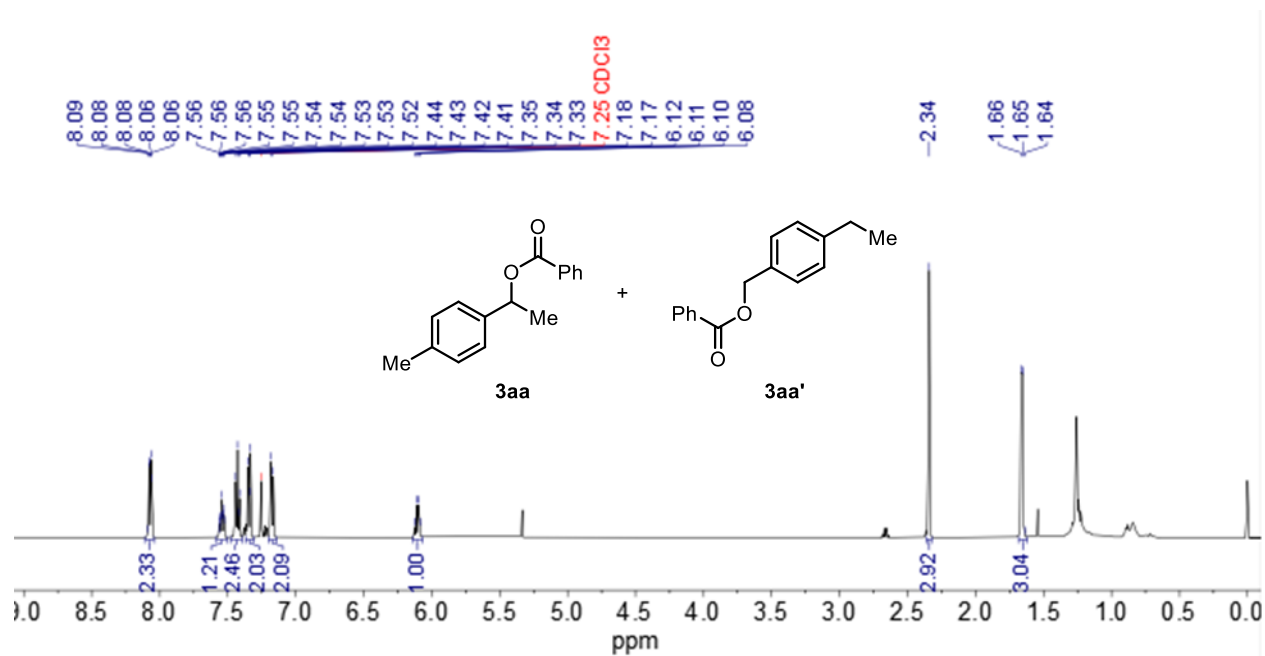
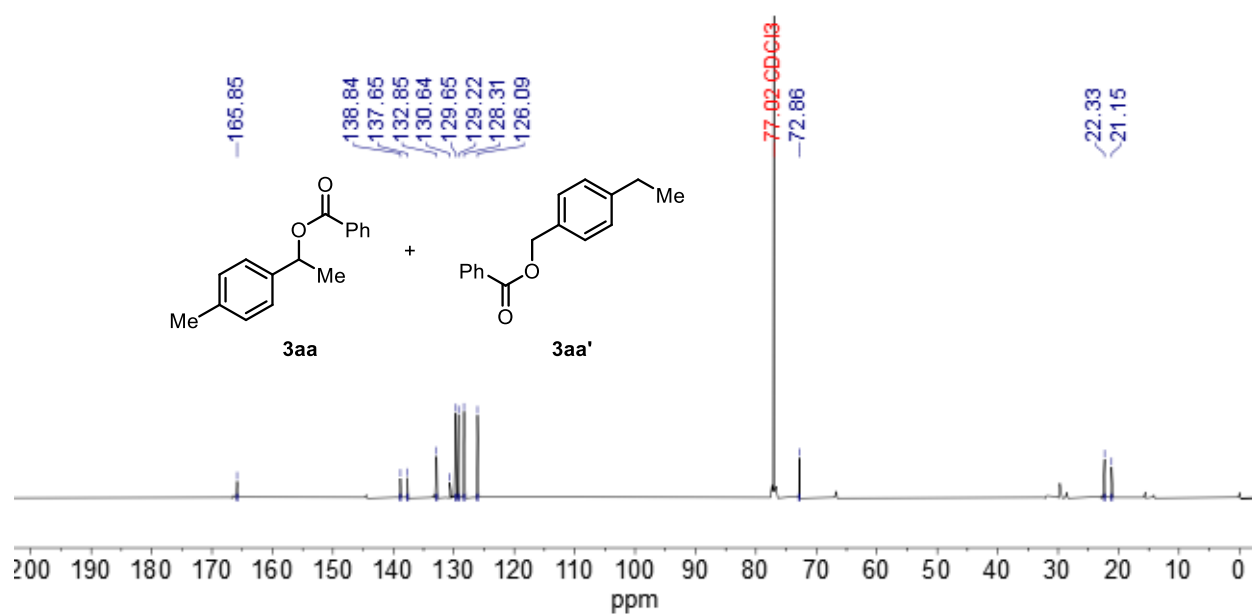
^1H NMR (500 MHz, CDCl_3) of **3x** ^{13}C NMR (126 MHz, CDCl_3) of **3x**

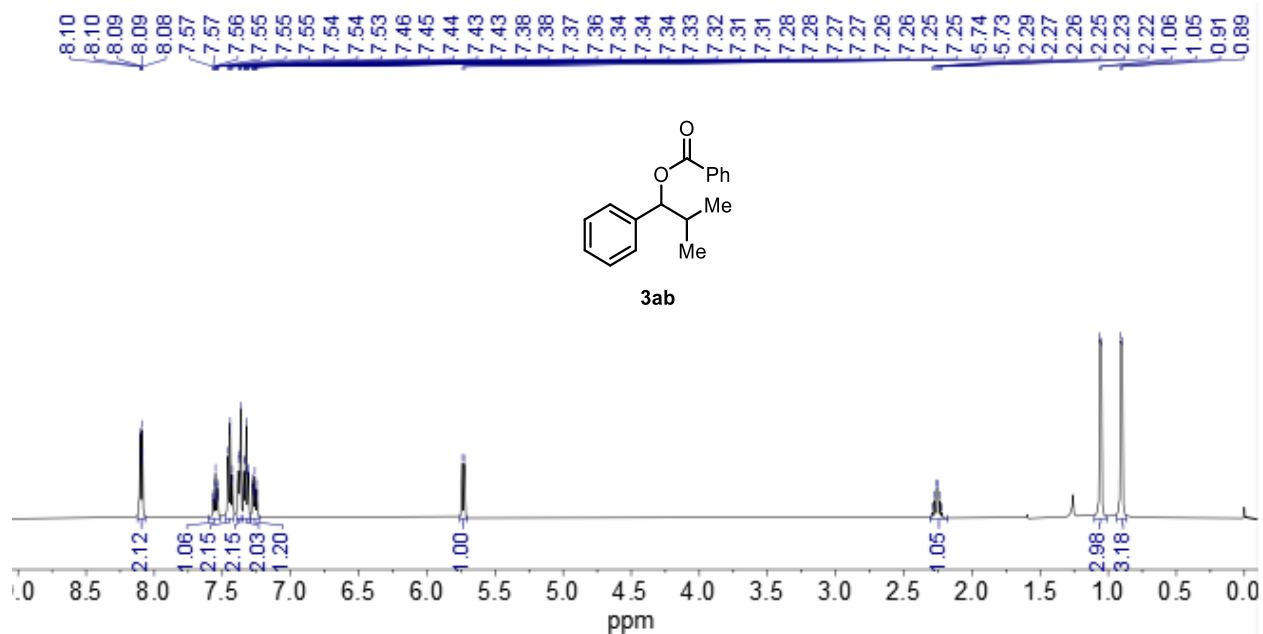
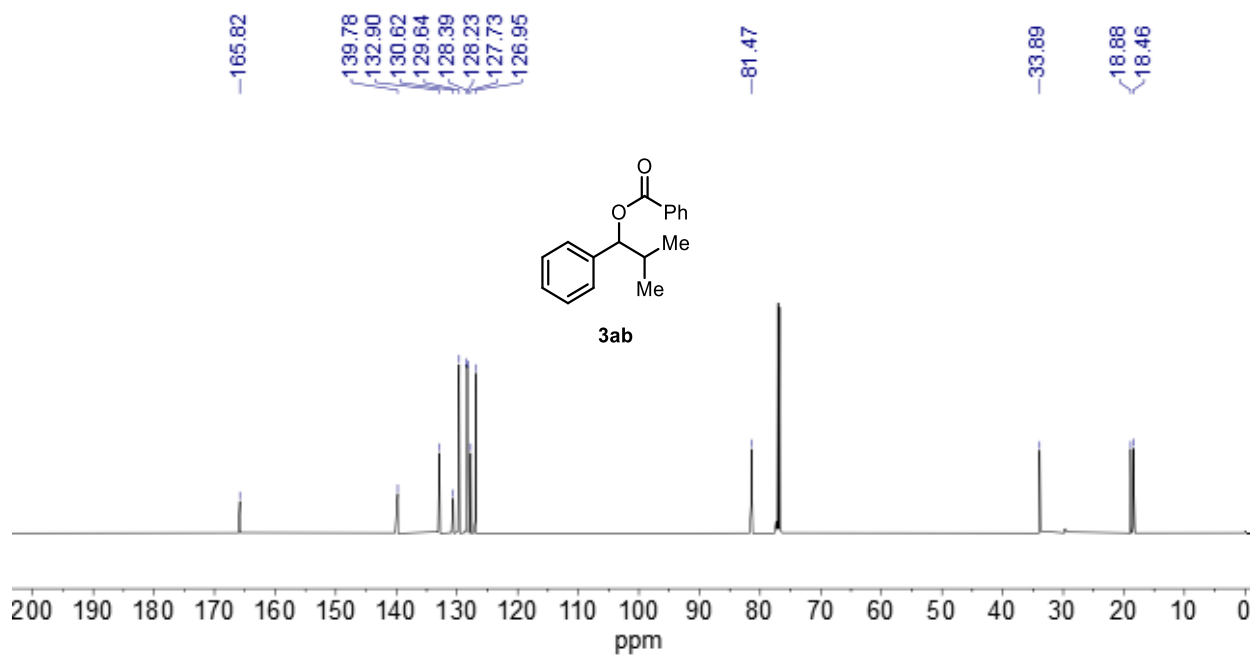
^1H NMR (500 MHz, CDCl_3) of **3y** **^{13}C NMR (126 MHz, CDCl_3) of **3y****

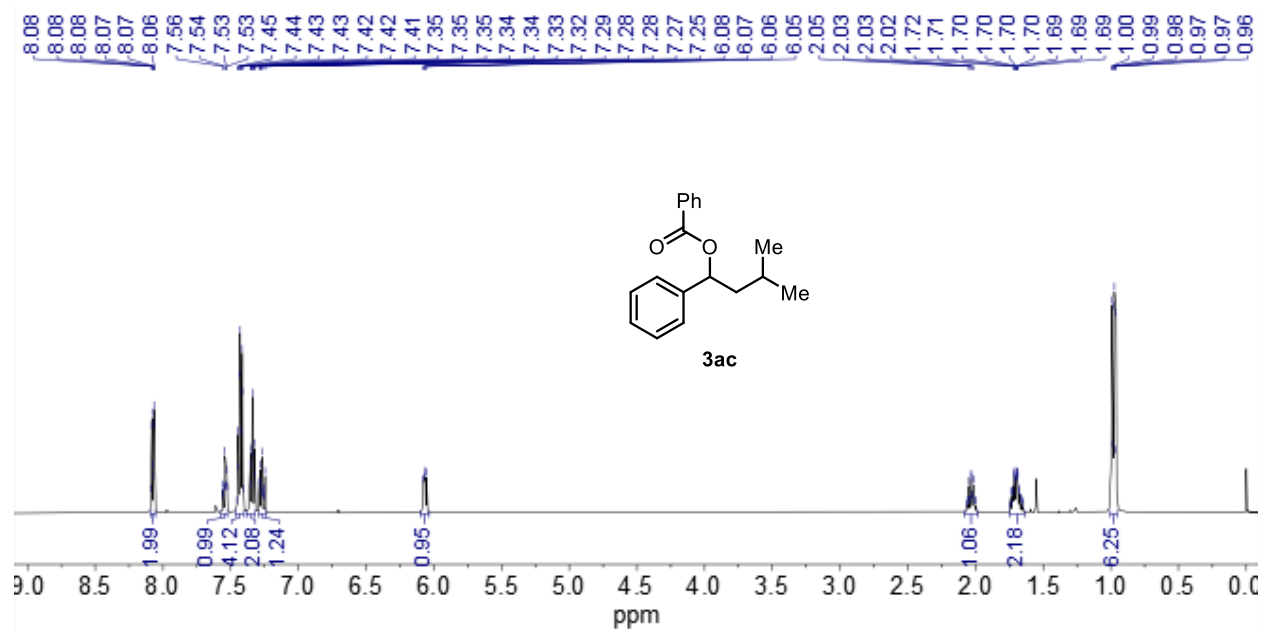
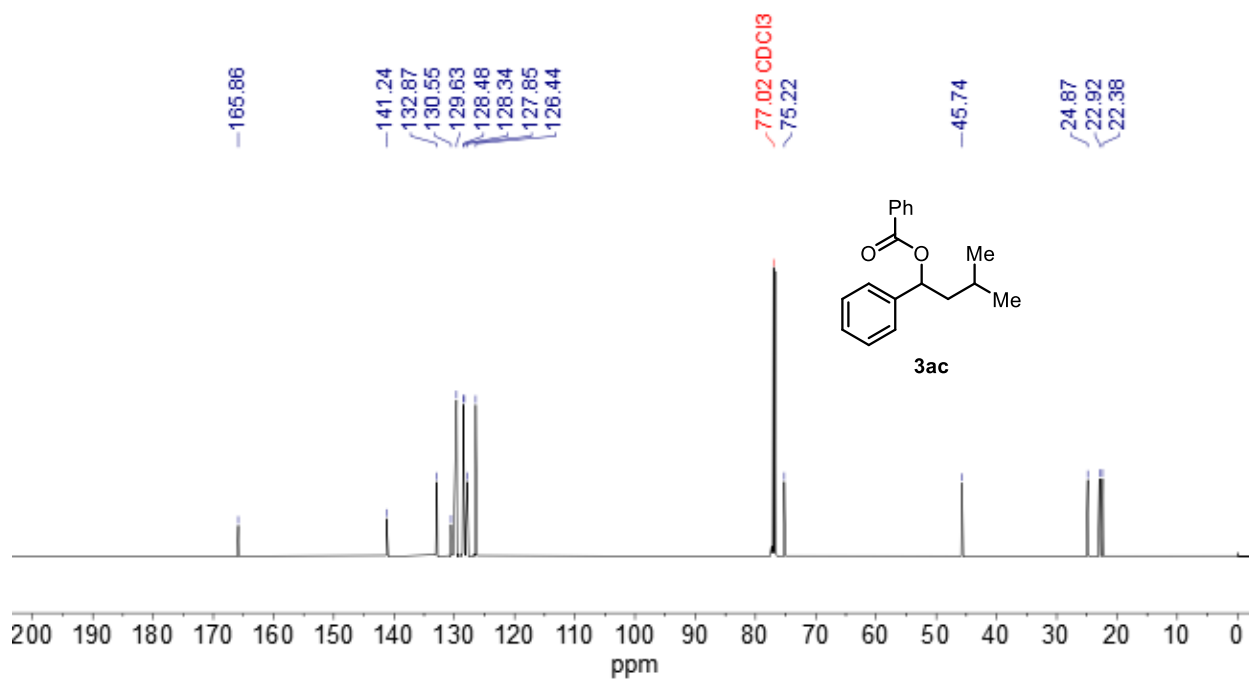
^{19}F NMR (377 MHz, CDCl_3) of **3y**

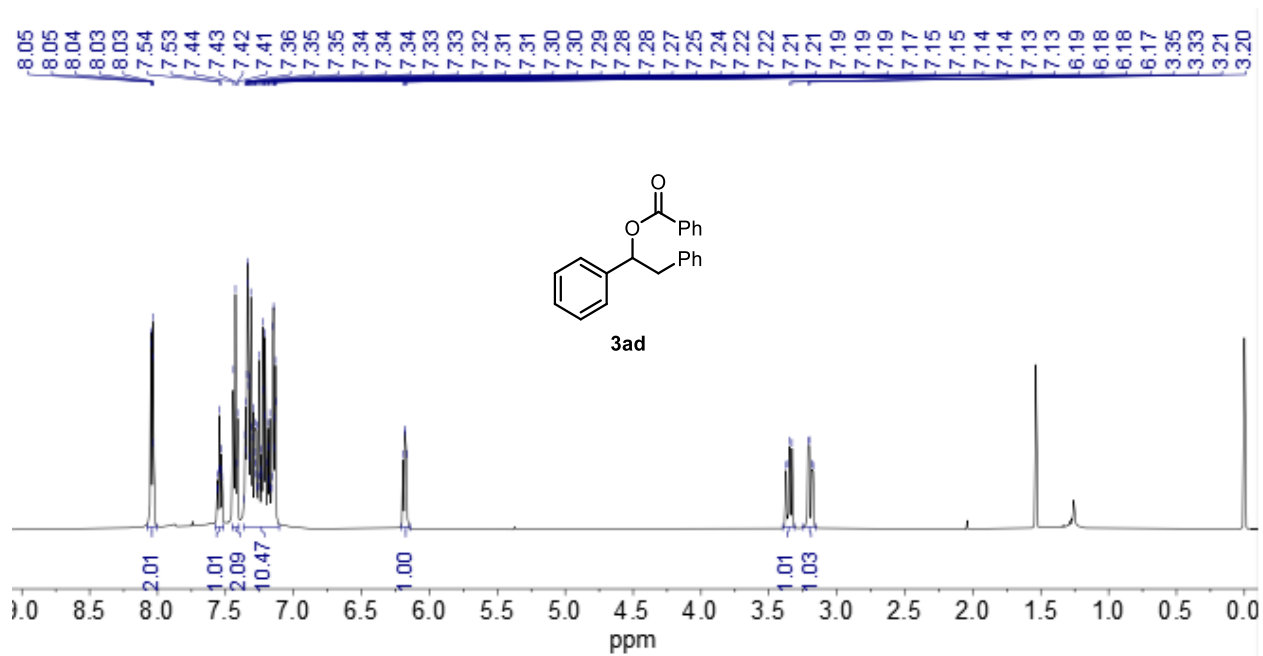
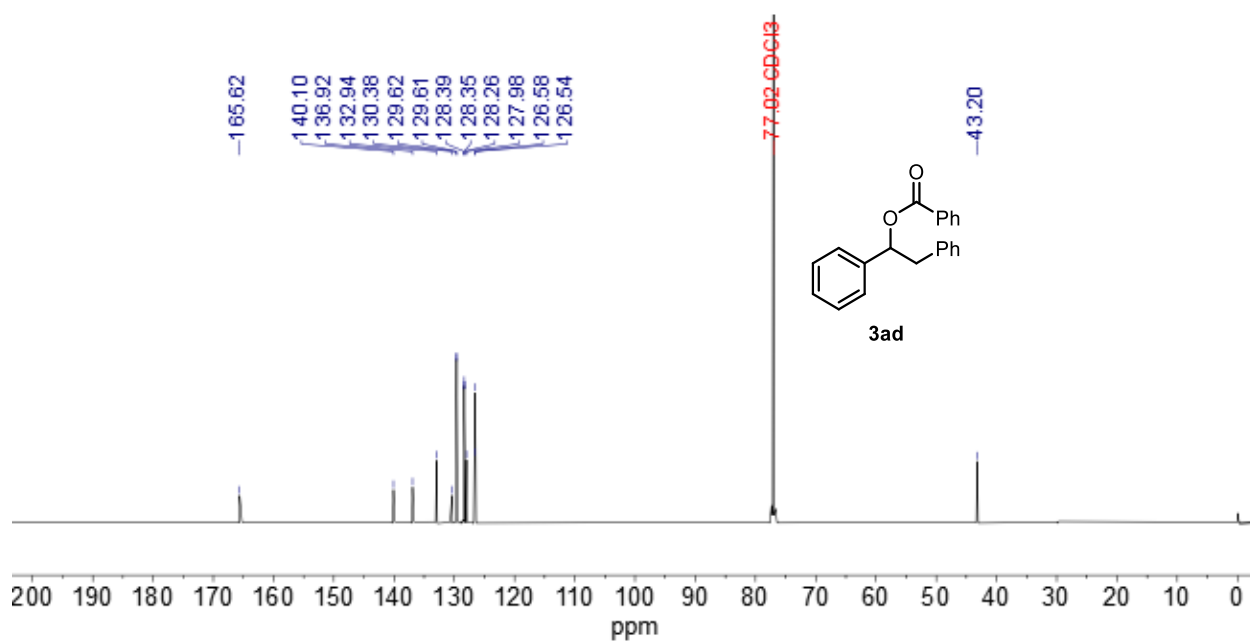


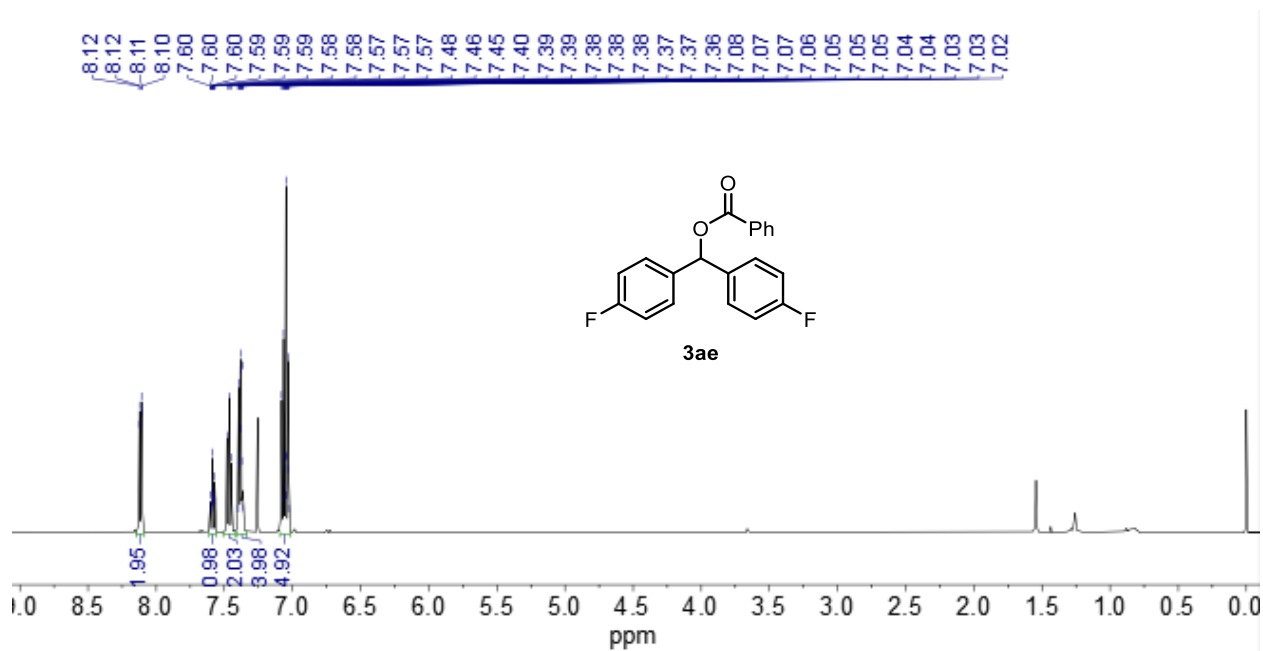
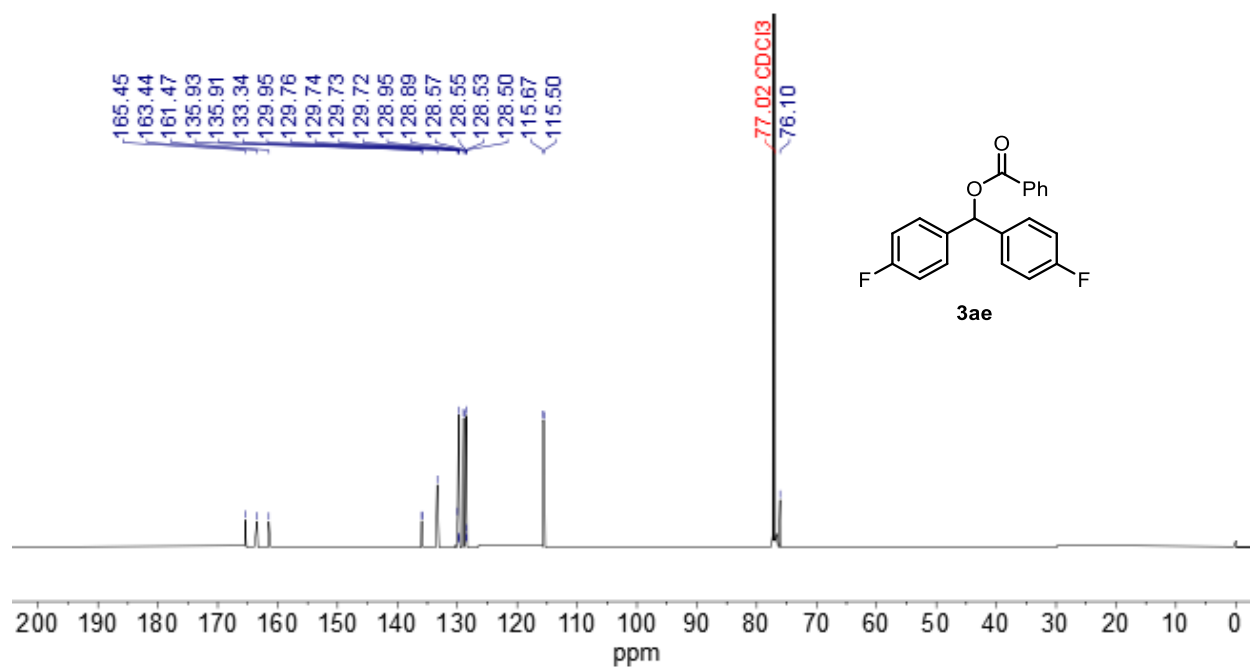
^1H NMR (500 MHz, CDCl_3) of **3z** ^{13}C NMR (126 MHz, CDCl_3) of **3z**

^1H NMR (500 MHz, CDCl_3) of **3aa** ^{13}C NMR (126 MHz, CDCl_3) of **3aa**

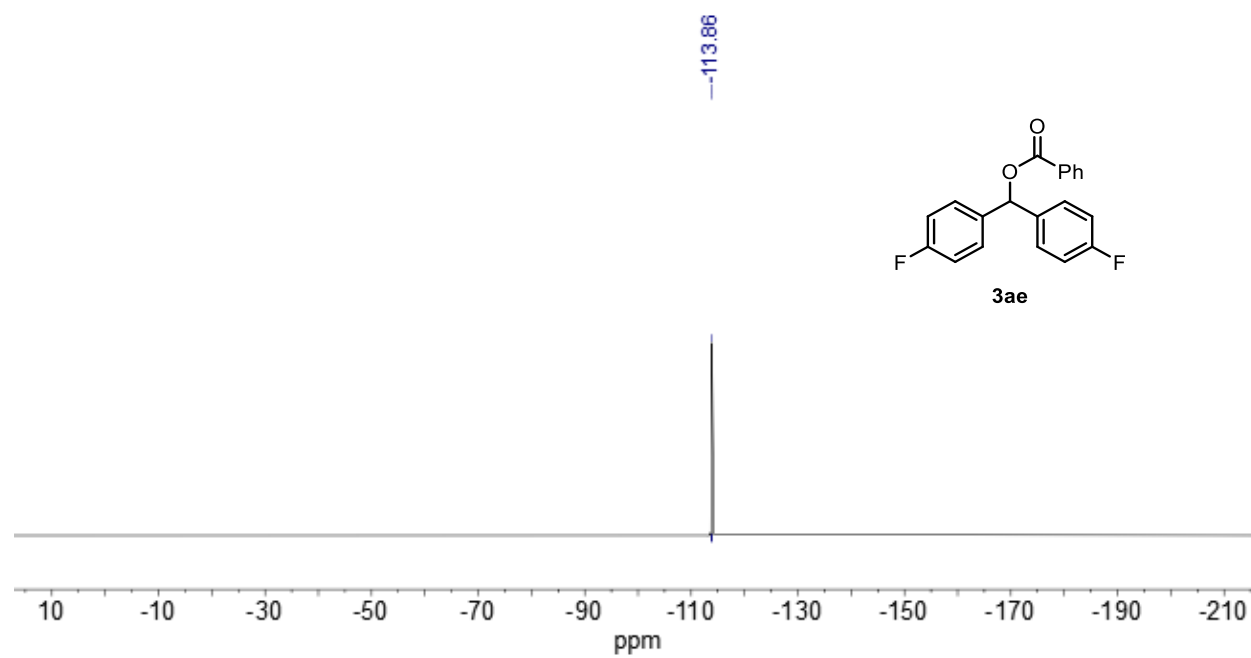
^1H NMR (500 MHz, CDCl_3) of **3ab** **^{13}C NMR (126 MHz, CDCl_3) of **3ab****

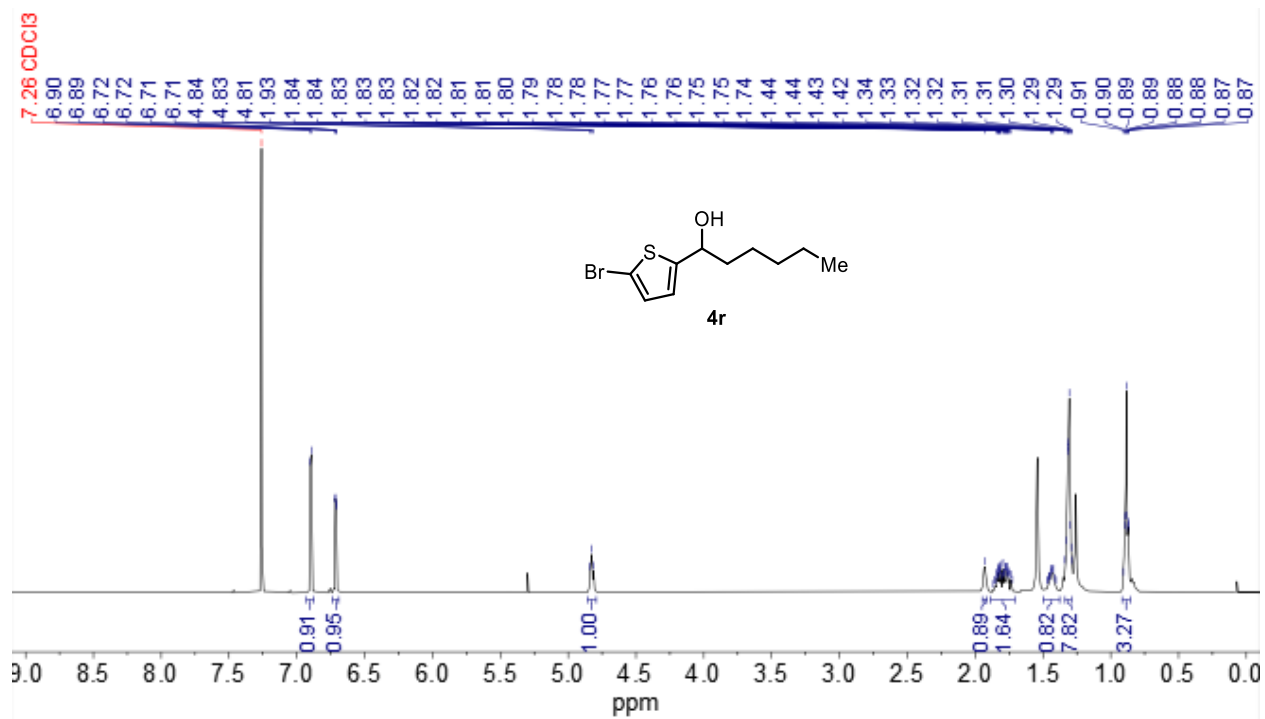
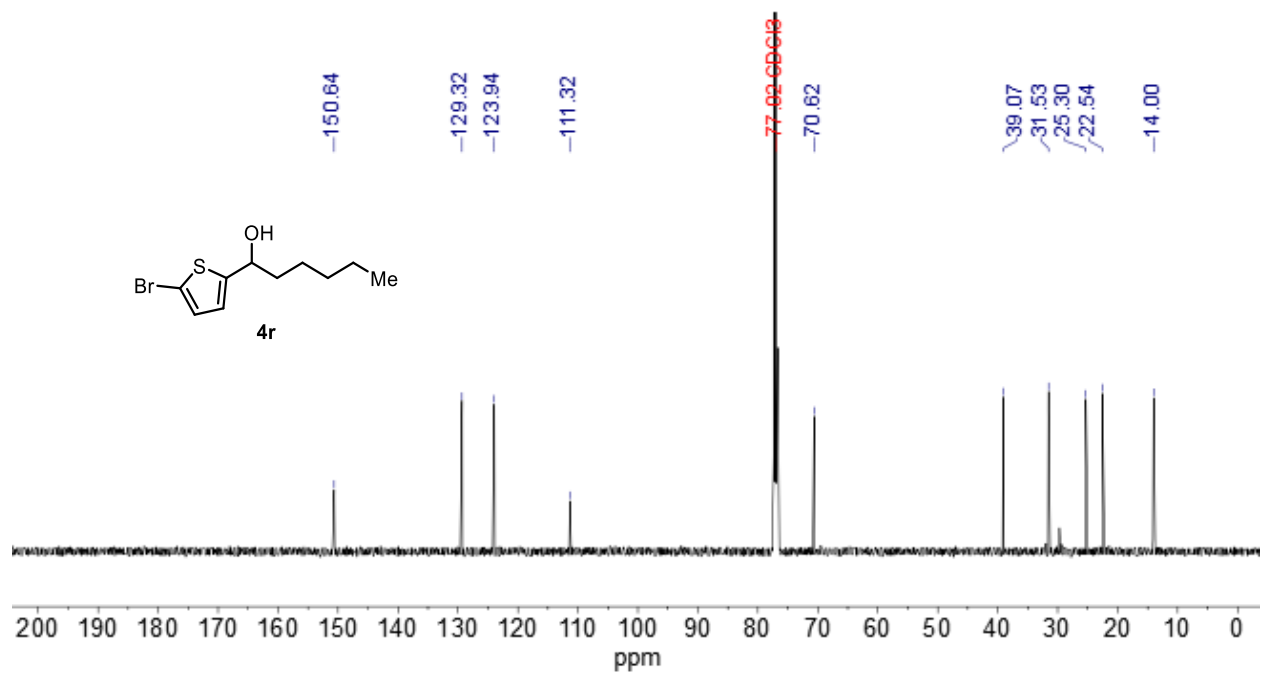
¹H NMR (500 MHz, CDCl₃) of 3ac**¹³C NMR (126 MHz, CDCl₃) of 3ac**

¹H NMR (500 MHz, CDCl₃) of 3ad**¹³C NMR (126 MHz, CDCl₃) of 3ad**

¹H NMR (500 MHz, CDCl₃) of **3ae****¹³C NMR** (126 MHz, CDCl₃) of **3ae**

^{19}F NMR (377 MHz, CDCl_3) of **3ae**



^1H NMR (500 MHz, CDCl_3) of **4r** **^{13}C NMR (126 MHz, CDCl_3) of **4r****

Appendix B: Supporting Information Chapter 3

3B.I. General Considerations

Reagents. All reagents were purchased and used as received unless otherwise noted. 3,5-Bis(trifluoromethyl)benzene-1-sulfonyl chloride, *tert*-butylamine, acetic acid, *tert*-butanol, and Cs₂CO₃ (99.99%) were purchased from Ambeed, TCI America, Sigma Aldrich, and Thermo Scientific. Unless otherwise stated, heterobenzylic C–H substrates and nucleophile coupling partners were acquired from commercial sources (Oakwood, Combi-Blocks, Enamine, AK Scientific, TCI America, Ambeed, or Sigma-Aldrich, Chem-Impex) and used as received, prepared following literature procedures, or sourced from the Merck Building Block Collection (MBBC) of Merck, Kenilworth, NJ. Anhydrous α,α,α -trifluorotoluene (PhCF₃) was purchased from Sigma Aldrich and stored with 4Å molecular sieves in the glovebox under N₂ atmosphere. All the reagents were used without further purification.

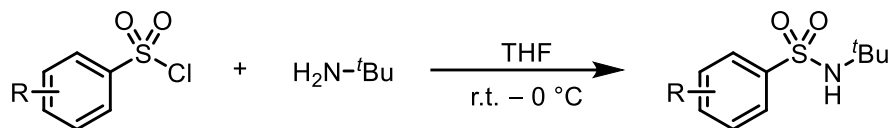
Photochemical Setup. ABI Tuna Blue 23W LED lamp (Product ID: B073V5V5JP) was the primary lighting source. The reaction vial was placed approximately 5 cm away from the lighting source and cooled by an electric fan to maintain the reaction temperature at 25 °C.

Other photochemical equipment. Philips EL/mdTQS 23W T2 (Product ID: 046677414016); Kessil PR160-440nm lamp (Product ID: L414G90708).

Characterization. ¹H, ¹³C, ¹⁹F and all the 2D NMR spectra were recorded on Bruker 400 MHz or Bruker 500 MHz spectrometers and chemical shifts are reported in parts per million (ppm). ¹H NMR spectra were referenced to tetramethylsilane at 0.00 ppm and ¹³C NMR spectra were referenced to CDCl₃ at 77.16 ppm. Column chromatography was performed using a Biotage Isolera One® with reusable 25 g, 40 g, and 120 g SiliaSep PREMIUM flash cartridges, 25 g and 50 g Sfär® cartridges or standard silica cartridges. High-resolution mass spectra were obtained using a Thermo Q Exactive™ Plus (ESI or ASAP-MS) by the mass spectrometry facility at the University of Wisconsin.

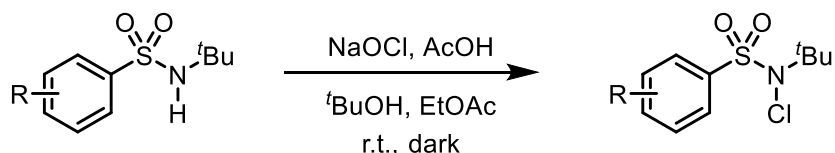
3B.II. Experimental Procedures for Preparations of Compounds

General Procedure (I) for Synthesis of Sulfonamides

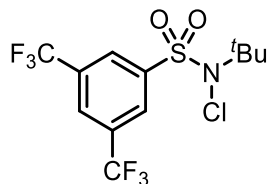


A 50-mL round bottom flask was charged with aryl sulfonyl chloride (10.0 mmol), tetrahydrofuran (THF, 15 mL), and a Teflon stir bar. The reaction was cooled to 0 °C. Then 2.2 mL of *tert*-butylamine (20.0 mmol, 2 equiv) was added dropwise. The reaction was allowed to warm up to room temperature and stirred overnight. Upon completion, the reaction was diluted with diethyl ether (Et₂O), washed with 2.0 M NaOH aqueous solution, 3 times with 1.0 M HCl aqueous solution, once with brine, then dried with MgSO₄. The organic solvent was evaporated under vacuum and the crude mixture was carried to the next step.

General Procedure (II) for Synthesis of *N*-Chlorosulfonamides



To a 100-mL foil wrapped round bottom flask under N₂, the crude mixture from previous step was dissolved in a mixture of ethyl acetate (EtOAc, 18 mL) and *tert*-butanol (0.96 mL, 10.0 mmol, 1.0 equiv). 44 mL of sodium hypochlorite aqueous solution (1.5 M in water) was added followed by acetic acid (5.7 mL, 10.0 equiv). The reaction was allowed to stir at room temperature overnight. Upon completion, the reaction was diluted with Et₂O, and washed three times with NaHCO₃ aqueous solution, once with water, once with brine, and dried with MgSO₄. The organic solvent was evaporated under vacuum and the crude mixture was purified via column chromatography. *General storage: N-chlorosulfonamide reagents were stored in the freezer when not in use but could be handled on the benchtop without risk of decomposition.*



N-(*tert*-butyl)-*N*-chloro-3,5-bis(trifluoromethyl)benzenesulfonamide, **2**

Reaction run using 3,5-bis(trifluoromethyl)benzenesulfonyl chloride (6.25 g, 20.0 mmol, 1.0 equiv), 4.4 mL of *tert*-butylamine (40.0 mmol, 2.0 equiv), and THF (30 mL) following the general procedure I for synthesis of sulfonamide. Reaction run using EtOAc (36 mL), *tert*-butanol (1.52 mL, 20.0 mmol, 1.0 equiv), 88 mL of sodium hypochlorite aqueous solution (1.5 M in water), and acetic acid (11.4 mL, 10.0 equiv) following the general procedure II for synthesis of *N*-chlorosulfonamide. Yield = 3.60 g (47%) of colorless oil.

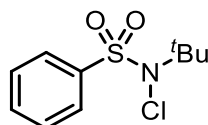
Purification: normal phase silica gel column chromatography with 5:1 pentane:ethyl acetate

Spectral data available in the literature: Yes¹

¹H NMR (CDCl₃, 500 MHz): δ 8.40 (s, 2H), 8.13 (s, 1H), 1.58 (s, 9H) ppm.

¹³C NMR (CDCl₃, 126 MHz): δ 141.12, 132.81 (q, J = 34.6 Hz), 129.08 (q, J = 3.9 Hz), 127.14 (p, J = 3.6 Hz), 122.39 (q, J = 273.4 Hz), 69.57, 29.36 ppm.

¹⁹F NMR (CDCl₃, 377 MHz): -62.92 ppm.



N-(*tert*-butyl)-*N*-chlorobenzesulfonamide

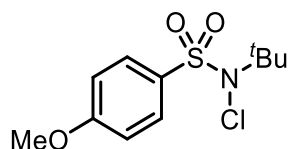
Reaction run using benzenesulfonyl chloride (1.76 g, 10.0 mmol, 1.0 equiv) following the general procedure I and II. Yield = 793 mg (32%) of clear colorless oil.

Purification: normal phase silica gel column chromatography with 5:1 pentane:ethyl acetate

Spectral data available in the literature: Yes²

¹H NMR (CDCl₃, 500 MHz): δ 7.99 (dd, J = 8.4, 1.3 Hz, 2H), 7.67 – 7.59 (m, 1H), 7.54 (t, J = 7.7 Hz, 1H), 1.50 (s, 9H) ppm.

¹³C NMR (CDCl₃, 126 MHz): δ 138.51, 133.58, 128.89, 128.84, 68.16, 29.18 ppm.



N-(*tert*-butyl)-*N*-chloro-4-methoxybenzenesulfonamide

Reaction run using 4-methoxybenzenesulfonyl chloride (2.06 g, 10.0 mmol, 1.0 equiv) following the general procedure I and II. Yield = 781 mg (39%) of white solid.

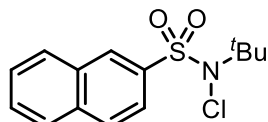
Purification: normal phase silica gel column chromatography with 5:1 pentane:ethyl acetate

Spectral data available in the literature: No

¹H NMR (CDCl₃, 500 MHz): δ 8.42 – 8.37 (m, 2H), 7.94 (dd, J = 8.6, 0.8 Hz, 1H), 7.89 (dd, J = 8.6, 2.3 Hz, 1H), 7.59 (dd, J = 4.4, 0.9 Hz, 1H), 5.13 (q, J = 6.9 Hz, 1H), 1.88 (d, J = 6.9 Hz, 3H) ppm.

¹³C NMR (CDCl₃, 126 MHz): δ 163.68, 131.18, 129.90, 114.00, 77.02, 67.91, 55.68, 29.18 ppm.

HRMS m/z: [M+H]⁺ calculated for C₁₁H₁₆ClNO₃S: 278.0612, Found: 278.0607.



N-(*tert*-butyl)-*N*-chloro-2-naphthalenesulfonamide

Reaction run using 2-naphthalenesulfonyl chloride (2.27 g, 10.0 mmol, 1.0 equiv) following the general procedure I and II. Yield = 1.35 g (45%) of white solid.

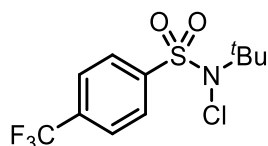
Purification: normal phase silica gel column chromatography with 5:1 pentane:ethyl acetate

Spectral data available in the literature: No

¹H NMR (CDCl₃, 500 MHz): δ 8.57 – 8.53 (m, 1H), 8.03 – 7.90 (m, 4H), 7.71 – 7.60 (m, 2H), 1.54 (s, 9H) ppm.

¹³C NMR (CDCl₃, 126 MHz): δ 135.38, 135.26, 131.91, 130.75, 129.52, 129.29, 129.08, 127.95, 127.60, 123.60, 68.26, 29.28 ppm.

HRMS m/z: [M+H]⁺ calculated for C₁₄H₁₆ClNO₂S: 298.0663, Found: 298.0655.



N-(*tert*-butyl)-*N*-chloro-4-(trifluoromethyl)benzenesulfonamide

Reaction run using 4-(trifluoromethyl)phenylsulfonyl chloride (2.45 g, 10.0 mmol, 1.0 equiv) following the general procedure I and II. Yield = 476 mg of yellow oil.

Purification: normal phase silica gel column chromatography with 5:1 pentane:ethyl acetate

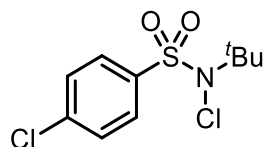
Spectral data available in the literature: No

¹H NMR (CDCl₃, 500 MHz): δ 141.99 (q, J = 1.5 Hz), 135.20 (q, J = 33.2 Hz), 129.38, 126.01 (q, J = 3.7 Hz), 122.06 (q, J = 273.0 Hz), 68.79, 29.28 ppm.

¹³C NMR (CDCl₃, 126 MHz): δ 151.11, 151.17 (d, J = 249.6 Hz), 146.15, 137.01, 136.35, 130.14 (d, J = 15.0 Hz), 112.99 (d, J = 29.1 Hz), 111.59 (d, J = 1.5 Hz), 5.21, 26.21 ppm.

¹⁹F NMR (CDCl₃, 377 MHz): -63.21 ppm.

HRMS m/z: [M+H]⁺ calculated for C₁₁H₁₃ClF₃NO₂S: 333.0646, Found: 333.0640.



N-(*tert*-butyl)-*N*-chloro-4-chlorobenzenesulfonamide

Reaction run using 4-chlorophenylsulfonyl chloride (2.11 g, 10.0 mmol, 1.0 equiv) following the general procedure I and II. Yield = 925 mg (33%) of white solid.

Purification: normal phase silica gel column chromatography with 5:1 pentane:ethyl acetate

Spectral data available in the literature: No

¹H NMR (CDCl₃, 500 MHz): δ 8.42 – 8.37 (m, 2H), 7.94 (dd, J = 8.6, 0.8 Hz, 1H), 7.89 (dd, J = 8.6, 2.3 Hz, 1H), 7.59 (dd, J = 4.4, 0.9 Hz, 1H), 5.13 (q, J = 6.9 Hz, 1H), 1.88 (d, J = 6.9 Hz, 3H) ppm.

¹³C NMR (CDCl₃, 126 MHz): δ 140.30, 136.93, 130.32, 129.19, 68.47, 29.23 ppm.

HRMS m/z: [M+H]⁺ calculated for C₁₀H₁₃Cl₂NO₂S: 282.0117, Found: 282.0113.

General Procedure (III) for Chlorination of Heterobenzylic C–H Substrate (0.20 mmol scale)

N-(*tert*-butyl)-*N*-chloro-3,5-bis(trifluoromethyl)benzenesulfonamide (115.1 – 307.0 mg, 0.30 – 0.80 mmol, 1.5 – 4.0 equiv) and benzylic substrate (if solid, 0.20 mmol, 1.0 equiv) were added to a 24-mL glass vial under air. The vial was then moved to a purging glove box under N₂ atmosphere. Cs₂CO₃ (97.7 mg, 0.30 mmol, 1.5 equiv), α,α,α -trifluorotoluene (1.0 mL), and benzylic substrate (if liquid, 0.20 mmol, 1.0 equiv) were added to the reaction vial. The vial was sealed in the glove box and taken out to photochemical setup. The reaction was carried out under irradiation of one blue LED lamp (~ 450 nm) with stirring for 20 hours. When the reaction finished, mesitylene (28 μ L, 0.20 mmol) was added as internal standard. An aliquot (50 μ L) was withdrawn and filtered through a celite plug for ¹H NMR analysis to detect formation of product and consumption of starting material. After ¹H NMR analysis, the crude reaction was filtered through a silica plug using acetonitrile, evaporated under vacuum, and purified by column chromatography.

General Procedure (IV) for Chlorination of Heterobenzylic C–H Substrate (0.50 mmol scale)

N-(*tert*-butyl)-*N*-chloro-3,5-bis(trifluoromethyl)benzenesulfonamide (287.8 – 767.5 mg, 0.75 – 2.00 mmol, 1.5 – 4.0 equiv) and benzylic substrate (if solid, 0.50 mmol, 1.0 equiv) were added to a 24-mL glass vial under air. The vial was then moved to a purging glove box under N₂ atmosphere. Cs₂CO₃ (244.4 mg, 0.75 mmol, 1.5 equiv), α,α,α -trifluorotoluene (2.5 mL), and benzylic substrate (if liquid, 0.50 mmol, 1.0 equiv) were added to the reaction vial. The vial was sealed in the glove box and taken out to photochemical setup. The reaction was carried out under irradiation of two blue LED lamps (~ 450 nm) with stirring for the indicated amount of time. When the reaction finished, mesitylene (70 μ L, 0.50 mmol) was added as internal standard. An aliquot (50 μ L) was withdrawn and filtered through a celite plug for ¹H NMR analysis to detect formation of product and consumption of starting material. After ¹H NMR analysis, the crude reaction was filtered through a silica plug using acetonitrile, evaporated under vacuum, and purified by column chromatography.

General Procedure (V) for Chlorination of Heterobenzylic C–H Substrate (5.00 mmol scale)

N-(*tert*-butyl)-*N*-chloro-3,5-bis(trifluoromethyl)benzenesulfonamide (2878.0 or 7674.6 mg, 7.5 or 20 mmol, 1.5 or 4.0 equiv) and benzylic substrate (if solid, 5.00 mmol, 1.0 equiv) were added to a 250-mL round bottom flask. The flask was then moved to a purging glove box under N₂ atmosphere. Cs₂CO₃ (2443.7 mg, 7.5 mmol, 1.5 equiv), α,α,α -trifluorotoluene (25 mL), and benzylic substrate (if liquid, 5.0 mmol, 1.0 equiv) were added to the reaction flask. The flask was sealed with a septum, secured with electrical tape in the glove box and taken out to photochemical setup. The reaction was carried out under irradiation of two blue LED lamps (~ 450 nm) with stirring for 20 hours. When the reaction finished, mesitylene (70 μ L, 0.50 mmol) was added as internal standard. An aliquot (50 μ L) was withdrawn and filtered through a celite plug for ¹H NMR analysis to detect formation of product and consumption of starting material. After ¹H NMR analysis, the crude reaction was filtered through a silica plug using acetonitrile, evaporated under vacuum, and purified by column chromatography.

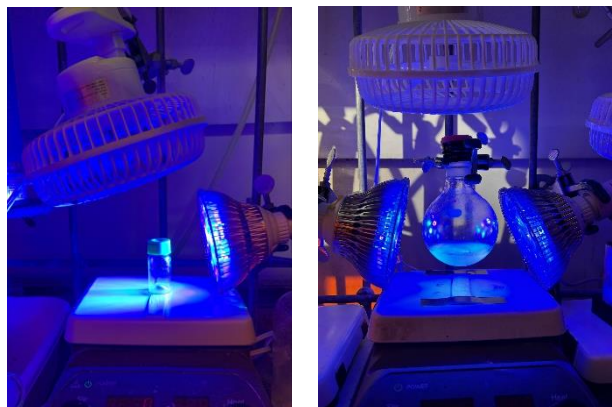


Figure 3B.1. Photochemical Setup for Normal Scale Reaction (Left) and Scale-Up Reaction (Right).

General Procedure (VI) for Chlorination of Heterobenzylic C–H Substrate (0.05 mmol scale)

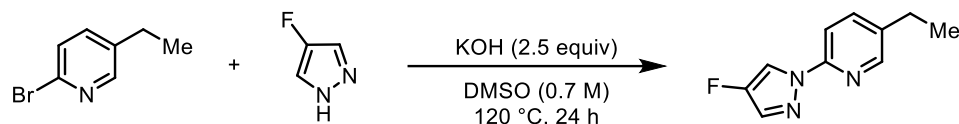
N-(*tert*-butyl)-*N*-chloro-3,5-bis(trifluoromethyl)benzenesulfonamide (38.4 – 76.7 mg, 0.10 – 0.20 mmol, 2.0 – 4.0 equiv) and benzylic substrate (if solid, 0.05 mmol, 1.0 equiv) were added to a 24-mL glass vial under air. The vial was then moved to a purging glove box under N₂ atmosphere. Cs₂CO₃ (24.4 mg, 0.075 mmol, 1.5 equiv), α,α,α -trifluorotoluene (0.25 mL), and benzylic substrate (if liquid, 0.05 mmol, 1.0 equiv) were added to the reaction vial. The vial was sealed in the glove box and taken out to photochemical setup. The reaction was carried out under irradiation of one blue LED lamp (~ 450 nm) with stirring for 20 hours. When the reaction finished, mesitylene (7 μ L, 0.05 mmol) was added as internal standard. An aliquot (50 μ L) was withdrawn and filtered through a celite plug for ¹H NMR analysis to detect formation of product and consumption of starting material.

General Procedure (VII) for Heterobenzylic Chloride Displacement with Nucleophiles (0.10 mmol scale)

Following chlorination in general procedure (III), mesitylene (70 μ L, 0.50 mmol) was added as internal standard. An aliquot (50 μ L) was withdrawn for ¹H NMR analysis to detect formation of product and consumption of starting material. After ¹H NMR analysis, the ¹H NMR sample was added back into the reaction vial. The crude reaction mixture was filtered through a silica plug using dichloromethane and concentrated under vacuum. A stock solution of heterobenzylic chloride was prepared with DMF in a 5-mL volumetric flask. Each 1-mL addition of this stock equaled to 0.10 mmol of heterobenzylic chloride at 0.1 M concentration. The nucleophile (0.20 mmol, 2.0 equiv), KI (19.9 mg, 0.12 mmol, 1.2 equiv), Cs₂CO₃ (39.1 – 117.3 mg, 0.12 – 0.36 mmol, 1.2 – 3.6 equiv), and a Teflon magnetic stir bar were added to a 4-mL glass vial under air. The vial was charged with 1 mL of the heterobenzylic chloride stock solution (0.1 mmol, 1 equiv). The vial was then sealed by a PTFE-lined pierceable cap and set to stir at 70°C on a stirring hot plate in an aluminum block at 550 rpm for 16 hours. When the reaction finished, the mixture was cooled down to room temperature. The crude reaction mixture was diluted with EtOAc and washed twice with 5% LiCl aqueous solution in a separatory funnel. The organic phase was collected in a 250-mL Erlenmeyer flask. The aqueous phase was returned to the separatory funnel and extracted with EtOAc. All the organic phase was combined, washed with brine, and dried over MgSO₄. The mixture was evaporated under vacuum and the crude mixture was purified by column chromatography.

3B.III. Starting Material Syntheses

(1b) – 5-ethyl-2-(4-fluoro-1H-pyrazol-1-yl)pyridine



Reaction Setup: 2-bromo-5-ethylpyridine (186.1 mg, 1.00 mmol, 1.0 equiv), 4-fluoro-1H-pyrazole (86.1 mg, 1.00 mmol, 1.0 equiv), and potassium hydroxide (140.3 mg, 2.50 mmol, 2.5 equiv) were added to an 8-mL glass vial under air. Anhydrous DMSO (0.7 M, 1.50 mL) was added to the reaction vial. The reaction was carried out at 120 °C with stirring for 24 hours. Upon completion, the reaction was allowed to cool to room temperature and diluted with Et₂O. The crude reaction mixture was washed once with saturated NH₄Cl aqueous solution, once with water, once with brine, and dried with MgSO₄. The organic solvent was evaporated under vacuum. Yield = 56.3 mg (29%) of white solid.

Purification: normal phase silica gel column chromatography with 9:1 pentane:ethyl acetate

Spectral data available in the literature: No

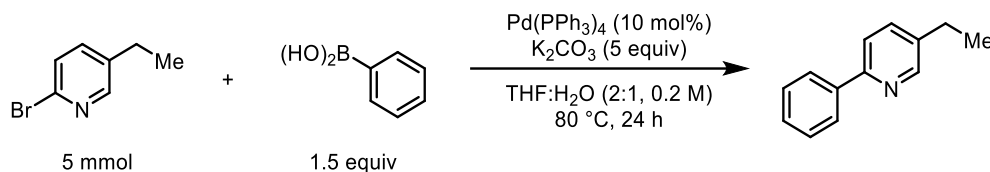
¹H NMR (CDCl₃, 500 MHz): δ 8.22 (d, *J* = 2.2 Hz, 1H), 7.88 – 7.82 (m, 1H), 7.64 (dd, *J* = 8.4, 2.3 Hz, 1H), 7.56 (dd, *J* = 4.3, 1.0 Hz, 1H), 2.68 (q, *J* = 7.6 Hz, 2H), 1.27 (t, *J* = 7.7 Hz, 3H) ppm.

¹³C NMR (CDCl₃, 126 MHz): δ 152.03, 150.05, 149.67, 147.20, 138.13, 137.42, 129.36 (d, *J* = 14.8 Hz), 112.79 (d, *J* = 29.0 Hz), 111.28 (d, *J* = 1.5 Hz), 25.53, 15.34 ppm.

¹⁹F NMR (CDCl₃, 377 MHz): -174.91 ppm.

HRMS m/z: [M+H]⁺ calculated for C₁₀H₁₀FN₃:192.0932, Found: 192.0929.

(1c) – 2-phenyl-5-ethylpyridine



Reaction Setup: 2-bromo-5-ethylpyridine (930.3 mg, 5.00 mmol, 1.0 equiv), phenylboronic acid (914.5 mg, 7.50 mmol, 1.5 equiv), tetrakis(triphenylphosphine)palladium(0) (577.8 mg, 0.50 mmol, 10 mol%), and potassium carbonate (3455.1 mg, 25.0 mmol, 5.0 equiv) were added to a 200-mL round bottom flask under air. The reaction flask was put under vacuum and backfilled with nitrogen three times. THF (16.5 mL) and water (8.5 mL) were added to the reaction. The reaction was carried out at 80 °C with stirring for 24 hours. Upon completion, the reaction was allowed to cool to room temperature and diluted with Et₂O. The crude reaction mixture was washed three times with water, once with brine, and dried with MgSO₄. The organic solvent was evaporated under vacuum. Yield = 678.3 mg (74%) of white solid.

Purification: normal phase silica gel column chromatography with 1:1 pentane:ethyl acetate

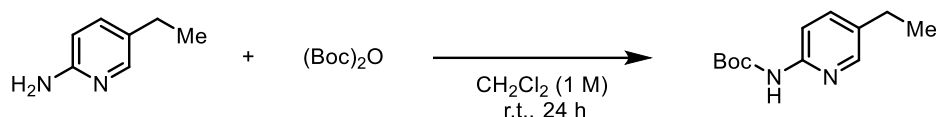
Spectral data available in the literature: No

¹H NMR (CDCl₃, 500 MHz): δ 8.56 – 8.52 (m, 1H), 8.00 – 7.94 (m, 2H), 7.66 (dd, J = 8.1, 0.9 Hz, 1H), 7.58 (ddt, J = 8.1, 2.3, 0.7 Hz, 1H), 7.50 – 7.43 (m, 2H), 7.43 – 7.36 (m, 1H), 2.70 (q, J = 7.6 Hz, 2H), 1.29 (t, J = 7.6 Hz, 3H) ppm.

¹³C NMR (CDCl₃, 126 MHz): δ 155.09, 149.41, 139.49, 137.74, 136.09, 128.70, 126.72, 120.17, 25.81, 15.34 ppm.

HRMS m/z: [M+H]⁺ calculated for C₁₃H₁₃N: 184.1121, Found: 184.1119.

(1d) – tert-butyl (5-ethylpyridin-2-yl)carbamate



Reaction Setup: 5-ethylpyridin-2-amine (610.8 mg, 5.00 mmol, 1.0 equiv) was dissolved in dichloromethane (5 mL) in 24-mL glass vial under air. Di-*tert*-butyl dicarbonate (1.20 g, 5.50 mmol, 1.1 equiv) was slowly added to the reaction vial via syringe. The reaction was carried out at room temperature with stirring overnight. Upon completion, the crude reaction mixture was diluted with dichloromethane, washed three times with water, once with brine, and dried with MgSO₄. The organic solvent was evaporated under vacuum. Yield = 258.0 mg (23%) of white solid.

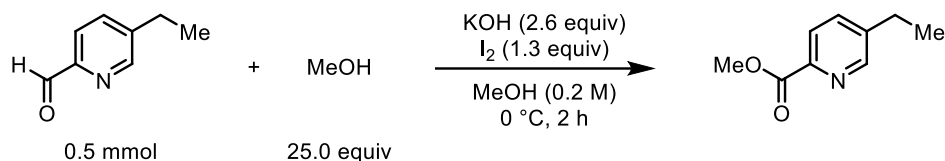
Purification: normal phase silica gel column chromatography with 5:1 pentane:ethyl acetate

Spectral data available in the literature: No

¹H NMR (CDCl₃, 500 MHz): δ 8.08 (dd, J = 2.4, 0.8 Hz, 1H), 7.84 (d, J = 8.5 Hz, 1H), 7.52 – 7.46 (m, 2H), 2.59 (q, J = 7.6 Hz, 2H), 1.53 (s, 9H), 1.22 (t, J = 7.6 Hz, 3H) ppm.

¹³C NMR (CDCl₃, 126 MHz): δ 152.52, 149.94, 146.93, 137.65, 134.01, 111.93, 80.77, 28.33, 25.41, 15.52 ppm.

HRMS m/z: [M+H]⁺ calculated for C₁₂H₁₈N₂O₂: 223.1441, Found: 223.1437.

(1g) – methyl 5-ethylpicolinate

Reaction Setup: 5-ethylpicolinaldehyde (67.6 mg, 0.50 mmol, 1.0 equiv) was dissolved in methanol (0.5 mL, 12.5 mmol, 25.0 equiv) in 4-mL glass vial under air. A solution of potassium hydroxide (72.9 mg, 1.3 mmol, 2.6 equiv) was prepared in methanol (0.75 mL) and slowly added to the reaction vial. A solution of iodine (164.9 mg, 0.65 mmol, 1.3 equiv) in methanol (0.75 mL) and added to the reaction mixture. The reaction was carried out at 0 °C with stirring for 2 hours. Upon completion, the crude reaction mixture was diluted with Et₂O and extracted with aqueous NaHSO₃ solution (5 mL). The organic layer was washed three times with water, once with brine, and dried with MgSO₄. The organic solvent was evaporated under vacuum. Yield = 36.5 mg (48%) of clear colorless oil.

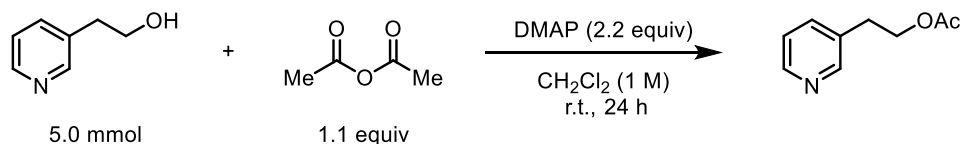
Purification: normal phase silica gel column chromatography with 1:1 pentane:ethyl acetate

Spectral data available in the literature: No

¹H NMR (CDCl₃, 500 MHz): δ 8.57 (d, J = 2.2 Hz, 1H), 8.05 (d, J = 8.0 Hz, 1H), 7.65 (dd, J = 8.0, 2.2 Hz, 1H), 3.99 (s, 3H), 2.73 (q, J = 7.6 Hz, 2H), 1.28 (t, J = 7.6 Hz, 3H) ppm.

¹³C NMR (CDCl₃, 126 MHz): δ 165.85, 149.70, 145.59, 143.40, 136.08, 124.96, 52.74, 26.13, 14.94 ppm.

HRMS m/z: [M+H]⁺ calculated for C₉H₁₁NO₂ 166.0863, Found: 166.0863.

(1p) – 2-(pyridine-3-yl)ethyl acetate

Reaction Setup: 2-(pyridin-3-yl)ethan-1-ol (615.8 mg, 5.00 mmol, 1.0 equiv) and DMAP (1.34 g, 11 mmol, 2.2 equiv) were dissolved in dichloromethane (5.0 mL) in 24-mL glass vial under air. Acetic anhydride (520 μL, 5.50 mmol, 1.1 equiv) was slowly added to the reaction vial via syringe. The reaction was carried out at room temperature with stirring overnight. Upon completion, the crude reaction mixture was diluted with ethyl acetate (20 mL) and extracted with sat. NaHCO₃ solution. The organic layer was washed three times with water, once with brine, and dried with MgSO₄. The organic solvent was evaporated under vacuum. Yield = 811.9 mg (98%) of clear colorless oil.

Purification: normal phase silica gel column chromatography with 1:4 pentane:ethyl acetate

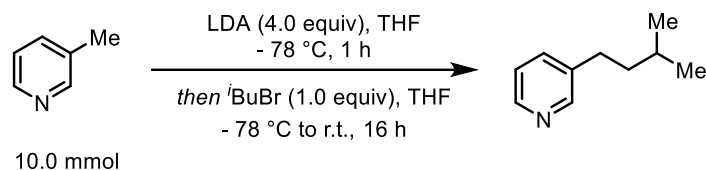
Spectral data available in the literature: No

¹H NMR (CDCl₃, 500 MHz): δ 8.55 (d, J = 3.7 Hz, 1H), 7.61 (ddt, J = 8.2, 4.7, 2.4 Hz, 1H), 7.21 – 7.11 (m, 2H), 4.46 (t, J = 6.8 Hz, 2H), 3.12 (t, J = 6.8 Hz, 2H), 2.02 (s, 3H) ppm.

^{13}C NMR (CDCl_3 , 126 MHz): δ 171.02, 158.07, 149.52, 136.38, 123.38, 121.64, 63.61, 37.40, 20.95 ppm.

HRMS m/z : $[\text{M}+\text{H}]^+$ calculated for $\text{C}_9\text{H}_{11}\text{NO}_2$: 166.0863, Found: 166.0862.

(1s) – 3-isopentylpyridine



Reaction Setup³: Lithium diisopropylamide solution (20 mL, 40 mmol, 4.0 equiv, [2M in tetrahydrofuran]) and anhydrous tetrahydrofuran (45 mL) were added under nitrogen at -78°C to a flame dried 200-mL round bottom flask. A solution of 3-methylpyridine (970 μL , 10 mmol, 1.0 equiv) in tetrahydrofuran (5 mL) was added dropwise under nitrogen at -78°C over 10 minutes. The reaction mixture was stirred for one hour at -78°C . After one hour, a solution of isobutyl bromide (1.08 mL, 10 mmol, 1.0 equiv) in tetrahydrofuran (5 mL) was added dropwise under nitrogen at -78°C over ten minutes. The reaction mixture was stirred for 16 hours and allowed to warm from -78°C to room temperature. Upon completion, the crude reaction mixture was diluted with saturated aqueous ammonium chloride solution. The aqueous layer was extracted three times with 30 mL of ethyl acetate. The combined organic layers were dried with MgSO_4 . The organic solvent was evaporated under vacuum. Yield = 711.0 mg (47%) of yellow oil.

Purification: normal phase silica gel column chromatography with 5:1 pentane:ethyl acetate

Spectral data available in the literature: Yes⁴

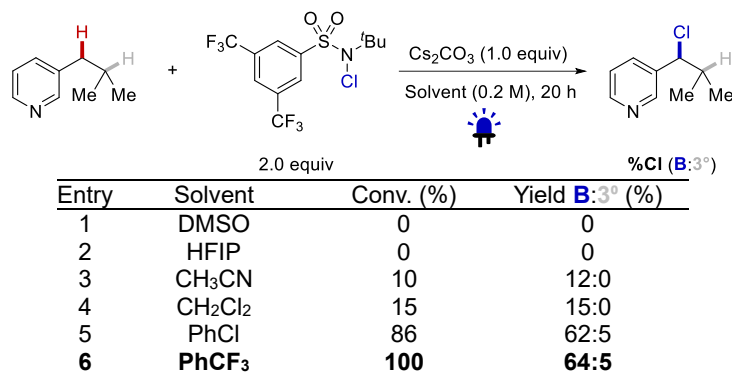
^1H NMR (CDCl_3 , 500 MHz): δ 8.47 – 8.40 (m, 2H), 7.48 (dt, $J = 7.9, 2.0$ Hz, 1H), 7.19 (ddd, $J = 7.8, 4.8, 0.9$ Hz, 1H), 2.64 – 2.57 (m, 2H), 1.59 (dp, $J = 13.1, 6.6$ Hz, 1H), 1.53 – 1.47 (m, 2H), 0.94 (d, $J = 6.6$ Hz, 6H) ppm.

^{13}C NMR (CDCl_3 , 126 MHz): δ 149.96, 147.18, 138.14, 135.68, 123.22, 77.02, 40.42, 30.88, 27.61, 22.44 ppm.

3B.IV. Reaction Optimization

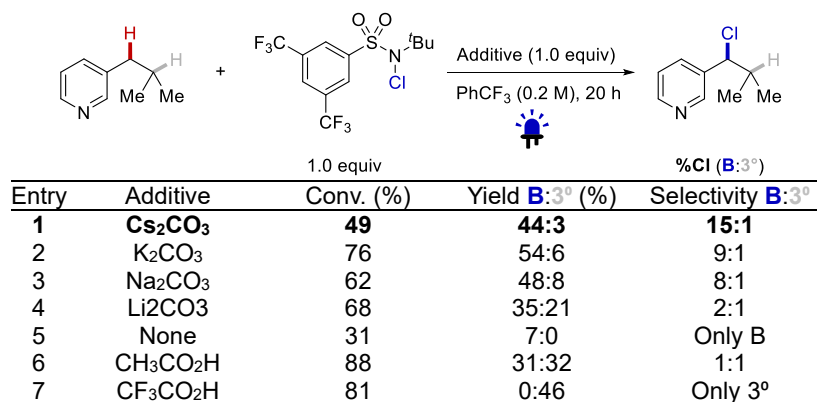
Optimization of reaction conditions were conducted according to general procedure (III) or (IV), with variations specified in each table. Reaction yields were monitored by ^1H NMR spectroscopy.

Table 3B.1. Solvent Screen^a



^aConv., conversion.

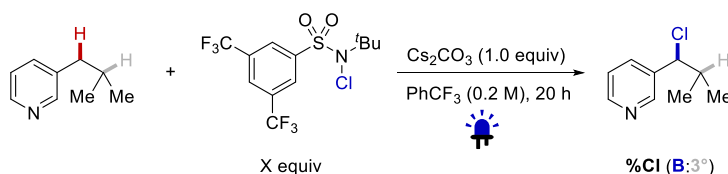
Table 3B.2. Additive Screen^a



^aConv., conversion.

Table 3B.3. Chlorination of 3-Isobutylpyridine with Various N-Chloro Reagents^a

Entry	Reagent	Conv. (%)	Yield B:3° (%)
1		66	36:6
2 – 6:			
2	Ar: C ₆ H ₅	35	5:4
3	Ar: 4-ClC ₆ H ₄	84	50:4
4	Ar: 4-(CF ₃)C ₆ H ₄	80	41:6
5	Ar: 4-(MeO)C ₆ H ₄	79	30:3
6	Ar: 3,5-(CF ₃) ₂ C ₆ H ₃	100	62:4

^aConv., conversion.Table 3B.4. Loading of *N*-(*tert*-butyl)-*N*-chloro-3,5 – bis (trifluoromethyl) benzenesulfonamide (2)^a

Entry	X (equiv)	Conv. (%)	Yield B:3° (%)	Selectivity B:3°
1	1.0	55	34:3	11:1
2	1.5	80	55:5	11:1
3	2.0	90	64:5	13:1
4^b	2.0	90	62:4	16:1

^aConv., conversion. ^b1.5 equiv of Cs₂CO₃.

3B.V. Computational Methods for Bond Dissociation Free Energy Analysis

- *Computational Details*

All density functional theory calculations, *i.e.*, structure optimizations, frequencies and final single-point energies, were calculated using TURBOMOLE 7.5.1¹⁵ program package. The lowest energy structures were searched with CREST⁶ and xTB⁷ program packages using the default iMTD-GC algorithm with GFN2-xTB. The conformer ensembles were then further refined with CENSO⁸ running parts 0–2. All ground state structures had zero imaginary frequencies.

The dispersion corrected hybrid functional PBE0-D4^{9,10} with def2-TZVP¹¹ basis sets was used for calculation of geometries and vibrational frequencies. Final single-point energy calculations were done using resolution-of-identity random-phase approximation (RI-RPA)^{12,13} with PBE0-D4/def2-QZVPP gas-phase orbitals. The core orbitals were kept frozen for computation of correlation energy. The (multipole accelerated) resolution-of-identity approximation for Coulomb term^{14,15} with corresponding auxiliary basis sets^{16,17} was used. Additionally, the *m4* grid and default convergence criteria of 10^{-6} and 10^{-7} were used for density and energy, respectively. For RI-RPA calculations the *m5* grid was used.

Solvation effects were included with COSMO¹⁸ in structure optimization and frequency calculations using the dielectric constant for α,α,α -trifluorotoluene ($\epsilon = 9.18$). For final single-point energies, the COSMO-RS model was used as implemented in COSMOthermX19 program package^{19–22} using BP_TZVPD_FINE_19.ctd parameter file based on BP86^{23,24}/def2-TZVPD²⁵ level of theory. The Gibbs free energy in solution was then calculated according to published protocol: $G = E_{\text{gas}}(\text{SCF}) + G_{\text{thermo}} + G_{\text{solv,1M}}$,²⁶ where $E_{\text{gas}}(\text{SCF})$ is the final single-point energy of the system in gas-phase, G_{thermo} is the chemical potential calculated at the optimization level using qRRHO approximation by Grimme,²⁷ and $G_{\text{solv,1M}}$ is the solvation free energy of each species in toluene from COSMO-RS. All thermodynamic functions were calculated at 298.15 K and vibrational frequencies were used without scaling. The reference state for the Gibbs free energies is 1 M.^{22,26}

• **Bond Dissociation Free Energies**

The homolytic bond dissociation free energies (BDFEs) for R–X bonds, where X is Cl or H, were calculated as

$$\Delta G_{298K} = G_{298K}(R \bullet) + G_{298K}(X \bullet) - G_{298K}(R - X) \quad (\text{Eq. 1})$$

Where $G_{298K}(R \bullet)$ and $G_{298K}(X \bullet)$ are the free energies of the radical species and $G_{298K}(R-X)$ is the free energy of the ground state species. **Error! Reference source not found.** summarizes the BDFEs of substrate **1a** and the investigated N-Cl reagents and **Error! Reference source not found.** lists Δ BDFE and ΔG values between the N-Cl reagents and substrate **1a**, see Figure 3B.2 for details.

Table 3B.5. BDFE (kcal·mol⁻¹) values for substrate **1a** and N-Cl reagents

Compound	BDFE(H)	BDFE(Cl)
1a-C(1°)	100.2	78.0
1a-C(2°)	87.0	65.2
1	134.3	80.4
2	118.8	65.6
3	117.7	57.8
4	107.7	52.0
5	107.7	48.6
6	107.0	47.8
7	101.9	44.4
8	99.4	40.9

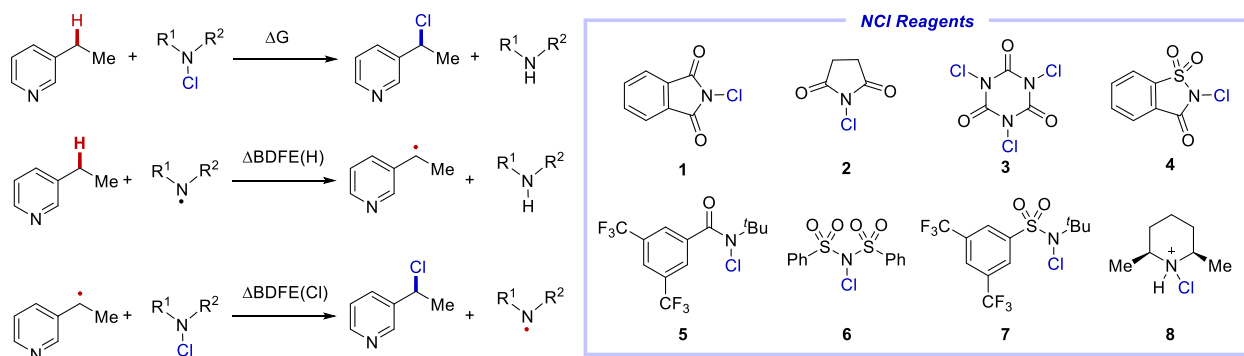


Figure 3B.2. The individual HAT and XAT steps, and the overall reaction used to calculate the Δ BDFE and ΔG , respectively.

Table 3B.6. Reaction free energies (kcal·mol⁻¹) for individual HAT/XAT steps and for overall chlorination reaction.

Substrate	N-Cl Reagent	Center Type	$\Delta\text{BDFE(H)}$	$\Delta\text{BDFE(Cl)}$	ΔG
1a	1	C(1°)	-34.1	2.4	-31.7
1a	1	C(2°)-benzylic	-47.3	15.3	-32.1
1a	2	C(1°)	-18.6	-12.4	-31.0
1a	2	C(2°)-benzylic	-31.8	0.4	-31.4
1a	3	C(1°)	-17.5	-20.2	-37.6
1a	3	C(2°)-benzylic	-30.7	-7.3	-38.0
1a	4	C(1°)	-7.5	-26.0	-33.5
1a	4	C(2°)-benzylic	-20.7	-13.1	-33.8
1a	5	C(1°)	-7.5	-29.4	-36.8
1a	5	C(2°)-benzylic	-20.7	-16.5	-37.2
1a	6	C(1°)	-6.8	-30.2	-36.9
1a	6	C(2°)-benzylic	-20.0	-17.3	-37.3
1a	7	C(1°)	-1.7	-33.5	-35.2
1a	7	C(2°)-benzylic	-14.9	-20.7	-35.6
1a	8	C(1°)	0.8	-37.1	-36.3
1a	8	C(2°)-benzylic	-12.4	-24.2	-36.7

- *Raw Energies*

Table 3B.7. Absolute energies (a.u.) for compound **1a**

Compound	Position	$E(\text{PBE0/TZ})$	G_{thermo}	$G_{\text{solv,1M}}$	$E(\text{PBE0/QZ})$	$E(\text{RPA})$
1a	C(1°/2°)-H	-326.6572173	0.1139440	-0.0105968	-326.6703604	-326.9540465
	C(1°)•	-325.9884387	0.1022243	-0.0103306	-326.0009415	-326.2663156
	C(2°)•	-326.0127723	0.1030013	-0.0107653	-326.0253328	-326.2877308
	C(1°)-Cl	-786.1273102	0.1030013	-0.0132845	-786.1511202	-786.1763031
	C(2°)-Cl	-786.1281607	0.1029556	-0.0127069	-786.1522989	-786.1774333

Table 3B.8. Absolute energies (a.u.) for the N-Cl reagents

Species	Compound	$E(\text{PBE0/TZ})$	G_{thermo}	$G_{\text{solV,1M}}$	$E(\text{PBE0/QZ})$	$E(\text{RPA})$
N-H	1	-512.7463166	0.0845439	-0.0151739	-512.7593769	-513.0845425
	2	-360.4413458	0.0629442	-0.0129288	-360.4451773	-360.7142526
	3	-1424.6501291	0.0247420	-0.0172461	-1424.6858117	-1424.4979745
	4	-947.8880881	0.0825671	-0.0192646	-947.9139473	-948.0080902
	5	-1231.5536362	0.2000876	-0.0176590	-1231.6087436	-1232.4899731
	6	-1615.1065718	0.1755323	-0.0269802	-1615.1630277	-1615.2136655
	7	-1666.7000031	0.1984041	-0.0199324	-1666.7697937	-1667.4202219
	8	-330.7297731	0.1984536	-0.0702013	-330.6812905	-331.0699128
N•	1	-512.0447767	0.0719139	-0.0154002	-512.0272709	-512.3410284
	2	-359.7318569	0.0474310	-0.0114692	-359.7382772	-359.9942531
	3	-1423.9471341	0.0110569	-0.0154215	-1423.9859154	-1423.7819948
	4	-947.2020404	0.0709770	-0.0174562	-947.2311150	-947.3101304
	5	-1230.8744631	0.1913159	-0.0153096	-1230.9314875	-1231.7953973
	6	-1614.4260733	0.1648181	-0.0271536	-1614.4821019	-1614.5157376
	7	-1666.0297083	0.1902875	-0.0181223	-1666.1017090	-1666.7349702
	8	-330.0629272	0.1853018	-0.0681157	-330.0171361	-330.3838235
N-Cl	1	-972.1610180	0.0717425	-0.0158761	-972.1896571	-972.2563832
	2	-819.8574853	0.0500933	-0.0139576	-819.8763339	-819.8867903
	3	-1884.0537475	0.0119101	-0.0177472	-1884.1056828	-1883.6605423
	4	-1407.2991289	0.0698000	-0.0190234	-1407.3423278	-1407.1781374
	5	-1690.9617018	0.1885317	-0.0168139	-1691.0326580	-1691.6564781
	6	-2074.5146304	0.1639535	-0.0264506	-2074.5871050	-2074.3796885
	7	-2126.1107651	0.1873053	-0.0198548	-2126.1960046	-2126.5889552
	8	-790.1342917	0.1850124	-0.0684469	-790.1038394	-790.2362883

3B.VI. Additional Screening Data with Benzylic C–H Substrates and Azoles

High-Throughput Experiment Procedure for Nucleophilic Displacement of 3-(1-chloroethyl)pyridine, 3a

A 24-mL glass vial was charged with Cs₂CO₃ (500 mg, 1.53 mmol) and a magnetic stir bar on the benchtop under air. 2-methylbutan-2-ol (*tert*-amyl alcohol, 15.2 mL) was added to the vial. 120 μL of the Cs₂CO₃ stock solution was dispensed as a slurry to 1-mL microvials (Analytical Sales, Cat. No. 96F610) in 96-well reaction microplates (Analytical Sales, Cat. No. 96960). The solvent was removed under vacuum and a magnetic stir bar was added into each microvial.

A second 24-mL glass vial was charged with potassium iodide (KI, 500 mg, 3.01 mmol) and a magnetic stir bar on the benchtop under air. *N,N*-dimethylformamide (DMF, 5.9 mL) was added to the vial. The vial was allowed to stir on a magnetic plate until all KI was completely dissolved. 24 μL of the KI stock solution was dispensed to each microvial using a multichannel pipette. Another 24-mL glass vial was charged with 3-(1-chloroethyl)pyridine (**3a**, 500 mg, 3.53 mmol) and a magnetic stir bar on the benchtop under air. DMF (8.3 mL) was added to the vial. The vial was allowed to stir on a magnetic plate for 15 minutes. 25 μL of the **3a** stock solution was dispensed to each microvial using a multichannel pipette. Each nucleophilic coupling partner was ordered pre-weighed in a 4-mL glass vial. DMF (300 – 500 μL) and a magnetic stir bar were added to the 4-mL glass vials. The vials containing the nucleophilic coupling partners were allowed to stir on a magnetic stir plate for 5 minutes. 50 μL of each nucleophilic coupling partner was dispensed to the corresponding microvial. Once the solution dosing was completed, the plates were covered by a perfluoroalkoxy alkane (PFA) film (Analytical Sales, Cat. No. 96967), two silicon rubber mats (Analytical Sales, Cat. No. 96965), and an aluminum cover, which was tightly sealed by 9 screws. The sealed plates were placed inside a heating block with stirring at 70 °C for 16 hours.

After 16 hours, the plate was removed from the heating block and allowed to cool to room temperature. 2 μL of each reaction mixture was transferred to an UPLC analytical plate (Analytical Sales, Cat. No. 96355) using a multichannel pipette. 200 μL of DMSO was added to each well. The analytical plate was sealed and injected into Waters UPLC-MS instrument for analysis.

Nucleophile selection using cheminformatic analysis

To each class of nucleophiles, the nucleophilic displacement products of 3-ethyl-5-phenylpyridine were enumerated and filtered based on molecular weight (≤ 500), lipophilicity (5.0 – 6.0), numbers of hydrogen bond donors, incompatible functional groups. Proprietary compounds were removed from the selections. Then, the nucleophiles were featurized followed by dimensionality reduced using Principle Component Analysis. The k-means clustering was done on the set of principal components that covered >95% variability in the chemical space. Clusters were visualized using *t*-SNE mapping. While the C–H substrate was switched to 3-ethylpyridine due to experimental issues, the selections that were made initially were mapped onto the clustering map to deliver the final *t*-SNE maps.

Note: Azoles were selected manually without computational clustering.

The following amine, alcohol, and carboxylic acid nucleophiles are included in Figure 3.6

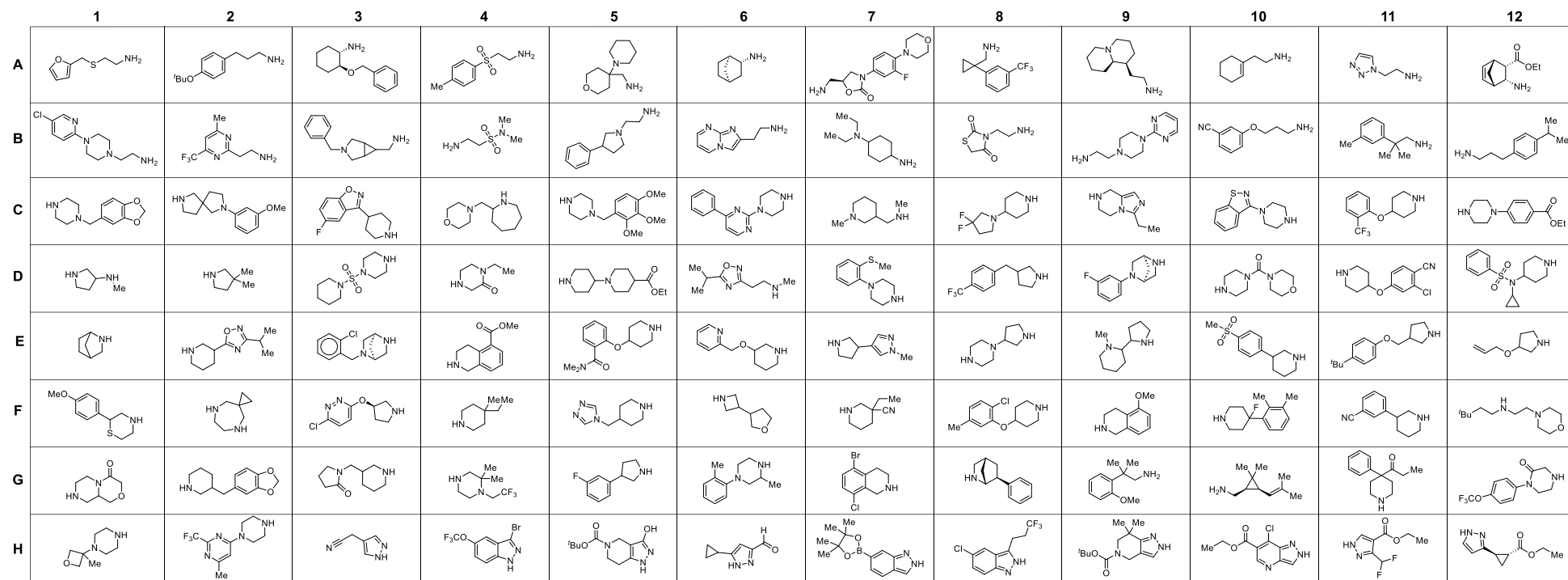


Figure 3B.3. Nitrogen-based nucleophiles in Figure 3.6.

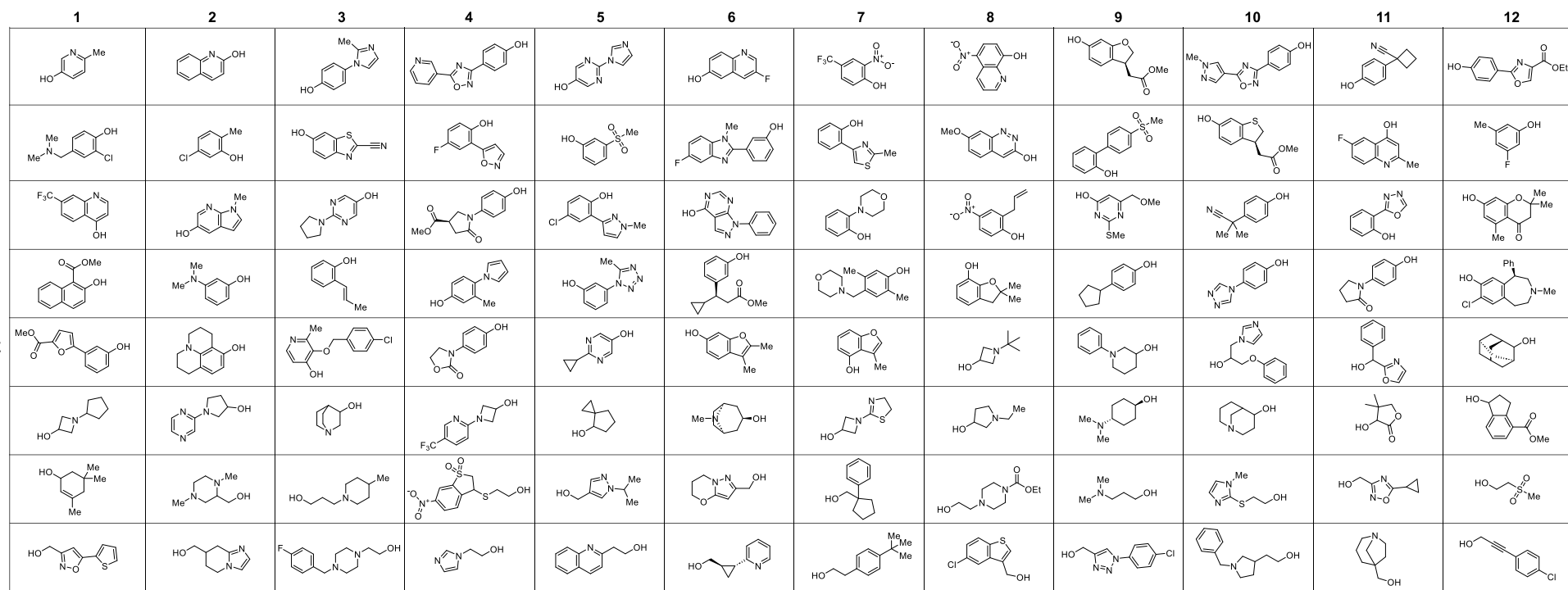


Figure 3B.4. Alcohol nucleophiles in Figure 3.6.

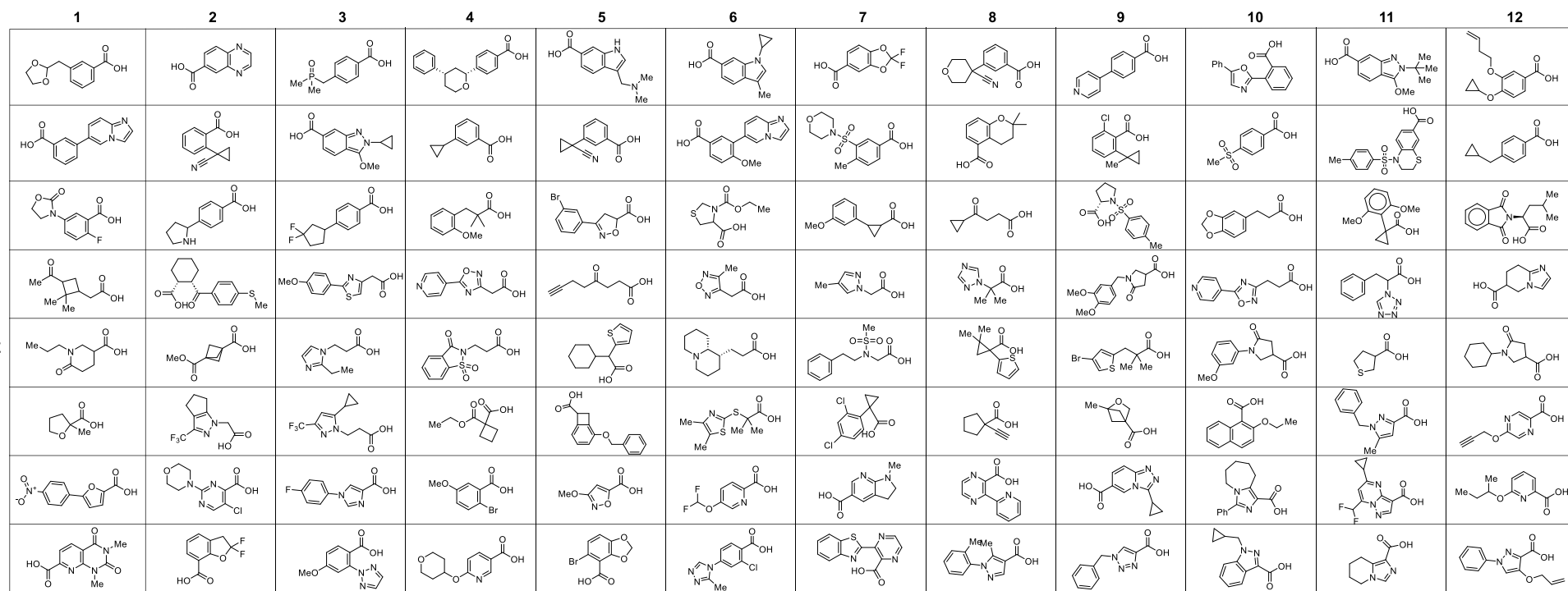


Figure 3B.5. Carboxylic acid nucleophiles in Figure 3.6.

More nucleophiles were tested for displacement of heterobenzyl chlorides and included below.

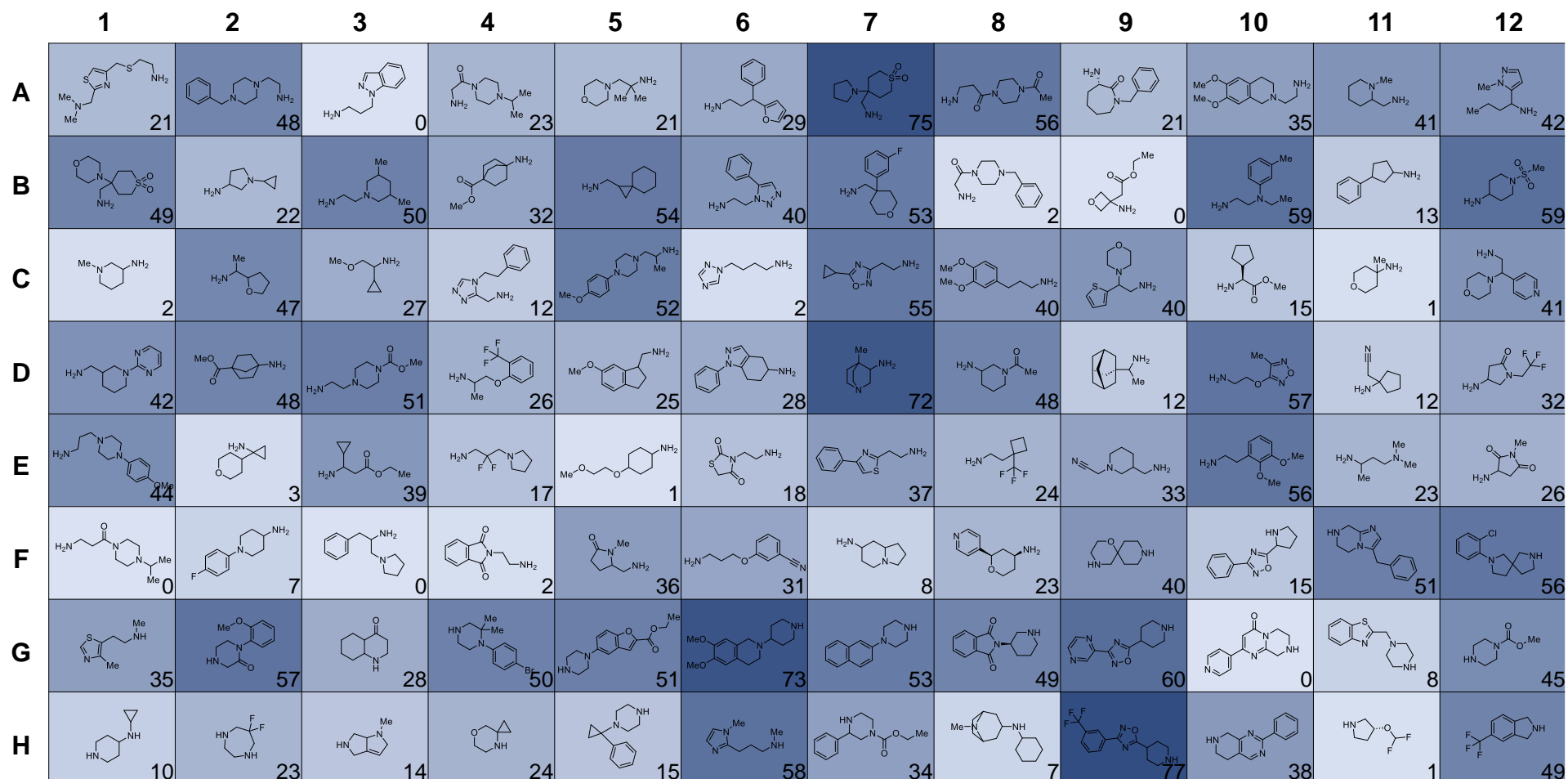


Figure 3B.6. 96-Well Plate Display of Selected Amines for High-Throughput Experiments not included in Figure 3.6.

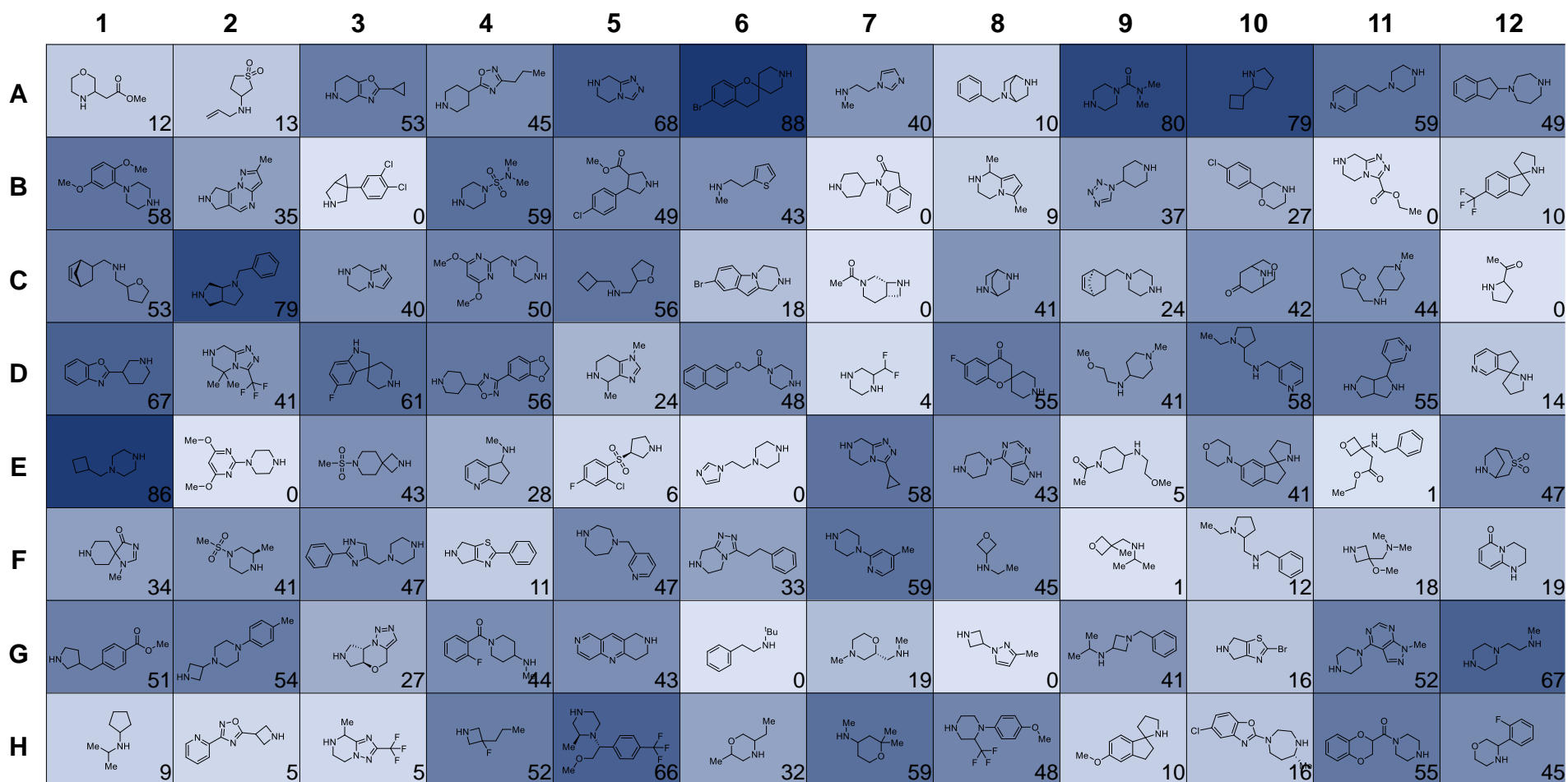


Figure 3B.7. 96-Well Plate Display of Selected Amines for High-Throughput Experiments not included in Figure 3.6.

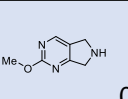
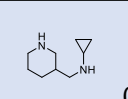
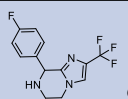
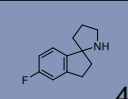
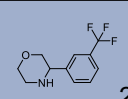
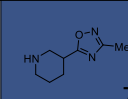
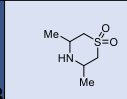
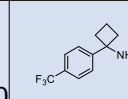
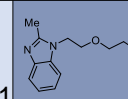
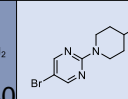
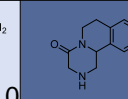
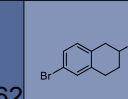
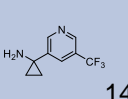
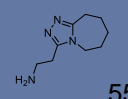
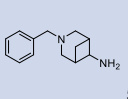
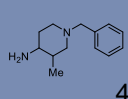
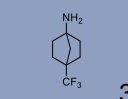
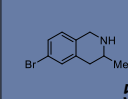
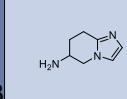
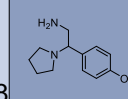
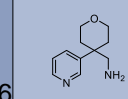
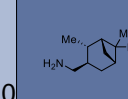
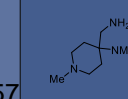
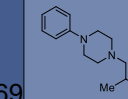
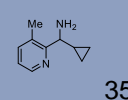
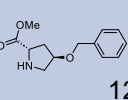
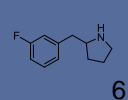
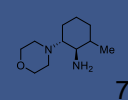
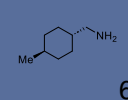
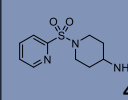
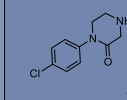
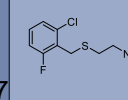
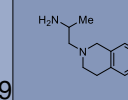
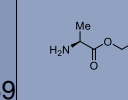
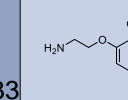
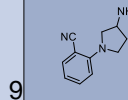
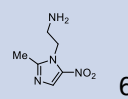
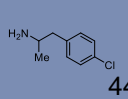
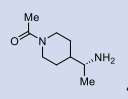
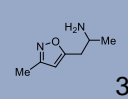
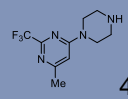
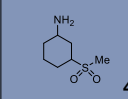
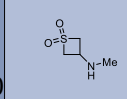
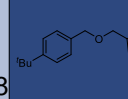
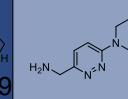
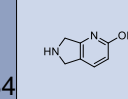
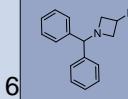
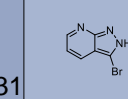
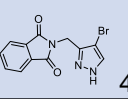
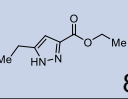
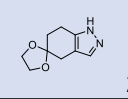
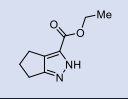
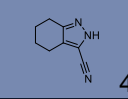
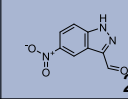
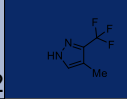
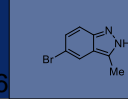
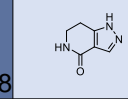
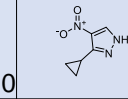
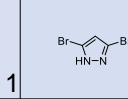
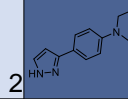
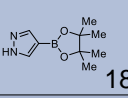
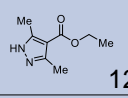
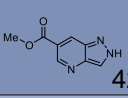
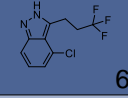
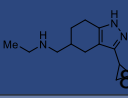
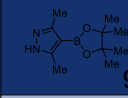
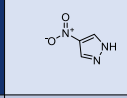
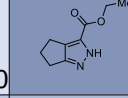
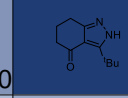
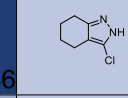
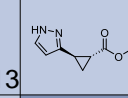
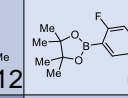
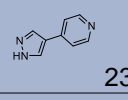
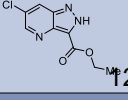
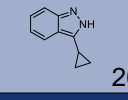
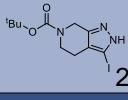
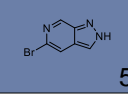
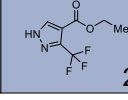
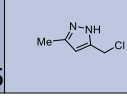
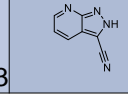
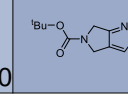
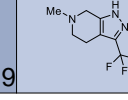
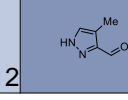
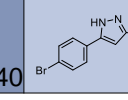
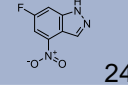
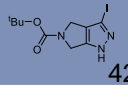
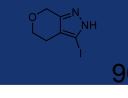
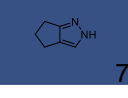
	1	2	3	4	5	6	7	8	9	10	11	12
A	 0	 0	 9	 40	 26	 73	 0	 1	 40	 0	 62	 40
B	 14	 55	 5	 44	 35	 53	 8	 36	 20	 57	 69	 47
C	 35	 12	 61	 72	 60	 41	 47	 29	 39	 33	 9	 27
D	 6	 44	 4	 30	 40	 40	 18	 79	 34	 6	 31	 23
E	 4	 8	 2	 1	 46	 22	 96	 58	 0	 1	 2	 66
F	 18	 12	 42	 65	 80	 91	 0	 40	 86	 13	 12	 0
G	 23	 12	 26	 25	 51	 25	 13	 20	 29	 12	 40	 13
H	 24	 42	 90	 75								

Figure 3B.8. 96-Well Plate Display of Selected Amines for High-Throughput Experiments not included in Figure 3.6.

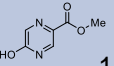
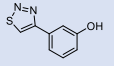
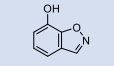
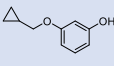
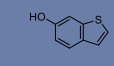
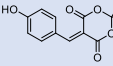
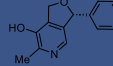
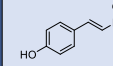
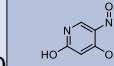
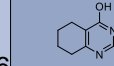
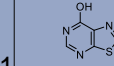
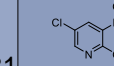
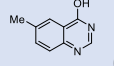
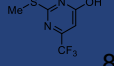
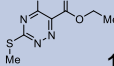
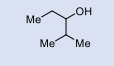
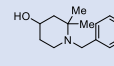
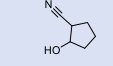
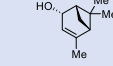
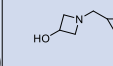
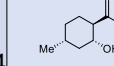
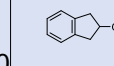
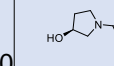
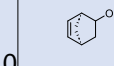
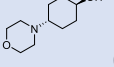
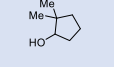
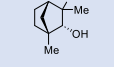
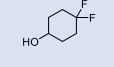
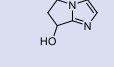
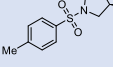
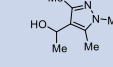
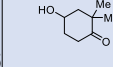
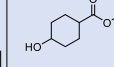
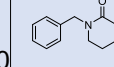
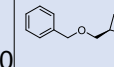
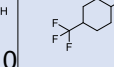
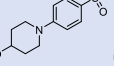
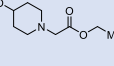
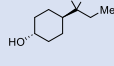
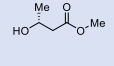
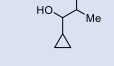
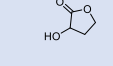
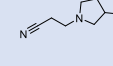
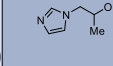
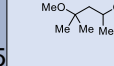
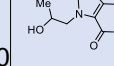
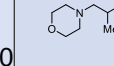
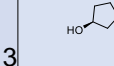
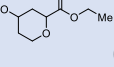
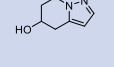
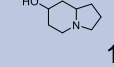
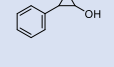
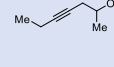
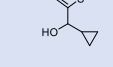
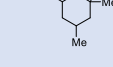
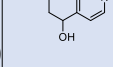
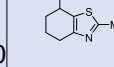
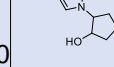
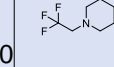
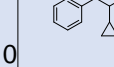
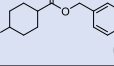
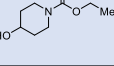
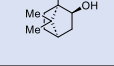
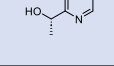
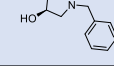
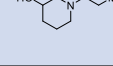
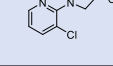
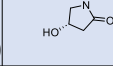
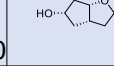
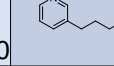
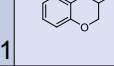
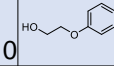
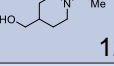
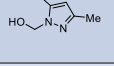
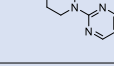

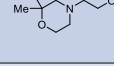
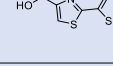
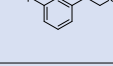
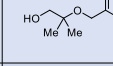

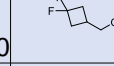
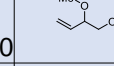
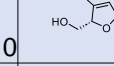
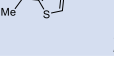
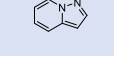
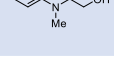
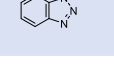
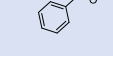
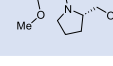
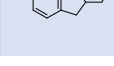
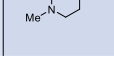
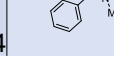
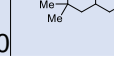
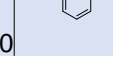
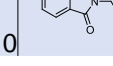
	1	2	3	4	5	6	7	8	9	10	11	12
A	 14	 0	 1	 1	 52	 0	 73	 0	 16	 31	 31	 36
B	 0	 83	 12	 0	 0	 0	 0	 4	 0	 0	 0	 0
C	 0	 0	 0	 0	 1	 0	 6	 1	 0	 0	 0	 0
D	 0	 0	 0	 0	 0	 0	 0	 25	 0	 0	 3	 0
E	 0	 5	 13	 0	 0	 0	 0	 0	 0	 0	 0	 0
F	 0	 0	 0	 1	 0	 4	 0	 0	 0	 11	 0	 0
G	 12	 9	 0	 9	 10	 0	 1	 0	 0	 0	 0	 0
H	 2	 0	 1	 0	 0	 0	 1	 4	 0	 0	 0	 0

Figure 3B.9. 96-Well Plate Display of Selected Alcohols for High-Throughput Experiments not included in Figure 3.6.

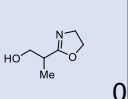
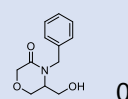
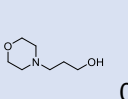
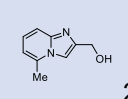
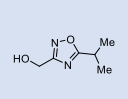
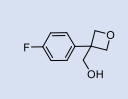
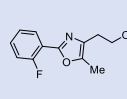
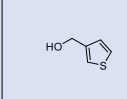
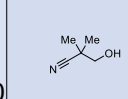
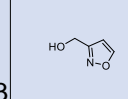
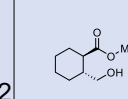
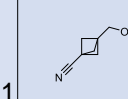
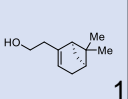
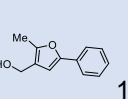
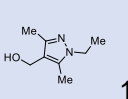
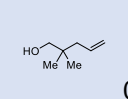
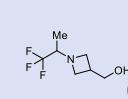
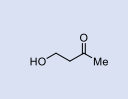
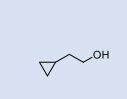
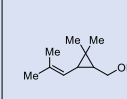
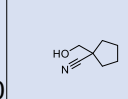
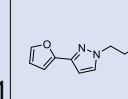
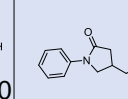
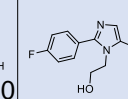
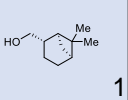
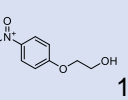
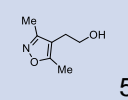
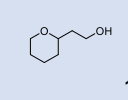
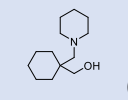
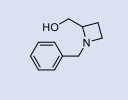
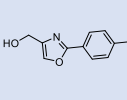
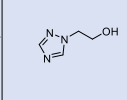
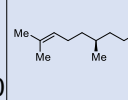
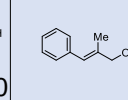
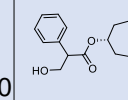
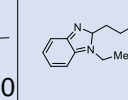
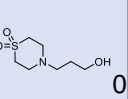
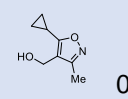
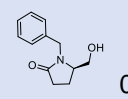
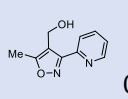
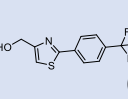
	1	2	3	4	5	6	7	8	9	10	11	12
A	 0	 0	 0	 2	 1	 1	 0	 0	 3	 2	 1	 3
B	 1	 1	 1	 0	 0	 0	 1	 0	 1	 0	 0	 0
C	 1	 1	 5	 1	 0	 0	 0	 0	 0	 0	 0	 1
D	 0	 0	 0	 0	 0							

Figure 3B.10. 96-Well Plate Display of Selected Alcohols for High-Throughput Experiments not included in Figure 3.6.

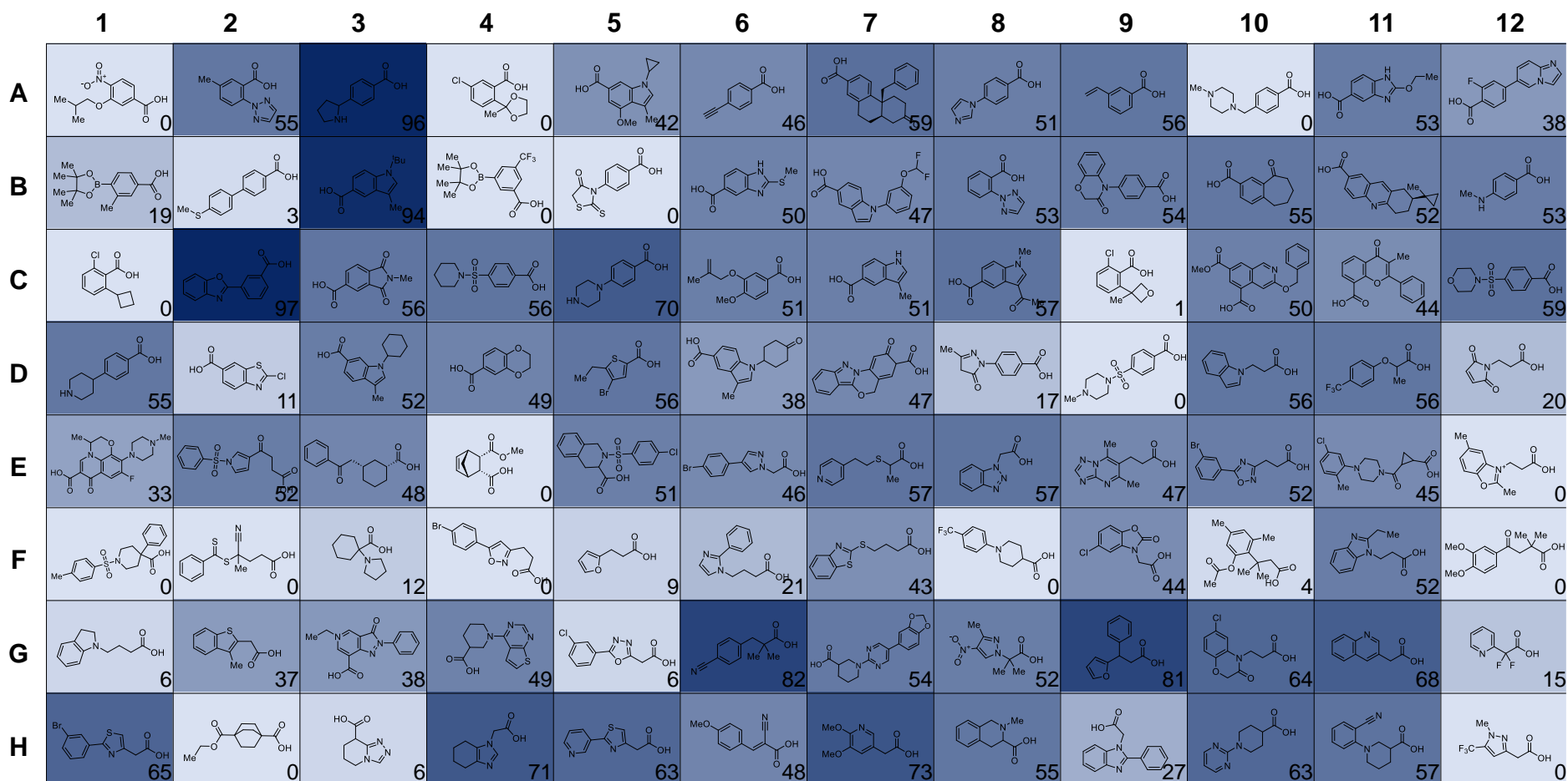


Figure 3B.11. 96-Well Plate Display of Selected Carboxylic Acids for High-Throughput Experiments not included in Figure 3.6.

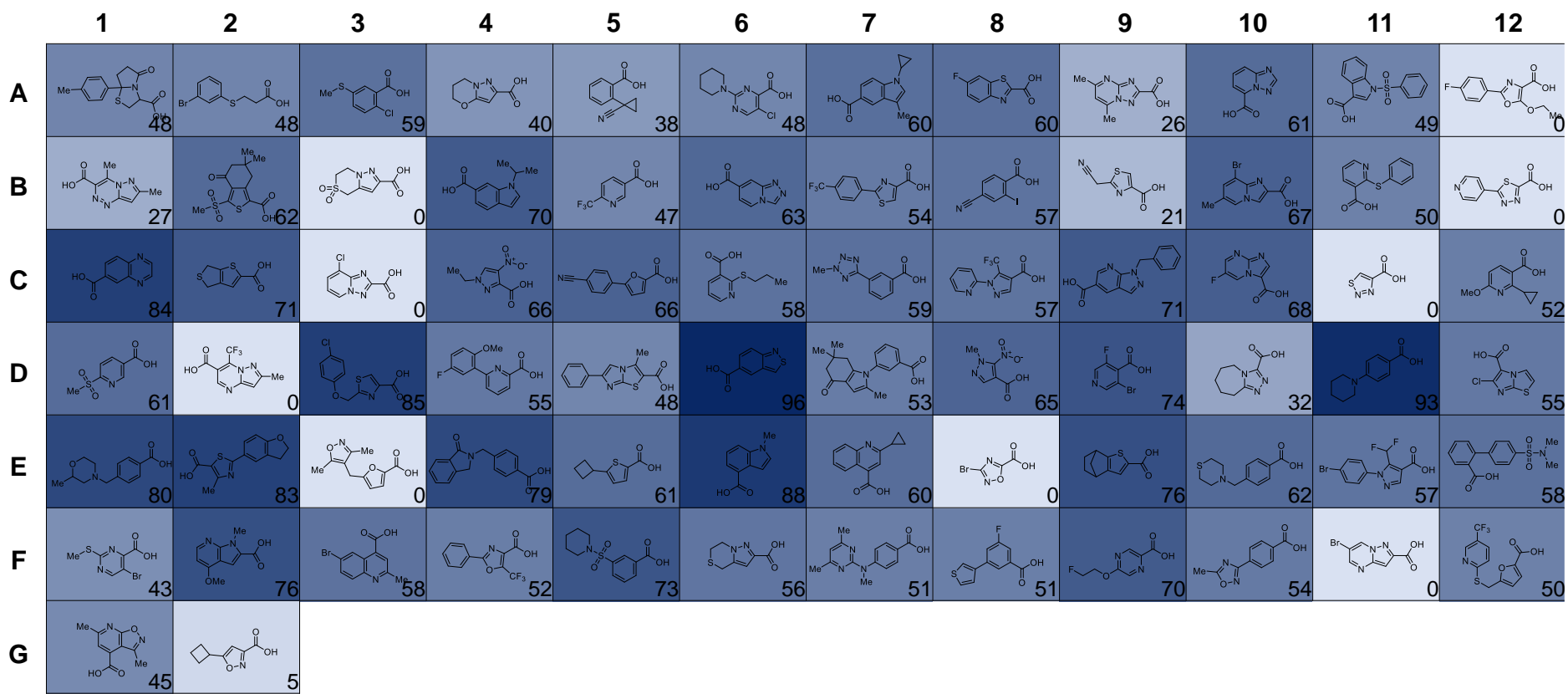


Figure 3B.12. 96-Well Plate Display of Selected Carboxylic Acids for High-Throughput Experiments not included in Figure 3.6

3B.VII. Additional Experiments and Observations

Assessment of other Heterobenzylic C–H Substrates

Not all substrates tested afforded good reactivity in the chlorination reaction, and a survey of suboptimal results are provided in Figure 3B.13.

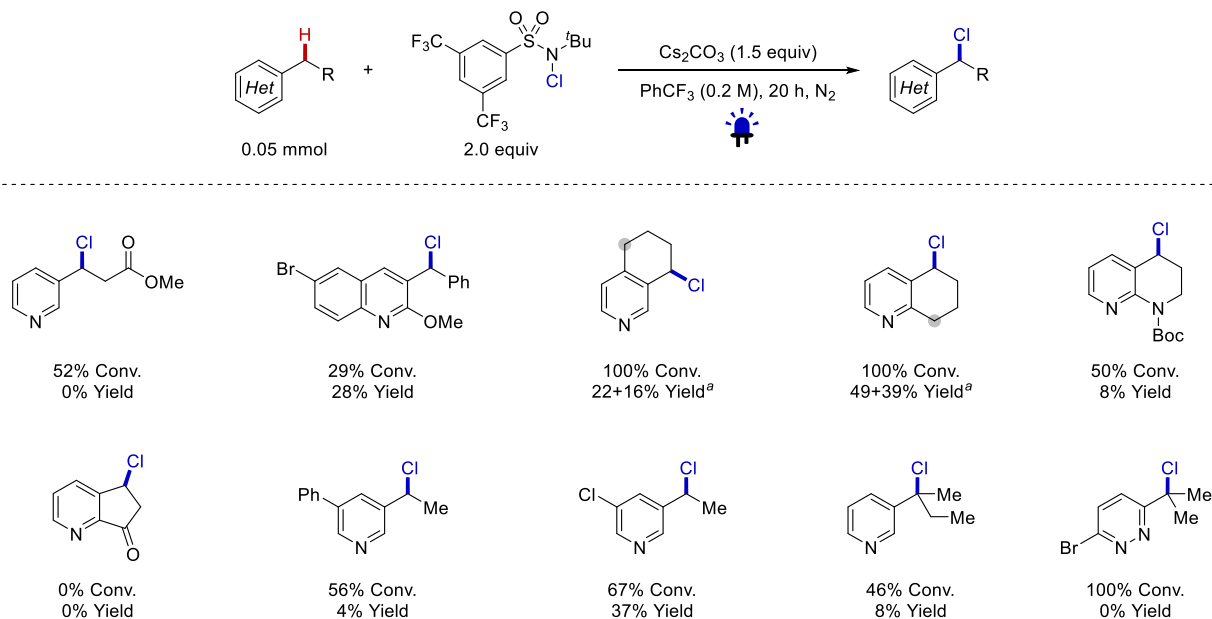


Figure 3B.13. Screening data with additional benzylic C–H substrates. Conv., conversion. ^a4-hour reaction time

The chlorination reaction also was tested with 2- and 4-alkyl substituted heteroaromatics. The results are provided in Figure 3B.14.

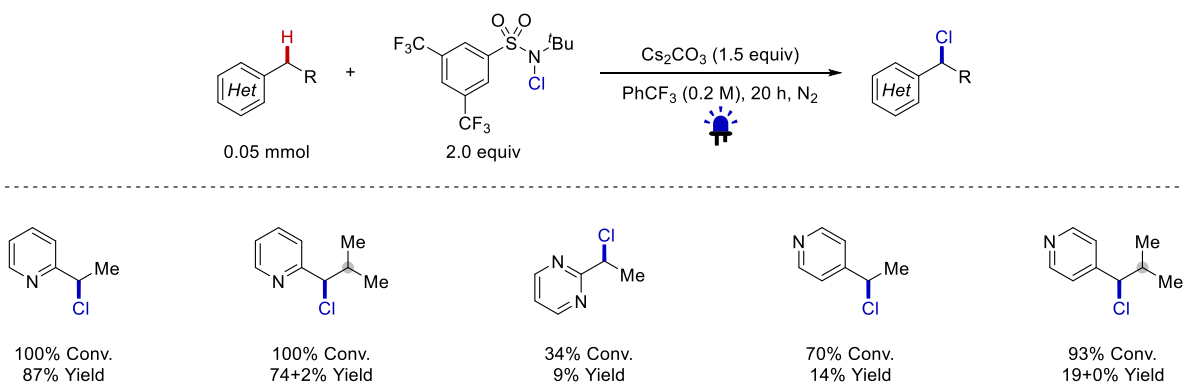
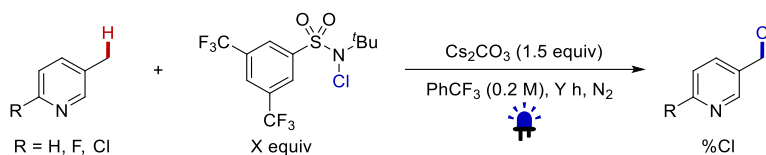


Figure 3B.14. Screening data with additional benzylic C–H substrates. Conv., conversion.

Byproduct Analysis of 3-Methylpyridine and Derivatives

Chlorination reactions of 3-methylpyridine, 2-fluoro-5-methylpyridine, and 2-chloro-5-methylpyridine were conducted with two different reaction times of 8 and 20 hours. The results are provided in Table 3B.9.

Table 3B.9. Chlorination data of 3-methylpyridine and derivatives



Entry	R	X (equiv)	Y (h)	Conv. (%)	%Cl	%di-Cl
1	H	2.0	8	42	37	5
2	H	2.0	20	83	36	0
3	F	4.0	8	42	40	3
4	F	4.0	20	60	44	0
5	Cl	4.0	8	35	28	1
6	Cl	4.0	20	35	32	0

^aConv., conversion.

Note: Multiple byproducts were detected in UPLC analysis for entry 1. The possible byproducts are provided in Figure 3B.15.

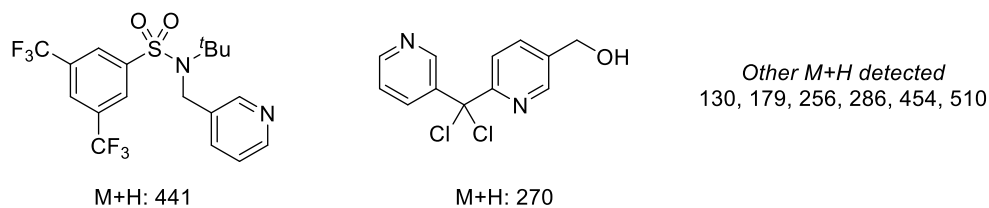
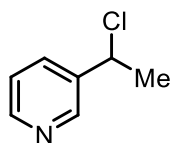


Figure 3B.15. Byproducts detected in UPLC analysis.

3B. VIII. Characterization of Compounds



3-(1-chloroethyl)pyridine, **3a**

Reaction run using 3-ethylbenzene **1a** (56.0 μ L, 0.50 mmol, 1.0 equiv) and *N*-(*tert*-butyl)-*N*-chloro-3,5-bis(trifluoromethyl)benzenesulfonamide **2** (384.0 mg, 1.00 mmol, 2.0 equiv) following the general procedure IV. ^1H NMR Yield = 86%.

Purification: normal phase silica gel column chromatography with 9:1 pentane:ethyl acetate

Spectral data available in the literature: No

^1H NMR (CDCl_3 , 500 MHz): δ 8.65 (s, 1H), 8.57 (s, 1H), 7.79 (dt, $J = 8.0, 2.0$ Hz, 1H), 7.32 (dd, $J = 8.0, 4.8$ Hz, 1H), 5.11 (q, $J = 6.8$ Hz, 1H), 1.87 (d, $J = 6.9$ Hz, 3H) ppm.

^{13}C NMR (CDCl_3 , 126 MHz): δ 149.57, 148.01, 138.42, 134.14, 123.62, 55.73, 26.37 ppm.

HRMS m/z : $[\text{M}+\text{H}]^+$ calculated for $\text{C}_7\text{H}_8\text{ClN}$: 142.0418, Found: 142.0419.

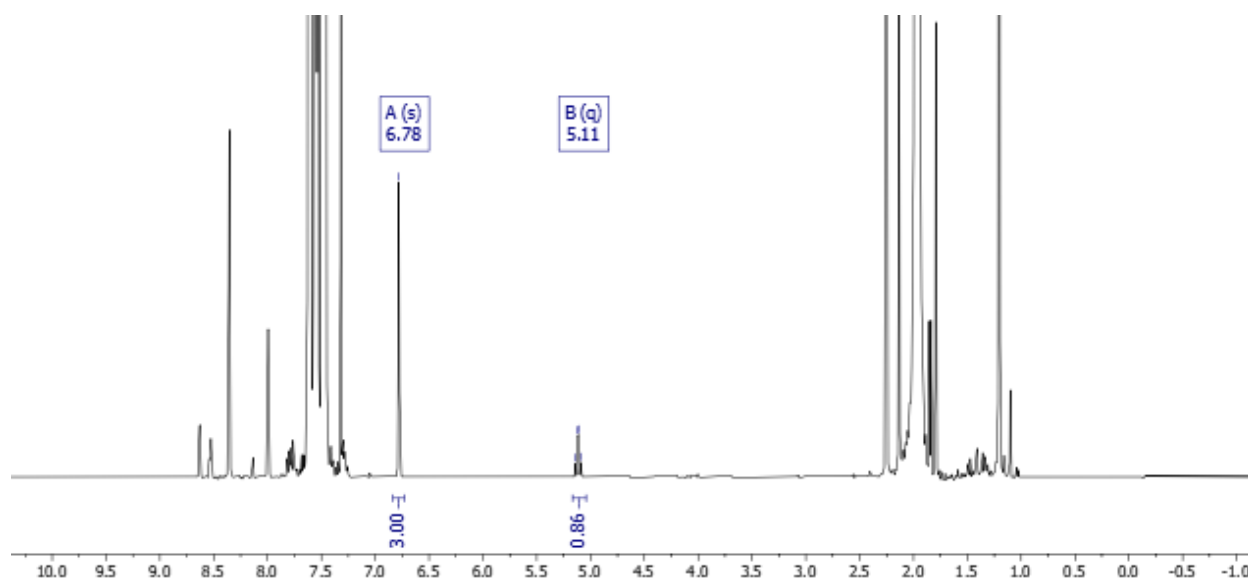
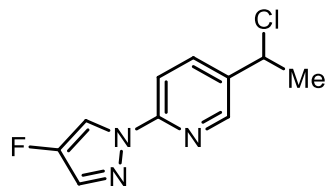


Figure 3B.16. Crude ^1H NMR Spectrum (CDCl_3 , 400 MHz, 25 $^\circ\text{C}$) of the reaction mixture for **1a** following the addition of 0.5 mmol (70 μ L) of mesitylene as an external standard (6.78 ppm). The resolved benzylic protons for **3a** is labeled and integrated.



5-(1-chloroethyl)-2-(4-fluoro-1H-pyrazol-1-yl)pyridine, **3b**

Reaction run using 5-ethyl-2-(4-fluoro-1H-pyrazol-1-yl)pyridine **1b** (38.2 mg, 0.20 mmol, 1.0 equiv) and *N*-(*tert*-butyl)-*N*-chloro-3,5-bis(trifluoromethyl)benzenesulfonamide **2** (230.2 mg, 0.60 mmol, 3.0 equiv) following the general procedure III. Yield = 36.5 mg (81%) of white solid.

Purification: normal phase silica gel column chromatography with 9:1 pentane:ethyl acetate

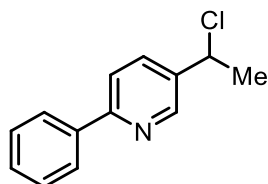
Spectral data available in the literature: No

¹H NMR (CDCl₃, 500 MHz): δ 8.42 – 8.37 (m, 2H), 7.94 (dd, *J* = 8.6, 0.8 Hz, 1H), 7.89 (dd, *J* = 8.6, 2.3 Hz, 1H), 7.59 (dd, *J* = 4.4, 0.9 Hz, 1H), 5.13 (q, *J* = 6.9 Hz, 1H), 1.88 (d, *J* = 6.9 Hz, 3H) ppm.

¹³C NMR (CDCl₃, 126 MHz): δ 151.11, 151.17 (d, *J* = 249.6 Hz), 146.15, 137.01, 136.35, 130.14 (d, *J* = 15.0 Hz), 112.99 (d, *J* = 29.1 Hz), 111.59 (d, *J* = 1.5 Hz), 5.21, 26.21 ppm.

¹⁹F NMR (CDCl₃, 377 MHz): -174.09 ppm.

HRMS *m/z*: [M+H]⁺ calculated for C₁₀H₉ClFN₃: 226.0542, Found: 226.0538.



5-(1-chloroethyl)-2-phenylpyridine, **3c**

Reaction run using 2-phenyl-5-ethylpyridine **1c** (36.7 mg, 0.20 mmol, 1.0 equiv) and *N*-(*tert*-butyl)-*N*-chloro-3,5-bis(trifluoromethyl)benzenesulfonamide **2** (115.1 mg, 0.30 mmol, 1.5 equiv) following the general procedure III. Yield = 33.0 mg (76%) of yellow oil in a mixture with 14% of remaining C–H starting material.

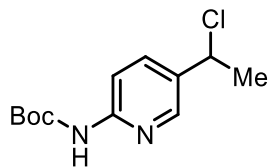
Purification: normal phase silica gel column chromatography with 2:1 pentane:ethyl acetate

Spectral data available in the literature: No

¹H NMR (CDCl₃, 500 MHz): δ 8.71 (dd, *J* = 2.3, 0.7 Hz, 1H), 8.03 – 7.98 (m, 2H), 7.84 (dd, *J* = 8.3, 2.4 Hz, 1H), 7.74 (dd, *J* = 8.2, 0.9 Hz, 1H), 7.50 – 7.41 (m, 3H), 5.16 (q, *J* = 6.8 Hz, 1H), 1.90 (d, *J* = 6.9 Hz, 3H) ppm.

¹³C NMR (CDCl₃, 126 MHz): δ 157.39, 147.85, 138.79, 136.65, 134.91, 128.77, 126.91, 120.36, 55.72, 26.25 ppm.

HRMS *m/z*: [M+H]⁺ calculated for C₁₃H₁₂ClN: 218.0731, Found: 218.0728.



tert-butyl (5-(1-chloroethyl)pyridin-2-yl)carbamate, **3d**

Reaction run using *tert*-butyl (5-ethylpyridin-2-yl)carbamate **1d** (44.5 mg, 0.20 mmol, 1.0 equiv) and *N*-(*tert*-butyl)-*N*-chloro-3,5-bis(trifluoromethyl)benzenesulfonamide **2** (153.5 mg, 0.40 mmol, 2.0 equiv) following the general procedure III. Yield = 24.1 mg (47%) of white solid.

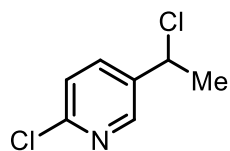
Purification: normal phase silica gel column chromatography with 5:1 pentane:ethyl acetate

Spectral data available in the literature: No

¹H NMR (CDCl₃, 500 MHz): δ 8.43 (s, 1H), 8.31 (d, J = 2.5 Hz, 1H), 7.98 (d, J = 8.7 Hz, 1H), 7.75 (dd, J = 8.7, 2.5 Hz, 1H), 5.07 (q, J = 6.8 Hz, 1H), 1.85 (d, J = 6.8 Hz, 3H), 1.55 (s, 9H) ppm.

¹³C NMR (CDCl₃, 126 MHz): δ 152.49, 152.21, 145.92, 136.58, 132.93, 112.26, 81.17, 55.81, 28.34, 26.25 ppm.

HRMS m/z: [M+H]⁺ calculated for C₁₂H₁₇ClN₂O₂: 257.1051, Found: 257.1047.



2-chloro-5-(1-chloroethyl)pyridine, **3e**

Reaction run using 2-chloro-5-ethylpyridine **1e** (28.3 mg, 0.20 mmol, 1.0 equiv) and *N*-(*tert*-butyl)-*N*-chloro-3,5-bis(trifluoromethyl)benzenesulfonamide **2** (307.0 mg, 0.80 mmol, 4.0 equiv) following the general procedure III. Yield = 30.0 mg (85%) of yellow oil.

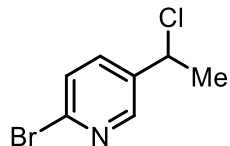
Purification: normal phase silica gel column chromatography with 4:1 pentane:ethyl acetate

Spectral data available in the literature: No

¹H NMR (CDCl₃, 500 MHz): δ 8.39 (d, J = 2.6 Hz, 1H), 7.74 (dd, J = 8.3, 2.6 Hz, 1H), 7.36 – 7.30 (m, 1H), 5.07 (q, J = 6.8 Hz, 1H), 1.84 (d, J = 6.9 Hz, 3H) ppm.

¹³C NMR (CDCl₃, 126 MHz): δ 151.17, 147.75, 137.38, 137.05, 124.38, 77.27, 77.02, 76.77, 54.67, 26.26 ppm.

HRMS m/z: [M+H]⁺ calculated for C₇H₇Cl₂N: 176.0028, Found: 176.0025.



2-bromo-5-(1-chloroethyl)pyridine, **3f**

Reaction run using 2-bromo-5-ethylpyridine **1f** (37.2 mg, 0.20 mmol, 1.0 equiv) and *N*-(*tert*-butyl)-*N*-chloro-3,5-bis(trifluoromethyl)benzenesulfonamide **2** (307.0 mg, 0.80 mmol, 4.0 equiv) following the general procedure III. Yield = 33.6 mg (76%) of yellow oil.

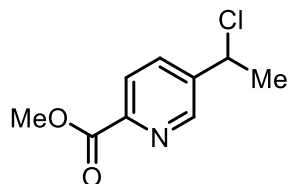
Purification: normal phase silica gel column chromatography with 5:1 pentane:ethyl acetate

Spectral data available in the literature: No

¹H NMR (CDCl₃, 500 MHz): δ 8.37 (d, *J* = 2.7 Hz, 1H), 7.64 (dd, *J* = 8.3, 2.7 Hz, 1H), 7.49 (d, *J* = 8.2 Hz, 1H), 5.05 (q, *J* = 6.9 Hz, 1H), 1.84 (d, *J* = 6.9 Hz, 3H) ppm.

¹³C NMR (CDCl₃, 126 MHz): δ 148.21, 141.75, 137.80, 136.80, 128.19, 54.69, 26.23 ppm.

HRMS *m/z*: [M+H]⁺ calculated for C₇H₇Cl₂N: 176.0028, Found: 176.0025.



Methyl 5-(1-chloroethyl)picolinate, **3g**

Reaction run using methyl 5-ethylpicolinate **1g** (33.0 mg, 0.20 mmol, 1.0 equiv) and *N*-(*tert*-butyl)-*N*-chloro-3,5-bis(trifluoromethyl)benzenesulfonamide **2** (230.2 mg, 0.60 mmol, 3.0 equiv) following the general procedure III. Yield = 30.7 mg (81%) of yellow oil in a mixture with 30% of remaining C–H starting material.

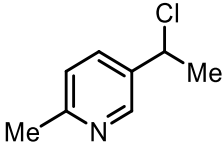
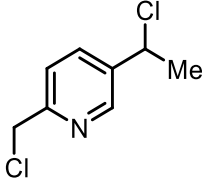
Purification: normal phase silica gel column chromatography with 1:1 pentane:ethyl acetate

Spectral data available in the literature: No

¹H NMR (CDCl₃, 500 MHz): δ 8.71 (d, *J* = 2.3 Hz, 1H), 8.11 (dd, *J* = 8.1, 0.8 Hz, 1H), 7.90 (dd, *J* = 8.1, 2.3 Hz, 1H), 5.12 (q, *J* = 6.8 Hz, 1H), 3.98 (s, 3H), 1.84 (d, *J* = 6.9 Hz, 3H) ppm.

¹³C NMR (CDCl₃, 126 MHz): δ 165.16, 148.05, 147.56, 141.80, 135.04, 125.05, 54.76, 52.89, 26.17 ppm.

HRMS *m/z*: [M+H]⁺ calculated for C₈H₈ClNO₂: 200.0478, Found: 200.0472.

	
5-(1-chloroethyl)-2-methylpyridine, 3h	5-(1-chloroethyl)-2-(chloromethyl)pyridine, 3h'

Reaction run using 5-ethyl-2-methylpyridine **1h** (26.4 μ L, 0.20 mmol, 1.0 equiv) and *N*-(*tert*-butyl)-*N*-chloro-3,5-bis(trifluoromethyl)benzenesulfonamide **2** (153.5 mg, 0.40 mmol, 2.0 equiv) following the general procedure III. Yield = 13.5 mg (43%) of **3h** as yellow oil and 4.2 mg (11%) of **3h'** as clear, colorless oil.

Purification: normal phase silica gel column chromatography with 5:1 pentane:ethyl acetate

Spectral data available in the literature: No

NMR spectroscopic data for **3h**

¹H NMR (CDCl₃, 500 MHz): δ 8.50 (d, *J* = 2.4 Hz, 1H), 7.67 (dd, *J* = 8.1, 2.5 Hz, 1H), 7.16 (d, *J* = 8.1 Hz, 1H), 5.09 (q, *J* = 6.8 Hz, 1H), 2.56 (s, 3H), 1.85 (d, *J* = 6.8 Hz, 3H) ppm.

¹³C NMR (CDCl₃, 126 MHz): δ 158.54, 147.25, 135.42, 134.47, 123.23, 55.84, 26.32, 24.16 ppm.

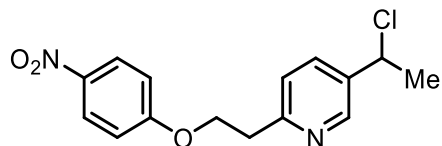
HRMS *m/z*: [M+H]⁺ calculated for C₈H₁₀ClN: 156.0575, Found: 156.0575.

NMR spectroscopic data for **3h'**

¹H NMR (CDCl₃, 500 MHz): δ 8.59 (d, *J* = 2.4 Hz, 1H), 7.82 (dd, *J* = 8.2, 2.4 Hz, 1H), 7.49 (d, *J* = 8.1 Hz, 1H), 5.11 (q, *J* = 6.8 Hz, 1H), 4.67 (s, 2H), 1.87 (d, *J* = 6.9 Hz, 3H) ppm.

¹³C NMR (CDCl₃, 126 MHz): δ 156.55, 147.66, 137.86, 135.28, 122.77, 55.28, 46.29, 26.32 ppm.

HRMS *m/z*: [M+H]⁺ calculated for C₈H₉Cl₂N: 190.0185, Found: 190.0185.



5-(1-chloroethyl)-2-(2-(4-nitrophenoxy)ethyl)pyridine, **3i**

Reaction run using methyl 5-ethyl-2-(2-(4-nitrophenoxy)ethyl)pyridine **1i** (54.5 mg, 0.20 mmol, 1.0 equiv) and *N*-(*tert*-butyl)-*N*-chloro-3,5-bis(trifluoromethyl)benzenesulfonamide **2** (153.5 mg, 0.40 mmol, 2.0 equiv) following the general procedure III. Yield = 42.5 mg (69%) of yellow oil.

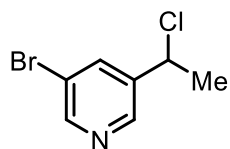
Purification: normal phase silica gel column chromatography with 3:1 pentane:ethyl acetate

Spectral data available in the literature: No

¹H NMR (CDCl₃, 500 MHz): δ 8.59 – 8.55 (m, 1H), 8.21 – 8.14 (m, 2H), 7.73 (ddd, J = 8.1, 2.4, 0.5 Hz, 1H), 7.27 (d, J = 8.4 Hz, 1H), 6.99 – 6.92 (m, 2H), 5.10 (q, J = 6.8 Hz, 1H), 4.48 (t, J = 6.6 Hz, 2H), 3.30 (t, J = 6.6 Hz, 2H), 1.86 (d, J = 6.8 Hz, 3H) ppm.

¹³C NMR (CDCl₃, 126 MHz): δ 163.81, 157.74, 147.73, 141.56, 136.58, 134.70, 125.89, 123.68, 114.51, 67.70, 55.60, 37.34, 26.29 ppm.

HRMS m/z: [M+H]⁺ calculated for C₁₅H₁₇ClN₂O: 307.0849, Found: 307.0840.



3-bromo-5-(1-chloroethyl)pyridine, **3j**

Reaction run using 3-bromo-5-ethylpyridine **1j** (37.2 mg, 0.20 mmol, 1.0 equiv) and *N*-(*tert*-butyl)-*N*-chloro-3,5-bis(trifluoromethyl)benzenesulfonamide **2** (306.9 mg, 0.80 mmol, 4.0 equiv) following the general procedure III. Yield = 28.0 mg (63%) of yellow oil.

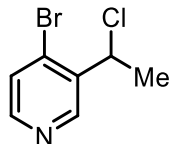
Purification: normal phase silica gel column chromatography with 4:1 pentane:ethyl acetate

Spectral data available in the literature: No

¹H NMR (CDCl₃, 500 MHz): δ 8.62 (d, J = 2.2 Hz, 1H), 8.55 (d, J = 1.9 Hz, 1H), 7.92 (dt, J = 2.1, 1.1 Hz, 1H), 5.05 (q, J = 6.9 Hz, 1H), 1.85 (d, J = 6.9 Hz, 3H) ppm.

¹³C NMR (CDCl₃, 126 MHz): δ 150.69, 146.10, 140.02, 136.81, 120.84, 54.62, 26.27 ppm.

HRMS m/z: [M+H]⁺ calculated for C₇H₇BrClN: 219.9523, Found: 219.9522.



4-bromo-3-(1-chloroethyl)pyridine, **3k**

Reaction run using 4-bromo-3-ethylpyridine hydrochloride **1k** (53.4 mg, 0.20 mmol, 1.0 equiv), *N*-(*tert*-butyl)-*N*-chloro-3,5-bis(trifluoromethyl)benzenesulfonamide **2** (230.2 mg, 0.60 mmol, 3.0 equiv), and Cs₂CO₃ (162.9 mg, 0.5 mmol, 2.5 equiv) following the general procedure III. Yield = 21.4 mg (49%) of brown oil.

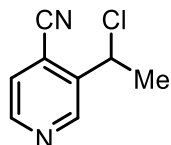
Purification: normal phase silica gel column chromatography with 1:1 pentane:ethyl acetate

Spectral data available in the literature: No

¹H NMR (CDCl₃, 500 MHz): δ 8.82 (s, 1H), 8.30 (d, *J* = 5.3 Hz, 1H), 7.49 (d, *J* = 5.3 Hz, 1H), 5.49 (q, *J* = 7.0 Hz, 1H), 2.10 (d, *J* = 7.0 Hz, 2H) ppm.

¹³C NMR (CDCl₃, 126 MHz): δ 149.68, 149.56, 138.10, 133.36, 127.86, 44.06, 25.48 ppm.

HRMS *m/z*: [M+H]⁺ calculated for C₇H₇BrClN: 219.9523, Found: 219.9522.



3-(1-chloroethyl)isonicotinonitrile, **3l**

Reaction run using 3-ethylisonicotinonitrile **1l** (26.4 mg, 0.20 mmol, 1.0 equiv) and *N*-(*tert*-butyl)-*N*-chloro-3,5-bis(trifluoromethyl)benzenesulfonamide **2** (306.9 mg, 0.80 mmol, 4.0 equiv) following the general procedure III. Yield = 20.0 mg (60%) of brown oil.

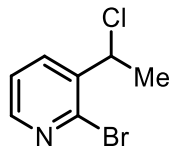
Purification: normal phase silica gel column chromatography with 1:1 pentane:ethyl acetate

Spectral data available in the literature: No

¹H NMR (CDCl₃, 500 MHz): δ 9.02 (s, 1H), 8.73 (d, *J* = 5.0 Hz, 1H), 7.52 (dd, *J* = 5.0, 0.8 Hz, 1H), 5.38 (q, *J* = 6.9 Hz, 1H), 1.97 (d, *J* = 6.9 Hz, 3H) ppm.

¹³C NMR (CDCl₃, 126 MHz): δ 149.92, 149.52, 139.25, 125.33, 118.81, 114.64, 52.85, 25.60 ppm.

HRMS *m/z*: [M+H]⁺ calculated for C₈H₇ClN₂: 167.0371, Found: 167.0369.



2-bromo-3-(1-chloroethyl)pyridine, **3m**

Reaction run using 2-bromo-3-ethylpyridine **1m** (37.2 mg, 0.20 mmol, 1.0 equiv) and *N*-(*tert*-butyl)-*N*-chloro-3,5-bis(trifluoromethyl)benzenesulfonamide **2** (230.2 mg, 0.60 mmol, 3.0 equiv) following the general procedure III. Yield = 26.7 mg (61%) of clear colorless oil.

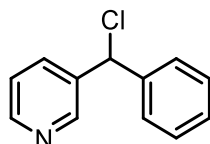
Purification: normal phase silica gel column chromatography with 4:1 pentane:ethyl acetate

Spectral data available in the literature: No

¹H NMR (CDCl₃, 500 MHz): δ 8.30 (dd, *J* = 4.7, 1.9 Hz, 1H), 7.96 (ddd, *J* = 7.8, 1.9, 0.5 Hz, 1H), 7.33 (ddd, *J* = 7.7, 4.7, 0.5 Hz, 1H), 5.45 (q, *J* = 6.8 Hz, 1H), 1.81 (d, *J* = 6.8 Hz, 3H) ppm.

¹³C NMR (CDCl₃, 126 MHz): δ 149.51, 141.78, 139.28, 136.56, 123.40, 55.98, 25.77 ppm.

HRMS *m/z*: [M+H]⁺ calculated for C₇H₇BrClN: 219.9523, Found: 219.9520.



3-(chloro(phenyl)methyl)pyridine, **3n**

Reaction run using 3-benzylpyridine **1n** (33.8 mg, 0.20 mmol, 1.0 equiv) and *N*-(*tert*-butyl)-*N*-chloro-3,5-bis(trifluoromethyl)benzenesulfonamide **2** (115.1 mg, 0.30 mmol, 1.5 equiv) following the general procedure III. Yield = 46.2 mg (59%) of yellow oil.

Purification: normal phase silica gel column chromatography with 2:1 pentane:ethyl acetate

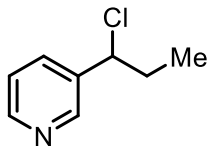
Spectral data available in the literature: No

¹H NMR (CDCl₃, 500 MHz): δ 8.65 (d, *J* = 2.4 Hz, 1H), 8.55 (dd, *J* = 4.8, 1.7 Hz, 1H), 7.75 (ddd, *J* = 8.0, 3.1, 1.3 Hz, 1H), 7.43 – 7.35 (m, 4H), 7.35 – 7.31 (m, 1H), 7.29 (ddd, *J* = 8.0, 4.7, 0.9 Hz, 1H), 6.14 (s, 1H) ppm.

¹³C NMR (CDCl₃, 126 MHz): δ 149.35, 148.99, 139.95, 136.87, 135.29, 128.80, 128.50, 127.66, 123.39, 61.53 ppm.

HRMS *m/z*: [M+H]⁺ calculated for C₁₂H₁₀ClN: 204.0575, Found: 204.0575.

Scale-up: reaction run using 3-benzylpyridine **1n** (845.0 mg, 5.00 mmol, 1.0 equiv) and *N*-(*tert*-butyl)-*N*-chloro-3,5-bis(trifluoromethyl)benzenesulfonamide **2** (2878.0 mg, 7.50 mmol, 1.5 equiv) following the general procedure V. Yield = 733.2 mg (72%) of yellow oil.



3-(chloro(phenyl)methyl)pyridine, **3o**

Reaction run using 3-propylpyridine **1o** (60.6 mg, 0.50 mmol, 1.0 equiv) and *N*-(*tert*-butyl)-*N*-chloro-3,5-bis(trifluoromethyl)benzenesulfonamide **2** (383.7 mg, 1.00 mmol, 2.0 equiv) following the general procedure IV. Yield = 46.2 mg (59%) of yellow oil.

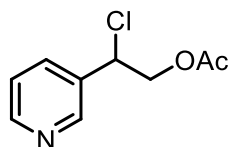
Purification: normal phase silica gel column chromatography with 10:1 pentane:ethyl acetate

Spectral data available in the literature: No

¹H NMR (CDCl₃, 500 MHz): δ 8.59 (d, *J* = 2.4 Hz, 1H), 8.54 (dd, *J* = 4.8, 1.6 Hz, 1H), 7.73 (dt, *J* = 7.9, 2.0 Hz, 1H), 7.29 (ddd, *J* = 7.9, 4.9, 0.9 Hz, 1H), 4.79 (dd, *J* = 8.0, 6.3 Hz, 1H), 2.20 – 2.00 (m, 2H), 1.01 (t, *J* = 7.3 Hz, 3H) ppm.

¹³C NMR (CDCl₃, 126 MHz): δ 149.53, 148.43, 137.34, 134.48, 123.54, 62.30, 33.07, 11.47 ppm.

HRMS m/z: [M+H]⁺ calculated for C₈H₁₀ClN: 156.0575, Found: 156.0574.



2-chloro-2-(pyridin-3-yl)ethyl acetate, **3p**

Reaction run using 2-(pyridin-3-yl)ethyl acetate **1p** (33.0 mg, 0.20 mmol, 1.0 equiv) and *N*-(*tert*-butyl)-*N*-chloro-3,5-bis(trifluoromethyl)benzenesulfonamide **2** (230.2 mg, 0.60 mmol, 3.0 equiv) following the general procedure III. Yield = 20.0 mg (50%) of yellow oil.

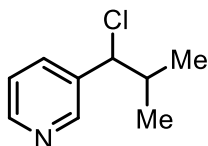
Purification: normal phase silica gel column chromatography with 1:1 pentane:ethyl acetate

Spectral data available in the literature: No

¹H NMR (CDCl₃, 500 MHz): δ 8.59 (ddd, *J* = 4.9, 1.9, 1.0 Hz, 1H), 7.73 (td, *J* = 7.7, 1.8 Hz, 1H), 7.48 (dt, *J* = 7.8, 1.0 Hz, 1H), 7.26 (ddd, *J* = 6.2, 4.8, 1.1 Hz, 1H), 5.16 (dd, *J* = 7.4, 5.7 Hz, 1H), 4.69 – 4.56 (m, 2H), 2.05 (s, 3H) ppm.

¹³C NMR (CDCl₃, 126 MHz): δ 170.47, 156.58, 149.50, 137.05, 123.53, 122.59, 66.80, 59.52, 20.71 ppm.

HRMS m/z: [M+H]⁺ calculated for C₉H₁₀ClNO₂: 200.0473, Found: 200.0472.



3-(1-chloro-2-methylpropyl)pyridine, **3q**

Reaction run using 3-isobutylpyridine **1q** (29.7 mg, 0.20 mmol, 1.0 equiv) and *N*-(*tert*-butyl)-*N*-chloro-3,5-bis(trifluoromethyl)benzenesulfonamide **2** (153.5 mg, 0.40 mmol, 2.0 equiv) following the general procedure III. Yield = 21.7 mg (64%) of brown oil.

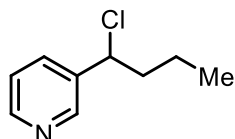
Purification: normal phase silica gel column chromatography with 1:4 pentane:ethyl acetate

Spectral data available in the literature: No

¹H NMR (CDCl₃, 500 MHz): δ 8.58 – 8.51 (m, 2H), 7.72 (dt, *J* = 7.9, 2.0 Hz, 1H), 7.30 (dd, *J* = 7.8, 4.1 Hz, 1H), 4.67 (d, *J* = 7.3 Hz, 1H), 2.31 – 2.18 (m, *J* = 6.7 Hz, 1H), 1.10 (d, *J* = 6.6 Hz, 3H), 0.90 (d, *J* = 6.8 Hz, 3H) ppm.

¹³C NMR (CDCl₃, 126 MHz): δ 149.33, 148.75, 136.59, 135.06, 123.35, 67.54, 36.55, 19.92, 19.22 ppm.

HRMS *m/z*: [M+H]⁺ calculated for C₉H₁₂ClN: 170.0731, Found: 170.0730.



3-(1-chlorobutyl)pyridine, **3r**

Reaction run using 3-butylpyridine **1r** (27.0 mg, 0.20 mmol, 1.0 equiv) and *N*-(*tert*-butyl)-*N*-chloro-3,5-bis(trifluoromethyl)benzenesulfonamide **2** (153.5 mg, 0.40 mmol, 2.0 equiv) following the general procedure III. Yield = 11.2 mg (33%) of yellow oil.

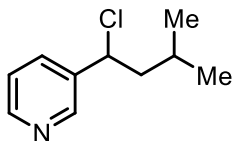
Purification: normal phase silica gel column chromatography with 1:1 pentane:ethyl acetate

Spectral data available in the literature: No

¹H NMR (CDCl₃, 500 MHz): 8.61 – 8.53 (m, 2H), 7.74 (dddd, *J* = 7.9, 2.3, 1.6, 0.5 Hz, 1H), 7.30 (ddd, *J* = 7.9, 4.8, 0.9 Hz, 1H), 4.88 (dd, *J* = 8.3, 6.3 Hz, 1H), 2.19 – 2.07 (m, 1H), 1.99 (ddt, *J* = 14.0, 9.7, 6.1 Hz, 1H), 1.52 (dddd, *J* = 14.9, 12.7, 9.7, 7.4, 5.2 Hz, 1H), 1.45 – 1.31 (m, 1H), 0.95 (t, *J* = 7.4 Hz, 3H) ppm.

¹³C NMR (CDCl₃, 126 MHz): δ 149.58, 148.45, 137.61, 134.47, 123.59, 60.46, 41.86, 20.16, 13.37 ppm.

HRMS *m/z*: [M+H]⁺ calculated for C₉H₁₀ClNO₂: 200.0473, Found: 200.0472.



3-(1-chloro-3-methylbutyl)pyridine, **3s**

Reaction run using 3-isopentylpyridine **1s** (29.8 mg, 0.20 mmol, 1.0 equiv) and *N*-(*tert*-butyl)-*N*-chloro-3,5-bis(trifluoromethyl)benzenesulfonamide **2** (153.5 mg, 0.40 mmol, 2.0 equiv) following the general procedure III. Yield = 18.2 mg (50%) of yellow oil.

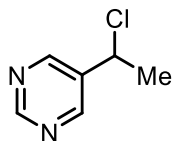
Purification: normal phase silica gel column chromatography with 1:1 pentane:ethyl acetate

Spectral data available in the literature: No

¹H NMR (CDCl₃, 500 MHz): δ 8.60 (d, *J* = 2.2 Hz, 1H), 8.55 (dd, *J* = 4.8, 1.6 Hz, 1H), 7.74 (dt, *J* = 7.9, 2.0 Hz, 1H), 7.30 (ddd, *J* = 7.9, 4.7, 0.9 Hz, 1H), 4.93 (dd, *J* = 9.0, 6.1 Hz, 1H), 2.07 (ddd, *J* = 13.7, 9.0, 5.9 Hz, 1H), 1.88 – 1.64 (m, 2H), 0.95 (dd, *J* = 6.5, 4.3 Hz, 6H) ppm.

¹³C NMR (CDCl₃, 126 MHz): δ 149.58, 148.41, 137.73, 134.47, 123.62, 58.99, 48.66, 25.62, 22.43, 21.68 ppm.

HRMS *m/z*: [M+H]⁺ calculated for C₁₀H₁₄ClN: 184.0888, Found: 184.0887.



5-(1-chloroethyl)pyrimidine, **3t**

Reaction run using 5-ethylpyrimidine **1t** (54.1 mg, 0.50 mmol, 1.0 equiv) and *N*-(*tert*-butyl)-*N*-chloro-3,5-bis(trifluoromethyl)benzenesulfonamide **2** (575.6 mg, 1.50 mmol, 3.0 equiv) following the general procedure IV. ^1H NMR Yield = 65% of brown oil.

Purification: normal phase silica gel column chromatography with 1:4 pentane:ethyl acetate

Spectral data available in the literature: No

^1H NMR (CDCl_3 , 500 MHz): δ 9.15 (s, 1H), 8.79 (s, 2H), 5.06 (q, $J = 6.9$ Hz, 1H), 1.88 (d, $J = 6.9$ Hz, 3H) ppm.

^{13}C NMR (CDCl_3 , 126 MHz): δ 158.34, 155.18, 136.12, 52.95, 25.87 ppm.

HRMS m/z : $[\text{M}+\text{H}]^+$ calculated for $\text{C}_6\text{H}_7\text{ClN}_2$: 143.0370, Found: 143.0369.

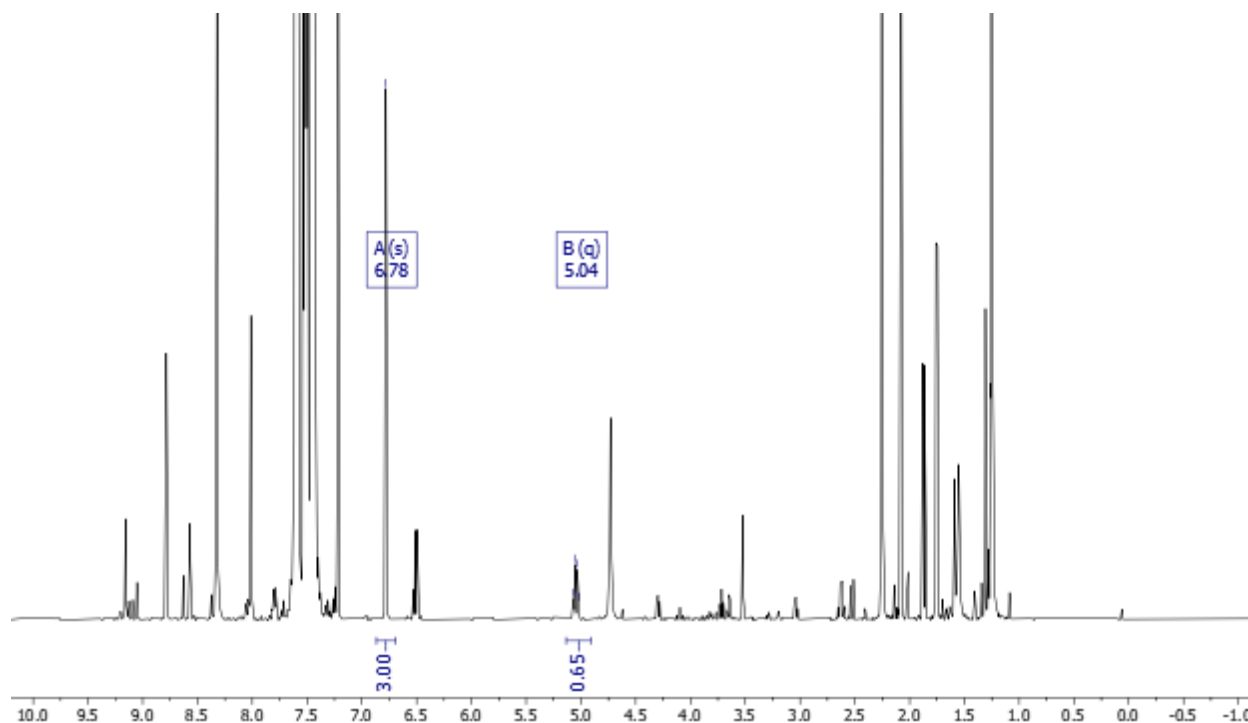
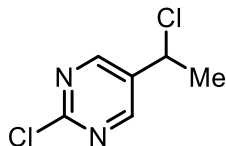


Figure 3B.17. Crude ^1H NMR Spectrum (CDCl_3 , 400 MHz, 25 $^\circ\text{C}$) of the reaction mixture for **1t** following the addition of 0.5 mmol (70 μL) of mesitylene as an external standard (6.78 ppm). The resolved benzylic protons for **3t** is labeled and integrated.



2-chloro-5-(1-chloroethyl)pyrimidine, **3u**

Reaction run using 2-chloro-5-ethylpyrimidine **1u** (71.3 mg, 0.50 mmol, 1.0 equiv) and *N*-(*tert*-butyl)-*N*-chloro-3,5-bis(trifluoromethyl)benzenesulfonamide **2** (767.5 mg, 2.00 mmol, 4.0 equiv) following the general procedure IV. Yield = 62.0 mg (70%) of yellow oil in a mixture with 9% of remaining C–H starting material.

Purification: normal phase silica gel column chromatography with 5:1 pentane:ethyl acetate

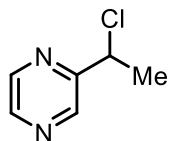
Spectral data available in the literature: No

¹H NMR (CDCl₃, 500 MHz): δ 8.67 (s, 2H), 5.07 (q, J = 6.9 Hz, 1H), 1.88 (d, J = 6.9 Hz, 3H) ppm.

¹³C NMR (CDCl₃, 126 MHz): δ 160.94, 157.90, 134.85, 52.01, 25.82 ppm.

HRMS m/z: [M+H]⁺ calculated for C₆H₆Cl₂N₂: 176.9981, Found: 176.9981.

Scale-up: reaction run using 2-chloro-5-ethylpyrimidine **1u** (713.0 mg, 5.00 mmol, 1.0 equiv) and *N*-(*tert*-butyl)-*N*-chloro-3,5-bis(trifluoromethyl)benzenesulfonamide **2** (7674.6 mg, 20.0 mmol, 4.0 equiv) following the general procedure V. Yield = 823.2 mg (72%) of yellow oil.



2-(1-chloroethyl)pyrazine, **3v**

Reaction run using 2-ethylpyrazine **1v** (5.4 mg, 0.05 mmol, 1.0 equiv) and *N*-(*tert*-butyl)-*N*-chloro-3,5-bis(trifluoromethyl)benzenesulfonamide **2** (56.1 mg, 0.15 mmol, 3.0 equiv) following the general procedure VI. ¹H NMR Yield = 67%.

Spectral data available in the literature: Yes.¹ Spectral data for **3v** was consistent with reported data.

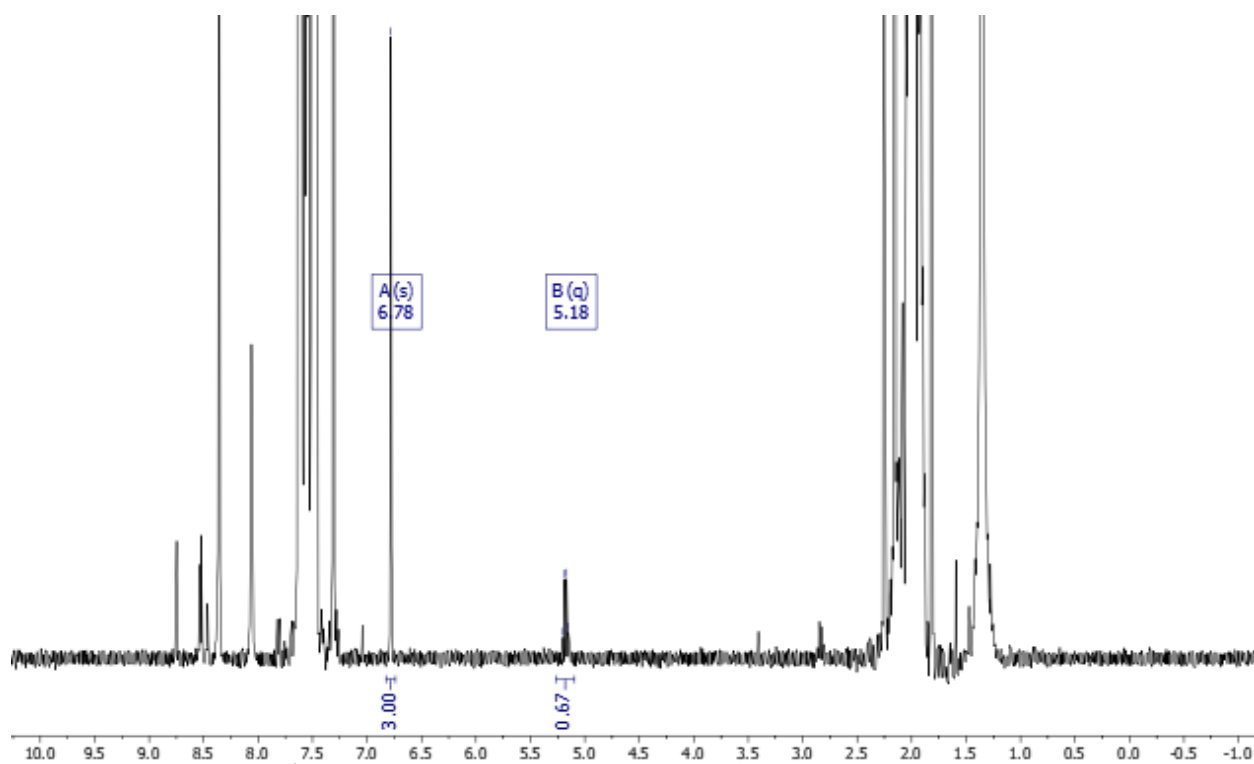
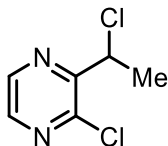


Figure 3B.18. Crude ¹H NMR Spectrum (CDCl₃, 400 MHz, 25 °C) of the reaction mixture for **1v** following the addition of 0.2 mmol (7 μL) of mesitylene as an external standard (6.78 ppm). The resolved benzylic protons for **3v** is labeled and integrated.



2-chloro-3-(1-chloroethyl)pyrazine, **3x**

Reaction run using 2-chloro-3-ethylpyrazine **1x** (28.5 mg, 0.20 mmol, 1.0 equiv) and *N*-(*tert*-butyl)-*N*-chloro-3,5-bis(trifluoromethyl)benzenesulfonamide **2** (306.9 mg, 0.80 mmol, 4.0 equiv) following the general procedure III. Yield = 16.5 mg (47%) of yellow oil.

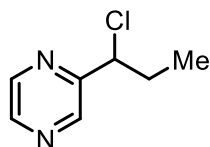
Purification: normal phase silica gel column chromatography with 3:1 pentane:ethyl acetate

Spectral data available in the literature: No

¹H NMR (CDCl₃, 500 MHz): δ 8.54 (d, J = 2.4 Hz, 1H), 8.34 (d, J = 2.4 Hz, 1H), 5.55 (q, J = 6.7 Hz, 1H), 1.93 (d, J = 6.7 Hz, 3H) ppm.

¹³C NMR (CDCl₃, 126 MHz): δ 153.63, 147.77, 143.47, 142.45, 142.44, 53.30, 22.35 ppm.

HRMS m/z: [M+H]⁺ calculated for C₆H₆Cl₂N₂: 176.9981, Found: 176.9982.



2-(1-chloropropyl)pyrazine, **3y**

Reaction run using 2-propylpyrazine **1y** (61.1 mg, 0.50 mmol, 1.0 equiv) and *N*-(*tert*-butyl)-*N*-chloro-3,5-bis(trifluoromethyl)benzenesulfonamide **2** (575.6 mg, 1.50 mmol, 3.0 equiv) following the general procedure IV. Yield = 30.6 mg (39%) of brown oil.

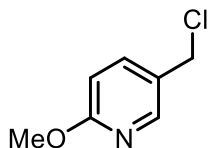
Purification: normal phase silica gel column chromatography with 1:1 pentane:ethyl acetate

Spectral data available in the literature: No

¹H NMR (CDCl₃, 500 MHz): δ 8.73 (d, J = 1.6 Hz, 1H), 8.52 (dd, J = 2.5, 1.5 Hz, 1H), 8.50 (d, J = 2.5 Hz, 1H), 4.89 (dd, J = 7.9, 6.3 Hz, 1H), 1.02 (t, J = 7.3 Hz, 3H) ppm.

¹³C NMR (CDCl₃, 126 MHz): δ 155.52, 143.97, 143.81, 143.74, 62.50, 31.09, 11.15 ppm.

HRMS m/z: [M+H]⁺ calculated for C₇H₉ClN₂: 157.0527, Found: 157.0527.



5-(chloromethyl)-2-methoxypyridine, **3z**

Reaction run using 2-methoxy-5-methylpyridine **1z** (24.6 mg, 0.20 mmol, 1.0 equiv) and *N*-(*tert*-butyl)-*N*-chloro-3,5-bis(trifluoromethyl)benzenesulfonamide **2** (115.1 mg, 0.30 mmol, 1.5 equiv) following the general procedure III. Yield = 10.6 mg (34%) of clear colorless oil.

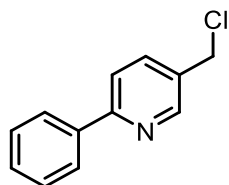
Purification: normal phase silica gel column chromatography with 5:1 pentane:ethyl acetate

Spectral data available in the literature: No

¹H NMR (CDCl₃, 500 MHz): δ 8.17 – 8.12 (m, 1H), 7.62 (dd, *J* = 8.6, 2.5 Hz, 1H), 6.75 (dd, *J* = 8.6, 0.7 Hz, 1H), 4.55 (s, 2H), 3.94 (s, 3H) ppm.

¹³C NMR (CDCl₃, 126 MHz): δ 164.20, 146.71, 139.19, 126.16, 111.28, 53.60, 43.38 ppm.

HRMS *m/z*: [M+H]⁺ calculated for C₇H₈ClNO: 158.0367, Found: 158.0367.



5-(chloromethyl)-2-phenylpyridine, **3aa**

Reaction run using 2-phenyl-5-methylpyridine **1aa** (33.8 mg, 0.20 mmol, 1.0 equiv) and *N*-(*tert*-butyl)-*N*-chloro-3,5-bis(trifluoromethyl)benzenesulfonamide **2** (230.2 mg, 0.60 mmol, 3.0 equiv) following the general procedure III. Yield = 17.2 mg (42%) of white solid.

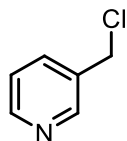
Purification: normal phase silica gel column chromatography with 19:1 dichloromethane:ethyl acetate

Spectral data available in the literature: No

¹H NMR (CDCl₃, 500 MHz): δ 8.69 (d, *J* = 2.3 Hz, 1H), 8.03 – 7.96 (m, 2H), 7.81 (dd, *J* = 8.2, 2.3 Hz, 1H), 7.74 (dd, *J* = 8.1, 0.9 Hz, 1H), 7.53 – 7.39 (m, 3H), 4.64 (s, 2H) ppm.

¹³C NMR (CDCl₃, 126 MHz): δ 157.57, 149.47, 138.77, 137.05, 131.54, 129.27, 128.82, 126.98, 120.42, 43.16 ppm.

HRMS *m/z*: [M+H]⁺ calculated for C₁₂H₁₀ClN: 204.0575, Found: 204.0575.



3-(1-chloromethyl)pyridine, **3ab**

Reaction run using 3-methylpyridine **1ab** (18.8 μL , 0.20 mmol, 1.0 equiv) and *N*-(*tert*-butyl)-*N*-chloro-3,5-bis(trifluoromethyl)benzenesulfonamide **2** (230.2mg, 0.40 mmol, 2.0 equiv) following the general procedure III. ^1H NMR Yield = 37%.

Spectral data available in the literature: Yes.² Spectral data for **3ab** was consistent with reported data.

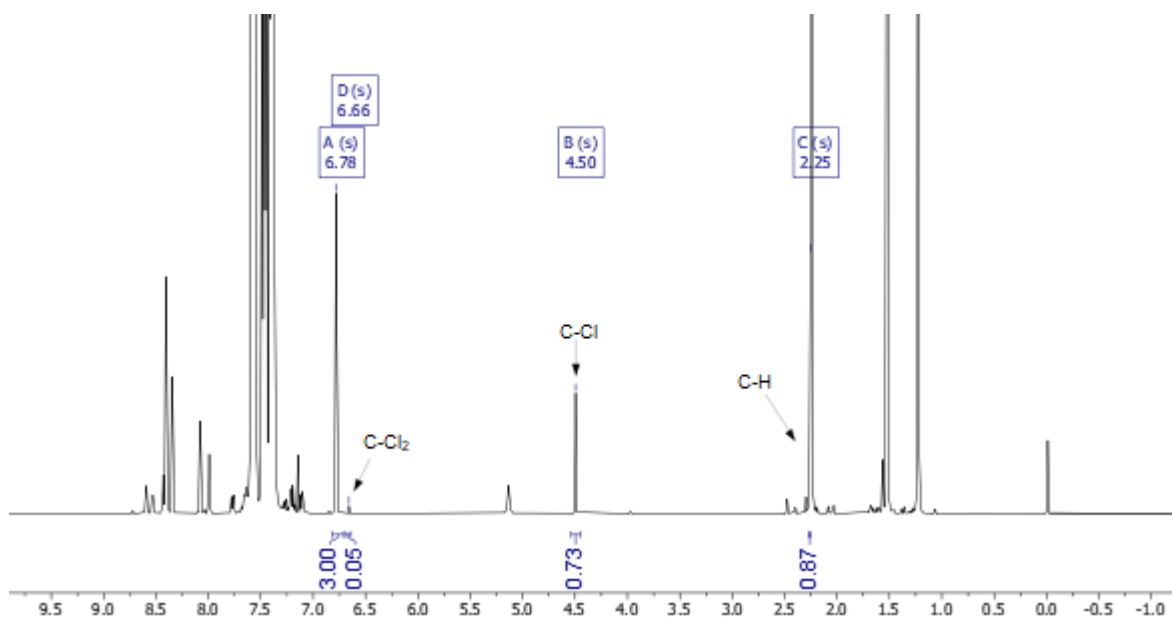
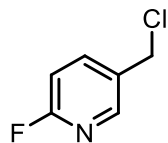


Figure 3B.19. Crude ^1H NMR Spectrum (CDCl_3 , 400 MHz, 25 $^\circ\text{C}$) of the reaction mixture for **1ab** following the addition of 0.05 mmol (7 μL) of mesitylene as an external standard (6.78 ppm). The resolved benzylic protons for **3ab** are labeled and integrated.



5-(chloromethyl)-2-fluoropyridine, **3ac**

Reaction run using 2-fluoro-5-methylpyridine **1ac** (5.6 mg, 0.05 mmol, 1.0 equiv) and *N*-(*tert*-butyl)-*N*-chloro-3,5-bis(trifluoromethyl)benzenesulfonamide **2** (76.7 mg, 0.20 mmol, 4.0 equiv) following the general procedure VI. ¹H NMR Yield = 44%.

Spectral data available in the literature: Yes.³ Spectral data for **3ac** was consistent with reported data.

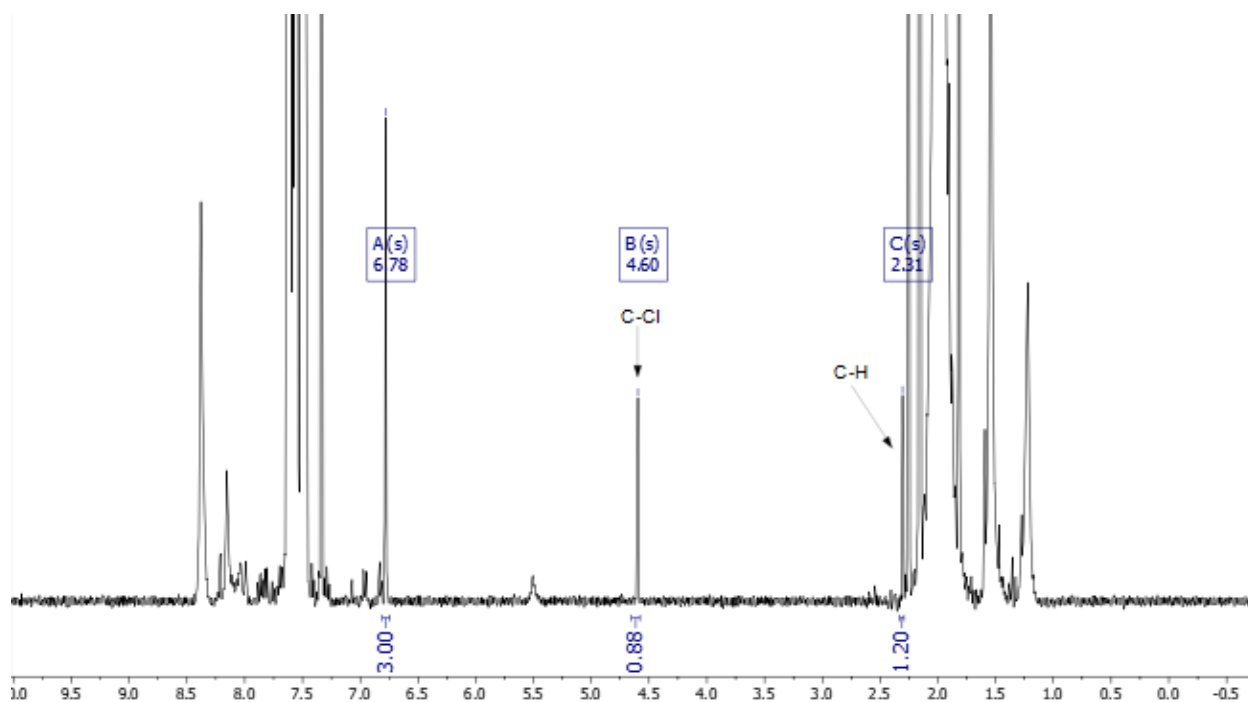
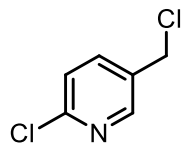


Figure 3B.20. Crude ¹H NMR Spectrum (CDCl₃, 400 MHz, 25 °C) of the reaction mixture for **1ac** following the addition of 0.05 mmol (7 μL) of mesitylene as an external standard (6.78 ppm). The resolved benzylic protons for **3ac** are labeled and integrated.



5-(chloromethyl)-2-chloropyridine, **3ad**

Reaction run using 2-chloro-5-methylpyridine **1ad** (6.4 mg, 0.05 mmol, 1.0 equiv) and *N*-(*tert*-butyl)-*N*-chloro-3,5-bis(trifluoromethyl)benzenesulfonamide **2** (76.7 mg, 0.20 mmol, 4.0 equiv) following the general procedure VI. ¹H NMR Yield = 36%.

Spectral data available in the literature: Yes.⁴ Spectral data for **3ad** was consistent with reported data.

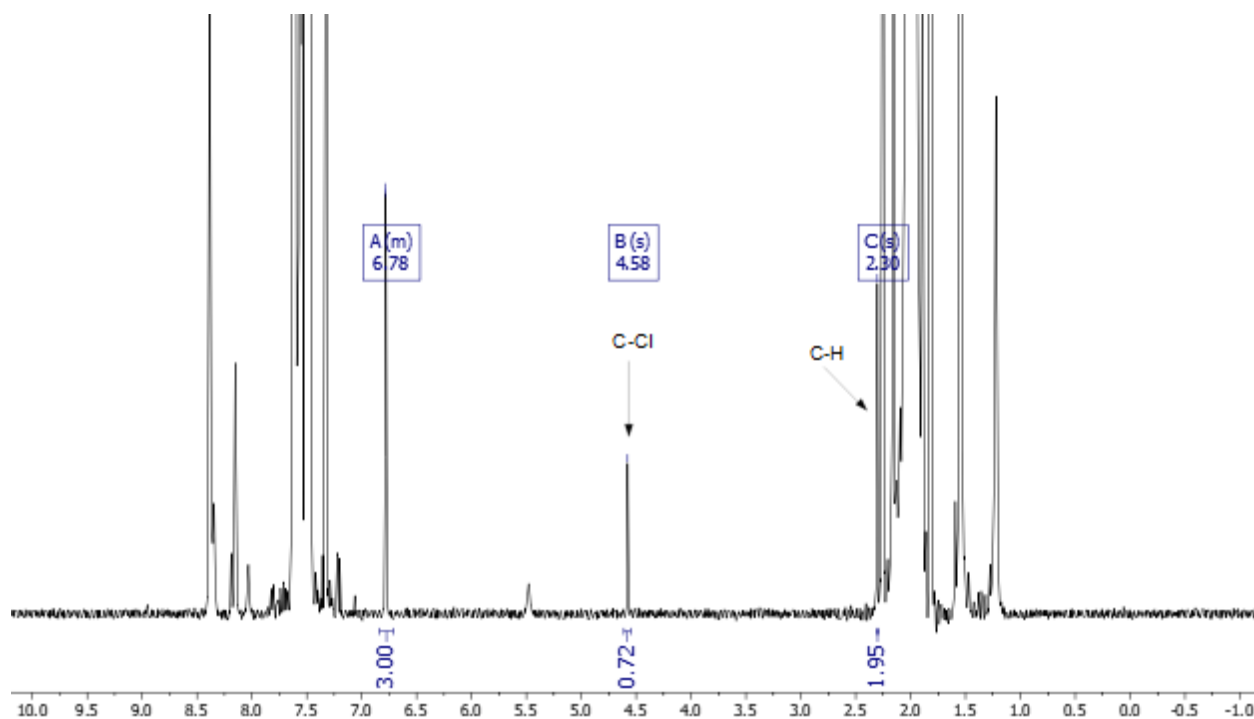
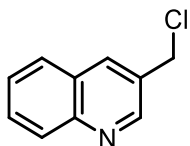


Figure 3B.21. Crude ¹H NMR Spectrum (CDCl₃, 400 MHz, 25 °C) of the reaction mixture for **1ad** following the addition of 0.05 mmol (7 μL) of mesitylene as an external standard (6.78 ppm). The resolved benzylic protons for **3ad** are labeled and integrated.



3-(chloromethyl)quinoline, **3ae**

Reaction run using 3-methylquinoline **1ae** (28.6 mg, 0.20 mmol, 1.0 equiv) and *N*-(*tert*-butyl)-*N*-chloro-3,5-bis(trifluoromethyl)benzenesulfonamide **2** (230.2 mg, 0.60 mmol, 3.0 equiv) following the general procedure III. Yield = 17.5 mg (49%) of yellow oil.

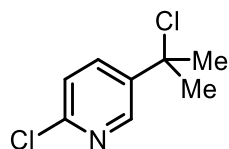
Purification: normal phase silica gel column chromatography with 2:1 pentane:ethyl acetate

Spectral data available in the literature: No

¹H NMR (CDCl₃, 500 MHz): δ 8.16 (d, *J* = 2.3 Hz, 1H), 8.12 (d, *J* = 8.4 Hz, 1H), 7.82 (dd, *J* = 8.1, 1.4 Hz, 1H), 7.74 (ddd, *J* = 8.4, 6.7, 1.5 Hz, 1H), 7.62 – 7.54 (m, 1H), 4.78 (s, 2H) ppm.

¹³C NMR (CDCl₃, 126 MHz): δ 150.73, 147.80, 135.49, 135.45, 130.31, 130.04, 130.01, 129.36, 127.87, 127.84, 127.55, 127.22, 127.19, 43.49 ppm.

HRMS *m/z*: [M+H]⁺ calculated for C₁₀H₈ClN: 178.0418, Found: 178.0418.



2-chloro-5-(2-chloropropan-2-yl)pyridine, **3af**

Reaction run using 2-chloro-5-isopropylpyridine **1af** (31.1 mg, 0.20 mmol, 1.0 equiv) and *N*-(*tert*-butyl)-*N*-chloro-3,5-bis(trifluoromethyl)benzenesulfonamide **2** (307.0 mg, 0.80 mmol, 4.0 equiv) following the general procedure III. Yield = 21.2 mg (56%) of clear, colorless oil.

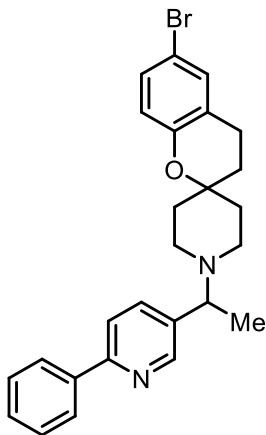
Purification: normal phase silica gel column chromatography with 9:1 pentane:ethyl acetate

Spectral data available in the literature: No

¹H NMR (CDCl₃, 500 MHz): δ 8.55 (d, *J* = 2.7 Hz, 1H), 7.88 (dd, *J* = 8.4, 2.7 Hz, 1H), 7.31 (dd, *J* = 8.3, 0.7 Hz, 1H), 1.98 (s, 6H) ppm.

¹³C NMR (CDCl₃, 126 MHz): δ 150.59, 146.59, 140.86, 136.71, 123.77, 77.02, 66.53, 34.00 ppm.

HRMS *m/z*: [M+H]⁺ calculated for C₈H₉Cl₂N: 190.0185, Found: 190.0183.



6-bromo-1'-(1-(6-phenylpyridin-3-yl)ethyl)spiro[chromane-2,4'-piperidine], **4ca**

Chlorination: Reaction run using methyl 2-phenyl-5-ethylpyridine **1c** (91.6 mg, 0.50 mmol, 1.0 equiv) and N-(tert-butyl)-N-chloro-3,5-bis(trifluoromethyl)benzenesulfonamide **2** (287.8 mg, 0.75 mmol, 1.5 equiv) following the general procedure IV. ^1H NMR Yield = 68%.

Nucleophilic displacement: Reaction run using 6-bromospiro[chromane-2,4'-piperidine] (56.4 mg, 0.20 mmol, 2.0 equiv) following the general procedure VII. Yield = 14.0 mg (30%) of yellow oil.

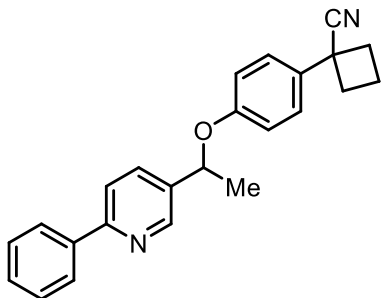
Purification: normal phase silica gel column chromatography with 2:1 dichloromethane:ethyl acetate

Spectral data available in the literature: No

^1H NMR (CDCl_3 , 500 MHz): δ 8.64 (dd, $J = 2.2, 1.0$ Hz, 1H), 8.03 – 7.97 (m, 2H), 7.78 – 7.66 (m, 2H), 7.51 – 7.46 (m, 1H), 7.43 – 7.37 (m, 1H), 7.18 – 7.12 (m, 2H), 6.70 – 6.65 (m, 1H), 3.59 (q, $J = 6.7$ Hz, 1H), 2.78 (d, $J = 11.3$ Hz, 1H), 2.72 (t, $J = 6.8$ Hz, 2H), 2.56 (d, $J = 11.1$ Hz, 1H), 2.50 – 2.41 (m, 2H), 1.83 (dq, $J = 13.7, 3.2$ Hz, 2H), 1.76 (t, $J = 6.8$ Hz, 2H), 1.71 – 1.53 (m, 2H), 1.44 (d, $J = 6.7$ Hz, 3H). ppm.

^{13}C NMR (CDCl_3 , 126 MHz): δ 156.14, 152.53, 149.30, 139.25, 138.00, 135.79, 131.95, 130.13, 128.74, 125.80, 123.63, 120.14, 119.15, 111.79, 72.90, 61.98, 46.52, 45.46, 34.81, 31.47, 21.48, 19.05 ppm.

HRMS m/z: $[\text{M}+\text{H}]^+$ calculated for $\text{C}_{26}\text{H}_{27}\text{BrN}_2\text{O}$: 463.1374, Found: 463.1380.



1-(4-(1-(6-phenylpyridin-3-yl)ethoxy)phenyl)cyclobutane-1-carbonitrile, **4cb**

Chlorination: Reaction run using methyl 2-phenyl-5-ethylpyridine **1c** (91.6 mg, 0.50 mmol, 1.0 equiv) and *N*-(*tert*-butyl)-*N*-chloro-3,5-bis(trifluoromethyl)benzenesulfonamide **2** (287.8 mg, 0.75 mmol, 1.5 equiv) following the general procedure IV. ¹H NMR Yield = 79%.

Nucleophilic displacement: Reaction run using 1-(4-hydroxyphenyl)cyclobutane-1-carbonitrile (34.6 mg, 0.20 mmol, 2.0 equiv) following the general procedure VII. Yield = 31.1 mg (88%) of yellow oil.

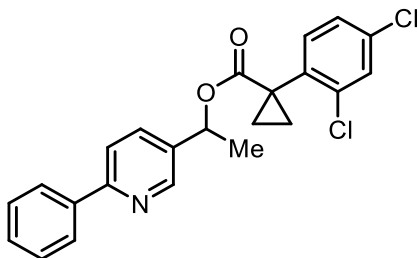
Purification: normal phase silica gel column chromatography with 4:1 petroleum ether:ethyl acetate

Spectral data available in the literature: No

¹H NMR (CDCl₃, 500 MHz): δ 8.70 (d, J = 2.2 Hz, 1H), 8.01 – 7.95 (m, 2H), 7.77 (dd, J = 8.2, 2.3 Hz, 1H), 7.71 (dd, J = 8.2, 0.8 Hz, 1H), 7.50 – 7.43 (m, 2H), 7.43 – 7.37 (m, 1H), 7.31 – 7.24 (m, 2H), 6.93 – 6.86 (m, 2H), 5.42 (q, J = 6.4 Hz, 1H), 2.76 (dddd, J = 12.9, 8.8, 4.1, 2.0 Hz, 2H), 2.59 – 2.48 (m, 2H), 2.37 (dp, J = 11.6, 8.8 Hz, 1H), 2.02 (dtt, J = 11.5, 9.0, 4.5 Hz, 1H), 1.70 (d, J = 6.5 Hz, 3H) ppm.

¹³C NMR (CDCl₃, 126 MHz): δ 157.02, 147.53, 138.93, 136.53, 134.12, 132.33, 129.04, 128.76, 126.83, 124.53, 120.49, 116.25, 73.83, 39.59, 34.72, 24.10, 16.96 ppm.

HRMS m/z: [M+Na]⁺ calculated for C₂₄H₂₂N₂O: 377.1624, Found: 377.1617.



1-(6-phenylpyridin-3-yl)ethyl 1-(2,4-dichlorophenyl)cyclopropane-1-carboxylate, **4cc**

Chlorination: Reaction run using methyl 2-phenyl-5-ethylpyridine **1c** (91.6 mg, 0.50 mmol, 1.0 equiv) and *N*-(*tert*-butyl)-*N*-chloro-3,5-bis(trifluoromethyl)benzenesulfonamide **2** (287.8 mg, 0.75 mmol, 1.5 equiv) following the general procedure IV. ¹H NMR Yield = 64%

Nucleophilic displacement: Reaction run using 1-(2,4-dichlorophenyl)cyclopropane-1-carboxylic acid (46.2 mg, 0.20 mmol, 2.0 equiv) following the general procedure VII. Yield = 19.1 mg (47%) of clear colorless oil.

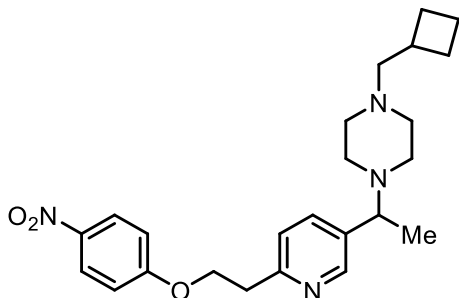
Purification: normal phase silica gel column chromatography with 4:1 petroleum ether:ethyl acetate

Spectral data available in the literature: No

¹H NMR (CDCl₃, 500 MHz): δ 7.66 (dd, *J* = 8.2, 0.9 Hz, 1H), 7.52 (dd, *J* = 8.2, 2.4 Hz, 1H), 7.49 – 7.44 (m, 2H), 7.43 – 7.38 (m, 2H), 7.26 – 7.20 (m, 2H), 5.92 (q, *J* = 6.6 Hz, 1H), 1.81 – 1.67 (m, 2H), 1.19 (tdd, *J* = 9.1, 6.4, 3.4 Hz, 2H) ppm.

¹³C NMR (CDCl₃, 126 MHz): δ 172.24, 156.98, 147.50, 139.00, 137.57, 136.11, 135.25, 134.37, 133.82, 132.38, 129.26, 129.01, 128.75, 126.96, 126.89, 120.15, 108.11, 70.92, 27.66, 22.00, 17.70 ppm.

HRMS *m/z*: [M+H]⁺ calculated for C₂₃H₁₉Cl₂NO₂: 412.0866, Found: 412.0861.



1-(cyclobutylmethyl)-4-(1-(6-(2-(4-nitrophenoxy)ethyl)pyridin-3-yl)ethyl)piperazine, **4ia**

Chlorination: Reaction run using methyl 5-ethyl-2-(2-(4-nitrophenoxy)ethyl)pyridine **1i** (54.5 mg, 0.50 mmol, 1.0 equiv) and *N*-(*tert*-butyl)-*N*-chloro-3,5-bis(trifluoromethyl)benzenesulfonamide **2** (153.5 mg, 1.00 mmol, 2.0 equiv) following the general procedure IV with one LED light. ^1H NMR Yield = 79%

Nucleophilic displacement: Reaction run using 1-(cyclobutylmethyl)piperazine (30.9 mg, 0.20 mmol, 2.0 equiv) following the general procedure VII. Yield = 4.1 mg (10%) of yellow solid.

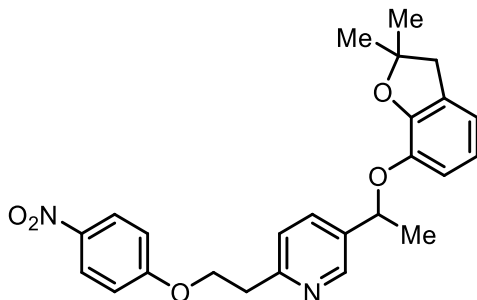
Purification: X-Bridge Prep C-18 5 μm , 19 x 150 mm LC column with 8% NH_4^+ at 25 mL/min flowrate

Spectral data available in the literature: No

^1H NMR (CDCl_3 , 500 MHz): δ 8.46 (d, $J = 2.1$ Hz, 1H), 8.21 – 8.14 (m, 2H), 7.58 (dd, $J = 7.9$, 2.3 Hz, 1H), 7.20 (d, $J = 7.9$ Hz, 1H), 6.99 – 6.93 (m, 2H), 4.47 (t, $J = 6.7$ Hz, 2H), 3.46 (q, $J = 6.8$ Hz, 1H), 3.27 (t, $J = 6.7$ Hz, 2H), 2.84 – 2.29 (m, 11H), 2.12 – 2.02 (m, 2H), 1.95 – 1.84 (m, 1H), 1.84 – 1.75 (m, 1H), 1.74 – 1.65 (m, 2H), 1.36 (d, $J = 6.7$ Hz, 3H) ppm.

^{13}C NMR (CDCl_3 , 126 MHz): δ 163.91, 156.38, 149.16, 141.52, 137.01, 135.65, 125.88, 123.39, 114.54, 67.92, 64.61, 61.88, 53.16, 49.46, 37.31, 33.29, 28.04, 19.20, 18.80 ppm.

HRMS m/z : $[\text{M}+\text{H}]^+$ calculated for $\text{C}_{24}\text{H}_{32}\text{N}_4\text{O}_3$: 425.2547, Found: 425.2544.



5-(1-((2,2-dimethyl-2,3-dihydrobenzofuran-7-yl)oxy)ethyl)-2-(2-(4-nitrophenoxy)ethyl)pyridine, **4ib**

Chlorination: Reaction run using methyl 5-ethyl-2-(2-(4-nitrophenoxy)ethyl)pyridine **1i** (136.2 mg, 0.50 mmol, 1.0 equiv) and *N*-(*tert*-butyl)-*N*-chloro-3,5-bis(trifluoromethyl)benzenesulfonamide **2** (383.7 mg, 1.00 mmol, 2.0 equiv) following the general procedure IV with one LED light. ^1H NMR Yield = 67%

Nucleophilic displacement: Reaction run using 2,2-dimethyl-2,3-dihydrobenzofuran-7-ol (32.8 mg, 0.20 mmol, 2.0 equiv) following the general procedure VII. Yield = 6.3 mg (15%) of yellow oil.

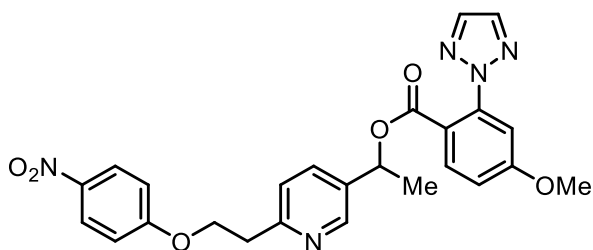
Purification: normal phase silica gel column chromatography with 5:1 dichloromethane:ethyl acetate

Spectral data available in the literature: No

^1H NMR (CDCl_3 , 500 MHz): δ 8.55 (d, $J = 2.3$ Hz, 1H), 8.21 – 8.13 (m, 2H), 7.72 (dd, $J = 8.0$, 2.3 Hz, 1H), 7.20 (d, $J = 8.0$ Hz, 1H), 6.96 – 6.91 (m, 2H), 6.74 (ddt, $J = 6.4$, 2.3, 1.1 Hz, 1H), 6.66 – 6.61 (m, 2H), 5.49 (q, $J = 6.5$ Hz, 1H), 4.45 (t, $J = 6.7$ Hz, 2H), 3.26 (t, $J = 6.7$ Hz, 2H), 2.97 (s, 2H), 1.66 (d, $J = 6.5$ Hz, 3H), 1.47 (s, 6H) ppm.

^{13}C NMR (CDCl_3 , 126 MHz): δ 163.89, 156.75, 148.57, 147.76, 141.97, 141.52, 136.83, 134.30, 129.01, 125.88, 123.50, 120.23, 118.62, 116.95, 114.53, 87.34, 75.05, 67.89, 43.17, 37.36, 28.23, 23.74 ppm.

HRMS m/z : $[\text{M}+\text{H}]^+$ calculated for $\text{C}_{25}\text{H}_{26}\text{N}_2\text{O}_5$: 435.1915, Found: 435.1907.



1-(6-(2-(4-nitrophenoxy)ethyl)pyridin-3-yl)ethyl 4-methoxy-2-(2H-1,2,3-triazol-2-yl)benzoate, **4ic**

Chlorination: Reaction run using methyl 5-ethyl-2-(2-(4-nitrophenoxy)ethyl)pyridine **1i** (136.2 mg, 0.50 mmol, 1.0 equiv) and *N*-(*tert*-butyl)-*N*-chloro-3,5-bis(trifluoromethyl)benzenesulfonamide **2** (383.7 mg, 1.00 mmol, 2.0 equiv) following the general procedure IV with one LED light. ^1H NMR Yield = 74%.

Nucleophilic displacement: Reaction run using 4-methoxy-2-(2H-1,2,3-triazol-2-yl)benzoic acid (28.6 mg, 0.20 mmol, 1.0 equiv) following the general procedure VII. Yield = 18.0 mg (37%) of clear colorless oil.

Purification: normal phase silica gel column chromatography with 1:4 petroleum ether:ethyl acetate

Spectral data available in the literature: No

^1H NMR (CDCl_3 , 500 MHz): δ 8.45 (d, $J = 2.3$ Hz, 1H), 8.20 – 8.14 (m, 2H), 7.80 (d, $J = 8.7$ Hz, 1H), 7.49 (dd, $J = 8.0, 2.4$ Hz, 1H), 7.21 – 7.17 (m, 2H), 7.00 (dd, $J = 8.7, 2.5$ Hz, 1H), 6.97 – 6.92 (m, 2H), 5.95 (q, $J = 6.6$ Hz, 1H), 4.46 (t, $J = 6.5$ Hz, 2H), 3.89 (s, 3H), 3.27 (t, $J = 6.5$ Hz, 2H), 1.45 (d, $J = 6.7$ Hz, 3H) ppm.

^{13}C NMR (CDCl_3 , 126 MHz): δ 165.25, 163.81, 162.48, 157.25, 147.83, 141.54, 140.37, 135.44, 134.89, 134.57, 132.27, 125.89, 123.38, 119.40, 114.75, 114.49, 110.80, 70.95, 67.81, 55.88, 37.33, 21.77 ppm.

HRMS m/z : $[\text{M}+\text{Na}]^+$ calculated for $\text{C}_{25}\text{H}_{23}\text{N}_5\text{O}_6$: 512.1541, Found: 512.1536.

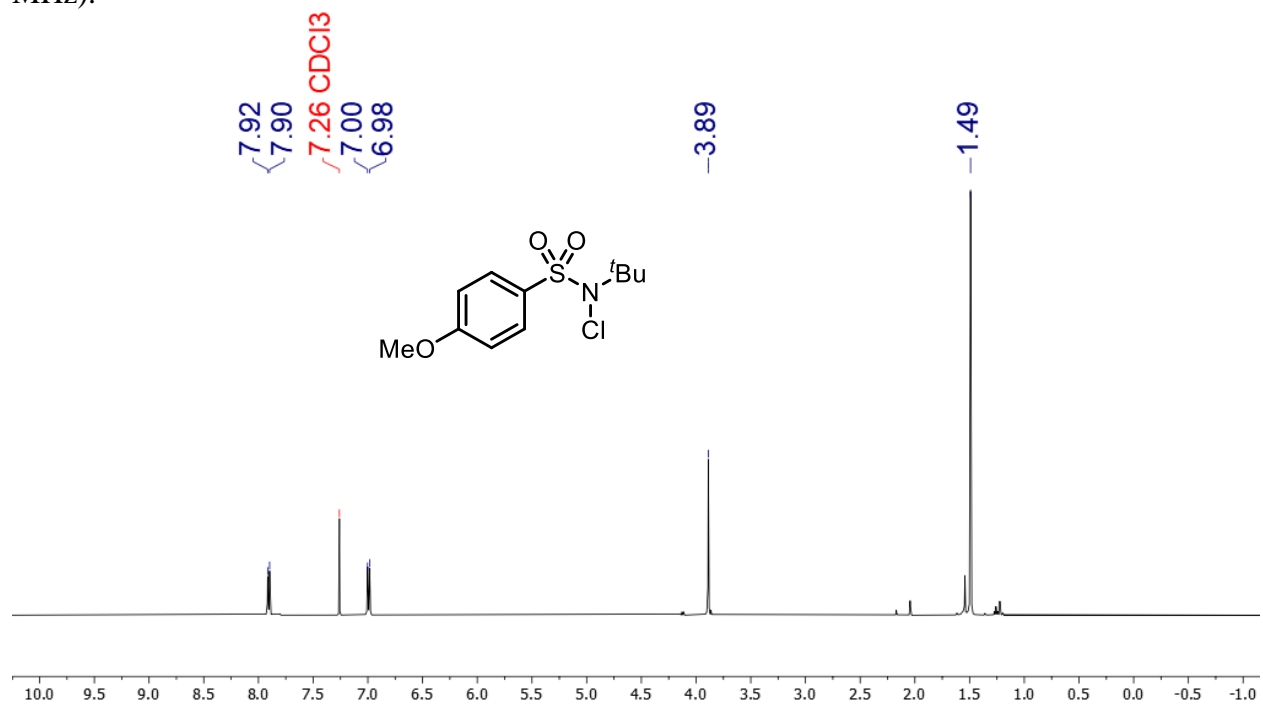
3B. XIII. Reference

- 1 Tierney, M. M.; Crespi, S.; Ravelli, D.; Alexanian, E. J. Identifying Amidyl Radicals for Intermolecular C–H Functionalizations. *J. Org. Chem.* **2019**, *84*, 12983–12991.
- 2 Heuger, G.; Göttlich, R. Intermolecular Addition Reactions of *N*-alkyl-*N*-chlorosulfonamides to Unsaturated Compounds. *Beilstein J. Org. Chem.* **2015**, *11*, 1226–1234.
- 3 McMillan, A. J.; Siénkowska, M.; Lorenzo, P. D.; Gransbury, G. K.; Chilton, N. F.; Salamone, M.; Ruffoni, A.; Bietti, M.; Leonori, D. Practical and Selective sp³ C–H bond Chlorination via Aminium Radicals. *Angew. Chem. Int. Ed.* **2021**, *60*, 7132–7139.
- 4 Fukuyama, T.; Nishikawa, T.; Yamada, K.; Ravelli, D.; Fagnoni, M.; Ryu, I. Photocatalyzed Site-Selective C(sp³)–H Functionalization of Alkylpyridines at Non-Benzyllic Positions. *Org. Lett.* **2017**, *19*, 6436–6439.
- 5 Balasubramani, S. G.; Chen, G. P.; Coriani, S.; Diedenhofen, M.; Frank, M. S.; Franzke, Y. J.; Furche, F.; Grotjahn, R.; Harding, M. E.; Hättig, C.; Hellweg, A.; Helmich-Paris, B.; Holzer, C.; Huniar, U.; Kaupp, M.; Khah, A. M.; Khani, S. K.; Müller, T.; Mack, F.; Nguyen, B. D.; Parker, S. M.; Perlt, E.; Rappoport, D.; Reiter, K.; Roy, S.; Rückert, M.; Schmitz, G.; Sierka, M.; Tapavicza, E.; Tew, D. P.; Wüllen, C. V.; Voora, V. K.; Weigend, F.; Wodyński, A.; Yu, J. M. TURBOMOLE: Modular Program Suite for Ab Initio Quantum-Chemical and Condensed-Matter Simulations. *J. Chem. Phys.* **2020**, *152*, 184107.
- 6 Pracht, P.; Bohle, F.; Grimme, S. Automated Exploration of the Low-Energy Chemical Space with Fast Quantum Chemical Methods. *Phys. Chem. Chem. Phys.* **2020**, *22*, 7169–7192.
- 7 Grimme, S.; Bannwarth, C.; Shushkov, P. A Robust and Accurate Tight-Binding Quantum Chemical Method for Structures, Vibrational Frequencies, and Noncovalent Interactions of Large Molecular Systems Parametrized for All spd-Block Elements (*Z* = 1–86). *J. Chem. Theory Comput.* **2017**, *13*, 1989–2009.
- 8 Grimme, S.; Bohle, F.; Hansen, A.; Pracht, P.; Spicher, S.; Stahn, M. Efficient Quantum Chemical Calculation of Structure Ensembles and Free Energies for Nonrigid Molecules. *J. Phys. Chem. A* **2021**, *125*, 4039–4054.
- 9 Adamo, C.; Barone, V. Toward Reliable Density Functional Methods without Adjustable Parameters: The PBE0 Model. *J. Chem. Phys.* **1999**, *110*, 6158–6170.
- 10 Caldeweyher, E.; Ehlert, S.; Hansen, A.; Neugebauer, H.; Spicher, S.; Bannwarth, C.; Grimme, S. A Generally Applicable Atomic-Charge Dependent London Dispersion Correction. *J. Chem. Phys.* **2019**, *150*, 154122.
- 11 Weigend, F.; Ahlrichs, R. Balanced Basis Sets of Split Valence, Triple Zeta Valence and Quadruple Zeta Valence Quality for H to Rn: Design and Assessment of Accuracy. *Phys. Chem. Chem. Phys.* **2005**, *7*, 3297–3305.
- 12 Eshuis, H.; Bates, J. E.; Furche, F. Electron Correlation Methods Based on the Random Phase Approximation. *Theor. Chem. Acc.* **2012**, *131*, 1084.
- 13 Eshuis, H.; Yarkony, J.; Furche, F. Fast Computation of Molecular Random Phase Approximation Correlation Energies Using Resolution of the Identity and Imaginary Frequency Integration. *J. Chem. Phys.* **2010**, *132*, 234114.

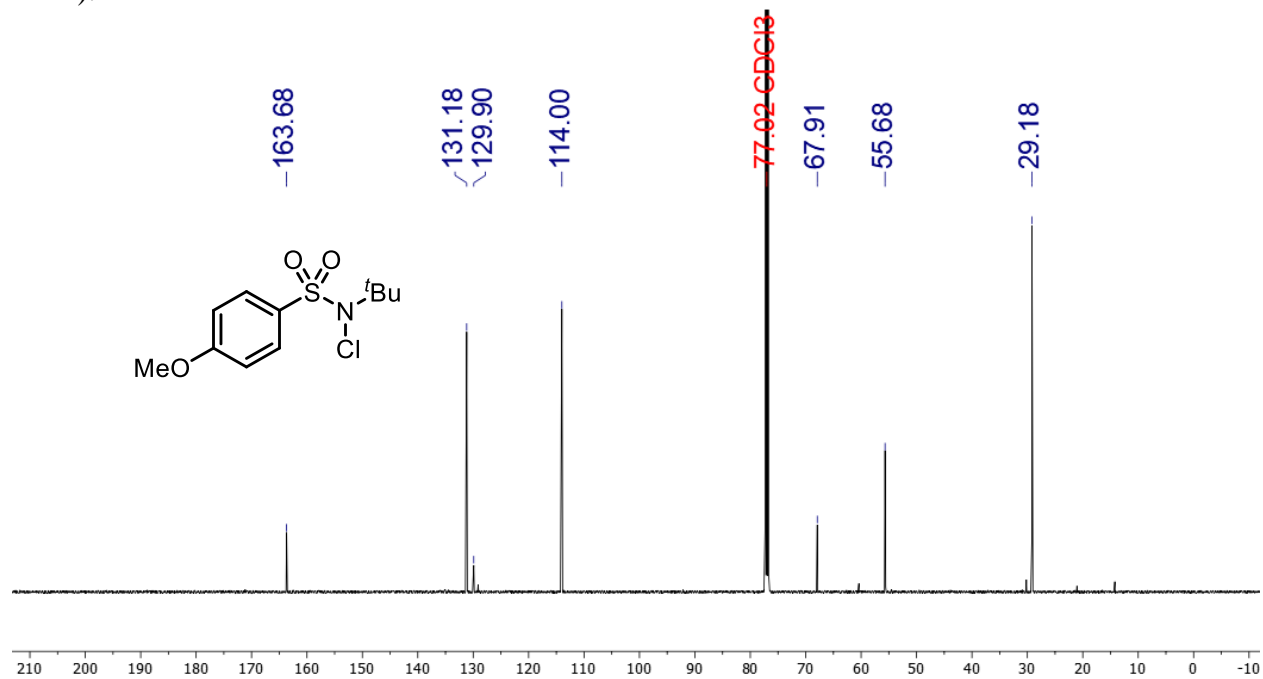
- 14 Eichkorn, K.; Treutler, O.; Öhm, H.; Häser, M.; Ahlrichs, R. Auxiliary Basis Sets to Approximate Coulomb Potentials. *Chem. Phys. Lett.* **1995**, *240*, 283–290.
- 15 Sierka, M.; Hogekamp, A.; Ahlrichs, R. Fast Evaluation of the Coulomb Potential for Electron Densities Using Multipole Accelerated Resolution of Identity Approximation. *J. Chem. Phys.* **2003**, *118*, 9136–9148.
- 16 Weigend, F. Accurate Coulomb-Fitting Basis Sets for H to Rn. *Phys. Chem. Chem. Phys.* **2006**, *8*, 1057–1065.
- 17 Weigend, F.; Häser, M.; Patzelt, H.; Ahlrichs, R. RI-MP2: Optimized Auxiliary Basis Sets and Demonstration of Efficiency. *Chem. Phys. Lett.* **1998**, *294*, 143–152.
- 18 Schäfer, A.; Klamt, A.; Sattel, D.; Lohrenz, J. C. W.; Eckert, F. COSMO Implementation in TURBOMOLE: Extension of an Efficient Quantum Chemical Code towards Liquid Systems. *Phys. Chem. Chem. Phys.* **2000**, *2*, 2187–2193.
- 19 Klamt, A. COSMOtherm, 19; COSMOlogic GmbH & Co. KG, a Dassault Systèmes company.: 2019.
- 20 Eckert, F.; Klamt, A. Fast Solvent Screening via Quantum Chemistry: COSMO-RS Approach. *AIChE J.* **2002**, *48*, 369–385.
- 21 Klamt, A.; Jonas, V.; Bürger, T.; Lohrenz, J. C. W. Refinement and Parametrization of COSMO-RS. *J. Phys. Chem. A* **1998**, *102*, 5074–5085.
- 22 Klamt, A. Conductor-like Screening Model for Real Solvents: A New Approach to the Quantitative Calculation of Solvation Phenomena. *J. Phys. Chem.* **1995**, *99*, 2224–2235.
- 23 Becke, A. D. Density-Functional Exchange-Energy Approximation with Correct Asymptotic Behavior. *Phys. Rev. A* **1988**, *38*, 3098–3100.
- 24 Perdew, J. P. Density-Functional Approximation for the Correlation Energy of the Inhomogeneous Electron Gas. *Phys. Rev. B* **1986**, *33*, 8822–8824.
- 25 Rappoport, D.; Furche, F. Property-Optimized Gaussian Basis Sets for Molecular Response Calculations. *J. Chem. Phys.* **2010**, *133*, 134105.
- 26 Hellweg, A.; Eckert, F. Brick by Brick Computation of the Gibbs Free Energy of Reaction in Solution Using Quantum Chemistry and COSMO-RS. *AIChE J.* **2017**, *63*, 3944–3954.
- 27 Grimme, S. Supramolecular Binding Thermodynamics by Dispersion-Corrected Density Functional Theory. *Chem. Eur. J.* **2012**, *18*, 9955–9964.
- 1 Wang, Y.; Huang, W.; Wang, C.; Qu, J.; Chen, Y. Nickel-Catalyzed Formal Aminocarbonylation of Secondary Benzyl Chlorides with Isocyanides. *Org. Lett.* **2020**, *22*, 4245–4249.
- 2 Zheng, D.; Mao, L.-L.; Zhu, X.-H.; Zhou, A.-X. NMP-Mediated Chlorination of Aliphatic Alcohols with Aryl Sulfonyl Chloride for the Synthesis of Alkyl Chlorides. *Synth. Commun.* **2018**, *48*, 2793–2800.
- 3 Pesti, J. A.; Huhn, G. F.; Yin, J.; Xin, Y.; Fortunak, J. M.; Earl, R. A. Efficient Pyridinylmethyl Functionalization: Synthesis of 10,10-Bis[(2-fluoro-4-pyridinyl)methyl]-9(10*H*)-anthracenone (DMP 543), an Acetylcholine Release Enhancing Agent. *J. Org. Chem.* **2000**, *65*, 7718–7722.
- 4 Emerson, C. R.; Zakharov, L. N.; Blakemore, P. R. Investigation of Functionalized α -chloroalkyllithiums for a Stereospecific Reagent-Controlled Homologation Approach to the Analgesic Alkaloid (-)-Epibatidine. *Chem. Eur. J.* **2013**, *19*, 16342–16356.

3B.XIV. NMR Spectroscopic Data

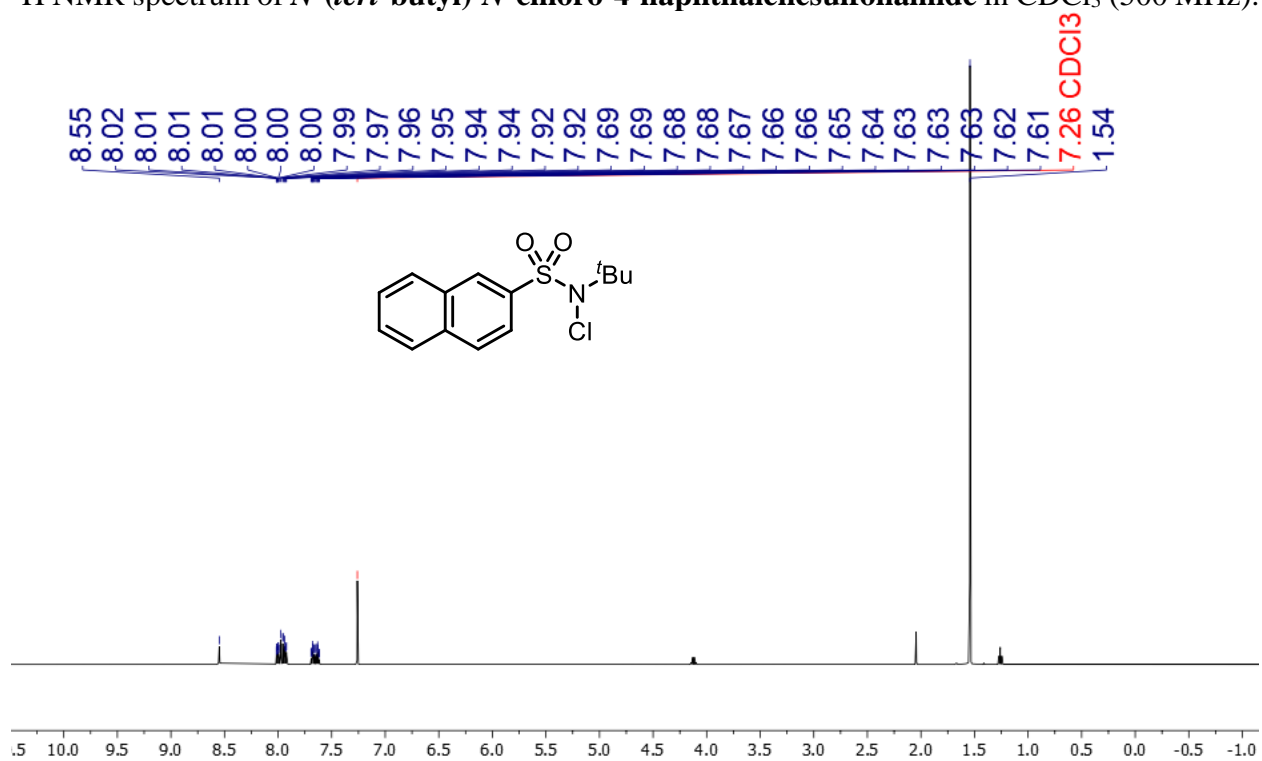
¹H NMR spectrum of *N*-(*tert*-butyl)-*N*-chloro-4-methoxybenzenesulfonamide in CDCl₃ (500 MHz).



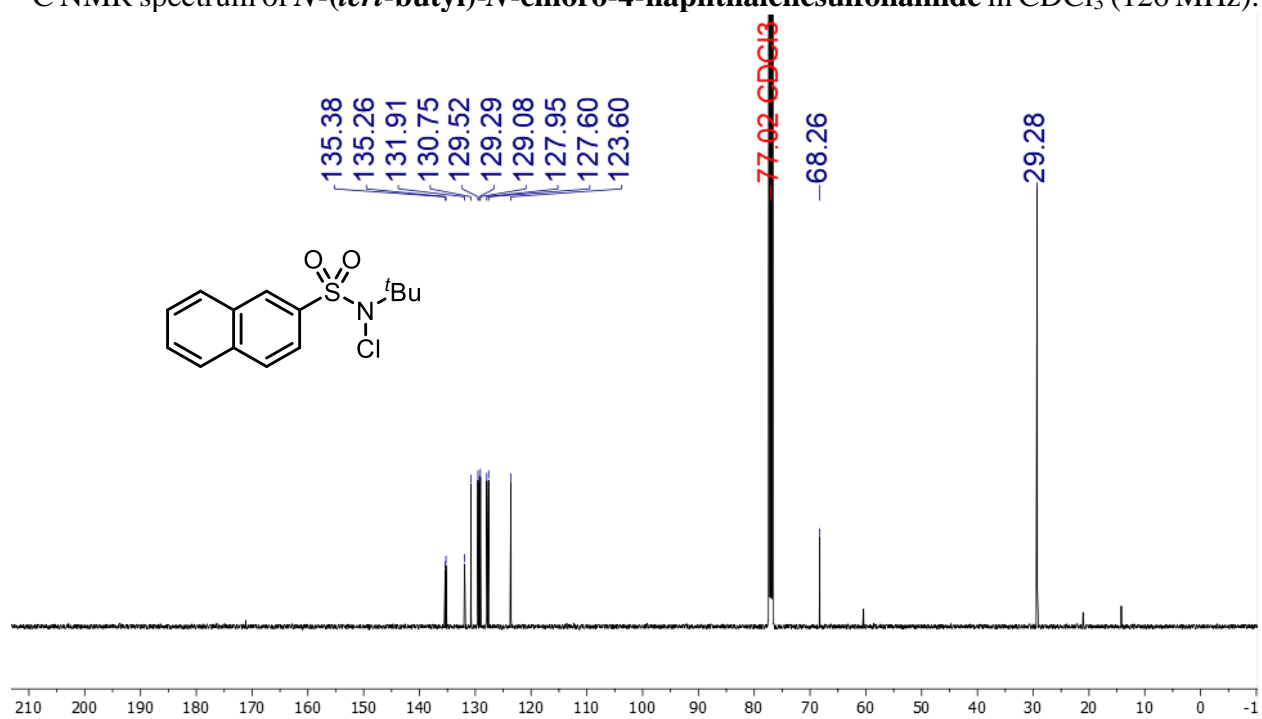
¹³C NMR spectrum of *N*-(*tert*-butyl)-*N*-chloro-4-methoxybenzenesulfonamide in CDCl₃ (126 MHz).



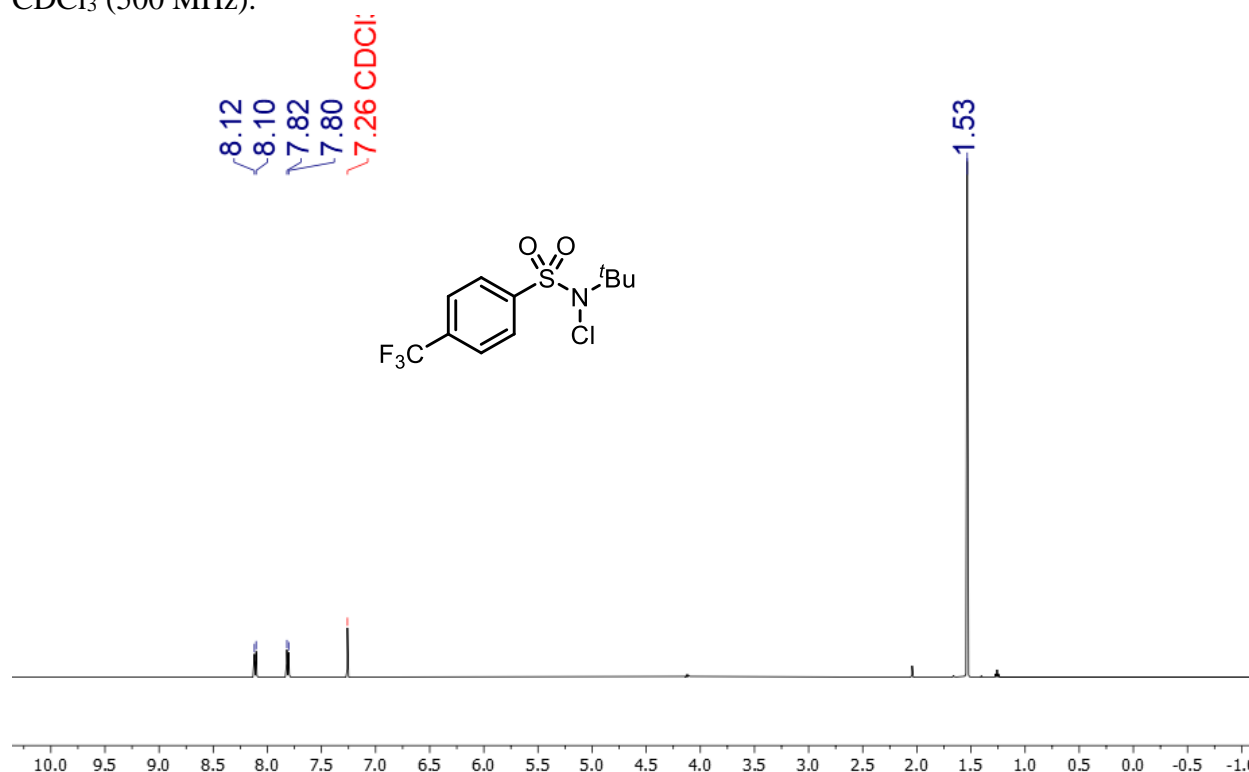
^1H NMR spectrum of *N*-(*tert*-butyl)-*N*-chloro-4-naphthalenesulfonamide in CDCl_3 (500 MHz).



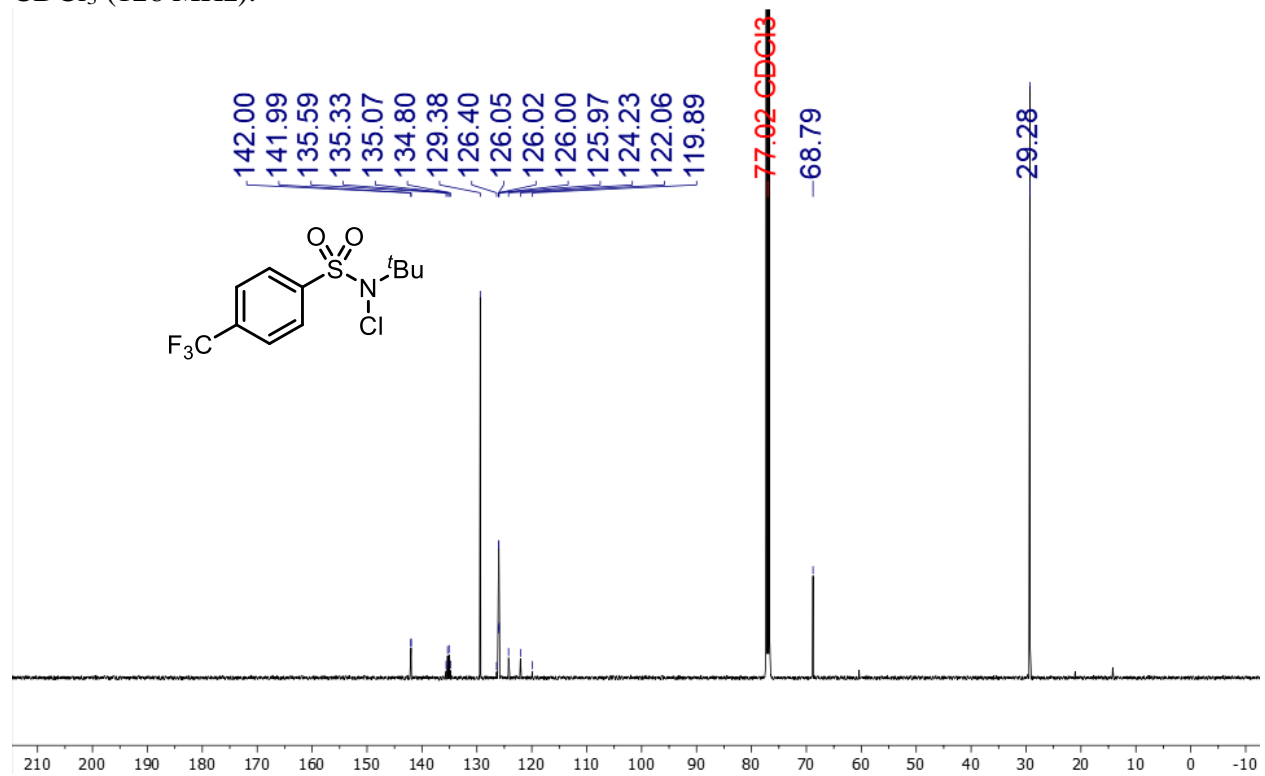
^{13}C NMR spectrum of *N*-(*tert*-butyl)-*N*-chloro-4-naphthalenesulfonamide in CDCl_3 (126 MHz).



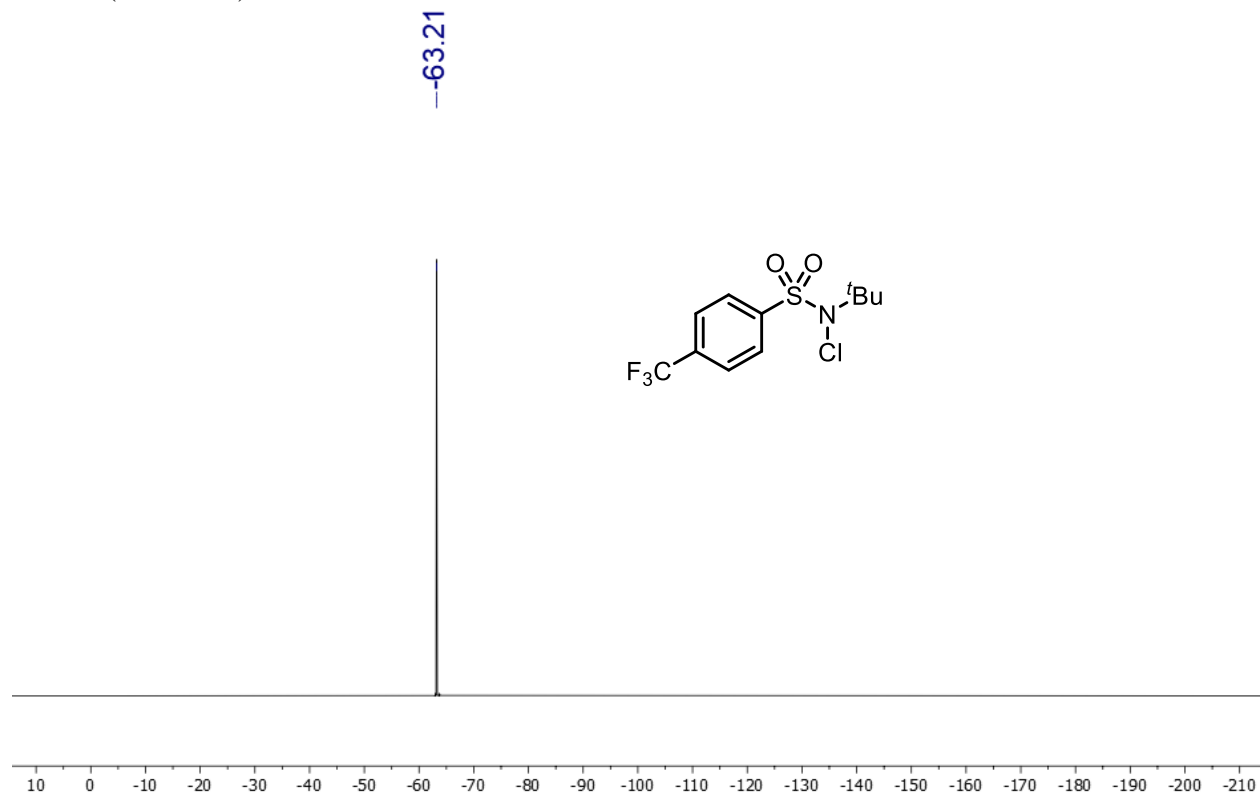
^1H NMR spectrum of *N*-(*tert*-butyl)-*N*-chloro-4-(trifluoromethyl)benzenesulfonamide in CDCl_3 (500 MHz).



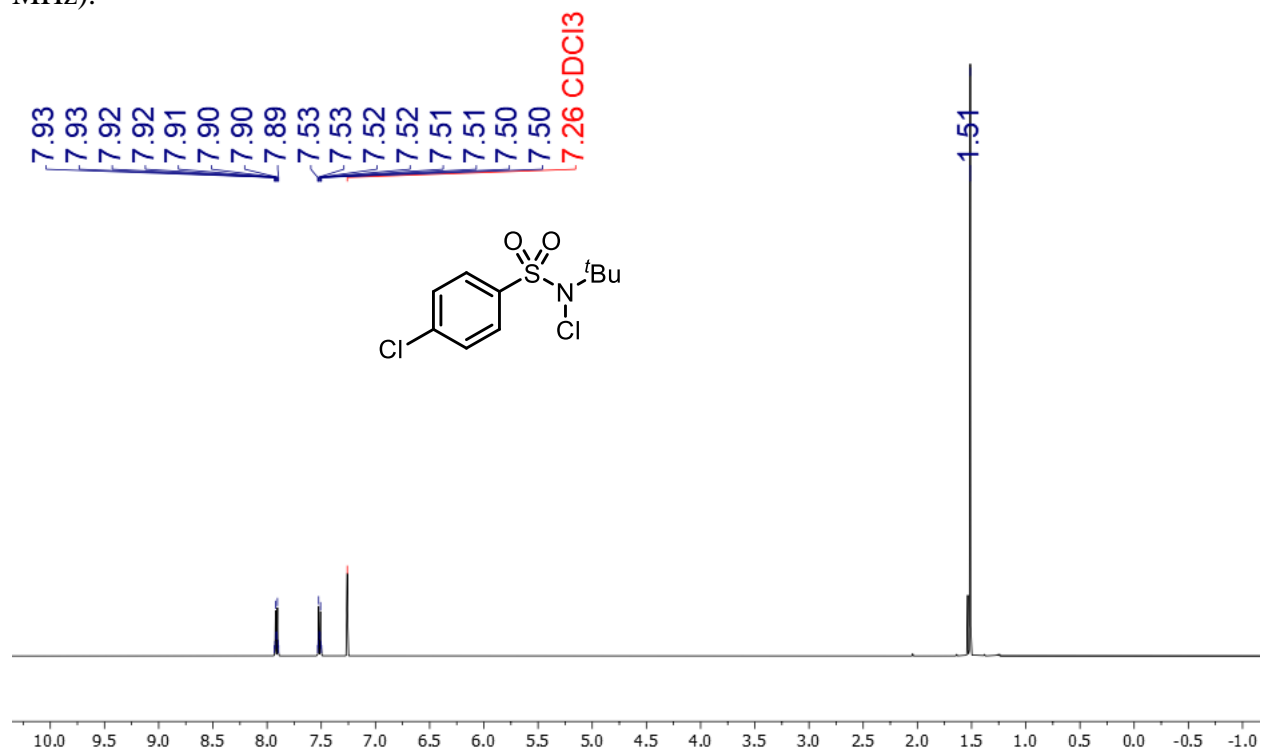
^{13}C NMR spectrum of *N*-(*tert*-butyl)-*N*-chloro-4-(trifluoromethyl)benzenesulfonamide in CDCl_3 (126 MHz).



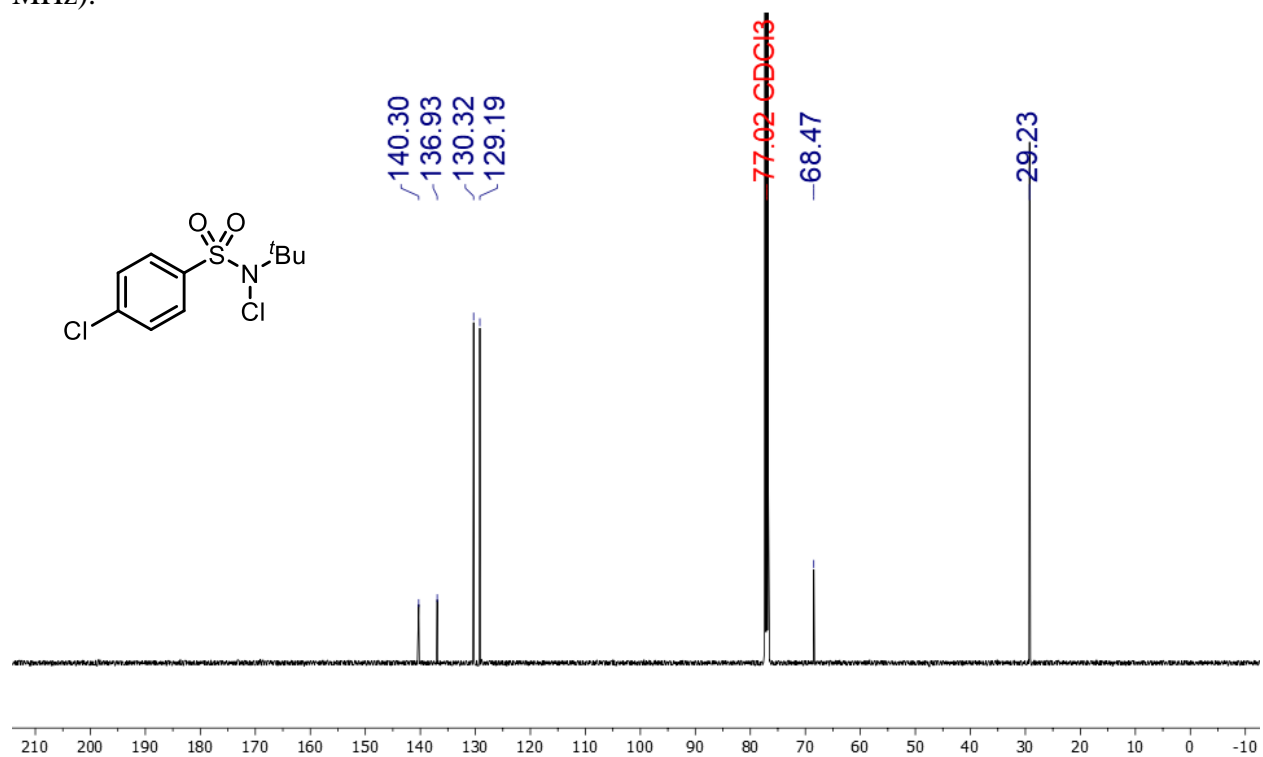
^{19}F NMR spectrum of *N*-(*tert*-butyl)-*N*-chloro-4-(trifluoromethyl)benzenesulfonamide in CDCl_3 (377 MHz).



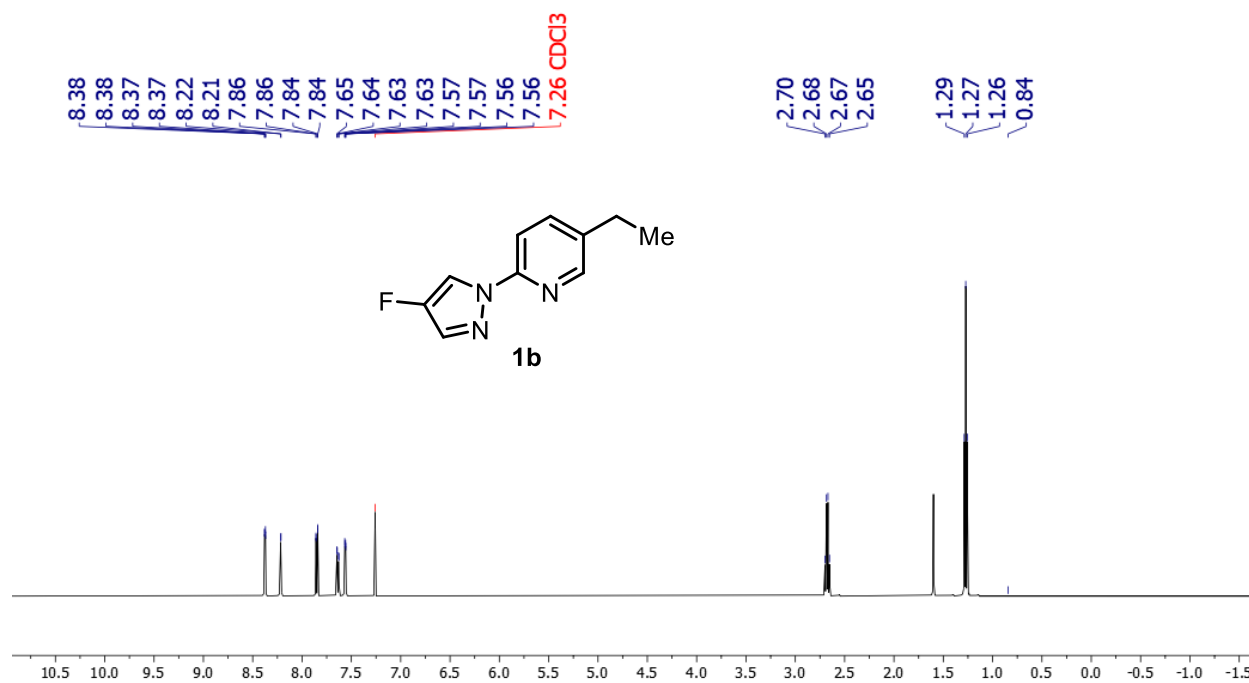
^1H NMR spectrum of *N*-(*tert*-butyl)-*N*-chloro-4-chlorobenzenesulfonamide in CDCl_3 (500 MHz).



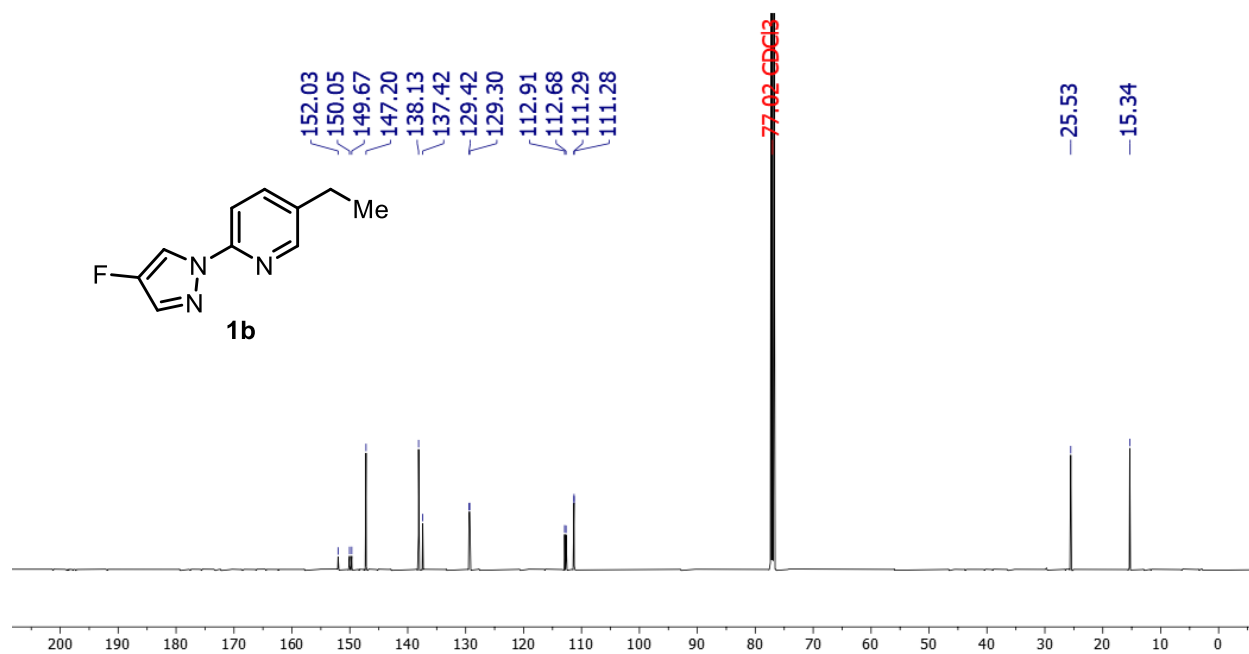
^{13}C NMR spectrum of *N*-(*tert*-butyl)-*N*-chloro-4-chlorobenzenesulfonamide in CDCl_3 (126 MHz).



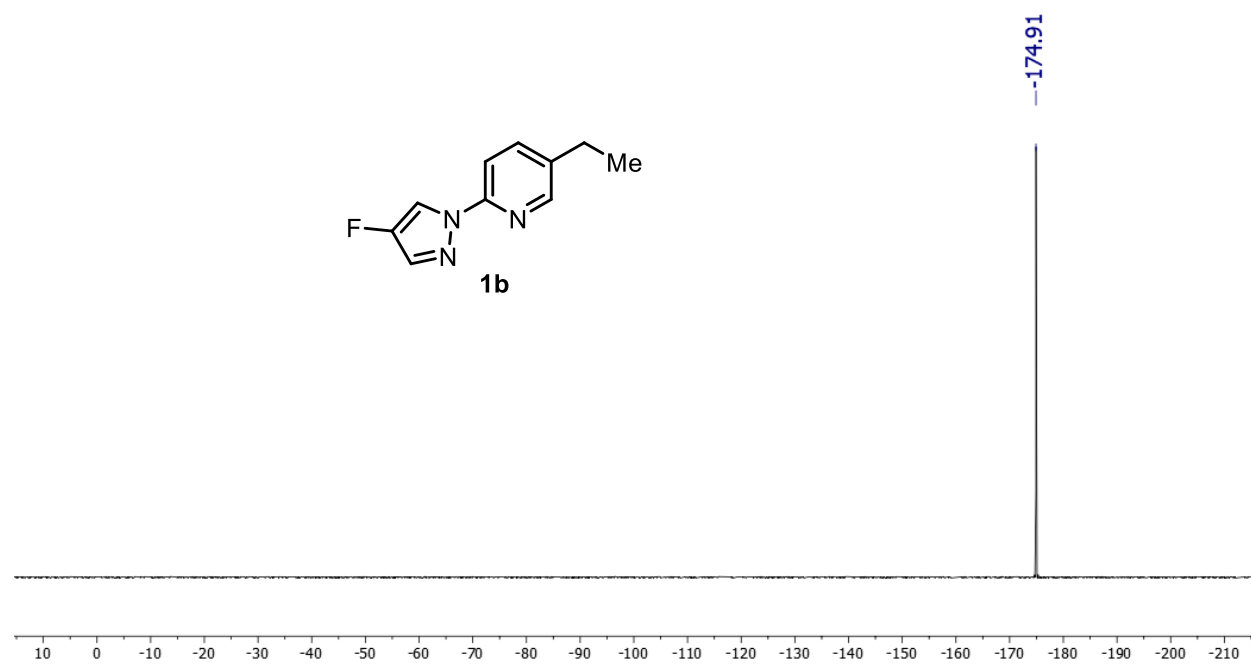
^1H NMR spectrum of **1b** in CDCl_3 (500 MHz).



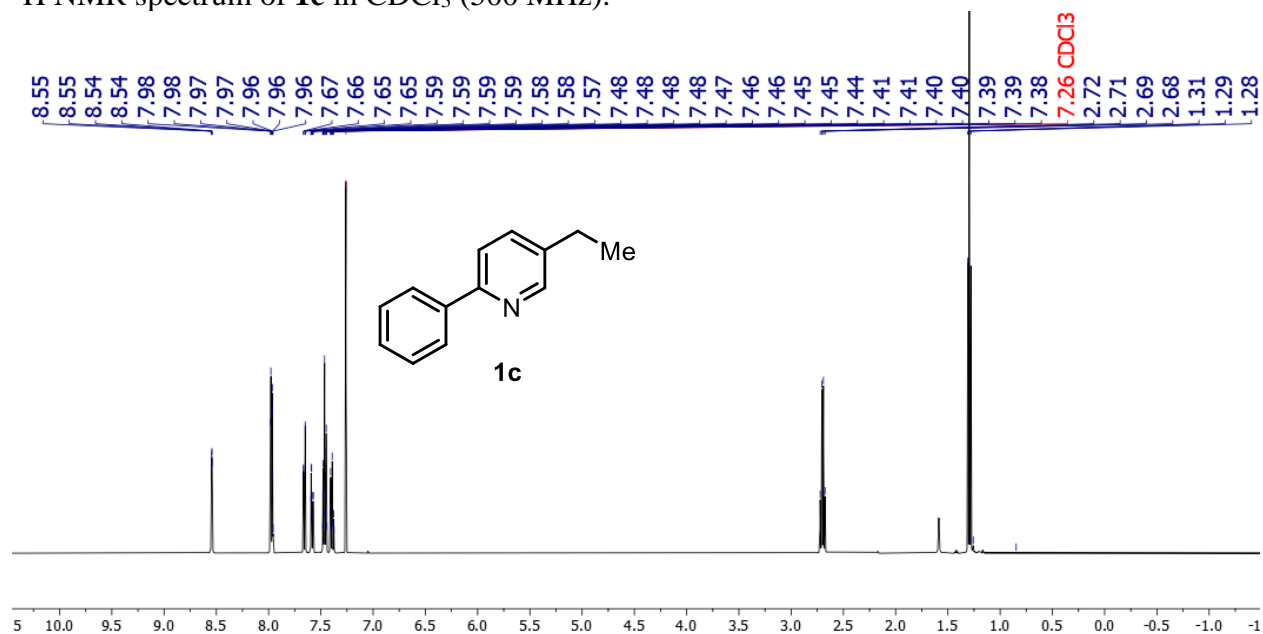
^{13}C NMR spectrum of **1b** in CDCl_3 (126 MHz).



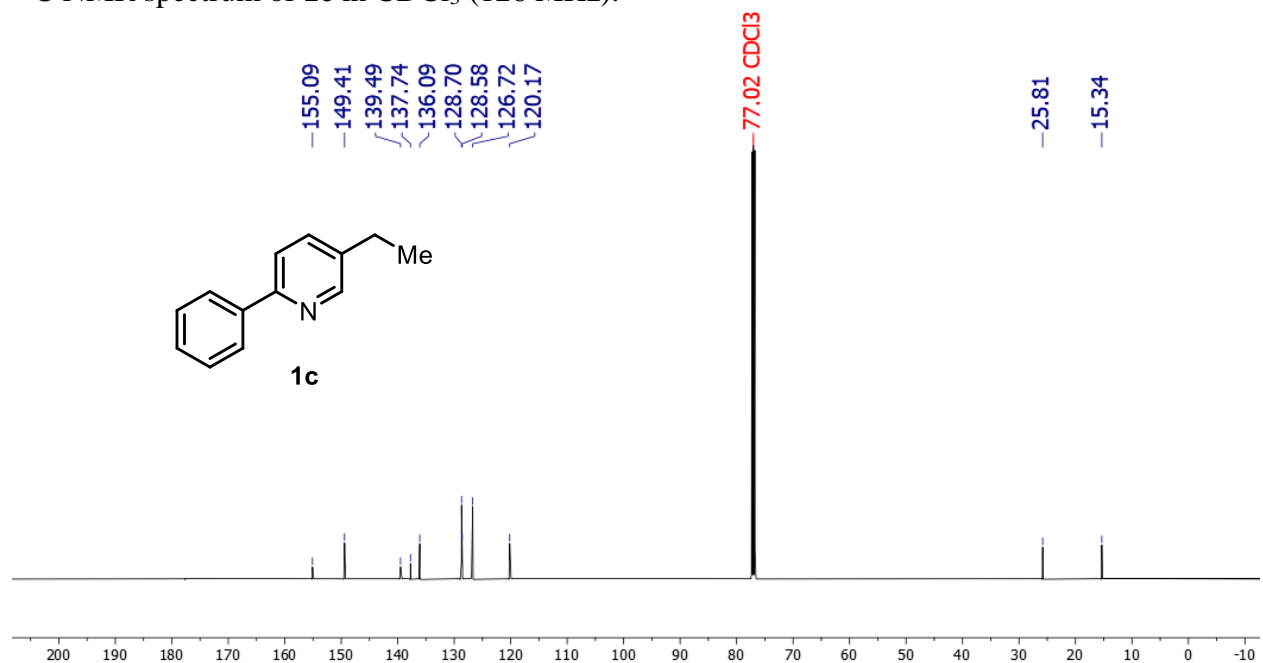
^{19}F NMR spectrum of **1b** in CDCl_3 (377 MHz).



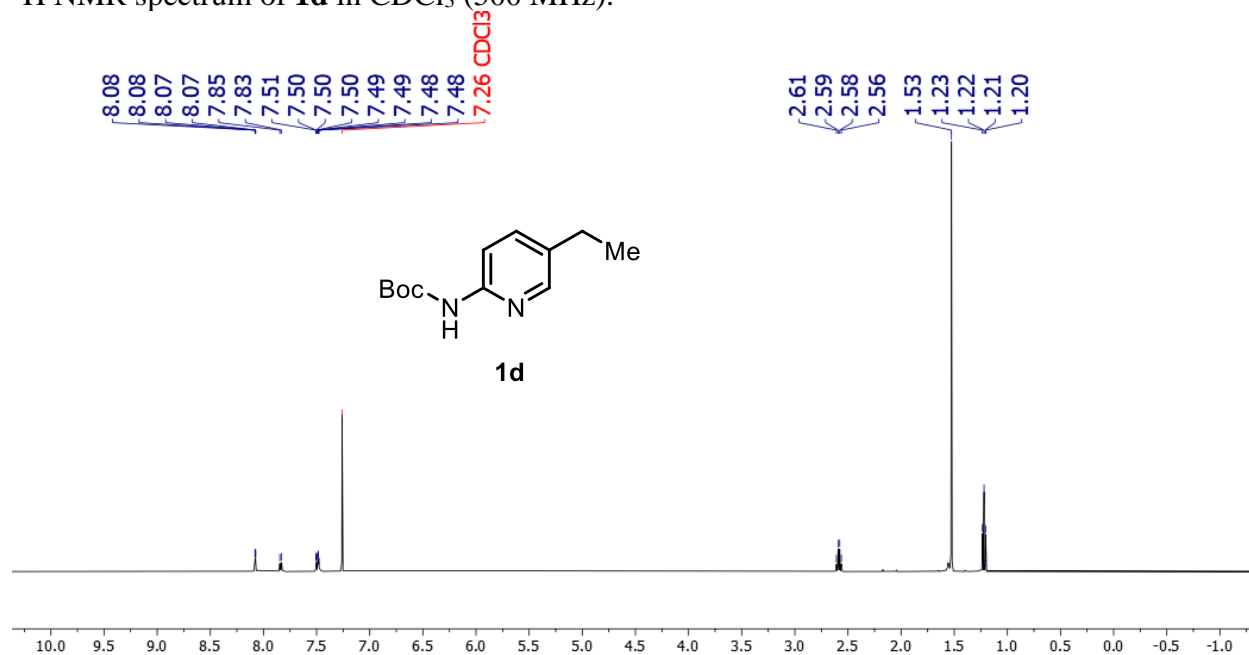
^1H NMR spectrum of **1c** in CDCl_3 (500 MHz).



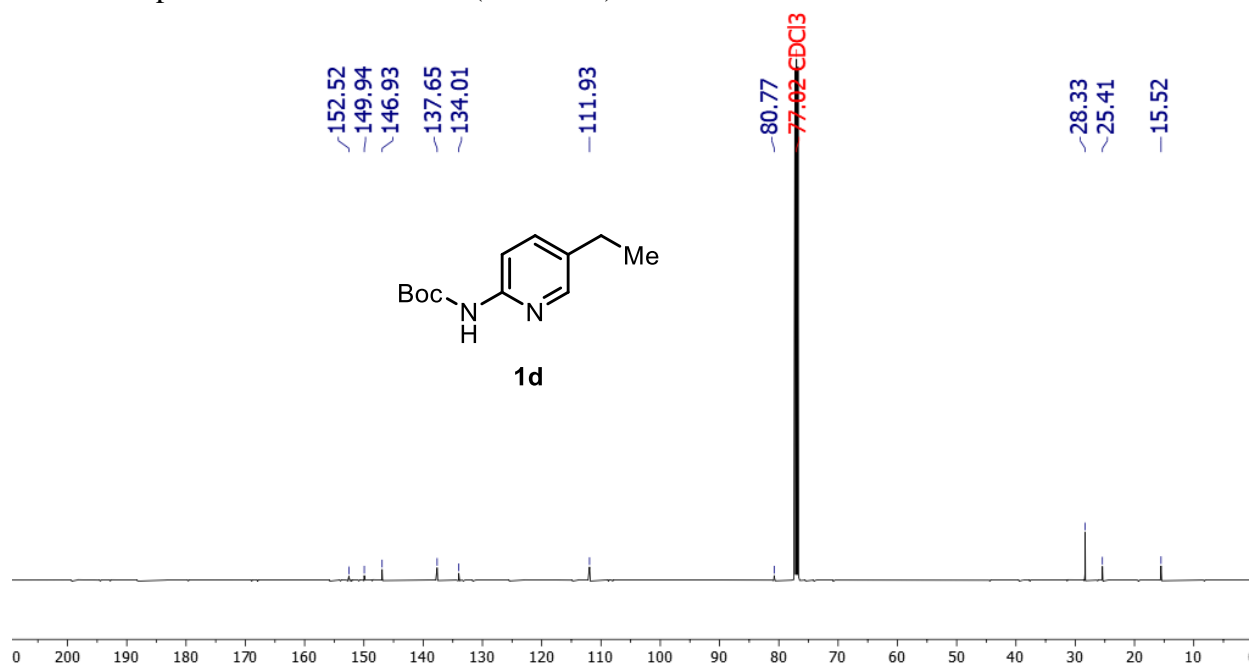
^{13}C NMR spectrum of **1c** in CDCl_3 (126 MHz).



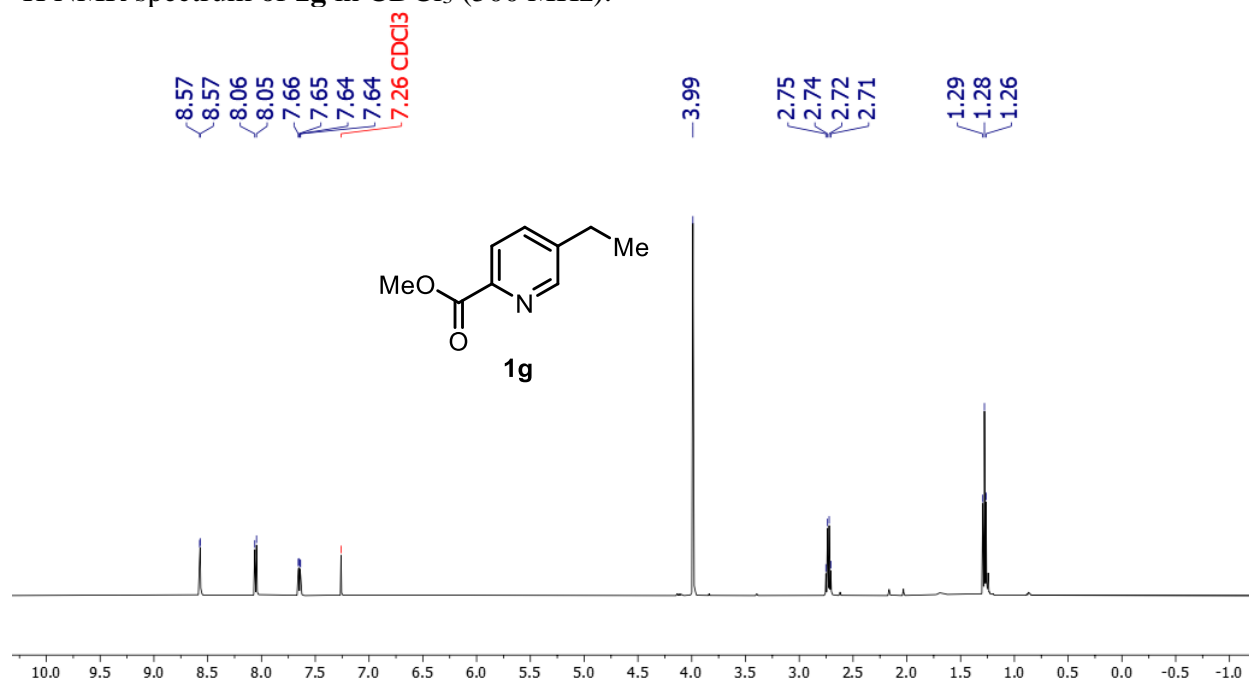
^1H NMR spectrum of **1d** in CDCl_3 (500 MHz).



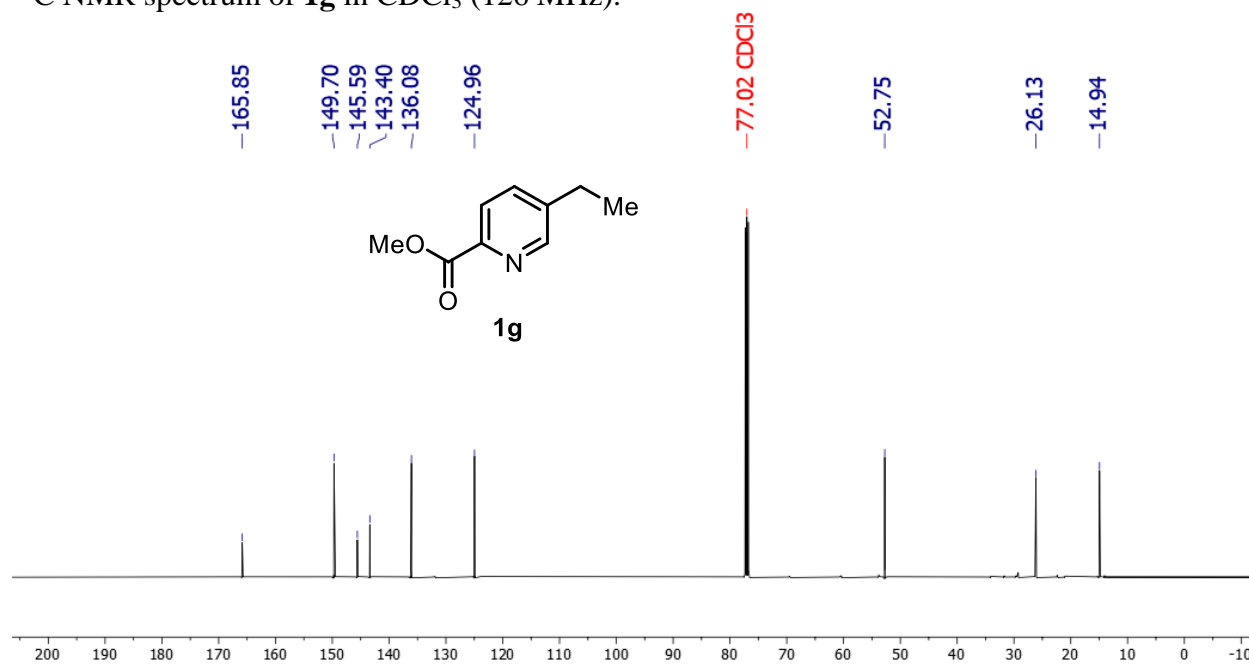
^{13}C NMR spectrum of **1d** in CDCl_3 (126 MHz).



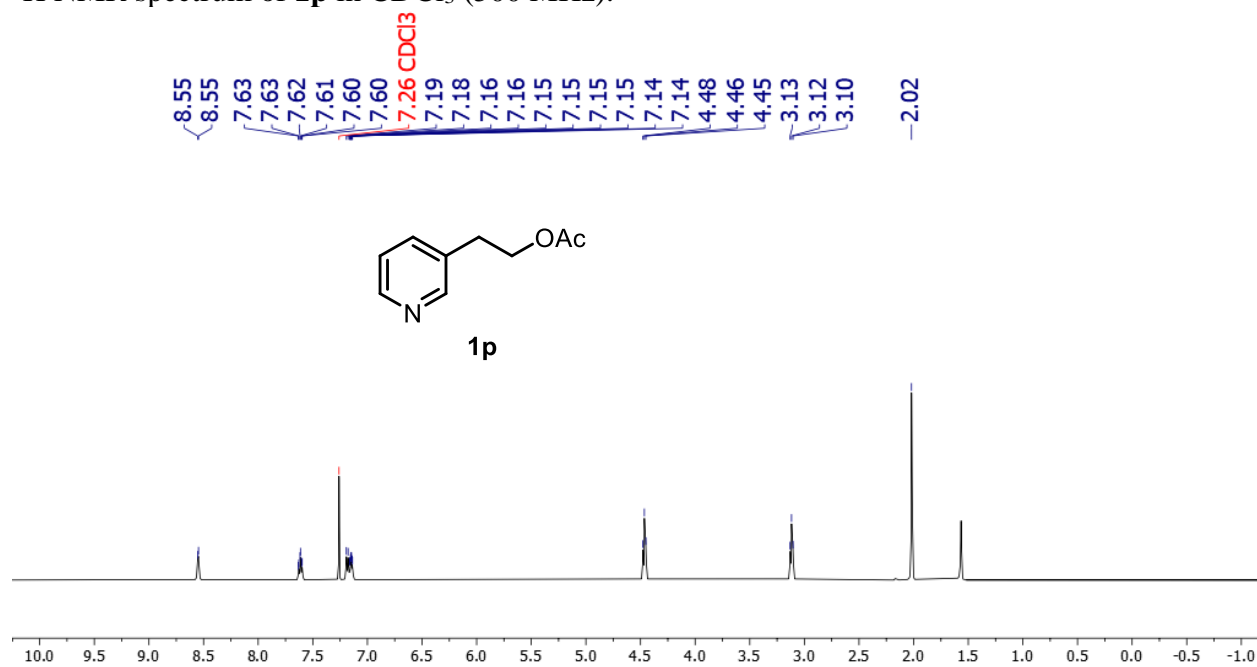
^1H NMR spectrum of **1g** in CDCl_3 (500 MHz).



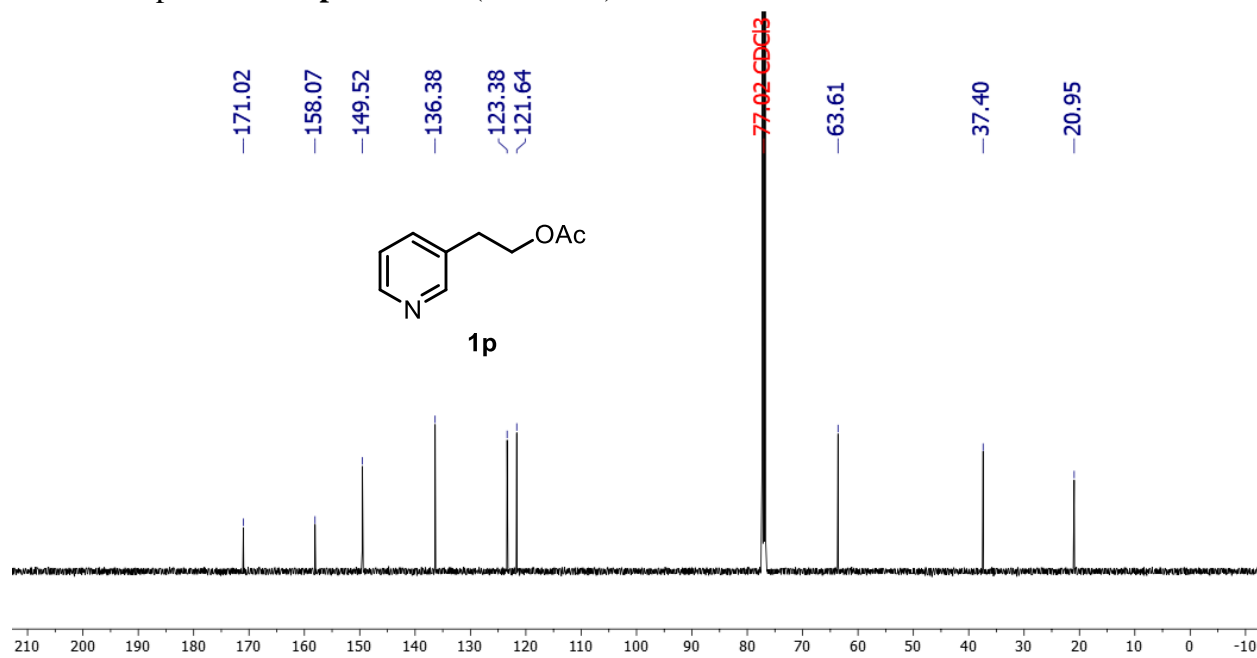
^{13}C NMR spectrum of **1g** in CDCl_3 (126 MHz).



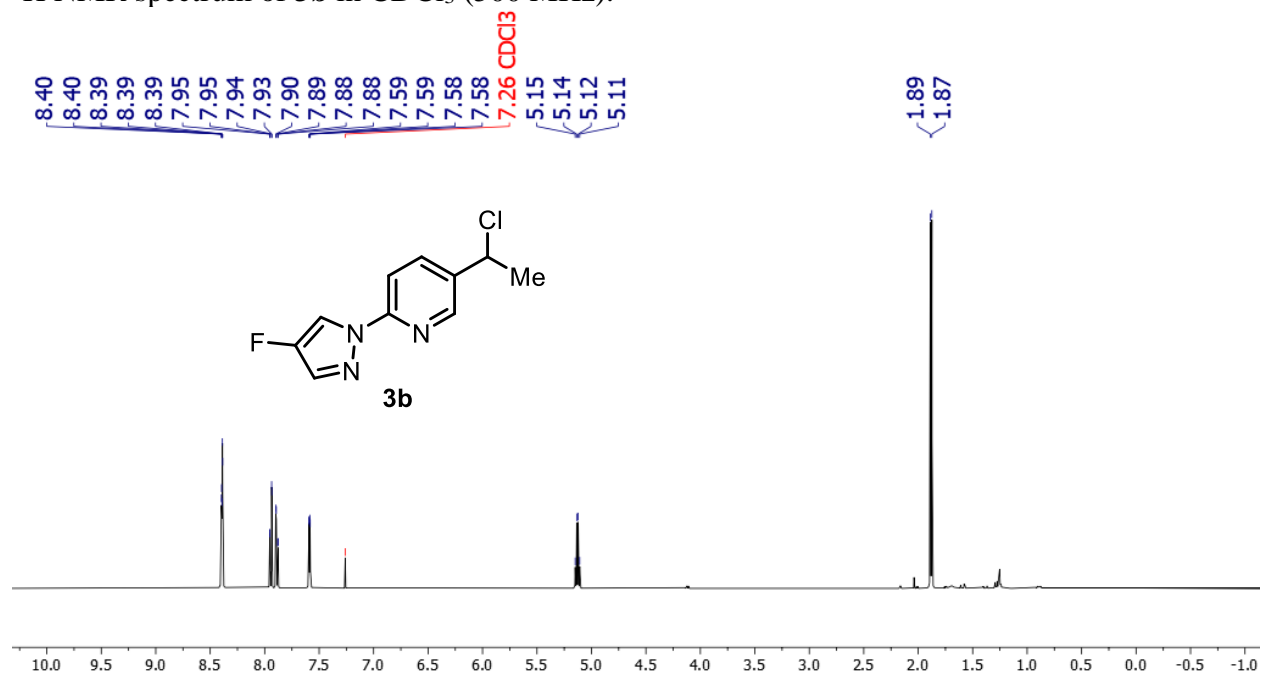
^1H NMR spectrum of **1p** in CDCl_3 (500 MHz).



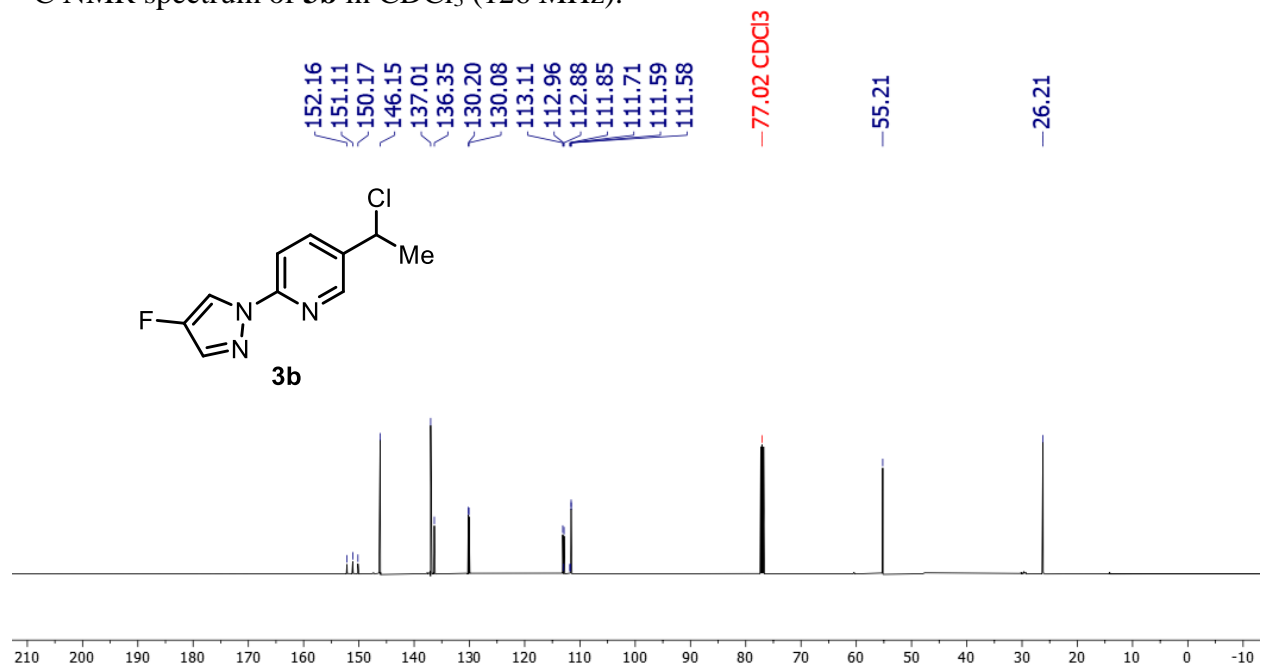
^{13}C NMR spectrum of **1p** in CDCl_3 (126 MHz).



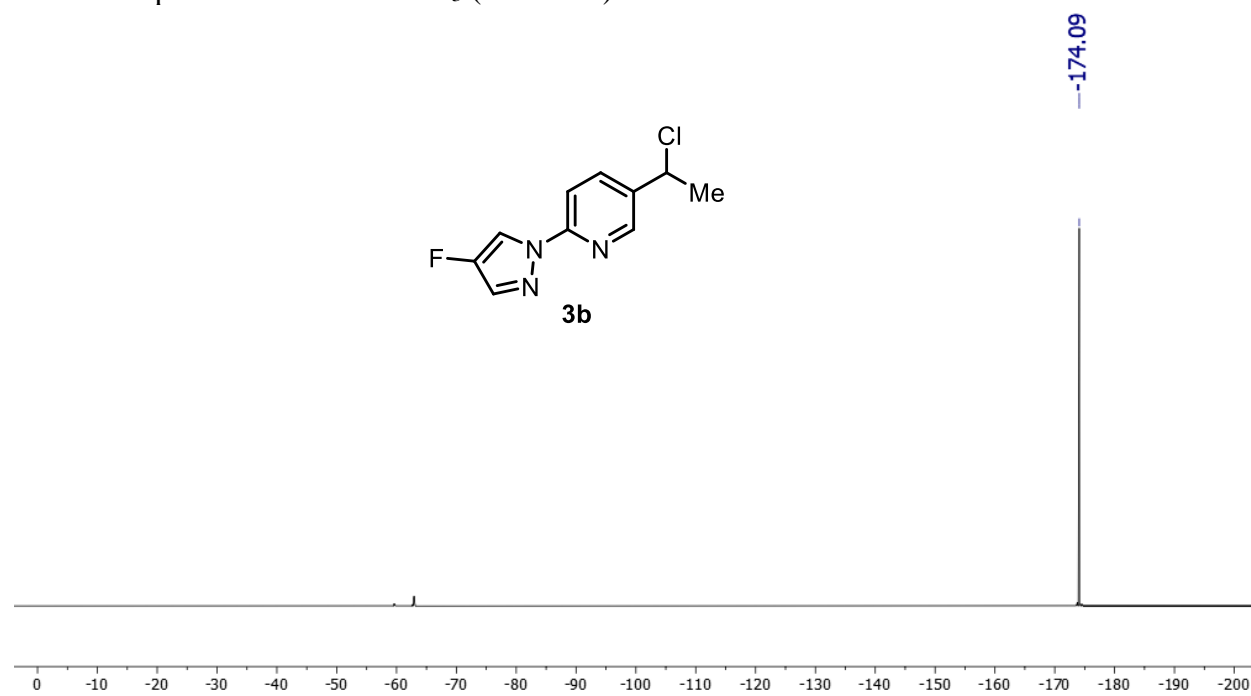
^1H NMR spectrum of **3b** in CDCl_3 (500 MHz).



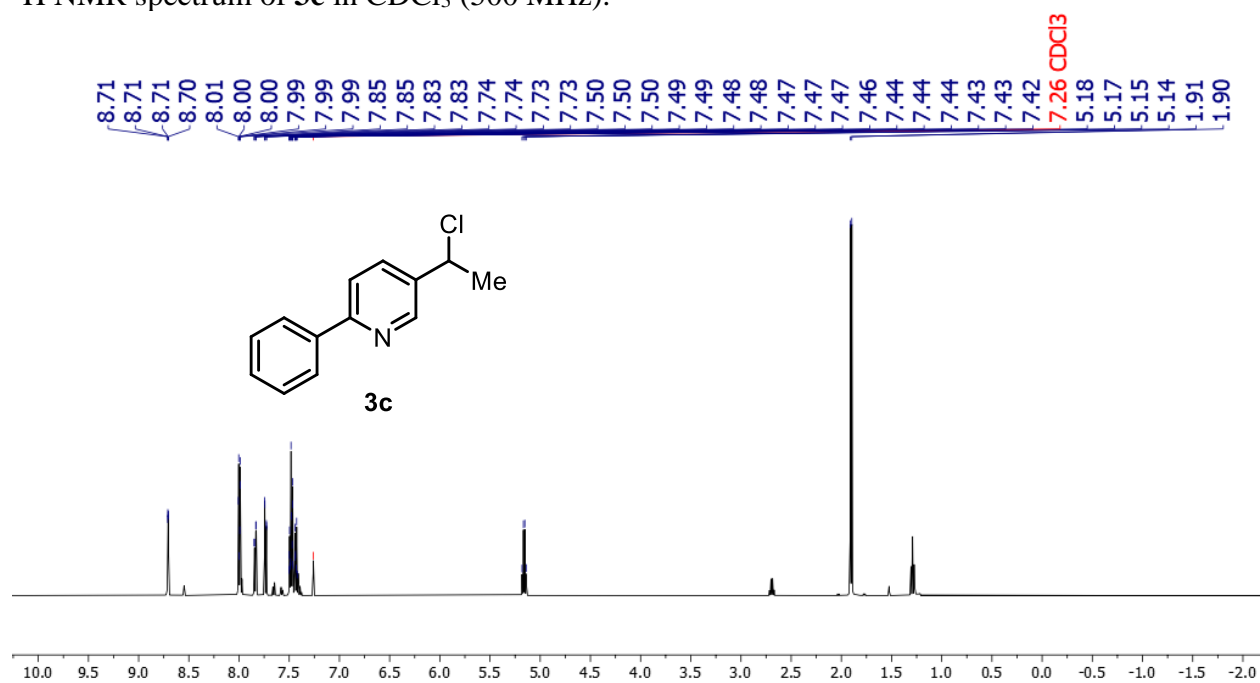
^{13}C NMR spectrum of **3b** in CDCl_3 (126 MHz).



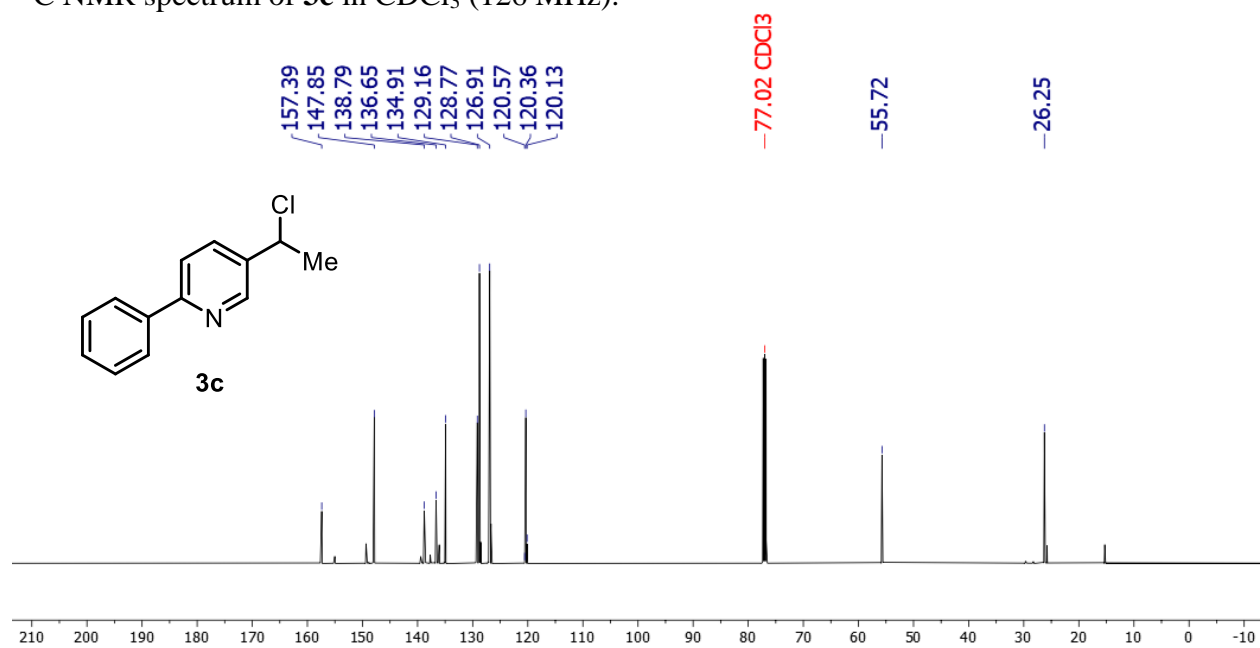
^{19}F NMR spectrum of **3b** in CDCl_3 (377 MHz).



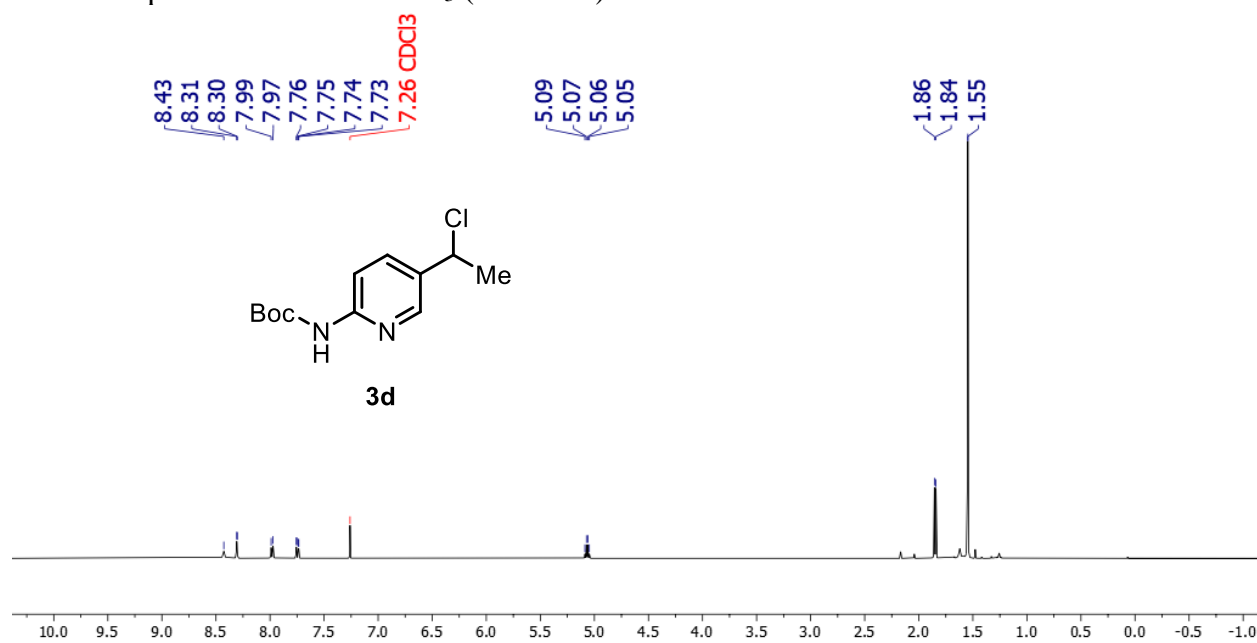
^1H NMR spectrum of **3c** in CDCl_3 (500 MHz).



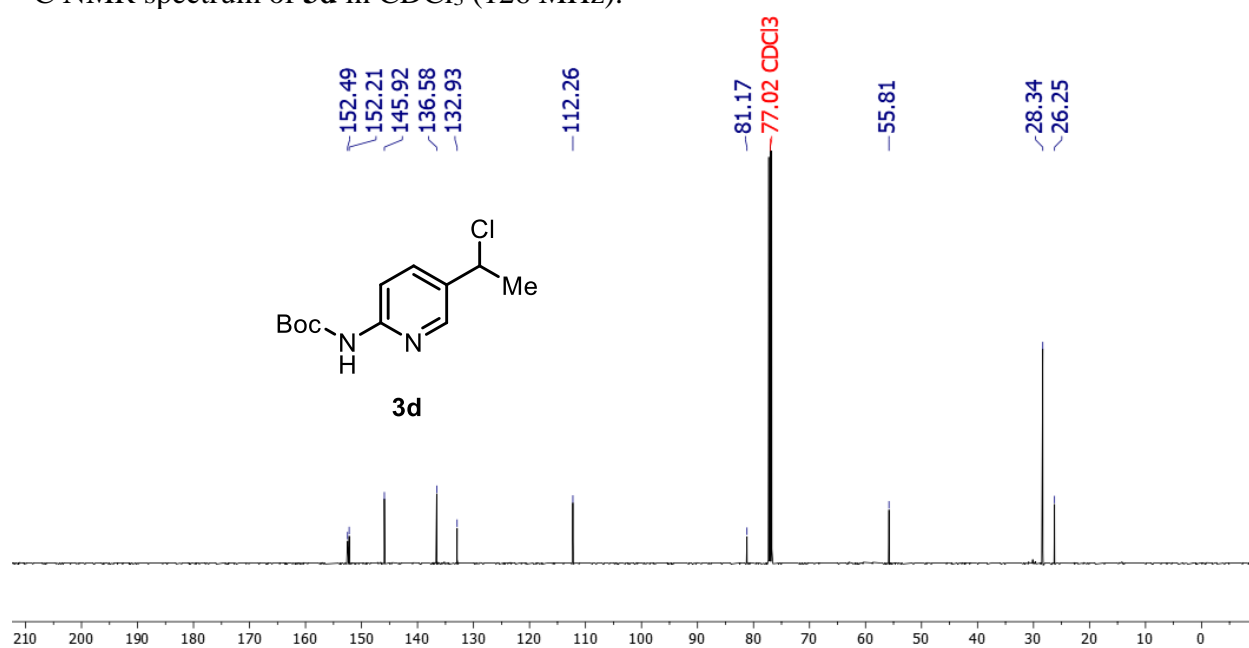
^{13}C NMR spectrum of **3c** in CDCl_3 (126 MHz).



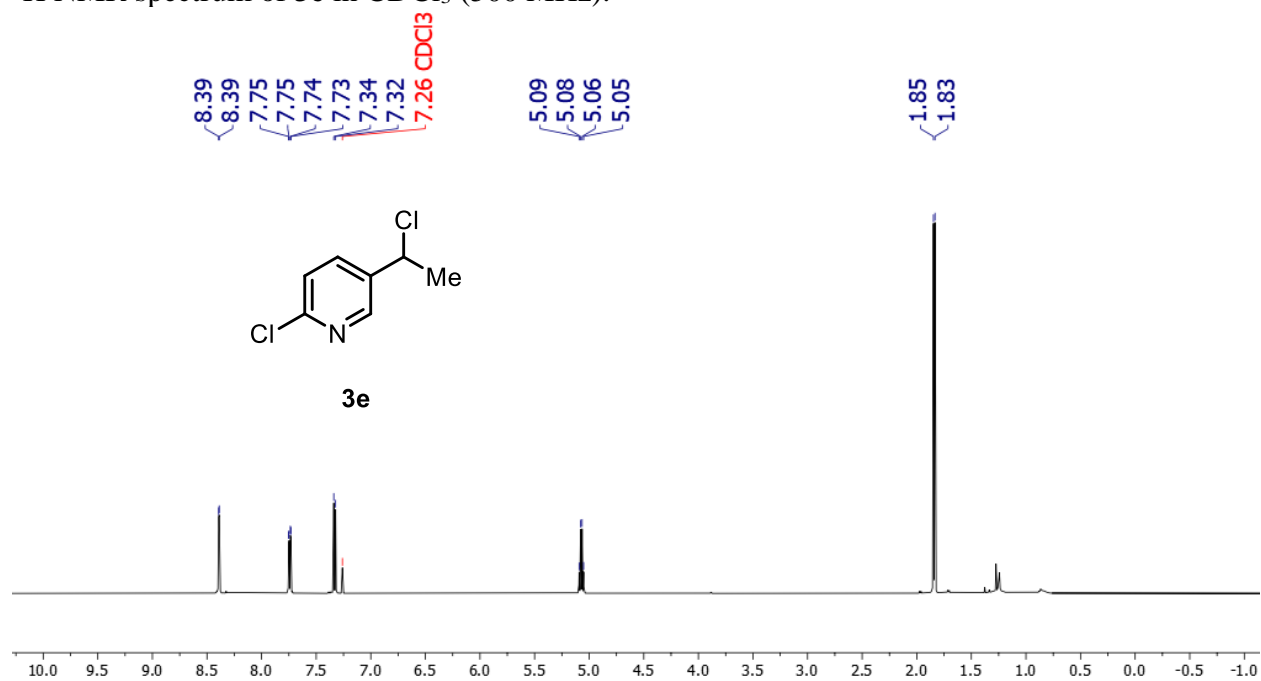
^1H NMR spectrum of **3d** in CDCl_3 (500 MHz).



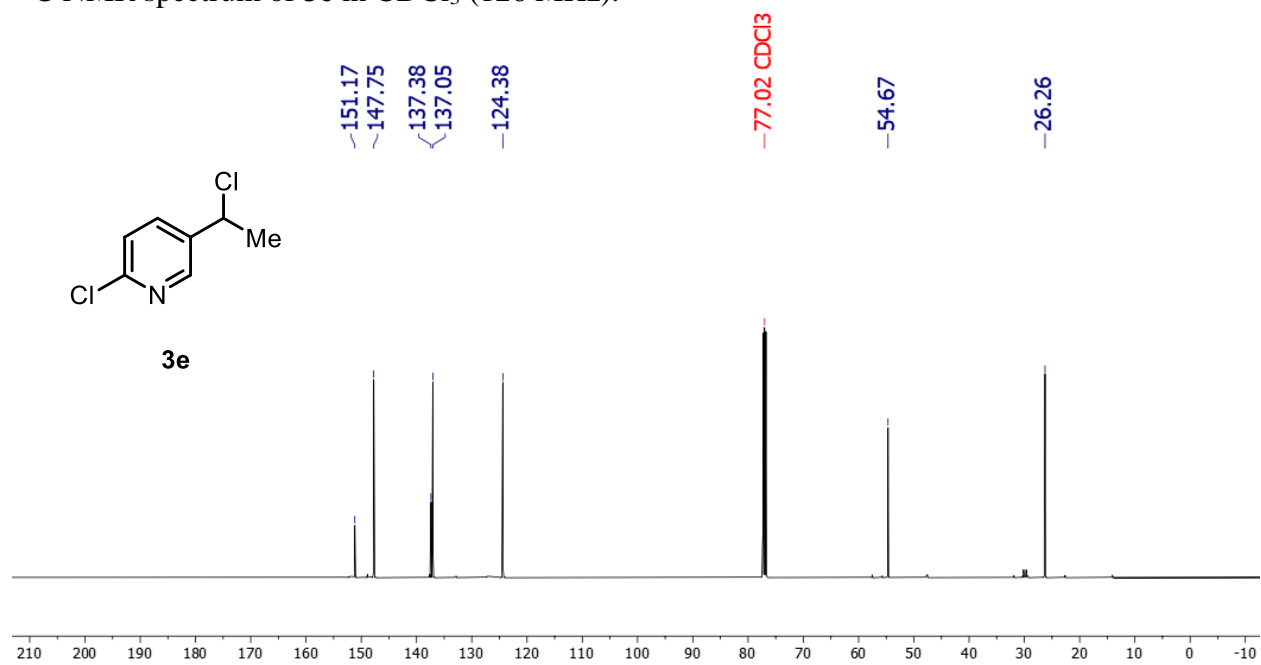
^{13}C NMR spectrum of **3d** in CDCl_3 (126 MHz).



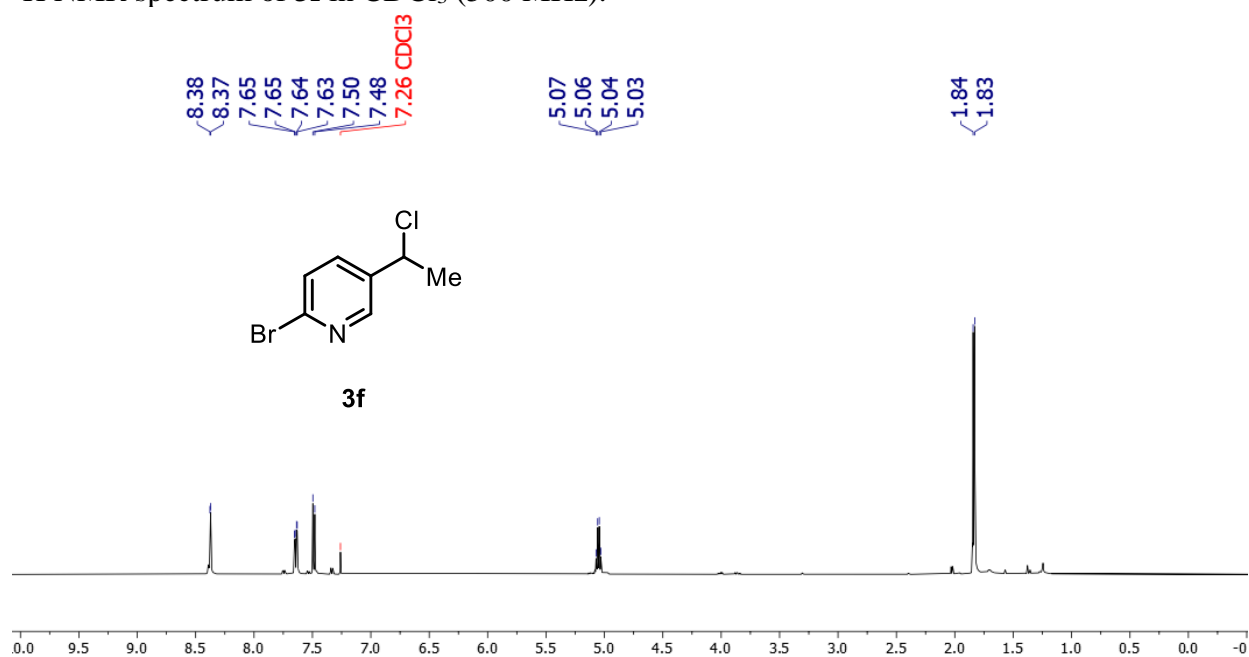
^1H NMR spectrum of **3e** in CDCl_3 (500 MHz).



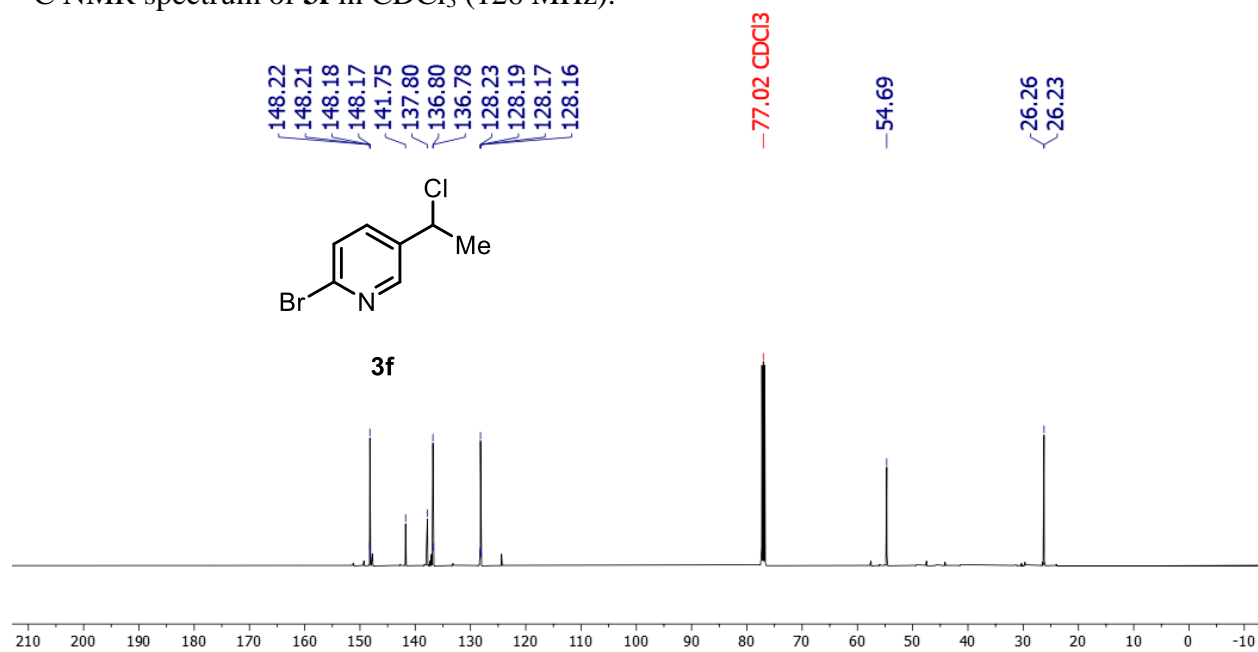
^{13}C NMR spectrum of **3e** in CDCl_3 (126 MHz).



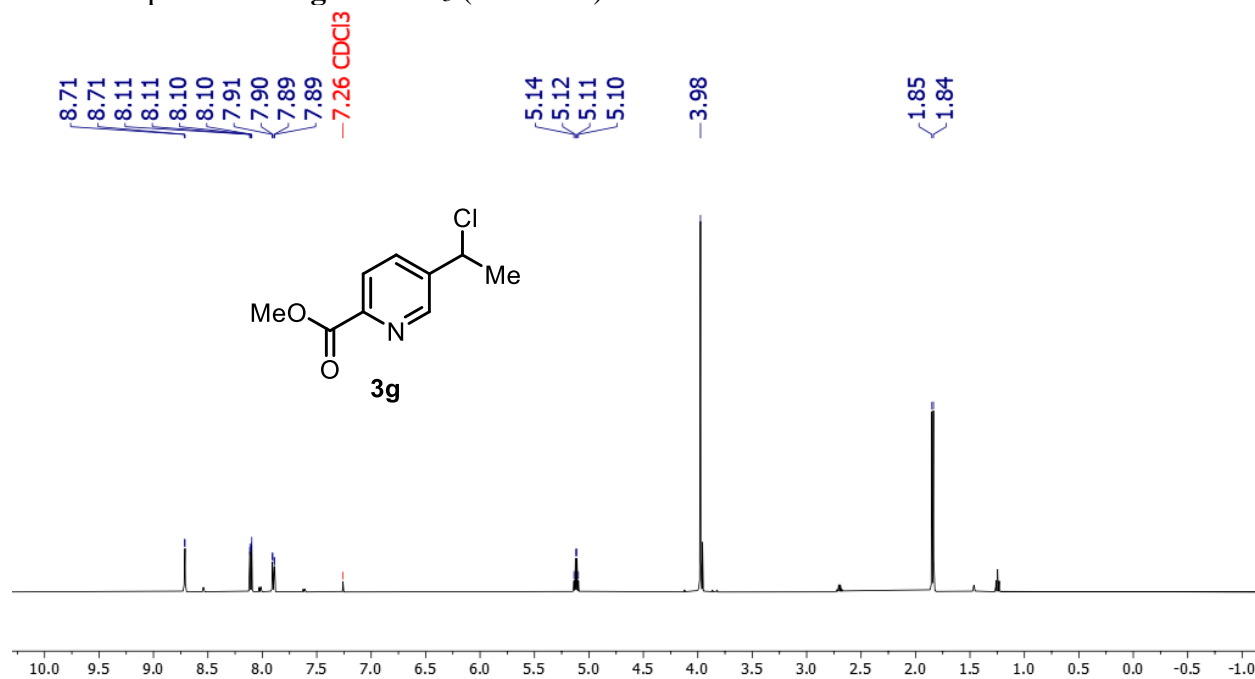
^1H NMR spectrum of **3f** in CDCl_3 (500 MHz).



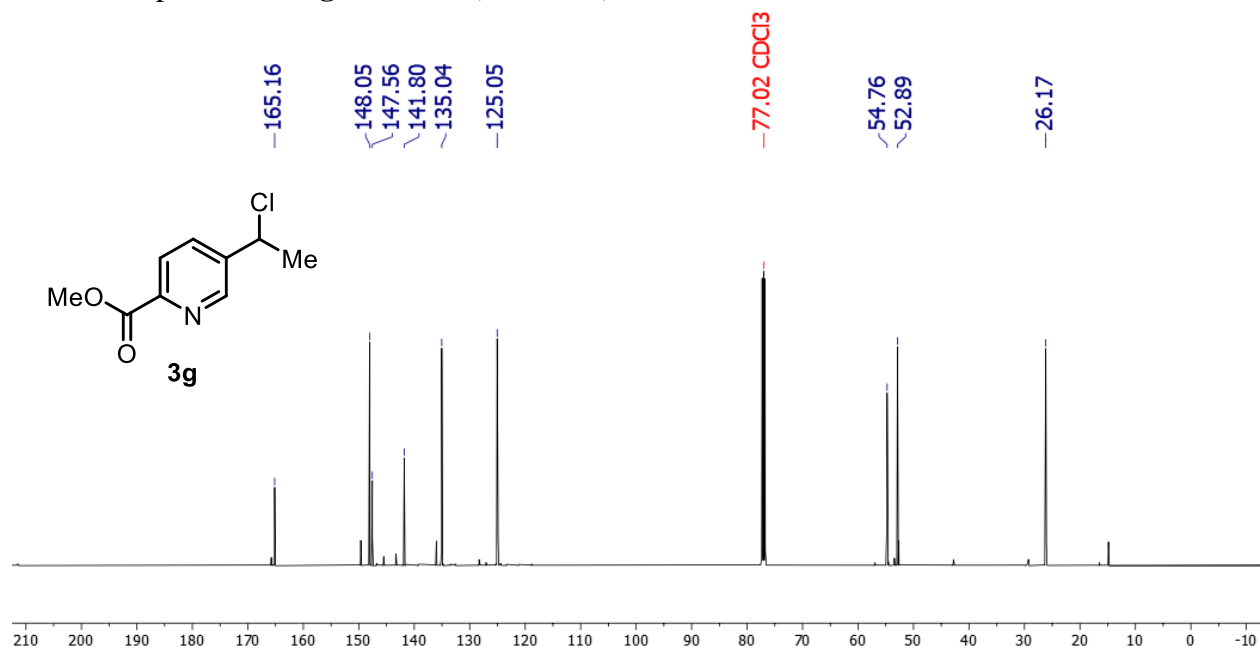
^{13}C NMR spectrum of **3f** in CDCl_3 (126 MHz).



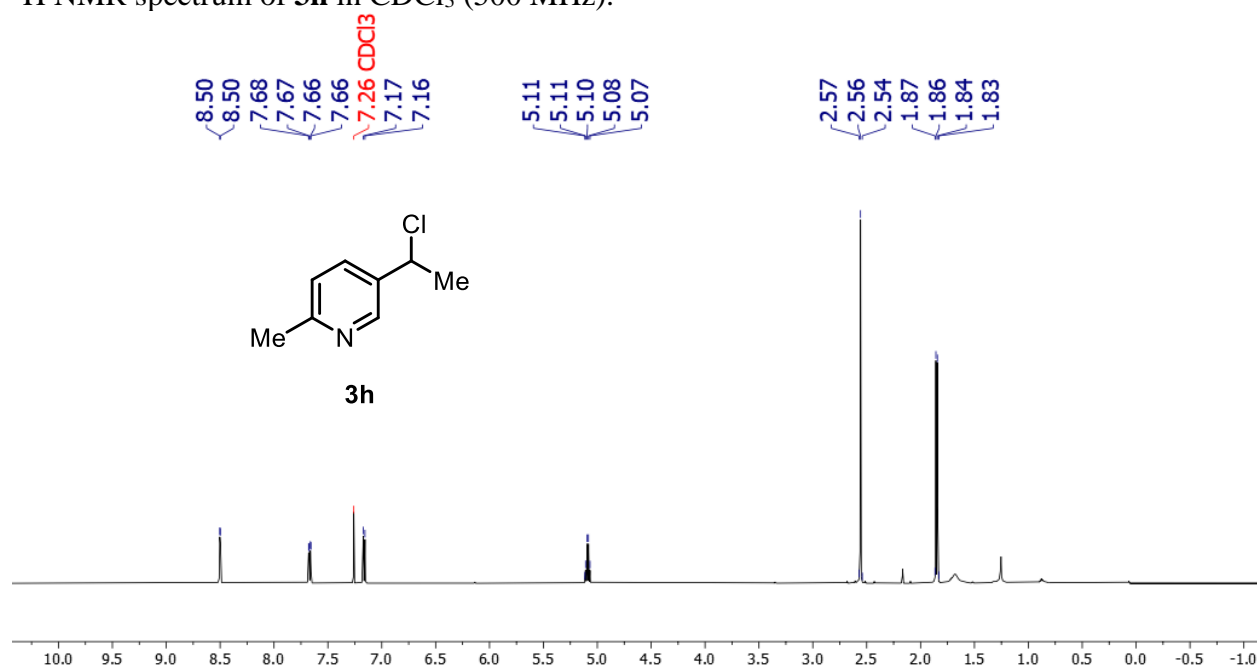
^1H NMR spectrum of **3g** in CDCl_3 (500 MHz).



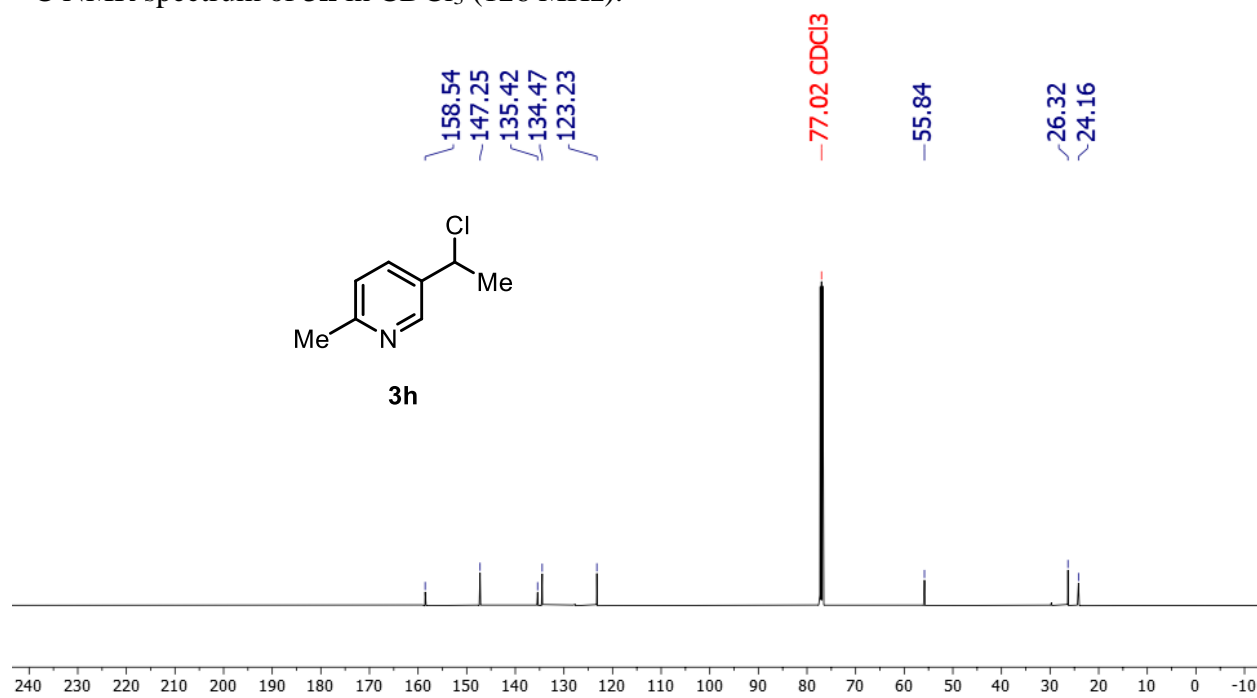
^{13}C NMR spectrum of **3g** in CDCl_3 (126 MHz).



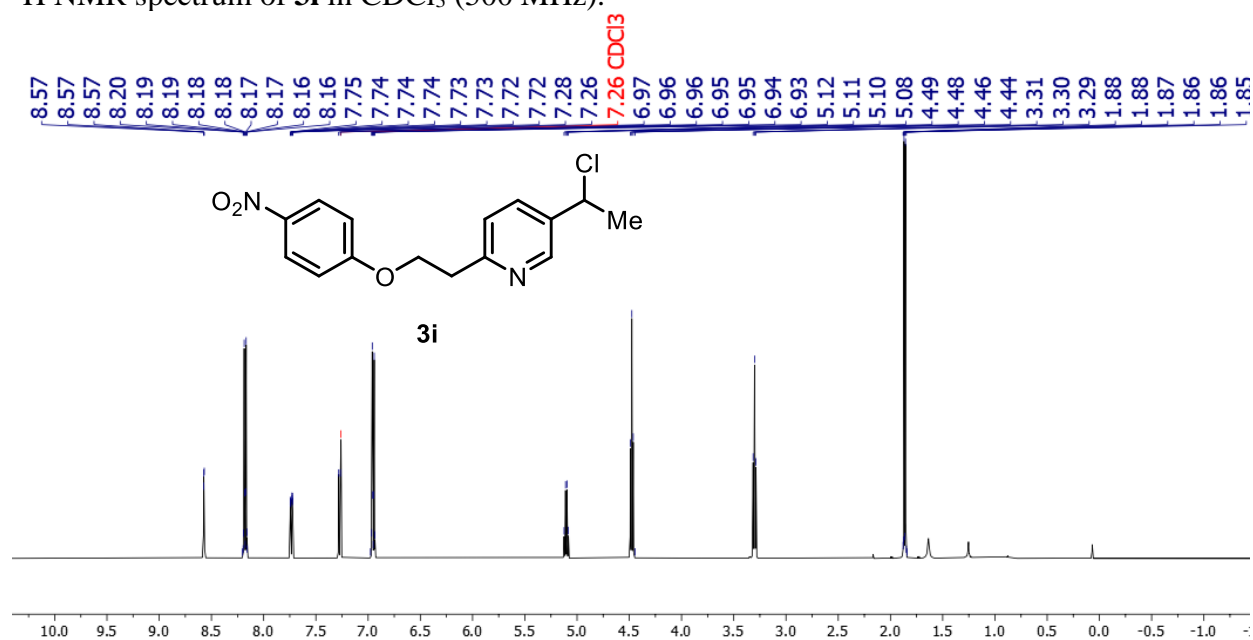
^1H NMR spectrum of **3h** in CDCl_3 (500 MHz).



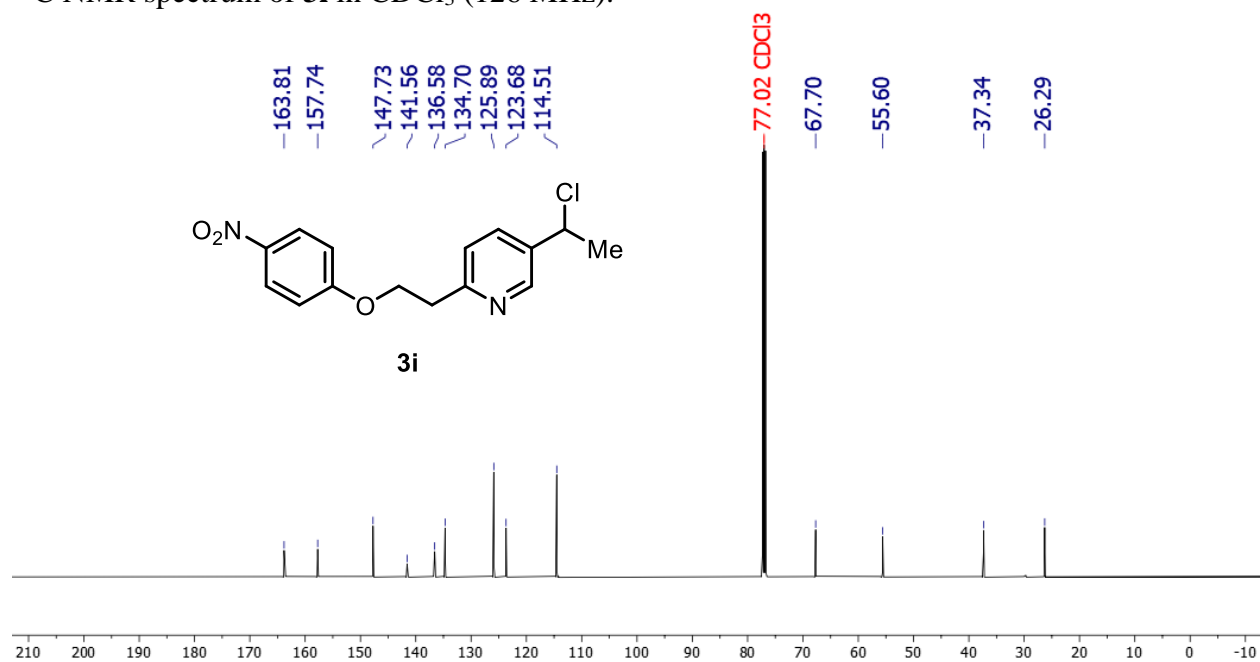
^{13}C NMR spectrum of **3h** in CDCl_3 (126 MHz).



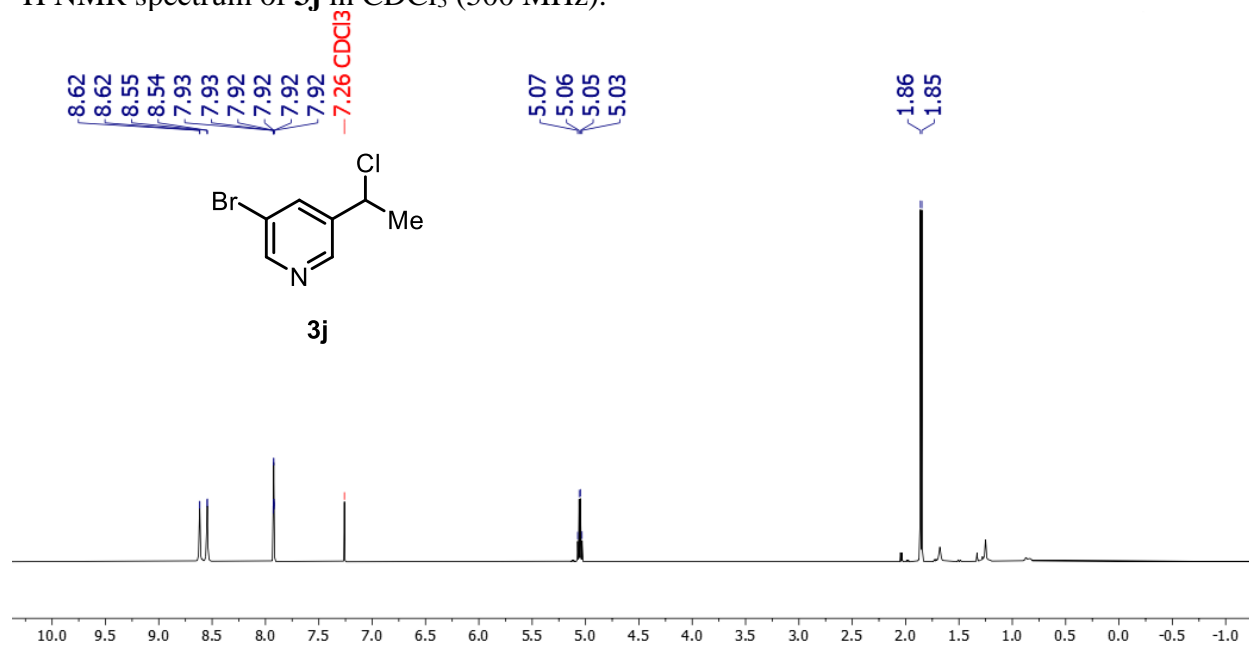
^1H NMR spectrum of **3i** in CDCl_3 (500 MHz).



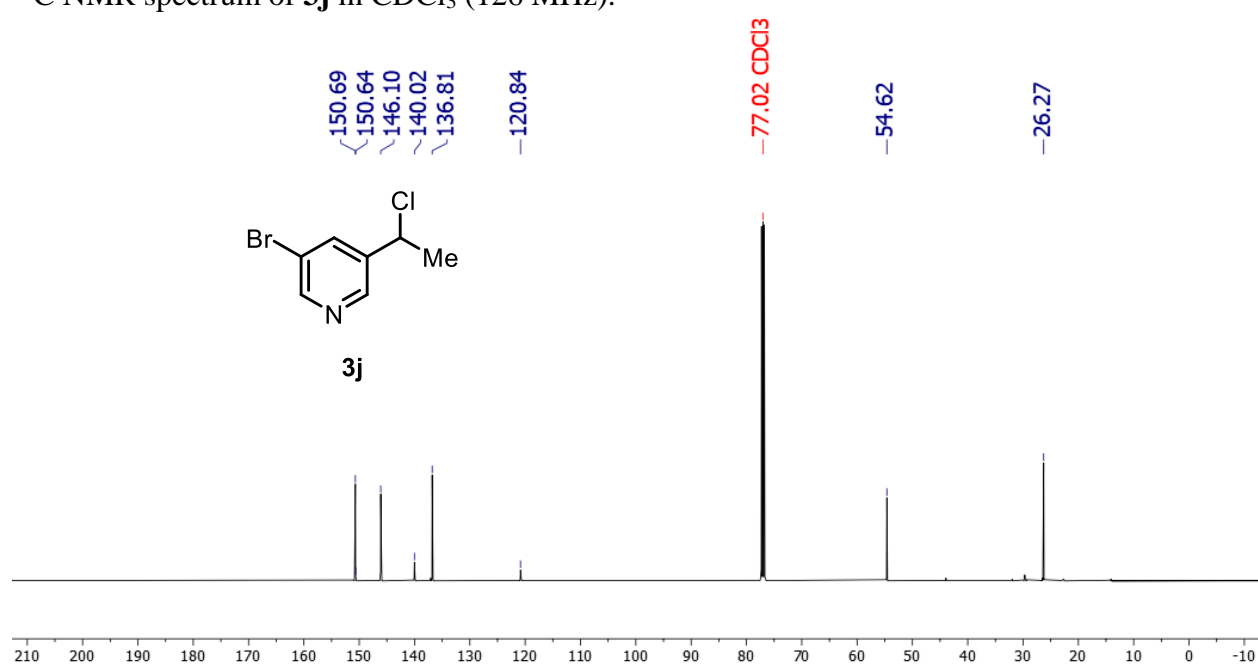
^{13}C NMR spectrum of **3i** in CDCl_3 (126 MHz).



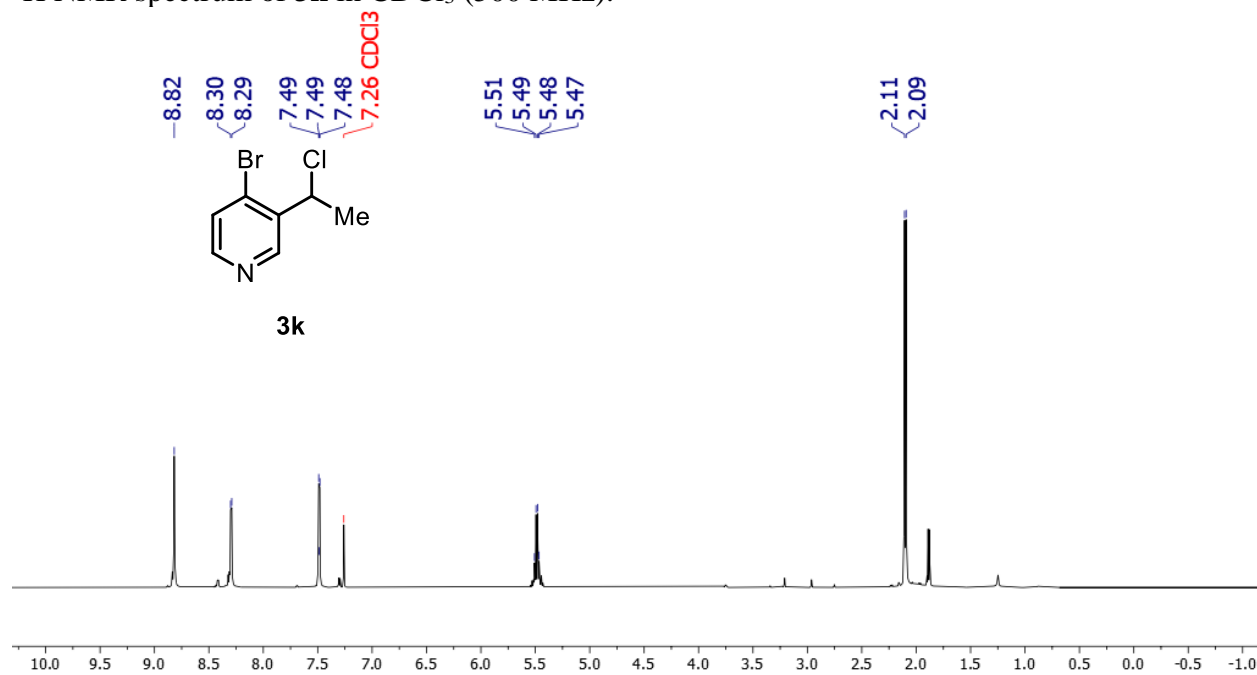
^1H NMR spectrum of **3j** in CDCl_3 (500 MHz).



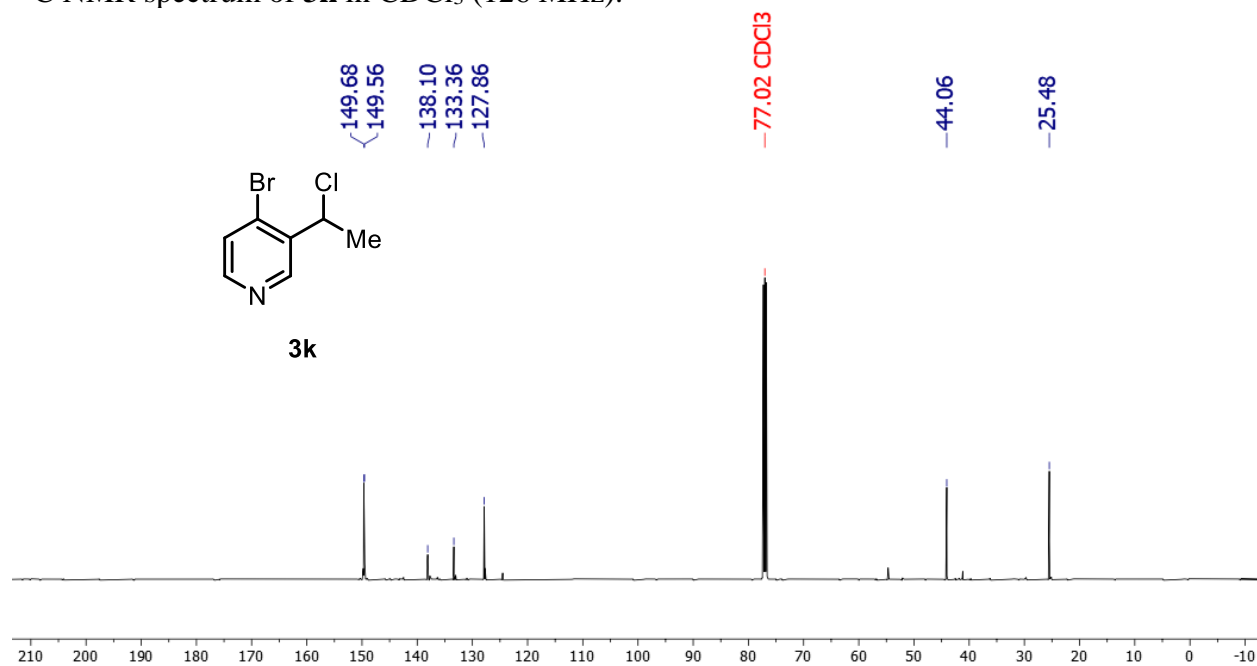
^{13}C NMR spectrum of **3j** in CDCl_3 (126 MHz).



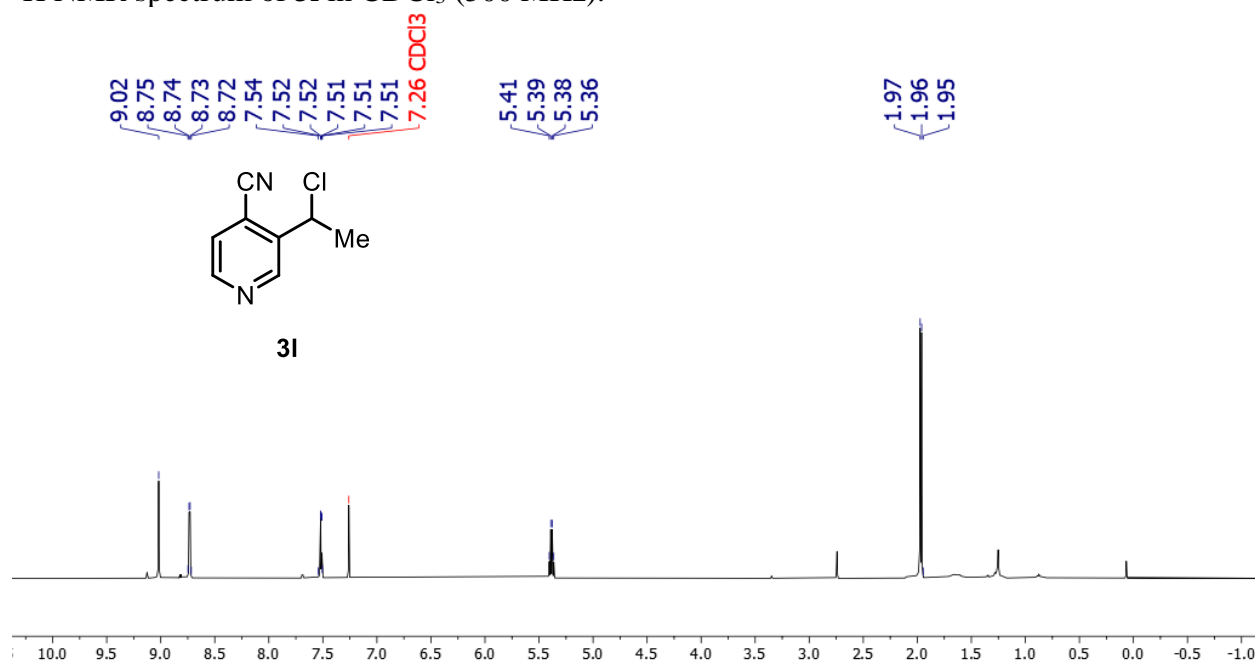
^1H NMR spectrum of **3k** in CDCl_3 (500 MHz).



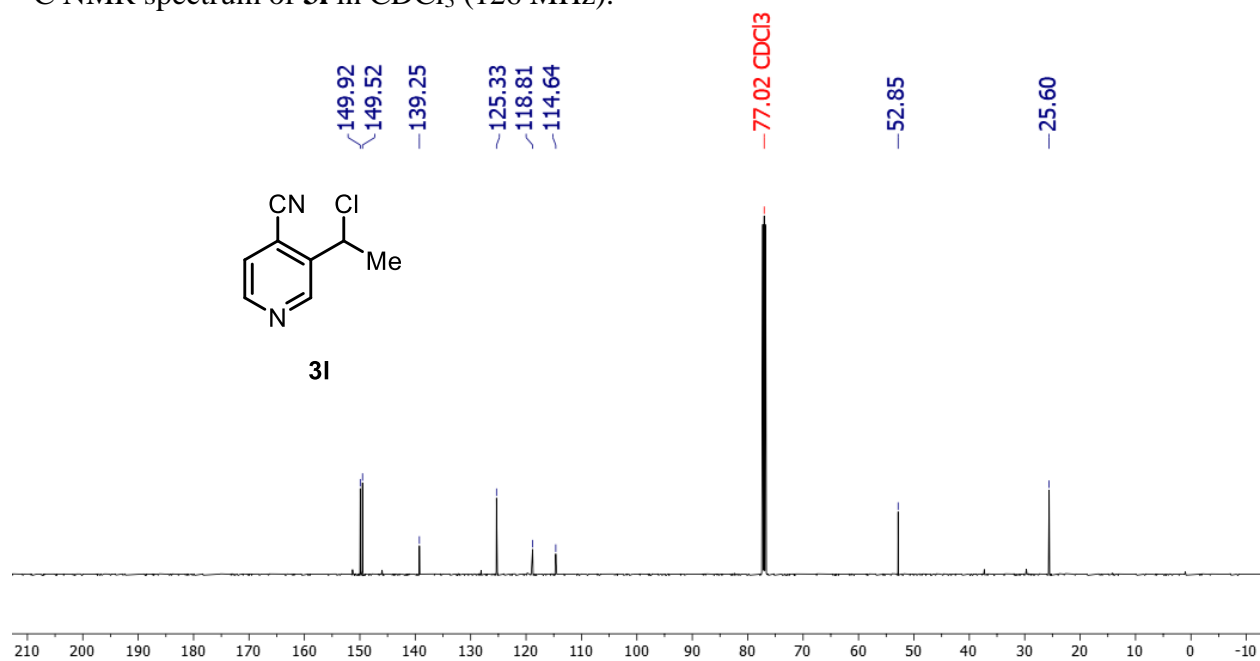
^{13}C NMR spectrum of **3k** in CDCl_3 (126 MHz).



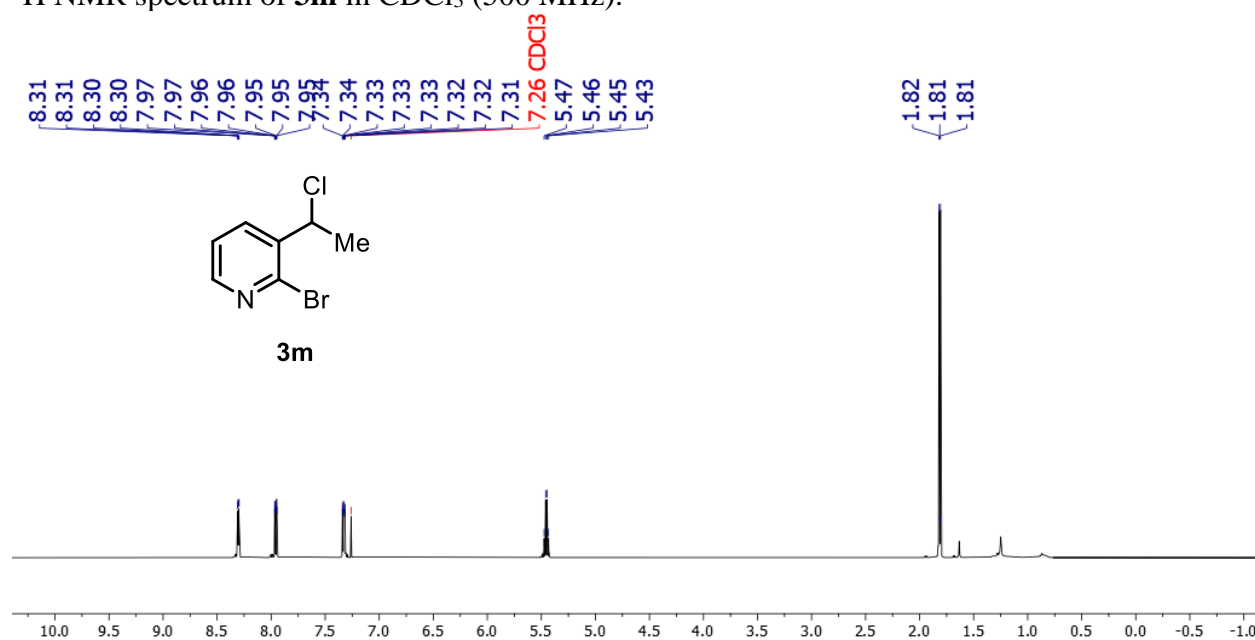
^1H NMR spectrum of **31** in CDCl_3 (500 MHz).



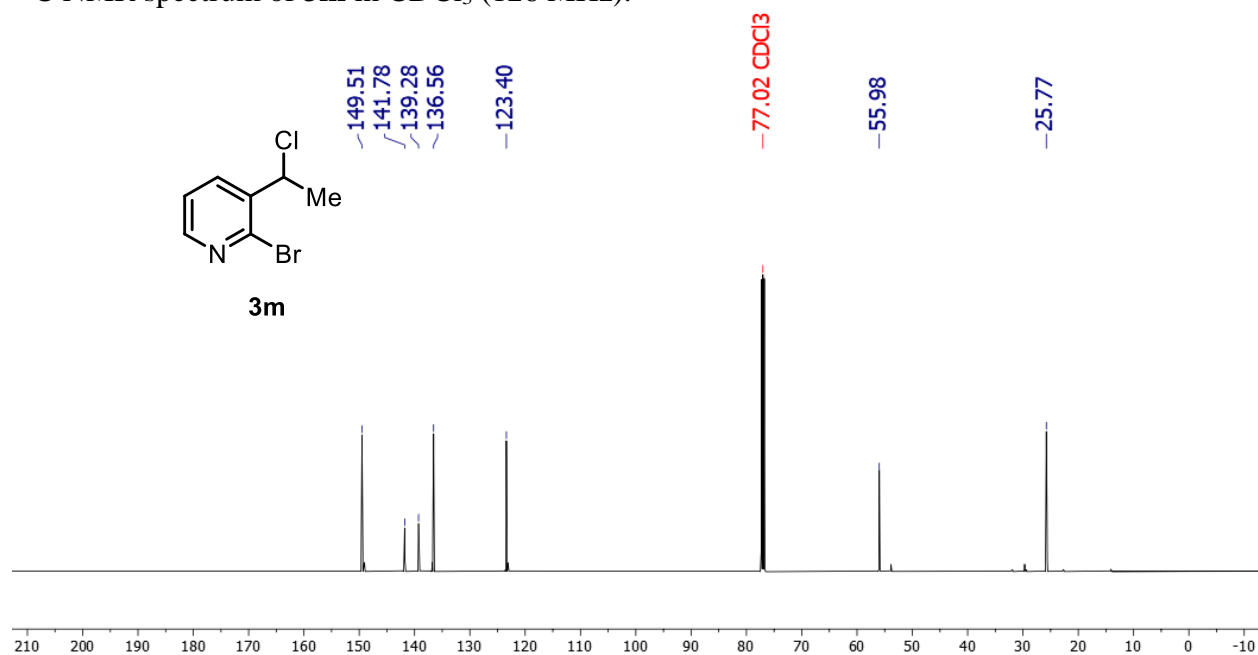
^{13}C NMR spectrum of **31** in CDCl_3 (126 MHz).



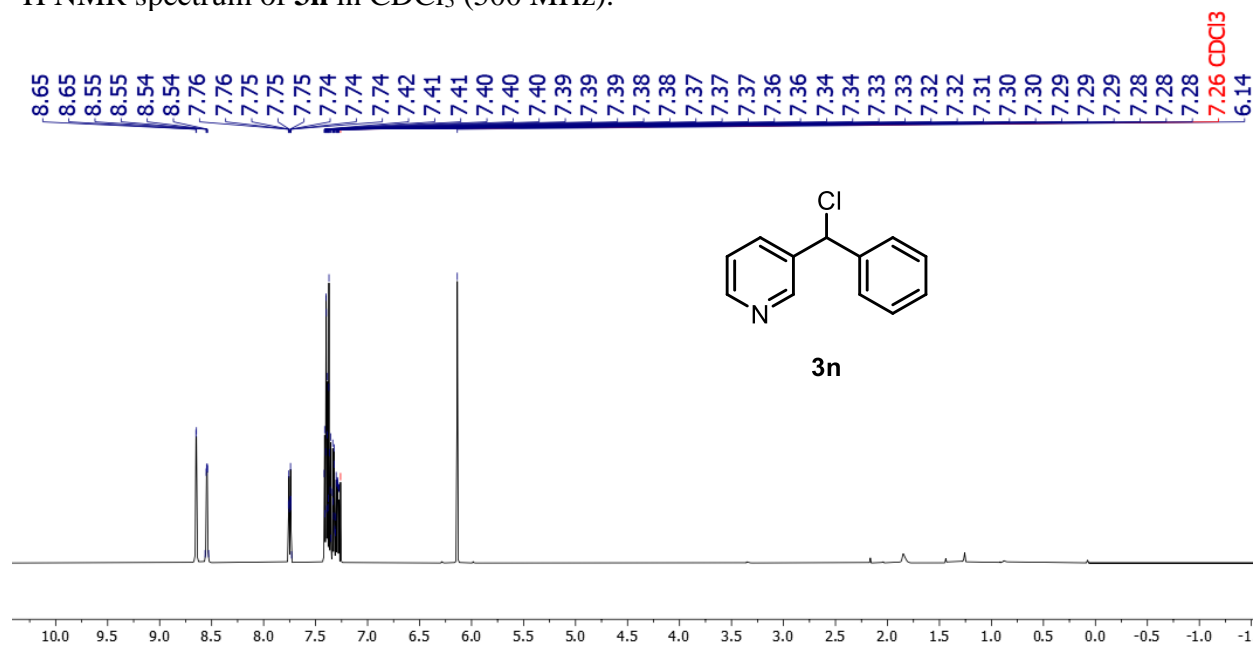
^1H NMR spectrum of **3m** in CDCl_3 (500 MHz).



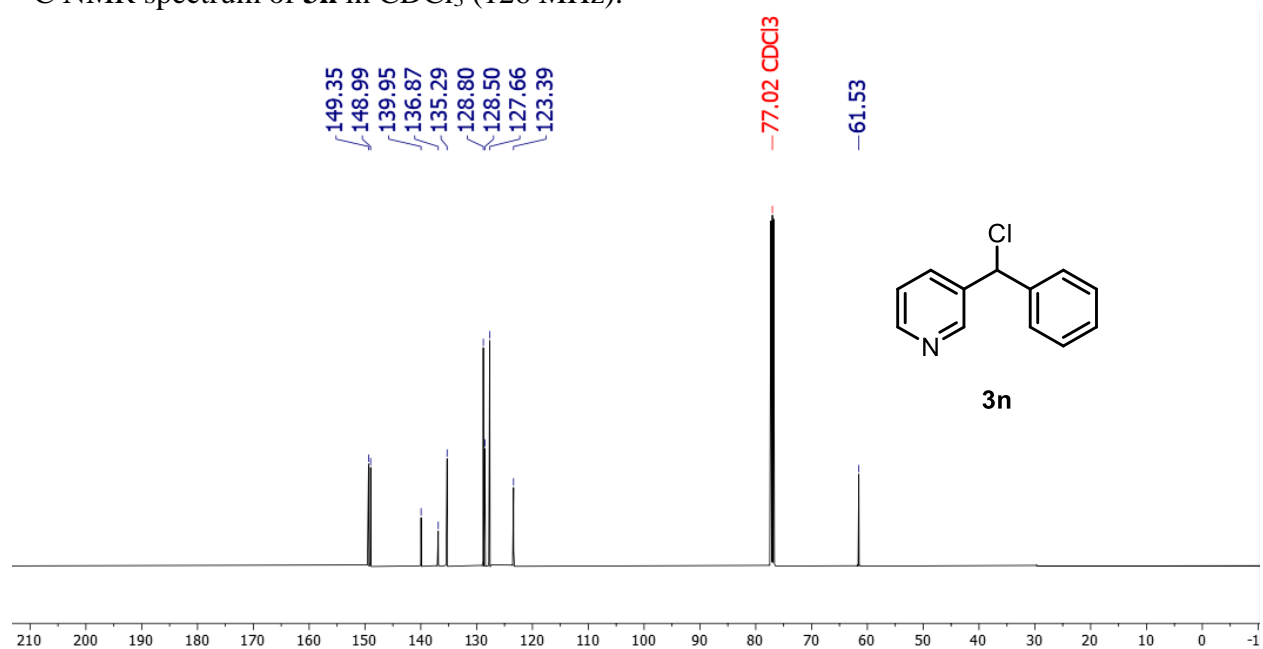
^{13}C NMR spectrum of **3m** in CDCl_3 (126 MHz).



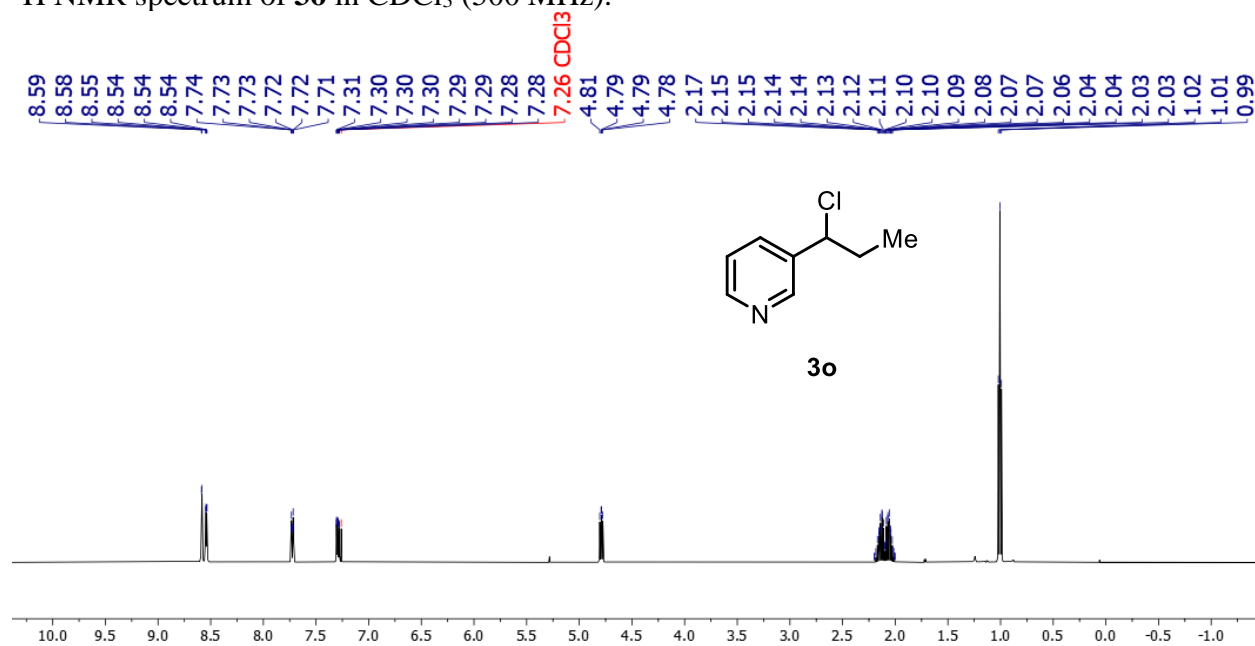
^1H NMR spectrum of **3n** in CDCl_3 (500 MHz).



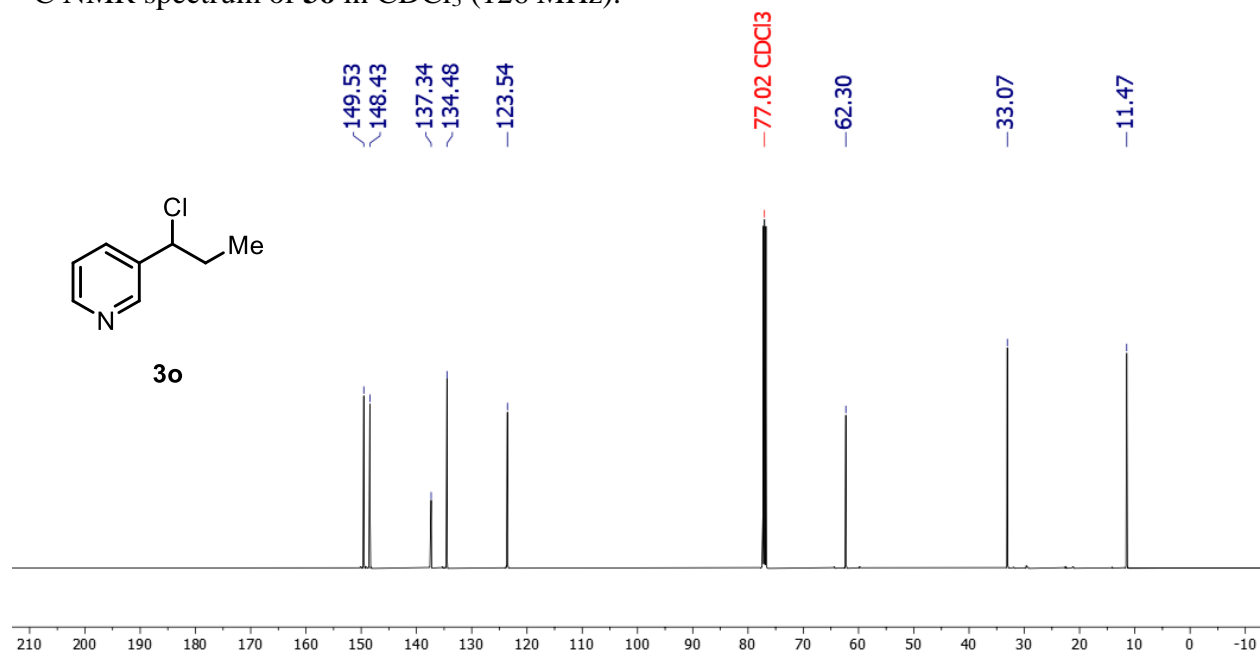
^{13}C NMR spectrum of **3n** in CDCl_3 (126 MHz).



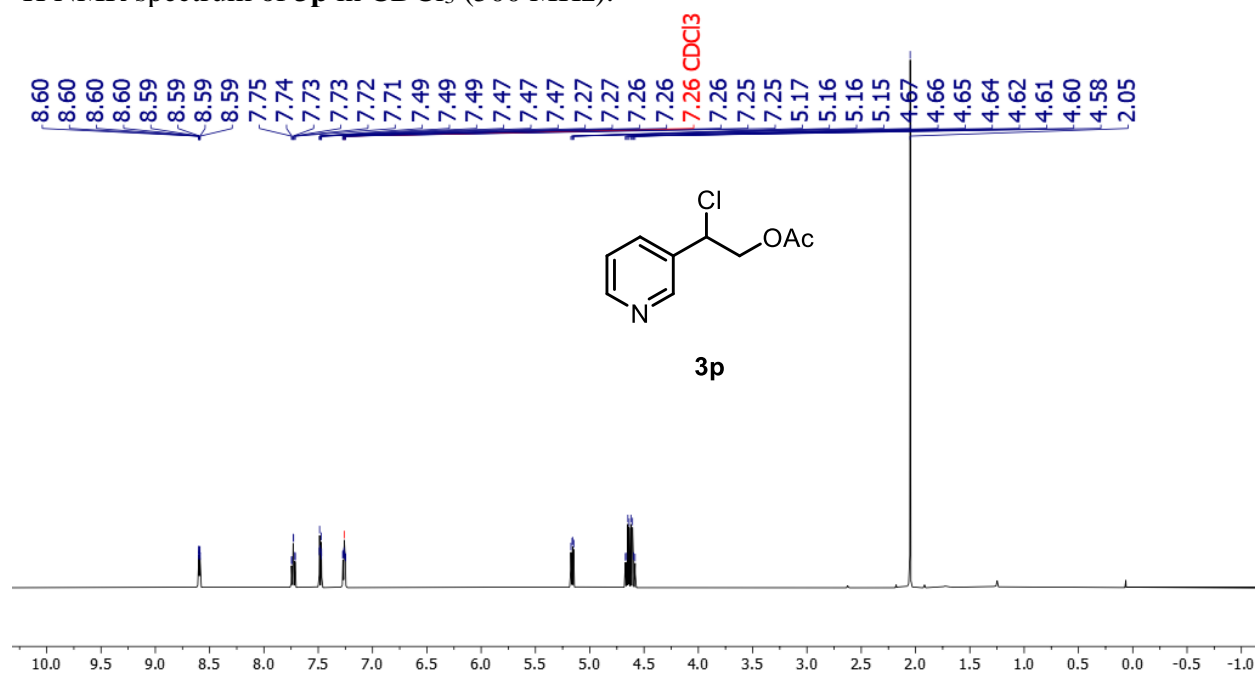
^1H NMR spectrum of **3o** in CDCl_3 (500 MHz).



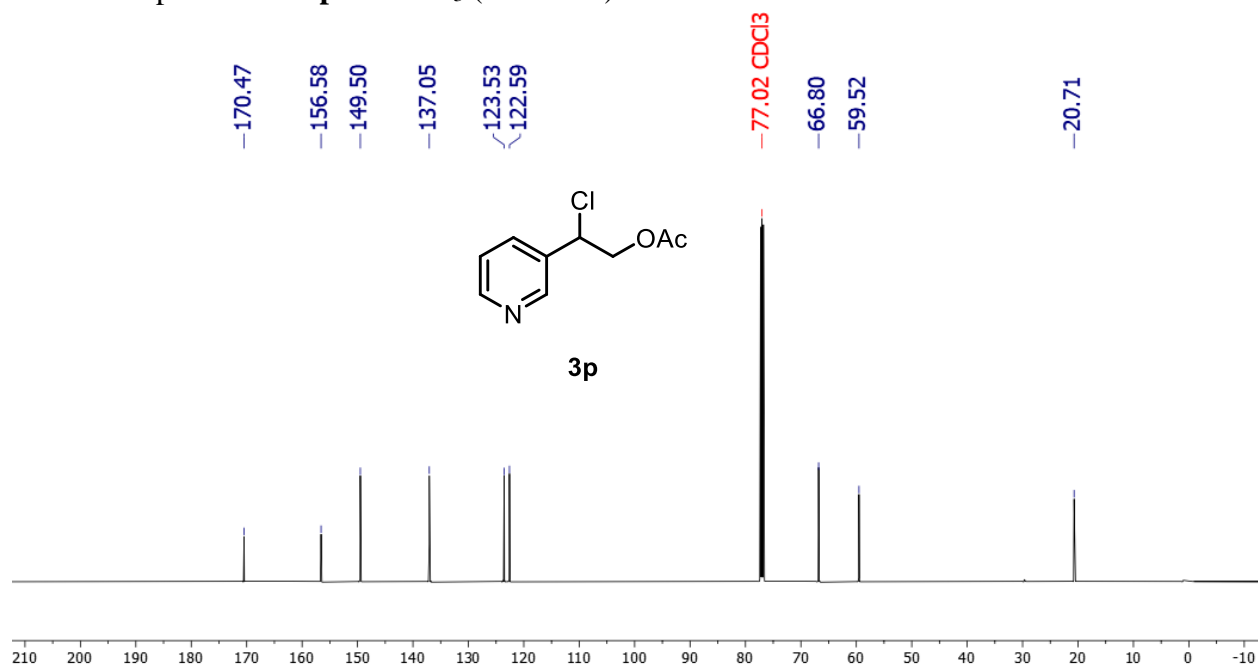
^{13}C NMR spectrum of **3o** in CDCl_3 (126 MHz).



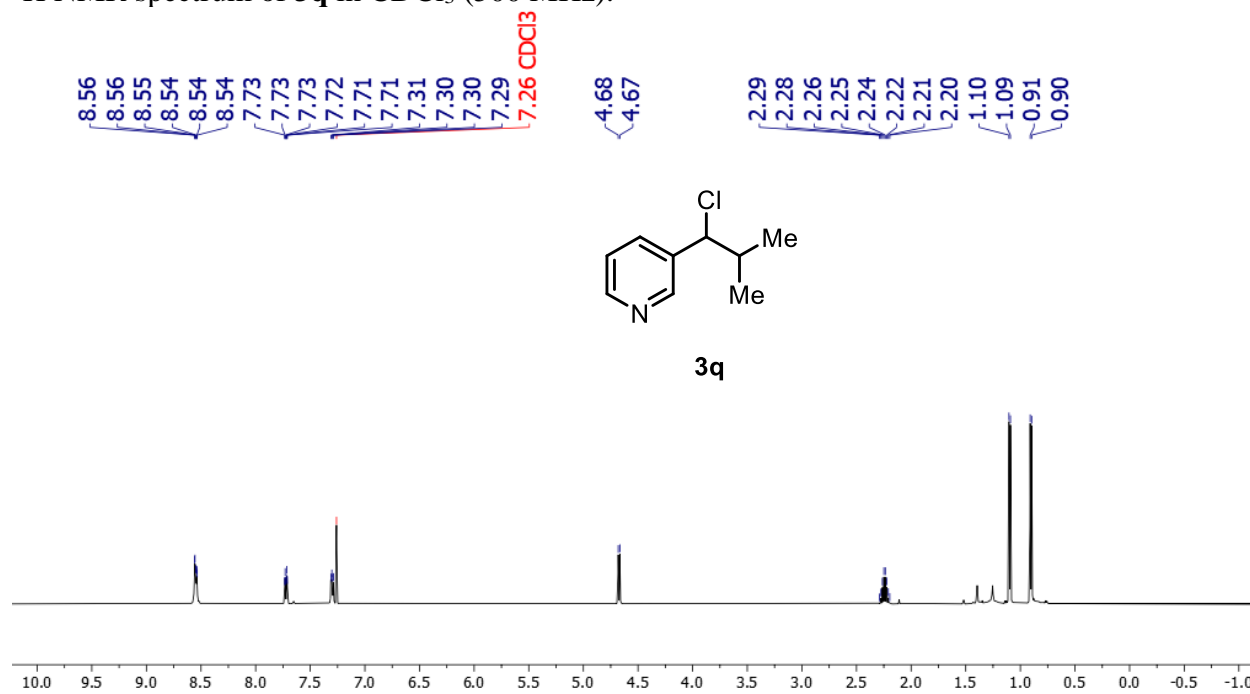
^1H NMR spectrum of **3p** in CDCl_3 (500 MHz).



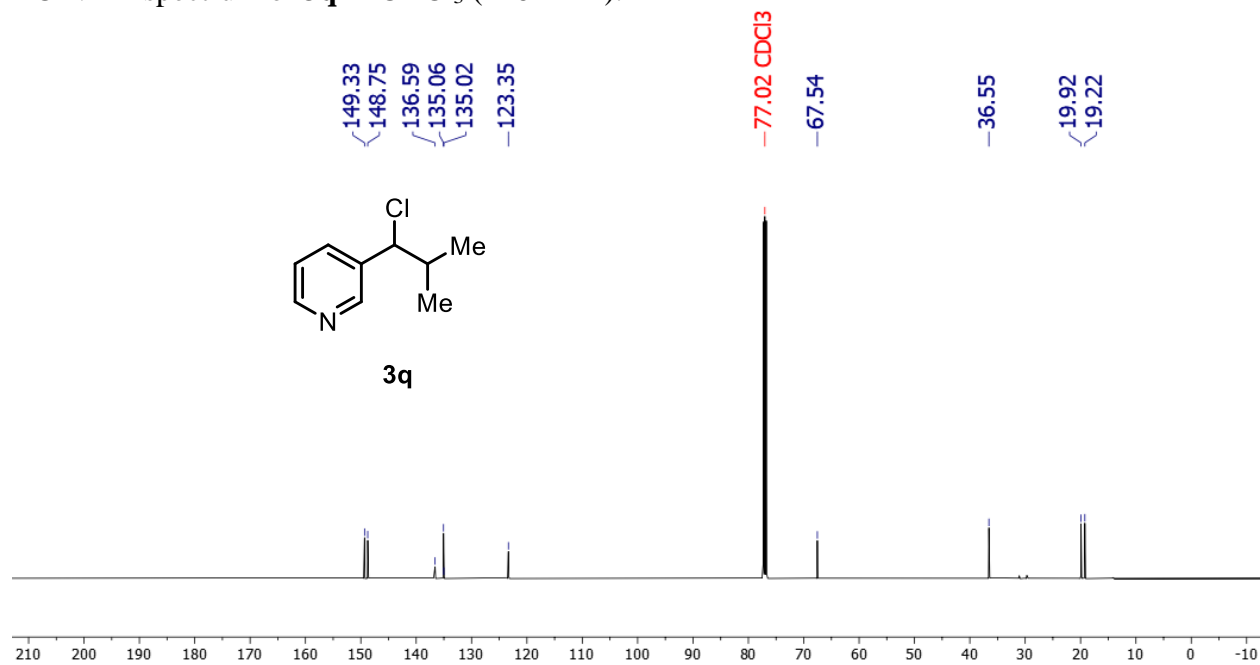
^{13}C NMR spectrum of **3p** in CDCl_3 (126 MHz).



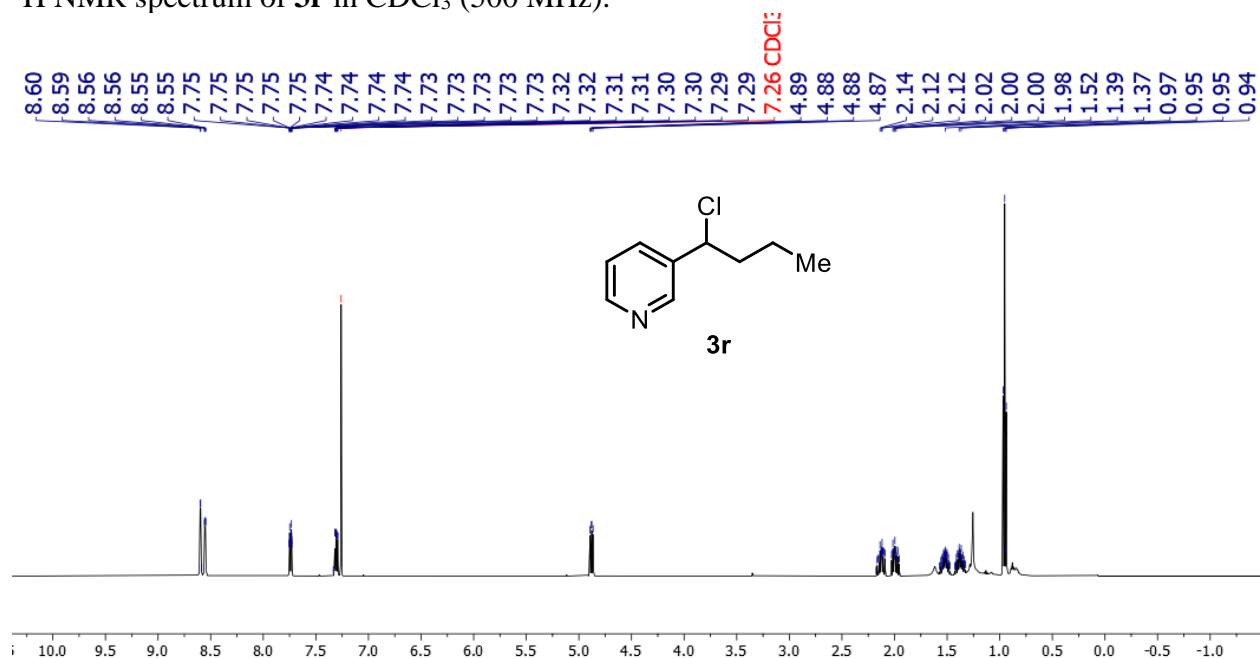
^1H NMR spectrum of **3q** in CDCl_3 (500 MHz).



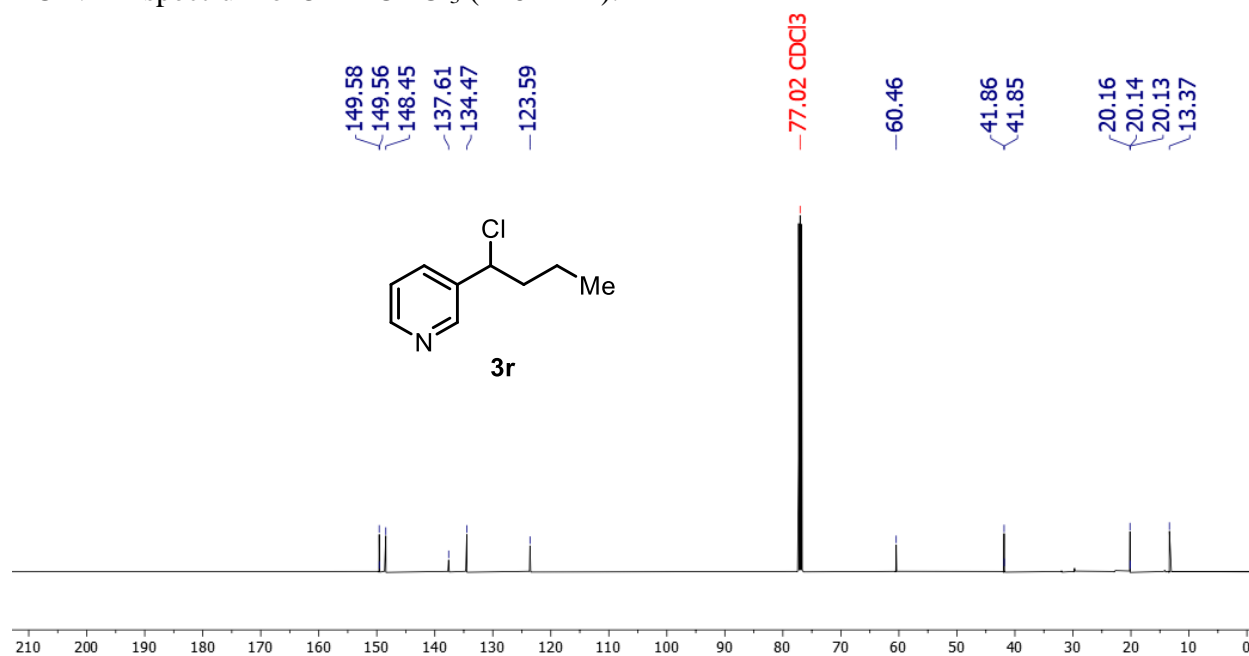
^{13}C NMR spectrum of **3q** in CDCl_3 (126 MHz).



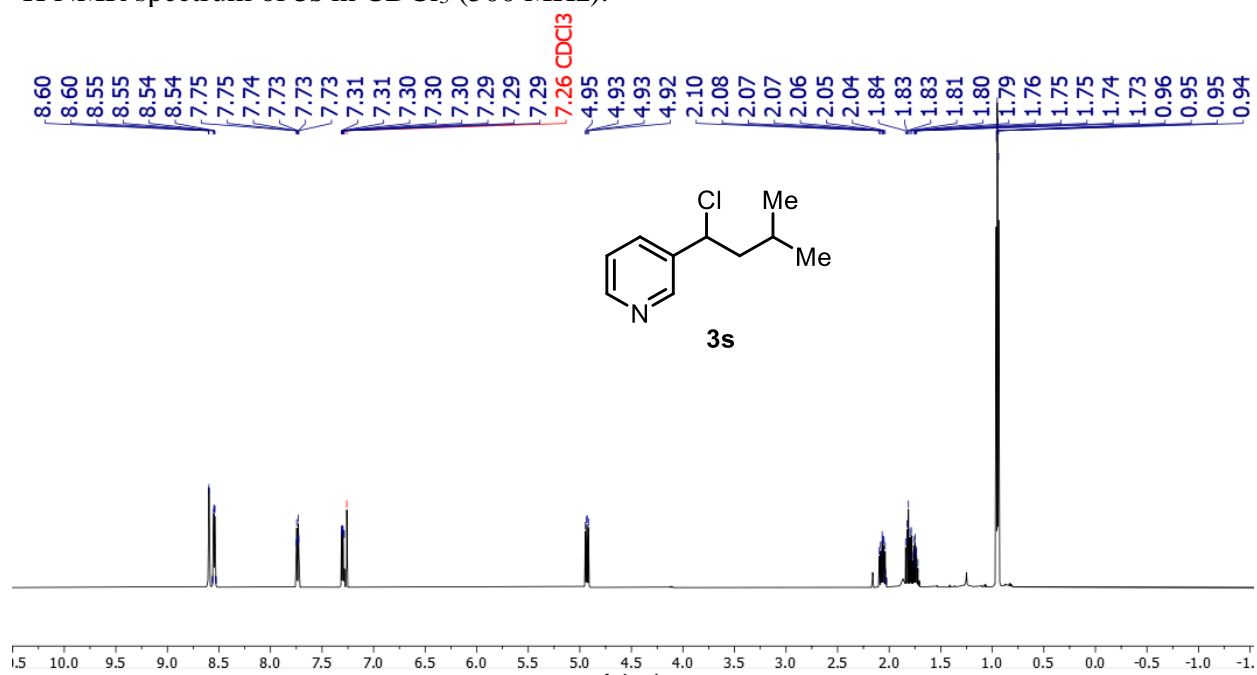
^1H NMR spectrum of **3r** in CDCl_3 (500 MHz).



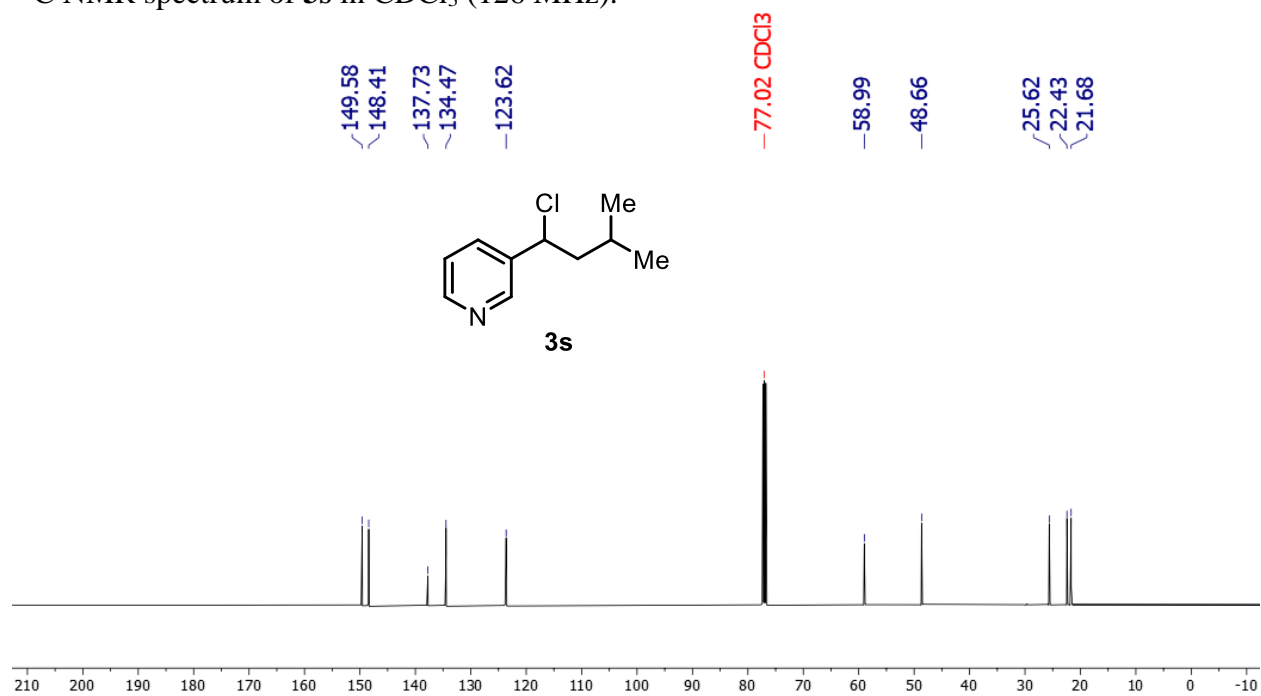
^{13}C NMR spectrum of **3r** in CDCl_3 (126 MHz).



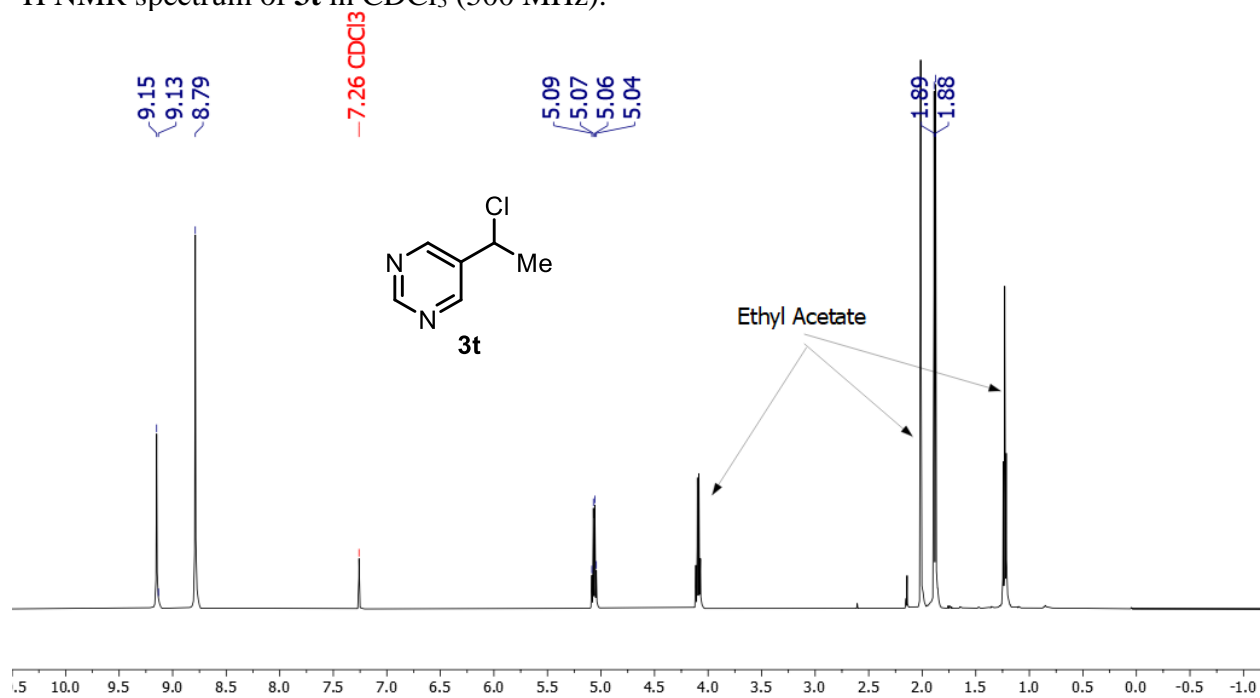
^1H NMR spectrum of **3s** in CDCl_3 (500 MHz).



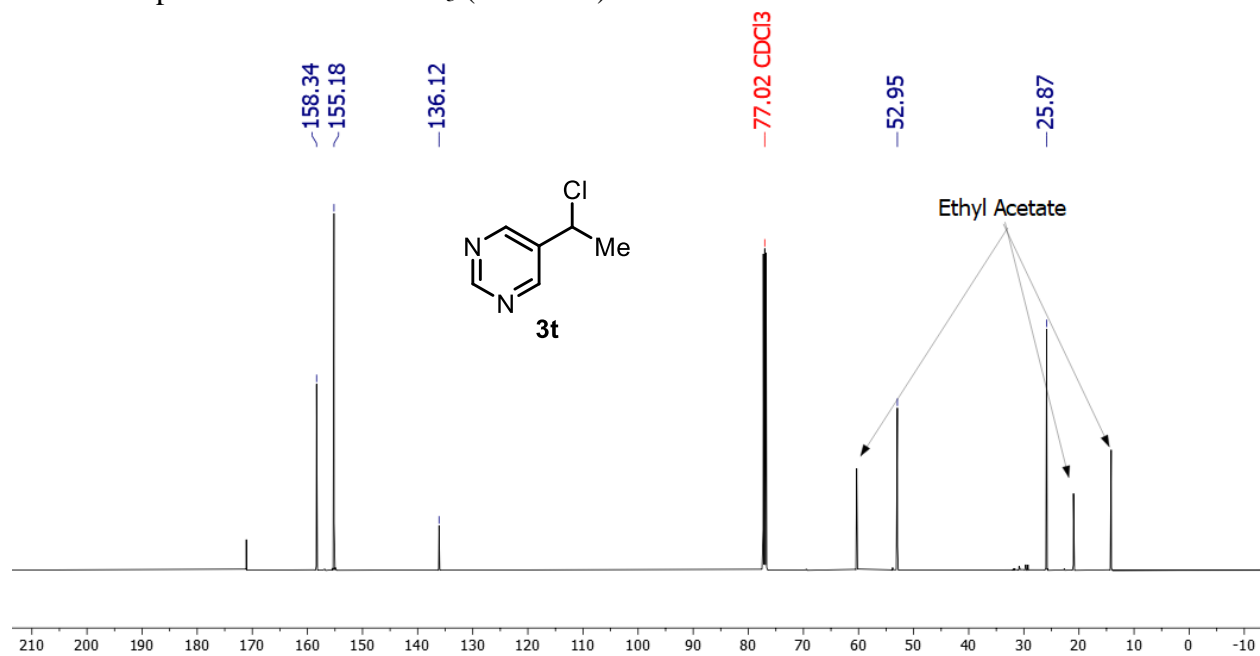
^{13}C NMR spectrum of **3s** in CDCl_3 (126 MHz).



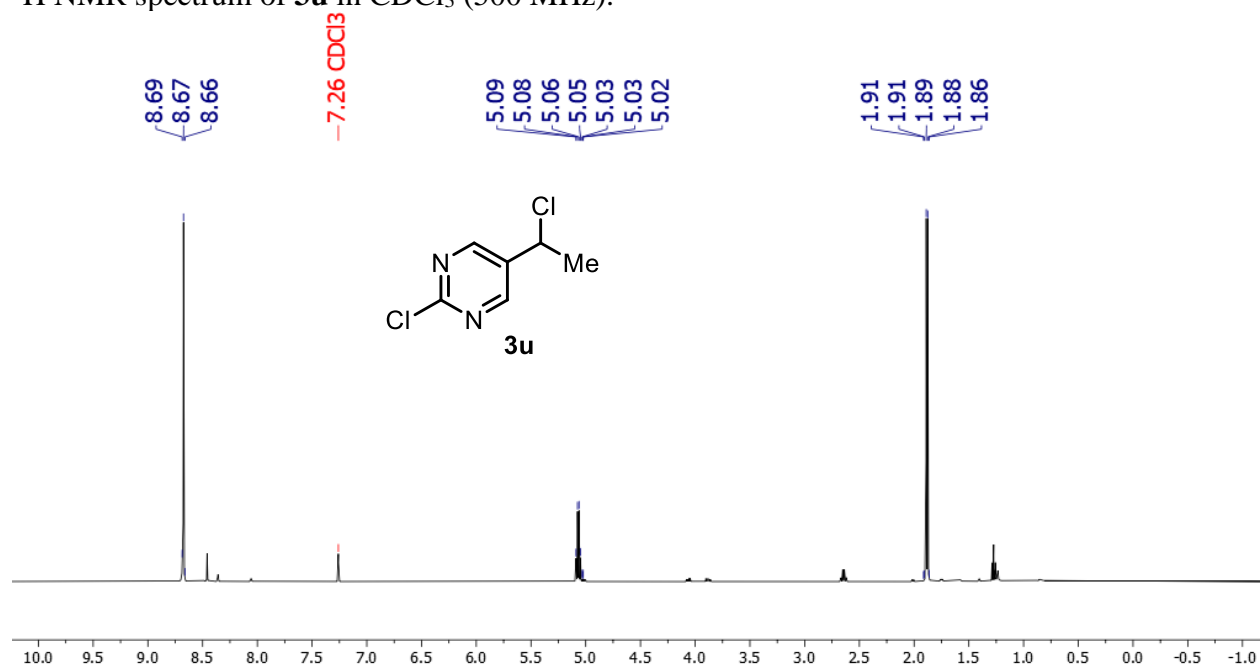
^1H NMR spectrum of **3t** in CDCl_3 (500 MHz).



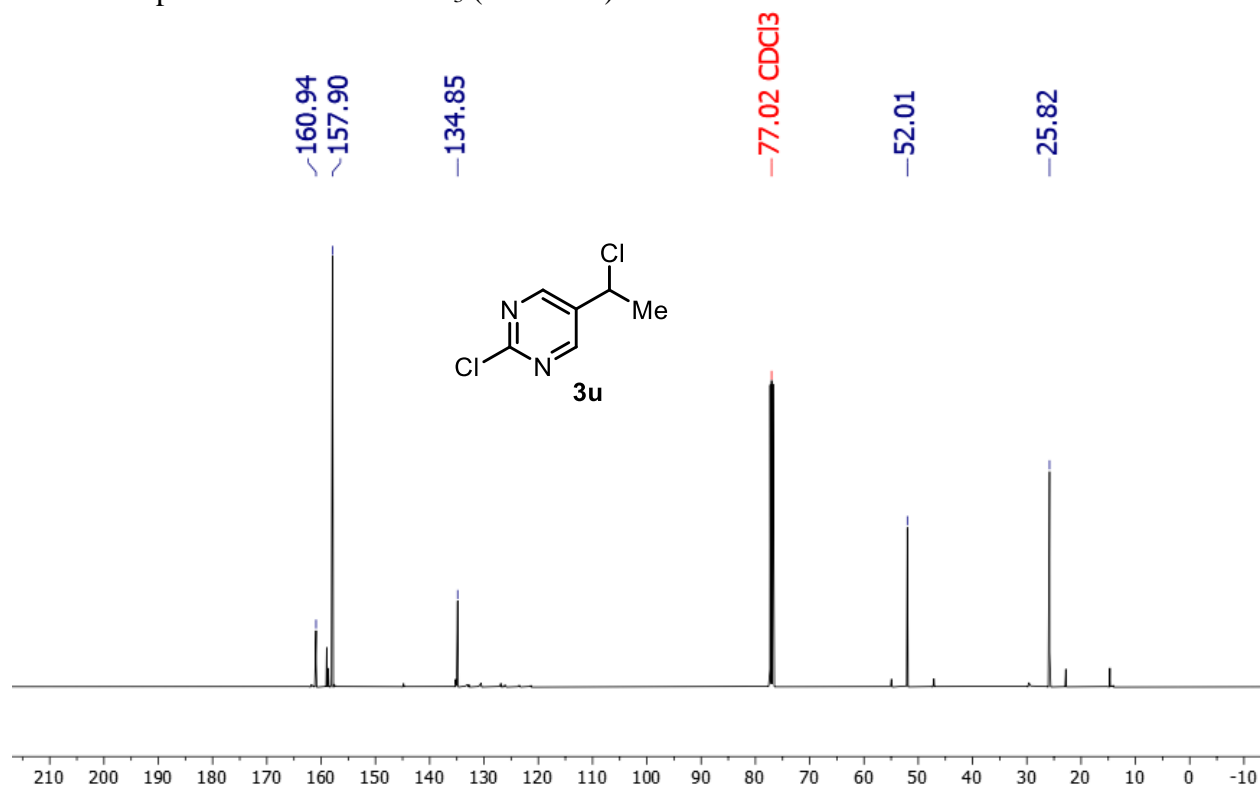
^{13}C NMR spectrum of **3t** in CDCl_3 (126 MHz).



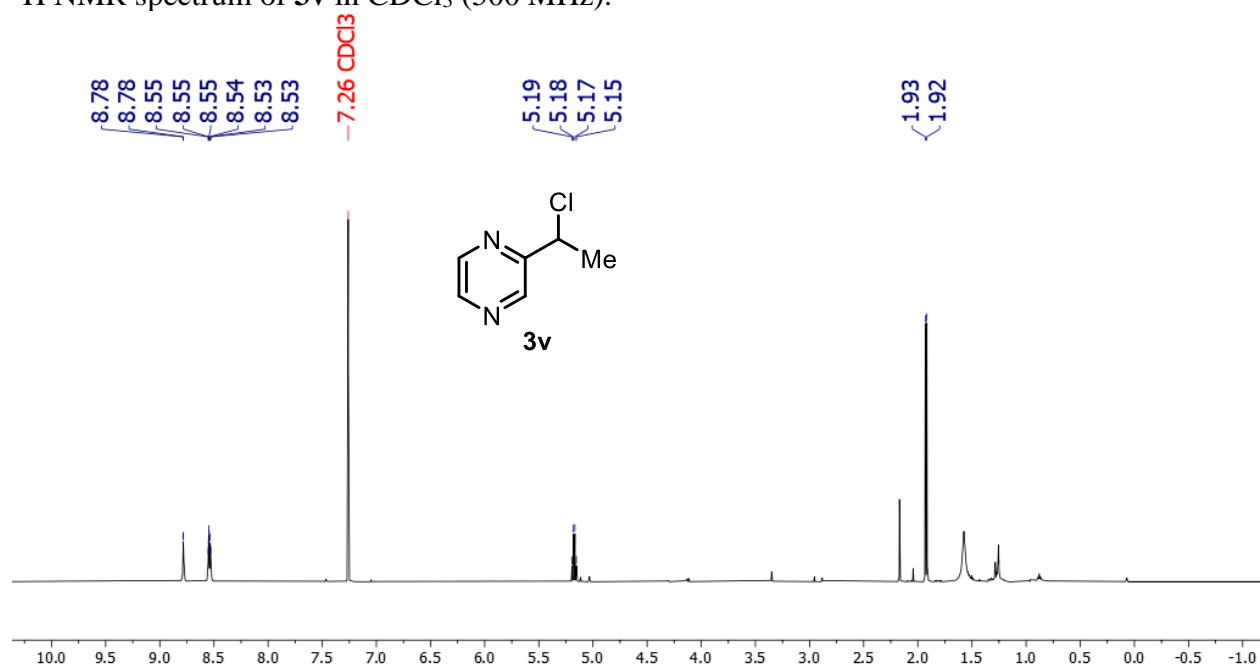
^1H NMR spectrum of **3u** in CDCl_3 (500 MHz).



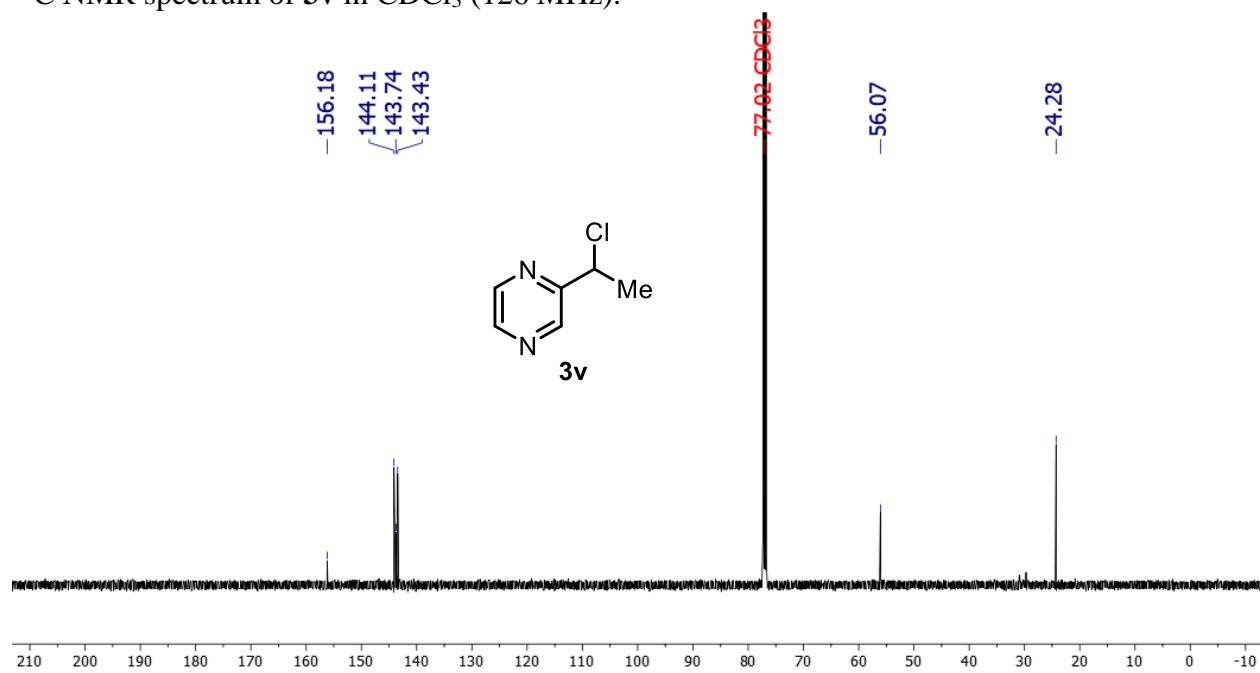
^{13}C NMR spectrum of **3u** in CDCl_3 (126 MHz).



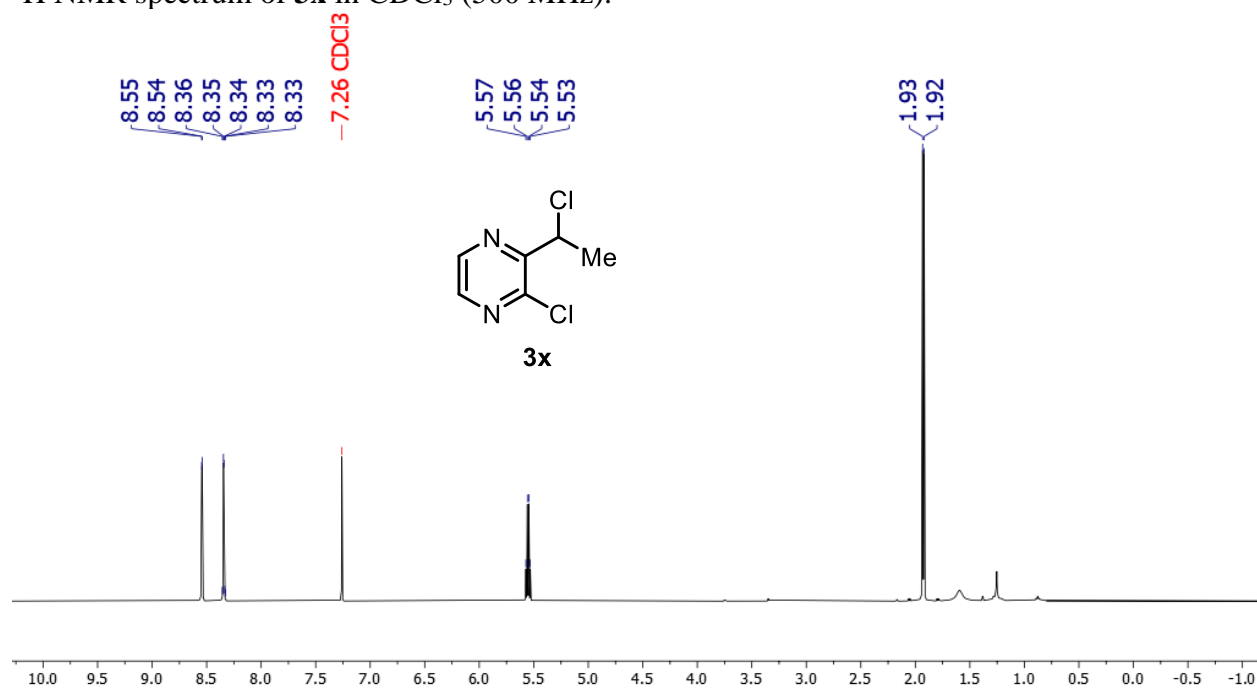
^1H NMR spectrum of **3v** in CDCl_3 (500 MHz).



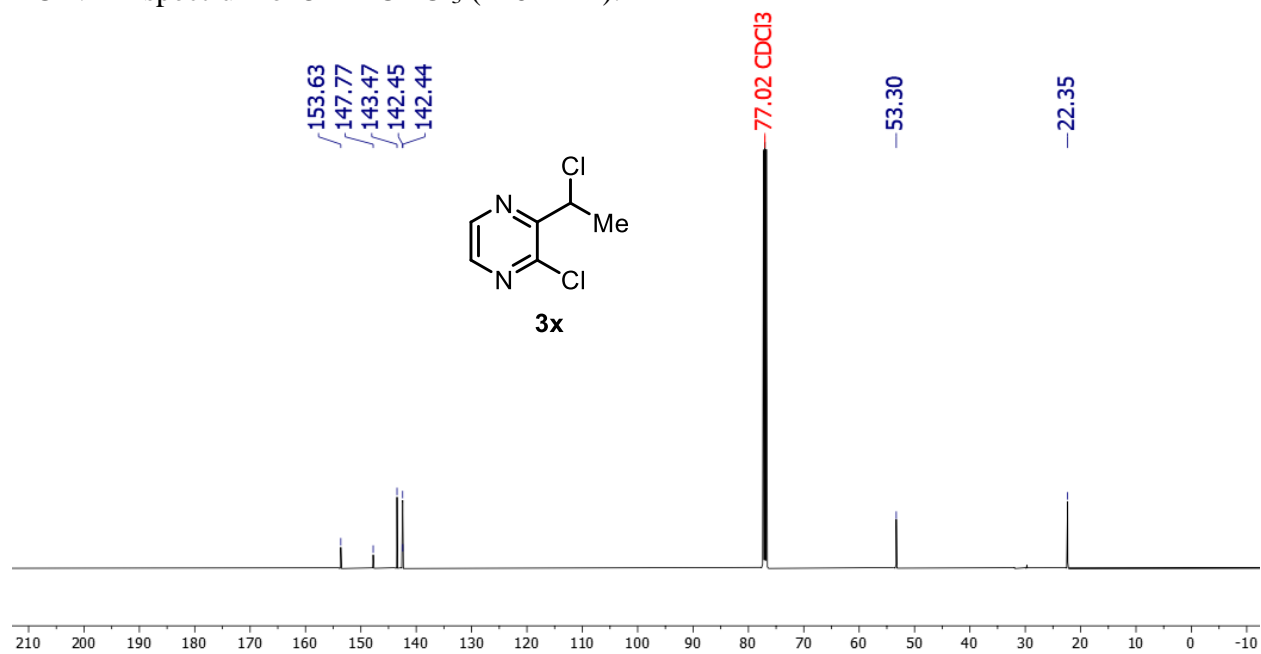
^{13}C NMR spectrum of **3v** in CDCl_3 (126 MHz).



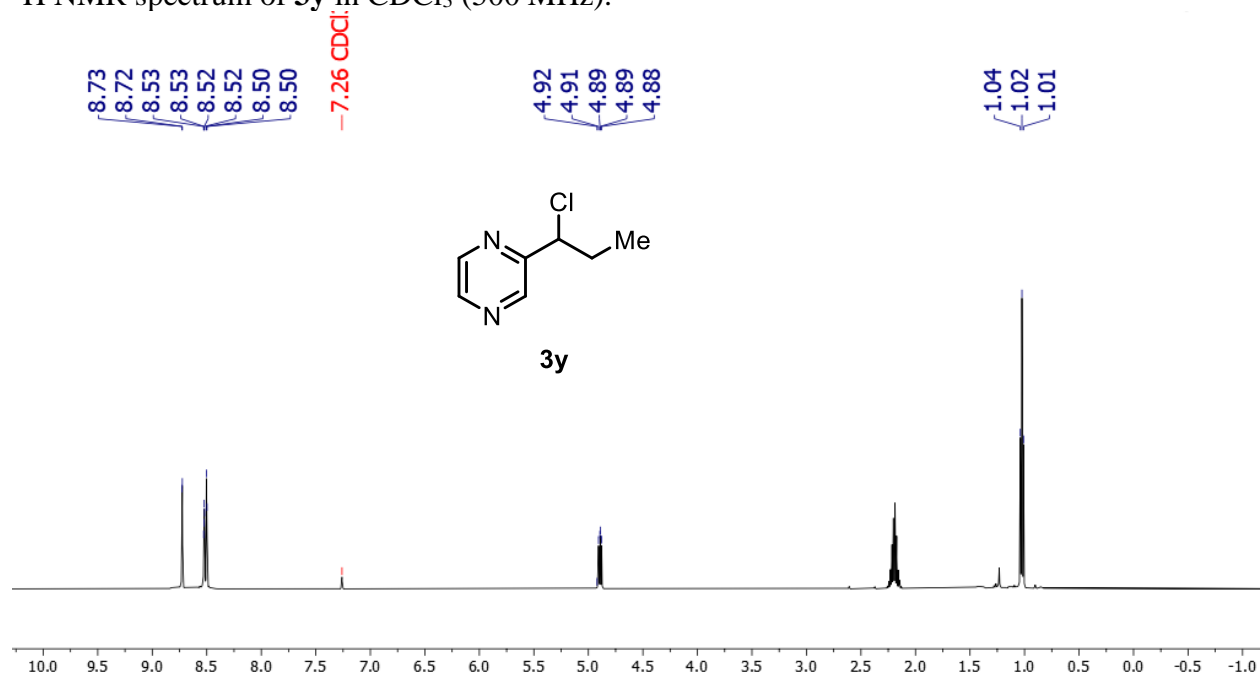
^1H NMR spectrum of **3x** in CDCl_3 (500 MHz).



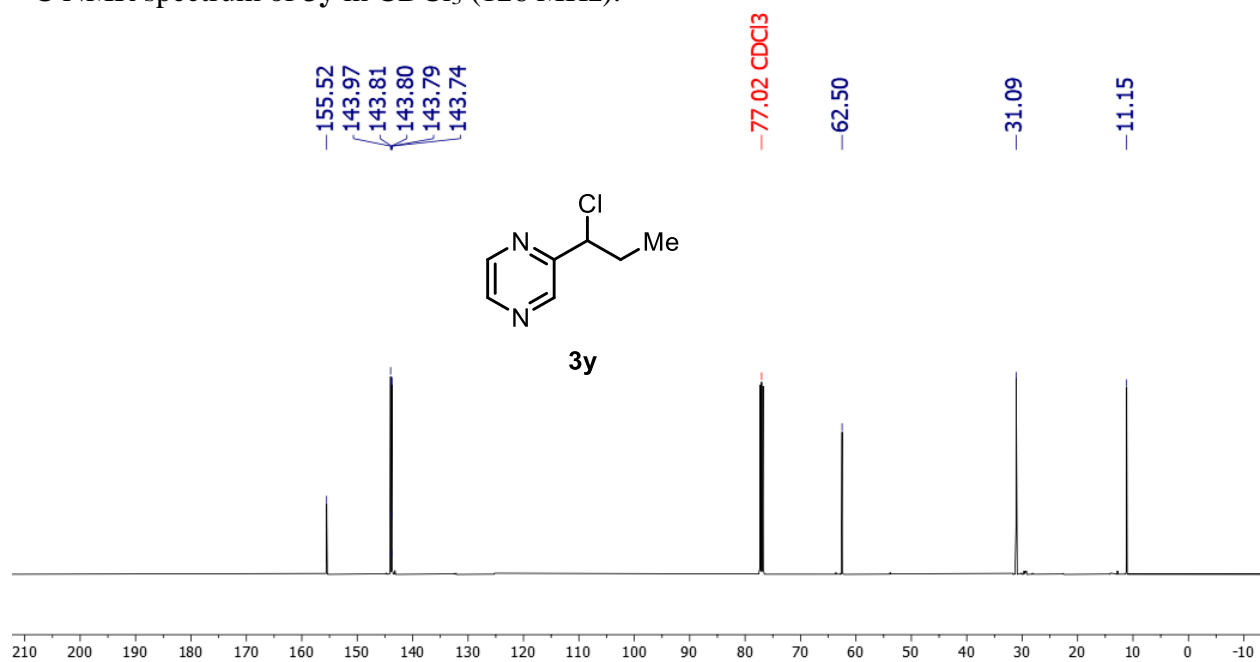
^{13}C NMR spectrum of **3x** in CDCl_3 (126 MHz).



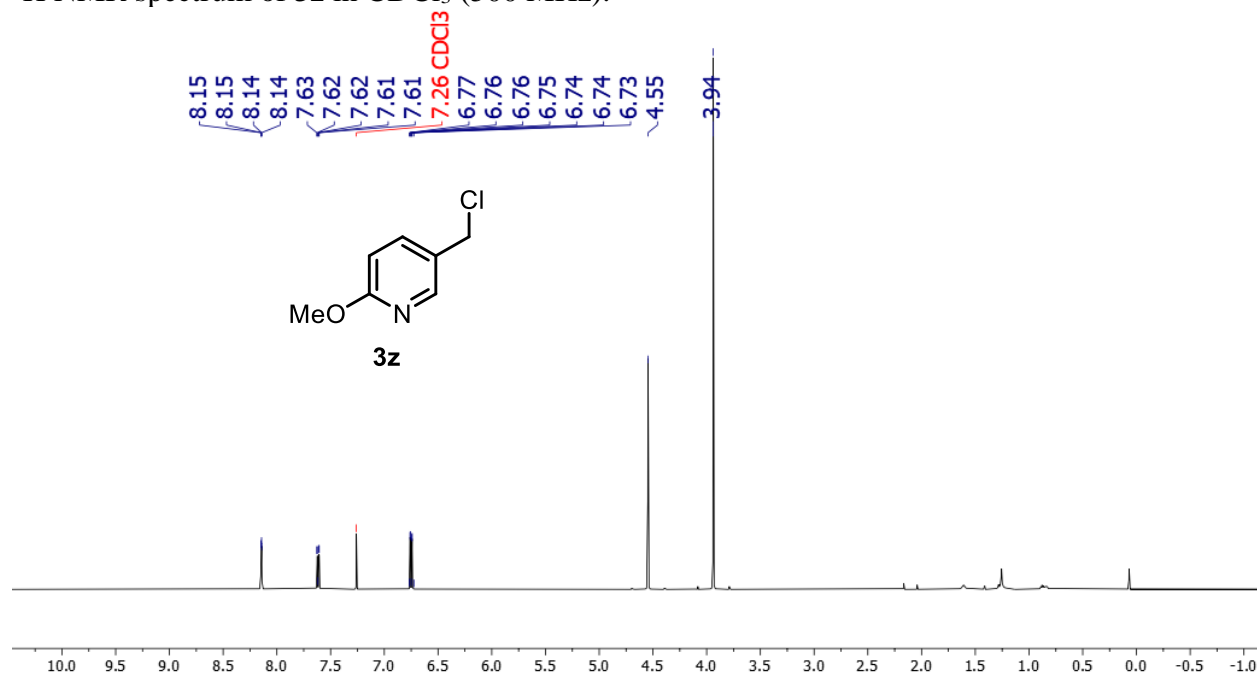
^1H NMR spectrum of **3y** in CDCl_3 (500 MHz).



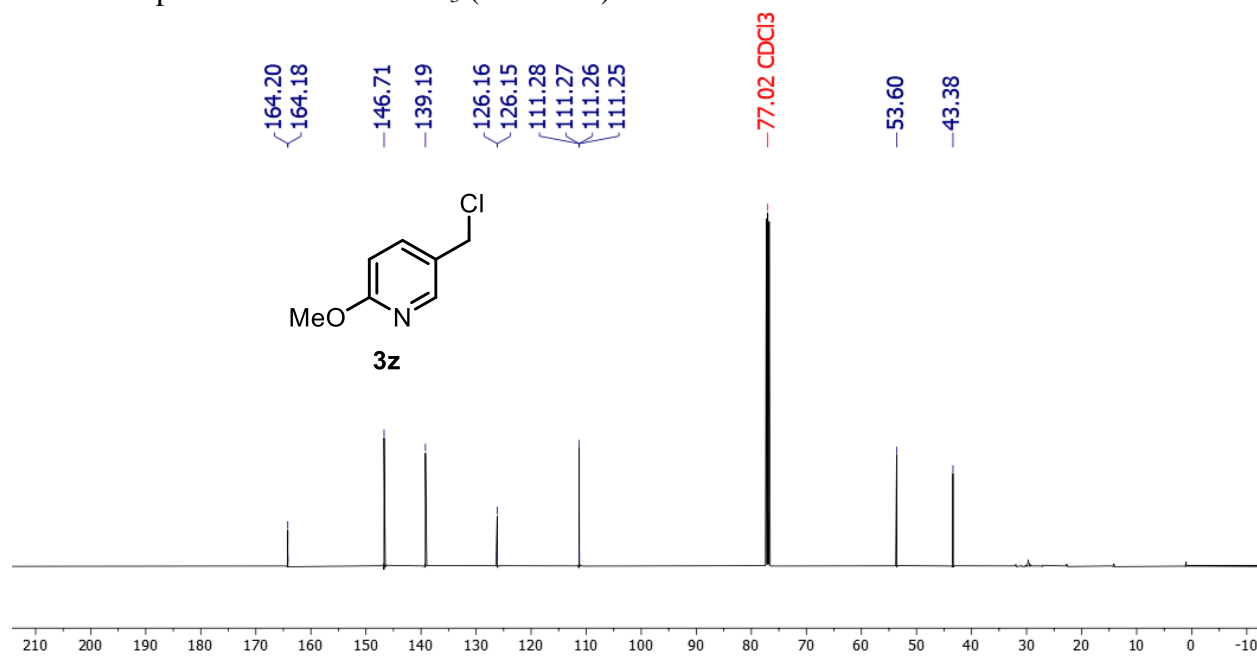
^{13}C NMR spectrum of **3y** in CDCl_3 (126 MHz).



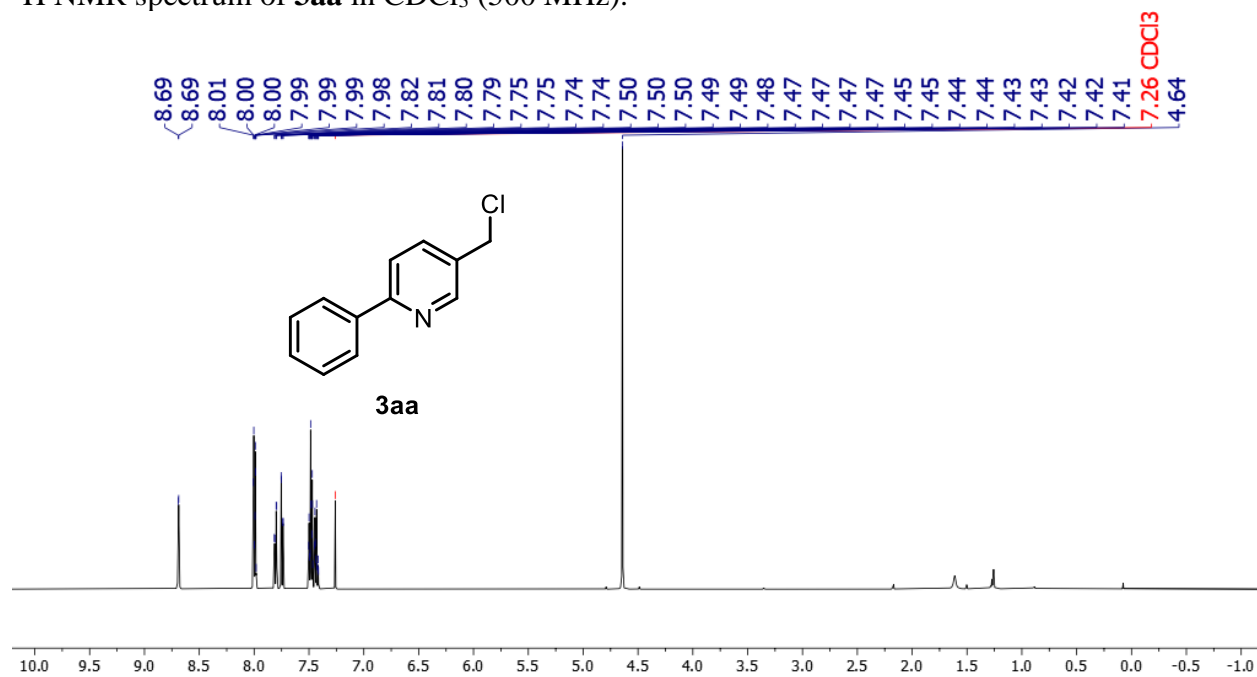
^1H NMR spectrum of **3z** in CDCl_3 (500 MHz).



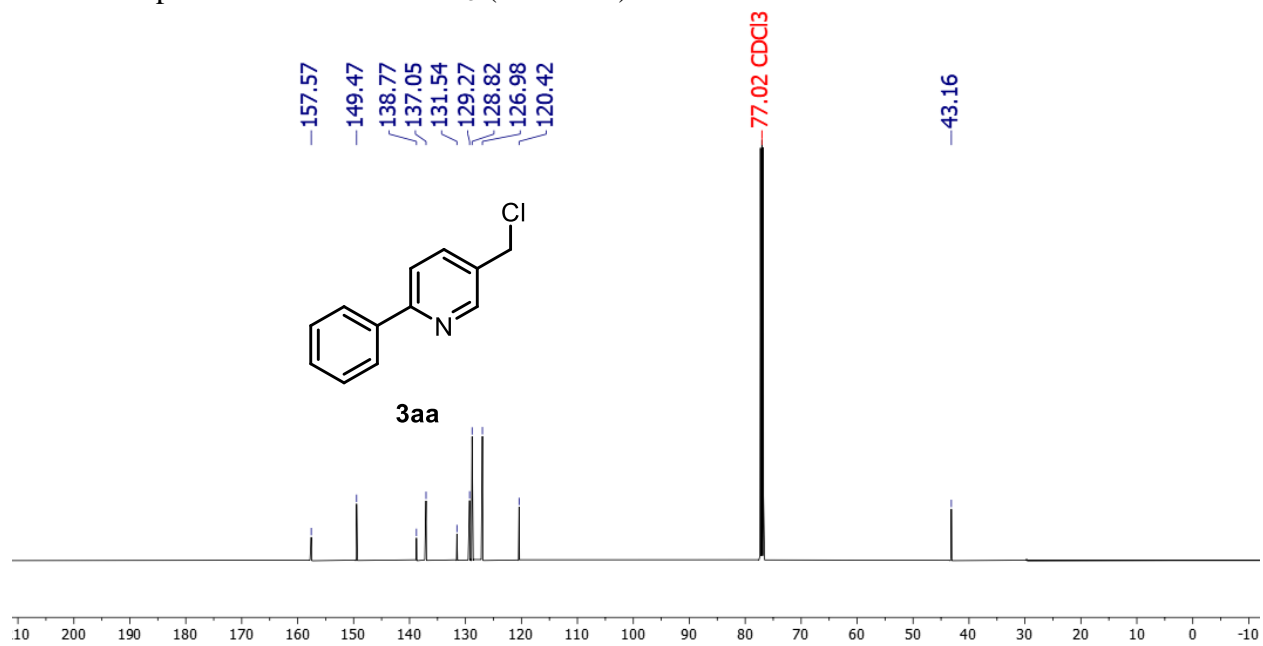
^{13}C NMR spectrum of **3z** in CDCl_3 (126 MHz).



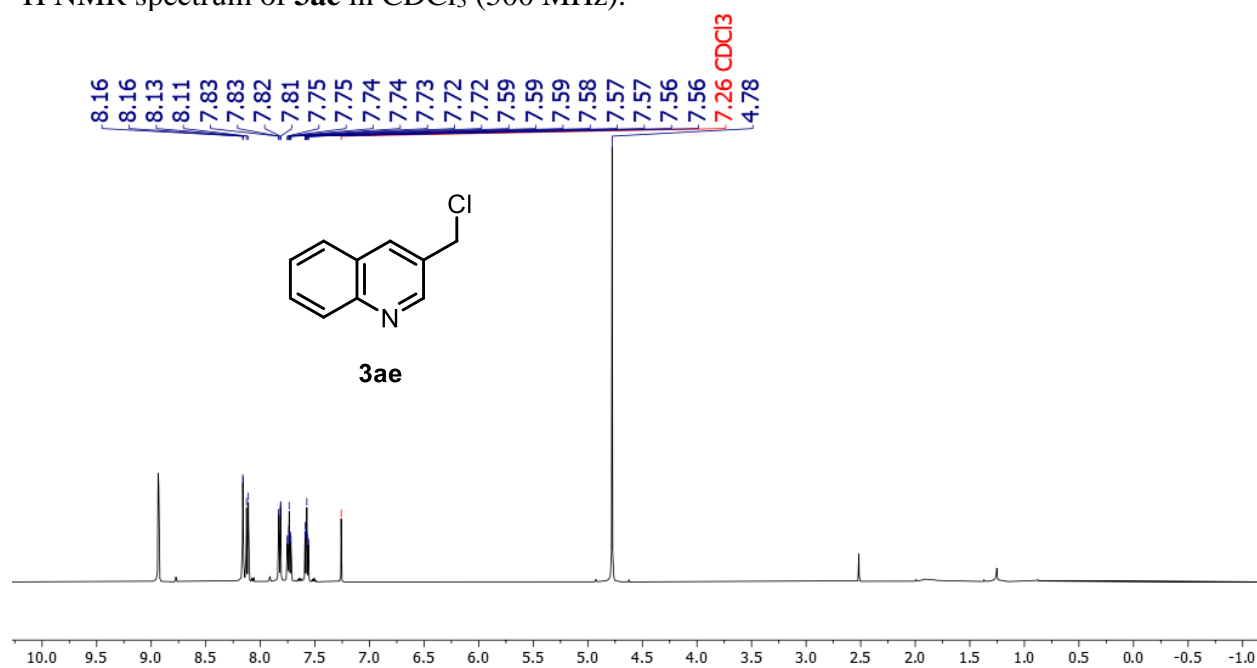
^1H NMR spectrum of **3aa** in CDCl_3 (500 MHz).



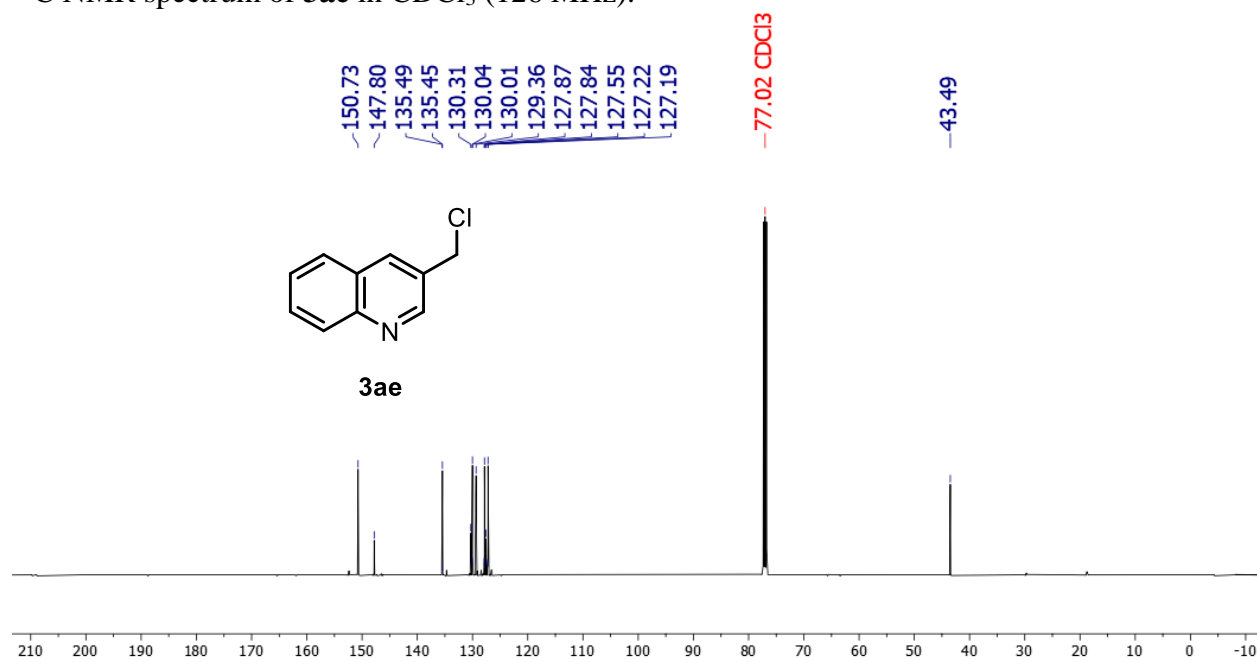
^{13}C NMR spectrum of **3aa** in CDCl_3 (126 MHz).



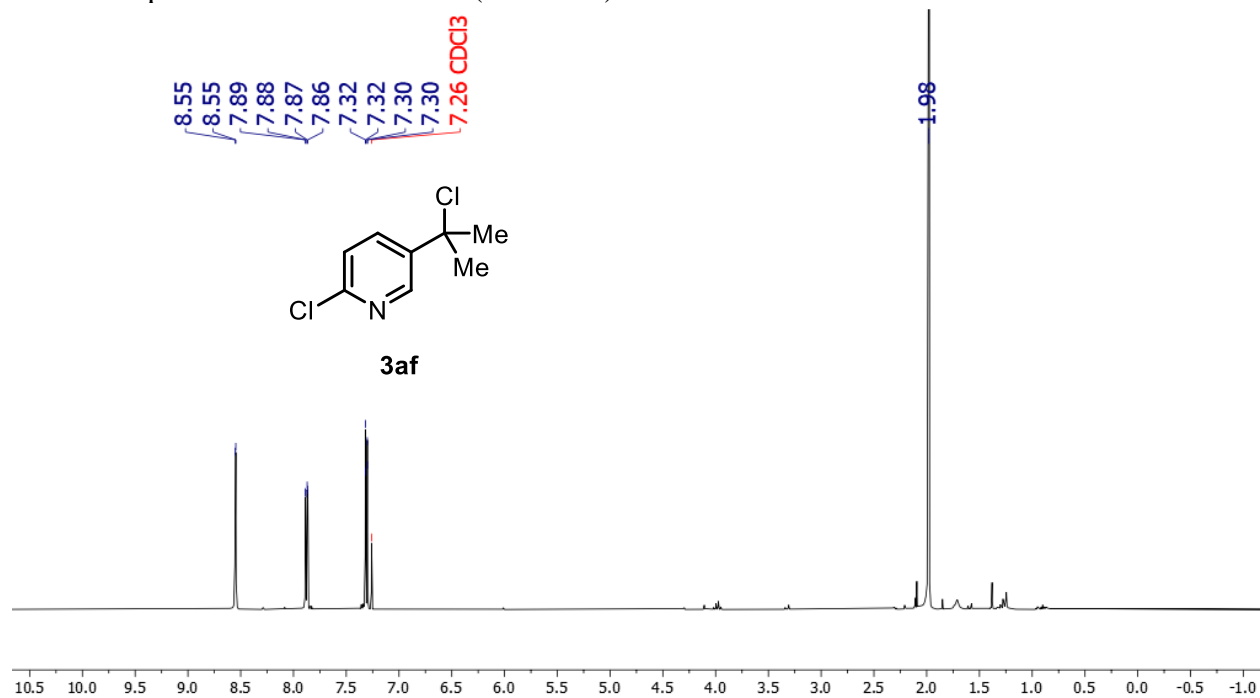
^1H NMR spectrum of **3ae** in CDCl_3 (500 MHz).



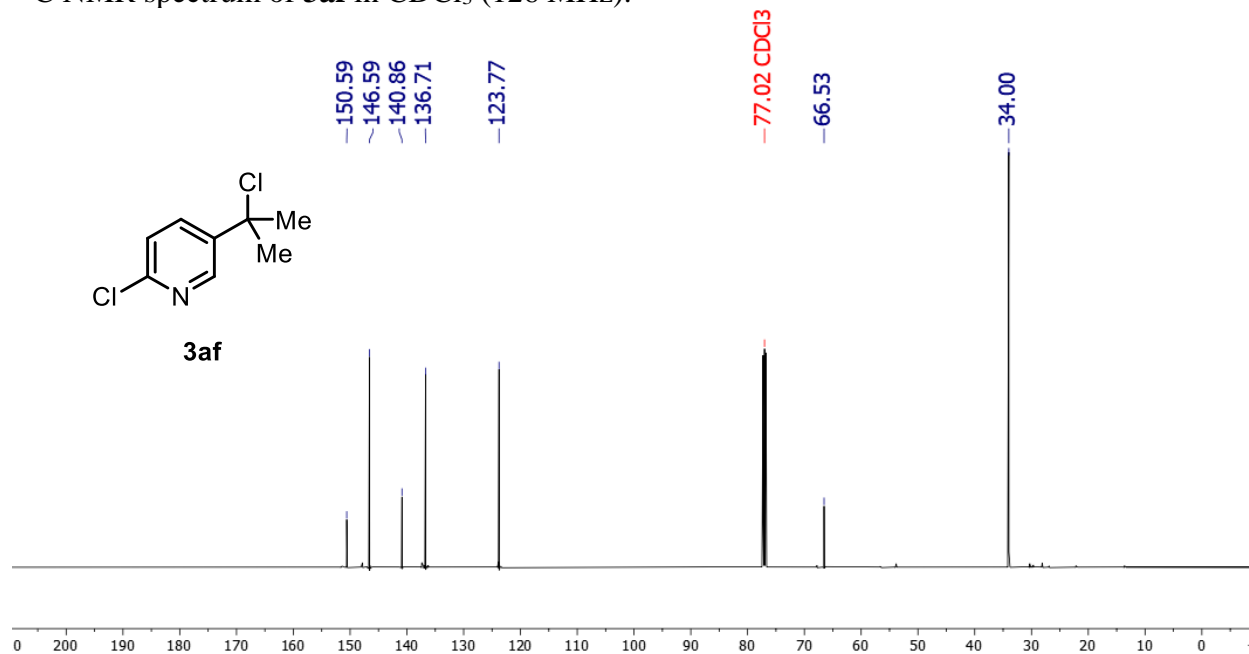
^{13}C NMR spectrum of **3ae** in CDCl_3 (126 MHz).



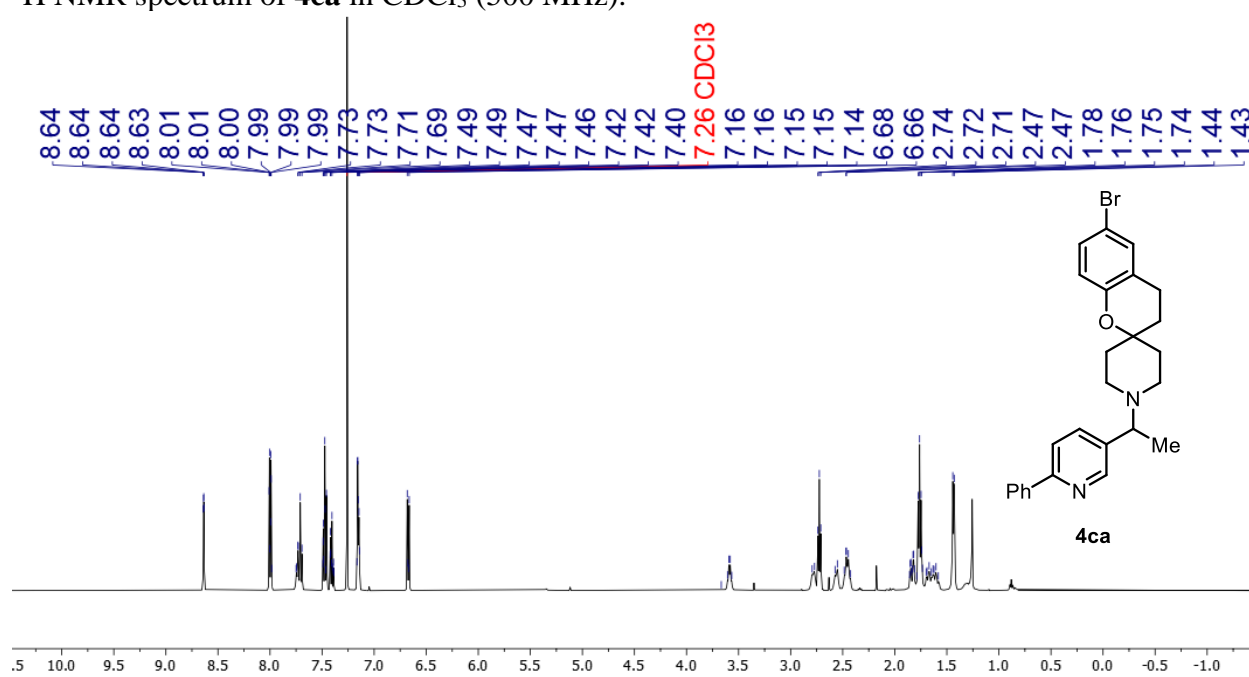
^1H NMR spectrum of **3af** in CDCl_3 (500 MHz).



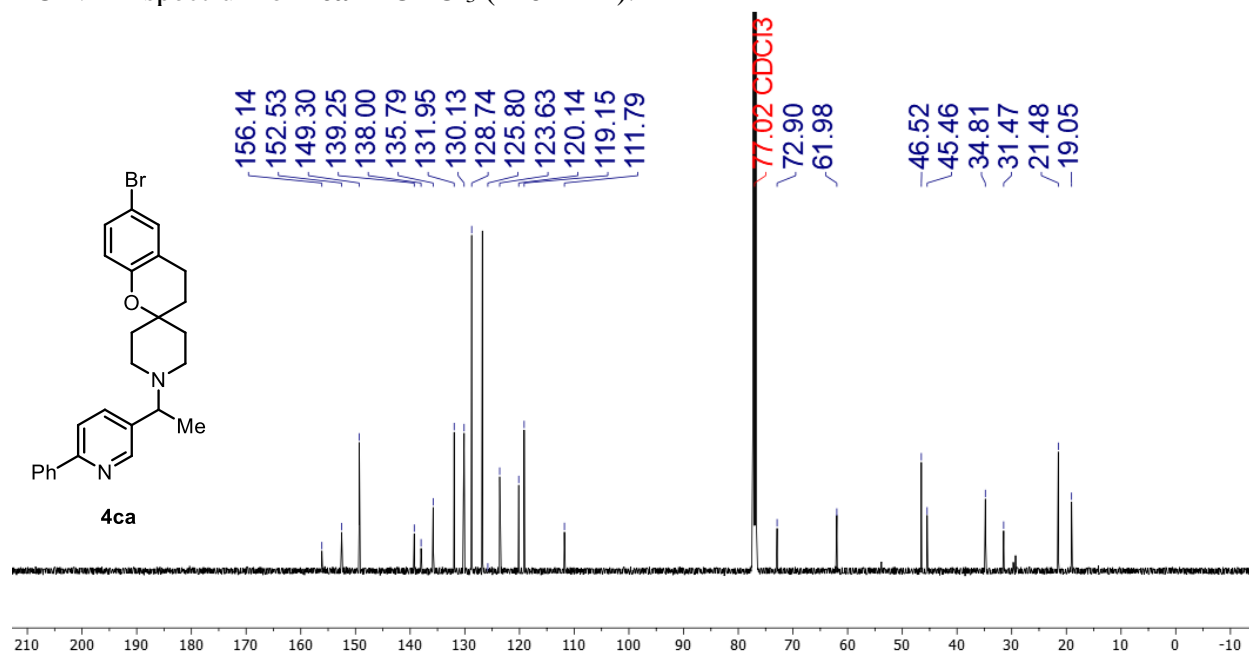
^{13}C NMR spectrum of **3af** in CDCl_3 (126 MHz).



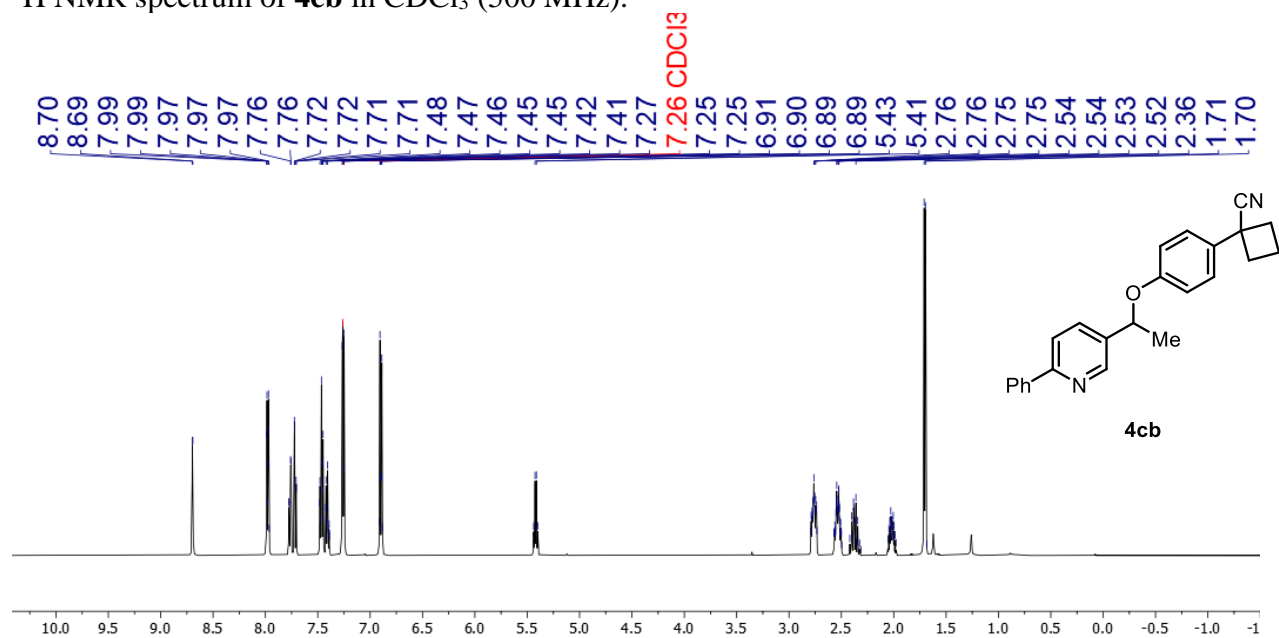
^1H NMR spectrum of **4ca** in CDCl_3 (500 MHz).



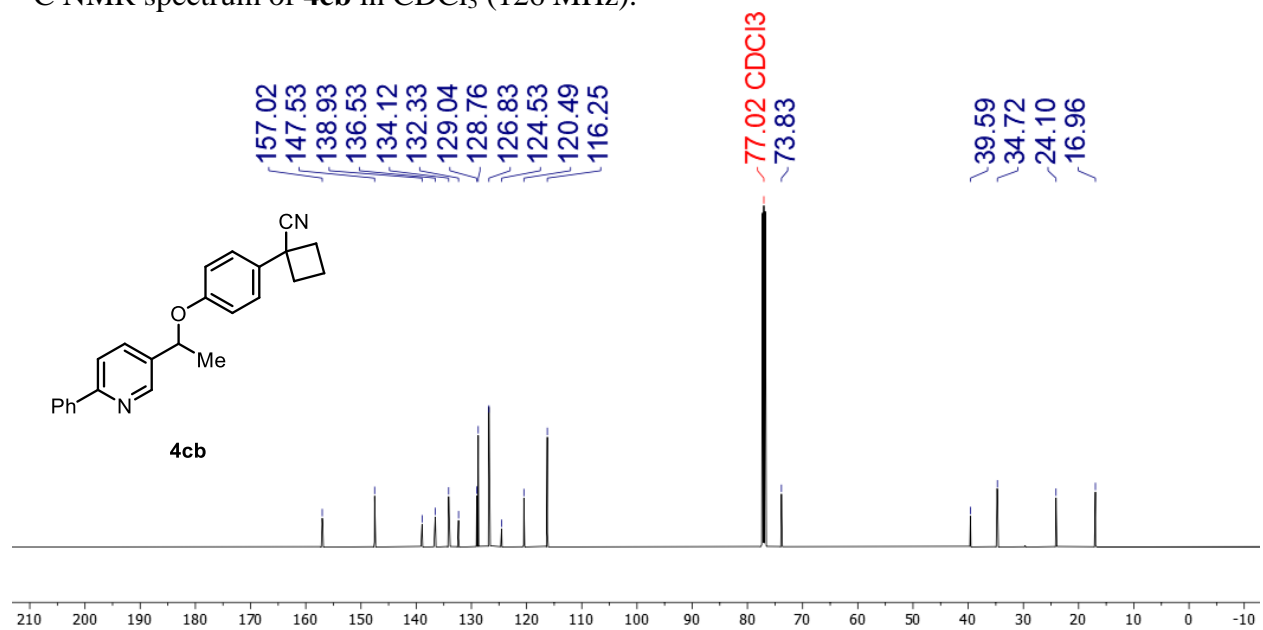
^{13}C NMR spectrum of **4ca** in CDCl_3 (126 MHz).



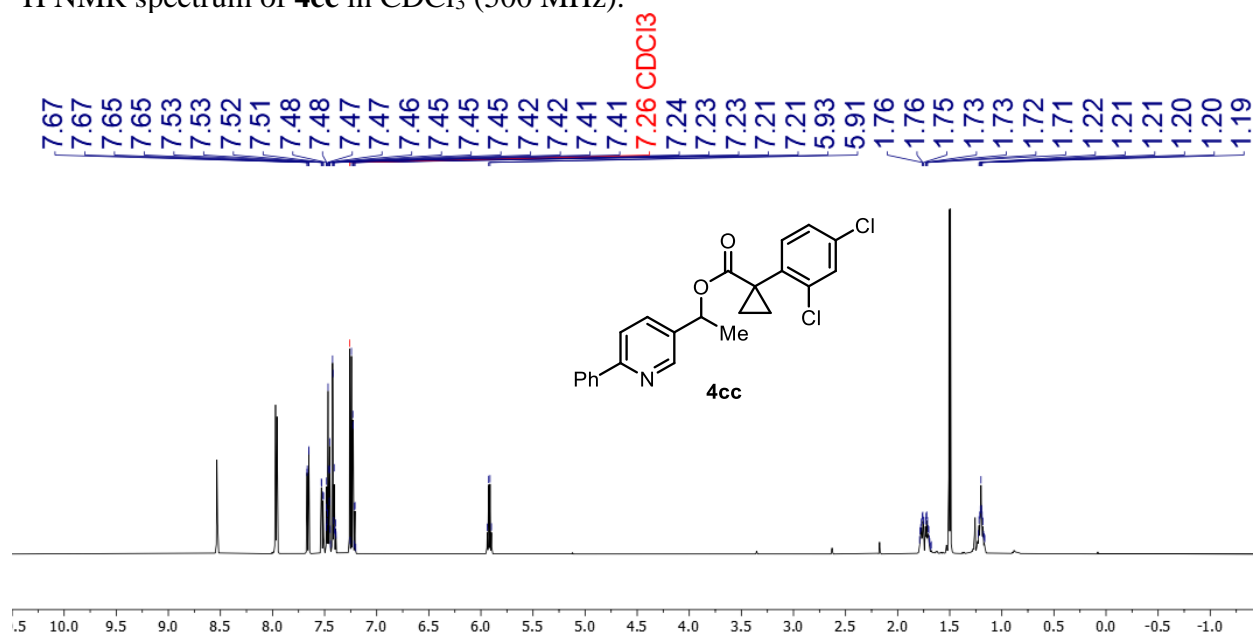
^1H NMR spectrum of **4cb** in CDCl_3 (500 MHz).



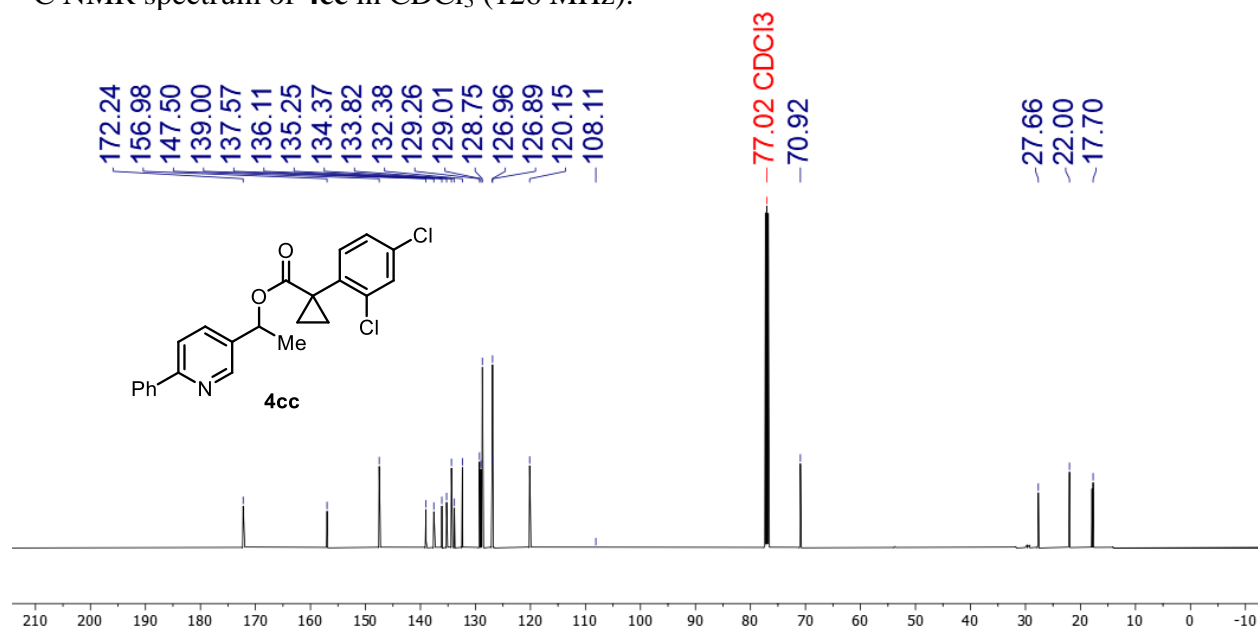
^{13}C NMR spectrum of **4cb** in CDCl_3 (126 MHz).



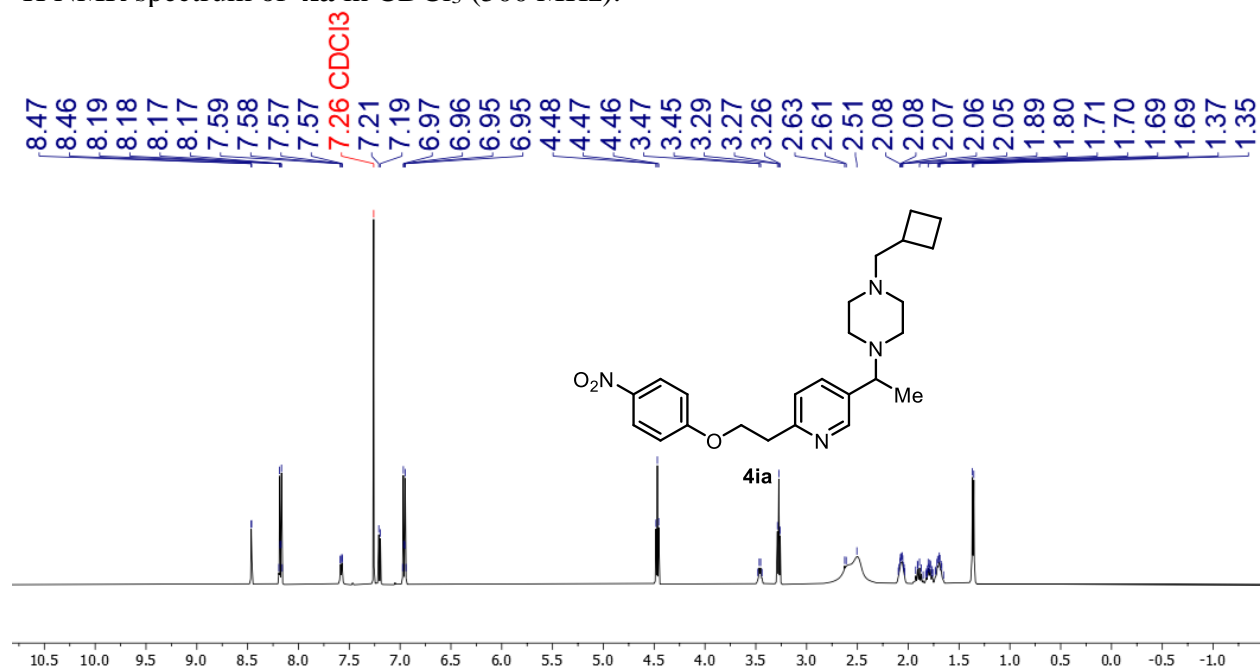
^1H NMR spectrum of **4cc** in CDCl_3 (500 MHz).



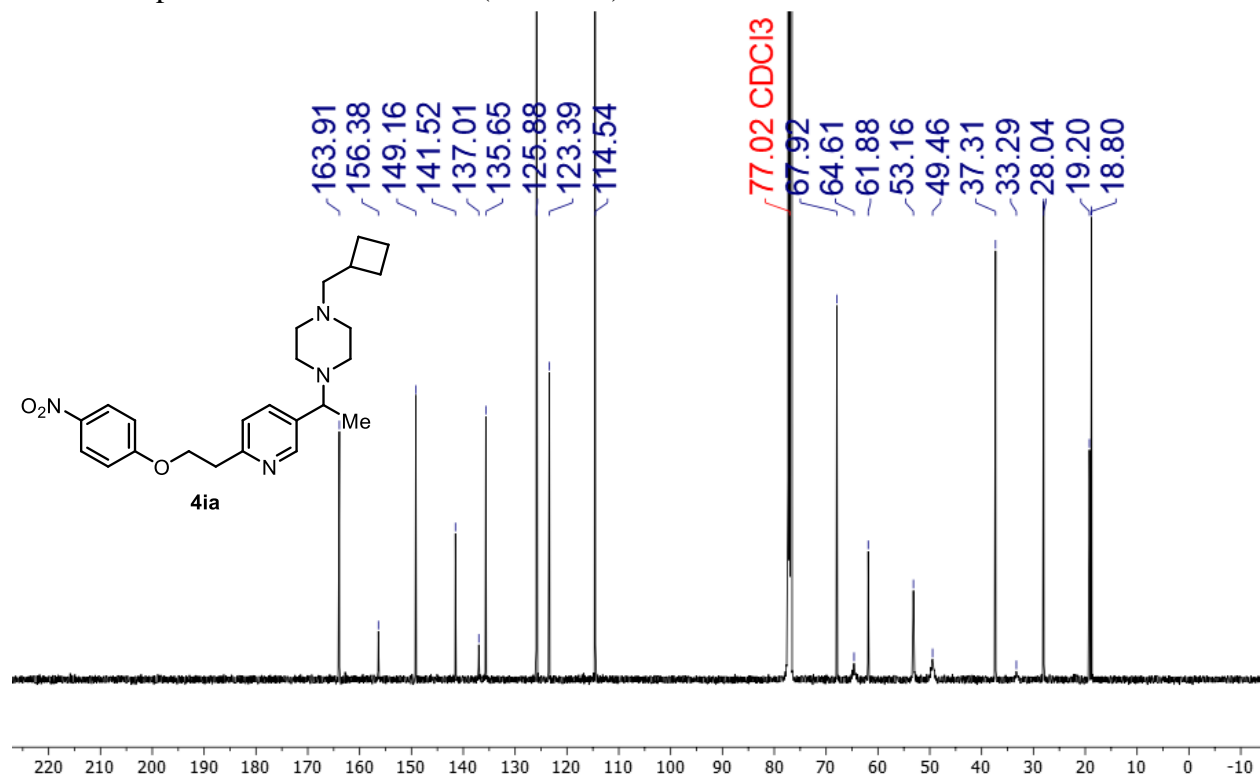
^{13}C NMR spectrum of **4cc** in CDCl_3 (126 MHz).



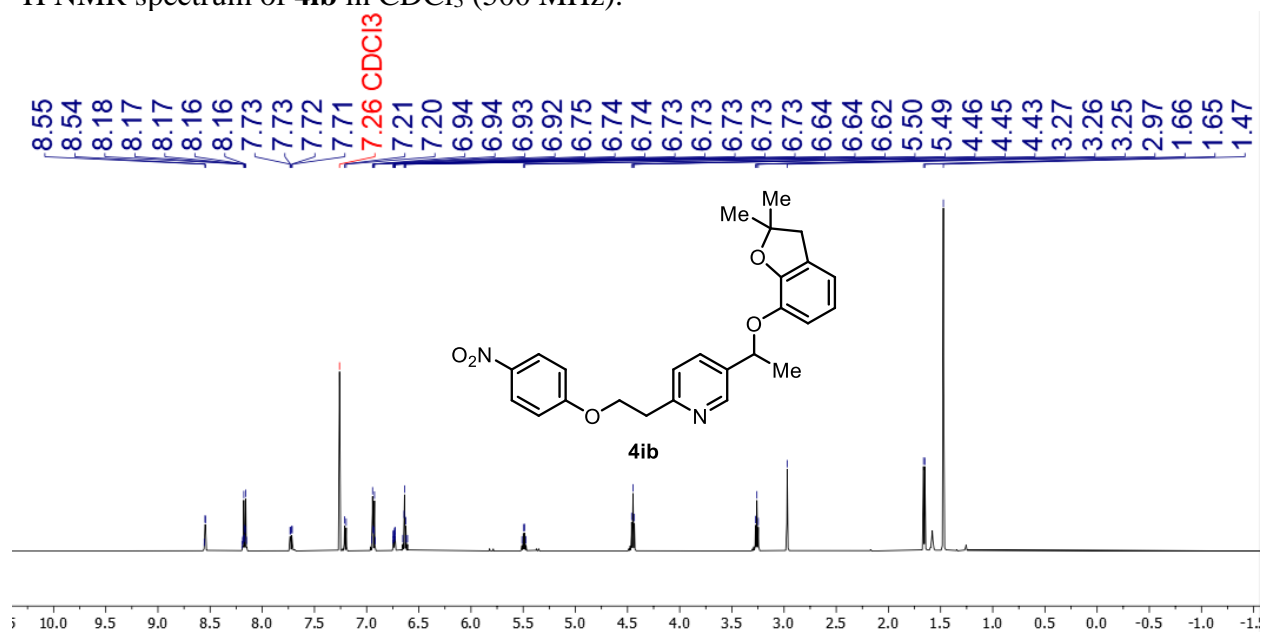
^1H NMR spectrum of **4ia** in CDCl_3 (500 MHz).



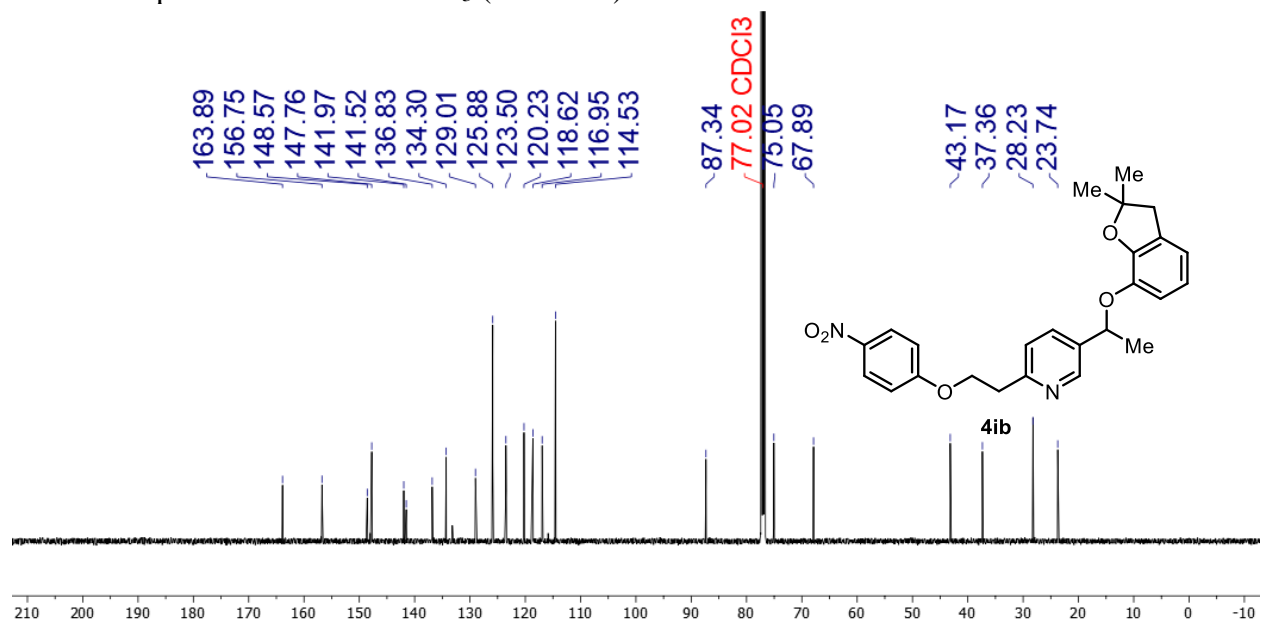
^{13}C NMR spectrum of **4ia** in CDCl_3 (126 MHz).



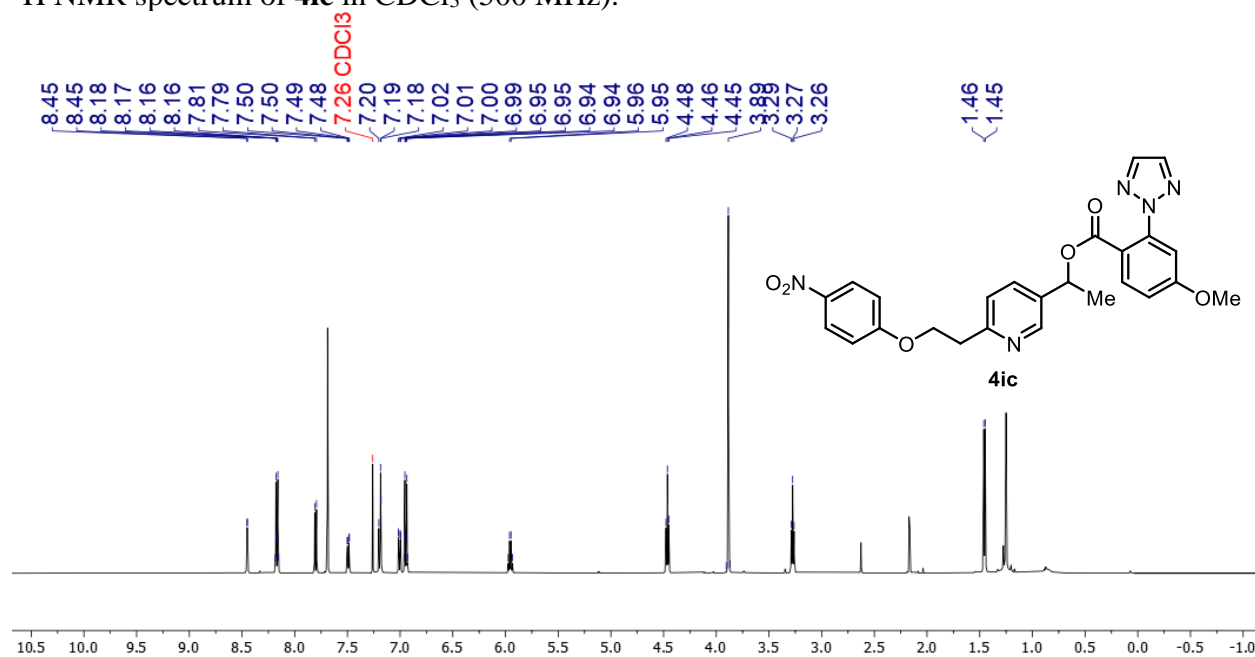
^1H NMR spectrum of **4ib** in CDCl_3 (500 MHz).



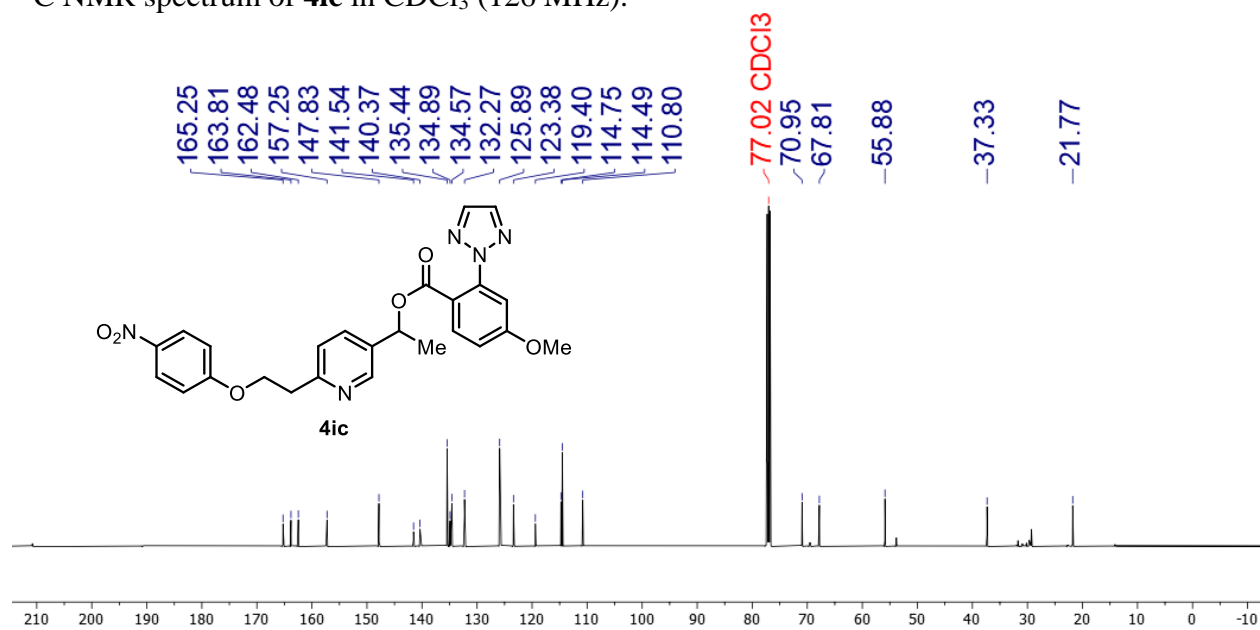
^{13}C NMR spectrum of **4ib** in CDCl_3 (126 MHz).



^1H NMR spectrum of **4ic** in CDCl_3 (500 MHz).



^{13}C NMR spectrum of **4ic** in CDCl_3 (126 MHz).



Appendix C: Supporting Information Chapter 4

4C.I. General Considerations

All reagents were purchased from commercial sources and used as received. Nearly identical performance was observed when using reagents from different commercial sources. Cu salts were purchased from Strem Chemicals and Sigma-Aldrich. C–H substrates and nucleophiles were purchased from Oakwood, Combi-Blocks, Enamine, AK Scientific, TCI America, Ark-Pharm, Ambeed, or Sigma-Aldrich. Nosyl protected amines were synthesized from the corresponding primary amines according to a literature procedure.¹ 3-Phenylpropyl trifluoroacetamide was synthesized according to a literature procedure.² NFSI was purchased from Ark-Pharm and Oakwood. Bathophenanthroline and other ligands were purchased from Aldrich, Ambeed, or Strem. The boron reagents were purchased from Sigma-Aldrich, Oakwood, or Combi-Blocks.

All fluorination reaction solids were weighed out on the benchtop, while liquids were added in an inert atmosphere (N₂) glovebox. Retention in performance can be obtained by setting up the fluorination reaction on the benchtop with backfilling or sparging of the reaction vessel with N₂. The fluorine displacement reactions were all set-up on the benchtop under air. The displacement step can produce catalytic quantities of HF (quenches on the reaction vial), so it is recommended to have ready access to a tube of calcium gluconate in case of accidental exposure to the reaction mixture. ¹H, ¹³C, and ¹⁹F NMR spectra were recorded on a Bruker Avance III 400 spectrometer at 25 °C (¹H 400.1 MHz, ¹³C 100.6 MHz, ¹⁹F 376.5 MHz) or a Bruker Avance III 500 spectrometer at 25 °C (¹H 500.1 MHz, ¹³C 125.7 MHz, ¹⁹F 470.6 MHz), except where noted otherwise, and chemical shifts are reported in parts per million (ppm). NMR spectra were referenced to residual CHCl₃ at 7.26 ppm (¹H) and CDCl₃ at 77.16 ppm (¹³C). All ¹⁹F NMR spectra were absolutely referenced to their respective solvent peaks in the ¹H NMR spectrum. Chromatography was performed using an automated Biotage Isolera® with reusable 25 g Biotage® Sfar Silica HC D cartridges for normal phase or 60 g Biotage® SNAP Ultra C18 cartridges for reversed phase. High-resolution mass spectra were obtained using a Thermo Q Exactive™ Plus via (ASAP-MS) by the mass spectrometry facility at the University of Wisconsin.

4C.II. General Procedure for Benzylic C–H Fluorination and NMR Quantitation

Warning: This reaction evolves gas from protonation of Li₂CO₃, which is able to pressurize the reaction vial. Be sure to take appropriate safety precautions.

Set-up: On the benchtop, a disposable 4 mL glass vial was charged with MeB(OH)₂ (0.6 mmol, 35.9 mg, 2 equiv), Li₂CO₃ (0.9 mmol, 66.5 mg, 3 equiv), N-fluorobenzenesulfonimide (NFSI; 0.75 mmol, 236.5 mg, 2.5 equiv), and a Teflon stir bar. The vial was sealed by a PTFE-lined pierceable cap. Bathophenanthroline (BPhen, 0.0216 mmol, 7.2 mg, 0.072 equiv) was weighed into a secondary vial with a Teflon stir bar. Both vials were then transferred to a purging glovebox under N₂(g). In the glovebox, CuOAc (0.018 mmol, 2.2 mg, 0.06 equiv) was weighed into the vial containing BPhen. Chlorobenzene (1.8 mL) was added to this vial and the vial is stirred to form a deep red 0.01 M stock solution of copper catalyst. The C–H substrate (0.3 mmol, 1 equiv) was weighed into the vial containing the rest of the reaction components, and then 0.6 mL of the copper catalyst solution was transferred to the reaction vial to give a 0.5 M mixture with a 2 mol% catalyst

loading. The solution color changes from red to blue/green. This reaction vial is then removed from the glovebox and set to stir at 45 °C on a stirring hotplate in an aluminum block at 600 rpm for 16 h.

Work-up: At the end of the reaction, the mixture often becomes a light blue paste. The cap of the vial is loosened to vent the pressure build-up from the reaction. Dibromomethane (0.3 mmol, 21 μL , 1 equiv) and trifluorotoluene (0.3 mmol, 37 μL , 1 equiv) are then added as ^1H and ^{19}F NMR standards, respectively. The mixture is then diluted with CDCl_3 (0.6 mL), mixed, and a 30 μL aliquot is taken and filtered over a 1-inch celite plug directly into an NMR tube using CDCl_3 (in a few cases, dilution was done with dichloromethane or CHCl_3). The amount of benzyl fluoride product is then quantified relative to the two added internal standards. For more information on the quantitation method, see Section 4C.VII.

Reaction tip:

- The fluorination reaction is highly temperature sensitive, so it is recommended to use a hot plate with a thermocouple.
- For scale up reactions, it may be beneficial to use DCM or acetone as the solvent to improve homogeneity of the reaction.

4C.III. General Procedure for Catalyzed Benzyl Fluoride Displacement

Warning: This reaction gradually produces HF, which is seemingly quenched via etching of the inside of the borosilicate vial. This reaction could degrade glass reaction vessels.

Set-up: Following NMR quantitation of the benzyl fluoride product, sodium dithionite (1 equiv with respect to the amount of NFSI used, ~150-250 mg) is added with 100 μ L water directly to the reaction vial. The reaction is then stirred for 15 min to quench the remaining NFSI (*warning:* dithionite oxidation results in protonation of remaining Li_2CO_3 ,³ leading to further pressure build-up). This typically changes the reaction to a red color. The chunky mixture is then filtered over a 3-inch pad of silica or celite into a disposable 15 mL glass vial using dichloromethane as the eluent (silica is preferred if the benzyl fluoride tolerates it). After flushing to a filtrate volume of 5 mL, MgSO_4 (3-7 equiv, ~300 mg) is added to the vial and it is allowed to dry for 10 min. Meanwhile, the nucleophile (0.75 mmol, 2.5 equiv) is weighed into another disposable 15 mL glass vial with a Teflon coated stir bar. The benzyl fluoride-containing solution is filtered over a 1-inch celite plug into the 15 mL vial containing the nucleophile, and then 1 mL of additional dichloromethane is used to flush the plug and bring the final reaction volume to 6 mL (0.05 M). The vessel is then sealed with a PTFE-lined pierceable cap and hexafluoroisopropanol (HFIP; 3 mmol, 315 μ L, 10 equiv) and/or $\text{BF}_3 \cdot \text{Et}_2\text{O}$ (0.03 mmol, 3.7 μ L, 0.1 equiv) is added to catalyze fluoride displacement. The reaction is stirred overnight. An aliquot of this reaction solution is then taken for ^1H NMR analysis to determine whether it is complete. Reactions showing incomplete fluoride conversion are subjected to harsher displacement conditions (i.e., heated to 45 $^\circ\text{C}$ in an aluminum block on a hotplate or additional $\text{BF}_3 \cdot \text{Et}_2\text{O}$ is added). The final solution is concentrated on a rotovap and purified using automated flash column chromatography to yield the desired functionalization product.

Reaction tips:

- Lewis basic functional groups disrupt fluoride displacement. When using coupling partners with Lewis basic groups, it is typically required to use additional BF_3 to enact displacement (>0.25 equiv BF_3 is common, *cf.* Substrates **37** and **42**).
- Protonation of Lewis basic groups may also be helpful for enabling displacement reactivity (*cf.* Substrate **31**)

4C.IV. Procedure for 3 mmol Scale Fluorination/Functionalization Sequence to Prepare 46

Fluorination: On the benchtop, a disposable 20 mL glass vial was charged with MeB(OH)₂ (6 mmol, 359 mg, 2 equiv), Li₂CO₃ (9 mmol, 665 mg, 3 equiv), NFSI (7.5 mmol, 2.365 g, 2.5 equiv), and a Teflon stir bar. The vial was sealed by a PTFE-lined pierceable cap. Bathophenanthroline (BPhen, 0.072 mmol, 23.9 mg, 0.024 equiv) was weighed into a secondary vial with a Teflon stir bar. Both vials were then transferred to a purging glovebox under N₂(g). In the glovebox, CuOAc (0.06 mmol, 7.4 mg, 0.02 equiv) was weighed into the vial containing BPhen followed by addition of chlorobenzene (6 mL, 0.5 M). This solution was allowed to stir for 3 minutes to form a deep red solution. 1-chloro-3-phenylpropane (3 mmol, 429 μL, 1 equiv) was then weighed into the vial containing the rest of the reaction components and the copper catalyst solution was transferred to the reaction vial. The reaction vial was then sealed, removed from the glovebox, and set to stir at 45 °C in an aluminum block on a heated stir plate at 600 rpm for 16 h.

Functionalization: The cap was carefully opened to release built-up pressure (the septum may have been pierced with a needle instead). Dibromomethane was then added as an NMR standard (1 mmol, 70.2 μL, 0.33 equiv) and a 50 uL aliquot was taken and filtered over celite with 450 uL CDCl₃ directly into an NMR tube for NMR quantitation. To the reaction vial was added sodium dithionite (7.5 mmol, 1.305 g, 2.5 equiv) and water (500 uL) and this mixture was allowed to stir for 10 minutes uncapped. After quenching NFSI, the now chunky red-white mixture was filtered over a 3-inch pad of silica directly into a 250 mL round bottom flask using dichloromethane (54 mL, final concentration of 0.05 M). *p*-Cresol (7.5 mmol, 811 mg, 2.5 equiv) was added to the round bottom flask followed by HFIP (30 mmol, 3.159 mL, 10 equiv) and after initial agitation, the reaction was left to sit at room temperature for 16 h.

Work-up: A 100 μ L aliquot was taken from the now light gold solution for NMR analysis to detect formation of product and consumption of benzyl fluoride (^1H and ^{19}F). If any residual fluoride were detected, the vessel would have been warmed to 40 $^\circ\text{C}$ on an aluminum block or catalytic $\text{BF}_3 \cdot \text{Et}_2\text{O}$ would have been added. The reaction was concentrated on the rotovap at 40 $^\circ\text{C}$ to remove the solvent (chlorobenzene, dichloromethane, and HFIP) and the concentrated residue was purified by reverse phase chromatography using a 65% \rightarrow 100% MeOH in water gradient. The product fractions were collected and concentrated on the rotovap at 50 $^\circ\text{C}$ to yield 445 mg of the desired diarylalkane product 46, corresponding to 57% yield with respect to the starting C–H substrate).

4C.V. Screening Tables

Table 4C.1. Control Experiments Table

entry	control	MB	% SM	% C-N	% C-F(F ₂) ^a
1	No CuOAc	102	102	--	--
2	No BPhen	101	77	--	24
3	No NFSI	102	102	--	--
4	No Li ₂ CO ₃	70	70	--	--
5	No MeB(OH) ₂	103	103	--	--
6	Under Air	66	42	--	24

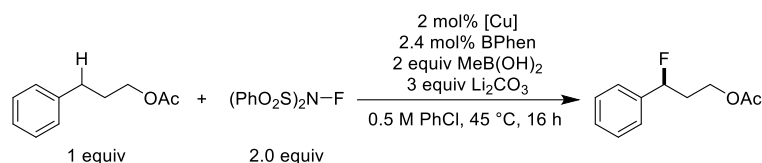
^aReactions run at 0.2 mmol scale. Calibrated ¹H NMR yields using mesitylene as an internal standard.

Table 4C.2. Solvent Screening Table

entry	solvent	MB	% SM	% C-N	% C-F(F ₂) ^a
1	DCM	76	9	--	64(3)
2	DCE	87	16	--	69(2)
3	MeCN	25	2	--	23
4	EtOAc	80	26	--	53(1)
5	acetone	71	--	--	68(3)
6	PhF	94	38	--	55(1)
7	PhCF ₃	89	38	--	50(1)
8	PhCl	98	19	--	76(3)
9	PhCl (0.4 M)	79	7	--	68(4)
10	PhCl (0.3 M)	85	9	--	72(4)
11	PhCl (0.2 M)	77	18	--	59
12	PhCl (0.1 M)	77	21	--	56

^aReactions run at 0.2 mmol scale. Calibrated ¹H NMR yields using mesitylene as an internal standard.

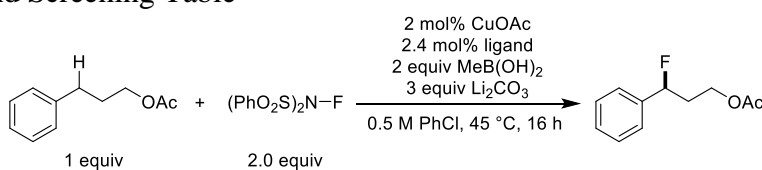
Table 4C.3. Cu Salt Screening Table



entry	Cu salt	MB	% SM	% C-N	% C-F(F ₂) ^a
1	CuI•DMS	74	5	--	64(5)
2	CuBr•DMS	80	9	--	68(3)
3	CuCl	88	17	--	68(3)
4	CuOAc	82	2	--	73(7)
5	Cu(MeCN) ₄ PF ₆	94	31	--	63
6	CuCN	102	92	--	10
7	Cu(OAc) ₂	90	9	5	76
8	Cu(OTf) ₂	100	100	--	--

^aReactions run at 0.2 mmol scale. Calibrated ¹H NMR yields using mesitylene as an internal standard.

Table 4C.4. Ligand Screening Table



entry	ligand	MB	% SM	% C-N	% C-F(F ₂) ^a	entry	ligand	MB	% SM	% C-N	% C-F(F ₂) ^a
1		93	7	0	81(5)	5		90	56	0	34
2		94	37	0	57	6		101	48	0	53
3*		101	56	0	45	7*		101	19	0	78(4)
4*		103	46	0	56(1)	8		91	29	0	61(1)

^aReactions run at 0.2 mmol scale. Calibrated ¹H NMR yields using mesitylene as an internal standard. *In an experiment with 2-(S)-acetoxy-4-phenylbutane, these three ligands formed the fluorinated product with an identical d.r. of 2:1 (avg yield 50%). It is unlikely that enantioselectivity would be observed in fluorination of achiral benzylic substrates when using the chiral ligands in entries 3 or 4.

Table 4C.5. Base Screening Table

entry	base/additive	MB	% SM	% C-N	% C-F(F ₂) ^a
1	K ₂ CO ₃	92	75	--	17
2	Na ₂ CO ₃	84	30	--	54
3	Li₂CO₃	97	13	--	78(6)
4	LiOAc	97	40	--	57
5	NaHCO ₃	70	12	--	58
6	Li ^t Bu	100	100	--	--
7	LiOTf	82	82	--	--
8	K ₃ PO ₄	99	99	--	--

^aReactions run at 0.2 mmol scale. Calibrated ¹H NMR yields using mesitylene as an internal standard.

Table 4C.6. Reductant Screening Table

entry	reductant	equiv	MB	% SM	% C-N	% C-F(F ₂) ^a
1		2	88	5	--	77(6)
2		2	40	--	--	37(3)
3		2	103	103	--	--
4		2	64	10	--	54
5		2	61	9	--	52

^aReactions run at 0.2 mmol scale. Calibrated ¹H NMR yields using mesitylene as an internal standard.

Table 4C.7. Reaction Stoichiometry Screening Table

entry	variation	MB	% SM	% C-N	% C-F(F ₂) ^a
1	standard cond.	95	2	--	80(5)
2	35 °C	93	44	--	48(1)
3	55 °C	92	3	--	74(10)
4	1 equiv. NFSI	90	34	--	52(2)
5	3 equiv. NFSI	98	7	--	89(5)
6	1 equiv. Li ₂ CO ₃	95	13	--	78(4)
7	2 equiv. Li ₂ CO ₃	93	5	--	82(6)
8	1 equiv. MeB(OH) ₂	95	12	--	79(4)
9	2.5 equiv. MeB(OH) ₂	97	3	--	87(7)
10	1 mol% BPhen	100	12	--	83(5)
11	4 mol% BPhen	103	103	--	0
12	1 mol% CuOAc/ 1 mol% BPhen	96	12	--	80(4)
13	10 mol% CuOAc/ 10 mol% BPhen	83	13	--	47(3)
14	10 mol% CuOAc/ 5 mol% BPhen	92	18	--	63(2)

^aReactions run at 0.2 mmol scale. Calibrated ¹H NMR yields using mesitylene as an internal standard. Mass balance in this table also accounts for formation of the benzyl ketone.

Table 4C.8. HFIP Loading Screening Table

entry	Nuc-H	equiv HFIP	% SM	% C-Nuc ^a
1		2	-	69
2		10	-	100
3		27	-	90

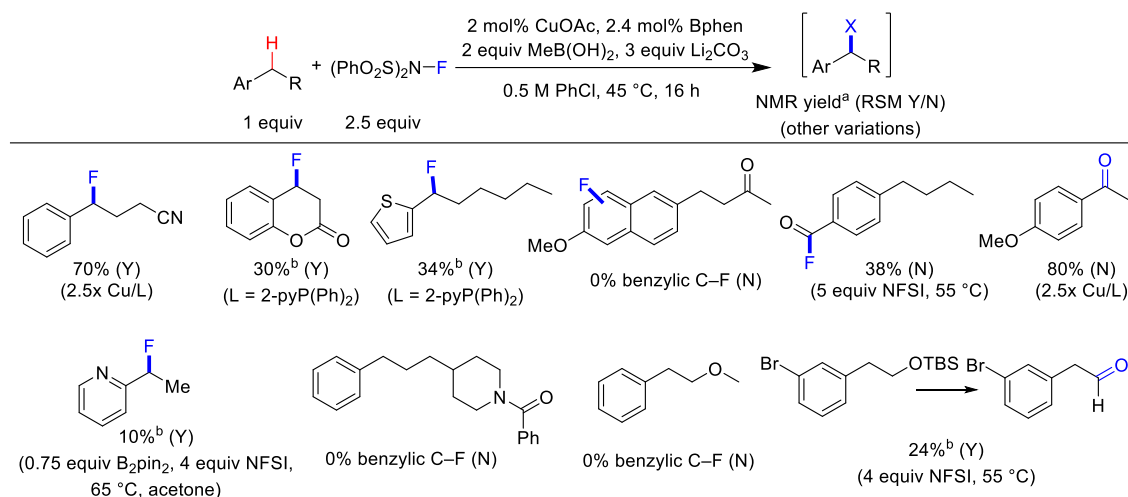
4		2	100	-
5		10	-	96
6		27	-	95

7		2	-	60
8		10	-	90
9		27	-	78

^aReactions run at 0.3 mmol scale. Calibrated ¹H NMR yields with respect to the benzyl fluoride using CH₂Br₂ as an internal standard. HFIP ether product is observed in reactions with 27 equiv HFIP.

4C.VI. Additional Experiments and Observations

Less Successful C–H Fluorination Substrates

Table 4C.9. Benzylic C–H fluorination results for substrates not included in Figure 4.3.

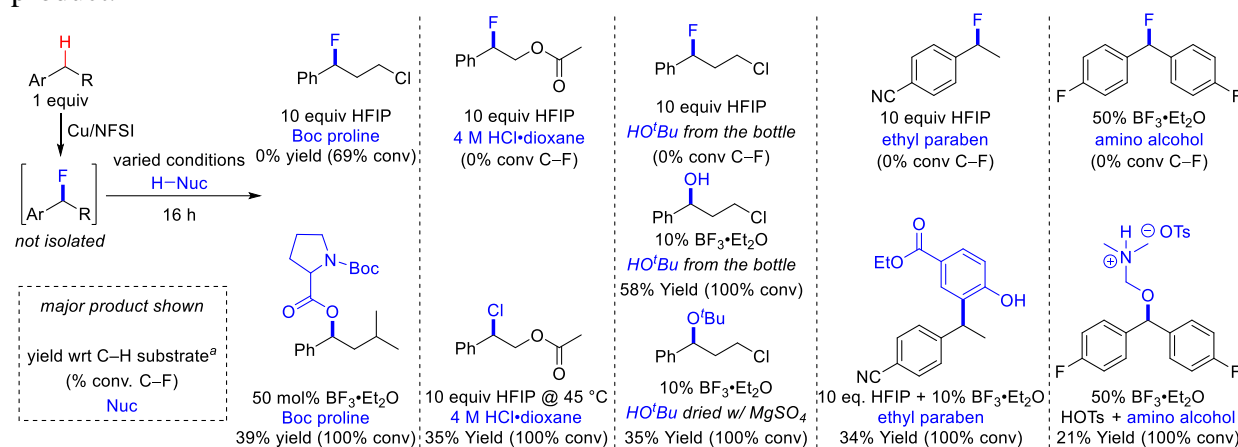
^aCalibrated ¹H NMR yields using dibromomethane as the internal standard. Reactions with (Y) indicates that remaining starting material was the major remaining mass balance component. Reactions with (N) indicates that all starting material was consumed. ^bHalf Cu/L loading, 1 equiv B₂pin₂ no MeB(OH)₂.

Discussion:

The collection of molecules in Table 4C.9 includes products omitted from the manuscript, typically because of low yields and observed deleterious side-reactivity (except for the alkylcyanide substrate, which was omitted because propylbenzene analogs are well-represented in Figure 4.3). The lactone substrate suffers from low yield because more forcing conditions result in a competitive dehydrogenation pathway to afford the α,β -unsaturated ester. The thiophene substrate showed very poor mass balance and no product was formed when BPhen was used as the ligand. Nabumetone (the ketone with a naphthalene ring) underwent complete conversion of starting material, but the only fluorination products observed were aryl fluorides. An aryl aldehyde substrate was tested for fluorination, but aldehydic C–H fluorination was observed, which agrees with a recently reported method for acyl fluoride generation.⁴ 4-Ethyl anisole oxidation resulted in complete conversion to *p*-methoxy acetophenone. The origin of ketone products likely traces back to C–F displacement by water from Li₂CO₃ to form the benzyl alcohol, which is oxidized *in situ* to the ketone (MeB(OH)₂ can also serve as a hydroxide source). It is also possible that the more electron-rich substrate oxidizes directly from the benzyl radical to a carbocation in solution, which is trapped by water and oxidized.⁵ 2-Ethyl pyridine fluorination resulted in a low yield of heterobenzylic fluoride. The nucleophilic pyridine likely coordinates to an electrophile *in situ*, which deactivates the C–H site to HAT. Ionic chemistries are typically more effective for fluorination of these types of heterobenzylic substrates.⁶ Benzylic substrates bearing an amide or ether functionality were not successfully fluorinated despite complete conversion of starting material. It is likely that the weak α -hetero C–H bonds compete for oxidation with the benzylic C–H site under these mildly basic conditions. A benzylic substrate with a TBS-protected alcohol was also tested in the fluorination reaction (92% conversion), but the TBS group is removed *in situ*, leading to an alcohol that is oxidized to an aldehyde (major observed product).

Observations Regarding Nucleophilic Coupling Partners

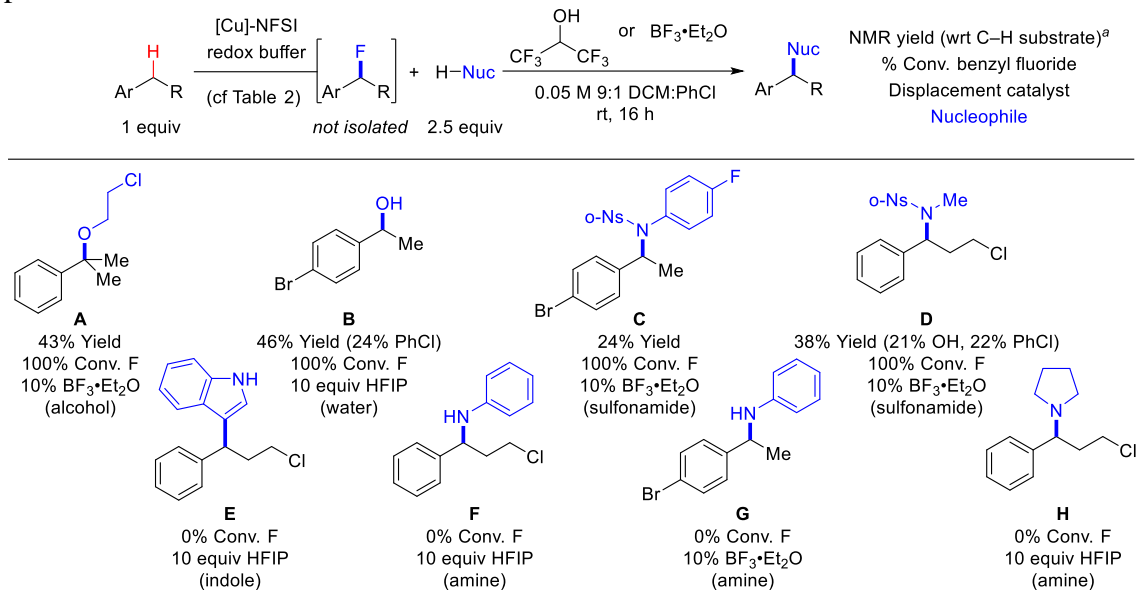
Table 4C.10. Comparisons between ineffective and effective conditions for forming desired product.



^aCalibrated ¹H NMR yields using dibromomethane as the internal standard. Yield calculated based on the starting C-H substrate. 2.5 equiv H-Nuc used, solvent is 9:1 DCM:PhCl at 0.05 M, and reactions run at room temperature unless otherwise noted. Product formation and conversion of starting material is improved from top to bottom.

Discussion:

Table 4C.10 shows how changes in conditions could be used to make certain classes of nucleophiles effective for the functionalization reaction. When using Boc proline as the nucleophile, HFIP was not able to catalyze product formation. In general, Lewis basic functional groups like carbamates resulted in obstruction of C-F activation reactivity. For Boc proline, product formation could be enabled by using 50 mol% BF₃·Et₂O as the catalyst. 2-Phenethylacetate has a C-F bond that is relatively recalcitrant towards activation (likely due to having an electron withdrawing group at the homobenzylic position). In order to activate the C-F bond for substitution by chloride, the reaction needed to be heated to 45 °C in an aluminum block on a hotplate. If *tert*-butanol is used as the nucleophile for displacement, HFIP does not catalyze displacement and BF₃·Et₂O must be used. This may support an S_N2-like pathway for displacement under HFIP-catalyzed conditions.⁷ If no precautions are taken to remove water when using *tert*-butanol as the nucleophile, the benzyl alcohol is formed as the product. If the reaction is dried with MgSO₄ and filtered before BF₃·Et₂O is added, the *tert*-butyl ether product is formed instead. In Figure 4.4, benzyl fluorides can be displaced by phenols like ethyl paraben in excellent yields when using HFIP as the catalyst. The benzyl fluoride from 4-ethyl benzonitrile is not activated under these conditions. In order to displace this electronically deactivated fluoride, BF₃·Et₂O must also be added as a catalyst. This result suggests that electron-deficient aryl rings can stabilize benzyl fluorides. It is possible to protonate Lewis basic groups (like amines), so they do not interfere with C-F activation. This allows an amino alcohol to be used as an effective coupling partner (or a pyridine, cf. **31**). An acid with a DCM-soluble non-nucleophilic counterion should be used to avoid formation of side products (for example, TFA is able to compete for fluoride displacement, so TFA salts should not be used).

Table 4C.11. Benzylic C–F displacement results for less effective C–H substrate/nucleophile pairs.

^aCalibrated ¹H NMR yields using dibromomethane as the internal standard. Yield calculated based on the starting C–H substrate.

Discussion:

Tertiary fluorides can be activated with BF₃·Et₂O for trapping by nucleophilic species, albeit the resulting products may have stability issues (the tertiary ether, 4C.11-A, decomposed after 2 days in DCM). For poor nucleophiles like water, it is possible for chlorobenzene to compete in fluoride displacement (4C.11-B and D). To avoid this issue, the fluorination reaction can be run in DCM. Another issue observed when using water as a nucleophile is that the resulting benzyl alcohol can serve as a nucleophile to form ethereal dimers of the starting material (this led to the relatively low yield of the benzyl alcohol **27** from 6-bromochromane). Ortho-nitro sulfonamide protecting groups can be used to protect primary amines to make competent nucleophiles, but the ortho-nosyl amines tend to have worse reactivity than para-nosyl amines in this reaction (compare 4C.11-C to **43**). Nucleophiles with very Lewis basic groups like amines can completely shut down displacement of the benzyl fluoride (4C.11-E, F, G, H). It is possible that these groups compete with the fluoride for hydrogen-bond donors and for BF₃·Et₂O. Efforts to drive these reactions forward with heat (45 °C in an aluminum block on a hotplate) were unsuccessful (testing at higher temperature would need to be done in a different solvent).

Site Selectivity for Fluorination of Benzylic C–H Bonds

Fluorination reactions were set up under standard conditions (see the general procedure in section 4C.II) except 5 equiv of each C–H substrate was employed (160 μ L PhMe, 1.5 mmol, 5 equiv; 185 μ L PhEt, 1.5 mmol, 5 equiv; 210 μ L cumene, 1.5 mmol, 5 equiv). Reactions were worked up in the standard fashion and analyzed via ^1H and $^{19}\text{F}\{^1\text{H}\}$ NMR spectroscopy. Product yields were determined relative to ^1H (CH_2Br_2 , 21 μ L, 0.3 mmol, 1 equiv) and ^{19}F (PhCF_3 , 37 μ L, 0.3 mmol, 1 equiv) internal standards.

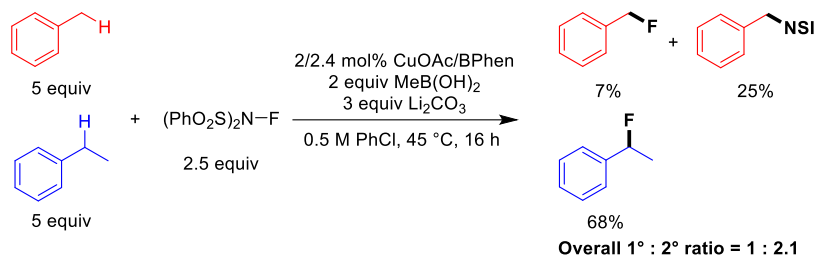


Figure 4C.1. Competition experiment for 1° vs. 2° benzylic C–H bond functionalization reactivity.

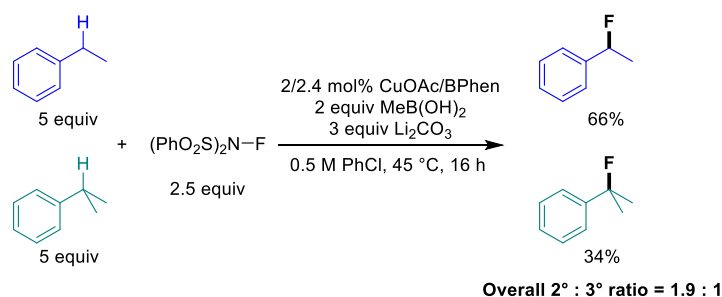
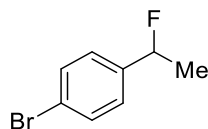


Figure 4C.2. Competition experiment for 2° vs. 3° benzylic C–H bond functionalization reactivity.

Similar selectivity preferences have been reported for photochemical benzylic fluorination reactions employing benzophenone and Selectfluor.⁸

4C.VII. Quantitative ^1H and ^{19}F NMR Spectra for Benzyl Fluoride Products

Processed (phase and baseline corrected) NMR spectra for the crude reaction mixtures of each of the benzyl fluoride products are shown below in red below. Peaks relevant to species of interest (monofluorides, difluorides, and starting material) have been picked, using the multiplet analysis tool in MestreNova. The dark blue overlays show idealized peak curves; inset spectra enlarging important resonances are included where appropriate. See figure captions for additional details.



(1) 1-bromo-4-(1-fluoroethyl)benzene: Prepared from 1-bromo-4-ethylbenzene (0.3 mmol, 42 μ L, 1.0 equiv) according to the general procedure in section 4C.II.

Spectra Available in the Literature (CAS): Yes⁹ (159298-87-0)

Benzyl Fluoride C–H Shift: ^1H NMR (CDCl_3 , 400 MHz): δ 5.59 (dq, $^2J_{(\text{H},\text{F})} = 47.4$ Hz, $^3J_{(\text{H},\text{H})} = 6.4$ Hz)

Calibrated ^1H NMR Yield from Benzylic Proton: 81%

Benzylic Fluoride Shift: ^{19}F NMR (CDCl_3 , 377 MHz): δ -168.05 (dq, $^2J_{(\text{H},\text{F})} = 48.2$ Hz, $^3J_{(\text{H},\text{F})} = 24.6$ Hz)

Calibrated ^{19}F NMR Yields from Benzylic Fluorides: 86% ($\text{CF}_2 - 11\%$)

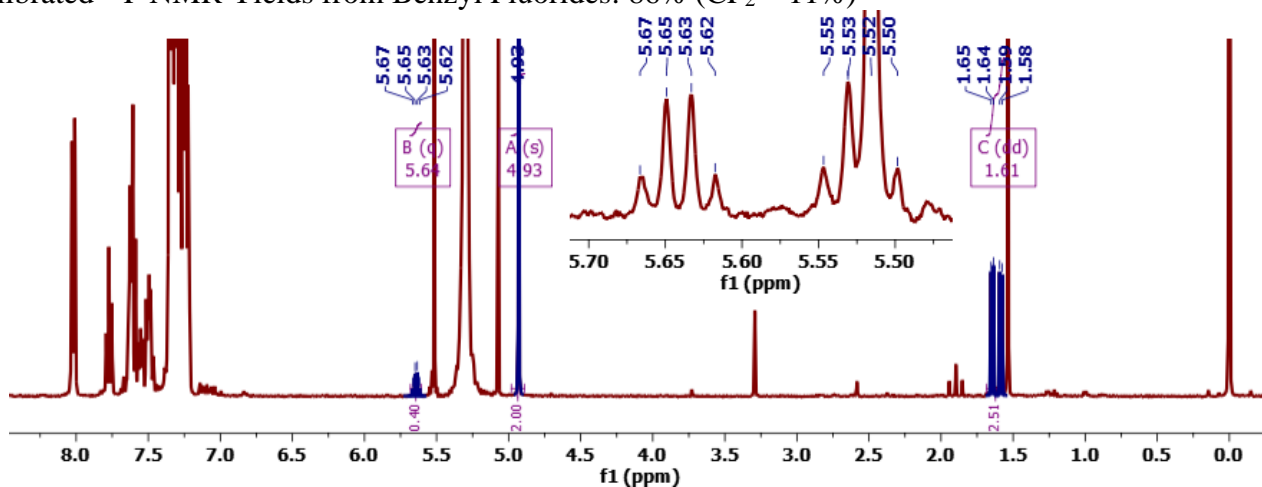


Figure 4C.3. Crude ^1H NMR Spectrum (CDCl_3 , 400 MHz, 25 $^\circ\text{C}$) of the reaction mixture following the addition of 0.3 mmol (21 μ L) of CH_2Br_2 as an internal standard (4.93 ppm). The resolved benzylic and methyl protons are labeled and integrated.

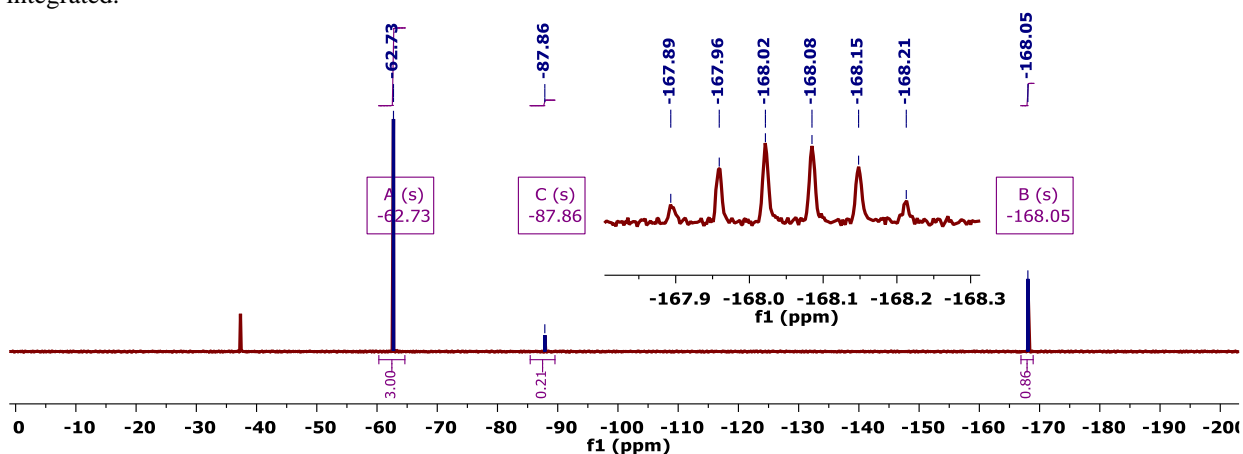
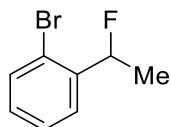


Figure 4C.4. Crude $^{19}\text{F}\{^1\text{H}\}$ NMR Spectrum (CDCl_3 , 377 MHz, 25 $^\circ\text{C}$) of the reaction mixture following the addition of 0.3 mmol (37 μ L) of PhCF_3 as an internal standard (-62.73 ppm). The mono- and di-fluoride (-168.05 and -87.86 ppm, respectively) are labeled and integrated. The inset shows an enlargement of the proton-coupled mono-fluoride.



(2) 1-bromo-2-(1-fluoroethyl)benzene: Prepared from 1-bromo-2-ethylbenzene (0.3 mmol, 41 μL , 1.0 equiv) according to the general procedure in section 4C.II with the following variations: 1 mol% CuOAc, 1.2 mol% BPhen, 1 equiv B₂pin₂ (in place of 2 equiv MeB(OH)₂), and 4 equiv NFSI operating at 55 °C.

Spectra Available in the Literature (CAS): Yes¹⁰ (1027513-77-4)

Benzyl Fluoride C–H Shift: ¹H NMR (CDCl₃, 400 MHz): δ 5.91 (dq, ²J_(H,F) = 46.5 Hz, ³J_(H,H) = 6.3 Hz)

Calibrated ¹H NMR Yield from Benzyl Fluoride Methyl Group: 50%

Benzylic Fluoride Shift: ¹⁹F NMR (CDCl₃, 377 MHz): δ -173.76 (dq, ²J_(H,F) = 48.3 Hz, ³J_(H,F) = 24.4 Hz)

Calibrated ¹⁹F NMR Yields from Benzyl Fluoride: 44%

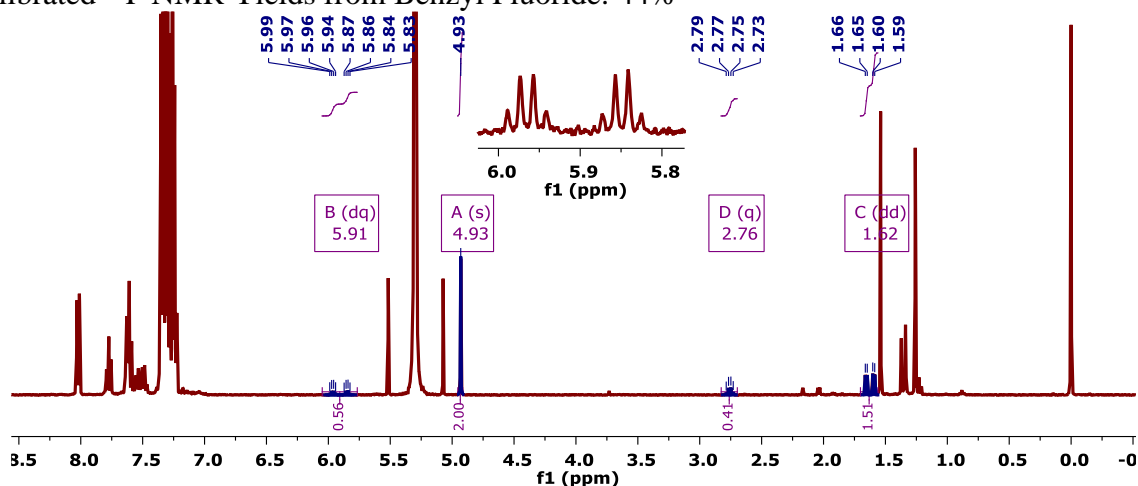


Figure 4C.5. Crude ¹H NMR Spectrum (CDCl₃, 400 MHz, 25 °C) of the reaction mixture following the addition of 0.3 mmol (21 μL) of CH₂Br₂ as an internal standard (4.93 ppm). The resolved product and starting material benzylic protons are labeled and integrated.

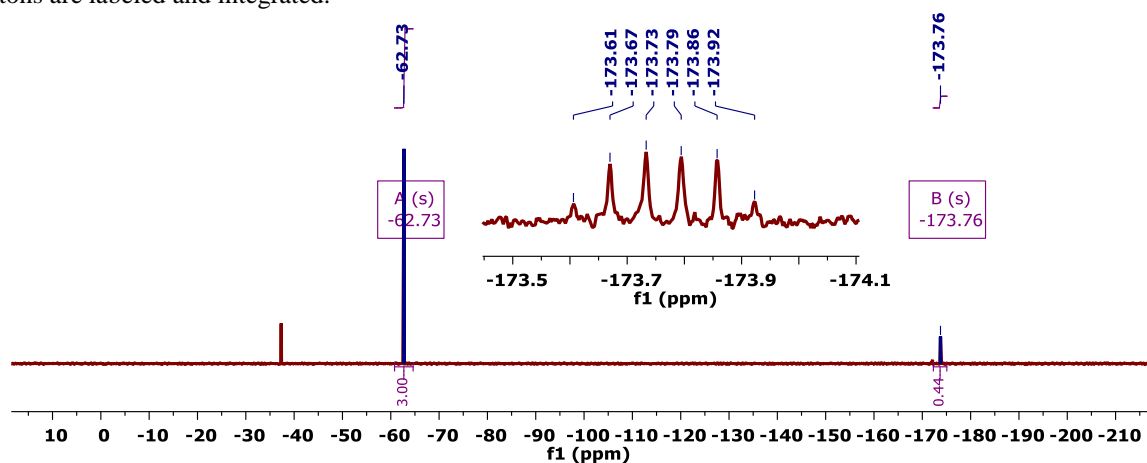
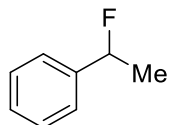


Figure 4C.6. Crude ¹⁹F{¹H} NMR Spectrum (CDCl₃, 377 MHz, 25 °C) of the reaction mixture following the addition of 0.3 mmol (37 μL) of PhCF₃ as an internal standard (-62.73 ppm). The mono-fluoride (-173.76 ppm) is labeled and integrated; the inset shows an enlargement of the proton-coupled mono-fluoride.



(3) (1-fluoroethyl)benzene: Prepared from ethylbenzene (0.3 mmol, 37 μ L, 1.0 equiv) according to the general procedure in section 4C.II.

Spectra Available in the Literature (CAS): Yes¹¹ (7100-97-2)

Benzyl Fluoride C–H Shift: ^1H NMR (CDCl_3 , 400 MHz): δ 5.62 (dq, $^2J_{(\text{H},\text{F})} = 47.8$ Hz, $^3J_{(\text{H},\text{H})} = 6.5$ Hz)

Calibrated ^1H NMR Yield from Benzylic Proton: 67%

Benzylic Fluoride Shift: ^{19}F NMR (CDCl_3 , 377 MHz): δ -167.02 (dq, $^2J_{(\text{H},\text{F})} = 47.8$ Hz, $^3J_{(\text{H},\text{F})} = 23.9$ Hz)

Calibrated ^{19}F NMR Yields from Benzylic Fluoride: 64% (CF_2 – 11%)

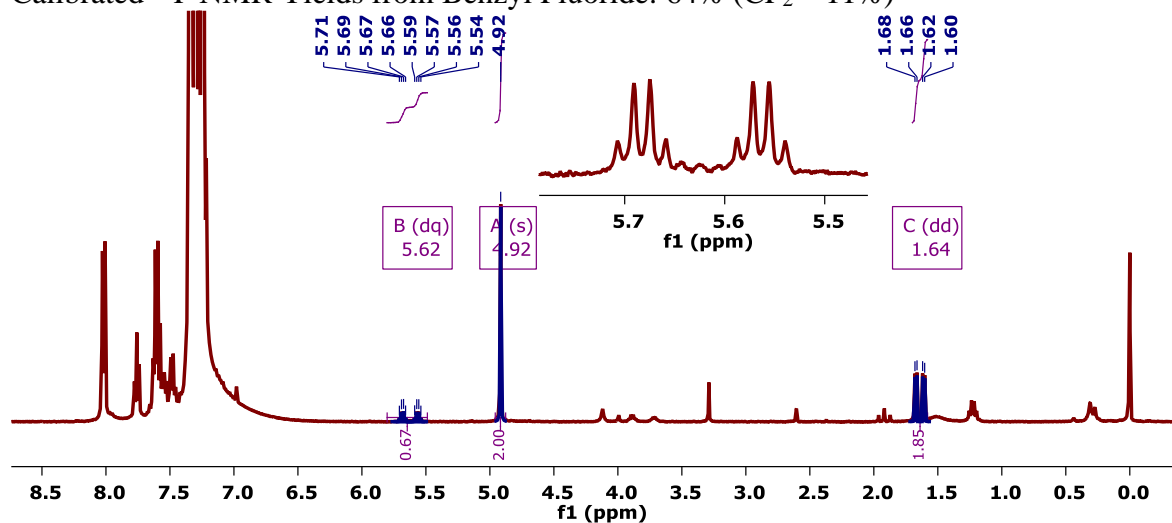


Figure 4C.7. Crude ^1H NMR Spectrum (CDCl_3 , 400 MHz, 25 $^\circ\text{C}$) of the reaction mixture following the addition of 0.3 mmol (21 μ L) of CH_2Br_2 as an internal standard (4.92 ppm). The resolved product benzylic and methyl protons are labeled and integrated.

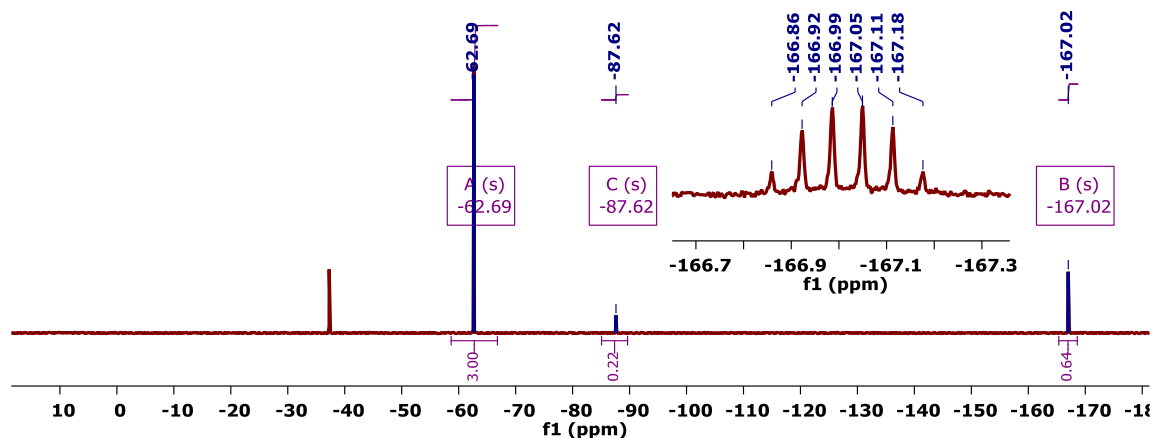
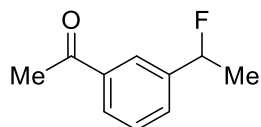


Figure 4C.8. Crude $^{19}\text{F}\{^1\text{H}\}$ NMR Spectrum (CDCl_3 , 377 MHz, 25 $^\circ\text{C}$) of the reaction mixture following the addition of 0.3 mmol (37 μ L) of PhCF_3 as an internal standard (-62.73 ppm). The mono- and di-fluoride (-167.02 and -87.62 ppm, respectively) are labeled and integrated. The inset shows an enlargement of the proton-coupled mono-fluoride.



(4) 1-(3-(1-fluoroethyl)phenyl)ethan-1-one: Prepared from 1-(3-ethylphenyl)ethan-1-one (0.3 mmol, 49.9 mg, 1.0 equiv) according to the general procedure in section 4C.II with the following variations: 1 mol% CuOAc, 1.2 mol% BPhen, 1 equiv B₂pin₂ (in place of 2 equiv MeB(OH)₂), and 4 equiv NFSI operating at 55 °C.

Spectra Available in the Literature (CAS): No (1550969-43-1)

Benzyl Fluoride C–H Shift: ¹H NMR (CDCl₃, 400 MHz): δ 5.61 (dq, ²J_(H,F) = 47.5 Hz, ³J_(H,H) = 6.5 Hz)

Calibrated ¹H NMR Yield from Benzyl Fluoride Methyl Group: 83%

Decoupled Benzyl Fluoride Shift: ¹⁹F NMR (CDCl₃, 377 MHz): δ -168.89 (s)

Calibrated ¹⁹F NMR Yields from Benzyl Fluoride: 75% (CF₂ – 20%)

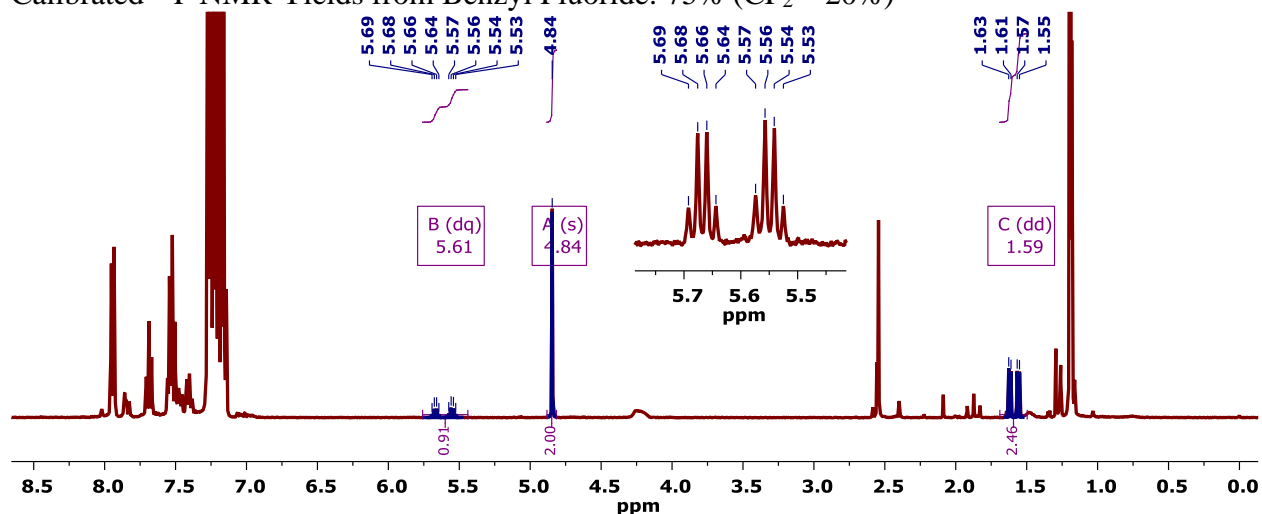


Figure 4C.9. Crude ¹H NMR Spectrum (CDCl₃, 400 MHz, 25 °C) of the reaction mixture following the addition of 0.3 mmol (21 μL) of CH₂Br₂ as an internal standard (4.84 ppm). The resolved product benzylic and methyl protons are labeled and integrated.

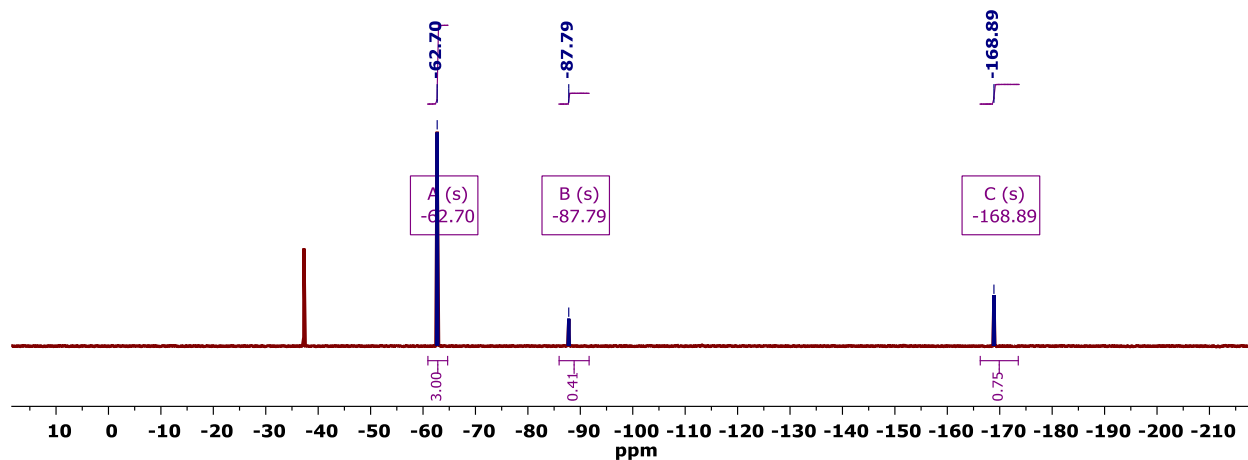
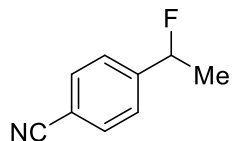


Figure 4C.10. Crude ¹⁹F{¹H} NMR Spectrum (CDCl₃, 377 MHz, 25 °C) of the reaction mixture following the addition of 0.3 mmol (37 μL) of PhCF₃ as an internal standard (-62.70 ppm). The mono- and di-fluoride (-168.89 and -87.79 ppm, respectively) are labeled and integrated.



(5) 4-(1-fluoroethyl)benzonitrile: Prepared from 4-ethylbenzonitrile (0.3 mmol, 41 μ L, 1.0 equiv) according to the general procedure in section 4C.II with the following variations: 1 mol% CuOAc, 1.2 mol% BPhen, 1 equiv B₂pin₂ (in place of 2 equiv MeB(OH)₂), and 4 equiv NFSI operating at 75 °C.

Spectra Available in the Literature (CAS): Yes⁸ (155671-14-0)

Benzyl Fluoride C–H Shift: ¹H NMR (CDCl₃, 400 MHz): δ 5.70 (dq, ²J_(H,F) = 47.4 Hz, ³J_(H,H) = 6.5 Hz)

Calibrated ¹H NMR Yield from Benzyl Fluoride Methyl Group: 56%

Decoupled Benzyl Fluoride Shift: ¹⁹F NMR (CDCl₃, 377 MHz): δ -172.67 (s)

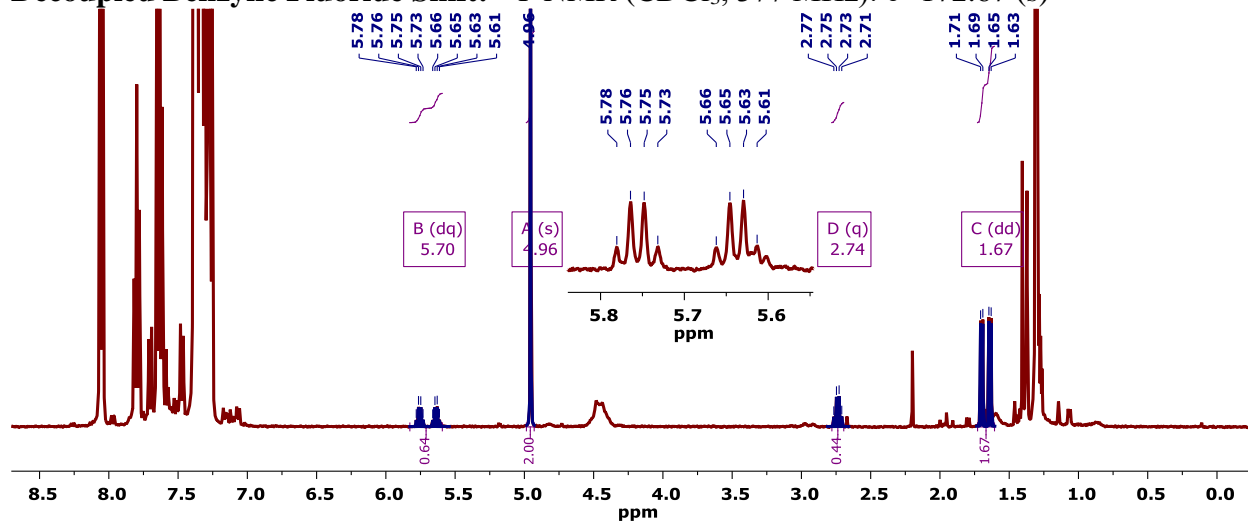


Figure 4C.11. Crude ¹H NMR Spectrum (CDCl₃, 400 MHz, 25 °C) of the reaction mixture following the addition of 0.3 mmol (21 μ L) of CH₂Br₂ as an internal standard (4.96 ppm). The resolved product benzylic and methyl protons are labeled and integrated. The residual starting material benzylic protons are likewise labeled and integrated.

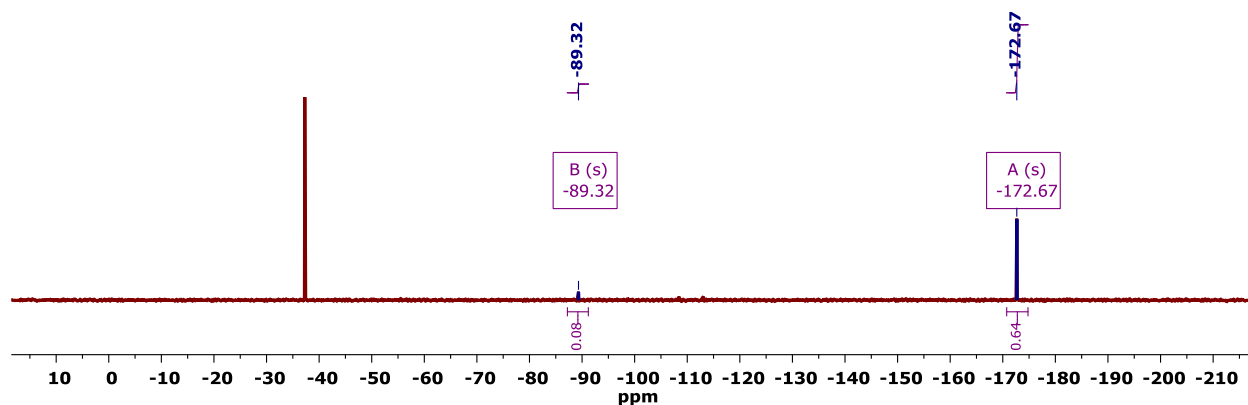
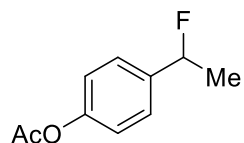


Figure 4C.12. Crude ¹⁹F{¹H} NMR Spectrum (CDCl₃, 377 MHz, 25 °C) of the reaction mixture. The mono- and difluoride (-172.67 and -89.32 ppm, respectively) are labeled and integrated.



(6) 4-(1-fluoroethyl)phenyl acetate: Prepared from 4-ethylphenyl acetate (0.3 mmol, 48 μ L, 1.0 equiv) according to the general procedure in section 4C.II with the following variations: 1 mol% CuOAc, 1.2 mol% BPhen, 1 equiv B₂pin₂ (in place of 2 equiv MeB(OH)₂), and 4 equiv NFSI operating at 55 °C.

Spectra Available in the Literature (CAS): Yes¹² (1487496-31-0)

Benzyl Fluoride C–H Shift: ¹H NMR (CDCl₃, 400 MHz): δ 5.62 (dq, ²J_(H,F) = 47.5 Hz, ³J_(H,H) = 6.4 Hz)

Calibrated ¹H NMR Yield from Benzyl Fluoride Methyl Group: 66%

Benzylic Fluoride Shift: ¹⁹F NMR (CDCl₃, 377 MHz): δ -166.40 (dq, ²J_(H,F) = 47.7 Hz, ³J_(H,F) = 23.9 Hz)

Calibrated ¹⁹F NMR Yields from Benzyl Fluoride: 63% (CF₂ – 7%)

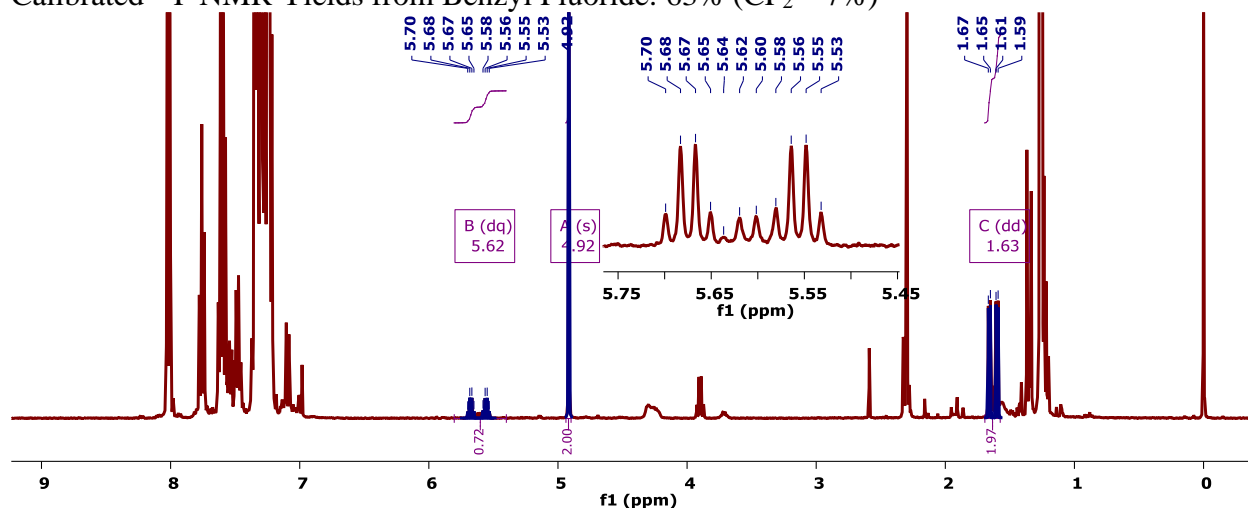


Figure 4C.13. Crude ¹H NMR Spectrum (CDCl₃, 400 MHz, 25 °C) of the reaction mixture following the addition of 0.3 mmol (21 μ L) of CH₂Br₂ as an internal standard (4.92 ppm). The resolved product benzylic and methyl protons are labeled and integrated.

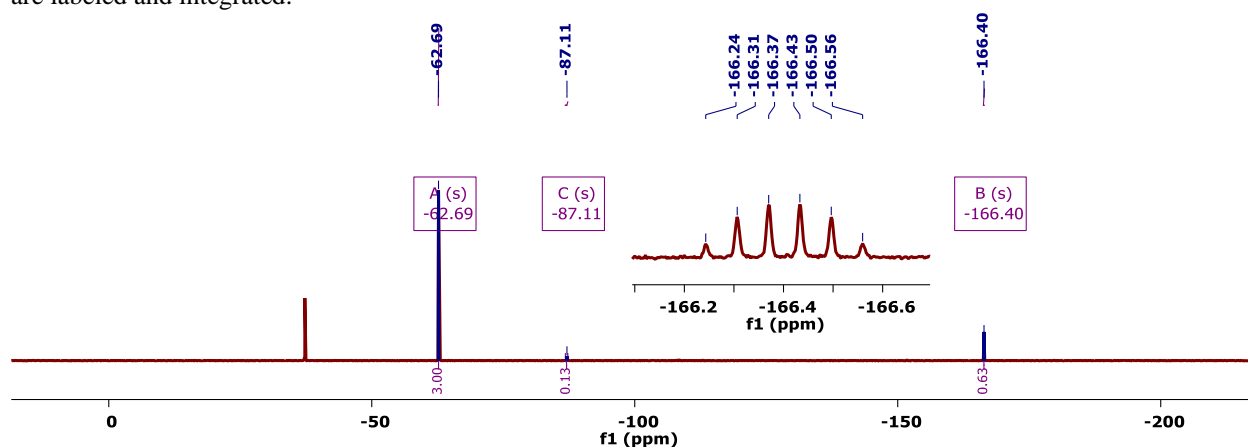
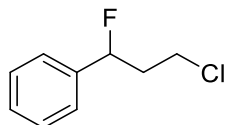


Figure 4C.14. Crude ¹⁹F{¹H} NMR Spectrum (CDCl₃, 377 MHz, 25 °C) of the reaction mixture following the addition of 0.3 mmol (37 μ L) of PhCF₃ as an internal standard (-62.69 ppm). The mono- and di-fluoride (-166.40 and -87.11 ppm, respectively) are labeled and integrated.



(7) (3-chloro-1-fluoropropyl)benzene: Prepared from (3-chloropropyl)benzene (0.3 mmol, 45 μL , 1.0 equiv) according to the general procedure in section 4C.II. When the reaction was repeated on 3 mmol scale, it was conducted in a 15 mL vial.

Spectra Available in the Literature (CAS): Yes¹³ (1487496-36-5)

Benzyl Fluoride C–H Shift: ^1H NMR (CDCl_3 , 400 MHz): δ 5.68 (ddd, $^2J_{(\text{H},\text{F})} = 47.8$ Hz, $^3J_{(\text{H},\text{H})} = 8.9$ & 3.8 Hz)

Calibrated ^1H NMR Yield from Benzyl Proton: 82% (0.3 mmol scale) or 68% (3 mmol scale)

Benzylic Fluoride Shift: ^{19}F NMR (CDCl_3 , 377 MHz): δ -179.43 (ddd, $^2J_{(\text{H},\text{F})} = 46.9$ Hz, $^3J_{(\text{H},\text{F})} = 31.3$ & 14.0 Hz)

Calibrated ^{19}F NMR Yield from Benzyl Fluoride: 75% (CF_2 – 5%)

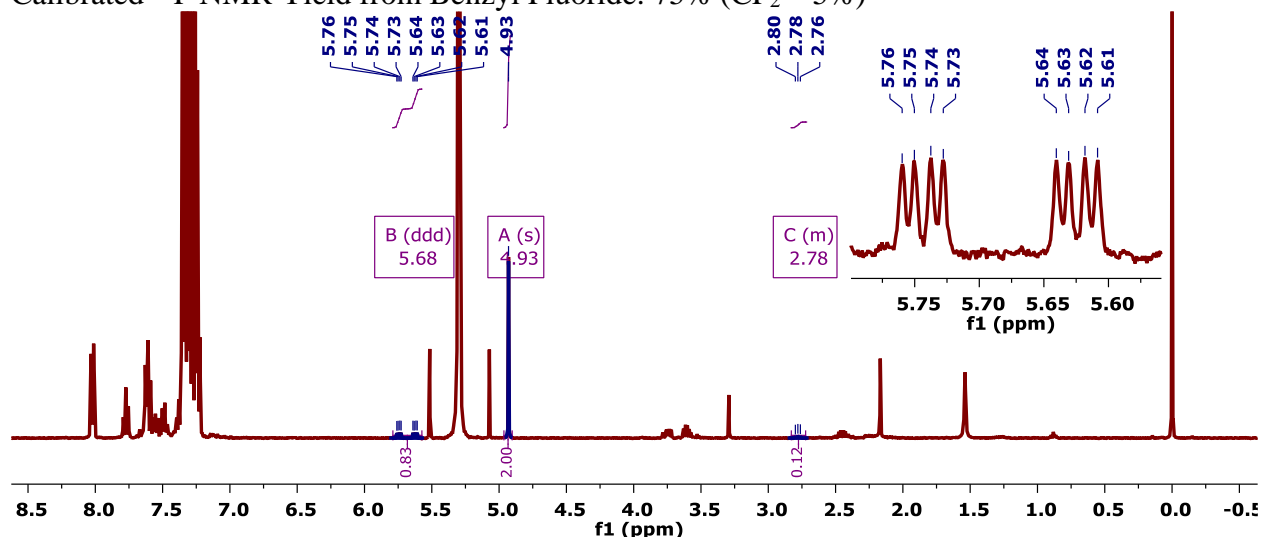


Figure 4C.15. Crude ^1H NMR Spectrum (CDCl_3 , 400 MHz, 25 $^\circ\text{C}$) of the reaction mixture following the addition of 0.3 mmol (21 μL) of CH_2Br_2 as an internal standard (4.93 ppm). The resolved product and starting material benzylic protons are labeled and integrated.

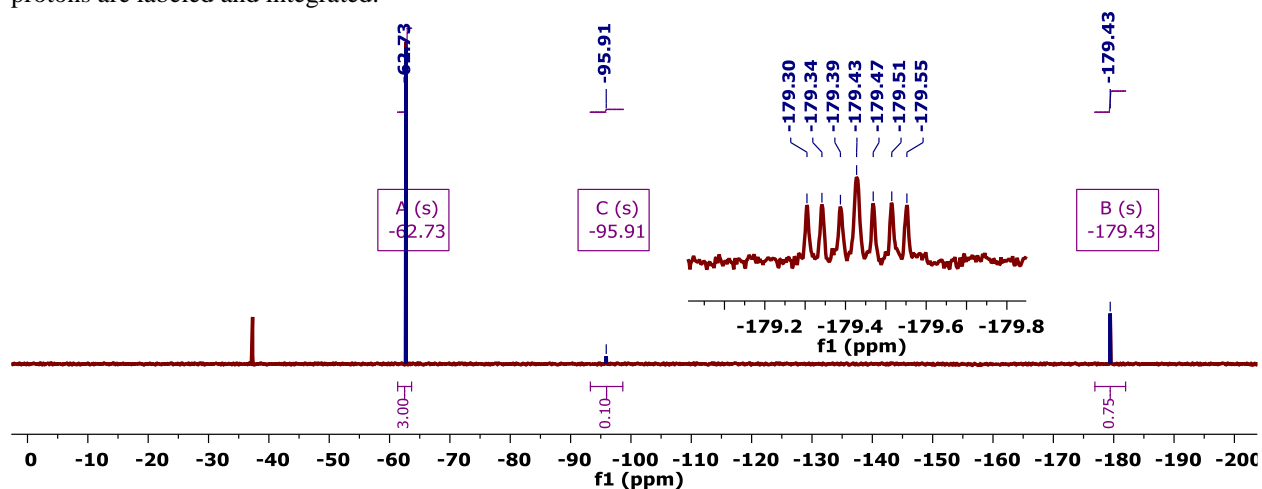
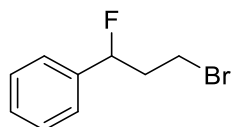


Figure 4C.16. Crude $^{19}\text{F}\{^1\text{H}\}$ NMR Spectrum (CDCl_3 , 377 MHz, 25 $^\circ\text{C}$) of the reaction mixture following the addition of 0.3 mmol (37 μL) of PhCF_3 as an internal standard (-62.73 ppm). The mono- and di-fluoride (-179.43 and -95.91 ppm, respectively) are labeled and integrated. The inset shows an enlargement of the proton coupled mono-fluoride.



(8) (3-bromo-1-fluoropropyl)benzene: Prepared from (3-bromopropyl)benzene (0.3 mmol, 46 μL , 1.0 equiv) according to the general procedure in section 4C.II. When the reaction was repeated on 3 mmol scale, it was conducted in a 15 mL vial.

Spectra Available in the Literature (CAS): Yes¹¹ (1428331-73-0)

Benzyl Fluoride C–H Shift: ^1H NMR (CDCl_3 , 400 MHz): δ 5.66 (ddd, $^2J_{(\text{H},\text{F})} = 47.7$ Hz, $^3J_{(\text{H},\text{H})} = 8.8$ & 3.9 Hz)

Calibrated ^1H NMR Yield from Benzyl Proton: 71% (0.3 mmol scale) or 67% (3 mmol scale)

Benzylic Fluoride Shift: ^{19}F NMR (CDCl_3 , 377 MHz): δ -179.33 (ddd, $^2J_{(\text{H},\text{F})} = 46.9$ Hz, $^3J_{(\text{H},\text{F})} = 31.3$ & 14.0 Hz)

Calibrated ^{19}F NMR Yield from Benzyl Fluoride: 68%

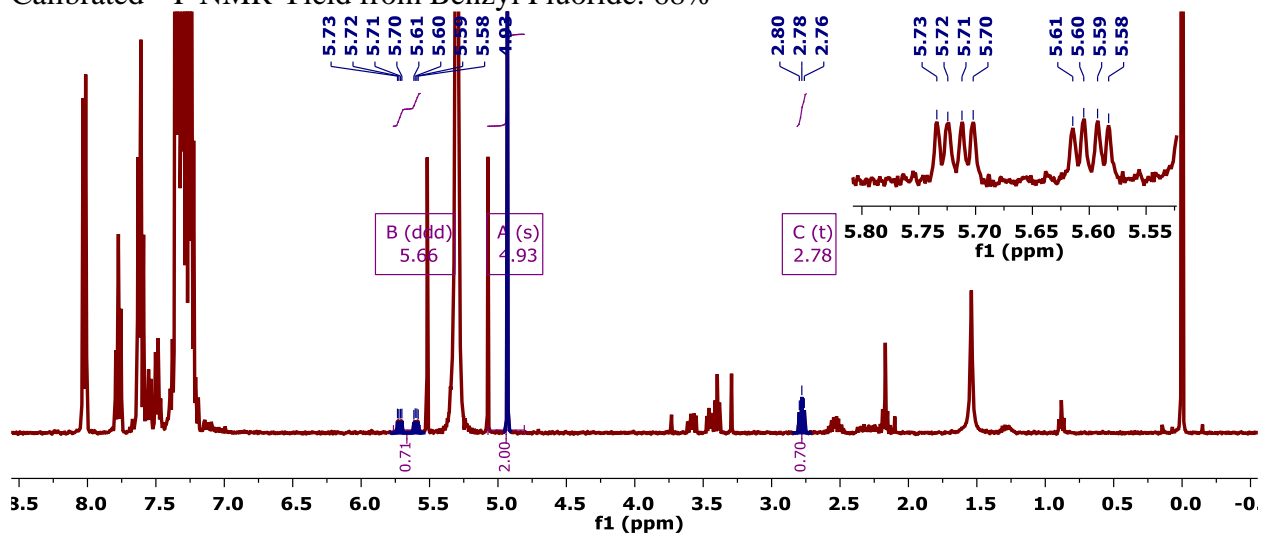


Figure 4C.17. Crude ^1H NMR Spectrum (CDCl_3 , 400 MHz, 25 $^\circ\text{C}$) of the reaction mixture following the addition of 0.3 mmol (21 μL) of CH_2Br_2 as an internal standard (4.93 ppm). The resolved product and starting material benzylic protons are labeled and integrated.

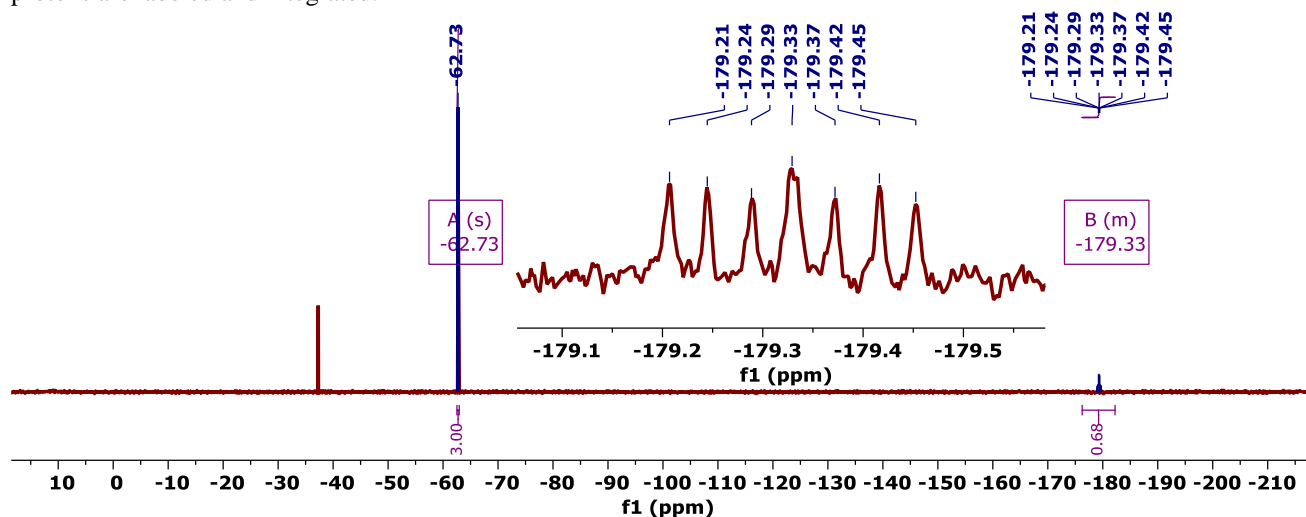
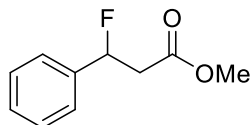


Figure 4C.18. Crude ^{19}F NMR Spectrum (CDCl_3 , 377 MHz, 25 $^\circ\text{C}$) of the reaction mixture following the addition of 0.3 mmol (37 μL) of PhCF_3 as an internal standard (-62.73 ppm). The mono-fluoride (-179.33) is labeled and integrated. The inset shows an enlargement of the proton-coupled mono-fluoride.



(9) Methyl 3-fluoro-3-phenylpropanoate: Prepared from methyl 3-phenylpropanoate (0.75 mmol, 47 μ L, 1.0 equiv) that was formed according to the general procedure in section 4C.II with the following variations: 1 mol% CuOAc, 1.2 mol% BPhen, 1 equiv B₂pin₂ (in place of 2 equiv MeB(OH)₂), and 4 equiv NFSI operating at 55 °C.

Spectra Available in the Literature (CAS): Yes⁸ (188941-05-1)

Benzyl Fluoride C–H Shift: ¹H NMR (CDCl₃, 400 MHz): δ 5.93 (ddd, ²J_(H,F) = 46.9 Hz, ³J_(H,H) = 9.2 & 4.1 Hz)

Calibrated ¹H NMR Yield from Benzyl Proton: 58%

Benzylic Fluoride Shift: ¹⁹F NMR (CDCl₃, 377 MHz): δ -173.16 (ddd, ²J_(H,F) = 46.4 Hz, ³J_(H,F) = 32.6 & 13.4 Hz)

Calibrated ¹⁹F NMR Yield from Benzyl Fluoride: 51% (CF₂ – 2%)

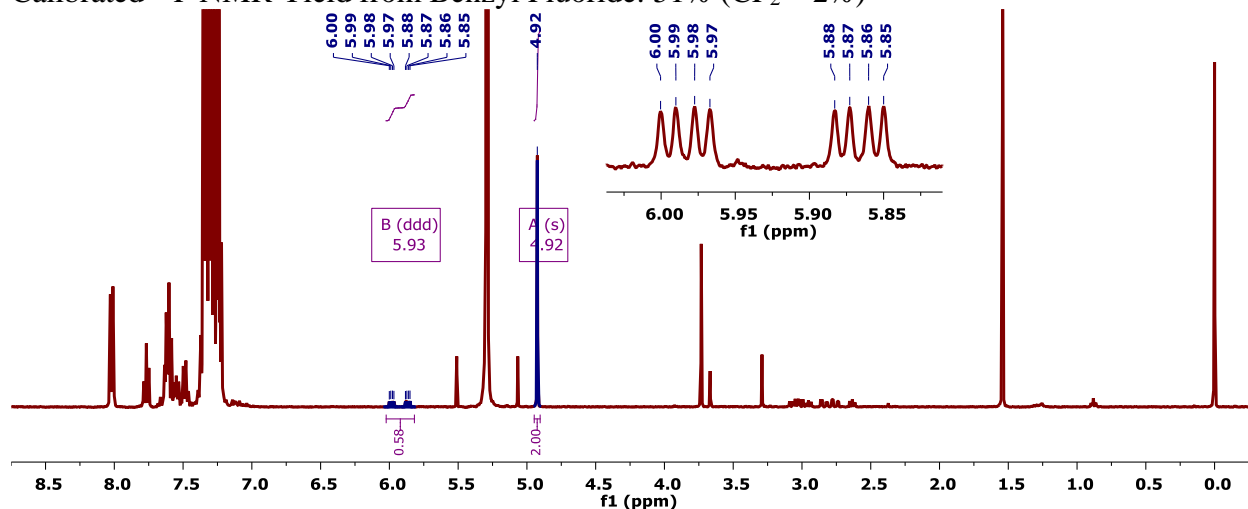


Figure 4C.19. Crude ¹H NMR Spectrum (CDCl₃, 400 MHz, 25 °C) of the reaction mixture following the addition of 0.3 mmol (21 μ L) of CH₂Br₂ as an internal standard (4.92 ppm). The resolved product benzylic protons are labeled and integrated.

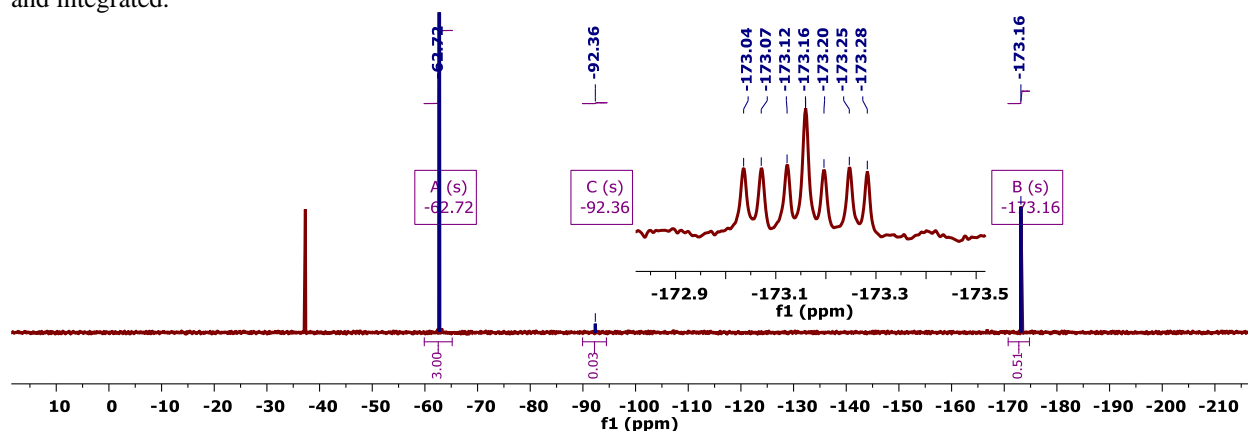
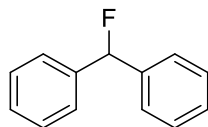


Figure 4C.20. Crude ¹⁹F{¹H} NMR Spectrum (CDCl₃, 377 MHz, 25 °C) of the reaction mixture following the addition of 0.3 mmol (37 μ L) of PhCF₃ as an internal standard (-62.72 ppm). The mono- and di-fluoride (-173.16 and -92.36 ppm, respectively) are labeled and integrated. The inset shows an enlargement of the proton-coupled mono-fluoride.



(10) (fluoromethylene)dibenzene: Prepared from diphenylmethane (0.3 mmol, 50.5 mg, 1.0 equiv) according to the general procedure in section 4C.II.

Spectra Available in the Literature (CAS): Yes⁸ (579-55-5)

Benzyl Fluoride C–H Shift: ¹H NMR (CDCl₃, 400 MHz): δ 6.47 (d, ²J_(H,F) = 47.4 Hz)

Calibrated ¹H NMR Yield from Benzyl Proton: 40%

Benzylic Fluoride Shift: ¹⁹F NMR (CDCl₃, 377 MHz): δ -166.73 (d, ²J_(H,F) = 47.5 Hz)

Calibrated ¹⁹F NMR Yield from Benzyl Fluoride: 40%

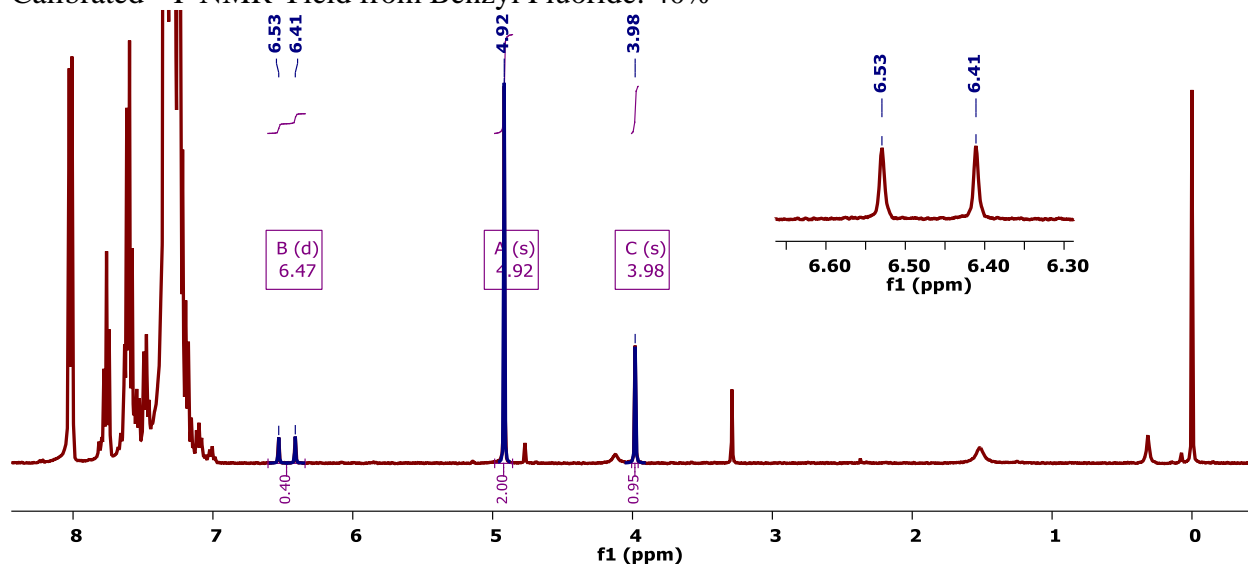


Figure 4C.21. Crude ¹H NMR Spectrum (CDCl₃, 400 MHz, 25 °C) of the reaction mixture following the addition of 0.3 mmol (21 μL) of CH₂Br₂ as an internal standard (4.92 ppm). The resolved product and starting material benzylic protons are labeled and integrated.

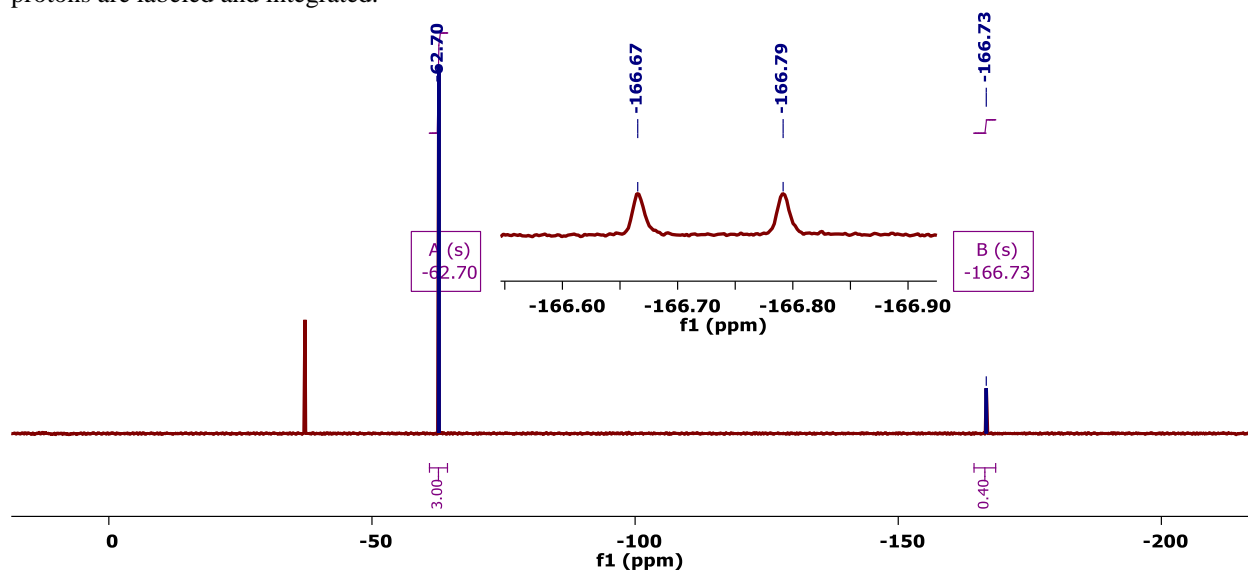
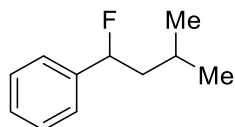


Figure 4C.22. Crude ¹⁹F{¹H} NMR Spectrum (CDCl₃, 377 MHz, 25 °C) of the reaction mixture following the addition of 0.3 mmol (37 μL) of PhCF₃ as an internal standard (-62.70 ppm). The mono-fluoride (-166.73) is labeled and integrated. The inset shows an enlargement of the proton-coupled mono-fluoride.



(11) (1-fluoro-3-methylbutyl)benzene: Prepared from isopentylbenzene (0.3 mmol, 52 μ L, 1.0 equiv) according to the general procedure in section 4C.II.

Spectra Available in the Literature (CAS): No (N/A)

Benzylic Fluoride C–H Shift: ^1H NMR (CDCl_3 , 400 MHz): δ 5.50 (ddd, $^2J_{(\text{H},\text{F})} = 48.2$ Hz, $^3J_{(\text{H},\text{H})} = 9.2$ & 4.3 Hz)

Calibrated ^1H NMR Yield from Benzylic Proton: 70%

Benzylic Fluoride Shift: ^{19}F NMR (CDCl_3 , 377 MHz): δ -174.31 (ddd, $^2J_{(\text{H},\text{F})} = 48.4$ Hz, $^3J_{(\text{H},\text{F})} = 33.6$ & 14.6 Hz)

Calibrated ^{19}F NMR Yield from Benzylic Fluoride: 65% (CF_2 – 6%)

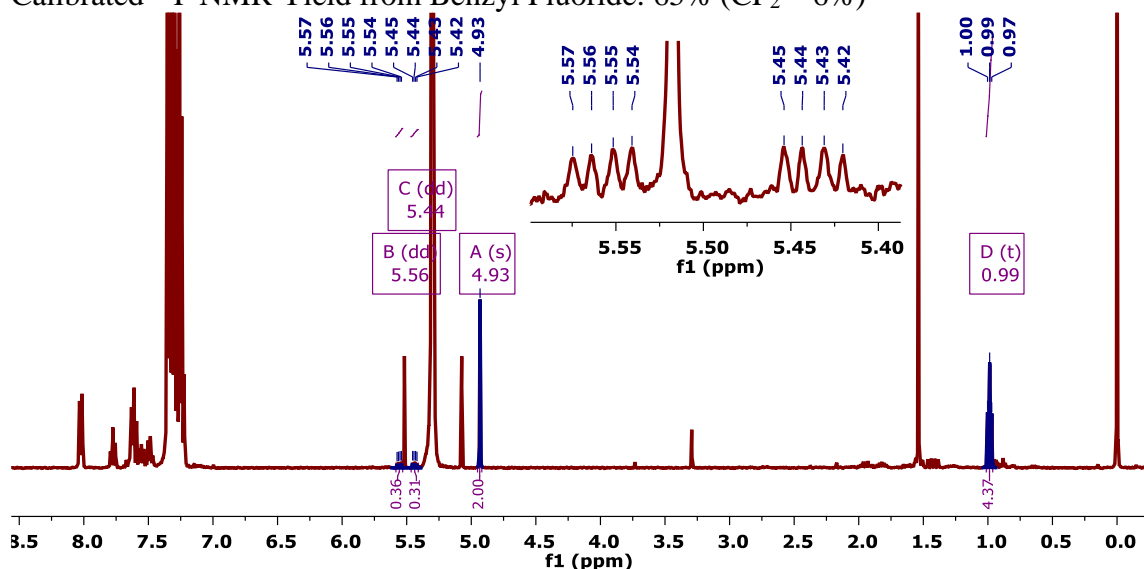


Figure 4C.23. Crude ^1H NMR Spectrum (CDCl_3 , 400 MHz, 25 $^\circ\text{C}$) of the reaction mixture following the addition of 0.3 mmol (21 μL) of CH_2Br_2 as an internal standard (4.93 ppm). The resolved product benzylic and methyl protons are labeled and integrated.

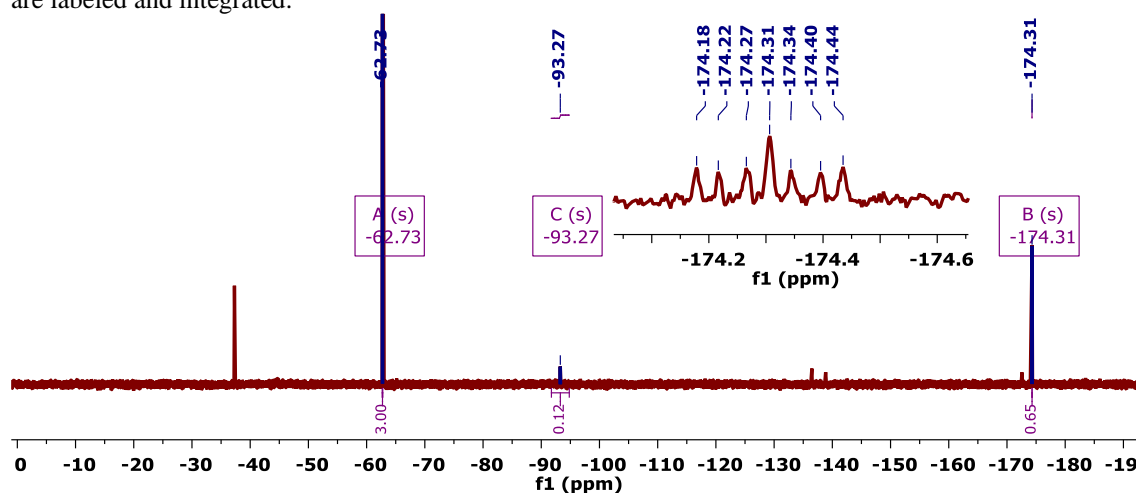
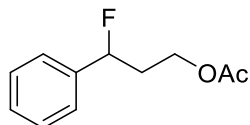


Figure 4C.2. Crude $^{19}\text{F}\{^1\text{H}\}$ NMR Spectrum (CDCl_3 , 377 MHz, 25 $^\circ\text{C}$) of the reaction mixture following the addition of 0.3 mmol (37 μL) of PhCF_3 as an internal standard (-62.73 ppm). The mono- and di-fluoride (-174.31 and -93.27 ppm, respectively) are labeled and integrated. The inset shows an enlargement of the proton-coupled mono-fluoride.



(12) 3-fluoro-3-phenylpropyl acetate: Prepared from 3-phenylpropyl acetate (0.3 mmol, 53 μ L, 1.0 equiv) according to the general procedure in section 4C.II.

Spectra Available in the Literature (CAS): Yes⁸ (412026-80-3)

Benzyl Fluoride C–H Shift: ^1H NMR (CDCl_3 , 400 MHz): δ 5.57 (ddd, $^2J_{(\text{H},\text{F})} = 47.8$ Hz, $^3J_{(\text{H},\text{H})} = 8.8$ & 4.3 Hz)

Calibrated ^1H NMR Yield from Benzyl Proton: 79%

Benzylic Fluoride Shift: ^{19}F NMR (CDCl_3 , 377 MHz): δ -177.40 (ddd, $^2J_{(\text{H},\text{F})} = 46.1$ Hz, $^3J_{(\text{H},\text{F})} = 30.1$ & 15.4 Hz)

Calibrated ^{19}F NMR Yield from Benzyl Fluoride: 74% (CF_2 – 3%)

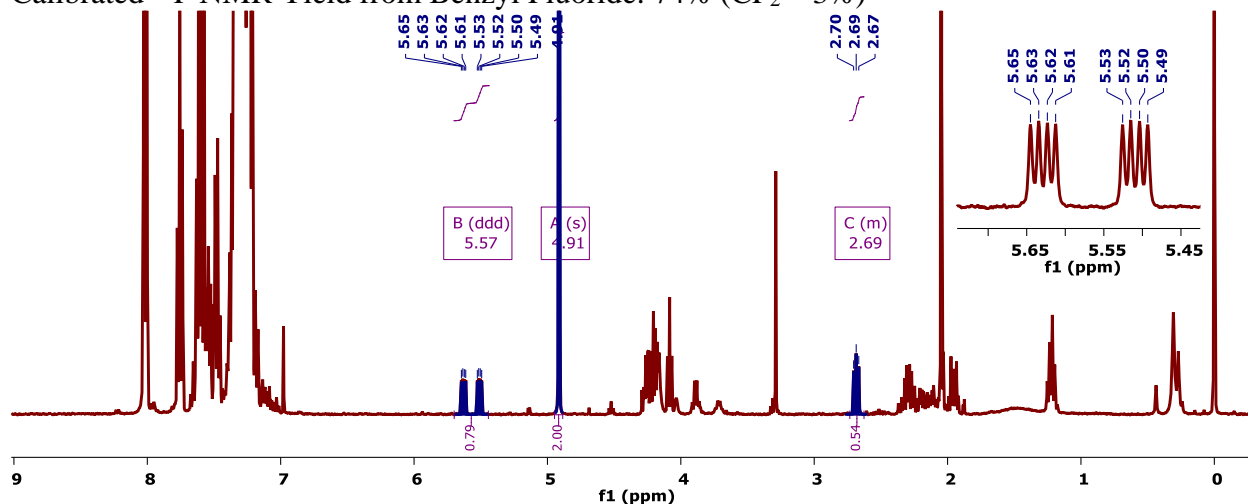


Figure 4C.25. Crude ^1H NMR Spectrum (CDCl_3 , 400 MHz, 25 $^\circ\text{C}$) of the reaction mixture following the addition of 0.3 mmol (21 μ L) of CH_2Br_2 as an internal standard (4.93 ppm). The resolved product and starting material benzylic protons are labeled and integrated.

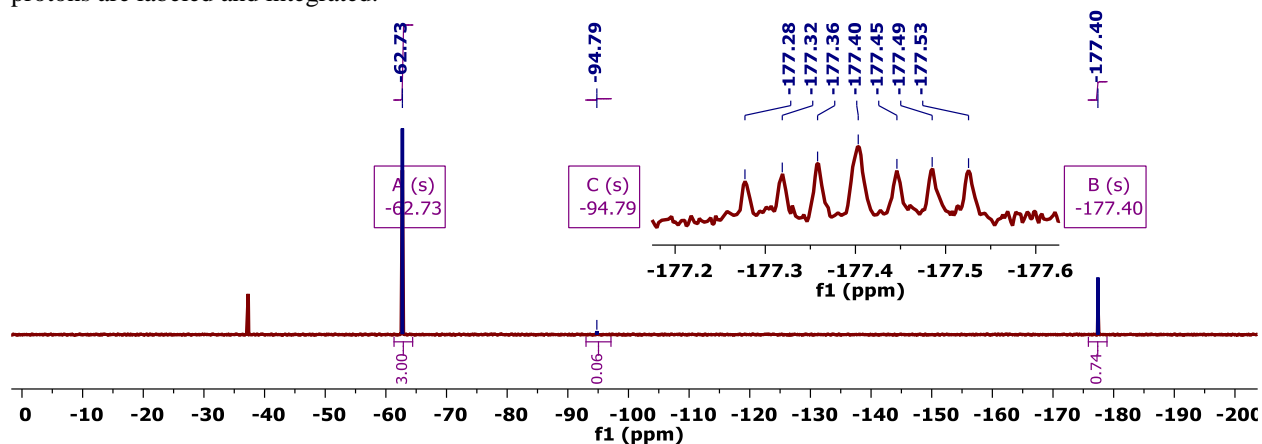
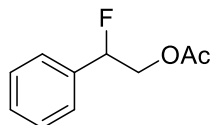


Figure 4C.26. Crude $^{19}\text{F}\{^1\text{H}\}$ NMR Spectrum (CDCl_3 , 377 MHz, 25 $^\circ\text{C}$) of the reaction mixture following the addition of 0.3 mmol (37 μ L) of PhCF_3 as an internal standard (-62.73 ppm). The mono- and di-fluoride (-177.40 and -94.79 ppm, respectively) are labeled and integrated. The inset shows an enlargement of the proton-coupled mono-fluoride.



(13) 2-fluoro-2-phenylethyl acetate: Prepared from phenethyl acetate (0.3 mmol, 54.6 mg, 1.0 equiv) according to the general procedure in section 4C.II with the following variations: 1 mol% CuOAc, 1.2 mol% BPhen, 1 equiv B₂pin₂ (in place of 2 equiv MeB(OH)₂), and 4 equiv NFSI operating at 55 °C in acetone.

Spectra Available in the Literature (CAS): Yes¹⁴ (33315-78-5)

Benzyl Fluoride C–H Shift: ¹H NMR (CDCl₃, 400 MHz): δ 5.58 (ddd, ²J_(H,F) = 48.6 Hz, ³J_(H,H) = 7.2 & 3.6 Hz)

Calibrated ¹H NMR Yield from Benzylic Proton: 53%

Decoupled Benzylic Fluoride Shift: ¹⁹F NMR (CDCl₃, 377 MHz): δ -184.35 (s)

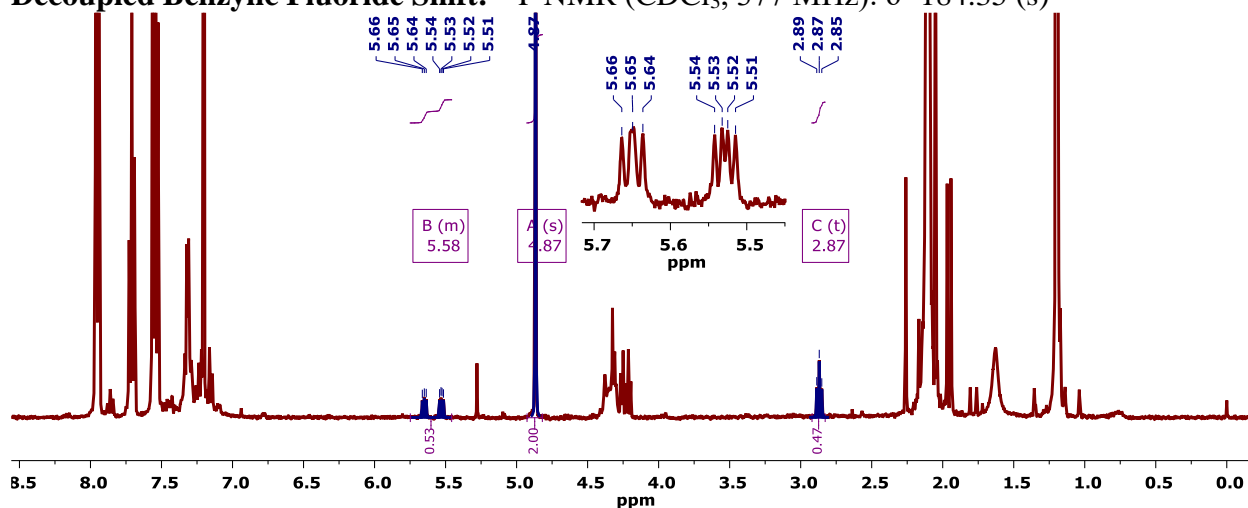


Figure 4C.27. Crude ¹H NMR Spectrum (CDCl₃, 400 MHz, 25 °C) of the reaction mixture following the addition of 0.3 mmol (21 μL) of CH₂Br₂ as an internal standard (4.87 ppm). The resolved product and starting material benzylic protons are labeled and integrated.

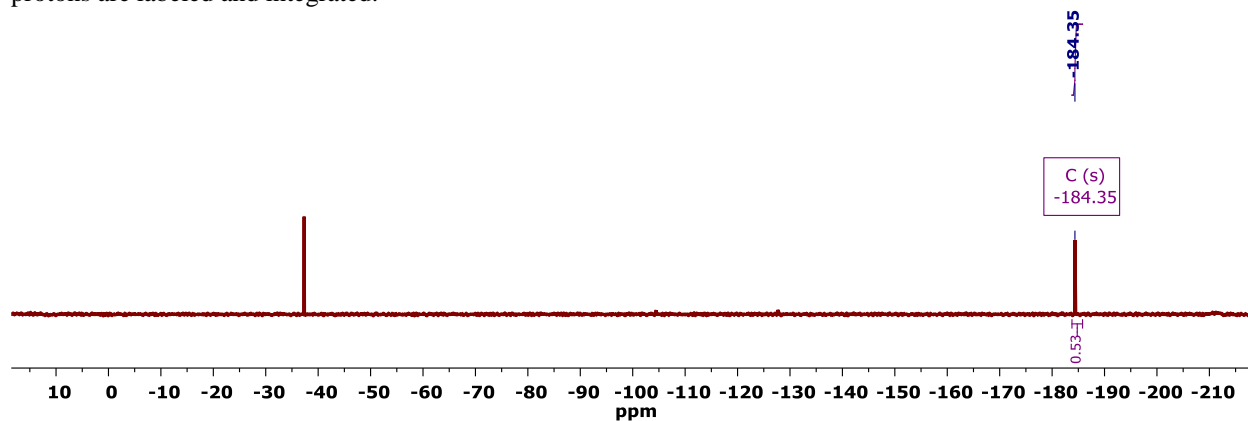
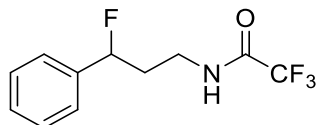


Figure 4C.28. Crude ¹⁹F{¹H} NMR Spectrum (CDCl₃, 377 MHz, 25 °C) of the reaction mixture. The mono-fluoride (-184.35) is labeled and integrated.



(14) 2,2,2-trifluoro-*N*-(3-fluoro-3-phenylpropyl)acetamide: Prepared from 2,2,2-trifluoro-*N*-(3-phenylpropyl)acetamide (0.3 mmol, 70 mg, 1.0 equiv) according to the general procedure in section 4C.II.

Spectra Available in the Literature (CAS): No (N/A)

Benzyl Fluoride C–H Shift: ^1H NMR (CDCl_3 , 400 MHz): δ 5.60 (ddd, $^2J_{(\text{H,F})} = 48.2$ Hz, $^3J_{(\text{H,H})} = 8.7$ & 3.0 Hz)

Calibrated ^1H NMR Yield from Benzyl Proton: 63%

Benzylic Fluoride Shift: ^{19}F NMR (CDCl_3 , 377 MHz): δ -183.75 (ddd, $^2J_{(\text{H,F})} = 48.0$ Hz, $^3J_{(\text{H,F})} = 30.2$ & 17.3 Hz)

Calibrated ^{19}F NMR Yield from Benzyl Fluoride: 63%

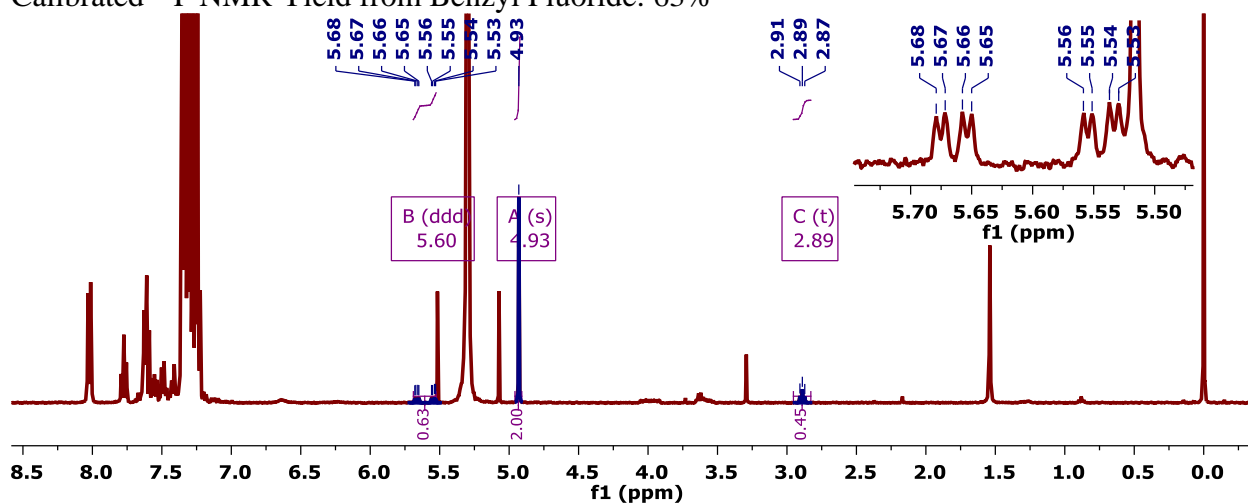


Figure 4C.29. Crude ^1H NMR Spectrum (CDCl_3 , 400 MHz, 25 °C) of the reaction mixture following the addition of 0.3 mmol (21 μL) of CH_2Br_2 as an internal standard (4.93 ppm). The resolved product and starting material benzylic protons are labeled and integrated.

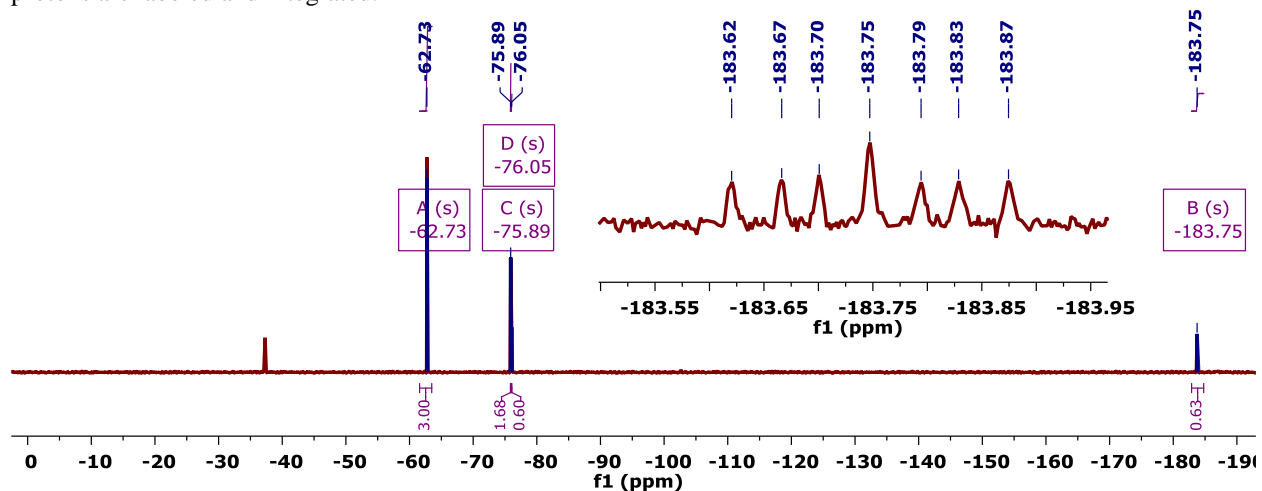
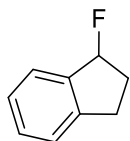


Figure 4C.30. Crude $^{19}\text{F}\{^1\text{H}\}$ NMR Spectrum (CDCl_3 , 377 MHz, 25 °C) of the reaction mixture following the addition of 0.3 mmol (37 μL) of PhCF_3 as an internal standard (-62.73 ppm). The benzylic fluoride (-183.75 ppm) and CF_3 groups (starting material and product) are labeled and integrated; the inset shows an enlargement of the proton-coupled mono-fluoride.



(15) 1-fluoro-2,3-dihydro-1H-indene: Prepared from indane (0.3 mmol, 37 μ L, 1.0 equiv) according to the general procedure in section 4C.II with the following variations: 0.5 equiv MeB(OH)₂ operating at 35 $^{\circ}$ C.

Spectra Available in the Literature (CAS): Yes¹⁵ (62393-01-5)

Benzyl Fluoride C–H Shift: ¹H NMR (CDCl₃, 400 MHz): δ 5.99 (ddd, ²J_(H,F) = 58.1 Hz, ³J_(H,H) = 6.1 & 2.8 Hz)

Calibrated ¹H NMR Yield from Benzyl Proton: 60%

Benzylic Fluoride Shift: ¹⁹F NMR (CDCl₃, 377 MHz): δ -159.91 (dt, ²J_(H,F) = 56.3 Hz, ³J_(H,F) = 27.2 Hz)

Calibrated ¹⁹F NMR Yield from Benzyl Fluoride: 49%

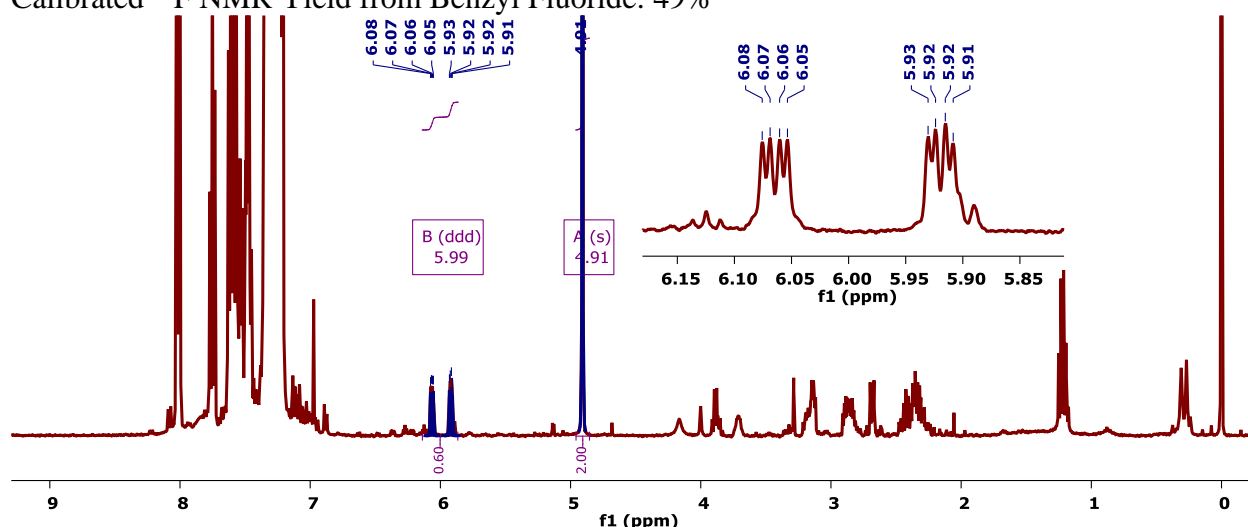


Figure 4C.31. Crude ¹H NMR Spectrum (CDCl₃, 400 MHz, 25 $^{\circ}$ C) of the reaction mixture following the addition of 0.3 mmol (21 μ L) of CH₂Br₂ as an internal standard (4.91 ppm). The resolved product benzylic proton is labeled and integrated.

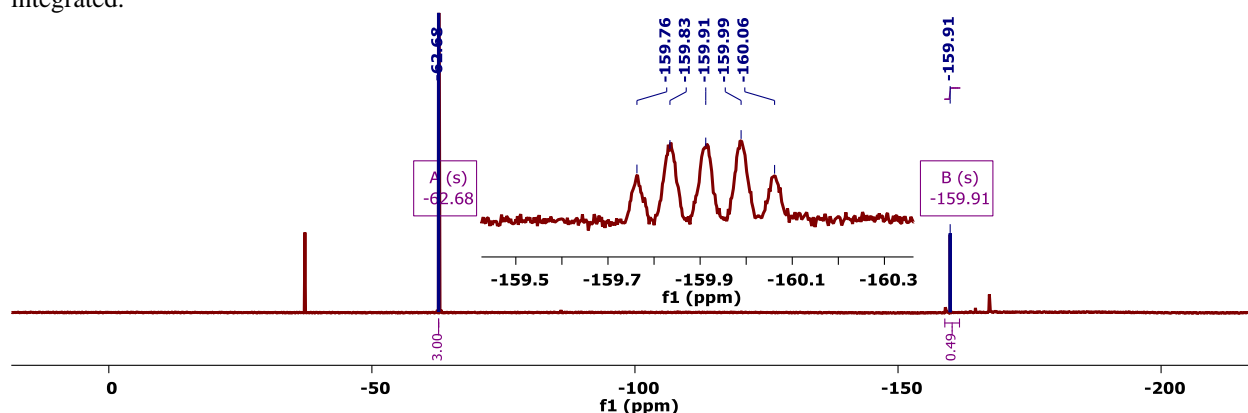
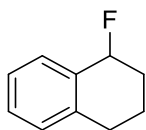


Figure 4C.32. Crude ¹⁹F{¹H} NMR Spectrum (CDCl₃, 377 MHz, 25 $^{\circ}$ C) of the reaction mixture following the addition of 0.3 mmol (37 μ L) of PhCF₃ as an internal standard (-62.68 ppm). The mono-fluoride (-159.91) is labeled and integrated. The inset shows an enlargement of the proton-coupled mono-fluoride.



(16) 1-fluoro-1,2,3,4-tetrahydronaphthalene: Prepared from 1,2,3,4-tetrahydronaphthalene (0.3 mmol, 41 μ L, 1.0 equiv) according to the general procedure in section II with the following variations: 0.5 equiv MeB(OH)₂ operating at 35 $^{\circ}$ C.

Spectra Available in the Literature (CAS): No (62462-11-7)

Benzyl Fluoride C–H Shift: ¹H NMR (CDCl₃, 400 MHz): δ 5.54 (dt, ²J_(H,F) = 51.8 Hz, ³J_(H,H) = 3.9 Hz)

Calibrated ¹H NMR Yield from Benzyl Proton: 61%

Benzylic Fluoride Shift: ¹⁹F NMR (CDCl₃, 377 MHz): δ -155.88 (m)

Calibrated ¹⁹F NMR Yield from Benzyl Fluoride: 57%

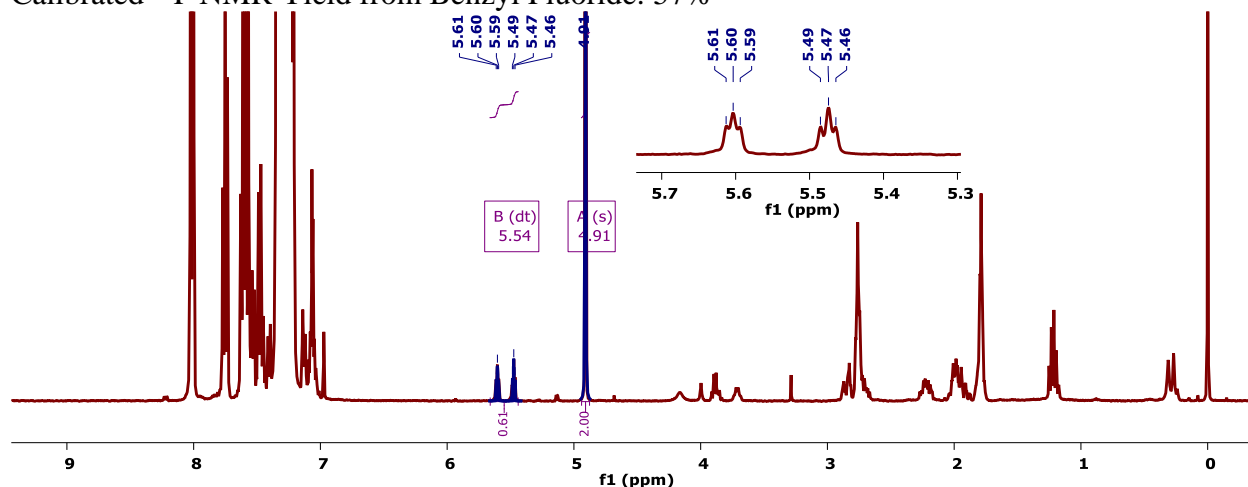


Figure 4C.33. Crude ¹H NMR Spectrum (CDCl₃, 400 MHz, 25 $^{\circ}$ C) of the reaction mixture following the addition of 0.3 mmol (21 μ L) of CH₂Br₂ as an internal standard (4.91 ppm). The resolved product benzylic proton is labeled and integrated.

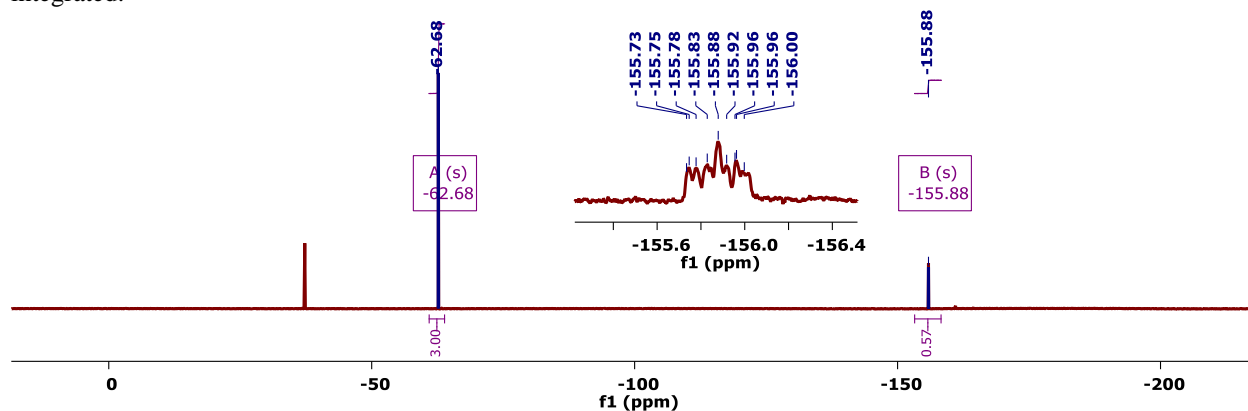
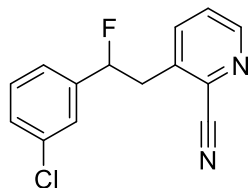


Figure 4C.34. Crude ¹⁹F{¹H} NMR Spectrum (CDCl₃, 377 MHz, 25 $^{\circ}$ C) of the reaction mixture following the addition of 0.3 mmol (37 μ L) of PhCF₃ as an internal standard (-62.68 ppm). The mono-fluoride (-155.88) is labeled and integrated. The inset shows an enlargement of the proton-coupled mono-fluoride.



(17) 3-(2-(3-chlorophenyl)-2-fluoroethyl)picolinonitrile: Prepared from 3-(3-chlorophenethyl)picolinonitrile (0.3 mmol, 73 mg, 1.0 equiv) according to the general procedure in section 4C.II with the following variations: 1 mol% CuOAc, 1.2 mol% BPhen, 1 equiv B₂pin₂ (in place of 2 equiv MeB(OH)₂), and 4 equiv NFSI operating at 75 °C.

Spectra Available in the Literature (CAS): No (N/A)

Benzyl Fluoride C–H Shift: ¹H NMR (CDCl₃, 400 MHz): δ 5.71 (ddd, ²J_(H,F) = 53.6 Hz, ³J_(H,H) = 5.4 Hz)

Calibrated ¹H NMR Yield from Benzyl Proton: 45%

Benzylic Fluoride Shift: ¹⁹F NMR (CDCl₃, 377 MHz): δ -178.75 (ddd, ²J_(H,F) = 47.9 Hz, ³J_(H,F) = 29.9 & 19.0 Hz)

Calibrated ¹⁹F NMR Yield from Benzyl Fluoride: 39%

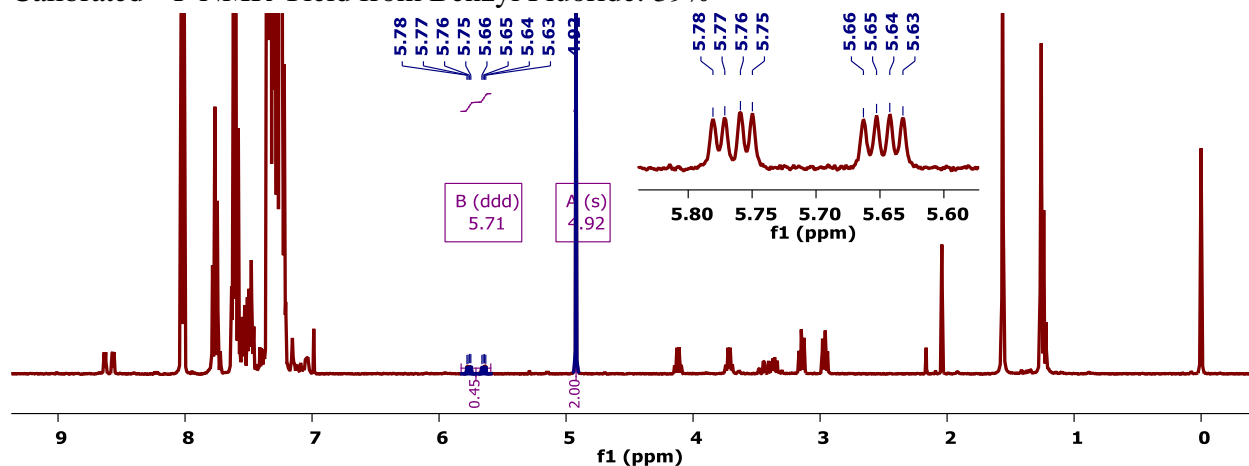


Figure 4C.35. Crude ¹H NMR Spectrum (CDCl₃, 400 MHz, 25 °C) of the reaction mixture following the addition of 0.3 mmol (21 μL) of CH₂Br₂ as an internal standard (4.92 ppm). The resolved product benzylic proton is labeled and integrated.

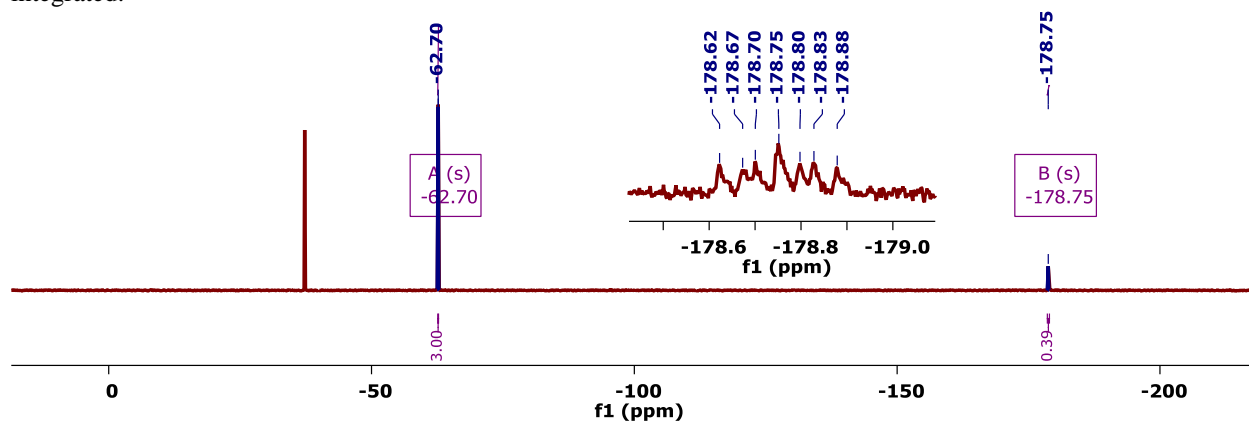
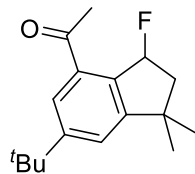


Figure 4C.36. Crude ¹⁹F{¹H} NMR Spectrum (CDCl₃, 377 MHz, 25 °C) of the reaction mixture following the addition of 0.3 mmol (37 μL) of PhCF₃ as an internal standard (-62.70 ppm). The mono-fluoride (-178.75) is labeled and integrated. The inset shows an enlargement of the proton-coupled mono-fluoride.



(18) 1-(6-(tert-butyl)-3-fluoro-1,1-dimethyl-2,3-dihydro-1H-inden-4-yl)ethan-1-one:

Prepared from celestolide (0.3 mmol, 73 mg, 1.0 equiv) according to the general procedure in section 4C.II.

Spectra Available in the Literature (CAS): Yes⁹ (1500096-10-5)

Benzyl Fluoride C–H Shift: ¹H NMR (CDCl₃, 400 MHz): δ 6.45 (dd, ²J_(H,F) = 53.6 Hz, ³J_(H,H) = 5.4 Hz)

Calibrated ¹H NMR Yield from Benzyl Proton: 86%

Benzylic Fluoride Shift: ¹⁹F NMR (CDCl₃, 377 MHz): δ -158.62 (ddd, ²J_(H,F) = 54.2 Hz, ³J_(H,F) = 34.1 & 23.5 Hz)

Calibrated ¹⁹F NMR Yield from Benzyl Fluoride: 90% (CF₂ – 6%)

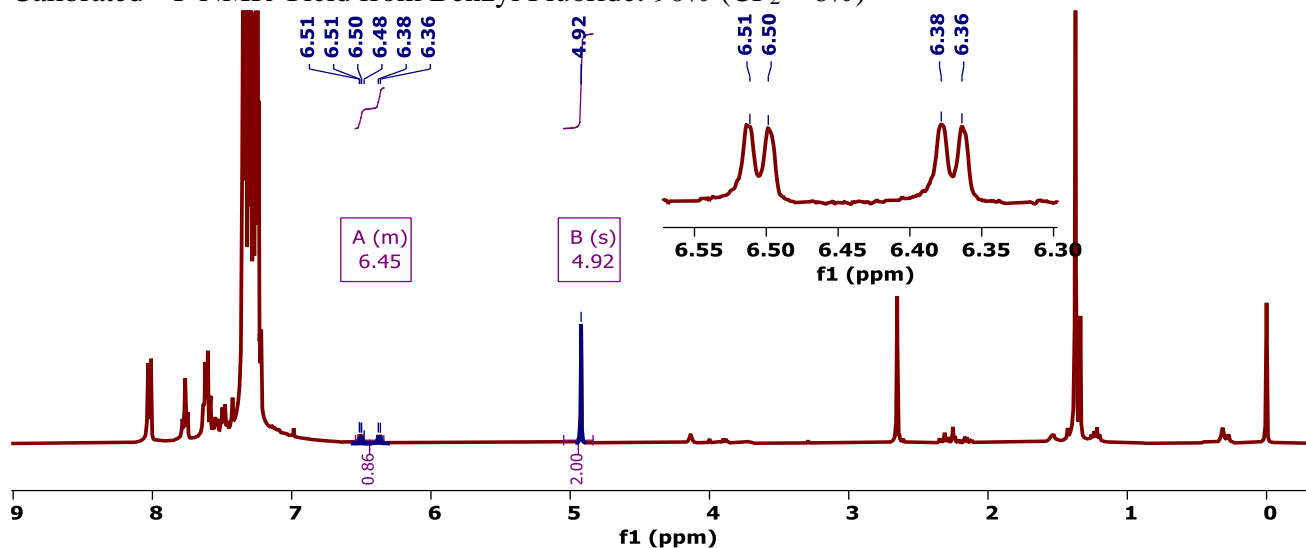


Figure 4C.37. Crude ¹H NMR Spectrum (CDCl₃, 400 MHz, 25 °C) of the reaction mixture following the addition of 0.3 mmol (21 μL) of CH₂Br₂ as an internal standard (4.92 ppm). The resolved product benzylic proton is labeled and integrated.

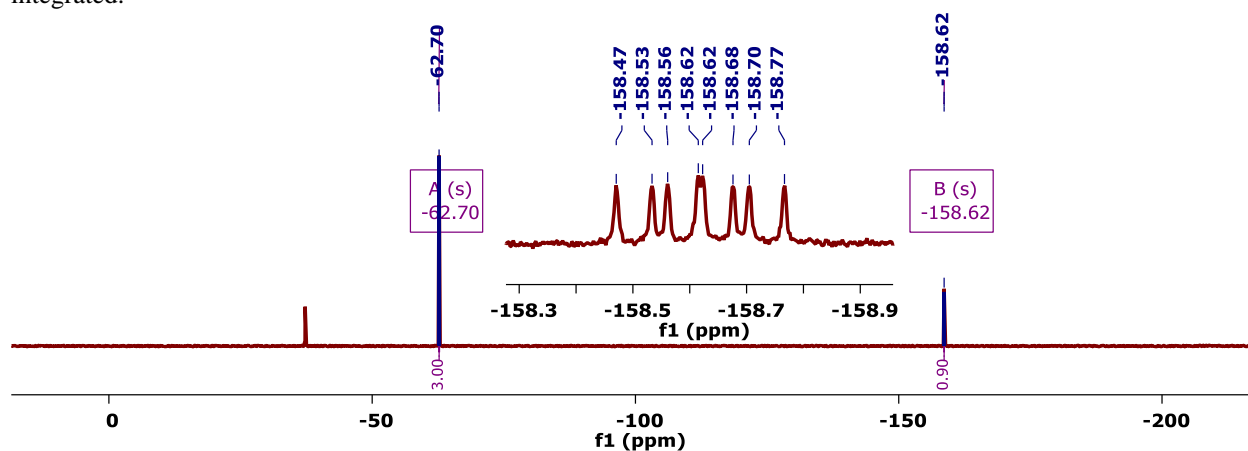
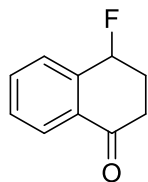


Figure 4C.38. Crude ¹⁹F{¹H} NMR Spectrum (CDCl₃, 377 MHz, 25 °C) of the reaction mixture following the addition of 0.3 mmol (37 μL) of PhCF₃ as an internal standard (-62.70 ppm). The mono-fluoride (-158.62) is labeled and integrated. The inset shows an enlargement of the proton-coupled mono-fluoride.



(19) 4-fluoro-3,4-dihydronaphthalen-1(2H)-one: Prepared from 1-tetralone (0.3 mmol, 41 μ L, 1.0 equiv) formed according to the general procedure in section 4C.II with the following variations: 1 mol% CuOAc, 1.2 mol% BPhen, 1 equiv B₂pin₂ (in place of 2 equiv MeB(OH)₂), and 4 equiv NFSI operating at 75 °C in acetone.

Spectra Available in the Literature (CAS): Yes¹⁶ (587853-65-4)

Benzyl Fluoride C–H Shift: ¹H NMR (CDCl₃, 400 MHz): δ 5.74 (dt, ²J_(H,F) = 50.5 Hz, ³J_(H,H) = 5.0 Hz)

Calibrated ¹H NMR Yield from Benzyl Proton: 38%

Benzylic Fluoride Shift: ¹⁹F NMR (CDCl₃, 377 MHz): δ -170.59 (m)

Calibrated ¹⁹F NMR Yield from Benzyl Fluoride: 44%

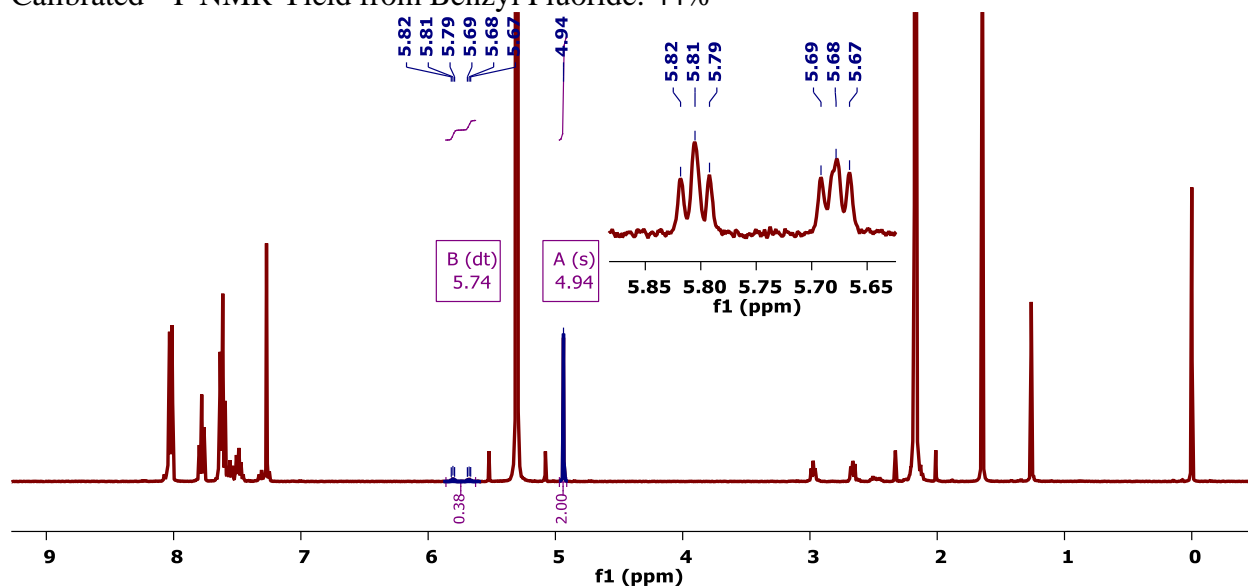


Figure 4C.39. Crude ¹H NMR Spectrum (CDCl₃, 400 MHz, 25 °C) of the reaction mixture following the addition of 0.3 mmol (21 μ L) of CH₂Br₂ as an internal standard (4.94 ppm). The resolved product benzylic proton is labeled and integrated.

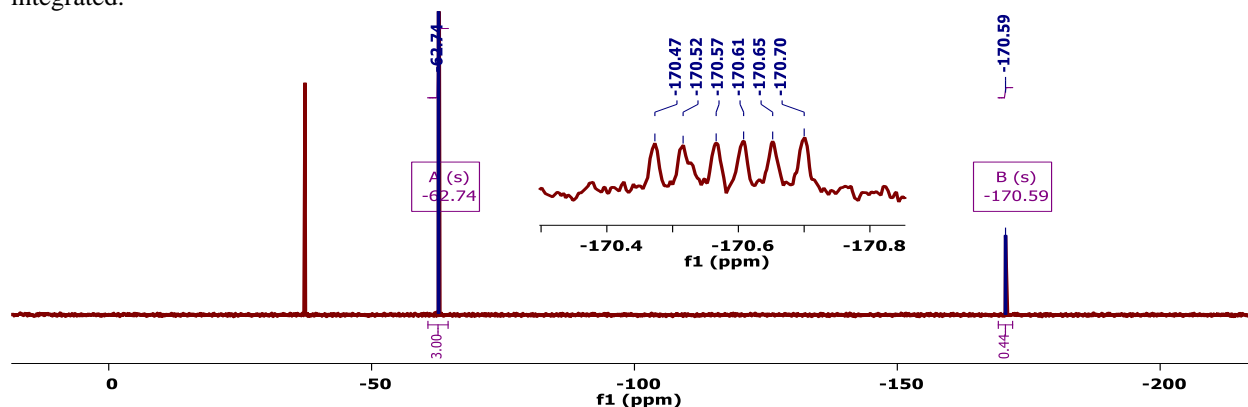
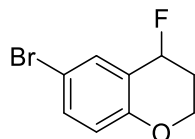


Figure 4C.40. Crude ¹⁹F{¹H} NMR Spectrum (CDCl₃, 377 MHz, 25 °C) of the reaction mixture following the addition of 0.3 mmol (37 μ L) of PhCF₃ as an internal standard (-62.74 ppm). The mono-fluoride (-170.59) is labeled and integrated. The inset shows an enlargement of the proton-coupled mono-fluoride.



(20) 6-bromo-4-fluorochromane: Prepared from 6-bromochromane (0.3 mmol, 44 μ L, 1.0 equiv) according to the general procedure in section 4C.II with the following variations: 0.5 equiv MeB(OH)₂ operating at 35 $^{\circ}$ C.

Spectra Available in the Literature (CAS): No (1780938-64-8)

Benzyl Fluoride C–H Shift: ¹H NMR (CDCl₃, 400 MHz): δ 5.43 (dt, ²J_(H,F) = 52.4 Hz, ³J_(H,H) = 3.4 Hz)

Calibrated ¹H NMR Yield from Benzylic Proton: 62%

Benzylic Fluoride Shift: ¹⁹F NMR (CDCl₃, 377 MHz): δ -153.79 (ddd, ²J_(H,F) = 50.6 Hz, ³J_(H,F) = 34.3 & 16.4 Hz)

Calibrated ¹⁹F NMR Yields from Benzylic Fluoride: 60%

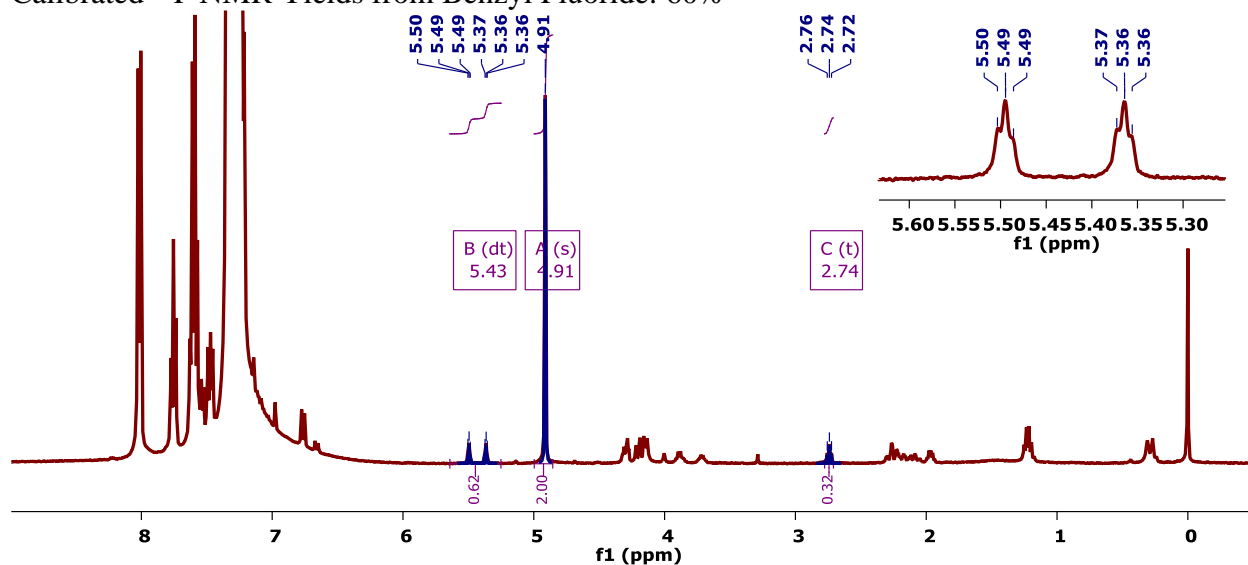


Figure 4C.41. Crude ¹H NMR Spectrum (CDCl₃, 400 MHz, 25 $^{\circ}$ C) of the reaction mixture following the addition of 0.3 mmol (21 μ L) of CH₂Br₂ as an internal standard (4.91 ppm). The resolved product and starting material benzylic protons are labeled and integrated.

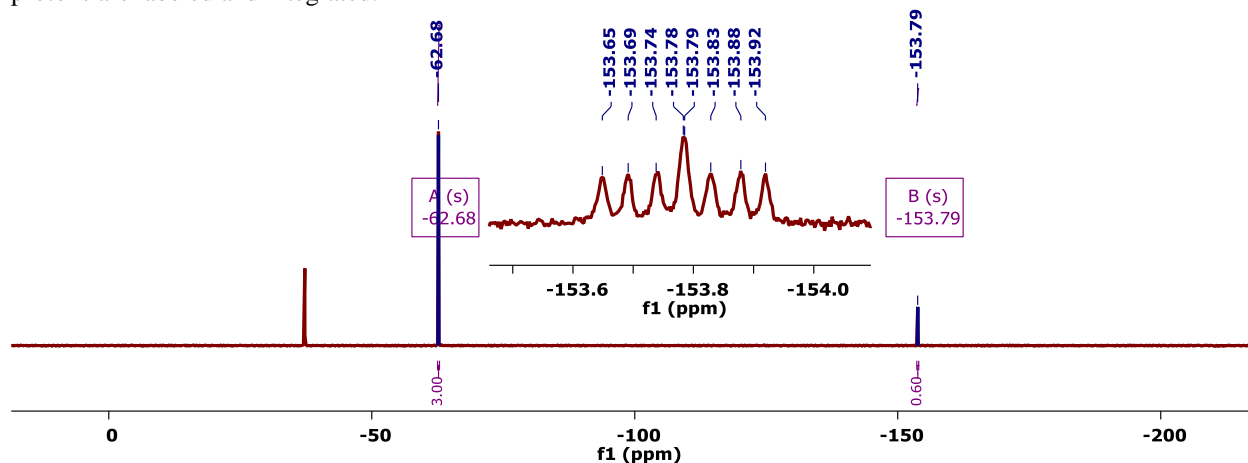
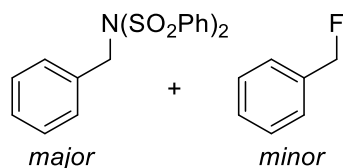


Figure 4C.42. Crude ¹⁹F{¹H} NMR Spectrum (CDCl₃, 377 MHz, 25 $^{\circ}$ C) of the reaction mixture following the addition of 0.3 mmol (37 μ L) of PhCF₃ as an internal standard (-62.68 ppm). The mono-fluoride (-153.79) is labeled and integrated. The inset shows an enlargement of the proton-coupled mono-fluoride.



(21) (fluoromethyl)benzene: Prepared from toluene (0.3 mmol, 32 μ L, 1.0 equiv) according to the general procedure in section 4C.II with the following variations: 1 mol% CuOAc, 1.2 mol% BPhen, 1 equiv B₂pin₂ (in place of 2 equiv MeB(OH)₂), and 4 equiv NFSI operating at 55 °C in acetone.

Spectra Available in the Literature (CAS): Yes¹⁷ (70869-03-3), Yes⁸ (350-50-5)

Benzyl Fluoride C–H Shift: ¹H NMR (CDCl₃, 400 MHz): δ 5.37 (d, ²J_(H,F) = 47.9 Hz)

Calibrated ¹H NMR Yield from Benzylic Proton(s): 59% (C–N), 12% (C–F), 6% (C–F₂)

Benzylic Fluoride Shift: ¹⁹F NMR (CDCl₃, 377 MHz): δ -206.64 (t, ²J_(H,F) = 47.3 Hz)

Calibrated ¹⁹F NMR Yields from Benzyl Fluoride(s): 8% (C–F), 8% (C–F₂)

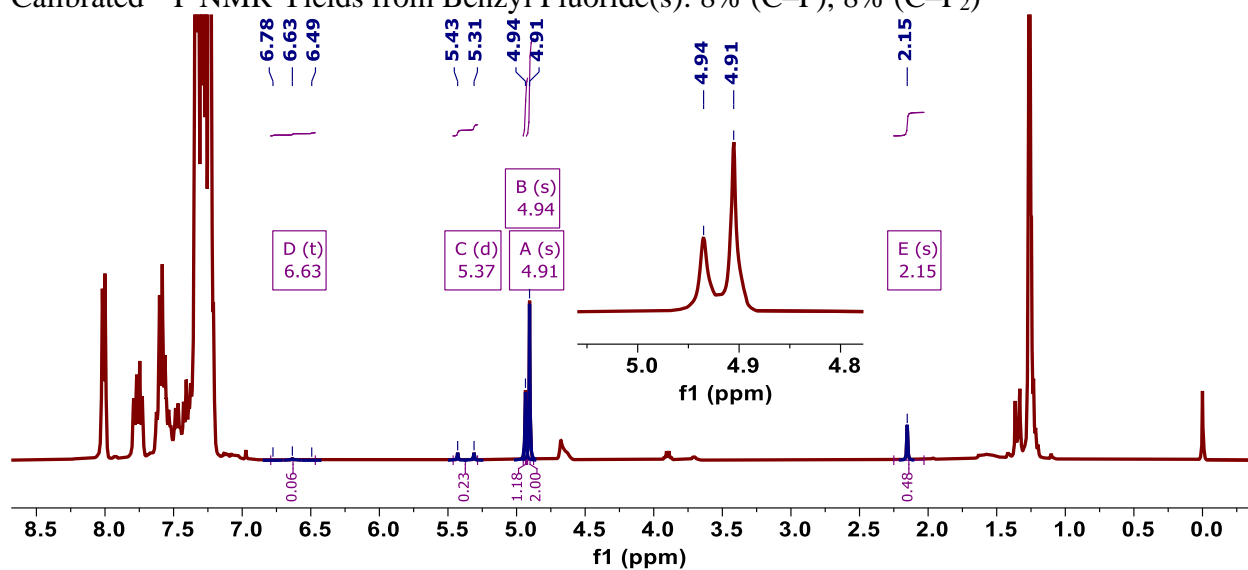


Figure 4C.43. Crude ¹H NMR Spectrum (CDCl₃, 400 MHz, 25 °C) of the reaction mixture following the addition of 0.3 mmol (21 μ L) of CH₂Br₂ as an internal standard (4.91 ppm). The resolved product and starting material benzylic protons are labeled and integrated.

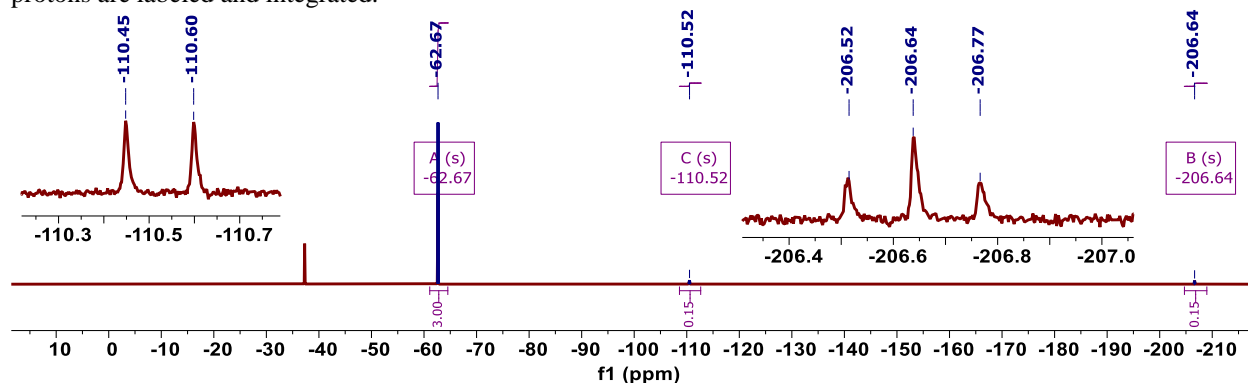
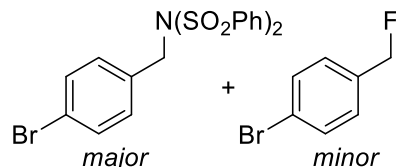


Figure 4C.44. Crude ¹⁹F{¹H} NMR Spectrum (CDCl₃, 377 MHz, 25 °C) of the reaction mixture following the addition of 0.3 mmol (37 μ L) of PhCF₃ as an internal standard (-62.67 ppm). The mono-fluoride (-206.64 ppm) and di-fluoride (-110.52 ppm) are labeled and integrated. The insets show enlargements of the proton-coupled resonances.



(22) 1-bromo-4-(fluoromethyl)benzene: Prepared from 4-bromotoluene (0.3 mmol, 37 μ L, 1.0 equiv) according to the general procedure in section II with the following variations: 1 mol% CuOAc, 1.2 mol% BPhen, 1 equiv B₂pin₂ (in place of 2 equiv MeB(OH)₂), and 4 equiv NFSI operating at 55 °C.

Spectra Available in the Literature (CAS): Yes¹⁷ (1361033-82-0), Yes¹⁴ (459-49-4)

Benzyl Fluoride C–H Shift: ¹H NMR (CDCl₃, 400 MHz): δ 5.32 (d, ²J_(H,F) = 47.7 Hz)

Calibrated ¹H NMR Yield from Benzylic Proton(s): 44% (C–N), 8% (C–F), 10% (C–F₂)

Benzyl Fluoride Shift: ¹⁹F NMR (CDCl₃, 377 MHz): δ -208.09 (t, ²J_(H,F) = 47.7 Hz)

Calibrated ¹⁹F NMR Yields from Benzyl Fluoride: 7% (C–F), 10% (C–F₂)

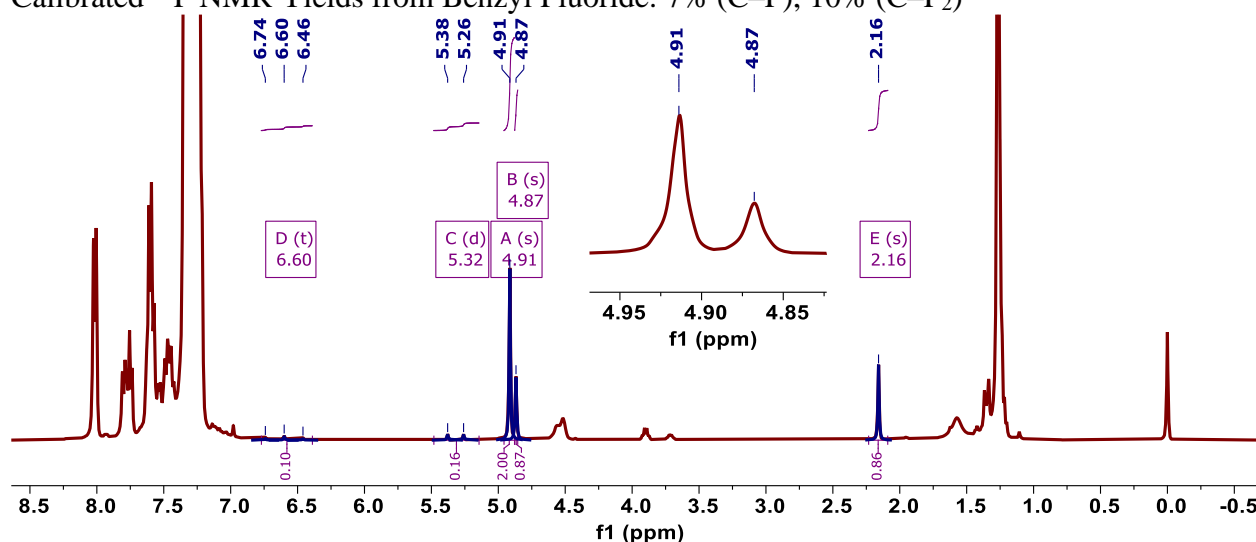


Figure 4C.45. Crude ¹H NMR Spectrum (CDCl₃, 400 MHz, 25 °C) of the reaction mixture following the addition of 0.3 mmol (21 μ L) of CH₂Br₂ as an internal standard (4.91 ppm). The resolved product and starting material benzylic protons are labeled and integrated.

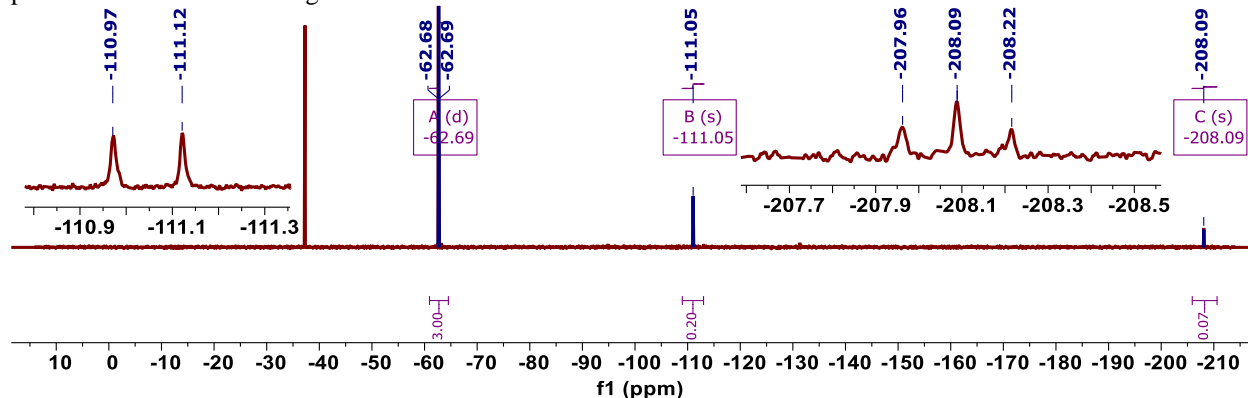
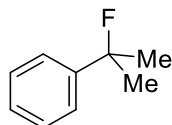


Figure 4C.46. Crude ¹⁹F{¹H} NMR Spectrum (CDCl₃, 377 MHz, 25 °C) of the reaction mixture following the addition of 0.3 mmol (37 μ L) of PhCF₃ as an internal standard (-62.69 ppm). The mono-fluoride (-208.09 ppm) and the di-fluoride (-111.05 ppm) are labeled and integrated. The insets show enlargements of the proton-coupled resonances.



(23) (2-fluoropropan-2-yl)benzene: Prepared from cumene (0.3 mmol, 42 μL , 1.0 equiv) according to the general procedure in section 4C.II.

Spectra Available in the Literature (CAS): Yes⁸ (74185-81-2)

Fluoride Product Methyl C–H Shift: ^1H NMR (CDCl_3 , 400 MHz): δ 1.68 (d, $^3J_{(\text{H},\text{F})} = 21.9$ Hz)

Calibrated ^1H NMR Yield from Benzyl Fluoride Methyl Protons: 92%

Benzylic Fluoride Shift: ^{19}F NMR (CDCl_3 , 377 MHz): δ -137.39 (hept, $^3J_{(\text{H},\text{F})} = 21.8$ Hz)

Calibrated ^{19}F NMR Yields from Benzyl Fluoride: 85%

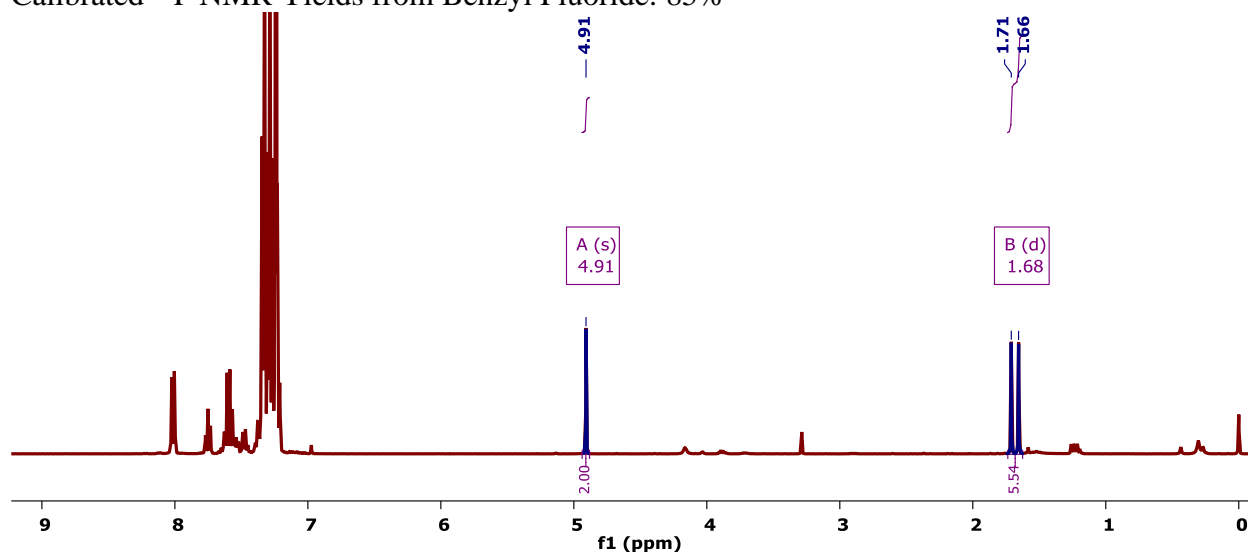


Figure 4C.47. Crude ^1H NMR Spectrum (CDCl_3 , 400 MHz, 25 $^\circ\text{C}$) of the reaction mixture following the addition of 0.3 mmol (21 μL) of CH_2Br_2 as an internal standard (4.91 ppm). The resolved product aromatic and methyl protons are labeled and integrated.

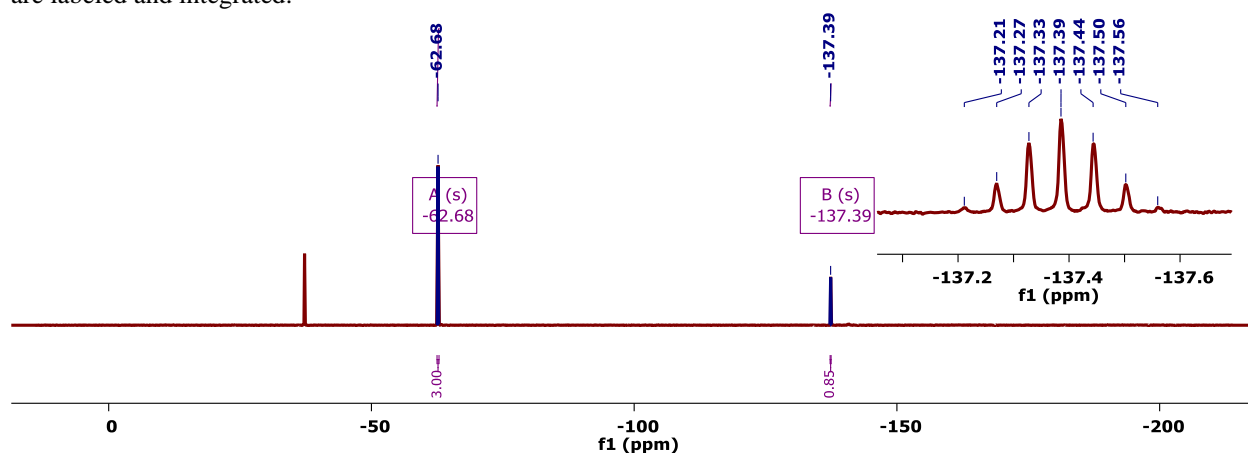
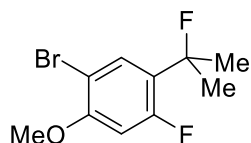


Figure 4C.48. Crude $^{19}\text{F}\{^1\text{H}\}$ NMR Spectrum (CDCl_3 , 377 MHz, 25 $^\circ\text{C}$) of the reaction mixture following the addition of 0.3 mmol (37 μL) of PhCF_3 as an internal standard (-62.69 ppm). The benzyl-fluoride (-137.39) is labeled and integrated. The inset shows an enlargement of the proton-coupled fluorine resonance.



(24) 1-bromo-4-fluoro-5-(2-fluoropropan-2-yl)-2-methoxybenzene: Prepared from 1-bromo-4-fluoro-5-isopropyl-2-methoxybenzene (0.3 mmol, 74 mg, 1.0 equiv) according to the general procedure in section 4C.II.

Spectra Available in the Literature (CAS): No (N/A)

Fluoride Product Aromatic C–H Shift: ^1H NMR (CDCl_3 , 400 MHz): δ 6.61 (d, $^3J_{(\text{H},\text{F})} = 12.8$ Hz)

Calibrated ^1H NMR Yield from Benzyl Fluoride Aromatic Proton: 84%

Benzyl Fluoride Product Fluorine Shifts: ^{19}F NMR (CDCl_3 , 377 MHz): δ -112.96 (dt, $^3J_{(\text{H},\text{F})} = 14.4$ Hz, $^4J_{(\text{H},\text{F})} = 7.6$ Hz), -135.16 (hd, $^3J_{(\text{H},\text{F})} = 22.8$ Hz, $^4J_{(\text{H},\text{F})} = 6.7$ Hz)

Calibrated ^{19}F NMR Yields from Benzyl Fluoride: 82%

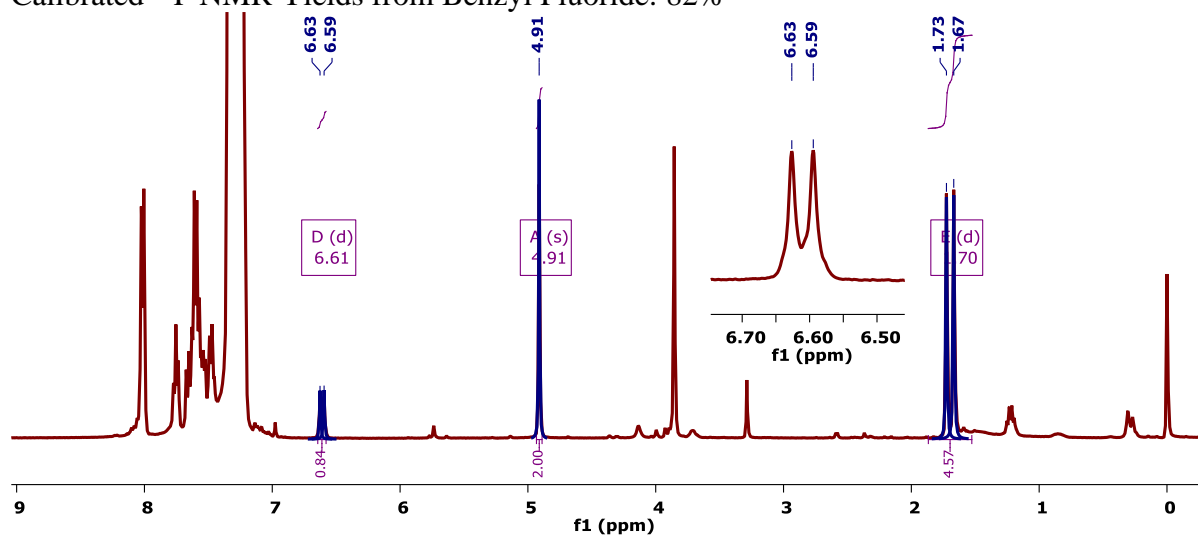


Figure 4C.49. Crude ^1H NMR Spectrum (CDCl_3 , 400 MHz, 25 °C) of the reaction mixture following the addition of 0.3 mmol (21 μL) of CH_2Br_2 as an internal standard (4.91 ppm). The resolved product aromatic and methyl protons are labeled and integrated.

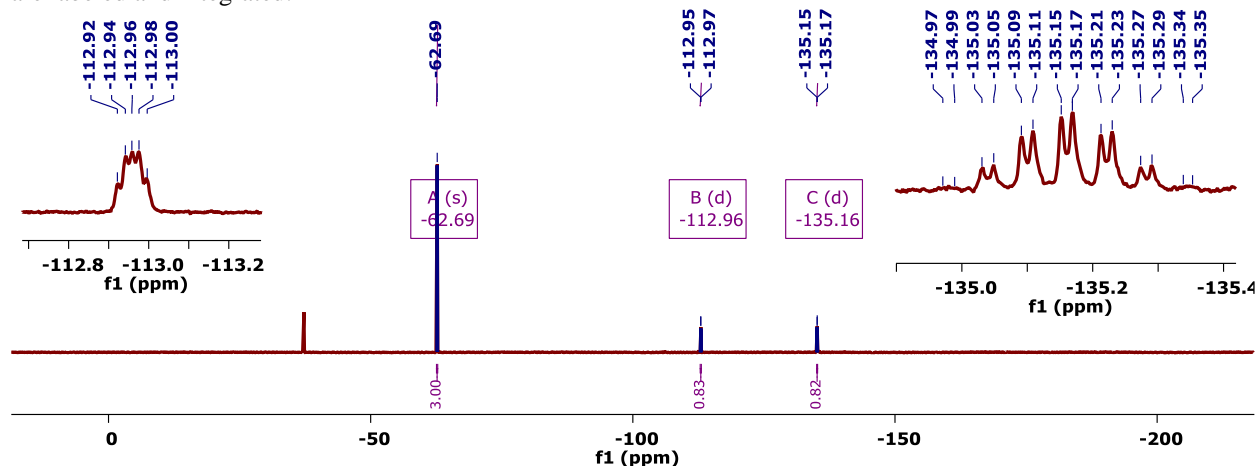
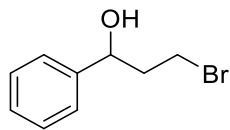


Figure 4C.50. Crude $^{19}\text{F}\{^1\text{H}\}$ NMR Spectrum (CDCl_3 , 377 MHz, 25 °C) of the reaction mixture following the addition of 0.3 mmol (37 μL) of PhCF_3 as an internal standard (-62.69 ppm). The aryl-fluoride (-112.96) and benzyl-fluoride (-135.16) are labeled and integrated. The inset shows an enlargement of the proton-coupled fluorine resonances.

4C.VIII. Characterization Data for Isolated Cross Coupling Products



(25) 3-bromo-1-phenylpropan-1-ol: Prepared from benzyl fluoride **8** (0.3 mmol scale, 65% NMR yield) that was formed according to the general procedure in section 4C.II. The ensuing displacement step followed the general procedure in section 4C.III and used water (0.75 mmol, 13.5 μ L, 2.5 equiv) as the nucleophile with HFIP (3.0 mmol, 315 μ L, 10 equiv) as the displacement catalyst.

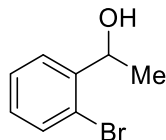
Purification: Normal phase silica gel chromatography was used with a gradient of 0% \rightarrow 10% EtOAc in pentane.

Isolated Yield from Benzyl Fluoride: 64%, 27.4 mg of yellow oil

Spectra Available in the Literature (CAS): Yes¹⁸ (34052-63-6)

¹H NMR (CDCl₃, 500 MHz): δ 7.39 – 7.35 (m, 4H), 7.33 – 7.28 (m, 1H), 4.92 (dd, J = 8.4, 4.7 Hz, 1H), 3.59 (ddd, J = 10.0, 8.2, 6.0 Hz, 1H), 3.42 (dt, J = 10.0, 6.1 Hz, 1H), 2.32 (ddt, J = 14.3, 8.3, 5.9 Hz, 1H), 2.18 (dddd, J = 14.5, 8.2, 6.3, 4.6 Hz, 1H), 2.03 (bs, 1H).

¹³C NMR (CDCl₃, 126 MHz): δ 143.6, 128.7, 127.9, 125.8, 72.3, 41.6, 30.2.



(26) 1-(2-bromophenyl)ethan-1-ol: Prepared from benzyl fluoride **2** (0.3 mmol scale, 44% NMR yield) that was formed according to the general procedure in section 4C.II with the following variations: 1 mol% CuOAc, 1.2 mol% BPhen, 1 equiv B₂pin₂ (in place of 2 equiv MeB(OH)₂), and 4 equiv NFSI operating at 75 °C. The ensuing displacement step followed the general procedure in section 4C.III and used water (0.75 mmol, 13.5 μ L, 2.5 equiv) as the nucleophile with HFIP (3.0 mmol, 315 μ L, 10 equiv) as the displacement catalyst.

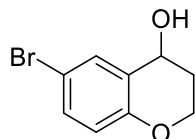
Table 4C.12. Purification: Reverse phase silica gel chromatography was used with a gradient of 50% \rightarrow 85% MeOH in water. The product was extracted with 1:1 ether:pentane.

Isolated Yield from Benzyl Fluoride: 87%, 22.9 mg of colorless oil.

Spectra Available in the Literature (CAS): Yes¹⁹ (5411-56-3)

¹H NMR (CDCl₃, 500 MHz): δ 7.60 (dd, J = 7.8, 1.7 Hz, 1H), 7.51 (dd, J = 7.9, 1.2 Hz, 1H), 7.35 (td, J = 7.6, 1.2 Hz, 1H), 7.13 (td, J = 7.7, 1.7 Hz, 1H), 5.24 (q, J = 6.4 Hz, 1H), 1.49 (d, J = 6.4 Hz, 3H).

¹³C NMR (CDCl₃, 126 MHz): δ 144.6, 132.7, 128.8, 127.9, 126.7, 121.7, 69.2, 23.6.



(27) 6-bromochroman-4-ol: Prepared from benzyl fluoride **20** (0.3 mmol scale, 57% NMR yield) that was formed according to the general procedure in section 4C.II with the following variations: 0.5 equiv MeB(OH)₂ operating at 35 °C. The ensuing displacement step followed the general procedure in section 4C.III and used water (0.75 mmol, 13.5 μL, 2.5 equiv) as the nucleophile with HFIP (3.0 mmol, 315 μL, 10 equiv) as the displacement catalyst.

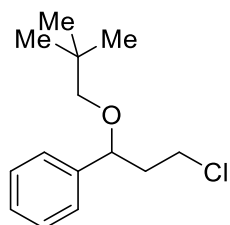
Table 4C.13. Purification: Reverse phase silica gel chromatography was used with a gradient of 50%→85% MeOH in water. The product was extracted with 1:1 ether:pentane.

Isolated Yield from Benzyl Fluoride: 34%, 13.1 mg of colorless oil.

Spectra Available in the Literature (CAS): Yes²⁰ (18385-77-8)

¹H NMR (CDCl₃, 500 MHz): δ 7.45 (d, *J* = 2.5 Hz, 1H), 7.28 (dd, *J* = 8.7, 2.5 Hz, 1H), 6.73 (d, *J* = 8.7 Hz, 1H), 4.76 (t, *J* = 4.3 Hz, 1H), 4.31 – 4.21 (m, 2H), 2.18 – 1.98 (m, 2H), 1.87 (bs, 1H).

¹³C NMR (CDCl₃, 126 MHz): δ 153.7, 132.5, 132.1, 126.3, 119.0, 112.4, 63.0, 62.2, 30.6.



(28) (3-chloro-1-(neopentyloxy)propyl)benzene: Prepared from benzyl fluoride **7** (0.3 mmol scale, 76% NMR yield) that was formed according to the general procedure in section 4C.II. The ensuing displacement step followed the general procedure in section 4C.III and used neopentyl alcohol (0.75 mmol, 81.4 μL, 2.5 equiv) as the nucleophile with BF₃•Et₂O (0.03 mmol, 3.7 μL, 0.1 equiv) as the displacement catalyst. The nucleophile was dried in 1 mL DCM with MgSO₄ prior to use.

Purification: Reverse phase silica gel chromatography was used with a gradient of 70%→100% MeOH in water. The product was extracted with 1:1 ether:pentane.

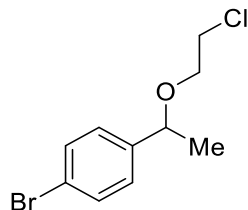
Isolated Yield from Benzyl Fluoride: 51%, 28.2 mg of light yellow oil.

Spectra Available in the Literature (CAS): No (2173346-35-3)

¹H NMR (CDCl₃, 500 MHz): δ 7.35 (t, *J* = 7.5 Hz, 2H), 7.32 – 7.26 (m, 3H), 4.42 (dd, *J* = 9.2, 4.1 Hz, 1H), 3.78 (ddd, *J* = 10.6, 8.6, 5.8 Hz, 1H), 3.59 (ddd, *J* = 11.0, 6.4, 5.1 Hz, 1H), 3.03 (d, *J* = 8.5 Hz, 1H), 2.90 (d, *J* = 8.5 Hz, 1H), 2.21 (ddt, *J* = 14.5, 9.2, 5.5 Hz, 1H), 2.00 (dddd, *J* = 14.6, 8.6, 6.4, 4.1 Hz, 1H), 0.91 (s, 9H).

¹³C NMR (CDCl₃, 126 MHz): δ 142.3, 128.4, 127.5, 126.4, 79.5, 78.9, 41.9, 41.6, 32.1, 26.7.

HRMS (ESI) m/z: [M-H]⁺ Calcd for C₁₄H₂₀ClO 239.1197; Found 239.1197.



(29) 1-bromo-4-(1-(2-chloroethoxy)ethyl)benzene: Prepared from benzyl fluoride **1** (0.3 mmol scale, 74% NMR yield) that was formed according to the general procedure in section 4C.II. The ensuing displacement step followed the general procedure in section 4C.III and used 2-chloroethanol (0.75 mmol, 50.3 μ L, 2.5 equiv) as the nucleophile with HFIP (3.0 mmol, 315 μ L, 10 equiv) as the displacement catalyst.

Purification: Normal phase silica gel chromatography was used with a gradient of 0% \rightarrow 20% EtOAc in pentane.

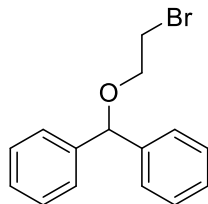
Isolated Yield from Benzyl Fluoride: 60%, 35.3 mg of colorless amorphous solid.

Spectra Available in the Literature (CAS): No (N/A)

$^1\text{H NMR}$ (CDCl_3 , 500 MHz): δ 7.48 (d, J = 8.4 Hz, 2H), 7.21 (d, J = 8.4 Hz, 2H), 4.43 (q, J = 6.5 Hz, 1H), 3.62 – 3.53 (m, 4H), 1.44 (d, J = 6.5 Hz, 3H).

$^{13}\text{C NMR}$ (CDCl_3 , 126 MHz): δ 142.4, 131.7, 127.9, 121.4, 77.9, 68.7, 43.0, 23.9.

HRMS (ESI) m/z: $[\text{M}+\text{NH}_4]^+$ Calcd for $\text{C}_{10}\text{H}_{16}\text{BrClNO}$ 280.0098; Found 280.0100.



(30) ((2-bromoethoxy)methylene)dibenzene: Prepared from benzyl fluoride **10** (0.3 mmol scale, 46% NMR yield) that was formed according to the general procedure in section 4C.II. The ensuing displacement step followed the general procedure in section 4C.III and used 2-bromoethanol (0.75 mmol, 53.2 μ L, 2.5 equiv) as the nucleophile with HFIP (3.0 mmol, 315 μ L, 10 equiv) as the displacement catalyst.

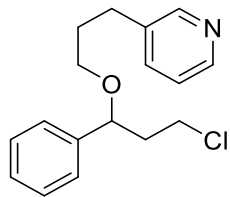
Purification: Reverse phase silica gel chromatography was used with a gradient of 50% \rightarrow 85% MeOH in water. The product was extracted with 1:1 ether:pentane.

Isolated Yield from Benzyl Fluoride: 80%, 32.3 mg of white solid.

Spectra Available in the Literature (CAS): Yes²¹ (91-01-0)

$^1\text{H NMR}$ (CDCl_3 , 500 MHz): δ 7.40 – 7.31 (m, 8H), 7.30 – 7.24 (m, 2H), 5.44 (s, 1H), 3.79 (t, J = 6.3 Hz, 2H), 3.53 (t, J = 6.2 Hz, 2H).

$^{13}\text{C NMR}$ (CDCl_3 , 126 MHz): δ 141.7, 128.4, 127.7, 127.0, 83.9, 68.9, 30.6.



(31) 3-(3-(3-chloro-1-phenylpropoxy)propyl)pyridine: Prepared from benzyl fluoride **7** (0.3 mmol scale, 78% NMR yield) that was formed according to the general procedure in section 4C.II. The ensuing displacement step followed the general procedure in section 4C.III and used 3-(3-pyridyl)-1-propanol (0.75 mmol, 43 μ L, 2.5 equiv) that was protonated with methanesulfonic acid (0.75 mmol, 48.7 μ L, 2.5 equiv) as the nucleophile with both HFIP (3.0 mmol, 315 μ L, 10 equiv) and $\text{BF}_3 \cdot \text{Et}_2\text{O}$ (0.15 mmol, 18.5 μ L, 0.5 equiv) as the displacement catalysts. The nucleophile was dried in 1 mL DCM with MgSO_4

Purification: An extraction with DCM and sodium bicarbonate was used to remove MsOH and BF_3 from pyridine. The organic phase was collected, dried with MgSO_4 , concentrated on the rotovap and then subjected to chromatography with a gradient of 20% \rightarrow 60% EtOAc in pentane.

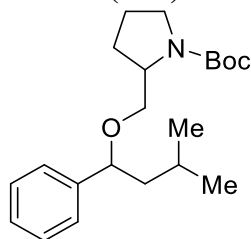
Isolated Yield from Benzyl Fluoride: 36%, 24.1 mg of slightly yellow oil.

Spectra Available in the Literature (CAS): No (N/A)

^1H NMR (CDCl_3 , 500 MHz): δ 8.44 (t, $J = 2.1$ Hz, 2H), 7.47 (dt, $J = 7.8, 2.0$ Hz, 1H), 7.38 – 7.33 (m, 2H), 7.33 – 7.28 (m, 3H), 7.19 (dd, $J = 7.8, 4.8$ Hz, 1H), 4.47 (dd, $J = 8.7, 4.6$ Hz, 1H), 3.75 (ddd, $J = 10.7, 8.5, 5.4$ Hz, 1H), 3.54 (dt, $J = 11.0, 5.7$ Hz, 1H), 3.38 (dt, $J = 9.5, 6.1$ Hz, 1H), 3.30 (dt, $J = 9.5, 6.1$ Hz, 1H), 2.76 – 2.61 (m, 2H), 2.25 (ddt, $J = 14.3, 8.8, 5.5$ Hz, 1H), 2.02 (dddd, $J = 14.4, 8.5, 5.9, 4.6$ Hz, 1H), 1.87 (tt, $J = 8.0, 6.2$ Hz, 2H).

^{13}C NMR (CDCl_3 , 126 MHz): δ 149.9, 147.3, 141.7, 137.2, 135.9, 128.6, 127.8, 126.5, 123.3, 78.7, 67.7, 41.7, 41.0, 31.2, 29.6.

HRMS (ESI) m/z : $[\text{M}+\text{H}]^+$ Calcd for $\text{C}_{17}\text{H}_{21}\text{ClNO}$ 290.1306; Found 290.1302.



(32) *tert*-butyl (2R)-2-((3-methyl-1-phenylbutoxy)methyl)pyrrolidine-1-carboxylate:

Prepared from benzyl fluoride **11** (0.3 mmol scale, 76% NMR yield) that was formed according to the general procedure in section 4C.II. The ensuing displacement step followed the general procedure in section 4C.III and used *N*-Boc-DL-prolinol (0.75 mmol, 151 mg, 2.5 equiv) as the nucleophile with $\text{BF}_3 \cdot \text{Et}_2\text{O}$ (0.15 mmol, 18.5 μ L, 0.5 equiv) as the displacement catalyst.

Purification: Silica gel chromatography was used with a gradient of 0% \rightarrow 20% EtOAc in pentane.

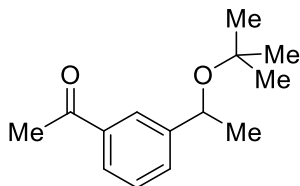
Isolated Yield from Benzyl Fluoride: 49%, 38.8 mg of colorless oil.

Spectra Available in the Literature (CAS): No (N/A)

^1H NMR (CDCl_3 , 500 MHz): δ 7.34 – 7.29 (m, 2H), 7.28 – 7.23 (m, 3H), 4.34 – 4.16 (m, 1H), 4.04 – 3.73 (m, 1H), 3.43 – 3.01 (m, 4H), 2.06 – 1.85 (m, 3H), 1.86 – 1.65 (m, 4H), 1.47 – 1.42 (m, 2H), 1.44 – 1.31 (m, 9H), 0.96 – 0.85 (m, 6H).

^{13}C NMR (CDCl_3 , 126 MHz): δ 154.4, 143.3, 128.3, 127.3, 126.4, 81.2, 80.6, 79.1, 70.0, 69.6, 68.8, 56.8, 56.5, 47.9, 47.8, 46.7, 46.4, 29.1, 28.5, 24.8, 24.8, 23.2, 23.0, 22.2.

HRMS (ESI) m/z : $[\text{M}+\text{Na}]^+$ Calcd for $\text{C}_{21}\text{H}_{33}\text{NNaO}_3$ 370.2353; Found 370.2348.



(33) 1-(3-(1-(*tert*-butoxy)ethyl)phenyl)ethan-1-one: Prepared from benzyl fluoride **4** (0.3 mmol scale, 80% NMR yield) that was formed according to the general procedure in section 4C.II with the following variations: 1 mol% CuOAc, 1.2 mol% BPhen, 1 equiv B₂pin₂ (in place of 2 equiv MeB(OH)₂), and 4 equiv NFSI operating at 55 °C. The ensuing displacement step followed the general procedure in section 4C.III and used *tert*-butanol (0.75 mmol, 71.7 μL, 2.5 equiv) as the nucleophile with BF₃•Et₂O (0.03 mmol, 3.7 μL, 0.1 equiv) as the displacement catalyst. The nucleophile was dried in 1 mL DCM with MgSO₄ prior to use.

Purification: Reverse phase silica gel chromatography was used with a gradient of 70%→100% MeOH in water. The product was extracted with 1:1 ether:pentane.

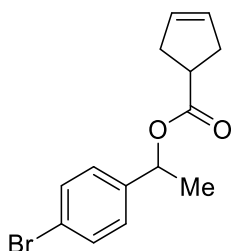
Isolated Yield from Benzyl Fluoride: 66%, 35.5 mg of colorless oil.

Spectra Available in the Literature (CAS): No (N/A)

¹H NMR (CDCl₃, 500 MHz): δ 7.93 (s, 1H), 7.80 (d, *J* = 7.8 Hz, 1H), 7.59 (d, *J* = 7.6 Hz, 1H), 7.41 (t, *J* = 7.7 Hz, 1H), 4.72 (q, *J* = 6.5 Hz, 1H), 2.61 (s, 3H), 1.38 (d, *J* = 6.5 Hz, 3H), 1.16 (s, 9H).

¹³C NMR (CDCl₃, 126 MHz): δ 198.3, 148.2, 137.1, 130.4, 128.4, 126.7, 125.3, 83.5, 74.4, 69.5, 28.5, 26.7, 26.6, 25.0.

HRMS (ESI) *m/z*: [M+Na]⁺ Calcd for C₁₄H₂₀NaO₂ 243.1356; Found 243.1353.



(34) 1-(4-bromophenyl)ethyl cyclopent-3-ene-1-carboxylate: Prepared from benzyl fluoride **1** (0.3 mmol scale, 72% NMR yield) that was formed according to the general procedure in section 4C.II. The ensuing displacement step followed the general procedure in section 4C.III and used cyclopent-3-ene-1-carboxylic acid (0.75 mmol, 77.6 μL, 2.5 equiv) as the nucleophile with BF₃•Et₂O (0.03 mmol, 3.7 μL, 0.1 equiv) as the displacement catalyst.

Purification: Normal phase silica gel chromatography was used with a gradient of 0%→20% EtOAc in pentane.

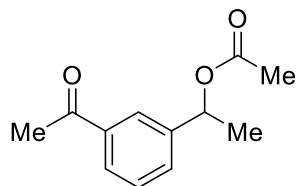
Isolated Yield from Benzyl Fluoride: 57%, 36.1 mg of clear, colorless liquid.

Spectra Available in the Literature (CAS): No (N/A)

¹H NMR (CDCl₃, 500 MHz): δ 7.47 (d, *J* = 8.5 Hz, 2H), 7.22 (d, *J* = 8.4 Hz, 2H), 5.84 (q, *J* = 6.6 Hz, 1H), 5.69 – 5.60 (m, 2H), 3.13 (tt, *J* = 9.0, 7.5 Hz, 1H), 2.73 – 2.54 (m, 4H), 1.51 (d, *J* = 6.7 Hz, 3H).

¹³C NMR (CDCl₃, 126 MHz): δ 175.2, 140.9, 131.6, 128.9, 127.8, 121.7, 71.5, 41.6, 36.2, 22.1.

HRMS (ESI) *m/z*: [M+Na]⁺ Calcd for C₁₄H₁₅BrNaO₂ 317.0148; Found 317.0147.



(35) 1-(3-acetylphenyl)ethyl acetate: Prepared from benzyl fluoride **4** (0.3 mmol scale, 76% NMR yield) that was formed according to the general procedure in section 4C.II with the following variations: 1 mol% CuOAc, 1.2 mol% BPhen, 1 equiv B₂pin₂ (in place of 2 equiv MeB(OH)₂), and 4 equiv NFSI operating at 55 °C. The ensuing displacement step followed the general procedure in section 4C.III and used acetic acid (0.75 mmol, 43 μL, 2.5 equiv) as the nucleophile with HFIP (3.0 mmol, 315 μL, 10 equiv) as the displacement catalyst.

Purification: Normal phase silica gel chromatography was used with a gradient of 0%→20% EtOAc in pentane.

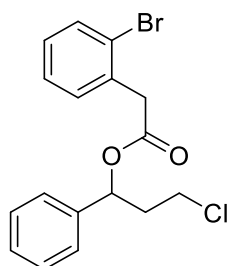
Isolated Yield from Benzyl Fluoride: 80%, 37.8 mg of colorless oil.

Spectra Available in the Literature (CAS): No (N/A)

¹H NMR (CDCl₃, 500 MHz): δ 7.95 (s, 1H), 7.88 (dd, *J* = 7.7, 1.4 Hz, 1H), 7.55 (d, *J* = 7.6 Hz, 1H), 7.45 (t, *J* = 7.7 Hz, 1H), 5.92 (q, *J* = 6.7 Hz, 1H), 2.62 (s, 3H), 2.09 (s, 3H), 1.56 (d, *J* = 6.7 Hz, 3H).

¹³C NMR (CDCl₃, 126 MHz): δ 197.8, 170.2, 142.4, 137.4, 130.8, 128.8, 127.9, 125.8, 71.9, 26.7, 22.2, 21.3.

HRMS (ESI) m/z: [M+Na]⁺ Calcd for C₁₂H₁₄NaO₃ 229.0835; Found 229.0832.



(36) 3-chloro-1-phenylpropyl 2-(2-bromophenyl)acetate: Prepared from benzyl fluoride **7** (0.3 mmol scale, 72% NMR yield) that was formed according to the general procedure in section 4C.II. The ensuing displacement step followed the general procedure in section 4C.III and used 2-(2-bromophenyl)acetic acid (0.75 mmol, 161.3 mg, 2.5 equiv) as the nucleophile with HFIP (3.0 mmol, 315 μL, 10 equiv) as the displacement catalyst.

Purification: Normal phase silica gel chromatography was used with a gradient of 0%→20% EtOAc in pentane.

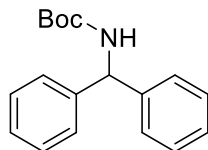
Isolated Yield from Benzyl Fluoride: 64%, 50.5 mg of yellow solid.

Spectra Available in the Literature (CAS): No (N/A)

¹H NMR (CDCl₃, 500 MHz): δ 7.58 (d, *J* = 7.9 Hz, 1H), 7.38 – 7.23 (m, 7H), 7.15 (ddd, *J* = 8.8, 6.0, 3.0 Hz, 1H), 5.98 (dd, *J* = 8.4, 5.3 Hz, 1H), 3.89 – 3.78 (m, 2H), 3.52 (dt, *J* = 10.9, 7.0 Hz, 1H), 3.43 (dt, *J* = 10.9, 6.4 Hz, 1H), 2.38 (ddt, *J* = 14.5, 8.3, 6.2 Hz, 1H), 2.18 (dtd, *J* = 14.3, 7.1, 5.3 Hz, 1H).

¹³C NMR (CDCl₃, 126 MHz): δ 169.5, 139.3, 134.1, 132.8, 131.4, 129.0, 128.6, 128.3, 127.6, 126.4, 125.0, 73.8, 41.9, 40.6, 39.1.

HRMS (ESI) m/z: [M+Na]⁺ Calcd for C₁₇H₁₆BrClNaO₂ 390.9893; Found 390.9886.



(37) *tert*-butyl benzhydrylcarbamate: Prepared from benzyl fluoride **10** (0.3 mmol scale, 44% NMR yield) that was formed according to the general procedure in section 4C.II. The ensuing displacement step followed the general procedure in section 4C.III and used Boc carbamate (0.75 mmol, 87.9 mg, 2.5 equiv) as the nucleophile with $\text{BF}_3 \cdot \text{Et}_2\text{O}$ (0.15 mmol, 18.5 μL , 0.5 equiv) as the displacement catalyst.

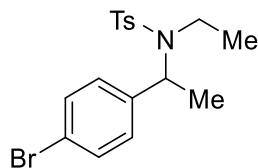
Purification: Normal phase silica gel chromatography was used with a gradient of 0%→20% EtOAc in pentane.

Isolated Yield from Benzyl Fluoride: 70%, 26.2 mg of white solid.

Spectra Available in the Literature (CAS): Yes²² (21420-61-1)

¹H NMR (CDCl_3 , 500 MHz): δ 7.35 – 7.30 (m, 4H), 7.29 – 7.22 (m, 6H), 5.92 (bs, 1H), 5.15 (bs, 1H), 1.44 (bs, 9H).

¹³C NMR (CDCl_3 , 126 MHz): δ 155.0, 142.1, 128.6, 127.3, 127.2, 79.8, 58.4, 28.4.



(38) *N*-(1-(4-bromophenyl)ethyl)-*N*-ethyl-4-methylbenzenesulfonamide: Prepared from benzyl fluoride **1** (0.3 mmol scale, 56% NMR yield) that was formed according to the general procedure in section 4C.II with the following variations: 1 mol% CuOAc, 1.2 mol% BPhen, 1 equiv B_2pin_2 (in place of 2 equiv $\text{MeB}(\text{OH})_2$), and 4 equiv NFSI operating at 45 °C with DCM as the solvent instead of PhCl. The ensuing displacement step followed the general procedure in section 4C.III and used *N*-ethyl-4-methylbenzenesulfonamide (0.75 mmol, 149.4 mg, 2.5 equiv) as the nucleophile with $\text{BF}_3 \cdot \text{Et}_2\text{O}$ (0.03 mmol, 3.7 μL , 0.1 equiv) as the displacement catalyst.

Purification: Reverse phase chromatography was used with a gradient of 65%→100% MeOH in water. Solvent was removed directly on the rotovap at elevated temperatures.

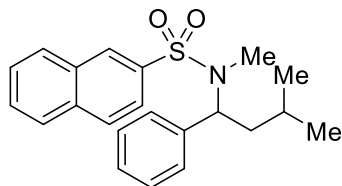
Isolated Yield from Benzyl Fluoride: 78%, 50 mg of white solid.

Spectra Available in the Literature (CAS): No (N/A)

¹H NMR (CDCl_3 , 500 MHz): δ 7.73 (d, J = 8.3 Hz, 2H), 7.41 (d, J = 8.5 Hz, 2H), 7.30 (d, J = 8.0 Hz, 2H), 7.16 (d, J = 8.5 Hz, 2H), 5.14 (q, J = 7.1 Hz, 1H), 3.20 – 3.02 (m, J = 7.3 Hz, 2H), 2.44 (s, 3H), 1.37 (d, J = 7.1 Hz, 3H), 0.93 (t, J = 7.1 Hz, 3H).

¹³C NMR (CDCl_3 , 126 MHz): δ 143.1, 139.7, 138.4, 131.4, 129.7, 129.2, 127.1, 121.5, 54.7, 38.9, 21.5, 16.7, 16.6.

HRMS (ESI) *m/z*: $[\text{M}+\text{Na}]^+$ Calcd for $\text{C}_{17}\text{H}_{20}\text{BrNNaO}_2\text{S}$ 404.0290; Found 404.0287.



(39) *N*-methyl-*N*-(3-methyl-1-phenylbutyl)naphthalene-2-sulfonamide: Prepared from benzyl fluoride **11** (0.3 mmol scale, 70% NMR yield) that was formed according to the general procedure in section 4C.II. The ensuing displacement step followed the general procedure in section 4C.III and used *N*-methyl-2-naphthylsulfonamide (0.75 mmol, 166 mg, 2.5 equiv) as the nucleophile with $\text{BF}_3 \cdot \text{Et}_2\text{O}$ (0.03 mmol, 3.7 μL , 0.1 equiv) as the displacement catalyst.

Purification: Normal phase silica gel chromatography was used with a gradient of 0%→20% EtOAc in pentane.

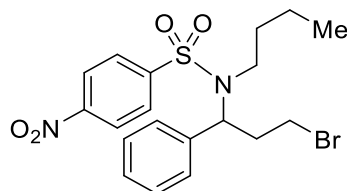
Isolated Yield from Benzyl Fluoride: 82%, 63.1 mg of white solid.

Spectra Available in the Literature (CAS): No (N/A)

^1H NMR (CDCl_3 , 500 MHz): δ 8.32 (s, 1H), 7.89 (t, J = 8.4 Hz, 3H), 7.71 (dd, J = 8.7, 1.9 Hz, 1H), 7.66 – 7.55 (m, 2H), 7.28 – 7.21 (m, 5H), 5.29 (dd, J = 8.4, 7.0 Hz, 1H), 2.69 (s, 3H), 1.84 – 1.74 (m, 1H), 1.56 – 1.43 (m, 2H), 0.90 (dd, J = 13.0, 6.3 Hz, 6H).

^{13}C NMR (CDCl_3 , 126 MHz): δ 138.5, 137.1, 134.6, 132.1, 129.1, 129.1, 128.5, 128.4, 128.4, 128.1, 127.8, 127.7, 127.4, 122.7, 58.2, 39.6, 28.8, 24.8, 22.7, 22.4.

HRMS (ESI) m/z : $[\text{M}+\text{Na}]^+$ Calcd for $\text{C}_{22}\text{H}_{25}\text{NNaO}_2\text{S}$ 390.1498; Found 390.1495.



(40) *N*-(3-bromo-1-phenylpropyl)-*N*-butyl-4-nitrobenzenesulfonamide: Prepared from benzyl fluoride **8** (0.3 mmol scale, 67% NMR yield) that was formed according to the general procedure in section 4C.II with DCM as the solvent instead of PhCl. The ensuing displacement step followed the general procedure in section 4C.III and used *N*-butyl-4-nitrobenzenesulfonamide (0.75 mmol, 193.7 mg, 2.5 equiv) as the nucleophile with $\text{BF}_3 \cdot \text{Et}_2\text{O}$ (0.03 mmol, 3.7 μL , 0.1 equiv) as the displacement catalyst. The nucleophile was dried in 1 mL DCM with MgSO_4 prior to use.

Purification: Reverse phase chromatography was used with 65%→100% MeOH in water. Solvent was removed directly on the rotovap at elevated temperatures.

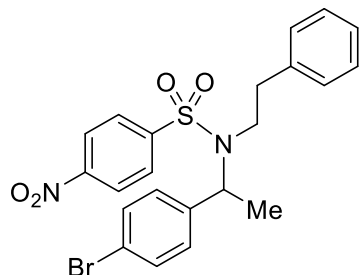
Isolated Yield from Benzyl Fluoride: 62%, 56.3 mg of colorless oil.

Spectra Available in the Literature (CAS): No (N/A)

^1H NMR (CDCl_3 , 500 MHz): δ 8.26 (d, J = 8.7 Hz, 2H), 7.88 (d, J = 8.7 Hz, 2H), 7.31 – 7.25 (m, 3H), 7.20 – 7.14 (m, 2H), 5.15 (dd, J = 8.9, 6.3 Hz, 1H), 3.43 (dt, J = 10.3, 6.0 Hz, 1H), 3.26 (ddd, J = 10.4, 8.4, 5.9 Hz, 1H), 3.14 (ddd, J = 9.8, 6.0, 3.7 Hz, 2H), 2.67 (ddt, J = 14.6, 8.9, 5.8 Hz, 1H), 2.37 (dt, J = 14.7, 7.3 Hz, 1H), 1.56 – 1.45 (m, 1H), 1.41 – 1.29 (m, 1H), 1.18 (h, J = 7.4 Hz, 2H), 0.83 (t, J = 7.4 Hz, 3H).

^{13}C NMR (CDCl_3 , 126 MHz): δ 149.7, 146.8, 136.3, 128.9, 128.7, 128.3, 128.2, 124.1, 60.1, 46.1, 35.3, 32.7, 29.7, 20.1, 13.6.

HRMS (ESI) m/z : $[\text{M}+\text{Na}]^+$ Calcd for $\text{C}_{19}\text{H}_{23}\text{BrN}_2\text{NaO}_4\text{S}$ 477.0454; Found 477.0448.



(41) *N*-(1-(4-bromophenyl)ethyl)-4-nitro-*N*-phenethylbenzenesulfonamide: Prepared from benzyl fluoride **1** (0.3 mmol scale, 83% NMR yield) that was formed according to the general procedure in section II with DCM as the solvent instead of PhCl. The ensuing displacement step followed the general procedure in section III and used *N*-phenethyl-4-nitrobenzenesulfonamide (0.75 mmol, 229.8 mg, 2.5 equiv) as the nucleophile with $\text{BF}_3 \cdot \text{Et}_2\text{O}$ (0.03 mmol, 3.7 μL , 0.1 equiv) as the displacement catalyst. The nucleophile was dried in 1 mL DCM with MgSO_4 prior to use. Purification: Reverse phase chromatography was used with 65% \rightarrow 100% MeOH in water. Solvent was removed directly on the rotovap at elevated temperatures.

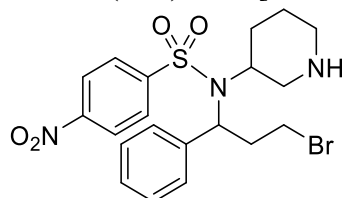
Isolated Yield from Benzyl Fluoride: 42%, 51.4 mg of white solid.

Spectra Available in the Literature (CAS): No (N/A)

$^1\text{H NMR}$ (CDCl_3 , 500 MHz): δ 8.34 (d, $J = 8.8$ Hz, 2H), 8.02 (d, $J = 8.9$ Hz, 2H), 7.46 (d, $J = 8.5$ Hz, 2H), 7.27 – 7.22 (m, 2H), 7.22 – 7.16 (m, 3H), 6.96 (d, $J = 7.0$ Hz, 2H), 5.22 (q, $J = 7.1$ Hz, 1H), 3.31 (ddd, $J = 14.8, 11.4, 5.5$ Hz, 1H), 3.19 (ddd, $J = 14.8, 11.3, 5.2$ Hz, 1H), 2.80 (td, $J = 12.8, 11.3, 5.5$ Hz, 1H), 2.38 (td, $J = 12.8, 11.3, 5.5$ Hz, 1H), 1.39 (d, $J = 7.1$ Hz, 3H).

$^{13}\text{C NMR}$ (CDCl_3 , 126 MHz): δ 149.9, 146.7, 138.5, 138.1, 131.8, 129.2, 128.7, 128.6, 128.2, 126.7, 124.4, 122.3, 55.6, 46.4, 37.6, 16.8.

HRMS (ESI) m/z : $[\text{M}+\text{Na}]^+$ Calcd for $\text{C}_{22}\text{H}_{21}\text{BrN}_2\text{NaO}_4\text{S}$ 511.0298; Found 511.0295.



Boc from the Nuc-H piperidine
was removed under displacement conditions

(42) *tert*-butyl 3-((*N*-(3-bromo-1-phenylpropyl)-4-nitrophenyl)sulfonamido)piperidine-1-carboxylate: Prepared from benzyl fluoride **8** (0.3 mmol scale, 63% NMR yield) that was formed according to the general procedure in section 4C.II with DCM as the solvent instead of PhCl. The ensuing displacement step followed the general procedure in section 4C.III and used 3-((4-nitrophenyl)sulfonamido)-*N*-Boc-piperidine (0.75 mmol, 289.1 mg, 2.5 equiv) as the nucleophile with $\text{BF}_3 \cdot \text{Et}_2\text{O}$ (0.45 mmol, 55.5 μL , 1.5 equiv) as the displacement catalyst.

Purification: Reverse phase chromatography was used with 65% \rightarrow 100% MeOH in water. Solvent was removed directly on the rotovap at elevated temperatures.

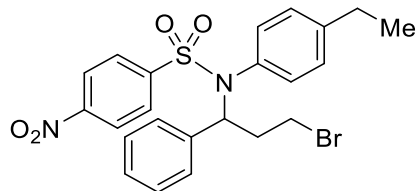
Isolated Yield from Benzyl Fluoride: 23%, 21.0 mg of yellow oil.

Spectra Available in the Literature (CAS): No (N/A)

$^1\text{H NMR}$ (CDCl_3 , 500 MHz): δ 8.43 – 8.25 (m, 2H), 8.12 – 7.96 (m, 2H), 7.40 – 7.28 (m, 5H), 5.82 (t, $J = 6.6$ Hz, 1H), 4.90 (bs, 1H), 3.56 – 3.18 (m, 7H), 2.55 – 2.44 (m, 1H), 2.39 – 2.20 (m, 1H), 1.86 – 1.70 (m, 1H), 1.70 – 1.62 (m, 1H), 1.53 – 1.43 (m, 2H).

$^{13}\text{C NMR}$ (CDCl_3 , 126 MHz): δ 150.1, 146.5, 139.7, 139.7, 128.8, 128.4, 128.4, 128.3, 126.2, 124.6, 124.6, 75.8, 49.6, 39.6, 39.5, 30.9, 28.7, 28.6, 22.4.

HRMS (ESI) m/z : $[\text{M}+\text{CO}_2+\text{Na}]^+$ Calcd for $\text{C}_{21}\text{H}_{24}\text{BrN}_3\text{NaO}_6\text{S}$ 548.0461; Found 548.0462.



(43) *N*-(3-bromo-1-phenylpropyl)-*N*-(4-ethylphenyl)-4-nitrobenzenesulfonamide: Prepared from benzyl fluoride **8** (0.3 mmol scale, 68% NMR yield) that was formed according to the general procedure in section 4C.II with DCM as the solvent instead of PhCl. The ensuing displacement step followed the general procedure in section 4C.III and used *N*-4-ethylphenyl-4-nitrobenzenesulfonamide (0.75 mmol, 229.8 mg, 2.5 equiv) as the nucleophile with $\text{BF}_3 \cdot \text{Et}_2\text{O}$ (0.15 mmol, 18.5 μL , 0.5 equiv) as the displacement catalyst. The nucleophile was dried in 1 mL DCM with MgSO_4 prior to use.

Purification: Reverse phase chromatography was used with 65%→100% MeOH in water.

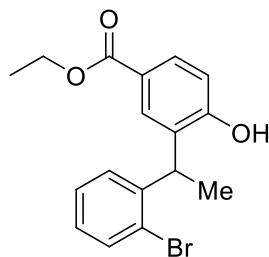
Isolated Yield from Benzyl Fluoride: 70%, 72 mg of yellow oil.

Spectra Available in the Literature (CAS): No (N/A)

^1H NMR (CDCl_3 , 500 MHz): δ 8.25 (d, J = 8.8 Hz, 2H), 7.84 (d, J = 8.8 Hz, 2H), 7.29 (t, J = 7.3 Hz, 1H), 7.24 (t, J = 7.4 Hz, 2H), 7.03 (t, J = 7.0 Hz, 4H), 6.48 (d, J = 7.9 Hz, 2H), 5.74 (t, J = 7.6 Hz, 1H), 3.38 (dt, J = 10.3, 6.2 Hz, 1H), 3.23 (dt, J = 10.3, 7.1 Hz, 1H), 2.63 (q, J = 7.6 Hz, 2H), 2.43 – 2.27 (m, 2H), 1.22 (t, J = 7.6 Hz, 3H).

^{13}C NMR (CDCl_3 , 126 MHz): δ 149.8, 146.5, 145.7, 136.9, 132.3, 131.5, 128.8, 128.7, 128.7, 128.5, 128.4, 123.9, 61.7, 35.7, 29.4, 28.4, 15.1.

HRMS (ESI) m/z : $[\text{M}+\text{Na}]^+$ Calcd for $\text{C}_{23}\text{H}_{23}\text{BrN}_2\text{NaO}_4\text{S}$ 525.0454; Found 525.0452.



(44) 3-(1-(2-bromophenyl)ethyl)-4-hydroxy-ethylbenzoate: Prepared from benzyl fluoride **2** (0.3 mmol scale, 48% NMR yield) that was formed according to the general procedure in section 4C.II with the following variations: 1 mol% CuOAc , 1.2 mol% BPhen, 1 equiv B_2pin_2 (in place of 2 equiv $\text{MeB}(\text{OH})_2$), and 4 equiv NFSI operating at 75 °C. The ensuing displacement step followed the general procedure in section 4C.III and used ethyl paraben (0.75 mmol, 124.7 mg, 2.5 equiv) as the nucleophile with HFIP (3.0 mmol, 315 μL , 10 equiv) as the displacement catalyst.

Purification: Reverse phase silica gel chromatography was used with a gradient of 50%→85% MeOH in water. The product was extracted with 1:1 ether:pentane.

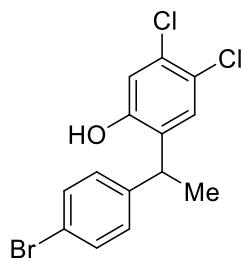
Isolated Yield from Benzyl Fluoride: 75%, 37.5 mg of colorless oil.

Spectra Available in the Literature (CAS): No (N/A)

^1H NMR (CDCl_3 , 500 MHz): δ 7.90 (d, J = 8.9 Hz, 2H), 7.55 (dd, J = 8.0, 1.2 Hz, 1H), 7.41 (dd, J = 7.8, 1.7 Hz, 1H), 7.25 (t, J = 7.6 Hz, 1H), 7.11 (td, J = 7.7, 1.7 Hz, 1H), 6.80 (d, J = 8.9 Hz, 2H), 5.69 (q, J = 6.3 Hz, 1H), 4.30 (q, J = 7.1 Hz, 2H), 1.64 (d, J = 6.3 Hz, 3H), 1.34 (t, J = 7.1 Hz, 3H).

^{13}C NMR (CDCl_3 , 126 MHz): δ 166.3, 161.2, 141.4, 132.8, 132.8, 131.5, 129.1, 129.1, 128.2, 126.8, 123.0, 121.5, 115.1, 74.9, 60.5, 22.6, 14.3.

HRMS (ESI) m/z : $[\text{M}+\text{Na}]^+$ Calcd for $\text{C}_{17}\text{H}_{17}\text{BrNaO}_3$ 371.0253; Found 371.0251.



(45) 2-(1-(4-bromophenyl)ethyl)-4,5-dichlorophenol: Prepared from benzyl fluoride **1** (0.3 mmol scale, 75% NMR yield) that was formed according to the general procedure in section 4C.II. The ensuing displacement step followed the general procedure in section 4C.III and used 3,4-dichlorophenol (0.75 mmol, 122.3 mg, 2.5 equiv) as the nucleophile with HFIP (3.0 mmol, 315 μ L, 10 equiv) as the displacement catalyst.

Purification: Reverse phase chromatography was used with a gradient of 65% \rightarrow 100% MeOH in water.

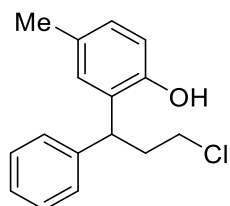
Isolated Yield from Benzyl Fluoride: 83%, 64.3 mg of yellow solid.

Spectra Available in the Literature (CAS): No (N/A)

$^1\text{H NMR}$ (CDCl_3 , 500 MHz): δ 7.42 (d, $J = 8.7$ Hz, 2H), 7.24 (s, 1H), 7.09 (d, $J = 8.6$ Hz, 2H), 6.84 (s, 1H), 4.97 (s, 1H), 4.29 (q, $J = 7.2$ Hz, 1H), 1.57 (d, $J = 7.3$ Hz, 3H).

$^{13}\text{C NMR}$ (CDCl_3 , 126 MHz): δ 152.1, 143.4, 132.4, 132.4, 131.8, 130.5, 129.2, 124.2, 120.5, 117.6, 37.7, 20.6.

HRMS (ESI) m/z: $[\text{M}-\text{H}]^-$ Calcd for $\text{C}_{14}\text{H}_{10}\text{BrCl}_2\text{O}$ 342.9298; Found 342.9300.



(46) 2-(3-chloro-1-phenylpropyl)-4-methylphenol: Prepared from benzyl fluoride **7** (0.3 mmol scale, 77% NMR yield) that was formed according to the general procedure in section 4C.II. The ensuing displacement step followed the general procedure in section 4C.III and used *p*-cresol (0.75 mmol, 81 mg, 2.5 equiv) as the nucleophile with HFIP (3.0 mmol, 315 μ L, 10 equiv) as the displacement catalyst.

Purification: Reverse phase silica gel chromatography was used with a gradient of 70% \rightarrow 100% MeOH in water. The product was extracted with 1:1 ether:pentane.

Isolated Yield from Benzyl Fluoride: 87%, 52.6 mg of off-white oil.

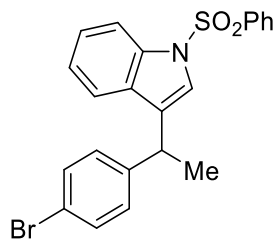
Isolated Yield from Benzyl Fluoride on 3 mmol Scale (see section IV): 84%, 445 mg of gold oil.

Spectra Available in the Literature (CAS): No (926890-10-0)

$^1\text{H NMR}$ (CDCl_3 , 500 MHz): δ 7.33 – 7.27 (m, 4H), 7.21 (tt, $J = 5.5, 2.5$ Hz, 1H), 7.02 (d, $J = 2.1$ Hz, 1H), 6.91 (dd, $J = 8.1, 2.2$ Hz, 1H), 6.64 (d, $J = 8.1$ Hz, 1H), 4.48 (s, 1H), 4.46 (t, $J = 7.8$ Hz, 1H), 3.54 – 3.44 (m, 2H), 2.60 – 2.44 (m, 2H), 2.28 (s, 3H).

$^{13}\text{C NMR}$ (CDCl_3 , 126 MHz): δ 151.1, 142.8, 130.2, 129.4, 128.7, 128.6, 128.2, 128.0, 126.7, 116.0, 43.3, 41.4, 37.2, 20.7.

HRMS (ESI) m/z: $[\text{M}-\text{Cl}]^+$ Calcd for $\text{C}_{16}\text{H}_{17}\text{O}$ 225.1274; Found 225.1271.



(47) 3-(1-(4-bromophenyl)ethyl)-1-(phenylsulfonyl)-1H-indole: Prepared from benzyl fluoride **1** (0.3 mmol scale, 78% NMR yield) that was formed according to the general procedure in section 4C.II. The ensuing displacement step followed the general procedure in section 4C.III and used 1-(phenylsulfonyl)indole (0.75 mmol, 193 mg, 2.5 equiv) as the nucleophile with HFIP (3.0 mmol, 315 μ L, 10 equiv) as the displacement catalyst.

Purification: Reverse phase silica gel chromatography was used with a gradient of 70% \rightarrow 100% MeOH in water. The product was extracted with 1:1 ether:pentane.

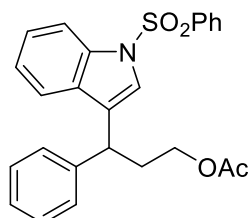
Isolated Yield from Benzyl Fluoride: 78%, 80.4 mg of white solid.

Spectra Available in the Literature (CAS): No (N/A)

^1H NMR (CDCl_3 , 500 MHz): δ 7.97 (d, J = 8.4 Hz, 1H), 7.87 (d, J = 7.2 Hz, 2H), 7.55 (t, J = 7.5 Hz, 1H), 7.45 (t, J = 7.9 Hz, 2H), 7.42 (d, J = 1.3 Hz, 1H), 7.36 (d, J = 8.5 Hz, 2H), 7.27 (ddd, J = 8.5, 6.9, 1.5 Hz, 1H), 7.15 – 7.07 (m, 2H), 7.02 (d, J = 8.5 Hz, 2H), 4.18 (q, J = 7.6 Hz, 1H), 1.64 (d, J = 7.1 Hz, 3H).

^{13}C NMR (CDCl_3 , 126 MHz): δ 143.9, 138.2, 135.7, 133.7, 131.6, 130.1, 129.2, 129.0, 127.2, 126.7, 124.8, 123.2, 122.9, 120.2, 120.2, 113.8, 36.4, 21.8.

HRMS (ESI) m/z : $[\text{M}+\text{Na}]^+$ Calcd for $\text{C}_{22}\text{H}_{18}\text{BrNNaO}_2\text{S}$ 462.0134; Found 462.0131.



(48) 3-phenyl-3-(1-(phenylsulfonyl)-1H-indol-3-yl)propylacetate: Prepared from benzyl fluoride **12** (0.3 mmol scale, 76% NMR yield) that was formed according to the general procedure in section 4C.II. The ensuing displacement step followed the general procedure in section 4C.III and used 1-(phenylsulfonyl)indole (0.75 mmol, 193 mg, 2.5 equiv) as the nucleophile with HFIP (3.0 mmol, 315 μ L, 10 equiv) as the displacement catalyst.

Purification: Reverse phase silica gel chromatography was used with a gradient of 70% \rightarrow 100% MeOH in water. The product was extracted with 1:1 ether:pentane.

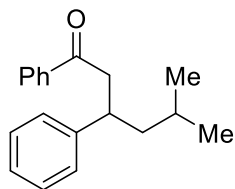
Isolated Yield from Benzyl Fluoride: 50%, 49.5 mg of white solid.

Spectra Available in the Literature (CAS): No (N/A)

^1H NMR (CDCl_3 , 500 MHz): δ 7.96 (d, J = 8.3 Hz, 1H), 7.86 (d, J = 7.3 Hz, 2H), 7.53 (t, J = 7.5 Hz, 1H), 7.49 (d, J = 1.1 Hz, 1H), 7.44 (t, J = 7.9 Hz, 2H), 7.29 – 7.21 (m, 4H), 7.22 – 7.16 (m, 3H), 7.10 (td, J = 7.6, 7.1, 1.0 Hz, 1H), 4.21 – 4.16 (m, 1H), 4.10 – 3.97 (m, 2H), 2.48 (dq, J = 13.6, 6.8 Hz, 1H), 2.29 (ddt, J = 13.7, 9.0, 6.0 Hz, 1H), 2.03 (s, 3H).

^{13}C NMR (CDCl_3 , 126 MHz): δ 170.9, 142.0, 138.1, 135.6, 133.7, 130.3, 129.2, 128.7, 127.7, 126.9, 126.7, 126.1, 124.9, 123.2, 122.7, 120.1, 113.8, 62.4, 39.2, 34.1, 20.9.

HRMS (ESI) m/z : $[\text{M}+\text{Na}]^+$ Calcd for $\text{C}_{25}\text{H}_{23}\text{NNaO}_4\text{S}$ 456.1240; Found 456.1234.



(49) 5-methyl-1,3-diphenylhexan-1-one: Prepared from benzyl fluoride **11** (0.3 mmol scale, 70% NMR yield) that was formed according to the general procedure in section 4C.II. The ensuing displacement step followed the general procedure in section 4C.III and used 1-phenyl-1-trimethylsiloxyethylene (0.75 mmol, 153.8 μ L, 2.5 equiv) as the nucleophile with $\text{BF}_3 \cdot \text{Et}_2\text{O}$ (0.03 mmol, 3.7 μ L, 0.1 equiv) as the displacement catalyst.

Purification: Normal phase silica gel chromatography was used with a gradient of 0% \rightarrow 20% EtOAc in pentane.

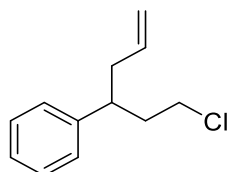
Isolated Yield from Benzyl Fluoride: 68%, 38.3 mg of colorless oil.

Spectra Available in the Literature (CAS): No (N/A)

$^1\text{H NMR}$ (CDCl_3 , 500 MHz): δ 7.89 (dd, $J = 8.4, 1.4$ Hz, 2H), 7.53 (t, $J = 7.4$ Hz, 1H), 7.42 (t, $J = 7.8$ Hz, 2H), 7.31 – 7.22 (m, 4H), 7.17 (t, $J = 7.0$ Hz, 1H), 3.45 (dtd, $J = 10.3, 6.9, 4.9$ Hz, 1H), 3.31 – 3.13 (m, 2H), 1.66 (ddd, $J = 13.4, 10.3, 4.7$ Hz, 1H), 1.50 (ddd, $J = 13.7, 9.3, 5.0$ Hz, 1H), 1.36 (dpd, $J = 9.3, 6.6, 4.8$ Hz, 1H), 0.91 (d, $J = 6.5$ Hz, 3H), 0.83 (d, $J = 6.7$ Hz, 3H).

$^{13}\text{C NMR}$ (CDCl_3 , 126 MHz): δ 199.1, 144.9, 137.3, 132.8, 128.5, 128.4, 128.0, 127.6, 126.2, 46.5, 45.5, 39.1, 25.4, 23.6, 21.6.

HRMS (ESI) m/z: $[\text{M}+\text{H}]^+$ Calcd for $\text{C}_{19}\text{H}_{23}\text{O}$ 267.1743; Found 267.1740.



(50) (1-chlorohex-5-en-3-yl)benzene: Prepared from benzyl fluoride **7** (0.3 mmol scale, 77% NMR yield) that was formed according to the general procedure in section 4C.II. The ensuing displacement step followed the general procedure in section 4C.III and used allyltrimethylsilane (0.75 mmol, 119.2 μ L, 2.5 equiv) as the nucleophile with both HFIP (3.0 mmol, 315 μ L, 10 equiv) and $\text{BF}_3 \cdot \text{Et}_2\text{O}$ (0.03 mmol, 3.7 μ L, 0.1 equiv) as the displacement catalysts.

Purification: Reverse phase silica gel chromatography was used with a gradient of 70% \rightarrow 100% MeOH in water. The product was extracted with 1:1 ether:pentane.

Isolated Yield from Benzyl Fluoride: 43%, 19.2 mg of colorless oil.

Spectra Available in the Literature (CAS): Yes²³ (276254-98-9)

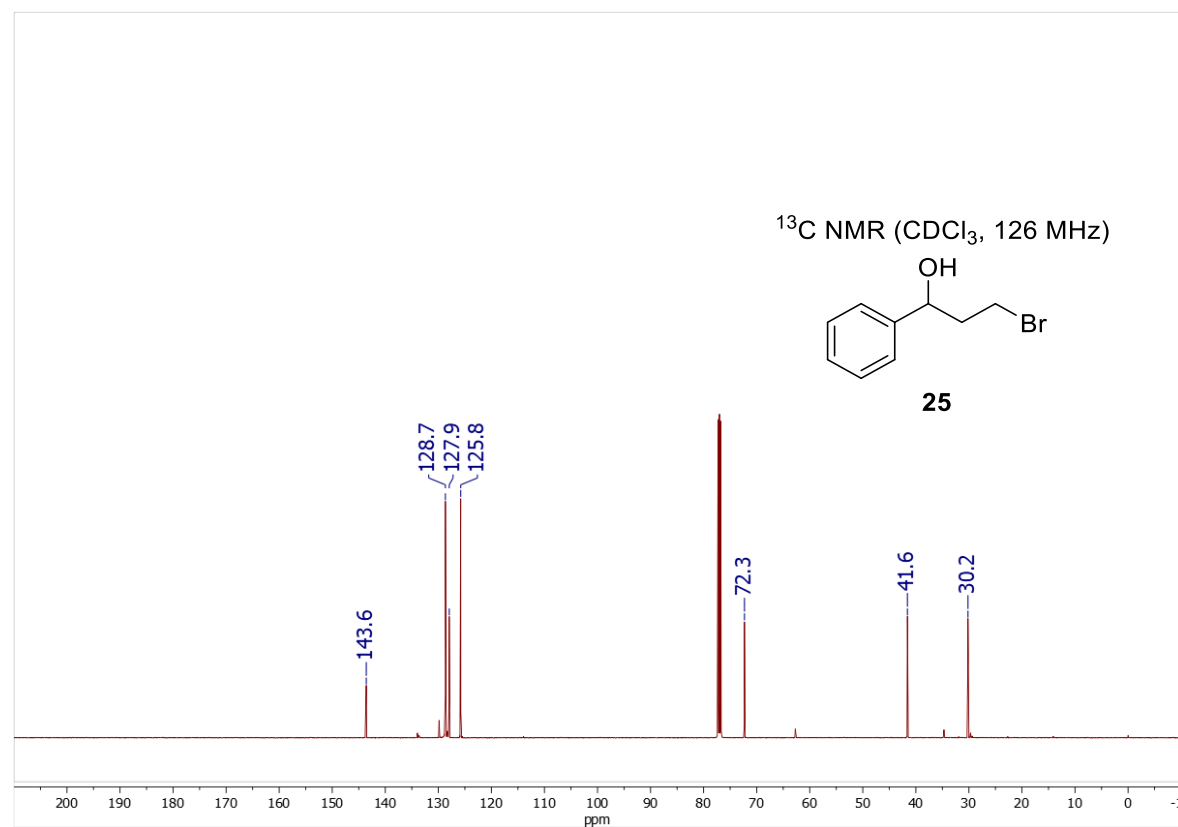
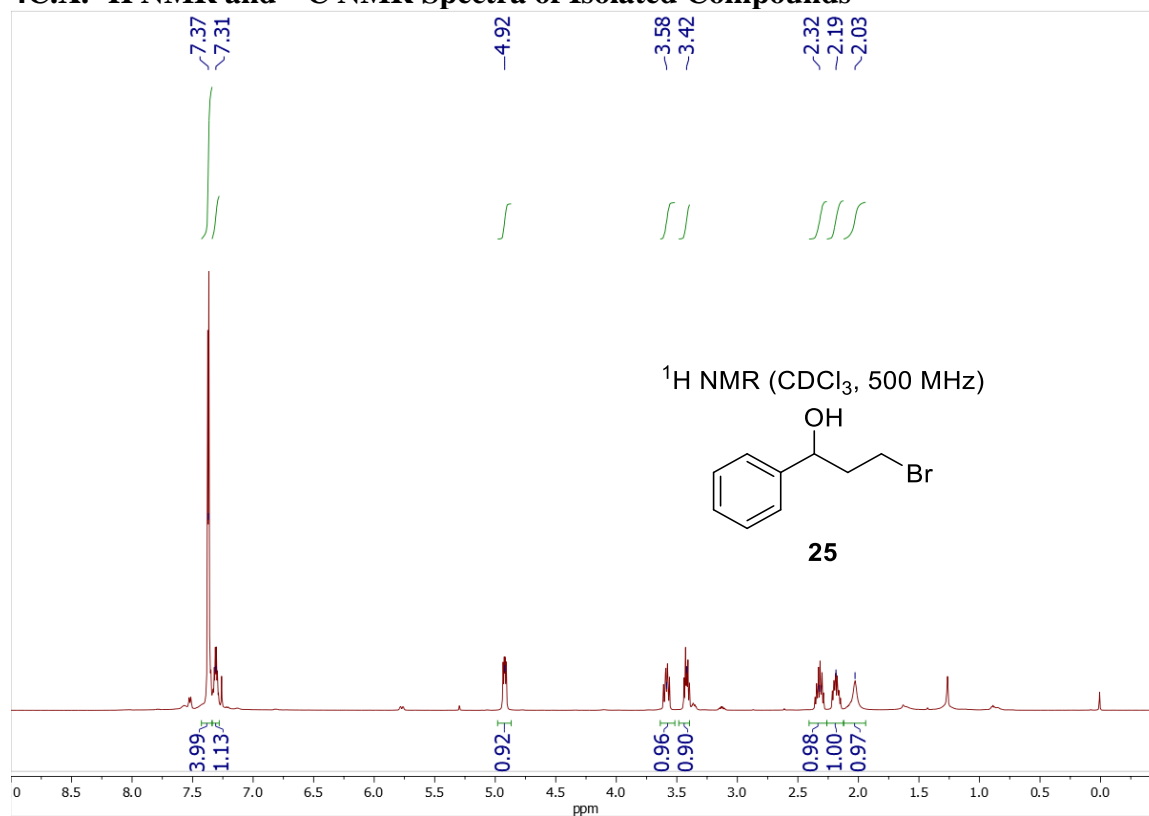
$^1\text{H NMR}$ (CDCl_3 , 500 MHz): δ 7.31 (t, $J = 7.5$ Hz, 2H), 7.22 (t, $J = 7.4$ Hz, 1H), 7.17 (d, $J = 6.7$ Hz, 2H), 5.67 (ddt, $J = 17.1, 10.1, 7.0$ Hz, 1H), 5.06 – 4.88 (m, 2H), 3.42 (ddd, $J = 10.8, 7.1, 4.8$ Hz, 1H), 3.26 (ddd, $J = 10.8, 8.7, 6.5$ Hz, 1H), 2.96 – 2.81 (m, 1H), 2.50 – 2.32 (m, 2H), 2.16 (dddd, $J = 13.4, 8.7, 7.1, 4.4$ Hz, 1H), 2.06 – 1.93 (m, 1H).

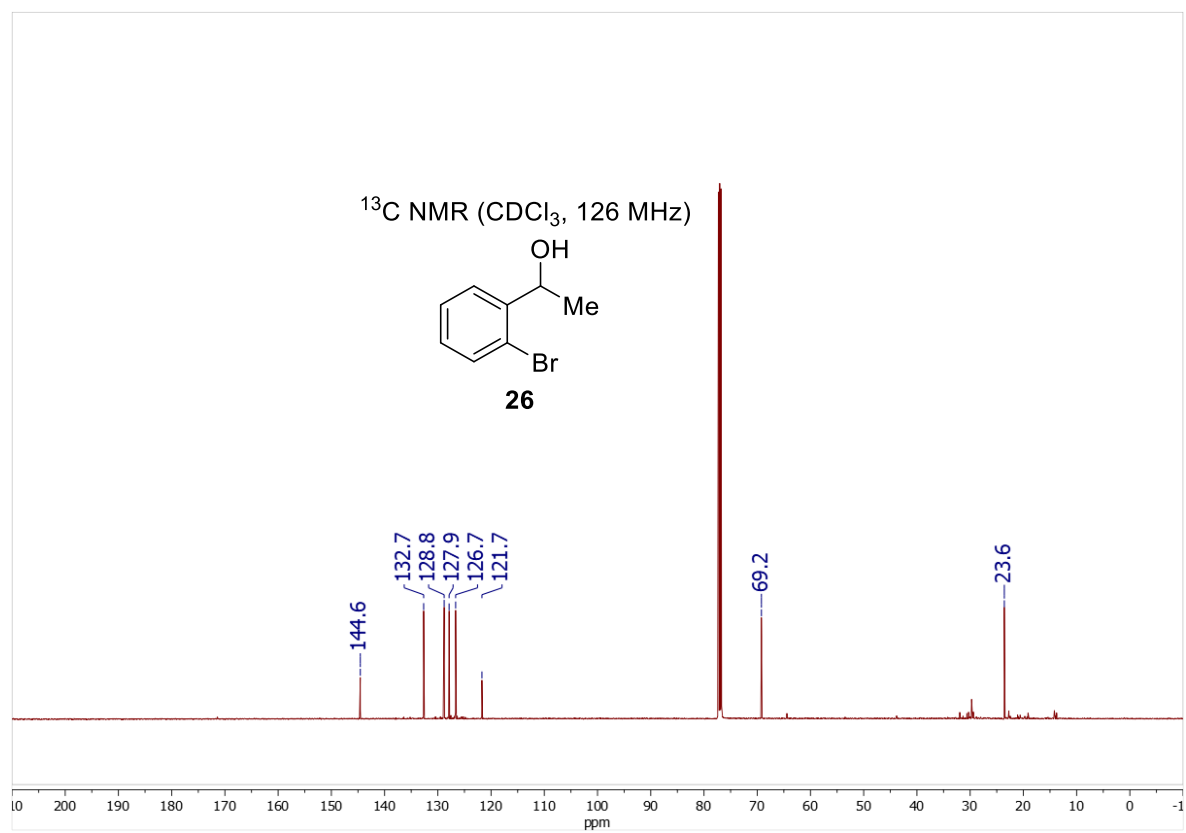
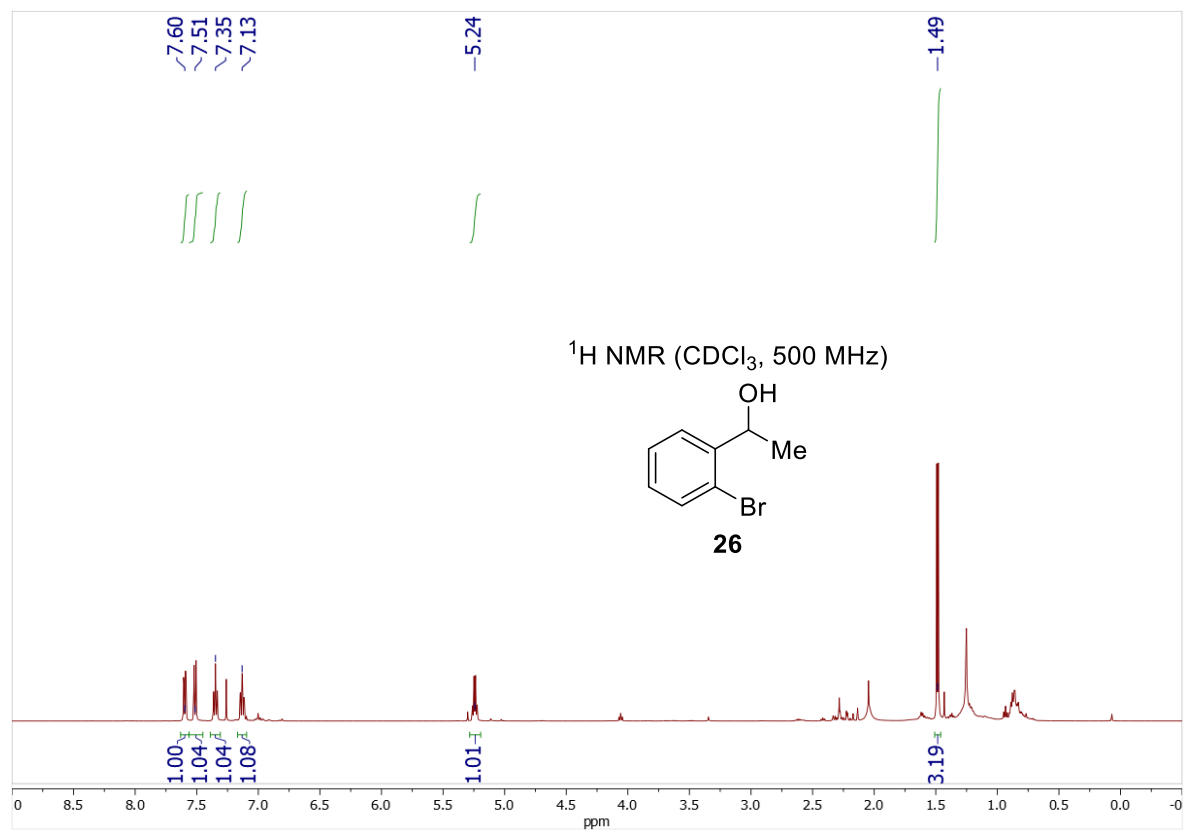
$^{13}\text{C NMR}$ (CDCl_3 , 126 MHz): δ 143.3, 136.3, 128.5, 127.6, 126.5, 116.4, 43.1, 42.8, 40.9, 38.6.

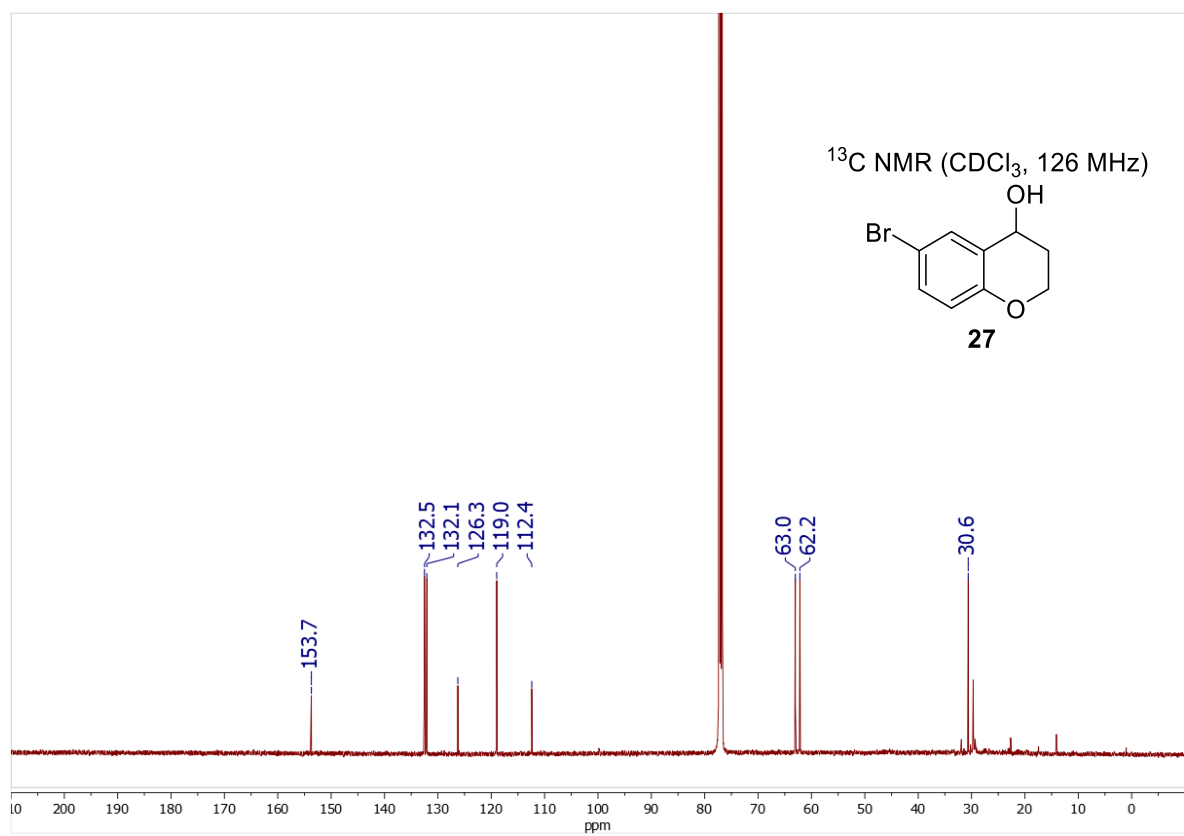
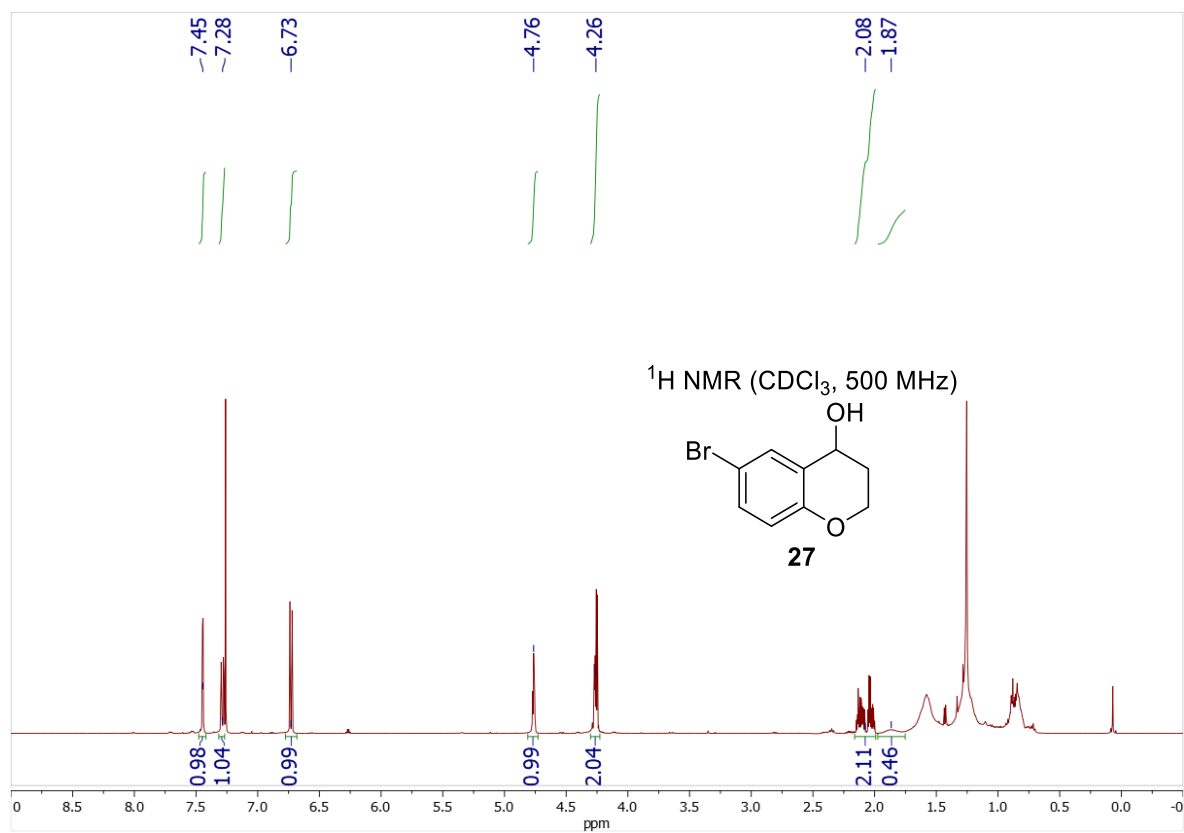
4C.X. Reference

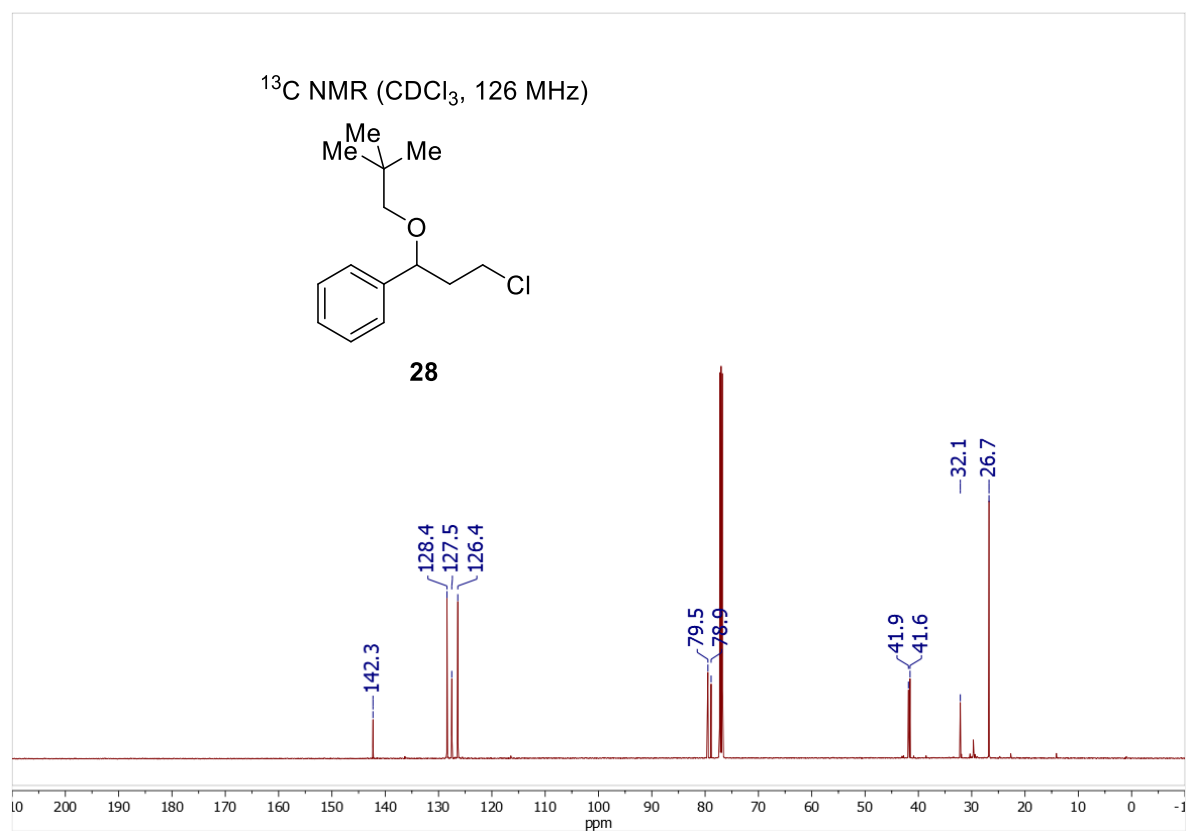
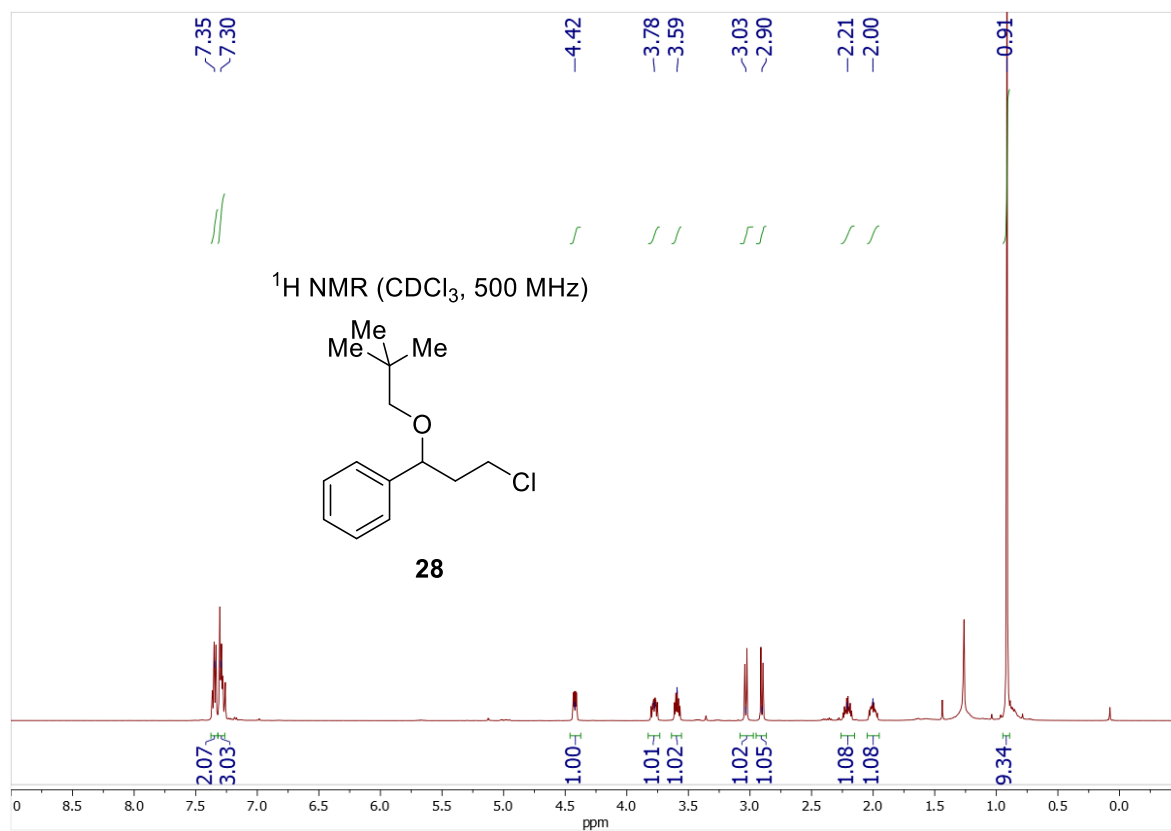
- 1 Gonçalves, C. R.; Lemmerer, M.; Teskey, C. J.; Adler, P.; Kaiser, D.; Maryasin, B.; González, L.; Maulide, N. A Unified Approach to the Chemoselective α -Functionalization of Amides with Heteroatom Nucleophiles. *J. Am. Chem. Soc.* **2019**, *46*, 18437-18443.
- 2 Pizsel, P. E.; Vasilopoulos, A.; Stahl, S. S. Oxidative Amide Coupling from Functionally Diverse Alcohols and Amines using Aerobic Copper/Nitroxyl Catalysis. *Angew. Chem. Int. Ed.* **2019**, *58*, 12211-12215.
- 3 Mayhew, S. G. The Redox Potential of Dithionite and SO₂; from Equilibrium Reactions with Flavodoxins, Methyl Viologen and Hydrogen Plus Hydrogenase. *Eur. J. Biochem.* **1978**, *85*, 535-547.
- 4 Meanwell, M.; Lehmann, J.; Eichenberger, M.; Martin, R. E.; Britton, R. Synthesis of Acyl Fluorides *via* Photocatalytic Fluorination of Aldehydic C–H Bonds. *Chem. Commun.* **2018**, *54*, 9985-9988.
- 5 Lee, B. J.; DeGlopper, K. S.; Yoon, T. P. Site-Selective Alkoxylation of Benzylic C–H Bonds by Photoredox Catalysis. *Angew. Chem. Int. Ed.* **2020**, *59*, 197-202.
- 6 Meanwell, M.; Adluri, B. S.; Yuan, Z.; Newton, J.; Prevost, P.; Nodwell, M. B.; Friesen, C. M.; Schaffer, P.; Martin, R. E.; Britton, R. Direct Heterobenzylic Fluorination, Difluorination and Trifluoromethylthiolation with Dibenzenesulfonamide Derivatives. *Chem. Sci.* **2018**, *9*, 5608-5613.
- 7 Champagne, P. A.; Pomarole, J.; Thérien, M.-E.; Benhassine, Y.; Beaulieu, S.; Legault, C. Y.; Paquin, J.-F. Enabling Nucleophilic Substitution Reactions of Activated Alkyl Fluorides Through Hydrogen Bonding. *Org. Lett.* **2013**, *15*, 2210-2213.
- 8 Xia, J.-B.; Zhu, C.; Chen, C. Visible Light-Promoted Metal-Free C–H Activation: Diarylketone-Catalyzed Selective Benzylic Mono- and Difluorination. *J. Am. Chem. Soc.* **2013**, *135*, 17494-17500.
- 9 Liu, W.; Groves, J.T. Manganese-Catalyzed Oxidative Benzylic C–H Fluorination by Fluoride Ions. *Angew. Chem. Int. Ed.* **2013**, *52*, 6024-6027.
- 10 Huang, X.; Liu, W.; Ren, H.; Neelamegam, R.; Hooker, J. M.; Groves, J. T. Late Stage Benzylic C–H Fluorination with [¹⁸F]Fluoride for PET Imaging. *J. Am. Chem. Soc.* **2014**, *136*, 6842-6845.
- 11 Bloom, S.; Pitts, C. R.; Woltornist, R.; Griswold, A.; Holl, M. G.; Lectka, T. Iron(II)-Catalyzed Benzylic Fluorination. *Org. Lett.* **2013**, *15*, 1722-1724.
- 12 Nodwell, M. B.; Bagai, A.; Halperin, S. D.; Martin, R. E.; Knust, H.; Britton, R. Direct Photocatalytic Fluorination of Benzylic C–H Bonds with *N*-Fluorobenzenesulfonimide. *Chem. Commun.* **2015**, *51*, 11783-11786.
- 13 Cantillo, D.; de Frutos, O.; Rincón, J. A.; Mateos, C.; Kappe, C. O. A Continuous-Flow Protocol for Light-Induced Benzylic Fluorinations. *J. Org. Chem.* **2014**, *79*, 8486-8490.
- 14 Bloom, S.; McCann, M.; Lectka, T. Photocatalyzed Benzylic Fluorination: Shedding “Light” on the Involvement of Electron Transfer. *Org. Lett.* **2014**, *16*, 6338-6341.
- 15 Sood, D. E.; Champion, S.; Dawson, D. M.; Chabbra, S.; Bode, B. E.; Sutherland, A.; Watson, A. J. B. Deoxyfluorination with CuF₂: Enabled by Using a Lewis Base Activating Group. *Angew. Chem. Int. Ed.* **2020**, *59*, 8460-8463.
- 16 Dinoiu, V.; Fukuhara, T.; Miura, K.; Yoneda, N. Electrochemical Partial Fluorination of Phenylacetic Acids Esters and 1-Tetralone. *J. Fluor. Chem.* **2003**, *121*, 227-231.

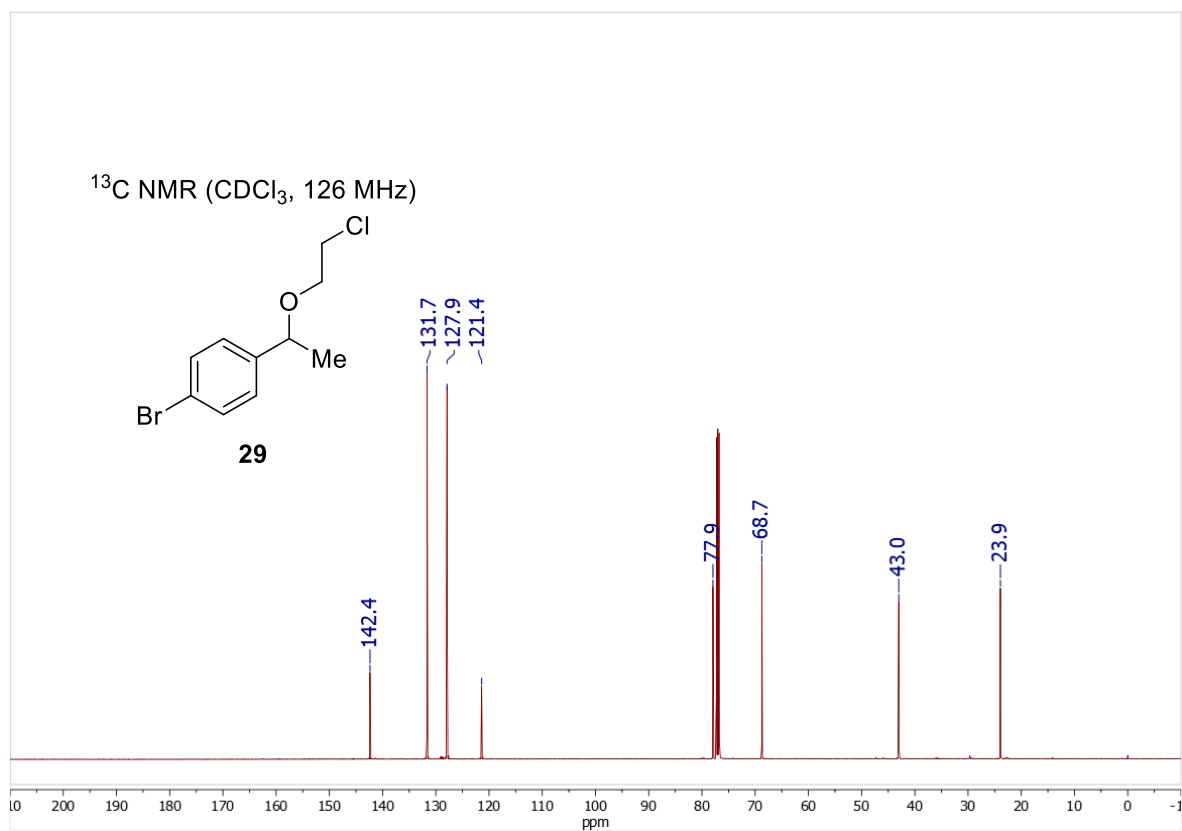
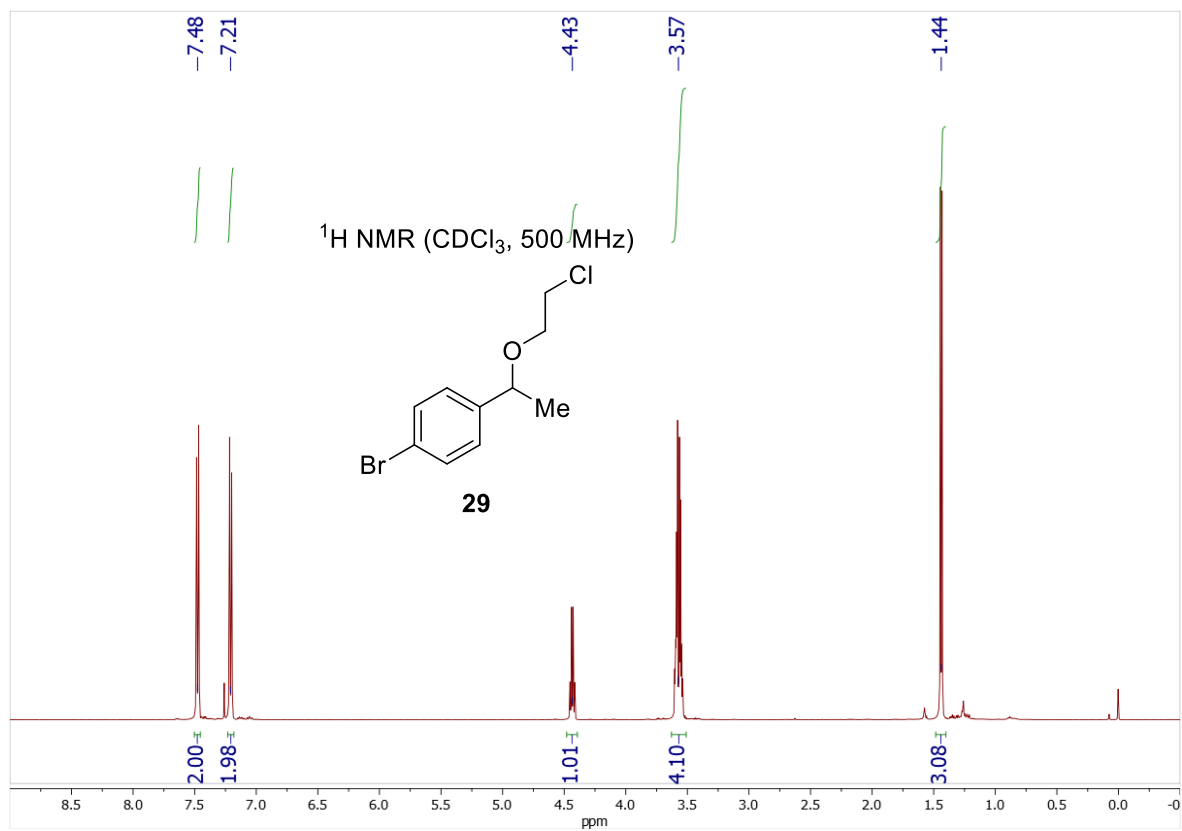
- 17 Ni, Z.; Zhang, Q.; Xiong, T.; Zheng, Y.; Li, Y.; Zhang, H.; Zhang, J.; Liu, Q. Highly Regioselective Copper-Catalyzed Benzylic C–H Amination by *N*-Fluorobenzenesulfonimide. *Angew. Chem. Int. Ed.* **2012**, *51*, 1244-1247.
- 18 Trahanovsky, W. S.; Fox, N. S. Oxidation of Organic Compounds with Cerium(IV). XIX. Effect of Alkyl Substitution on the Oxidative Cleavage of Alkylphenylmethanols. *J. Am. Chem. Soc.* **1974**, *96*, 7968-7974.
- 19 Bosson, J.; Nolan, S. P. N-Heterocyclic Carbene–Ruthenium Complexes for the Racemization of Chiral Alcohols. *J. Org. Chem.* **2010**, *75*, 2039-2043.
- 20 Ramadas, S.; Krupadanam, G. L. D. Enantioselective Acylation of Chroman-4-ols Catalyzed by Lipase from *Pseudomonas Cepecia* (Amano PS). *Tetrahedron: Asymmetry* **1997**, *8*, 3059-3066.
- 21 Darwish, K. M.; Salama, I.; Mostafa, S.; Gomaa, M. S.; Khafagy, E.-S.; Helal, M. A. Synthesis, Biological Evaluation, and Molecular Docking Investigation of Benzhydrol- and Indole-Based Dual PPAR- γ /FFAR1 Agonists. *Bioorg. Med. Chem. Lett.* **2018**, *28*, 1595-1602.
- 22 Dastbaravardeh, N.; Schnürch, M.; Mihovilovic, M. D. Ruthenium(0)-Catalyzed sp³ C–H Bond Arylation of Benzylic Amines Using Arylboronates. *Org. Lett.* **2012**, *14*, 1930-1933.
- 23 Yasuda, M.; Saito, T.; Ueba, M.; Baba, A. Direct Substitution of the Hydroxy Group in Alcohols with Silyl Nucleophiles Catalyzed by Indium Trichloride. *Angew. Chem. Int. Ed.* **2004**, *43*, 1414-1416.

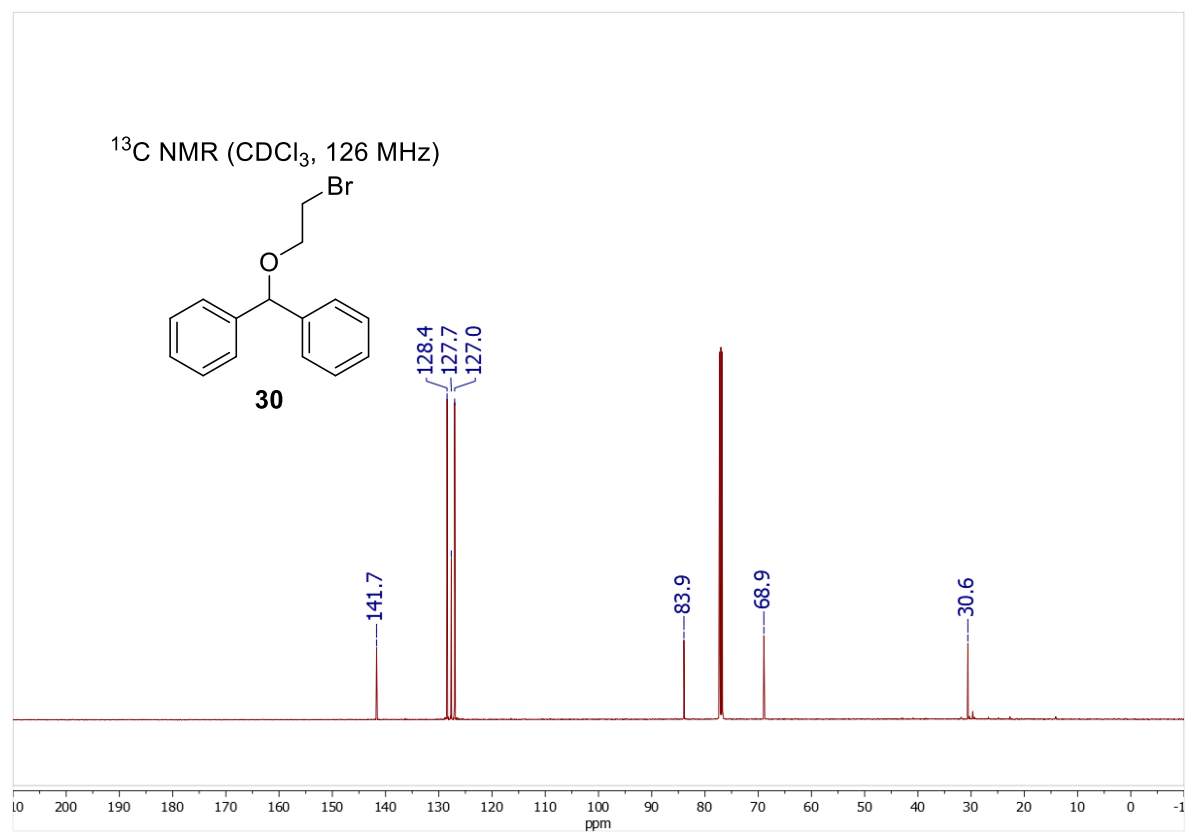
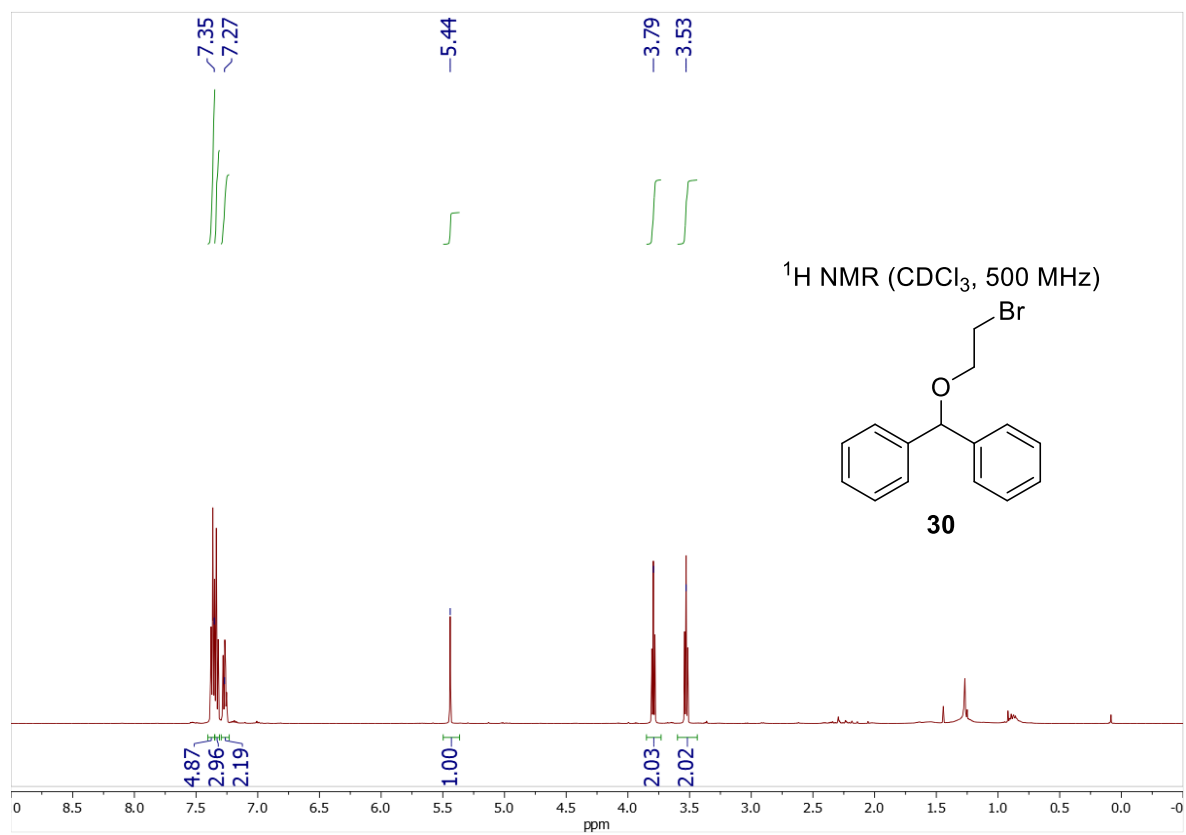
4C.X. ^1H NMR and ^{13}C NMR Spectra of Isolated Compounds

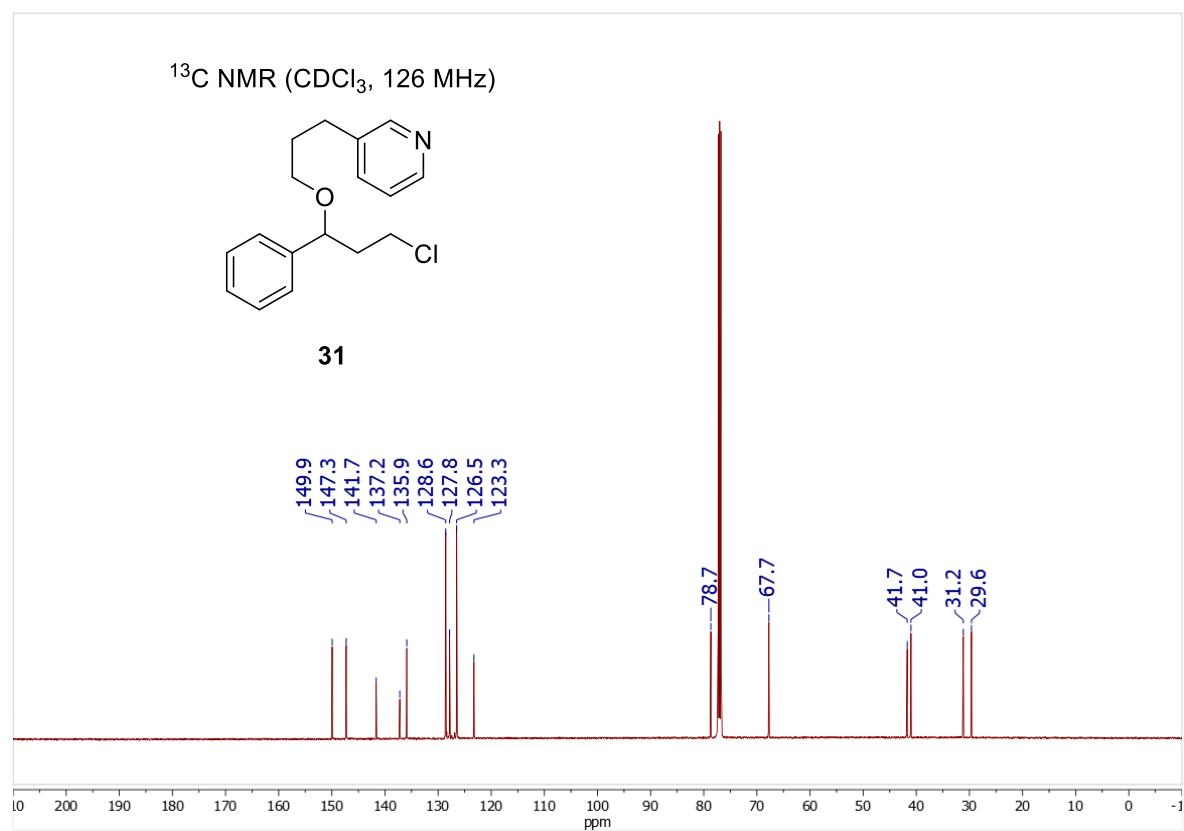
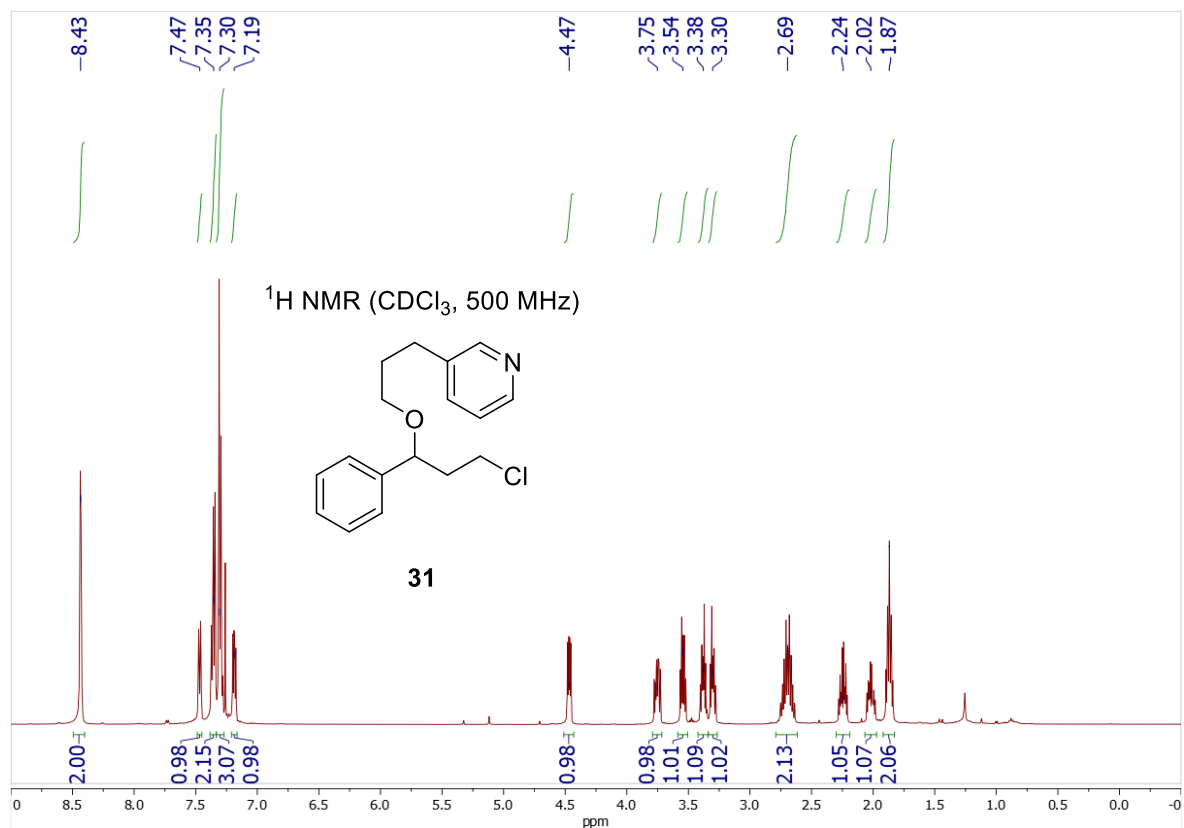


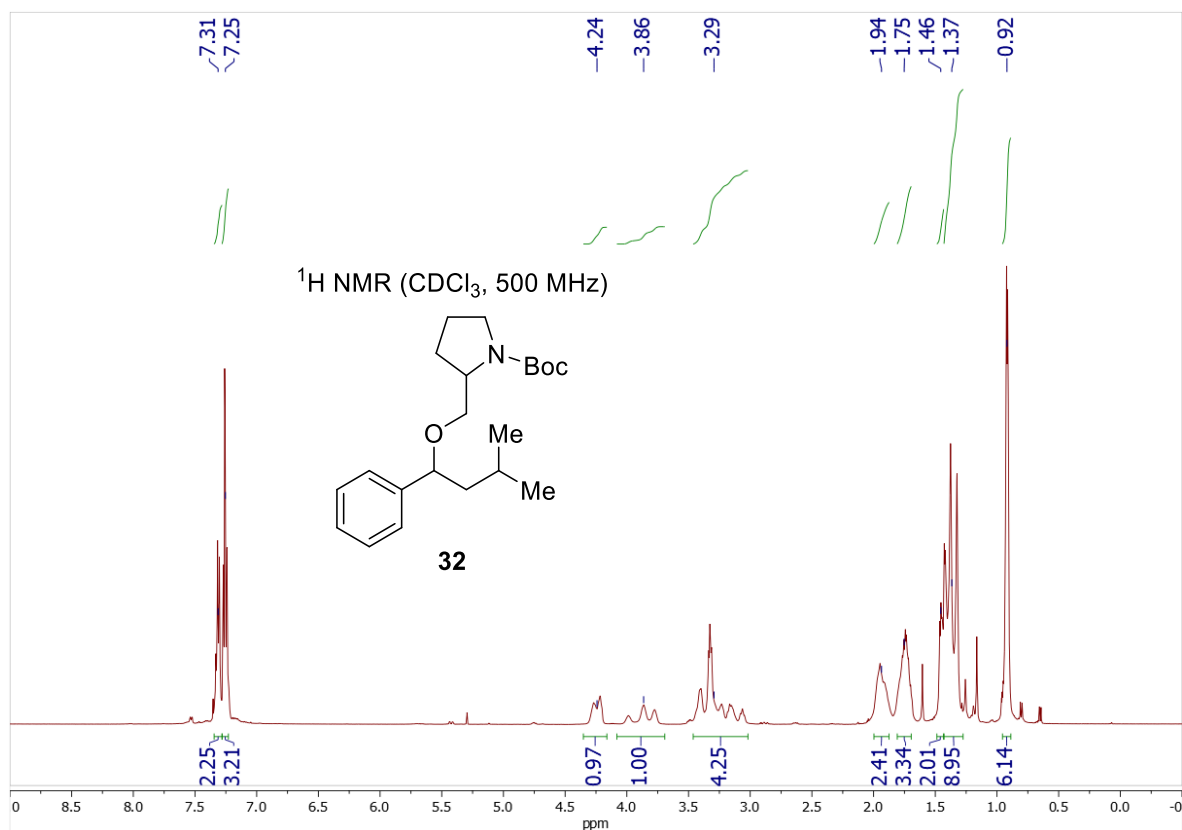




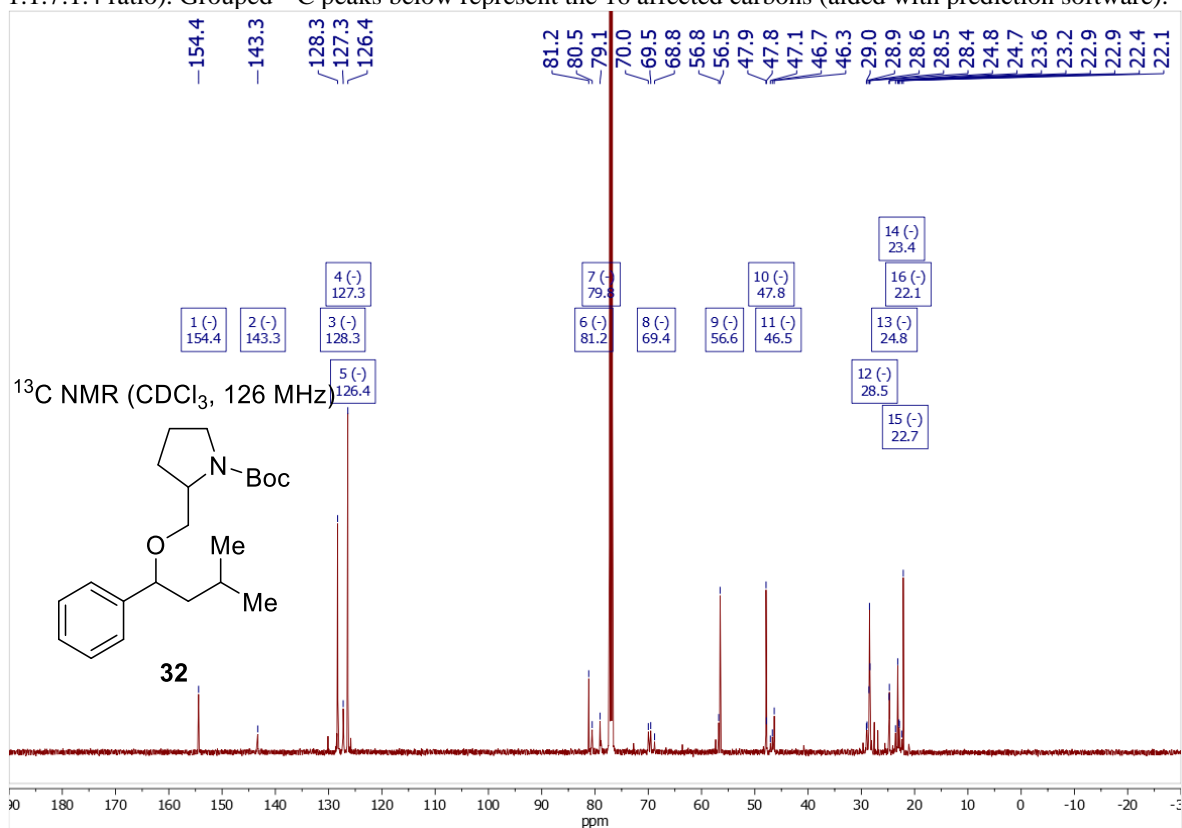


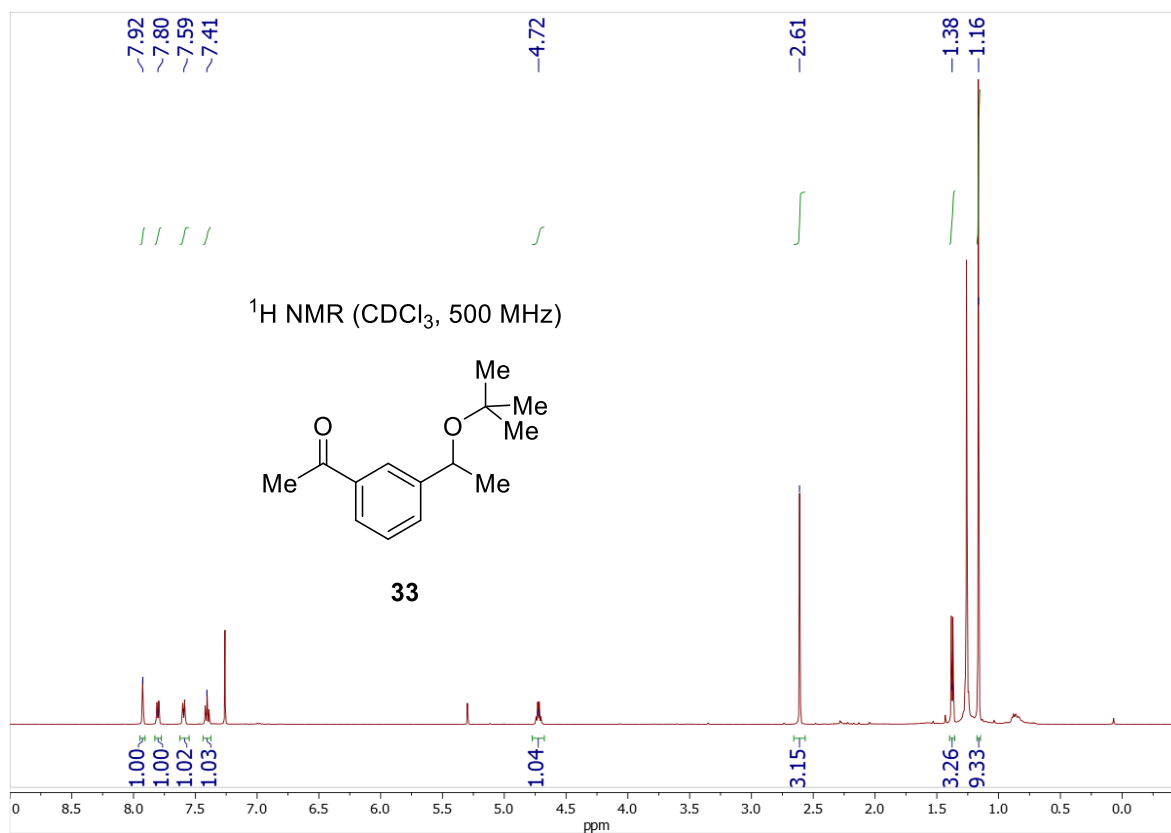




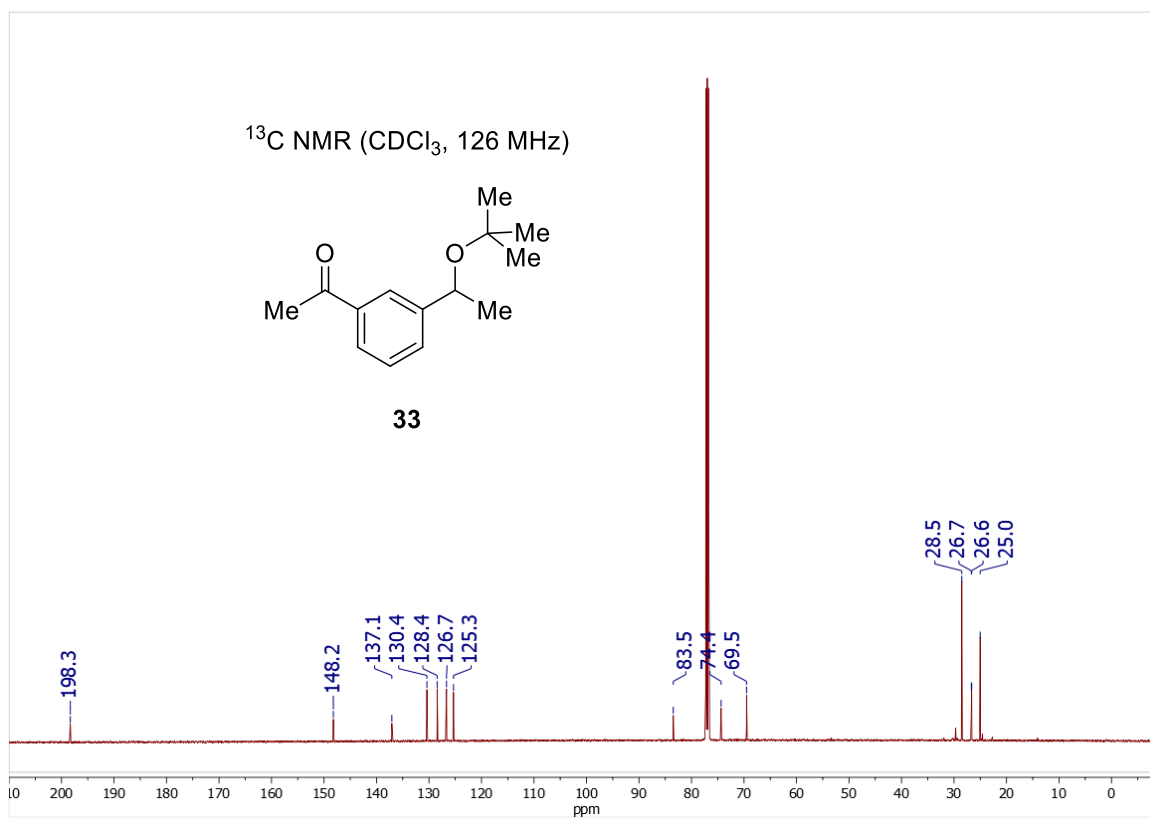


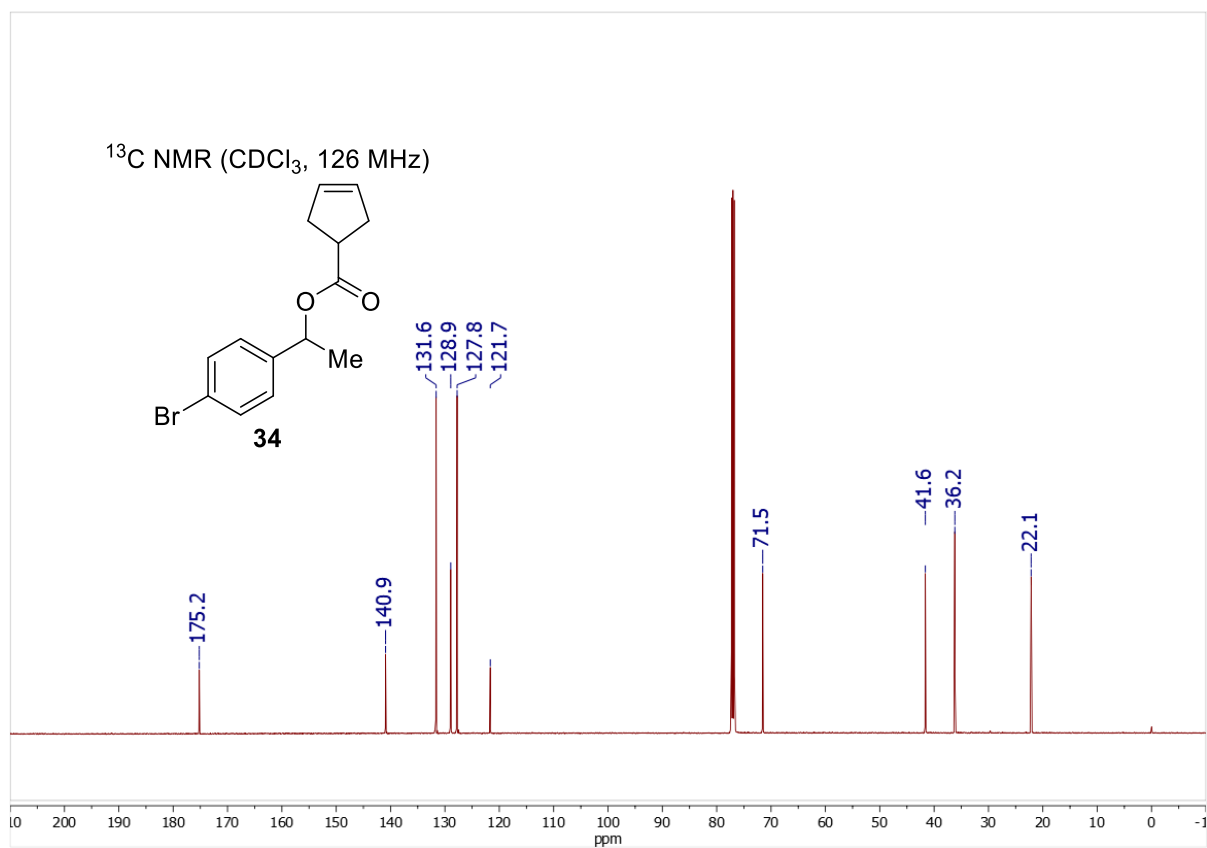
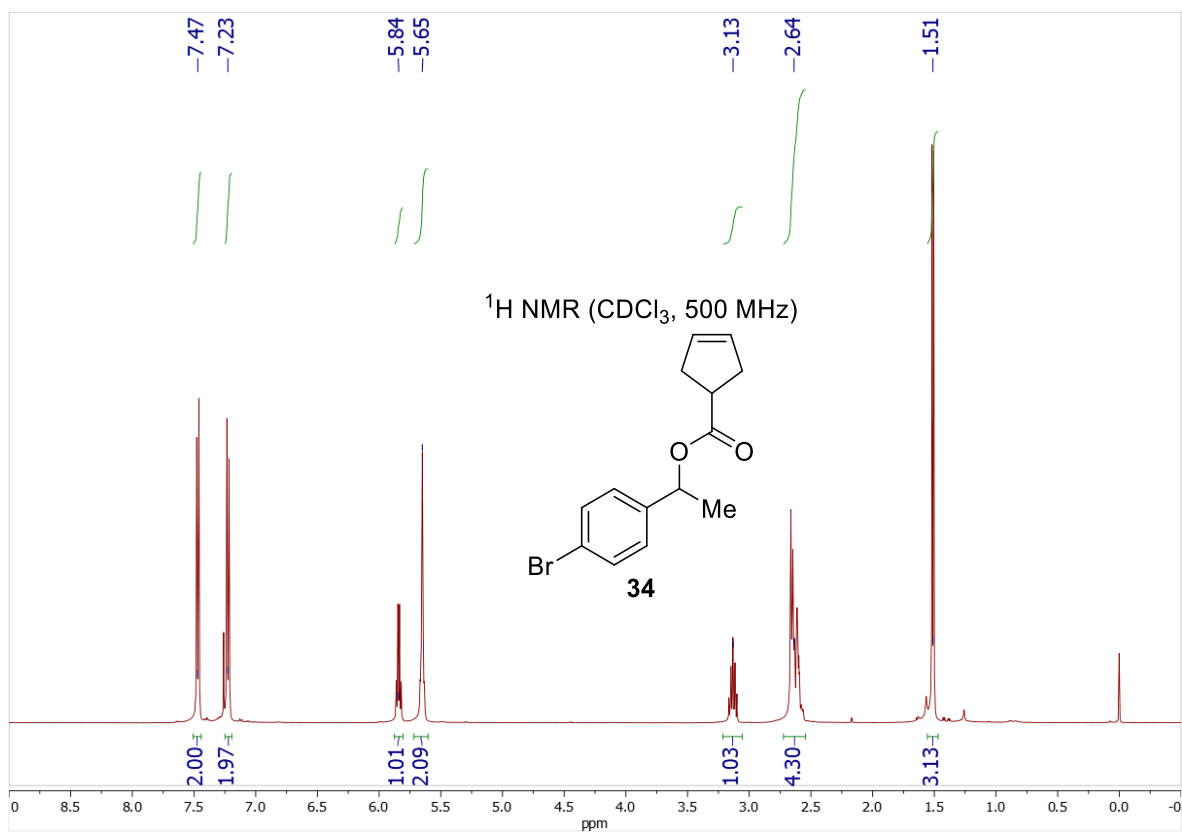
A combination of diastereomers and Boc rotamers make these spectra complex (*tert*-butyl peak above is 3 peaks with 1:1.7:1.4 ratio). Grouped ¹³C peaks below represent the 16 affected carbons (aided with prediction software).

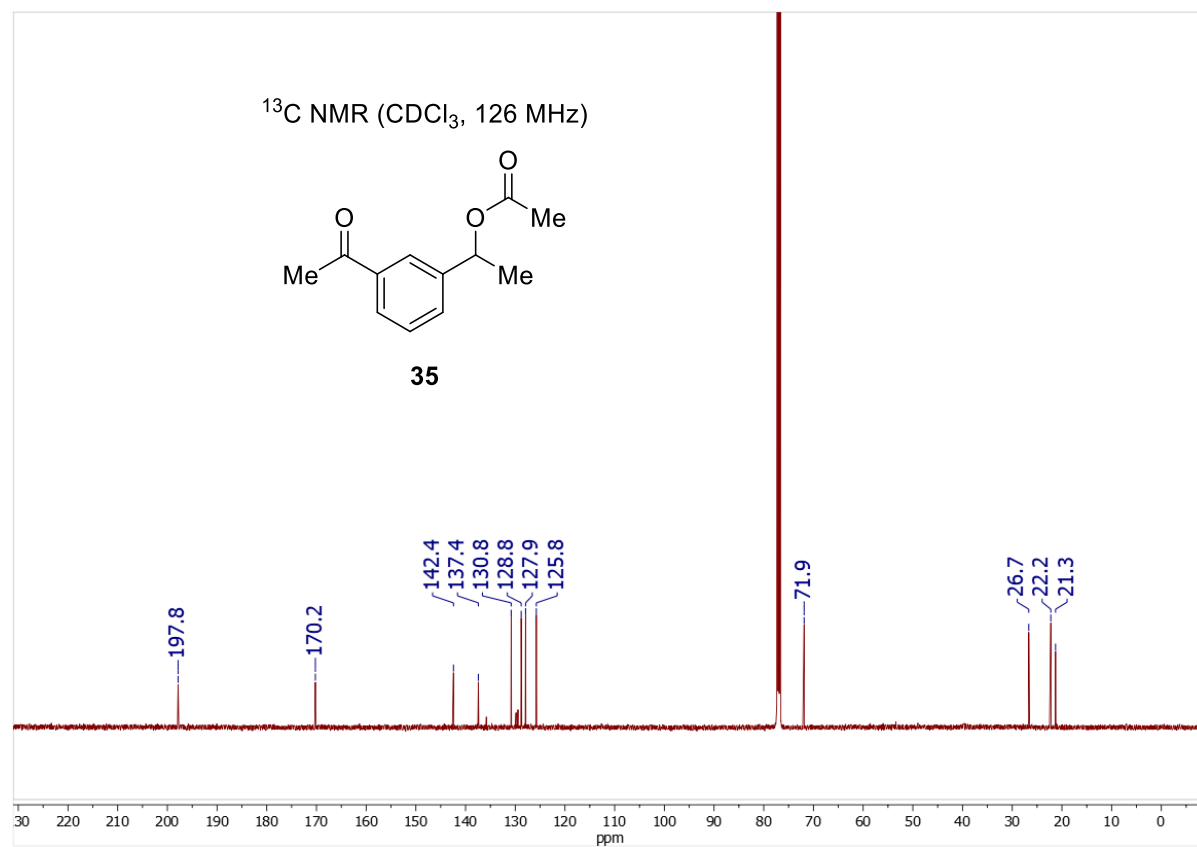
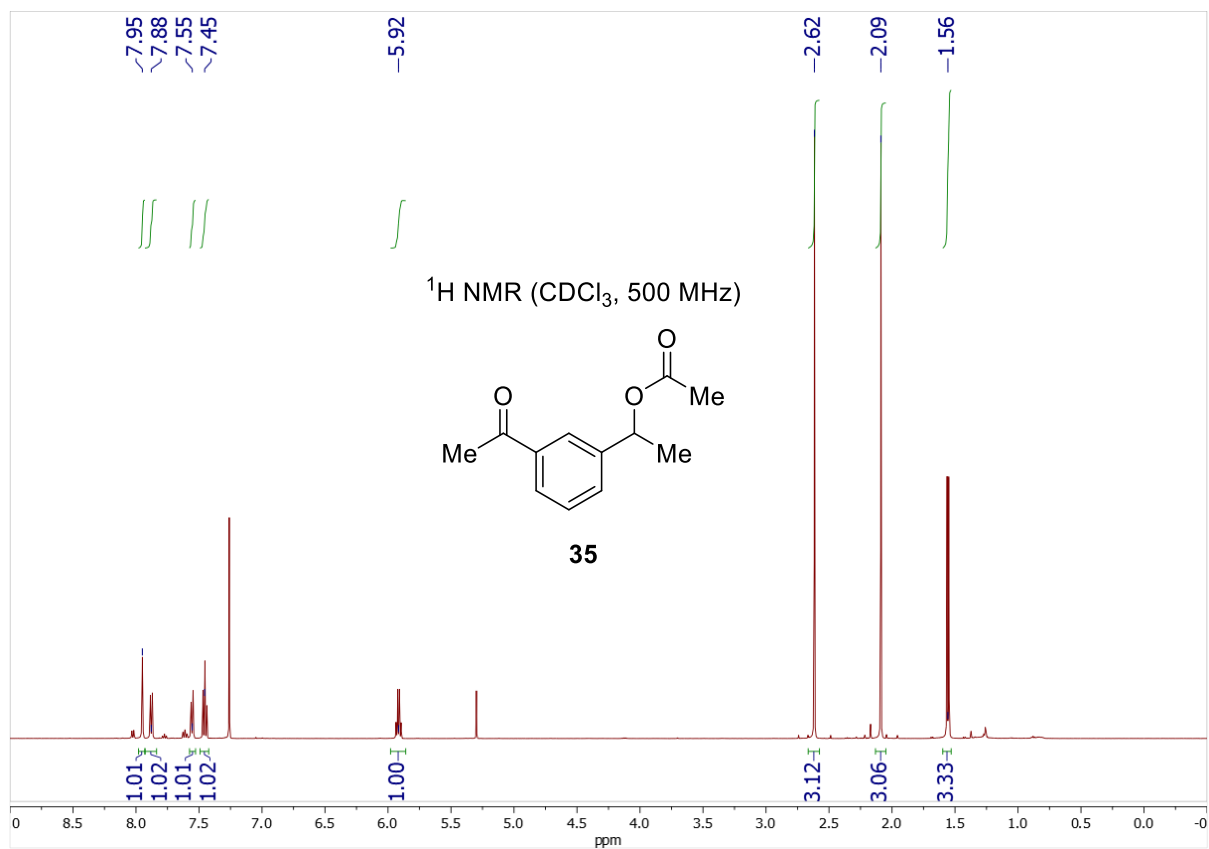


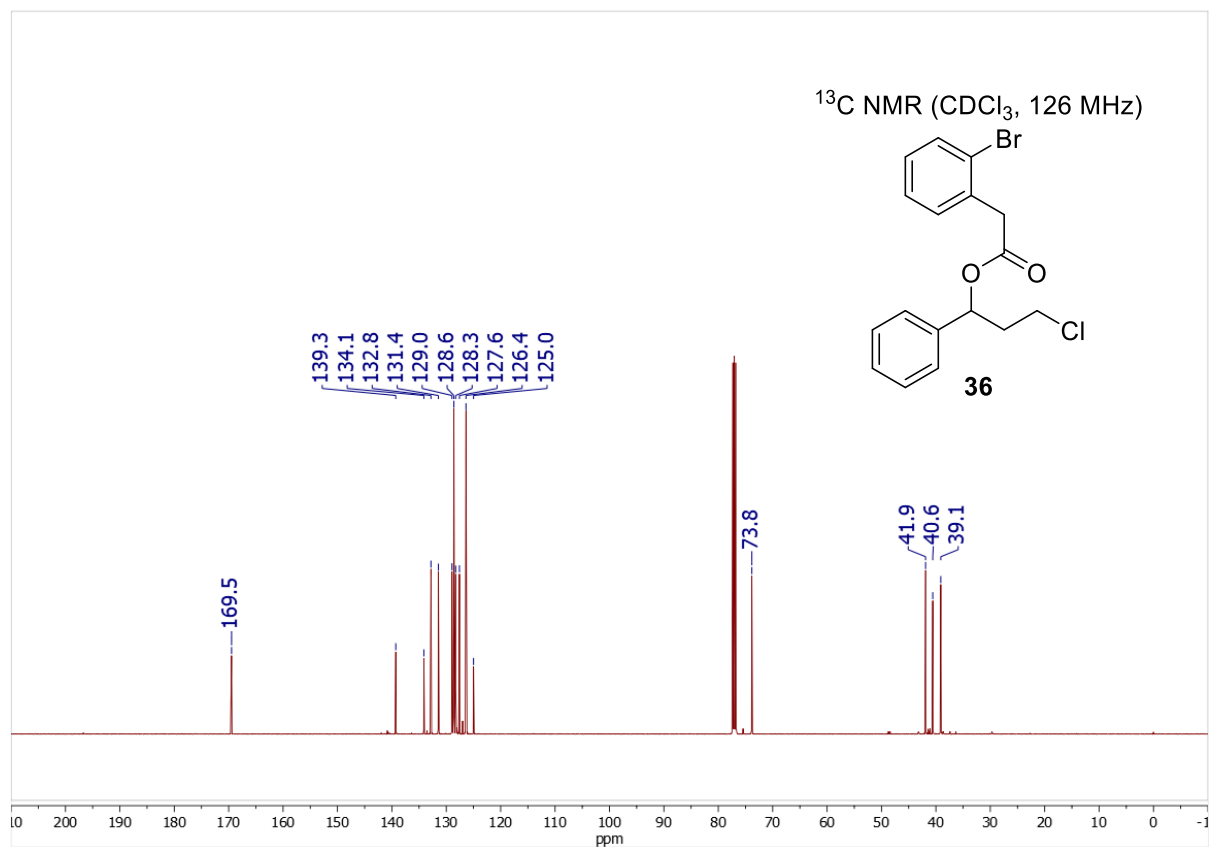
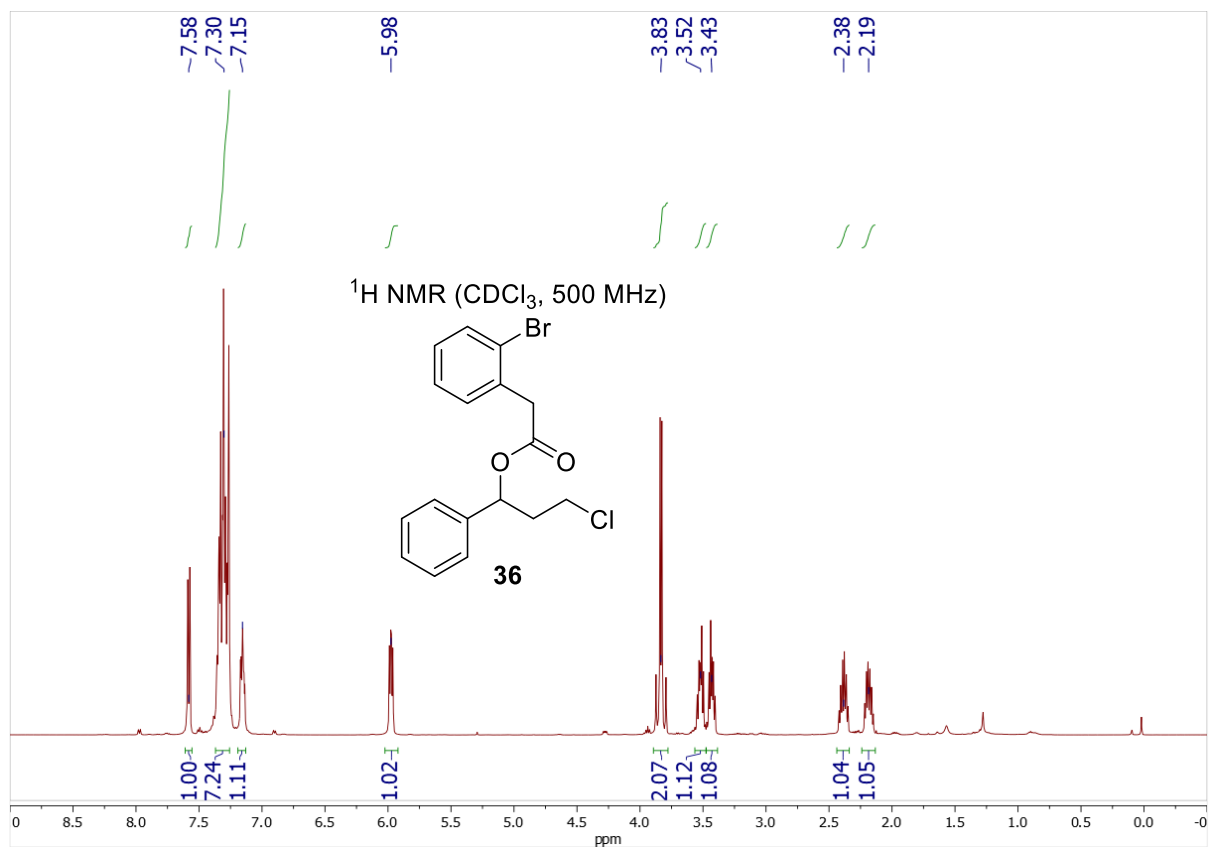


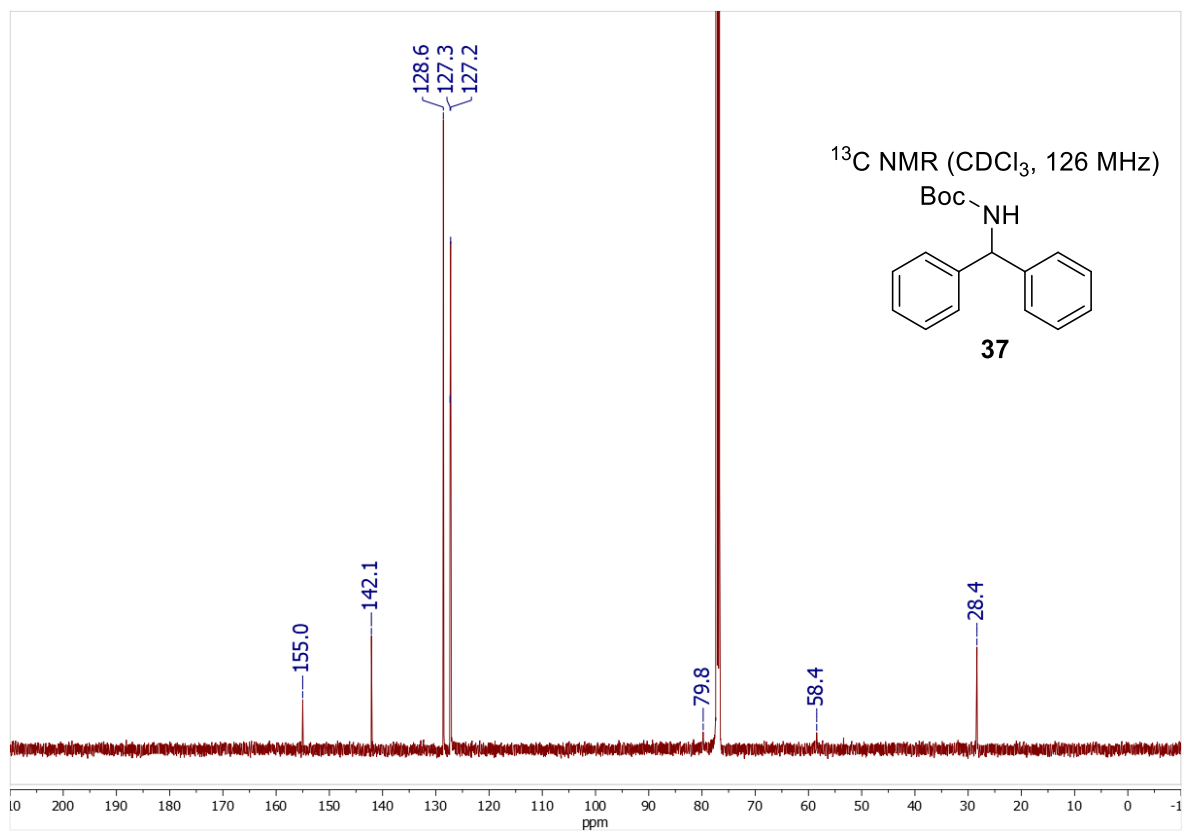
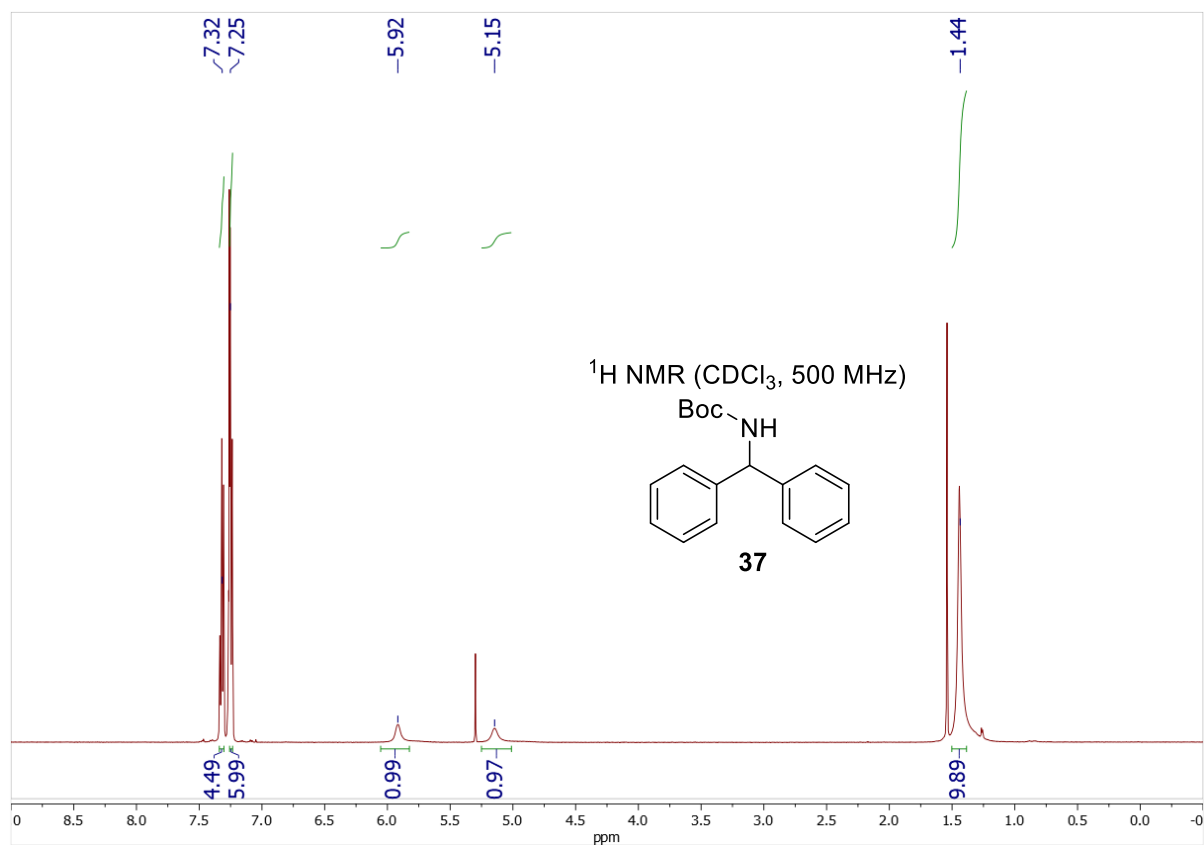
Seems to show a rotamer in the ¹³C spectrum (83.5 vs 74.4 and 26.6 vs 26.7):

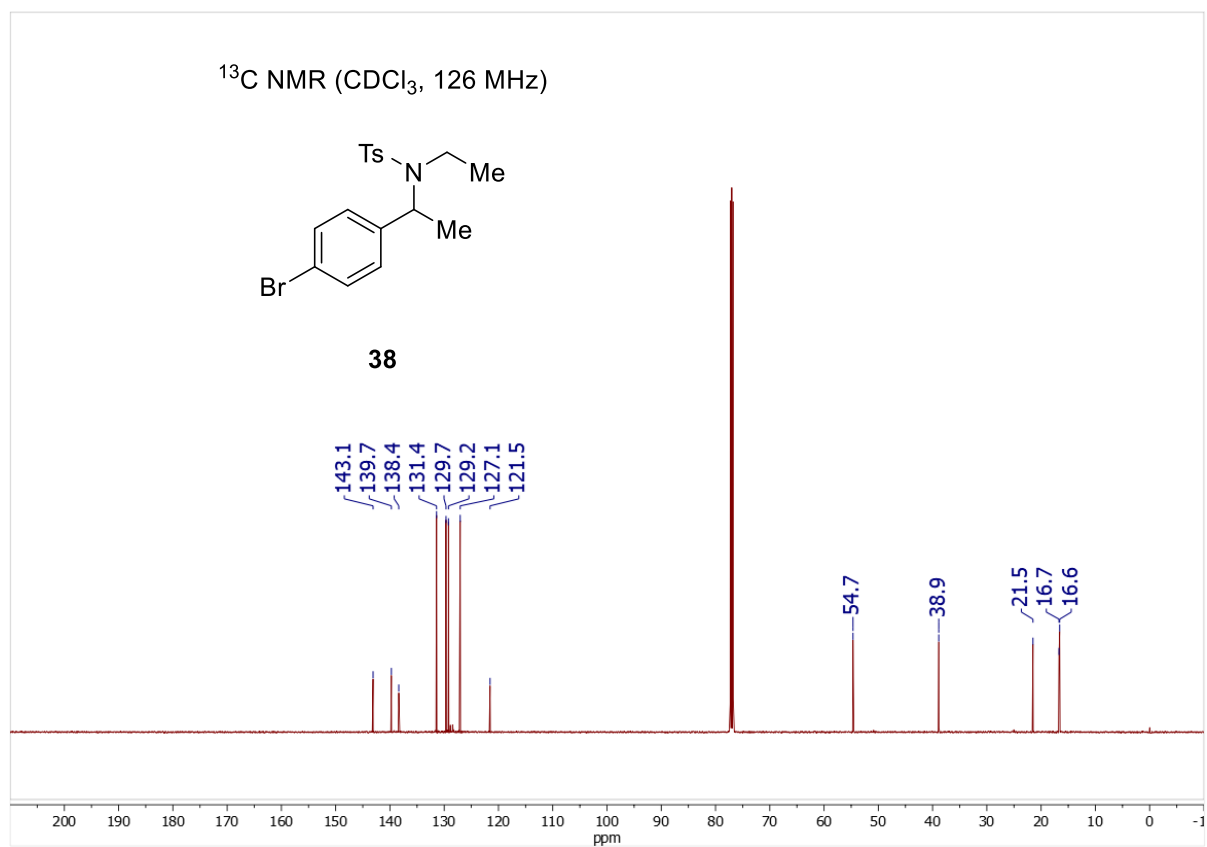
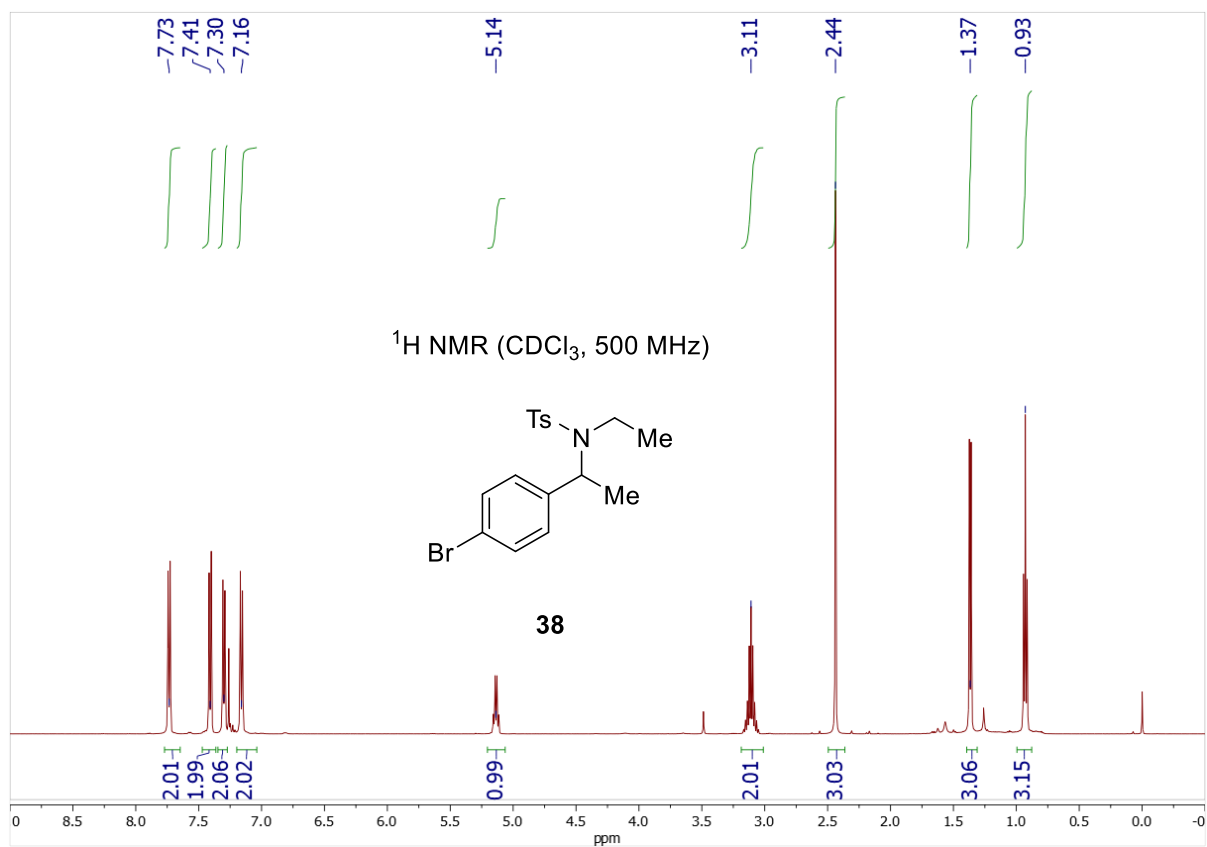


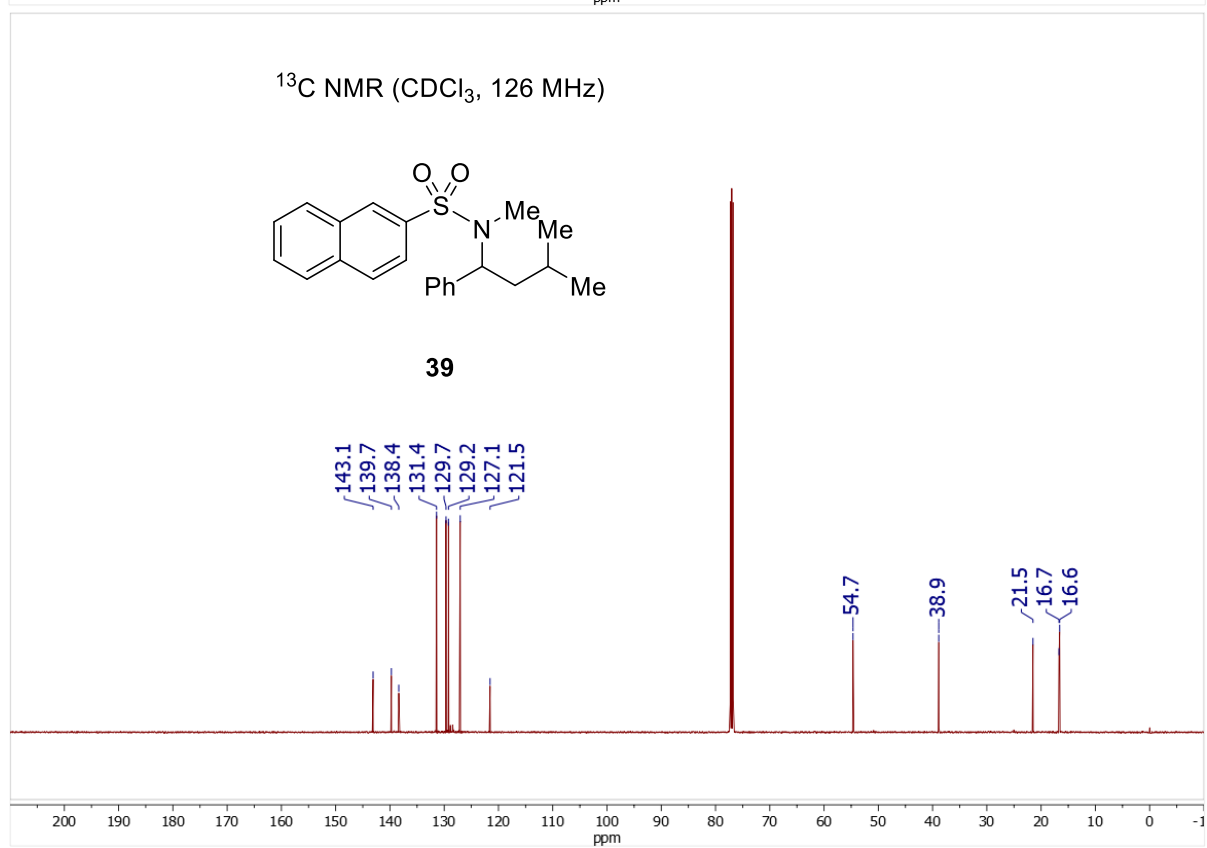
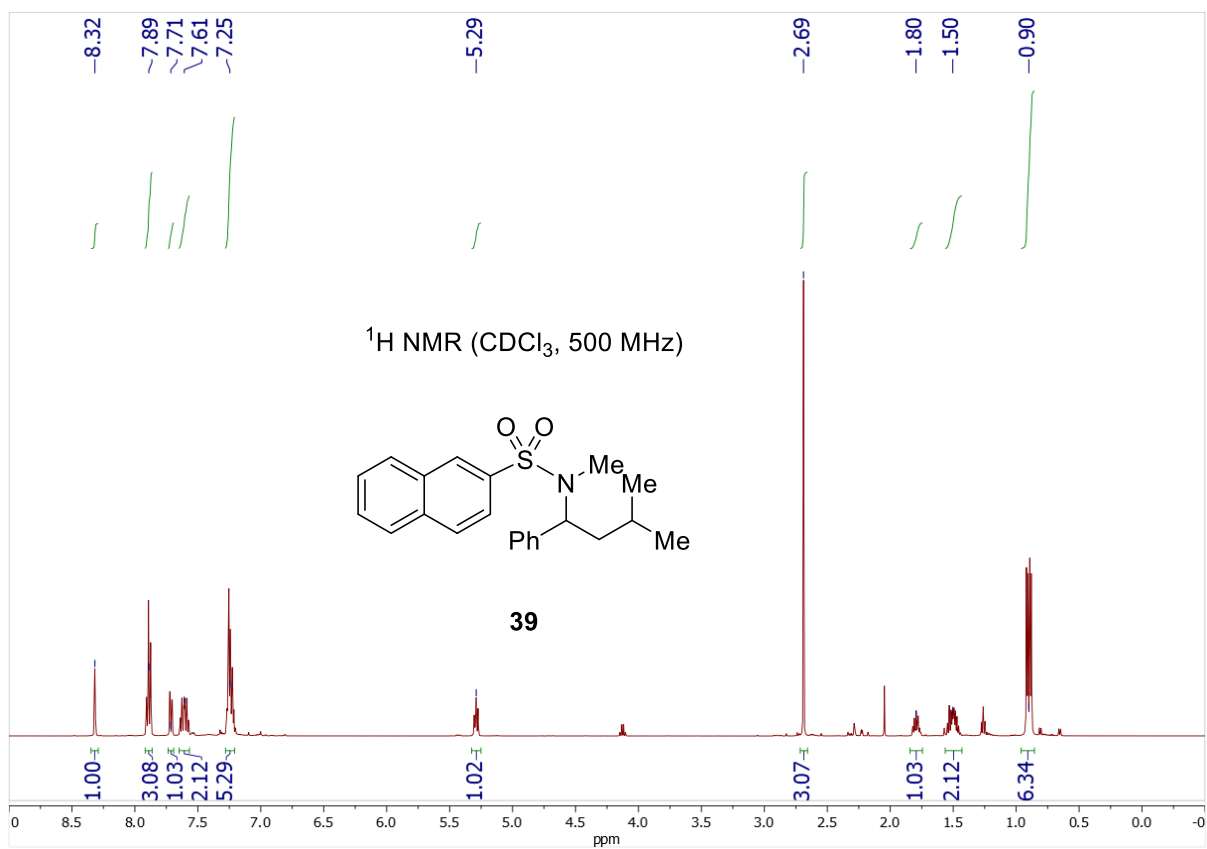


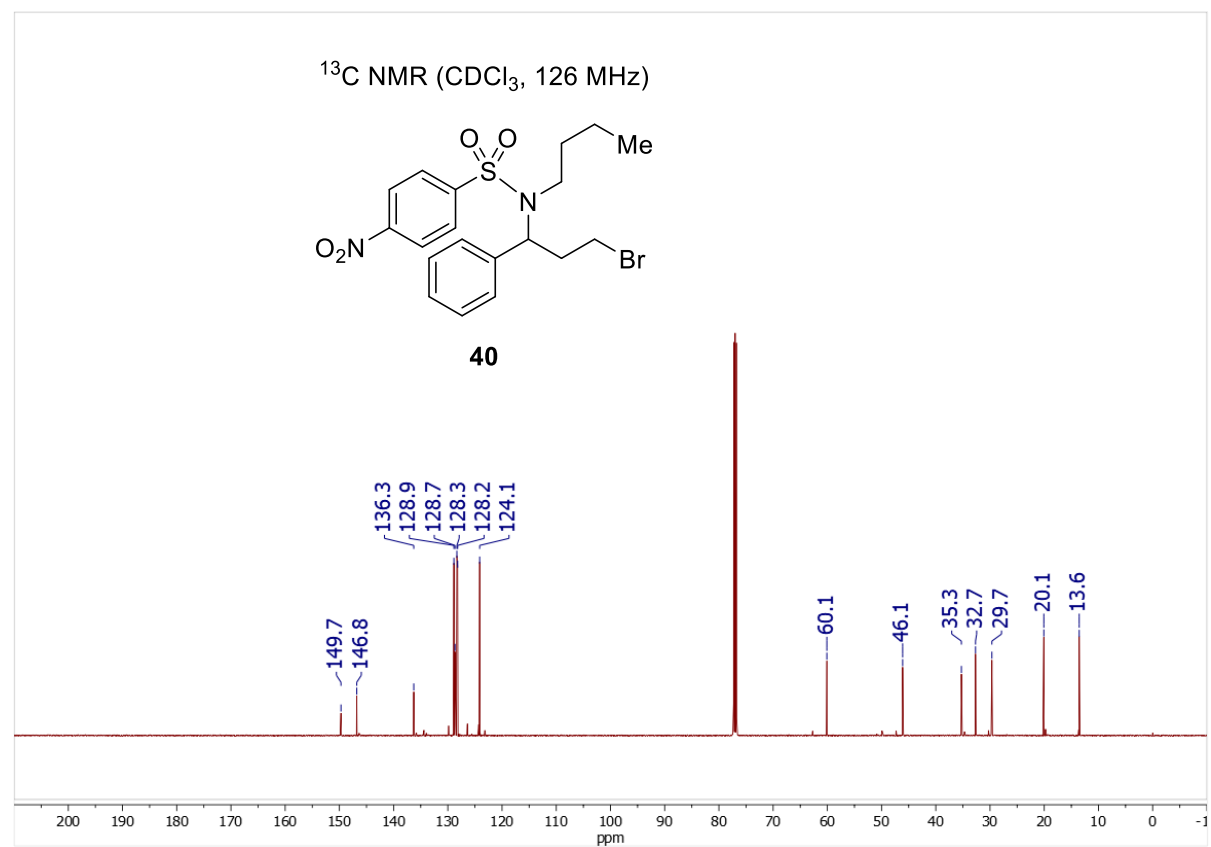
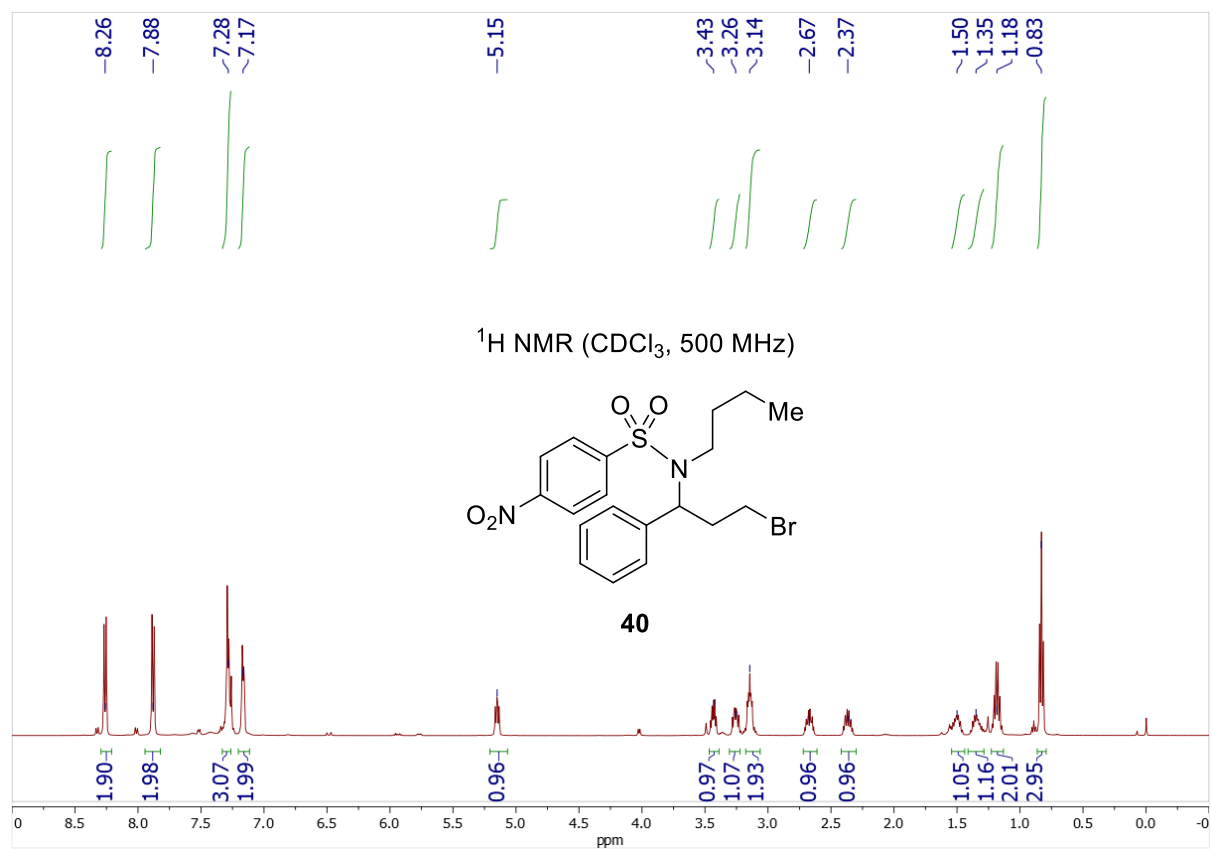


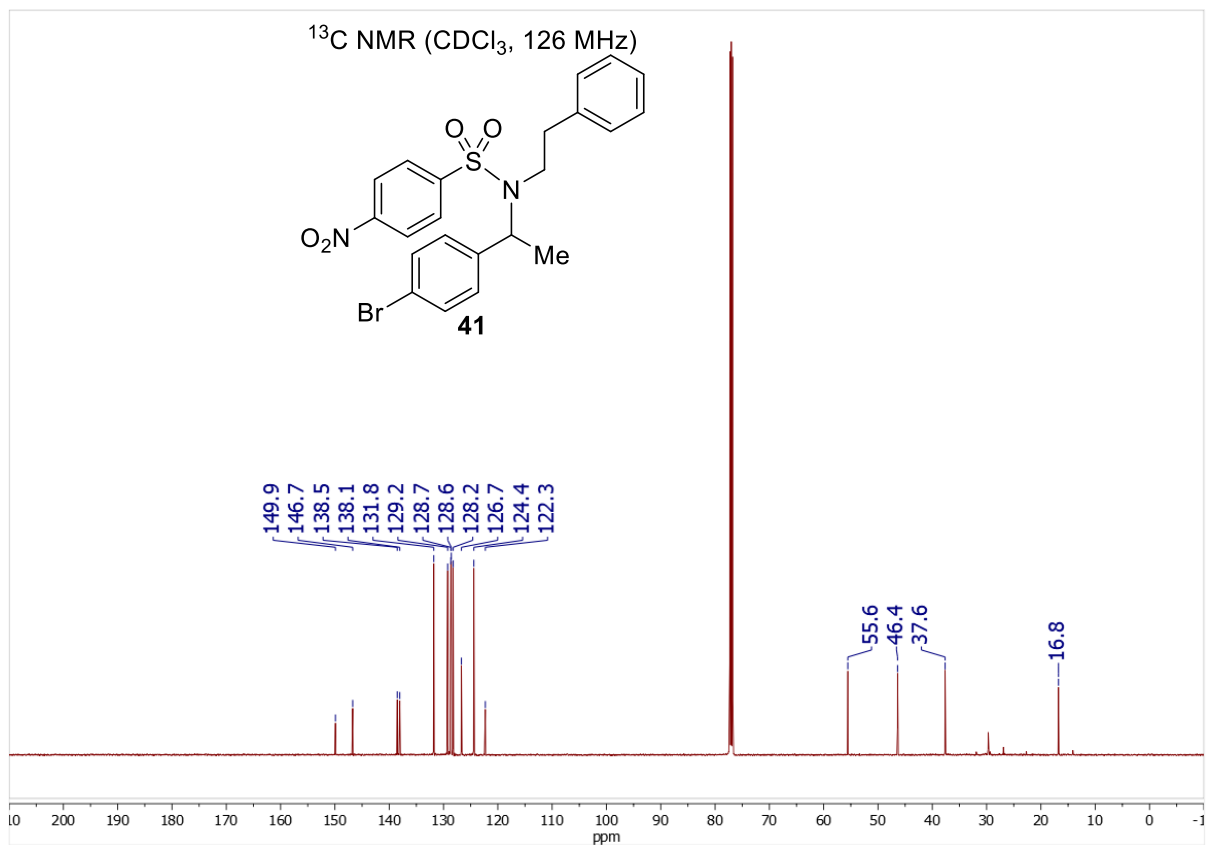
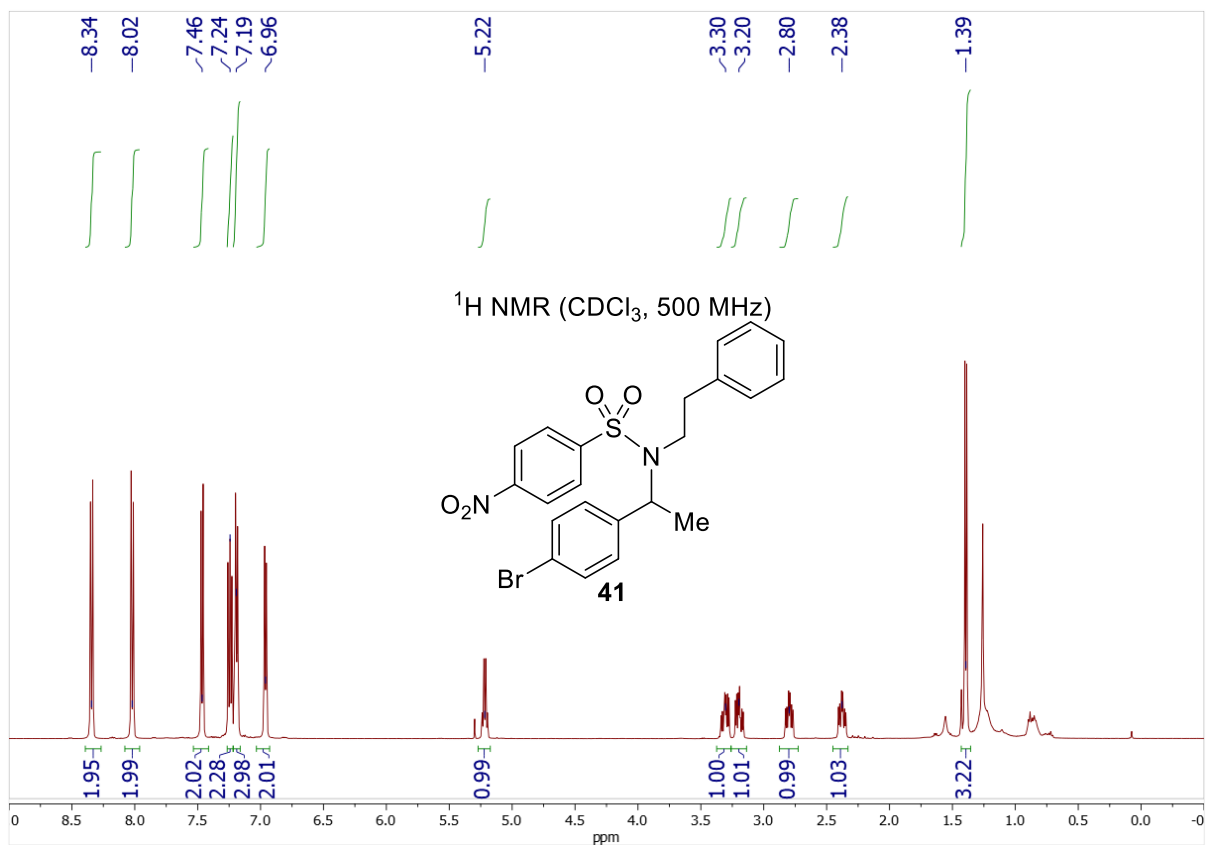


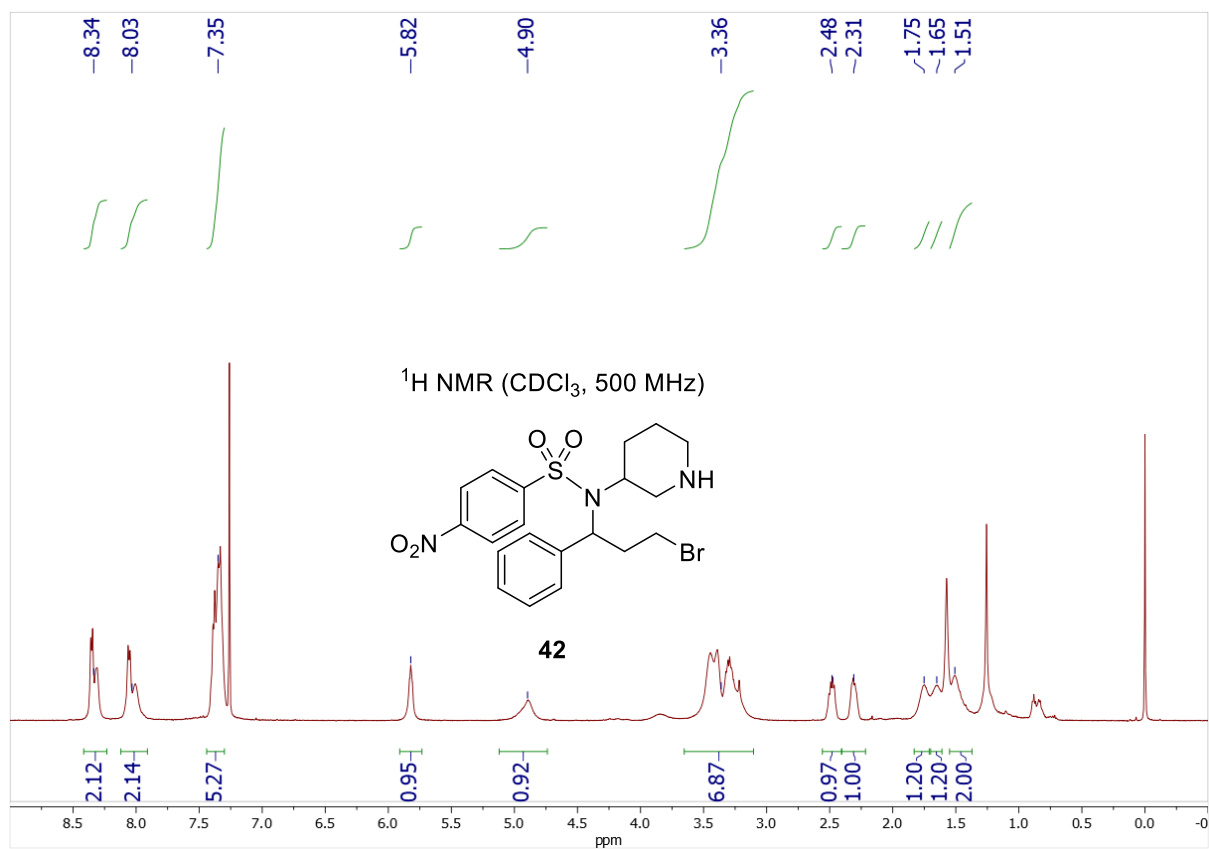




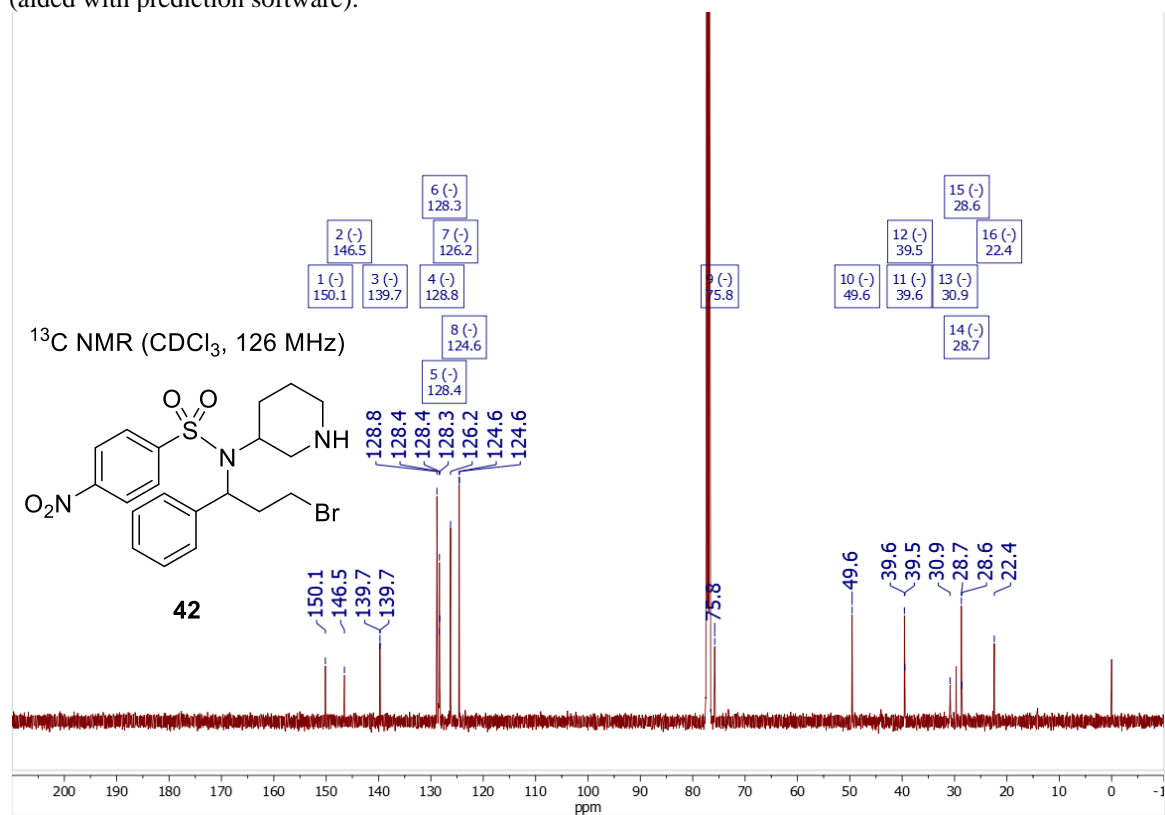


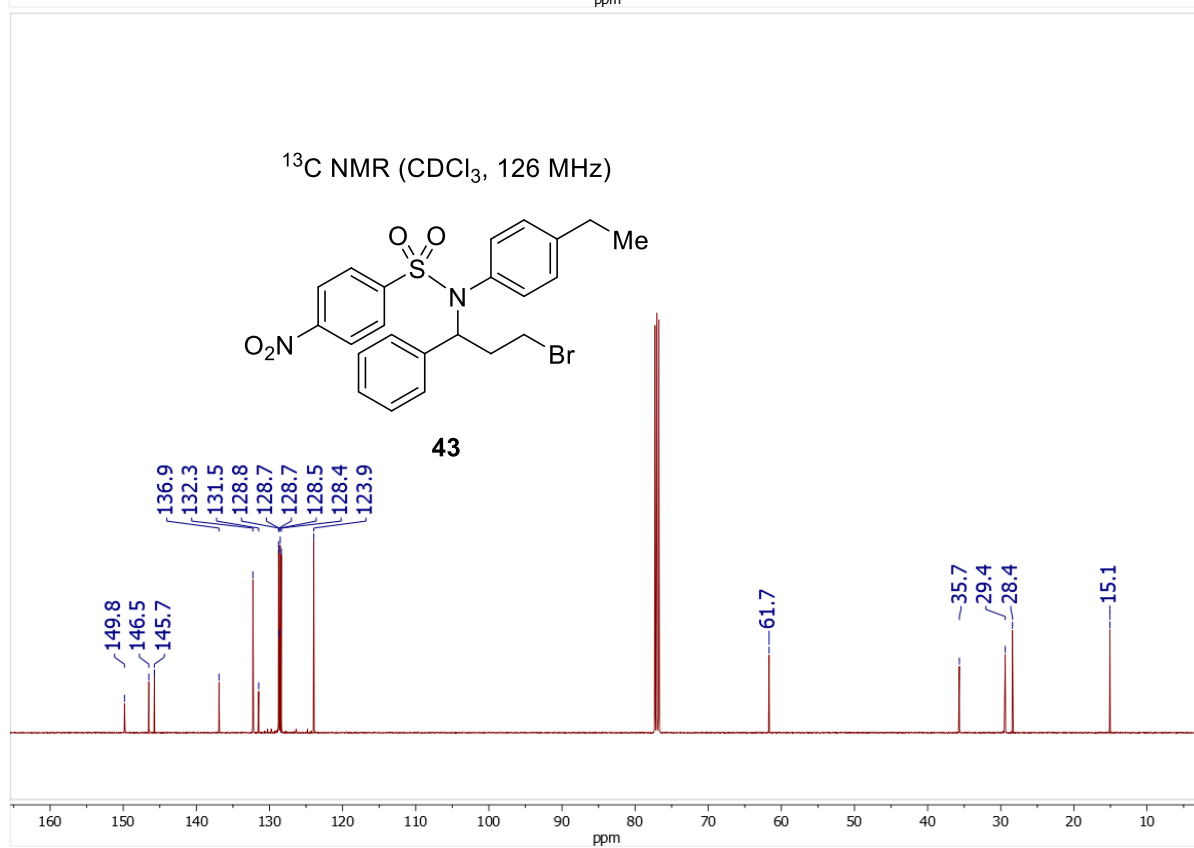
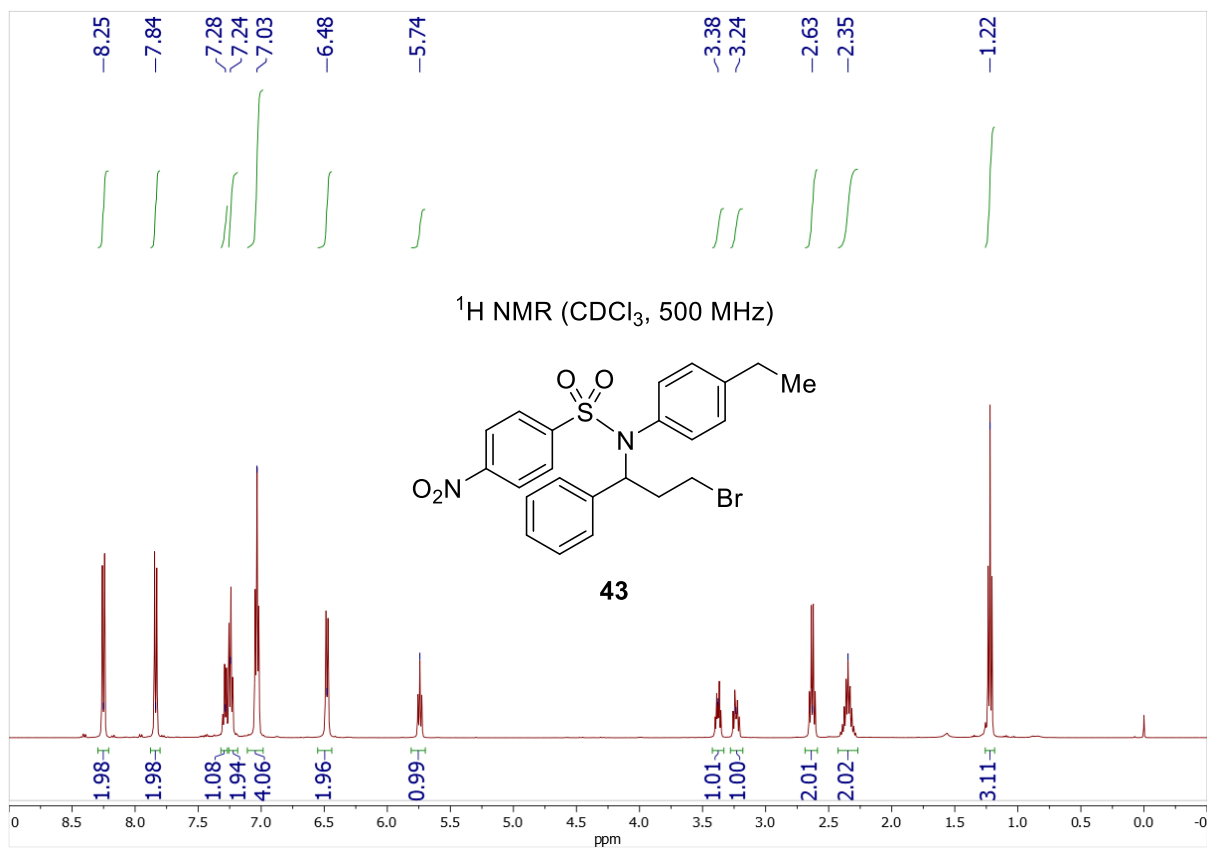


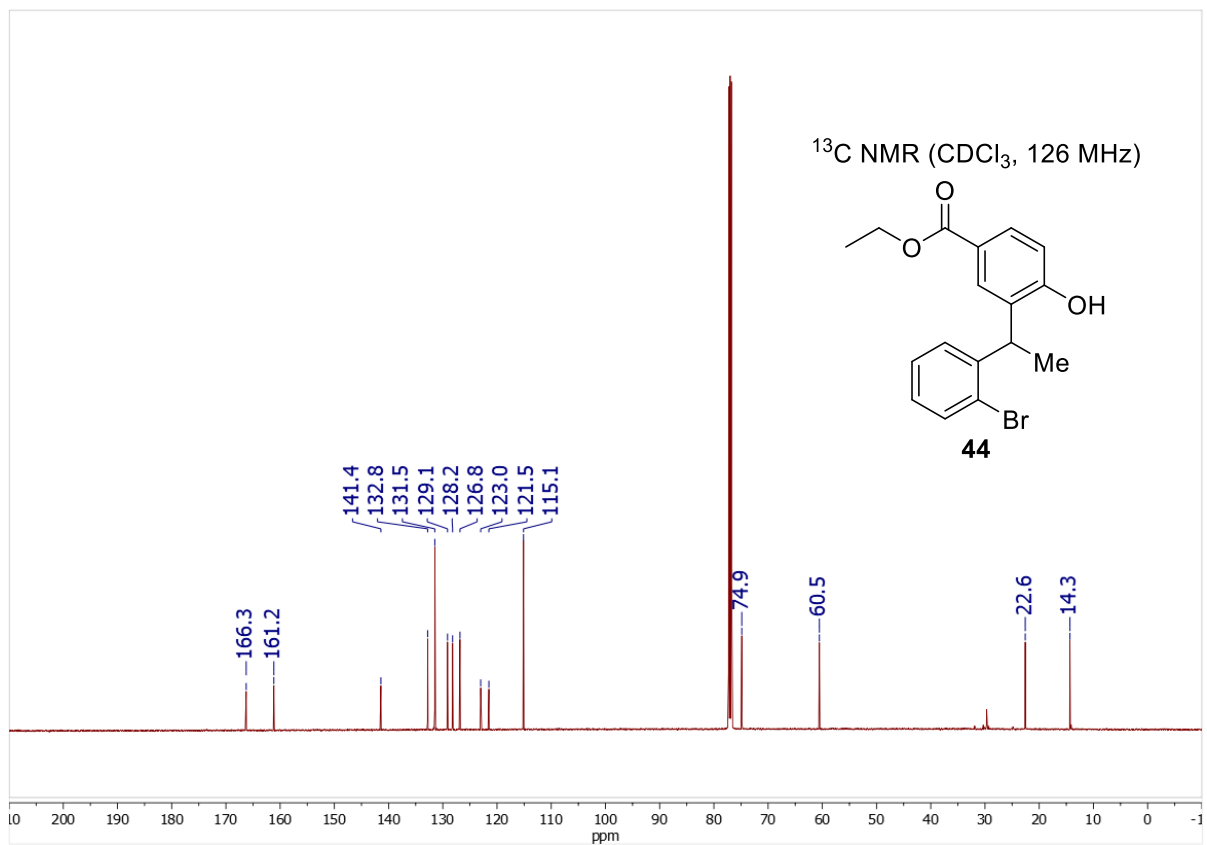
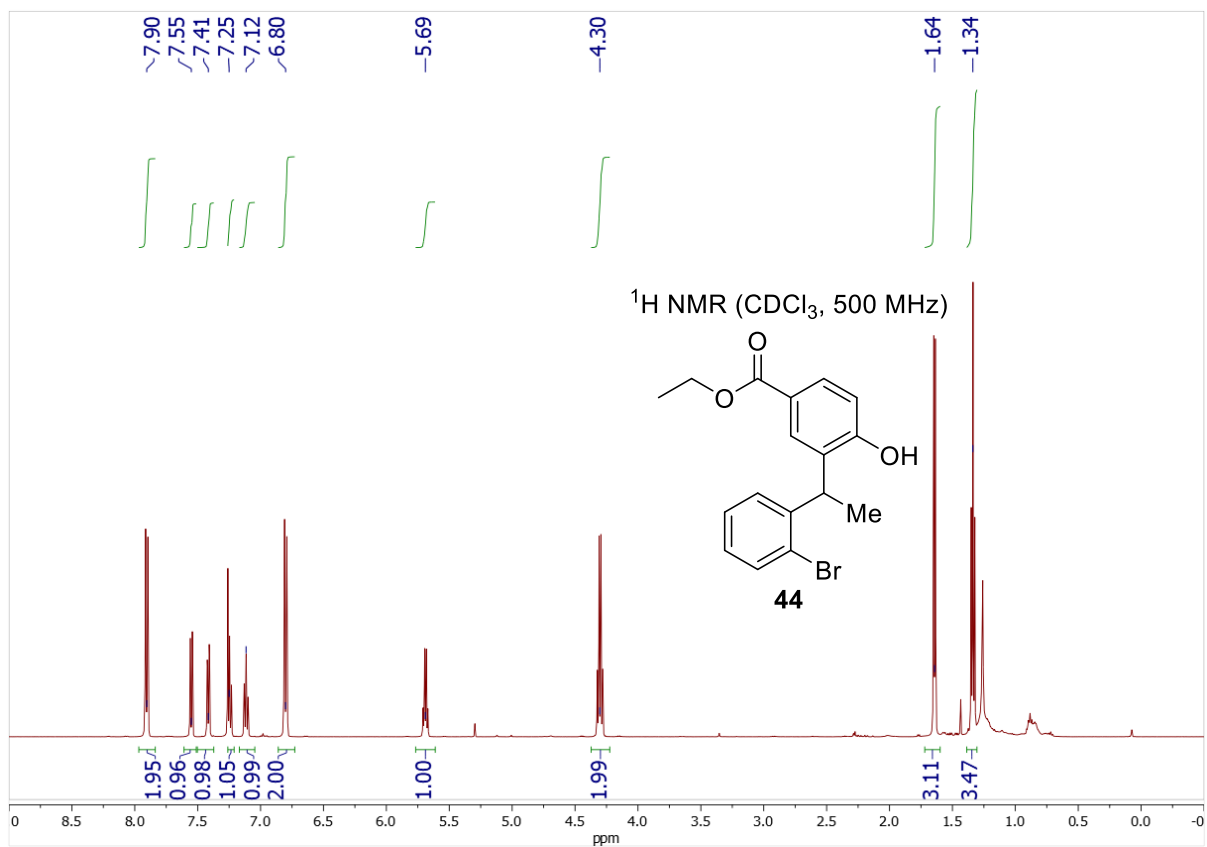


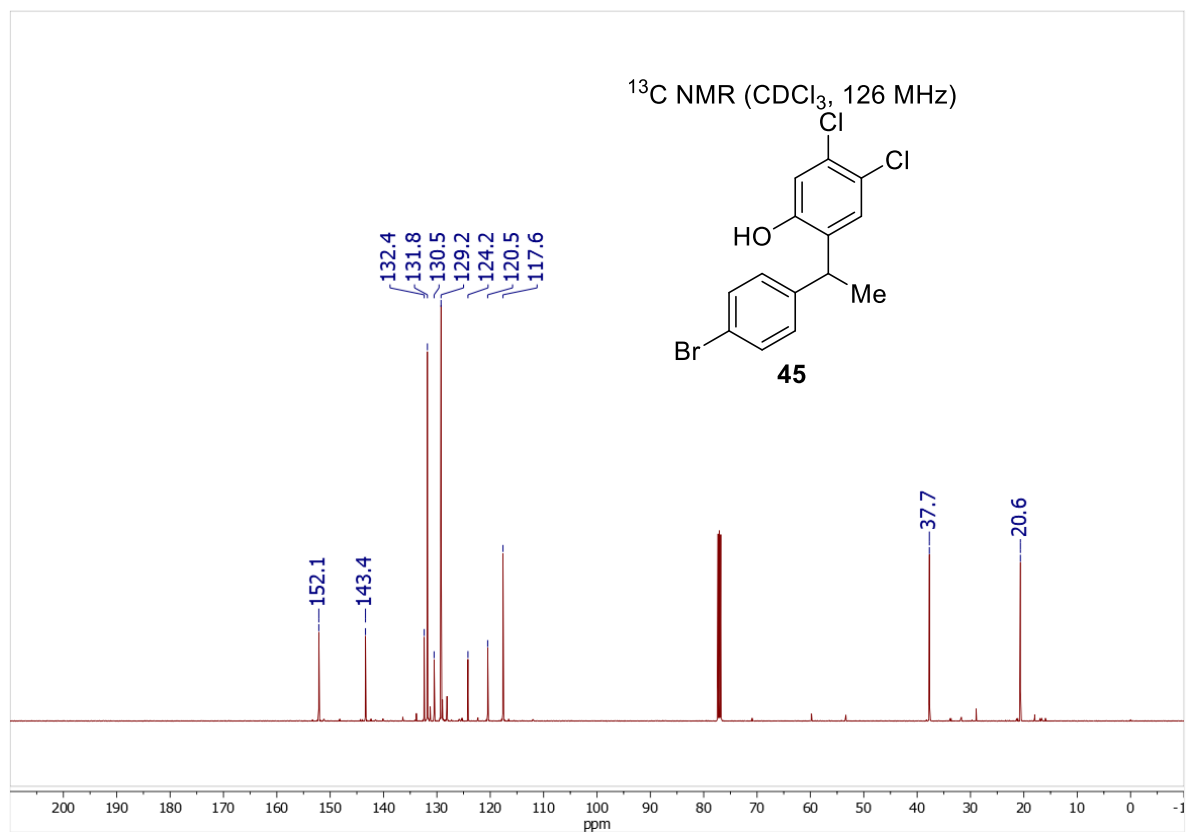
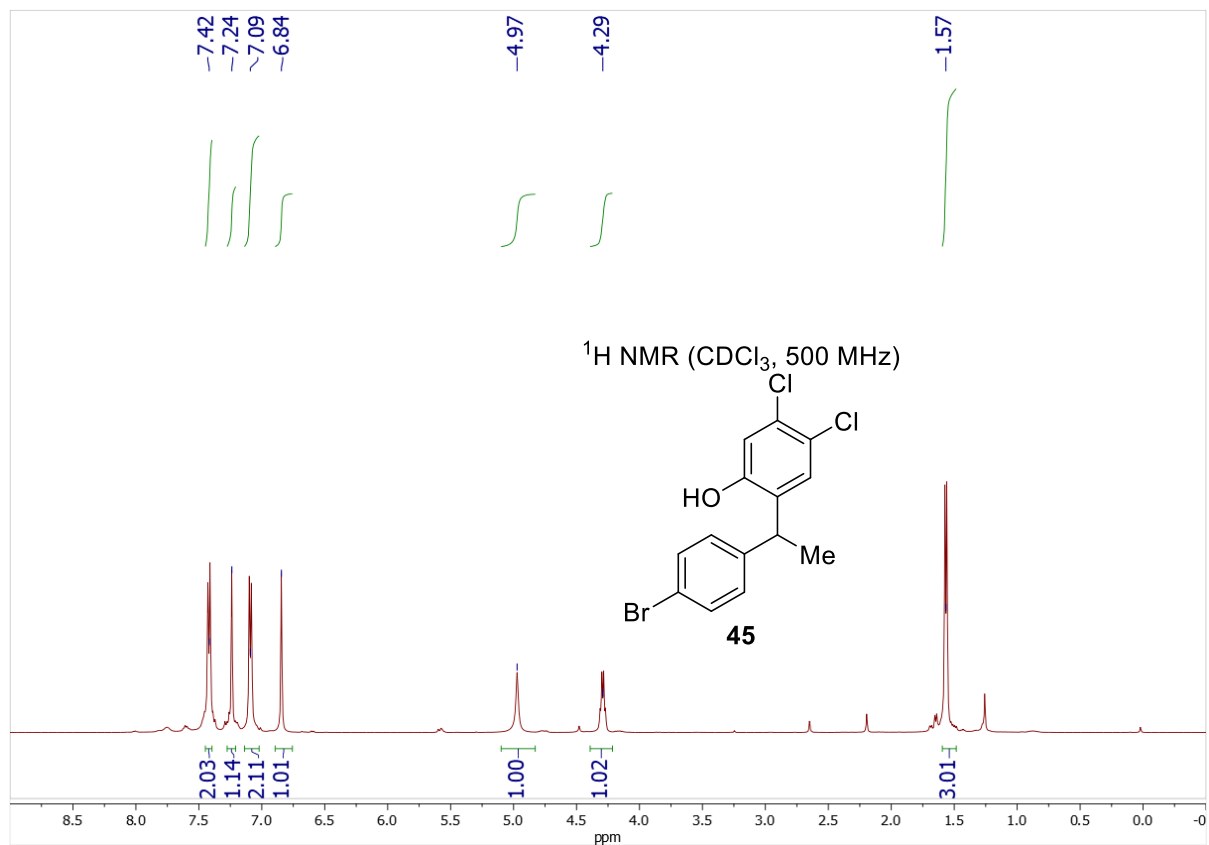


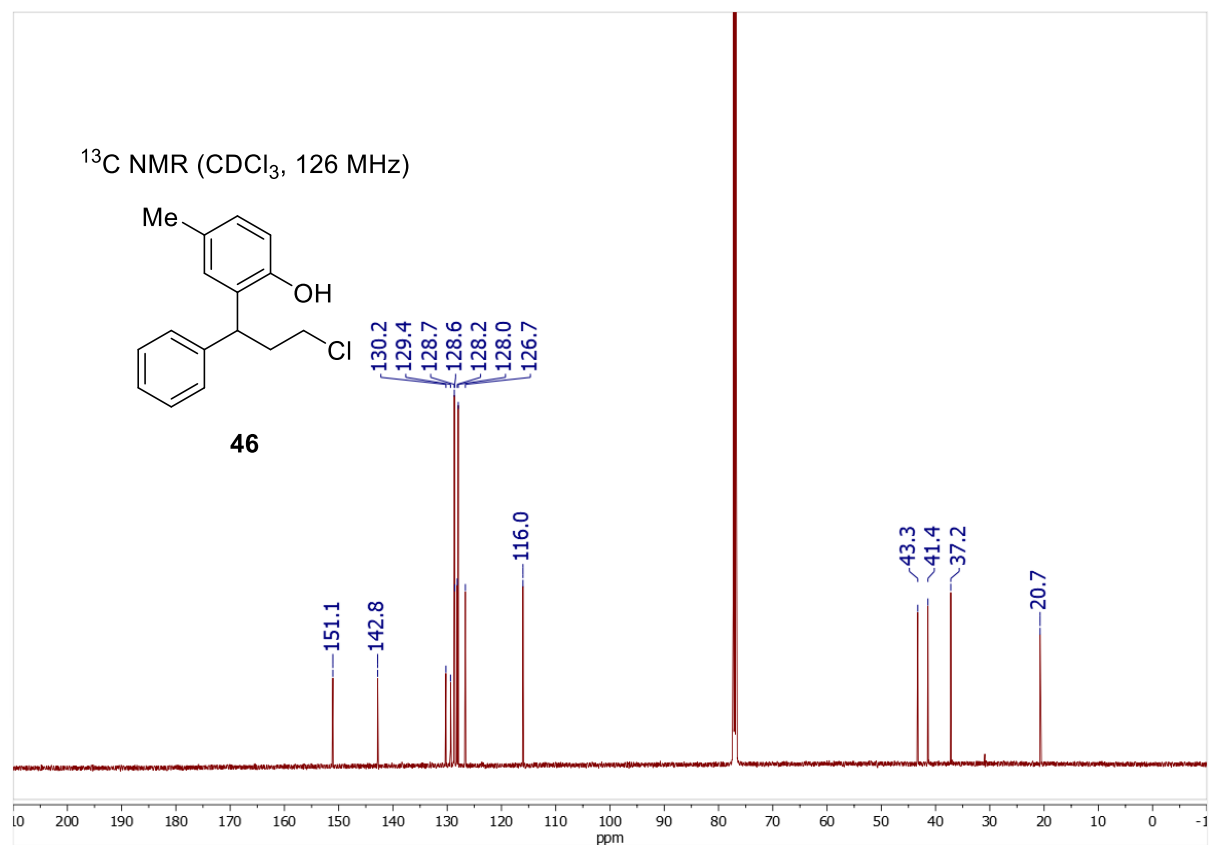
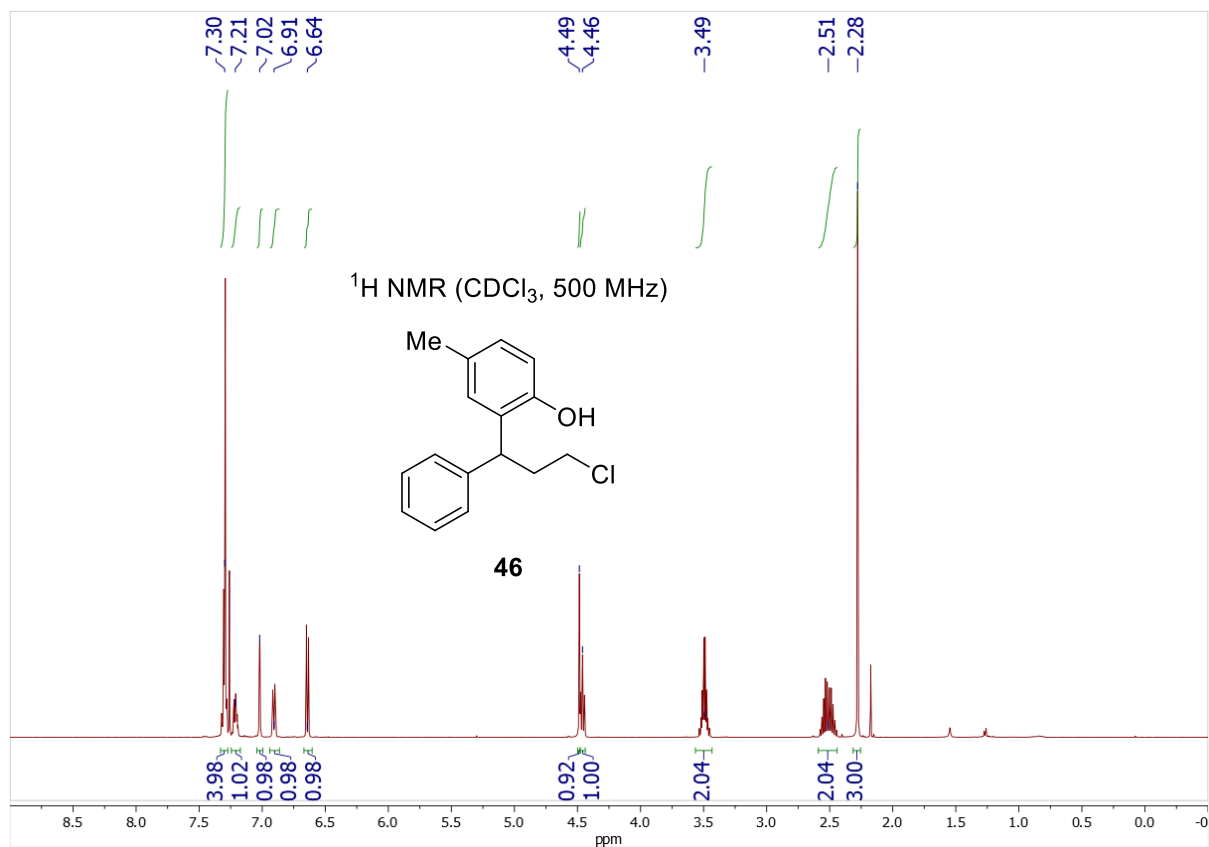
Diastereomers make these spectra complex. Diastereomeric ¹³C peaks are grouped below within the numbered boxes (aided with prediction software).

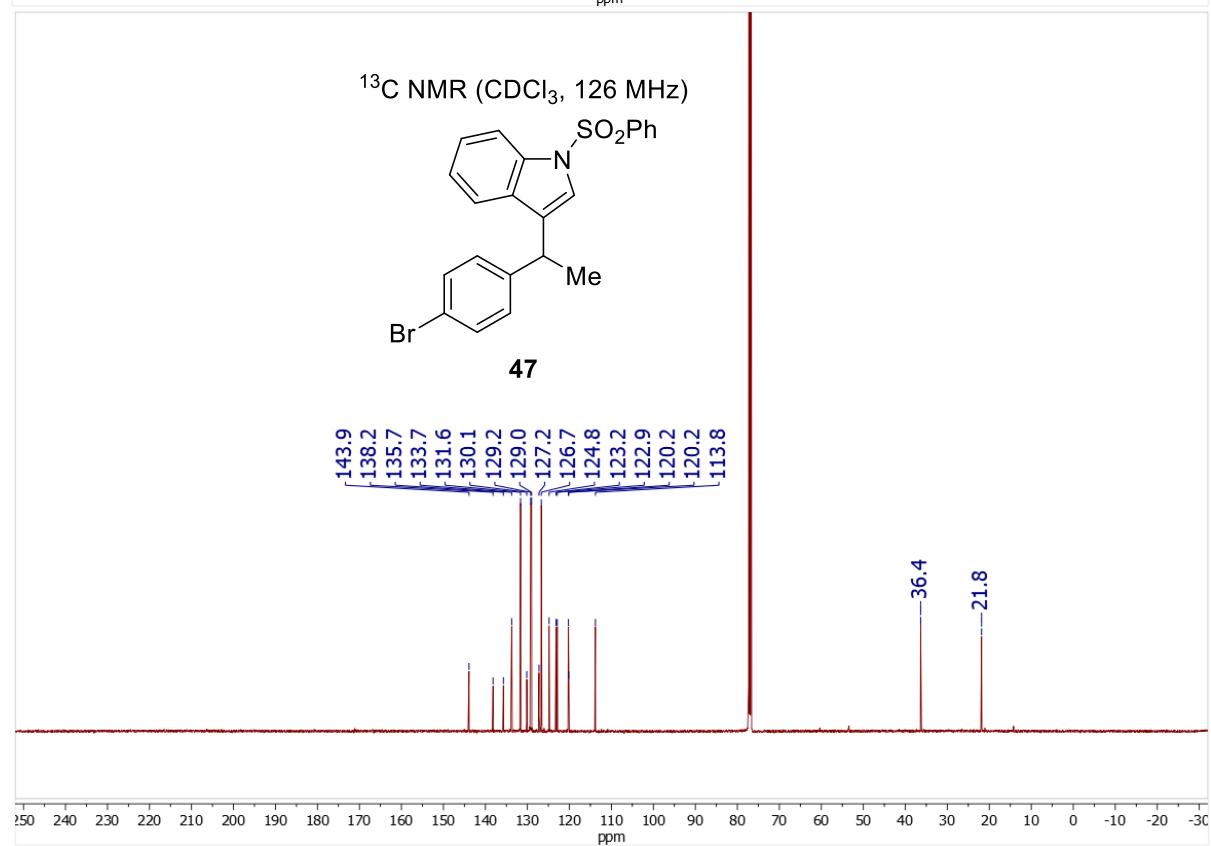
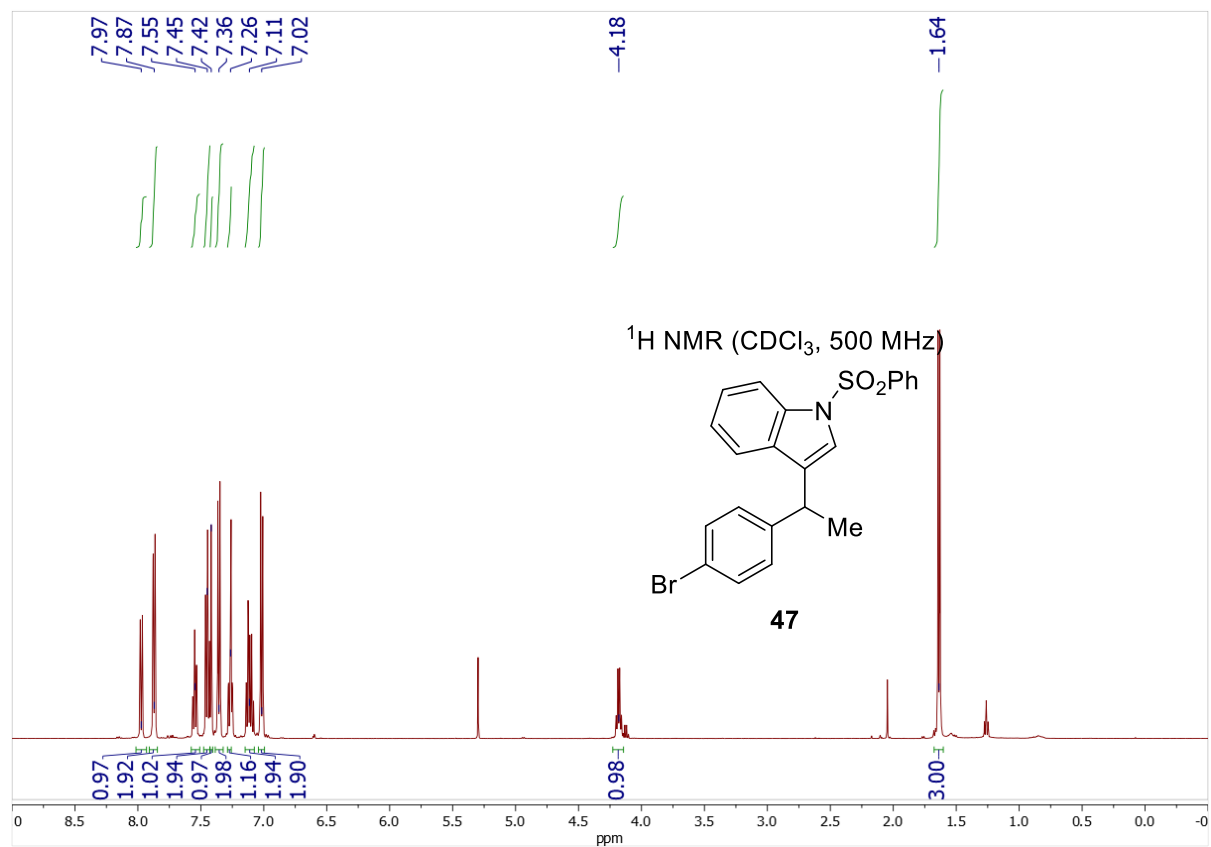


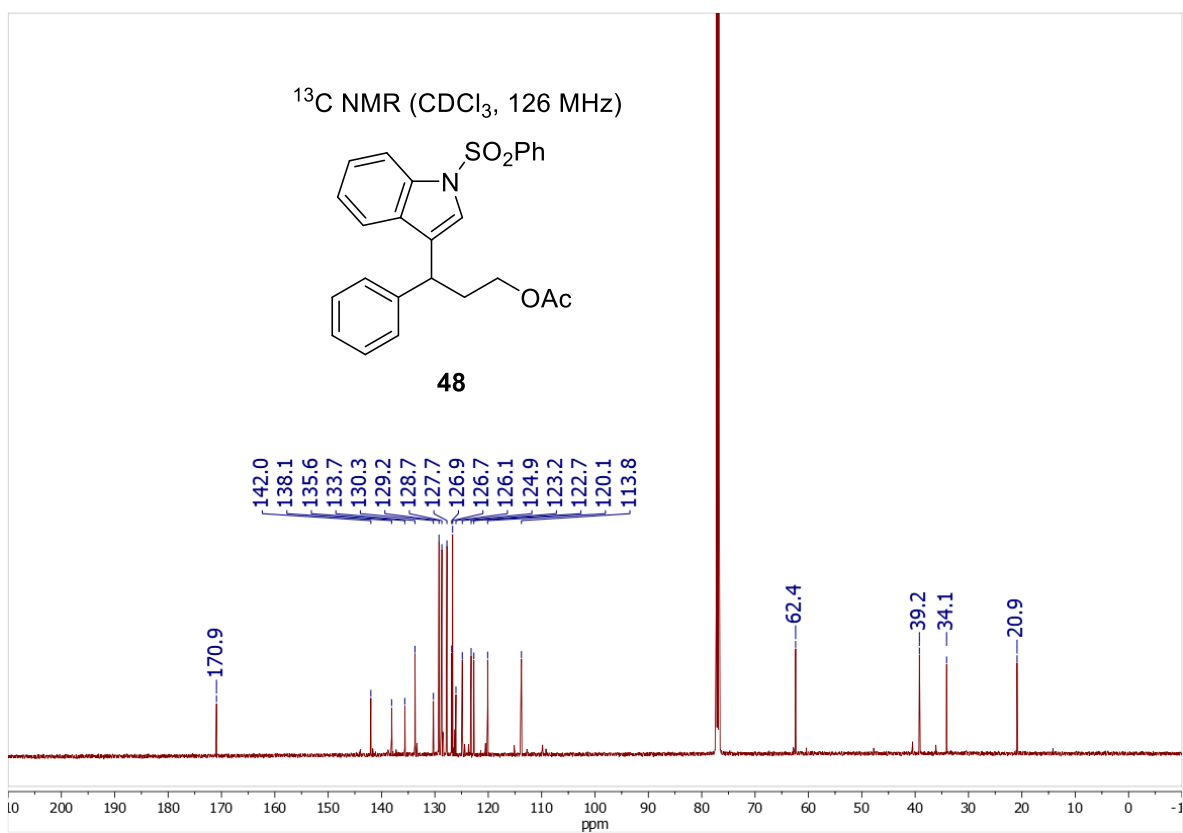
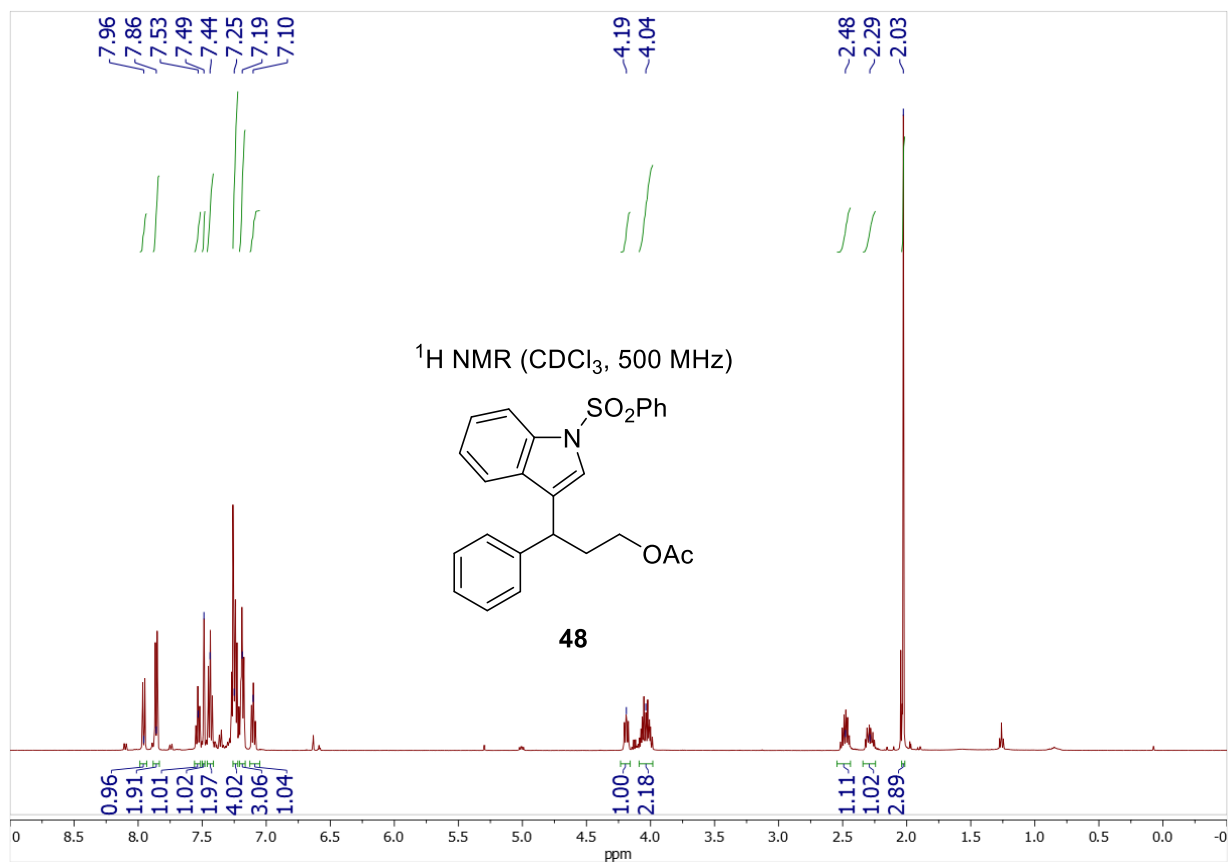


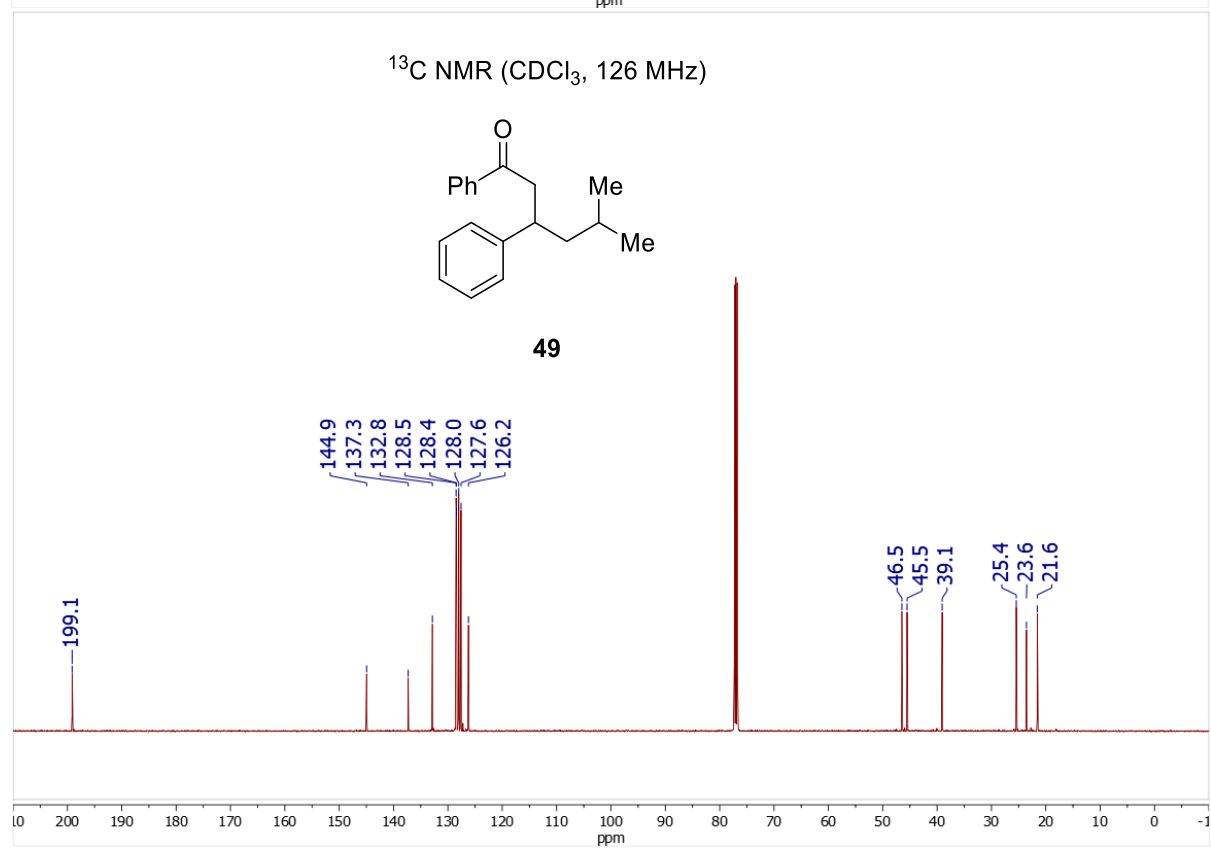
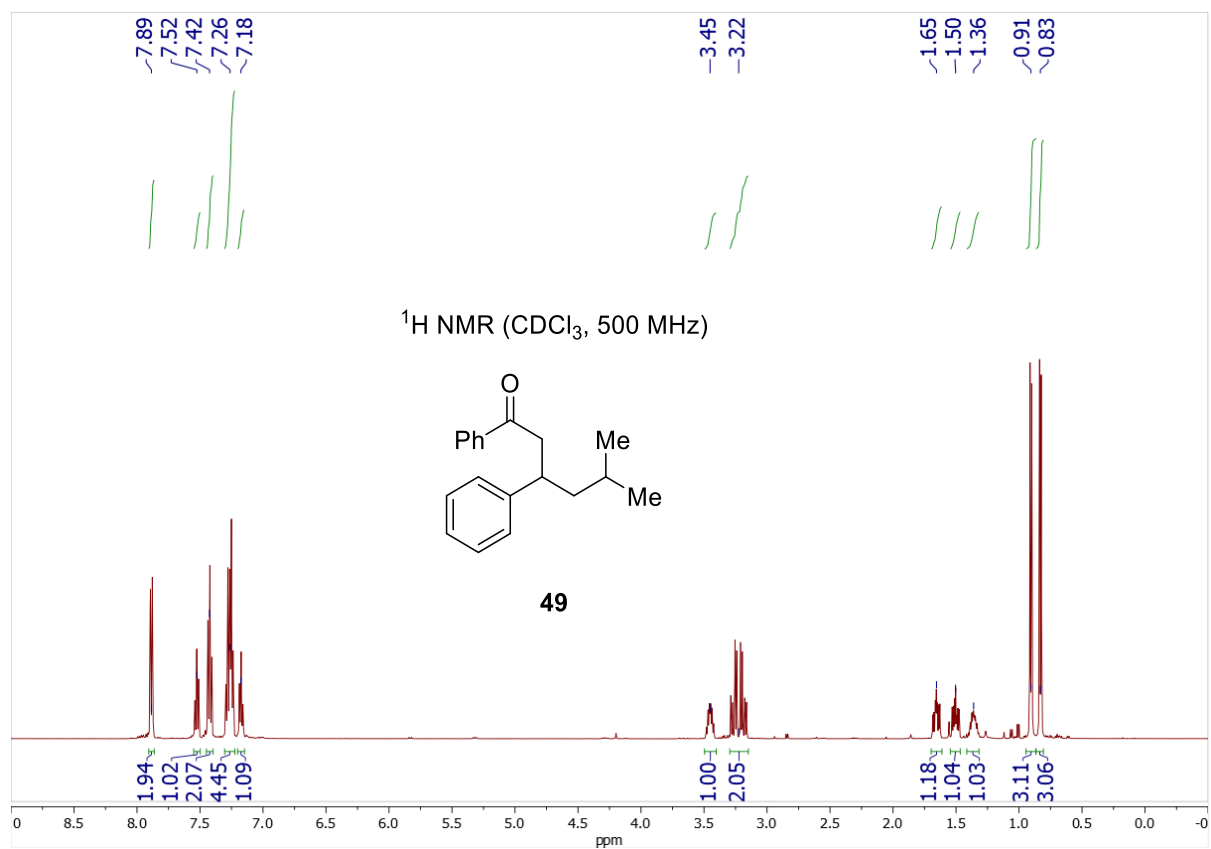


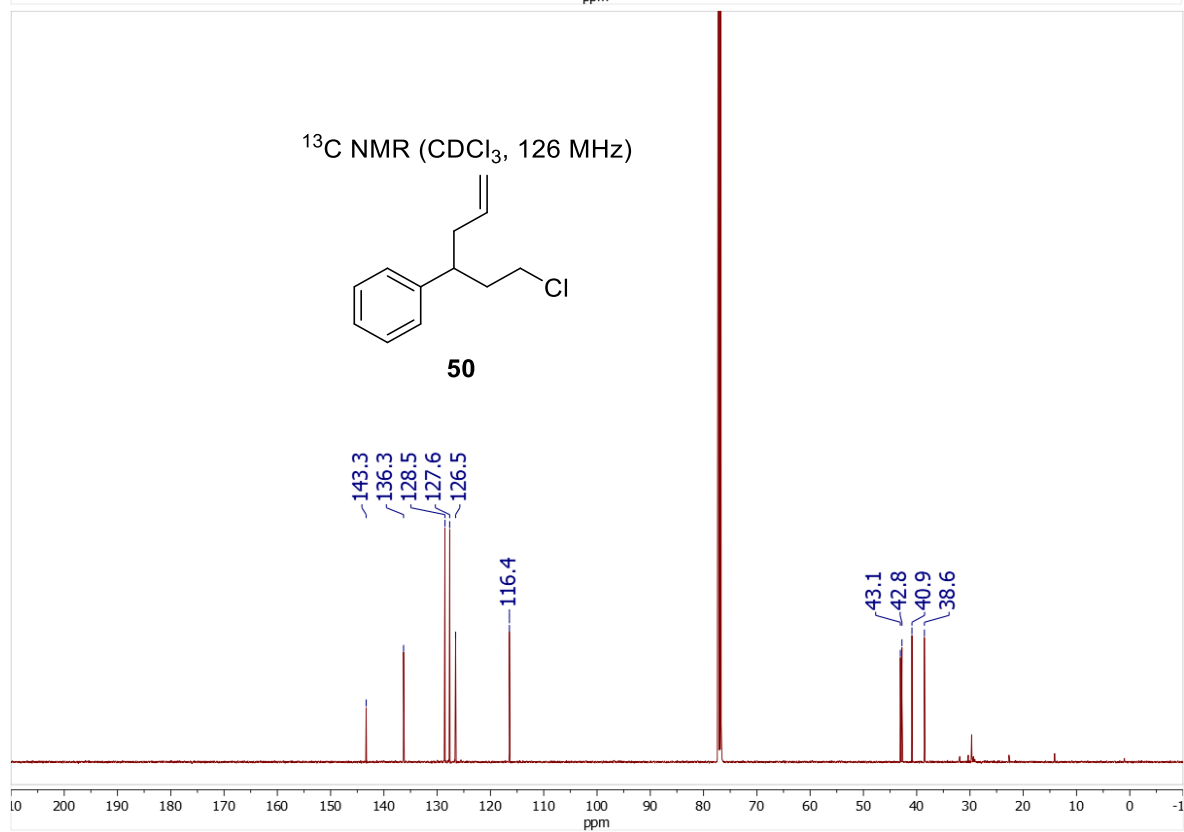
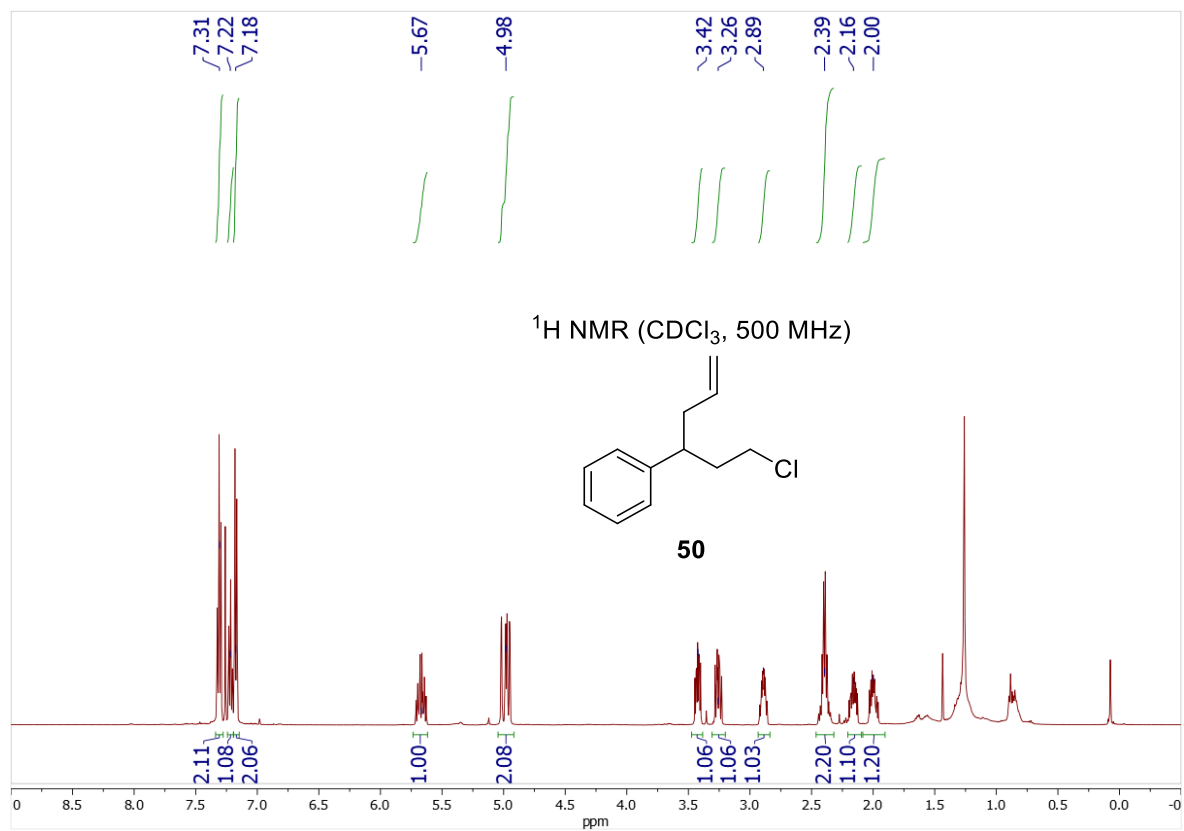












Appendix D: Supporting Information Chapter 5

5D.I. General Considerations

All reagents were purchased and used as received unless otherwise noted. Cu salts were purchased from Aldrich. Benzylic C–H substrates were purchased from Alfa Aesar, Ambeed, Ark Pharm, AstaTech, Chem-Impex, Combi-Blocks, Enamine, Matrix Chemicals, Millipore Sigma, Oakwood Chemicals and TCI America. Additives were purchased from Aldrich or TCI America. N-Fluorobenzenesulfonimide (NFSI) was purchased from Ark Pharm and Combi-Blocks. Diisopropyl phosphites were purchased from Aldrich, Oakwood Chemicals, Alfa Aesar and TCI America. All the reagents were used without further purification. Substrate **1q** was prepared with the procedure reported in literature.¹

¹H, ¹³C, ¹⁹F and all the 2D NMR spectra were recorded on Bruker 400 MHz or Bruker 500 MHz spectrometers and chemical shifts are reported in parts per million (ppm). ¹H NMR spectra were referenced to tetramethylsilane at 0.00 ppm and ¹³C NMR spectra were referenced to CDCl₃ at 77.16 ppm. Column chromatography was performed using a Biotage Isolera One® with reusable 25 g SNAP Ultra® cartridges, 25 g Sfär® cartridges or standard silica cartridges. Further purification of impure samples was conducted using preparative thin-layer chromatography with Analtech® Glass-Backed Silica G UNIPLATES®. High-resolution mass spectra were obtained using a Thermo Q Exactive™ Plus (ESI or ASAP-MS) by the mass spectrometry facility at the University of Wisconsin. Melting points were determined using a DigiMelt MPA160 SRS melting point apparatus.

5D.II. Experimental Procedures for Cross-Coupling Reactions

General Procedure (I) for Cross Coupling of N–H Nucleophiles and Benzylic C–H Substrates (pressure tube, temperature ≥ 50 °C)

Copper(I) chloride (2.0 mg, 0.020 mmol, 10 mol%), tetrabutylammonium chloride (2.8 mg, 0.020 mmol, 10 mol% or 16.8 mg, 0.060 mmol, 30 mol%), NFSI (94.6 mg, 0.30 mmol, 1.5 equiv), N–H nucleophile (0.50 mmol, 2.5 equiv) and benzylic substrate (if solid, 0.20 mmol, 1.0 equiv) were added to a glass pressure tube under air. The pressure tube was then moved to a glove box under N₂ atmosphere. Solvent (1.0 mL), benzylic substrate (if liquid, 0.20 mmol, 1.0 equiv) and diisopropyl phosphite (16.3 μ L, 0.10 mmol, 0.5 equiv) were added to the tube. The tube was sealed in the glove box and taken out to a hot plate. The sealed tube was heated at 50 °C with stirring for 16 h. When the reaction finished, the mixture was cooled down to room temperature. Then the mixture was evaporated under vacuum and the crude mixture was purified by column chromatography (silica gel, eluted by pentane:ethyl acetate = 20:1 to 4:1).

Trimethylsilyl triflate (3.6 μ L, 0.020 mmol, 10 mol%) or BF₃•OEt₂ (2.5 μ L, 0.020 mmol, 10 mol%) was added in the glove box when they were used as an additive instead of tetrabutylammonium chloride.

General Procedure (II) for Cross Coupling of N–H nucleophiles and Benzylic C–H Substrates (glass vial, temperature ≤ 40 °C)

Copper(I) chloride (2.0 mg, 0.020 mmol, 10 mol%), tetrabutylammonium chloride (5.6 mg, 0.020 mmol, 10 mol% or 16.8 mg, 0.060 mmol, 30 mol%), NFSI (94.6 mg, 0.30 mmol, 1.5 equiv), N–H nucleophile (0.50 mmol, 2.5 equiv) and benzylic substrate (if solid, 0.20 mmol, 1.0 equiv) were added under air to a 4 ml borosilicate glass vial containing a magnetic stir bar. Then the vial was capped with a pierceable Teflon cap. A needle was pierced through the cap to facilitate exchange of the vial headspace with the atmosphere. Then the vial was moved into a glove box, through three vacuum-nitrogen-backfill cycles. The needle was removed, and the vial was taken out of the glove box (now sealed under an inert gas). Solvent (1.0 mL), benzylic substrate (if liquid, 0.20 mmol, 1.0 equiv), and diisopropyl phosphite (16.3 μ L, 0.10 mmol, 0.5 equiv) were added into the vial by injection through the cap. The sealed vial was heated at 30 °C and stirred for 16 h. When the reaction finished, the mixture was cooled down to room temperature. Then the mixture was evaporated under vacuum and the crude mixture was purified by column chromatography (silica gel, eluted by pentane:ethyl acetate = 20:1 to 4:1).

5D.III. Optimization of the Reaction Conditions

Optimization of reaction conditions were conducted according to general procedure (I) or (II), with variations specified in each table. Reaction yields were monitored by ^1H NMR spectroscopy with 0.2 mmol mesitylene as the internal standard.

Table 5D.1. Assessment of ancillary ligands

Reaction scheme for Table 5D.1:

1a (0.2 mmol) + 2a (0.5 mmol) $\xrightarrow[\text{DCM:HFIP (7:3, 1 mL)}]{\text{CuCl (10 mol \%), Additive (10 mol \%), NFSI (1.5 equiv), (iPrO)}_2\text{P(O)H (0.5 equiv)}}$ 3aa (N^2) + $\text{3aa}'$ (N^1)
 16 h, 40°C, N_2

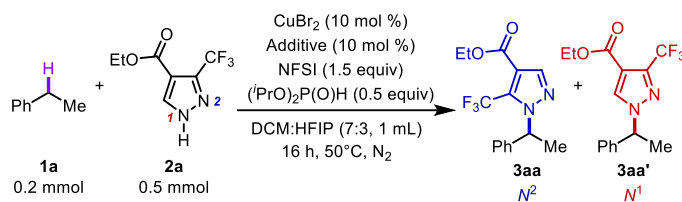
None					
37% (18+19) Yield 58% Conv.	50% (45+5) Yield 73% Conv.	11% (11+0) Yield 25% Conv.	14% (12+2) Yield 28% Conv.	18% (16+2) Yield 34% Conv.	6% (6+0) Yield 25% Conv.
10% (10+0) Yield 25% Conv.	29% (28+1) Yield 43% Conv.	74% (64+10) Yield 100% Conv.	51% (48+3) Yield 70% Conv.	7% (7+0) Yield 16% Conv.	9% (9+0) Yield 22% Conv.
12% (12+0) Yield 25% Conv.	0% (0+0) Yield 13% Conv.	19% (18+1) Yield 55% Conv.	60% (58+2) Yield 79% Conv.	30% (26+4) Yield 58% Conv.	68% (56+12) Yield 85% Conv.

Table 5D.2. Ligand comparison with selected nucleophiles

Reaction scheme for Table 5D.2:

1a (0.2 mmol) + 2a (0.5 mmol) $\xrightarrow[\text{DCM:HFIP (7:3, 1 mL)}]{\text{CuCl (10 mol \%), Additive (10 mol \%), NFSI (1.5 equiv), (iPrO)}_2\text{P(O)H (0.5 equiv)}}$ 3aa (N^2) + $\text{3aa}'$ (N^1)
 16 h, 40°C, N_2

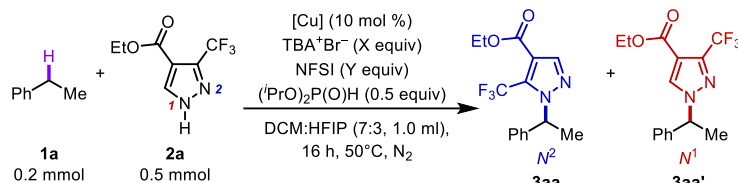
74% (64+10) Yield 100% Conv.	68% (56+12) Yield 85% Conv.	12% (12+0) Yield 25% Conv.
0% Yield 4% Conv.	61% (52+9) Yield 88% Conv.	25% (20+5) Yield 40% Conv.

Table 5D.3. Effect of different additives in controlling the regioselectivity^a

Entry	Additive	Conv. of 1a (%)	Yield of <i>N</i> -2 (%)	Yield of <i>N</i> -1 (%)	<i>N</i> -2: <i>N</i> -1
1	IMes ⁺ Cl ⁻	100	63	7	9.0:1
2	TBA ⁺ Br ⁻	100	72	4	18:1
3	TBA ⁺ NO ₃ ⁻	91	54	2	13:1
4	TBA ⁺ Cl ⁻	100	70	6	11.7:1
5	(none)	89	57	5	9.3:1
6	TBA ⁺ PF ₆ ⁻	91	57	11	5.8:1
7	TBA ⁺ HSO ₄ ⁻	100	57	10	5.7:1
8	TBA ⁺ BH ₂ ⁻	88	52	24	2.2:1
9	TBA ⁺ OTf ⁻	96	45	23	2.1:1
10	TBA ⁺ ClO ₄ ⁻	100	63	34	1.7:1
11	TBDMSCl	94	44	27	1.6:1
12	TMSCN	91	42	28	1.5:1
13	TIPSCl	91	36	29	1.2:1
14	TBA ⁺ BF ₄ ⁻	100	26	34	1:1.3
15	TEA ⁺ BF ₄ ⁻	97	35	43	1:1.2
16	(Ph) ₃ SiCl	97	34	37	1:1.1
17	TMSCl	94	30	47	1:1.8
18	BF ₃ •OEt ₂	91	6	60	1:10
19	TMSOTf	42	2	38	1:19
20 ^b	TMSOTf	100	1	66	1:66

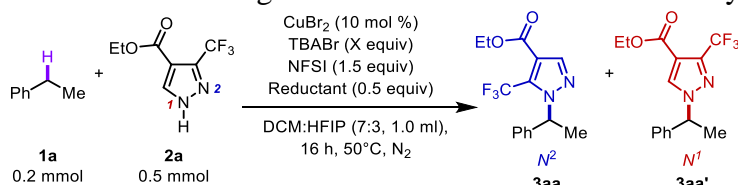
^aTBA, tetrabutylammonium; TEA, tetraethylammonium; TMS, trimethylsilyl; TIPS, triisopropylsilyl; TBDMS, *tert*-butyldimethyl; DCM, dichloromethane; HFIP, hexafluoroisopropanol; Conv., conversion. ^bReaction conducted at 60 °C.

Note: The screening of salts in this study indicate the imidazolium cation identified in previous screening results does not play an important role in reactivity or *N*¹/*N*² regioselectivity and can be replaced by tetrabutylammonium cation. When the additive contains a Lewis acid, such as TMSCl or BF₃•OEt₂, the regioselectivity switches to favor *N*¹.

Table 5D.4. Optimization of the reaction conditions with various solvents, Cu salts and temperature^a

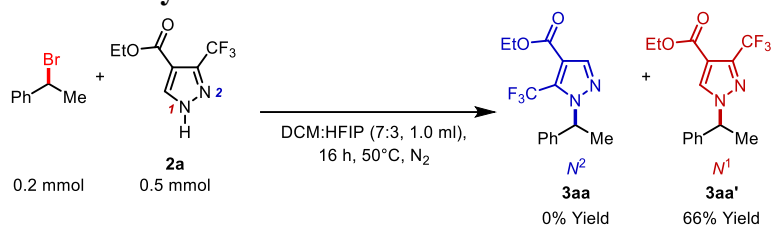
Entry	[Cu]	Solvent	X	Y	Z	Conv. of 1 (%)	Yield of N-2 (%)	Yield of N-1 (%)	N-2:N-1
1	CuCl	DCE	0.1	1.5	2.5	94	60	3	20:1
2	CuCl	PhH	0.1	1.5	2.5	58	12	0	–
3	CuCl	PhCl	0.1	1.5	2.5	91	48	0	–
4	CuCl	PhCF ₃	0.1	1.5	2.5	64	24	1	24:1
5	CuCl	PhNO ₂	0.1	1.5	2.5	64	12	1	12:1
6	CuCl	MeNO ₂	0.1	1.5	2.5	97	21	34	1:1.6
7	CuCl	DCM	0.1	1.5	2.5	100	48	8	6:1
8	CuCl	HFIP	0.1	1.5	2.5	91	2	39	1:19.5
10	CuCl	DCM:HFIP (8:2)	0.1	1.5	2.5	100	63	9	7:1
11	CuCl	DCM:HFIP (6:4)	0.1	1.5	2.5	100	45	16	2.8:1
12	CuCl	DCM:HFIP (7:3)	0.1	1.5	2.5	100	63	8	7.9:1
13	CuOAc	DCM:HFIP=7:3	0.1	1.5	2.5	94	66	6	11:1
14	CuI	DCM:HFIP=7:3	0.1	1.5	2.5	100	57	11	5.2:1
15	CuBr	DCM:HFIP=7:3	0.1	1.5	2.5	100	57	11	5.2:1
16	CuCl ₂	DCM:HFIP=7:3	0.1	1.5	2.5	100	60	10	6:1
17	CuBr ₂	DCM:HFIP=7:3	0.1	1.5	2.5	100	63	11	5.7:1
18	CuBr ₂	DCM:HFIP=7:3	0.1	1.0	2.5	94	60	8	7.5:1
19	CuBr ₂	DCM:HFIP=7:3	0.1	2.0	2.5	100	63	8	7.9:1
20	CuBr ₂	DCM:HFIP=7:3	0.1	1.5	2.5	100	69	6	11.5:1
21	CuBr ₂	DCM:HFIP=7:3	0.3	1.5	2.5	97	72	2	36:1
22	CuCl	DCM:HFIP=7:3	0.3 ^a	1.5	2.5	100	76	4	19:1
23	CuCl	DCM:HFIP=7:3	0.1 ^a	1.5	2.5	100	75	4	19:1

^aReactions were conducted with TBA⁺Cl⁻ instead of TBA⁺Br⁻. DCE, 1,2-dichloroethane; DCM, DCM; HFIP, hexafluoroisopropanol; Conv., conversion.

Table 5D.5. Investigation of various reductants with ethylbenzene as the substrate

Entry	Reductant	Conv. of 1 (%)	Yield of N-2 (%)	Yield of N-1 (%)	N-2:N-1
1	–	100	63	5	13:1
2	(MeO) ₂ P(O)H	100	33	5	6.6:1
3	(EtO) ₂ P(O)H	100	42	7	6.0:1
4	(iPrO) ₂ P(O)H	100	68	4	17:1
5	(tBuO) ₂ P(O)H	76	45	4	11:1
6	(ⁿ BuO) ₂ P(O)H	100	51	7	7.3:1
7	(MeO) ₂ MeSiH	91	48	3	16:1
8	(EtO) ₂ MeSiH	94	51	5	10:1
9	PhNHNHPh	28	4	0	–
10	EtCO ₂ NHNHCO ₂ Et	100	51	2	26:1
11	P(ⁿ Bu) ₃	88	54	6	9.0:1
12	Sodium Ascorbate	100	36	11	3.3:1

5D.IV. Displacement of Benzylic Bromide with 2a



2a (104 mg, 0.50 mmol, 2.5 equiv) was added to a glass pressure tube under air. The pressure tube was then moved to a glove box under N₂ atmosphere. DCM:HFIP (7:3, 1.0 mL) and (1-Bromoethyl)benzene (27.3 μ L, 0.20 mmol, 1.0 equiv) and were added to the tube. The tube was sealed in the glove box and taken out to a hot plate. The sealed tube was heated at 50 °C with stirring for 16 h. When the reaction finished, the mixture was cooled down to room temperature. Then an aliquot of the mixture was taken, diluted with CDCl₃. Reaction yield was monitored by ¹H NMR spectroscopy with 0.2 mmol mesitylene as the internal standard.

5D.V. Additional Screening Data with Benzylic C–H Substrates and Azoles

Not all substrates tested afforded good reactivity in the cross-coupling reactions, and a survey of suboptimal results are provided in Figure 5D.1. Ethylbenzene derivatives with electron-deficient *para*-substituents are less reactive toward C–H activation, and lower conversions and yields are observed (Figure 5D.1A and B). Pyridine-containing substrates do afford the desirable products but often with low yield (Figure 5D.1C). More electron-rich azoles appear to inhibit the C–N cross coupling reactivity, possibly reflecting coordination/inhibition of the copper catalyst or because they undergo side reactions with NFSI (Figure 5D.1D). The presence of large substituents near the benzylic C–H site also inhibits the conversion of the starting material (Figure 5D.1E). Reaction yields were monitored by ¹H NMR spectroscopy with 0.2 mmol mesitylene as the internal standard.

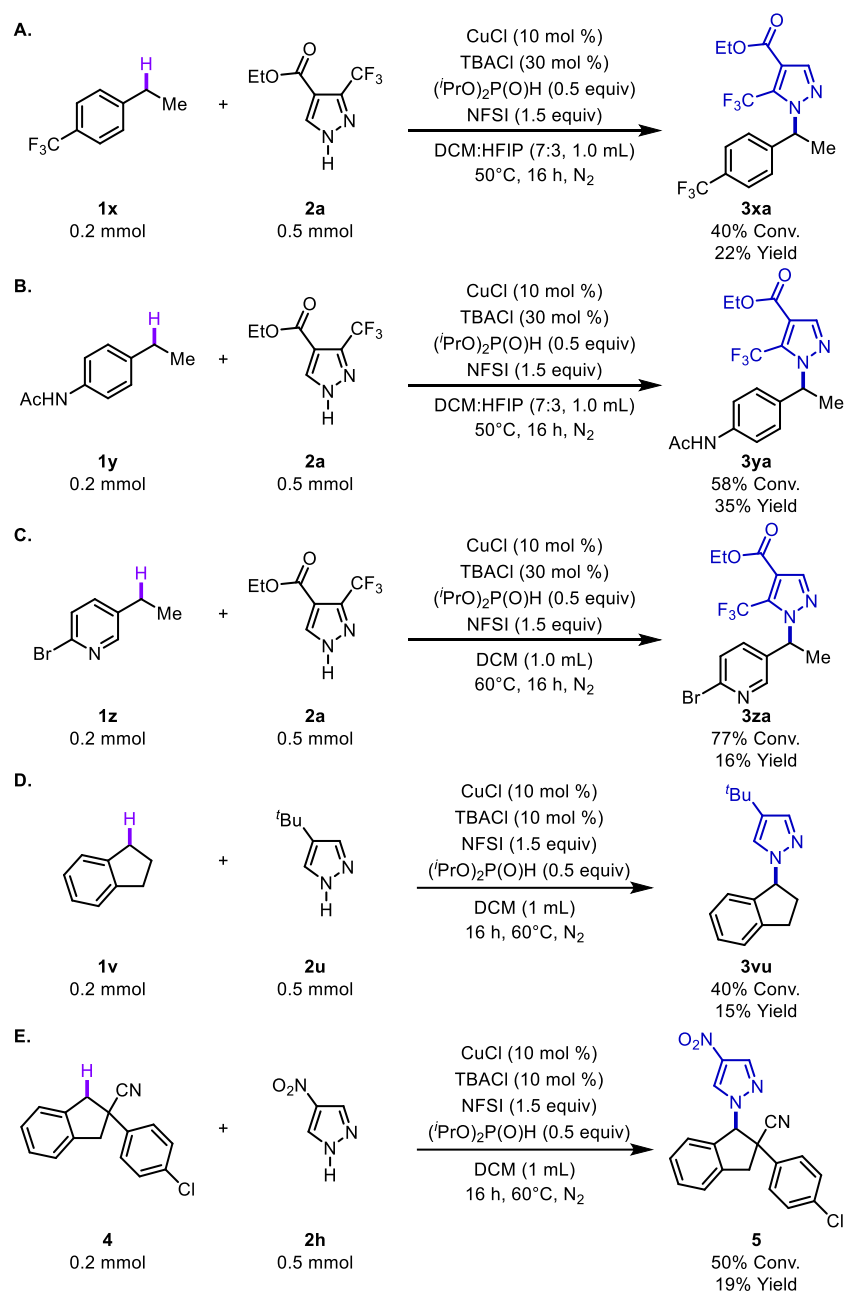


Figure 5D.1. Screening data with additional benzylic C–H substrates and azoles.

A selection of cross-coupling reactions of benzylic C–H substrates and azoles were further analyzed to insight the mass balance of this method.

- While TBABr has shown high selectivity for *N*-2 regioisomer in coupling reactions with **2a**, when electron-rich substrates like **1h** were employed, formation of brominated products on the arene were observed. Replacing TBABr with TBACl avoided this side reactivity (Figure 3B.2A).
- Minor side products were observed where the byproduct benzenesulfonimide from NFSI was introduced to the benzylic sites, especially when cyclic substrates were engaged (Figure 3B.2B and 3B.2C).

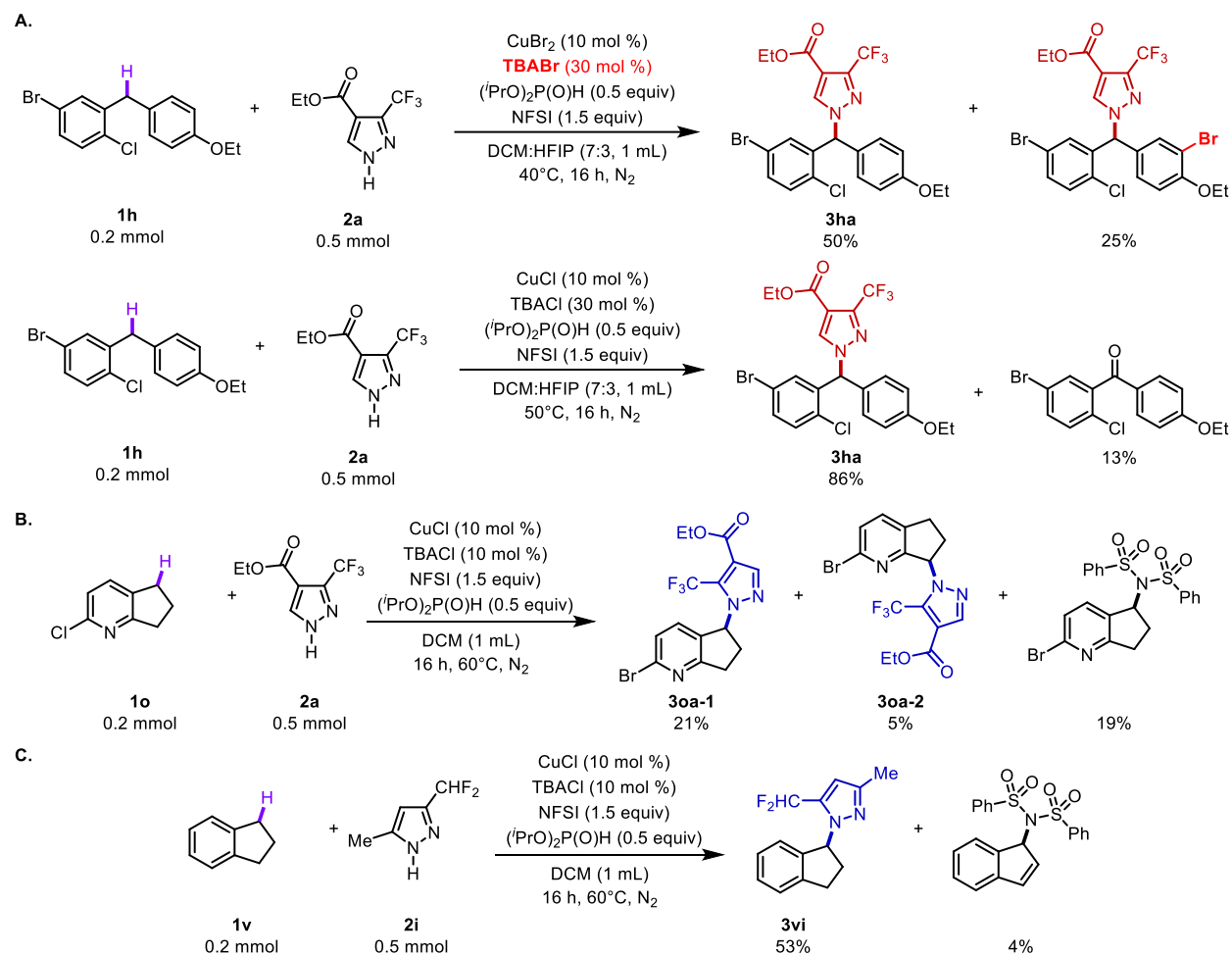


Figure 5D.2. Further analyses of reaction outcomes of cross couplings of benzylic C–H bonds and azoles

5D.VI. Characterization of Regioselectivity

A. Benzylic C–H cross coupling products with 2a

All the *N*-1 and *N*-2 regioisomers were assigned based on 2D NMR spectra (HSQC and HMBC), along with additional characteristics in the ^{13}C and ^{19}F NMR spectra.

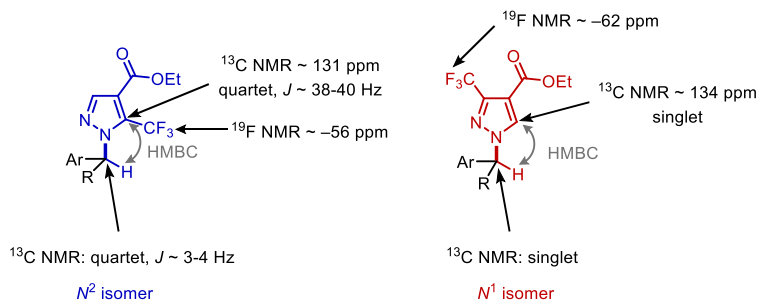


Figure 5D.3. Evidence for regioisomer assignment of benzylic C–H cross coupling products with 2a

B. Benzylic C–H cross coupling products with other ambidentate azoles

Regioisomers with other azoles were assigned based on 2D NMR spectra (HSQC and HMBC), literature values and/or the number of peaks in ^{13}C NMR spectra.

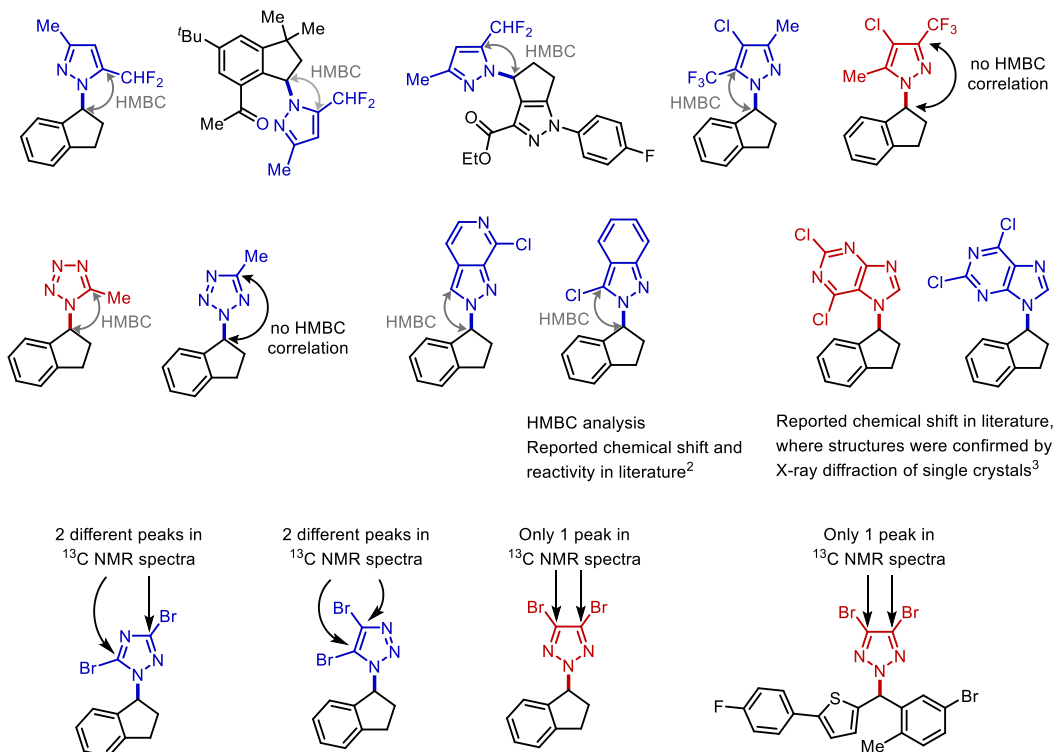


Figure 5D.4. Proof of regioisomer assignment for benzylic C–H cross coupling products with other ambidentate azoles.

5D.VII. Crystallization and Crystallographic Data for $[(\text{C}_6\text{H}_5)\text{N}(\text{CH}_3)_3]_2[\text{CuBr}_4]$ and **2a**

Preparation

Copper(I) bromide (28.7 mg, 0.2 mmol, 1.0 equiv) and trimethylphenylammonium bromide (129.7 mg, 0.6 mmol, 3.0 equiv) were weighed into a 4 mL borosilicate glass vial in a glove box under nitrogen atmosphere, followed by the addition of 1 mL 1,1,1,3,3,3-hexafluoroisopropanol. *N*-fluorobenzenesulfonimide (31.5 mg, 0.1 mmol, 0.5 equiv) was then added into the solution. The vial was then sealed with a Teflon cap and the reaction mixture was heated at 50°C for 30 min. After that, **2a** (166.5 mg, 0.4 mmol, 4.0 equiv) was added into the solution. The reaction mixture was then removed from the glovebox and heated at 50°C on a hot plate for 16 h before cooling down to room temperature. The 4 mL glass vial was uncapped and placed in a 15 mL borosilicate glass vial containing pentane. The 15 mL glass vial was then sealed with a 15 mL Teflon cap to allow vapor diffusion. Two kinds of crystals were found in the glass vial: blue crystal $[(\text{C}_6\text{H}_5)\text{N}(\text{CH}_3)_3]_2[\text{CuBr}_4]$ and colorless crystal **2a**.

Crystallographic Data for $[(\text{C}_6\text{H}_5)\text{N}(\text{CH}_3)_3]_2[\text{CuBr}_4]$

Data Collection

A blue crystal with approximate dimensions 0.14 x 0.01 x 0.005 mm³ was selected under oil under ambient conditions and attached to the tip of a MiTeGen MicroMount©. The crystal was mounted in a stream of cold nitrogen at 100(1) K and centered in the X-ray beam by using a video camera.

The crystal evaluation and data collection were performed on a Bruker Quazar SMART APEXII diffractometer with Mo K_α ($\lambda = 0.71073 \text{ \AA}$) radiation and a diffractometer to crystal distance of 4.96 cm.²

The initial cell constants were obtained from three series of ω scans at different starting angles. Each series consisted of 12 frames collected at intervals of 0.5° in a 6° range about ω with the exposure time of 30 seconds per frame. The reflections were successfully indexed by an automated indexing routine built in the APEXII program suite. The final cell constants were calculated from a set of 5662 strong reflections from the actual data collection.

The data were collected by using a full sphere data collection routine to survey reciprocal space to the extent of a full sphere to a resolution of 0.80 Å. A total of 28817 data were harvested by collecting 4 sets of frames with 0.6° scans in ω and ϕ with exposure times of 180 sec per frame. These highly redundant datasets were corrected for Lorentz and polarization effects. The absorption correction was based on fitting a function to the empirical transmission surface as sampled by multiple equivalent measurements.³

Structure Solution and Refinement

The systematic absences in the diffraction data were consistent for the space groups *Pn* and *P2/n*. The *E*-statistics strongly suggested the centrosymmetric space group *P2/n* that yielded chemically reasonable and computationally stable results of refinement.⁴⁻⁹

A successful solution by direct methods provided most non-hydrogen atoms from the *E*-map. The remaining non-hydrogen atoms were located in an alternating series of least-squares cycles and difference Fourier maps. All non-hydrogen atoms were refined with anisotropic displacement coefficients. All hydrogen atoms were included in the structure factor calculation at idealized

positions and were allowed to ride on the neighboring atoms with relative isotropic displacement coefficients.

The structure crystallizes as an inorganic salt with the formula $[(\text{C}_6\text{H}_5)\text{N}(\text{CH}_3)_3]_2[\text{CuBr}_4]$. Atom Br4 in the $[\text{CuBr}_4]^{2-}$ anion is disordered over two positions, with a major component occupancy of 58.5(16) %.

The structure also contains two trimethylaniline cations. One of these cations resides on a crystallographic general position and is fully occupied. The second cation is disordered over two different crystallographic sites. Both of these sites are crystallographic special positions corresponding to two-fold axes. Thus, this cation presents itself in the symmetry-independent unit as being 50% occupied at two different crystallographic sites and is equally disordered across the crystallographic two-fold axis at each site. This cation was refined with 1,2 and 1,3 distance restraints, as well as with atomic displacement parameter restraints and constraints.

The final least-squares refinement of 305 parameters against 4749 data resulted in residuals R (based on F^2 for $I \geq 2\sigma$) and wR (based on F^2 for all data) of 0.0453 and 0.0962, respectively. The final difference Fourier map was featureless.

Summary

Crystal Data for $\text{C}_{18}\text{H}_{28}\text{Br}_4\text{CuN}_2$ ($M = 655.60$ g/mol): monoclinic, space group $P2/n$ (no. 13), $a = 9.247(4)$ Å, $b = 8.397(3)$ Å, $c = 29.837(10)$ Å, $\beta = 93.608(11)^\circ$, $V = 2312.2(14)$ Å³, $Z = 4$, $T = 99.99$ K, $\mu(\text{Mo K}\alpha) = 7.862$ mm⁻¹, $D_{\text{calc}} = 1.883$ g/cm³, 28817 reflections measured ($2.736^\circ \leq 2\theta \leq 52.85^\circ$), 4749 unique ($R_{\text{int}} = 0.0705$, $R_{\text{sigma}} = 0.0545$) which were used in all calculations. The final R_1 was 0.0453 ($I > 2\sigma(I)$) and wR_2 was 0.0962 (all data).

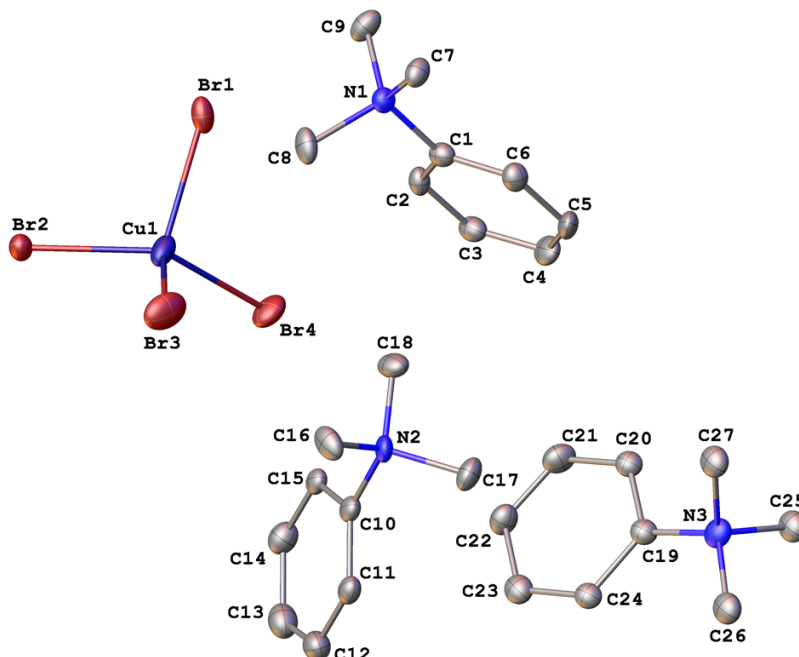


Figure 5D.5. A molecular drawing of $[(\text{C}_6\text{H}_5)\text{N}(\text{CH}_3)_3]_2[\text{CuBr}_4]$. The N,N,N-trimethylanilinium cations containing atoms N2 and N3 are 50% occupied. All atoms are shown with 50% probability ellipsoids. All H atoms and minor disorder components are omitted.

Table 5D.6. Crystal data and structure refinement for [(C₆H₅)N(CH₃)₃]₂[CuBr₄]

Empirical formula	[(C ₆ H ₅)N(CH ₃) ₃] ₂ [CuBr ₄]
Formula weight	655.60
Temperature/K	99.99
Crystal system	monoclinic
Space group	<i>P2/n</i>
<i>a</i> /Å	9.247(4)
<i>b</i> /Å	8.397(3)
<i>c</i> /Å	29.837(10)
α /°	90
β /°	93.608(11)
γ /°	90
Volume/Å ³	2312.2(14)
<i>Z</i>	4
ρ_{calc} /g/cm ³	1.883
μ /mm ⁻¹	7.862
<i>F</i> (000)	1276.0
Crystal size/mm ³	0.14 × 0.01 × 0.005
Radiation	Mo K α (λ = 0.71073)
2 Θ range for data collection/°	2.736 to 52.85
Index ranges	-11 ≤ <i>h</i> ≤ 11, -10 ≤ <i>k</i> ≤ 9, -37 ≤ <i>l</i> ≤ 35
Reflections collected	28817
Independent reflections	4749 [<i>R</i> _{int} = 0.0705, <i>R</i> _{sigma} = 0.0545]
Data/restraints/parameters	4749/95/305
Goodness-of-fit on <i>F</i> ²	1.067
Final <i>R</i> indexes [<i>I</i> ≥ 2 σ (<i>I</i>)]	<i>R</i> ₁ = 0.0453, <i>wR</i> ₂ = 0.0879
Final <i>R</i> indexes [all data]	<i>R</i> ₁ = 0.0727, <i>wR</i> ₂ = 0.0962
Largest diff. peak/hole / e Å ⁻³	0.70/-1.02

Crystallographic Data for 2a

Data Collection

A colorless crystal with approximate dimensions 0.50 x 0.40 x 0.40 mm³ was selected under oil under ambient conditions and attached to the tip of a MiTeGen MicroMount©. The crystal was mounted in a stream of cold nitrogen at 100(1) K and centered in the X-ray beam by using a video camera.

The crystal evaluation and data collection were performed on a Bruker SMART APEXII diffractometer with Cu K α ($\lambda = 1.54178 \text{ \AA}$) radiation and the diffractometer to crystal distance of 4.03 cm.⁴

The initial cell constants were obtained from three series of ω scans at different starting angles. Each series consisted of 50 frames collected at intervals of 0.5° in a 25° range about ω with an exposure time of 10 seconds per frame. The reflections were successfully indexed by an automated indexing routine built in the APEX3 program. The final cell constants were calculated from a set of 2234 strong reflections from the actual data collection.

The data were collected by using a full sphere data collection routine to survey reciprocal space to the extent of a full sphere to a resolution of 0.81 Å. A total of 3882 data were harvested by collecting 9 sets of frames with 0.6° scans in ω and ϕ with an exposure time 5-20 sec per frame. These highly redundant datasets were corrected for Lorentz and polarization effects. The absorption correction was based on fitting a function to the empirical transmission surface as sampled by multiple equivalent measurements.⁵

Structure Solution and Refinement

The systematic absences in the diffraction data were consistent for the space groups $P2_1/m$ and $P2_1$. The E -statistics strongly suggested the centrosymmetric space group $P2_1/m$ that yielded chemically reasonable and computationally stable results of refinement.⁶⁻¹¹

A successful solution by direct methods provided most non-hydrogen atoms from the E -map. The remaining non-hydrogen atoms were located in an alternating series of least-squares cycles and difference Fourier maps. All non-hydrogen atoms were refined with anisotropic displacement coefficients.

The molecule resides on a crystallographic mirror plane.

The final least-squares refinement of 99 parameters against 912 data resulted in residuals R (based on F^2 for $I \geq 2\sigma$) and wR (based on F^2 for all data) of 0.0305 and 0.0814, respectively. The final difference Fourier map was featureless.

Summary

Crystal Data for C₇H₇F₃N₂O₂ ($M = 208.15 \text{ g/mol}$): monoclinic, space group $P2_1/m$ (no. 11), $a = 6.7889(11) \text{ \AA}$, $b = 6.6884(5) \text{ \AA}$, $c = 9.9202(8) \text{ \AA}$, $\beta = 105.469(11)^\circ$, $V = 434.13(9) \text{ \AA}^3$, $Z = 2$, $T = 99.97 \text{ K}$, $\mu(\text{Cu K}\alpha) = 1.420 \text{ mm}^{-1}$, $D_{\text{calc}} = 1.592 \text{ g/cm}^3$, 3882 reflections measured ($9.25^\circ \leq 2\Theta \leq 144.162^\circ$), 912 unique ($R_{\text{int}} = 0.0278$, $R_{\text{sigma}} = 0.0202$) which were used in all calculations. The final R_1 was 0.0305 ($I > 2\sigma(I)$) and wR_2 was 0.0814 (all data).

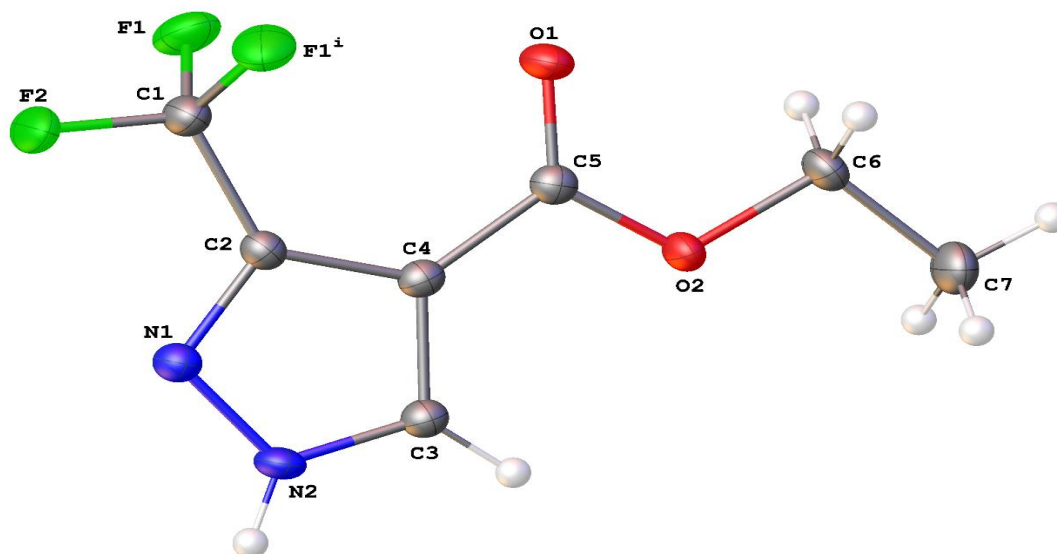


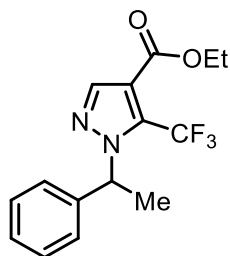
Figure 5D.6. A molecular drawing of **2a** shown with 50% probability ellipsoids for non-hydrogen atoms. [Symmetry code: (i) $x, 3/2 - y, z$.]

Table 5D.7. Crystal data and structure refinement for **2a**

Empirical formula	$C_7H_7F_3N_2O_2$
Formula weight	208.15
Temperature/K	99.97
Crystal system	monoclinic
Space group	$P2_1/m$
$a/\text{\AA}$	6.7889(11)
$b/\text{\AA}$	6.6884(5)
$c/\text{\AA}$	9.9202(8)
$\alpha/^\circ$	90
$\beta/^\circ$	105.469(11)
$\gamma/^\circ$	90
Volume/ \AA^3	434.13(9)
Z	2
$\rho_{\text{calc}}/\text{g/cm}^3$	1.592
μ/mm^{-1}	1.420
F(000)	212.0
Crystal size/ mm^3	$0.5 \times 0.4 \times 0.4$
Radiation	Cu $K\alpha$ ($\lambda = 1.54178$)
2θ range for data collection/ $^\circ$	9.25 to 144.162
Index ranges	$-7 \leq h \leq 8, -8 \leq k \leq 8, -12 \leq l \leq 12$
Reflections collected	3882
Independent reflections	912 [$R_{\text{int}} = 0.0278, R_{\text{sigma}} = 0.0202$]

Data/restraints/parameters	912/0/99
Goodness-of-fit on F ²	1.073
Final R indexes [I ≥ 2σ (I)]	R ₁ = 0.0305, wR ₂ = 0.0788
Final R indexes [all data]	R ₁ = 0.0343, wR ₂ = 0.0814
Largest diff. peak/hole / e Å ⁻³	0.28/-0.27

5D.VIII. Characterization of Compounds



Ethyl 1-(1-phenylethyl)-5-(trifluoromethyl)-1H-pyrazole-4-carboxylate, **3aa**

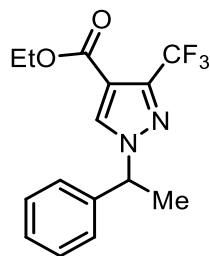
Reaction run using ethylbenzene **1a** (24.5 μL, 0.2 mmol, 1.0 equiv), ethyl 3-(trifluoromethyl)-1H-pyrazole-4-carboxylate **2a** (104.1 mg, 0.50 mmol, 2.5 equiv), and tetrabutylammonium chloride (5.6 mg, 0.02 mmol, 0.1 equiv) following the general procedure I (pressure tube). Yield = 47.3 mg (76%) of pale-yellow liquid. TLC (pentane:EtOAc, 9:1 v/v): R_f = 0.71.

¹H NMR (CDCl₃, 500 MHz): 7.99 (s, 1H), 7.40 – 7.19 (m, 5H), 5.79 (q, *J* = 6.9 Hz, 1H), 4.31 (q, *J* = 7.1 Hz, 2H), 1.94 (d, *J* = 6.9 Hz, 3H), 1.33 (t, *J* = 7.1 Hz, 3H) ppm.

¹³C NMR (CDCl₃, 126 MHz): 161.2, 141.5, 140.5, 131.4 (q, *J* = 40.1 Hz), 128.7, 128.1, 126.3, 119.7 (q, *J* = 271.2 Hz), 115.8 (q, *J* = 1.5 Hz), 61.1, 61.0 (q, *J* = 3.6 Hz), 22.1, 14.1 ppm.

¹⁹F NMR (CDCl₃, 377 MHz): -55.9 ppm.

HRMS Calculated for [C₁₅H₁₅F₃N₂O₂+H]⁺: 313.1158, Found: 313.1153.



Ethyl 1-(1-phenylethyl)-3-(trifluoromethyl)-1H-pyrazole-4-carboxylate, **3aa'**

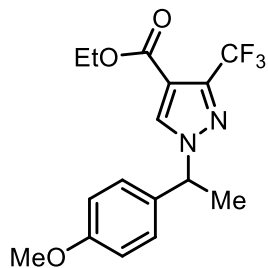
Reaction run using ethylbenzene **1a** (24.5 μL, 0.2 mmol, 1.0 equiv), ethyl 3-(trifluoromethyl)-1H-pyrazole-4-carboxylate **2a** (104.1 mg, 0.50 mmol, 2.5 equiv), and TMSOTf (3.6 μL, 0.02 mmol, 0.1 equiv) following the general procedure I (pressure tube). Yield = 39.6 mg (63%) of clear colorless liquid. TLC (pentane:EtOAc, 9:1 v/v): R_f = 0.38.

¹H NMR (CDCl₃, 500 MHz): 7.91 (s, 1H), 7.42 – 7.32 (m, 3H), 7.28 – 7.26 (m, 2H), 5.56 (q, *J* = 7.1 Hz, 1H), 4.29 (q, *J* = 7.1 Hz, 2H), 1.92 (d, *J* = 7.1 Hz, 3H), 1.32 (t, *J* = 7.1 Hz, 3H) ppm.

¹³C NMR (CDCl₃, 126 MHz): 161.0, 141.2 (q, *J* = 38.3 Hz), 139.4, 134.1, 129.1, 128.8, 126.7, 120.5 (q, *J* = 269.6 Hz), 113.2, 62.6, 61.0, 21.1, 14.1 ppm.

¹⁹F NMR (CDCl₃, 377 MHz): -61.9 ppm.

HRMS Calculated for [C₁₅H₁₅F₃N₂O₂+H]⁺: 313.1158, Found: 313.1157.



Ethyl 1-(1-(4-methoxyphenyl)ethyl)-3-(trifluoromethyl)-1H-pyrazole-4-carboxylate, **3ba'**

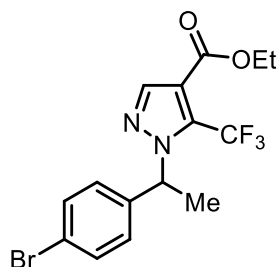
Reaction run using 4-ethylanisole **1b** (29.3 μL , 0.2 mmol, 1.0 equiv), ethyl 3-(trifluoromethyl)-1H-pyrazole-4-carboxylate **2a** (104.1 mg, 0.50 mmol, 2.5 equiv), and trimethylsilyl triflate (3.6 μL , 0.02 mmol, 0.1 equiv) at 60°C following the general procedure I (pressure tube). Yield = 54.7 mg (80%) of clear colorless liquid. TLC (pentane:EtOAc, 9:1 v/v): R_f = 0.42.

^1H NMR (CDCl_3 , 500 MHz): 7.84 (s, 1H), 7.26 – 7.20 (m, 2H), 6.94 – 6.86 (m, 2H), 5.51 (q, J = 7.0 Hz, 1H), 4.28 (q, J = 7.1 Hz, 2H), 3.81 (s, 3H), 1.89 (d, J = 7.0 Hz, 3H), 1.32 (t, J = 7.1 Hz, 3H) ppm.

^{13}C NMR (CDCl_3 , 126 MHz): 161.0, 159.8, 141.1 (q, J = 38.4 Hz), 133.8, 131.1, 128.1, 120.5 (q, J = 269.6 Hz), 114.4, 113.0, 62.1, 60.8, 55.3, 21.1, 14.1 ppm.

^{19}F NMR (CDCl_3 , 377 MHz): -61.9 ppm.

HRMS Calculated for $[\text{C}_{16}\text{H}_{17}\text{F}_3\text{N}_2\text{O}_3+\text{Na}]^+$: 365.1083, Found: 365.1089.



Ethyl 1-(1-(4-bromophenyl)ethyl)-5-(trifluoromethyl)-1H-pyrazole-4-carboxylate, **3ca**

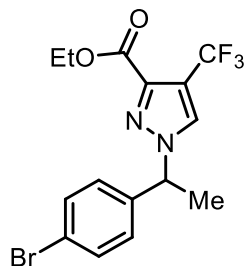
Reaction run using 4-bromoethylbenzene **1c** (27.5 μL , 0.2 mmol, 1.0 equiv), ethyl 3-(trifluoromethyl)-1H-pyrazole-4-carboxylate **2a** (104.1 mg, 0.50 mmol, 2.5 equiv), and tetrabutylammonium chloride (5.6 mg, 0.02 mmol, 0.1 equiv) following the general procedure I (pressure tube). Yield = 57.6 mg (74%) of clear colorless liquid. TLC (pentane:EtOAc, 9:1 v/v): R_f = 0.61.

^1H NMR (CDCl_3 , 500 MHz): 7.98 (s, 1H), 7.52 – 7.39 (m, 2H), 7.24 – 7.05 (m, 2H), 5.73 (q, J = 6.9 Hz, 1H), 4.31 (q, J = 7.1 Hz, 2H), 1.92 (d, J = 6.9 Hz, 3H), 1.34 (t, J = 7.1 Hz, 3H) ppm.

^{13}C NMR (CDCl_3 , 126 MHz): 161.1, 141.7, 139.5, 131.9, 131.4 (q, J = 39.9 Hz), 128.2, 122.3, 119.6 (q, J = 271.3 Hz), 115.9 (q, J = 1.6 Hz), 61.2, 60.5 (q, J = 3.4 Hz), 22.1, 14.1 ppm.

^{19}F NMR (CDCl_3 , 377 MHz): -55.9 ppm.

HRMS Calculated for $[\text{C}_{15}\text{H}_{14}\text{BrF}_3\text{N}_2\text{O}_2+\text{H}]^+$: 391.0264, Found: 391.0257.



Ethyl 1-(1-(4-bromophenyl)ethyl)-5-(trifluoromethyl)-1H-pyrazole-4-carboxylate, **3ca'**

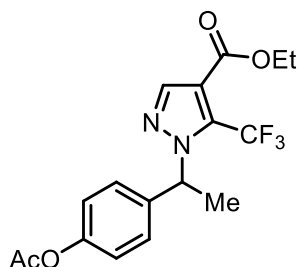
Reaction run using 4-bromoethylbenzene **1c** (27.5 μ L, 0.2 mmol, 1.0 equiv), ethyl 3-(trifluoromethyl)-1H-pyrazole-4-carboxylate **2a** (104.1 mg, 0.50 mmol, 2.5 equiv), and trimethylsilyl triflate (3.6 μ L, 0.02 mmol, 0.1 equiv) at 60°C following the general procedure I (pressure tube). Yield = 78.2 mg (35%) of pale-yellow semisolid. TLC (pentane:EtOAc, 9:1 v/v): R_f = 0.31. Mp: 89-90 °C

^1H NMR (CDCl_3 , 500 MHz): 7.92 (s, 1H), 7.71 – 7.41 (m, 2H), 7.18 – 7.11 (m, 2H), 5.51 (q, J = 7.1 Hz, 1H), 4.30 (q, J = 7.1 Hz, 2H), 1.90 (d, J = 7.1 Hz, 3H), 1.33 (t, J = 7.1 Hz, 3H) ppm.

^{13}C NMR (CDCl_3 , 126 MHz): 160.9, 141.4 (q, J = 38.6 Hz), 138.5, 134.0, 132.3, 128.3, 122.8, 120.4 (q, J = 269.7 Hz), 113.4 (d, J = 1.2 Hz), 62.0, 61.0, 21.0, 14.1 ppm.

^{19}F NMR (CDCl_3 , 377 MHz): -61.94 ppm.

HRMS Calculated for $[\text{C}_{15}\text{H}_{14}\text{BrF}_3\text{N}_2\text{O}_2+\text{Na}]^+$: 413.0083, Found: 413.0083.



Ethyl 1-(1-(4-acetoxyphenyl)ethyl)-5-(trifluoromethyl)-1H-pyrazole-4-carboxylate, **3da**

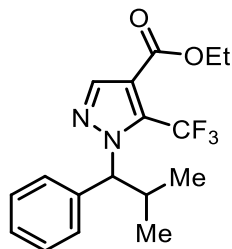
Reaction run using 4-ethylphenyl acetate **1d** (32.0 μ L, 0.2 mmol, 1.0 equiv), ethyl 3-(trifluoromethyl)-1H-pyrazole-4-carboxylate **2a** (104.1 mg, 0.50 mmol, 2.5 equiv), and tetrabutylammonium chloride (5.6 mg, 0.02 mmol, 0.1 equiv) following the general procedure I (pressure tube). Yield = 51.5 mg (70%) of brown solid. TLC (pentane:EtOAc, 9:1 v/v): R_f = 0.33. Mp: 88-90 °C

^1H NMR (CDCl_3 , 500 MHz): 7.98 (s, 1H), 7.34 – 7.28 (m, 2H), 7.10 – 7.01 (m, 2H), 5.77 (q, J = 6.9 Hz, 1H), 4.31 (q, J = 7.1 Hz, 2H), 2.28 (s, 3H), 1.93 (d, J = 6.9 Hz, 3H), 1.34 (t, J = 7.1 Hz, 3H) ppm.

^{13}C NMR (CDCl_3 , 126 MHz): 169.3, 161.1, 150.4, 141.6, 137.9, 131.3 (q, J = 40.0 Hz), 127.7, 121.8, 119.6 (q, J = 271.2 Hz), 115.8 (q, J = 1.6 Hz), 61.1, 60.5 (q, J = 3.4 Hz), 22.2, 21.1, 14.1 ppm.

^{19}F NMR (CDCl_3 , 377 MHz): -55.8 ppm.

HRMS Calculated for $[\text{C}_{17}\text{H}_{17}\text{F}_3\text{N}_2\text{O}_4+\text{H}]^+$: 371.1213, Found: 371.1218.



Ethyl 1-(2-methyl-1-phenylpropyl)-5-(trifluoromethyl)-1H-pyrazole-4-carboxylate, **3ea**

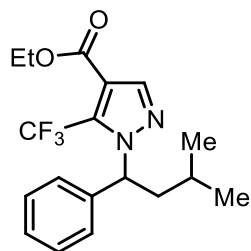
Reaction run using isobutylbenzene **1e** (31.4 μ L, 0.2 mmol, 1.0 equiv), ethyl 3-(trifluoromethyl)-1H-pyrazole-4-carboxylate **2a** (104.1 mg, 0.50 mmol, 2.5 equiv), and tetrabutylammonium chloride (5.6 mg, 0.02 mmol, 0.1 equiv) following the general procedure I (pressure tube). Yield = 45.8 mg (67%) of yellow liquid. TLC (pentane:EtOAc, 9:1 v/v): R_f = 0.47.

^1H NMR (CDCl_3 , 400 MHz): 7.98 (s, 1H), 7.57 – 7.46 (m, 2H), 7.41 – 7.26 (m, 3H), 4.96 (d, J = 10.6 Hz, 1H), 4.29 (q, J = 7.1 Hz, 2H), 2.94 (dh, J = 12.6, 6.4, 5.8 Hz, 1H), 1.33 (t, J = 7.1 Hz, 4H), 0.82 (d, J = 2.3 Hz, 3H), 0.80 (d, J = 2.0 Hz, 3H) ppm.

^{13}C NMR (CDCl_3 , 126 MHz): 161.3, 141.7, 138.1, 131.9 (q, J = 39.6 Hz), 128.5, 128.4, 128.2, 119.7 (q, J = 271.3 Hz), 115.1 (q, J = 1.5 Hz), 72.7 (q, J = 3.0 Hz), 61.1, 33.6, 19.9, 19.7, 14.1 ppm.

^{19}F NMR (CDCl_3 , 377 MHz): -54.9 ppm.

HRMS Calculated for $[\text{C}_{17}\text{H}_{19}\text{F}_3\text{N}_2\text{O}_2+\text{H}]^+$: 341.1471, Found: 341.1470.



Ethyl 1-(3-methyl-1-phenylbutyl)-5-(trifluoromethyl)-1H-pyrazole-4-carboxylate, **3fa**

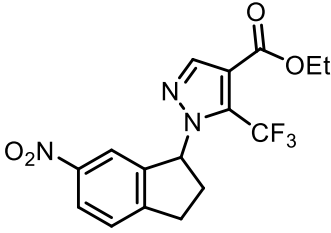
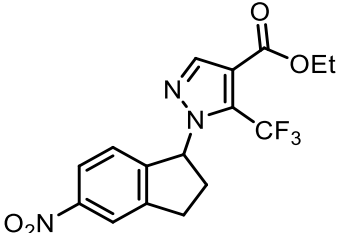
Reaction run using isopentylbenzene **1f** (34.7 μ L, 0.2 mmol, 1.0 equiv), ethyl 3-(trifluoromethyl)-1H-pyrazole-4-carboxylate **2a** (104.1 mg, 0.50 mmol, 2.5 equiv), and tetrabutylammonium chloride (5.6 mg, 0.02 mmol, 0.1 equiv) following the general procedure I (pressure tube). Yield = 42.1 mg (59%) of pale-yellow semisolid. TLC (pentane:EtOAc, 9:1 v/v): R_f = 0.67.

^1H NMR (CDCl_3 , 500 MHz): 7.99 (s, 1H), 7.38 – 7.25 (m, 5H), 5.63 (dd, J = 9.1, 6.0 Hz, 1H), 4.30 (q, J = 7.1 Hz, 2H), 2.50 (ddd, J = 14.5, 9.1, 5.8 Hz, 1H), 2.00 (ddd, J = 14.0, 7.9, 6.0 Hz, 1H), 1.42 – 1.36 (m, 1H), 1.33 (t, J = 7.1 Hz, 3H), 0.95 (d, J = 6.6 Hz, 3H), 0.92 (d, J = 6.6 Hz, 3H) ppm.

^{13}C NMR (CDCl_3 , 126 MHz): 141.5, 139.7, 131.72 (q, J = 39.7 Hz), 128.7, 128.2, 127.0, 119.7 (q, J = 271.3 Hz), 115.6 (q, J = 1.5 Hz), 63.9 (q, J = 3.1 Hz), 61.1, 45.1, 29.7, 24.9, 22.5, 21.9, 14.1 ppm.

^{19}F NMR (CDCl_3 , 377 MHz): -55.6 ppm.

HRMS Calculated for $[\text{C}_{18}\text{H}_{21}\text{F}_3\text{N}_2\text{O}_2+\text{Na}]^+$: 377.1447, Found: 377.1444.

	
Ethyl 1-(6-nitro-2,3-dihydro-1H-inden-1-yl)-5-(trifluoromethyl)-1H-pyrazole-4-carboxylate, 3ga-1	Ethyl 1-(5-nitro-2,3-dihydro-1H-inden-1-yl)-5-(trifluoromethyl)-1H-pyrazole-4-carboxylate, 3ga-2

Reaction run using 5-nitroindane **1g** (32.7 mg, 0.2 mmol, 1.0 equiv), ethyl 3-(trifluoromethyl)-1H-pyrazole-4-carboxylate **2a** (104.1 mg, 0.50 mmol, 2.5 equiv), copper(II) bromide (4.5 mg, 0.02 mmol, 0.1 equiv.), and tetrabutylammonium bromide (19.3 mg, 0.06 mmol, 0.3 equiv) following the general procedure I (pressure tube) and two regioisomers were isolated.

3ga-1: Yield = 14.5 mg (20%) of pale-yellow semisolid. TLC (pentane:EtOAc, 4:1 v/v): $R_f = 0.47$.

^1H NMR (CDCl_3 , 500 MHz): δ 8.20 (dd, $J = 8.4, 2.2$ Hz, 1H), 7.90 (s, 1H), 7.89 (d, $J = 2.1$ Hz, 1H), 7.49 (d, $J = 8.4$ Hz, 1H), 6.16 (dd, $J = 7.9, 6.0$ Hz, 1H), 4.35 (q, $J = 7.1$ Hz, 2H), 3.40 (ddd, $J = 17.0, 8.9, 5.2$ Hz, 1H), 3.11 (ddd, $J = 16.9, 8.8, 6.2$ Hz, 1H), 2.80 (dtd, $J = 13.6, 8.4, 5.2$ Hz, 1H), 2.61 (ddt, $J = 12.7, 9.0, 6.1$ Hz, 1H), 1.37 (t, $J = 7.1$ Hz, 3H) ppm

^{13}C NMR (CDCl_3 , 126 MHz): δ 160.9, 151.5, 147.7, 142.5, 141.9, 131.9 (q, $J = 40.0$ Hz), 125.8, 124.6, 120.0, 119.7 (q, $J = 271.3$ Hz), 115.9 (q, $J = 1.3$ Hz), 65.4 (q, $J = 3.5$ Hz), 61.3, 33.7, 31.0, 14.1 ppm.

^{19}F NMR (377 MHz, CDCl_3): -55.5 ppm.

HRMS Calculated for $[\text{C}_{16}\text{H}_{14}\text{F}_3\text{N}_3\text{O}_4 + \text{NH}_4]^+$: 387.1275, Found: 387.1271.

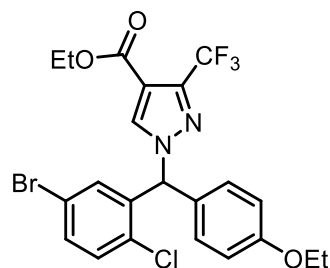
3ga-2: Yield = 9.8 mg (13%) of pale-yellow liquid. TLC (pentane:EtOAc, 4:1 v/v): $R_f = 0.59$.

^1H NMR (CDCl_3 , 500 MHz): δ 8.19 (d, $J = 2.1$ Hz, 1H), 8.09 (dd, $J = 8.4, 2.1$ Hz, 1H), 7.90 (s, 1H), 7.17 (d, $J = 8.3$ Hz, 1H), 6.15 (dd, $J = 8.2, 6.0$ Hz, 1H), 4.35 (q, $J = 7.1$ Hz, 2H), 3.40 (ddd, $J = 16.3, 9.0, 5.0$ Hz, 1H), 3.12 (dt, $J = 15.9, 7.6$ Hz, 1H), 2.81 (dtd, $J = 13.4, 8.4, 5.0$ Hz, 1H), 2.64 (ddt, $J = 13.1, 8.9, 6.3$ Hz, 1H), 1.37 (t, $J = 7.1$ Hz, 3H) ppm.

^{13}C NMR (CDCl_3 , 126 MHz): δ 160.9, 148.8, 147.0, 145.7, 142.4, 131.9 (q, $J = 40.0$ Hz), 125.1, 122.8, 120.5, 119.7 (q, $J = 271.5$ Hz), 115.9 (q, $J = 1.3$ Hz), 65.4 (q, $J = 3.5$ Hz), 61.3, 33.6, 30.7, 14.1 ppm.

^{19}F NMR (377 MHz, CDCl_3): -55.6 ppm.

HRMS Calculated for $[\text{C}_{16}\text{H}_{14}\text{F}_3\text{N}_3\text{O}_4 + \text{NH}_4]^+$: 387.1275, Found: 387.1271.



Ethyl 1-((5-bromo-2-chlorophenyl)(4-ethoxyphenyl)methyl)-3-(trifluoromethyl)-1H-pyrazole-4-carboxylate, **3ha'**

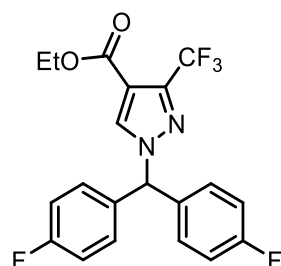
Reaction run using 4-(5-bromo-2-chlorobenzyl)phenyl ethyl ether **1h** (65.1 mg, 0.2 mmol, 1.0 equiv), ethyl 3-(trifluoromethyl)-1H-pyrazole-4-carboxylate **2a** (104.1 mg, 0.50 mmol, 2.5 equiv), and tetrabutylammonium chloride (5.6 mg, 0.02 mmol, 0.1 equiv) following the general procedure I (pressure tube). Yield = 91.5 mg (86%) of yellow solid. TLC (pentane:EtOAc, 9:1 v/v): R_f = 0.44. Mp: 84-87 °C

^1H NMR (CDCl_3 , 500 MHz): 7.74 (s, 1H), 7.44 (dd, J = 8.5, 2.3 Hz, 1H), 7.29 (d, J = 8.5 Hz, 1H), 7.07 – 7.01 (m, 2H), 6.98 (s, 1H), 6.95 – 6.88 (m, 2H), 6.81 (d, J = 2.3 Hz, 1H), 4.31 (q, J = 7.1 Hz, 2H), 4.05 (q, J = 7.0 Hz, 2H), 1.43 (t, J = 7.0 Hz, 3H), 1.34 (t, J = 7.1 Hz, 3H) ppm.

^{13}C NMR (CDCl_3 , 126 MHz): 160.9, 159.7, 142.3 (q, J = 38.5 Hz), 138.0, 136.1, 132.9, 132.5, 131.6, 131.3, 129.9, 126.7, 121.1, 120.2 (q, J = 269.9 Hz), 115.2, 113.2, 67.1, 63.6, 61.1, 14.8, 14.0 ppm.

^{19}F NMR (CDCl_3 , 377 MHz): -62.0 ppm.

HRMS Calculated for $[\text{C}_{22}\text{H}_{19}\text{BrClF}_3\text{N}_2\text{O}_3+\text{Na}]^+$: 553.0112, Found: 553.0112.



Ethyl 1-(bis(4-fluorophenyl)methyl)-3-(trifluoromethyl)-1H-pyrazole-4-carboxylate, **3ia'**

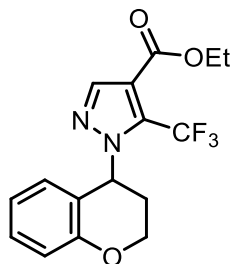
Reaction run using 4,4'-difluorodiphenylmethane **1i** (40.8 mg, 0.2 mmol, 1.0 equiv), ethyl 3-(trifluoromethyl)-1H-pyrazole-4-carboxylate **2a** (104.1 mg, 0.50 mmol, 2.5 equiv), copper(II) bromide (4.5 mg, 0.02 mmol, 0.1 equiv.), and tetrabutylammonium bromide (19.3 mg, 0.06 mmol, 0.3 equiv) following the general procedure I (pressure tube). Yield = 78.3 mg (95%) of yellow solid. TLC (pentane:EtOAc, 9:1 v/v): R_f = 0.30. Mp: 96-97 °C

^1H NMR (CDCl_3 , 500 MHz): 7.83 – 7.78 (m, 1H), 7.12 – 7.03 (m, 8H), 6.78 (s, 1H), 4.30 (q, J = 7.1 Hz, 2H), 1.33 (t, J = 7.1 Hz, 3H) ppm.

^{13}C NMR (CDCl_3 , 126 MHz): 162.8 (d, J = 249.1 Hz), 161.8, 160.8, 142.0 (q, J = 38.6 Hz), 135.4, 133.3 (d, J = 3.3 Hz), 129.9 (d, J = 8.3 Hz), 120.3 (q, J = 269.8 Hz), 116.2 (d, J = 21.8 Hz), 113.5, 69.3, 61.1, 14.0 ppm.

^{19}F NMR (CDCl_3 , 377 MHz): -61.97, -112.26 ppm.

HRMS Calculated for $[\text{C}_{20}\text{H}_{15}\text{F}_5\text{N}_2\text{O}_2+\text{Na}]^+$: 433.0946, Found: 433.0951.



Ethyl 1-(chroman-4-yl)-5-(trifluoromethyl)-1H-pyrazole-4-carboxylate, **3ja**

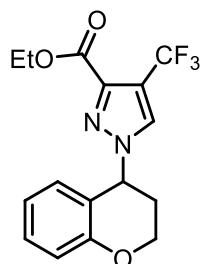
Reaction run using chroman **1j** (25.3 μ L, 0.2 mmol, 1.0 equiv), ethyl 3-(trifluoromethyl)-1H-pyrazole-4-carboxylate **2a** (104.1 mg, 0.50 mmol, 2.5 equiv), and tetrabutylammonium chloride (16.8 mg, 0.06 mmol, 0.3 equiv) following the general procedure I (pressure tube). Yield = 29.4 mg (43%) of yellow semisolid. TLC (pentane:EtOAc, 15:1 v/v): R_f = 0.51. **3ja'** (9.7 mg, 14%) was also isolated in this reaction.

^1H NMR (CDCl_3 , 500 MHz): 7.91 (s, 1H), 7.22 (ddd, J = 8.5, 6.9, 1.5 Hz, 1H), 6.92 (dd, J = 8.3, 1.0 Hz, 1H), 6.85 (td, J = 7.6, 1.1 Hz, 1H), 6.75 (dd, J = 7.9, 0.9 Hz, 1H), 5.82 (t, J = 5.7 Hz, 1H), 4.51 (dt, J = 11.6, 5.7 Hz, 1H), 4.34 (q, J = 7.2 Hz, 2H), 4.28 (dt, J = 10.8, 5.0 Hz, 1H), 2.45 (q, J = 5.6 Hz, 2H), 1.36 (t, J = 7.2 Hz, 3H) ppm.

^{13}C NMR (CDCl_3 , 126 MHz): 161.1, 155.2, 141.9, 132.0 (q, J = 39.9 Hz), 130.0, 128.6, 120.9, 119.8 (q, J = 271.2 Hz), 119.1, 117.6, 115.7 (d, J = 1.6 Hz), 62.8, 61.3, 55.4 (q, J = 3.6 Hz), 30.1, 14.1 ppm.

^{19}F NMR (CDCl_3 , 377 MHz): -55.7 ppm.

HRMS Calculated for $[\text{C}_{16}\text{H}_{15}\text{F}_3\text{N}_2\text{O}_3+\text{Na}]^+$: 363.0927, Found: 363.0918.



Ethyl 1-(chroman-4-yl)-4-(trifluoromethyl)-1H-pyrazole-3-carboxylate, **3ja'**

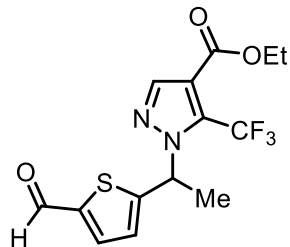
Reaction run using chroman **1j** (25.3 μ L, 0.2 mmol, 1.0 equiv), ethyl 3-(trifluoromethyl)-1H-pyrazole-4-carboxylate **2a** (104.1 mg, 0.50 mmol, 2.5 equiv), and trimethylsilyl triflate (3.6 μ L, 0.02 mmol, 0.1 equiv) at 60°C following the general procedure I (pressure tube). Yield = 25.4 mg (37%) of white solid. TLC (pentane:EtOAc, 9:1 v/v): R_f = 0.94. Mp: 86-88 °C

^1H NMR (CDCl_3 , 500 MHz): 7.71 (s, 1H), 7.33 (ddd, J = 8.6, 7.3, 1.7 Hz, 1H), 7.08 (dd, J = 8.1, 1.8 Hz, 1H), 6.97 (m, 2H), 5.58 (t, J = 4.3 Hz, 1H), 4.34 – 4.23 (m, 3H), 3.92 (td, J = 11.5, 2.5 Hz, 1H), 2.53 (dtd, J = 14.6, 3.9, 2.5 Hz, 1H), 2.43 (ddt, J = 14.7, 11.4, 4.3 Hz, 1H), 1.31 (t, J = 7.1 Hz, 3H) ppm.

^{13}C NMR (CDCl_3 , 126 MHz): 160.9, 155.5, 142.0 (q, J = 38.4 Hz), 135.3, 131.2, 130.5, 121.4, 120.4 (q, J = 269.8 Hz), 118.0, 116.4, 112.9, 61.5, 61.0, 56.7, 28.9, 14.0 ppm.

^{19}F NMR (CDCl_3 , 377 MHz): -62.0 ppm.

HRMS Calculated for $[\text{C}_{16}\text{H}_{15}\text{F}_3\text{N}_2\text{O}_3+\text{Na}]^+$: 363.0927, Found: 363.0922.



Ethyl 1-(1-(5-formylthiophen-2-yl)ethyl)-5-(trifluoromethyl)-1H-pyrazole-4-carboxylate, **3ka**

Reaction run using 5-ethyl-2-thiophenecarboxaldehyde **1k** (25.1 μ L, 0.2 mmol, 1.0 equiv), ethyl 3-(trifluoromethyl)-1H-pyrazole-4-carboxylate **2a** (104.1 mg, 0.50 mmol, 2.5 equiv), and tetrabutylammonium chloride (16.8 mg, 0.06 mmol, 0.3 equiv) following the general procedure I (pressure tube). Yield = 37.7 mg (54%) of pale-yellow liquid. TLC (pentane:EtOAc, 4:1 v/v): R_f = 0.52.

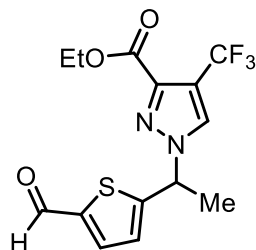
3ka' (13%) was observed in ^1H NMR analysis of the reaction crude, with 0.2 mmol mesitylene as the external standard.

^1H NMR (CDCl_3 , 500 MHz): δ 9.86 (s, 1H), 8.00 (s, 1H), 7.61 (d, J = 3.9 Hz, 1H), 7.05 (d, J = 3.9 Hz, 1H), 6.05 (q, J = 6.8 Hz, 1H), 4.33 (q, J = 7.1 Hz, 2H), 2.03 (d, J = 6.8 Hz, 3H), 1.35 (t, J = 7.1 Hz, 3H) ppm.

^{13}C NMR (CDCl_3 , 126 MHz): δ 182.8, 160.8, 153.1, 143.8, 142.2, 135.7, 131.2 (q, J = 40.2 Hz), 126.5, 116.1 (q, J = 1.3 Hz), 119.5 (q, J = 271.4 Hz), 61.3, 56.8 (q, J = 3.7 Hz), 22.9, 14.1 ppm.

^{19}F NMR (377 MHz, CDCl_3): -55.9 ppm.

HRMS Calculated for $[\text{C}_{14}\text{H}_{13}\text{BF}_3\text{N}_2\text{O}_3\text{S}+\text{Na}]^+$: 369.0491, Found: 369.0485.



Ethyl 1-(1-(5-formylthiophen-2-yl)ethyl)-4-(trifluoromethyl)-1H-pyrazole-3-carboxylate, **3ka'**

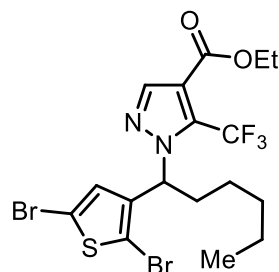
Reaction run using 5-ethyl-2-thiophenecarboxaldehyde **1k** (25.1 μ L, 0.2 mmol, 1.0 equiv), ethyl 3-(trifluoromethyl)-1H-pyrazole-4-carboxylate **2a** (104.1 mg, 0.50 mmol, 2.5 equiv), and trimethylsilyl triflate (3.6 μ L, 0.02 mmol, 0.1 equiv) at 60°C following the general procedure I (pressure tube). Yield = 34.6 mg (50%) of yellow semisolid. TLC (pentane:EtOAc, 9:1 v/v): R_f = 0.91.

^1H NMR (CDCl_3 , 500 MHz): 9.88 (s, 1H), 8.04 (s, 1H), 7.66 (d, J = 3.8 Hz, 1H), 7.11 (d, J = 3.8 Hz, 1H), 5.83 (q, J = 7.0 Hz, 1H), 4.31 (q, J = 7.1 Hz, 2H), 2.02 (d, J = 7.1 Hz, 3H), 1.34 (t, J = 7.1 Hz, 4H) ppm.

^{13}C NMR (CDCl_3 , 126 MHz): 182.8, 160.6, 152.2, 143.9, 141.8 (q, J = 38.7 Hz), 136.1, 133.7, 126.94, 120.2 (q, J = 269.8 Hz), 113.8, 61.1, 58.3, 21.8, 14.0 ppm.

^{19}F NMR (CDCl_3 , 377 MHz): -62.0 ppm.

HRMS Calculated for $[\text{C}_{14}\text{H}_{13}\text{F}_3\text{N}_2\text{O}_3\text{S}+\text{Na}]^+$: 369.0491, Found: 369.0487.



Ethyl 1-(1-(2,5-dibromothiophen-3-yl)hexyl)-5-(trifluoromethyl)-1H-pyrazole-4-carboxylate, **3a**

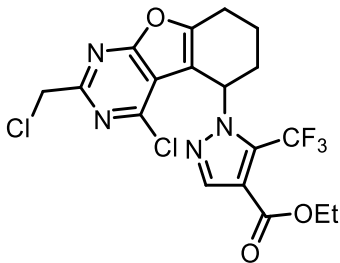
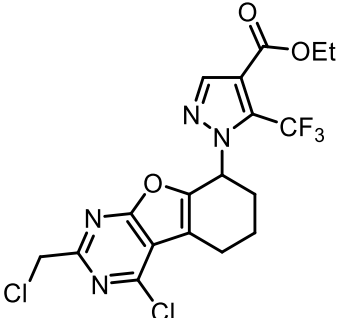
Reaction run using 2,5-dibromo-3-hexylthiophene **11** (42 μ L, 0.2 mmol, 1.0 equiv), ethyl 3-(trifluoromethyl)-1H-pyrazole-4-carboxylate **2a** (104.1 mg, 0.50 mmol, 2.5 equiv, and tetrabutylammonium chloride (16.8 mg, 0.06 mmol, 0.3 equiv) following the general procedure I (pressure tube). Yield = 68.7 mg (65%) of pale-yellow liquid. TLC (pentane:EtOAc, 9:1 v/v): R_f = 0.59.

^1H NMR (CDCl_3 , 500 MHz): 8.00 (s, 1H), 7.14 (s, 1H), 5.69 (dd, J = 8.7, 6.3 Hz, 1H), 4.32 (q, J = 7.1 Hz, 2H), 2.35 (dtd, J = 14.2, 9.2, 5.3 Hz, 1H), 2.03 (ddt, J = 13.5, 9.8, 6.1 Hz, 1H), 1.35 (t, J = 7.1 Hz, 3H), 1.32 – 1.25 (m, 4H), 1.26 – 1.19 (m, 1H), 1.16 – 1.08 (m, 1H), 0.88 – 0.83 (m, 3H) ppm.

^{13}C NMR (CDCl_3 , 126 MHz): 161.1, 142.0, 139.9, 132.0 (q, J = 40.1 Hz), 129.8, 119.5 (q, J = 271.6 Hz), 115.6, 111.7, 110.0, 61.2, 60.1 (q, J = 3.4 Hz), 36.0, 31.0, 25.5, 22.3, 14.1, 13.9 ppm.

^{19}F NMR (CDCl_3 , 377 MHz): -55.7 ppm.

HRMS Calculated for $[\text{C}_{17}\text{H}_{19}\text{BrF}_3\text{N}_2\text{O}_2\text{S}+\text{H}]^+$: 530.9559, Found: 530.9554.

	
Ethyl 1-(4-chloro-2-(chloromethyl)-5,6,7,8-tetrahydrobenzofuro[2,3-d]pyrimidin-5-yl)-5-(trifluoromethyl)-1H-pyrazole-4-carboxylate, 3ma-1	Ethyl 1-(4-chloro-2-(chloromethyl)-5,6,7,8-tetrahydrobenzofuro[2,3-d]pyrimidin-8-yl)-5-(trifluoromethyl)-1H-pyrazole-4-carboxylate, 3ma-2

Reaction run using 3-chloro-5-(chloromethyl)-8-oxa-4,6-diazatricyclo[7.4.0.0{2,7}]trideca-1(9),2,4,6-tetraene **1m** (51.4 mg, 0.2 mmol, 1.0 equiv), ethyl 3-(trifluoromethyl)-1H-pyrazole-4-carboxylate **2a** (104.1 mg, 0.50 mmol, 2.5 equiv), and tetrabutylammonium chloride (16.8 mg, 0.06 mmol, 0.3 equiv) following the general procedure II (glass vial) at 40 °C and two regioisomers were isolated.

3ma-1: Yield = 72.3 mg (45%) of yellow semisolid. TLC (pentane:EtOAc, 9:1 v/v): $R_f = 0.32$.

^1H NMR (CDCl_3 , 500 MHz): 7.89 (s, 1H), 5.87 (t, $J = 5.6$ Hz, 1H), 4.73 (s, 2H), 4.35 (q, $J = 7.1$ Hz, 2H), 3.11 (dtd, $J = 17.0, 5.5, 1.6$ Hz, 1H), 2.92 (dddd, $J = 17.0, 7.3, 5.5, 1.7$ Hz, 1H), 2.43 (q, $J = 5.9$ Hz, 2H), 2.30 – 2.18 (m, 1H), 2.00 (dh, $J = 17.2, 5.6$ Hz, 1H), 1.37 (t, $J = 7.1$ Hz, 3H) ppm.

^{13}C NMR (CDCl_3 , 126 MHz): 167.0, 161.1, 160.7, 153.4, 149.7, 142.0, 132.0 (q, $J = 40.3$ Hz), 119.6 (q, $J = 271.4$ Hz), 117.2, 116.3 (q, $J = 1.6$ Hz), 116.1, 61.3, 54.5 (q, $J = 3.9$ Hz), 46.2, 30.8, 21.0, 19.4, 14.1 ppm.

^{19}F NMR (CDCl_3 , 377 MHz): -55.8 ppm.

HRMS Calculated for $[\text{C}_{18}\text{H}_{15}\text{Cl}_2\text{F}_3\text{N}_4\text{O}_3+\text{H}]^+$: 463.0546, Found: 463.0543.

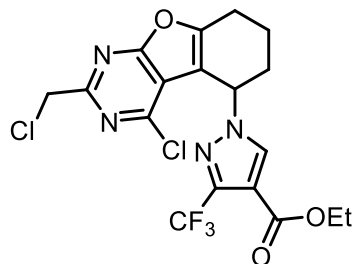
3ma-2: Yield = 8.1 mg (9%) of yellow semisolid. TLC (pentane:EtOAc, 4:1 v/v): $R_f = 0.39$.

^1H NMR (CDCl_3 , 500 MHz): 7.84 (s, 1H), 6.07 (t, $J = 4.5$ Hz, 2H), 4.73 (s, 2H), 4.34 (q, $J = 7.1$ Hz, 2H), 3.05 (dt, $J = 18.1, 5.1$ Hz, 1H), 2.86 (dt, $J = 17.5, 7.2$ Hz, 1H), 2.34 (ddt, $J = 16.8, 8.7, 2.8$ Hz, 1H), 2.26 – 2.09 (m, 2H), 2.08 – 1.95 (m, 2H), 1.36 (t, $J = 7.1$ Hz, 3H) ppm.

^{13}C NMR (CDCl_3 , 126 MHz): 167.1, 160.9, 160.2, 159.7, 151.6, 141.4, 131.4 (q, $J = 40.3$ Hz), 119.8 (q, $J = 271.6$ Hz), 116.7, 115.5, 109.3, 61.3, 54.2 (q, $J = 3.8$ Hz), 46.3, 31.2, 23.1, 18.2, 14.1 ppm.

^{19}F NMR (CDCl_3 , 377 MHz): -56.0 ppm.

HRMS Calculated for $[\text{C}_{18}\text{H}_{15}\text{Cl}_2\text{F}_3\text{N}_4\text{O}_3+\text{H}]^+$: 463.0546, Found: 463.0545.



Ethyl 1-(4-chloro-2-(chloromethyl)-5,6,7,8-tetrahydrobenzofuro[2,3-d]pyrimidin-5-yl)-3-(trifluoromethyl)-1H-pyrazole-4-carboxylate, **3ma'-1**

Reaction run using 3-chloro-5-(chloromethyl)-8-oxa-4,6-diazatricyclo[7.4.0.0{2,7}]trideca-1(9),2,4,6-tetraene **1m** (51.4 mg, 0.2 mmol, 1.0 equiv), ethyl 3-(trifluoromethyl)-1H-pyrazole-4-carboxylate **2a** (104.1 mg, 0.50 mmol, 2.5 equiv), and $\text{BF}_3 \cdot \text{Et}_2\text{O}$ (2.5 μL , 0.02 mmol, 0.1 equiv) at 60°C following the general procedure I (pressure tube) and two regioisomers were isolated.

3ma'-1: Yield = 52.6 mg (58%) of colorless semisolid. TLC (pentane: Et_2O , 1:1 v/v): $R_f = 0.18$.

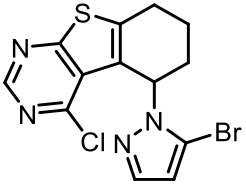
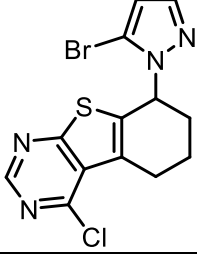
^1H NMR (CDCl_3 , 400 MHz): 7.93 (s, 1H), 5.65 (t, $J = 5.0$ Hz, 1H), 4.76 (s, 2H), 4.31 (q, $J = 7.2$ Hz, 2H), 3.12 (dt, $J = 17.4, 5.3$ Hz, 1H), 2.97 – 2.82 (m, 1H), 2.57 (dq, $J = 14.3, 4.7$ Hz, 1H), 2.48 – 2.31 (m, 1H), 2.04 (p, $J = 5.2$ Hz, 2H), 1.34 (t, $J = 7.1$ Hz, 3H) ppm.

^{13}C NMR (CDCl_3 , 126 MHz): 167.3, 161.7, 160.6, 153.9, 148.6, 142.2 (q, $J = 38.8$ Hz), 135.1, 120.2 (q, $J = 269.8$ Hz), 118.4, 115.9, 113.6, 61.1, 55.4, 46.2, 29.9, 21.1, 18.8, 14.1 ppm.

^{19}F NMR (CDCl_3 , 377 MHz): -62.1 ppm.

HRMS Calculated for $[\text{C}_{18}\text{H}_{15}\text{Cl}_2\text{F}_3\text{N}_4\text{O}_3 + \text{H}]^+$: 463.0546, Found: 463.0539.

3ma-1: Yield = 12.9 mg (14%) of yellow semisolid. TLC (pentane: EtOAc , 9:1 v/v): $R_f = 0.32$.

	
5-(5-bromo-1 <i>H</i> -pyrazol-1-yl)-4-chloro-5,6,7,8-tetrahydrobenzo[4,5]thieno[2,3- <i>d</i>]pyrimidine, 3nb-1	8-(5-bromo-1 <i>H</i> -pyrazol-1-yl)-4-chloro-5,6,7,8-tetrahydrobenzo[4,5]thieno[2,3- <i>d</i>]pyrimidine, 3nb-2

Reaction run using 4-chloro-5,6,7,8-tetrahydro[1]benzothieno[2,3-*d*]pyrimidine **1n** (44.8 mg, 0.2 mmol, 1.0 equiv), 3-bromopyrazole **2b** (73.5 mg, 0.50 mmol, 2.5 equiv), copper(II) bromide (4.5 mg, 0.02 mmol, 0.1 equiv.), and tetrabutylammonium bromide (19.3 mg, 0.06 mmol, 0.3 equiv) following the general procedure I (pressure tube) and two regioisomers were isolated.

3nb-1: Yield = 28.1 mg (38%) of white solid. (pentane:EtOAc, 2:1 v/v): $R_f = 0.48$.

$^1\text{H NMR}$ (CDCl_3 , 500 MHz): δ 8.72 (s, 1H), 7.39 (d, $J = 2.0$ Hz, 1H), 6.39 (d, $J = 1.9$ Hz, 1H), 6.18 (t, $J = 2.4$ Hz, 1H), 3.19 (ddd, $J = 17.8, 5.4, 2.1$ Hz, 1H), 3.02 – 2.81 (m, 1H), 2.33 (ddt, $J = 13.8, 5.0, 2.7$ Hz, 1H), 2.15 (tdd, $J = 13.7, 4.5, 2.9$ Hz, 1H), 2.04 (tddd, $J = 13.6, 11.3, 5.3, 2.5$ Hz, 1H), 1.96 – 1.86 (m, 1H) ppm.

$^{13}\text{C NMR}$ (CDCl_3 , 126 MHz): 168.8, 152.8, 152.0, 145.6, 139.8, 127.9, 122.7, 112.0, 109.2, 52.7, 29.9, 26.1, 17.0 ppm.

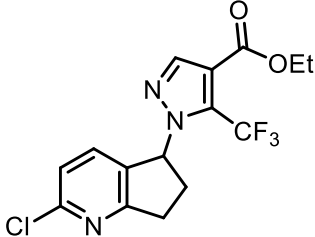
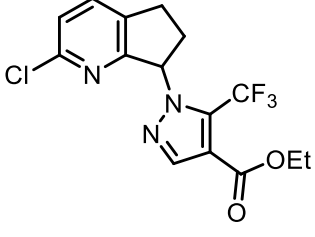
HRMS Calculated for $[\text{C}_{13}\text{H}_{10}\text{BrClN}_4\text{S}+\text{H}]^+$: 368.9571, Found: 368.9570.

3nb-2: Yield = 18.8 mg (25%) of white solid. (pentane:EtOAc, 2:1 v/v): $R_f = 0.06$.

$^1\text{H NMR}$ (CDCl_3 , 500 MHz): 8.75 (s, 1H), 7.56 (d, $J = 1.8$ Hz, 1H), 6.40 (d, $J = 1.9$ Hz, 1H), 5.86 (dd, $J = 7.7, 5.4$ Hz, 1H), 3.37 – 3.14 (m, 2H), 2.52 – 2.40 (m, 1H), 2.42 – 2.27 (m, 2H), 2.07 – 1.95 (m, 1H) ppm.

$^{13}\text{C NMR}$ (CDCl_3 , 126 MHz): 169.6, 154.5, 152.5, 141.3, 137.7, 131.0, 128.3, 112.8, 109.1, 55.6, 29.9, 26.1, 20.5 ppm.

HRMS Calculated for $[\text{C}_{13}\text{H}_{10}\text{BrClN}_4\text{S}+\text{H}]^+$: 368.9571, Found: 368.9571.

	
Ethyl 1-(2-chloro-6,7-dihydro-5H-cyclopenta[b]pyridin-5-yl)-5-(trifluoromethyl)-1H-pyrazole-4-carboxylate, 30a-1	Ethyl 1-(2-chloro-6,7-dihydro-5H-cyclopenta[b]pyridin-7-yl)-5-(trifluoromethyl)-1H-pyrazole-4-carboxylate, 30a-2

Reaction run using 2-chloro-6,7-dihydro-5H-cyclopenta[b]pyridine **1o** (30.7 mg, 0.2 mmol, 1.0 equiv), ethyl 3-(trifluoromethyl)-1H-pyrazole-4-carboxylate **2a** (104.1 mg, 0.50 mmol, 2.5 equiv), and tetrabutylammonium chloride (5.6 mg, 0.02 mmol, 0.1 equiv) following the general procedure I (pressure tube) at 60 °C and two regioisomers were isolated.

30a-1: Yield = 14.0 mg (20%) of light-yellow liquid. TLC (pentane:EtOAc, 4:1 v/v): $R_f = 0.27$.

^1H NMR (CDCl_3 , 400 MHz): δ 7.89 (s, 1H), 7.34 (d, $J = 8.1$ Hz, 1H), 7.17 (d, $J = 8.1$ Hz, 1H), 6.09 (dd, $J = 8.4, 5.2$ Hz, 1H), 4.34 (q, $J = 7.1$ Hz, 2H), 3.41 (ddd, $J = 17.1, 9.3, 5.5$ Hz, 1H), 3.11 (ddd, $J = 17.3, 8.9, 6.1$ Hz, 1H), 2.77 (dtd, $J = 14.0, 8.7, 5.5$ Hz, 1H), 2.57 (ddt, $J = 14.3, 9.3, 5.7$ Hz, 1H), 1.36 (t, $J = 7.1$ Hz, 3H) ppm.

^{13}C NMR (CDCl_3 , 126 MHz): δ 165.6, 160.9, 152.5, 142.3, 135.1, 132.3, 131.7 (q, $J = 39.9$ Hz), 122.4, 119.7 (q, $J = 271.2$ Hz), 115.9, 63.7 (q, $J = 3.5$ Hz), 61.4, 32.4, 31.6, 14.2 ppm.

^{19}F NMR (377 MHz, CDCl_3): -55.6 ppm.

HRMS Calculated for $[\text{C}_{15}\text{H}_{13}\text{ClF}_3\text{N}_3\text{O}_2+\text{H}]^+$: 360.0721, Found: 360.0717.

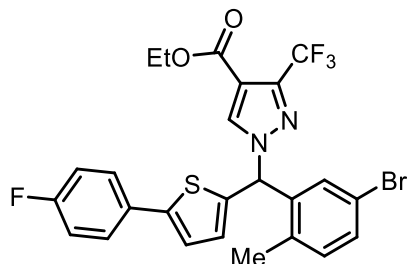
30a-2: Yield = 4.0 mg (6%) of light-yellow liquid. TLC (pentane:EtOAc, 9:1 v/v): $R_f = 0.16$.

^1H NMR (CDCl_3+DCM , 400 MHz): δ 7.89 (s, 1H), 7.62 (d, $J = 8.0$ Hz, 1H), 7.26 (d, $J = 8.3$ Hz, 3H), 6.05 (dd, $J = 8.6, 4.9$ Hz, 1H), 4.33 (qd, $J = 7.1, 1.7$ Hz, 2H), 3.24 (ddd, $J = 15.4, 9.0, 5.7$ Hz, 1H), 2.99 (ddd, $J = 16.3, 8.8, 5.2$ Hz, 1H), 2.77 (dtd, $J = 14.3, 8.7, 5.8$ Hz, 1H), 2.48 (ddt, $J = 14.1, 9.6, 5.1$ Hz, 1H), 1.35 (t, $J = 7.1$ Hz, 3H) ppm.

^{13}C NMR (CDCl_3 , 126 MHz): δ 161.1, 160.1, 150.7, 142.2, 136.4, 135.7, 131.7 (q, $J = 39.9$ Hz), 124.3, 119.7 (q, $J = 271.2$ Hz), 115.9, 65.52 (q, $J = 3.9$ Hz), 61.1, 31.7, 27.9, 14.1 ppm.

^{19}F NMR (377 MHz, CDCl_3): -55.7 ppm.

HRMS Calculated for $[\text{C}_{15}\text{H}_{13}\text{ClF}_3\text{N}_3\text{O}_2+\text{Na}]^+$: 382.0541, Found: 382.0538.



Ethyl 1-((5-bromo-2-methylphenyl)(5-(4-fluorophenyl)thiophen-2-yl)methyl)-3-(trifluoromethyl)-1H-pyrazole-4-carboxylate, **3pa'**

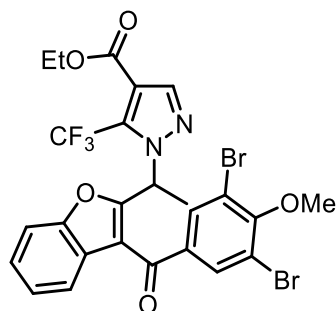
Reaction run using 2-(5-bromo-2-methylbenzyl)-5-(4-fluorophenyl)thiophene **1p** (68.6 mg, 0.2 mmol, 1.0 equiv), ethyl 3-(trifluoromethyl)-1H-pyrazole-4-carboxylate **2a** (104.1 mg, 0.50 mmol, 2.5 equiv), and tetrabutylammonium chloride (5.6 mg, 0.02 mmol, 0.1 equiv) following the general procedure II (glass vial) at 30 °C. Yield = 101.6 mg (90%) of yellow solid. TLC (pentane:EtOAc, 9:1 v/v): R_f = 0.56. Mp: 115–118 °C.

^1H NMR (CDCl_3 , 500 MHz): 7.94 (s, 1H), 7.57 – 7.49 (m, 2H), 7.43 (dd, J = 8.1, 2.1 Hz, 1H), 7.15 (d, J = 3.7 Hz, 1H), 7.11 (d, J = 8.2 Hz, 1H), 7.08 (t, J = 8.6 Hz, 2H), 7.02 (s, 1H), 6.85 (d, J = 2.0 Hz, 1H), 6.80 (dd, J = 3.8, 0.9 Hz, 1H), 4.33 (q, J = 7.1 Hz, 2H), 2.23 (s, 3H), 1.35 (t, J = 7.1 Hz, 3H) ppm.

^{13}C NMR (CDCl_3 , 126 MHz): 162.7 (d, J = 248.6 Hz), 160.8, 146.0, 142.3 (q, J = 38.6 Hz), 138.2, 137.4, 135.5, 134.87, 132.8, 132.1, 130.0, 129.7 (d, J = 3.4 Hz), 128.7, 127.7 (d, J = 8.2 Hz), 123.1, 120.4, 120.2 (q, J = 270.0 Hz), 116.1 (d, J = 21.9 Hz), 113.6, 63.1, 61.2, 18.8, 14.1 ppm.

^{19}F NMR (CDCl_3 , 377 MHz): -62.0, -113.2 ppm.

HRMS Calculated for $[\text{C}_{25}\text{H}_{19}\text{BrF}_4\text{N}_2\text{O}_2\text{S}+\text{NH}_4]^+$: 584.0625, Found: 584.0617.



Ethyl 1-(1-(3-(3,5-dibromo-4-methoxybenzoyl)benzofuran-2-yl)ethyl)-5-(trifluoromethyl)-1H-pyrazole-4-carboxylate, **3qa**

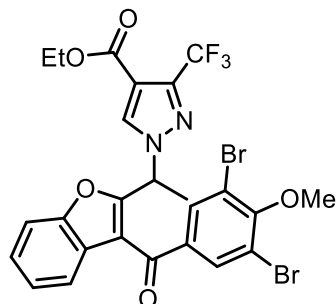
Reaction run using benzbromarone methyl ether **1q** (87.6 mg, 0.2 mmol, 1.0 equiv), ethyl 3-(trifluoromethyl)-1H-pyrazole-4-carboxylate **2a** (104.1 mg, 0.50 mmol, 2.5 equiv), and tetrabutylammonium chloride (5.6 mg, 0.02 mmol, 0.1 equiv) following the general procedure I (pressure tube). Yield = 99.0 mg (77%) of pale-yellow semisolid. TLC (pentane:EtOAc, 9:1 v/v): R_f = 0.42.

^1H NMR (CDCl_3 , 500 MHz): δ 7.99 (s, 1H), 7.94 (s, 2H), 7.60 (dt, J = 8.5, 0.9 Hz, 1H), 7.39 (ddd, J = 8.4, 7.0, 1.5 Hz, 1H), 7.27 (td, J = 7.5, 7.1, 0.8 Hz, 2H), 7.23 (dd, J = 8.0, 0.7 Hz, 1H), 6.37 (q, J = 6.9 Hz, 1H), 4.31 (qd, J = 7.2, 1.1 Hz, 2H), 3.98 (s, 3H), 2.08 (d, J = 6.9 Hz, 3H), 1.34 (t, J = 7.1 Hz, 3H) ppm.

^{13}C NMR (CDCl_3 , 126 MHz): δ 187.4, 160.9, 158.8, 158.3, 154.0, 141.9, 136.1, 133.7, 131.4 (q, J = 40.0 Hz), 126.0, 125.2, 124.4, 121.4, 119.4 (q, J = 271.3 Hz), 118.7, 117.1, 116.3 (q, J = 1.3 Hz), 112.2, 61.2, 60.9, 54.1 (q, J = 3.6 Hz), 19.5, 14.1 ppm.

^{19}F NMR (377 MHz, CDCl_3): -56.4 ppm.

HRMS Calculated for $[\text{C}_{25}\text{H}_{19}\text{Br}_2\text{F}_3\text{N}_2\text{O}_5+\text{H}]^+$: 642.9686, Found: 642.9687.



Ethyl 1-(1-(3-(3,5-dibromo-4-methoxybenzoyl)benzofuran-2-yl)ethyl)-3-(trifluoromethyl)-1H-pyrazole-4-carboxylate, **3qa'**

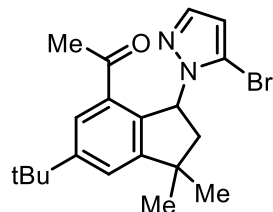
Reaction run using benzbromarone methyl ether **1q** (87.6 mg, 0.2 mmol, 1.0 equiv), ethyl 3-(trifluoromethyl)-1H-pyrazole-4-carboxylate **2a** (104.1 mg, 0.50 mmol, 2.5 equiv), and $\text{BF}_3 \cdot \text{Et}_2\text{O}$ (2.5 μL , 0.02 mmol, 0.1 equiv) following the general procedure I (pressure tube) at 60 °C. Yield = 58.0 mg (45%) of pale-yellow semisolid. TLC (pentane:EtOAc, 4:1 v/v): $R_f = 0.56$. Mp: 152-155 °C.

^1H NMR (CDCl_3 , 500 MHz): δ 8.31 (s, 1H), 8.01 (s, 2H), 7.59 (dt, $J = 8.4, 0.9$ Hz, 1H), 7.42 (ddd, $J = 8.5, 4.7, 3.8$ Hz, 1H), 7.30 (t, $J = 1.0$ Hz, 1H), 7.29 (d, $J = 0.8$ Hz, 1H), 6.06 (q, $J = 7.1$ Hz, 1H), 4.32 (q, $J = 7.1$ Hz, 2H), 4.00 (s, 3H), 2.06 (d, $J = 7.1$ Hz, 3H), 1.35 (t, $J = 7.1$ Hz, 3H) ppm.

^{13}C NMR (CDCl_3 , 126 MHz): δ 187.3, 160.8, 158.5, 158.2, 154.0, 141.7 (q, $J = 38.7$ Hz), 135.9, 134.8, 133.9, 126.3, 125.2, 124.6, 121.6, 120.3 (q, $J = 269.9$ Hz), 118.8, 117.7, 113.6, 112.2, 61.0, 60.9, 55.0, 18.8, 14.1 ppm.

^{19}F NMR (377 MHz, CDCl_3): -62.0 ppm.

HRMS Calculated for $[\text{C}_{25}\text{H}_{19}\text{Br}_2\text{F}_3\text{N}_2\text{O}_5 + \text{H}]^+$: 642.9686, Found: 642.9687.

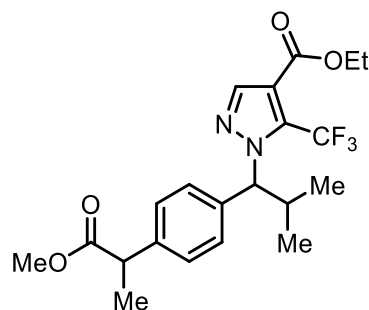


1-(3-(4-bromo-1H-pyrazol-1-yl)-6-(tert-butyl)-1,1-dimethyl-2,3-dihydro-1H-inden-4-yl)ethan-1-one, **3rb**
 Reaction run using celestolide **1r** (48.9 mg, 0.2 mmol, 1.0 equiv), 3-bromopyrazole **2b** (73.5 mg, 0.50 mmol, 2.5 equiv), and tetrabutylammonium chloride (5.6 mg, 0.02 mmol, 0.1 equiv) following the general procedure I (pressure tube). Yield = 54.2 mg (70%) of white solid. TLC (pentane:EtOAc, 9:1 v/v): R_f = 0.46. Mp: 88-90 °C

^1H NMR (CDCl_3 , 500 MHz): 7.63 (s, 1H), 7.42 (d, J = 1.8 Hz, 1H), 7.36 (d, J = 1.9 Hz, 1H), 6.40 (dd, J = 8.2, 6.5 Hz, 1H), 6.26 (d, 1H), 2.53 (dd, J = 13.1, 8.3 Hz, 1H), 2.35 (s, 3H), 2.09 (dd, J = 13.1, 6.5 Hz, 1H), 1.42 (s, 3H), 1.37 (s, 9H), 1.32 (s, 3H) ppm.

^{13}C NMR (CDCl_3 , 126 MHz): 199.9, 154.2, 152.4, 139.6, 135.4, 135.1, 125.1, 123.0, 113.8, 107.6, 61.6, 49.3, 42.4, 34.9, 31.4, 30.3, 29.3, 27.6 ppm.

HRMS Calculated for $[\text{C}_{20}\text{H}_{25}\text{BrN}_2\text{O}+\text{H}]^+$: 389.1223, Found: 389.1220.



Ethyl 1-(1-(4-(1-methoxy-1-oxopropan-2-yl)phenyl)-2-methylpropyl)-5-(trifluoromethyl)-1H-pyrazole-4-carboxylate, **3sa**

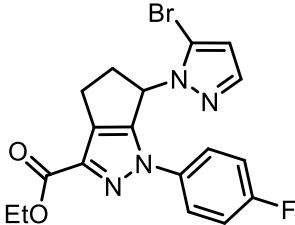
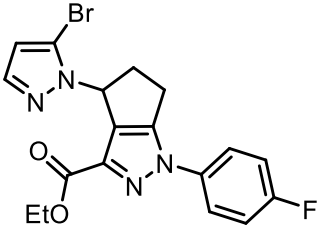
Reaction run using ibuprofen methyl ester **1s** (41.6 μL , 0.2 mmol, 1.0 equiv), ethyl 3-(trifluoromethyl)-1H-pyrazole-4-carboxylate **2a** (104.1 mg, 0.50 mmol, 2.5 equiv), and tetrabutylammonium chloride (5.6 mg, 0.02 mmol, 0.1 equiv) following the general procedure II (glass vial) at 40 °C. Yield = 55.7 mg (65%) of white solid. TLC (pentane:EtOAc, 9:1 v/v): R_f = 0.45. Mp: 83-86 °C.

^1H NMR (CDCl_3 , 500 MHz): 7.97 (s, 1H), 7.47 (d, J = 8.3 Hz, 2H), 7.25 (d, J = 8.3 Hz, 2H), 4.94 (d, J = 10.6 Hz, 1H), 4.29 (q, J = 7.1 Hz, 2H), 3.70 (q, J = 7.2 Hz, 1H), 3.65 (s, 3H), 2.97 – 2.86 (m, 1H), 1.47 (d, J = 7.2 Hz, 3H), 1.33 (t, J = 7.1 Hz, 3H), 0.81 (d, J = 6.8 Hz, 3H), 0.79 (d, J = 6.4 Hz, 3H) ppm.

^{13}C NMR (CDCl_3 , 126 MHz): 174.8 (d, J = 1.3 Hz), 161.3, 141.7, 140.6 (d, J = 1.0 Hz), 136.9, 131.9 (q, J = 39.8 Hz), 128.5, 127.6, 119.7 (q, J = 271.3 Hz), 115.1 (q, J = 1.5 Hz), 72.3 (q, J = 2.9 Hz), 61.1, 52.1, 45.1, 33.6, 20.0, 19.7, 18.5, 14.1 ppm.

^{19}F NMR (CDCl_3 , 377 MHz): -54.9 ppm.

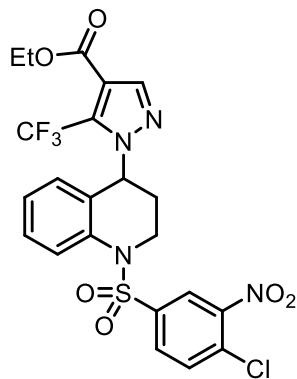
HRMS Calculated for $[\text{C}_{21}\text{H}_{25}\text{F}_3\text{N}_2\text{O}_4+\text{NH}_4]^+$: 444.2105, Found: 444.2101.

	
Ethyl 6-(5-bromo-1H-pyrazol-1-yl)-1-(4-fluorophenyl)-1,4,5,6-tetrahydrocyclopenta[<i>c</i>]pyrazole-3-carboxylate, 3tb-1	Ethyl 4-(5-bromo-1H-pyrazol-1-yl)-1-(4-fluorophenyl)-1,4,5,6-tetrahydrocyclopenta[<i>c</i>]pyrazole-3-carboxylate, 3tb-2

Reaction run ethyl 1-(4-fluorophenyl)-1,4,5,6-tetrahydrocyclopenta[*c*]pyrazole-3-carboxylate **1t** (54.5 mg, 0.2 mmol, 1.0 equiv), ethyl 3-(trifluoromethyl)-1H-pyrazole-4-carboxylate **2a** (104.1 mg, 0.50 mmol, 2.5 equiv), and tetrabutylammonium chloride (5.6 mg, 0.02 mmol, 0.1 equiv) following the general procedure I (pressure tube) and two regioisomers were isolated.

3tb-1: Yield = 36.0 mg (43%) of light yellow amorphous solid. TLC (pentane:EtOAc, 4:1 v/v): $R_f = 0.17$. $^1\text{H NMR}$ (CDCl_3 , 500 MHz): 7.99 – 7.61 (m, 2H), 7.50 (d, $J = 1.9$ Hz, 1H), 7.22 – 7.10 (m, 2H), 6.30 (d, $J = 1.9$ Hz, 1H), 6.09 (dd, $J = 8.4, 3.8$ Hz, 1H), 4.23 (qt, $J = 7.4, 3.8$ Hz, 2H), 3.38 (dddd, $J = 15.4, 8.9, 5.1, 1.3$ Hz, 1H), 3.22 (dtd, $J = 13.6, 8.6, 5.1$ Hz, 1H), 3.03 (ddd, $J = 15.4, 8.9, 4.4$ Hz, 1H), 2.80 (ddt, $J = 13.2, 8.6, 4.2$ Hz, 1H), 1.18 (t, $J = 7.1$ Hz, 3H) ppm. $^{13}\text{C NMR}$ (CDCl_3 , 126 MHz): 161.5 (d, $J = 247.6$ Hz), 161.4, 151.3, 140.6, 138.3, 135.7 (d, $J = 3.1$ Hz), 129.2, 122.2 (d, $J = 8.6$ Hz), 116.3 (d, $J = 23.0$ Hz), 112.4, 108.0, 60.9, 55.8, 39.5, 25.1, 14.2 ppm. $^{19}\text{F NMR}$ (CDCl_3 , 377 MHz): -114.2 ppm. HRMS Calculated for $[\text{C}_{18}\text{H}_{16}\text{BrFN}_4\text{O}_2 + \text{H}]^+$: 419.0513, Found: 419.0508.

3tb-2: Yield = 5.1 mg (6%) of light-yellow semisolid. TLC (pentane:EtOAc, 4:1 v/v): $R_f = 0.25$. $^1\text{H NMR}$ (CDCl_3 , 500 MHz): 7.45 (d, $J = 1.9$ Hz, 1H), 7.21 – 7.14 (m, 2H), 6.97 (t, $J = 8.6$ Hz, 2H), 6.24 (d, $J = 1.9$ Hz, 1H), 6.07 (q, $J = 4.4$ Hz, 1H), 4.42 (qd, $J = 7.1, 1.3$ Hz, 2H), 3.21 (qd, $J = 7.9, 3.8$ Hz, 2H), 3.02 – 2.89 (m, 1H), 2.86 – 2.74 (m, 1H), 1.40 (t, $J = 7.1$ Hz, 3H) ppm. $^{13}\text{C NMR}$ (CDCl_3 , 126 MHz): 162.2, 161.8 (d, $J = 248.1$ Hz), 146.6, 141.4, 138.4, 135.1, 134.7, 123.5 (d, $J = 8.7$ Hz), 116.0 (d, $J = 23.1$ Hz), 112.2, 108.9, 61.0, 56.9, 40.1, 22.4, 14.4 ppm. $^{19}\text{F NMR}$ (CDCl_3 , 377 MHz): -113.6 ppm. HRMS Calculated for $[\text{C}_{18}\text{H}_{16}\text{BrFN}_4\text{O}_2 + \text{H}]^+$: 419.0513, Found: 419.0509.



Ethyl 1-(1-((4-chloro-3-nitrophenyl)sulfonyl)-1,2,3,4-tetrahydroquinolin-4-yl)-5-(trifluoromethyl)-1H-pyrazole-4-carboxylate, **3ua**

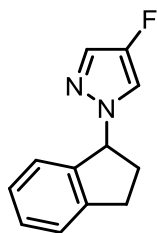
Reaction run using 1-(4-chloro-3-nitrobenzenesulfonyl)-1,2,3,4-tetrahydroquinoline **1u** (70.6 mg, 0.2 mmol, 1.0 equiv), ethyl 3-(trifluoromethyl)-1H-pyrazole-4-carboxylate **2a** (104.1 mg, 0.50 mmol, 2.5 equiv), and tetrabutylammonium chloride (5.6 mg, 0.02 mmol, 0.1 equiv) following the general procedure I (pressure tube). Yield = 47.0 mg (42%) of yellow semisolid. TLC (pentane:EtOAc, 4:1 v/v): R_f = 0.40.

^1H NMR (CDCl_3 , 500 MHz): 8.08 (d, J = 2.2 Hz, 1H), 7.90 (dd, J = 8.4, 1.1 Hz, 1H), 7.78 (dd, J = 8.5, 2.2 Hz, 1H), 7.71 (s, 1H), 7.63 (d, J = 8.5 Hz, 1H), 7.35 (ddd, J = 8.5, 7.2, 1.1 Hz, 2H), 7.14 (td, J = 7.6, 1.2 Hz, 1H), 6.68 (d, J = 7.4 Hz, 1H), 5.59 (t, J = 7.2 Hz, 1H), 4.33 (q, J = 7.1 Hz, 3H), 4.32 – 4.25 (m, 1H), 3.95 (ddd, J = 13.9, 9.3, 3.9 Hz, 1H), 2.22 – 2.09 (m, 2H), 1.35 (t, J = 7.1 Hz, 3H) ppm.

^{13}C NMR (CDCl_3 , 126 MHz) δ 160.7, 148.0, 142.1, 139.3, 136.2, 133.0, 132.1 (q, J = 39.8 Hz), 132.1, 131.2, 129.3, 128.5, 127.1, 126.5, 124.7, 124.7, 119.5 (q, J = 271.4 Hz), 115.7, 61.4, 56.9 (q, J = 3.2 Hz), 44.7, 28.5, 14.1 ppm.

^{19}F NMR (CDCl_3 , 377 MHz): -55.93 ppm.

HRMS Calculated for $[\text{C}_{22}\text{H}_{18}\text{ClF}_3\text{N}_4\text{O}_6\text{S}+\text{Na}]^+$: 581.0480, Found: 581.0478.



1-(2,3-dihydro-1H-inden-1-yl)-4-fluoro-1H-pyrazole, **3vc**

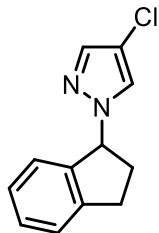
Reaction run using indane **1v** (24.5 μL , 0.2 mmol, 1.0 equiv), 4-fluoropyrazole **2c** (43.0 mg, 0.50 mmol, 2.5 equiv), and tetrabutylammonium chloride (5.6 mg, 0.02 mmol, 0.1 equiv) following the general procedure I (pressure tube) at 60 °C. Yield = 33.4 mg (82%) of yellow liquid. TLC (pentane:EtOAc, 9:1 v/v): R_f = 0.50.

^1H NMR (CDCl_3 , 400 MHz): 7.36 (d, J = 4.4 Hz, 1H), 7.34 – 7.28 (m, 2H), 7.22 (td, J = 7.0, 6.3, 2.3 Hz, 1H), 7.16 (d, J = 7.5 Hz, 1H), 7.07 (d, J = 4.7 Hz, 1H), 5.76 (t, J = 7.0 Hz, 1H), 3.12 (ddd, J = 16.0, 8.7, 5.2 Hz, 1H), 2.96 (ddd, J = 15.8, 8.4, 6.6 Hz, 1H), 2.68 (dtd, J = 13.5, 8.2, 5.2 Hz, 1H), 2.30 (ddt, J = 13.4, 8.7, 6.2 Hz, 1H) ppm.

^{13}C NMR (CDCl_3 , 101 MHz): 149.6 (d, J = 246.0 Hz), 143.8, 140.6, 129.0, 127.1, 126.1 (d, J = 13.5 Hz), 125.2, 124.8, 113.6 (d, J = 27.8 Hz), 68.0, 33.7, 30.4 ppm.

^{19}F NMR (CDCl_3 , 377 MHz): -176.5 ppm.

HRMS Calculated for $[\text{C}_{12}\text{H}_{11}\text{FN}_2+\text{H}]^+$: 203.0979, Found: 203.0978.



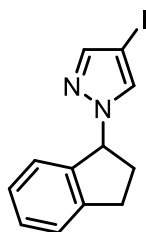
4-chloro-1-(2,3-dihydro-1H-inden-1-yl)-1H-pyrazole, **3vd**

Reaction run using indane **1v** (24.5 μ L, 0.2 mmol, 1.0 equiv), 4-chloropyrazole **2d** (51.3 mg, 0.50 mmol, 2.5 equiv), and tetrabutylammonium chloride (5.6 mg, 0.02 mmol, 0.1 equiv) following the general procedure I (pressure tube) at 60°C. Yield = 28.8 mg (66%) of colorless liquid. TLC (pentane:EtOAc, 9:1 v/v): R_f = 0.57.

^1H NMR (CDCl_3 , 500 MHz): 7.45 (s, 1H), 7.32 (m, 2H), 7.23 (ddd, J = 8.0, 6.5, 2.1 Hz, 1H), 7.17 (m, 2H), 5.81 (dd, J = 7.9, 5.6 Hz, 1H), 3.13 (ddd, J = 14.4, 8.6, 5.6 Hz, 1H), 2.96 (ddd, J = 15.7, 8.2, 6.4 Hz, 1H), 2.68 (dtd, J = 13.6, 8.2, 5.6 Hz, 1H), 2.33 (ddt, J = 11.9, 8.6, 5.9 Hz, 1H) ppm.

^{13}C NMR (CDCl_3 , 126 MHz): 144.0, 140.4, 137.7, 129.0, 127.1, 125.6, 125.2, 124.9, 109.8, 67.7, 33.7, 30.4 ppm.

HRMS Calculated for $[\text{C}_{12}\text{H}_{11}\text{ClN}_2\text{N}_2+\text{H}]^+$: 219.0684, Found: 219.0684.



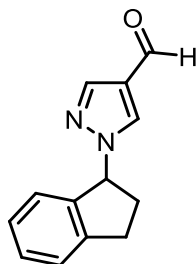
1-(2,3-dihydro-1H-inden-1-yl)-4-iodo-1H-pyrazole, **3ve**

Reaction run using indane **1v** (24.5 μ L, 0.2 mmol, 1.0 equiv), 4-iodopyrazole **2e** (97.0 mg, 0.50 mmol, 2.5 equiv), and tetrabutylammonium chloride (5.6 mg, 0.02 mmol, 0.1 equiv) following the general procedure I (pressure tube) at 60°C. Yield = 37.5 mg (60%) of light-yellow liquid. TLC (pentane:EtOAc, 9:1 v/v): R_f = 0.60.

^1H NMR (CDCl_3 , 400 MHz): 7.54 (s, 1H), 7.37 – 7.28 (m, 2H), 7.27 – 7.19 (m, 2H), 7.17 (d, J = 7.6 Hz, 1H), 5.87 (dd, J = 7.9, 5.5 Hz, 1H), 3.13 (ddd, J = 16.0, 8.6, 5.6 Hz, 1H), 2.96 (ddd, J = 15.7, 8.4, 6.1 Hz, 1H), 2.68 (dtd, J = 13.7, 8.2, 5.6 Hz, 1H), 2.33 (ddt, J = 14.1, 8.6, 5.8 Hz, 1H) ppm.

^{13}C NMR (CDCl_3 , 101 MHz): 144.4, 144.0, 140.4, 132.1, 129.1, 127.2, 125.2, 125.0, 67.5, 56.1, 33.9, 30.4 ppm.

HRMS Calculated for $[\text{C}_{12}\text{H}_{11}\text{IN}_2+\text{H}]^+$: 311.0040, Found: 311.0036.



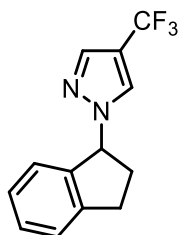
1-(2,3-dihydro-1H-inden-1-yl)-1H-pyrazole-4-carbaldehyde, **3vf**

Reaction run using indane **1v** (24.5 μ L, 0.2 mmol, 1.0 equiv), pyrazole-4-carboxaldehyde **2f** (48.0 mg, 0.50 mmol, 2.5 equiv), and tetrabutylammonium chloride (5.6 mg, 0.02 mmol, 0.1 equiv) following the general procedure I (pressure tube) at 60°C. Yield = 30.2 mg (71%) of light-yellow liquid. TLC (pentane:EtOAc, 9:1 v/v): R_f = 0.17.

^1H NMR (CDCl_3 , 400 MHz): 9.80 (s, 1H), 8.01 (s, 1H), 7.73 (s, 1H), 7.39 – 7.34 (m, 2H), 7.30 – 7.23 (m, 1H), 7.21 (d, J = 7.6 Hz, 1H), 5.90 (dd, J = 7.9, 4.9 Hz, 1H), 3.16 (ddd, J = 15.2, 8.5, 6.2 Hz, 1H), 3.00 (ddd, J = 16.1, 8.5, 5.4 Hz, 1H), 2.73 (dtd, J = 14.2, 8.2, 6.2 Hz, 1H), 2.41 (ddt, J = 13.7, 8.5, 5.2 Hz, 1H) ppm.

^{13}C NMR (CDCl_3 , 101 MHz): 184.1, 144.3, 141.0, 139.6, 131.1, 129.4, 127.3, 125.4, 125.0, 124.2, 67.5, 33.7, 30.4 ppm.

HRMS Calculated for $[\text{C}_{13}\text{H}_{12}\text{N}_2\text{O}+\text{H}]^+$: 213.1022, Found: 213.1021.



1-(2,3-dihydro-1H-inden-1-yl)-4-(trifluoromethyl)-1H-pyrazole, **3vg**

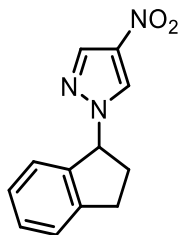
Reaction run using indane **1v** (24.5 μ L, 0.2 mmol, 1.0 equiv), 4-trifluoromethylpyrazole **2g** (68.0 mg, 0.50 mmol, 2.5 equiv), and tetrabutylammonium chloride (5.6 mg, 0.02 mmol, 0.1 equiv) following the general procedure I (pressure tube) at 60°C. Yield = 36.0 mg (71%) of colorless liquid. TLC (pentane:EtOAc, 9:1 v/v): R_f = 0.61.

^1H NMR (CDCl_3 , 500 MHz): 7.74 (s, 1H), 7.48 (s, 1H), 7.39 – 7.31 (m, 2H), 7.30 – 7.21 (m, 1H), 7.19 (d, J = 7.5 Hz, 1H), 5.89 (dd, J = 7.9, 5.3 Hz, 1H), 3.15 (ddd, J = 15.9, 8.6, 5.7 Hz, 1H), 2.99 (ddd, J = 15.9, 8.5, 5.9 Hz, 1H), 2.72 (dtd, J = 13.9, 8.2, 5.8 Hz, 1H), 2.38 (ddt, J = 13.9, 8.6, 5.6 Hz, 1H) ppm.

^{13}C NMR (CDCl_3 , 126 MHz): 144.1, 139.9, 137.1 (q, J = 2.8 Hz), 129.3, 127.3, 126.9 (q, J = 3.6 Hz), 125.3, 124.9, 122.7 (q, J = 265.9 Hz), 113.5 (q, J = 38.1 Hz), 67.5, 33.8, 30.4 ppm.

^{19}F NMR (CDCl_3 , 377 MHz): -56.3 ppm.

HRMS Calculated for $[\text{C}_{13}\text{H}_{11}\text{F}_3\text{N}_2+\text{H}]^+$: 253.0947, Found: 253.0944.

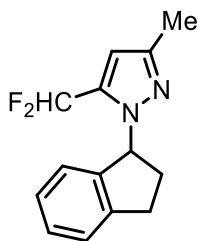


1-(2,3-dihydro-1H-inden-1-yl)-4-nitro-1H-pyrazole, **3vh**

Reaction run using indane **1v** (24.5 μ L, 0.2 mmol, 1.0 equiv), 4-nitropyrazole **2h** (56.5 mg, 0.50 mmol, 2.5 equiv), and tetrabutylammonium chloride (5.6 mg, 0.02 mmol, 0.1 equiv) following the general procedure I (pressure tube) at 60°C. Yield = 38.2 mg (83%) of dark yellow liquid. TLC (pentane:EtOAc, 9:1 v/v): R_f = 0.40.

^1H NMR (CDCl_3 , 400 MHz): 8.11 (s, 1H), 7.89 (s, 1H), 7.38 (d, J = 3.9 Hz, 2H), 7.29 (dt, J = 8.5, 4.2 Hz, 1H), 7.23 (d, J = 7.6 Hz, 1H), 5.87 (dd, J = 7.9, 4.6 Hz, 1H), 3.17 (ddd, J = 15.4, 8.5, 6.5 Hz, 1H), 3.02 (ddd, J = 16.2, 8.6, 5.1 Hz, 1H), 2.74 (dtd, J = 14.5, 8.2, 6.5 Hz, 1H), 2.41 (ddt, J = 13.5, 8.4, 4.9 Hz, 1H) ppm.

^{13}C NMR (CDCl_3 , 101 MHz): 144.4, 138.8, 136.0, 129.8, 127.5, 127.0, 125.5, 125.0, 68.3, 33.6, 30.3 ppm.
HRMS Calculated for $[\text{C}_{12}\text{H}_{11}\text{N}_3\text{O}_2+\text{Na}]^+$: 252.0743, Found: 252.0740.



5-(difluoromethyl)-1-(2,3-dihydro-1H-inden-1-yl)-3-methyl-1H-pyrazole, **3vi**

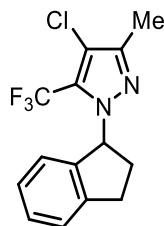
Reaction run using indane **1v** (24.5 μ L, 0.2 mmol, 1.0 equiv), 3-(difluoromethyl)-5-methyl-1H-pyrazole **2i** (66.0 mg, 0.50 mmol, 2.5 equiv), and tetrabutylammonium chloride (5.6 mg, 0.02 mmol, 0.1 equiv) following the general procedure I (pressure tube) in DCM. Yield = 25.7 mg (52%) of white solid. TLC (pentane:EtOAc, 9:1 v/v): R_f = 0.47. Mp: 75-77 °C.

^1H NMR (CDCl_3 , 500 MHz): 7.29 (d, J = 7.5 Hz, 1H), 7.25 (t, J = 7.3 Hz, 1H), 7.16 (t, J = 7.3 Hz, 1H), 6.99 (d, J = 7.6 Hz, 1H), 6.65 (t, J = 54.1 Hz, 1H), 6.28 (s, 1H), 5.93 (t, J = 7.9 Hz, 1H), 3.23 (ddd, J = 15.9, 9.1, 3.5 Hz, 1H), 2.97 (dt, J = 16.2, 8.3 Hz, 1H), 2.70 – 2.62 (m, 1H), 2.57 (dq, J = 13.1, 8.3 Hz, 1H), 2.22 (s, 3H) ppm.

^{13}C NMR (CDCl_3 , 126 MHz): 148.3, 143.3, 141.3, 136.1 (t, J = 26.0 Hz), 128.4, 126.8, 125.1, 124.1, 108.8 (t, J = 235.5 Hz), 106.4, 65.2, 32.9, 30.5, 13.6 ppm.

^{19}F NMR (CDCl_3 , 377 MHz): -109.1 (d, J = 307.2 Hz), -111.7 (d, J = 307.2 Hz) ppm.

HRMS Calculated for $[\text{C}_{14}\text{H}_{14}\text{F}_2\text{N}_2+\text{H}]^+$: 249.1198, Found: 249.1193.



4-chloro-1-(2,3-dihydro-1H-inden-1-yl)-3-methyl-5-(trifluoromethyl)-1H-pyrazole, **3vj**

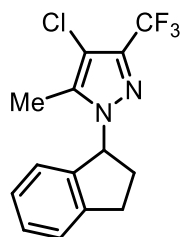
Reaction run using indane **1v** (24.5 μ L, 0.2 mmol, 1.0 equiv), 4-Chloro-3-trifluoromethyl-5-(methyl) pyrazole **2j** (92.3 mg, 0.50 mmol, 2.5 equiv), and tetrabutylammonium chloride (5.6 mg, 0.02 mmol, 0.1 equiv) following the general procedure I (pressure tube) in DCM. Yield = 32.7 mg (55%) of colorless liquid. TLC (pentane:Et₂O, 20:1 v/v): R_f = 0.56.

¹H NMR (CDCl₃, 500 MHz): 7.30 (d, J = 7.5 Hz, 1H), 7.30 – 7.25 (m, 1H), 7.18 (t, J = 7.3 Hz, 1H), 7.00 (d, J = 7.6 Hz, 1H), 5.89 (t, J = 7.4 Hz, 1H), 3.26 (ddd, J = 15.7, 9.0, 4.3 Hz, 1H), 2.97 (dt, J = 15.8, 7.9 Hz, 1H), 2.62 (dtt, J = 12.4, 8.5, 4.2 Hz, 1H), 2.54 (ddd, J = 13.1, 6.7, 1.7 Hz, 1H), 2.17 (s, 3H) ppm.

¹³C NMR (CDCl₃, 126 MHz): 146.9, 143.5, 140.6, 128.6, 127.8 (q, J = 37.6 Hz), 126.9, 125.1, 124.1, 120.0 (q, J = 270.2 Hz), 110.4, 65.7 (q, J = 2.3 Hz), 32.8, 30.6, 11.3 ppm.

¹⁹F NMR (CDCl₃, 377 MHz): -57.3 ppm.

HRMS Calculated for [C₁₄H₁₂ClF₃N₂+Na]⁺: 323.0533, Found: 323.0529.



4-chloro-1-(2,3-dihydro-1H-inden-1-yl)-5-methyl-3-(trifluoromethyl)-1H-pyrazole, **3vj'**

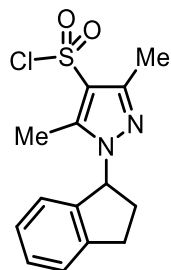
Reaction run using indane **1v** (24.5 μ L, 0.2 mmol, 1.0 equiv), 4-Chloro-3-trifluoromethyl-5-(methyl) pyrazole **2j** (92.3 mg, 0.50 mmol, 2.5 equiv), and BF₃•Et₂O (2.5 μ L, 0.02 mmol, 0.1 equiv) following the general procedure I (pressure tube) at 60°C. Yield = 27.9 mg (46%) of colorless liquid. TLC (pentane:EtOAc, 9:1 v/v): R_f = 0.63.

¹H NMR (CDCl₃, 500 MHz): 7.33 – 7.26 (m, 2H), 7.19 (td, J = 7.2, 1.6 Hz, 1H), 6.96 (d, J = 7.6 Hz, 1H), 5.90 (t, J = 7.9 Hz, 1H), 3.23 (ddd, J = 16.0, 9.2, 3.7 Hz, 1H), 3.01 (dt, J = 16.2, 8.2 Hz, 1H), 2.68 (dtd, J = 13.5, 8.5, 3.7 Hz, 1H), 2.50 (ddt, J = 13.4, 9.3, 7.8 Hz, 1H) ppm.

¹³C NMR (CDCl₃, 126 MHz): 143.4, 140.1, 137.7, 137.6 (q, J = 37.3 Hz), 129.0, 127.2, 125.4, 124.1, 120.9 (q, J = 269.3 Hz), 107.5, 66.6, 32.1, 30.7, 9.6 ppm.

¹⁹F NMR (CDCl₃, 377 MHz): -62.3 ppm.

HRMS Calculated for [C₁₄H₁₂ClF₃N₂+H]⁺: 301.0714, Found: 301.0710.



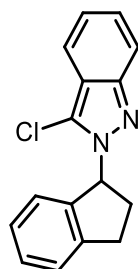
1-(2,3-dihydro-1H-inden-1-yl)-3,5-dimethyl-1H-pyrazole-4-sulfonyl chloride, **3vk**

Reaction run using indane **1v** (24.5 μ L, 0.2 mmol, 1.0 equiv), 3,5-dimethyl-1H-pyrazole-4-sulfonyl chloride **2k** (97.3 mg, 0.50 mmol, 2.5 equiv), and tetrabutylammonium chloride (5.6 mg, 0.02 mmol, 0.1 equiv) following the general procedure I (pressure tube) in DCM. Yield = 32.7 mg (53%) of white solid. TLC (pentane:EtOAc, 9:1 v/v): R_f = 0.37. Mp: 69-71 $^{\circ}$ C.

^1H NMR (CDCl_3 , 500 MHz): 7.33 (d, J = 7.5 Hz, 1H), 7.30 (t, J = 7.4 Hz, 1H), 7.20 (t, J = 7.3 Hz, 1H), 6.95 (d, J = 7.6 Hz, 1H), 5.83 (t, J = 7.7 Hz, 1H), 3.28 (ddd, J = 16.0, 9.0, 3.9 Hz, 1H), 3.02 (dt, J = 16.0, 8.1 Hz, 1H), 2.66 (m, 1H), 2.63 (s, 3H), 2.57 (dq, J = 13.2, 7.6 Hz, 1H), 2.42 (s, 3H) ppm.

^{13}C NMR (CDCl_3 , 126 MHz): 148.4, 143.4, 142.9, 139.9, 128.9, 127.1, 125.4, 123.8, 121.6, 64.2, 32.1, 30.7, 13.3, 10.9 ppm.

HRMS Calculated for $[\text{C}_{14}\text{H}_{15}\text{ClN}_2\text{O}_2\text{S}+\text{H}]^+$: 311.0616, Found: 311.0609.



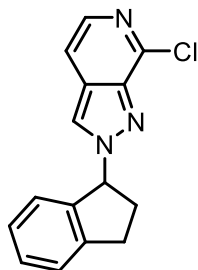
3-chloro-2-(2,3-dihydro-1H-inden-1-yl)-2H-indazole, **3vl**

Reaction run using indane **1v** (24.5 μ L, 0.2 mmol, 1.0 equiv), 3-chloroindazole **2l** (38.2 mg, 0.50 mmol, 2.5 equiv), and tetrabutylammonium chloride (5.6 mg, 0.02 mmol, 0.1 equiv) following the general procedure I (pressure tube) at 60 $^{\circ}$ C. Yield = 17.2 mg (32%) of colorless semisolid. TLC (pentane:EtOAc, 9:1 v/v): R_f = 0.71.

^1H NMR (CDCl_3 , 500 MHz): 7.68 (d, J = 8.1 Hz, 1H), 7.35 (d, J = 7.5 Hz, 1H), 7.31 (d, J = 7.3 Hz, 1H), 7.28 (d, J = 7.2 Hz, 1H), 7.18 (t, J = 7.5 Hz, 1H), 7.14 (t, J = 7.5 Hz, 1H), 7.07 (d, J = 8.5 Hz, 1H), 6.99 (d, J = 7.6 Hz, 1H), 6.22 (t, J = 7.9 Hz, 1H), 3.27 (ddd, J = 15.9, 9.1, 3.4 Hz, 2H), 3.06 (dt, J = 16.2, 8.3 Hz, 1H), 2.73 (ddt, J = 16.8, 8.4, 4.2 Hz, 2H), 2.56 (dq, J = 13.3, 8.2 Hz, 1H) ppm.

^{13}C NMR (CDCl_3 , 126 MHz): 143.3, 140.8, 140.3, 133.0, 128.6, 127.2, 126.9, 125.2, 124.4, 121.8, 121.2, 112.0, 110.1, 65.3, 32.1, 30.6 ppm.

HRMS Calculated for $[\text{C}_{16}\text{H}_{13}\text{ClN}_2+\text{H}]^+$: 269.0840, Found: 269.0838.



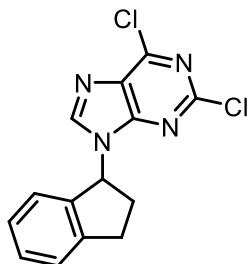
7-chloro-1-(2,3-dihydro-1H-inden-1-yl)-1H-pyrazolo[3,4-c]pyridine, **3vm**

Reaction run using indane **1v** (24.5 μ L, 0.2 mmol, 1.0 equiv), 7-chloro-1H-pyrazolo[3,4-c]pyridine **2m** (76.8 mg, 0.50 mmol, 2.5 equiv), and tetrabutylammonium chloride (5.6 mg, 0.02 mmol, 0.1 equiv) following the general procedure I (pressure tube) at 60°C. Yield = 16.0 mg (30%) of yellow semisolid. TLC (DCM:MeOH, 19:1 v/v): R_f = 0.60.

^1H NMR (CDCl_3 , 500 MHz): 7.90 (d, J = 5.8 Hz, 1H), 7.70 (s, 1H), 7.44 – 7.37 (m, 2H), 7.36 (d, J = 6.0 Hz, 1H), 7.31 – 7.22 (m, 3H), 6.31 (dd, J = 8.1, 4.7 Hz, 1H), 3.21 (ddd, J = 15.3, 8.4, 6.4 Hz, 1H), 3.07 (ddd, J = 16.2, 8.6, 5.2 Hz, 1H), 2.90 (dtd, J = 14.5, 8.3, 6.3 Hz, 1H), 2.50 (ddt, J = 13.6, 8.6, 5.0 Hz, 1H) ppm.

^{13}C NMR (CDCl_3 , 126 MHz): 144.5, 142.9, 142.9, 139.5, 137.2, 129.7, 127.5, 125.6, 125.5, 125.3, 122.3, 113.6, 69.5, 34.7, 30.5 ppm.

HRMS Calculated for $[\text{C}_{15}\text{H}_{12}\text{ClN}_3+\text{Na}]^+$: 292.0612, Found: 292.0607.



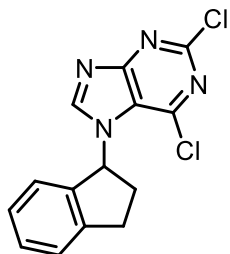
2,6-dichloro-9-(2,3-dihydro-1H-inden-1-yl)-9H-purine, **3vn**

Reaction run using indane **1v** (24.5 μ L, 0.2 mmol, 1.0 equiv), 2,6-dichloropurine **2n** (94.5 mg, 0.50 mmol, 2.5 equiv), and tetrabutylammonium chloride (5.6 mg, 0.02 mmol, 0.1 equiv) following the general procedure I (pressure tube) in DCM. Yield = 21.5 mg (35%) of white solid. TLC (pentane:EtOAc, 4:1 v/v): R_f = 0.26. Mp: 140-143 °C. **3vn'** (13.9 mg, 23%) was also isolated in this reaction.

^1H NMR (CDCl_3 , 400 MHz): 7.79 (s, 1H), 7.46 – 7.35 (m, 2H), 7.27 (d, J = 7.7 Hz, 1H), 7.16 (d, J = 7.6 Hz, 1H), 6.25 (dd, J = 7.8, 5.5 Hz, 1H), 3.22 (ddd, J = 14.7, 8.5, 5.9 Hz, 1H), 3.10 (ddd, J = 16.0, 8.2, 6.4 Hz, 1H), 2.87 (dtd, J = 13.9, 8.1, 5.8 Hz, 1H), 2.28 (ddt, J = 14.0, 8.5, 5.7 Hz, 1H) ppm.

^{13}C NMR (CDCl_3 , 101 MHz): 153.2, 153.0, 151.8, 144.3, 144.1, 138.7, 131.0, 129.8, 127.7, 125.6, 124.6, 59.9, 34.1, 30.5 ppm.

HRMS Calculated for $[\text{C}_{14}\text{H}_{10}\text{Cl}_2\text{N}_4+\text{H}]^+$: 305.0355, Found: 305.0353.

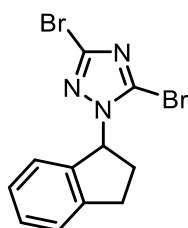


2,6-dichloro-7-(2,3-dihydro-1H-inden-1-yl)-7H-purine, **3vn'**

Reaction run using indane **1v** (24.5 μ L, 0.2 mmol, 1.0 equiv), 2,6-dichloropurine **2n** (94.5 mg, 0.50 mmol, 2.5 equiv), and $\text{BF}_3 \cdot \text{Et}_2\text{O}$ (2.5 μ L, 0.02 mmol, 0.1 equiv) following the general procedure I (pressure tube) at 60°C. Yield = 38.5 mg (63%) of white solid. TLC (pentane:EtOAc, 4:1 v/v): R_f = 0.11. Mp: 167-170 °C. ^1H NMR (CDCl_3 , 400 MHz): 7.79 (s, 1H), 7.54 – 7.41 (m, 2H), 7.36 (dt, J = 8.3, 4.0 Hz, 1H), 7.31 (d, J = 7.7 Hz, 1H), 6.47 (dd, J = 7.6, 4.2 Hz, 1H), 3.36 – 3.00 (m, 2H), 2.87 (dq, J = 15.1, 7.7 Hz, 1H), 2.28 (ddt, J = 13.1, 8.4, 4.6 Hz, 1H) ppm.

^{13}C NMR (CDCl_3 , 101 MHz): 164.0, 157.9, 153.2, 148.4, 144.7, 143.8, 137.5, 130.3, 128.0, 125.9, 125.2, 62.8, 35.5, 30.1 ppm.

HRMS Calculated for $[\text{C}_{14}\text{H}_{10}\text{Cl}_2\text{N}_4+\text{Na}]^+$: 327.0175, Found: 327.0173.

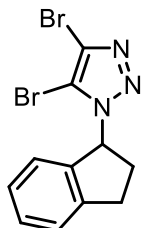


3,5-dibromo-1-(2,3-dihydro-1H-inden-1-yl)-1H-1,2,4-triazole, **3vo**

Reaction run using indane **1v** (24.5 μ L, 0.2 mmol, 1.0 equiv), 3,5-dibromo-1H-1,2,4-triazole **2o** (113.4 mg, 0.50 mmol, 2.5 equiv), and tetrabutylammonium chloride (5.6 mg, 0.02 mmol, 0.1 equiv) following the general procedure I (pressure tube) at 60°C. Yield = 53.1 mg (77%) of white solid. TLC (pentane:EtOAc, 9:1 v/v): R_f = 0.52. Mp: 83-86 °C.

^1H NMR (CDCl_3+DCM , 500 MHz): 7.37 – 7.28 (m, 2H), 7.24 – 7.16 (m, 1H), 7.08 (d, J = 7.6 Hz, 1H), 6.01 (dd, J = 8.2, 6.0 Hz, 1H), 3.32 (ddd, J = 15.9, 8.9, 4.9 Hz, 1H), 3.01 (ddd, J = 15.6, 8.5, 6.6 Hz, 1H), 2.67 (dtd, J = 13.4, 8.4, 5.0 Hz, 1H), 2.56 (ddt, J = 13.2, 8.9, 6.3 Hz, 1H) ppm.

^{13}C NMR (CDCl_3 , 126 MHz): 143.8, 140.4, 139.2, 129.3, 129.0, 127.1, 125.3, 124.1, 64.9, 31.9, 30.7 ppm. HRMS Calculated for $[\text{C}_{11}\text{H}_9\text{Br}_2\text{N}_3+\text{H}]^+$: 341.9236, Found: 341.9233.

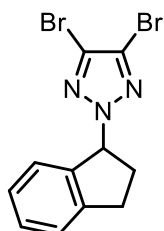


4,5-dibromo-1-(2,3-dihydro-1H-inden-1-yl)-1H-1,2,3-triazole, **3vp**

Reaction run using indane **1v** (24.5 μ L, 0.2 mmol, 1.0 equiv), 4,5-dibromo-1H-1,2,3-triazole **2p** (113.4 mg, 0.50 mmol, 2.5 equiv), and tetrabutylammonium chloride (5.6 mg, 0.02 mmol, 0.1 equiv) following the general procedure I (pressure tube) in DCM. Yield = 25.4 mg (37%) of colorless liquid. TLC (pentane:EtOAc, 9:1 v/v): R_f = 0.47. **3vp'** (59 mg, 8%) was also isolated in this reaction.

$^1\text{H NMR}$ (CDCl_3 , 500 MHz): 7.55 – 7.28 (m, 2H), 7.21 (t, J = 7.0 Hz, 1H), 7.11 (d, J = 7.7 Hz, 1H), 6.19 (dd, J = 8.4, 5.7 Hz, 1H), 3.38 (ddd, J = 15.8, 8.9, 5.3 Hz, 1H), 3.07 (ddd, J = 15.7, 8.6, 6.1 Hz, 1H), 2.77 (dtd, J = 13.9, 8.5, 5.4 Hz, 1H), 2.63 (ddt, J = 14.4, 8.8, 5.9 Hz, 1H) ppm.

$^{13}\text{C NMR}$ (CDCl_3 , 126 MHz): 144.0, 138.9, 129.4, 127.2, 125.3, 124.4, 123.4, 111.7, 66.1, 32.2, 30.9 ppm.
HRMS Calculated for $[\text{C}_{11}\text{H}_9\text{Br}_2\text{N}_3+\text{Na}]^+$: 363.9055, Found: 363.9053.

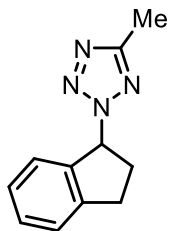


4,5-dibromo-2-(2,3-dihydro-1H-inden-1-yl)-2H-1,2,3-triazole, **3vp'**

Reaction run using indane **1v** (24.5 μ L, 0.2 mmol, 1.0 equiv), 4,5-dibromo-1H-1,2,3-triazole **2p** (113.4 mg, 0.50 mmol, 2.5 equiv), and $\text{BF}_3 \bullet \text{Et}_2\text{O}$ (2.5 μ L, 0.02 mmol, 0.1 equiv) following the general procedure I (pressure tube) at 60°C in DCM. Yield = 5.9 mg (8%) of colorless liquid. TLC (pentane:EtOAc, 9:1 v/v): R_f = 0.73.

$^1\text{H NMR}$ (CDCl_3 , 500 MHz): 7.34 – 7.30 (m, 1H), 7.24 – 7.18 (m, 1H), 6.10 (dd, J = 7.5, 5.9 Hz, 1H), 3.48 – 3.22 (m, 1H), 3.10 – 2.94 (m, 1H), 2.90 – 2.57 (m, 1H). ppm.

$^{13}\text{C NMR}$ (CDCl_3 , 126 MHz): 144.0, 138.9, 129.4, 127.2, 125.3, 124.4, 123.4, 111.7, 66.1, 32.2, 30.9 ppm.
HRMS Calculated for $[\text{C}_{11}\text{H}_9\text{Br}_2\text{N}_3+\text{Na}]^+$: 363.9052, Found: 363.9055.



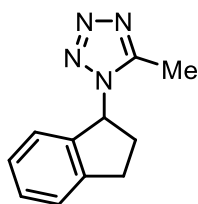
2-(2,3-dihydro-1H-inden-1-yl)-5-methyl-2H-tetrazole, **3vq**

Reaction run using indane **1v** (24.5 μ L, 0.2 mmol, 1.0 equiv), 5-methyl tetrazole **2q** (42.0 mg, 0.50 mmol, 2.5 equiv), and tetrabutylammonium chloride (5.6 mg, 0.02 mmol, 0.1 equiv) following the general procedure I (pressure tube) at 60°C in DCM. Yield = 20.0 mg (50%) of colorless liquid. TLC (pentane:Et₂O, 20:1 v/v): R_f = 0.30. **3vq'** (3.6 mg, 18%) was also isolated in this reaction.

¹H NMR (CDCl₃, 400 MHz): 7.56 – 7.29 (m, 2H), 7.24 – 6.93 (m, 2H), 6.36 (dd, *J* = 8.1, 5.2 Hz, 1H), 3.37 (ddd, *J* = 15.3, 8.6, 6.1 Hz, 1H), 3.07 (ddd, *J* = 15.9, 8.4, 5.8 Hz, 1H), 2.88 – 2.64 (m, 2H), 2.50 (s, 3H) ppm.

¹³C NMR (CDCl₃, 101 MHz): 163.1, 144.0, 139.2, 129.4, 127.1, 125.2, 124.8, 68.0, 32.1, 30.8, 11.0 ppm.

HRMS Calculated for [C₁₁H₁₂N₄+H]⁺: 201.1135, Found: 201.1132.



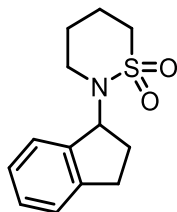
1-(2,3-dihydro-1H-inden-1-yl)-5-methyl-1H-tetrazole, **3vq'**

Reaction run using indane **1v** (24.5 μ L, 0.2 mmol, 1.0 equiv), 5-methyl tetrazole **2q** (42.0 mg, 0.50 mmol, 2.5 equiv), and BF₃•Et₂O (2.5 μ L, 0.02 mmol, 0.1 equiv) following the general procedure I (pressure tube) at 60°C. Yield = 16.7 mg (42%) of colorless liquid. TLC (pentane:Et₂O, 20:1 v/v): R_f = 0.30. **3vq** (15.2 mg, 37%) was also isolated in this reaction.

¹H NMR (CDCl₃, 600 MHz): 7.37 (d, *J* = 7.6 Hz, 1H), 7.34 (t, *J* = 7.3 Hz, 1H), 7.22 (t, *J* = 7.3 Hz, 0H), 6.99 (d, *J* = 7.7 Hz, 1H), 6.13 (dd, *J* = 8.4, 6.2 Hz, 1H), 3.33 (ddd, *J* = 16.2, 9.0, 4.8 Hz, 1H), 3.09 (ddd, *J* = 15.9, 8.8, 6.5 Hz, 1H), 2.81 (dtd, *J* = 13.5, 8.5, 4.8 Hz, 1H), 2.49 – 2.40 (m, 1H), 2.43 (s, 3H) ppm.

¹³C NMR (CDCl₃, 151 MHz): 150.9, 143.6, 138.5, 129.5, 127.4, 125.5, 124.1, 63.1, 32.6, 30.7, 9.5 ppm.

HRMS Calculated for [C₁₁H₁₂N₄+Na]⁺: 223.0954, Found: 223.0952.



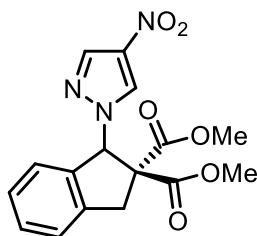
2-(2,3-dihydro-1H-inden-1-yl)-1,2-thiazinane 1,1-dioxide, **3vr**

Reaction run using indane **1v** (24.5 μ L, 0.2 mmol, 1.0 equiv), 1,4-propanesultam **2r** (67.5 mg, 0.50 mmol, 2.5 equiv), and tetrabutylammonium chloride (5.6 mg, 0.02 mmol, 0.1 equiv) following the general procedure I (pressure tube) in DCM. Yield = 23.5 mg (47%) of colorless liquid. TLC (pentane:EtOAc, 9:1 v/v): R_f = 0.13.

^1H NMR (CDCl_3 , 500 MHz): 7.40 – 7.30 (m, 1H), 7.28 – 7.19 (m, 3H), 5.67 (t, J = 8.0 Hz, 1H), 3.24 – 3.11 (m, 2H), 3.07 (ddd, J = 16.7, 8.8, 4.4 Hz, 1H), 3.03 – 2.90 (m, 2H), 2.85 (dt, J = 16.3, 8.4 Hz, 1H), 2.46 – 2.34 (m, 1H), 2.31 – 2.15 (m, 2H), 2.03 (dq, J = 13.3, 8.5 Hz, 1H), 1.64 (ddtq, J = 22.3, 13.6, 9.0, 4.1 Hz, 2H) ppm.

^{13}C NMR (CDCl_3 , 126 MHz): 143.6, 140.3, 128.1, 126.8, 124.9, 124.6, 59.7, 51.1, 43.8, 30.4, 29.3, 24.9, 24.2 ppm.

HRMS Calculated for $[\text{C}_{13}\text{H}_{17}\text{NO}_2\text{S}+\text{Na}]^+$: 274.0872, Found: 274.0868.



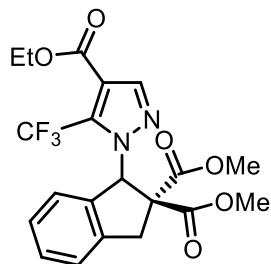
Dimethyl 1-(4-nitro-1H-pyrazol-1-yl)-1,3-dihydro-2H-indene-2,2-dicarboxylate, **3wh**

Reaction run using 2,2-dimethyl 1,3-dihydroindene-2,2-dicarboxylate **1w** (46.9 mg, 0.2 mmol, 1.0 equiv), 4-Nitropyrazole **2h** (56.0 mg, 0.50 mmol, 2.5 equiv), and tetrabutylammonium chloride (5.6 mg, 0.02 mmol, 0.1 equiv) following the general procedure I (pressure tube). Yield = 44.7 mg (65%) of yellow semisolid. TLC (pentane:EtOAc, 9:1 v/v): R_f = 0.10.

^1H NMR (CDCl_3 , 400 MHz): 8.03 (dd, J = 10.6, 0.6 Hz, 1H), 7.42 (td, J = 7.4, 1.2 Hz, 1H), 7.37 (d, J = 7.4 Hz, 1H), 7.32 (t, J = 7.6 Hz, 1H), 7.22 (d, J = 7.6 Hz, 1H), 6.60 (s, 1H), 4.09 (d, J = 16.8 Hz, 1H), 3.79 (s, 3H), 3.51 (s, 3H), 3.47 (d, J = 16.9 Hz, 1H) ppm.

^{13}C NMR (CDCl_3 , 101 MHz): 170.1, 167.6, 140.6, 136.3, 136.1, 135.9, 130.5, 129.4, 128.3, 125.23, 125.18, 71.3, 65.0, 53.6, 53.3, 38.8. ppm.

HRMS Calculated for $[\text{C}_{16}\text{H}_{15}\text{N}_3\text{O}_6\text{S}+\text{Na}]^+$: 368.0853, Found: 368.0846.



Dimethyl 1-(4-(ethoxycarbonyl)-5-(trifluoromethyl)-1*H*-pyrazol-1-yl)-1,3-dihydro-2*H*-indene-2,2-dicarboxylate, **3wa**

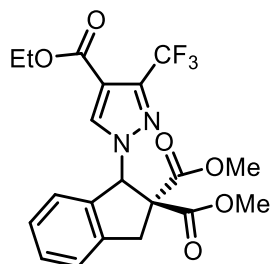
Reaction run using 2,2-dimethyl 1,3-dihydroindene-2,2-dicarboxylate **1w** (46.9 mg, 0.2 mmol, 1.0 equiv), ethyl 3-(trifluoromethyl)-1*H*-pyrazole-4-carboxylate **2a** (104.1 mg, 0.50 mmol, 2.5 equiv), and $\text{BF}_3 \cdot \text{Et}_2\text{O}$ (2.5 μL , 0.02 mmol, 0.1 equiv) following the general procedure I (pressure tube) at 60°C in DCM. Yield = 45.1 mg (51%) of yellow semisolid. TLC (pentane:EtOAc, 9:1 v/v): $R_f = 0.20$.

^1H NMR (CDCl_3 , 400 MHz): 7.79 (s, 1H), 7.41 – 7.29 (m, 2H), 7.25 – 7.16 (m, 2H), 6.82 (s, 1H), 4.39 (d, $J = 16.8$ Hz, 1H), 4.31 (q, $J = 7.1$ Hz, 2H), 3.76 (s, 3H), 3.51 (d, $J = 16.8$ Hz, 1H), 3.46 (s, 3H), 1.34 (t, $J = 7.1$ Hz, 3H) ppm.

^{13}C NMR (CDCl_3 , 101 MHz): 170.1, 167.4, 160.9, 142.6, 140.9, 138.4, 132.5 (q, $J = 39.9$ Hz), 129.9, 127.8, 125.0, 124.6, 119.6 (q, $J = 271.8$ Hz), 115.4, 68.4 (q, $J = 4.3$ Hz), 65.2, 61.2, 53.7, 53.0, 39.9, 14.1 ppm.

^{19}F NMR (CDCl_3 , 377 MHz): -56.6 ppm.

HRMS Calculated for $[\text{C}_{20}\text{H}_{19}\text{F}_3\text{N}_2\text{O}_6 + \text{H}]^+$: 441.1268, Found: 441.1262.



Dimethyl 1-(4-(ethoxycarbonyl)-3-(trifluoromethyl)-1*H*-pyrazol-1-yl)-1,3-dihydro-2*H*-indene-2,2-dicarboxylate, **3wa'**

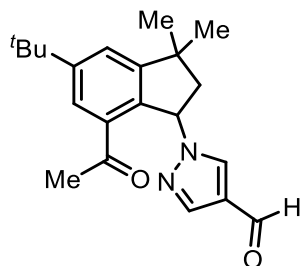
Reaction run using 2,2-dimethyl-1,3-dihydroindene-2,2-dicarboxylate **1w** (46.9 mg, 0.2 mmol, 1.0 equiv), ethyl 3-(trifluoromethyl)-1*H*-pyrazole-4-carboxylate **2a** (104.1 mg, 0.50 mmol, 2.5 equiv), and $\text{BF}_3 \cdot \text{Et}_2\text{O}$ (2.5 μL , 0.02 mmol, 0.1 equiv) following the general procedure I (pressure tube) at 60°C. Yield = 40.6 mg (46%) of white semisolid. TLC (pentane:EtOAc, 9:1 v/v): $R_f = 0.13$.

^1H NMR (CDCl_3 , 400 MHz): 7.79 (s, 1H), 7.41 – 7.29 (m, 2H), 7.25 – 7.16 (m, 2H), 6.82 (s, 1H), 4.39 (d, $J = 16.8$ Hz, 1H), 4.31 (q, $J = 7.1$ Hz, 2H), 3.76 (s, 3H), 3.51 (d, $J = 16.8$ Hz, 1H), 3.46 (s, 3H), 1.34 (t, $J = 7.1$ Hz, 3H) ppm.

^{13}C NMR (CDCl_3 , 101 MHz): 170.1, 167.4, 160.9, 142.6, 140.9, 138.4, 132.5 (q, $J = 39.9$ Hz), 129.9, 127.8, 125.0, 124.6, 119.6 (q, $J = 271.8$ Hz), 115.4, 68.4 (q, $J = 4.3$ Hz), 65.2, 61.2, 53.7, 53.0, 39.9, 14.1 ppm.

^{19}F NMR (CDCl_3 , 377 MHz): -56.6 ppm.

HRMS Calculated for $[\text{C}_{20}\text{H}_{19}\text{F}_3\text{N}_2\text{O}_6 + \text{H}]^+$: 441.1268, Found: 441.1262.



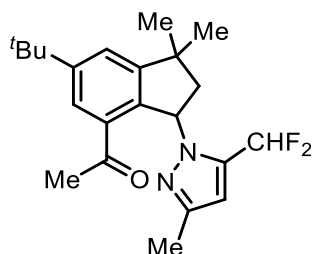
1-(7-acetyl-5-(tert-butyl)-3,3-dimethyl-2,3-dihydro-1H-inden-1-yl)-1H-pyrazole-4-carbaldehyde, **3rf**

Reaction run using celestolide **1r** (48.9 mg, 0.2 mmol, 1.0 equiv), pyrazole-4-carboxaldehyde **2f** (48.0 mg, 0.50 mmol, 2.5 equiv), and tetrabutylammonium chloride (5.6 mg, 0.02 mmol, 0.1 equiv) following the general procedure I (pressure tube) at 60°C. Yield = 61.0 mg (90%) of colorless semisolid. TLC (pentane:EtOAc, 4:1 v/v): $R_f = 0.29$.

^1H NMR (CDCl_3 , 500 MHz): 9.79 (s, 1H), 7.93 (s, 1H), 7.77 (d, $J = 1.8$ Hz, 1H), 7.74 (s, 1H), 7.48 (d, $J = 1.8$ Hz, 1H), 6.29 (dd, $J = 8.4, 3.9$ Hz, 1H), 2.54 (dd, $J = 13.8, 8.4$ Hz, 1H), 2.45 (s, 3H), 2.37 (dd, $J = 13.8, 3.9$ Hz, 1H), 1.40 (s, 10H), 1.34 (s, 3H), 1.30 (s, 3H) ppm.

^{13}C NMR (CDCl_3 , 126 MHz): 199.2, 184.3, 155.4, 153.8, 140.8, 134.4, 132.7, 126.2, 124.0, 123.1, 65.0, 49.0, 42.7, 35.1, 31.4, 30.3, 29.9, 27.8 ppm.

HRMS Calculated for $[\text{C}_{21}\text{H}_{26}\text{N}_2\text{O}_2 + \text{Na}]^+$: 361.1887, Found: 361.1880.



1-(6-(tert-butyl)-3-(5-(difluoromethyl)-3-methyl-1H-pyrazol-1-yl)-1,1-dimethyl-2,3-dihydro-1H-inden-4-yl)ethan-1-one, **3ri**

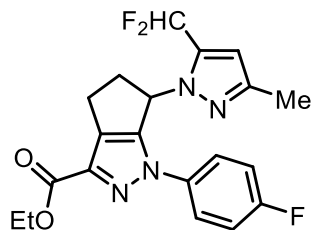
Reaction run using celestolide **1r** (48.9 mg, 0.2 mmol, 1.0 equiv), 3-(difluoromethyl)-5-methyl-1H-pyrazole **2i** (66.0 mg, 0.50 mmol, 2.5 equiv), and tetrabutylammonium chloride (5.6 mg, 0.02 mmol, 0.1 equiv) following the general procedure I (pressure tube) at 60°C in DCM. Yield = 38.7 mg (52%) of white solid. TLC (pentane:EtOAc, 9:1 v/v): $R_f = 0.56$. Mp: 113-116 °C.

^1H NMR (CDCl_3 , 400 MHz): 7.54 (d, $J = 1.8$ Hz, 1H), 7.39 (d, $J = 1.7$ Hz, 1H), 7.09 (dd, $J = 58.3, 53.1$ Hz, 1H), 6.19 (d, $J = 2.2$ Hz, 1H), 6.08 (t, $J = 7.9$ Hz, 1H), 2.51 (dd, $J = 12.9, 8.0$ Hz, 1H), 2.30 (s, 3H), 2.21 (dd, $J = 12.9, 7.9$ Hz, 1H), 2.14 (s, 3H), 1.47 (s, 3H), 1.36 (s, 9H), 1.27 (s, 3H) ppm.

^{13}C NMR (CDCl_3 , 101 MHz): 200.5, 153.8, 152.3, 147.4, 137.5 (dd, $J = 33.0, 24.4$ Hz), 135.7, 135.4, 124.4, 122.8, 109.8 (dd, $J = 235.3$ Hz, $J = 235.4$ Hz), 104.4 (dd, $J = 3.7, 2.4$ Hz), 61.9 (d, $J = 2.0$ Hz), 50.0, 42.1, 34.9, 31.5, 30.3, 28.8, 27.8, 13.6 ppm.

^{19}F NMR (CDCl_3 , 377 MHz): -106.96 (d, $J = 307.0$ Hz), -121.35 (d, $J = 307.0$ Hz) ppm.

HRMS Calculated for $[\text{C}_{22}\text{H}_{28}\text{F}_2\text{N}_2\text{O} + \text{Na}]^+$: 397.2062, Found: 297.2057.



Ethyl 6-(5-(difluoromethyl)-3-methyl-1H-pyrazol-1-yl)-1-(4-fluorophenyl)-1,4,5,6-tetrahydrocyclopenta[*c*]pyrazole-3-carboxylate, **3ti**

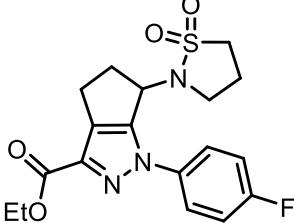
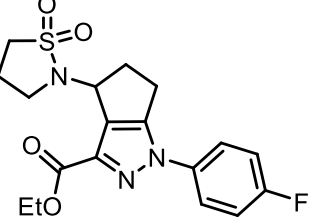
Reaction run using ethyl 1-(4-fluorophenyl)-1,4,5,6-tetrahydrocyclopenta[*c*]pyrazole-3-carboxylate **1t** (54.5 mg, 0.2 mmol, 1.0 equiv), 3-(difluoromethyl)-5-methyl-1H-pyrazole **2i** (66.0 mg, 0.50 mmol, 2.5 equiv), and tetrabutylammonium chloride (5.6 mg, 0.02 mmol, 0.1 equiv) following the general procedure I (pressure tube) at 50 °C in DCM. Yield = 33.6 mg (42%) of pale yellow amorphous solid. TLC (DCM:MeOH, 50:1 v/v): $R_f = 0.18$.

^1H NMR (CDCl_3 , 500 MHz): 7.72 – 7.65 (m, 2H), 7.20 – 7.13 (m, 2H), 6.99 (dd, $J = 56.5, 53.2$ Hz, 1H), 6.25 (d, $J = 1.9$ Hz, 1H), 5.86 (dd, $J = 8.6, 3.8$ Hz, 1H), 4.36 – 4.14 (m, 2H), 3.40 (dddd, $J = 15.1, 8.7, 5.1, 1.3$ Hz, 1H), 3.20 (dtd, $J = 13.6, 8.4, 5.0$ Hz, 1H), 2.99 (ddd, $J = 15.2, 8.6, 4.5$ Hz, 1H), 2.90 (ddt, $J = 13.2, 8.7, 4.2$ Hz, 1H), 2.21 (s, 3H), 1.19 (t, $J = 7.1$ Hz, 3H) ppm.

^{13}C NMR (CDCl_3 , 126 MHz): 161.7, 161.6 (d, $J = 247.6$ Hz), 151.5, 148.1, 138.2, 136.1 (dd, $J = 30.2, 25.0$ Hz), 135.7 (d, $J = 3.0$ Hz), 129.6, 122.3 (d, $J = 8.4$ Hz), 116.3 (d, $J = 23.1$ Hz), 109.2 (t, $J = 235.7$ Hz), 105.5 (t, $J = 3.8$ Hz), 61.0, 56.2 (d, $J = 2.4$ Hz), 39.8, 25.2, 14.1, 13.7 ppm.

^{19}F NMR (CDCl_3 , 377 MHz): -108.15 (d, $J = 307.6$ Hz), -114.20, -116.86 (d, $J = 307.8$ Hz) ppm.

HRMS Calculated for $[\text{C}_{20}\text{H}_{19}\text{F}_3\text{N}_4\text{O}_2 + \text{H}]^+$: 405.1533, Found: 405.1529.

	
Ethyl 4-(1,1-dioxidoisothiazolidin-2-yl)-1-(4-fluorophenyl)-1,4,5,6-tetrahydrocyclopenta[<i>c</i>]pyrazole-3-carboxylate, 3tt-1	Ethyl 4-(1,1-dioxidoisothiazolidin-2-yl)-1-(4-fluorophenyl)-1,4,5,6-tetrahydrocyclopenta[<i>c</i>]pyrazole-3-carboxylate, 3tt-2

Reaction run using ethyl 1-(4-fluorophenyl)-1,4,5,6-tetrahydrocyclopenta[*c*]pyrazole-3-carboxylate **1t** (54.5 mg, 0.2 mmol, 1.0 equiv), 1,3-propanesultam **2t** (50.0 μ L, 0.50 mmol, 2.5 equiv), and tetrabutylammonium chloride (5.6 mg, 0.02 mmol, 0.1 equiv) following the general procedure I (pressure tube) at 40 °C in DCM, and two regioisomers were isolated.

3tt-1: Yield = 39.0 mg (47%) of colorless semisolid. TLC (pentane:EtOAc, 1:2 v/v): R_f = 0.33.

^1H NMR (CDCl_3 , 500 MHz): 7.92 – 7.56 (m, 2H), 7.19 – 6.96 (m, 2H), 5.66 – 4.99 (m, 1H), 4.42 (qd, J = 7.1, 3.0 Hz, 2H), 3.36 – 3.11 (m, 5H), 3.03 – 2.89 (m, 2H), 2.85 (ddt, J = 13.6, 5.2, 2.8 Hz, 1H), 2.32 (dddd, J = 13.3, 9.0, 6.4, 2.6 Hz, 2H), 1.41 (t, J = 7.1 Hz, 3H). ppm.

^{13}C NMR (CDCl_3 , 126 MHz): 161.8, 161.6 (d, J = 247.9 Hz), 151.4, 139.0, 135.6 (d, J = 3.0 Hz), 128.4, 122.2 (d, J = 8.5 Hz), 116.4 (d, J = 23.0 Hz), 61.3, 51.3, 47.3, 42.7, 37.0, 25.2, 18.6, 14.4 ppm.

^{19}F NMR (CDCl_3 , 377 MHz): -113.9 ppm.

HRMS Calculated for $[\text{C}_{18}\text{H}_{20}\text{FN}_3\text{O}_4\text{S}+\text{H}]^+$: 394.1231, Found: 394.1226.

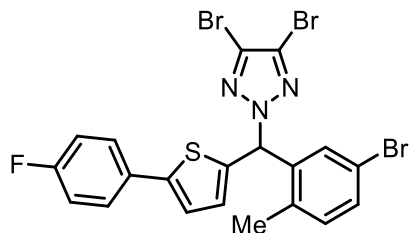
3tt-2: Yield = 4.0 mg (5%) of pale yellow amorphous solid. TLC (pentane:EtOAc, 1:1 v/v): R_f = 0.33.

^1H NMR (CDCl_3 , 500 MHz): 7.90 – 7.76 (m, 2H), 7.21 – 7.11 (m, 2H), 5.38 (dd, J = 8.1, 3.2 Hz, 1H), 4.42 (qd, J = 7.1, 1.4 Hz, 2H), 3.18 (dt, J = 9.1, 7.3 Hz, 1H), 3.11 (ddd, J = 12.7, 8.2, 6.8 Hz, 1H), 3.01 (dddd, J = 24.5, 13.6, 9.0, 7.1 Hz, 2H), 2.94 – 2.84 (m, 2H), 2.81 – 2.69 (m, 2H), 2.33 – 2.22 (m, 1H), 2.18 – 2.07 (m, 1H), 1.41 (t, J = 7.1 Hz, 3H) ppm.

^{13}C NMR (CDCl_3 , 126 MHz): 162.1, 161.7 (d, J = 247.8 Hz), 145.6, 138.2, 135.1 (d, J = 3.0 Hz), 134.6, 122.4 (d, J = 8.4 Hz), 116.2 (d, J = 23.0 Hz), 61.1, 51.1, 46.8, 40.7, 36.0, 22.8, 18.4, 14.1 ppm.

^{19}F NMR (CDCl_3 , 377 MHz): -114.1 ppm.

HRMS Calculated for $[\text{C}_{18}\text{H}_{20}\text{FN}_3\text{O}_4\text{S}+\text{H}]^+$: 394.1231, Found: 394.1229.



4,5-dibromo-2-((5-bromo-2-methylphenyl)(5-(4-fluorophenyl)thiophen-2-yl)methyl)-2H-1,2,3-triazole, **3pp'**

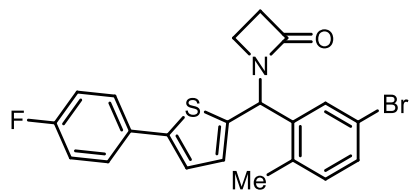
Reaction run using 2-(5-bromo-2-methylbenzyl)-5-(4-fluorophenyl)thiophene **1p** (68.6 mg, 0.2 mmol, 1.0 equiv), 4,5-Dibromo-1H-1,2,3-triazole **2p** (113.4 mg, 0.50 mmol, 2.5 equiv), and tetrabutylammonium chloride (5.6 mg, 0.02 mmol, 0.1 equiv) following the general procedure II (glass vial) procedure at 30 °C. Yield = 81.8 mg (70%) of colorless liquid. TLC (pentane:EtOAc, 9:1 v/v): $R_f = 0.51$.

^1H NMR (CDCl_3 , 500 MHz): 7.58 – 7.46 (m, 2H), 7.40 (d, $J = 7.4$ Hz, 2H), 7.20 (s, 1H), 7.09 (d, $J = 3.2$ Hz, 2H), 7.08 – 6.94 (m, 2 H), 6.84 (d, $J = 3.7$ Hz, 1H), 2.29 (s, 3H) ppm.

^{13}C NMR (CDCl_3 , 101 MHz): 162.6 (d, $J = 248.1$ Hz), 145.5, 137.6, 137.5, 134.6, 132.5, 132.1, 130.00, 129.95, 129.6, 127.6 (d, $J = 8.1$ Hz), 125.6, 122.8, 120.3, 116.0 (d, $J = 21.9$ Hz), 65.9, 18.9.

^{19}F NMR (CDCl_3 , 377 MHz): -113.6 ppm.

HRMS Calculated for $[\text{C}_{20}\text{H}_{13}\text{Br}_3\text{FN}_3\text{S}+\text{H}]^+$: 583.8437, Found: 583.8444.



4,5-dibromo-2-((5-bromo-2-methylphenyl)(5-(4-fluorophenyl)thiophen-2-yl)methyl)-2H-1,2,3-triazole, **3ps**

Reaction run using 2-(5-bromo-2-methylbenzyl)-5-(4-fluorophenyl)thiophene **1p** (68.6 mg, 0.2 mmol, 1.0 equiv), azetidin-2-one **2s** (35.0 mg, 0.50 mmol, 2.5 equiv), and tetrabutylammonium chloride (5.6 mg, 0.02 mmol, 0.1 equiv) following the general procedure II (glass vial) procedure at 30 °C. Yield = 68.5 mg (80%) of light-yellow liquid. TLC (pentane:EtOAc, 4:1 v/v): $R_f = 0.10$.

^1H NMR (CDCl_3 , 500 MHz): 7.57 – 7.48 (m, 2H), 7.41 (d, $J = 2.1$ Hz, 1H), 7.38 (dd, $J = 8.1, 2.1$ Hz, 1H), 7.15 – 7.06 (m, 2H), 7.06 (t, $J = 8.6$ Hz, 2H), 6.72 (d, $J = 3.8$ Hz, 1H), 6.43 (s, 1H), 3.38 (q, $J = 5.1, 4.5$ Hz, 1H), 3.24 (dt, $J = 5.7, 4.0$ Hz, 1H), 3.01 (t, $J = 4.2$ Hz, 2H), 2.29 (s, 3H) ppm.

^{13}C NMR (CDCl_3 , 101 MHz): 167.2, 162.5 (d, $J = 247.7$ Hz), 143.7, 140.7, 139.2, 135.1, 132.7, 131.3, 130.2 (d, $J = 3.5$ Hz), 129.9, 127.7, 127.4 (d, $J = 8.1$ Hz), 122.9, 119.8, 115.9 (d, $J = 21.8$ Hz), 53.8, 38.4, 36.1, 19.0 ppm.

^{19}F NMR (CDCl_3 , 471 MHz): -114.0 ppm.

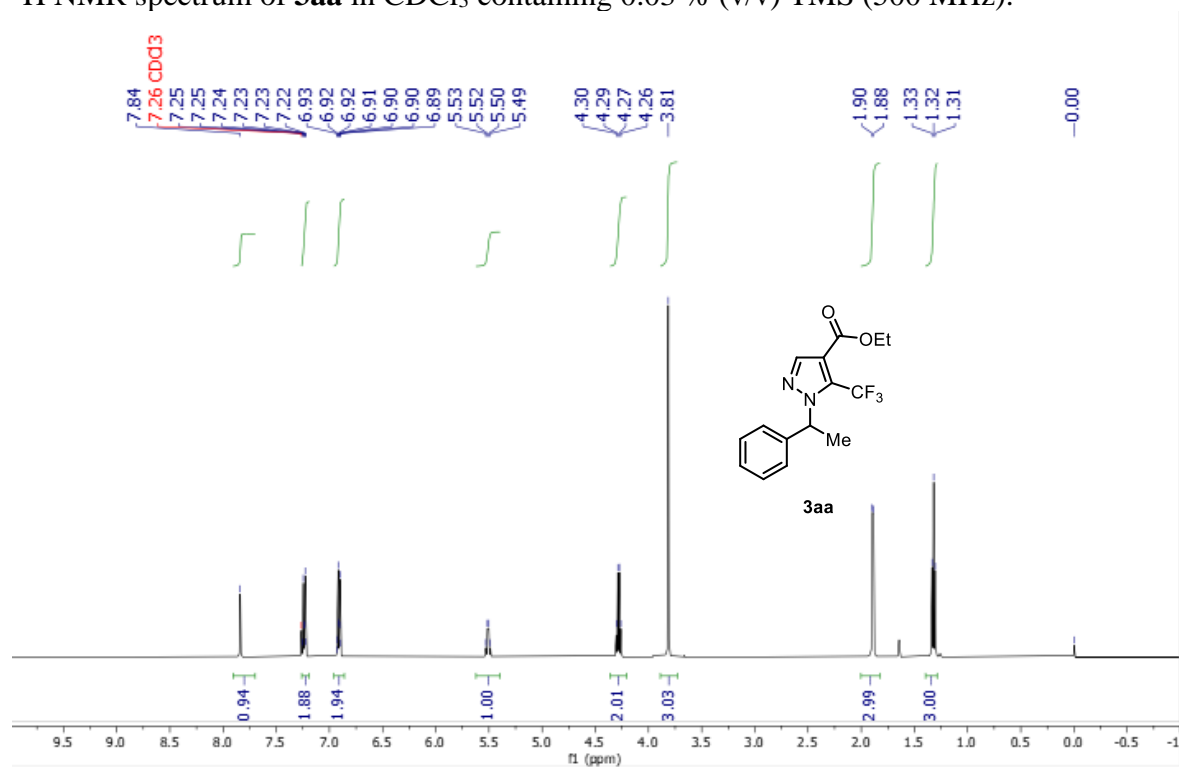
HRMS Calculated for $[\text{C}_{21}\text{H}_{17}\text{BrFNOS}+\text{H}]^+$: 452.0091, Found: 452.0089.

5D.IX. References

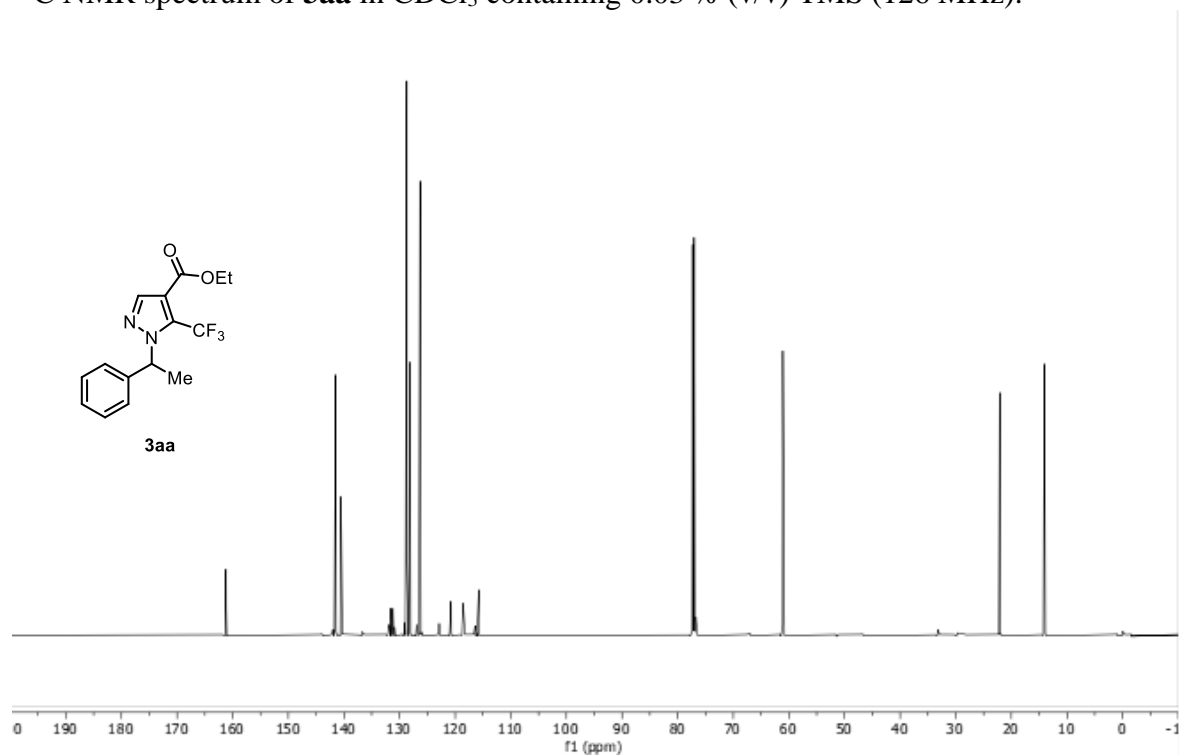
- 1 Hu, H.; Chen, S.-J.; Mandal, M.; Pratik, S. M.; Buss, J. A.; Krska, S. W.; Cramer, C. J.; Stahl, S. S. Copper-Catalysed Benzylic C–H Coupling with Alcohols via Radical Relay Enabled by Redox buffering. *Nat. Catal.* **2020**, *3*, 358–367.
- 2 Bruker-AXS (2016). *APEX3*. Version 2016.5-0. Madison, Wisconsin, USA.
- 3 Krause, L., Herbst-Irmer, R., Sheldrick, G. M. & Stalke, D. Comparison of Silver and Molybdenum Microfocus X-Ray Sources for Single-Crystal Structure Determination. *J. Appl. Cryst.* **2015**, *48*, 3–10.
- 4 Sheldrick, G. M. (2013b). *XPREF*. Version 2013/1. Georg-August-Universität Göttingen, Göttingen, Germany.
- 5 Sheldrick, G. M. (2013a). The *SHELX* homepage, <http://shelx.uni-ac.gwdg.de/SHELX/>.
- 6 Sheldrick, G. M. SHELXT-Integrated Space-Group and Crystal-Structure Determination. *Acta Cryst.* **2015**, *A71*, 3–8.
- 7 Sheldrick, G. M. Crystal Structure Refinement with *SHELX*. *Acta Cryst.* **2015**, *C71*, 3–8.
- 8 Dolomanov, O. V.; Bourhis, L. J.; Gildea, R. J.; Howard, J. A. K.; Puschmann, H. OLEX2: A Complete Structure Solution, Refinement and Analysis Program. *J. Appl. Cryst.* **2009**, *42*, 339–341.
- 9 Guzei, I. A. (2007-2013). *Programs Gn*. University of Wisconsin-Madison, Madison, Wisconsin, USA.

5D.X. NMR Spectroscopic Data

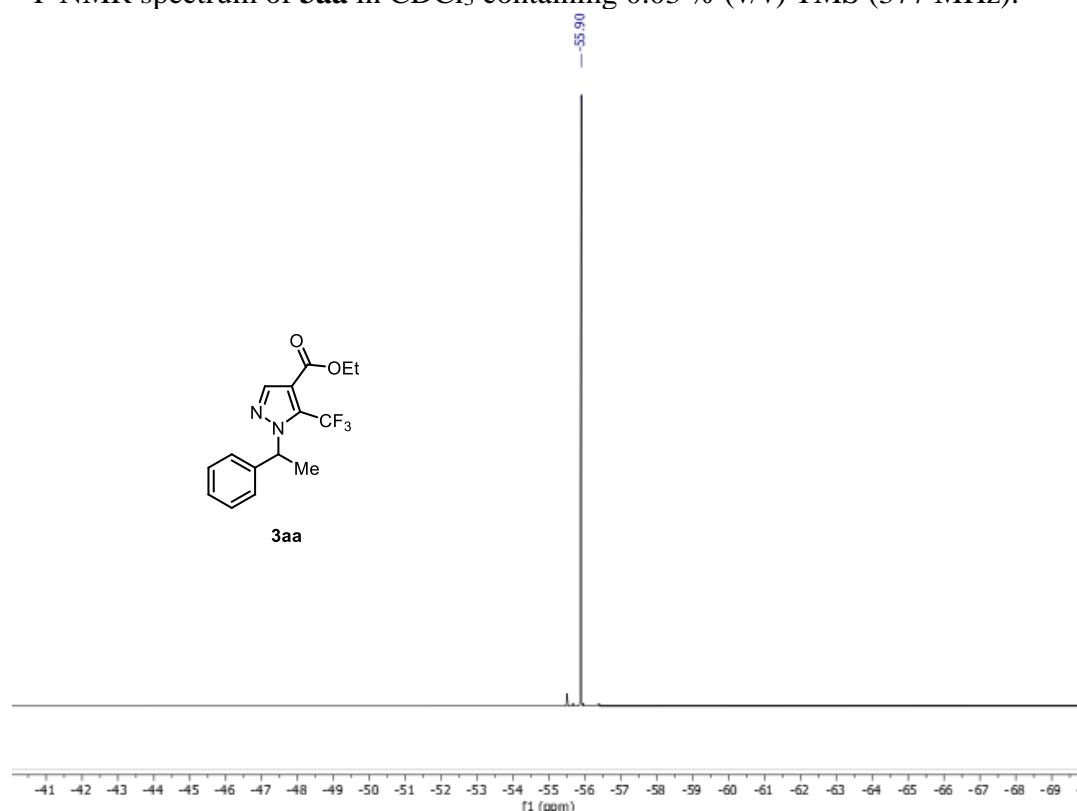
^1H NMR spectrum of **3aa** in CDCl_3 containing 0.03 % (v/v) TMS (500 MHz).



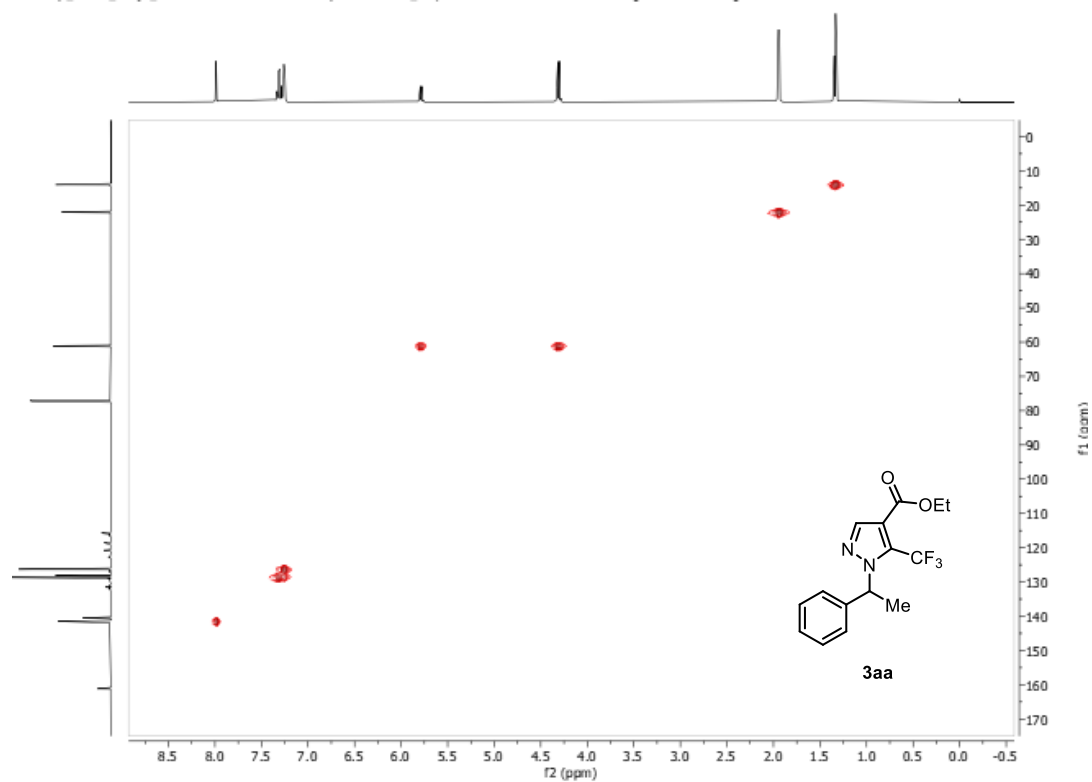
^{13}C NMR spectrum of **3aa** in CDCl_3 containing 0.03 % (v/v) TMS (126 MHz).



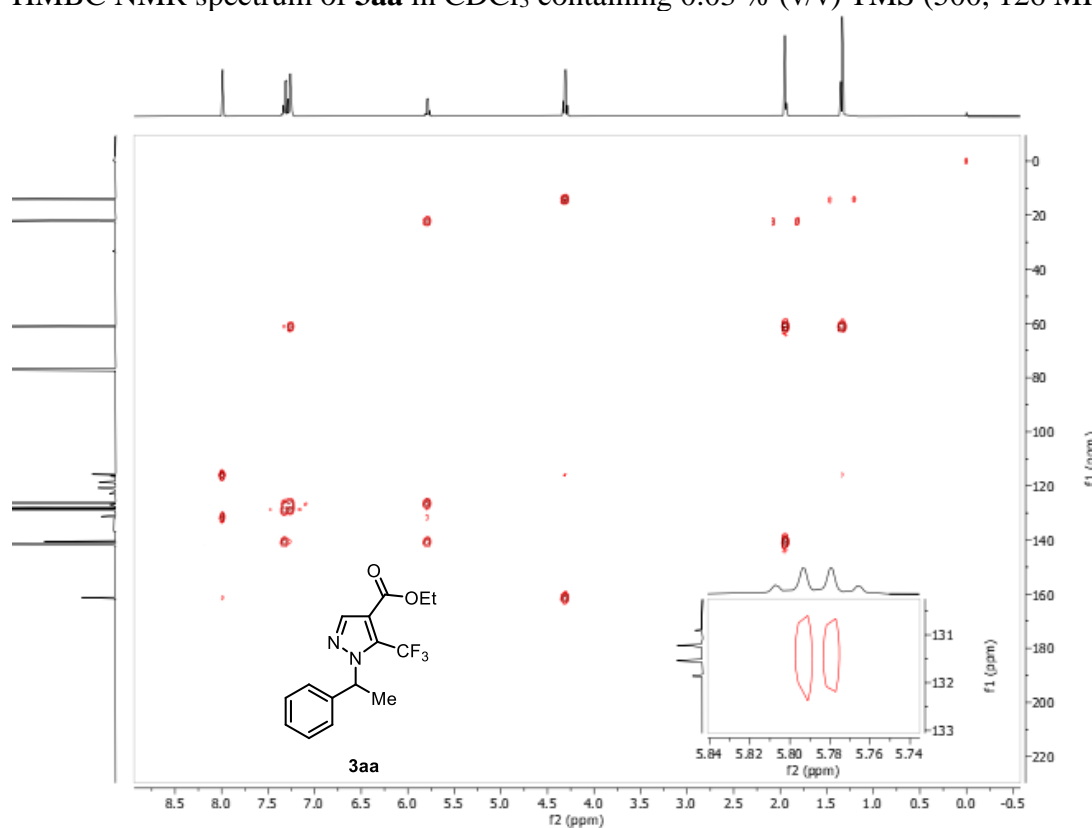
^{19}F NMR spectrum of **3aa** in CDCl_3 containing 0.03 % (v/v) TMS (377 MHz).



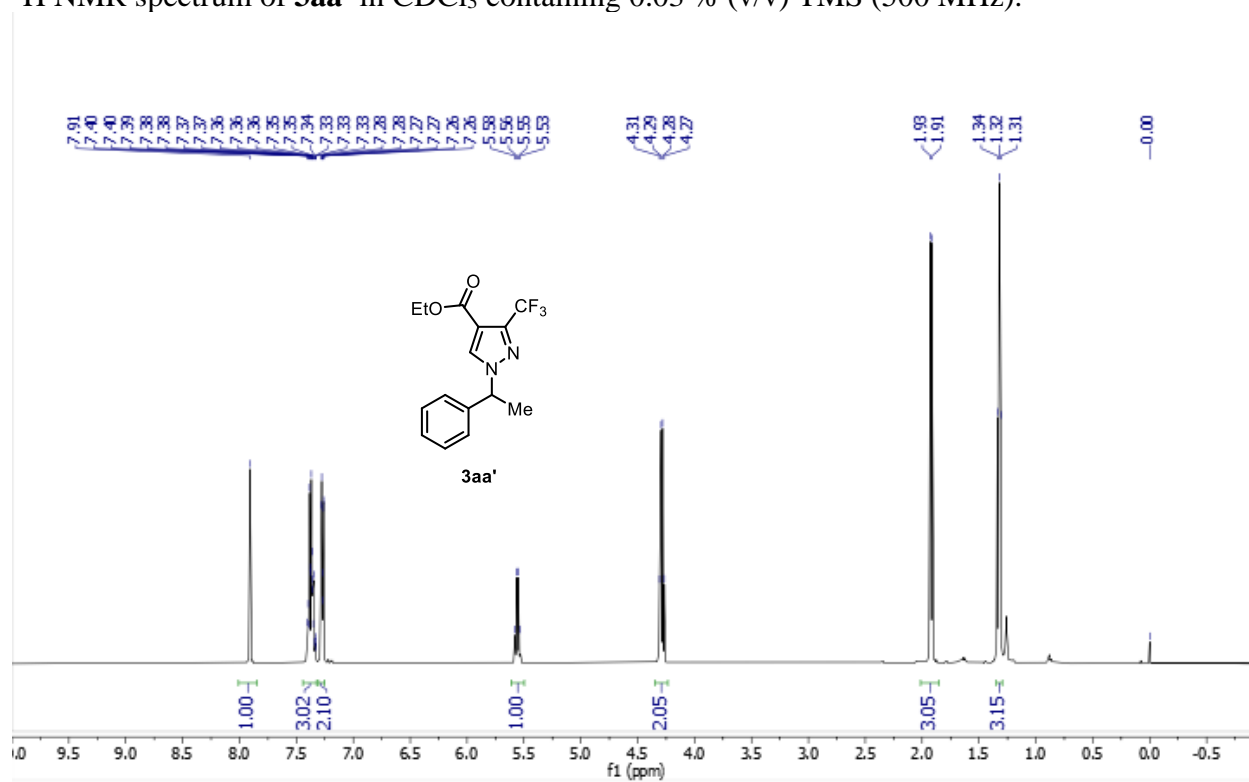
HSQC NMR spectrum of **3aa** in CDCl_3 containing 0.03 % (v/v) TMS (500, 126 MHz).



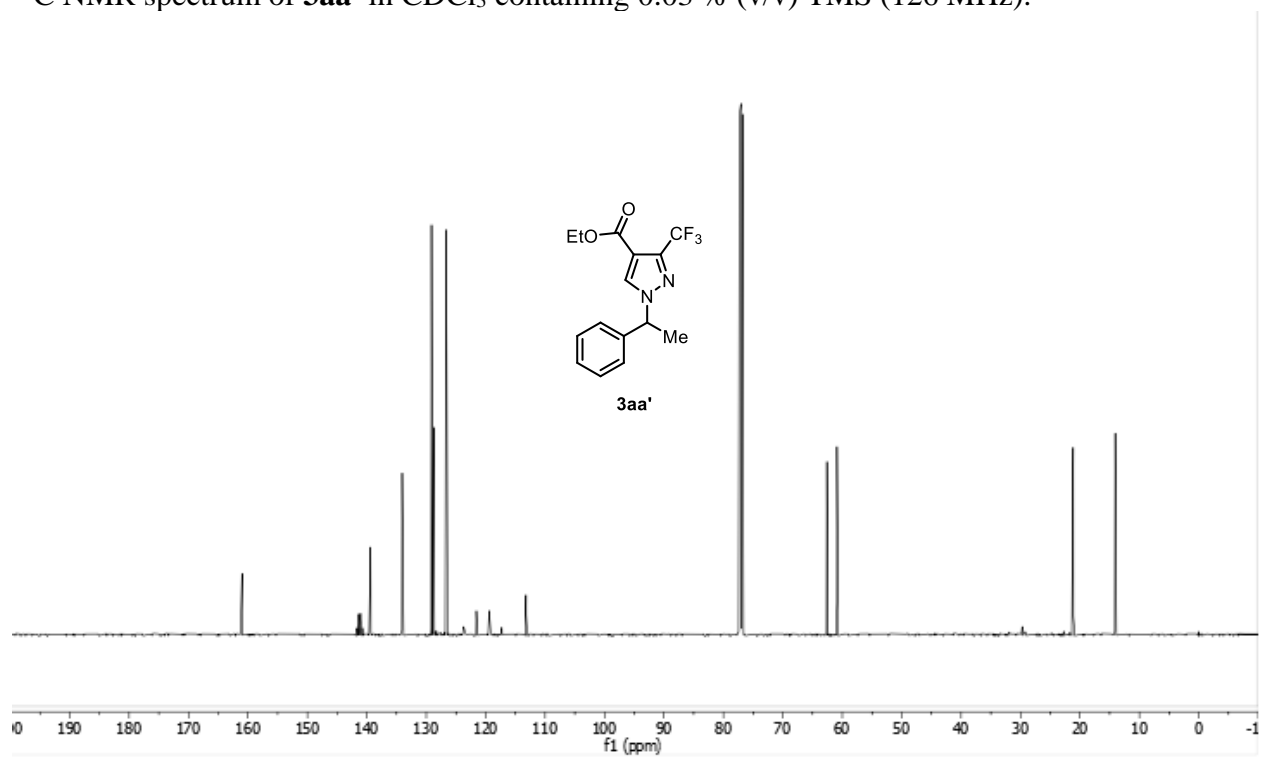
HMBC NMR spectrum of **3aa** in CDCl₃ containing 0.03 % (v/v) TMS (500, 126 MHz).



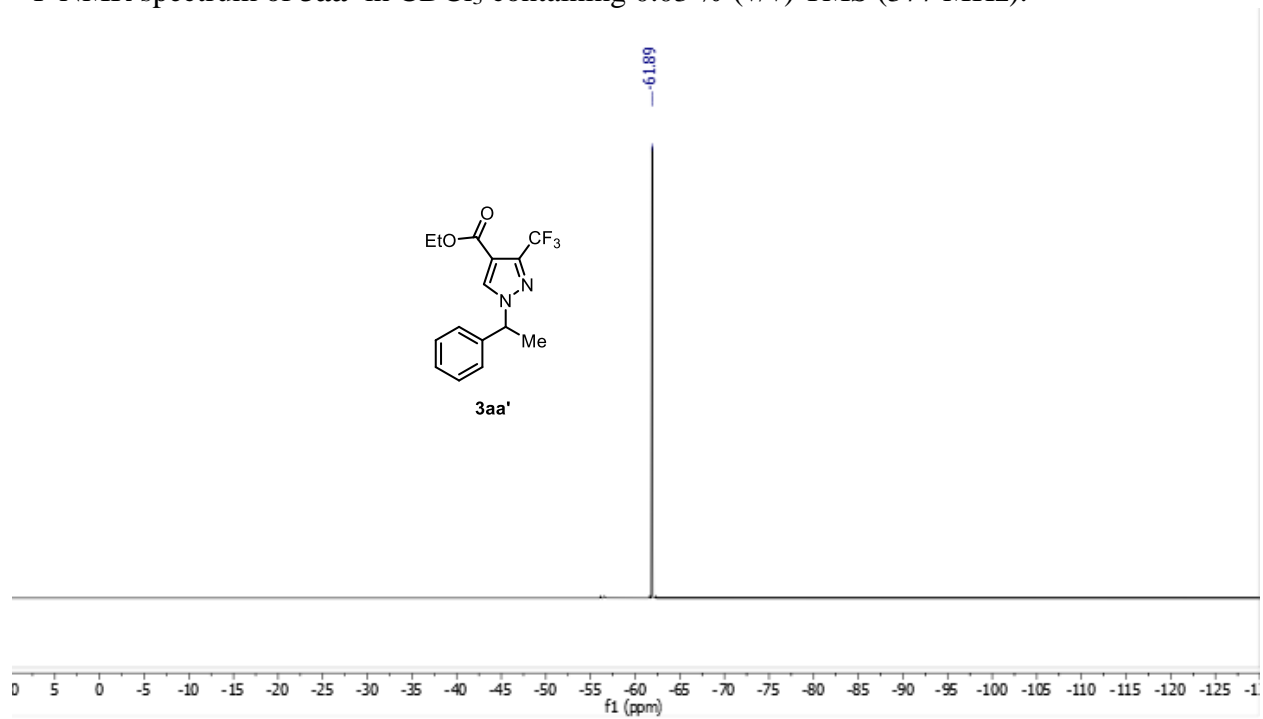
¹H NMR spectrum of **3aa'** in CDCl₃ containing 0.03 % (v/v) TMS (500 MHz).



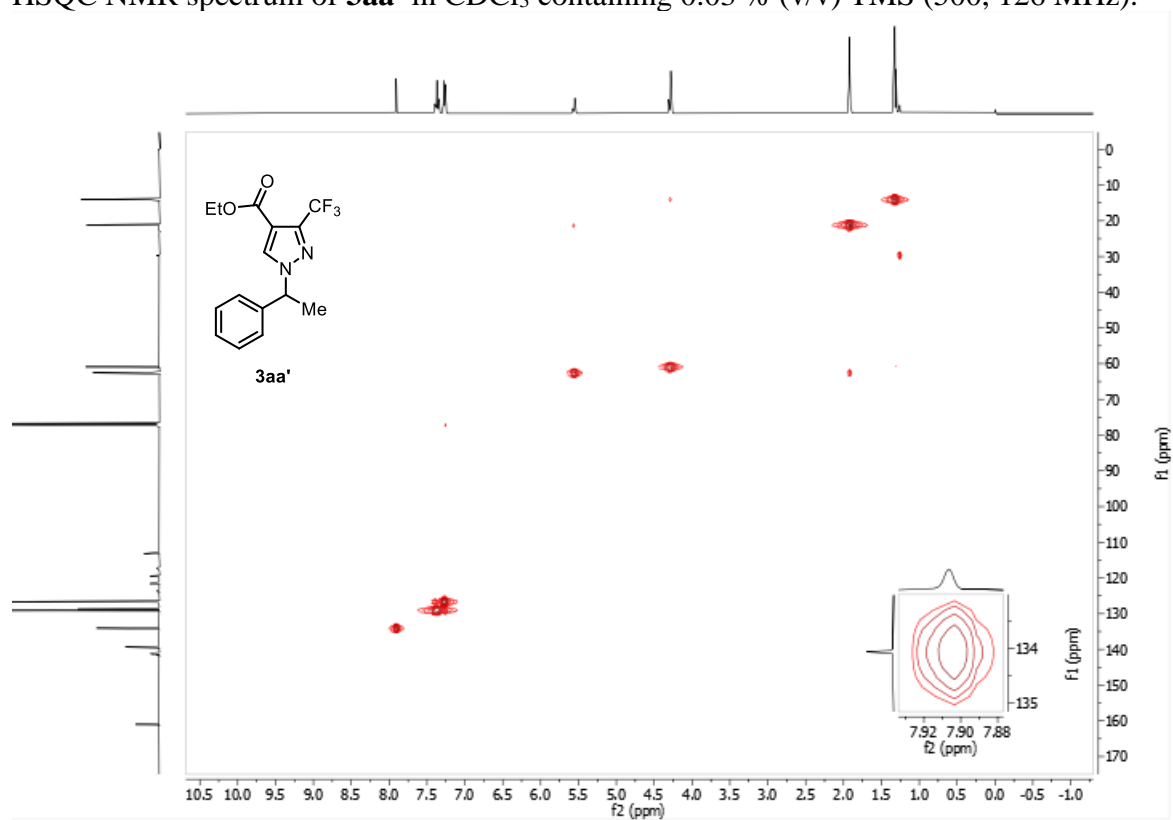
^{13}C NMR spectrum of **3aa'** in CDCl_3 containing 0.03 % (v/v) TMS (126 MHz).



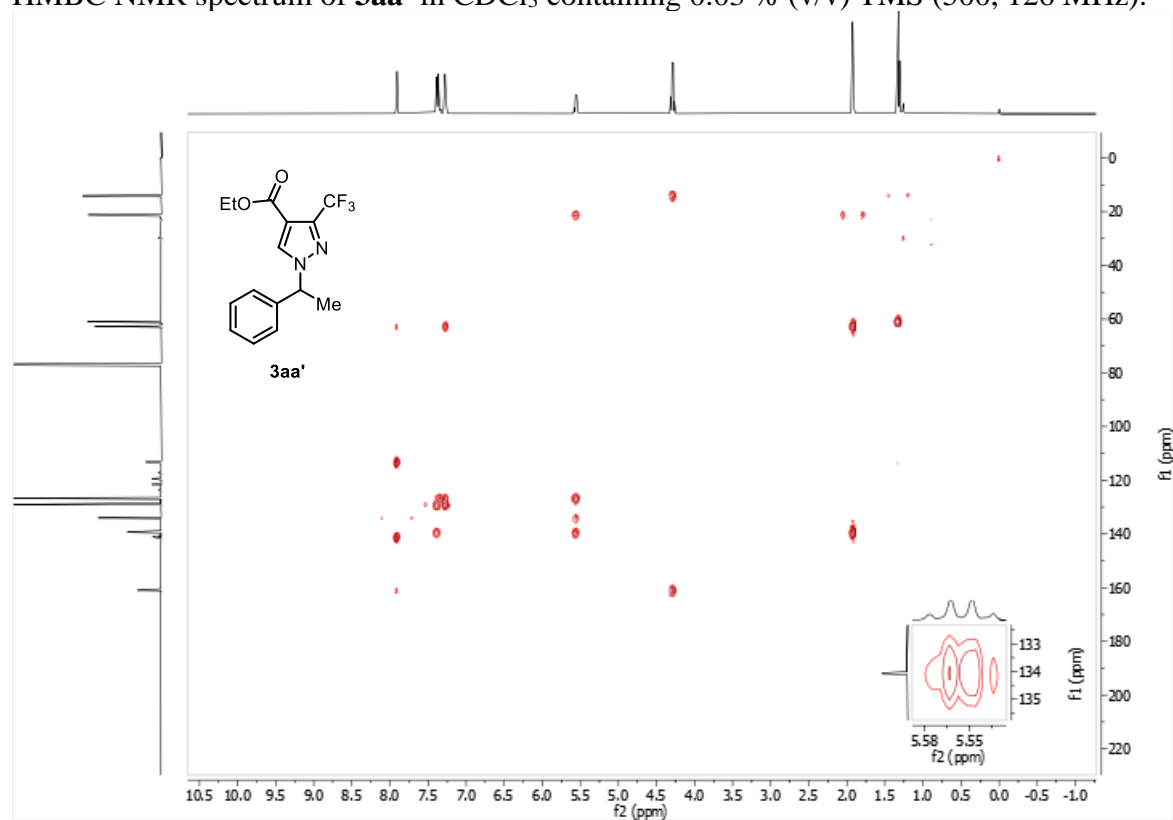
^{19}F NMR spectrum of **3aa'** in CDCl_3 containing 0.03 % (v/v) TMS (377 MHz).



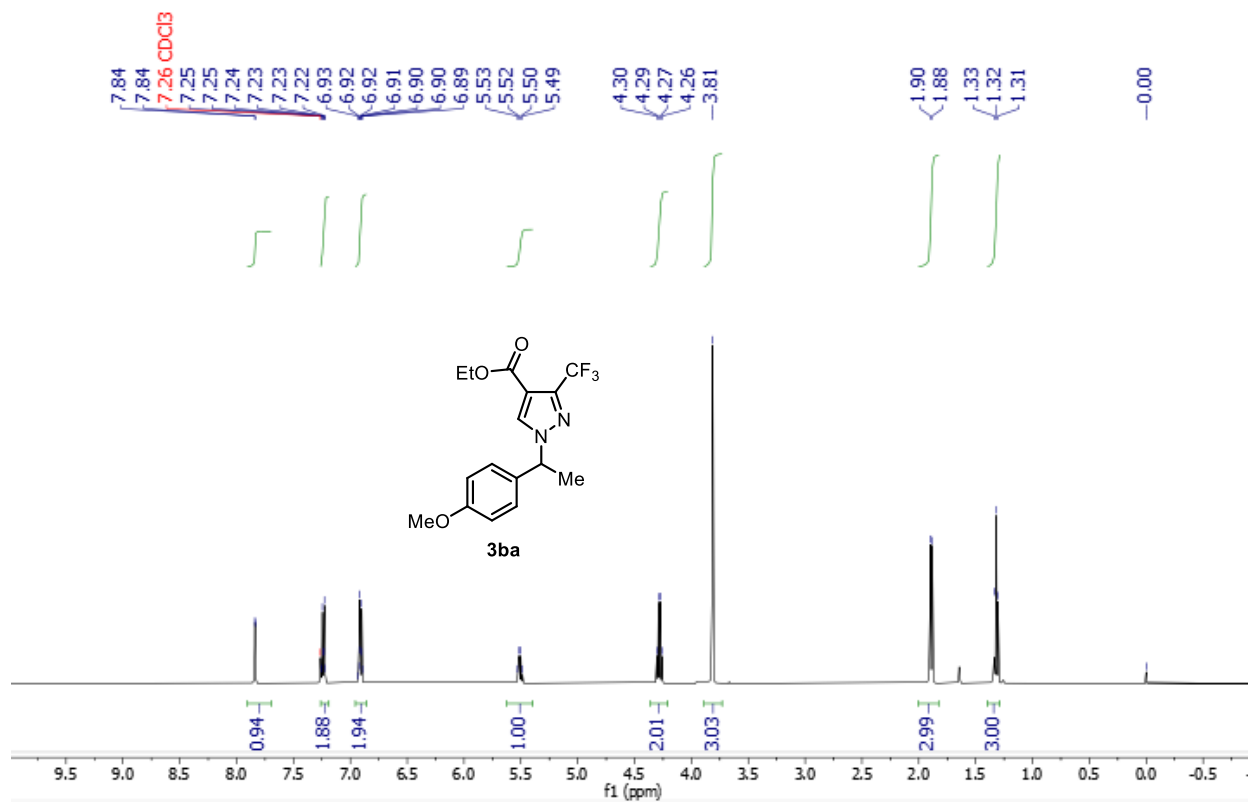
HSQC NMR spectrum of **3aa'** in CDCl₃ containing 0.03 % (v/v) TMS (500, 126 MHz).



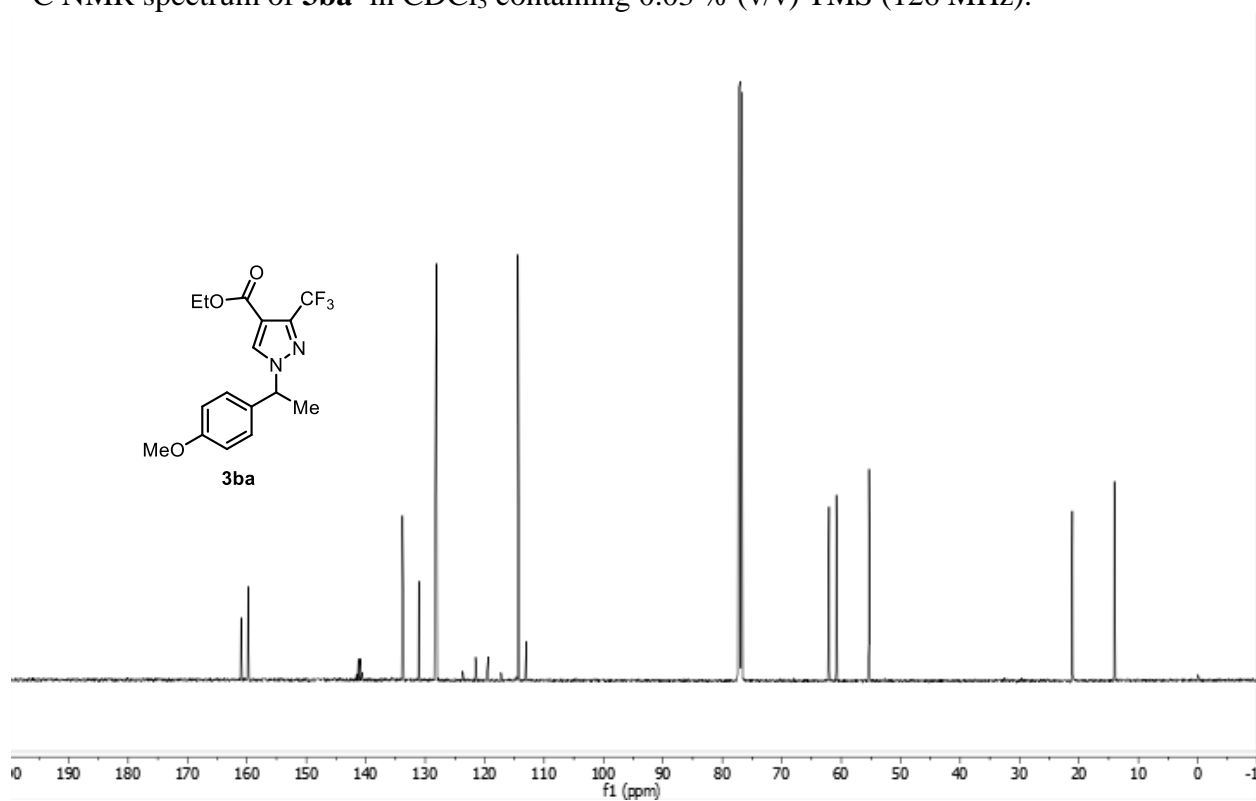
HMBC NMR spectrum of **3aa'** in CDCl₃ containing 0.03 % (v/v) TMS (500, 126 MHz).



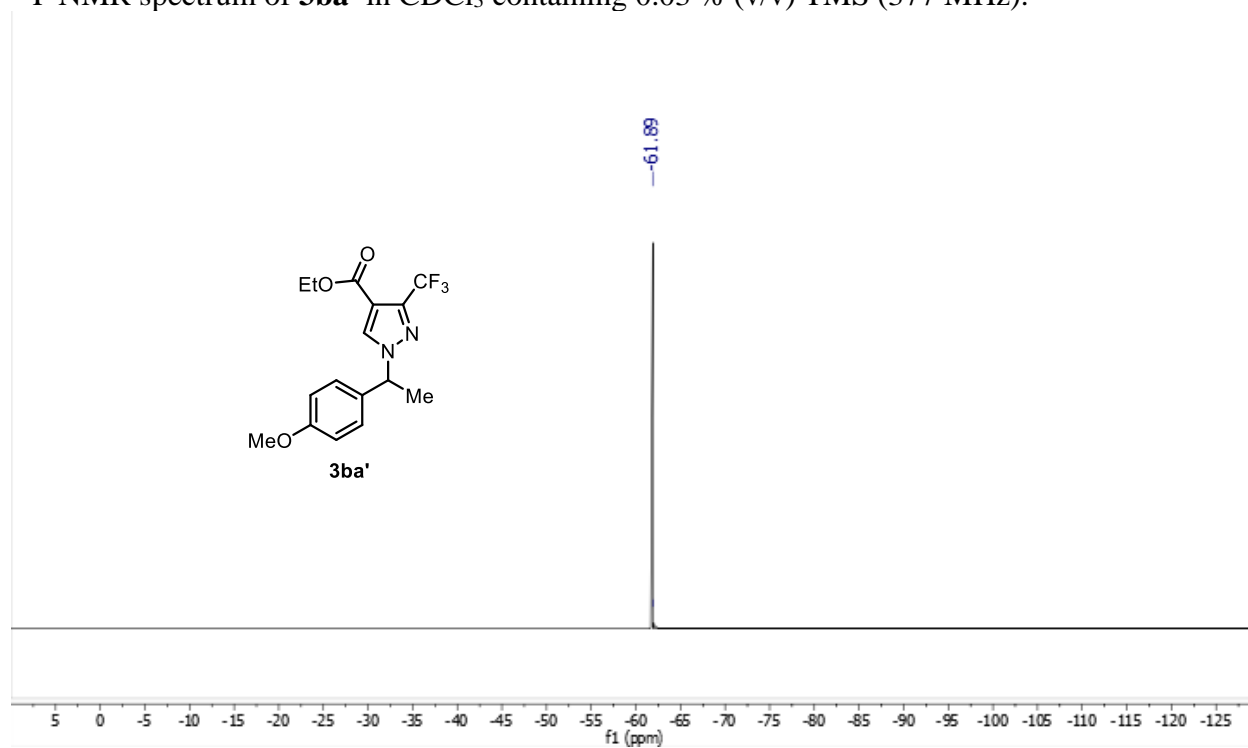
^1H NMR spectrum of **3ba**' in CDCl_3 containing 0.03 % (v/v) TMS (500 MHz).



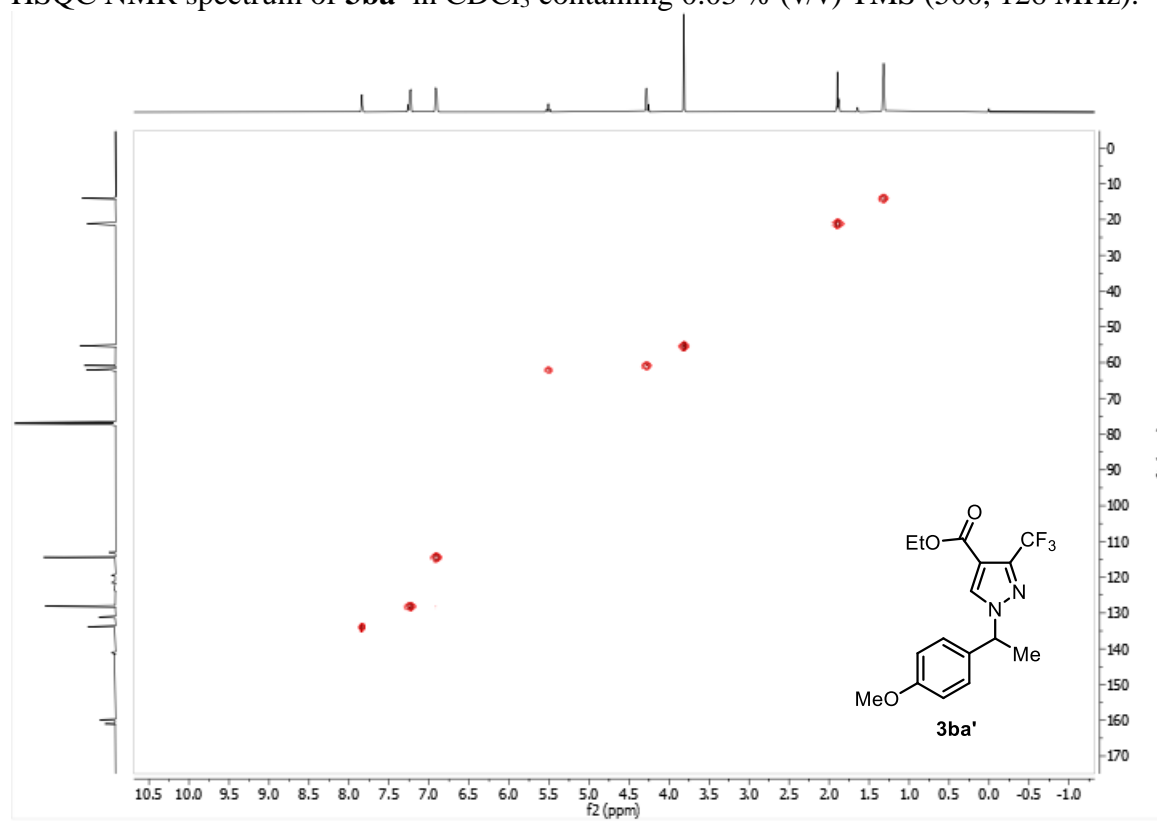
^{13}C NMR spectrum of **3ba**' in CDCl_3 containing 0.03 % (v/v) TMS (126 MHz).



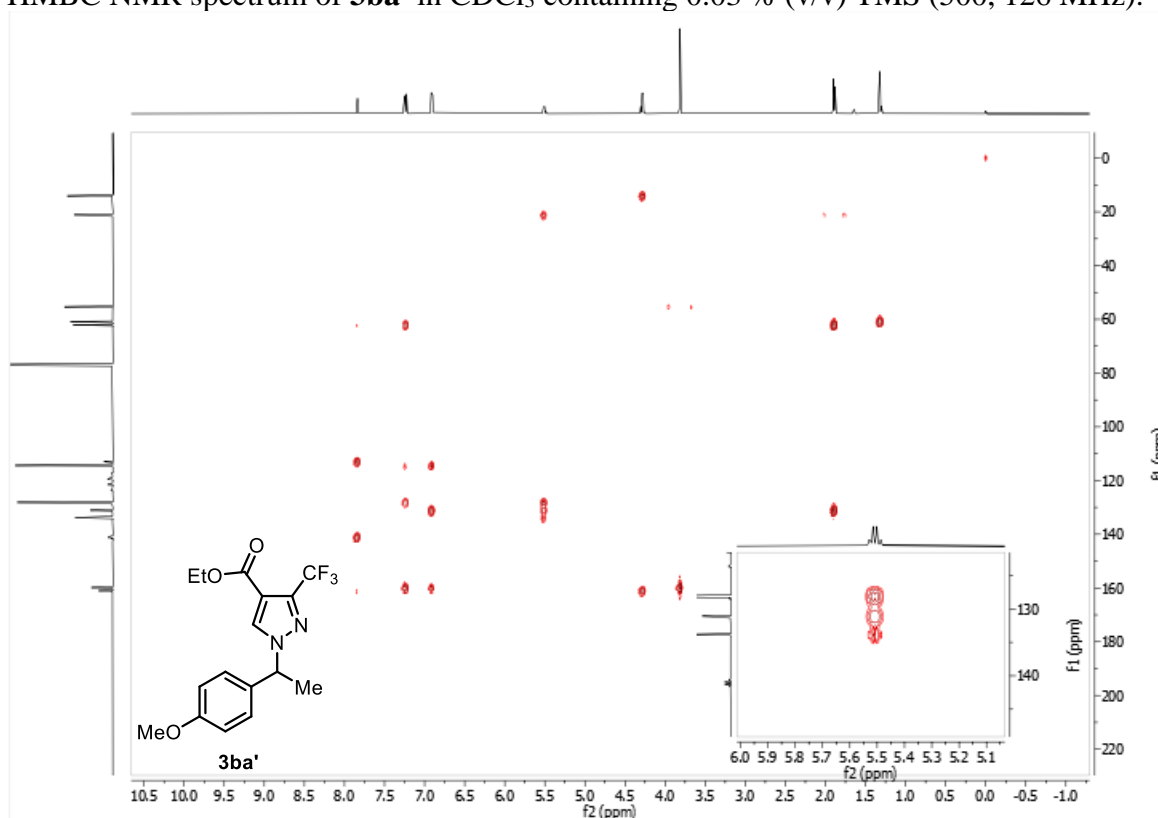
^{19}F NMR spectrum of **3ba'** in CDCl_3 containing 0.03 % (v/v) TMS (377 MHz).



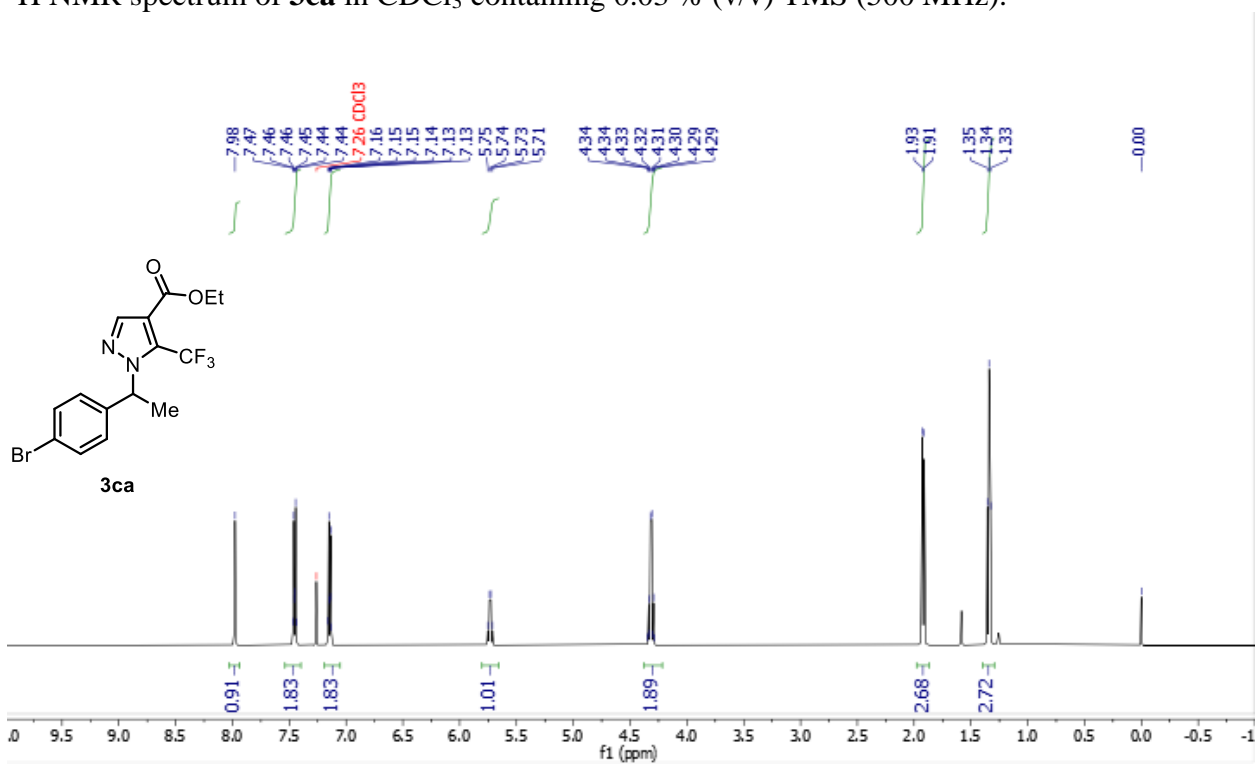
HSQC NMR spectrum of **3ba'** in CDCl_3 containing 0.03 % (v/v) TMS (500, 126 MHz).



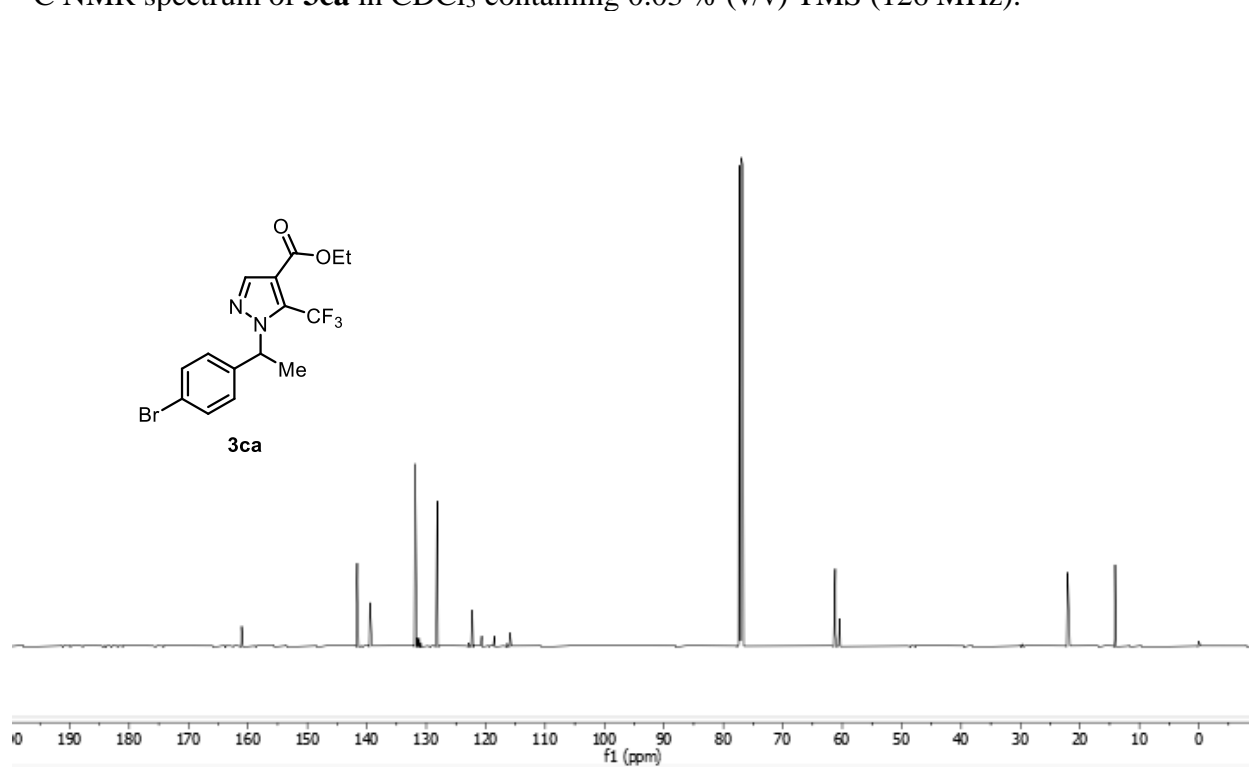
HMBC NMR spectrum of **3ba'** in CDCl₃ containing 0.03 % (v/v) TMS (500, 126 MHz).



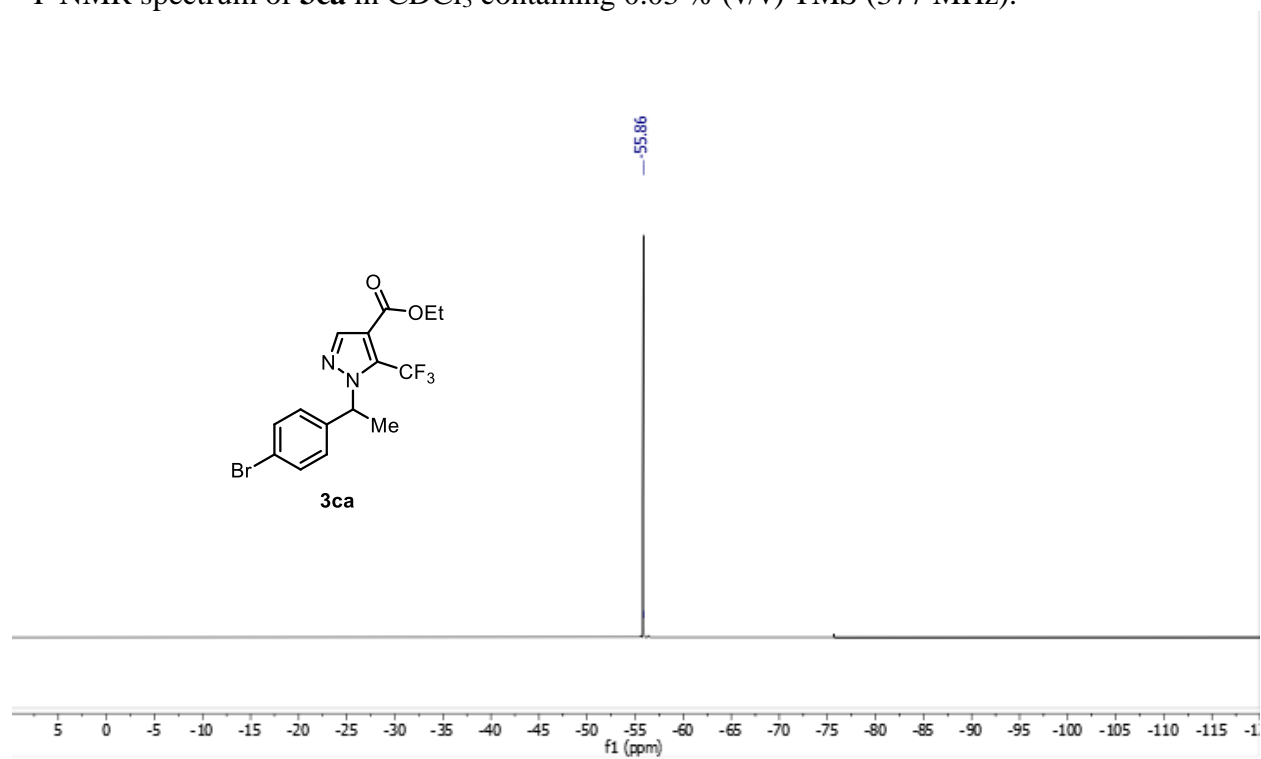
¹H NMR spectrum of **3ca** in CDCl₃ containing 0.03 % (v/v) TMS (500 MHz).



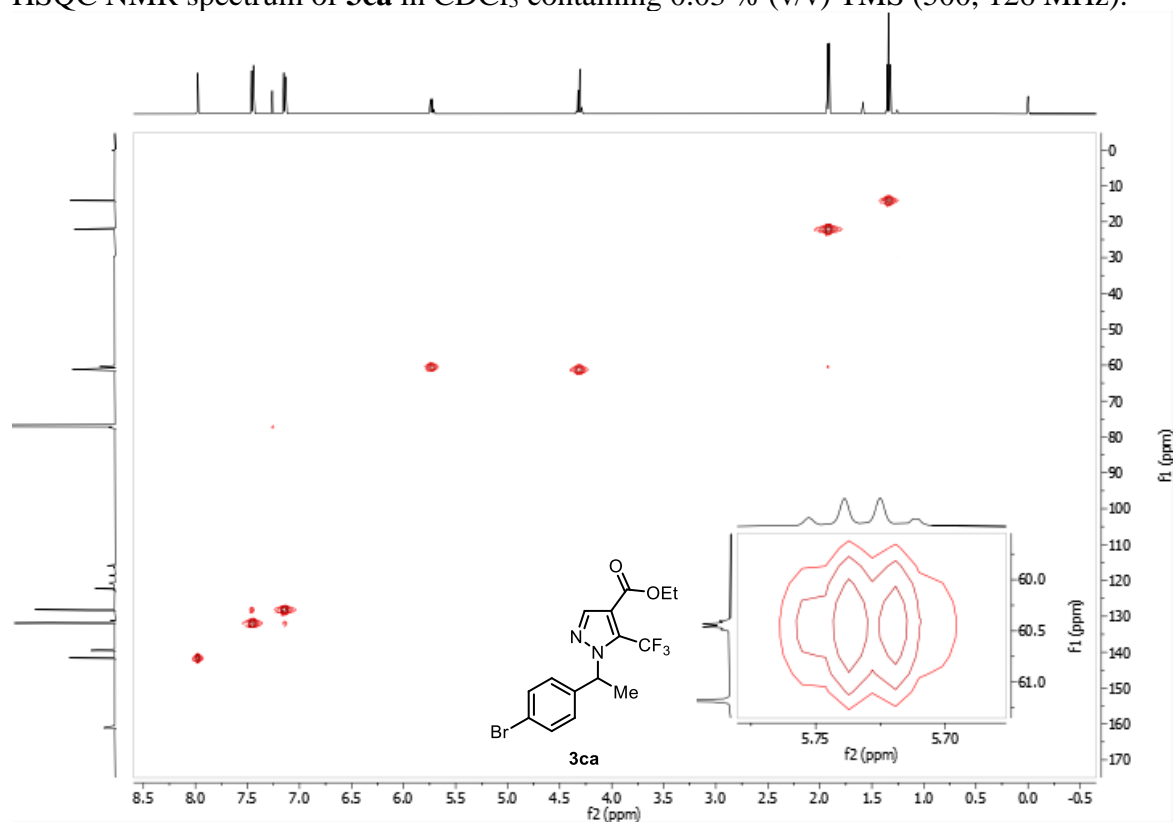
^{13}C NMR spectrum of **3ca** in CDCl_3 containing 0.03 % (v/v) TMS (126 MHz).



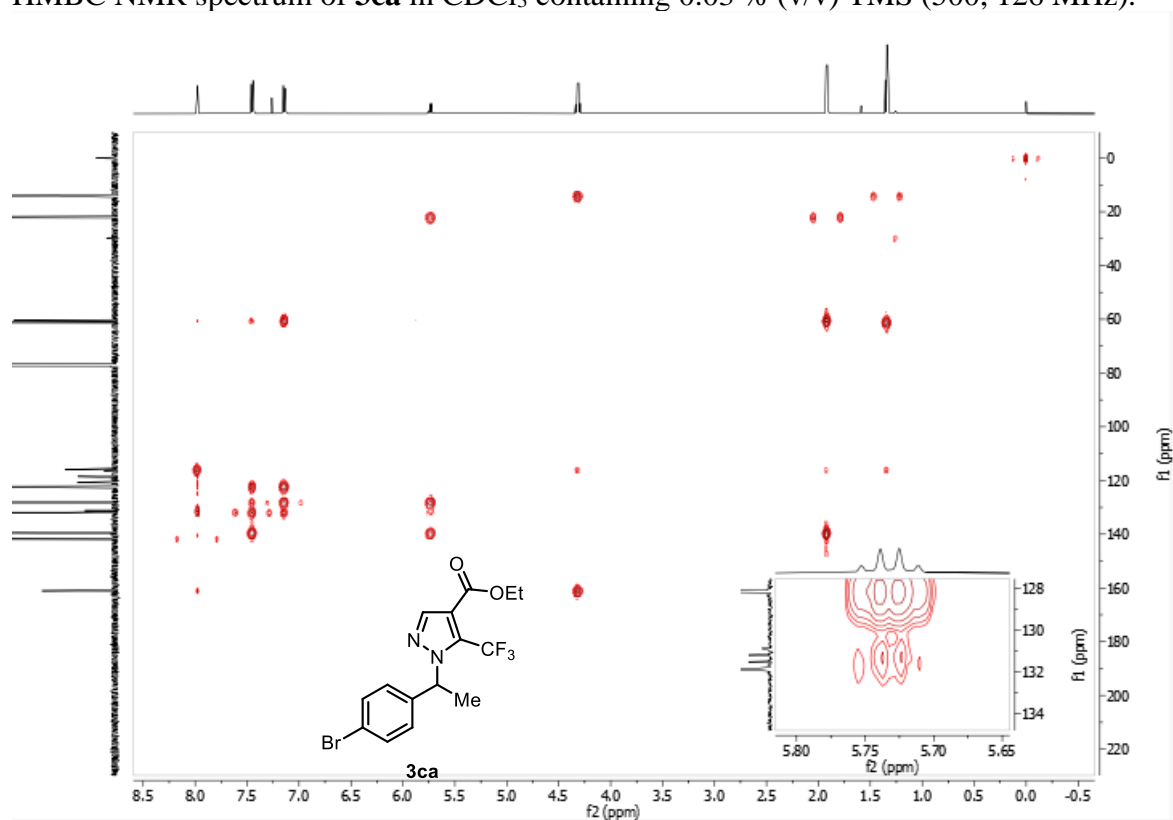
^{19}F NMR spectrum of **3ca** in CDCl_3 containing 0.03 % (v/v) TMS (377 MHz).



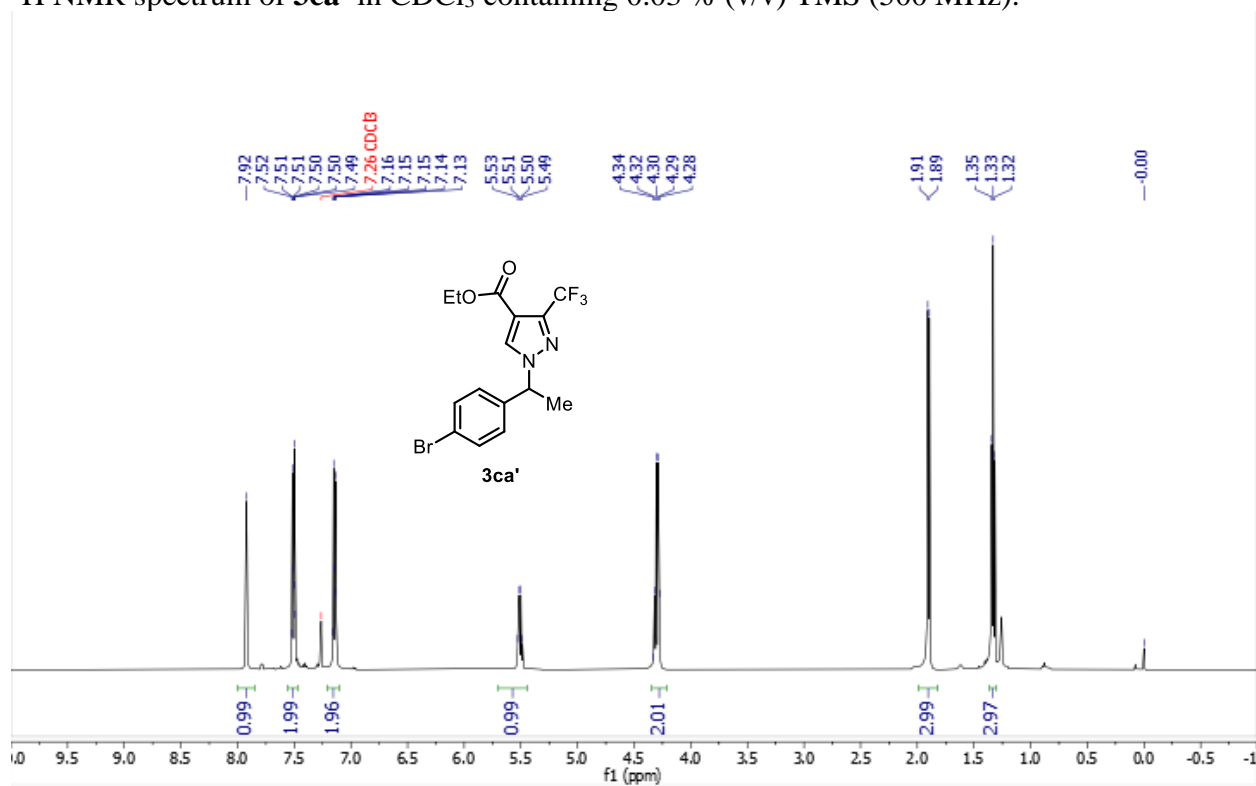
HSQC NMR spectrum of **3ca** in CDCl₃ containing 0.03 % (v/v) TMS (500, 126 MHz).



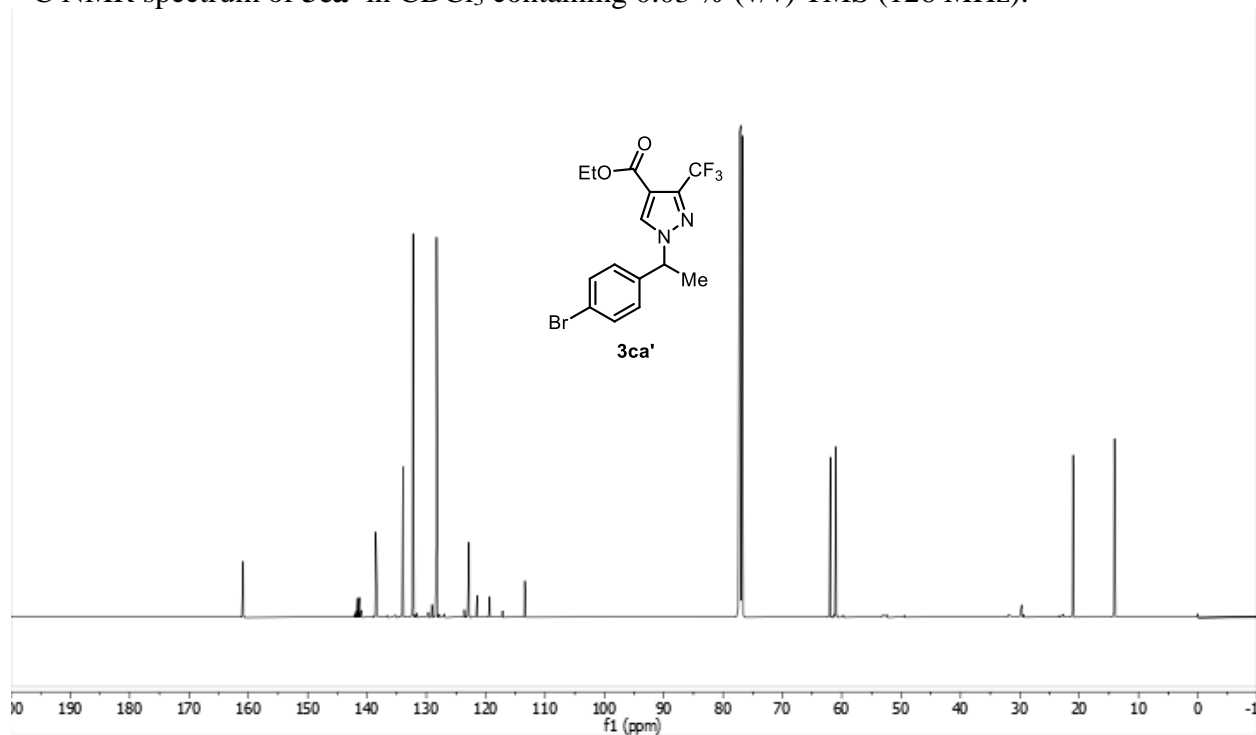
HMBC NMR spectrum of **3ca** in CDCl₃ containing 0.03 % (v/v) TMS (500, 126 MHz).



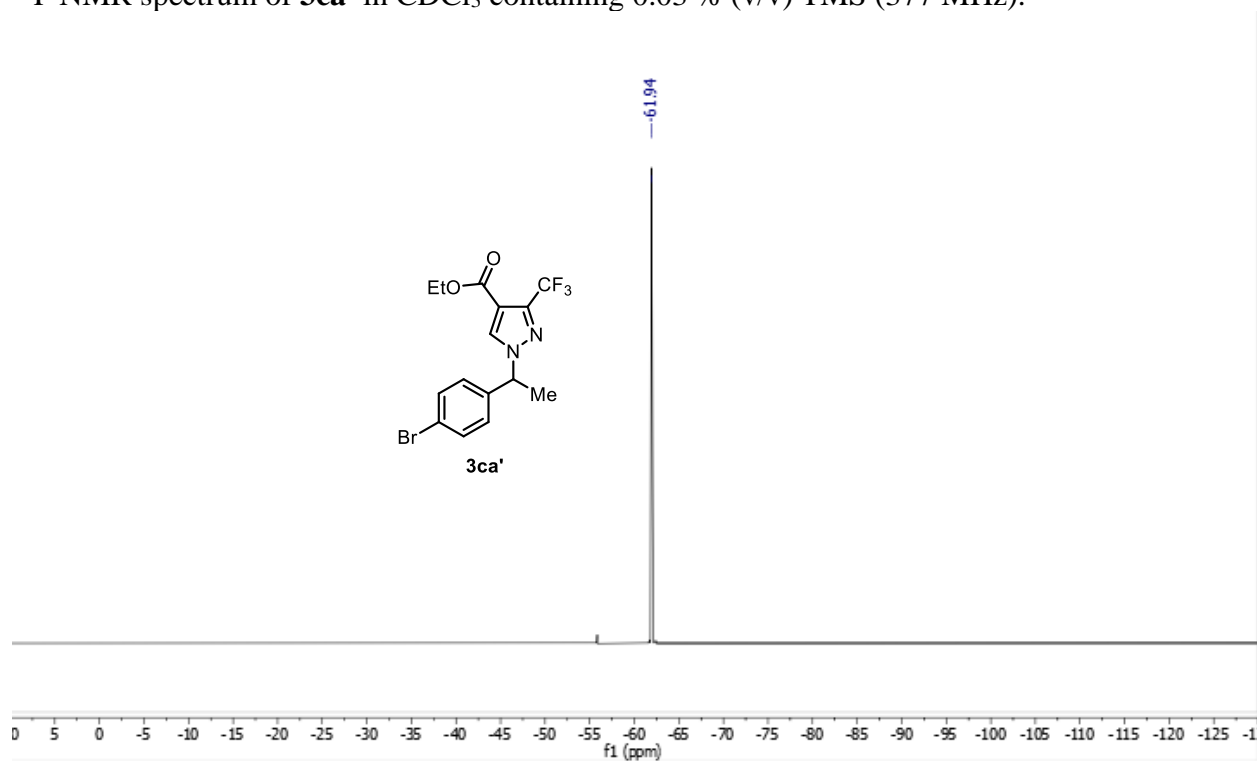
^1H NMR spectrum of **3ca'** in CDCl_3 containing 0.03 % (v/v) TMS (500 MHz).



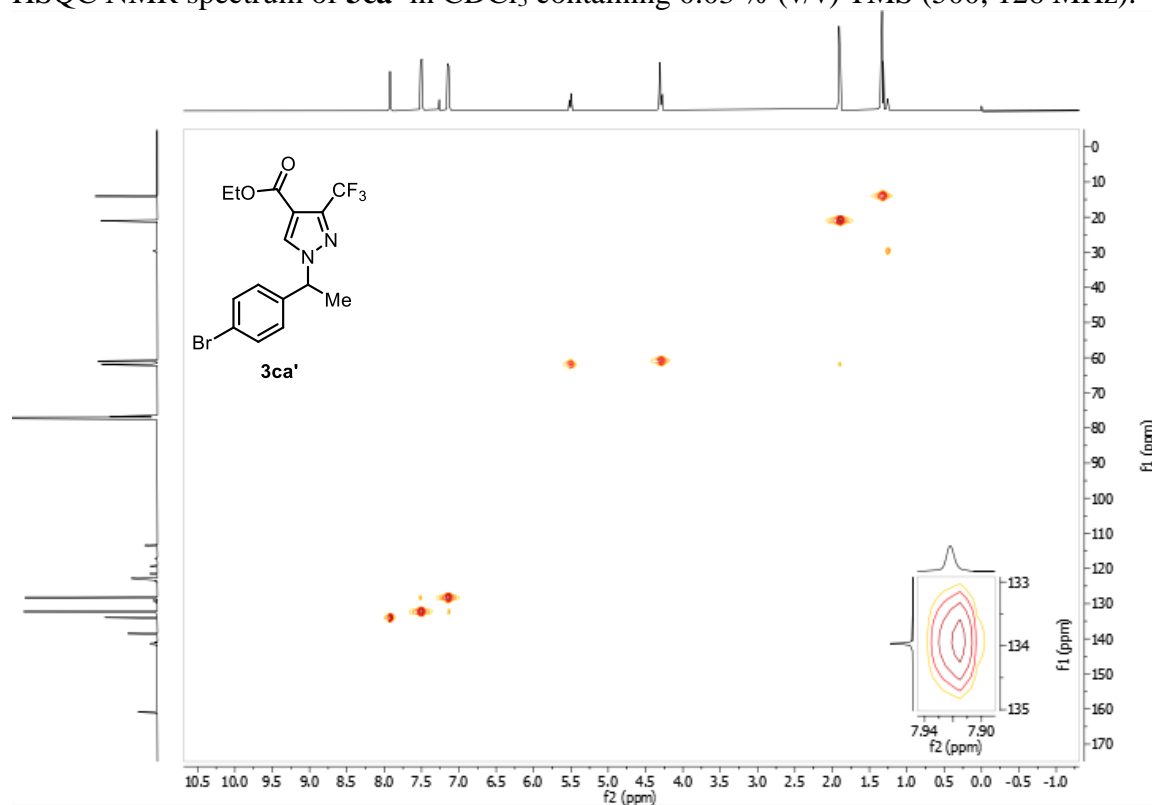
^{13}C NMR spectrum of **3ca'** in CDCl_3 containing 0.03 % (v/v) TMS (126 MHz).



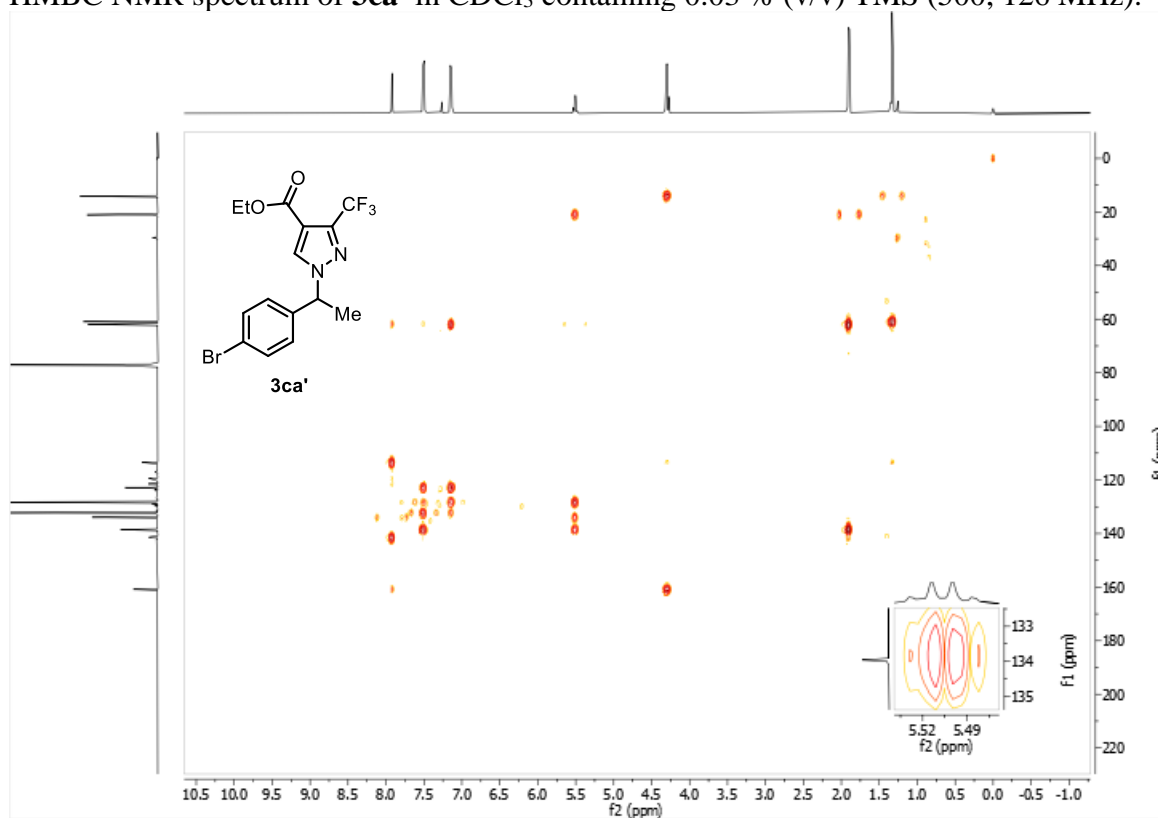
^{19}F NMR spectrum of **3ca'** in CDCl_3 containing 0.03 % (v/v) TMS (377 MHz).



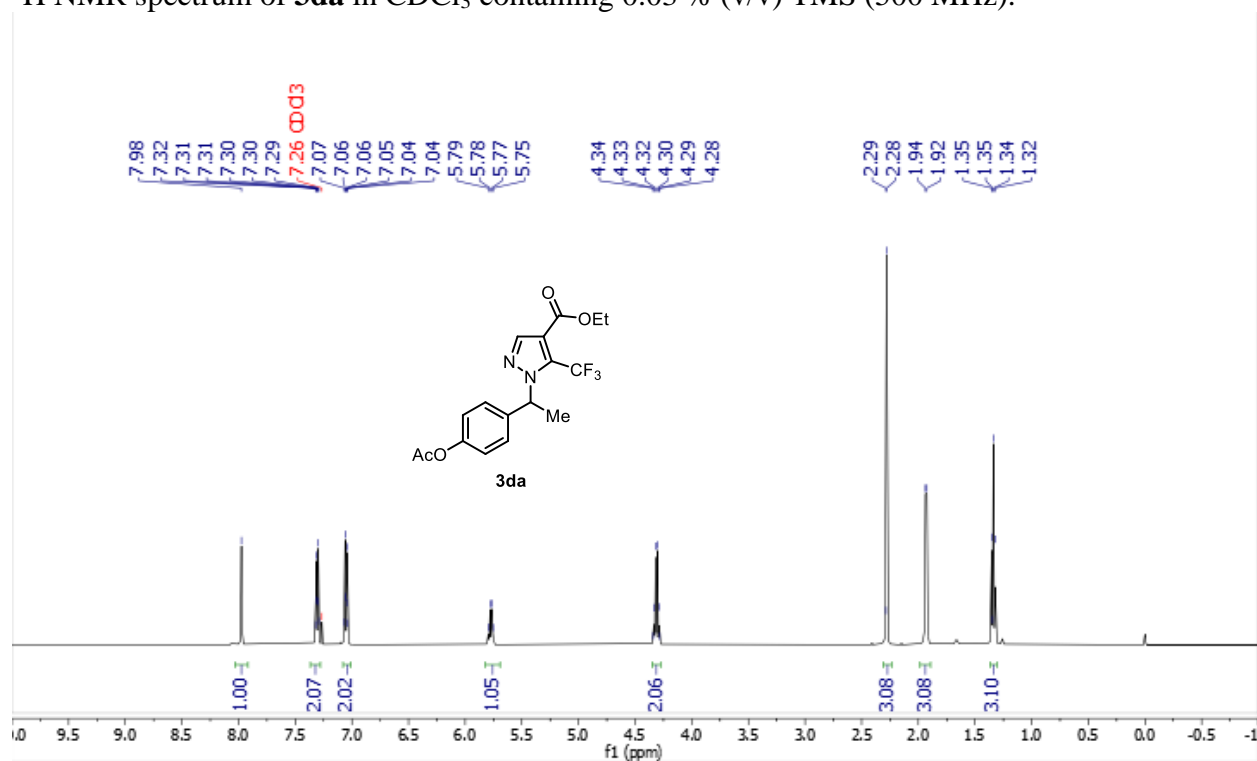
HSQC NMR spectrum of **3ca'** in CDCl_3 containing 0.03 % (v/v) TMS (500, 126 MHz).



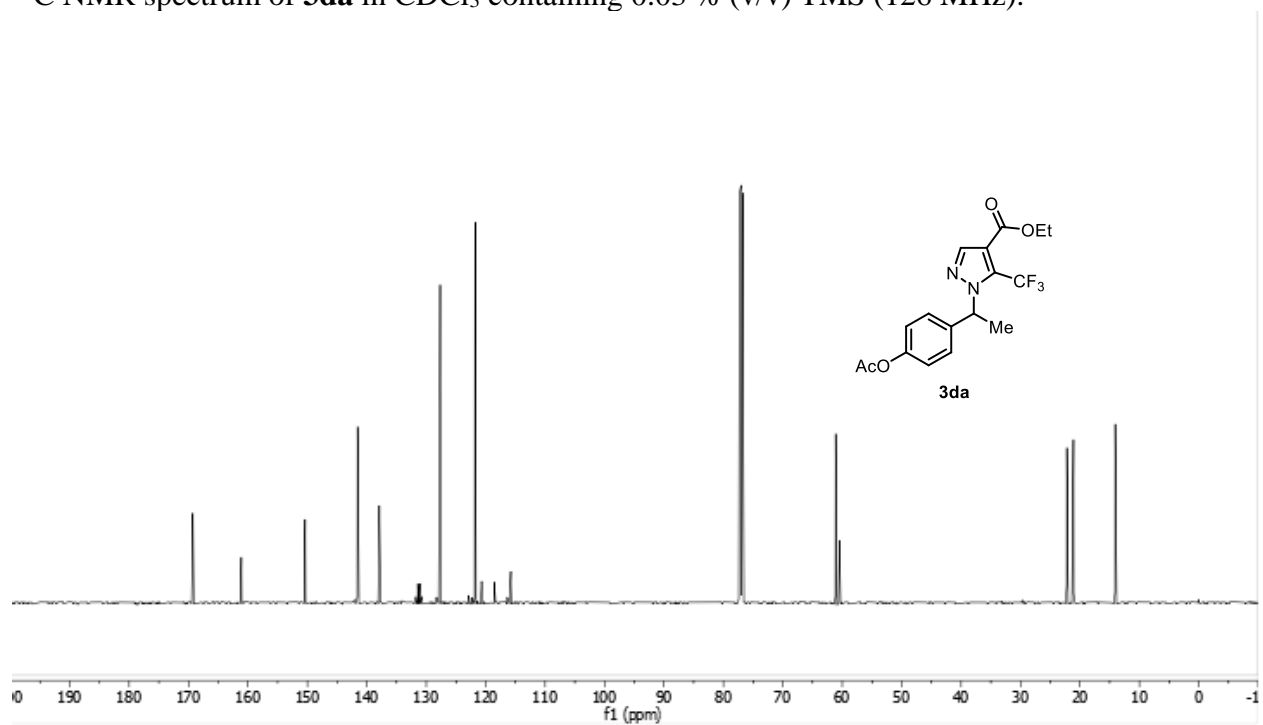
HMBC NMR spectrum of **3ca'** in CDCl₃ containing 0.03 % (v/v) TMS (500, 126 MHz).



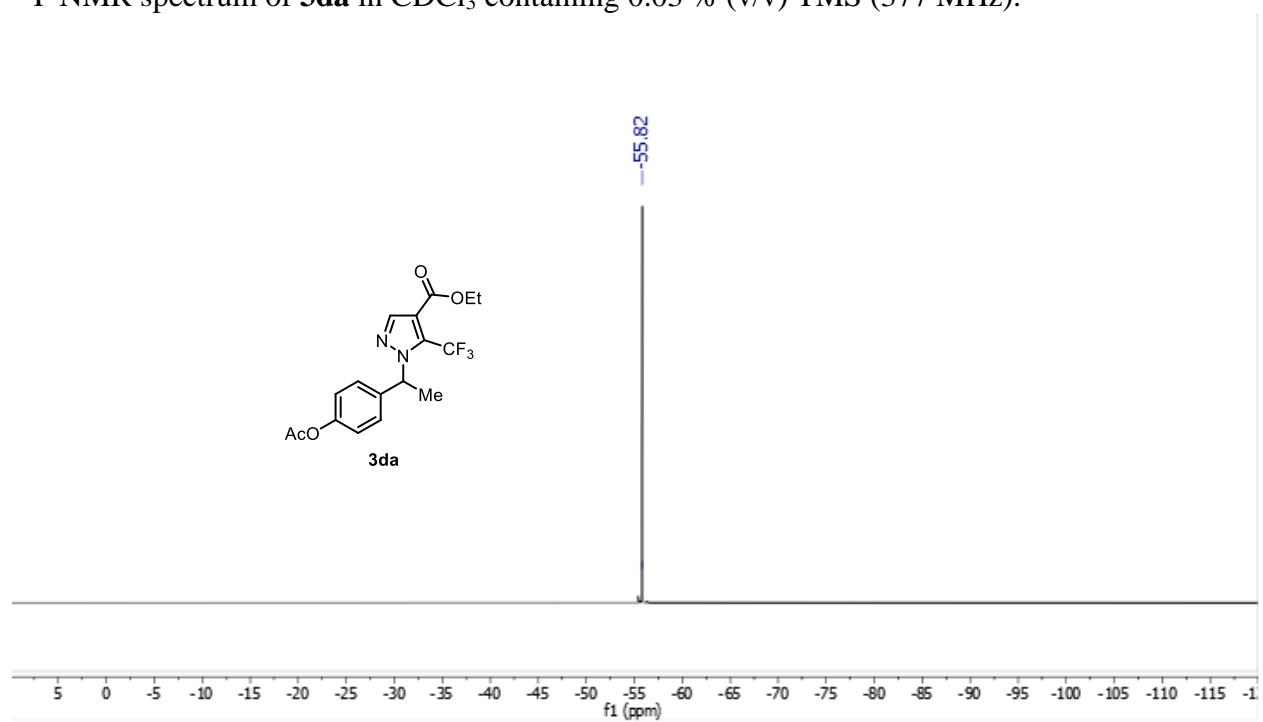
¹H NMR spectrum of **3da** in CDCl₃ containing 0.03 % (v/v) TMS (500 MHz).



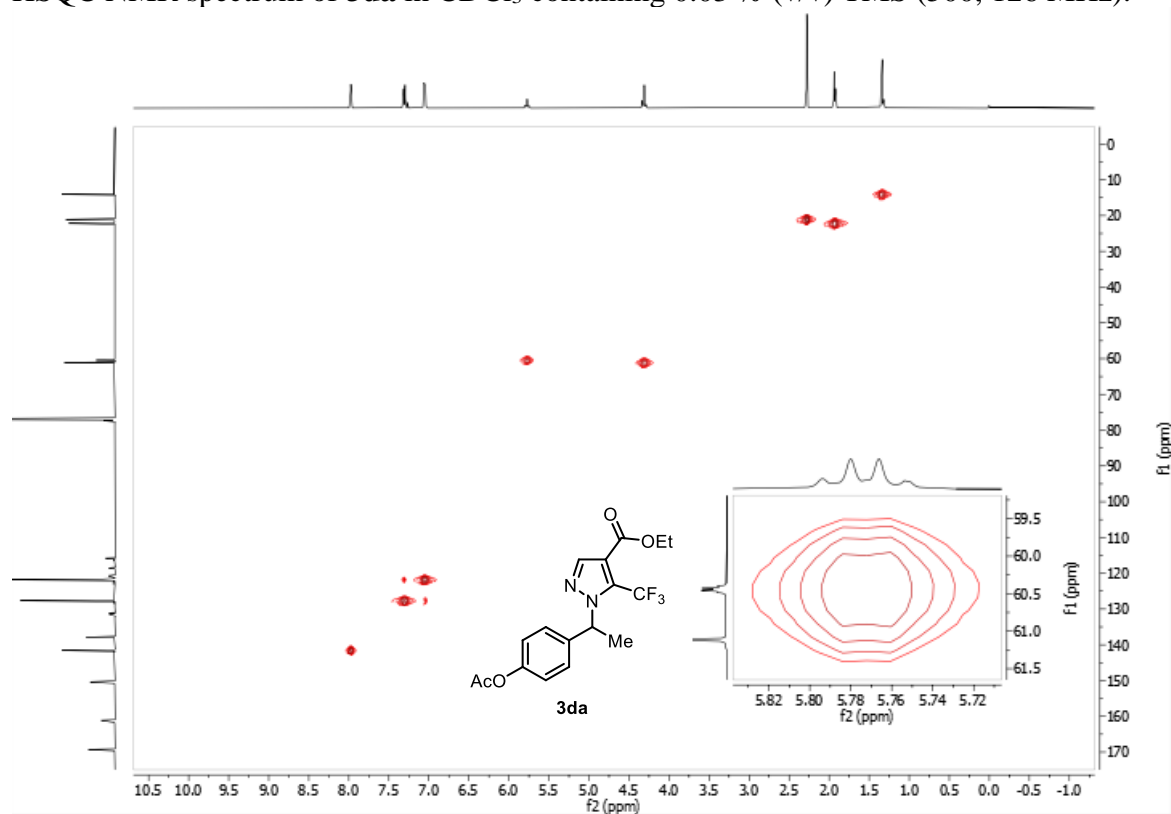
^{13}C NMR spectrum of **3da** in CDCl_3 containing 0.03 % (v/v) TMS (126 MHz).



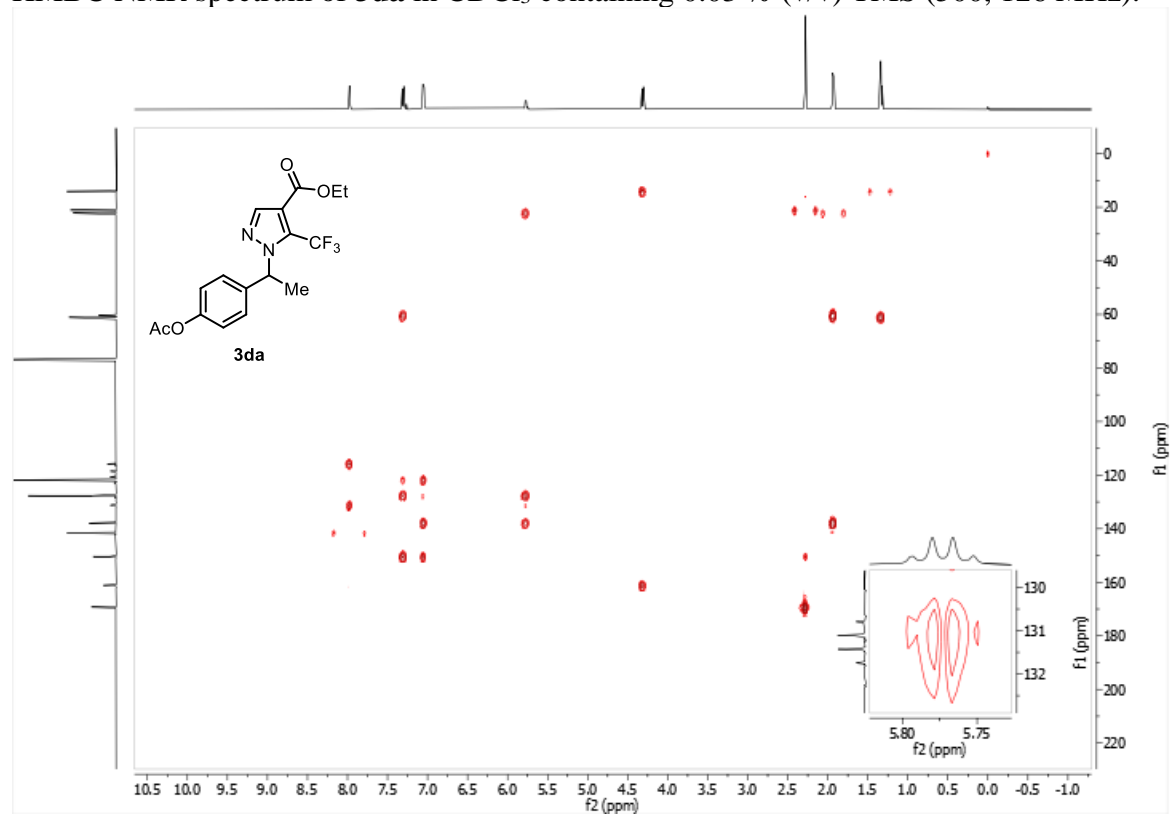
^{19}F NMR spectrum of **3da** in CDCl_3 containing 0.03 % (v/v) TMS (377 MHz).



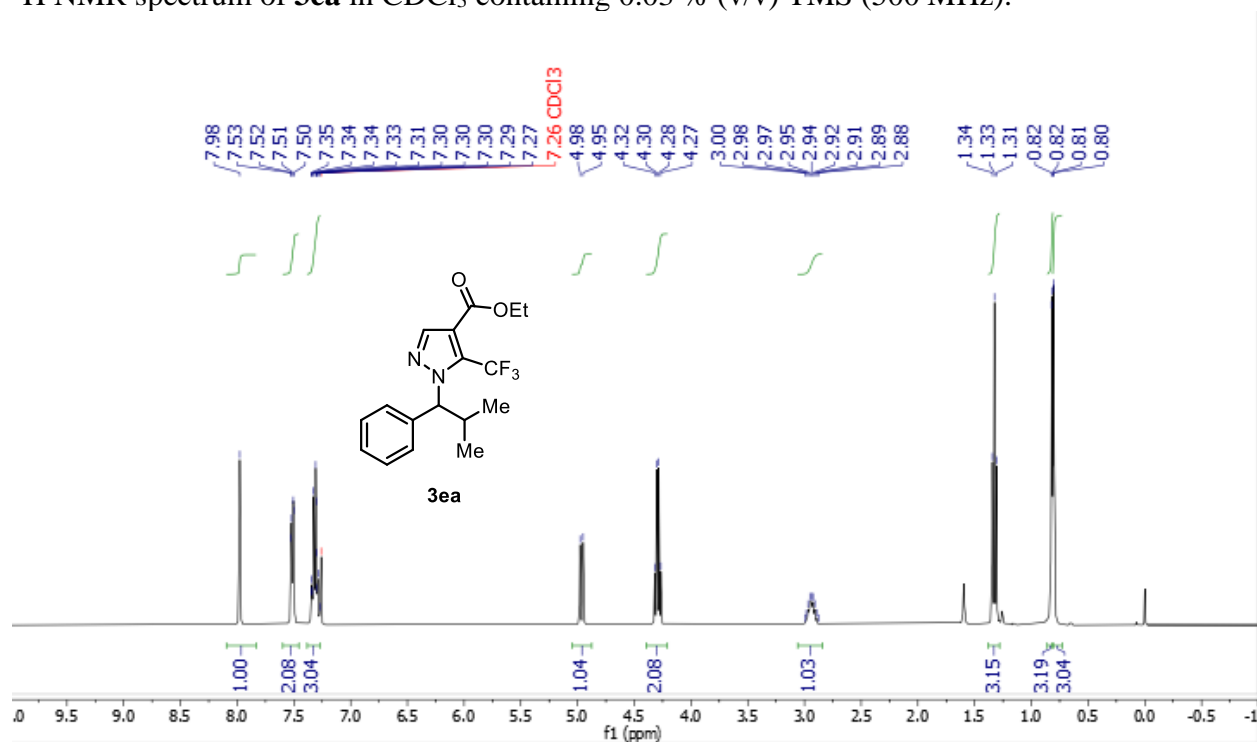
HSQC NMR spectrum of **3da** in CDCl₃ containing 0.03 % (v/v) TMS (500, 126 MHz).



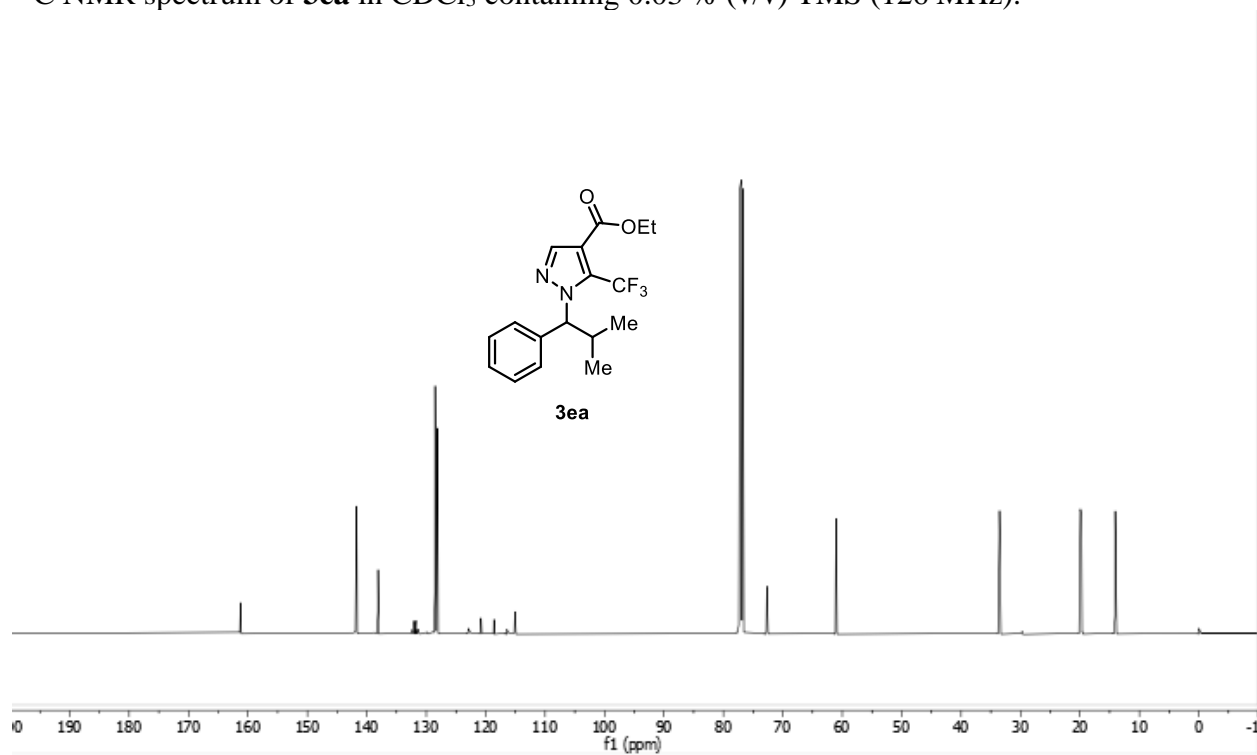
HMBC NMR spectrum of **3da** in CDCl₃ containing 0.03 % (v/v) TMS (500, 126 MHz).



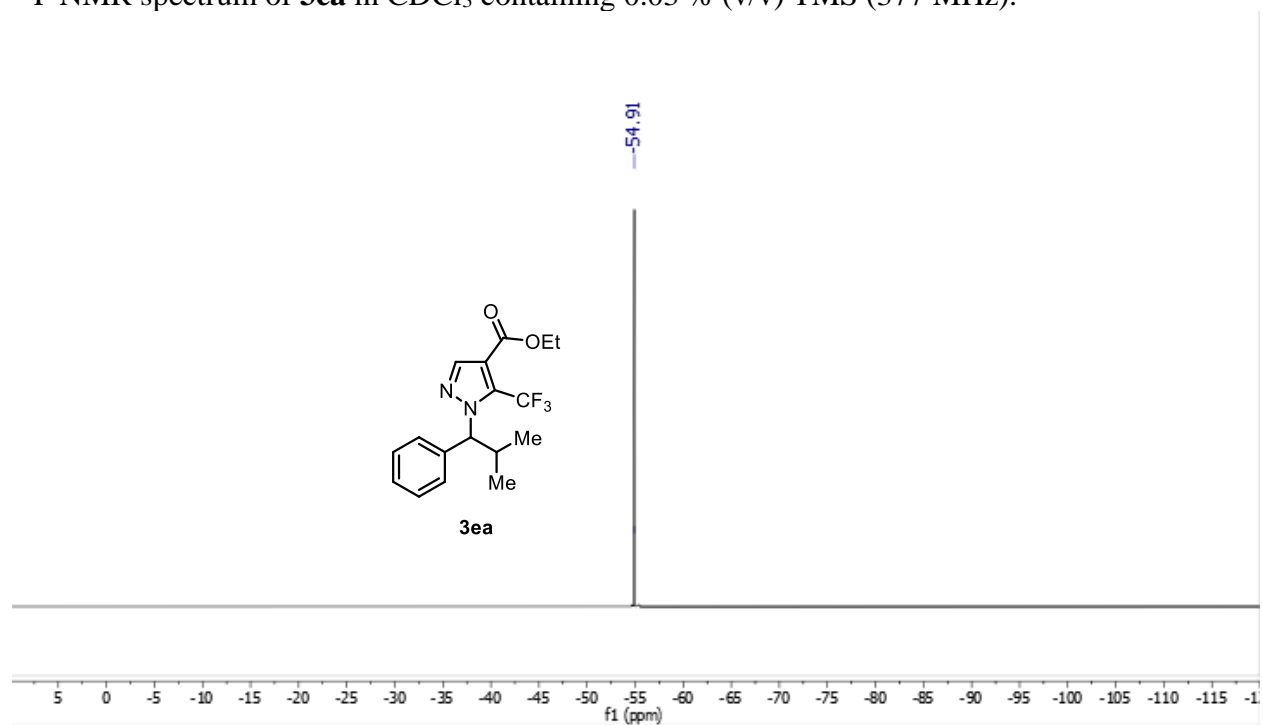
^1H NMR spectrum of **3ea** in CDCl_3 containing 0.03 % (v/v) TMS (500 MHz).



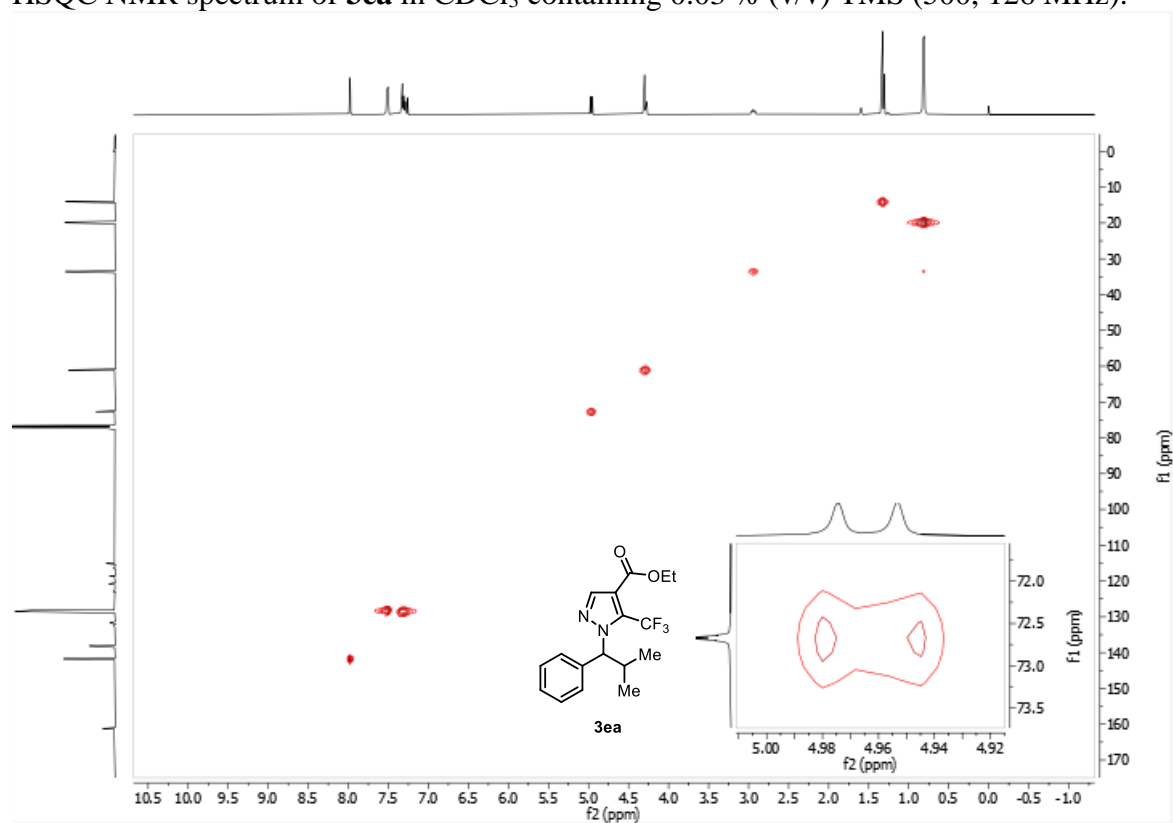
^{13}C NMR spectrum of **3ea** in CDCl_3 containing 0.03 % (v/v) TMS (126 MHz).



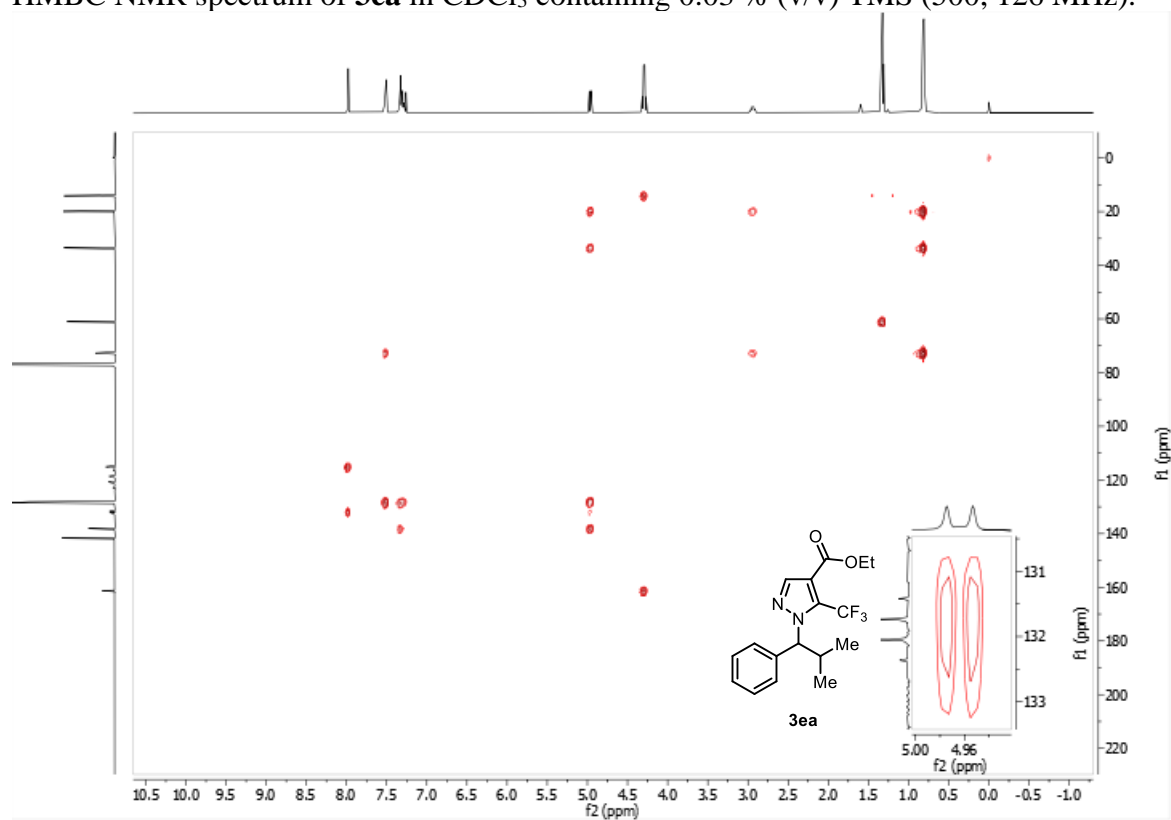
^{19}F NMR spectrum of **3ea** in CDCl_3 containing 0.03 % (v/v) TMS (377 MHz).



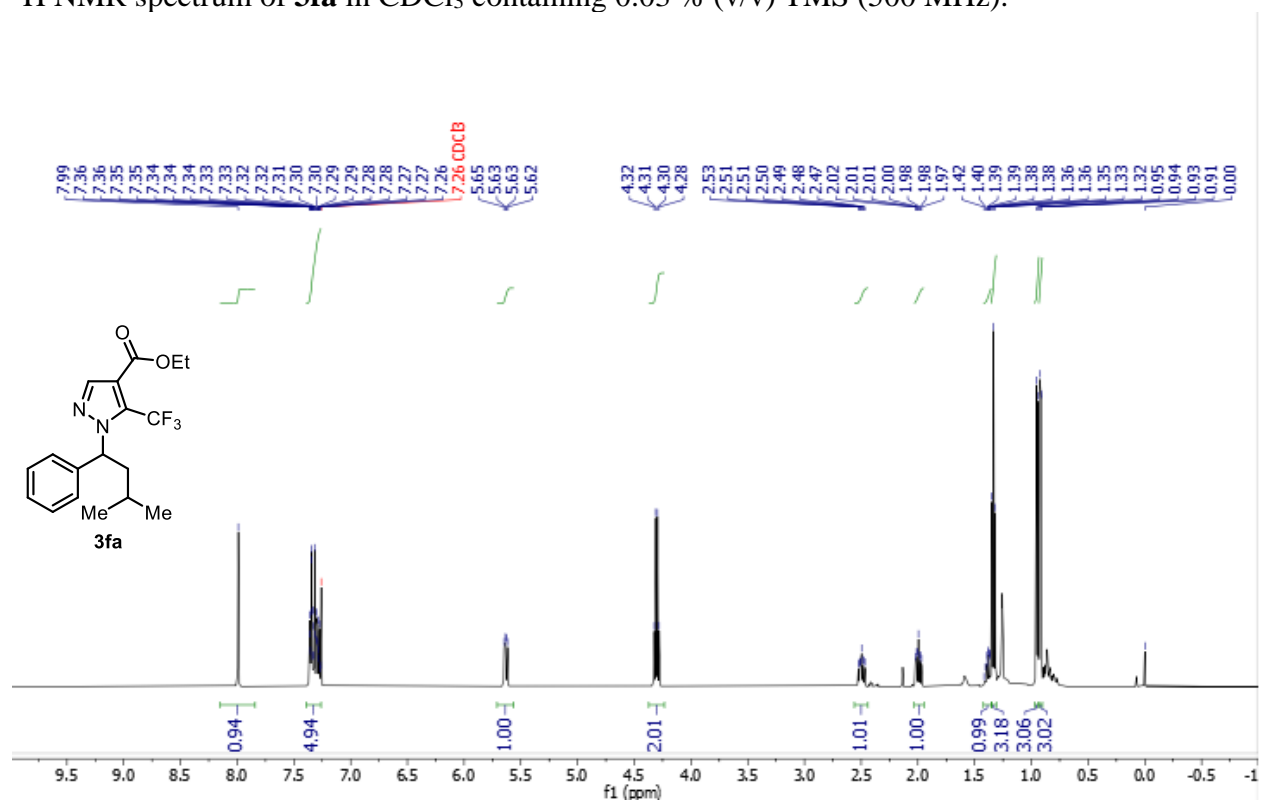
HSQC NMR spectrum of **3ea** in CDCl_3 containing 0.03 % (v/v) TMS (500, 126 MHz).



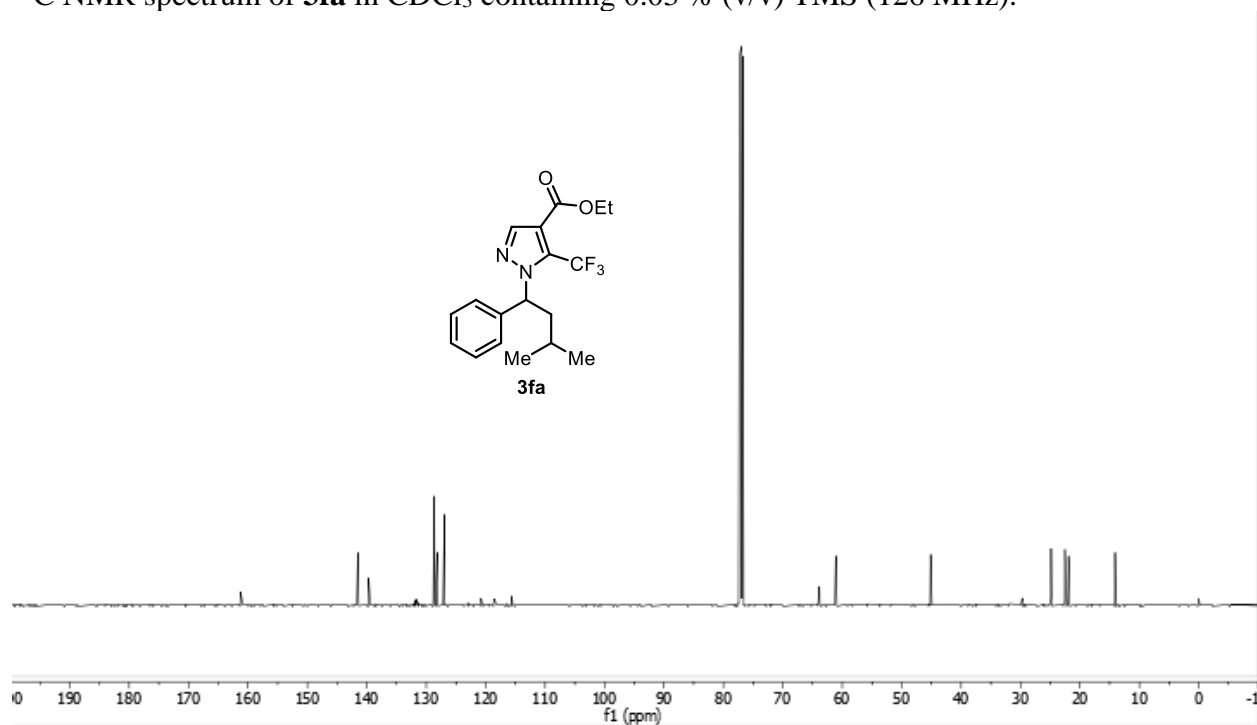
HMBC NMR spectrum of **3ea** in CDCl₃ containing 0.03 % (v/v) TMS (500, 126 MHz).



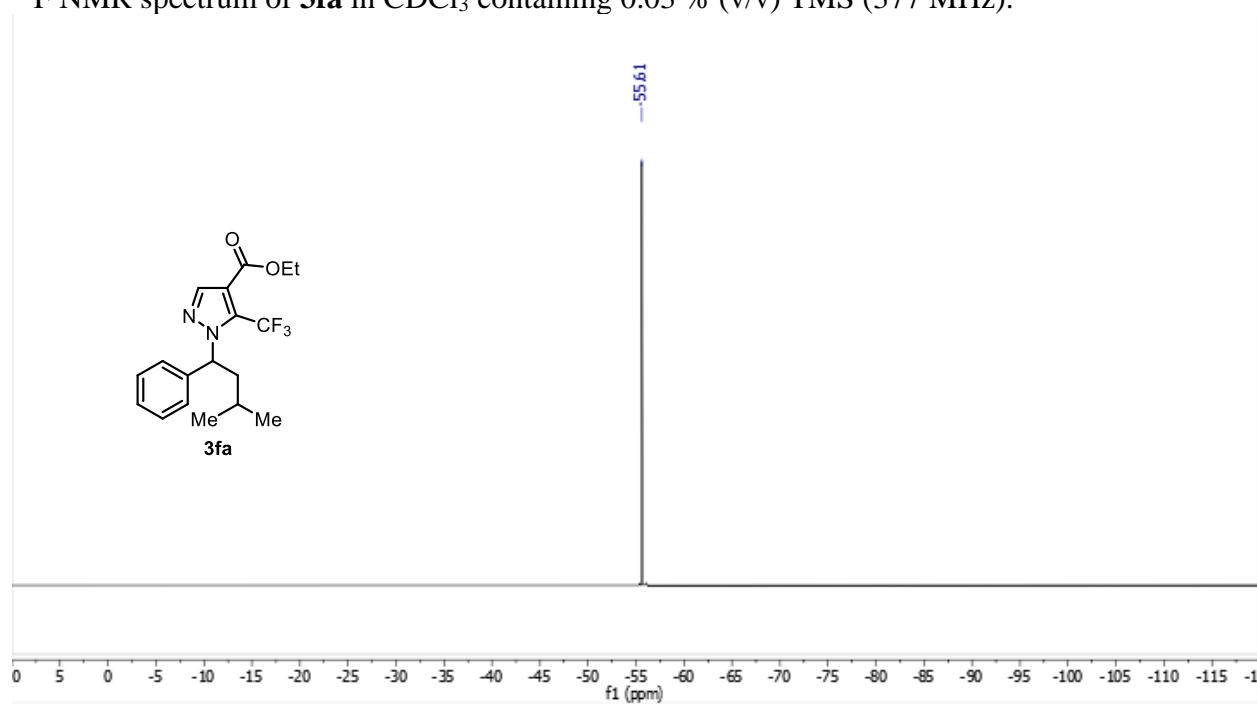
¹H NMR spectrum of **3fa** in CDCl₃ containing 0.03 % (v/v) TMS (500 MHz).



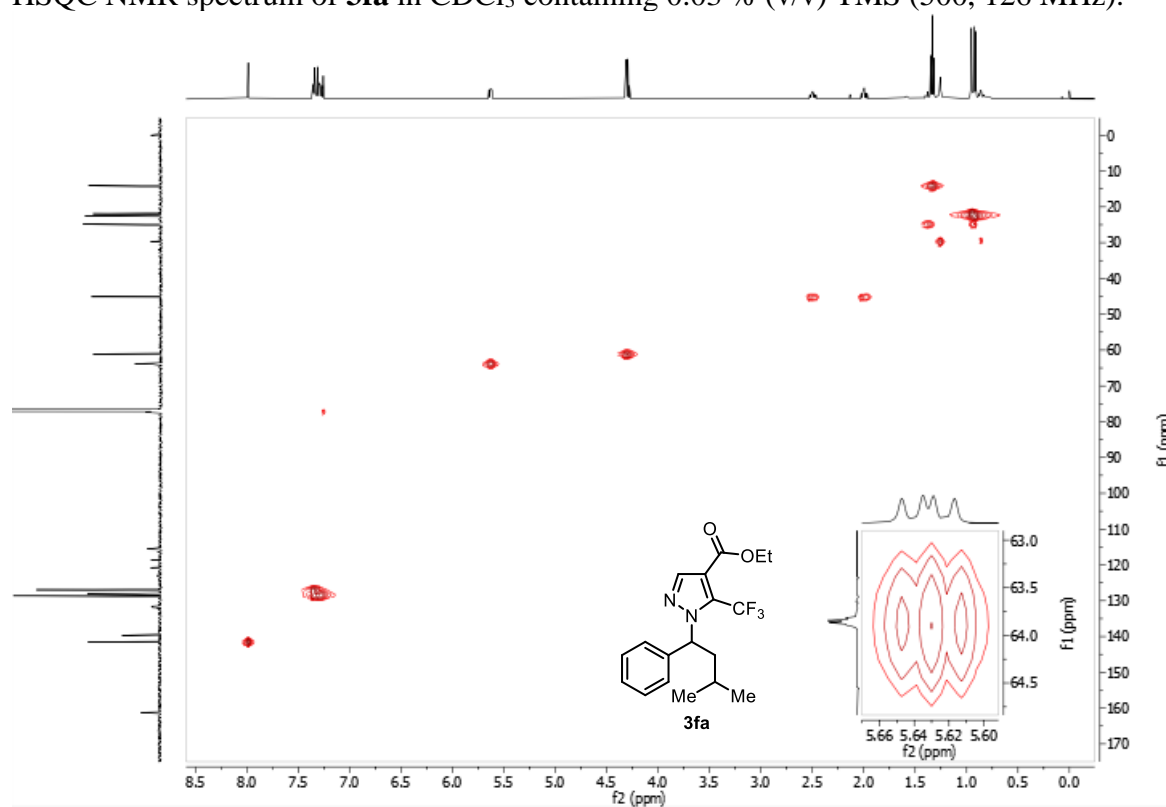
^{13}C NMR spectrum of **3fa** in CDCl_3 containing 0.03 % (v/v) TMS (126 MHz).



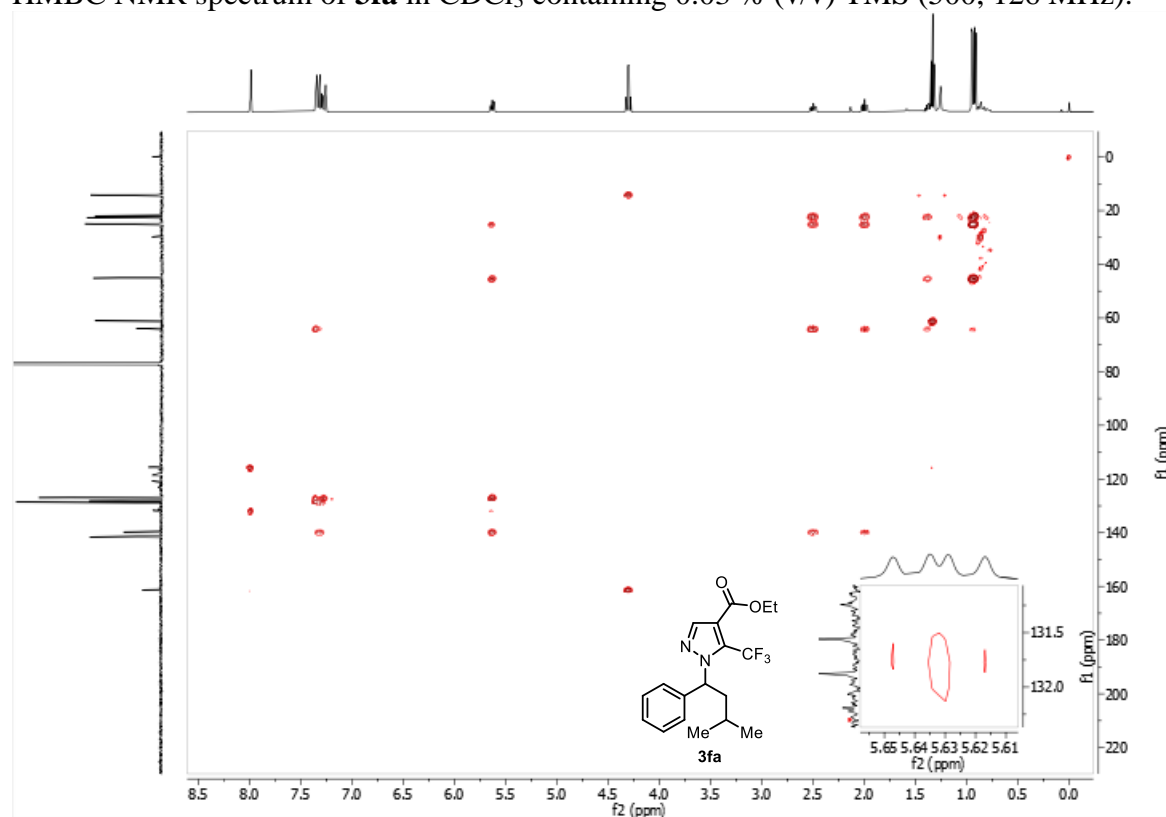
^{19}F NMR spectrum of **3fa** in CDCl_3 containing 0.03 % (v/v) TMS (377 MHz).



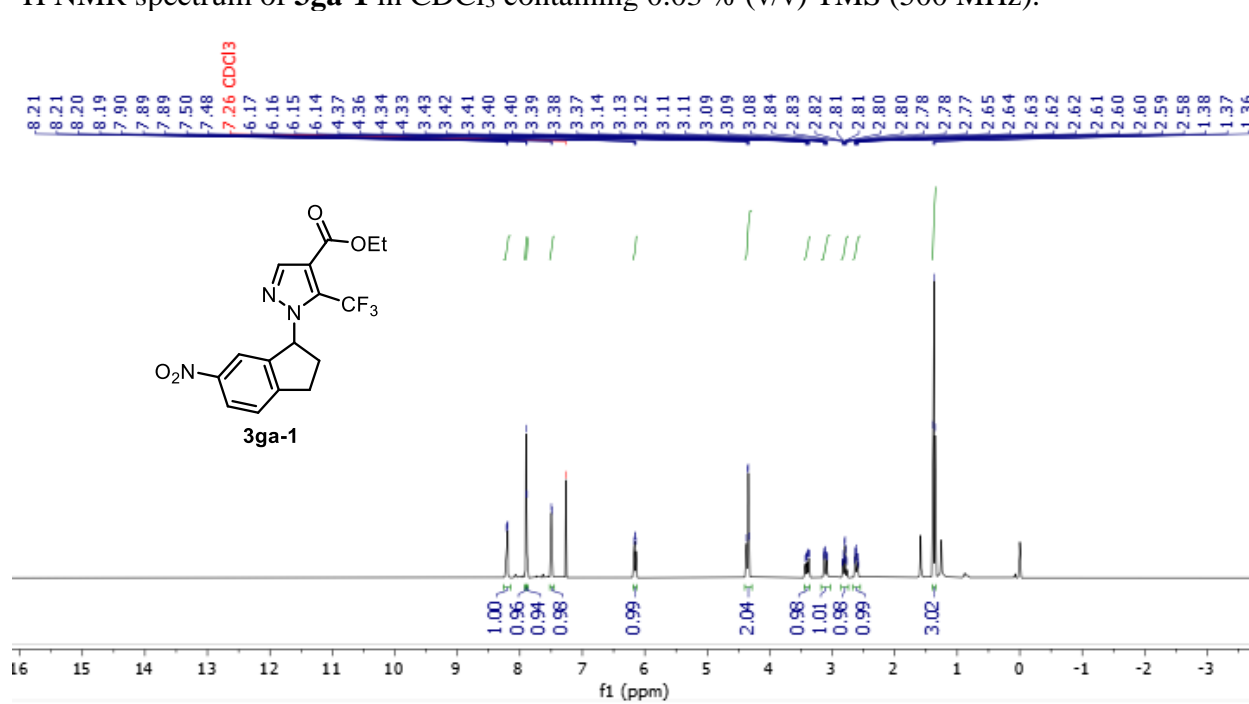
HSQC NMR spectrum of **3fa** in CDCl₃ containing 0.03 % (v/v) TMS (500, 126 MHz).



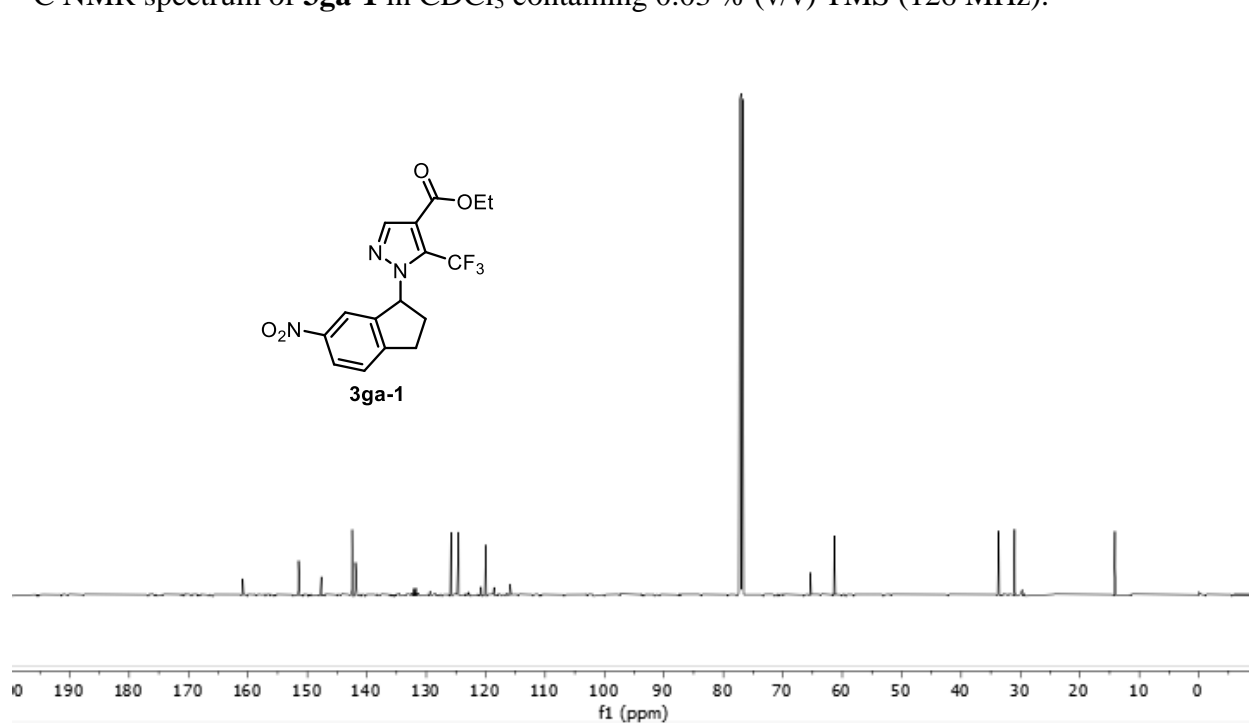
HMBC NMR spectrum of **3fa** in CDCl₃ containing 0.03 % (v/v) TMS (500, 126 MHz).



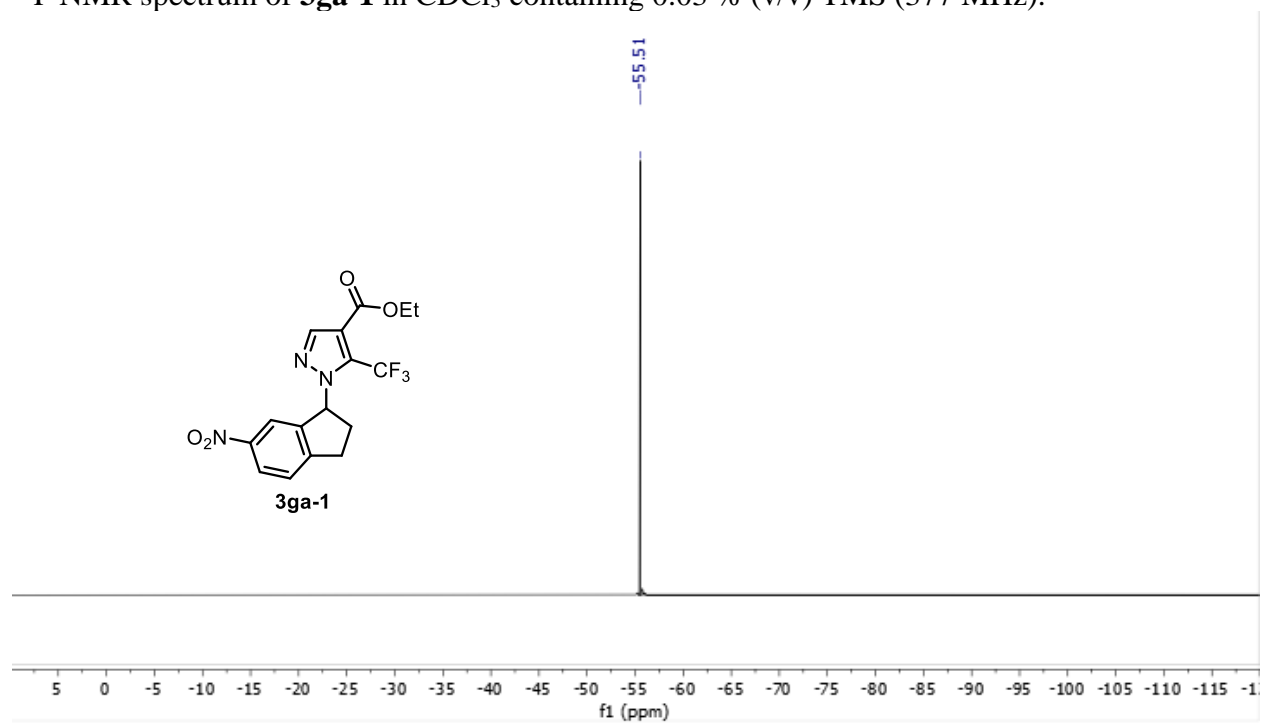
^1H NMR spectrum of **3ga-1** in CDCl_3 containing 0.03 % (v/v) TMS (500 MHz).



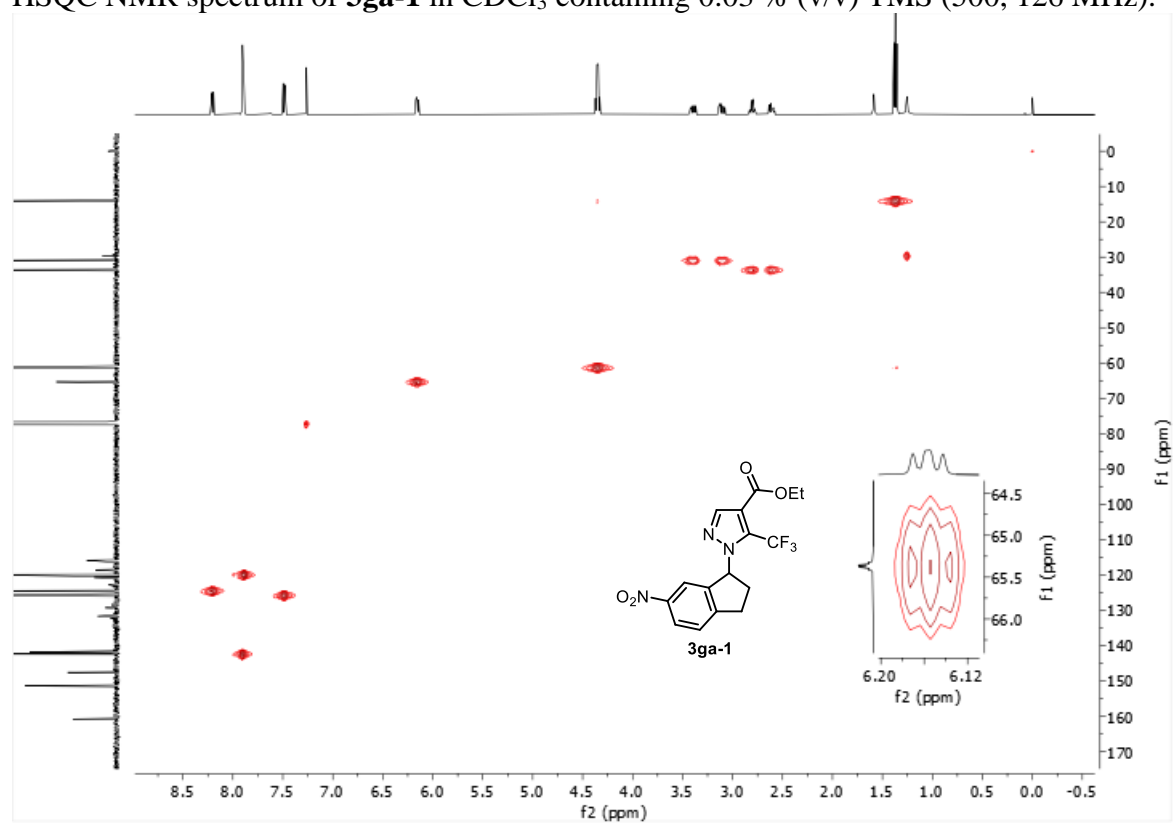
^{13}C NMR spectrum of **3ga-1** in CDCl_3 containing 0.03 % (v/v) TMS (126 MHz).



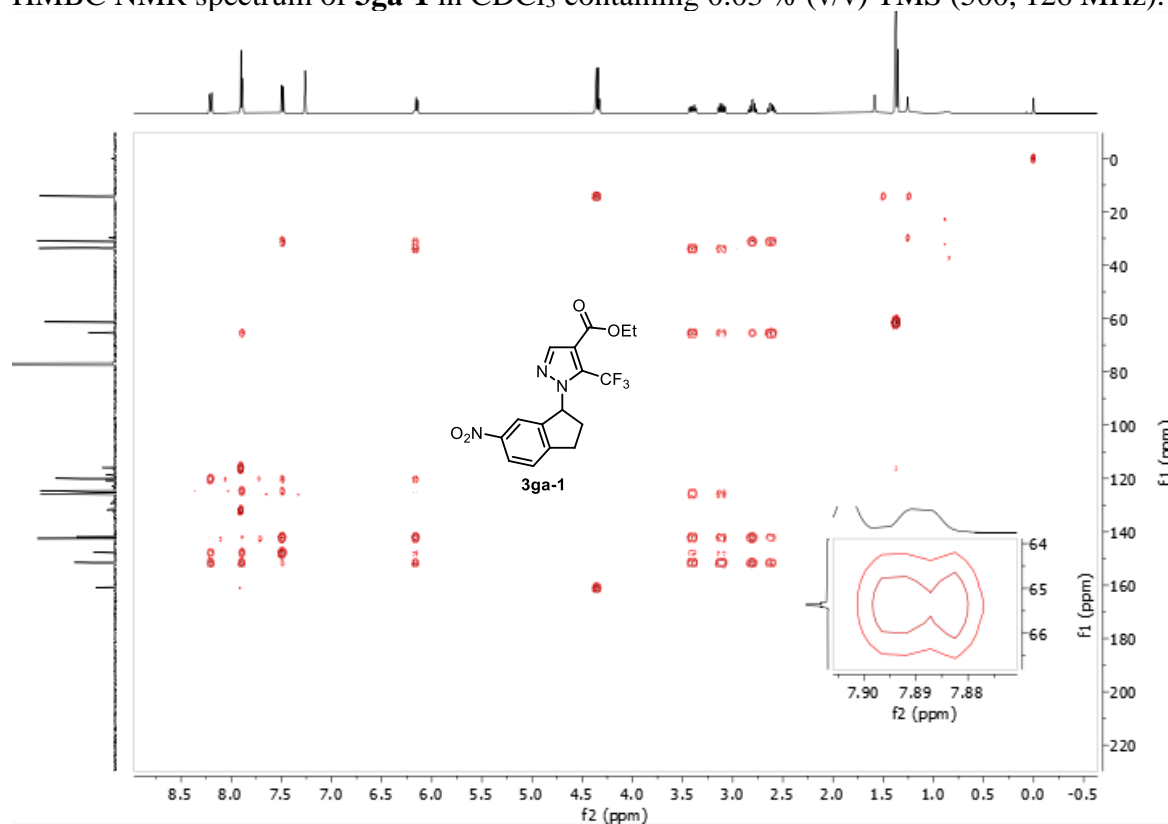
^{19}F NMR spectrum of **3ga-1** in CDCl_3 containing 0.03 % (v/v) TMS (377 MHz).



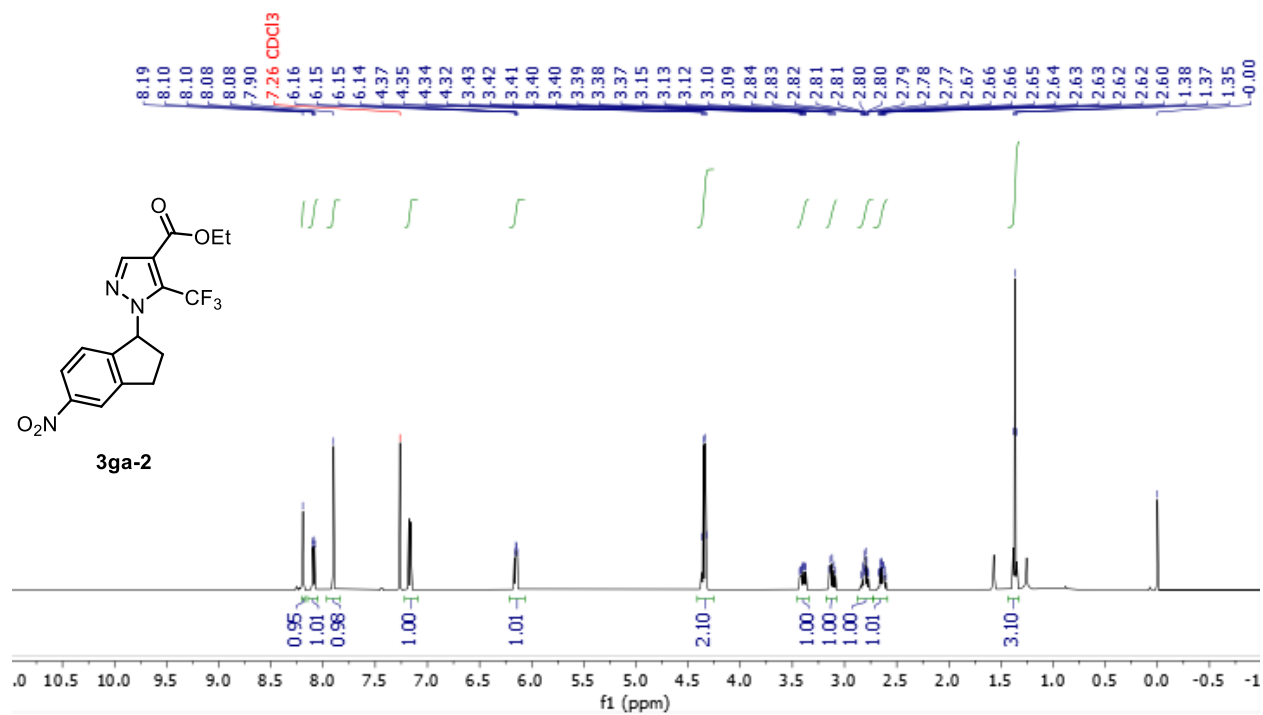
HSQC NMR spectrum of **3ga-1** in CDCl_3 containing 0.03 % (v/v) TMS (500, 126 MHz).



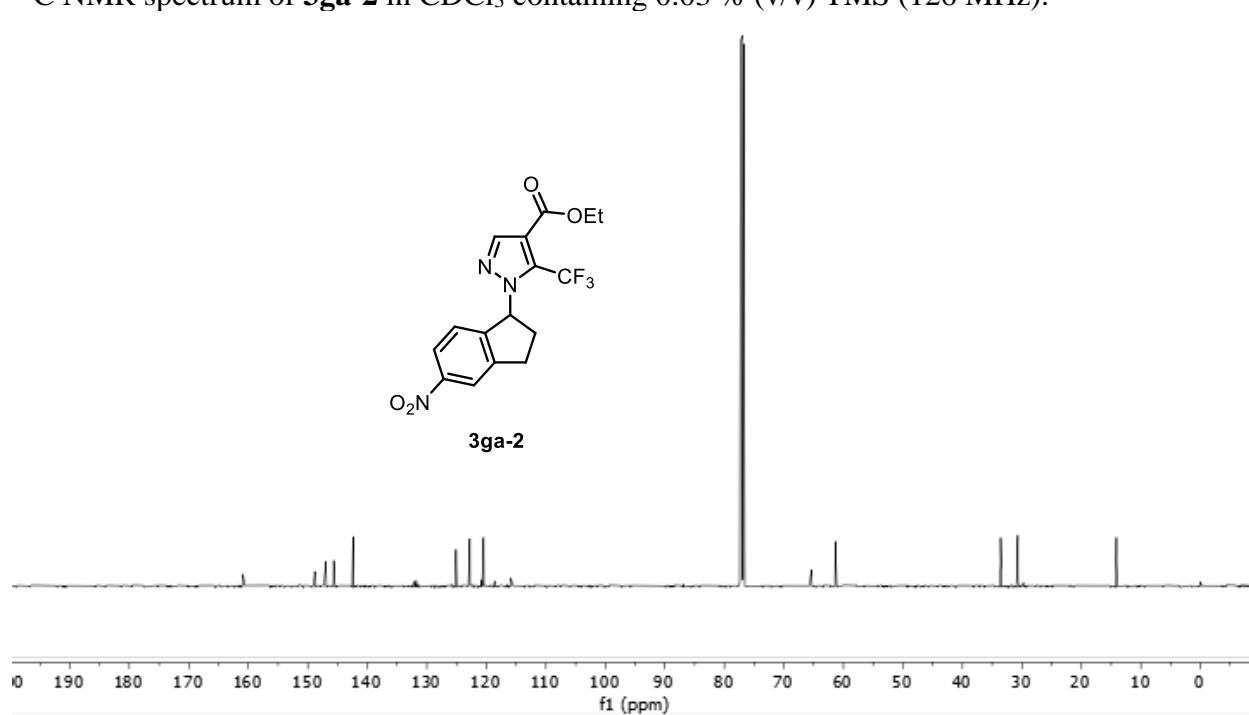
HMBC NMR spectrum of **3ga-1** in CDCl₃ containing 0.03 % (v/v) TMS (500, 126 MHz).



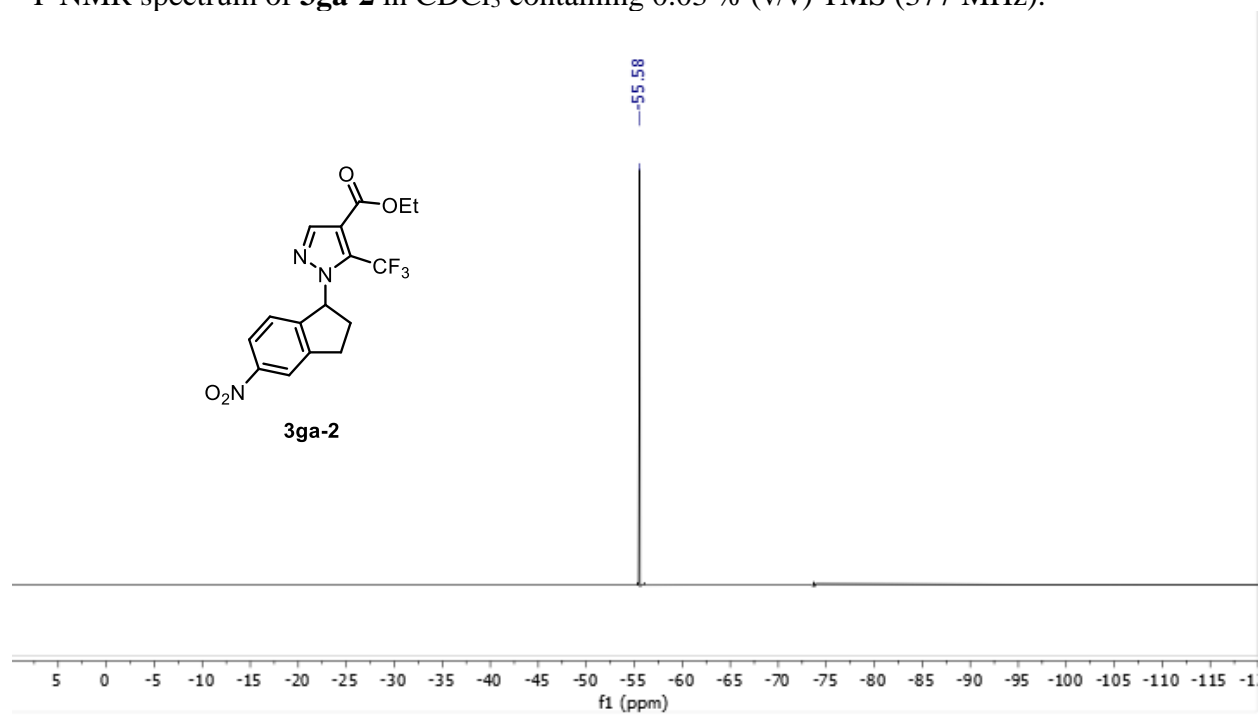
¹H NMR spectrum of **3ga-2** in CDCl₃ containing 0.03 % (v/v) TMS (500 MHz).



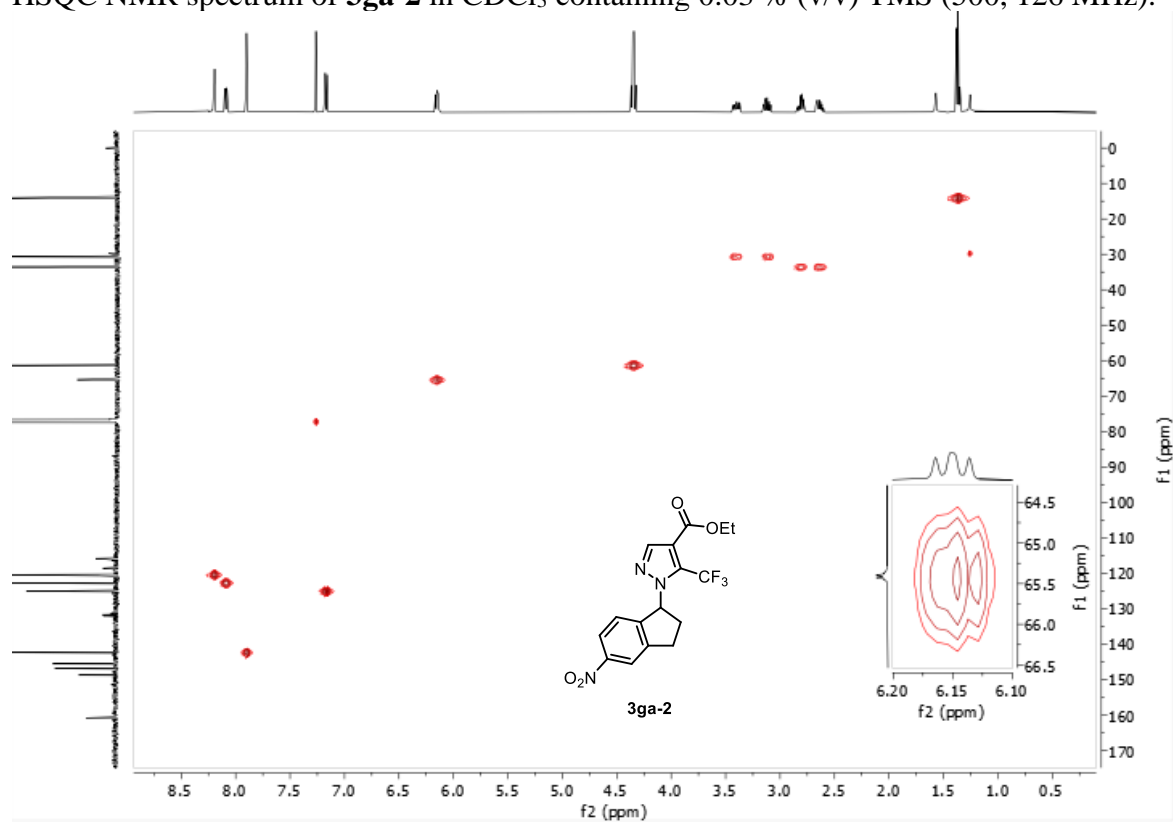
^{13}C NMR spectrum of **3ga-2** in CDCl_3 containing 0.03 % (v/v) TMS (126 MHz).



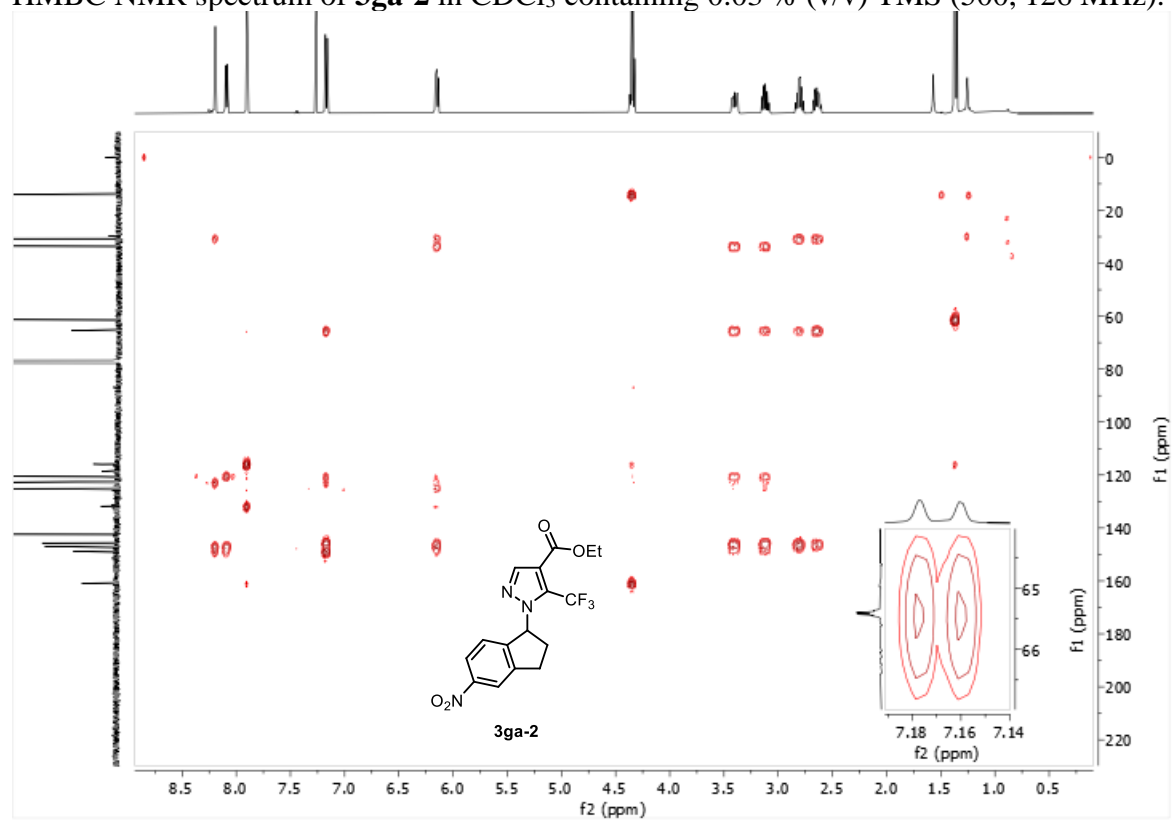
^{19}F NMR spectrum of **3ga-2** in CDCl_3 containing 0.03 % (v/v) TMS (377 MHz).



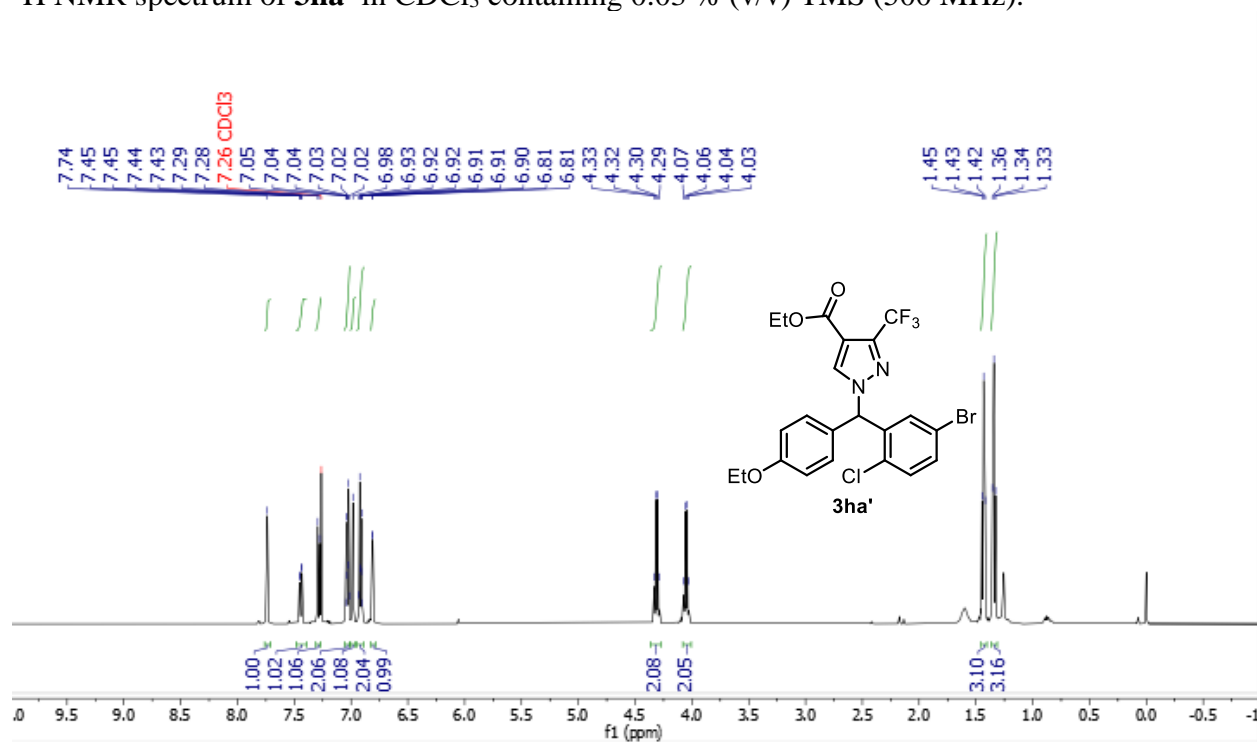
HSQC NMR spectrum of **3ga-2** in CDCl₃ containing 0.03 % (v/v) TMS (500, 126 MHz).



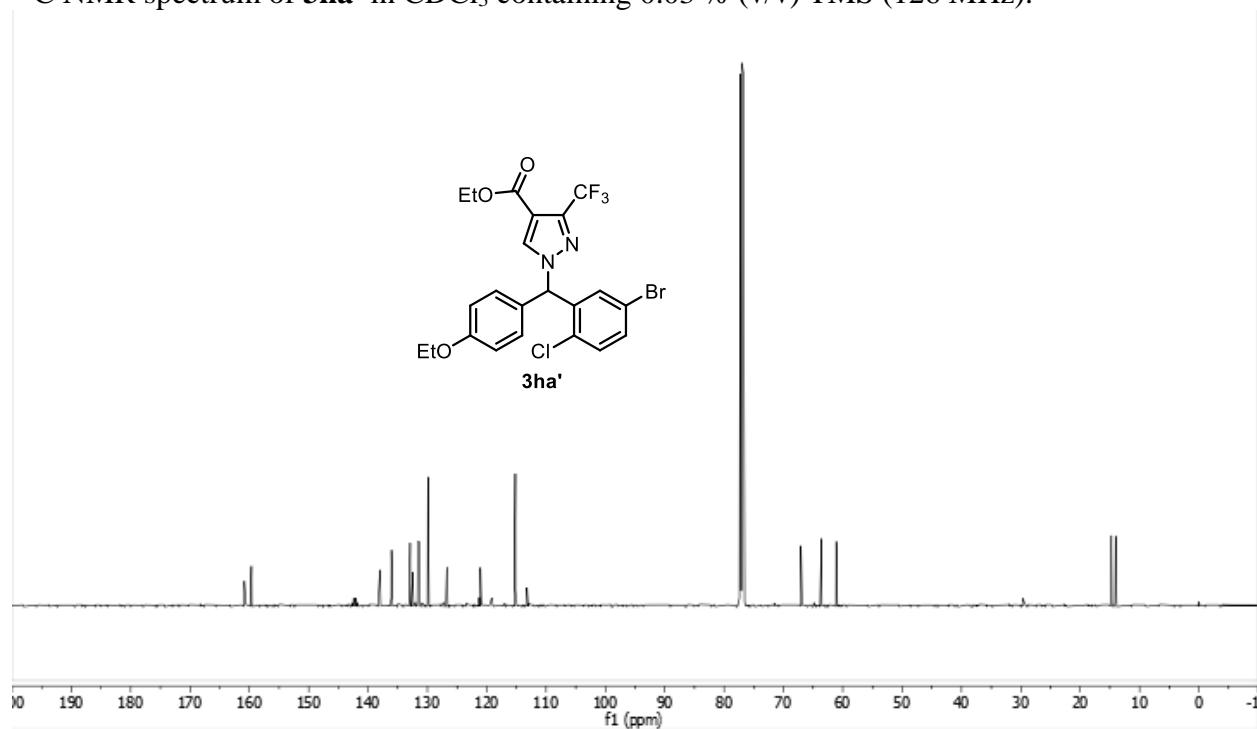
HMBC NMR spectrum of **3ga-2** in CDCl₃ containing 0.03 % (v/v) TMS (500, 126 MHz).



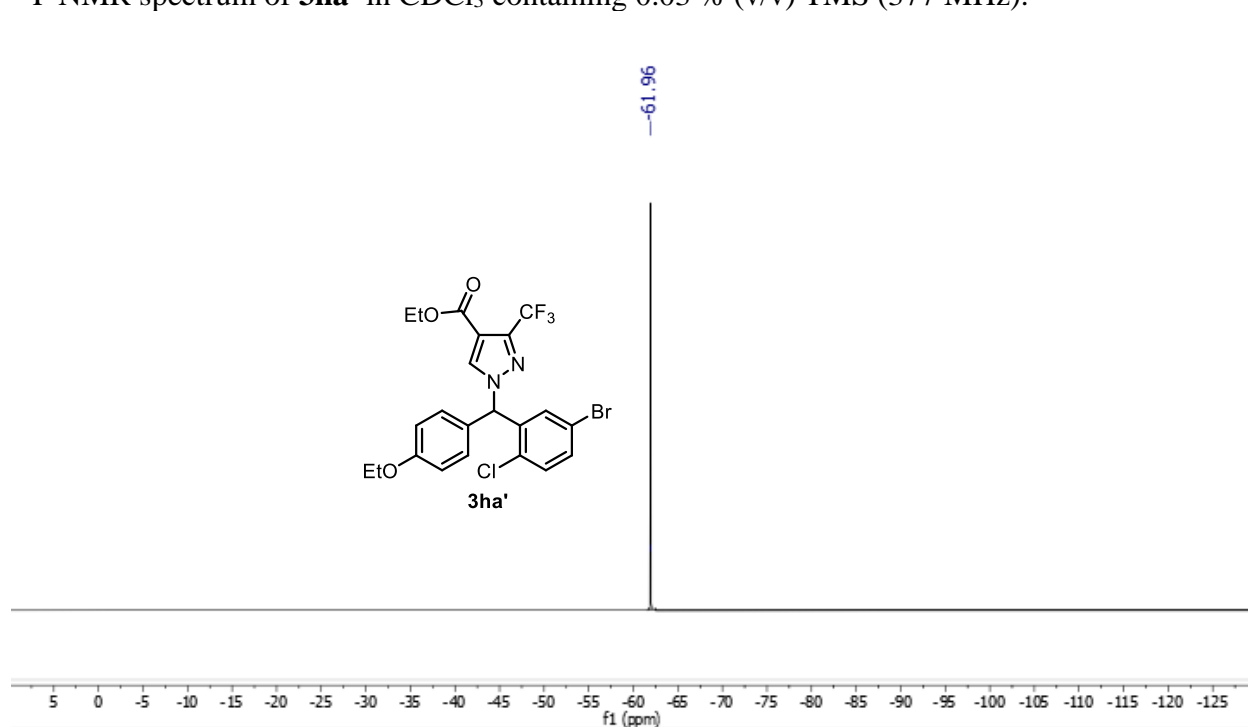
^1H NMR spectrum of **3ha'** in CDCl_3 containing 0.03 % (v/v) TMS (500 MHz).



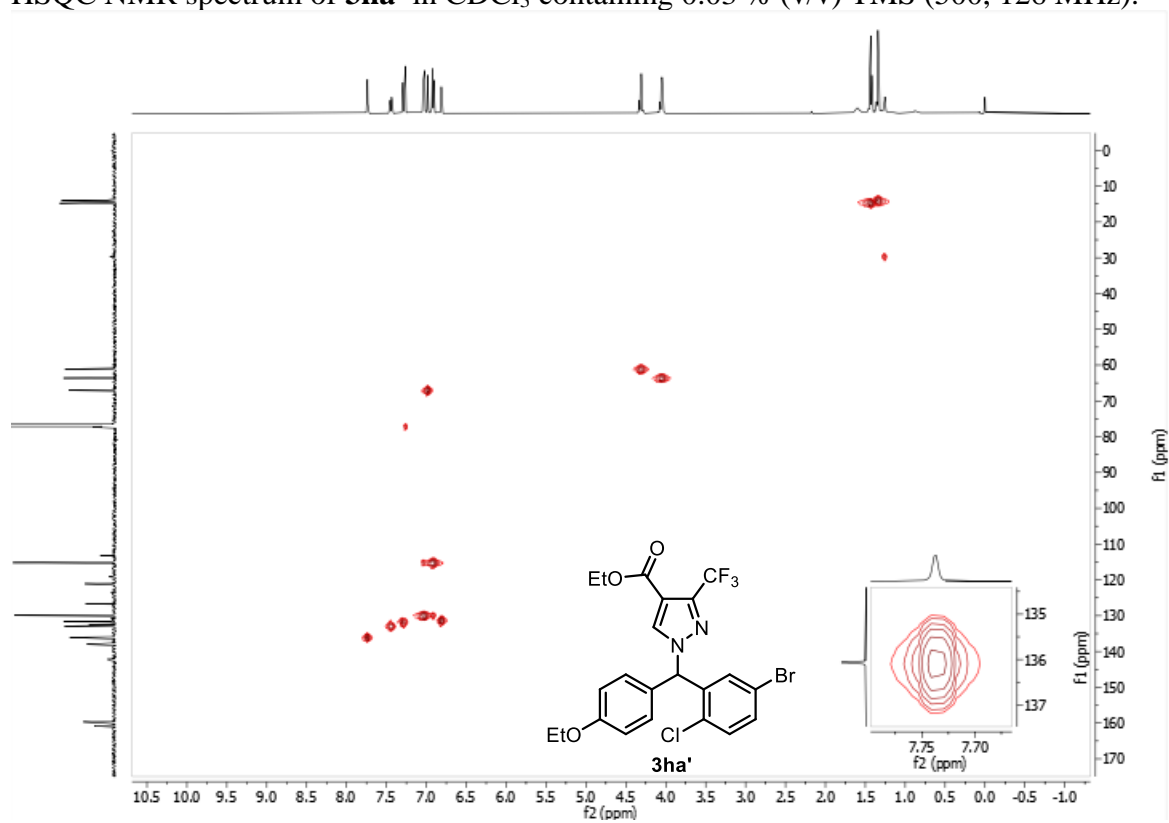
^{13}C NMR spectrum of **3ha'** in CDCl_3 containing 0.03 % (v/v) TMS (126 MHz).



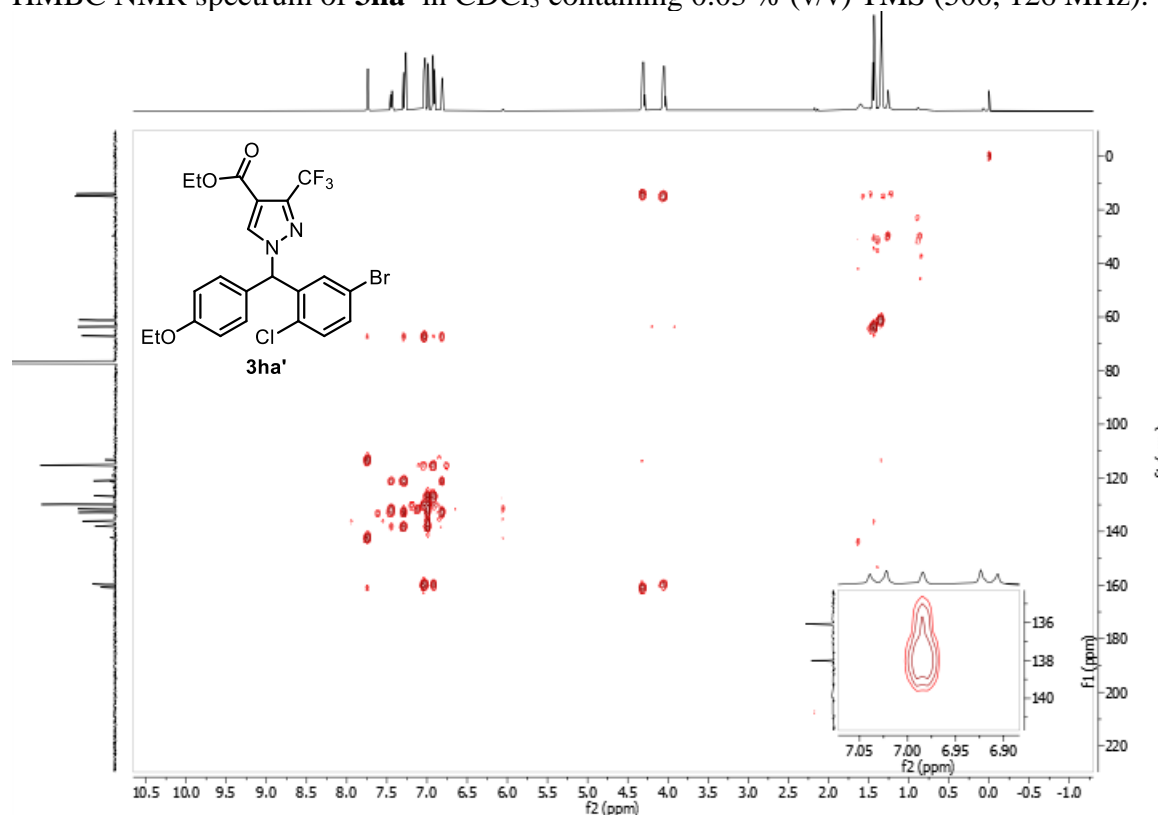
^{19}F NMR spectrum of **3ha'** in CDCl_3 containing 0.03 % (v/v) TMS (377 MHz).



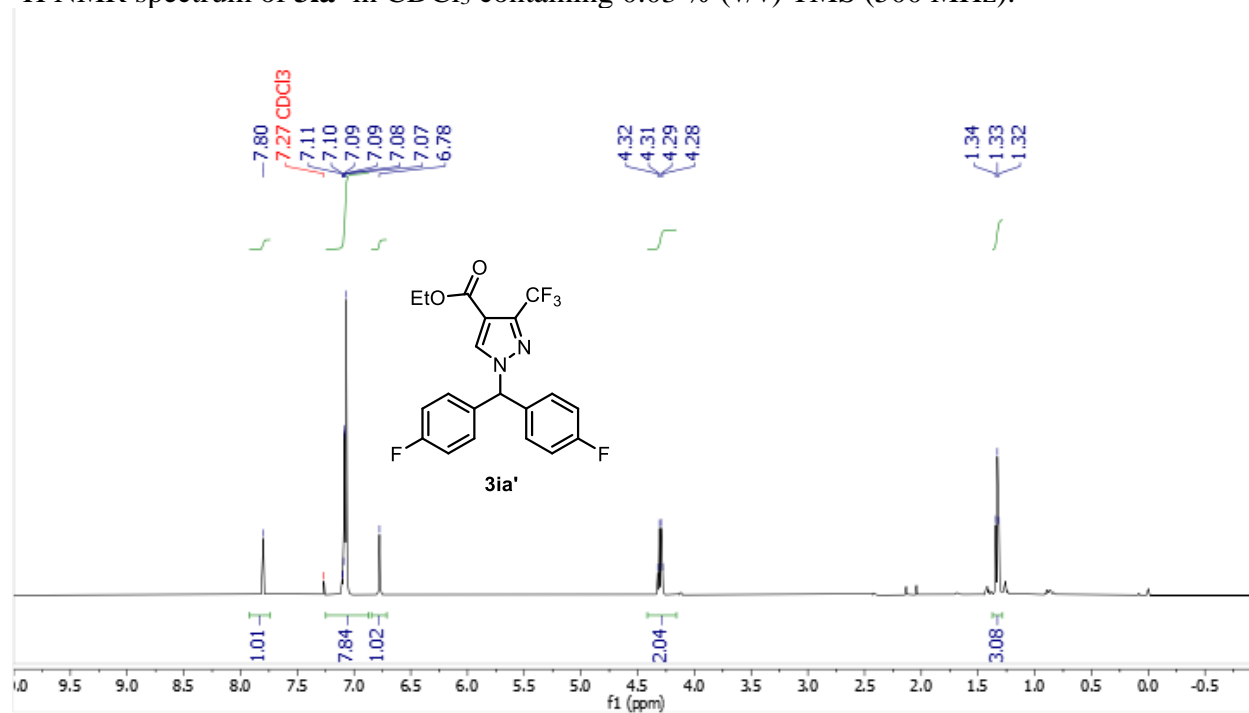
HSQC NMR spectrum of **3ha'** in CDCl_3 containing 0.03 % (v/v) TMS (500, 126 MHz).



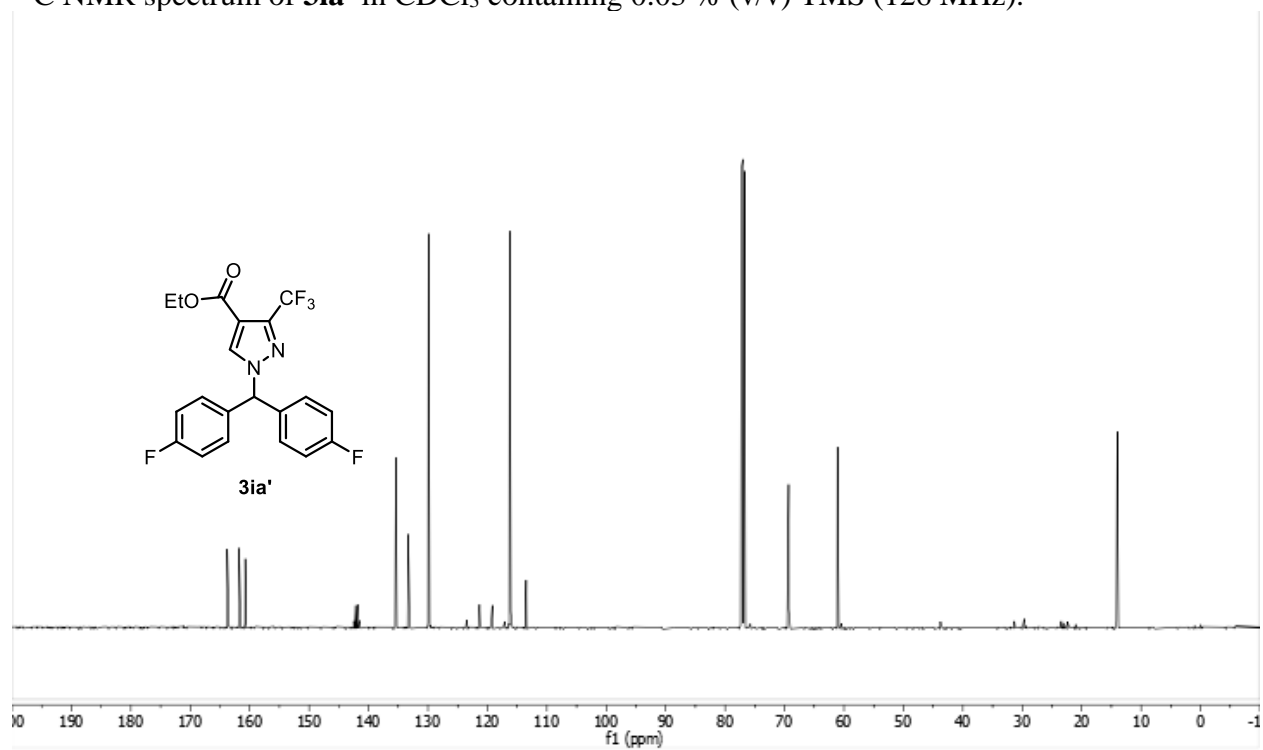
HMBC NMR spectrum of **3ha'** in CDCl₃ containing 0.03 % (v/v) TMS (500, 126 MHz).



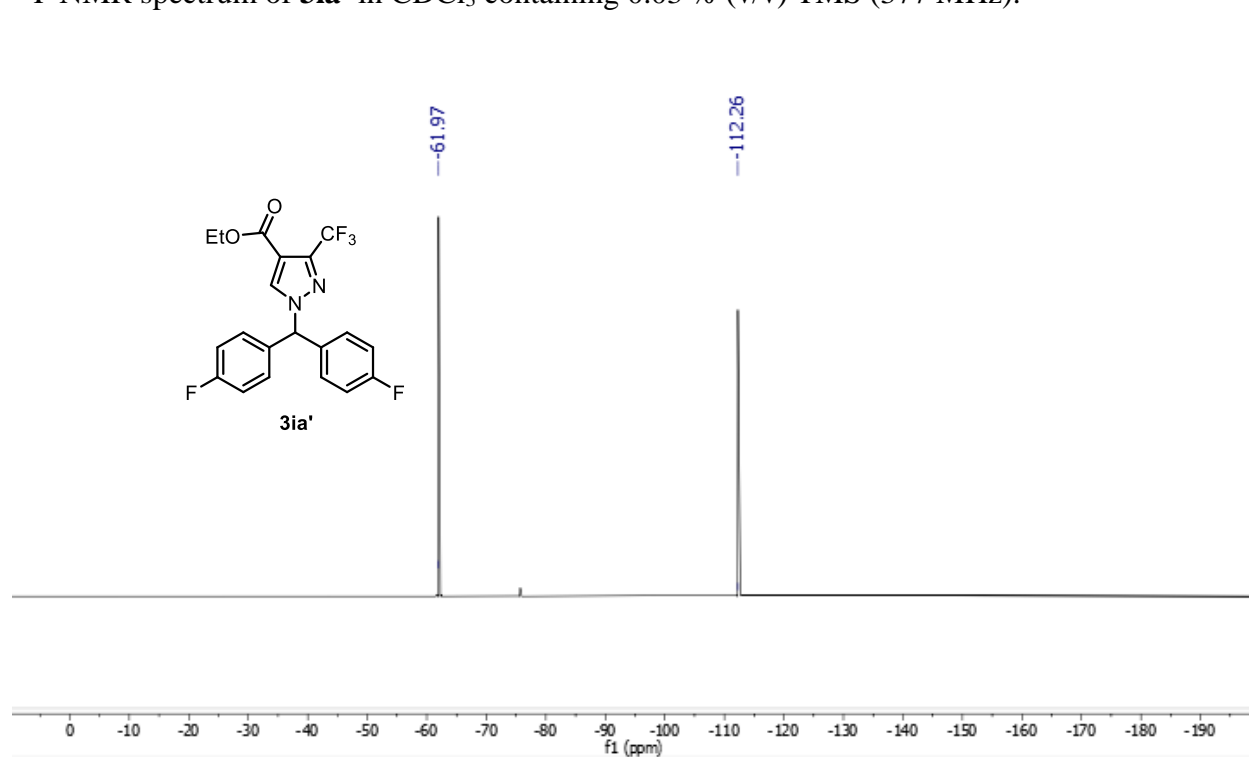
¹H NMR spectrum of **3ia'** in CDCl₃ containing 0.03 % (v/v) TMS (500 MHz).



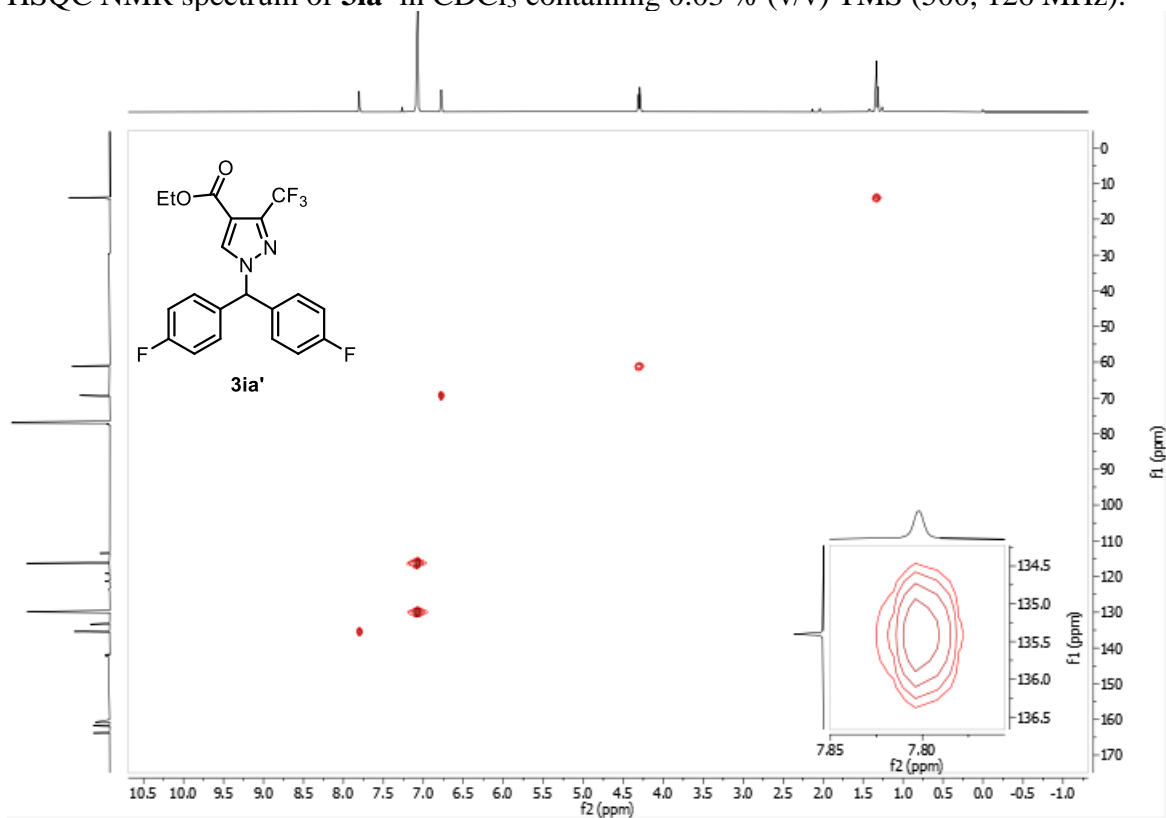
^{13}C NMR spectrum of **3ia'** in CDCl_3 containing 0.03 % (v/v) TMS (126 MHz).



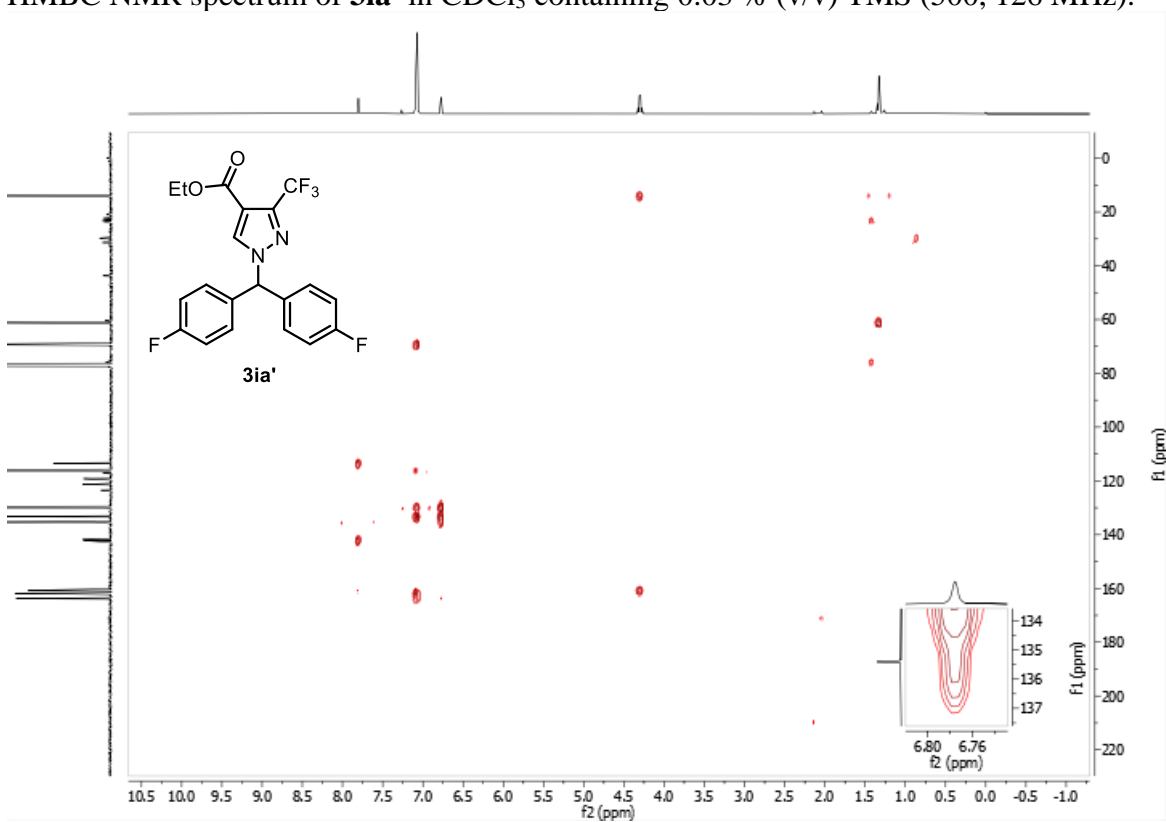
^{19}F NMR spectrum of **3ia'** in CDCl_3 containing 0.03 % (v/v) TMS (377 MHz).



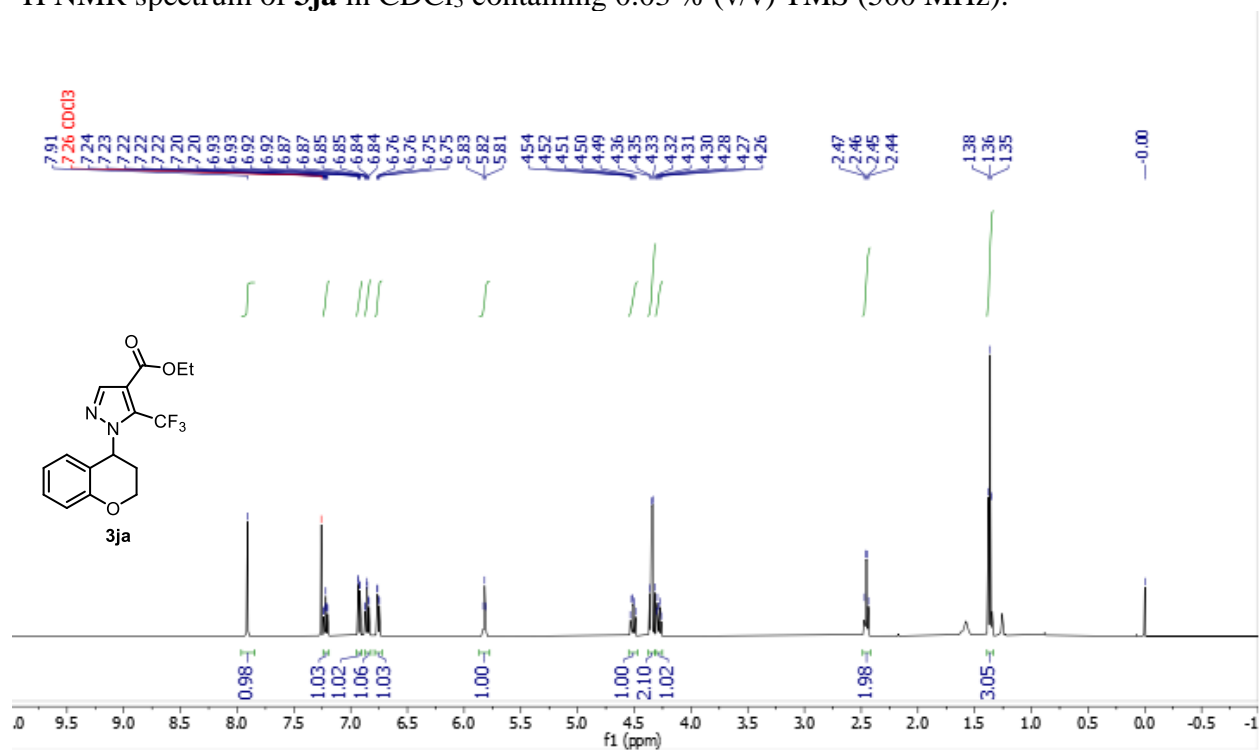
HSQC NMR spectrum of **3ia'** in CDCl₃ containing 0.03 % (v/v) TMS (500, 126 MHz).



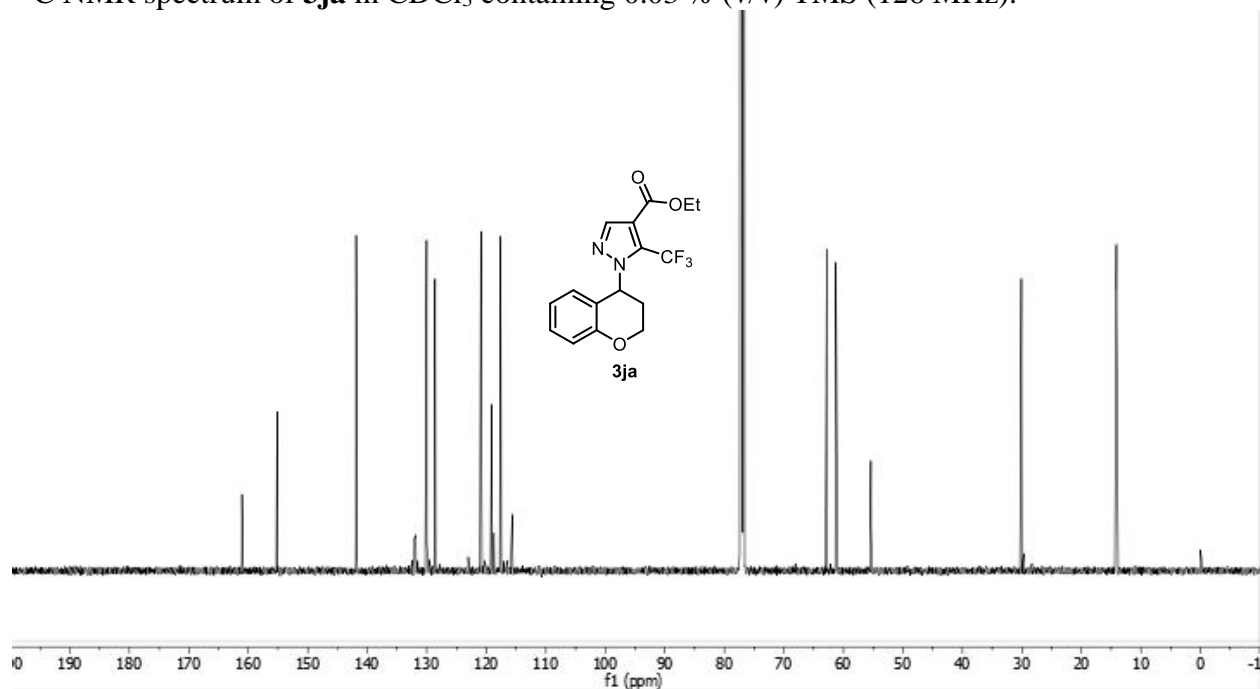
HMBC NMR spectrum of **3ia'** in CDCl₃ containing 0.03 % (v/v) TMS (500, 126 MHz).



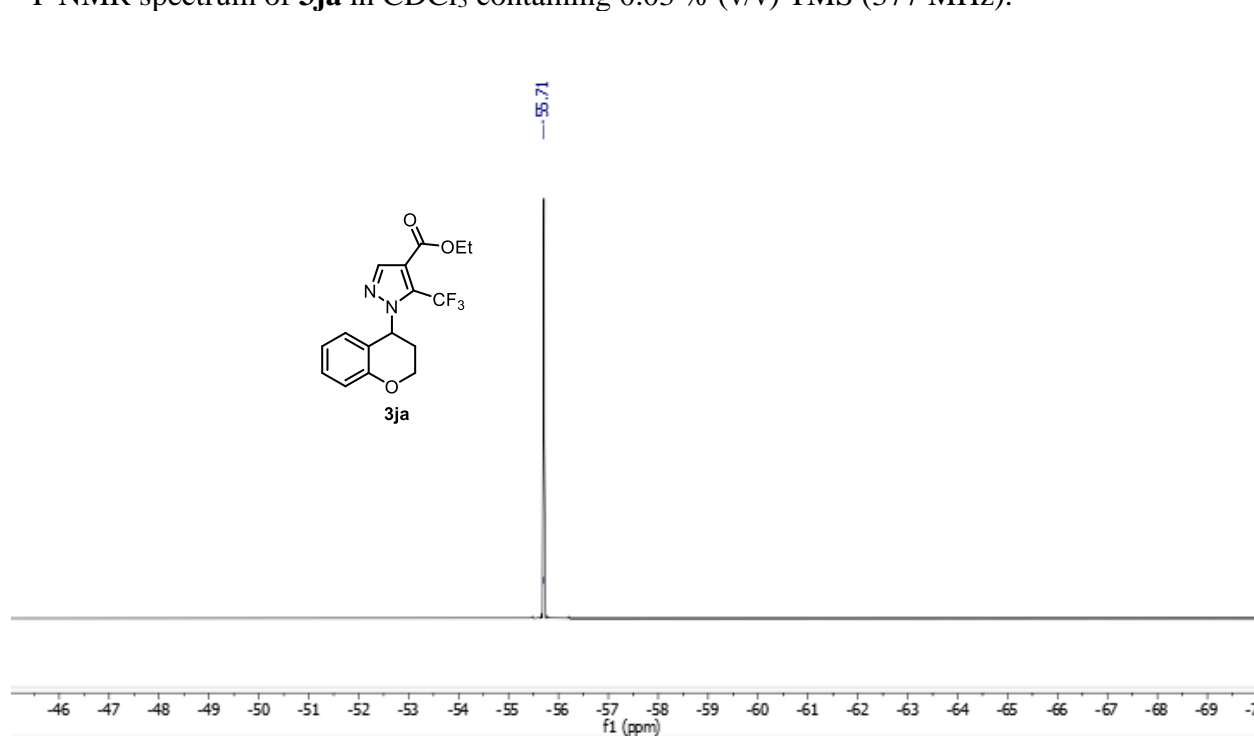
^1H NMR spectrum of **3ja** in CDCl_3 containing 0.03 % (v/v) TMS (500 MHz).



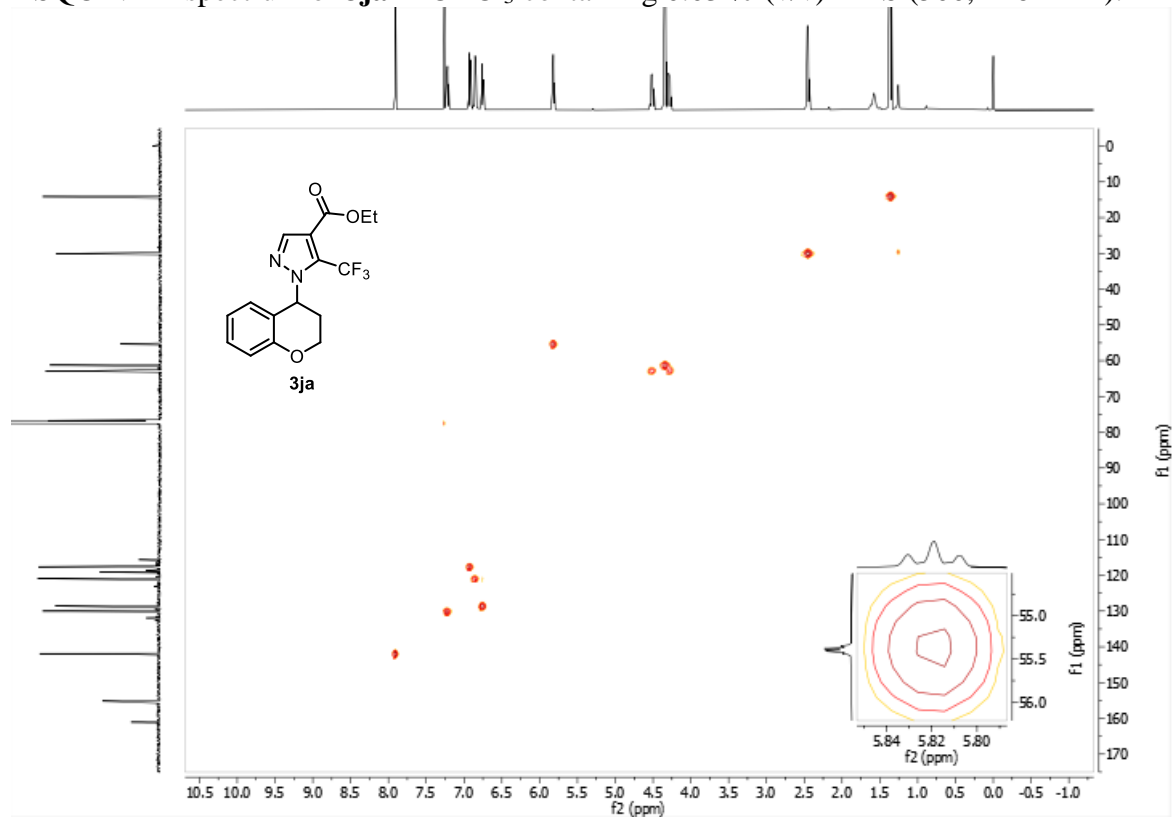
^{13}C NMR spectrum of **3ja** in CDCl_3 containing 0.03 % (v/v) TMS (126 MHz).



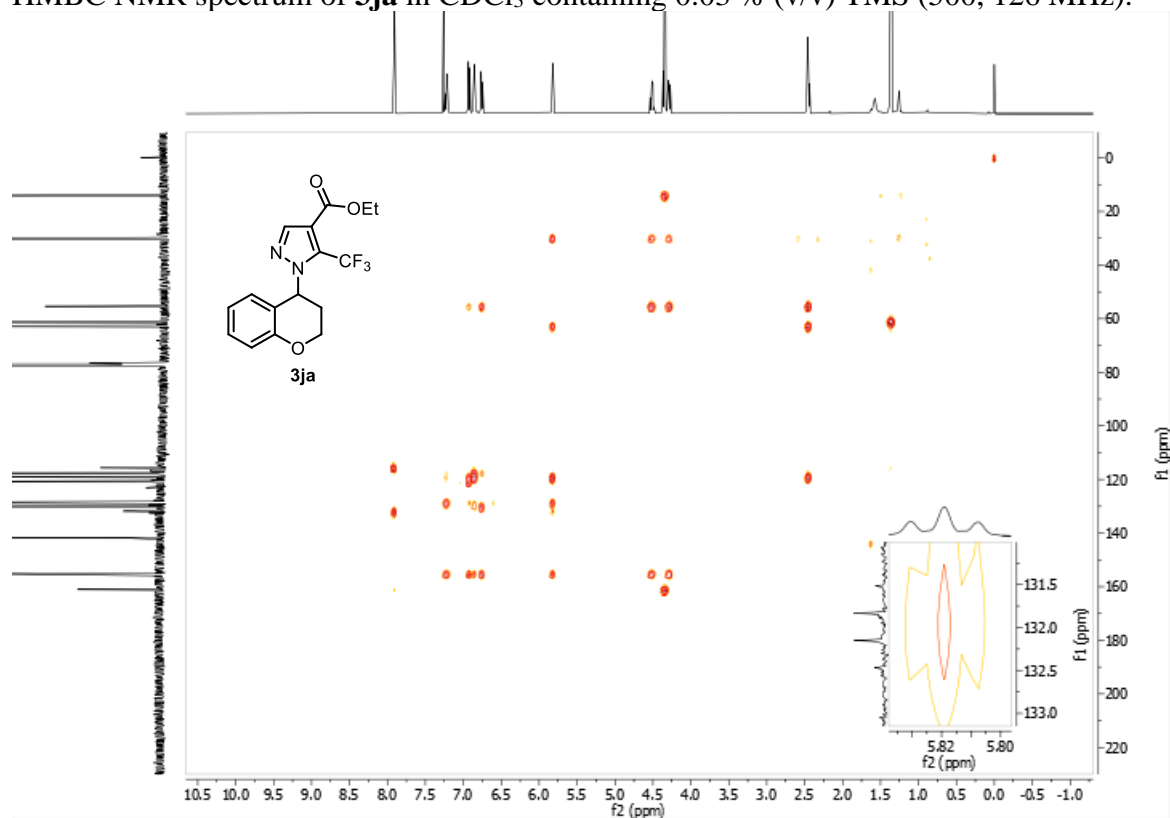
^{19}F NMR spectrum of **3ja** in CDCl_3 containing 0.03 % (v/v) TMS (377 MHz).



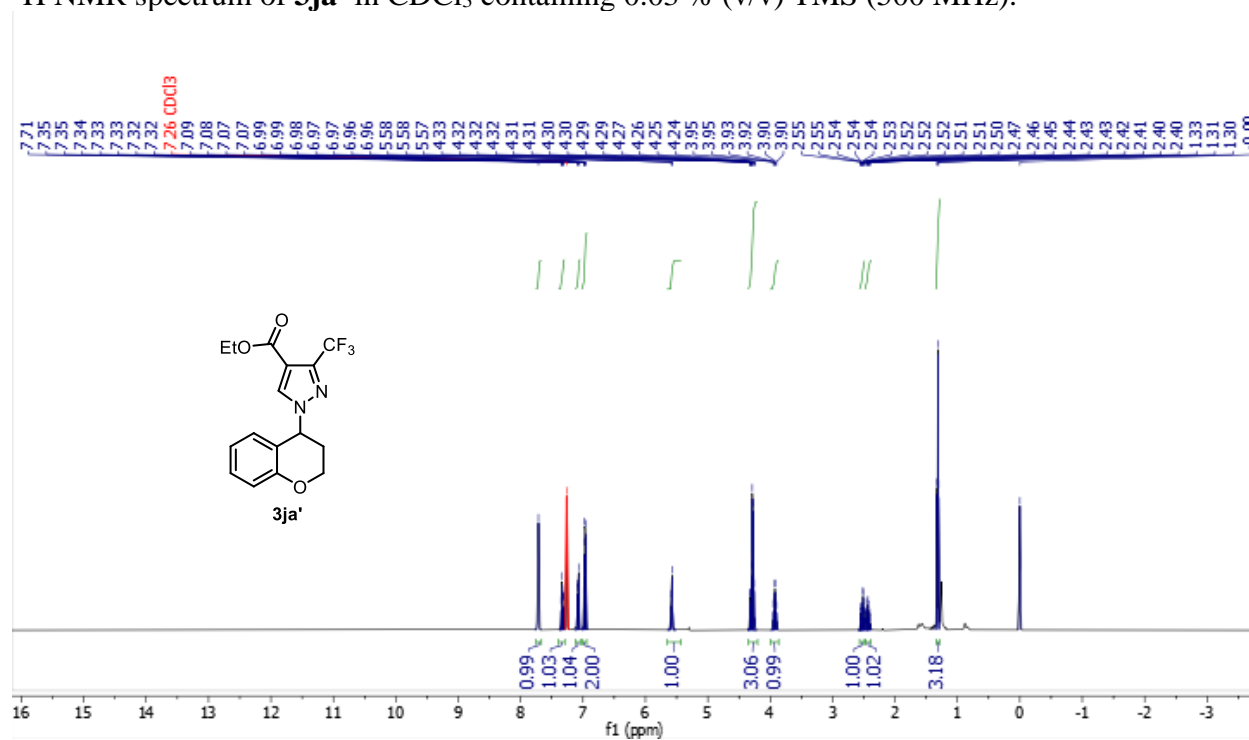
HSQC NMR spectrum of **3ja** in CDCl_3 containing 0.03 % (v/v) TMS (500, 126 MHz).



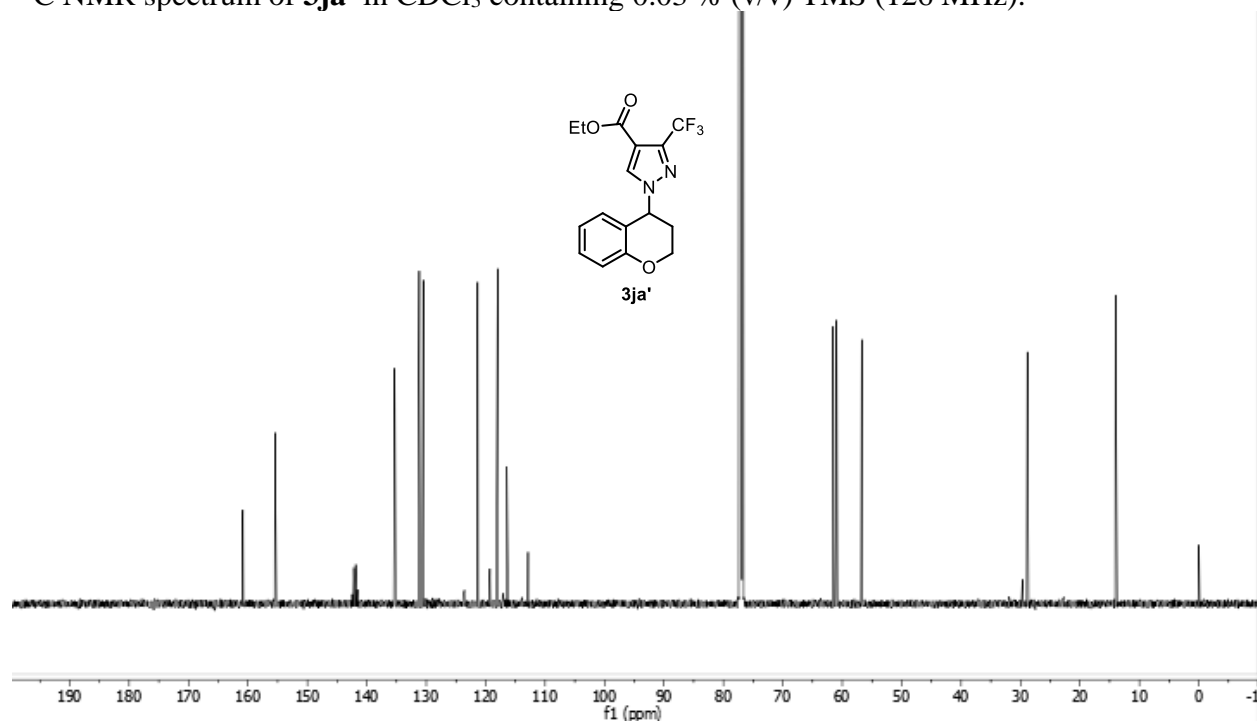
HMBC NMR spectrum of **3ja** in CDCl₃ containing 0.03 % (v/v) TMS (500, 126 MHz).



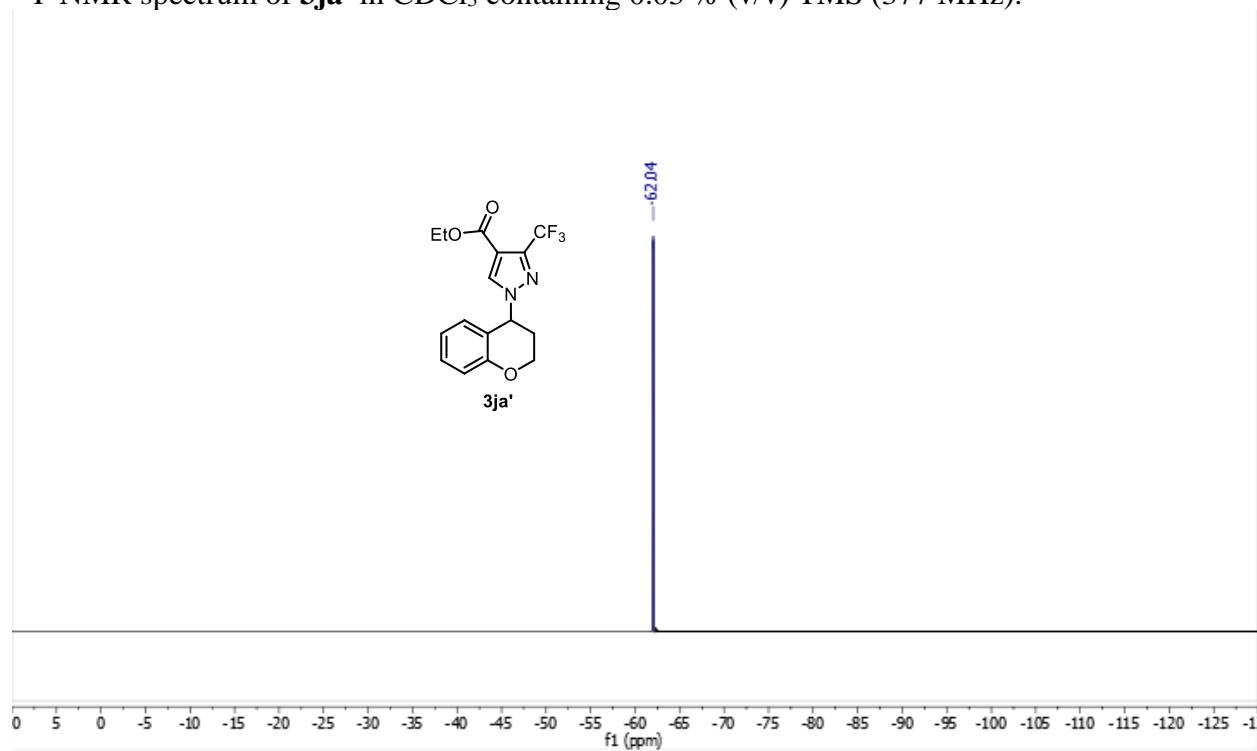
¹H NMR spectrum of **3ja'** in CDCl₃ containing 0.03 % (v/v) TMS (500 MHz).



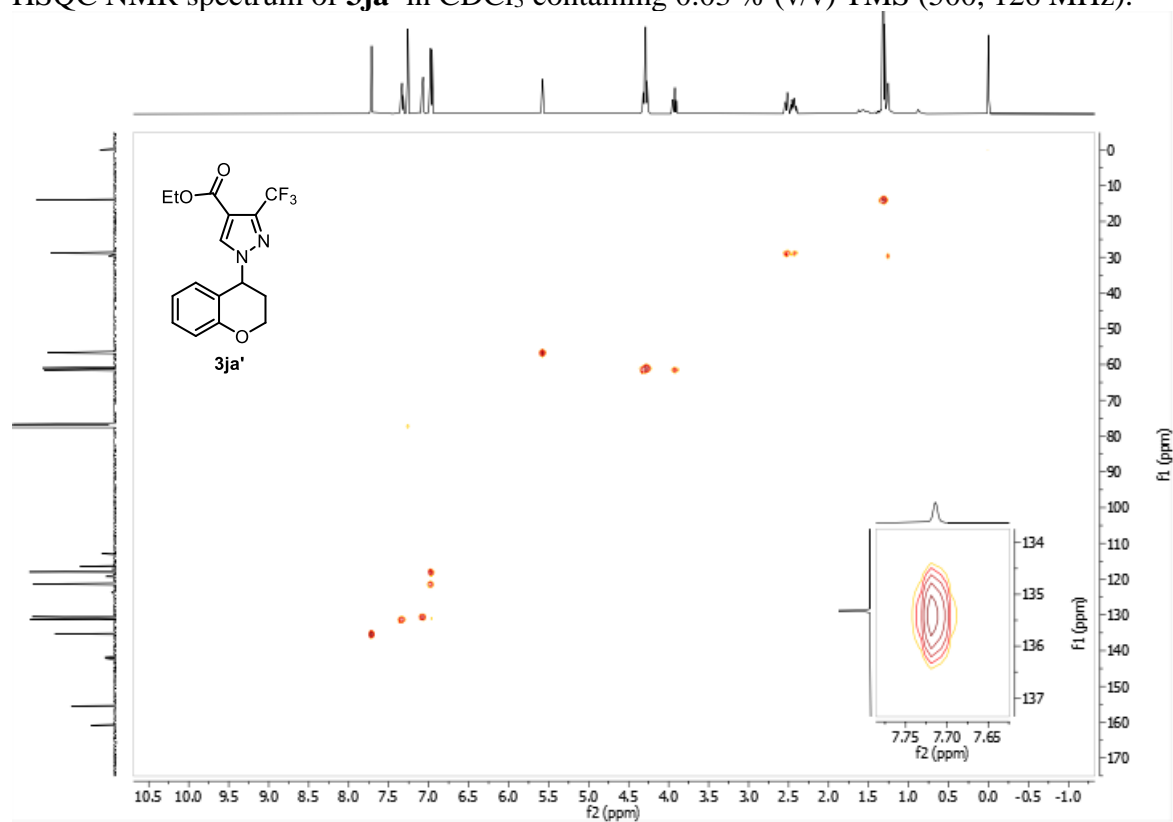
^{13}C NMR spectrum of **3ja'** in CDCl_3 containing 0.03 % (v/v) TMS (126 MHz).



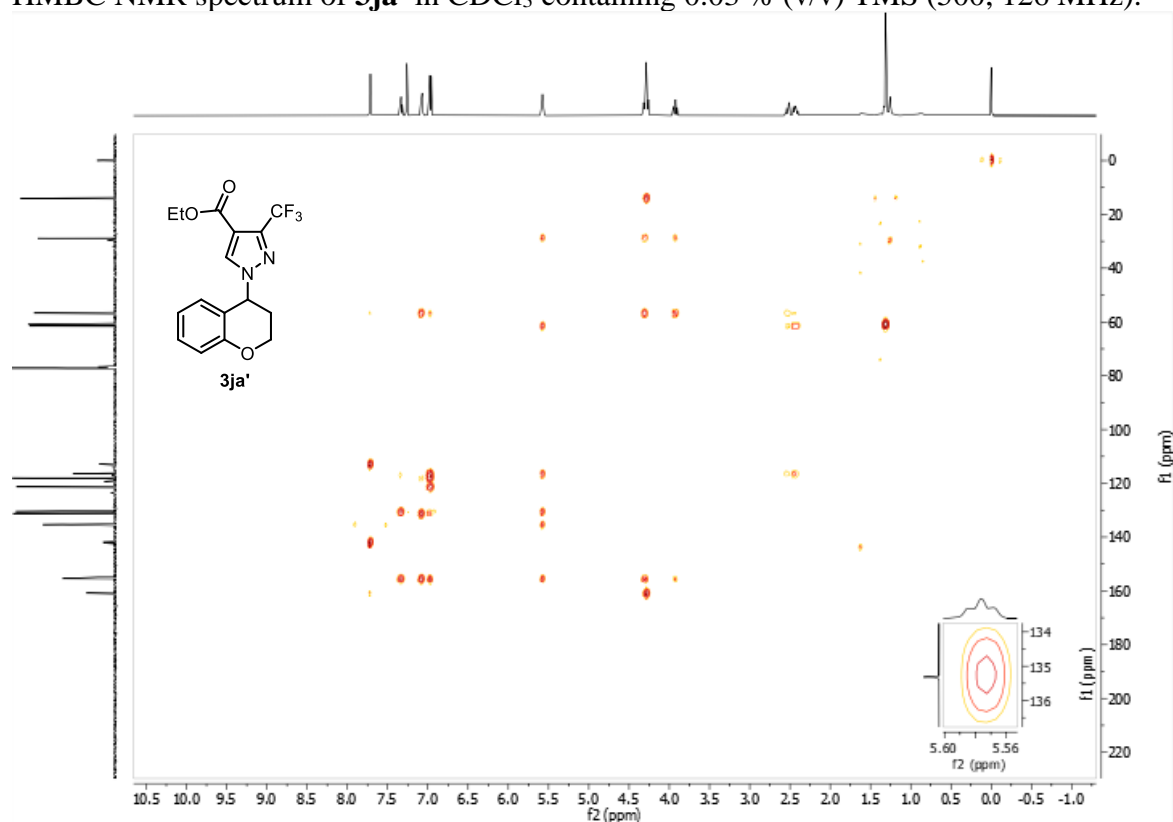
^{19}F NMR spectrum of **3ja'** in CDCl_3 containing 0.03 % (v/v) TMS (377 MHz).



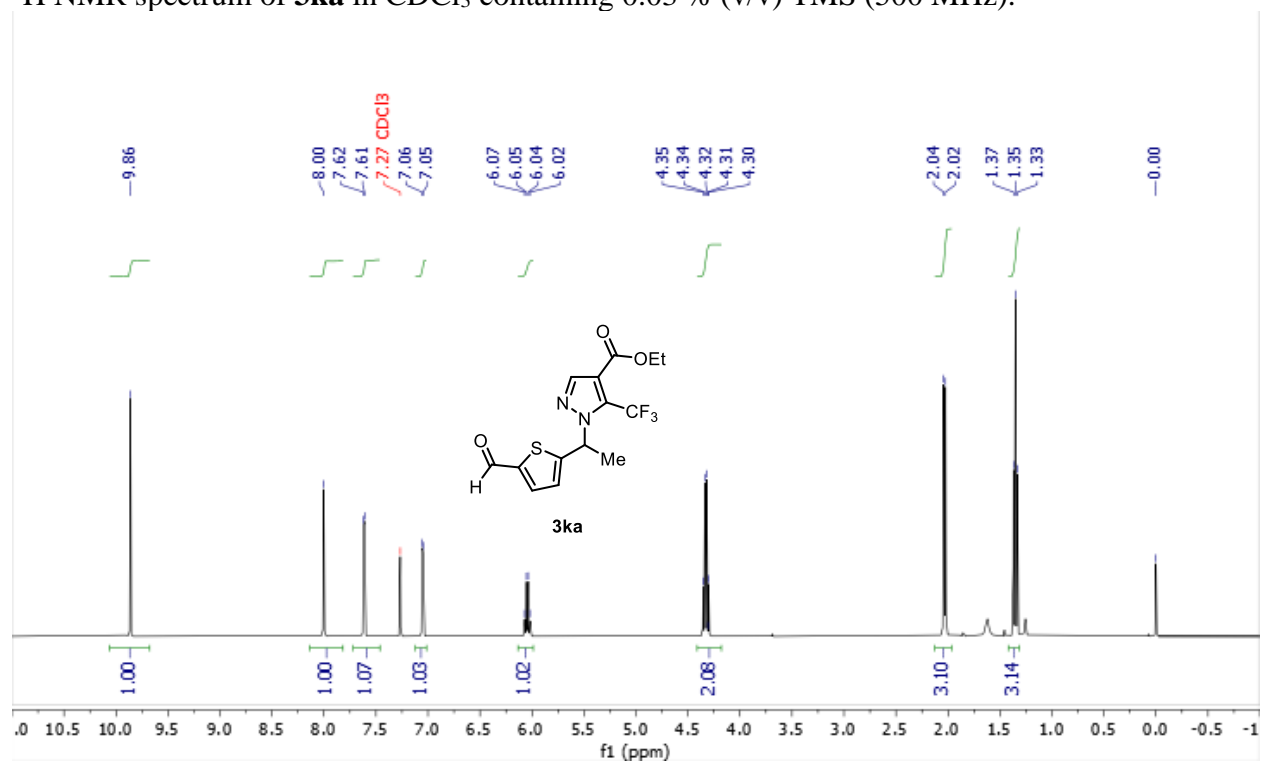
HSQC NMR spectrum of **3ja'** in CDCl₃ containing 0.03 % (v/v) TMS (500, 126 MHz).



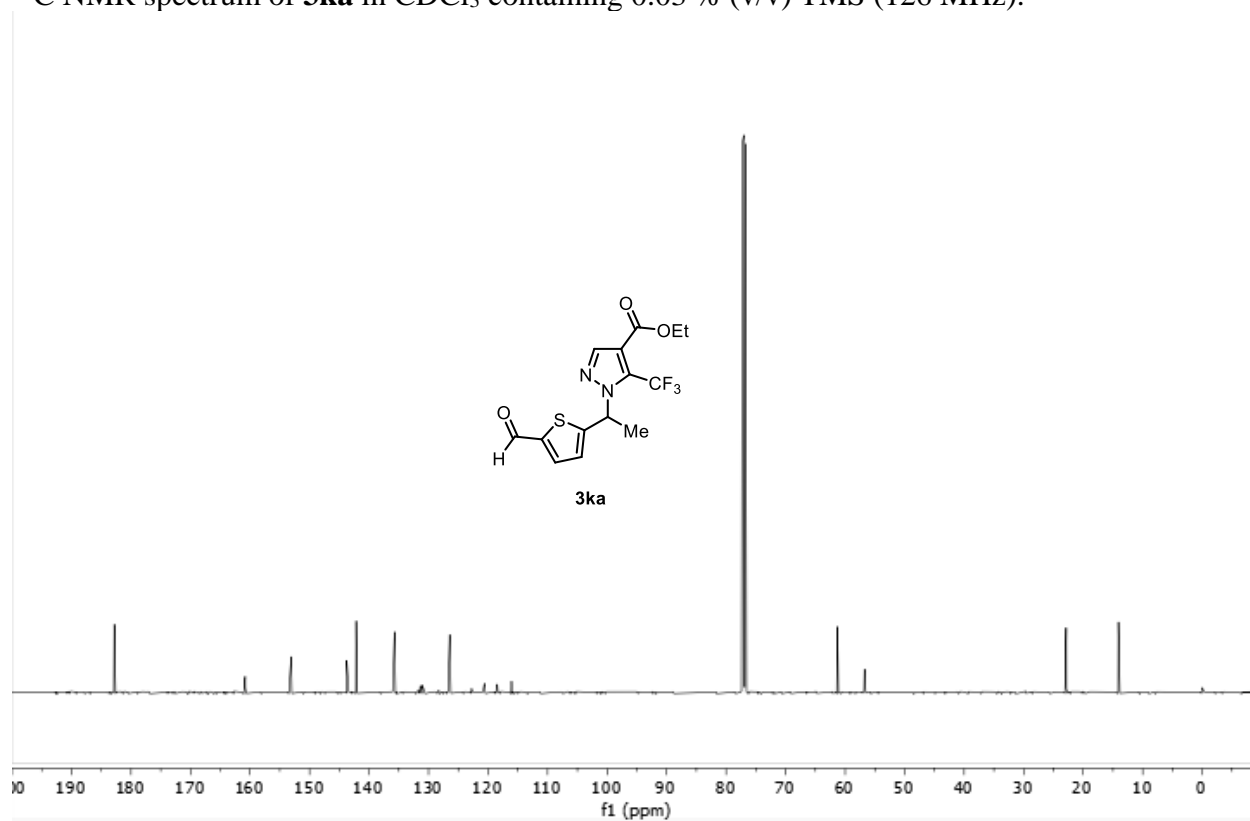
HMBC NMR spectrum of **3ja'** in CDCl₃ containing 0.03 % (v/v) TMS (500, 126 MHz).



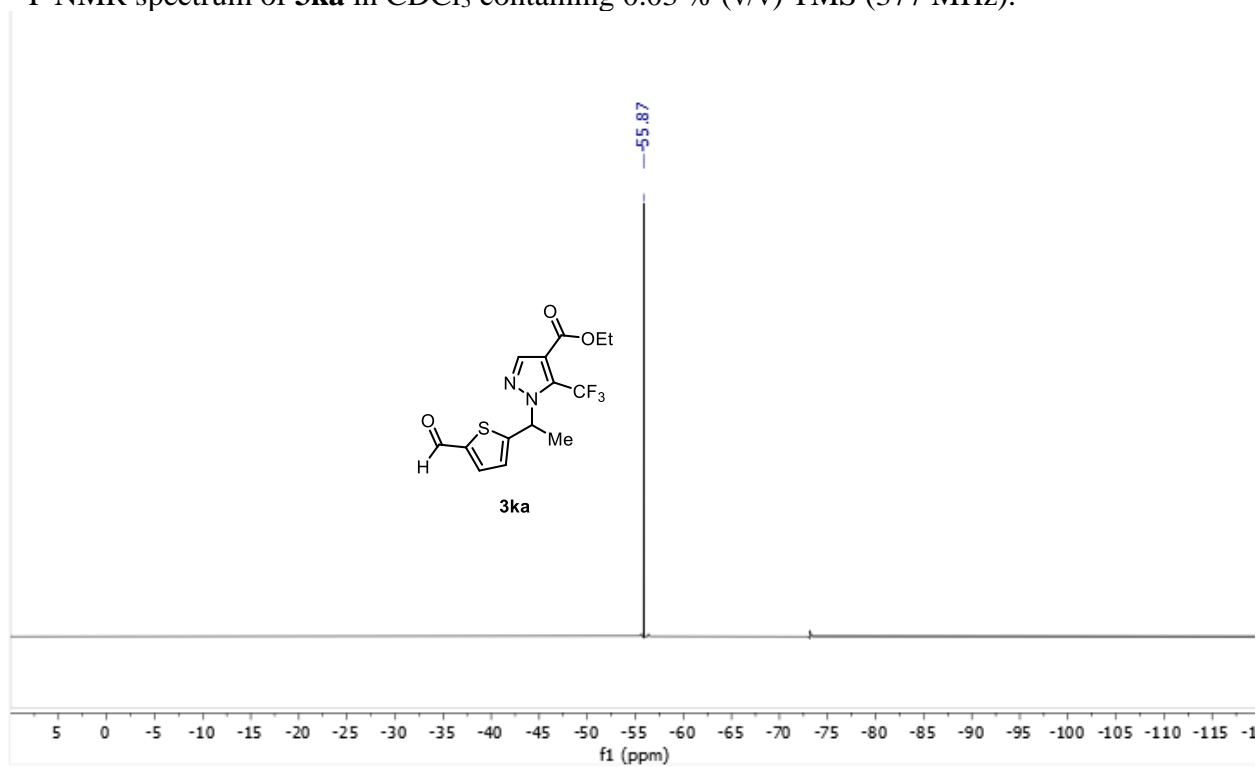
^1H NMR spectrum of **3ka** in CDCl_3 containing 0.03 % (v/v) TMS (500 MHz).



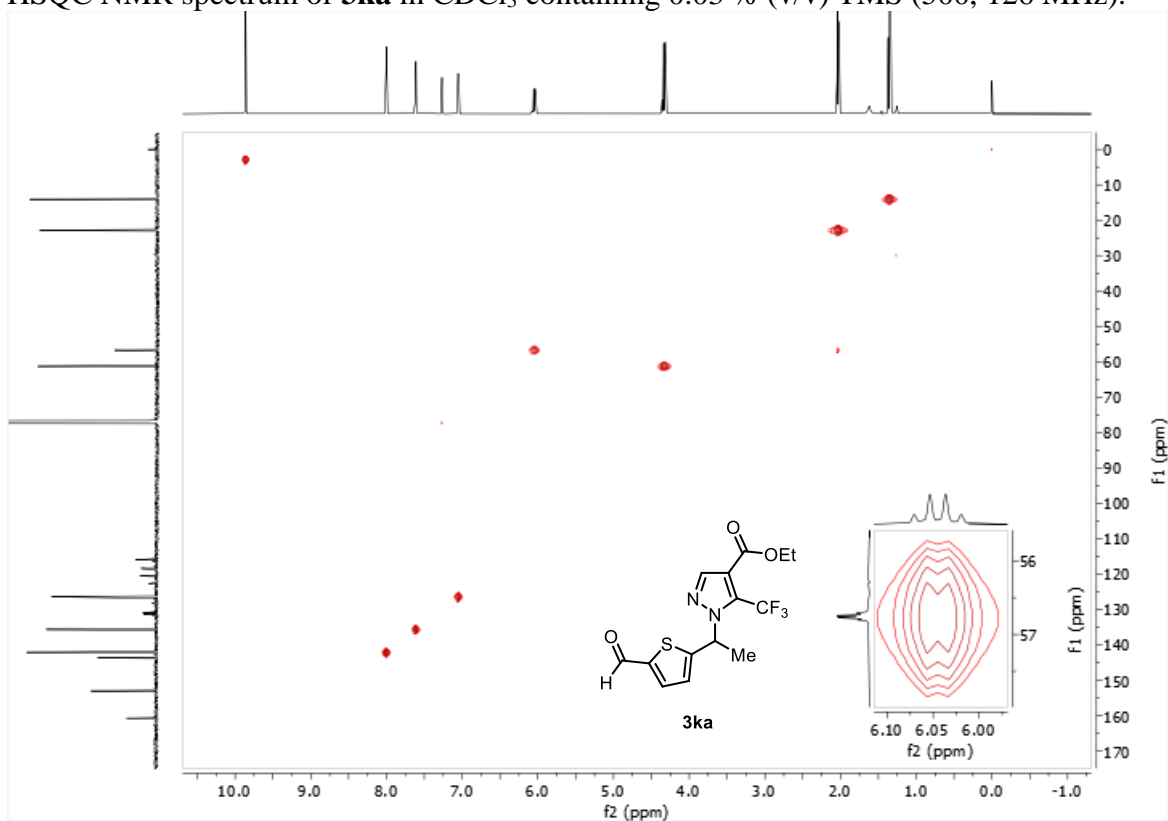
^{13}C NMR spectrum of **3ka** in CDCl_3 containing 0.03 % (v/v) TMS (126 MHz).



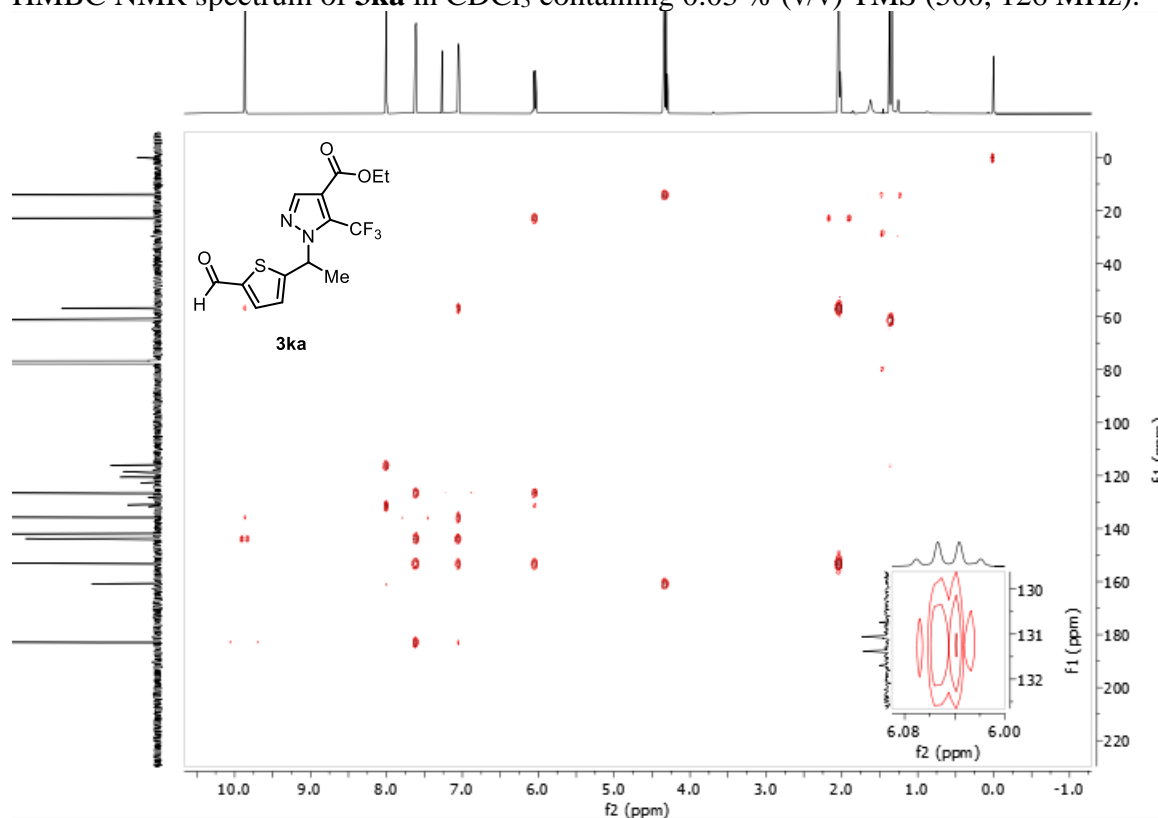
^{19}F NMR spectrum of **3ka** in CDCl_3 containing 0.03 % (v/v) TMS (377 MHz).



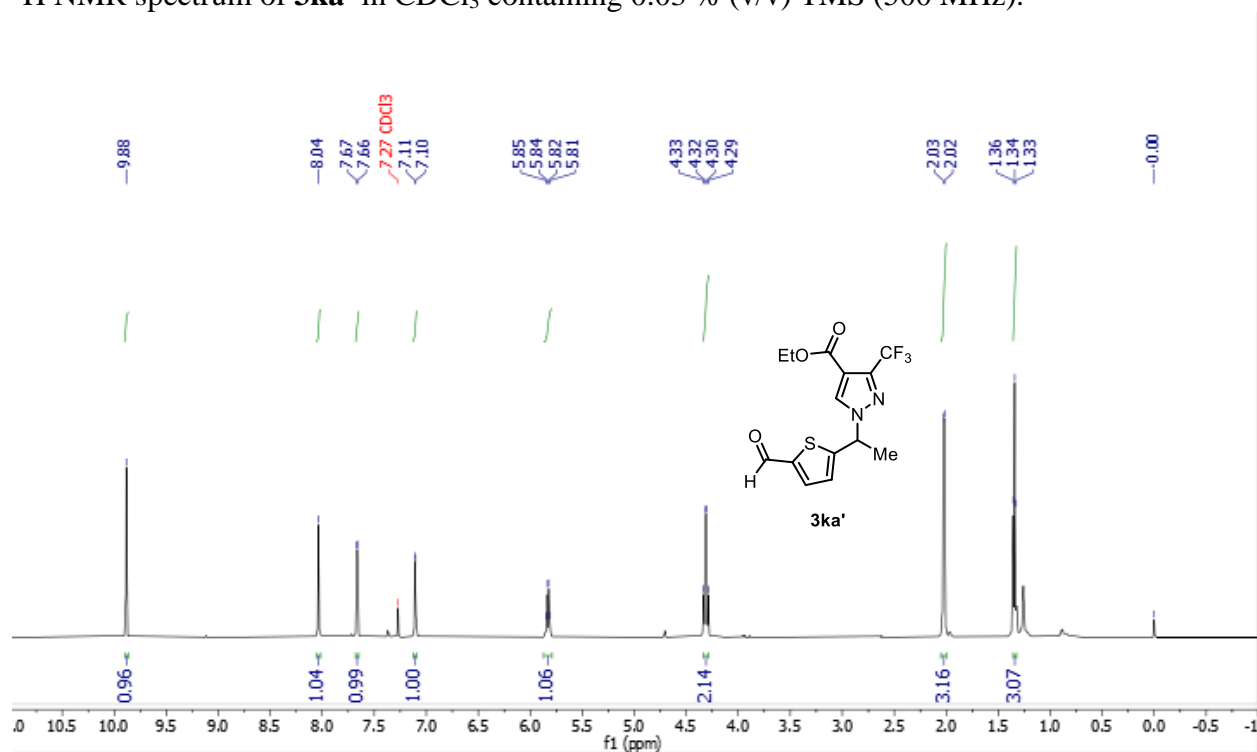
HSQC NMR spectrum of **3ka** in CDCl_3 containing 0.03 % (v/v) TMS (500, 126 MHz).



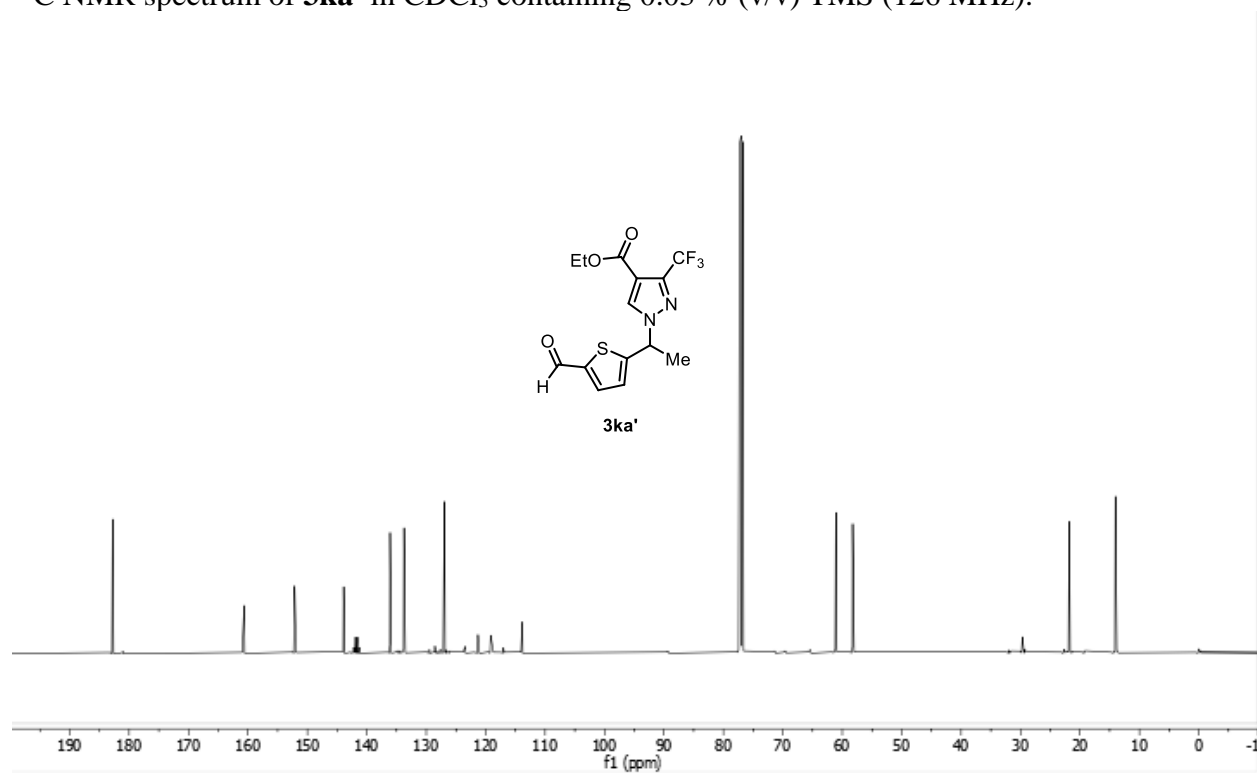
HMBC NMR spectrum of **3ka** in CDCl₃ containing 0.03 % (v/v) TMS (500, 126 MHz).



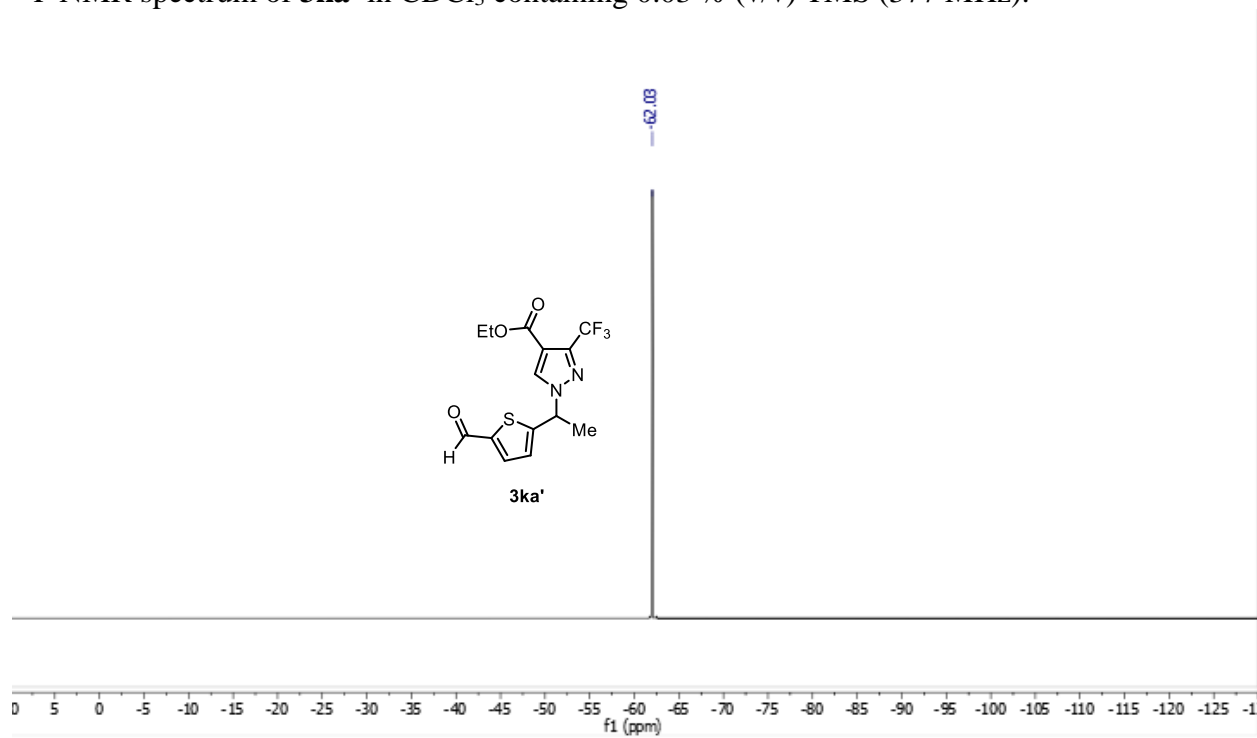
¹H NMR spectrum of **3ka'** in CDCl₃ containing 0.03 % (v/v) TMS (500 MHz).



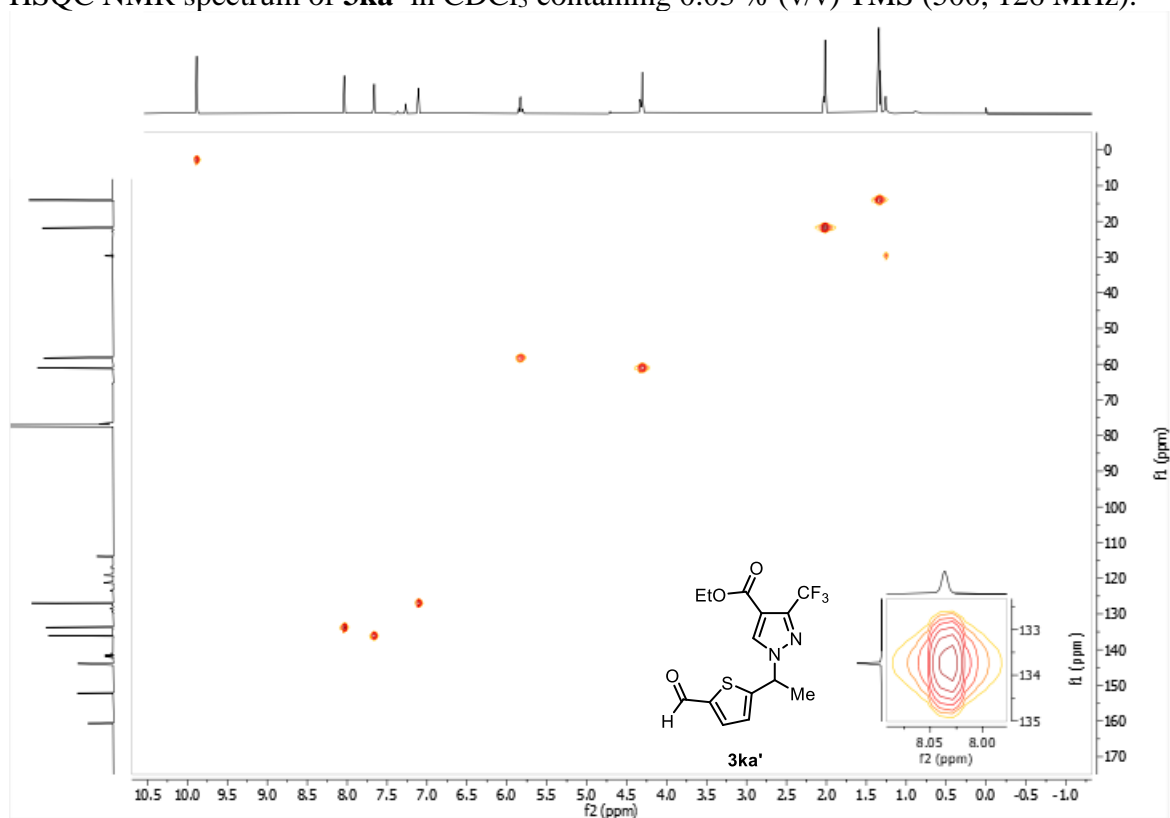
^{13}C NMR spectrum of **3ka'** in CDCl_3 containing 0.03 % (v/v) TMS (126 MHz).



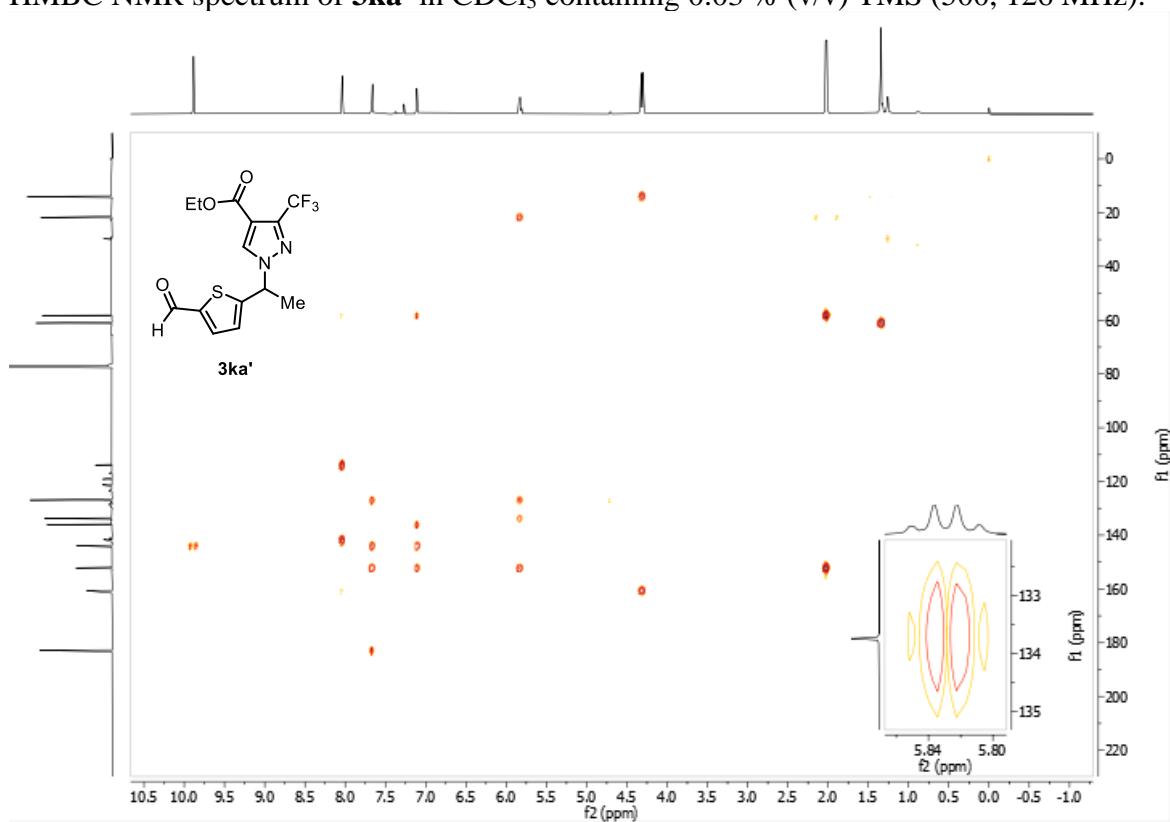
^{19}F NMR spectrum of **3ka'** in CDCl_3 containing 0.03 % (v/v) TMS (377 MHz).



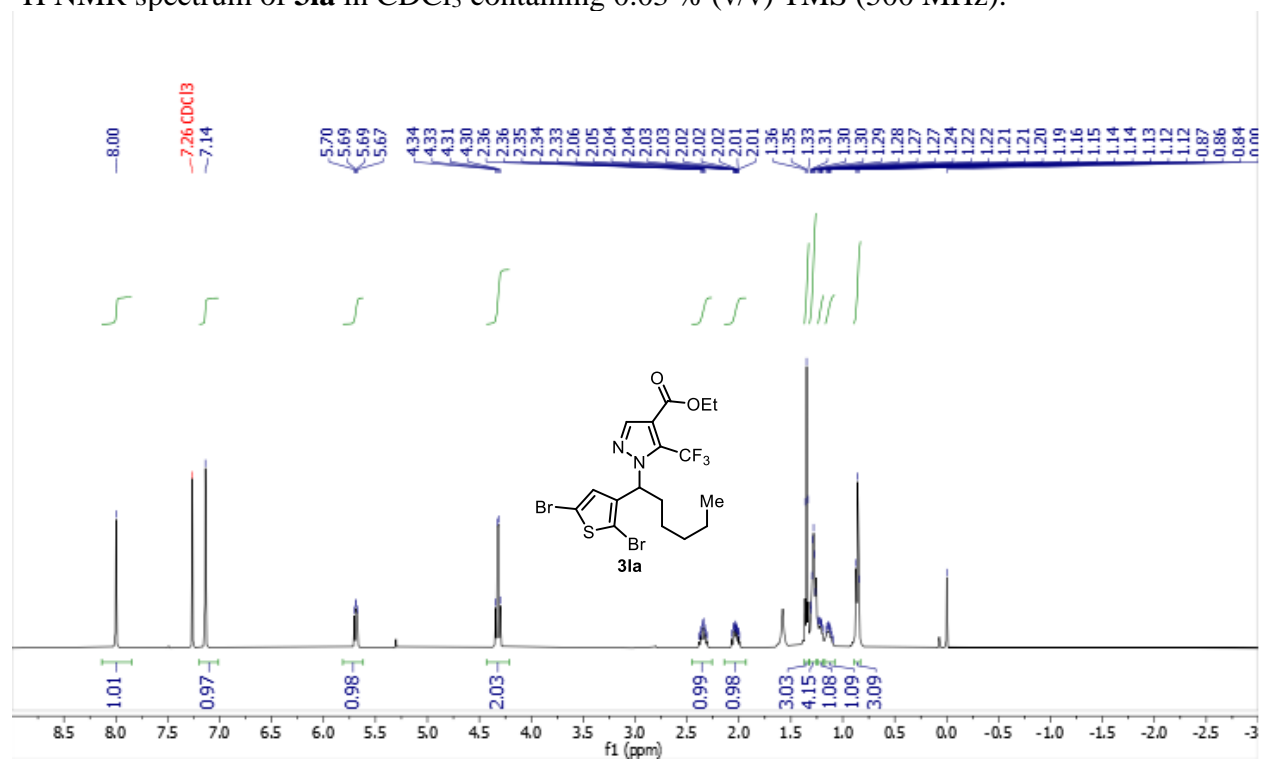
HSQC NMR spectrum of **3ka'** in CDCl₃ containing 0.03 % (v/v) TMS (500, 126 MHz).



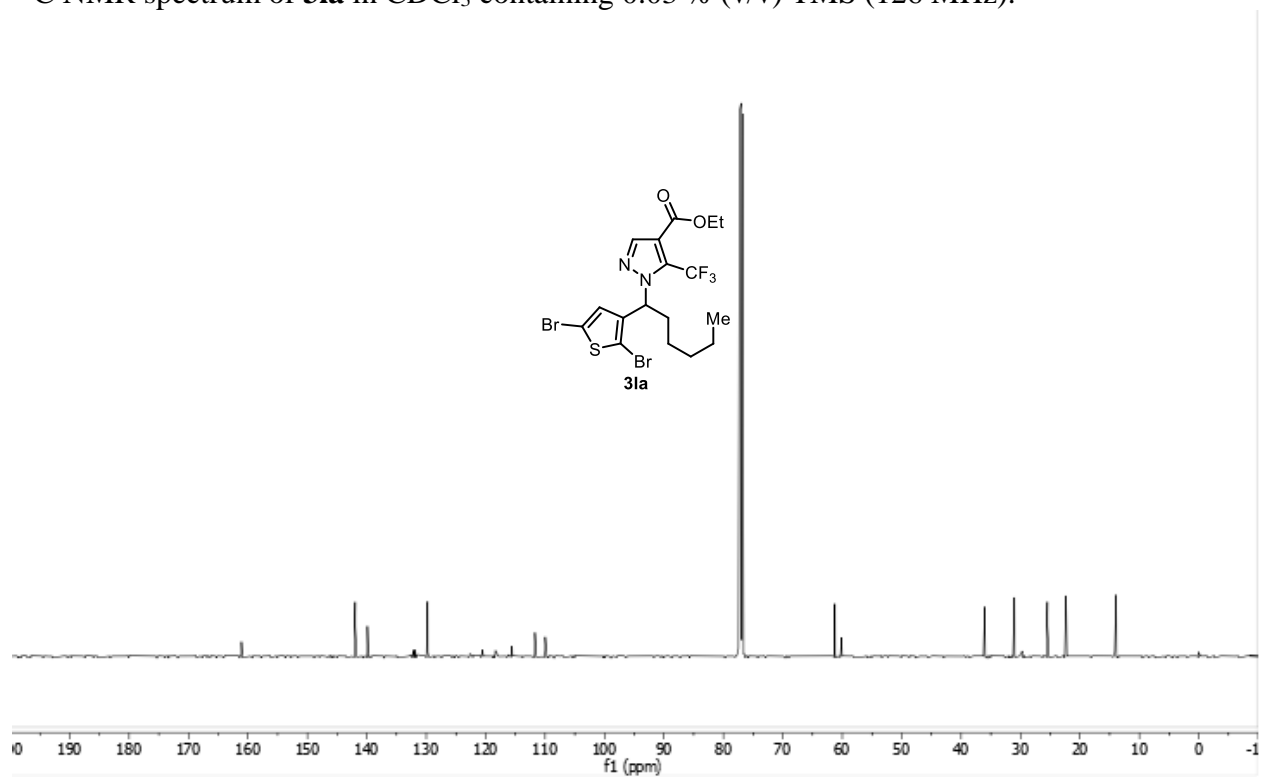
HMBC NMR spectrum of **3ka'** in CDCl₃ containing 0.03 % (v/v) TMS (500, 126 MHz).



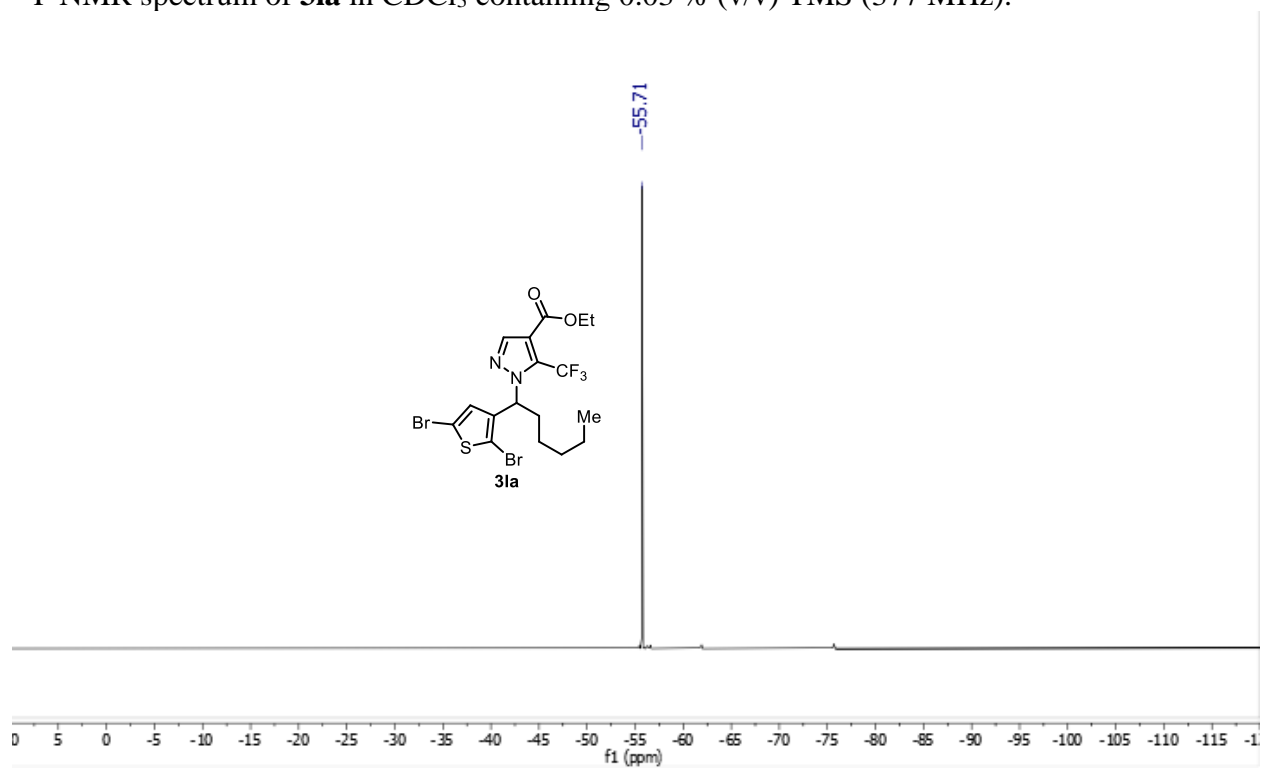
^1H NMR spectrum of **3la** in CDCl_3 containing 0.03 % (v/v) TMS (500 MHz).



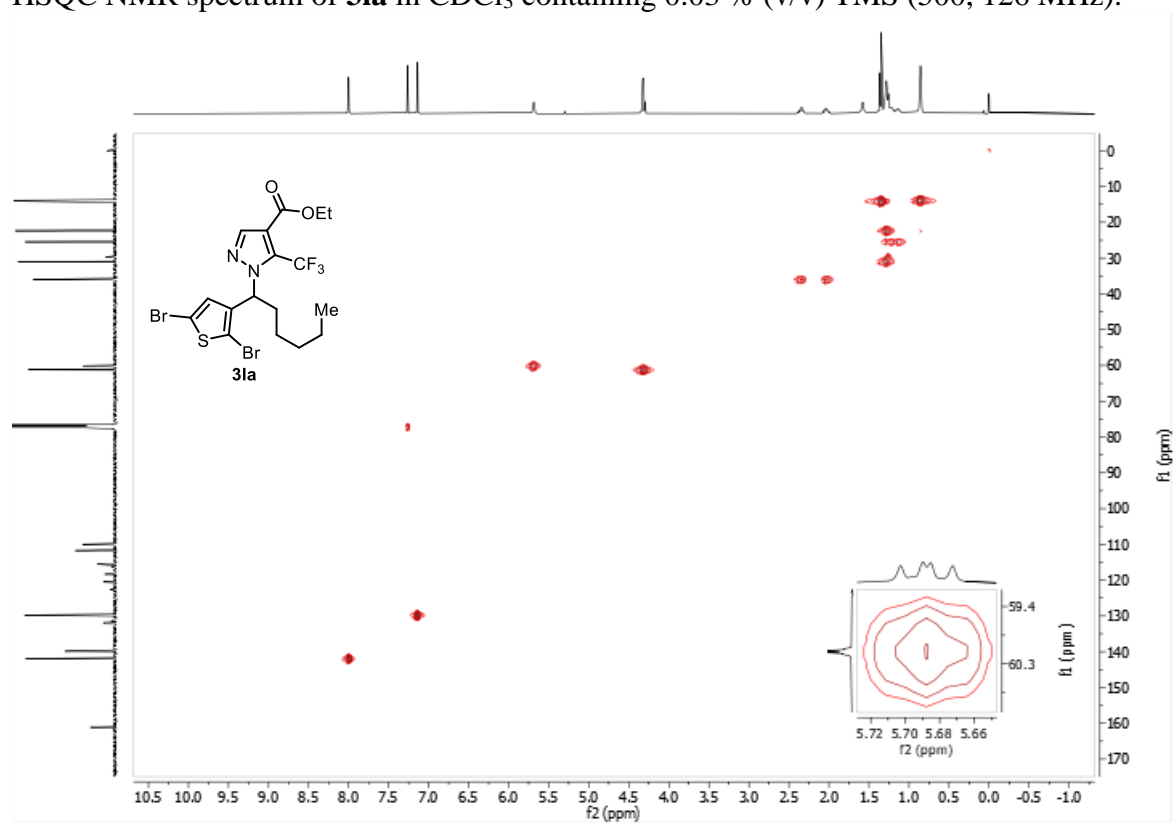
^{13}C NMR spectrum of **3la** in CDCl_3 containing 0.03 % (v/v) TMS (126 MHz).



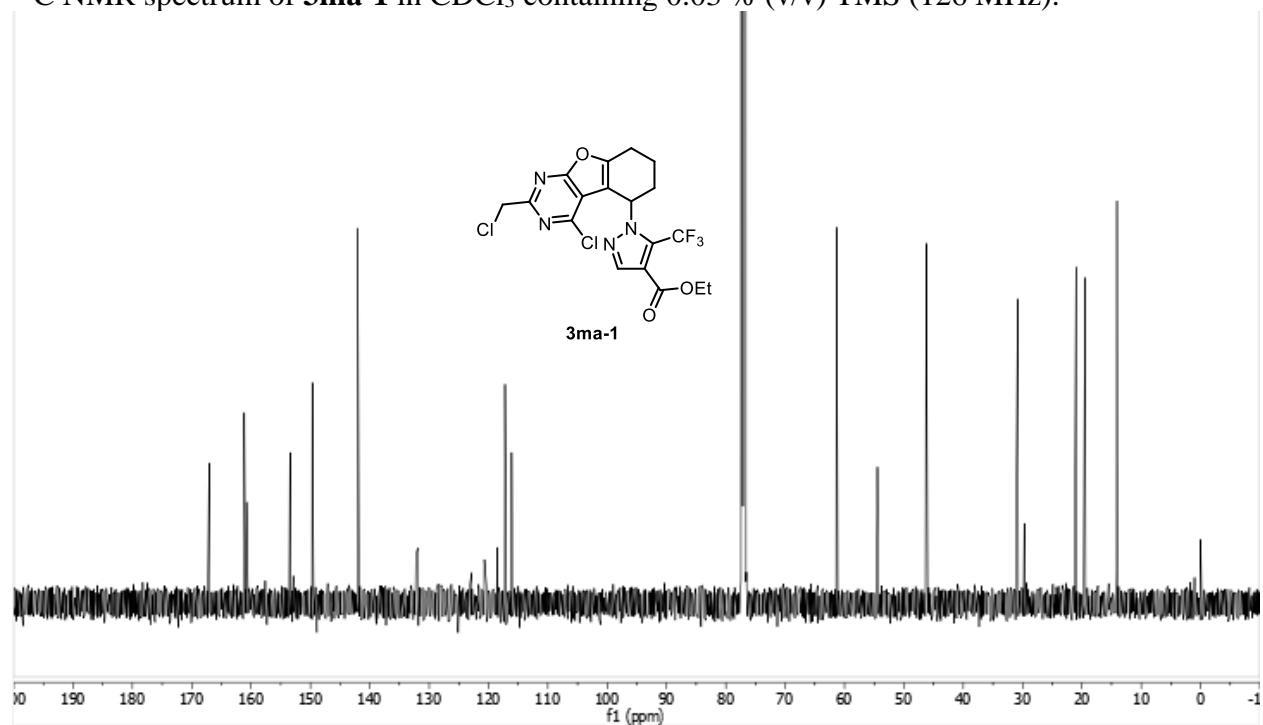
^{19}F NMR spectrum of **3la** in CDCl_3 containing 0.03 % (v/v) TMS (377 MHz).



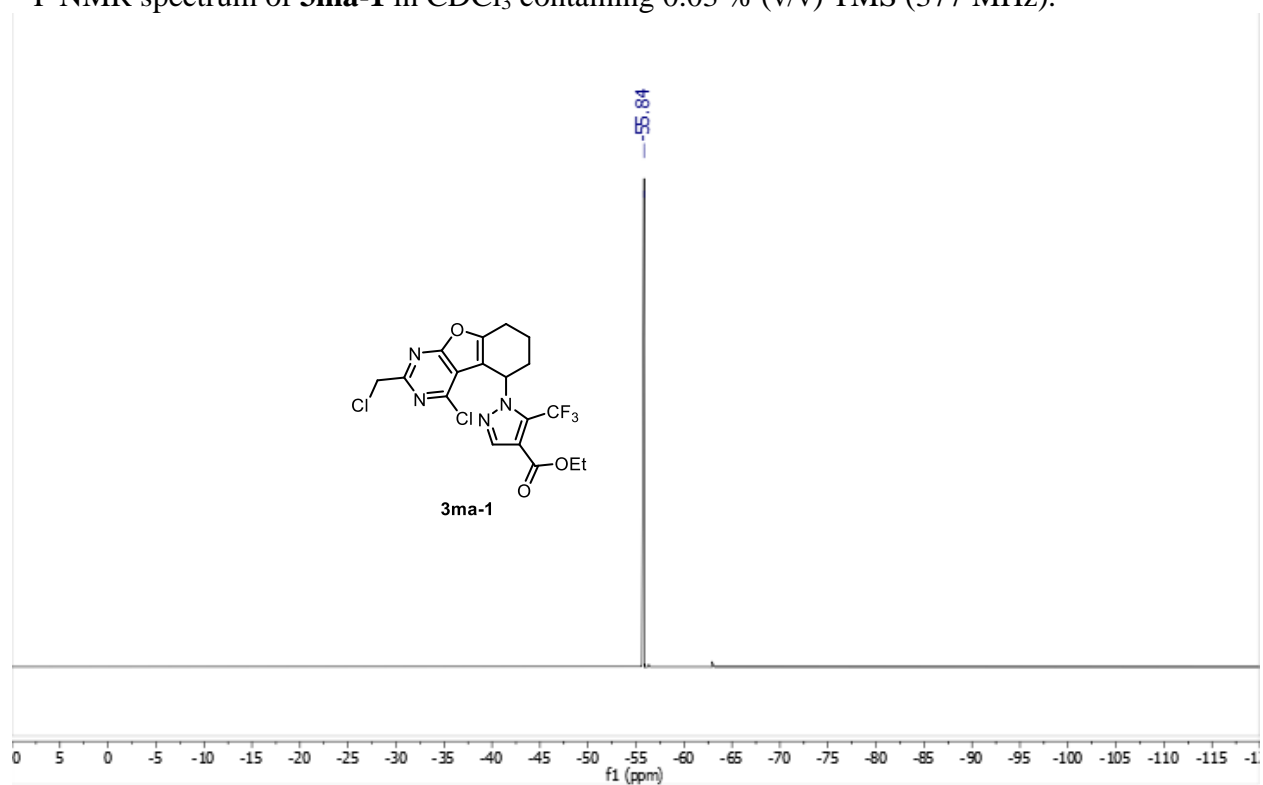
HSQC NMR spectrum of **3la** in CDCl_3 containing 0.03 % (v/v) TMS (500, 126 MHz).



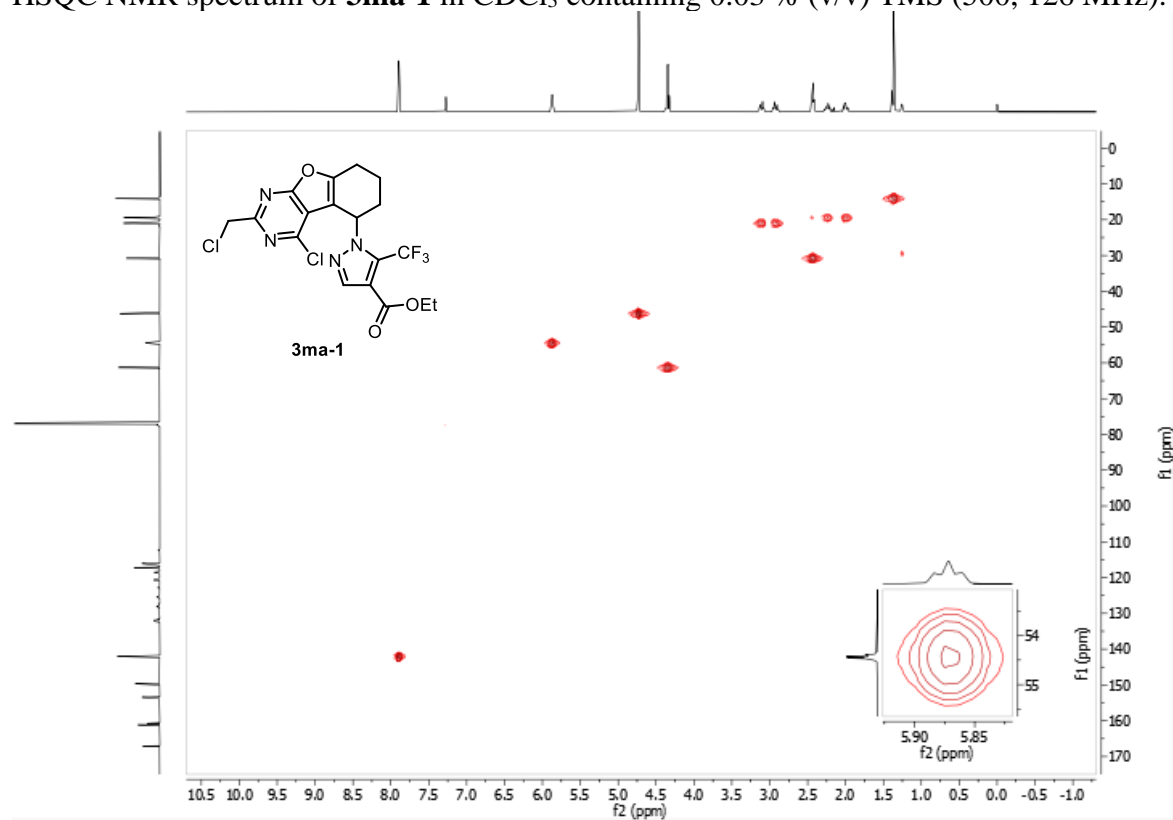
^{13}C NMR spectrum of **3ma-1** in CDCl_3 containing 0.03 % (v/v) TMS (126 MHz).



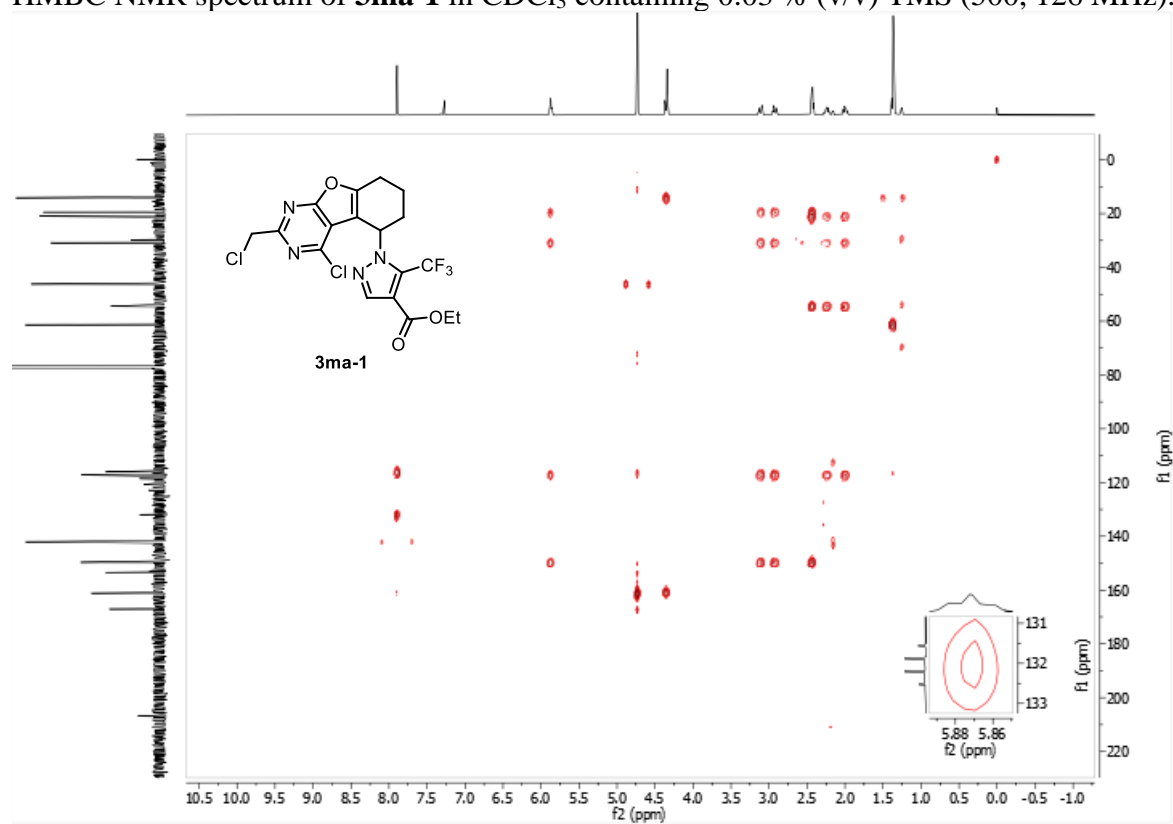
^{19}F NMR spectrum of **3ma-1** in CDCl_3 containing 0.03 % (v/v) TMS (377 MHz).



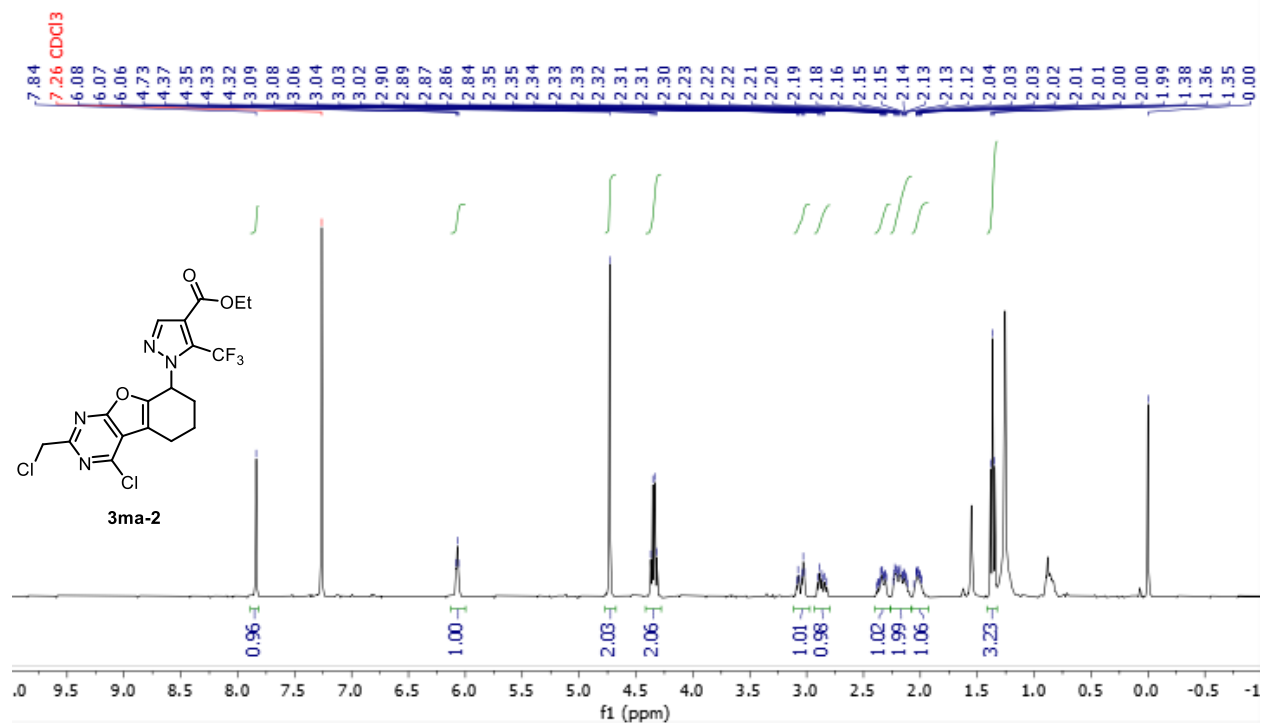
HSQC NMR spectrum of **3ma-1** in CDCl₃ containing 0.03 % (v/v) TMS (500, 126 MHz).



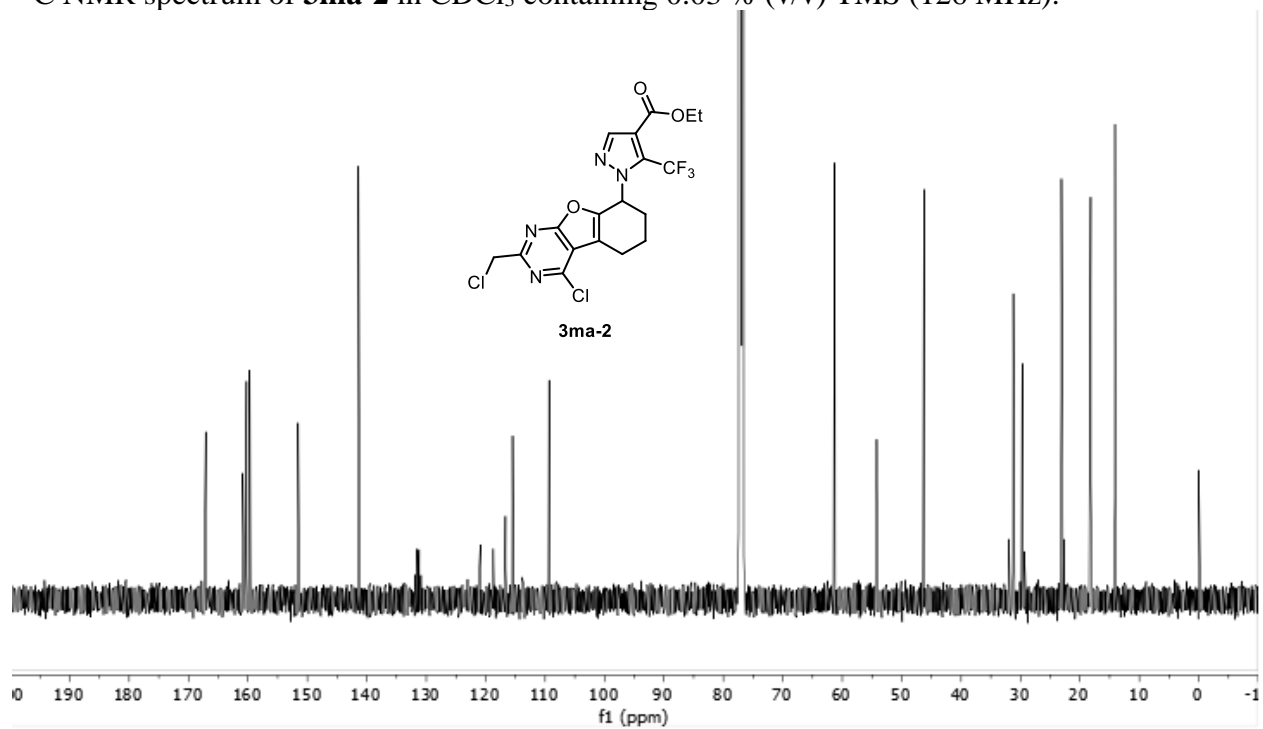
HMBC NMR spectrum of **3ma-1** in CDCl₃ containing 0.03 % (v/v) TMS (500, 126 MHz).



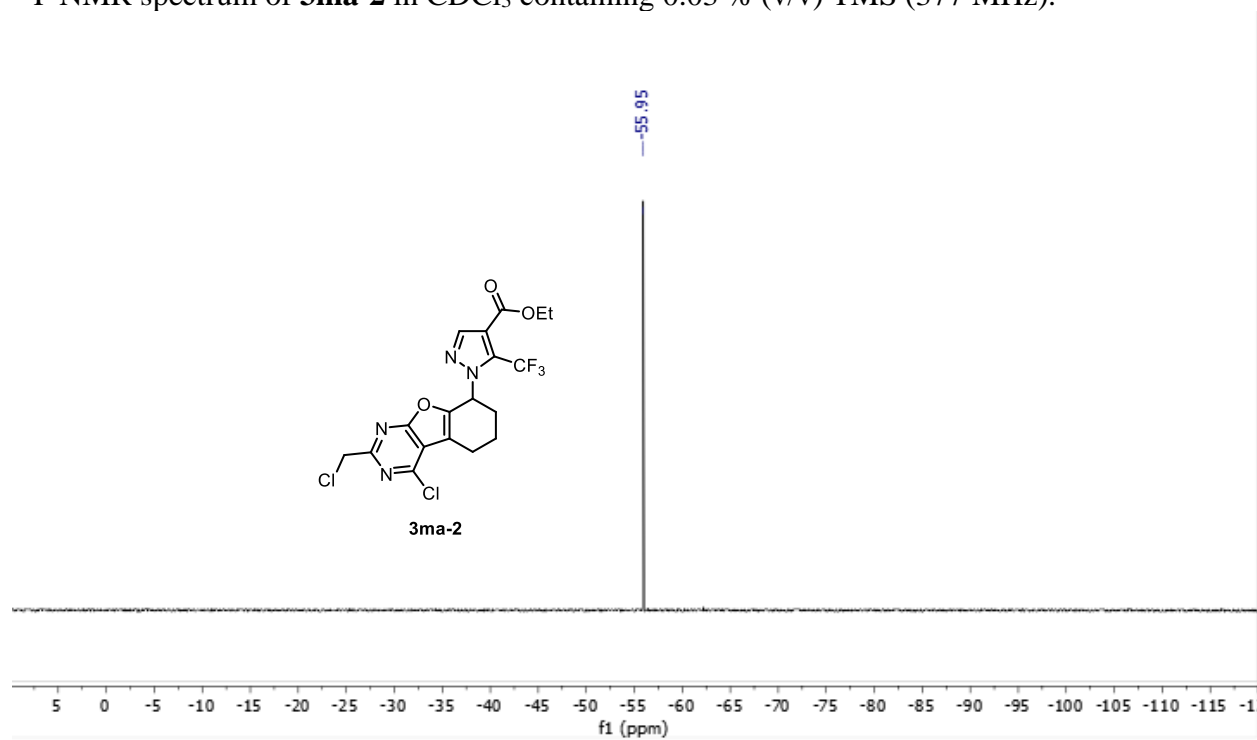
^1H NMR spectrum of **3ma-2** in CDCl_3 containing 0.03 % (v/v) TMS (500 MHz).



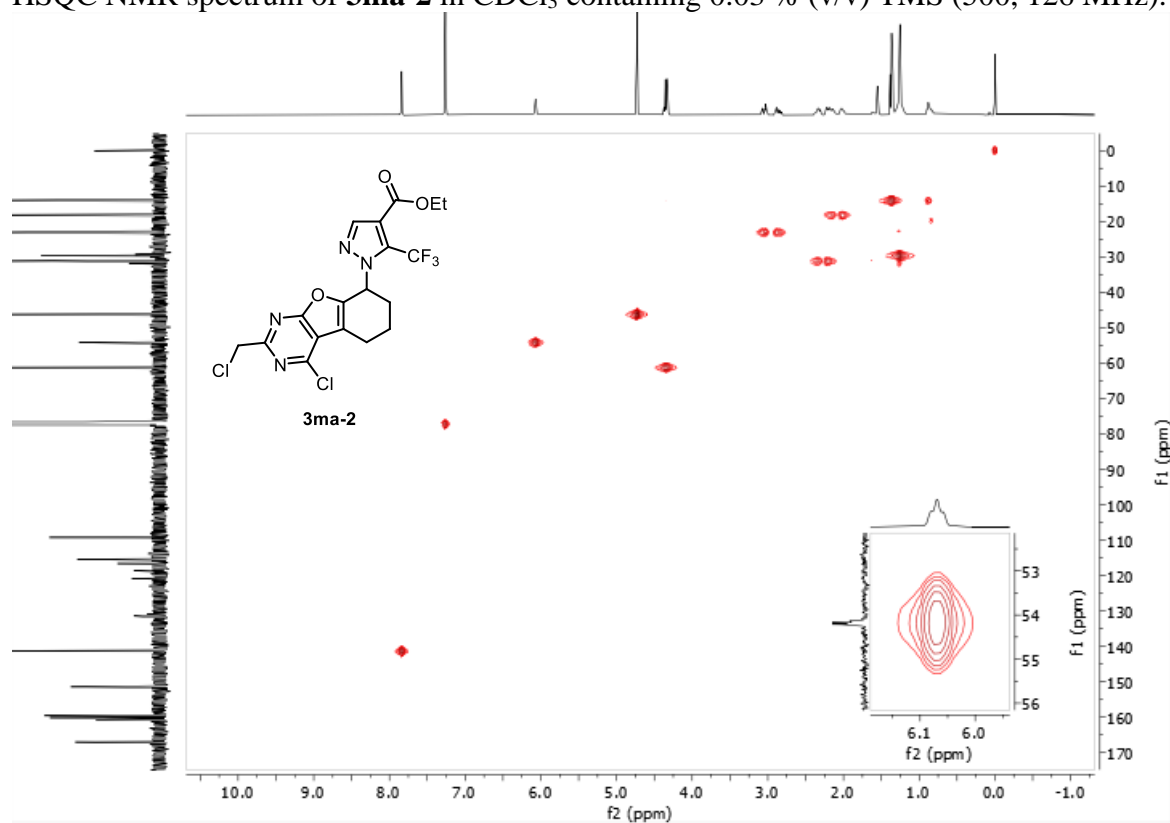
^{13}C NMR spectrum of **3ma-2** in CDCl_3 containing 0.03 % (v/v) TMS (126 MHz).



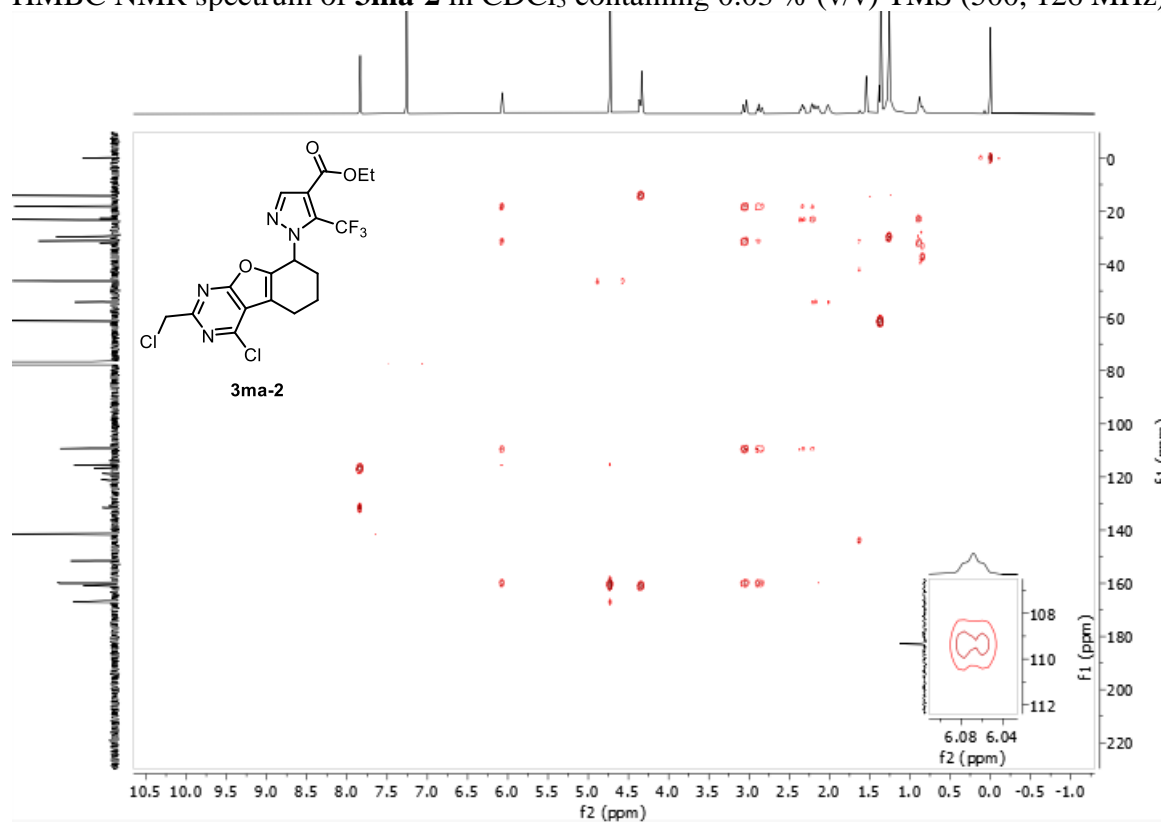
^{19}F NMR spectrum of **3ma-2** in CDCl_3 containing 0.03 % (v/v) TMS (377 MHz).



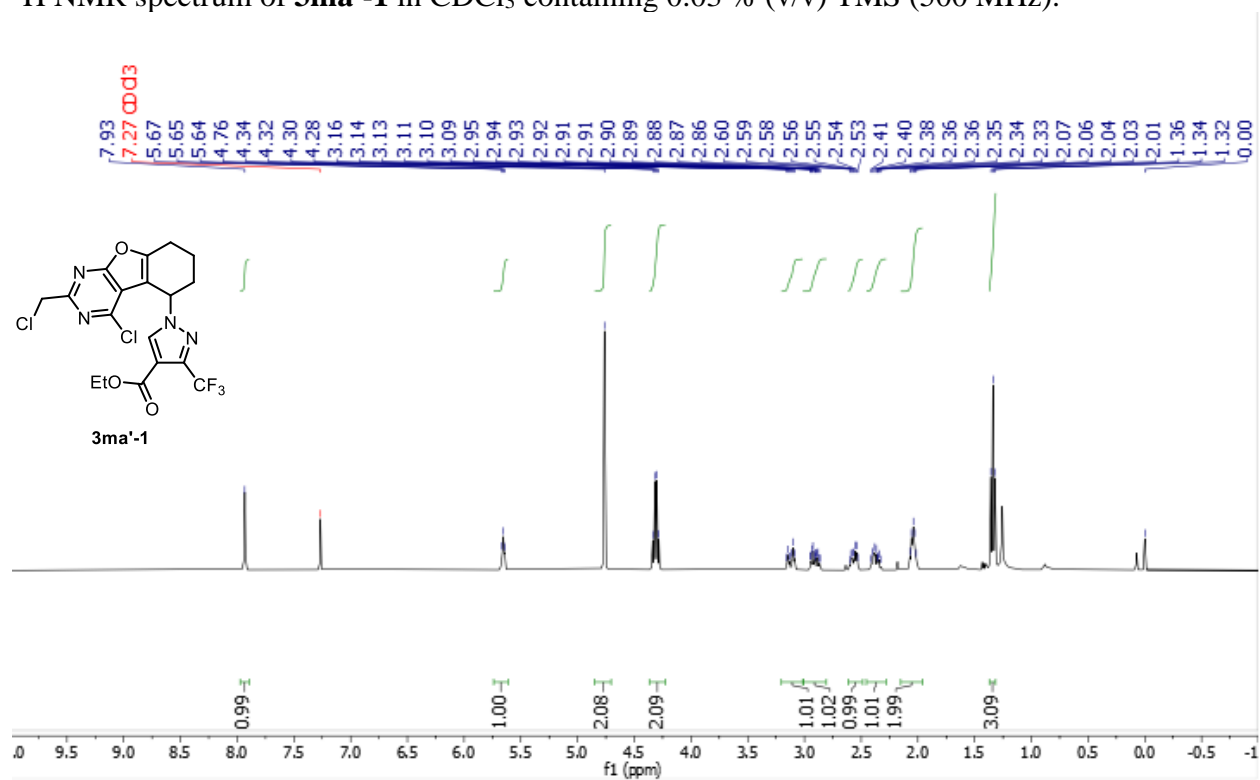
HSQC NMR spectrum of **3ma-2** in CDCl_3 containing 0.03 % (v/v) TMS (500, 126 MHz).



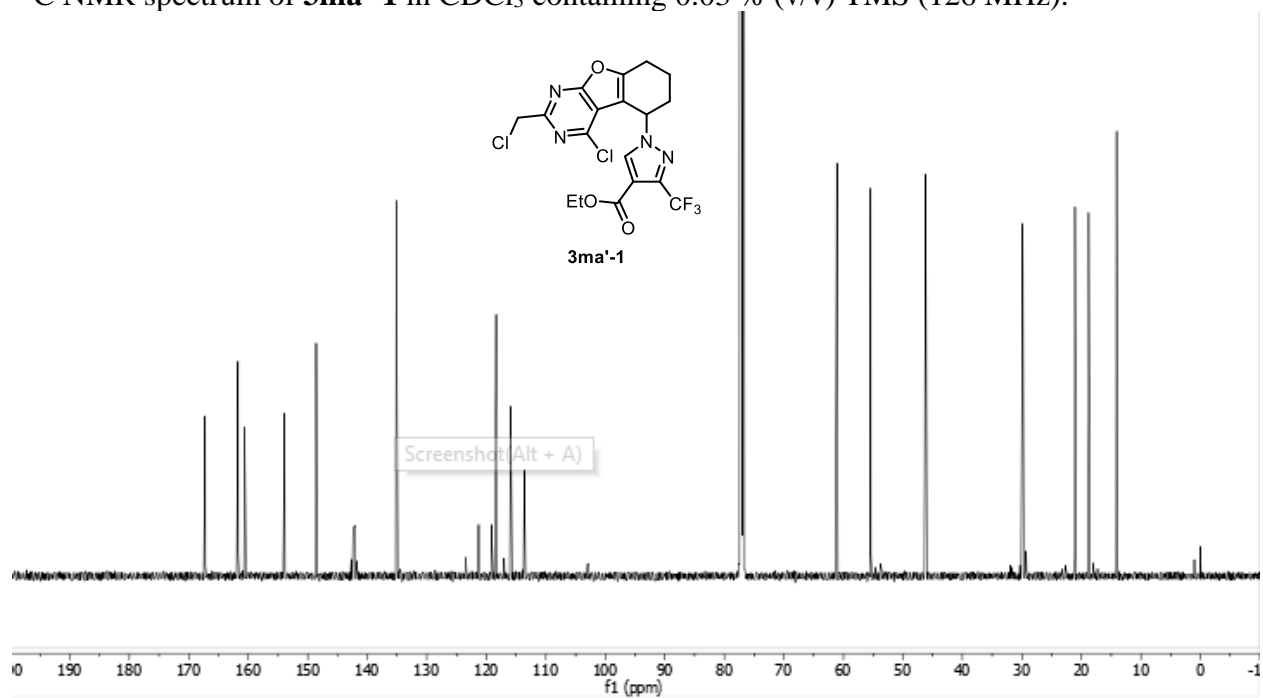
HMBC NMR spectrum of **3ma-2** in CDCl₃ containing 0.03 % (v/v) TMS (500, 126 MHz).



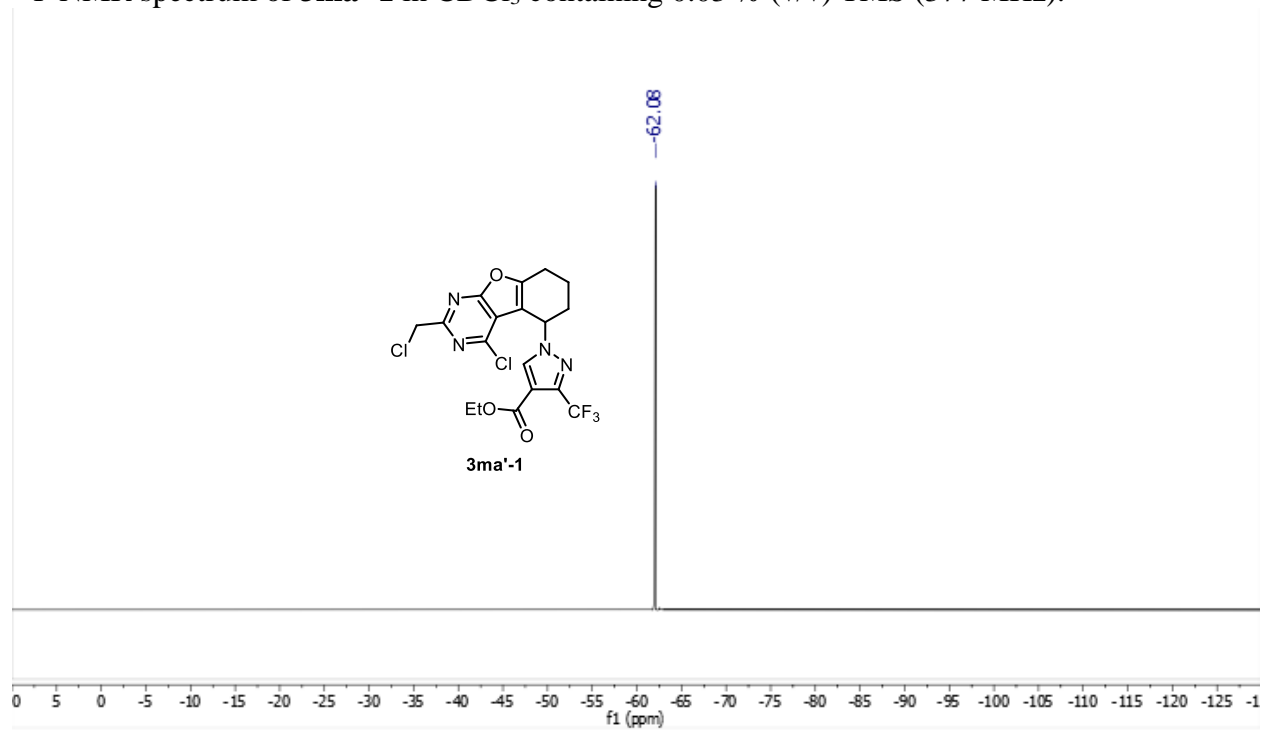
¹H NMR spectrum of **3ma'-1** in CDCl₃ containing 0.03 % (v/v) TMS (500 MHz).



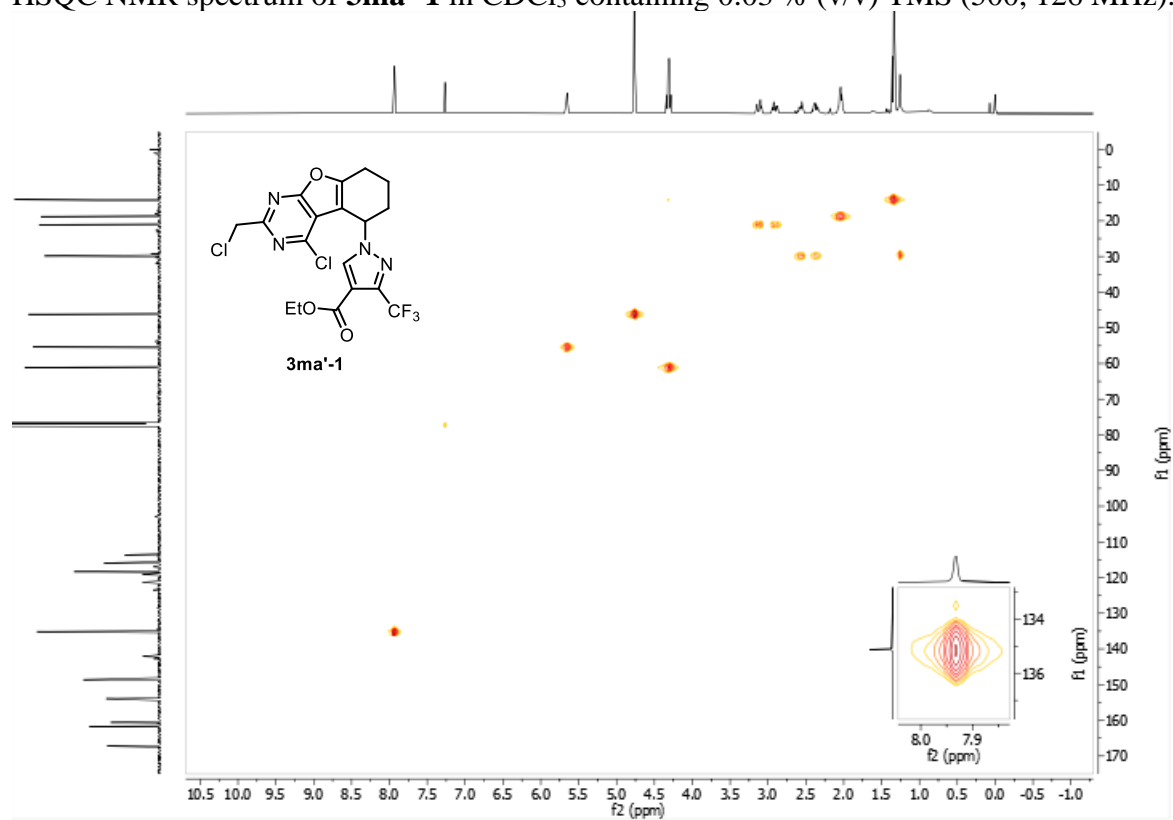
^{13}C NMR spectrum of **3ma'-1** in CDCl_3 containing 0.03 % (v/v) TMS (126 MHz).



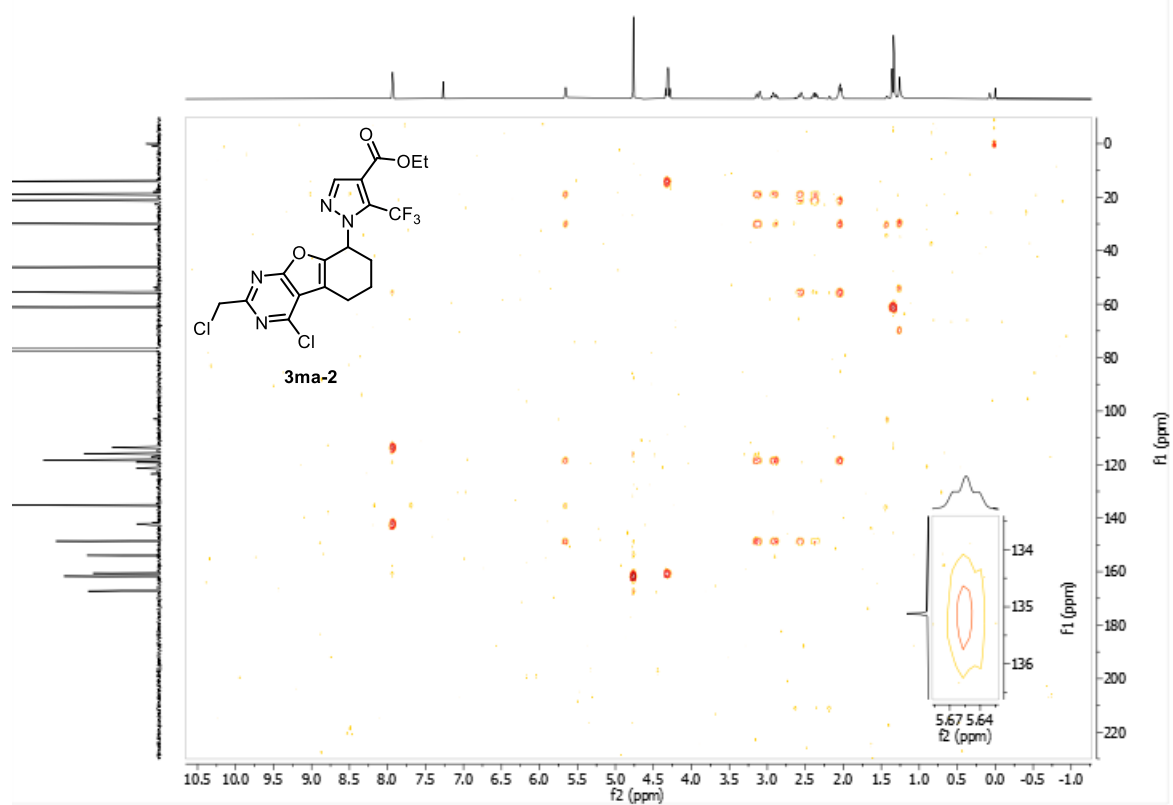
^{19}F NMR spectrum of **3ma'-1** in CDCl_3 containing 0.03 % (v/v) TMS (377 MHz).



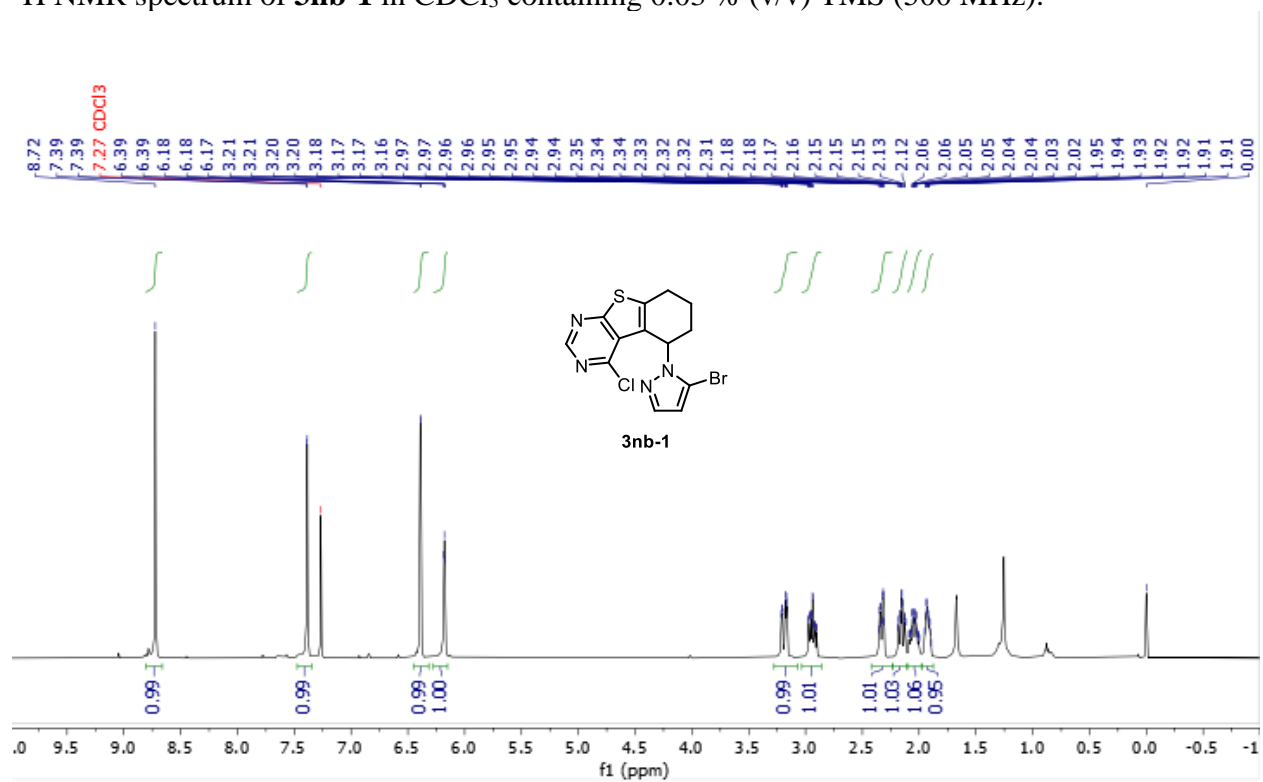
HSQC NMR spectrum of **3ma'-1** in CDCl₃ containing 0.03 % (v/v) TMS (500, 126 MHz).



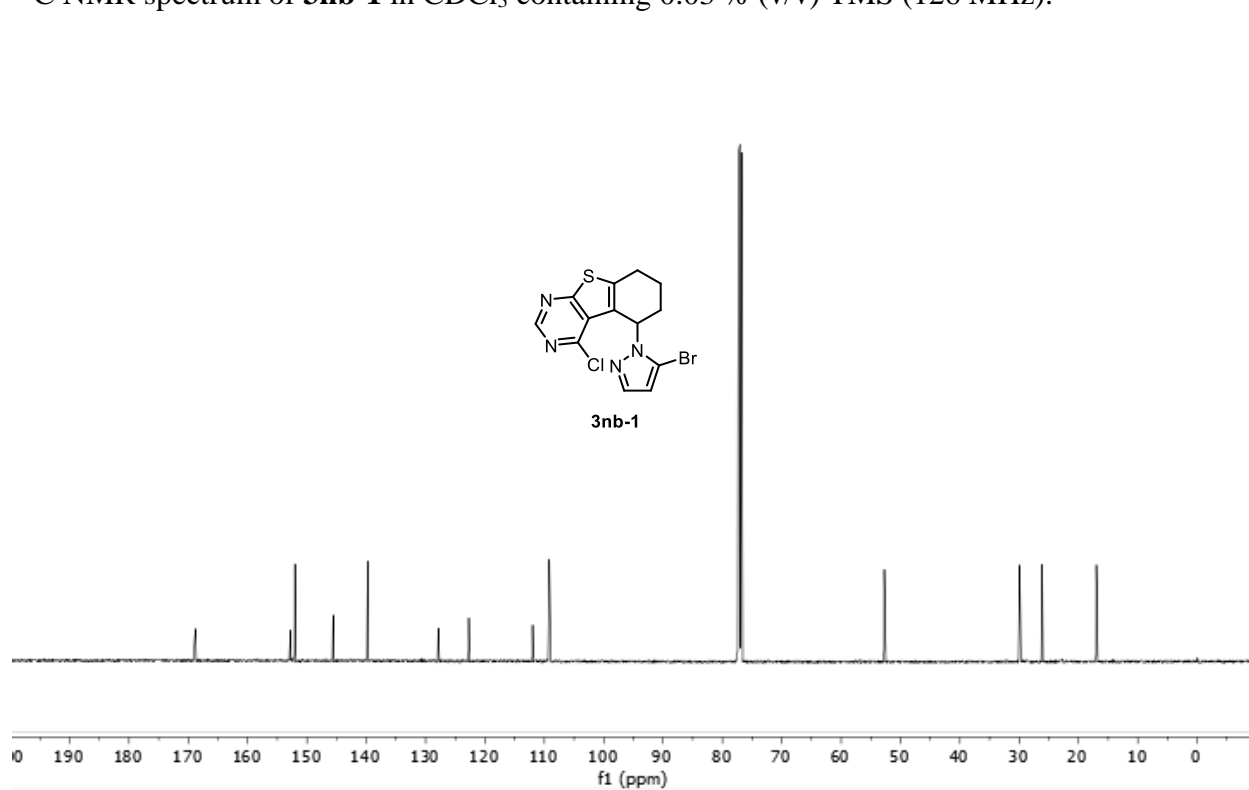
HMBC NMR spectrum of **3ma-1** in CDCl₃ containing 0.03 % (v/v) TMS (500, 126 MHz).



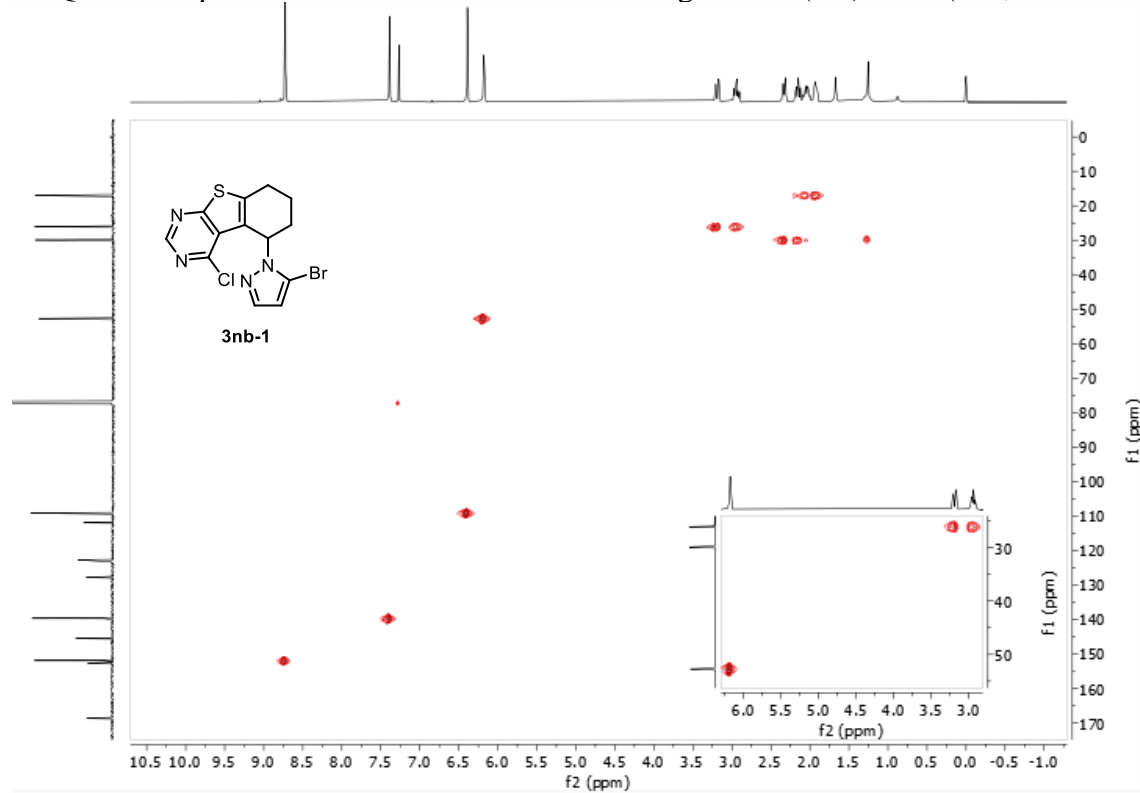
^1H NMR spectrum of **3nb-1** in CDCl_3 containing 0.03 % (v/v) TMS (500 MHz).



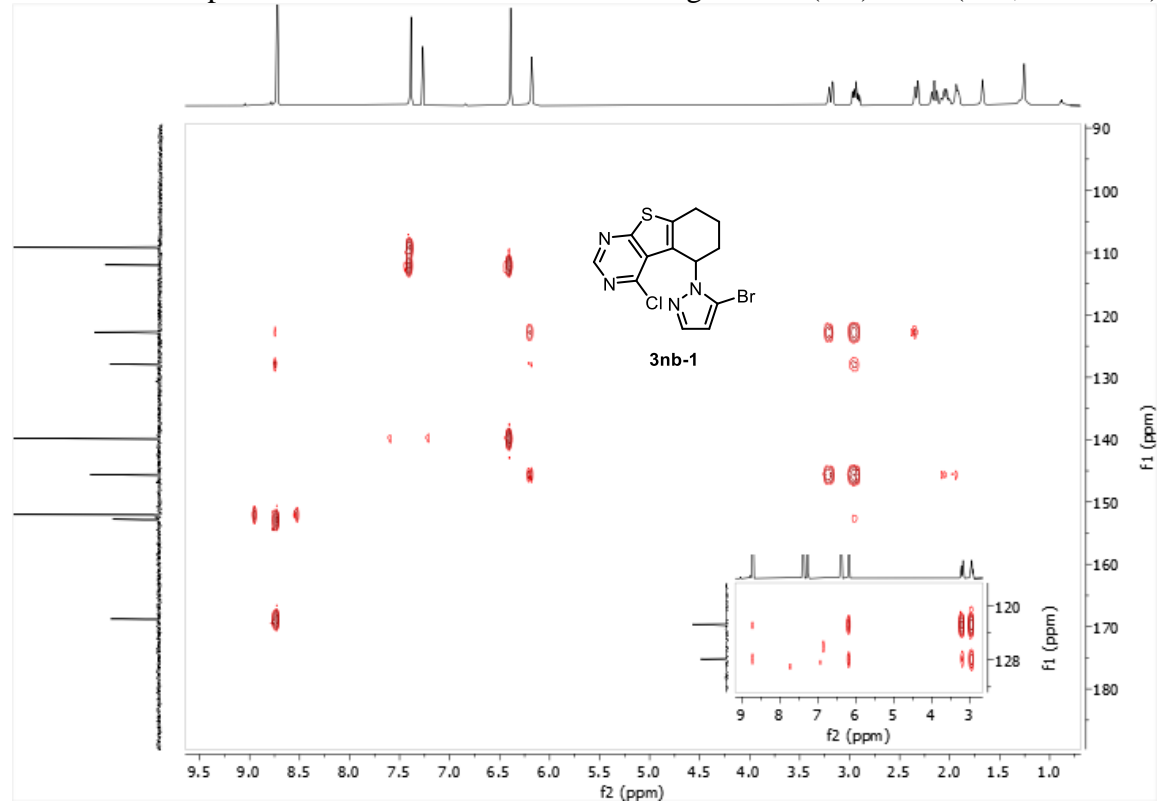
^{13}C NMR spectrum of **3nb-1** in CDCl_3 containing 0.03 % (v/v) TMS (126 MHz).



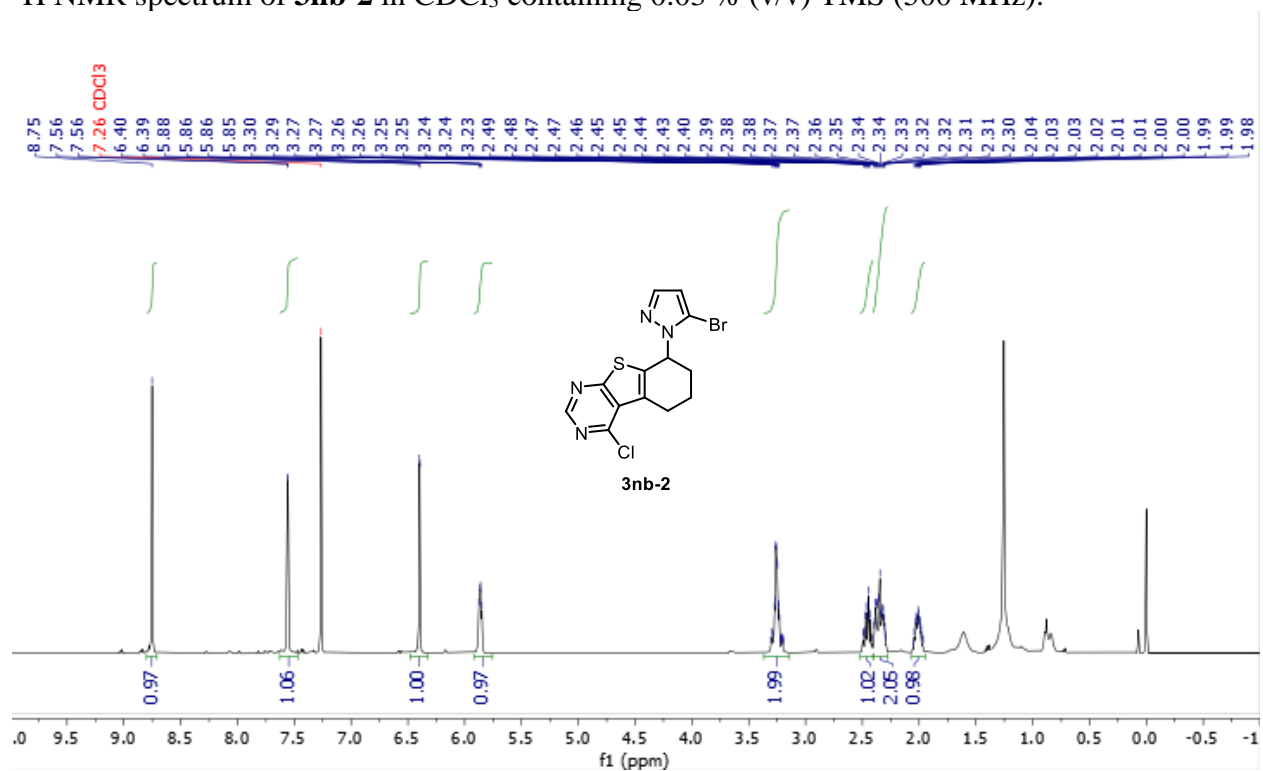
HSQC NMR spectrum of **3nb-1** in CDCl₃ containing 0.03 % (v/v) TMS (500, 126 MHz).



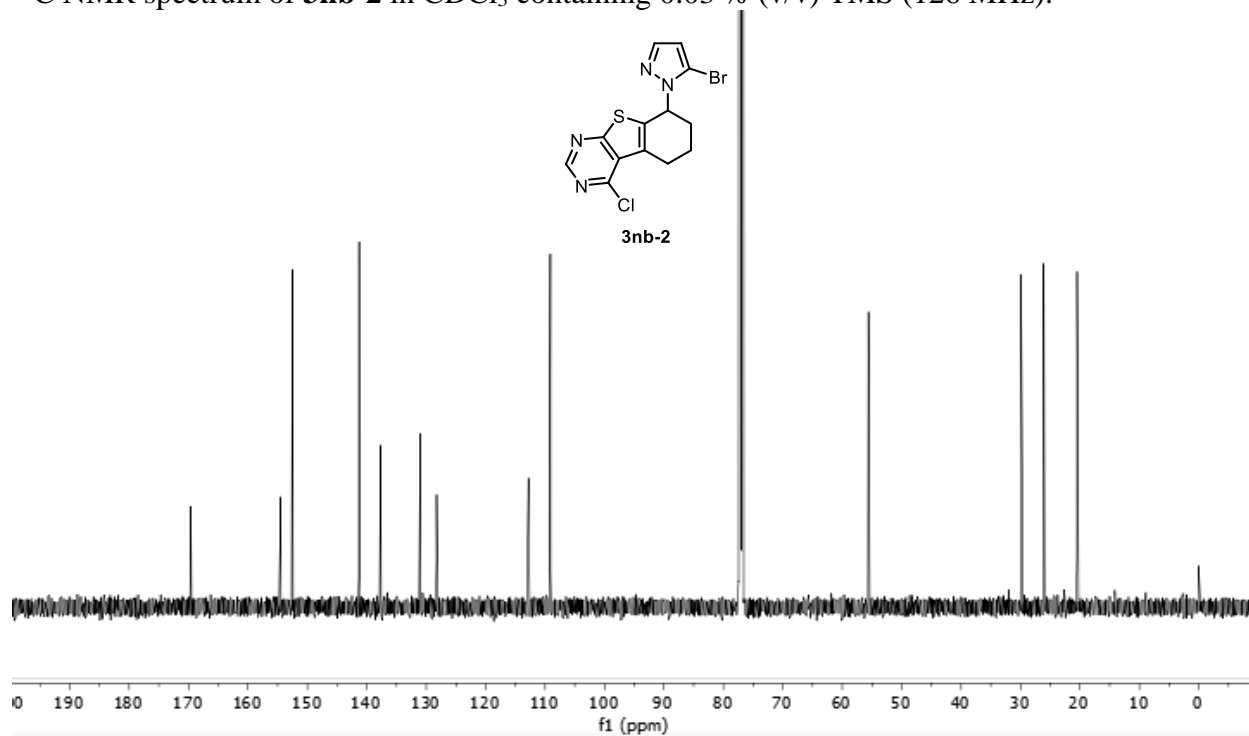
HMBC NMR spectrum of **3nb-1** in CDCl₃ containing 0.03 % (v/v) TMS (500, 126 MHz).



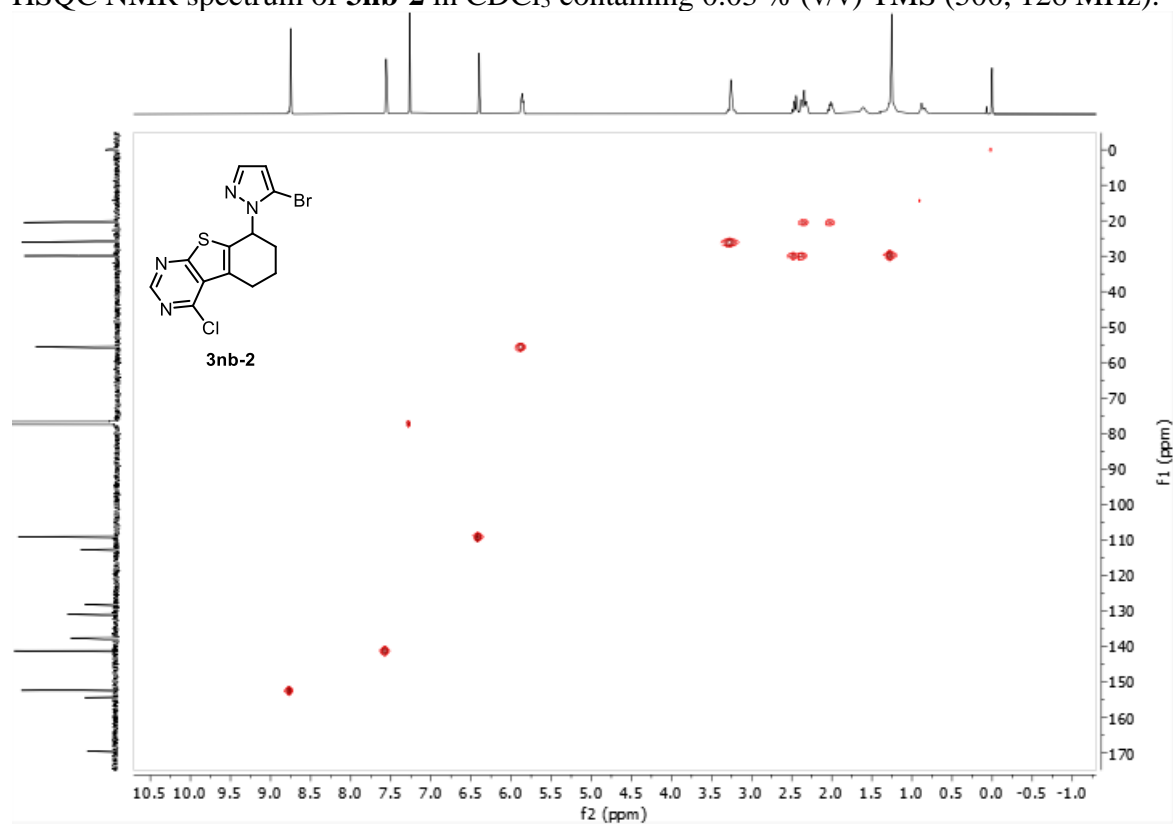
^1H NMR spectrum of **3nb-2** in CDCl_3 containing 0.03 % (v/v) TMS (500 MHz).



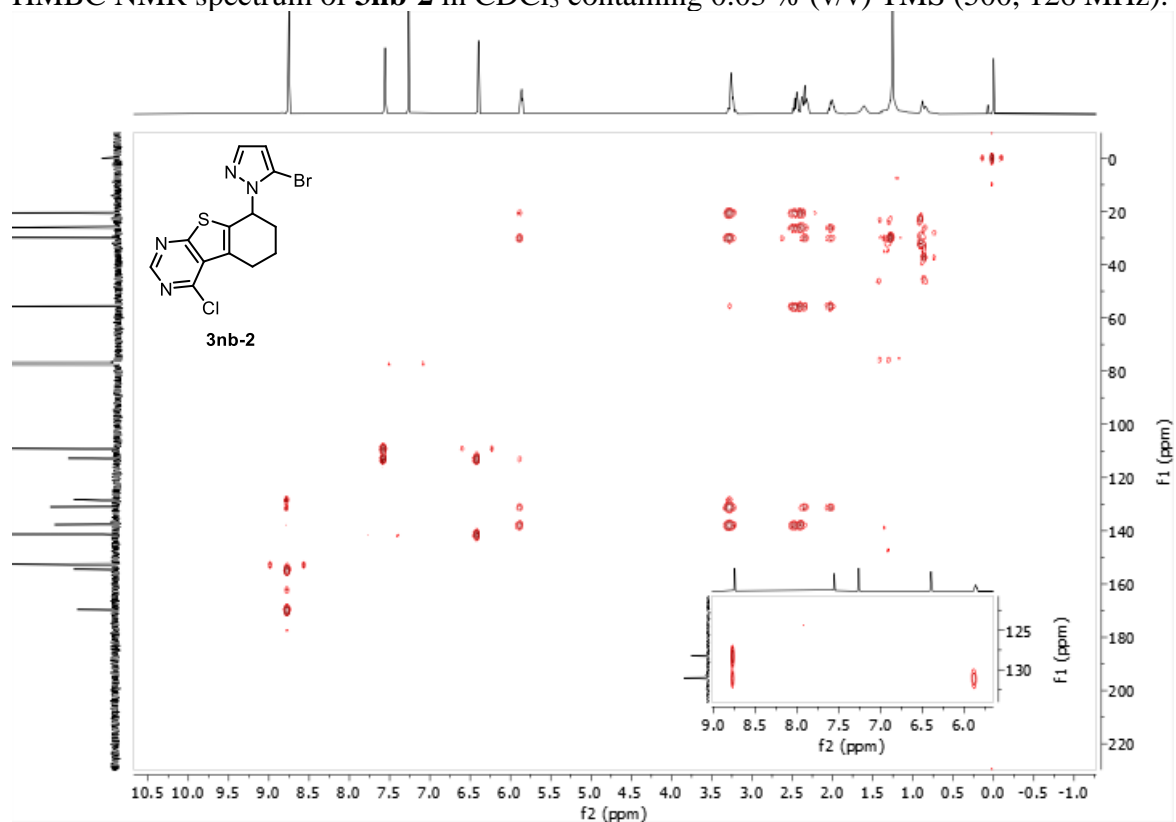
^{13}C NMR spectrum of **3nb-2** in CDCl_3 containing 0.03 % (v/v) TMS (126 MHz).



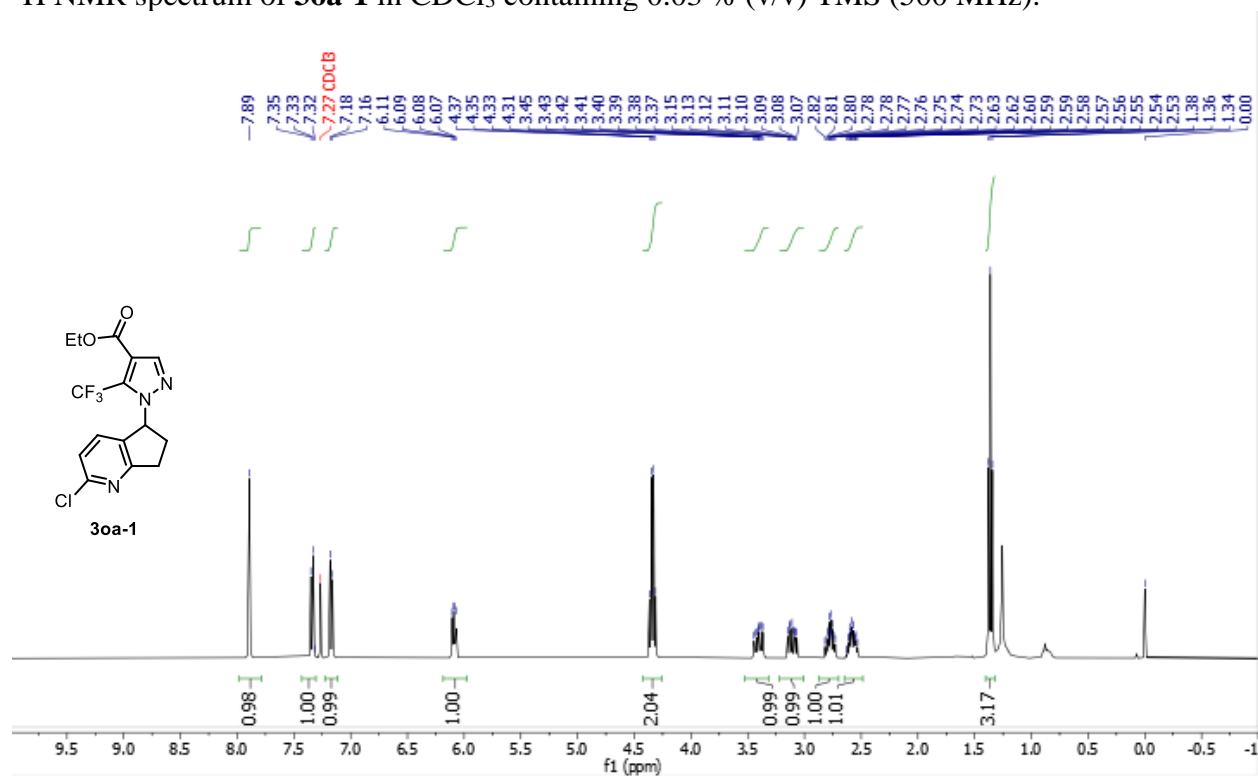
HSQC NMR spectrum of **3nb-2** in CDCl₃ containing 0.03 % (v/v) TMS (500, 126 MHz).



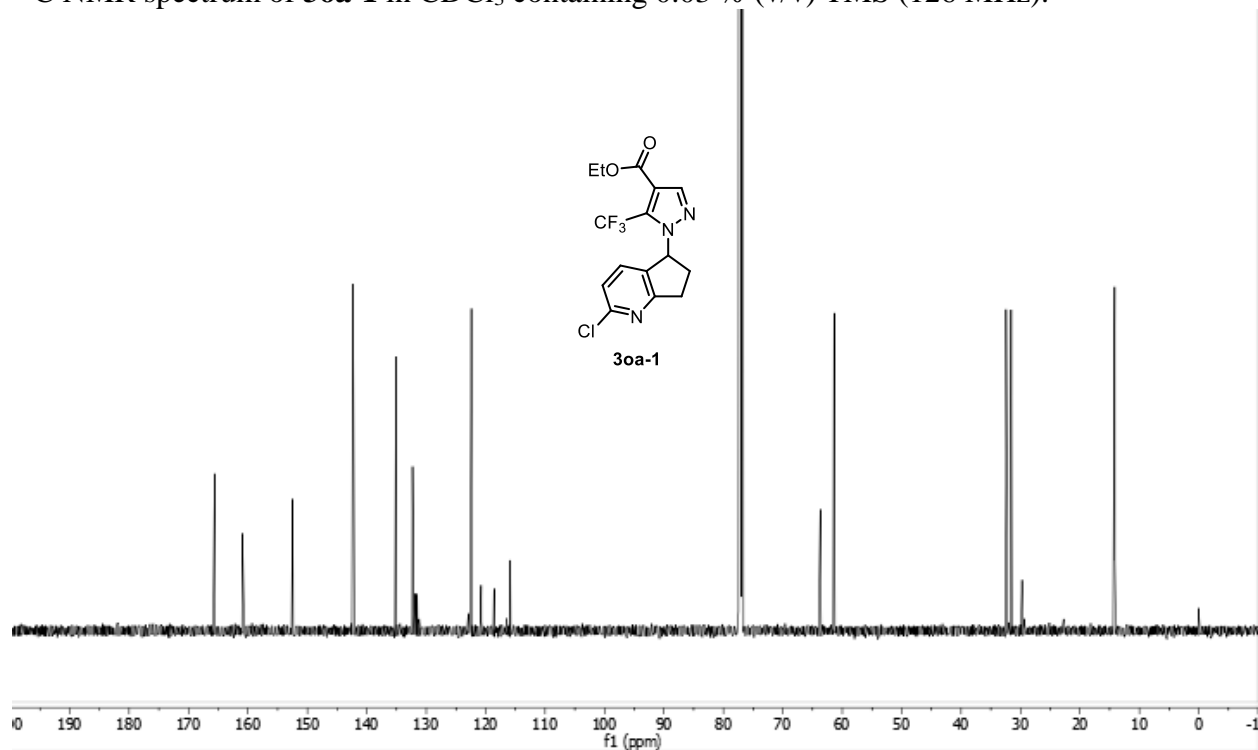
HMBC NMR spectrum of **3nb-2** in CDCl₃ containing 0.03 % (v/v) TMS (500, 126 MHz).



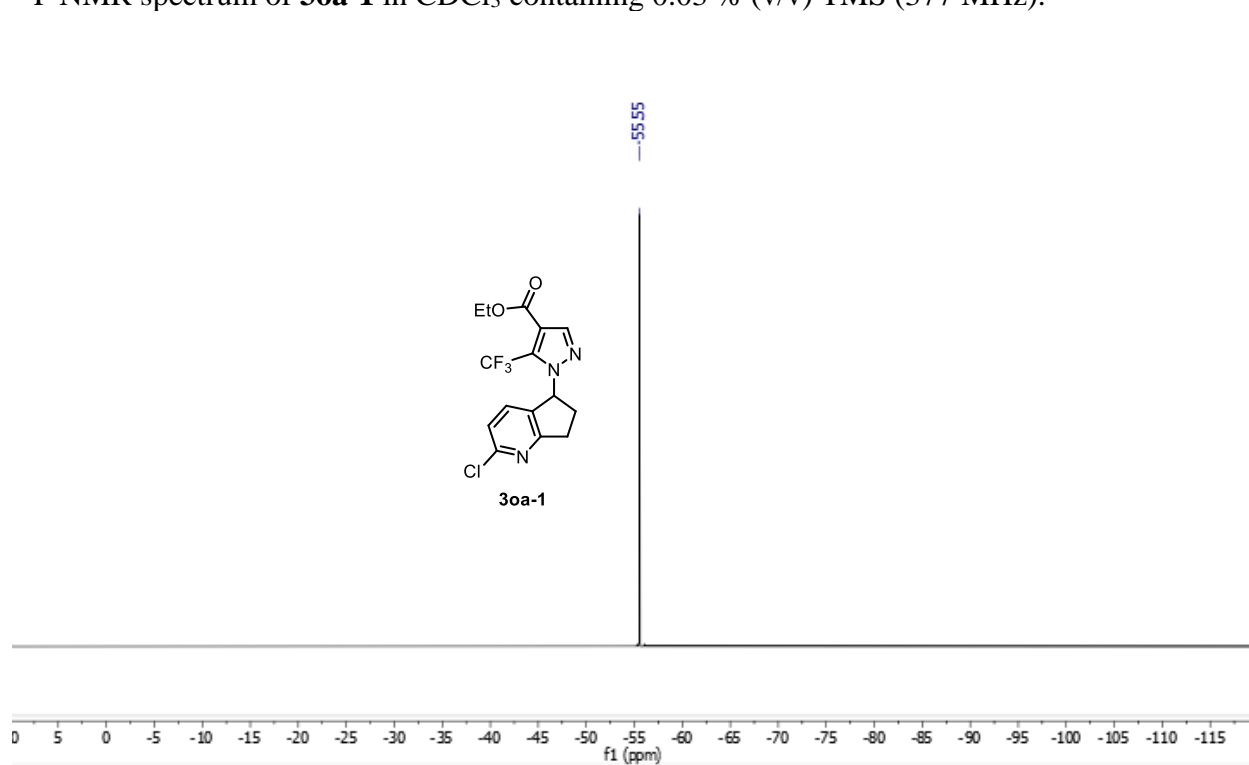
^1H NMR spectrum of **3oa-1** in CDCl_3 containing 0.03 % (v/v) TMS (500 MHz).



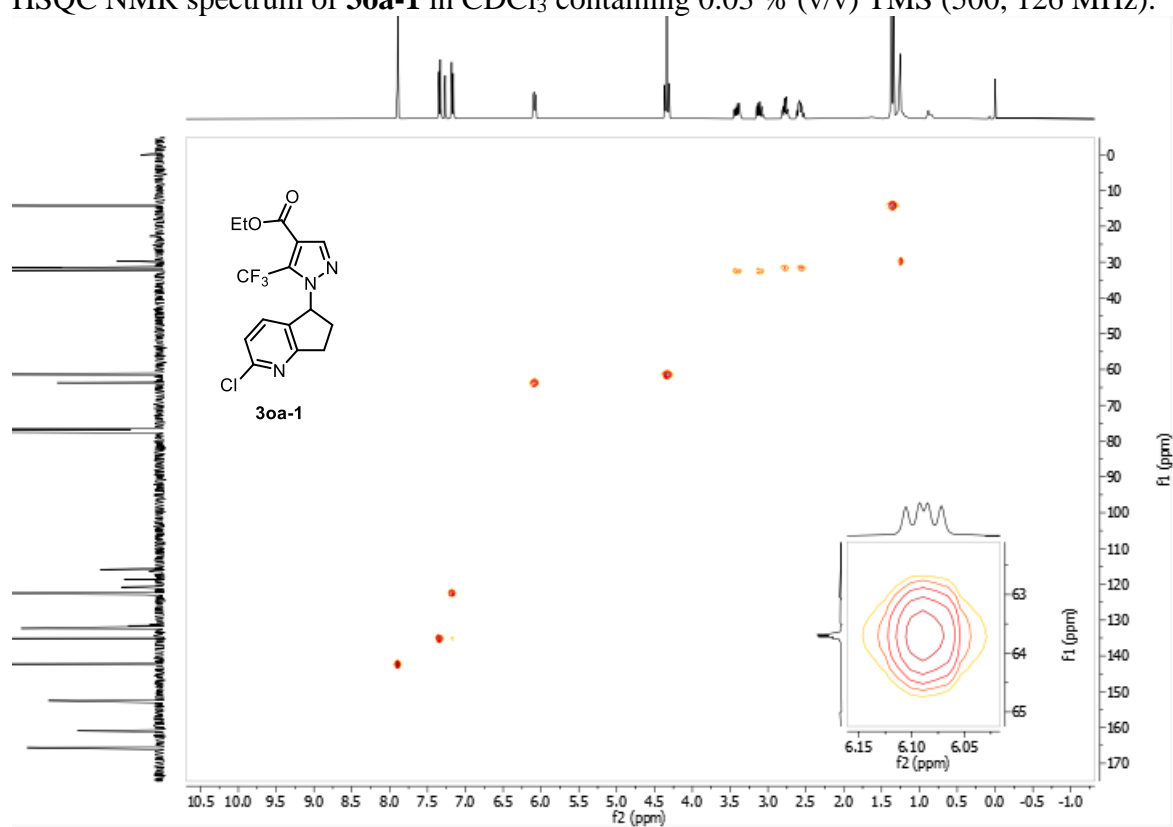
^{13}C NMR spectrum of **3oa-1** in CDCl_3 containing 0.03 % (v/v) TMS (126 MHz).



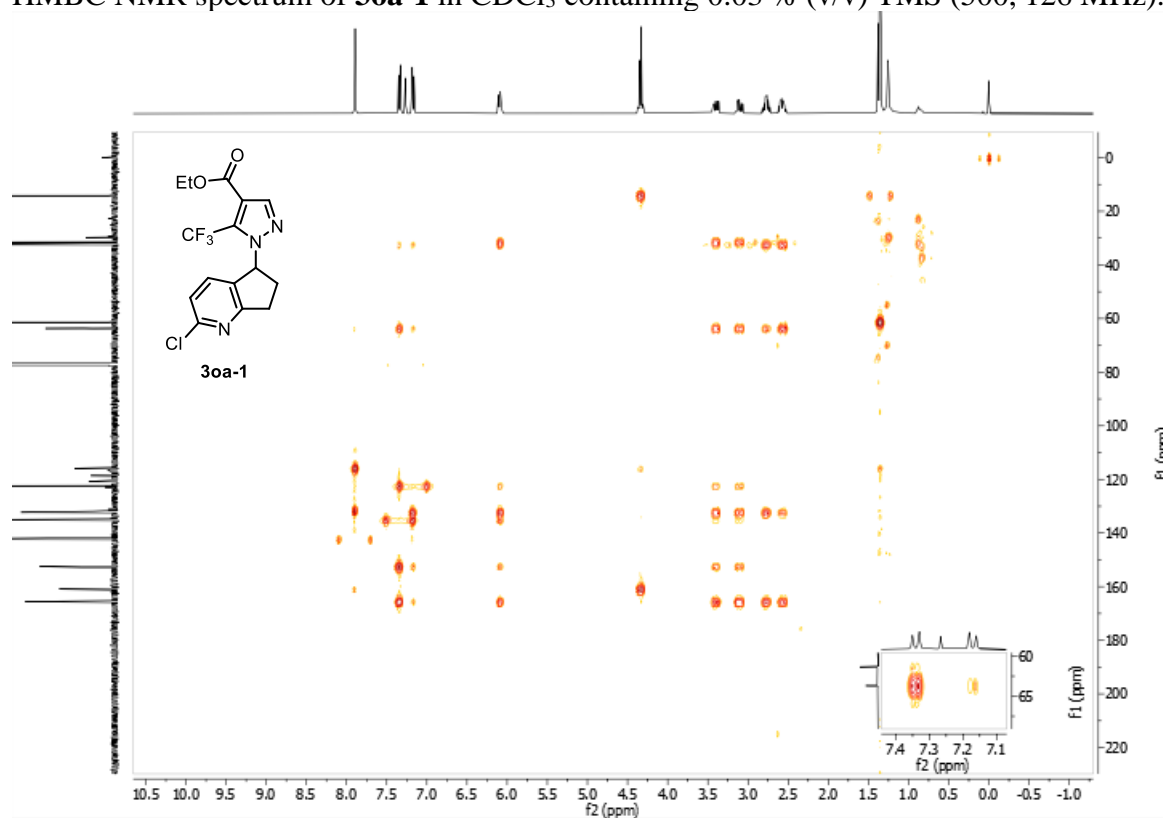
^{19}F NMR spectrum of **3oa-1** in CDCl_3 containing 0.03 % (v/v) TMS (377 MHz).



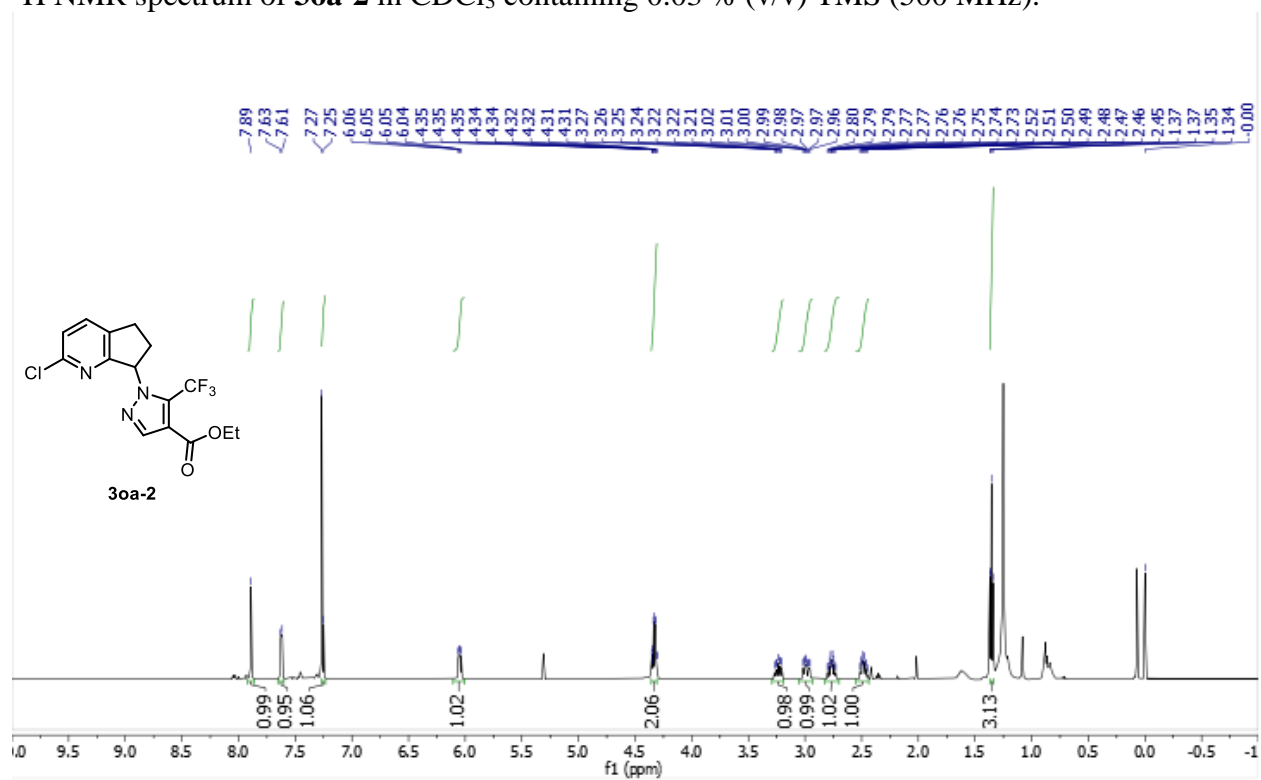
HSQC NMR spectrum of **3oa-1** in CDCl_3 containing 0.03 % (v/v) TMS (500, 126 MHz).



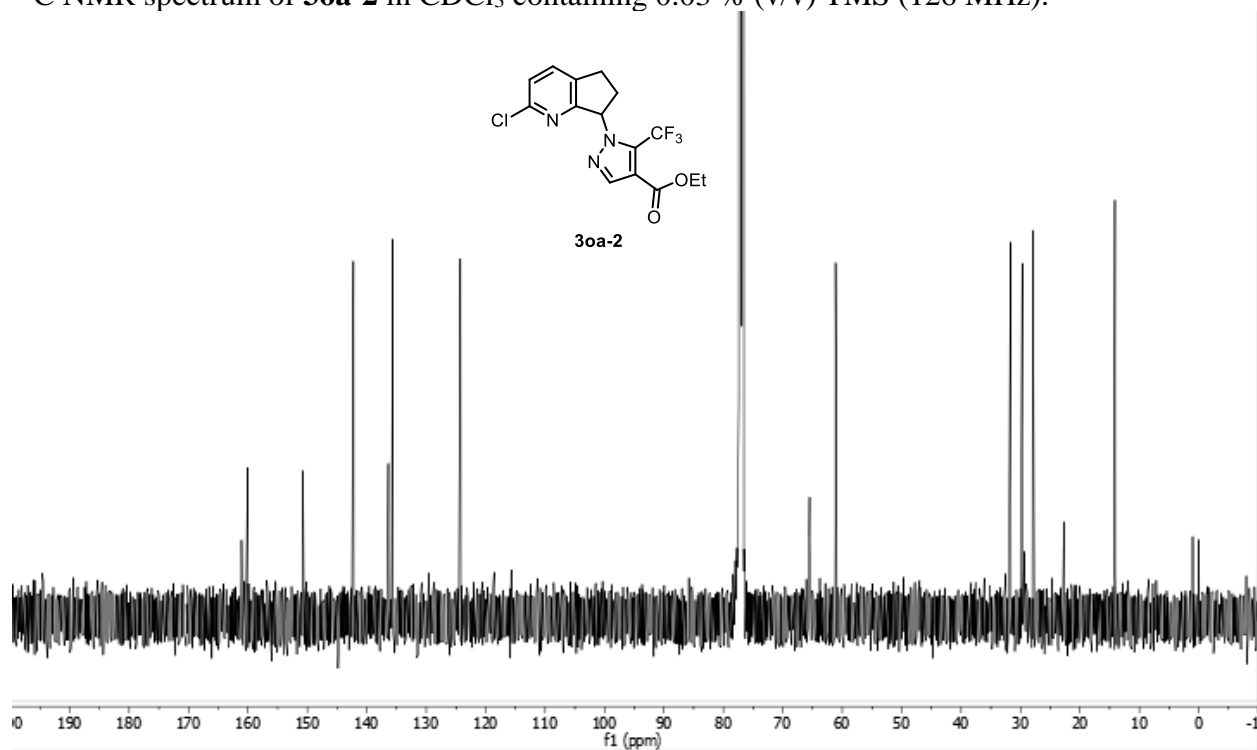
HMBC NMR spectrum of **3oa-1** in CDCl₃ containing 0.03 % (v/v) TMS (500, 126 MHz).



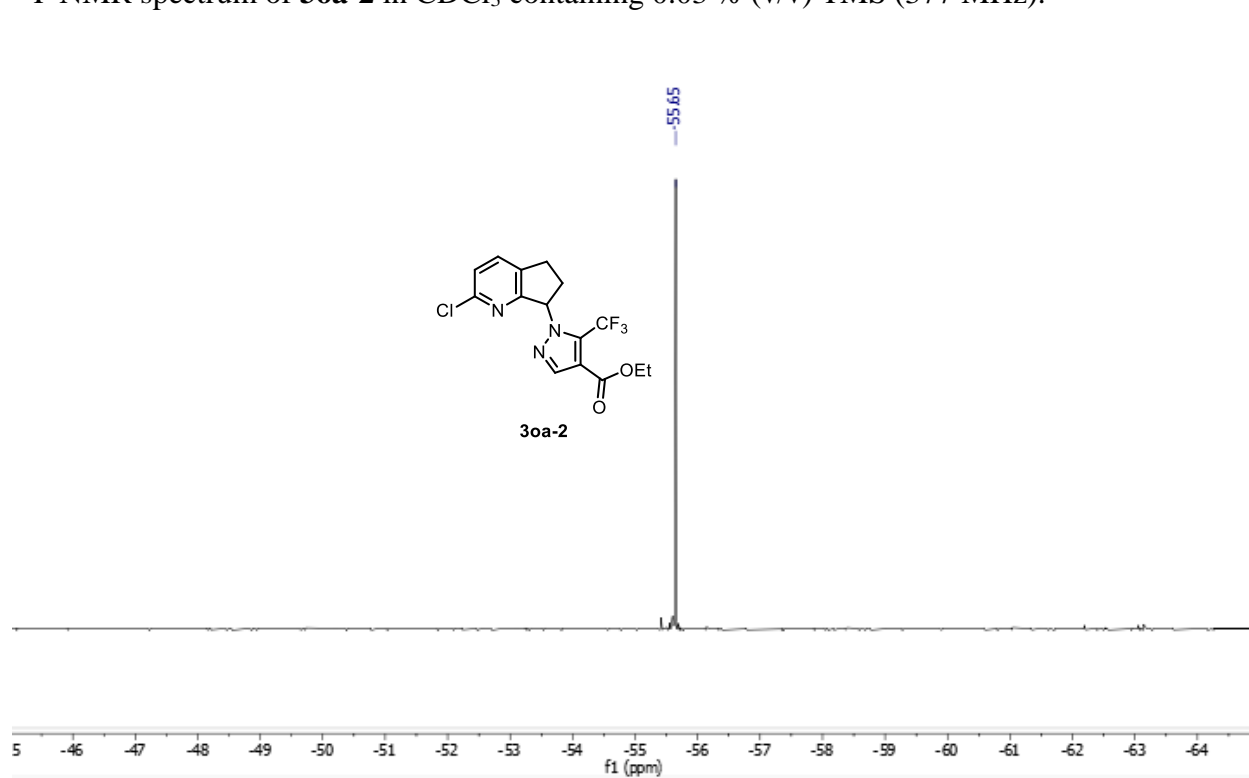
¹H NMR spectrum of **3oa-2** in CDCl₃ containing 0.03 % (v/v) TMS (500 MHz).



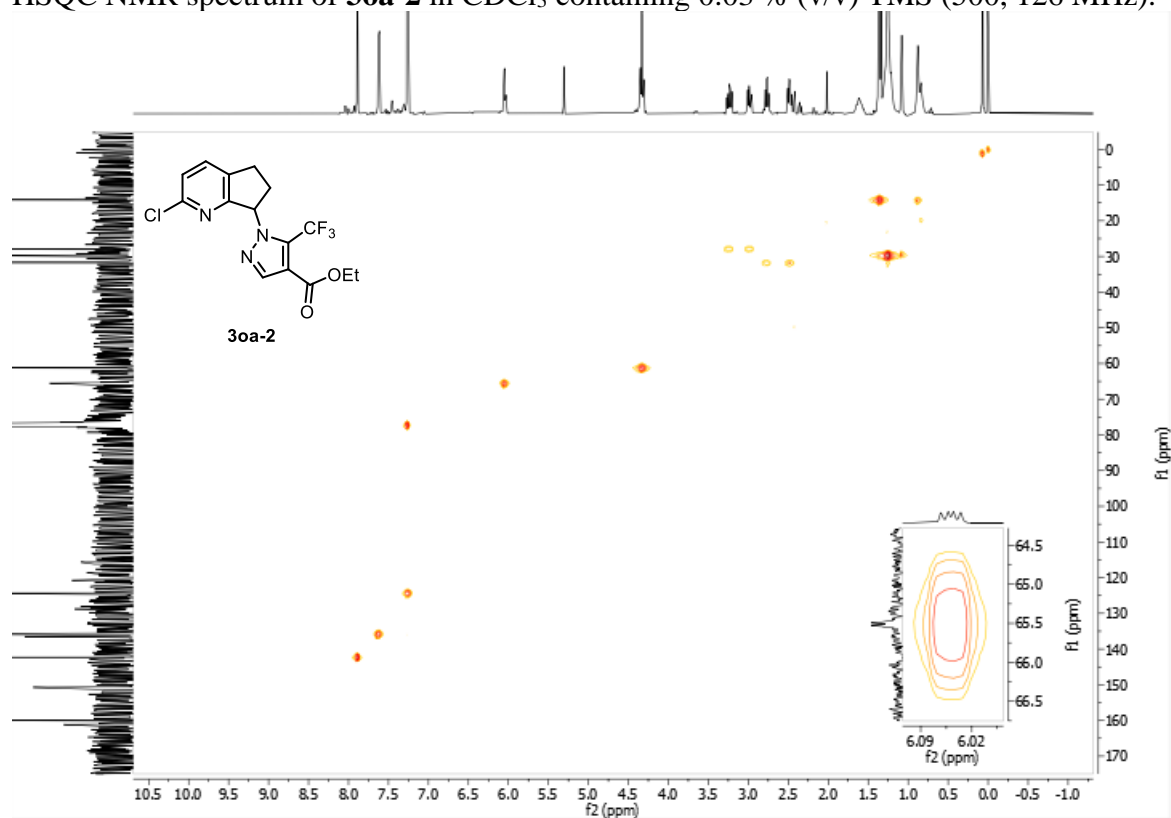
^{13}C NMR spectrum of **3oa-2** in CDCl_3 containing 0.03 % (v/v) TMS (126 MHz).



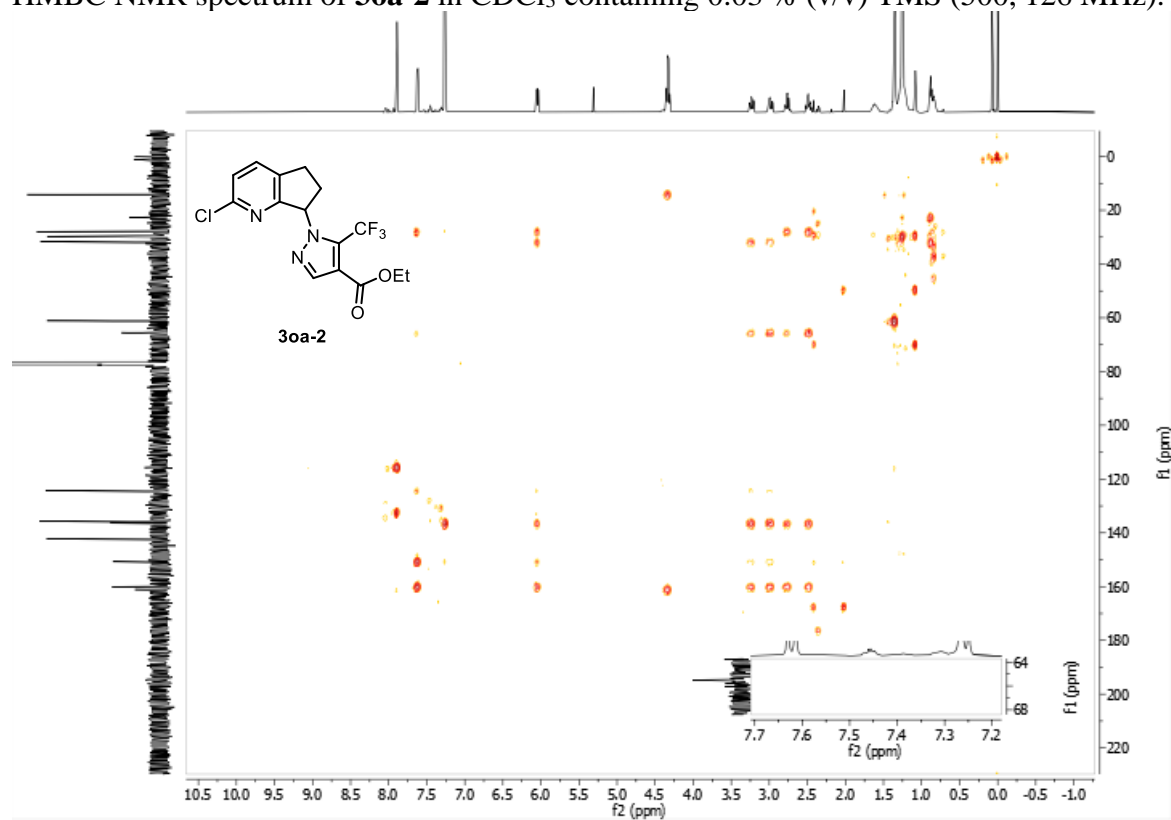
^{19}F NMR spectrum of **3oa-2** in CDCl_3 containing 0.03 % (v/v) TMS (377 MHz).



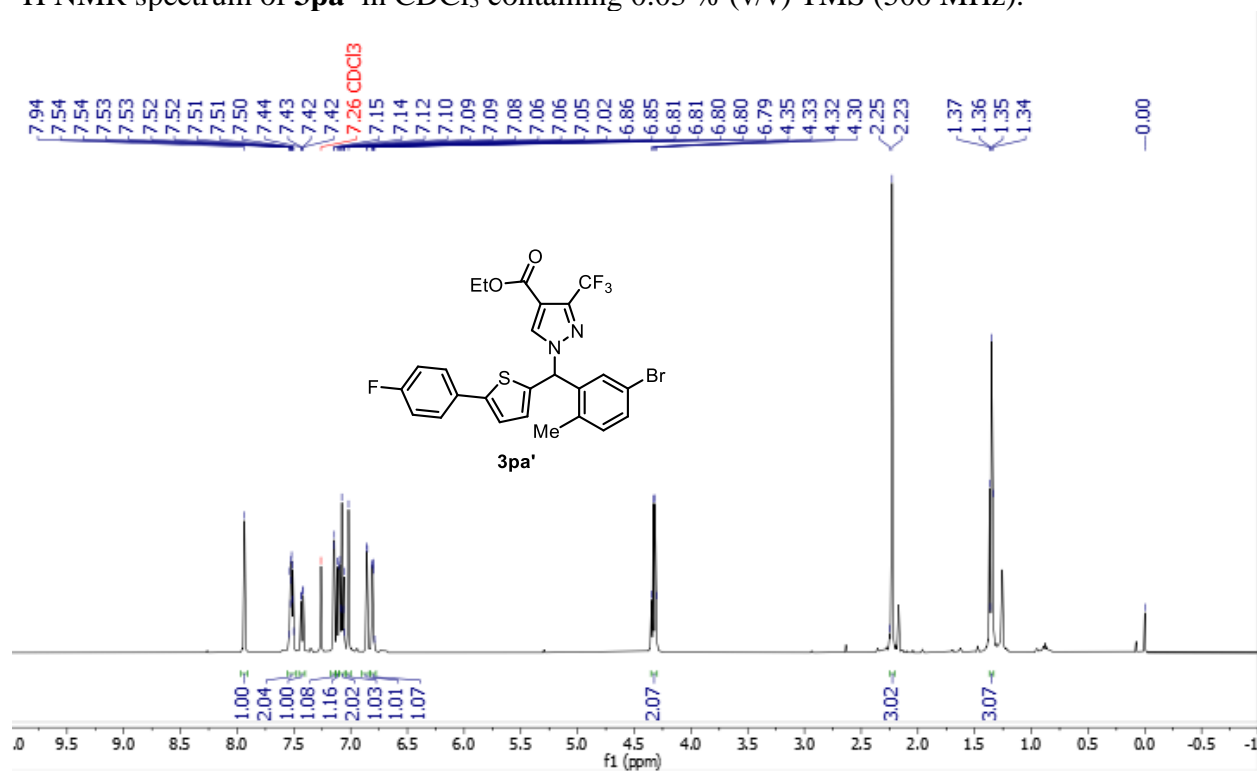
HSQC NMR spectrum of **3oa-2** in CDCl₃ containing 0.03 % (v/v) TMS (500, 126 MHz).



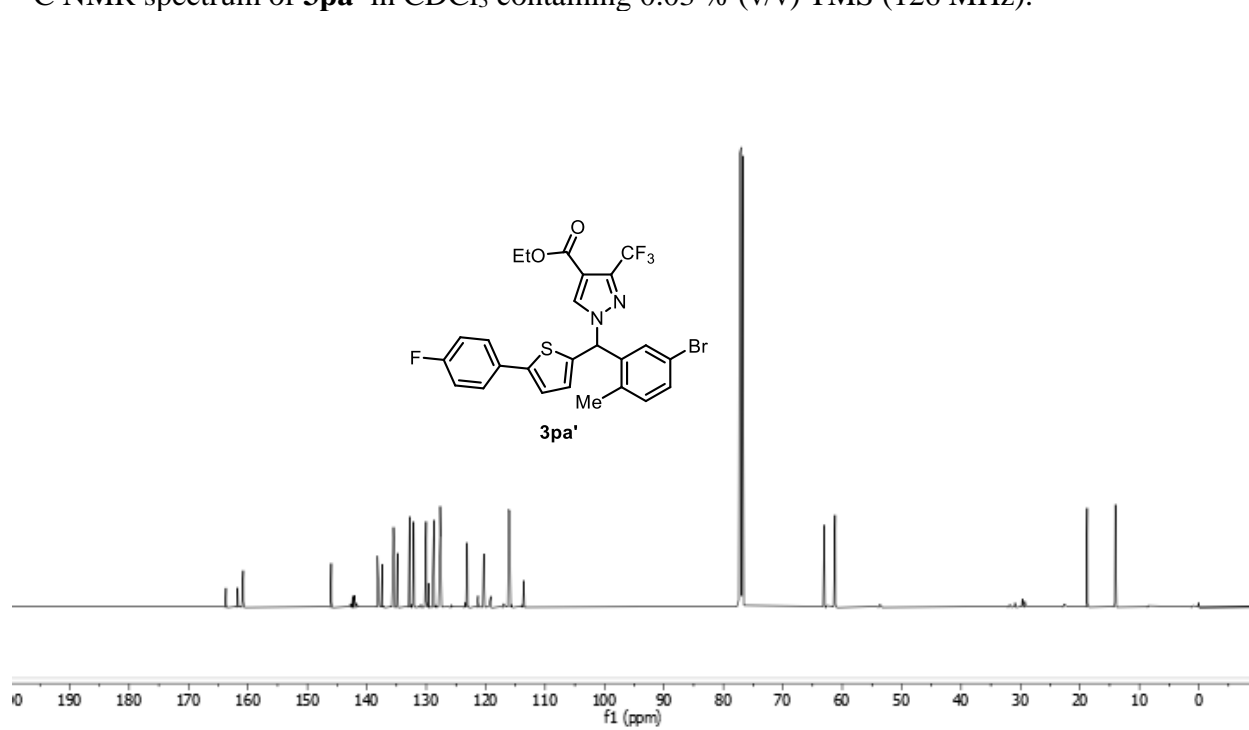
HMBC NMR spectrum of **3oa-2** in CDCl₃ containing 0.03 % (v/v) TMS (500, 126 MHz).



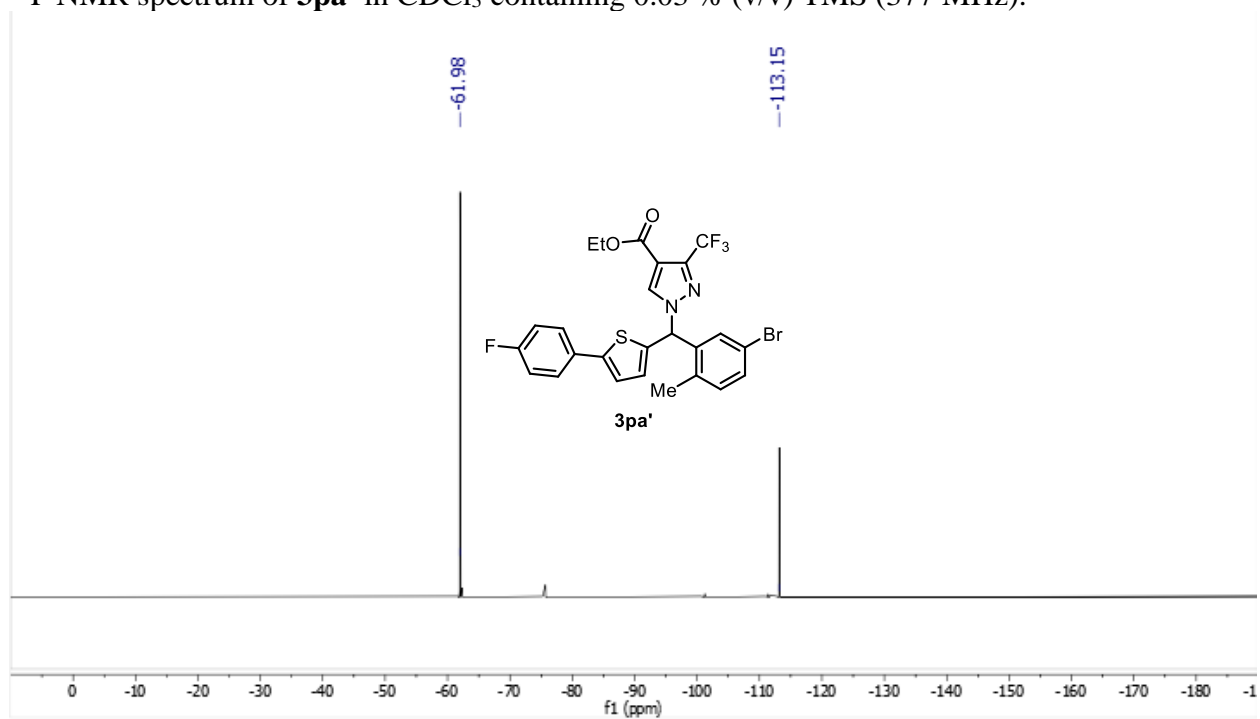
^1H NMR spectrum of **3pa'** in CDCl_3 containing 0.03 % (v/v) TMS (500 MHz).



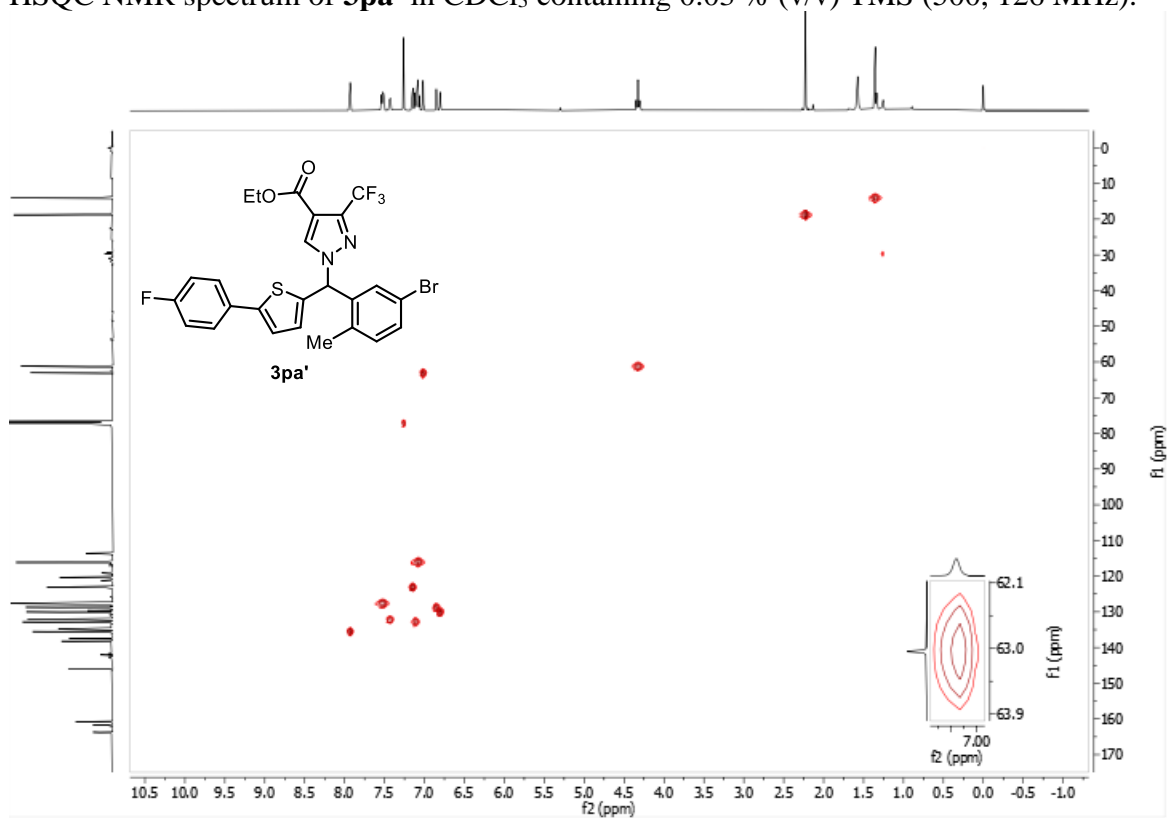
^{13}C NMR spectrum of **3pa'** in CDCl_3 containing 0.03 % (v/v) TMS (126 MHz).



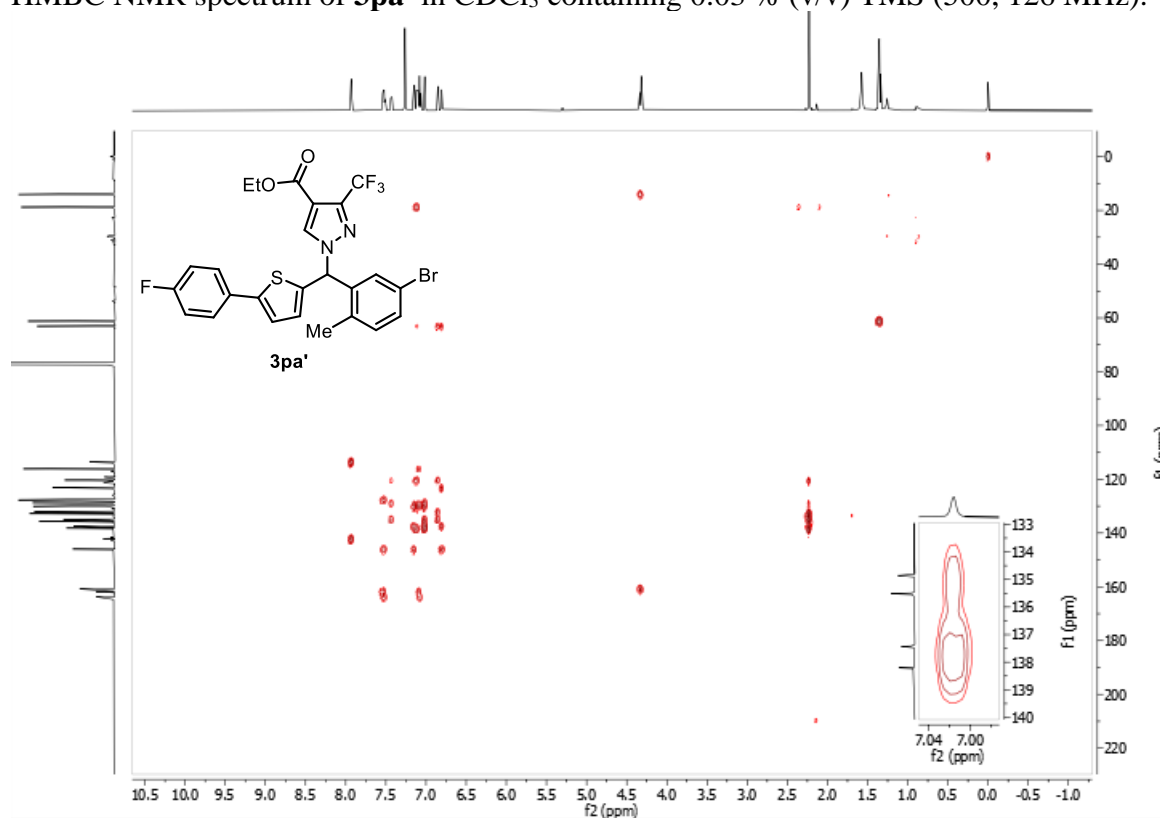
^{19}F NMR spectrum of **3pa'** in CDCl_3 containing 0.03 % (v/v) TMS (377 MHz).



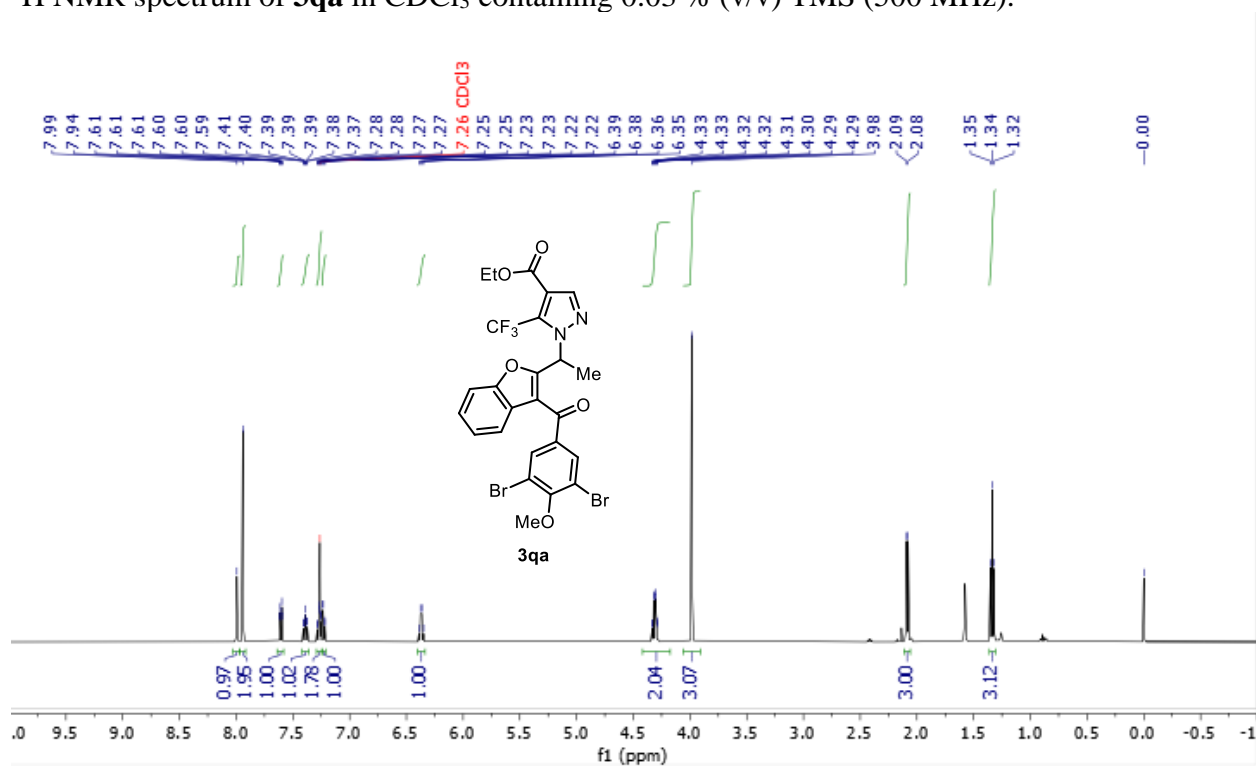
HSQC NMR spectrum of **3pa'** in CDCl_3 containing 0.03 % (v/v) TMS (500, 126 MHz).



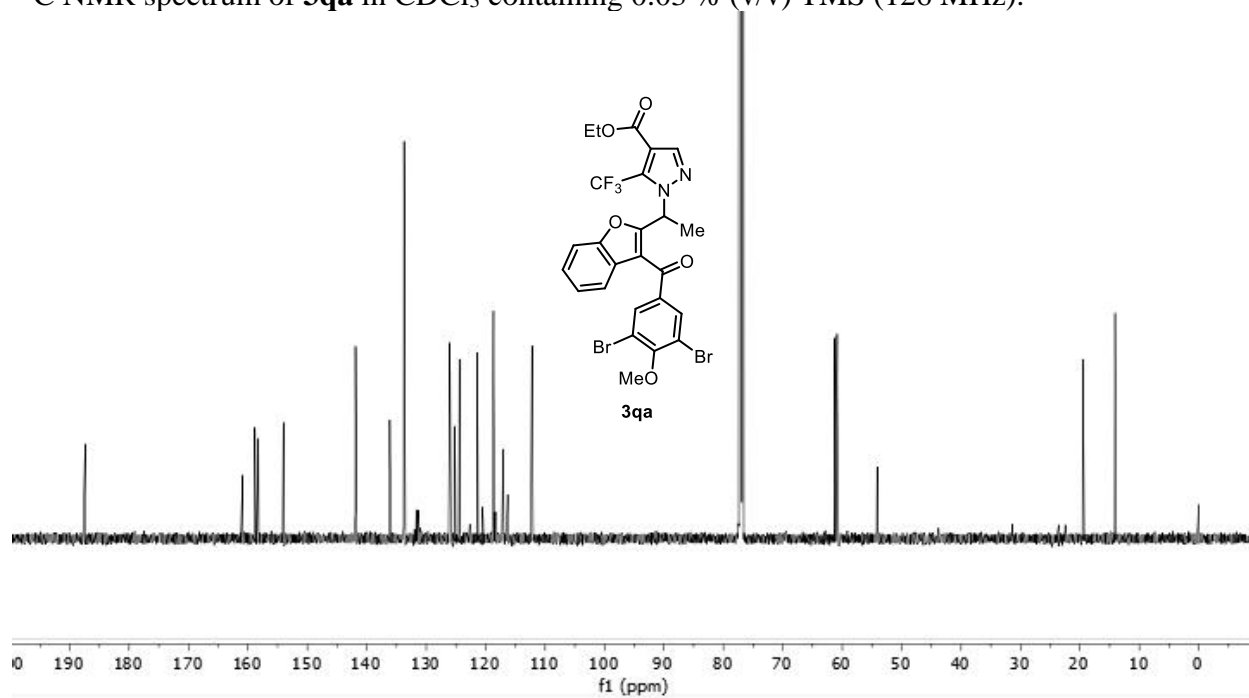
HMBC NMR spectrum of **3pa'** in CDCl₃ containing 0.03 % (v/v) TMS (500, 126 MHz).



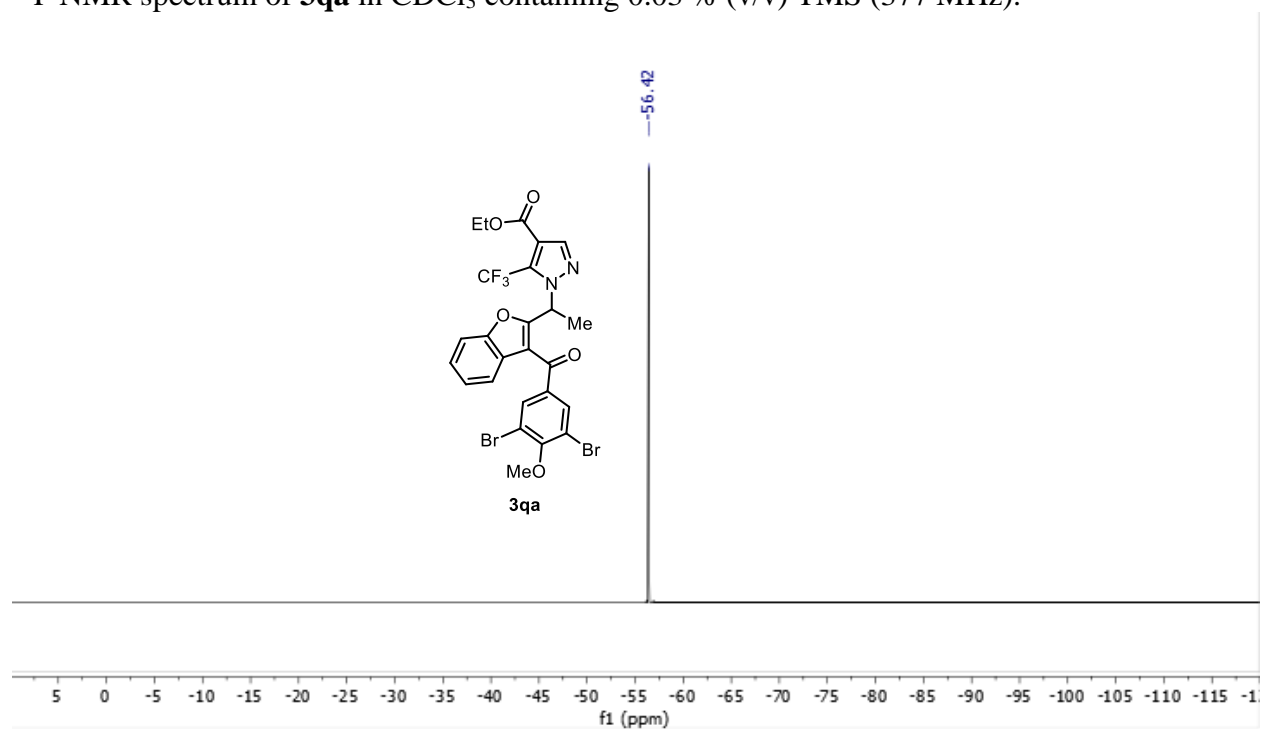
¹H NMR spectrum of **3qa** in CDCl₃ containing 0.03 % (v/v) TMS (500 MHz).



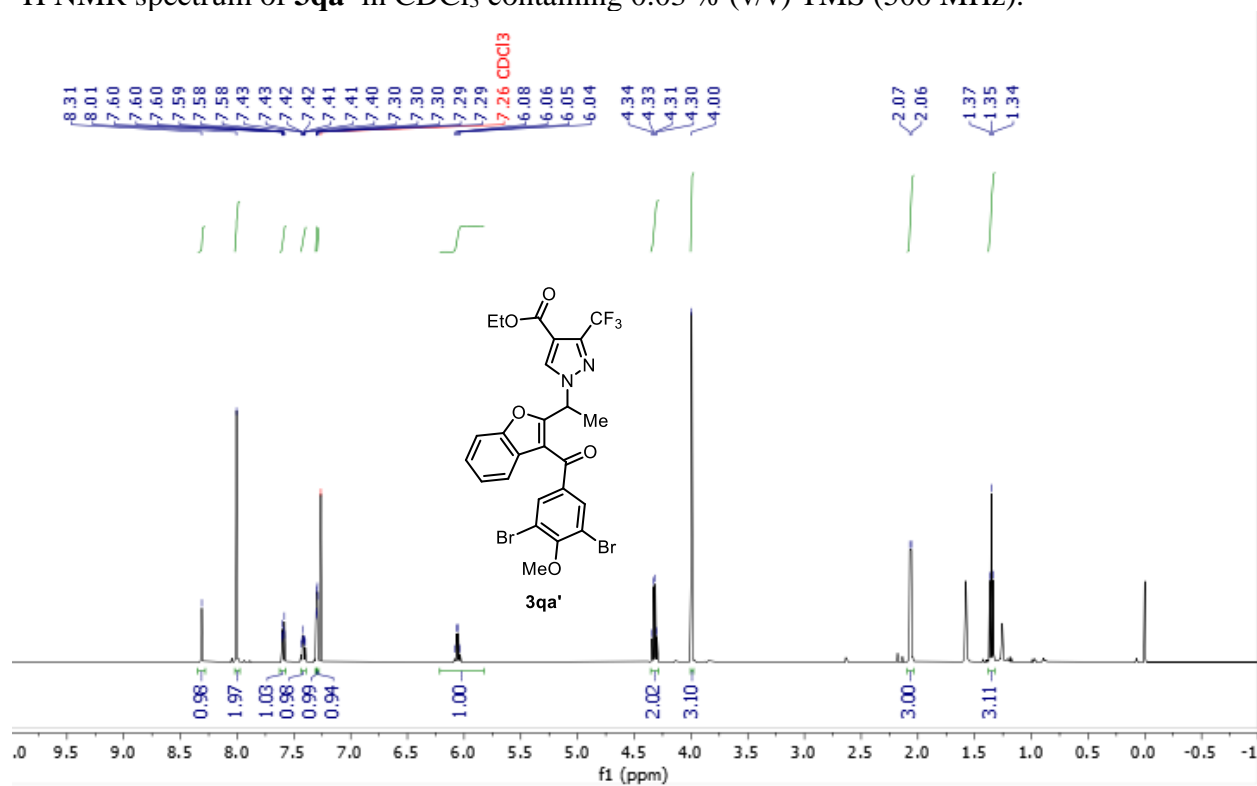
^{13}C NMR spectrum of **3qa** in CDCl_3 containing 0.03 % (v/v) TMS (126 MHz).



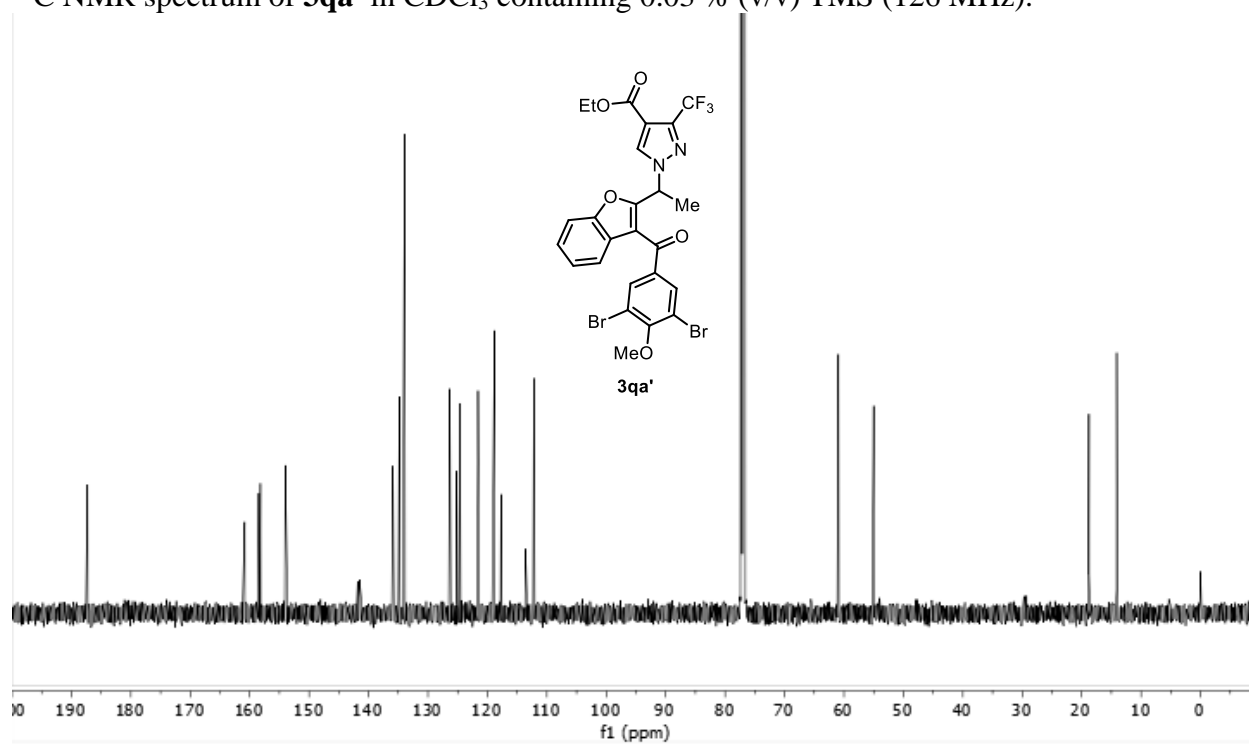
^{19}F NMR spectrum of **3qa** in CDCl_3 containing 0.03 % (v/v) TMS (377 MHz).



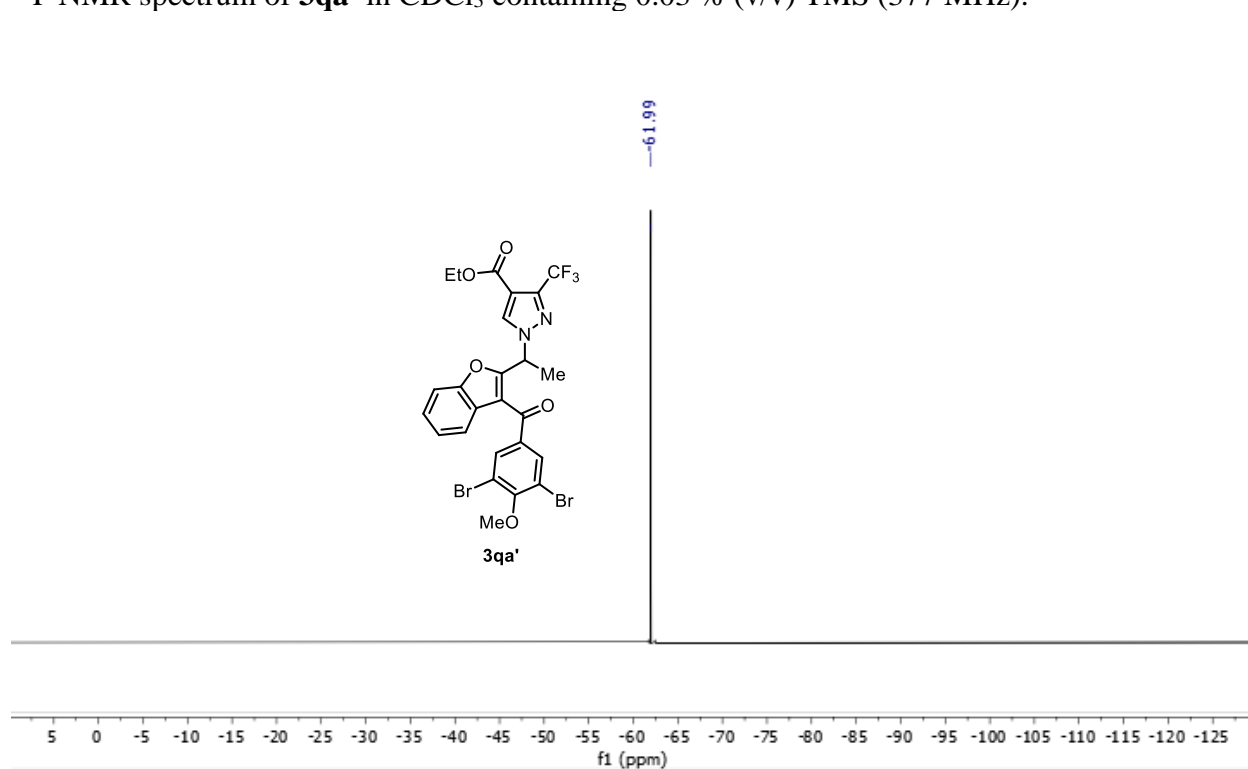
^1H NMR spectrum of **3qa'** in CDCl_3 containing 0.03 % (v/v) TMS (500 MHz).



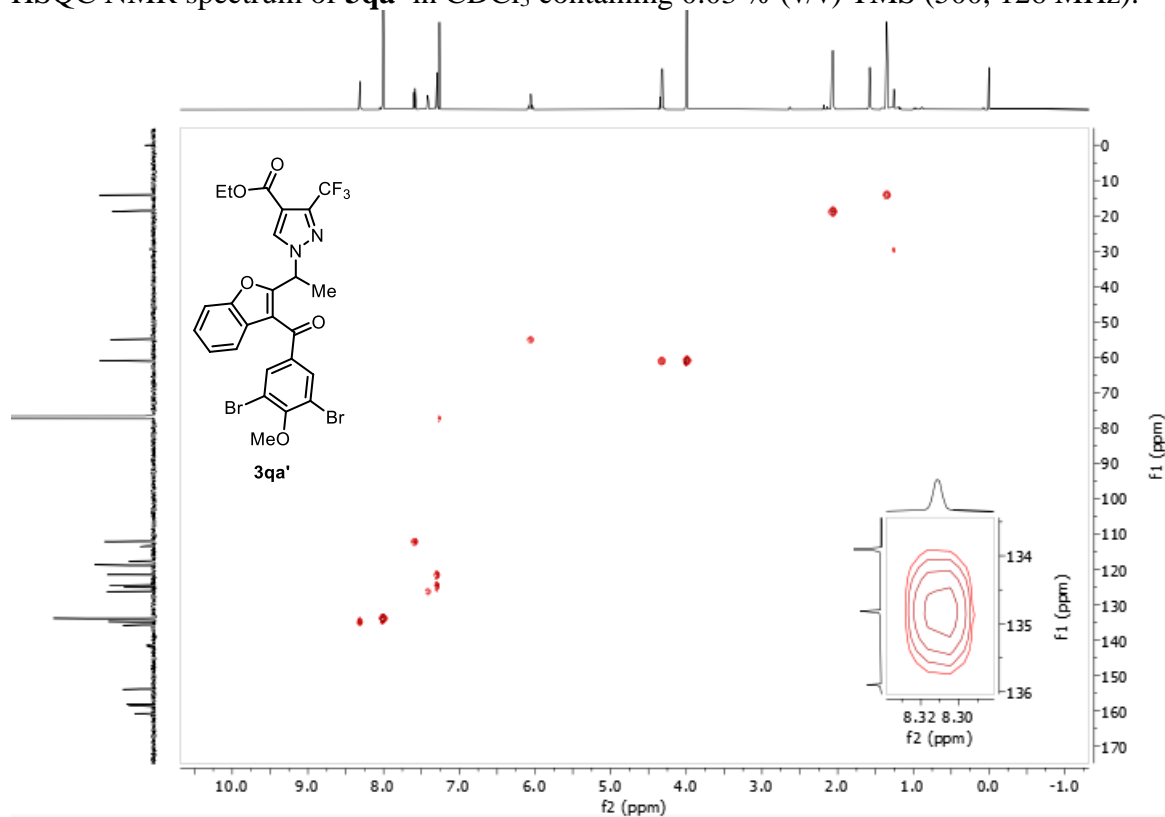
^{13}C NMR spectrum of **3qa'** in CDCl_3 containing 0.03 % (v/v) TMS (126 MHz).



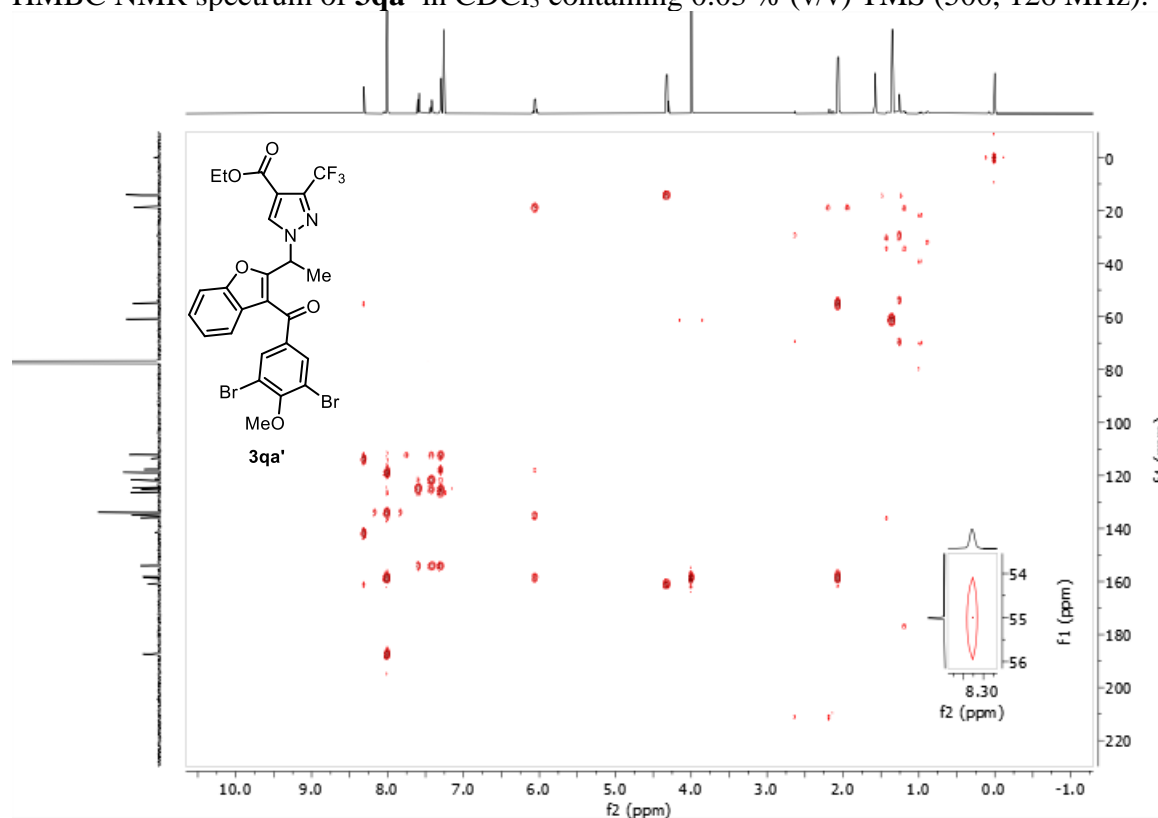
^{19}F NMR spectrum of **3qa'** in CDCl_3 containing 0.03 % (v/v) TMS (377 MHz).



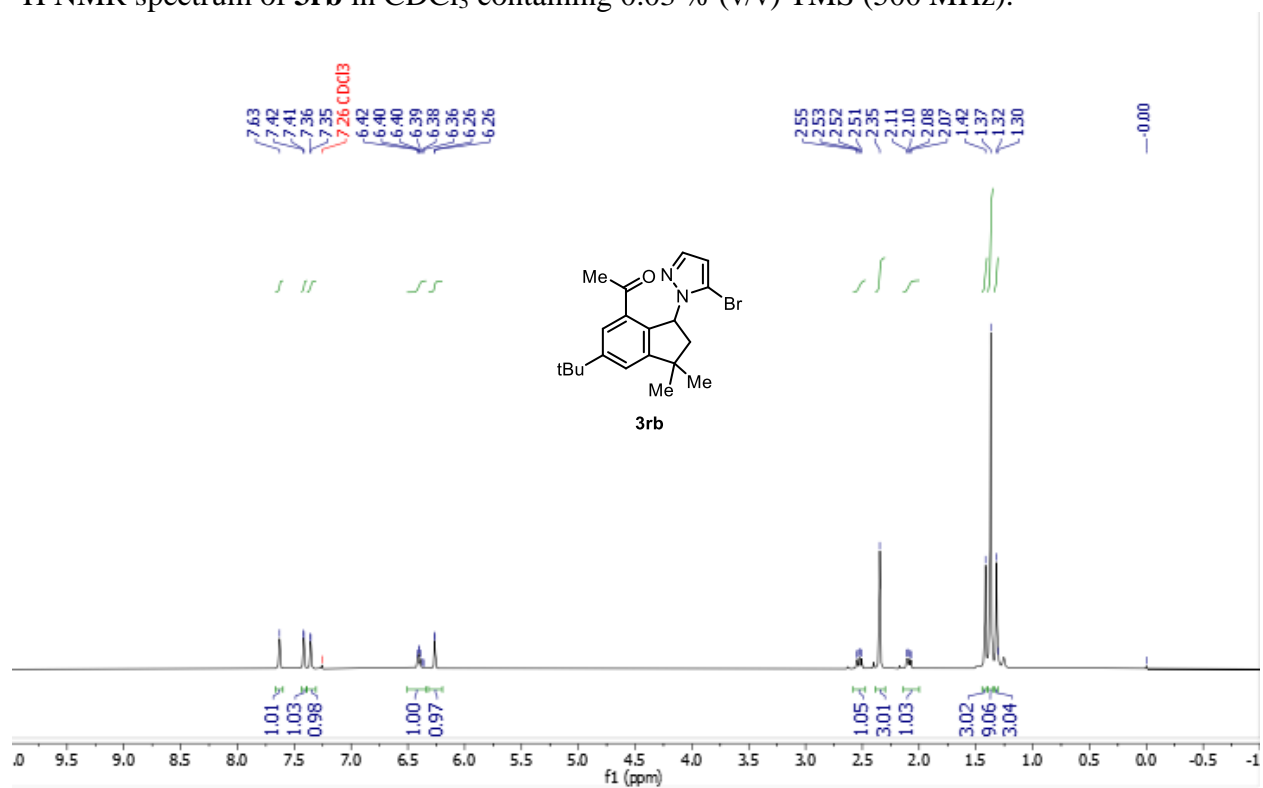
HSQC NMR spectrum of **3qa'** in CDCl_3 containing 0.03 % (v/v) TMS (500, 126 MHz).



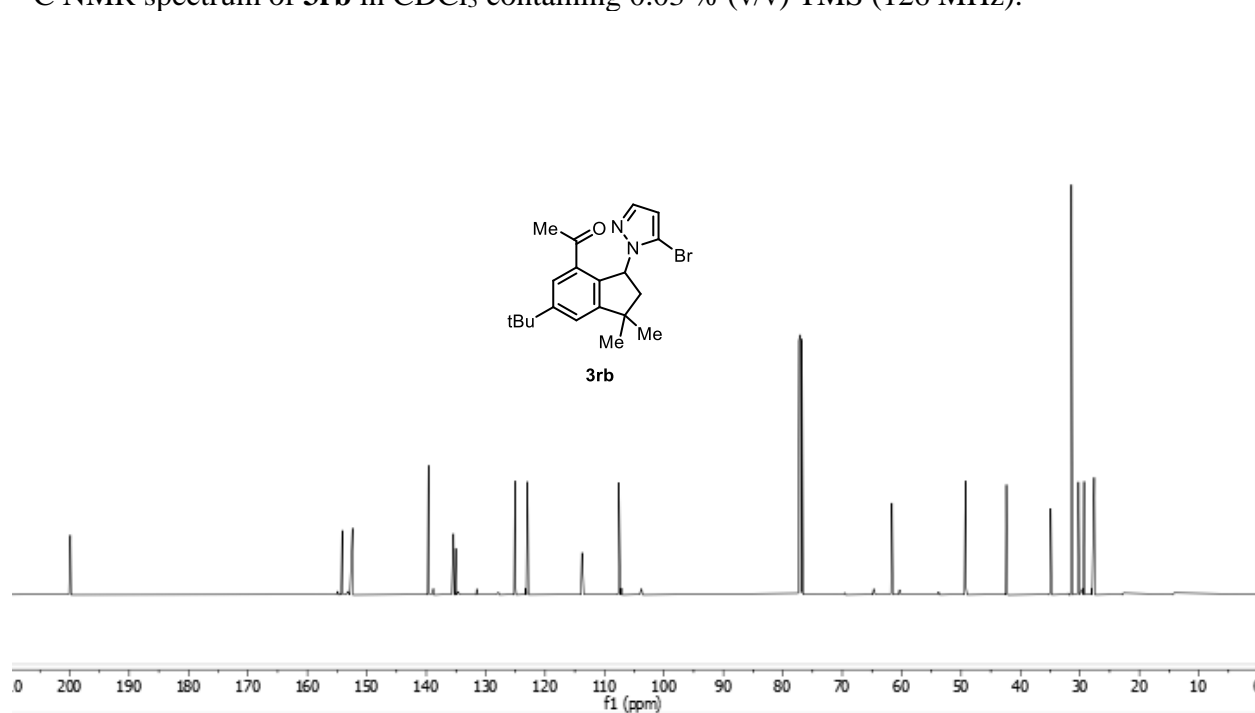
HMBC NMR spectrum of **3qa'** in CDCl₃ containing 0.03 % (v/v) TMS (500, 126 MHz).



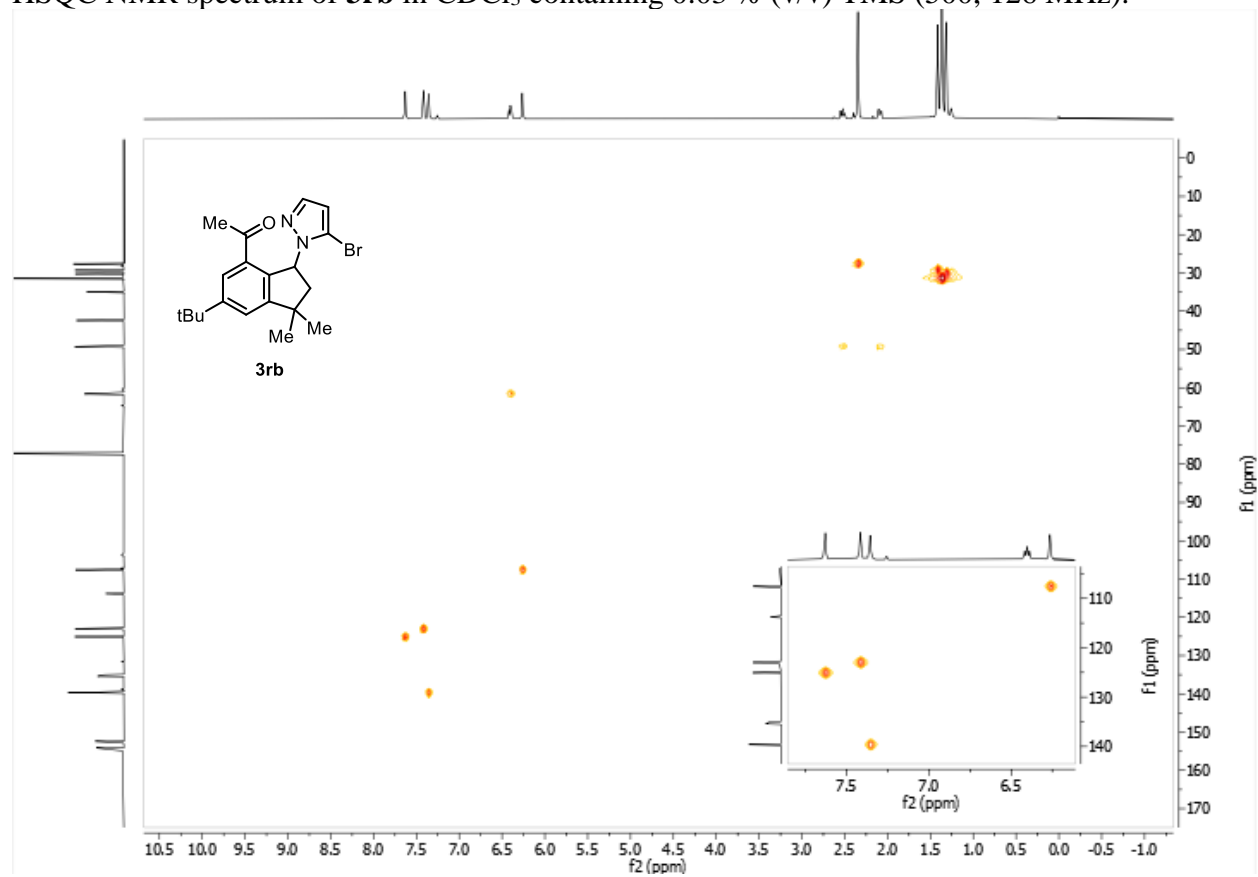
¹H NMR spectrum of **3rb** in CDCl₃ containing 0.03 % (v/v) TMS (500 MHz).



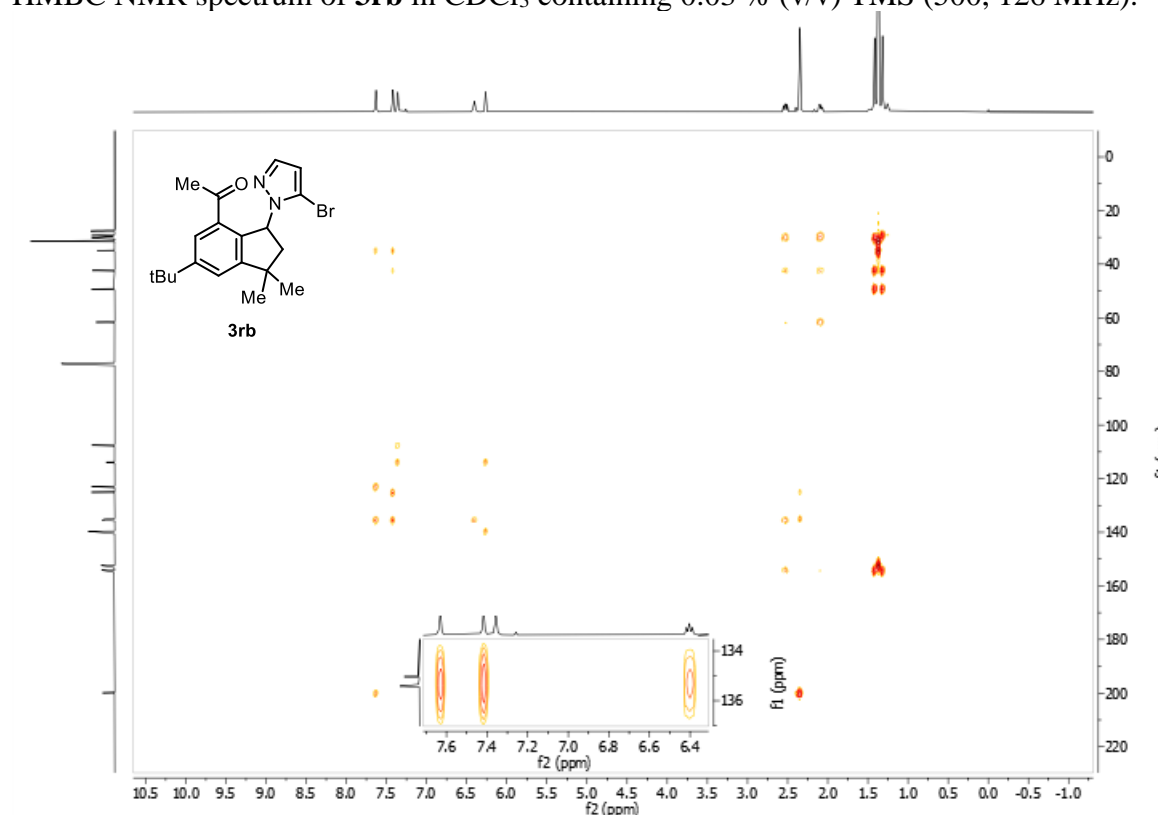
^{13}C NMR spectrum of **3rb** in CDCl_3 containing 0.03 % (v/v) TMS (126 MHz).



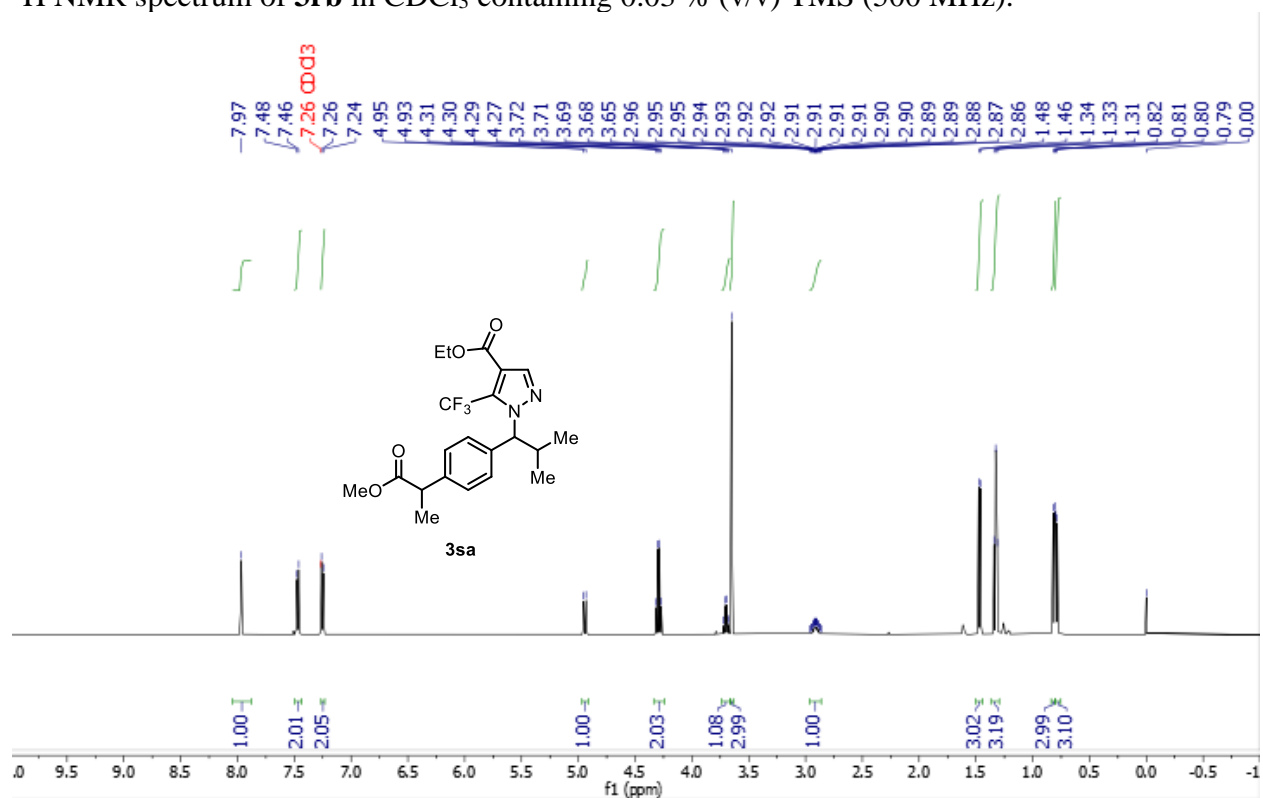
HSQC NMR spectrum of **3rb** in CDCl_3 containing 0.03 % (v/v) TMS (500, 126 MHz).



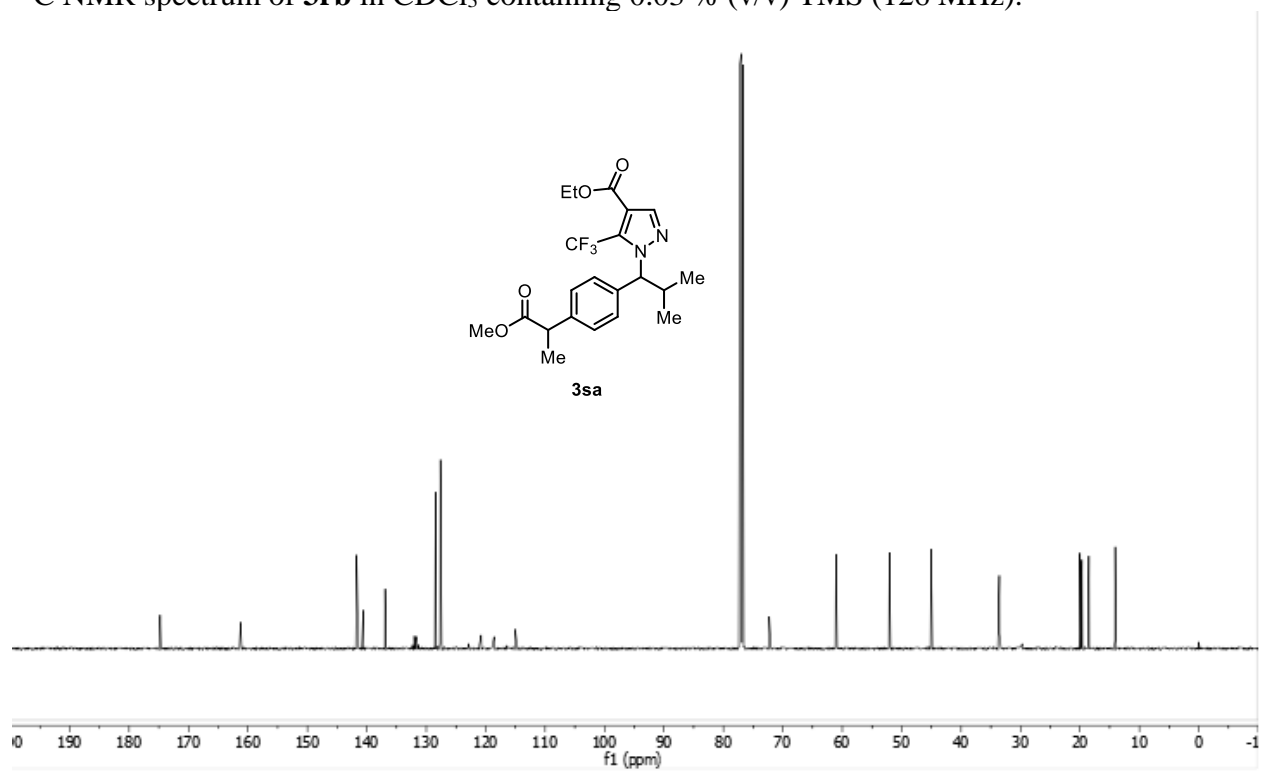
HMBC NMR spectrum of **3rb** in CDCl₃ containing 0.03 % (v/v) TMS (500, 126 MHz).



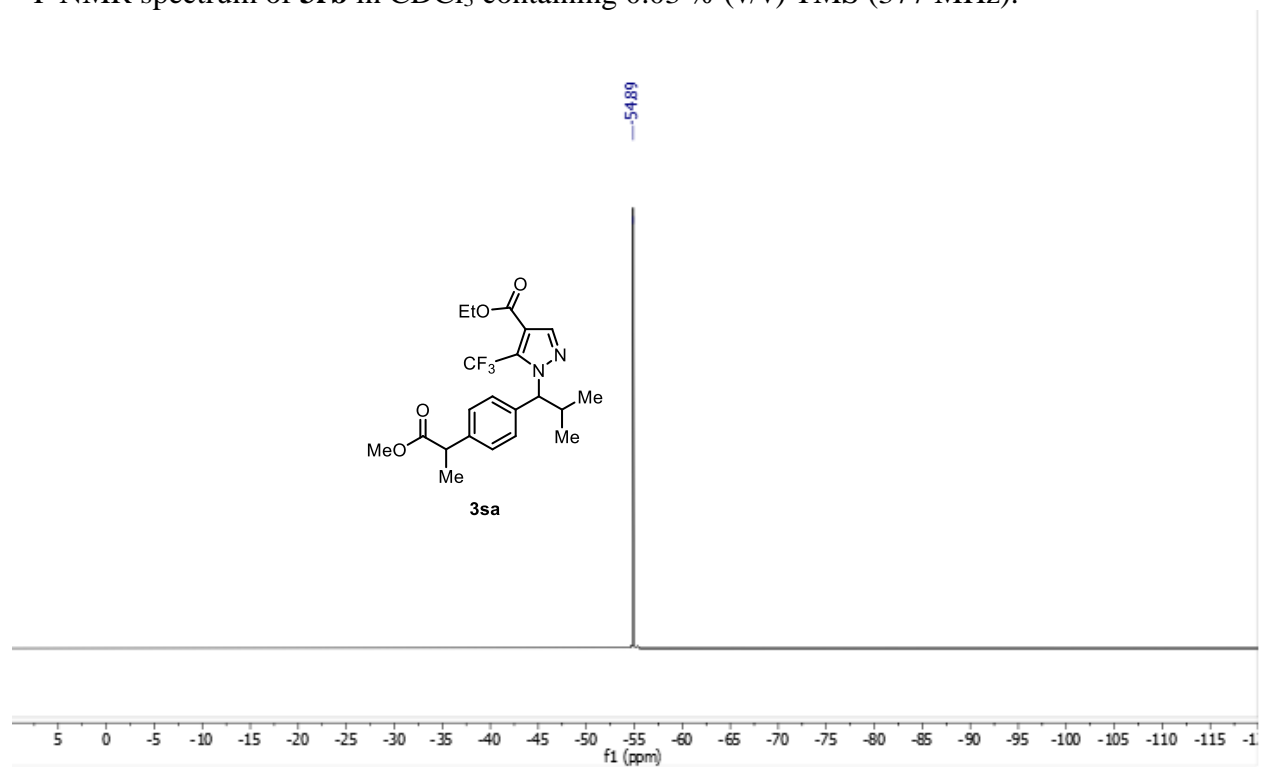
¹H NMR spectrum of **3rb** in CDCl₃ containing 0.03 % (v/v) TMS (500 MHz).



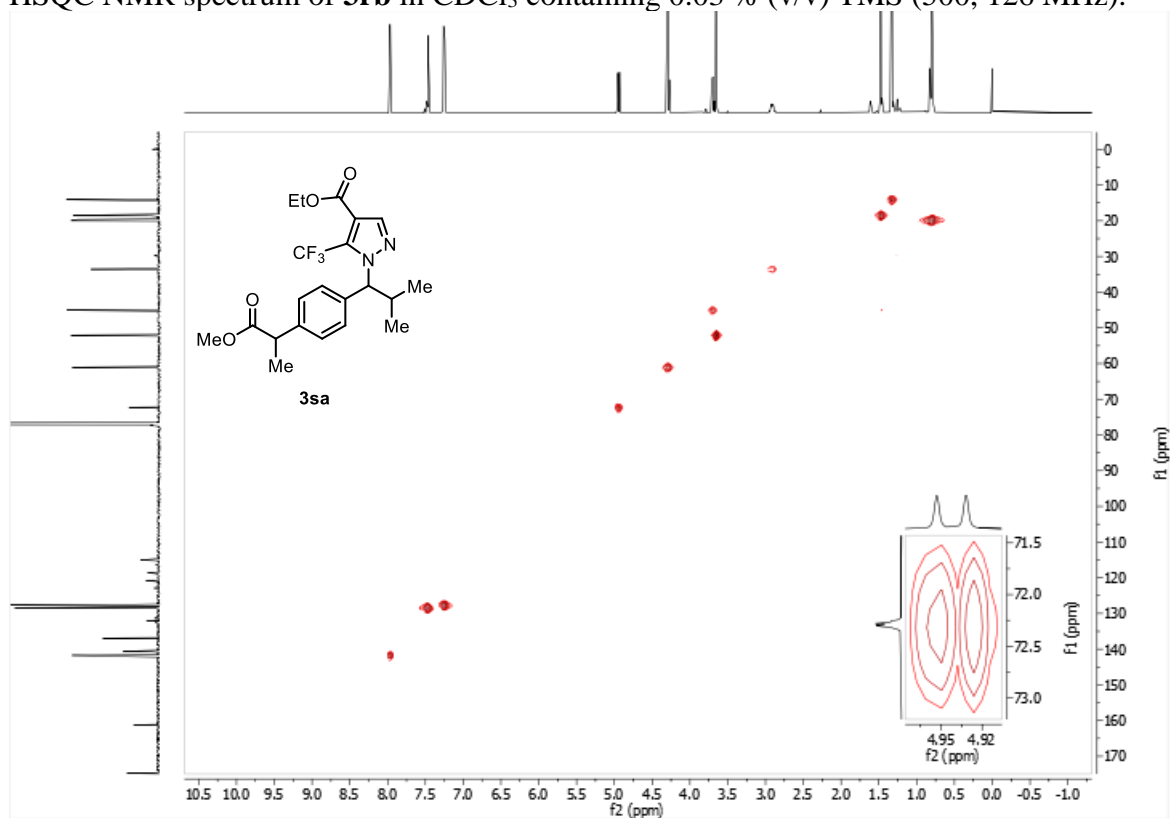
^{13}C NMR spectrum of **3rb** in CDCl_3 containing 0.03 % (v/v) TMS (126 MHz).



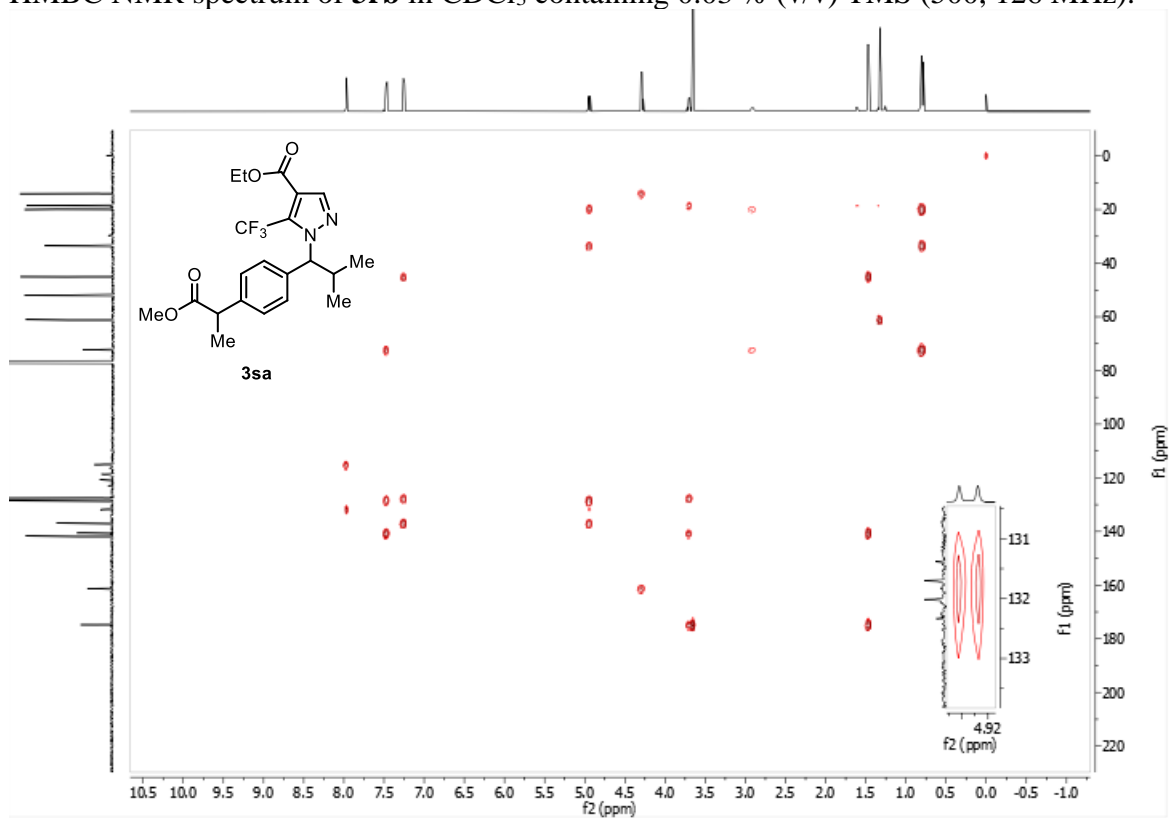
^{19}F NMR spectrum of **3rb** in CDCl_3 containing 0.03 % (v/v) TMS (377 MHz).



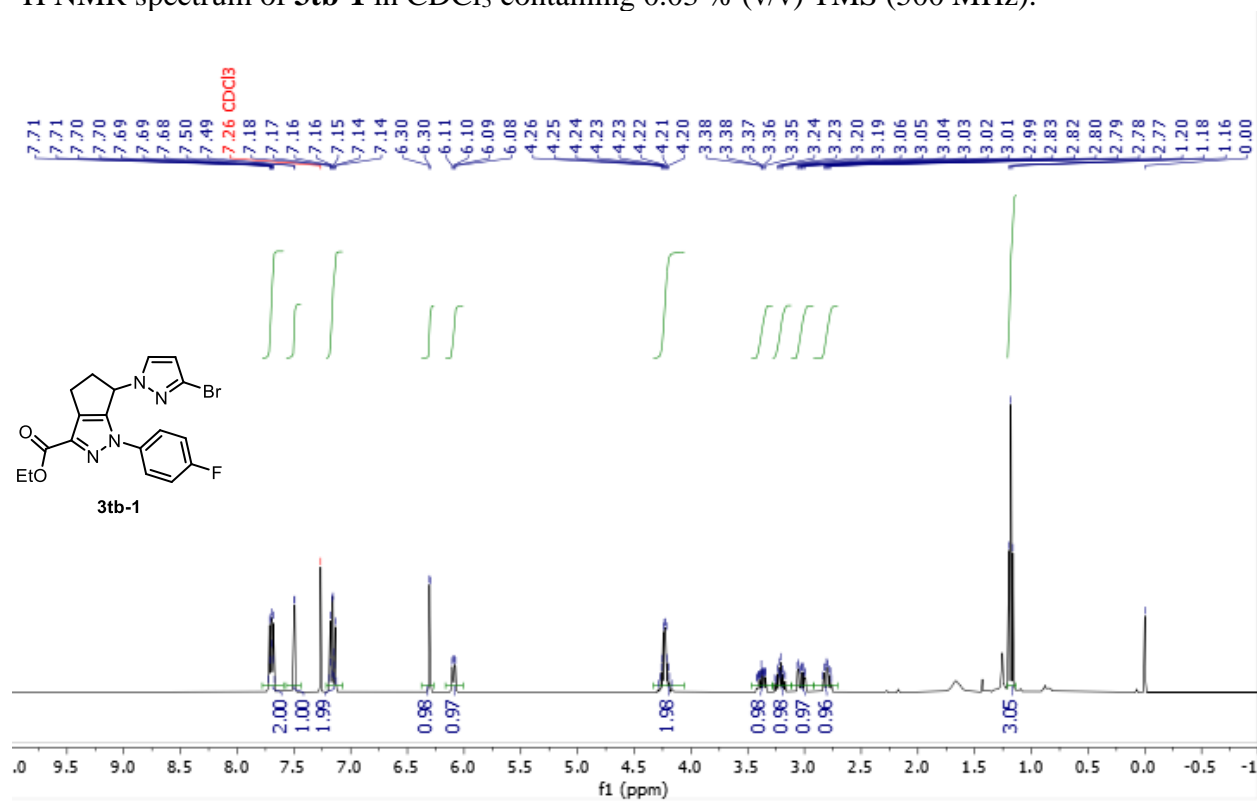
HSQC NMR spectrum of **3rb** in CDCl₃ containing 0.03 % (v/v) TMS (500, 126 MHz).



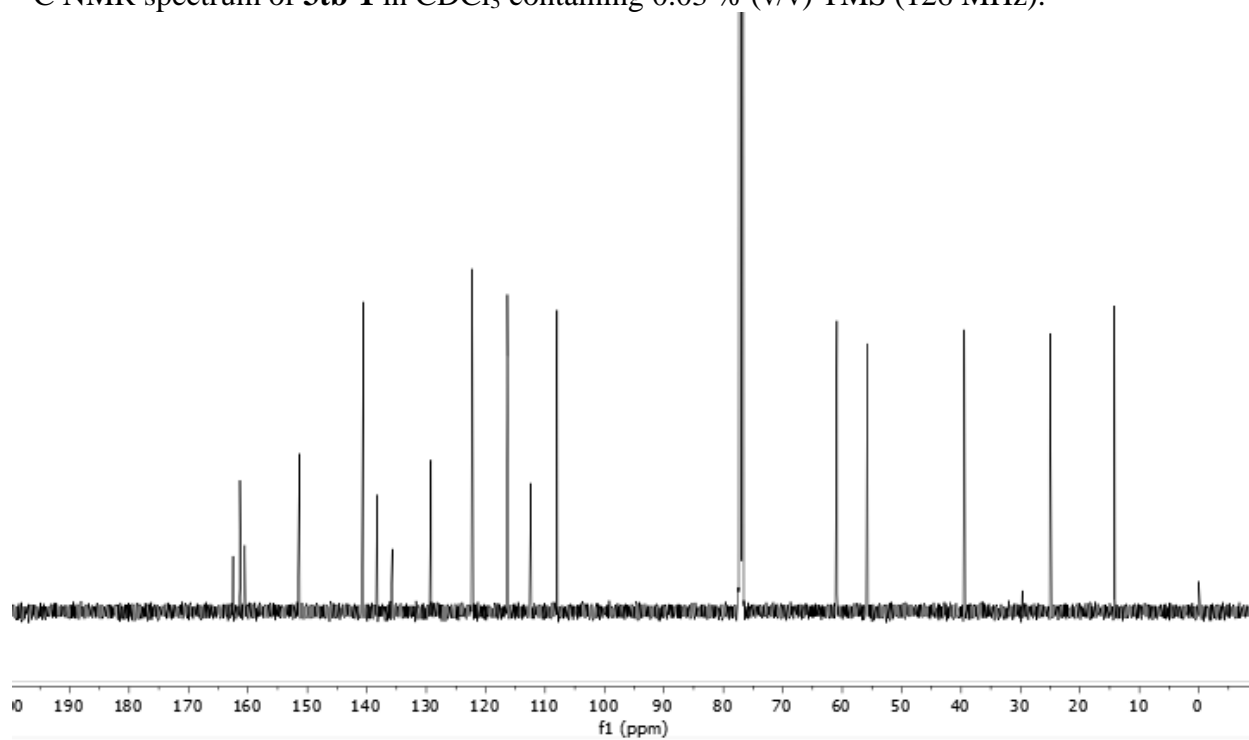
HMBC NMR spectrum of **3rb** in CDCl₃ containing 0.03 % (v/v) TMS (500, 126 MHz).



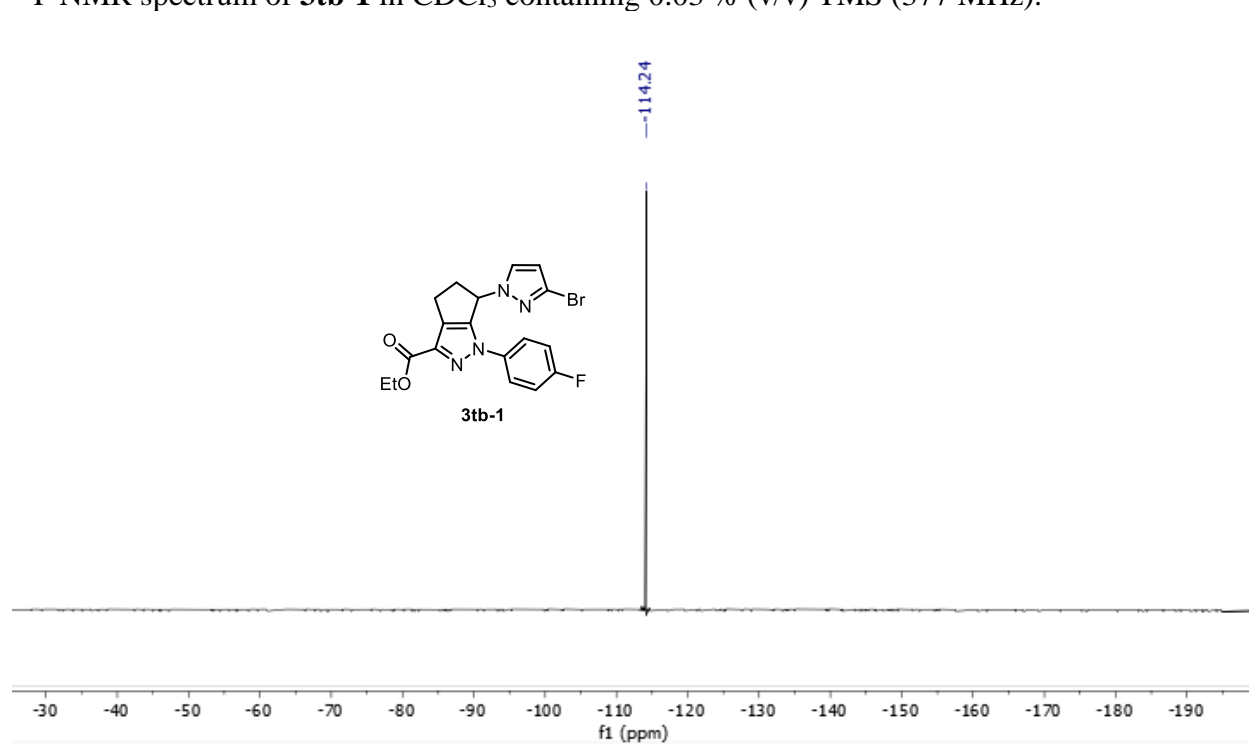
^1H NMR spectrum of **3tb-1** in CDCl_3 containing 0.03 % (v/v) TMS (500 MHz).



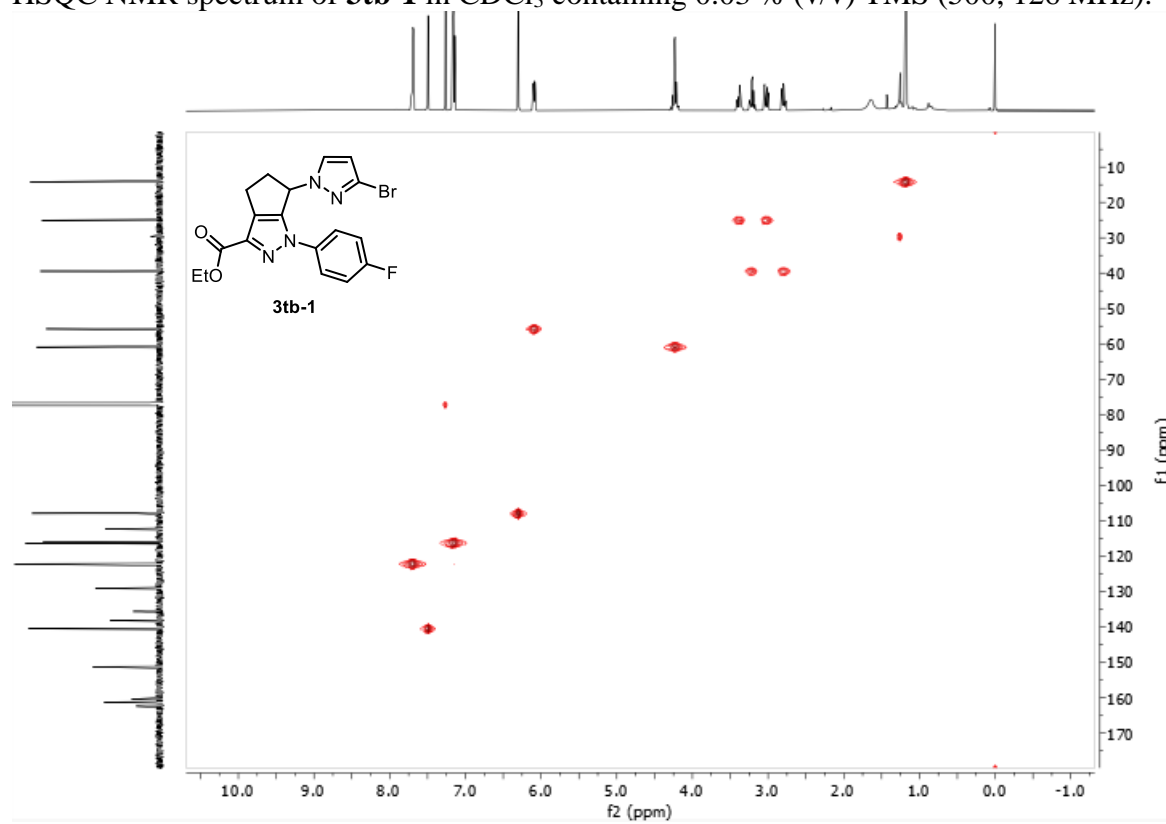
^{13}C NMR spectrum of **3tb-1** in CDCl_3 containing 0.03 % (v/v) TMS (126 MHz).



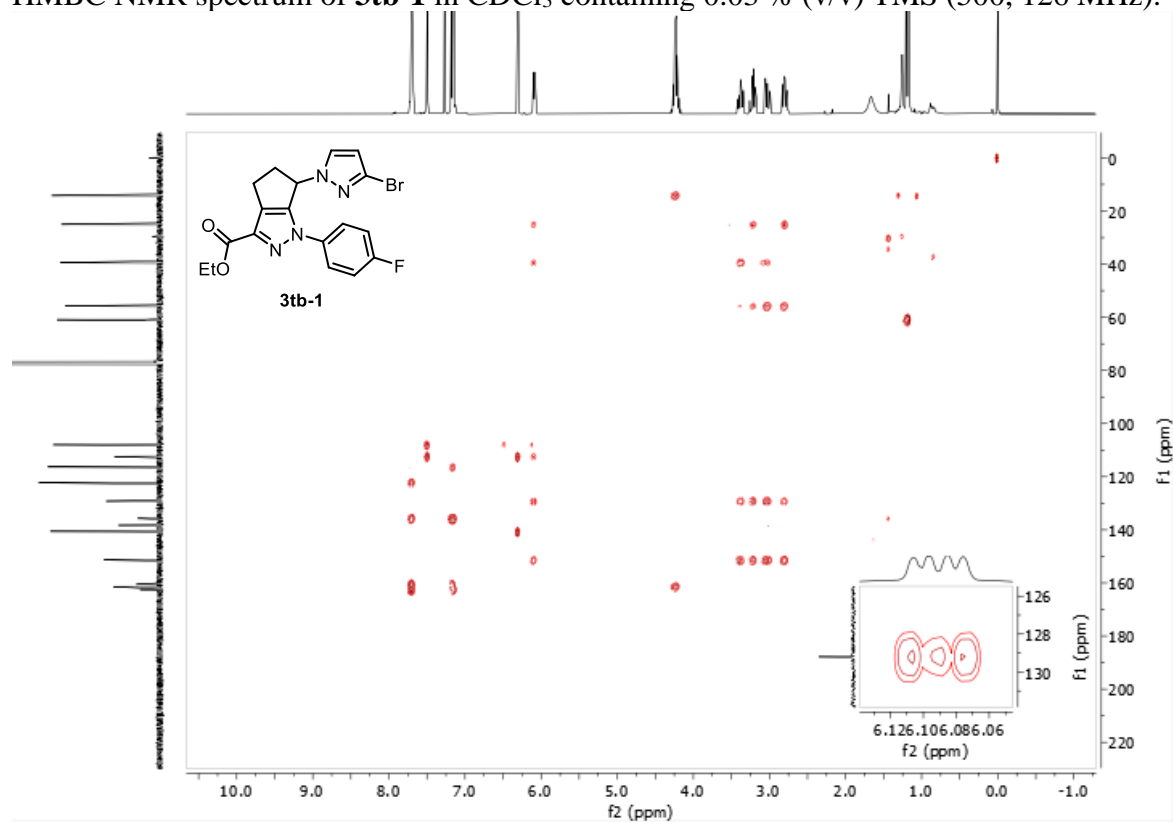
^{19}F NMR spectrum of **3tb-1** in CDCl_3 containing 0.03 % (v/v) TMS (377 MHz).



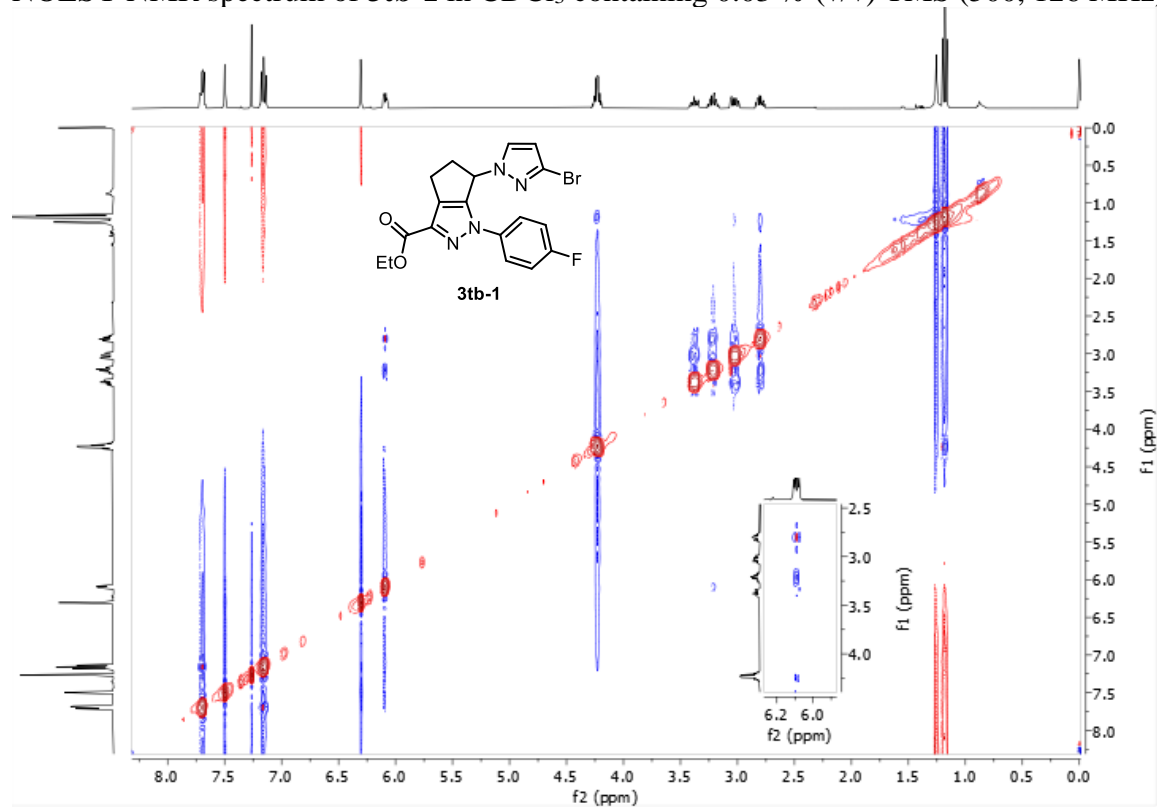
HSQC NMR spectrum of **3tb-1** in CDCl_3 containing 0.03 % (v/v) TMS (500, 126 MHz).



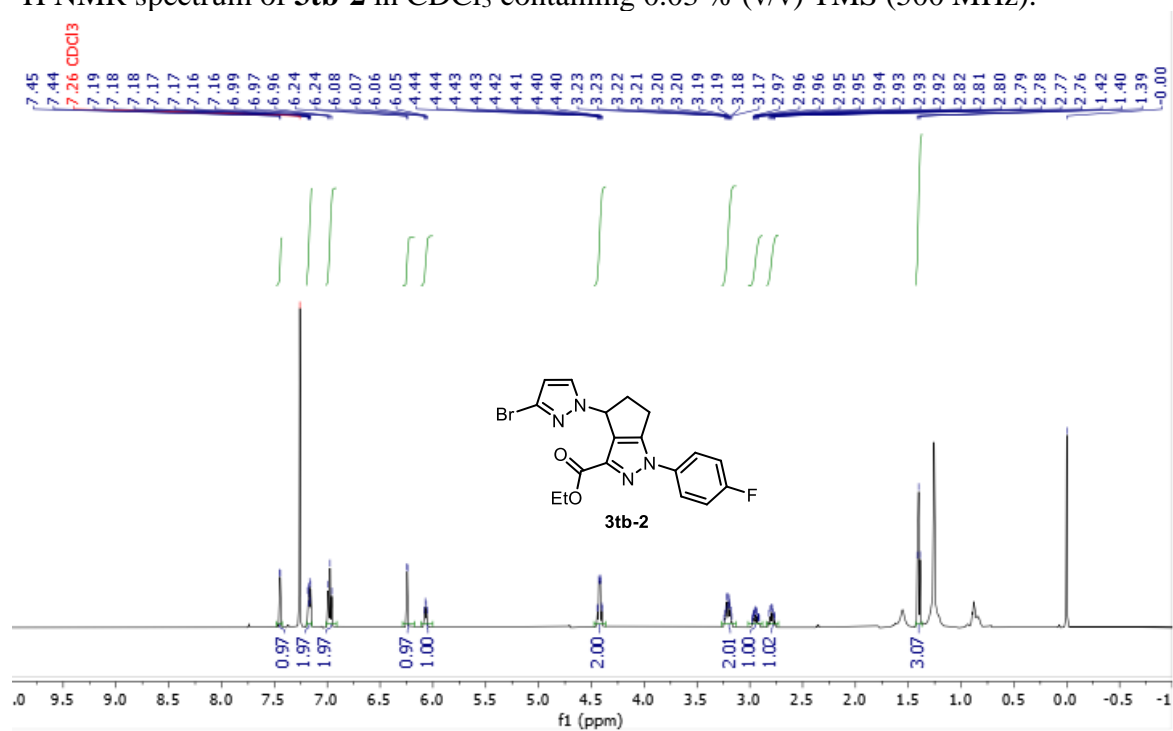
HMBC NMR spectrum of **3tb-1** in CDCl₃ containing 0.03 % (v/v) TMS (500, 126 MHz).



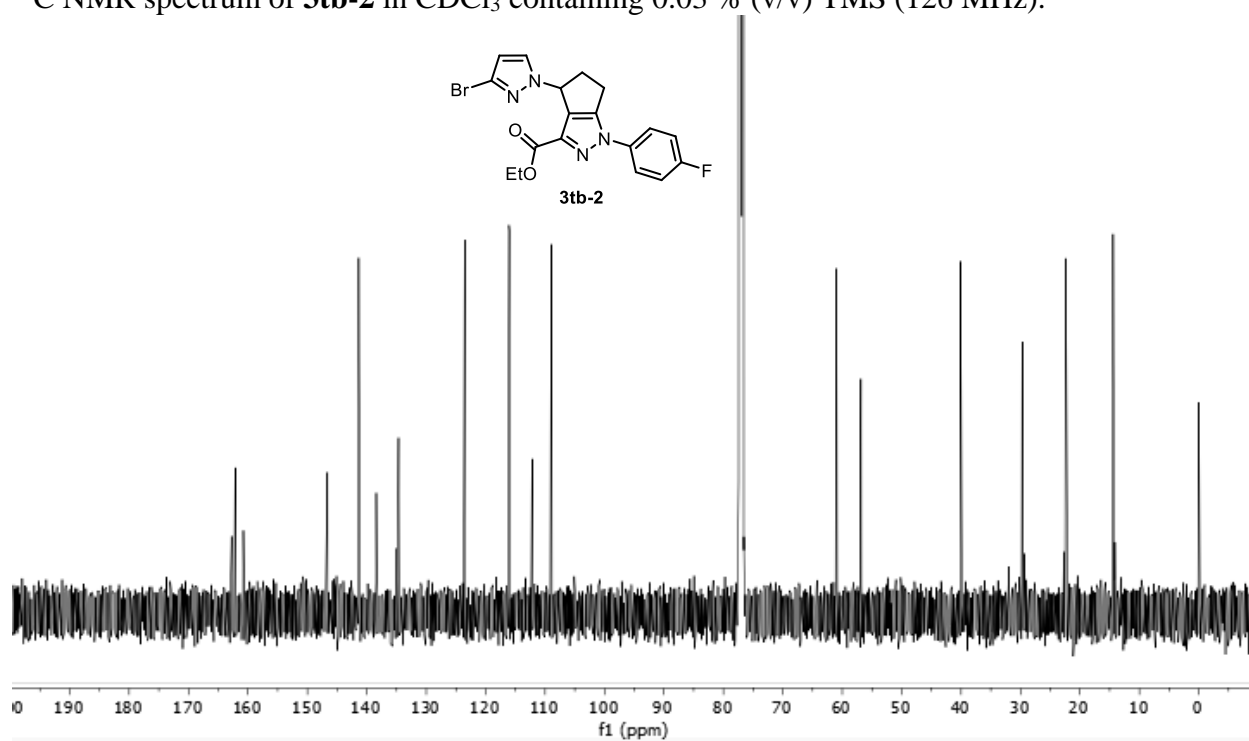
NOESY NMR spectrum of **3tb-1** in CDCl₃ containing 0.03 % (v/v) TMS (500, 126 MHz).



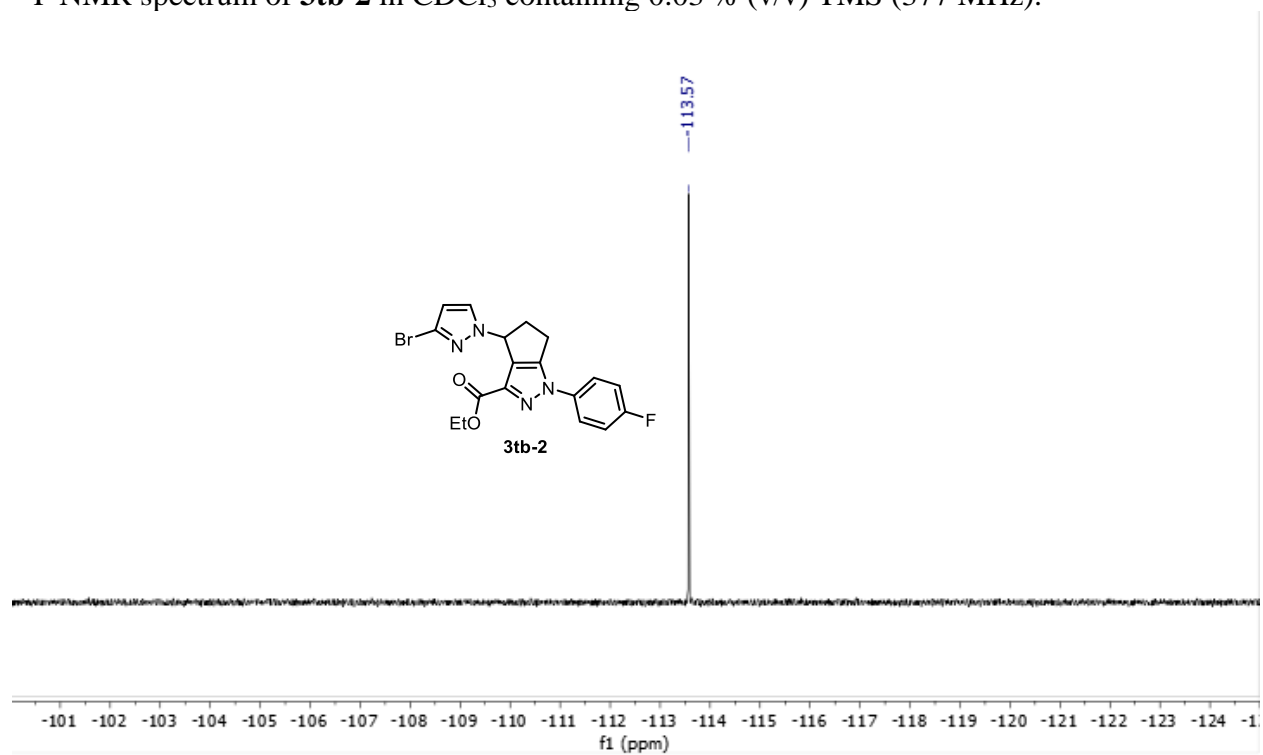
^1H NMR spectrum of **3tb-2** in CDCl_3 containing 0.03 % (v/v) TMS (500 MHz).



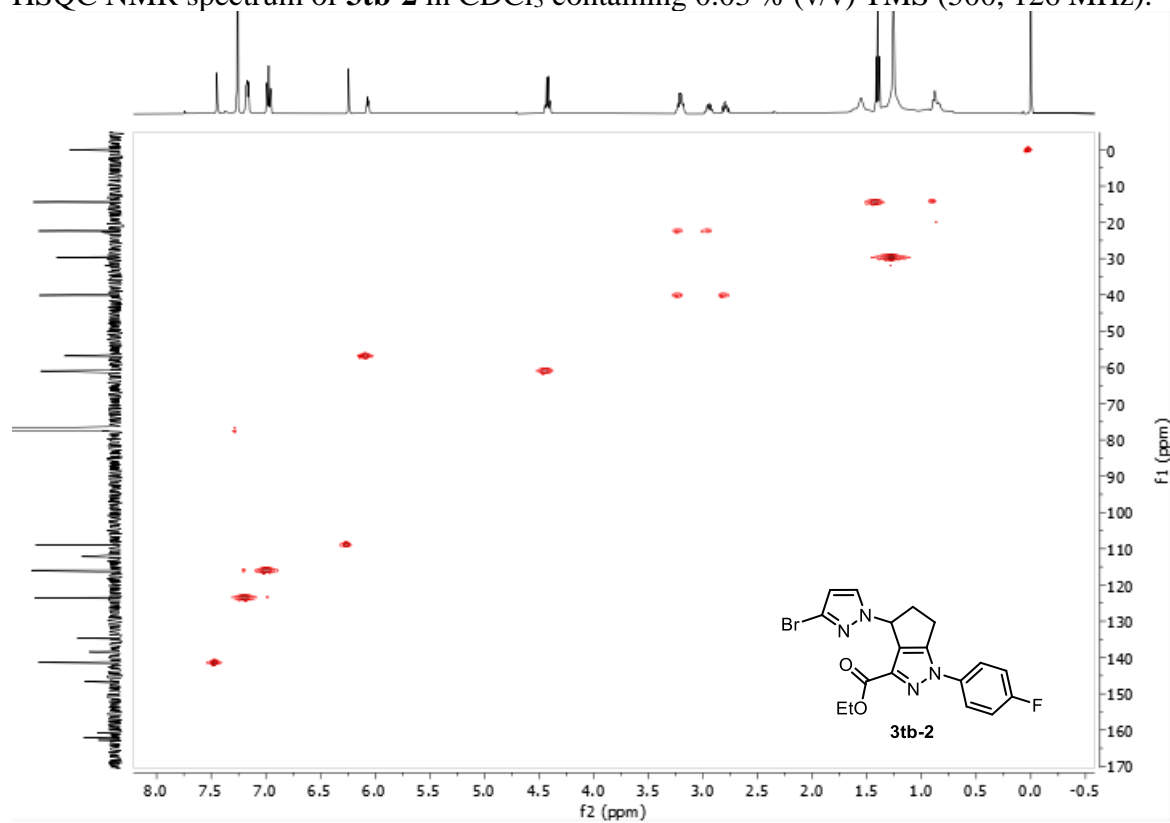
^{13}C NMR spectrum of **3tb-2** in CDCl_3 containing 0.03 % (v/v) TMS (126 MHz).



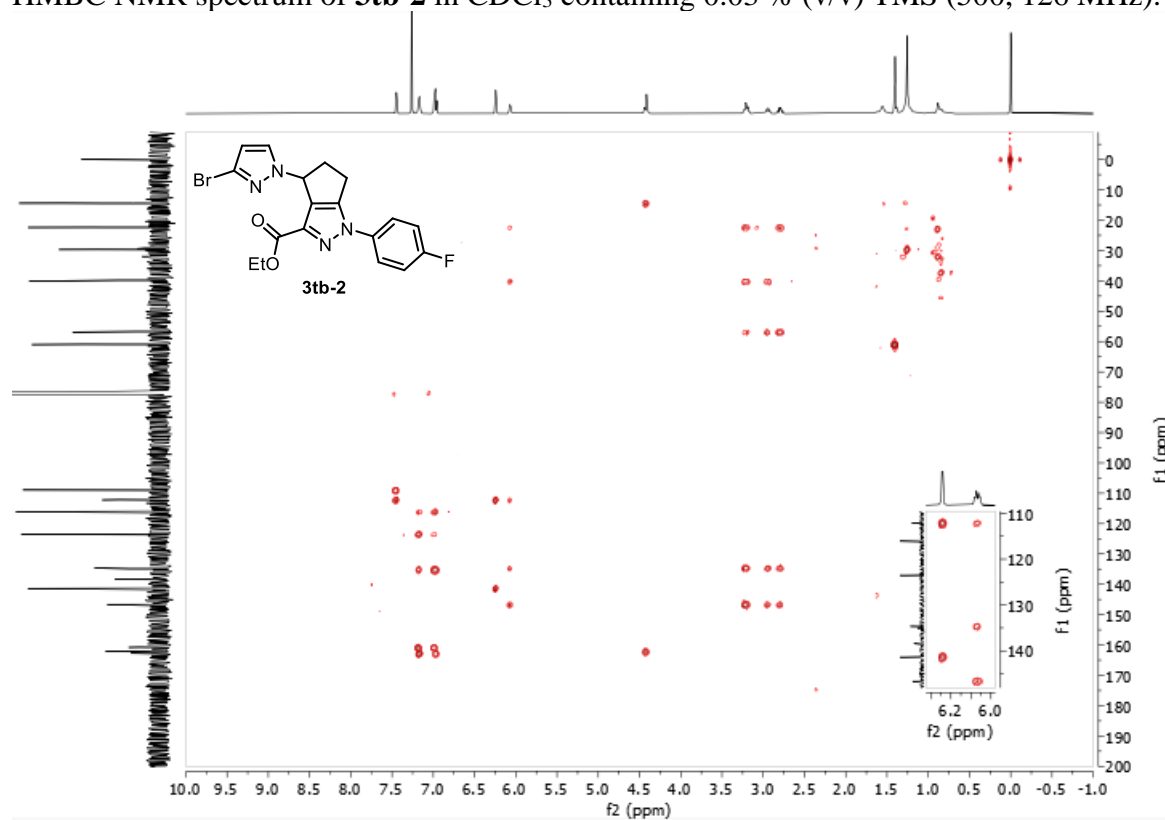
^{19}F NMR spectrum of **3tb-2** in CDCl_3 containing 0.03 % (v/v) TMS (377 MHz).



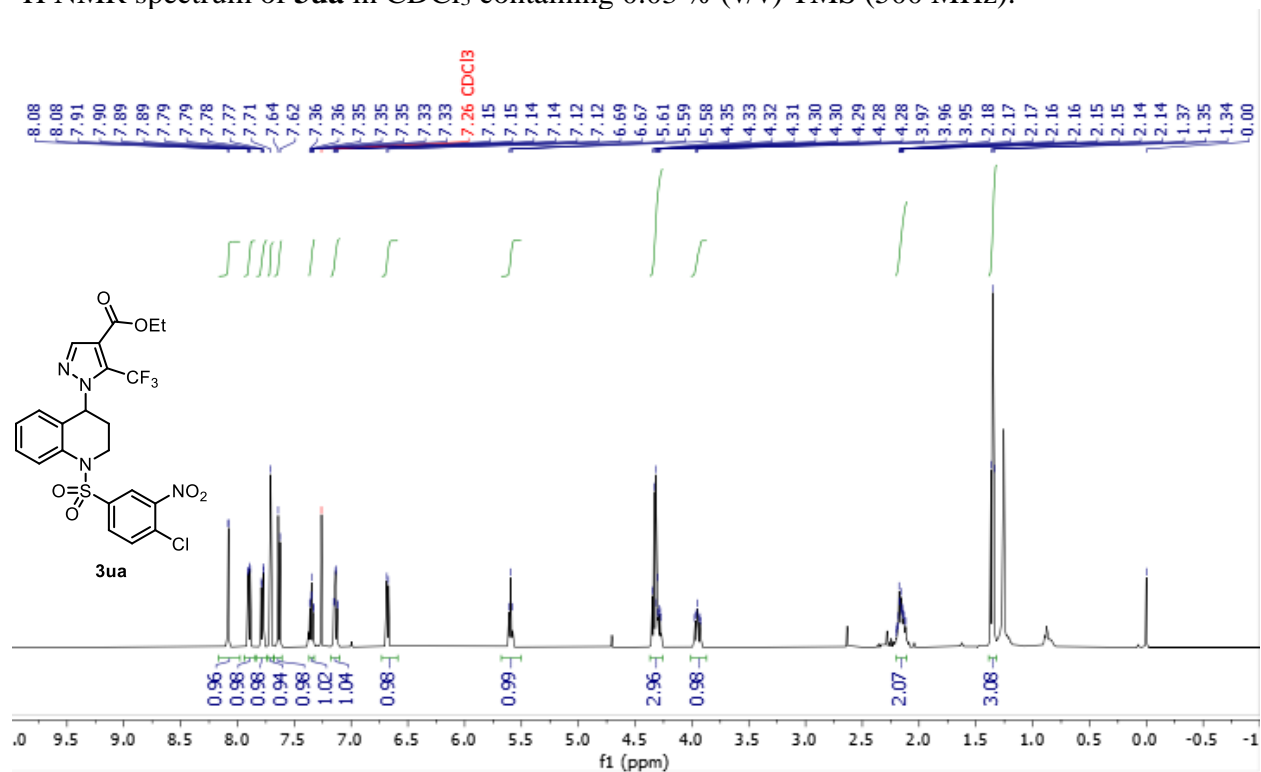
HSQC NMR spectrum of **3tb-2** in CDCl_3 containing 0.03 % (v/v) TMS (500, 126 MHz).



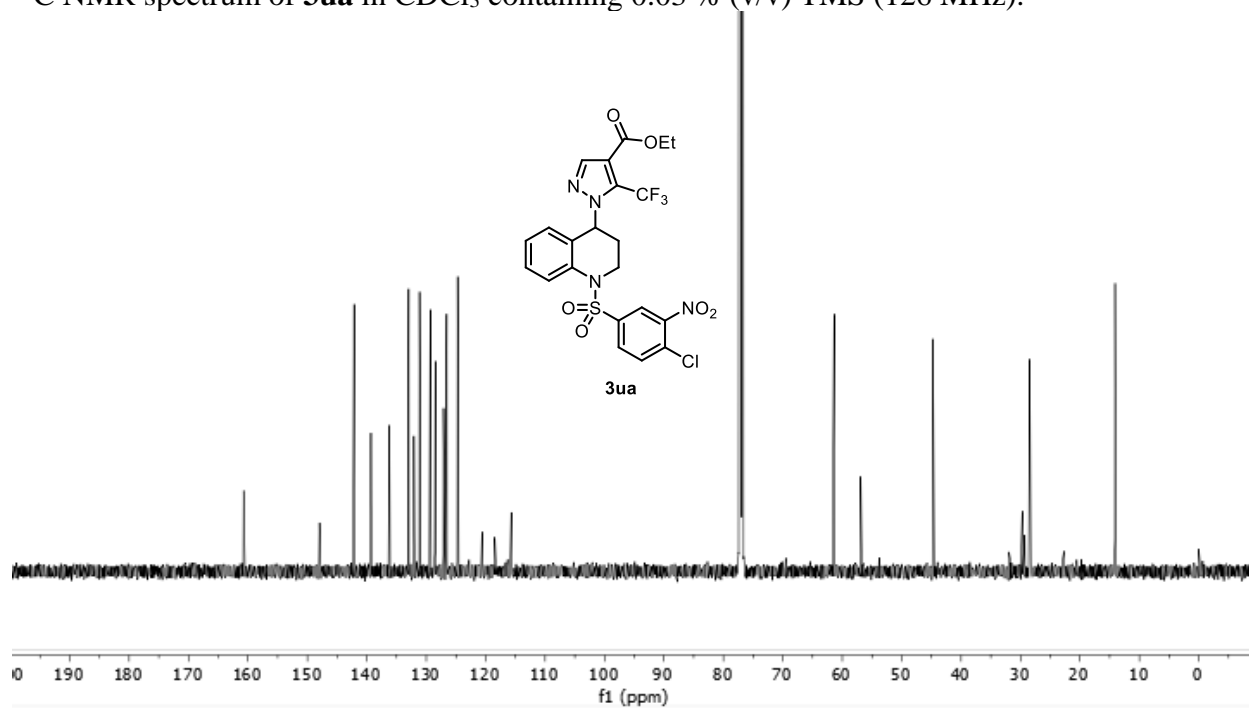
HMBC NMR spectrum of **3tb-2** in CDCl₃ containing 0.03 % (v/v) TMS (500, 126 MHz).



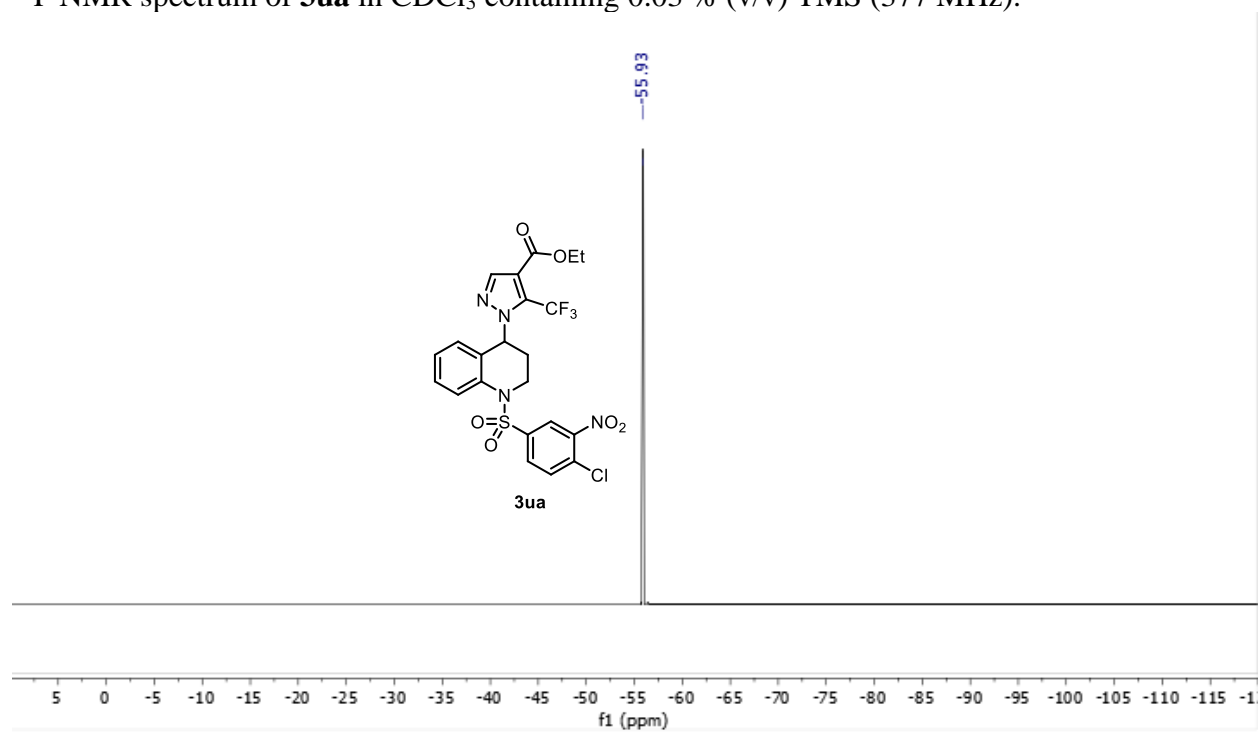
¹H NMR spectrum of **3ua** in CDCl₃ containing 0.03 % (v/v) TMS (500 MHz).



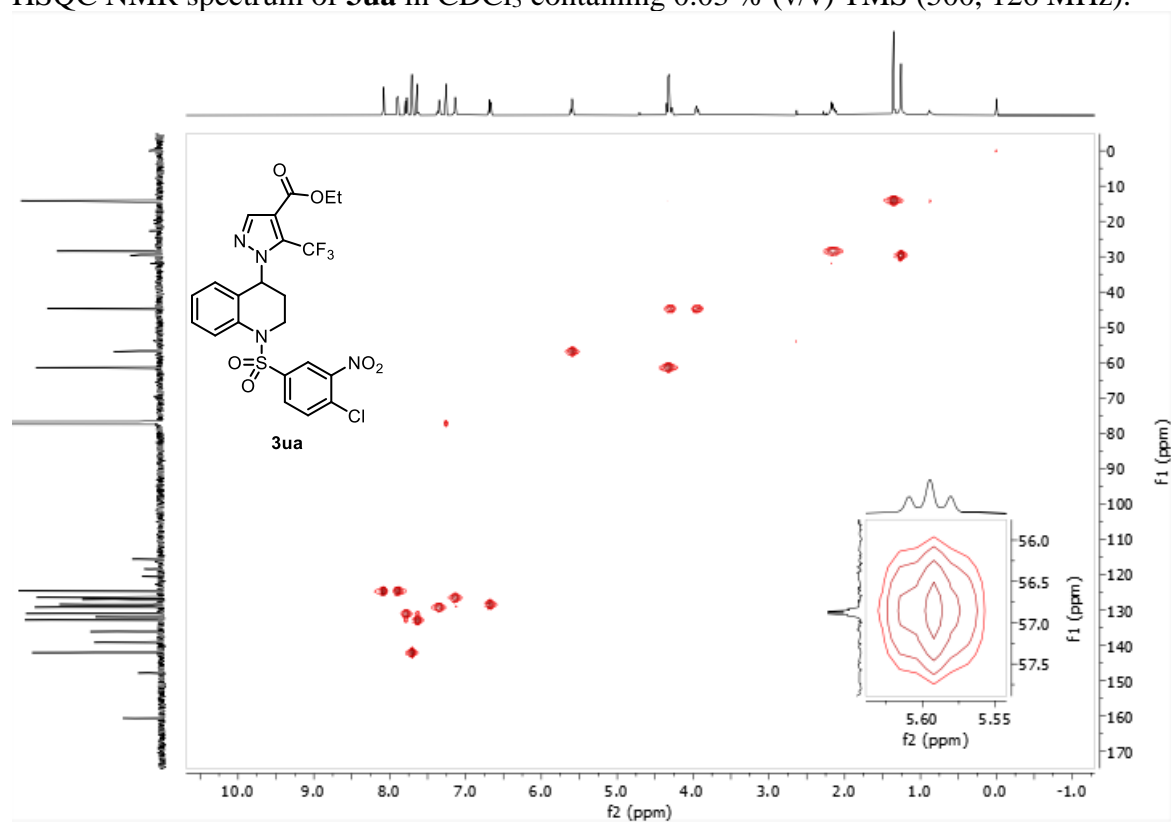
^{13}C NMR spectrum of **3ua** in CDCl_3 containing 0.03 % (v/v) TMS (126 MHz).



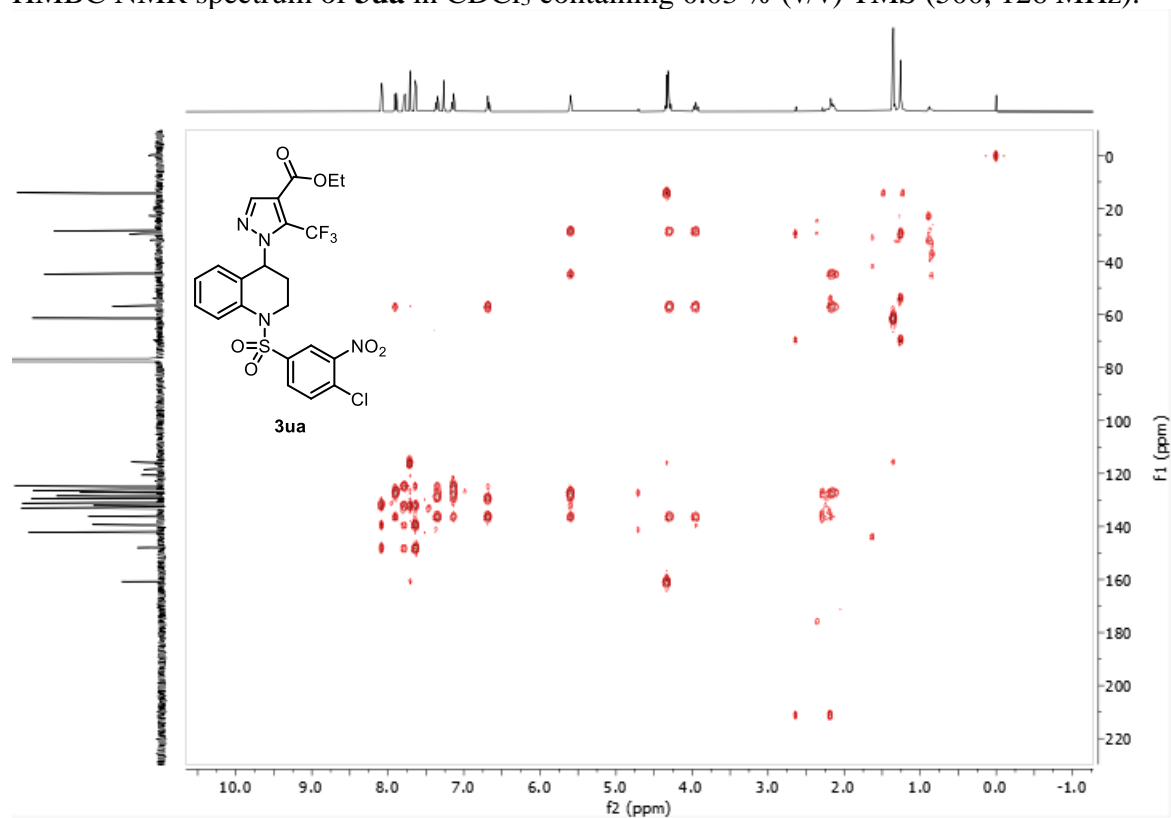
^{19}F NMR spectrum of **3ua** in CDCl_3 containing 0.03 % (v/v) TMS (377 MHz).



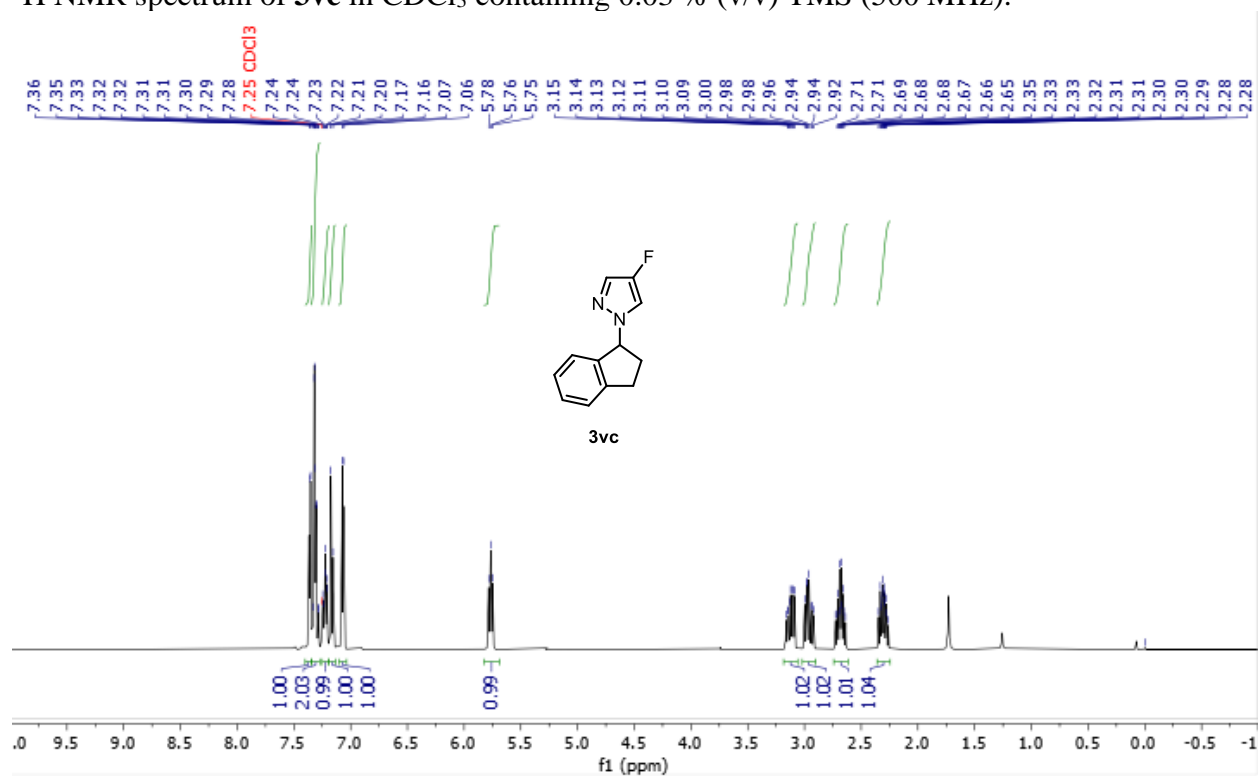
HSQC NMR spectrum of **3ua** in CDCl₃ containing 0.03 % (v/v) TMS (500, 126 MHz).



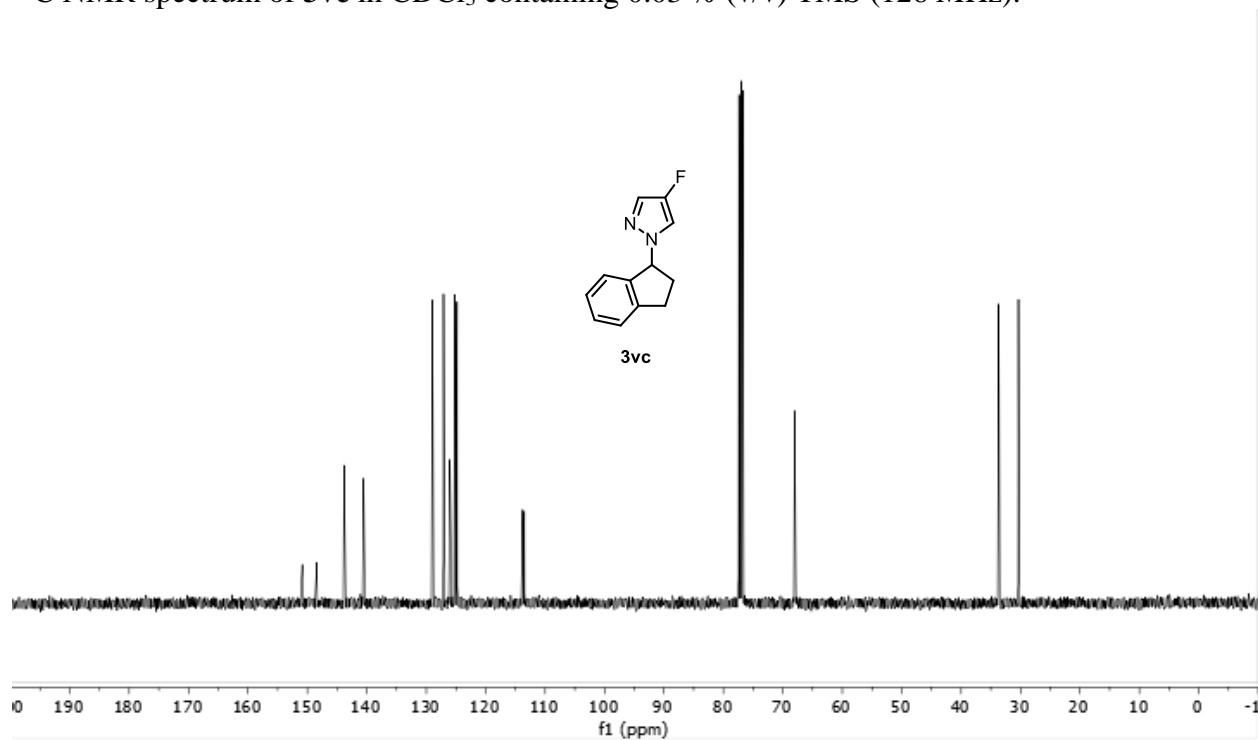
HMBC NMR spectrum of **3ua** in CDCl₃ containing 0.03 % (v/v) TMS (500, 126 MHz).



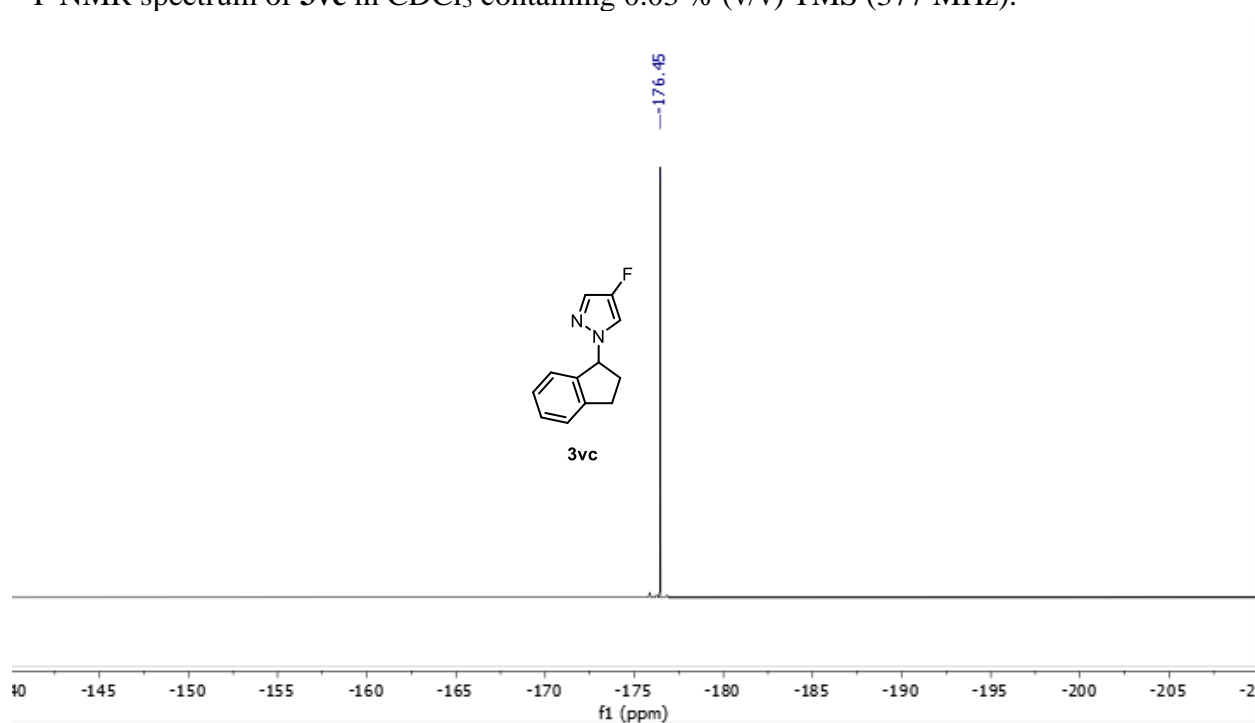
^1H NMR spectrum of **3vc** in CDCl_3 containing 0.03 % (v/v) TMS (500 MHz).



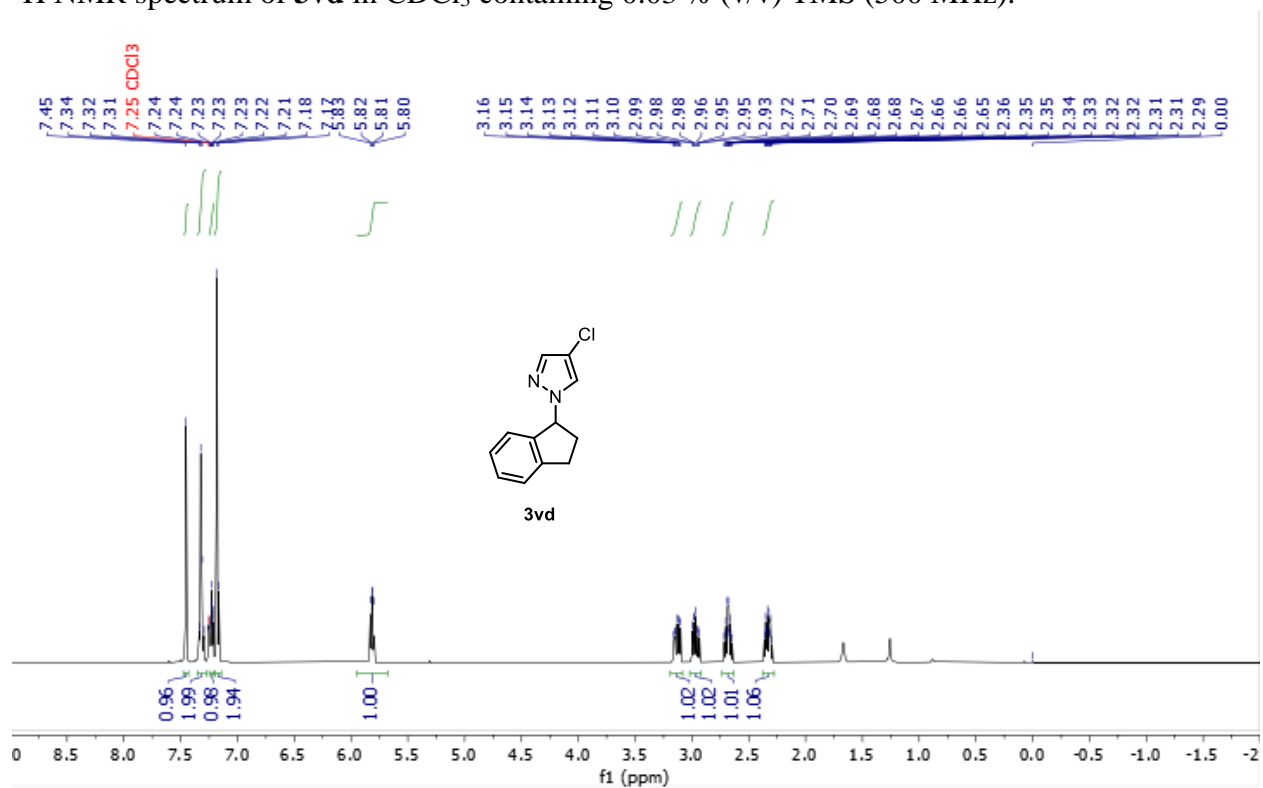
^{13}C NMR spectrum of **3vc** in CDCl_3 containing 0.03 % (v/v) TMS (126 MHz).



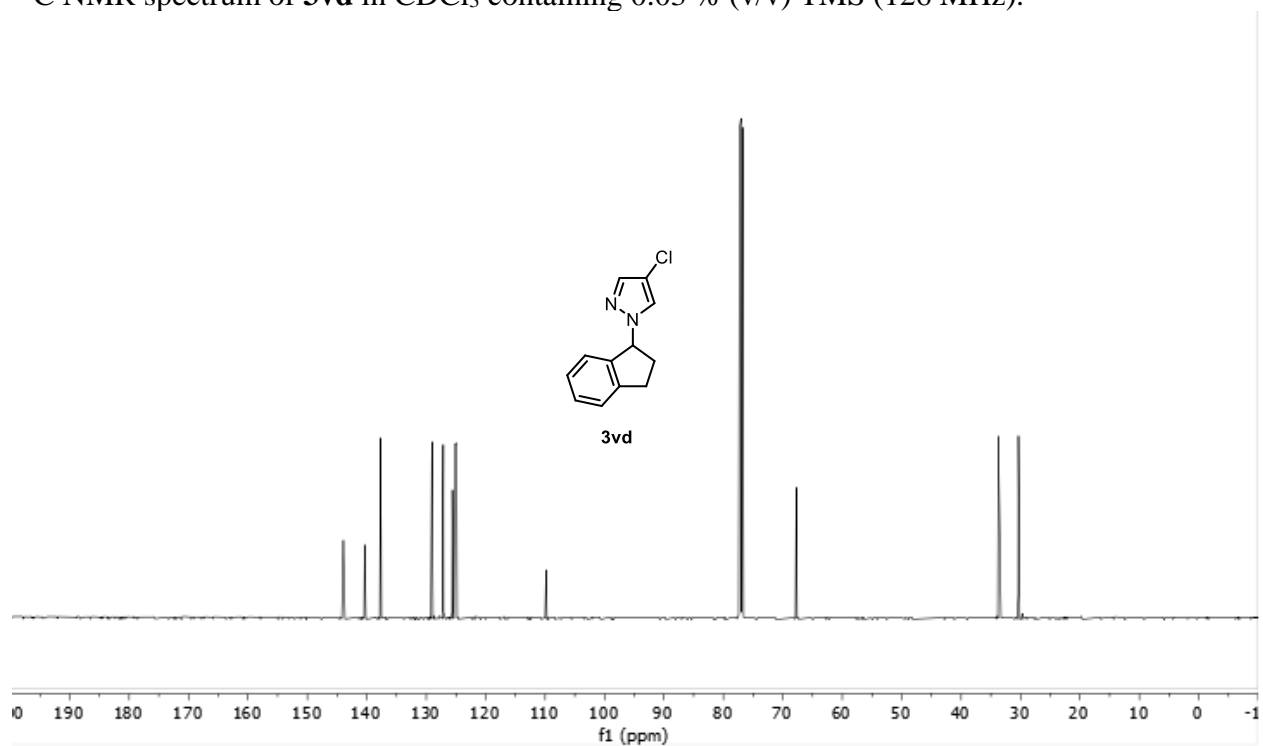
^{19}F NMR spectrum of **3vc** in CDCl_3 containing 0.03 % (v/v) TMS (377 MHz).



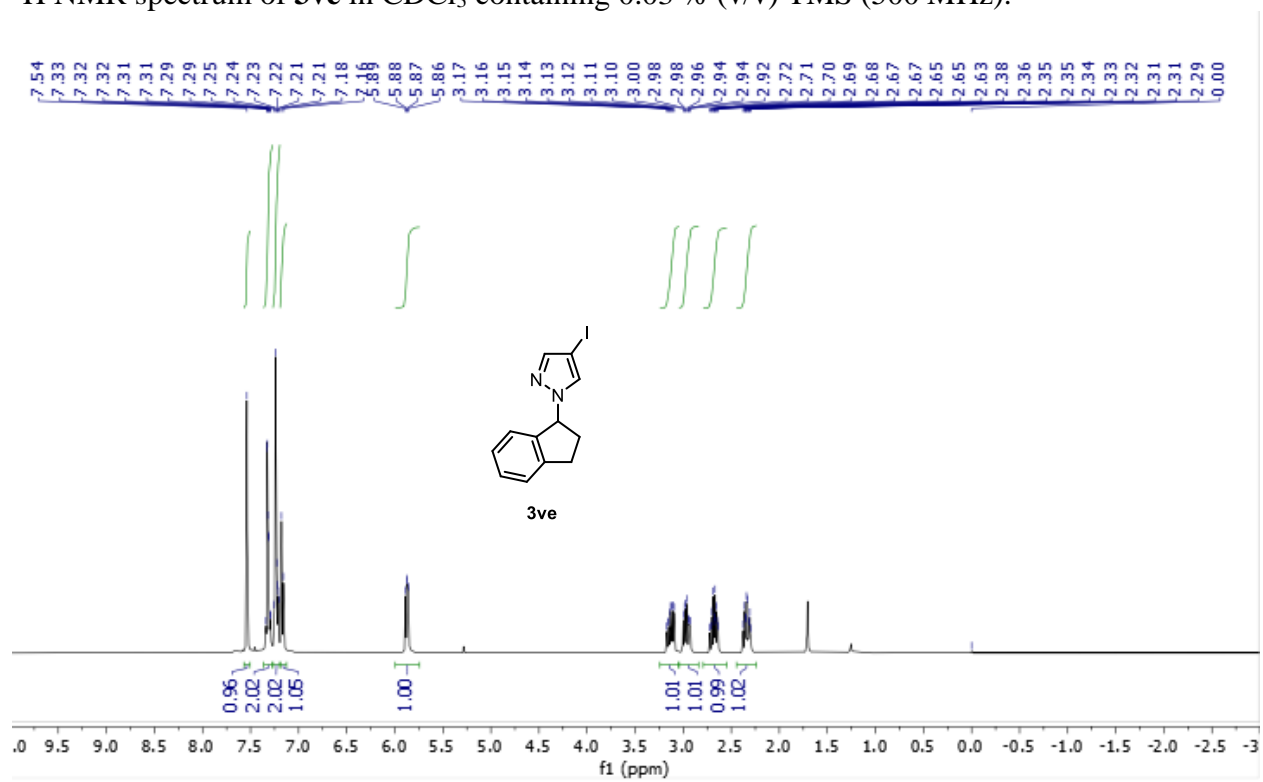
^1H NMR spectrum of **3vd** in CDCl_3 containing 0.03 % (v/v) TMS (500 MHz).



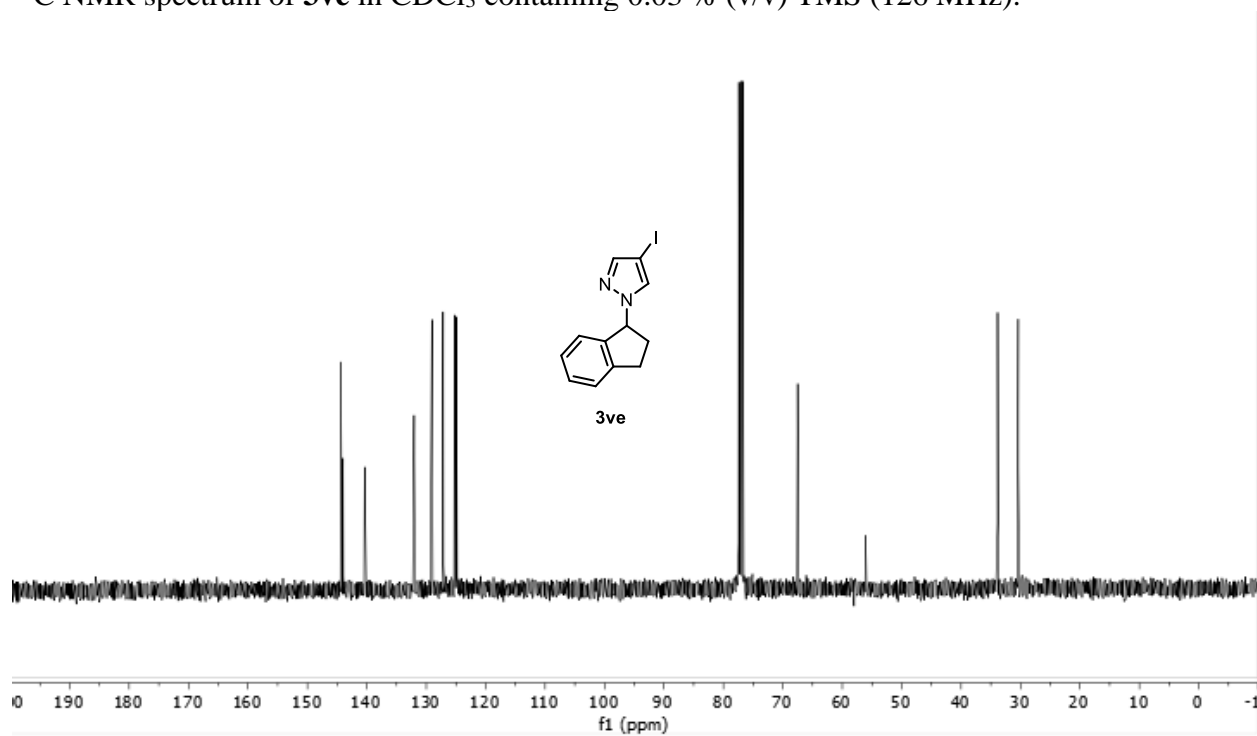
^{13}C NMR spectrum of **3vd** in CDCl_3 containing 0.03 % (v/v) TMS (126 MHz).



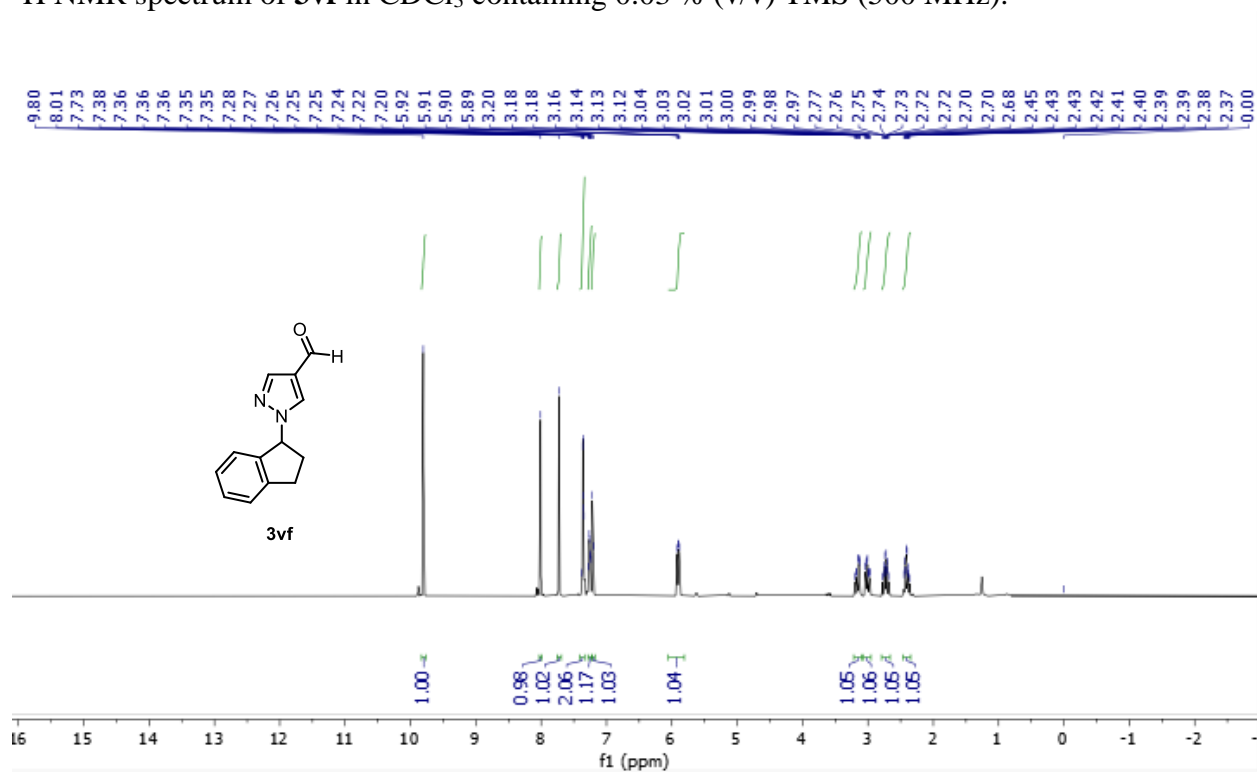
^1H NMR spectrum of **3ve** in CDCl_3 containing 0.03 % (v/v) TMS (500 MHz).



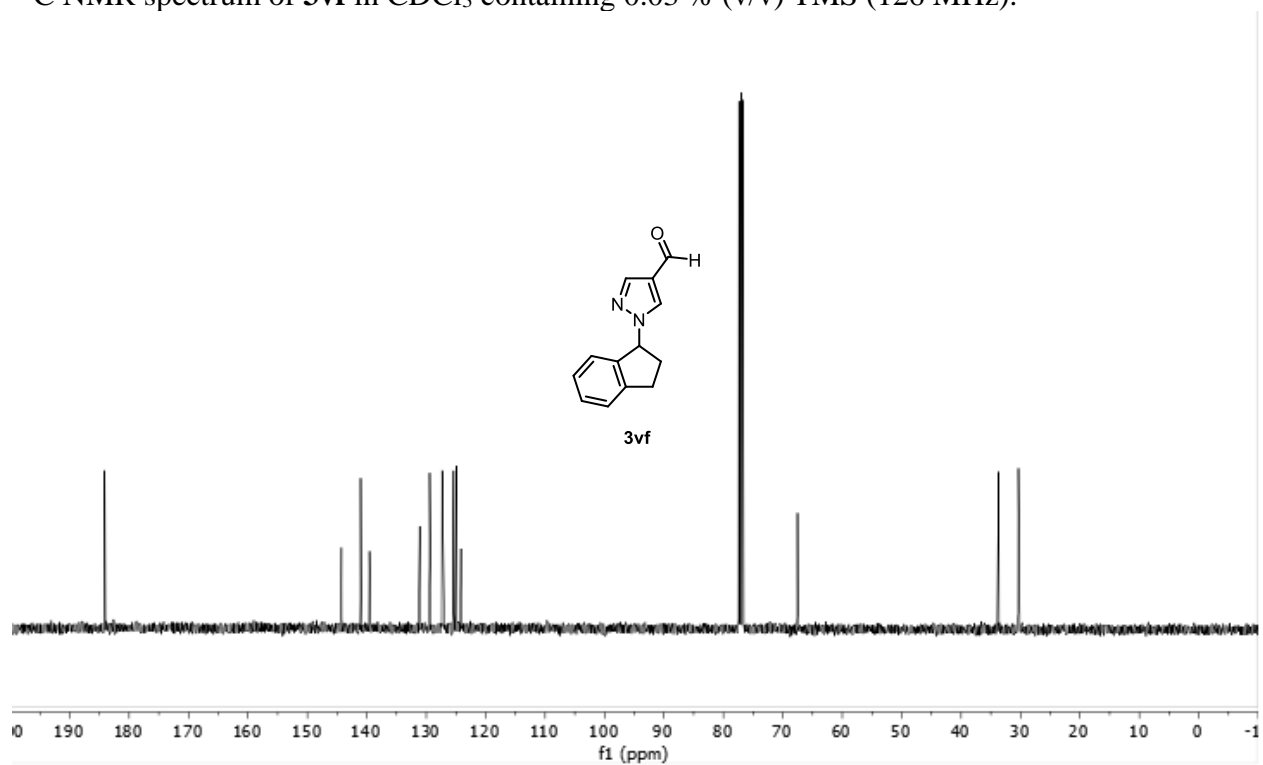
^{13}C NMR spectrum of **3ve** in CDCl_3 containing 0.03 % (v/v) TMS (126 MHz).



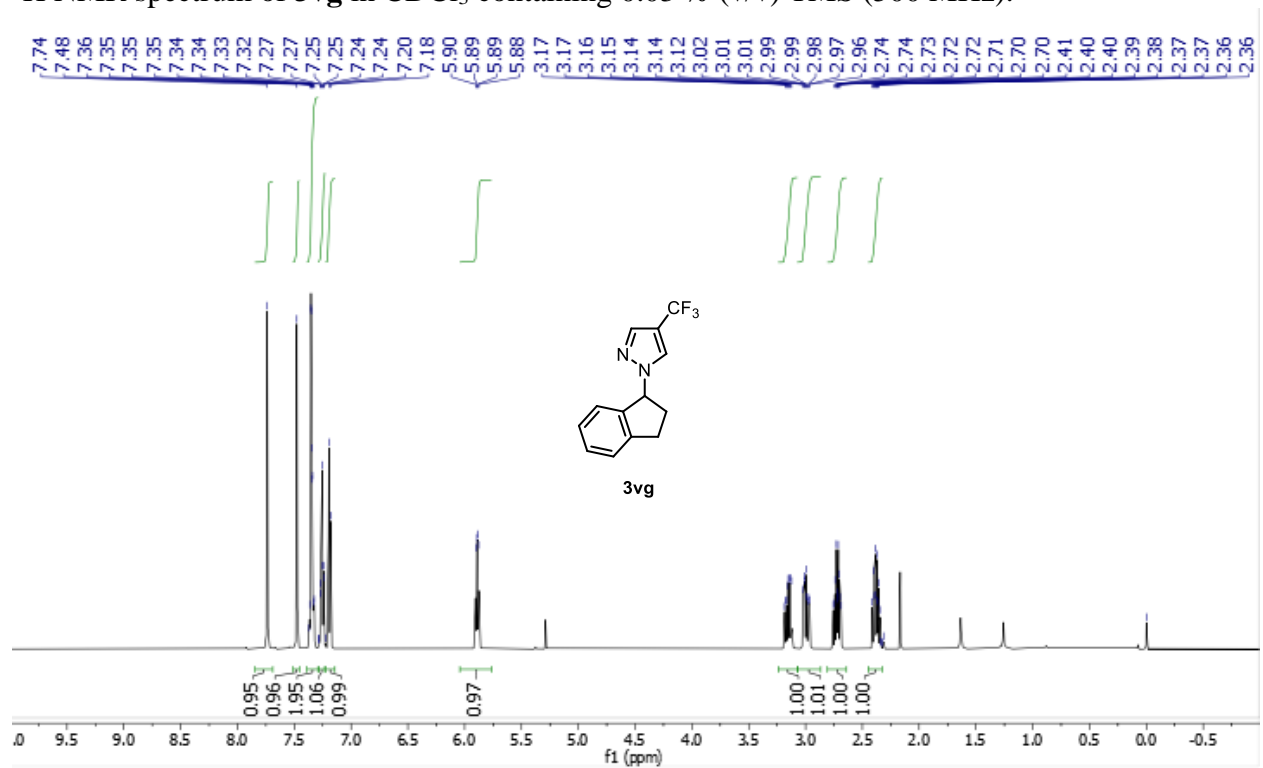
^1H NMR spectrum of **3vf** in CDCl_3 containing 0.03 % (v/v) TMS (500 MHz).



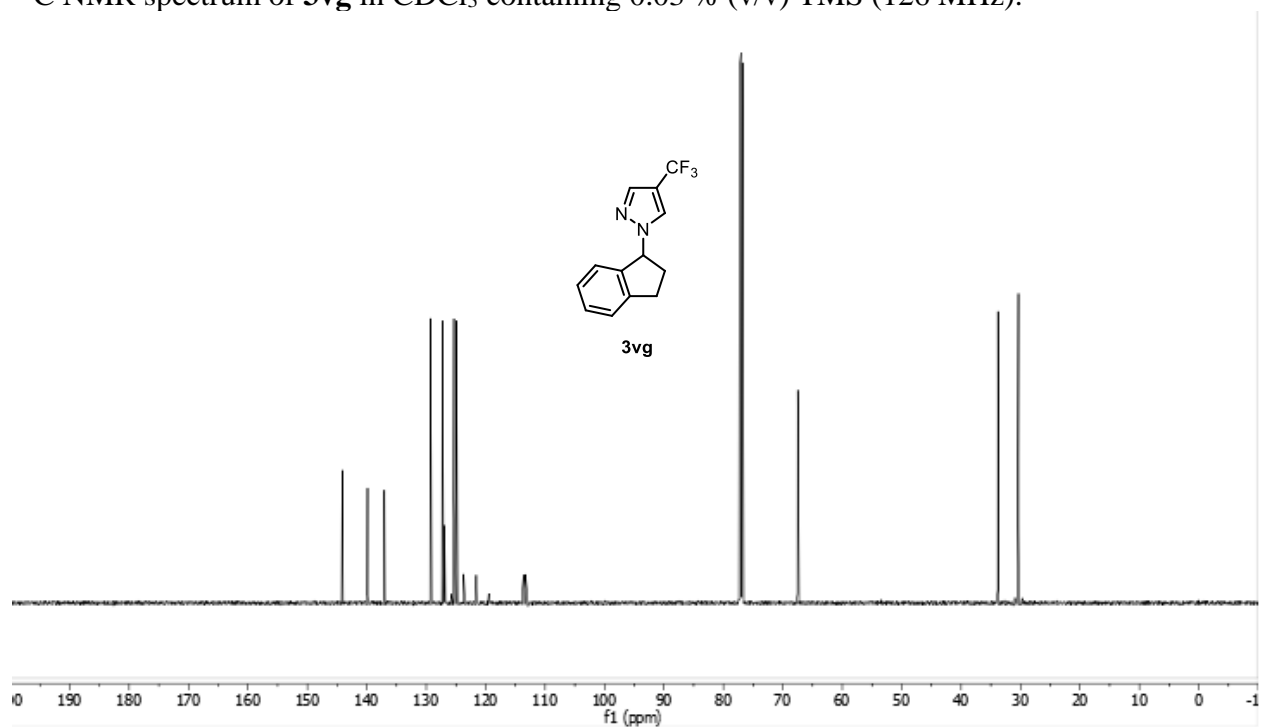
^{13}C NMR spectrum of **3vf** in CDCl_3 containing 0.03 % (v/v) TMS (126 MHz).



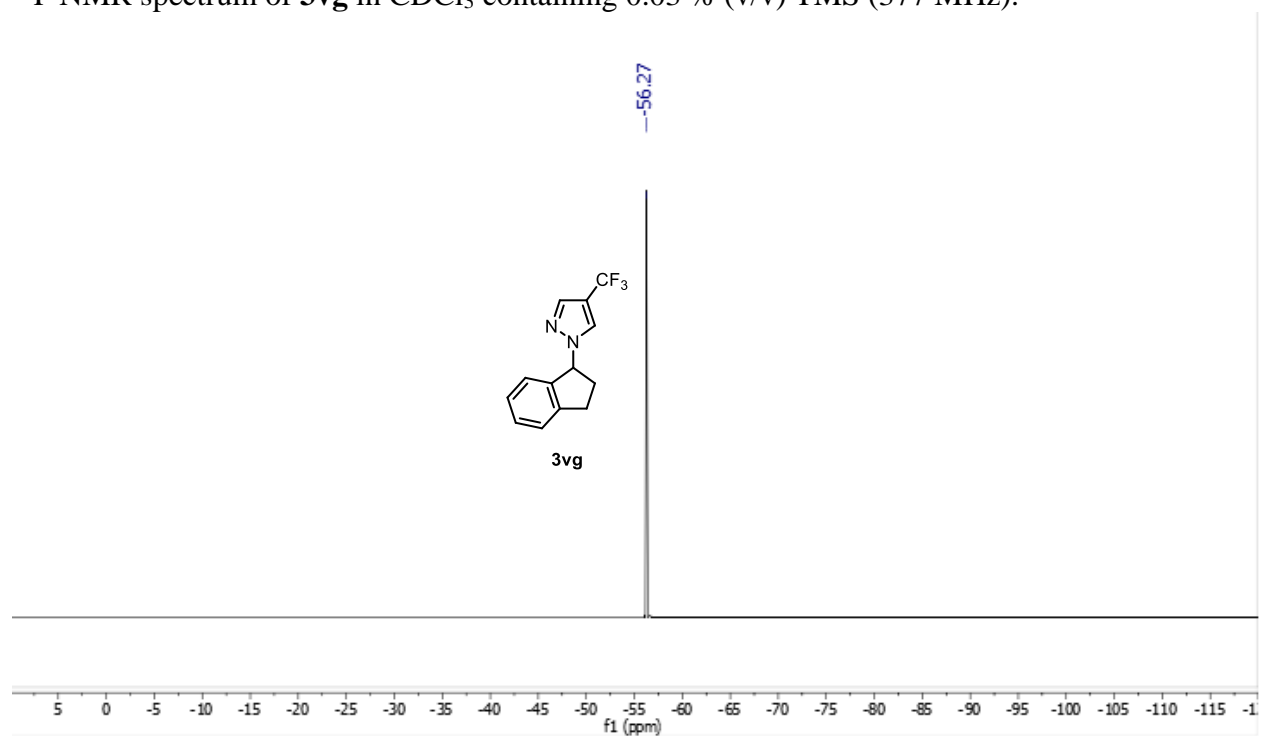
^1H NMR spectrum of **3vg** in CDCl_3 containing 0.03 % (v/v) TMS (500 MHz).



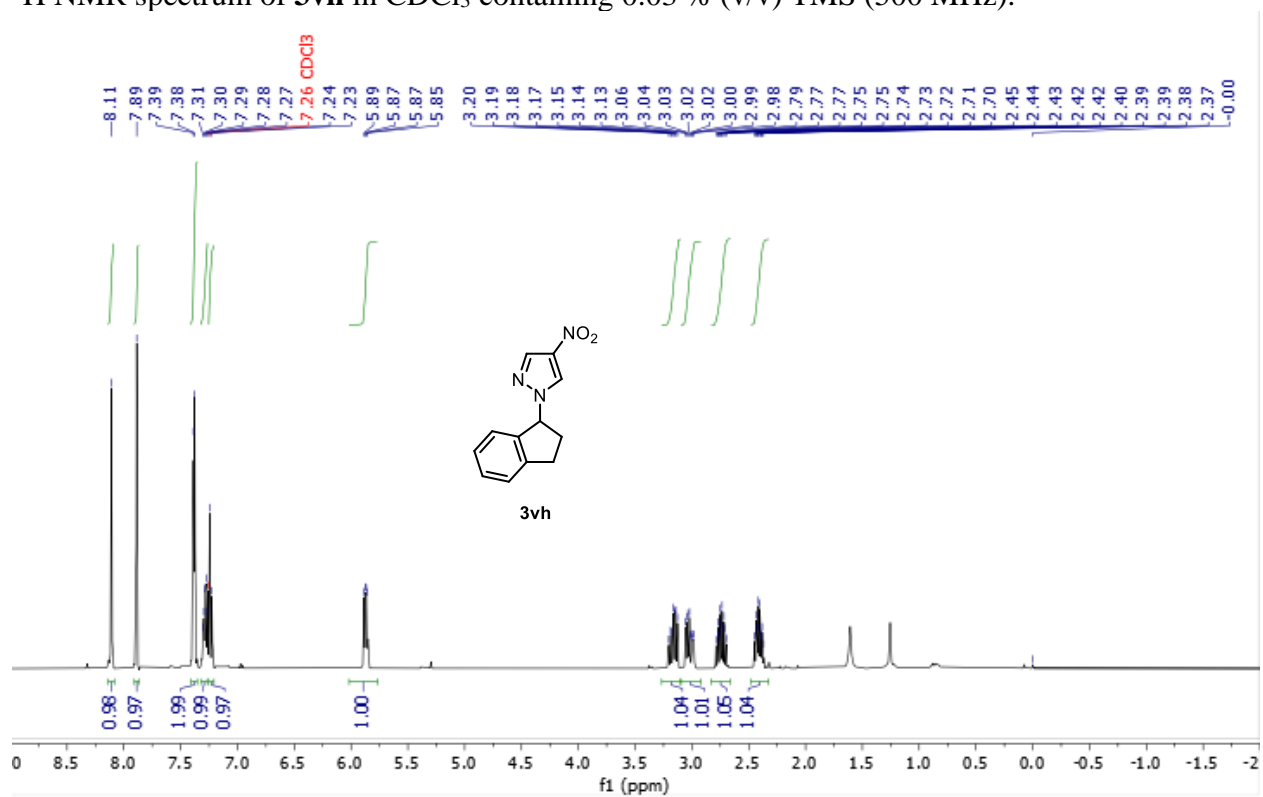
^{13}C NMR spectrum of **3vg** in CDCl_3 containing 0.03 % (v/v) TMS (126 MHz).



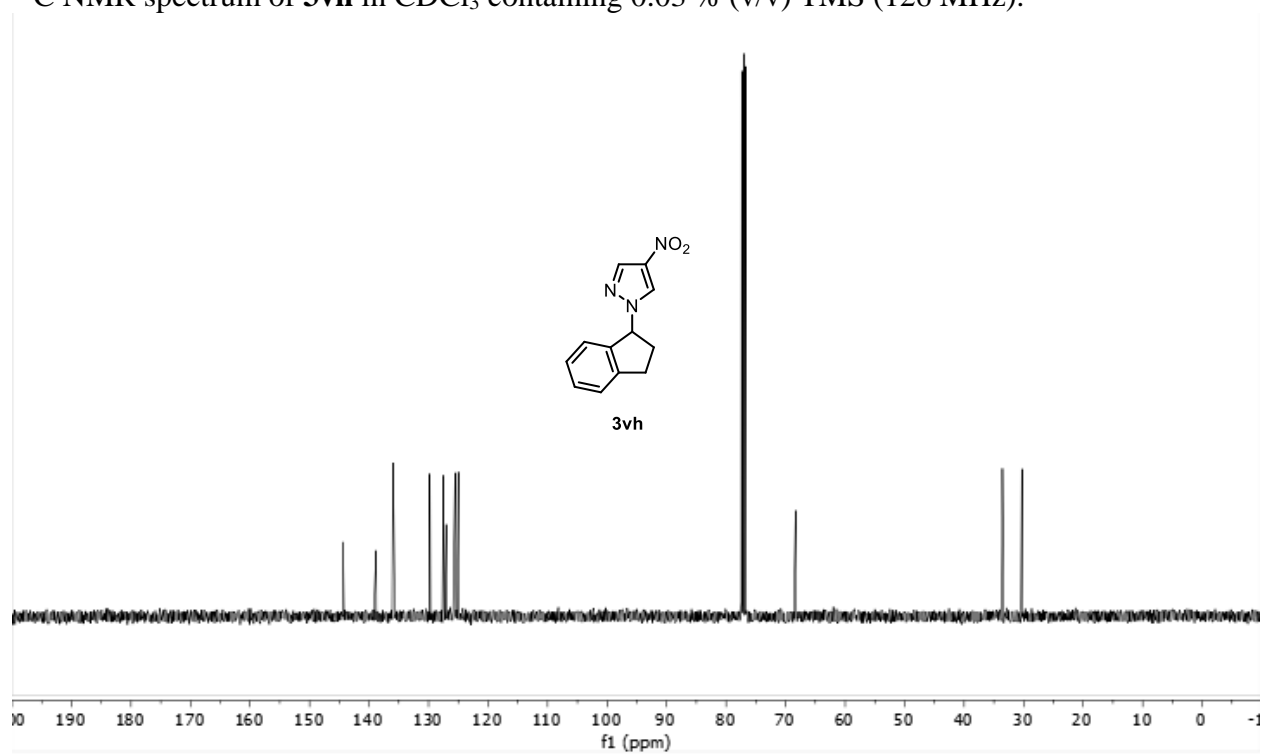
^{19}F NMR spectrum of **3vg** in CDCl_3 containing 0.03 % (v/v) TMS (377 MHz).



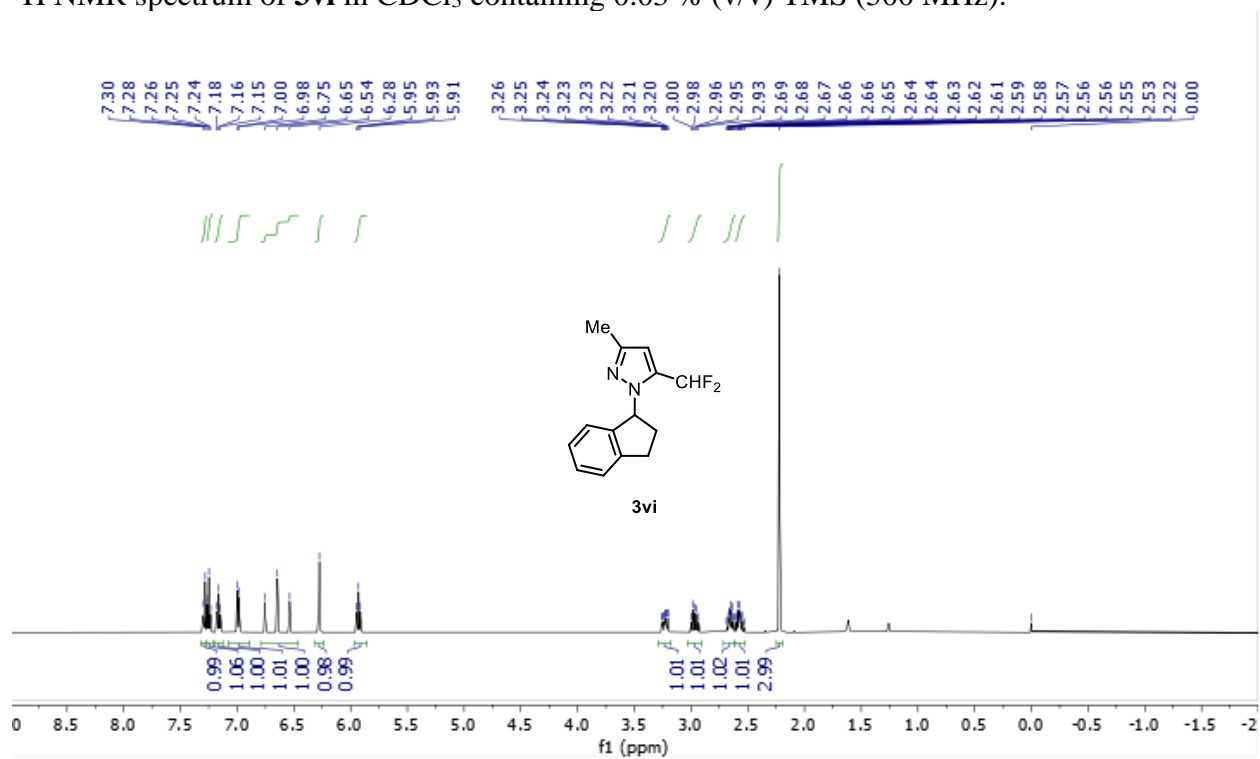
^1H NMR spectrum of **3vh** in CDCl_3 containing 0.03 % (v/v) TMS (500 MHz).



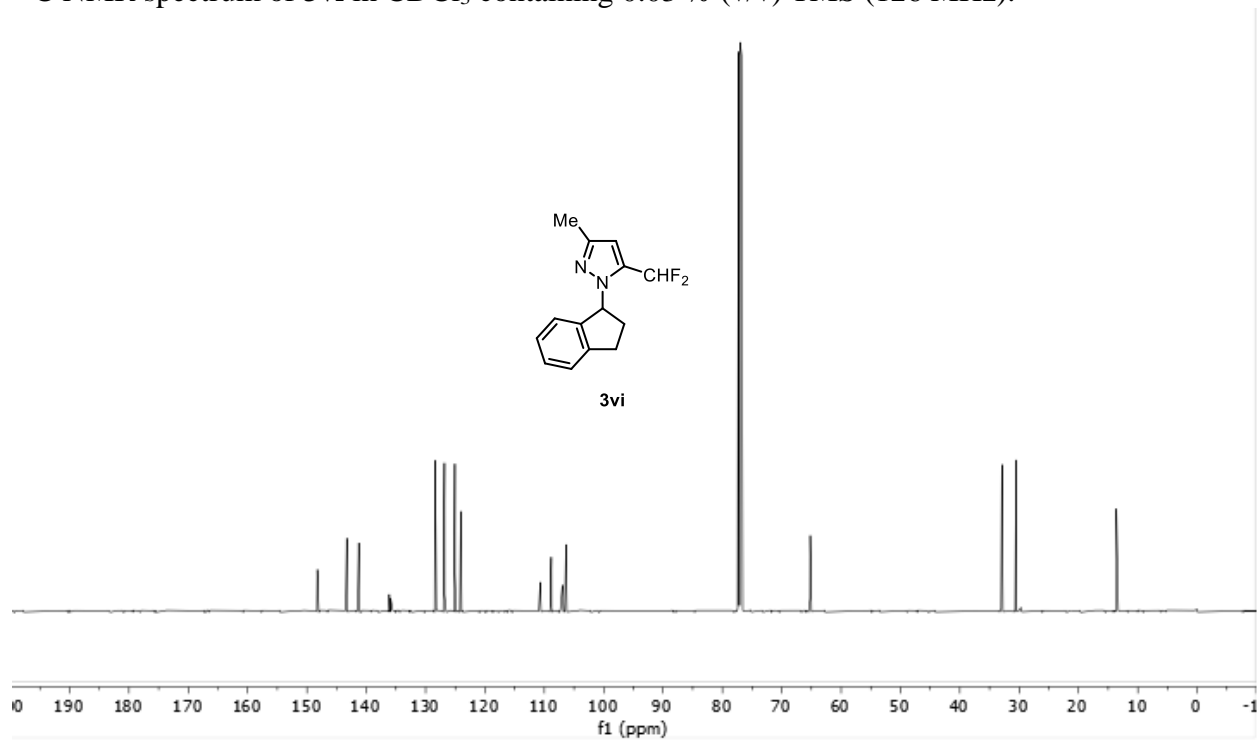
^{13}C NMR spectrum of **3vh** in CDCl_3 containing 0.03 % (v/v) TMS (126 MHz).



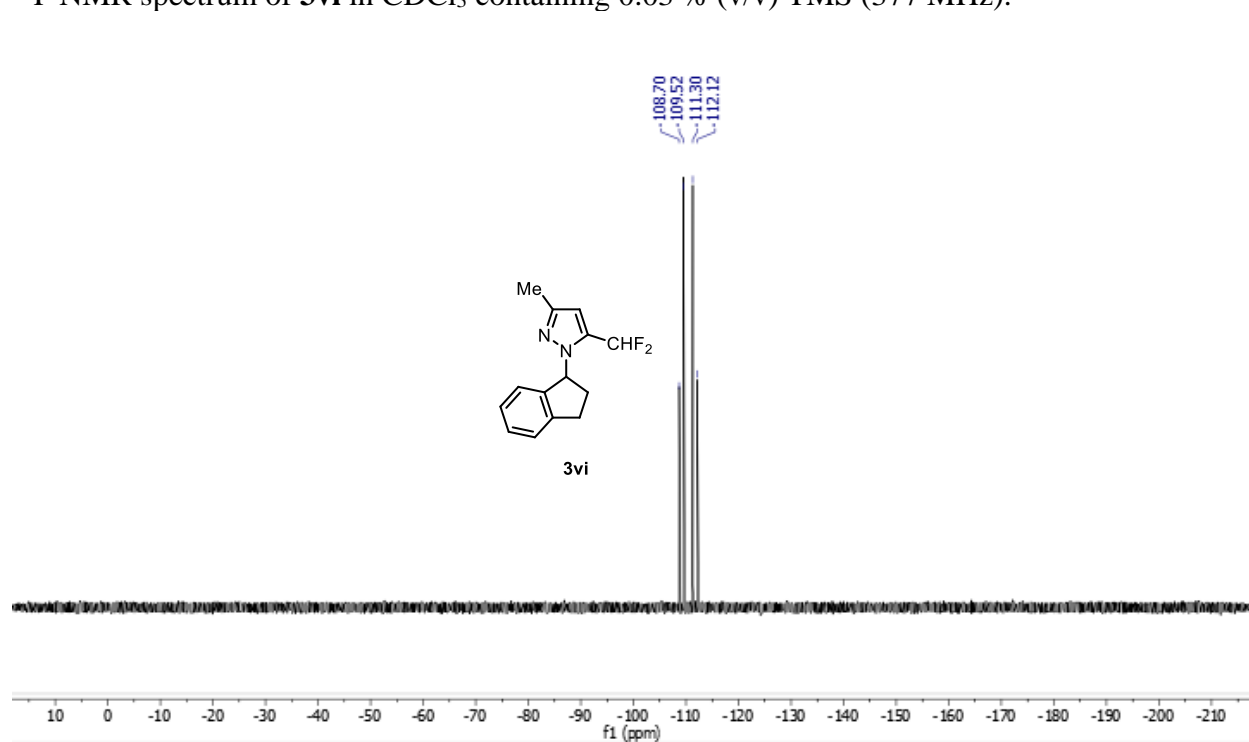
^1H NMR spectrum of **3vi** in CDCl_3 containing 0.03 % (v/v) TMS (500 MHz).



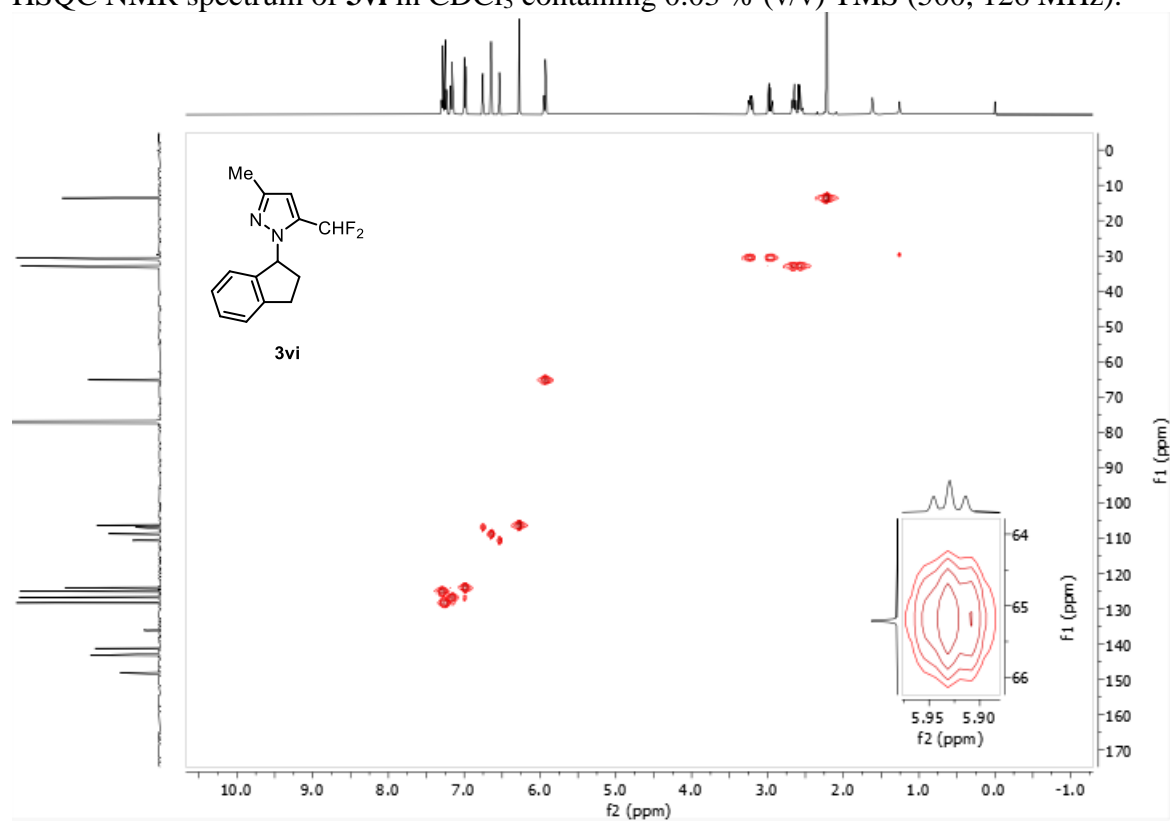
^{13}C NMR spectrum of **3vi** in CDCl_3 containing 0.03 % (v/v) TMS (126 MHz).



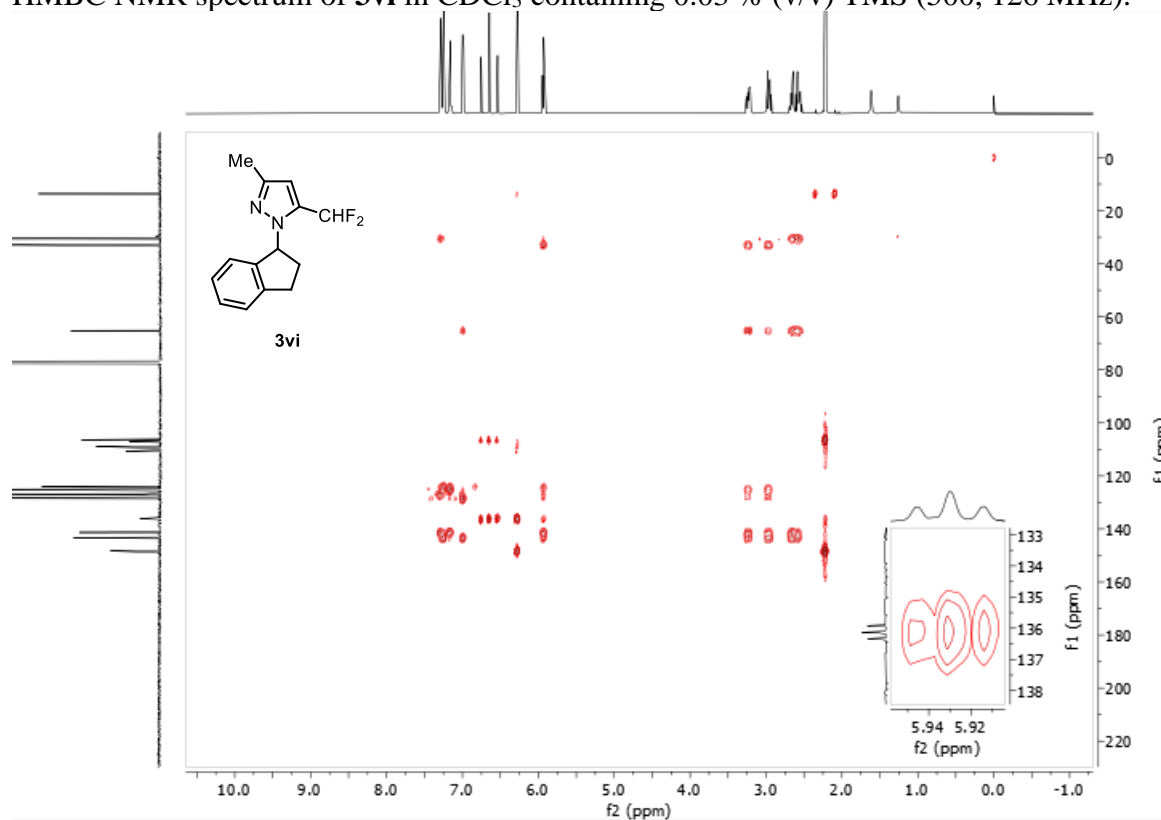
^{19}F NMR spectrum of **3vi** in CDCl_3 containing 0.03 % (v/v) TMS (377 MHz).



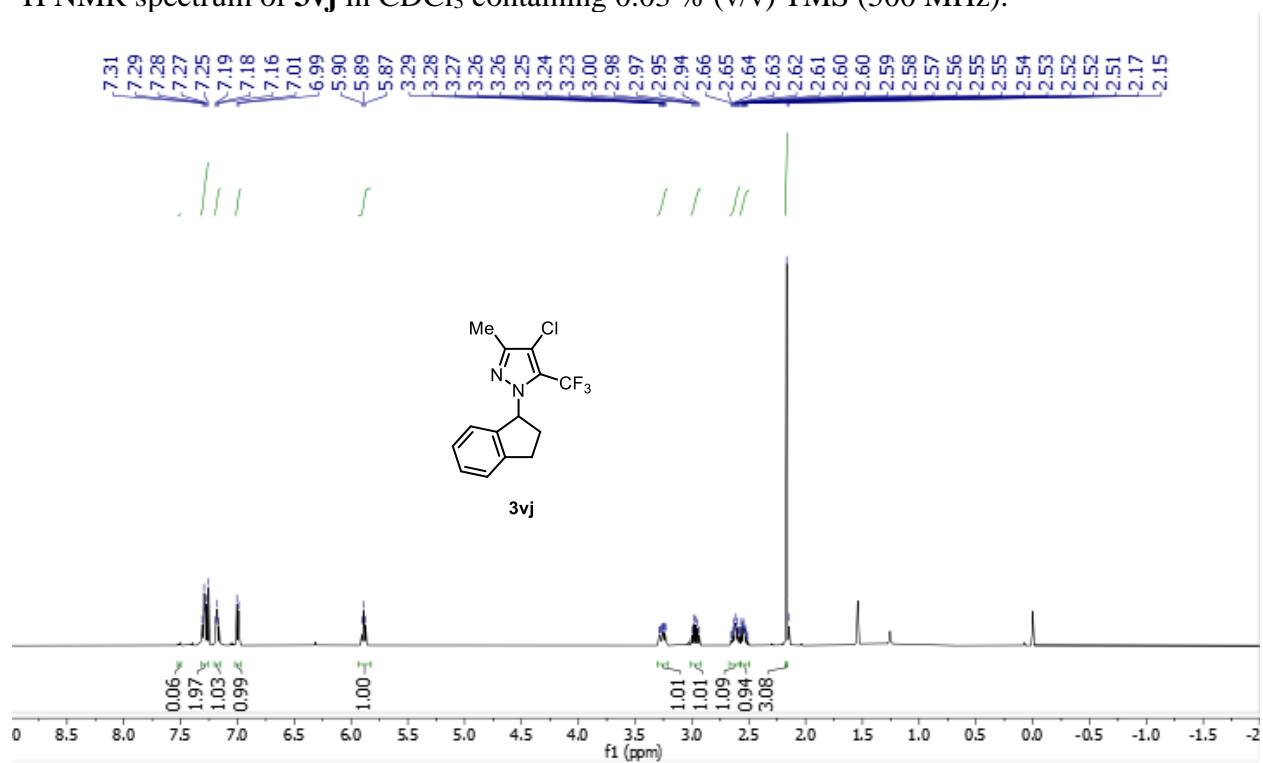
HSQC NMR spectrum of **3vi** in CDCl_3 containing 0.03 % (v/v) TMS (500, 126 MHz).



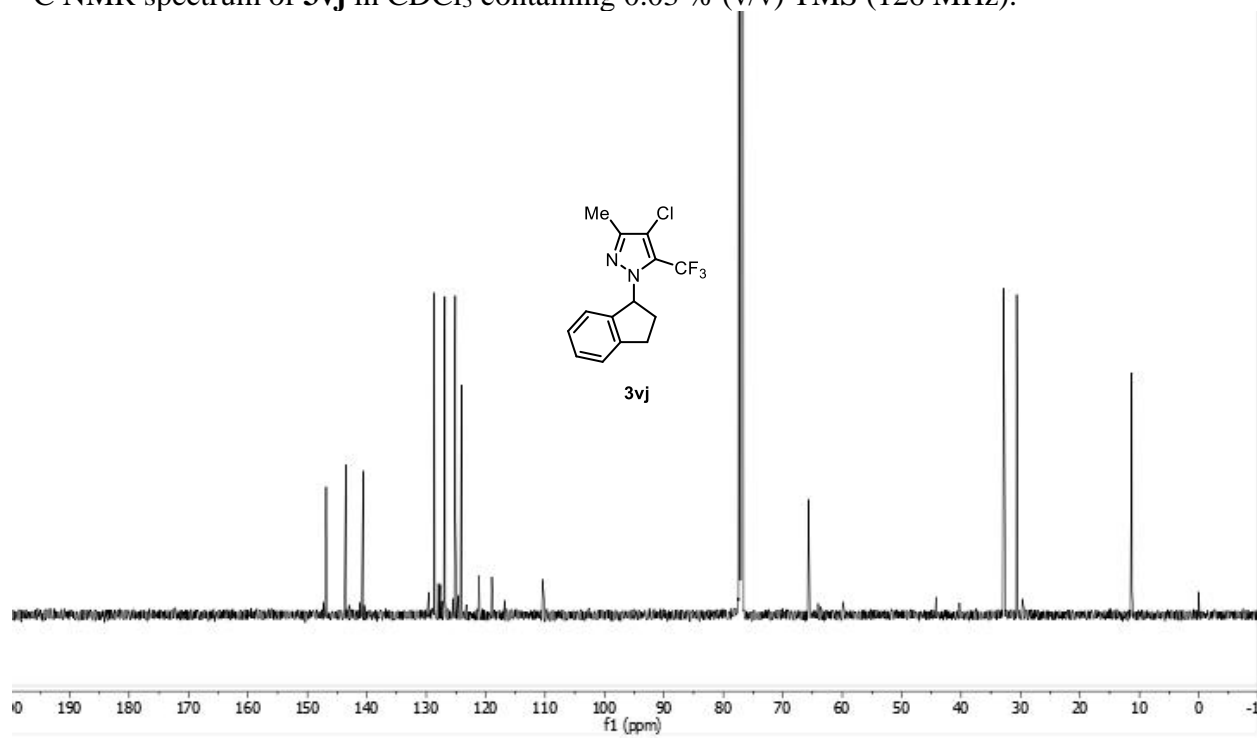
HMBC NMR spectrum of **3vi** in CDCl₃ containing 0.03 % (v/v) TMS (500, 126 MHz).



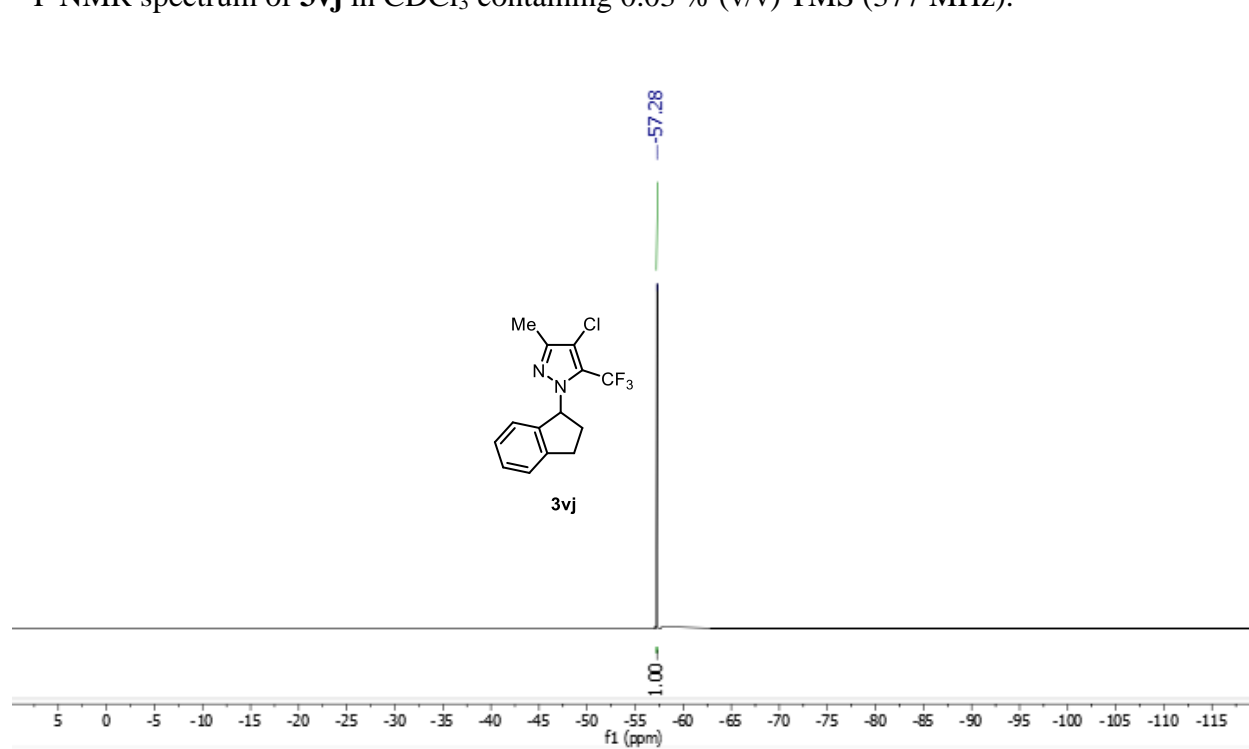
¹H NMR spectrum of **3vj** in CDCl₃ containing 0.03 % (v/v) TMS (500 MHz).



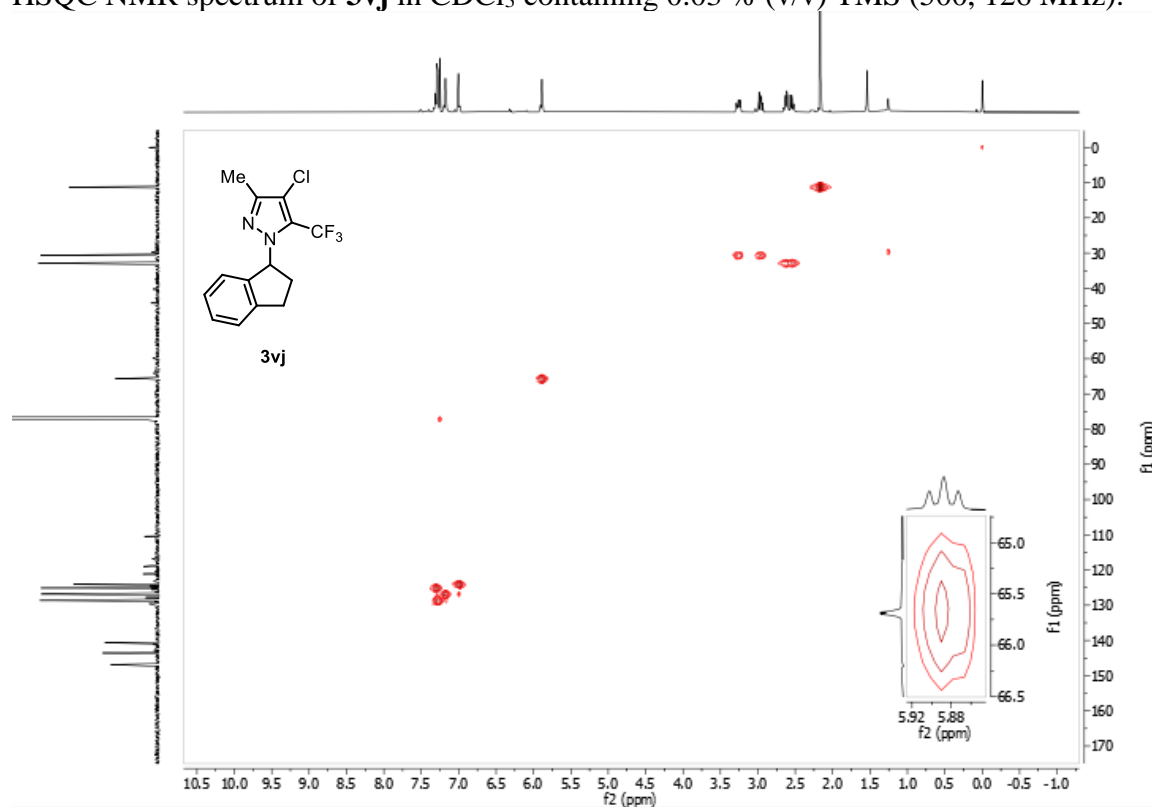
^{13}C NMR spectrum of **3vj** in CDCl_3 containing 0.03 % (v/v) TMS (126 MHz).



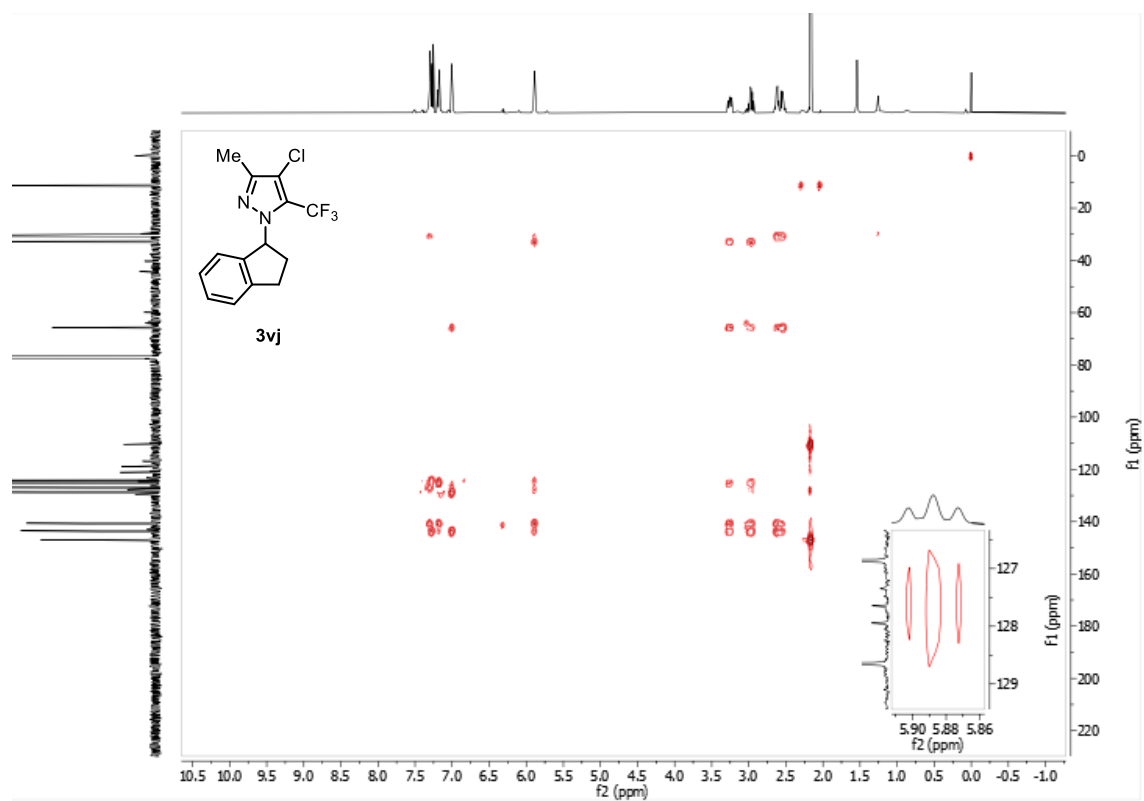
^{19}F NMR spectrum of **3vj** in CDCl_3 containing 0.03 % (v/v) TMS (377 MHz).



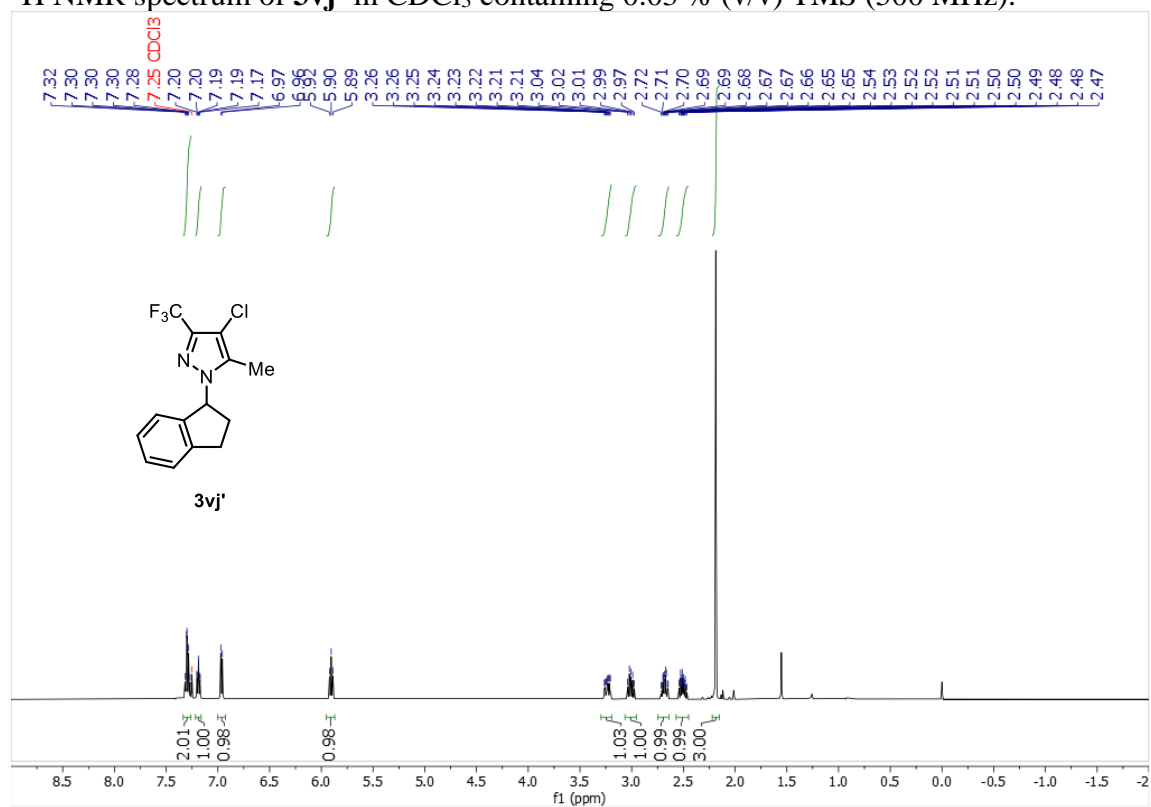
HSQC NMR spectrum of **3vj** in CDCl₃ containing 0.03 % (v/v) TMS (500, 126 MHz).



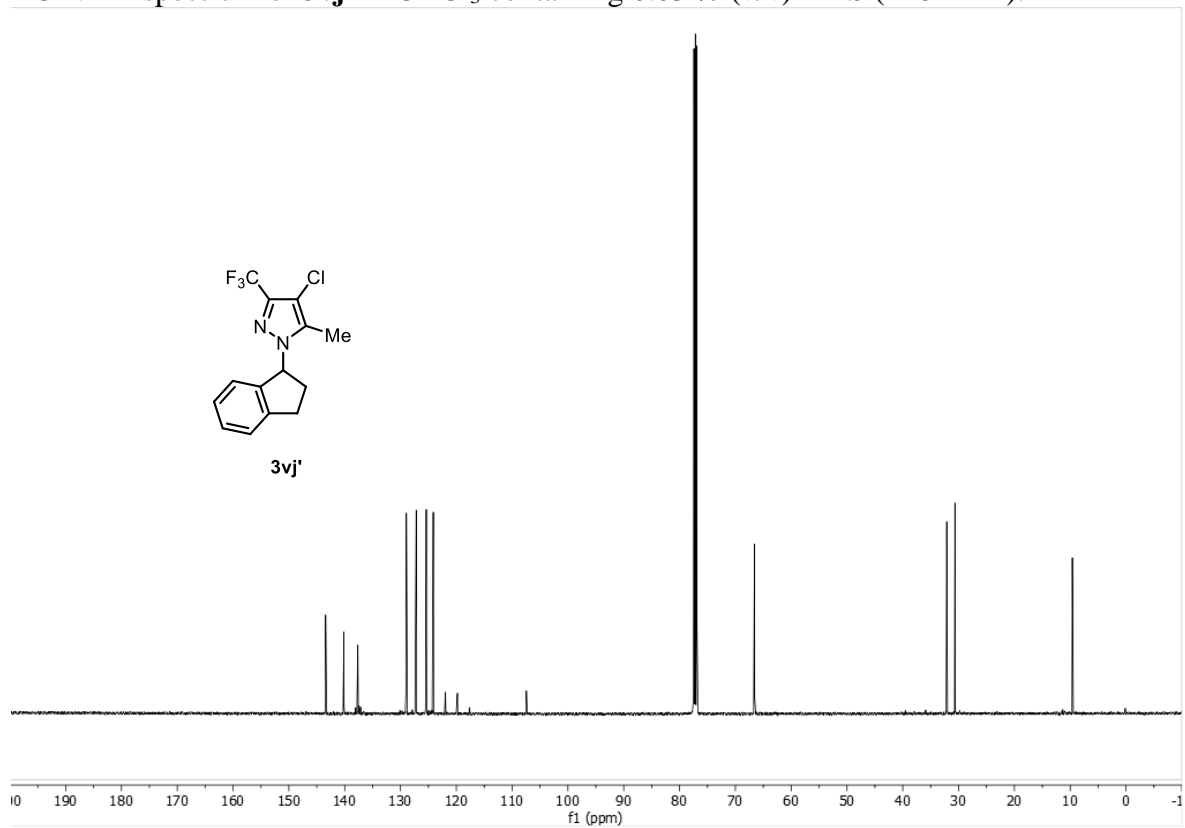
HMBC NMR spectrum of **3vj** in CDCl₃ containing 0.03 % (v/v) TMS (500, 126 MHz).



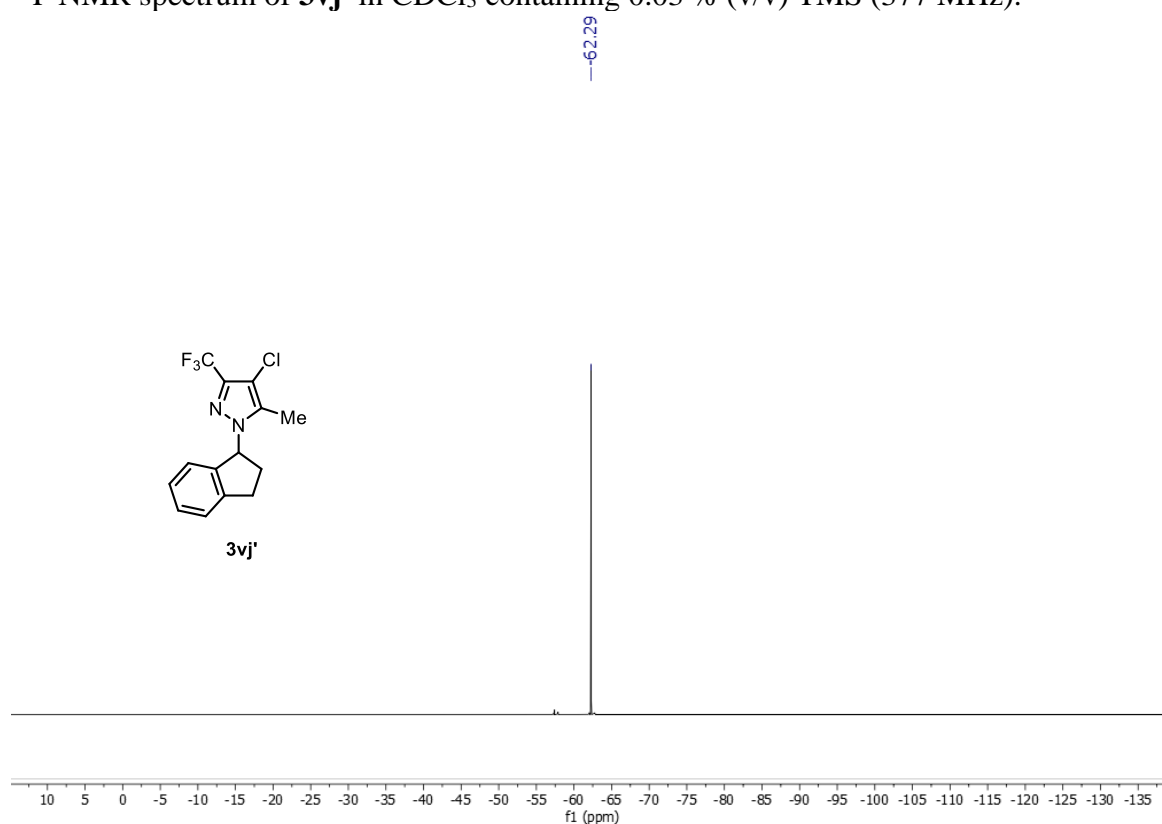
^1H NMR spectrum of **3vj'** in CDCl_3 containing 0.03 % (v/v) TMS (500 MHz).



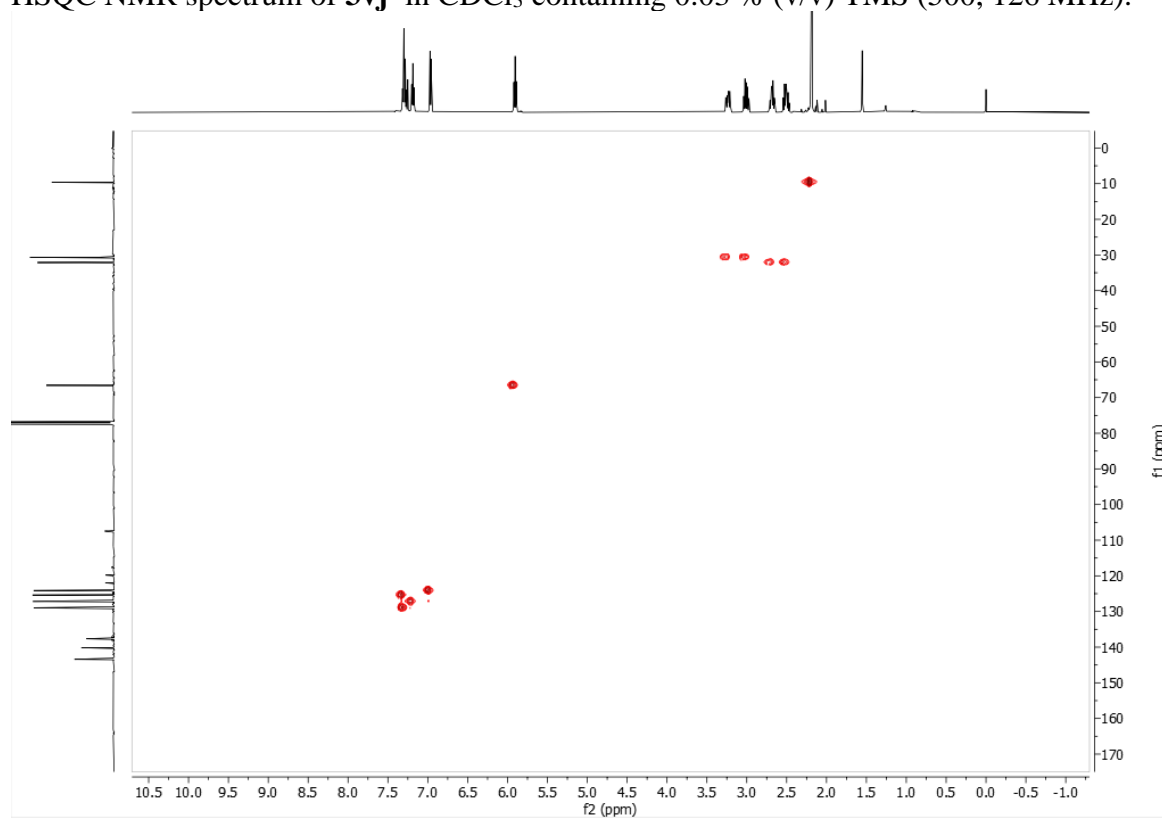
^{13}C NMR spectrum of **3vj'** in CDCl_3 containing 0.03 % (v/v) TMS (126 MHz).



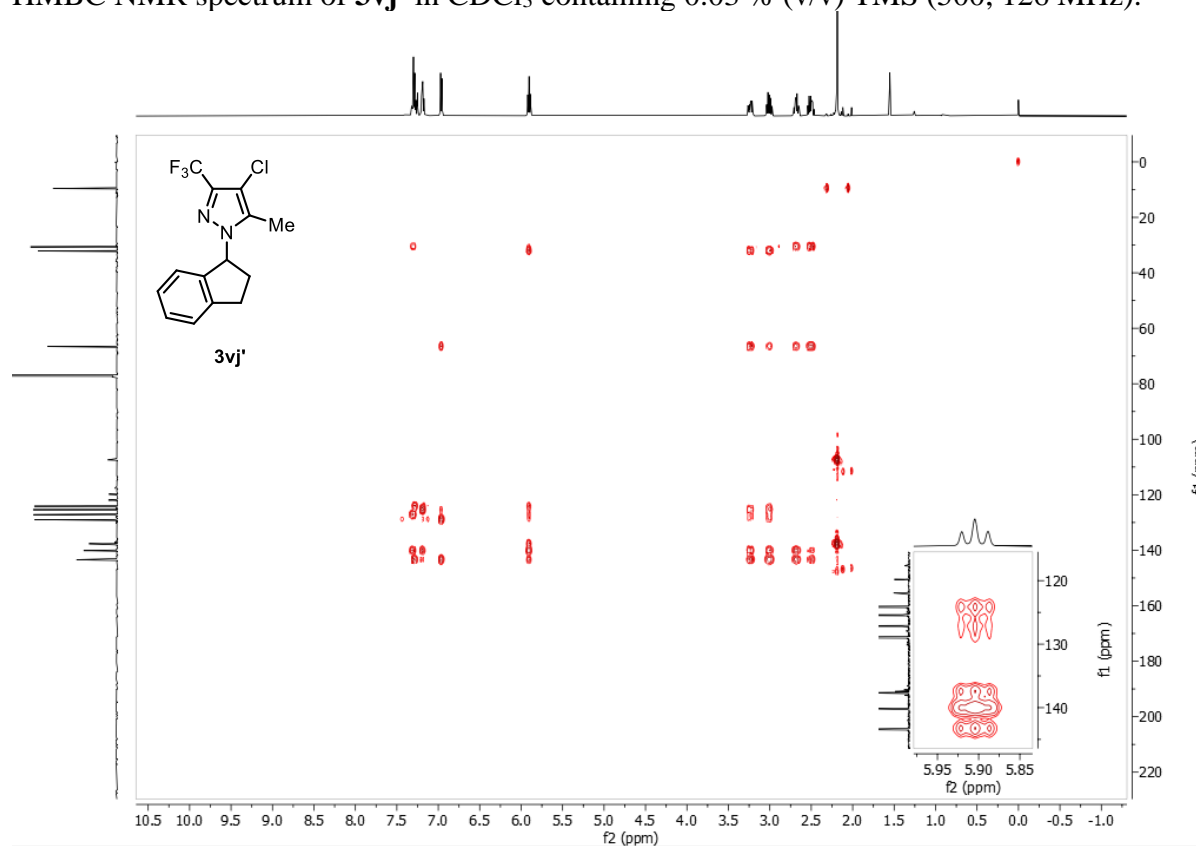
^{19}F NMR spectrum of **3vj'** in CDCl_3 containing 0.03 % (v/v) TMS (377 MHz).



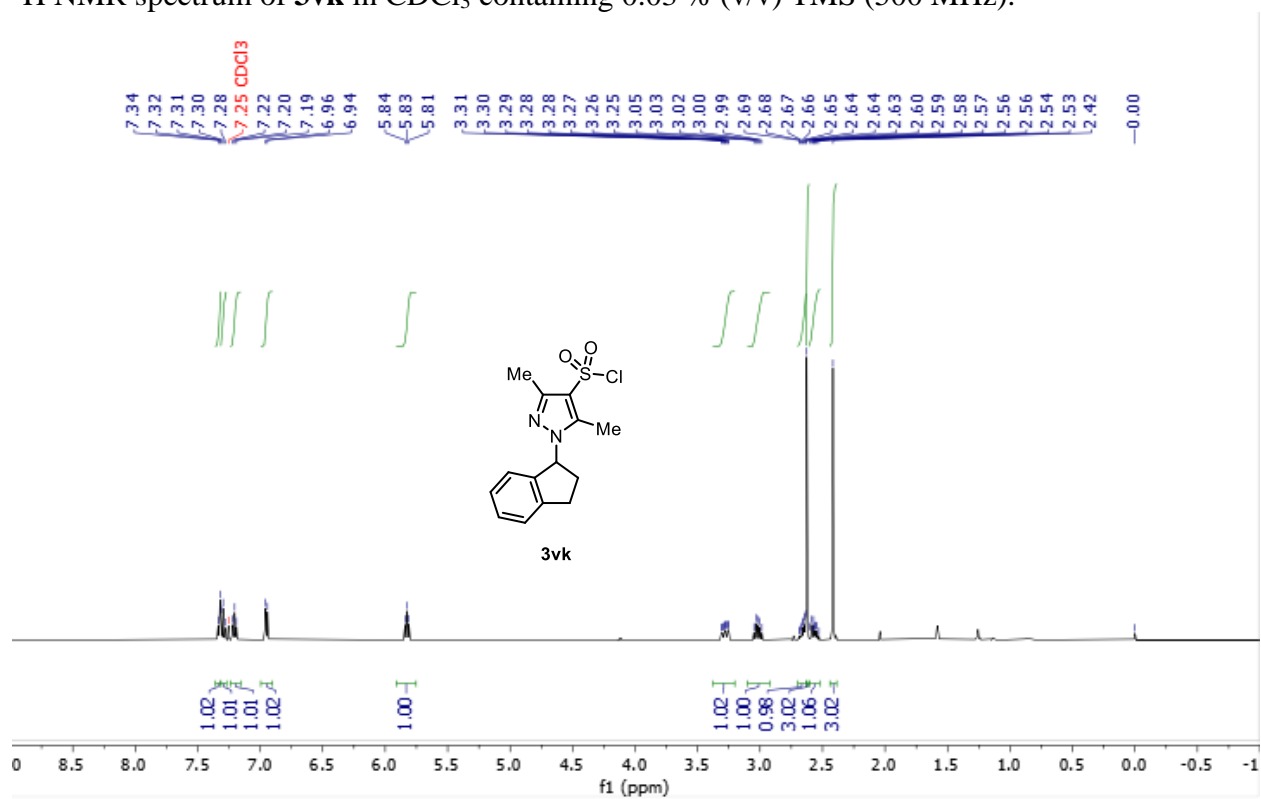
HSQC NMR spectrum of **3vj'** in CDCl_3 containing 0.03 % (v/v) TMS (500, 126 MHz).



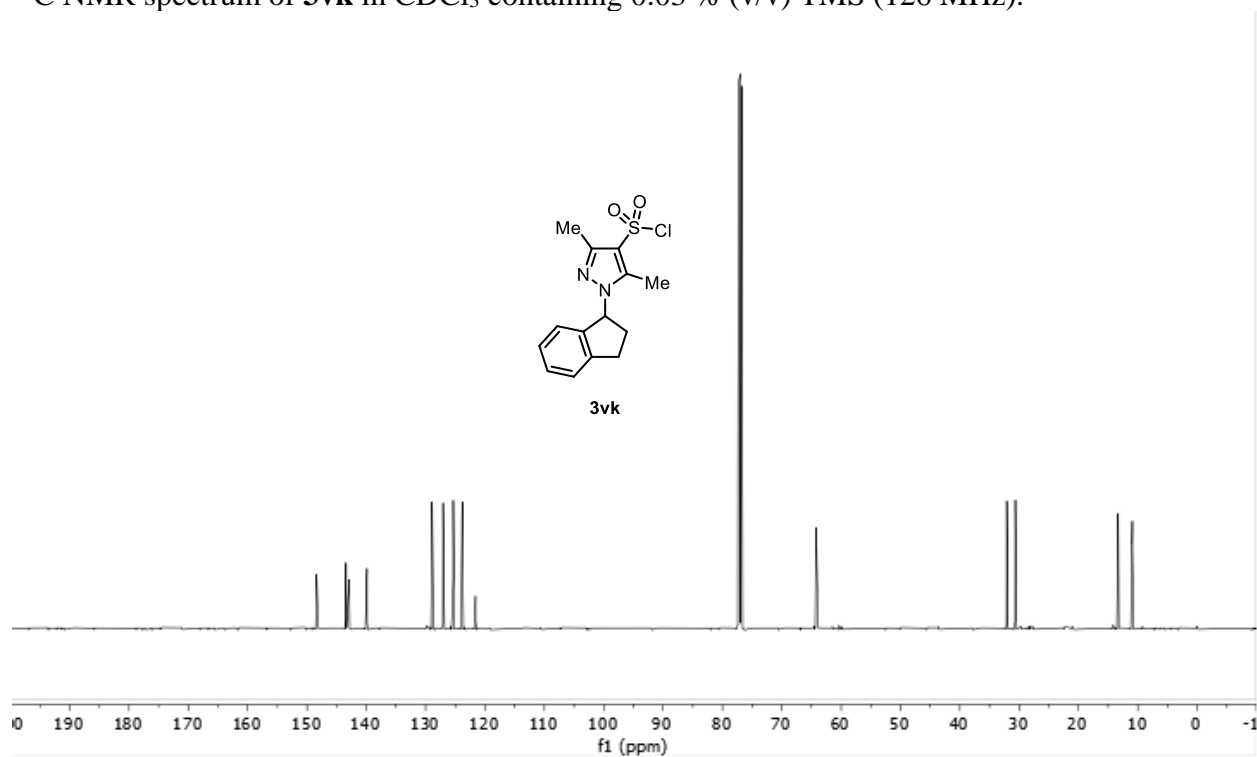
HMBC NMR spectrum of **3vj'** in CDCl₃ containing 0.03 % (v/v) TMS (500, 126 MHz).



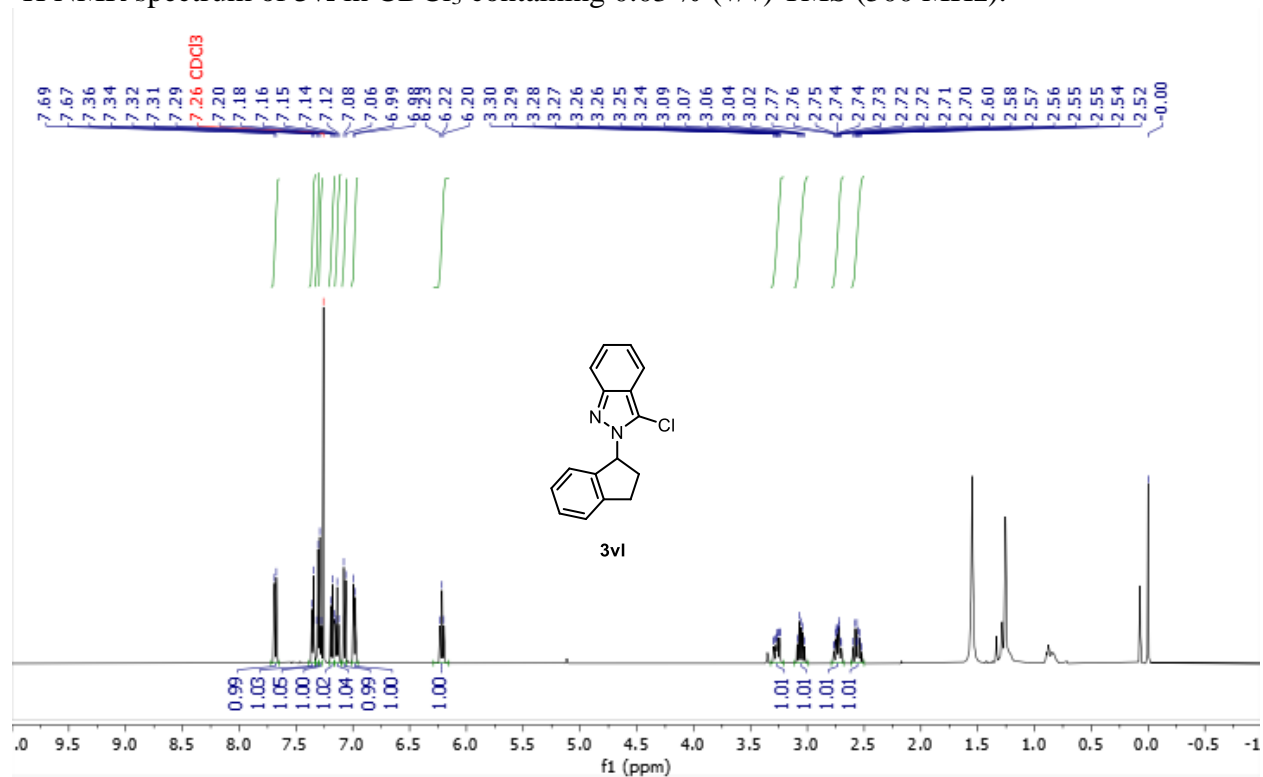
¹H NMR spectrum of **3vk** in CDCl₃ containing 0.03 % (v/v) TMS (500 MHz).



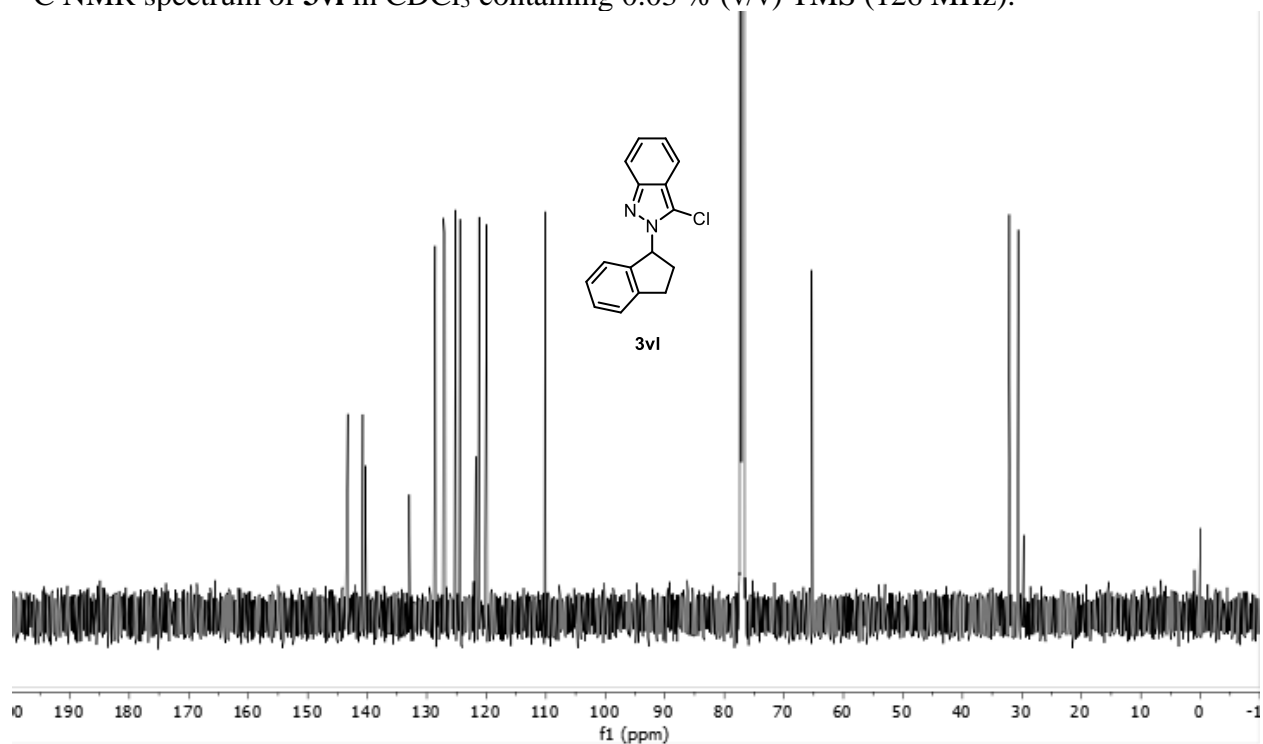
^{13}C NMR spectrum of **3vk** in CDCl_3 containing 0.03 % (v/v) TMS (126 MHz).



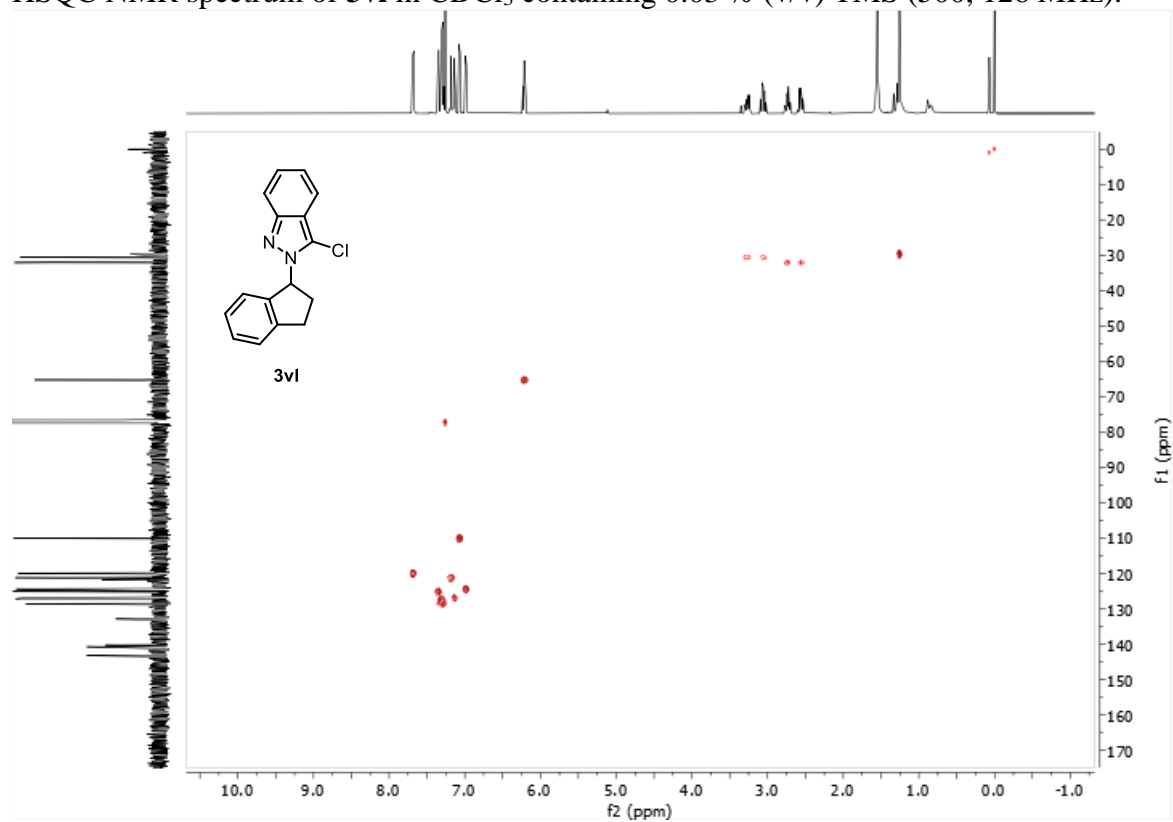
^1H NMR spectrum of **3vl** in CDCl_3 containing 0.03 % (v/v) TMS (500 MHz).



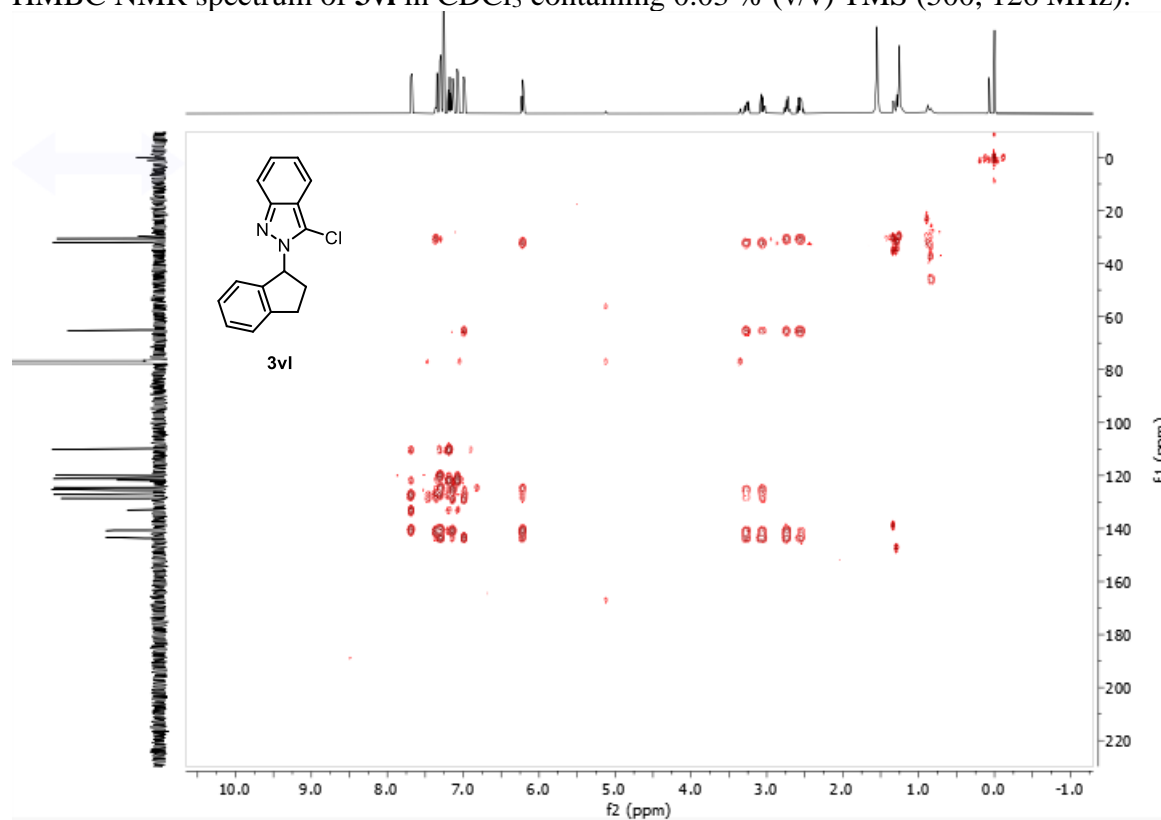
^{13}C NMR spectrum of **3vl** in CDCl_3 containing 0.03 % (v/v) TMS (126 MHz).



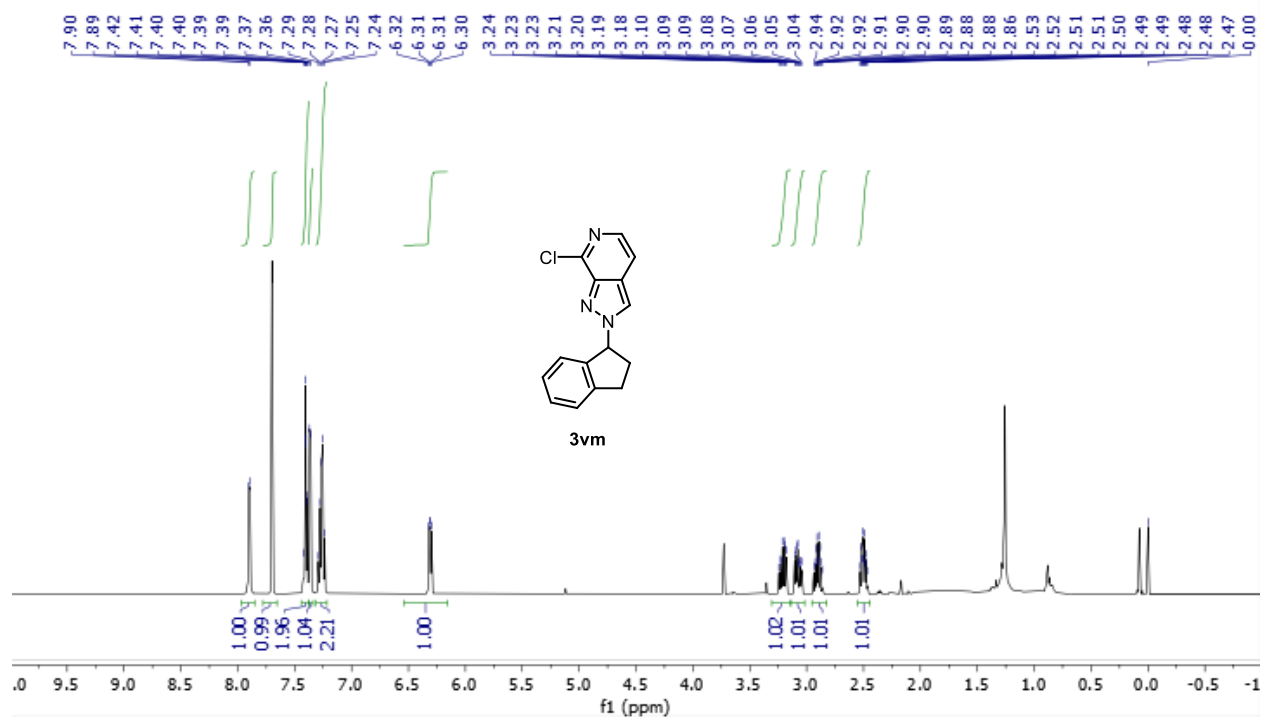
HSQC NMR spectrum of **3vl** in CDCl_3 containing 0.03 % (v/v) TMS (500, 126 MHz).



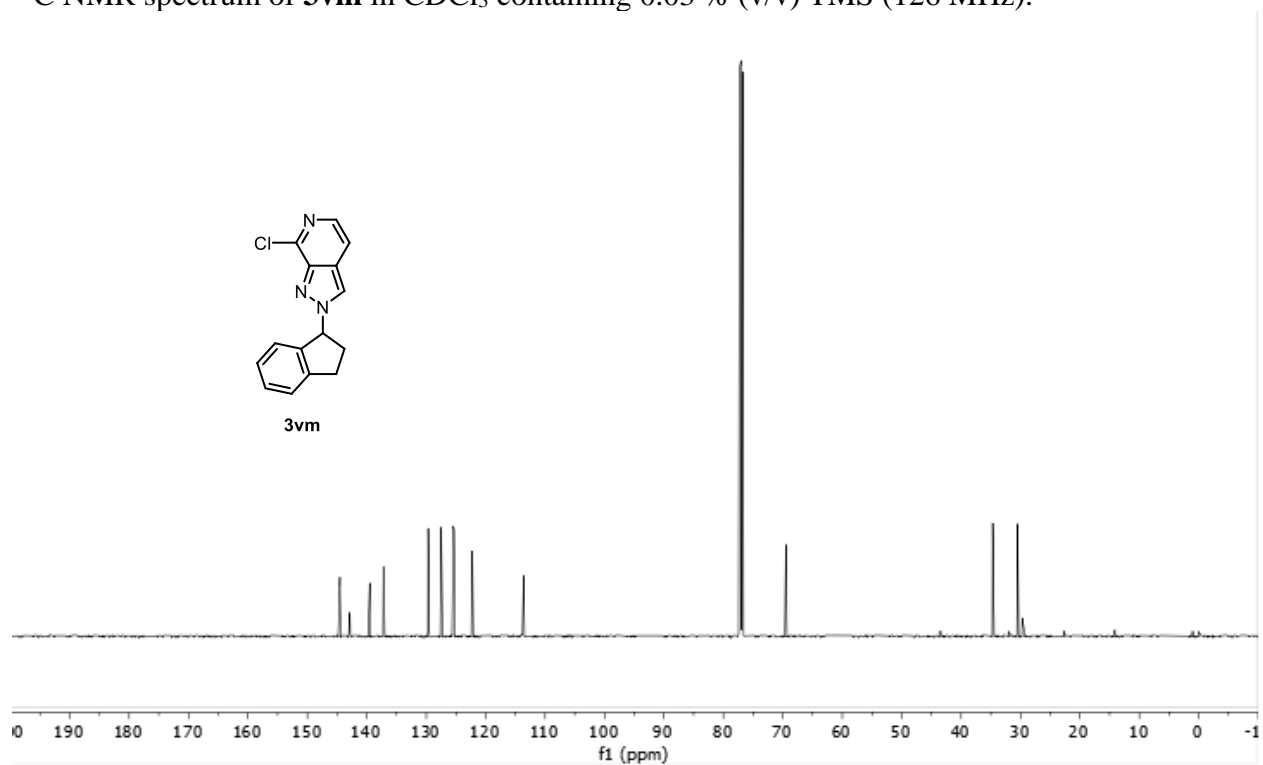
HMBC NMR spectrum of **3vl** in CDCl₃ containing 0.03 % (v/v) TMS (500, 126 MHz).



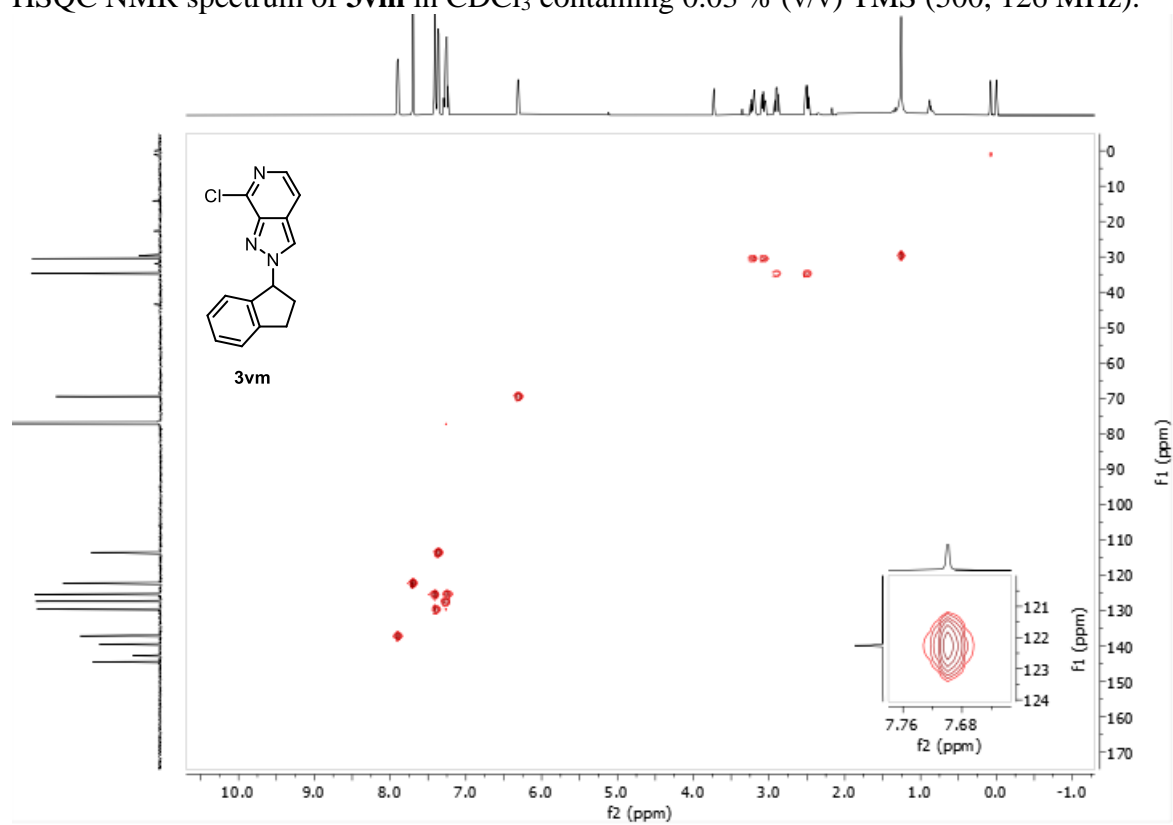
¹H NMR spectrum of **3vm** in CDCl₃ containing 0.03 % (v/v) TMS (500 MHz).



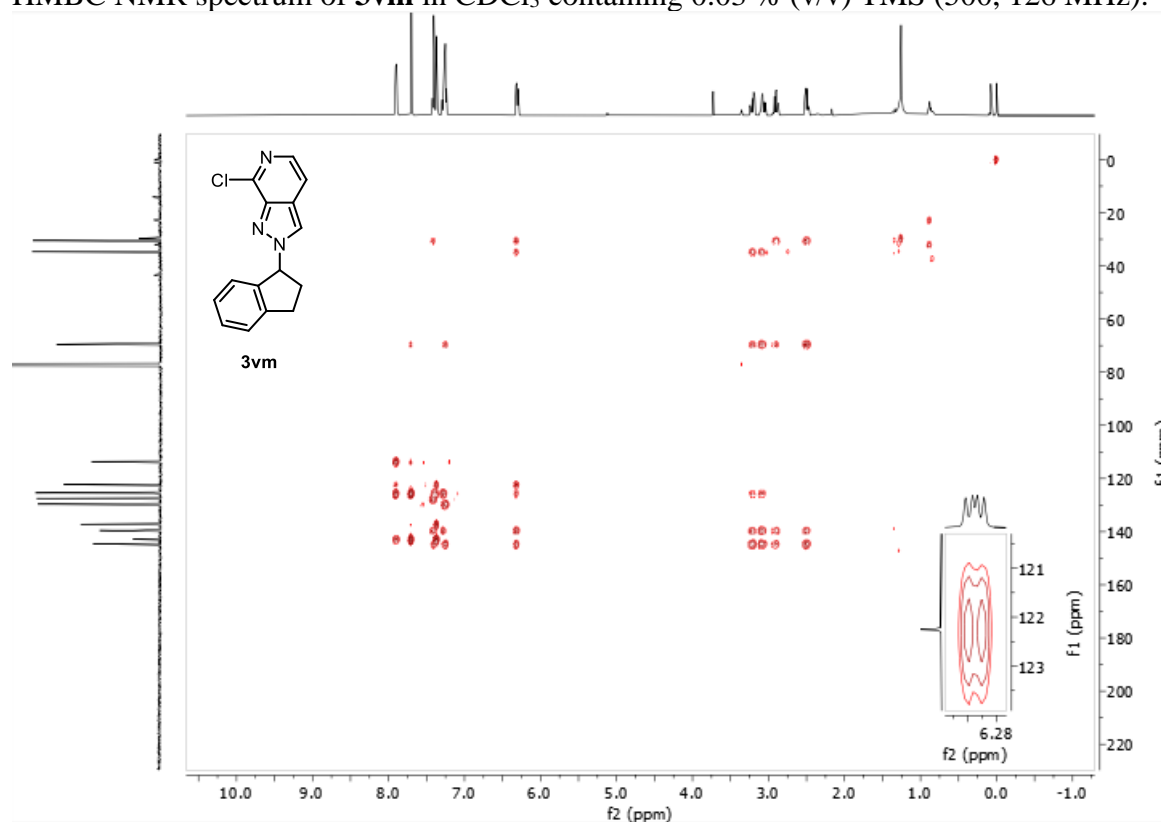
^{13}C NMR spectrum of **3vm** in CDCl_3 containing 0.03 % (v/v) TMS (126 MHz).



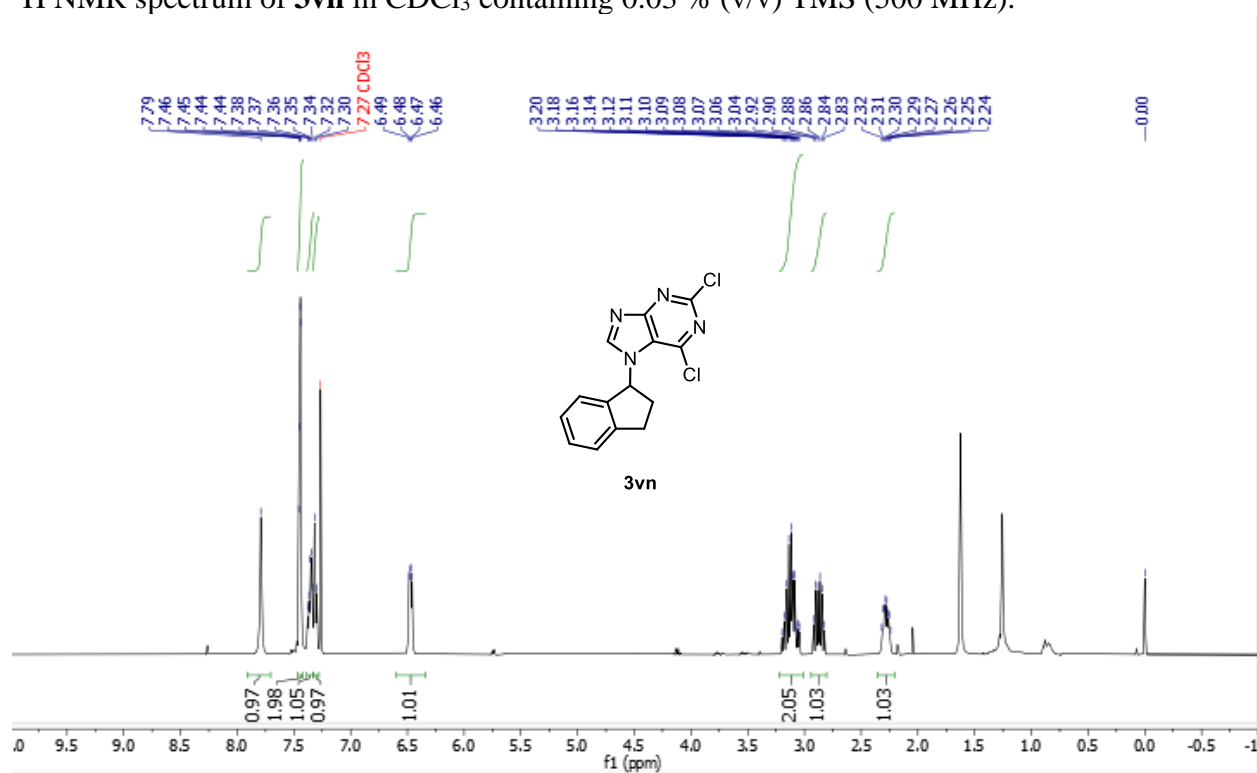
HSQC NMR spectrum of **3vm** in CDCl_3 containing 0.03 % (v/v) TMS (500, 126 MHz).



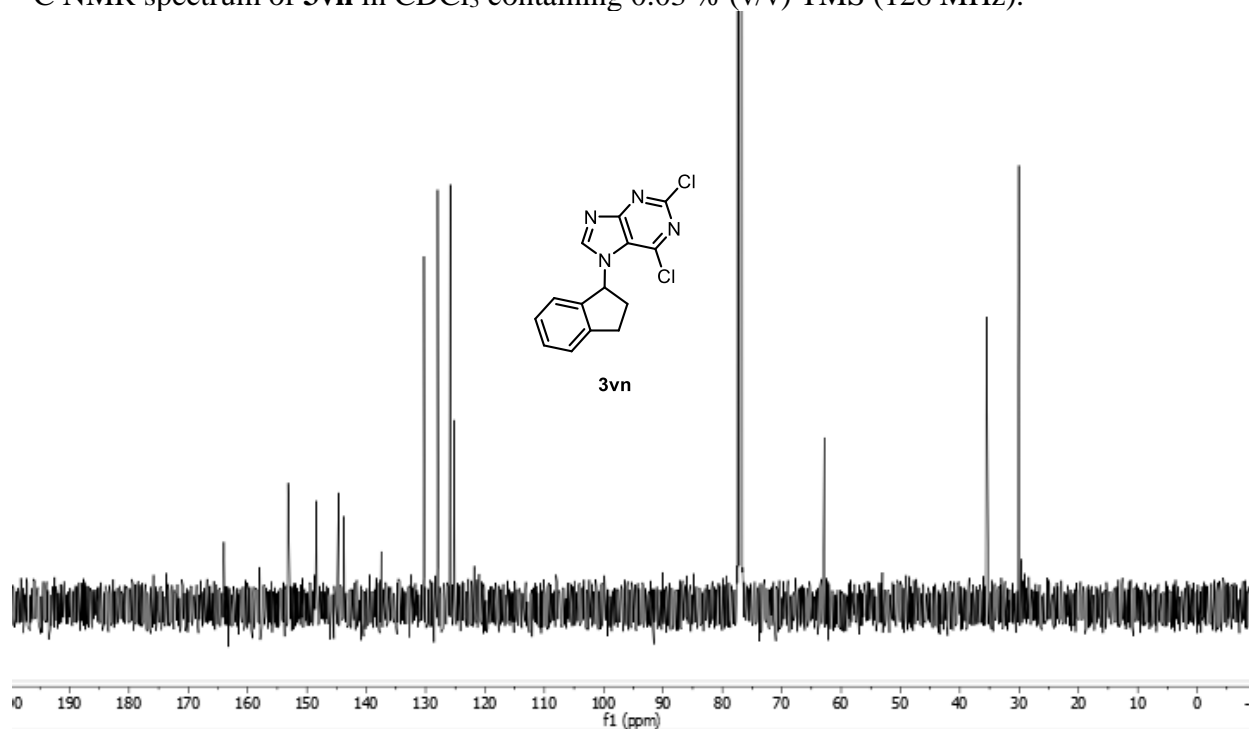
HMBC NMR spectrum of **3vm** in CDCl₃ containing 0.03 % (v/v) TMS (500, 126 MHz).



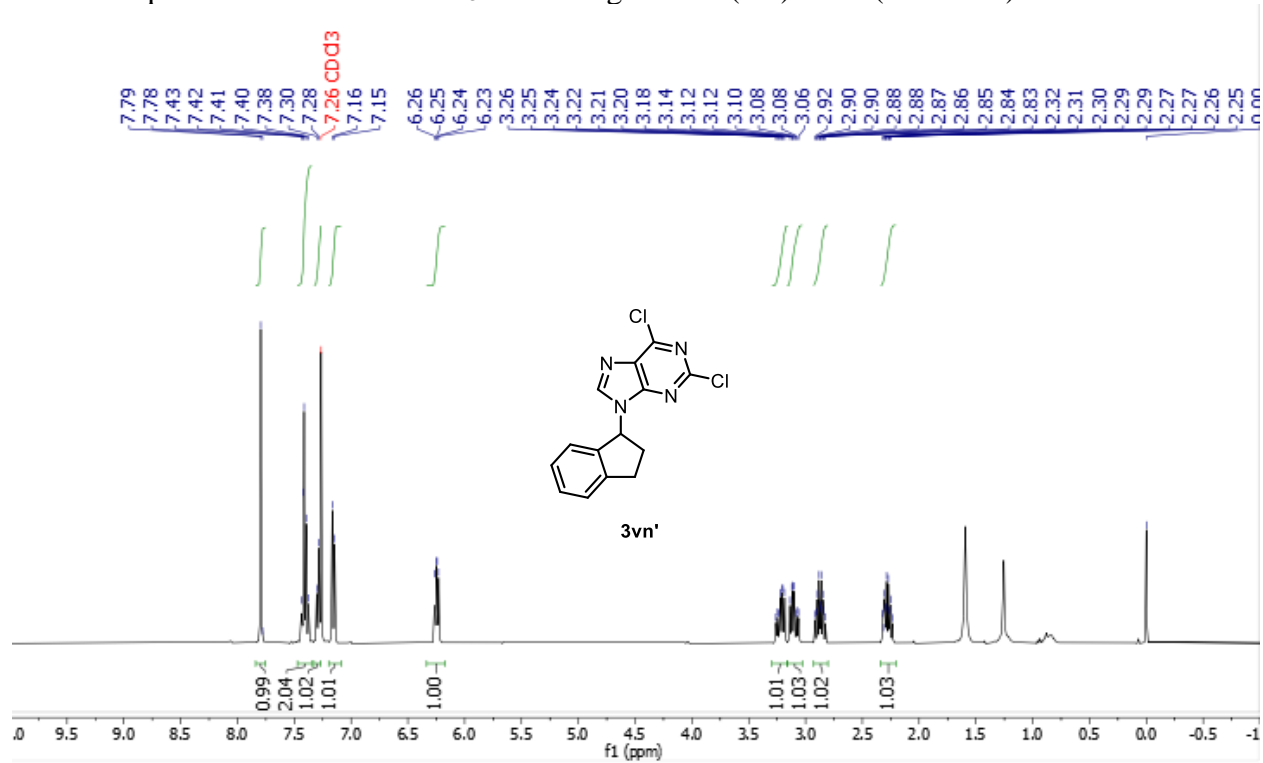
¹H NMR spectrum of **3vn** in CDCl₃ containing 0.03 % (v/v) TMS (500 MHz).



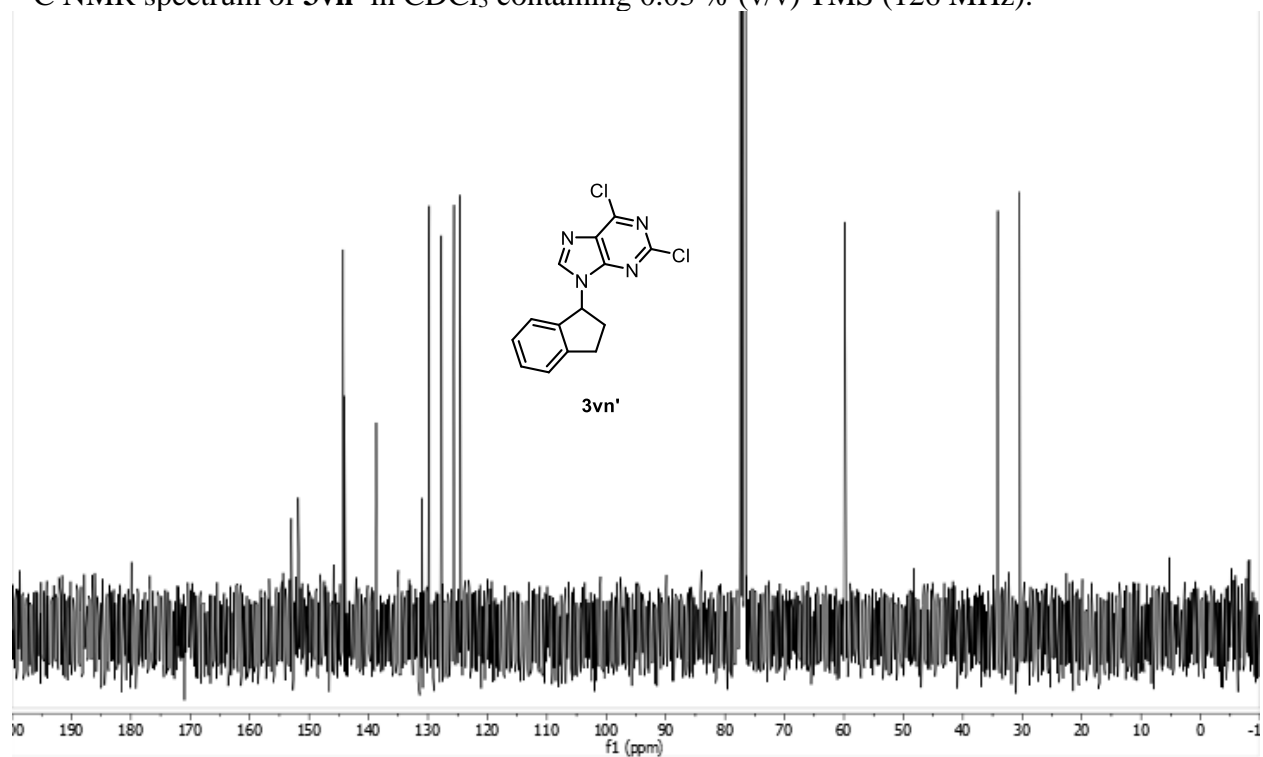
^{13}C NMR spectrum of **3vn** in CDCl_3 containing 0.03 % (v/v) TMS (126 MHz).



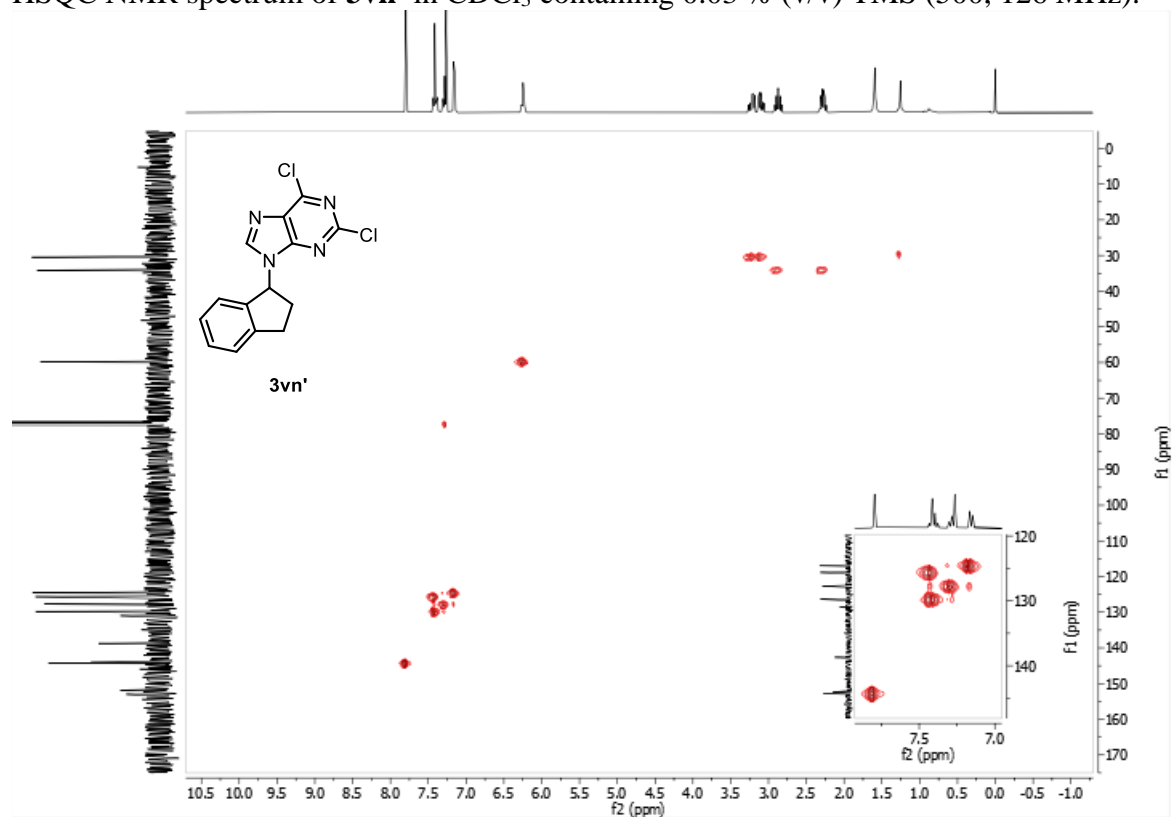
^1H NMR spectrum of **3vn'** in CDCl_3 containing 0.03 % (v/v) TMS (500 MHz).



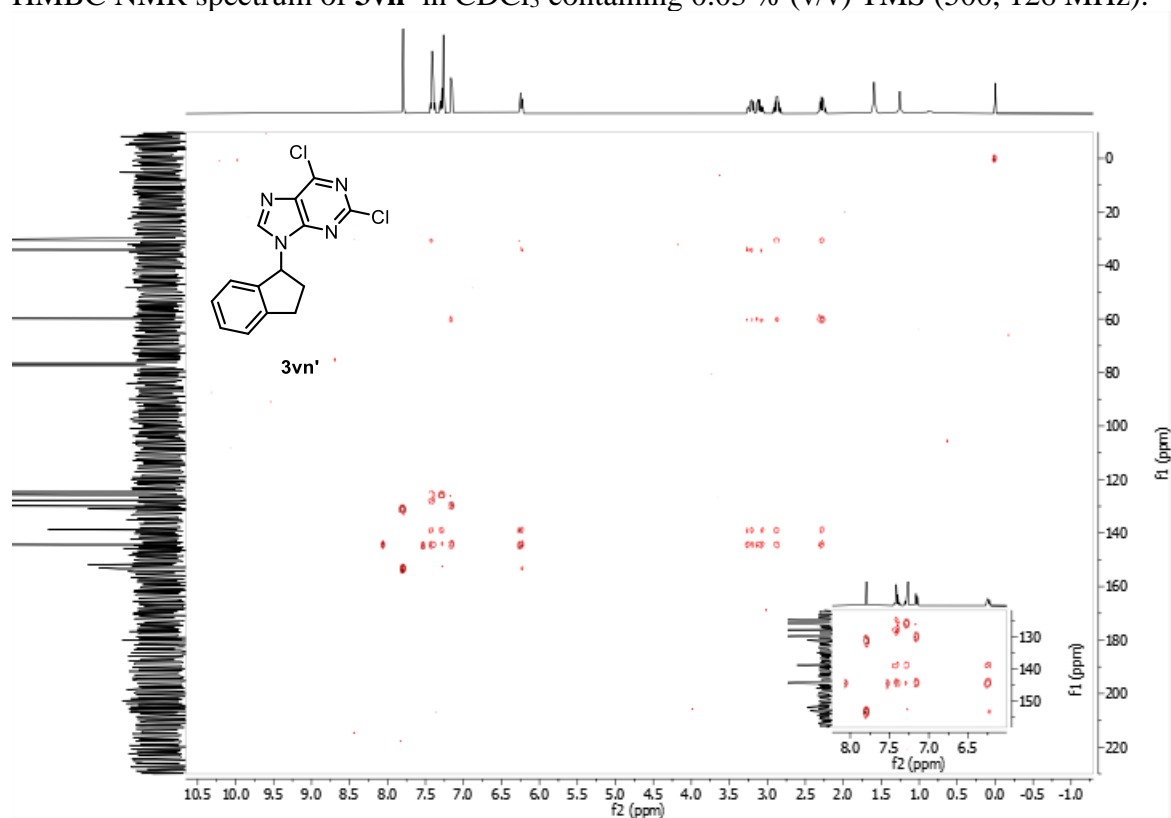
^{13}C NMR spectrum of **3vn'** in CDCl_3 containing 0.03 % (v/v) TMS (126 MHz).



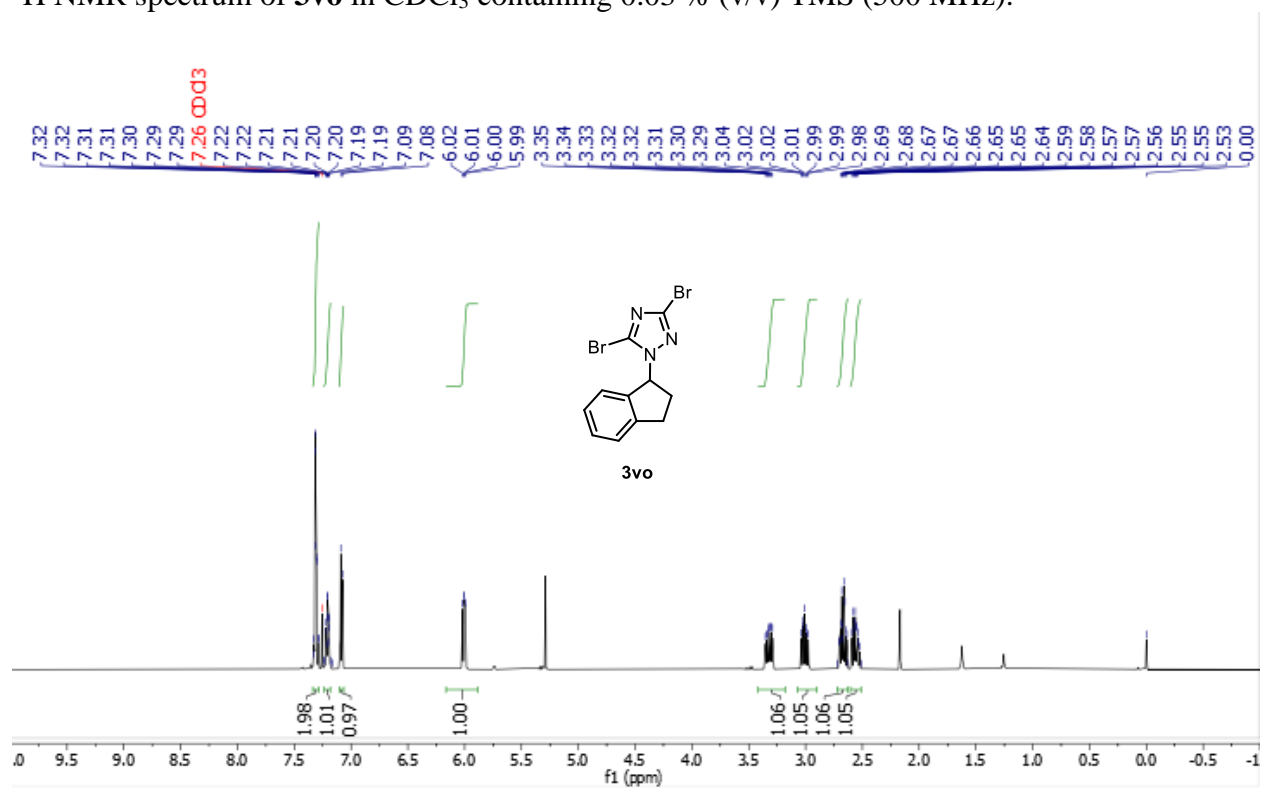
HSQC NMR spectrum of **3vn'** in CDCl_3 containing 0.03 % (v/v) TMS (500, 126 MHz).



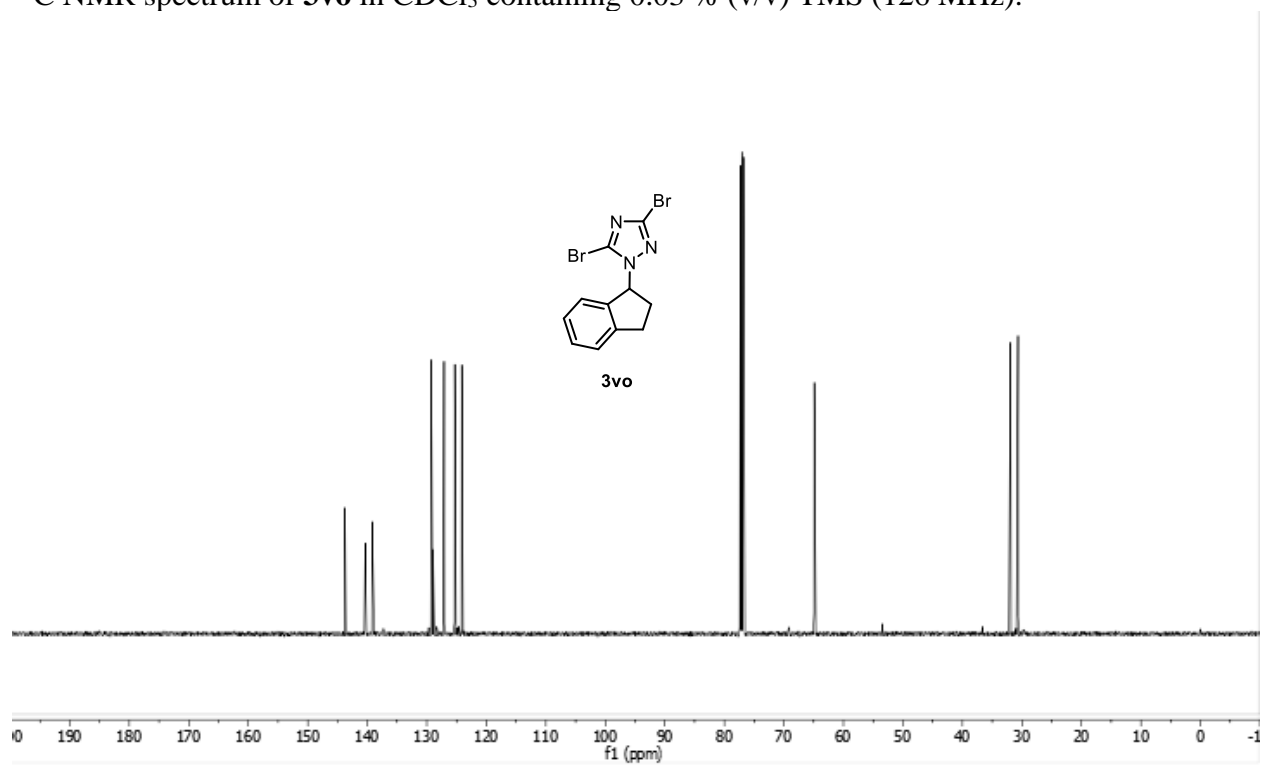
HMBC NMR spectrum of **3vn'** in CDCl₃ containing 0.03 % (v/v) TMS (500, 126 MHz).



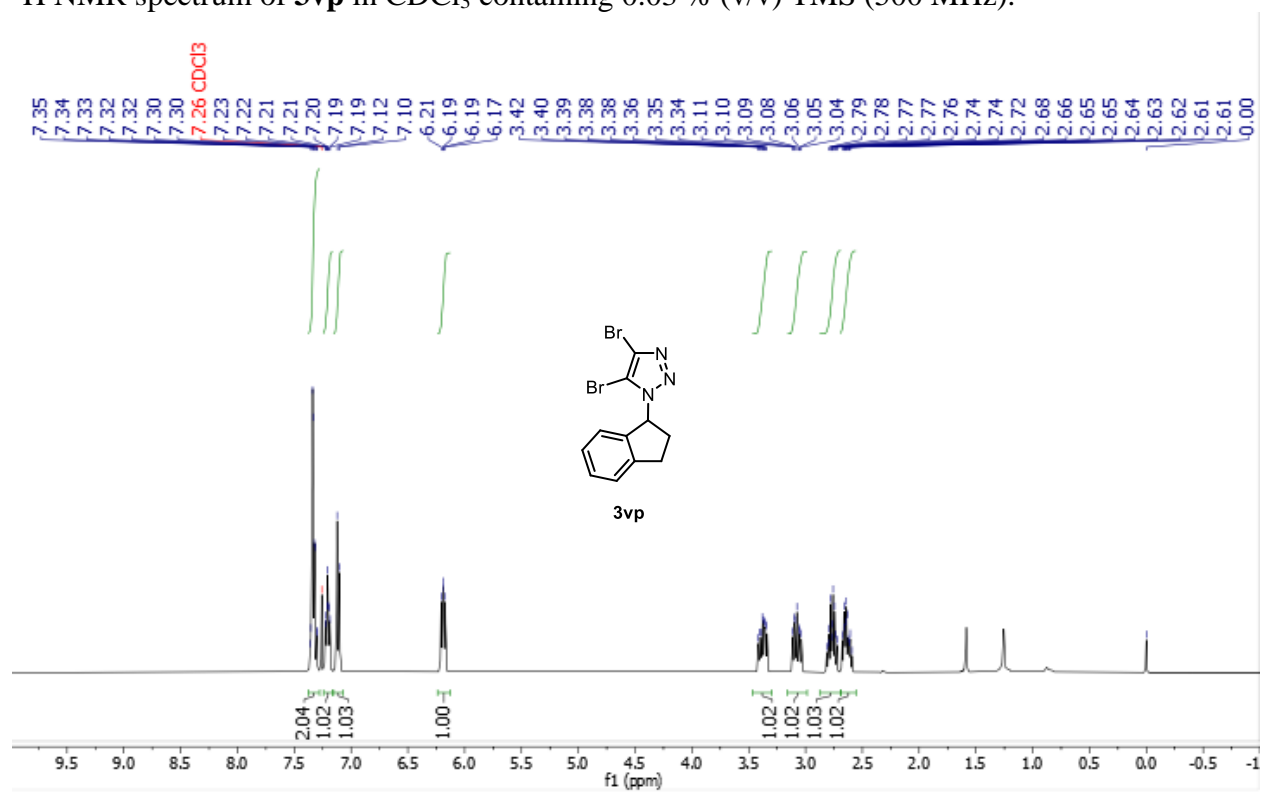
¹H NMR spectrum of **3vo** in CDCl₃ containing 0.03 % (v/v) TMS (500 MHz).



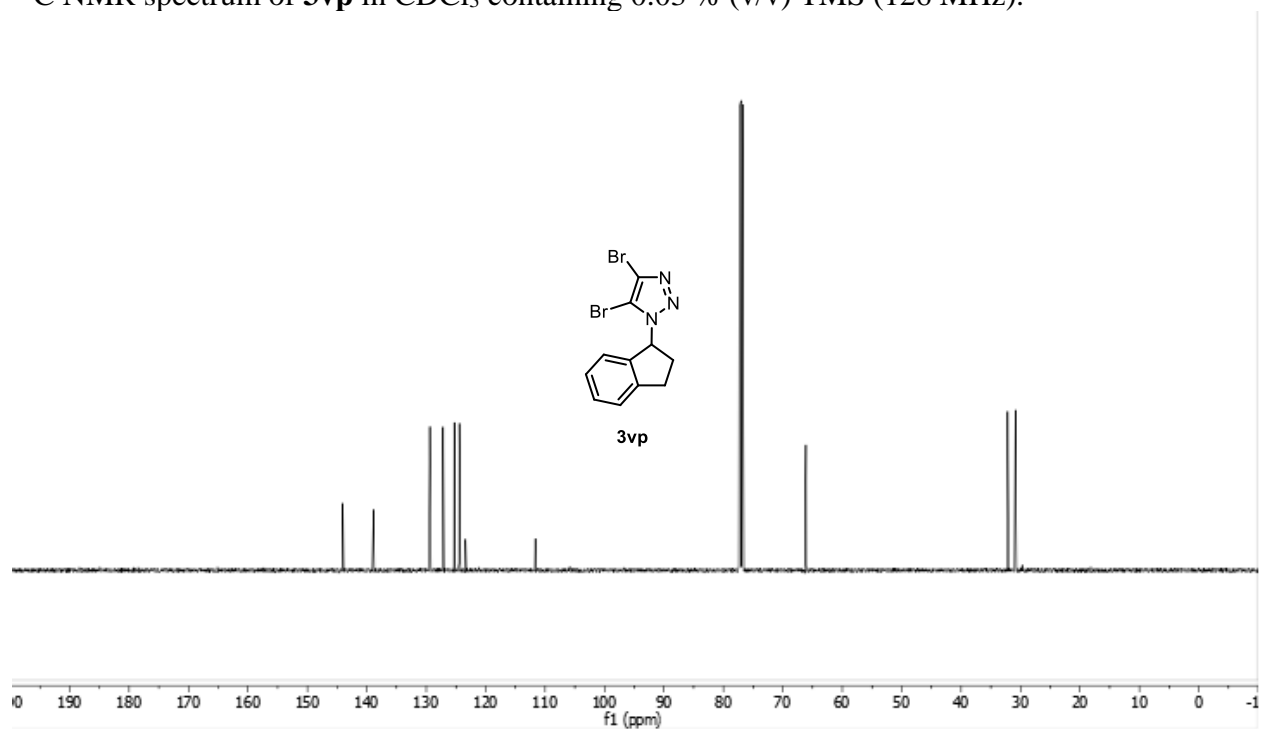
^{13}C NMR spectrum of **3vo** in CDCl_3 containing 0.03 % (v/v) TMS (126 MHz).



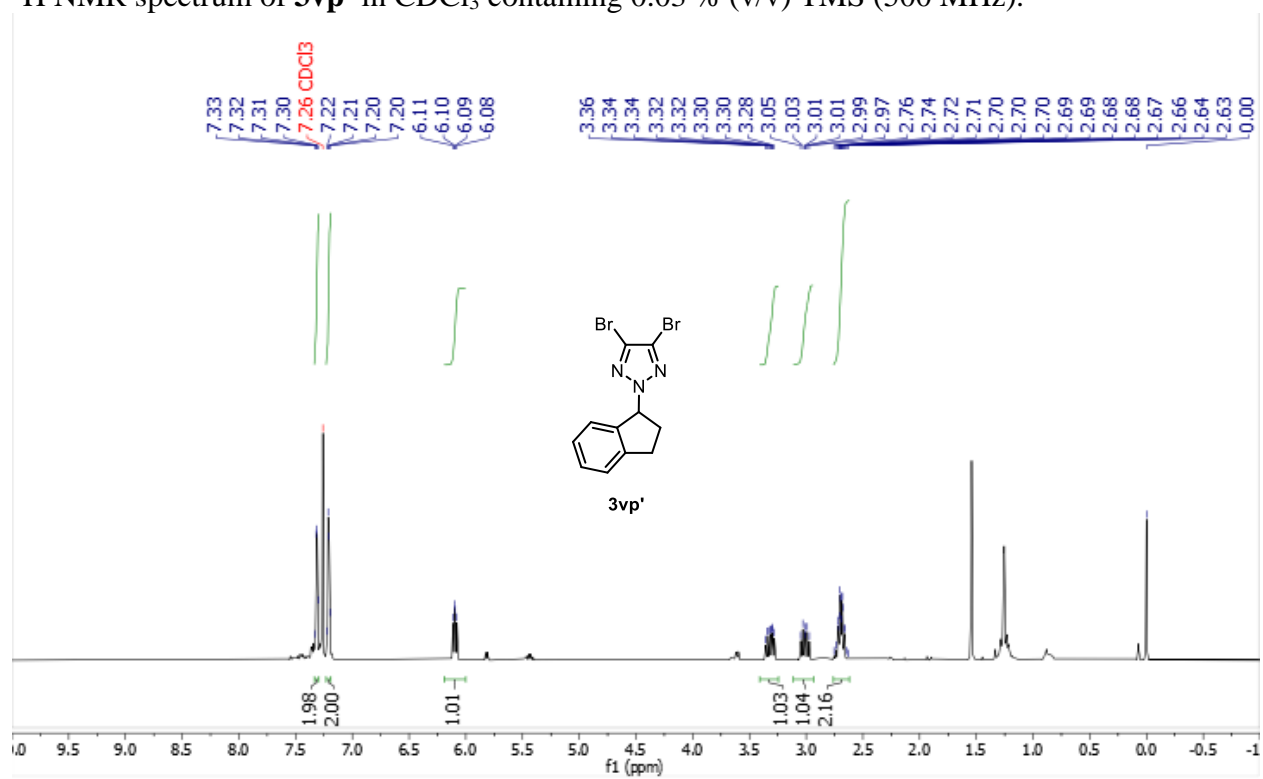
^1H NMR spectrum of **3vp** in CDCl_3 containing 0.03 % (v/v) TMS (500 MHz).



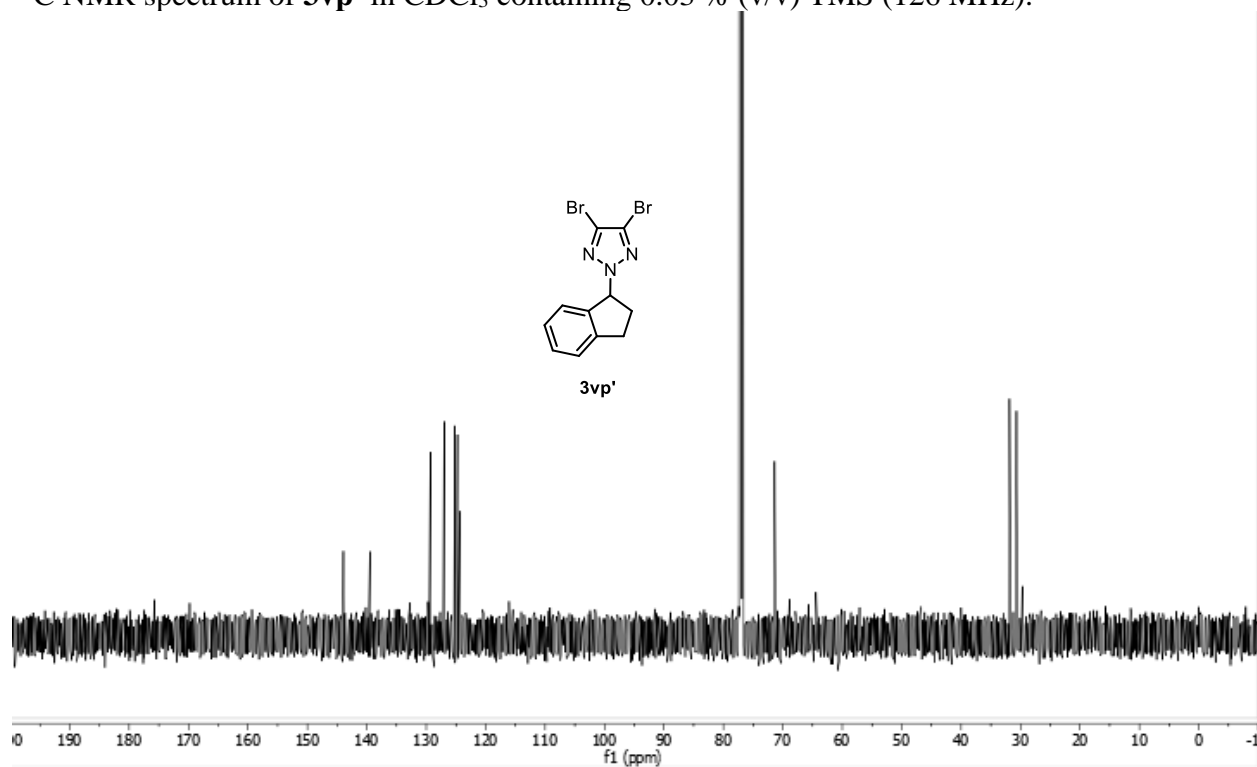
^{13}C NMR spectrum of **3vp** in CDCl_3 containing 0.03 % (v/v) TMS (126 MHz).



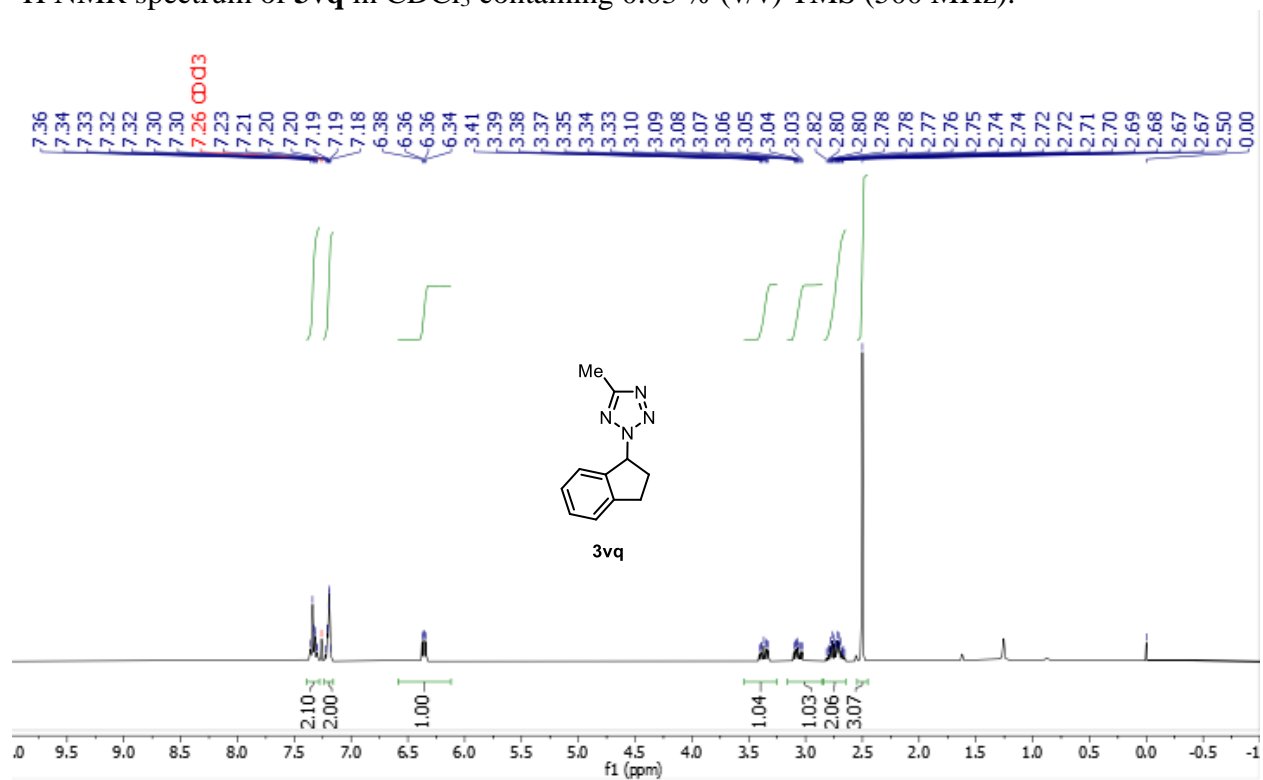
^1H NMR spectrum of **3vp'** in CDCl_3 containing 0.03 % (v/v) TMS (500 MHz).



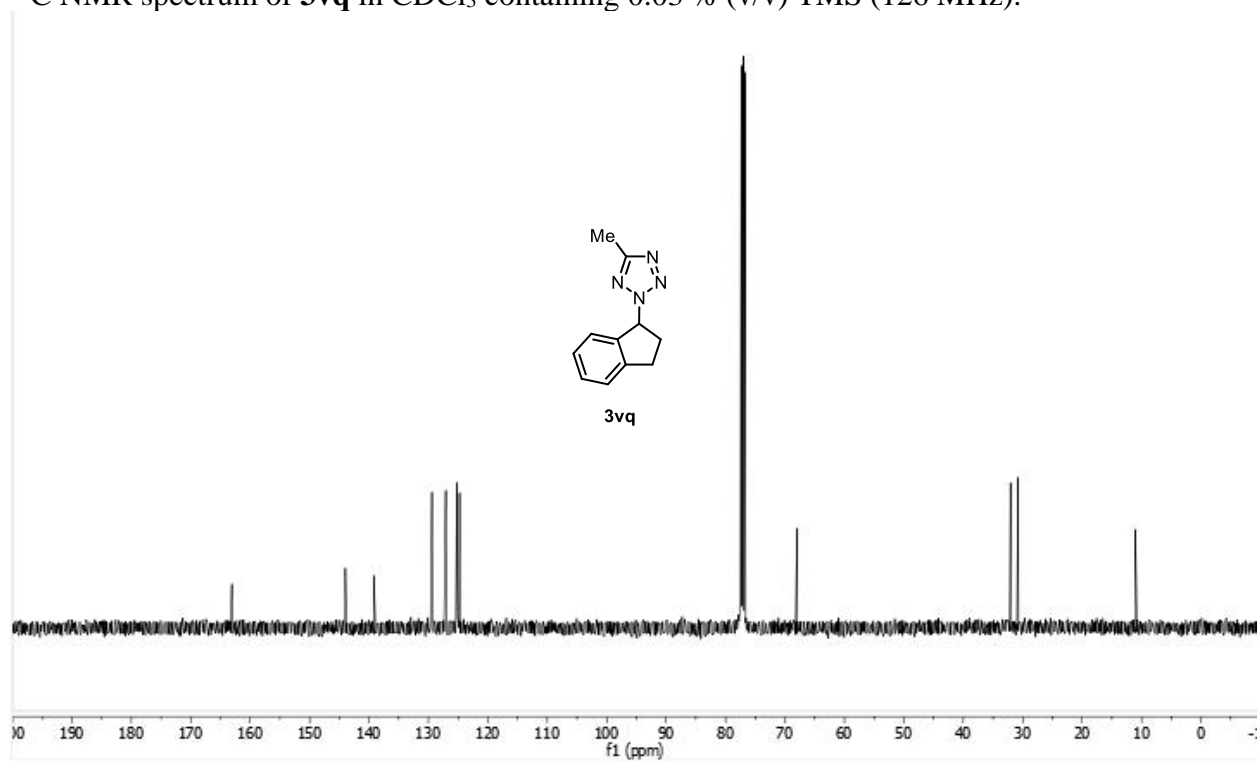
^{13}C NMR spectrum of **3vp'** in CDCl_3 containing 0.03 % (v/v) TMS (126 MHz).



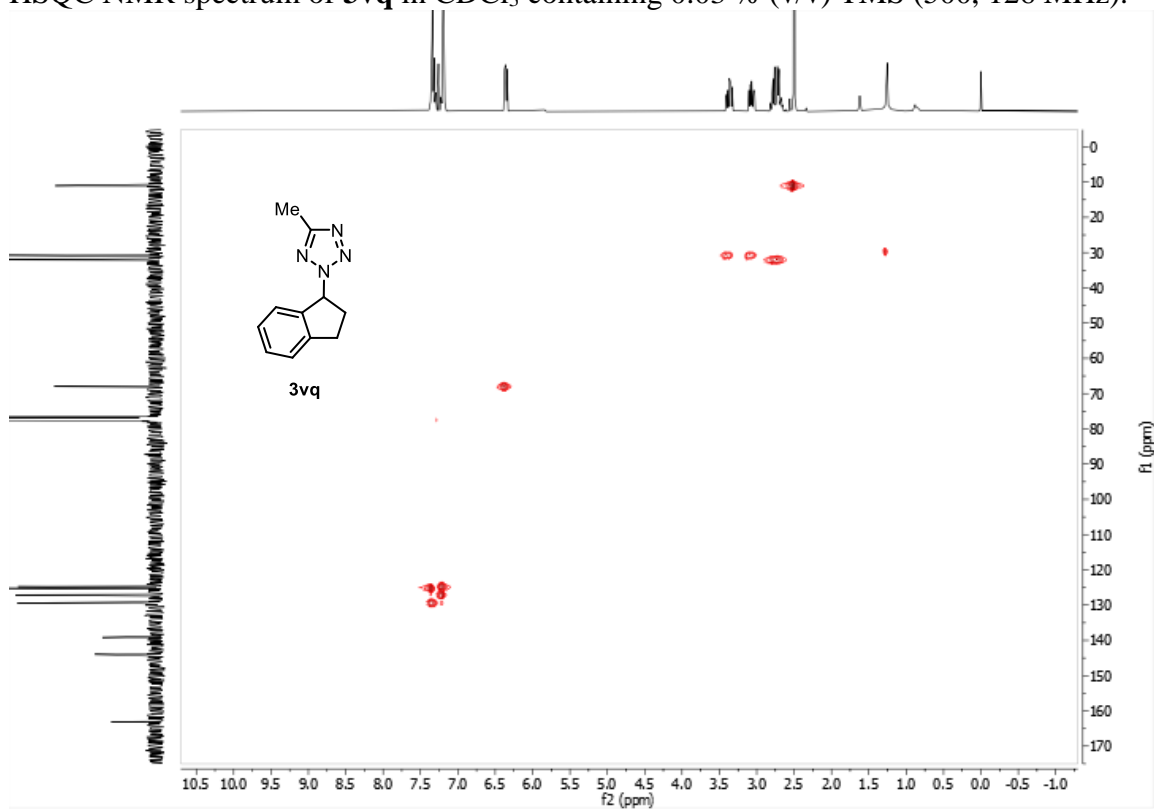
^1H NMR spectrum of **3vq** in CDCl_3 containing 0.03 % (v/v) TMS (500 MHz).



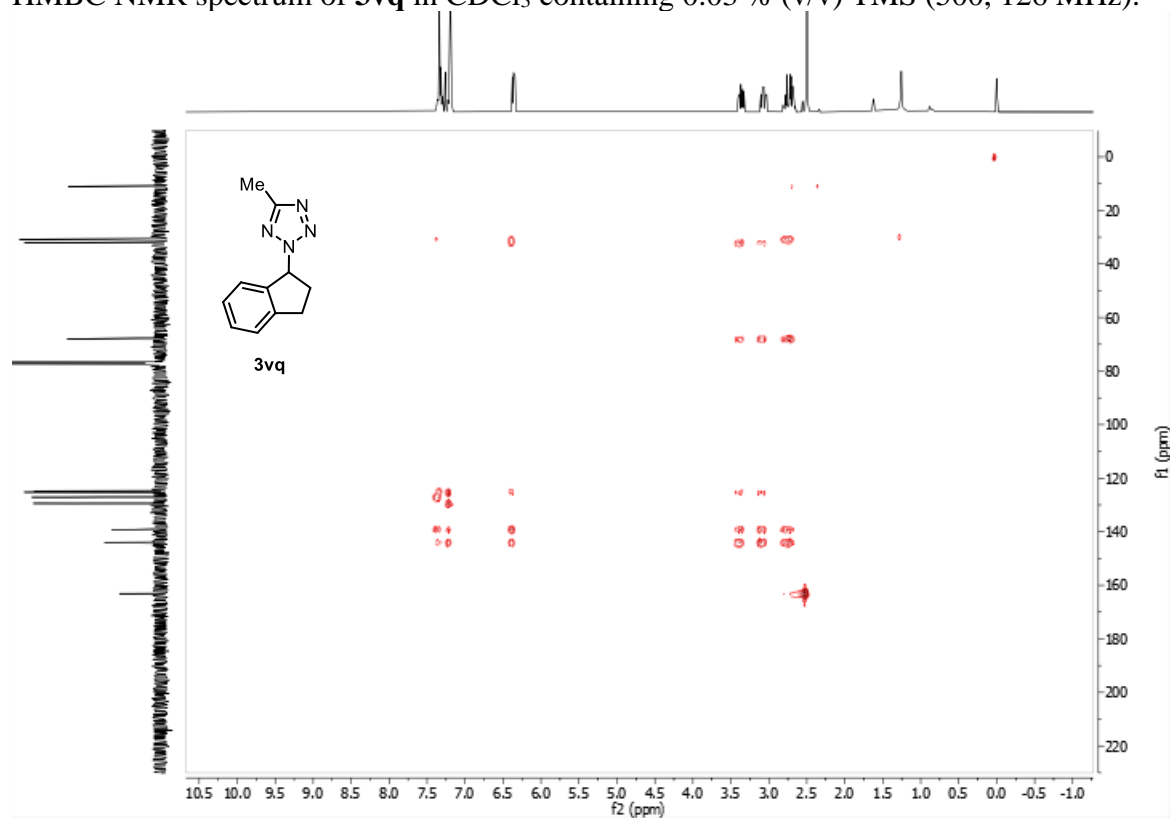
^{13}C NMR spectrum of **3vq** in CDCl_3 containing 0.03 % (v/v) TMS (126 MHz).



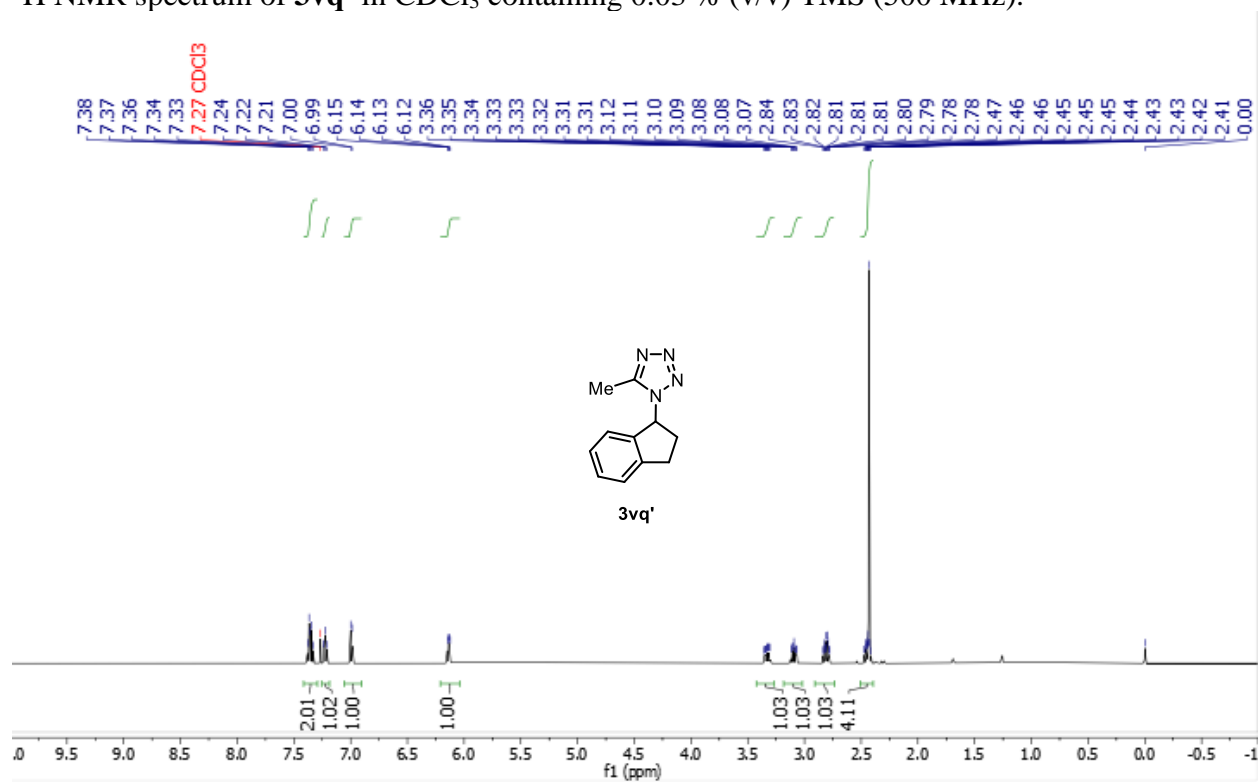
HSQC NMR spectrum of **3vq** in CDCl_3 containing 0.03 % (v/v) TMS (500, 126 MHz).



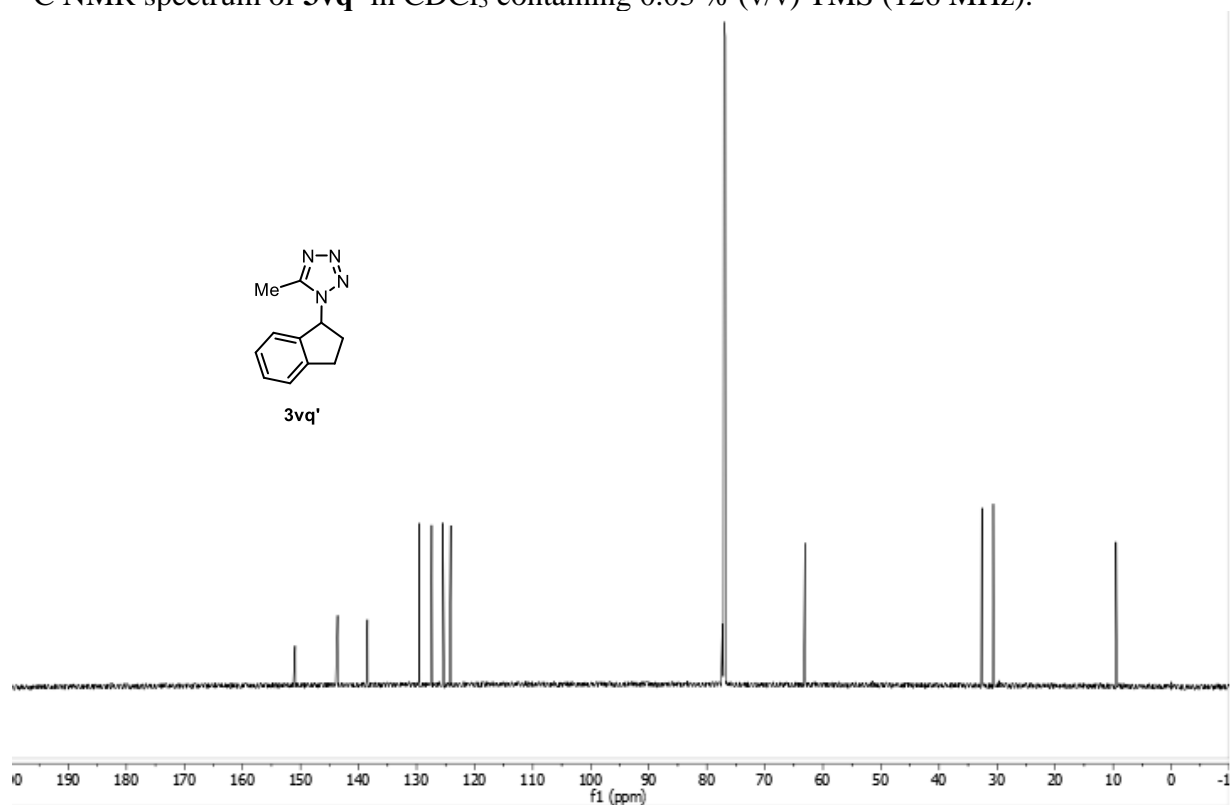
HMBC NMR spectrum of **3vq** in CDCl₃ containing 0.03 % (v/v) TMS (500, 126 MHz).



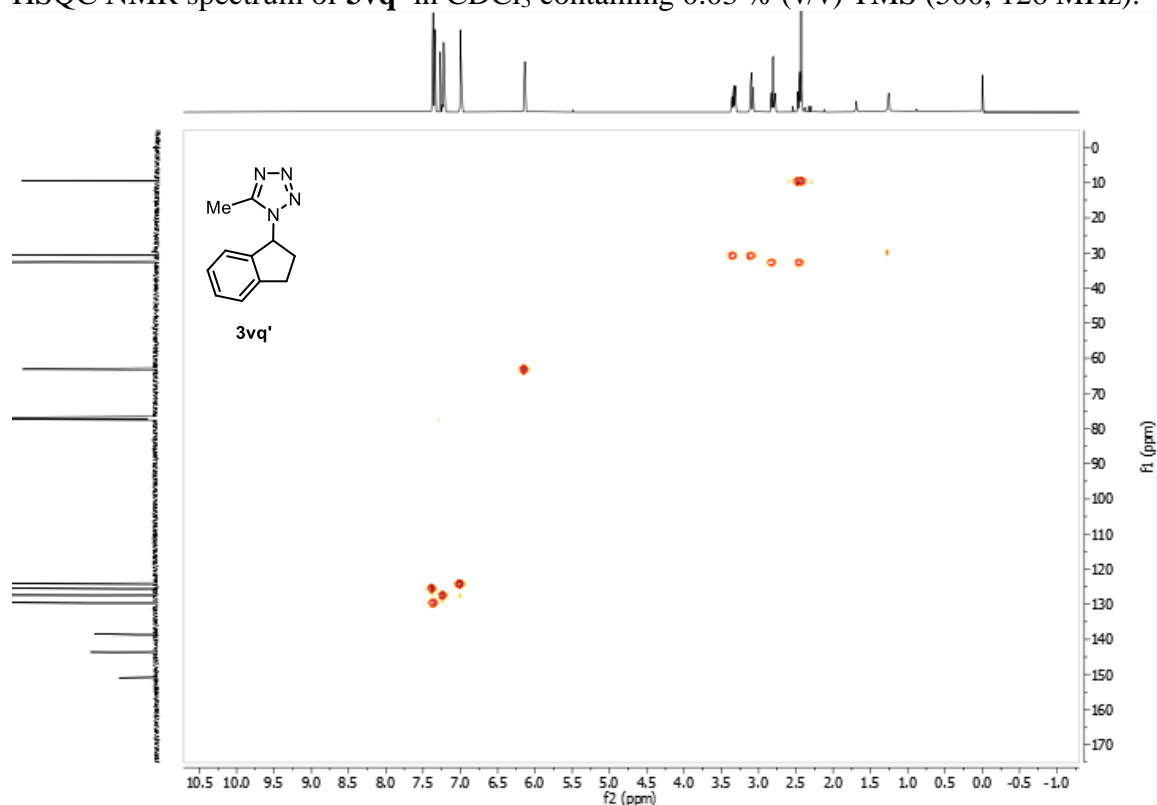
¹H NMR spectrum of **3vq'** in CDCl₃ containing 0.03 % (v/v) TMS (500 MHz).



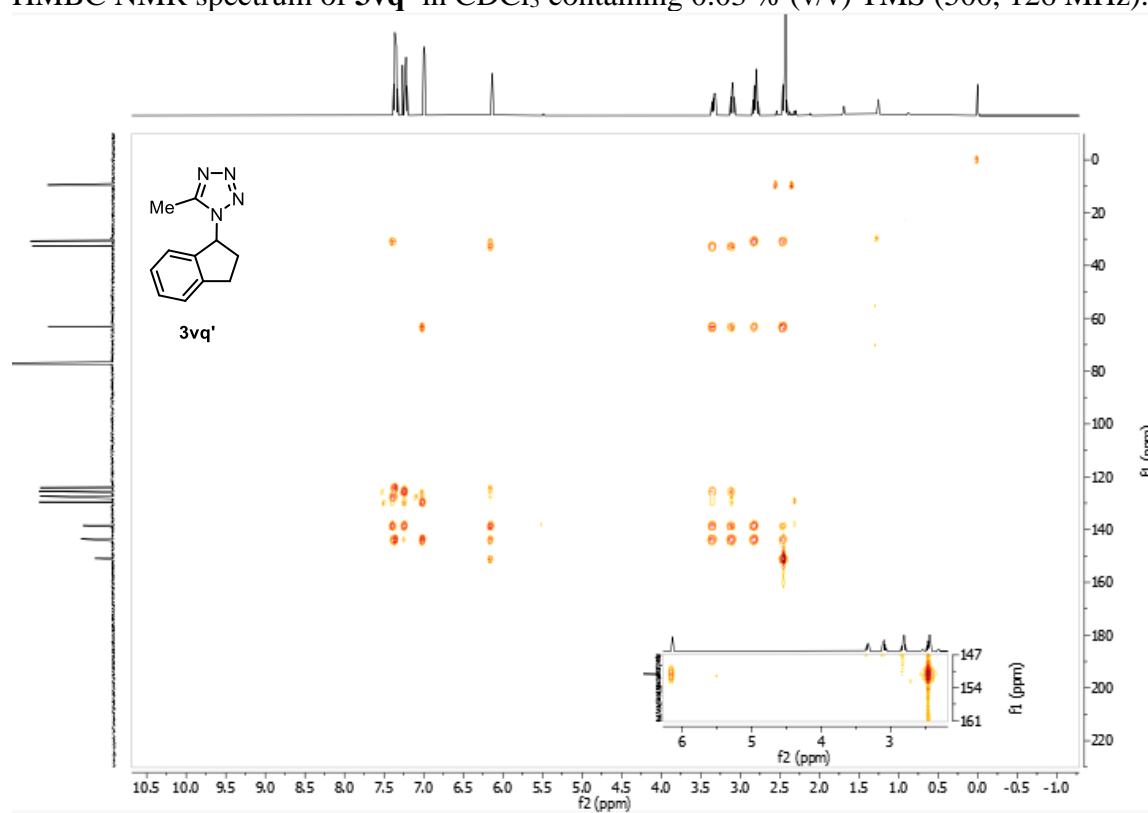
^{13}C NMR spectrum of **3vq'** in CDCl_3 containing 0.03 % (v/v) TMS (126 MHz).



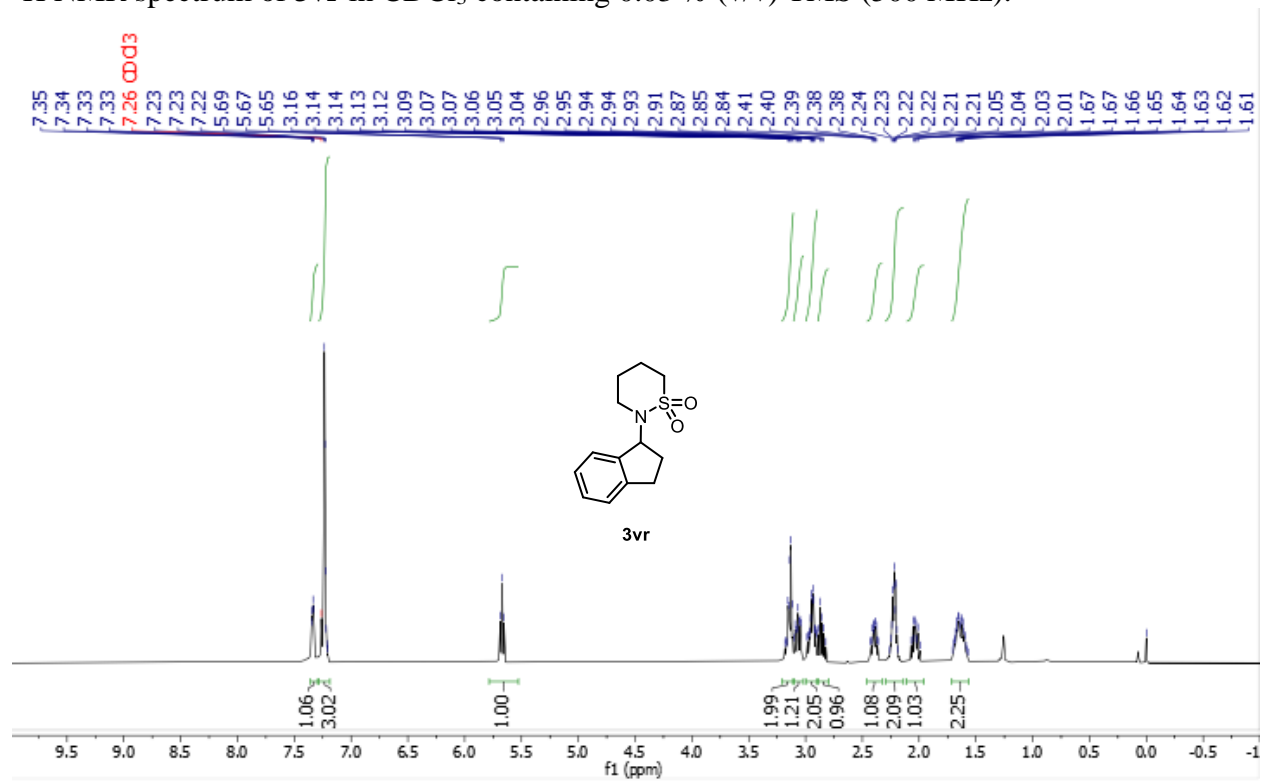
HSQC NMR spectrum of **3vq'** in CDCl_3 containing 0.03 % (v/v) TMS (500, 126 MHz).



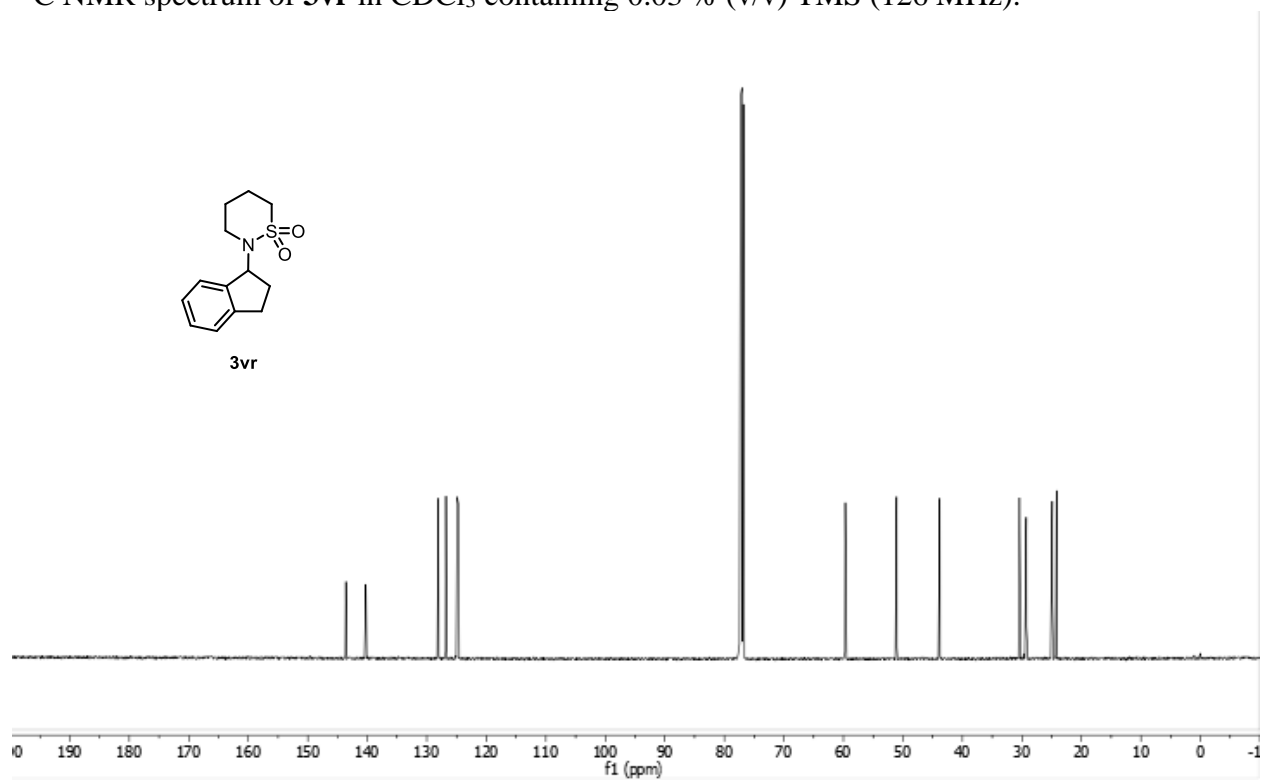
HMBC NMR spectrum of **3vq'** in CDCl₃ containing 0.03 % (v/v) TMS (500, 126 MHz).



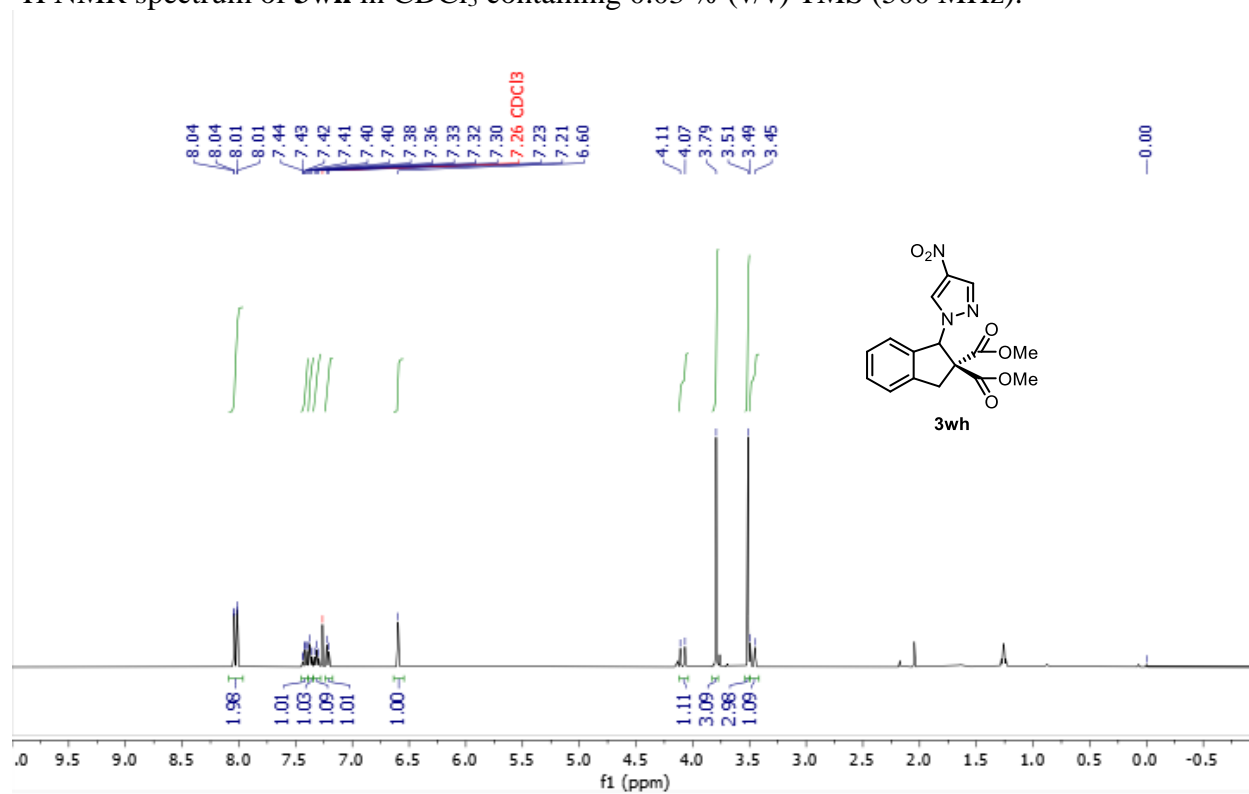
¹H NMR spectrum of **3vr** in CDCl₃ containing 0.03 % (v/v) TMS (500 MHz).



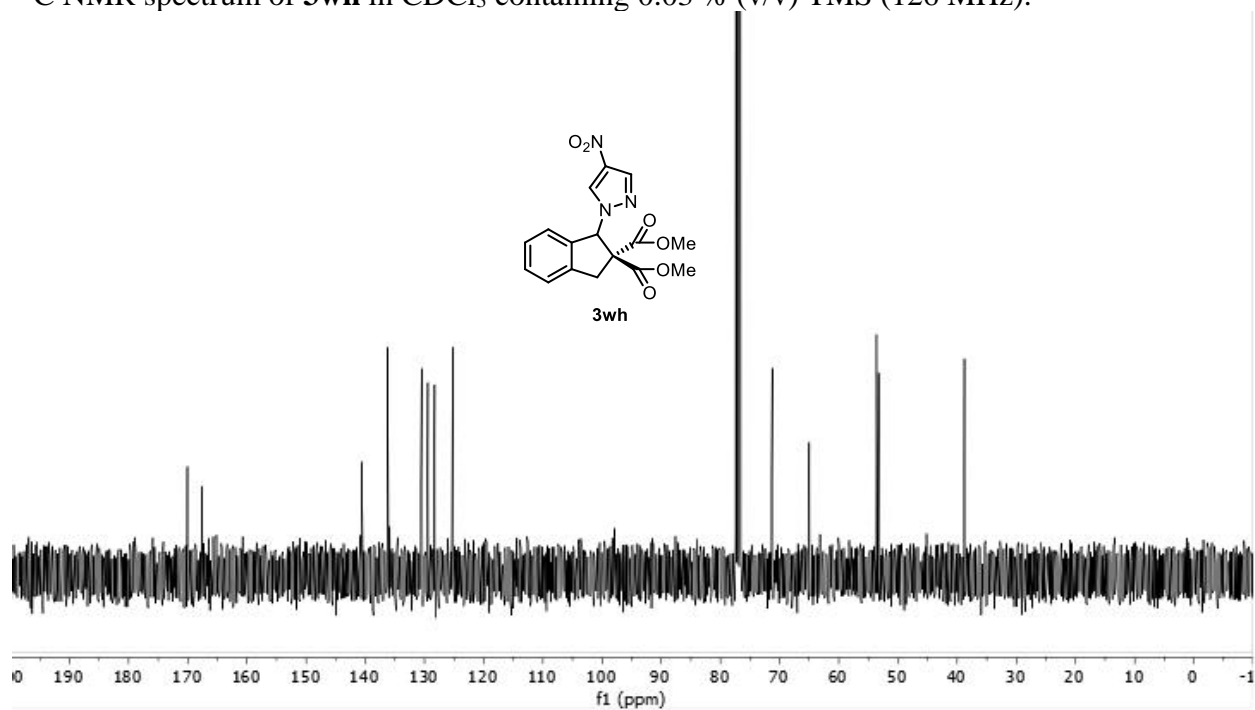
^{13}C NMR spectrum of **3vr** in CDCl_3 containing 0.03 % (v/v) TMS (126 MHz).



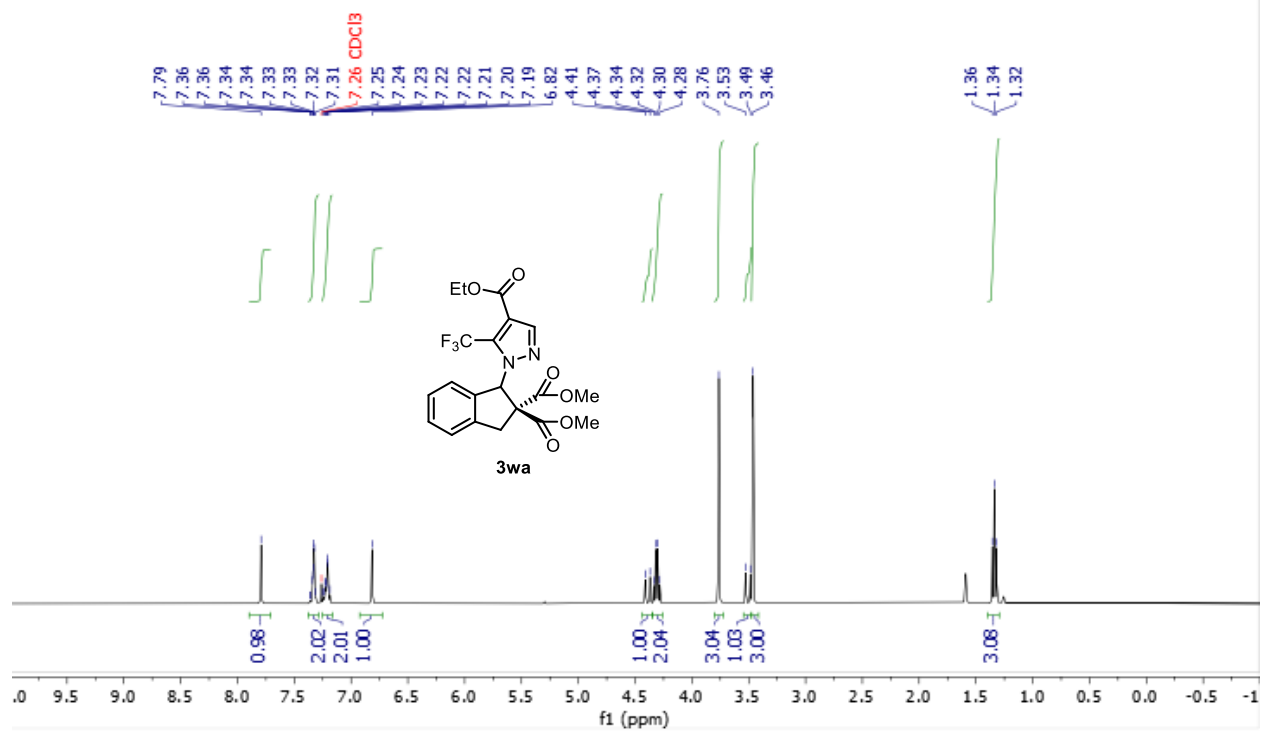
^1H NMR spectrum of **3wh** in CDCl_3 containing 0.03 % (v/v) TMS (500 MHz).



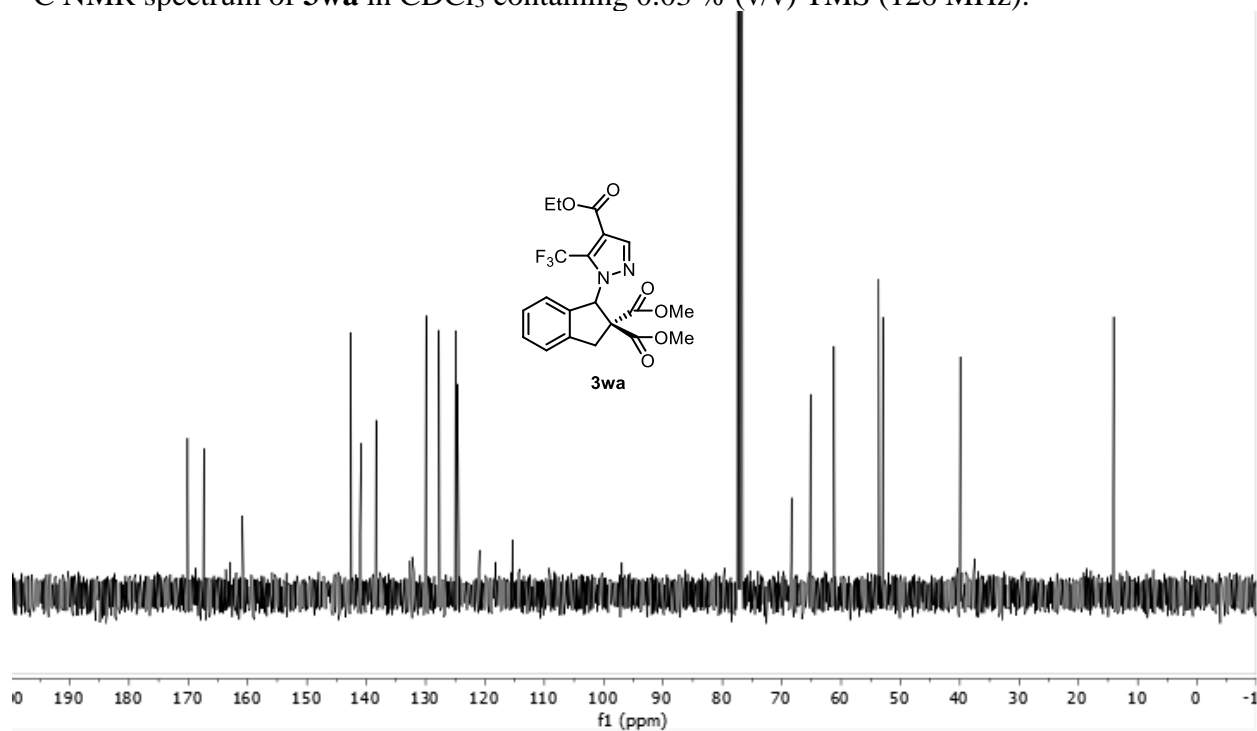
^{13}C NMR spectrum of **3wh** in CDCl_3 containing 0.03 % (v/v) TMS (126 MHz).



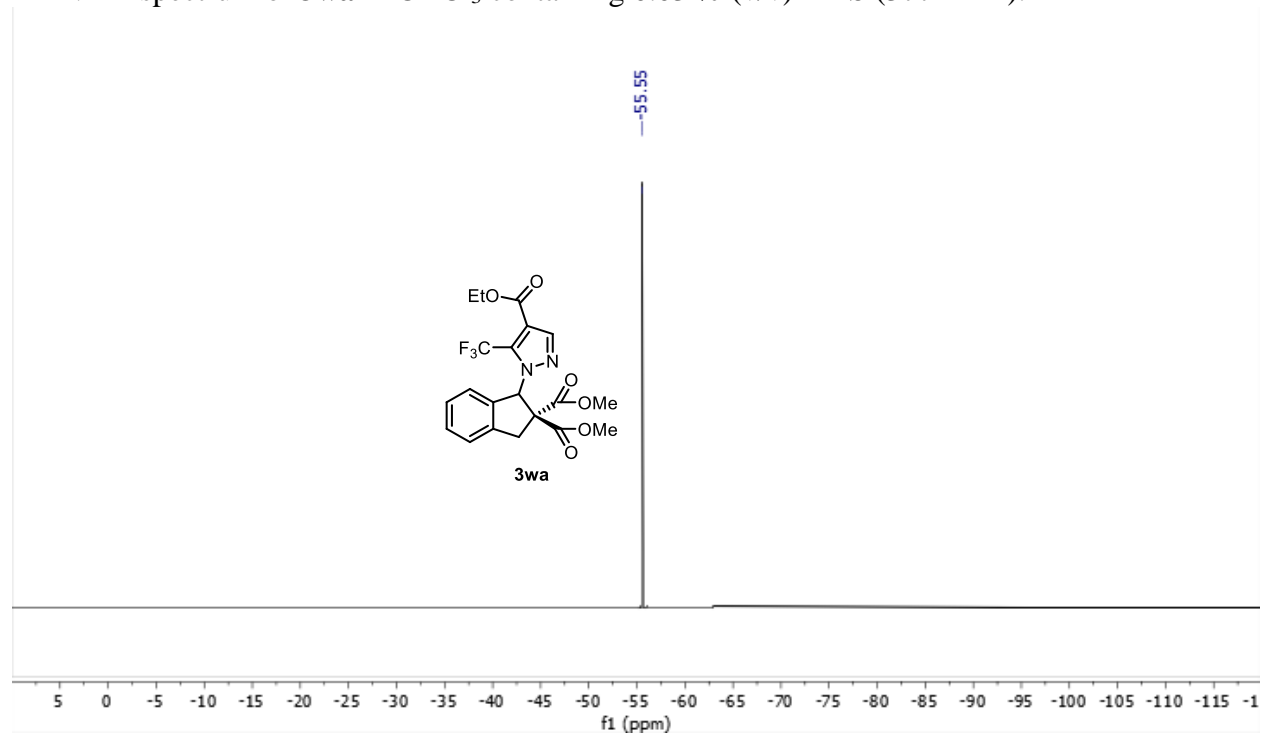
^1H NMR spectrum of **3wa** in CDCl_3 containing 0.03 % (v/v) TMS (500 MHz).



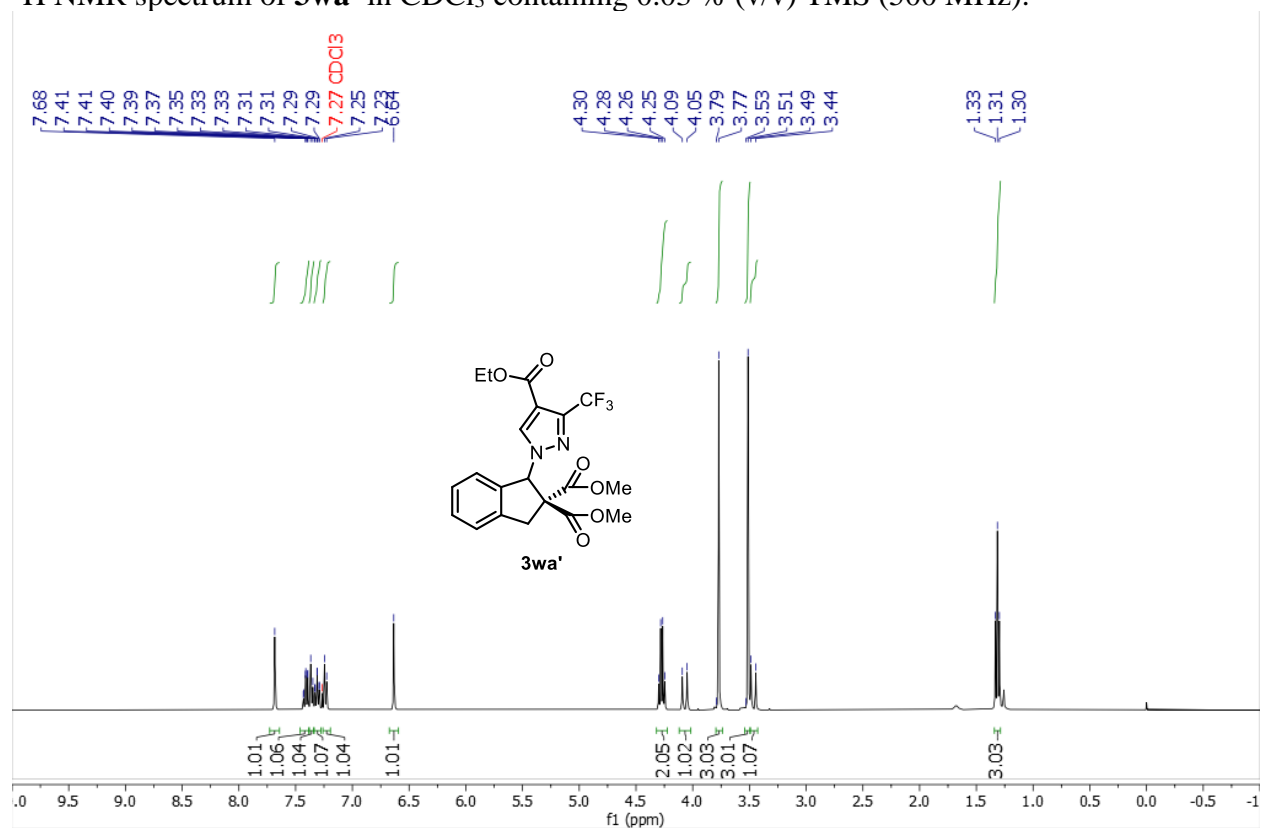
^{13}C NMR spectrum of **3wa** in CDCl_3 containing 0.03 % (v/v) TMS (126 MHz).



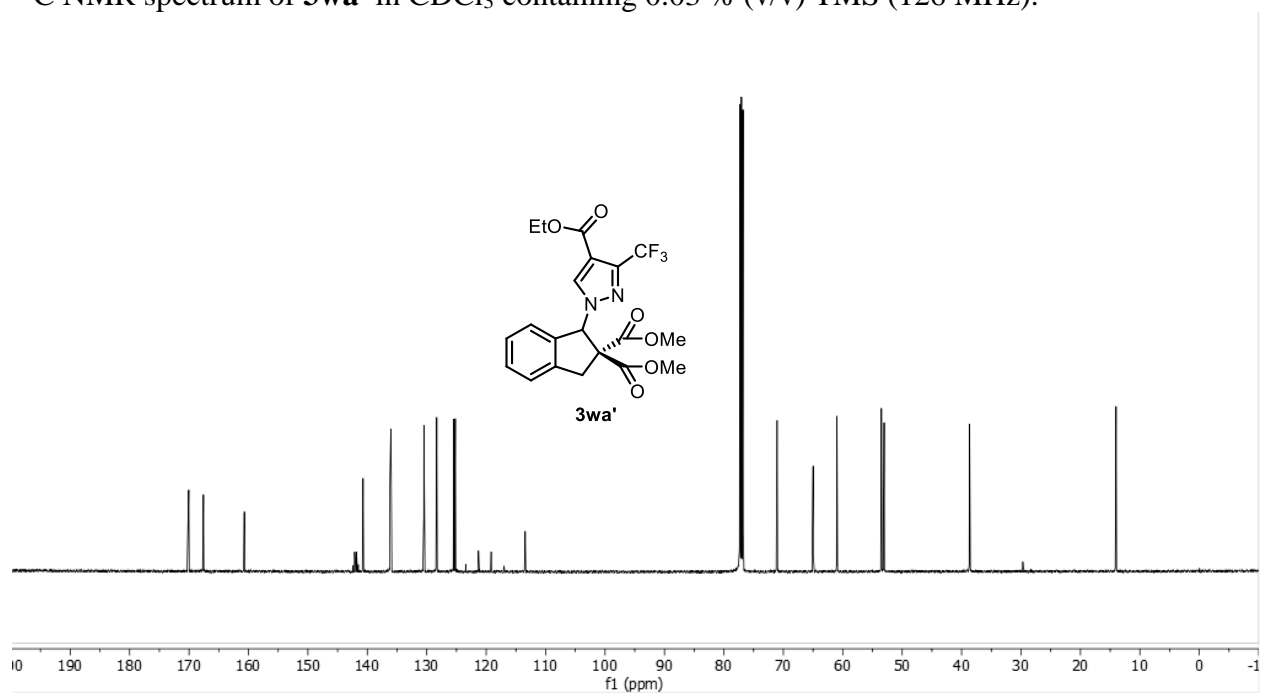
^{19}F NMR spectrum of **3wa** in CDCl_3 containing 0.03 % (v/v) TMS (377 MHz).



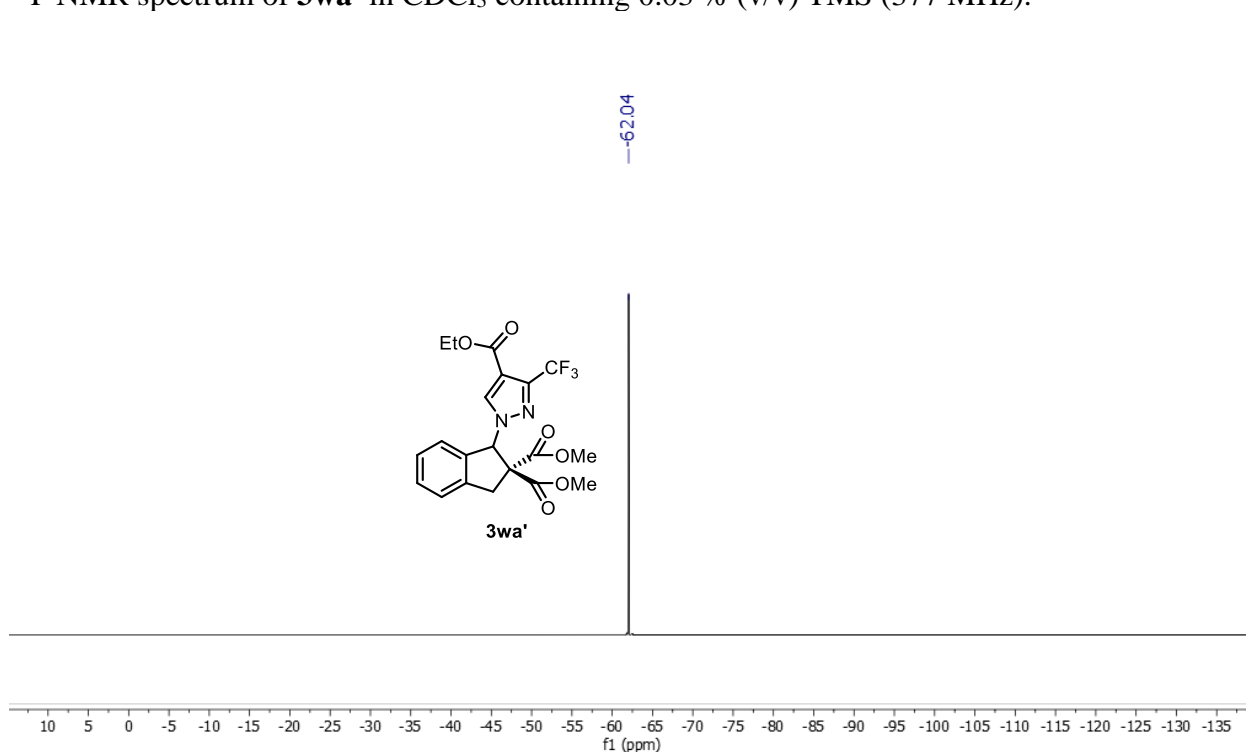
^1H NMR spectrum of **3wa'** in CDCl_3 containing 0.03 % (v/v) TMS (500 MHz).



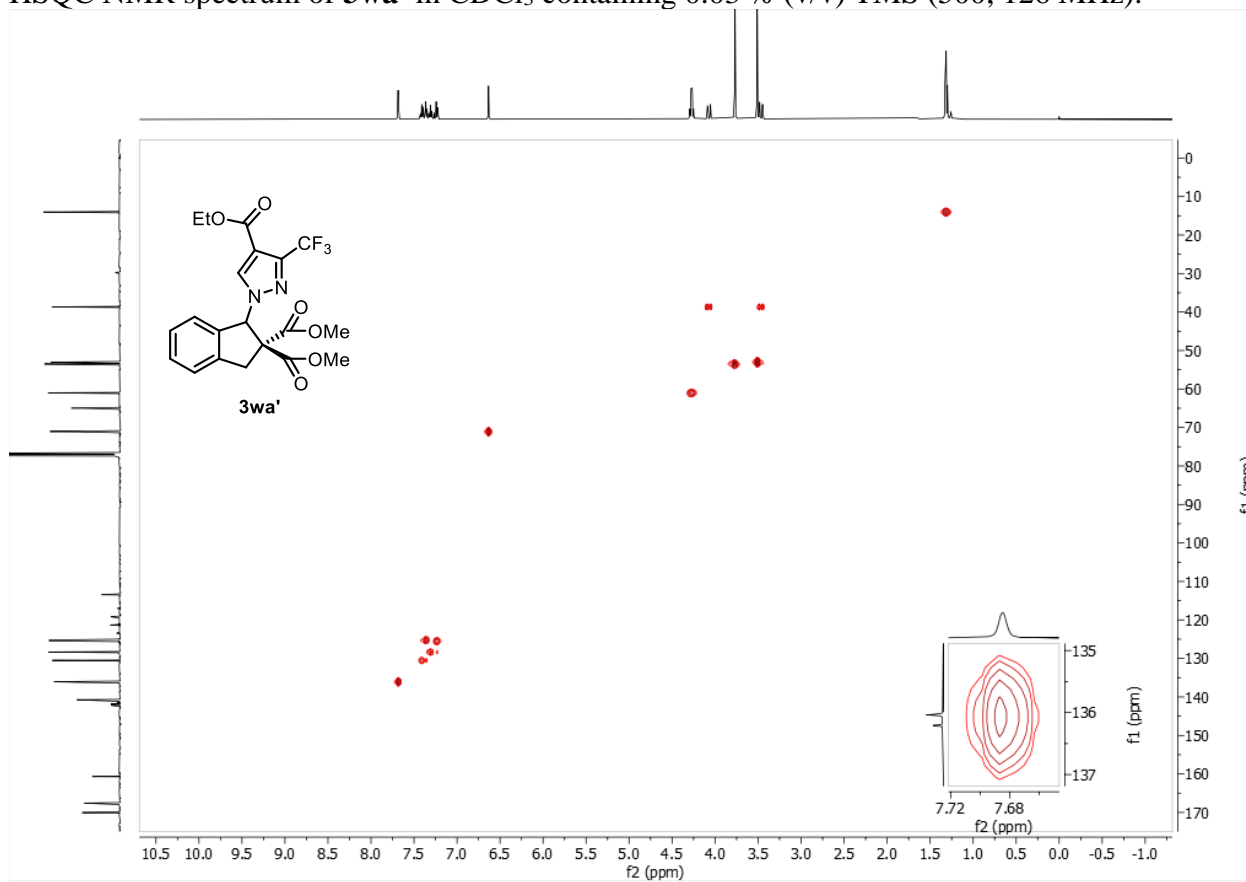
^{13}C NMR spectrum of **3wa'** in CDCl_3 containing 0.03 % (v/v) TMS (126 MHz).



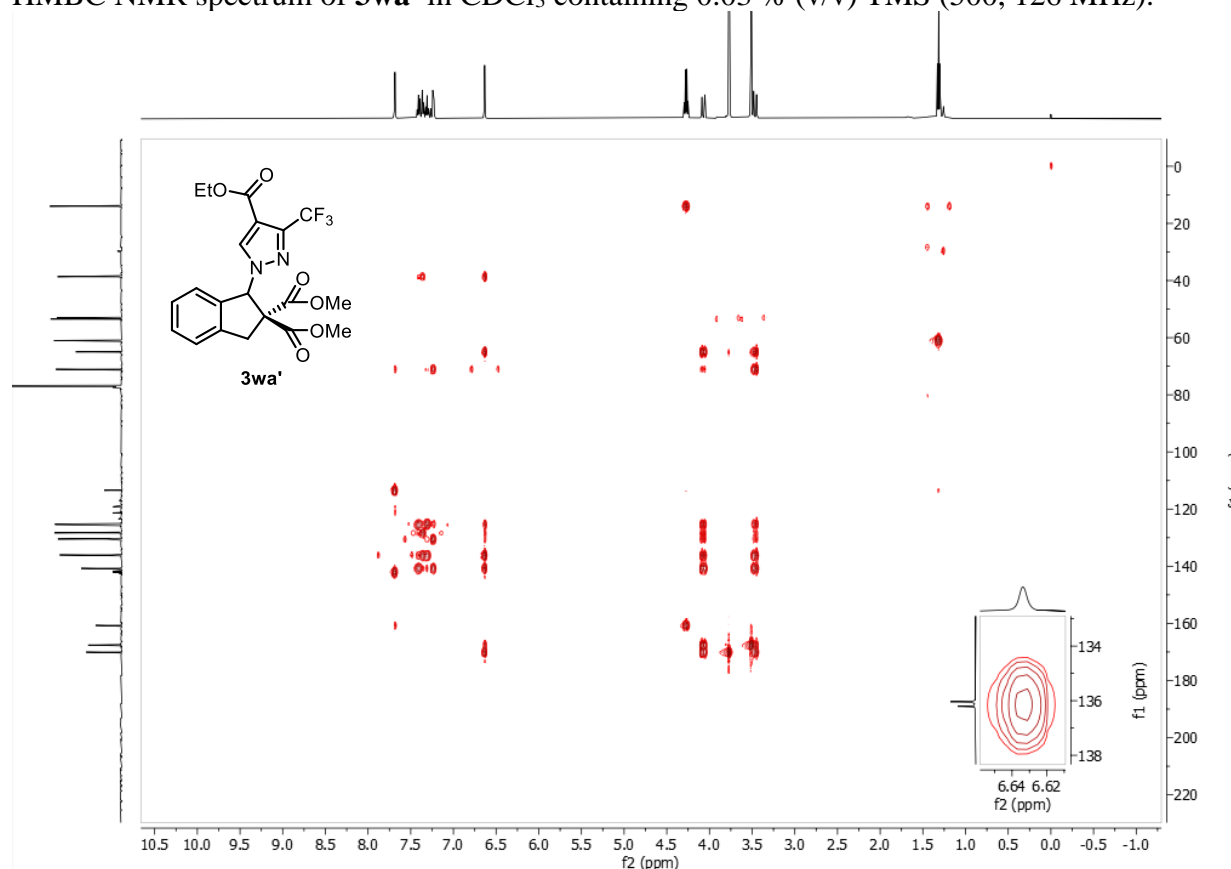
^{19}F NMR spectrum of **3wa'** in CDCl_3 containing 0.03 % (v/v) TMS (377 MHz).



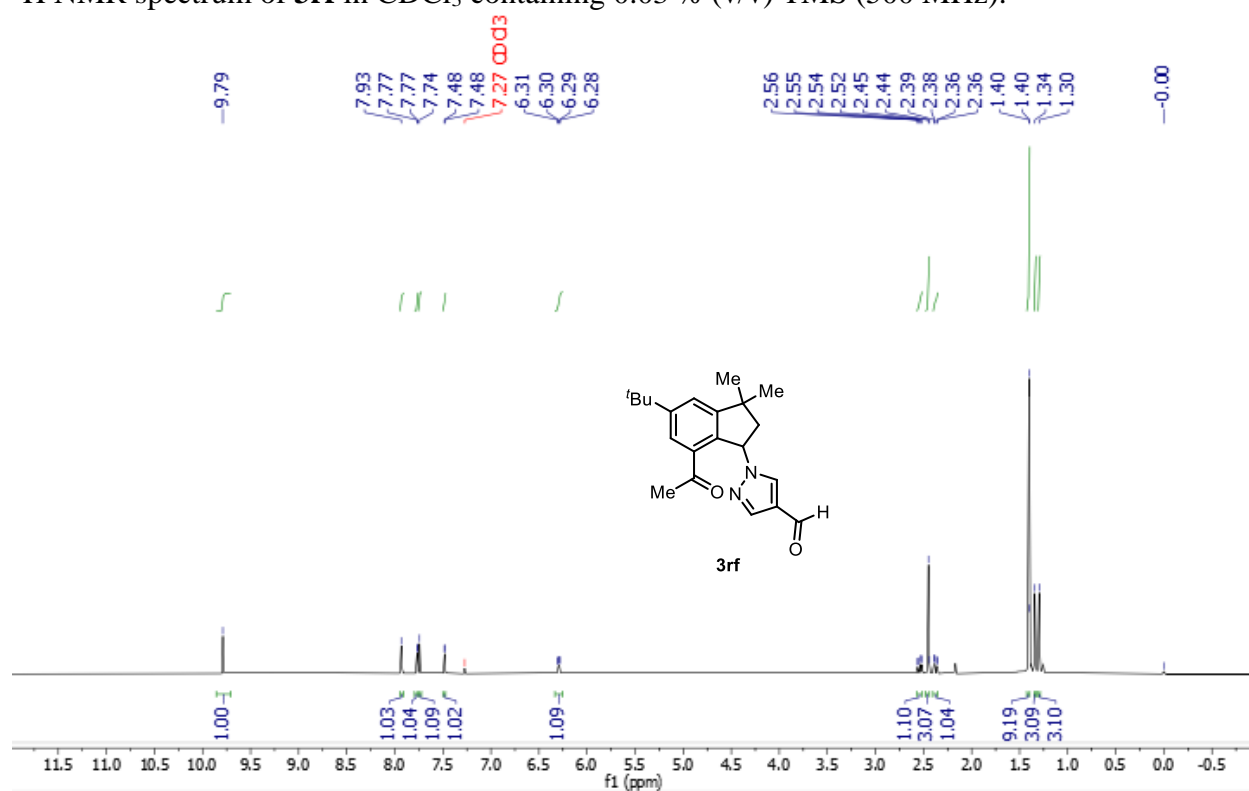
HSQC NMR spectrum of **3wa'** in CDCl_3 containing 0.03 % (v/v) TMS (500, 126 MHz).



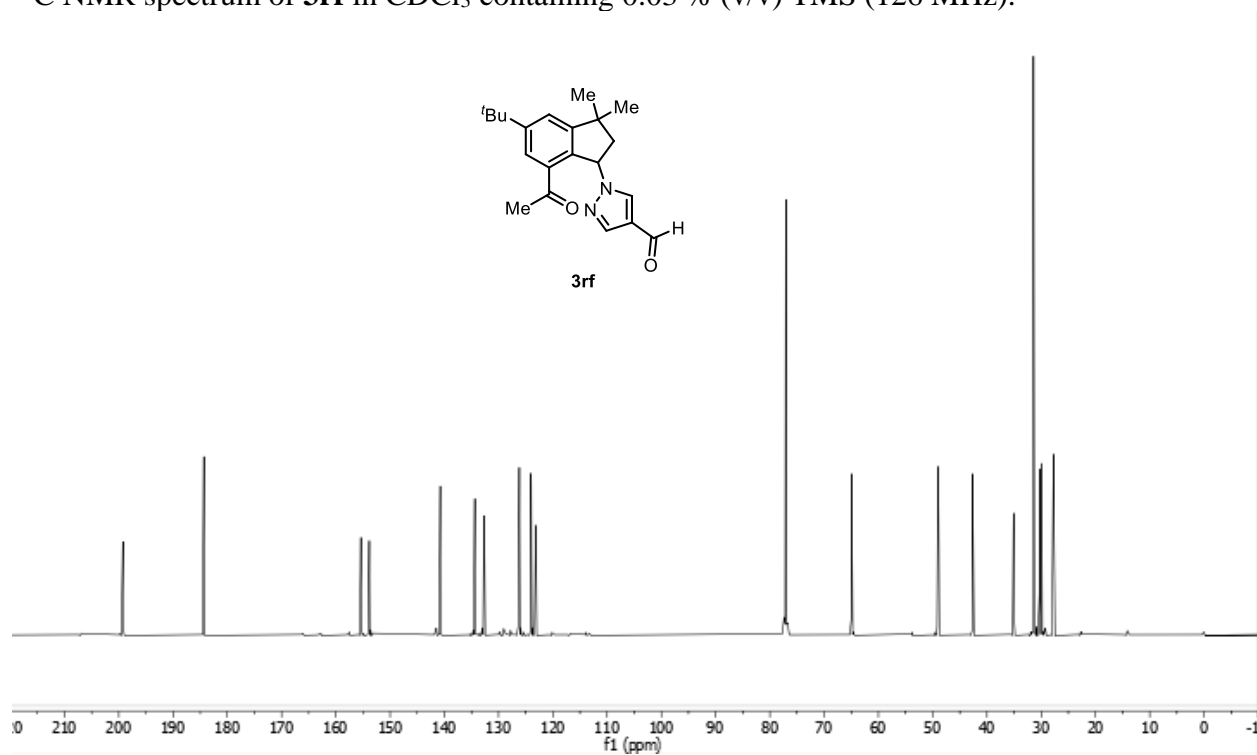
HMBC NMR spectrum of **3wa'** in CDCl₃ containing 0.03 % (v/v) TMS (500, 126 MHz).



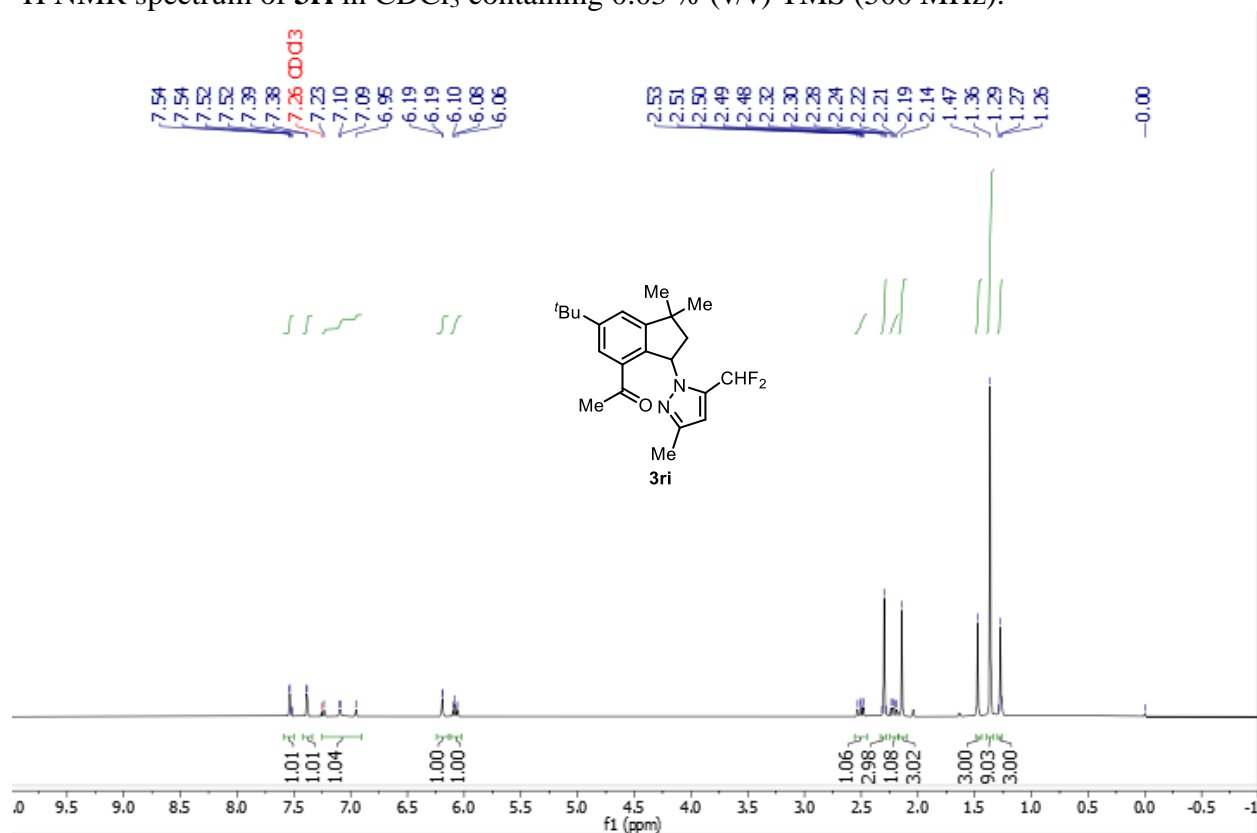
¹H NMR spectrum of **3rf** in CDCl₃ containing 0.03 % (v/v) TMS (500 MHz).



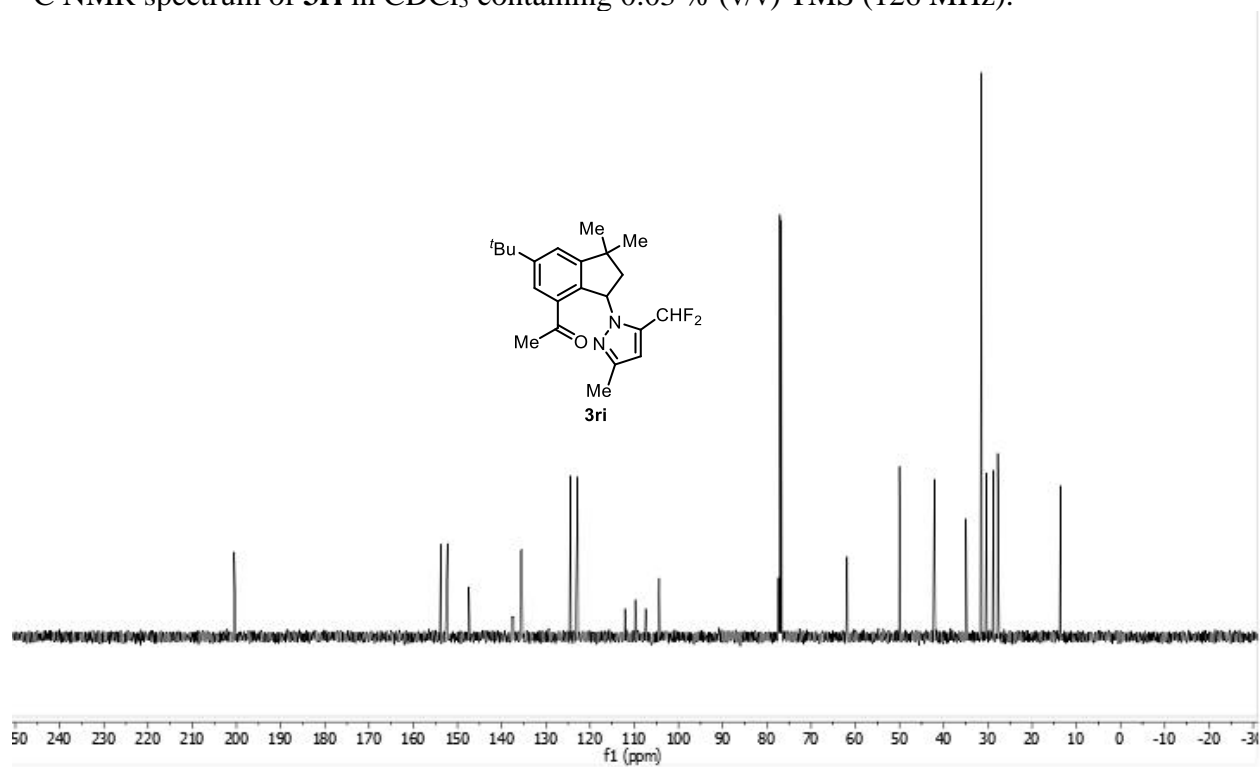
^{13}C NMR spectrum of **3rf** in CDCl_3 containing 0.03 % (v/v) TMS (126 MHz).



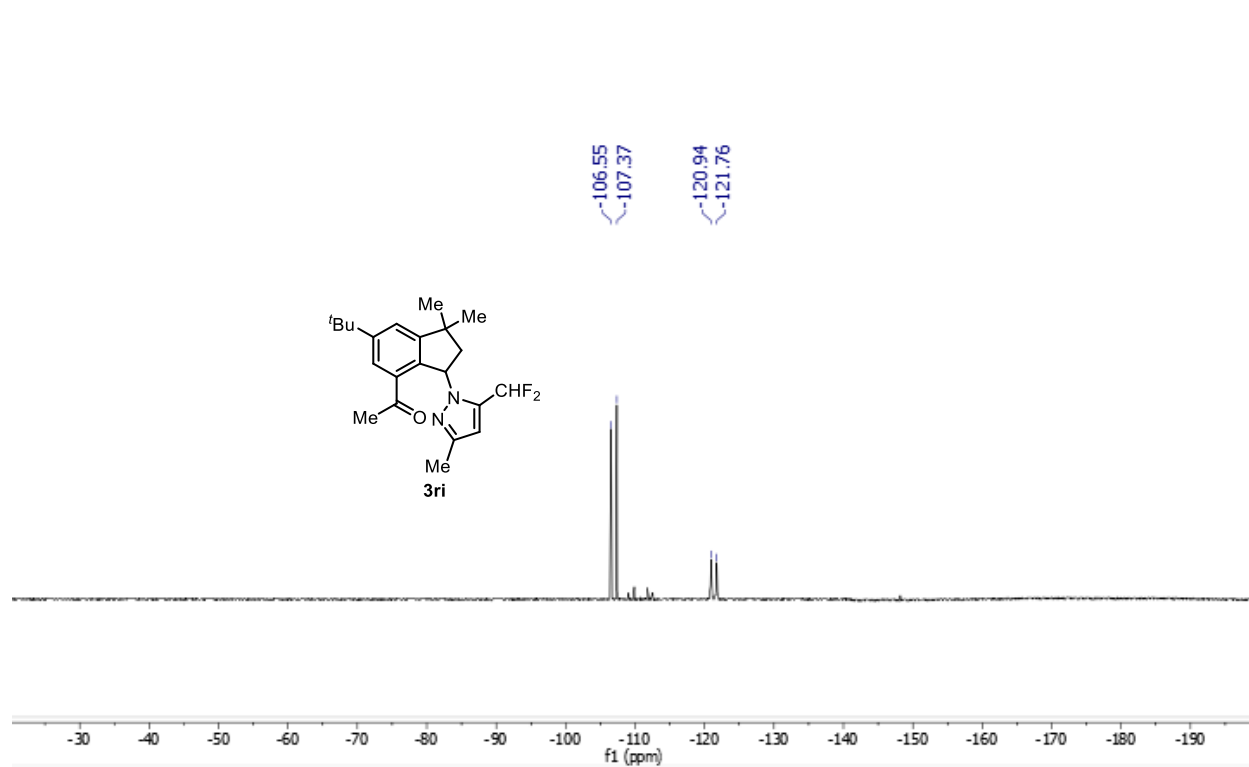
^1H NMR spectrum of **3ri** in CDCl_3 containing 0.03 % (v/v) TMS (500 MHz).



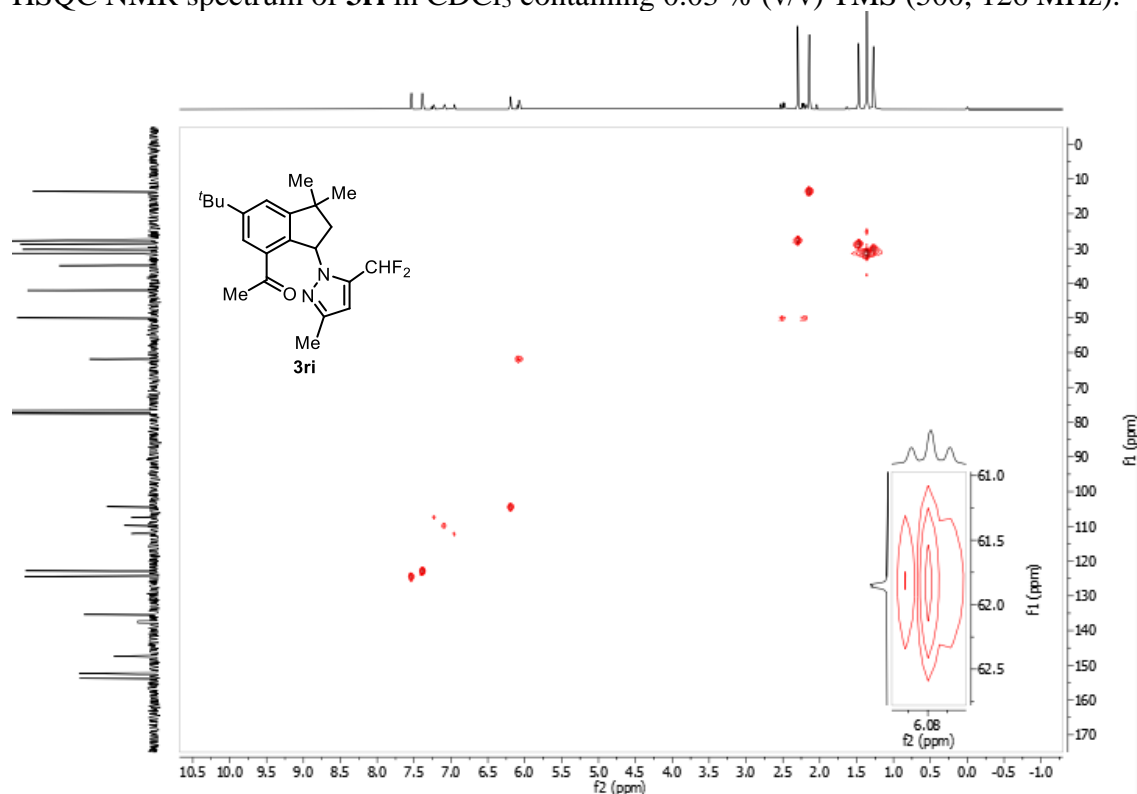
^{13}C NMR spectrum of **3ri** in CDCl_3 containing 0.03 % (v/v) TMS (126 MHz).



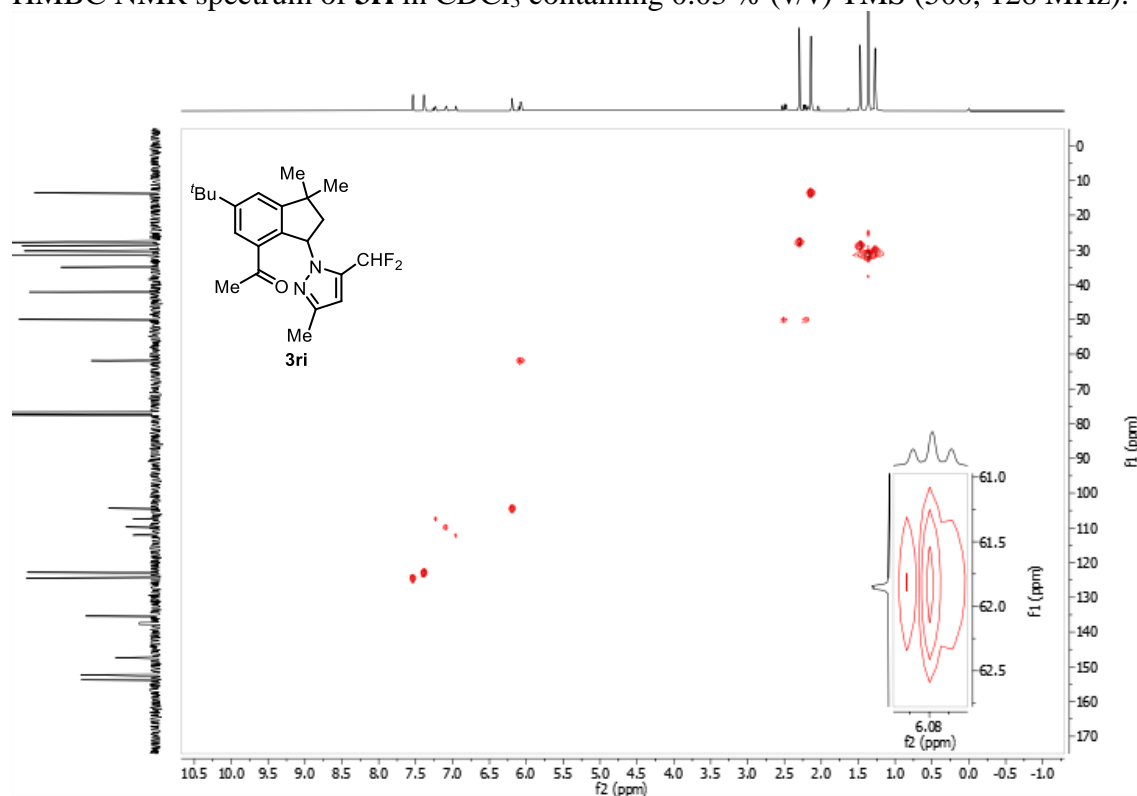
^{19}F NMR spectrum of **3ri** in CDCl_3 containing 0.03 % (v/v) TMS (377 MHz).



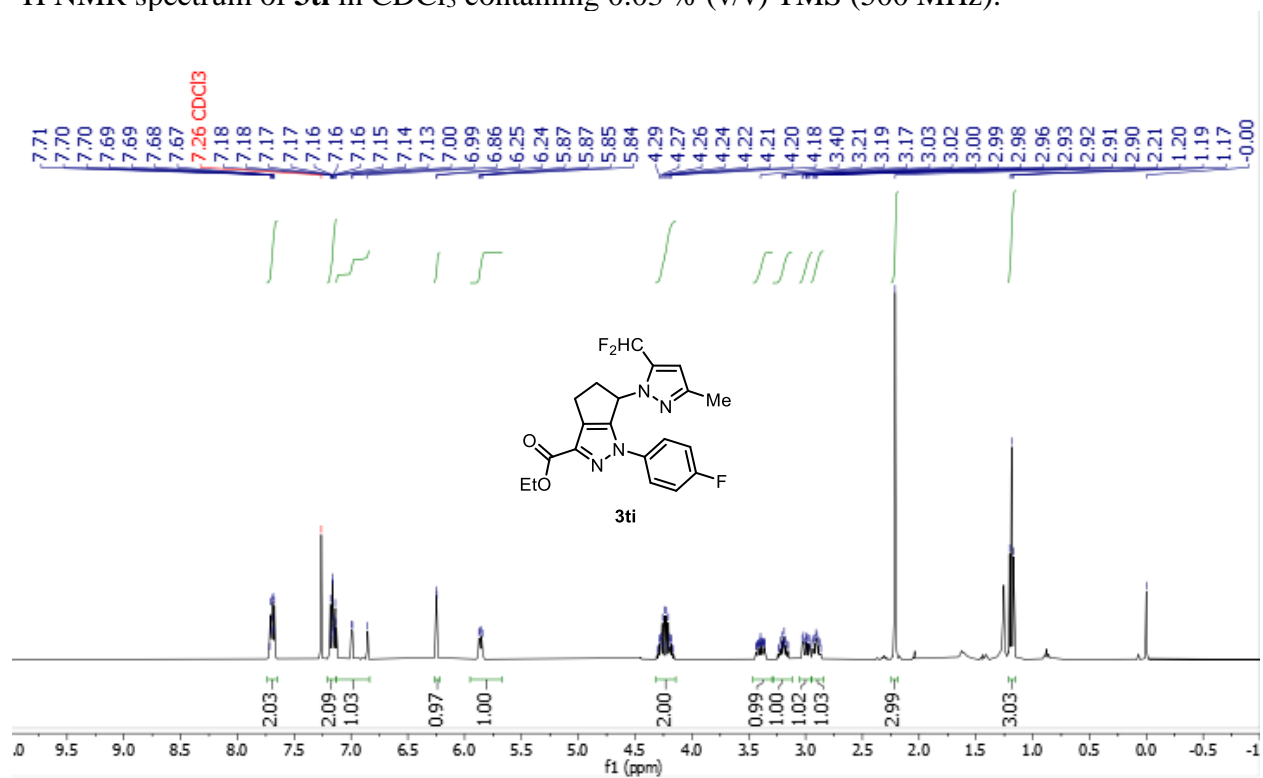
HSQC NMR spectrum of **3ri** in CDCl₃ containing 0.03 % (v/v) TMS (500, 126 MHz).



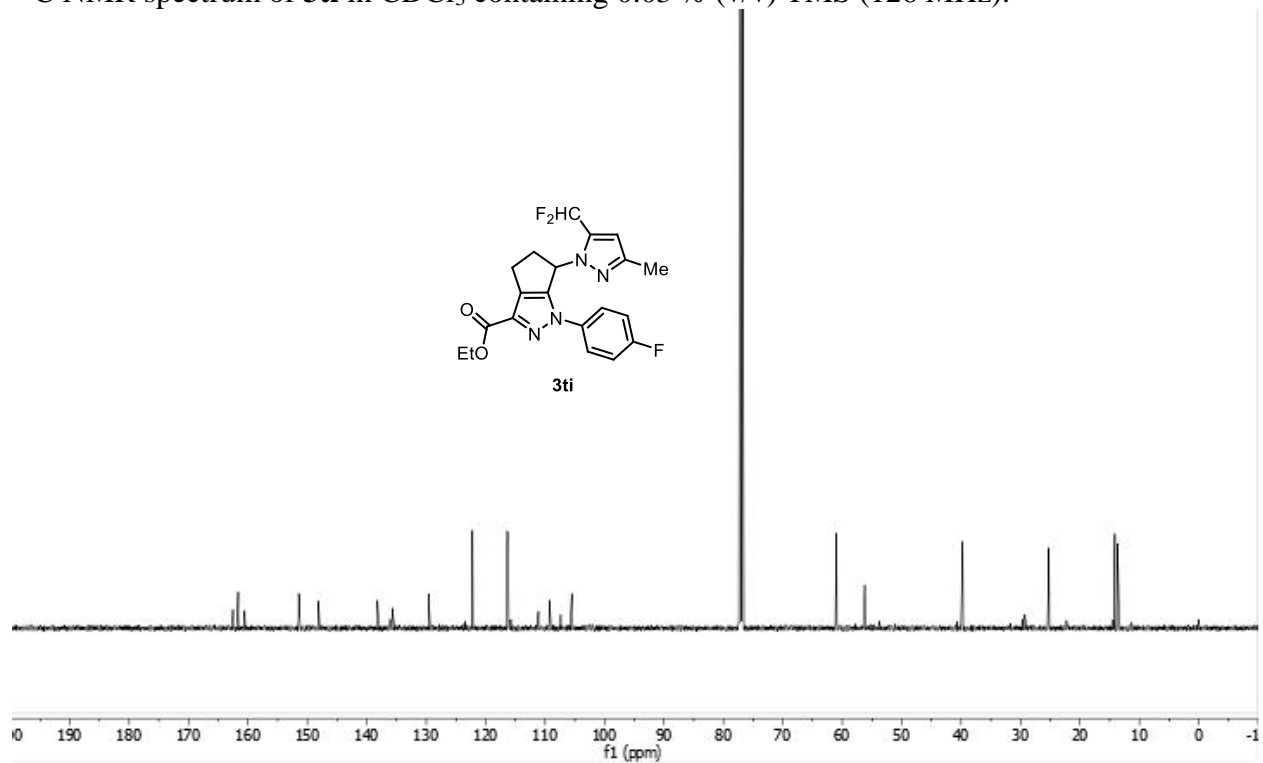
HMBC NMR spectrum of **3ri** in CDCl₃ containing 0.03 % (v/v) TMS (500, 126 MHz).



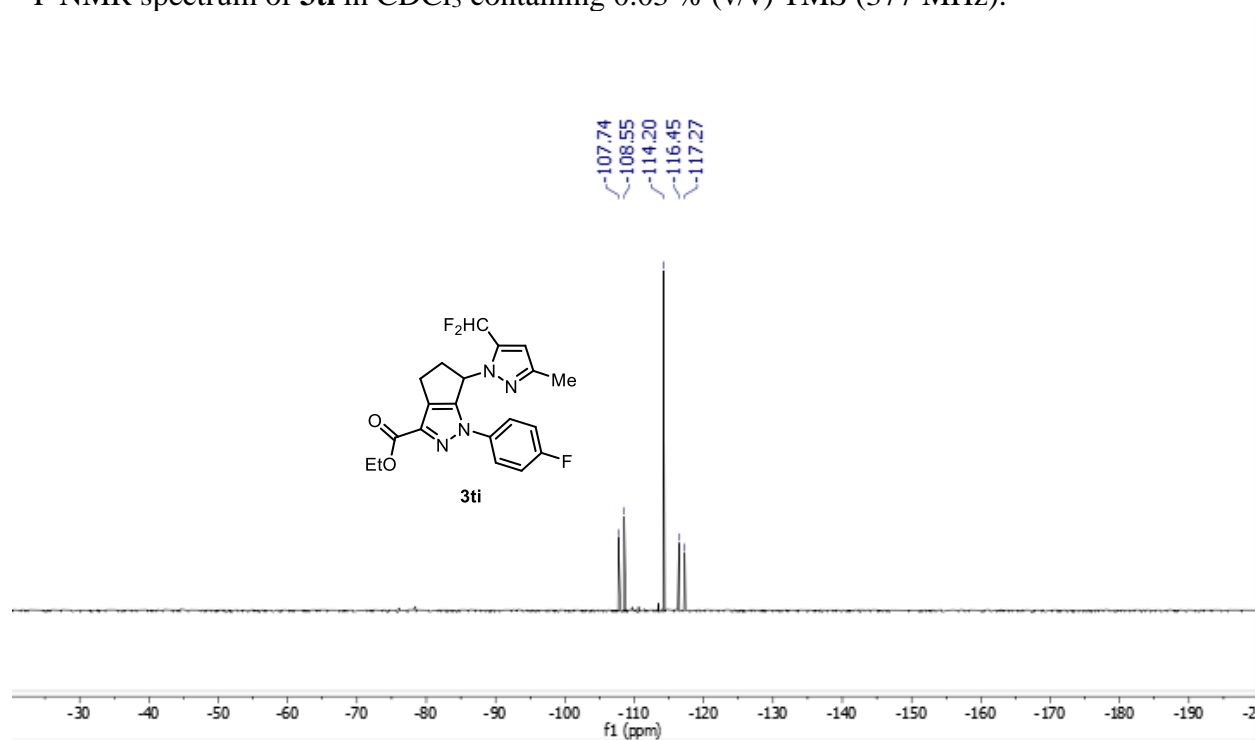
^1H NMR spectrum of **3ti** in CDCl_3 containing 0.03 % (v/v) TMS (500 MHz).



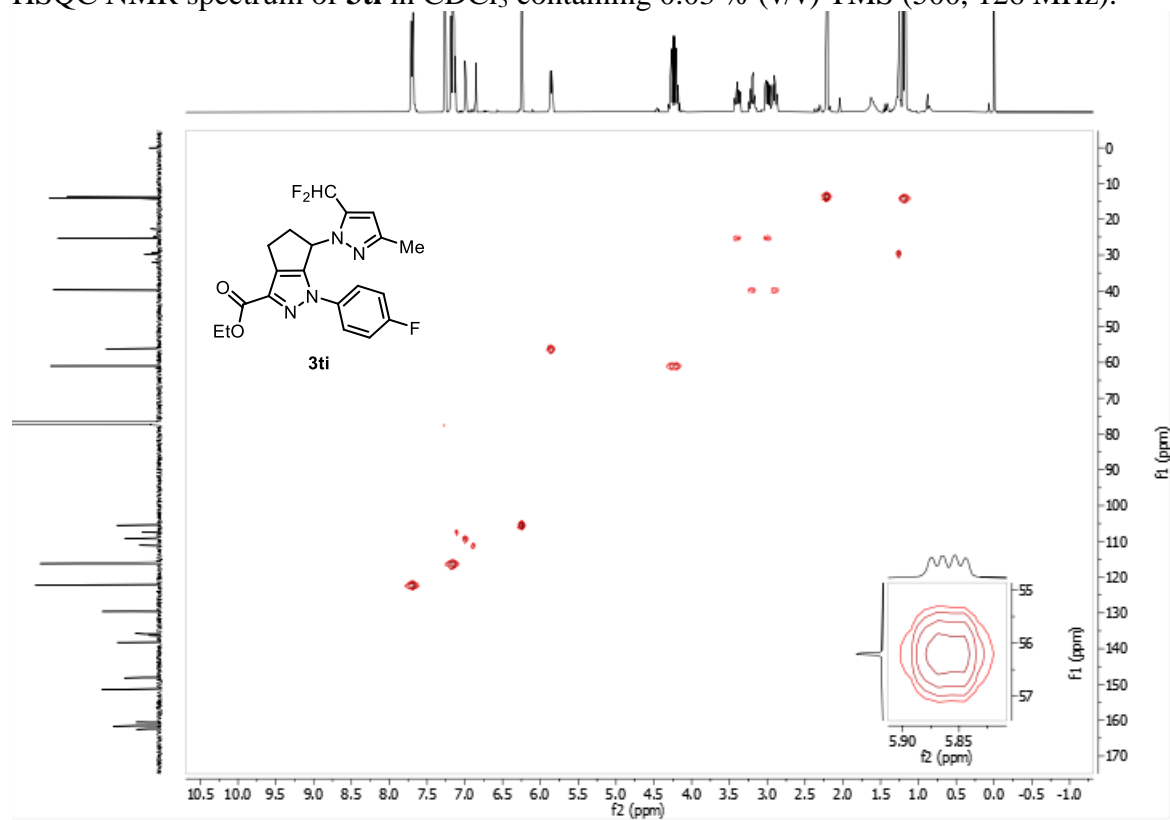
^{13}C NMR spectrum of **3ti** in CDCl_3 containing 0.03 % (v/v) TMS (126 MHz).



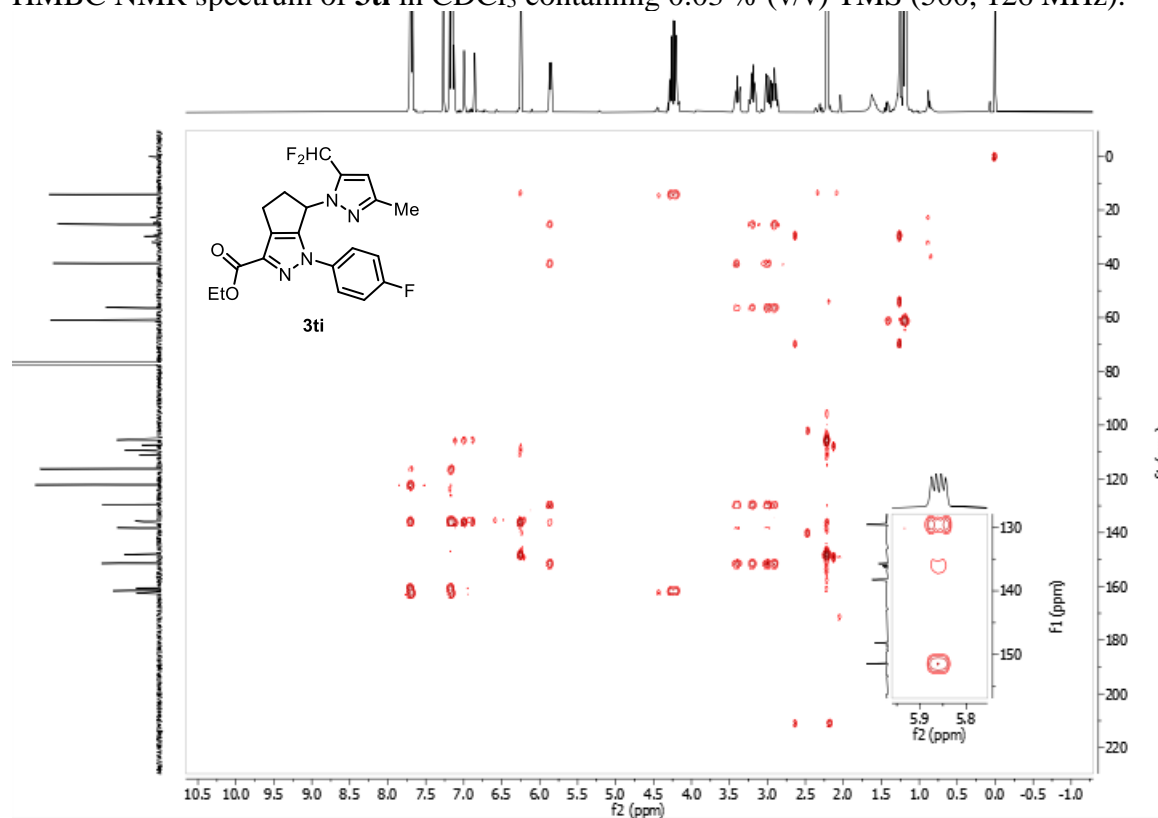
^{19}F NMR spectrum of **3ti** in CDCl_3 containing 0.03 % (v/v) TMS (377 MHz).



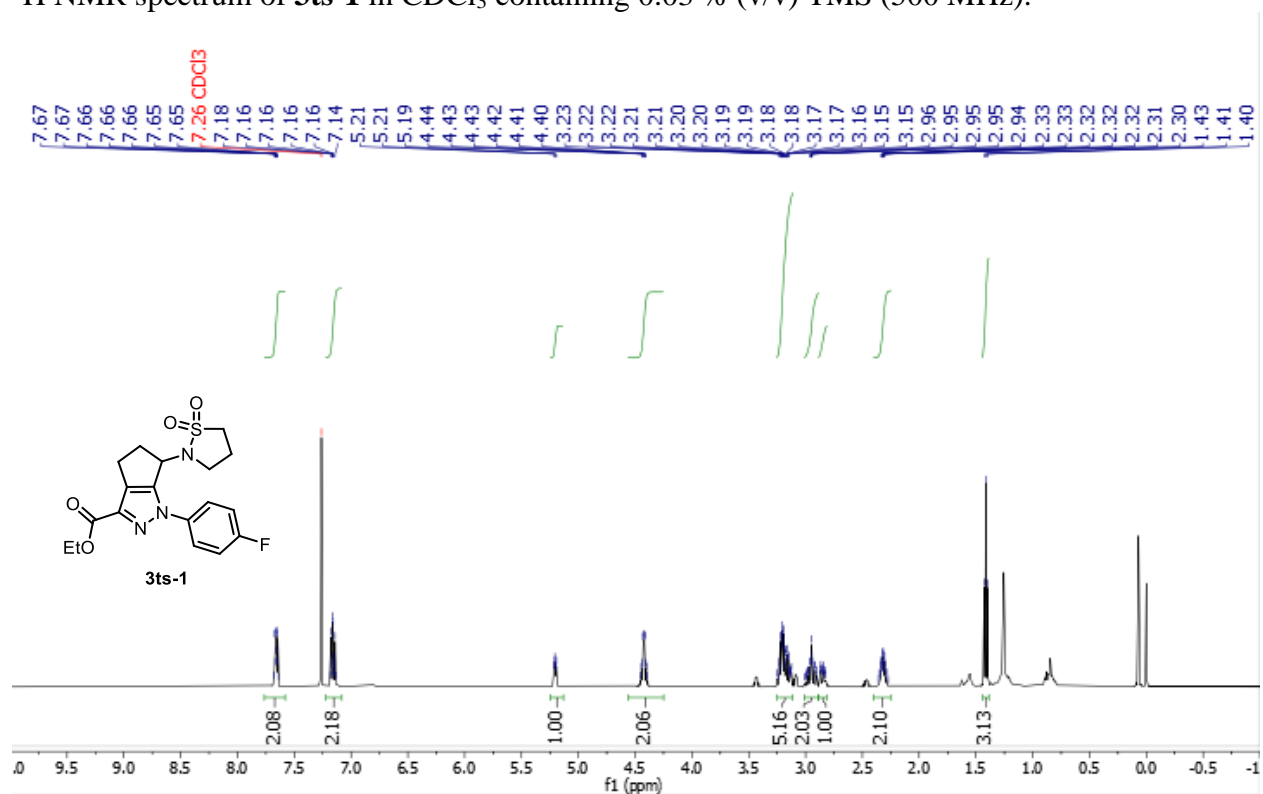
HSQC NMR spectrum of **3ti** in CDCl_3 containing 0.03 % (v/v) TMS (500, 126 MHz).



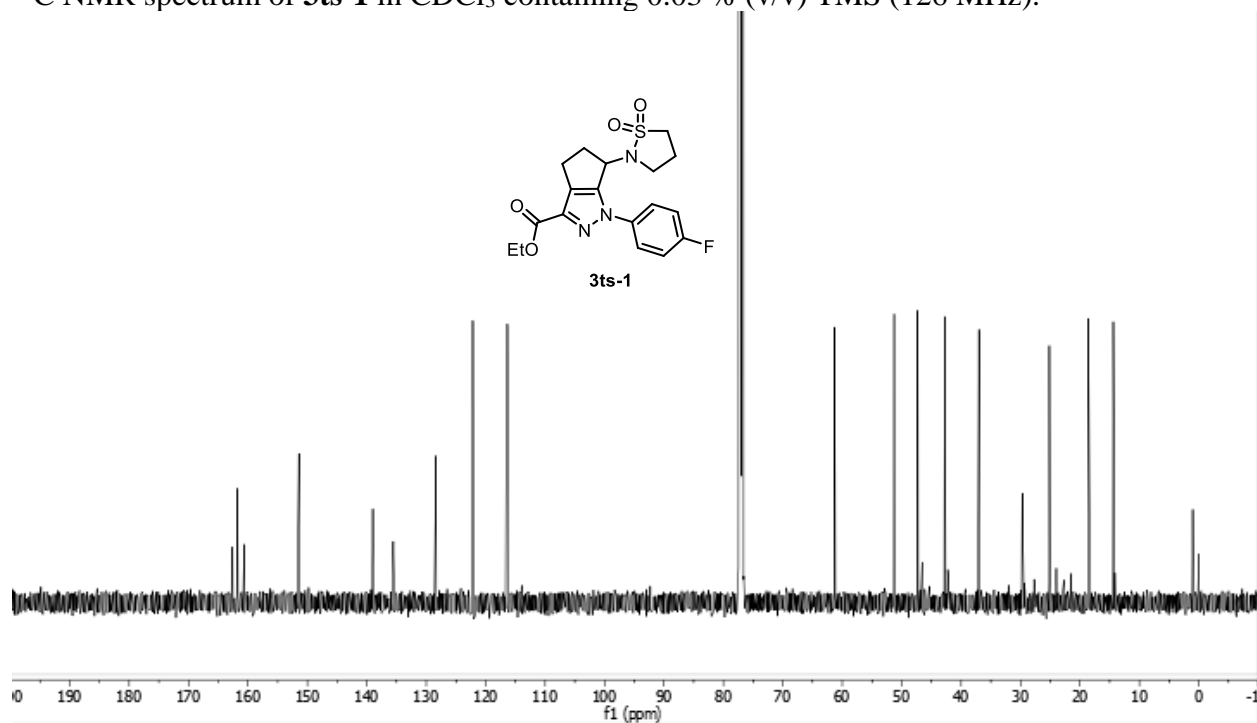
HMBC NMR spectrum of **3ti** in CDCl₃ containing 0.03 % (v/v) TMS (500, 126 MHz).



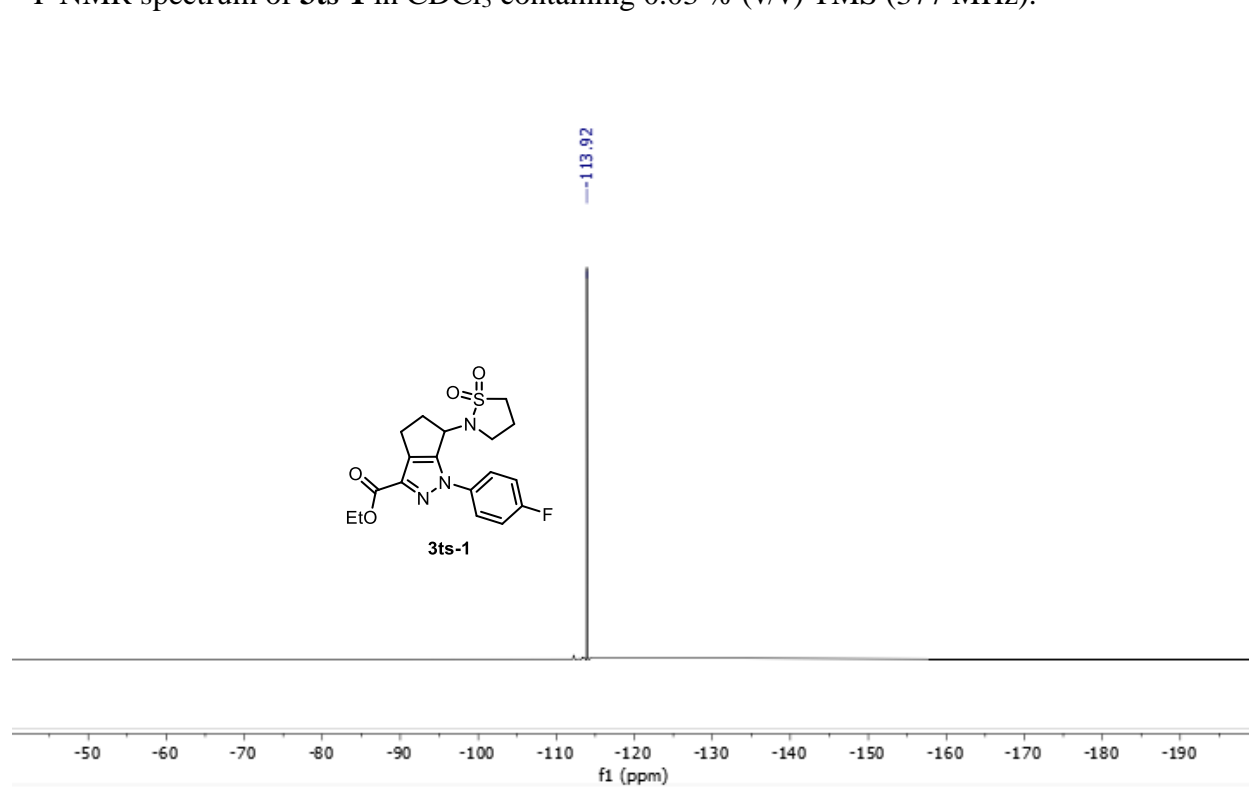
¹H NMR spectrum of **3ts-1** in CDCl₃ containing 0.03 % (v/v) TMS (500 MHz).



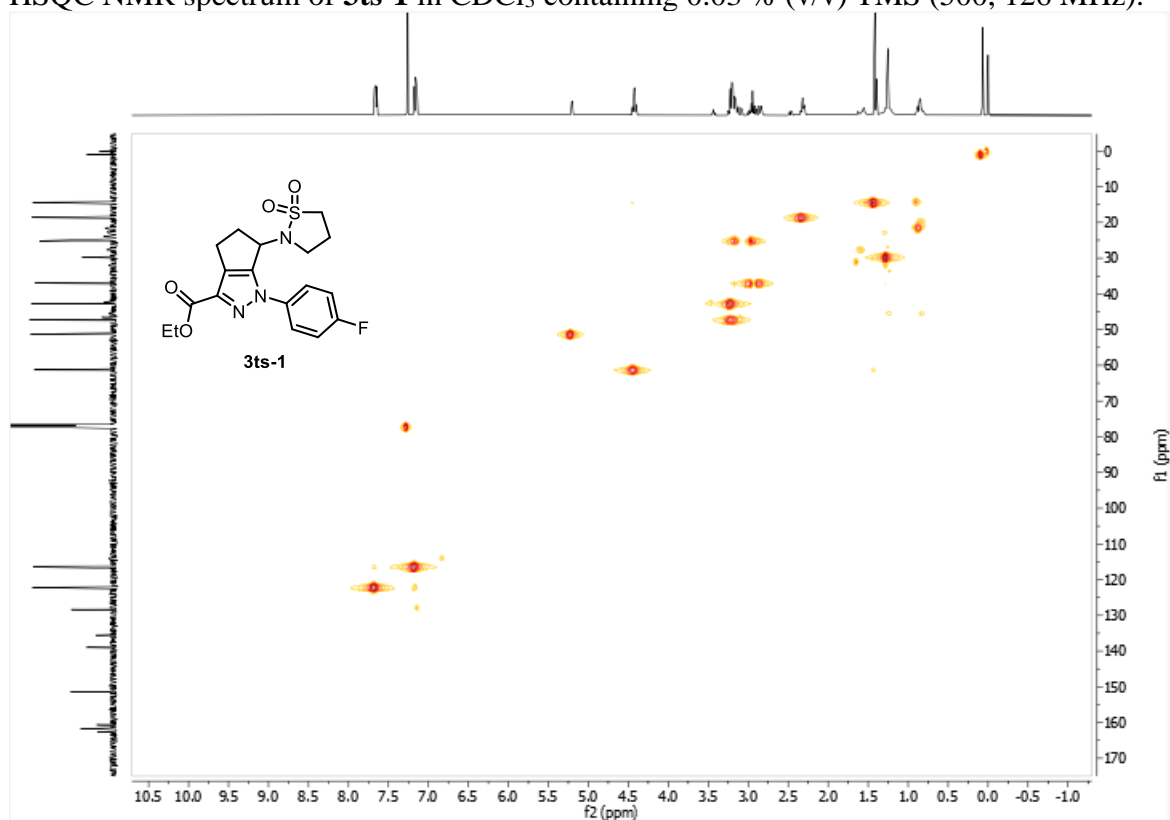
^{13}C NMR spectrum of **3ts-1** in CDCl_3 containing 0.03 % (v/v) TMS (126 MHz).



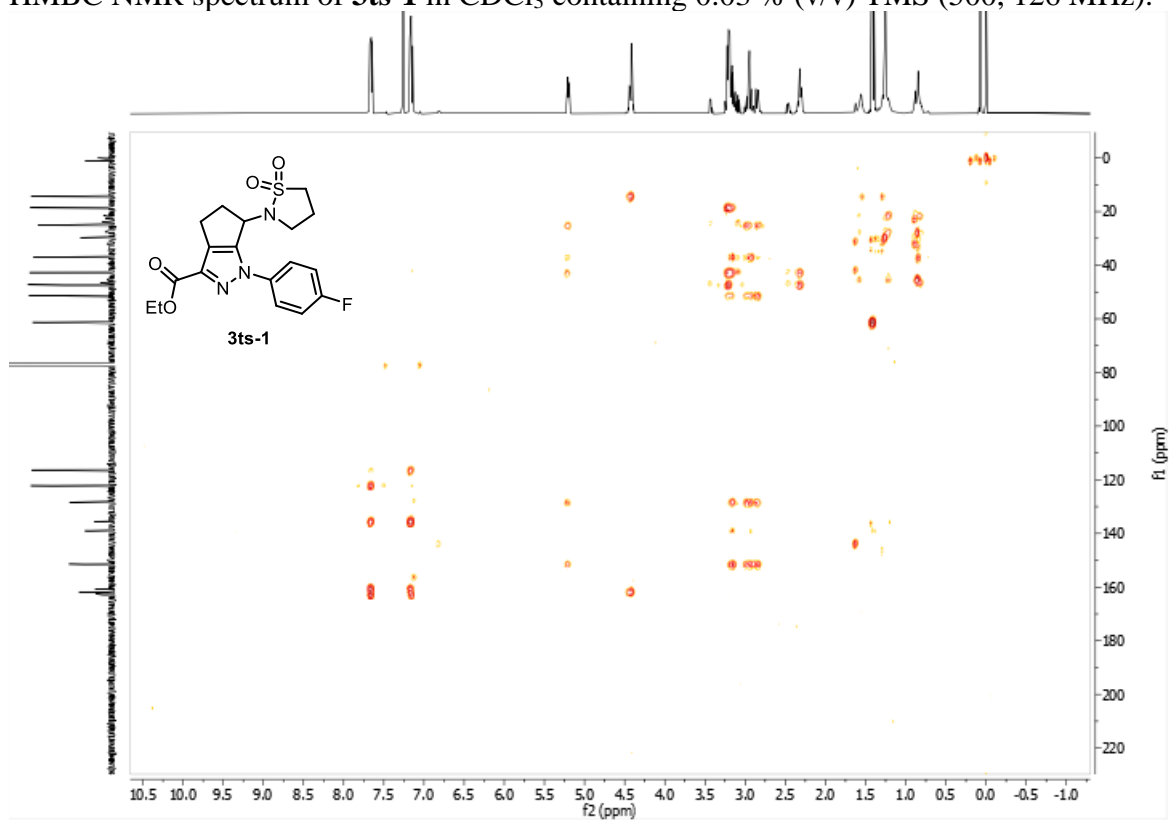
^{19}F NMR spectrum of **3ts-1** in CDCl_3 containing 0.03 % (v/v) TMS (377 MHz).



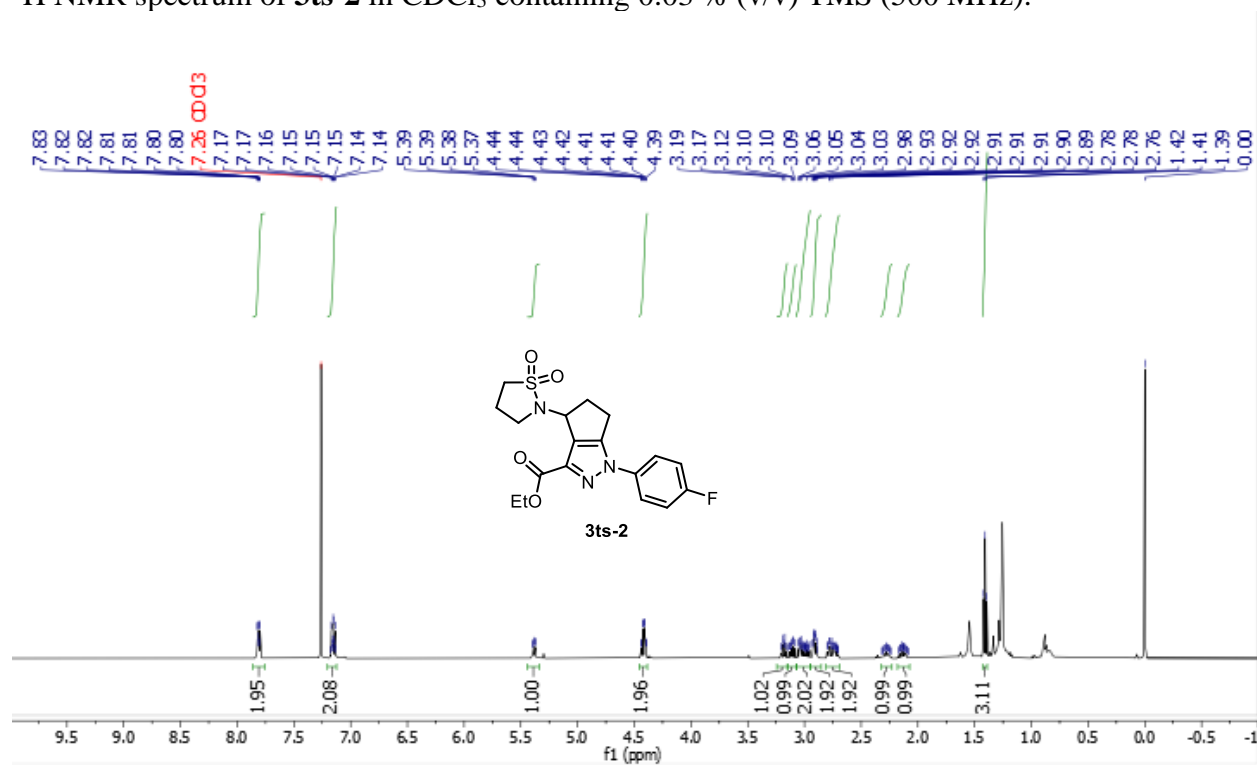
HSQC NMR spectrum of **3ts-1** in CDCl₃ containing 0.03 % (v/v) TMS (500, 126 MHz).



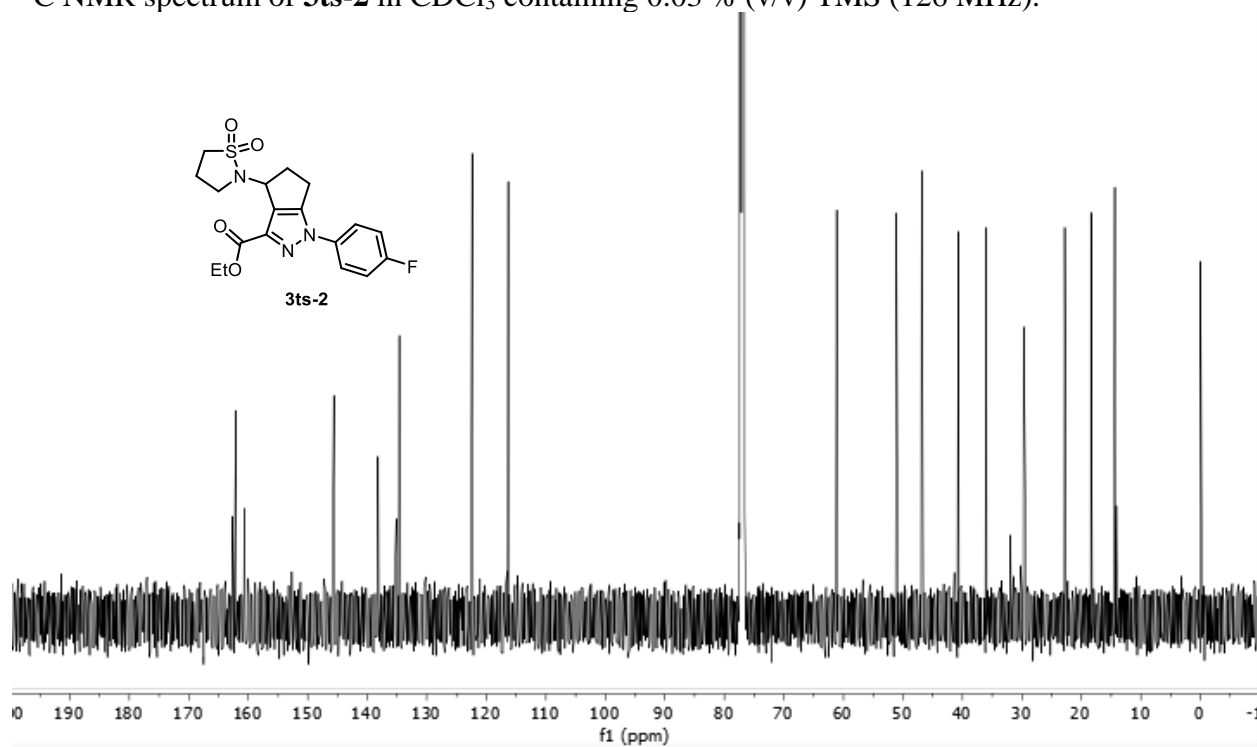
HMBC NMR spectrum of **3ts-1** in CDCl₃ containing 0.03 % (v/v) TMS (500, 126 MHz).



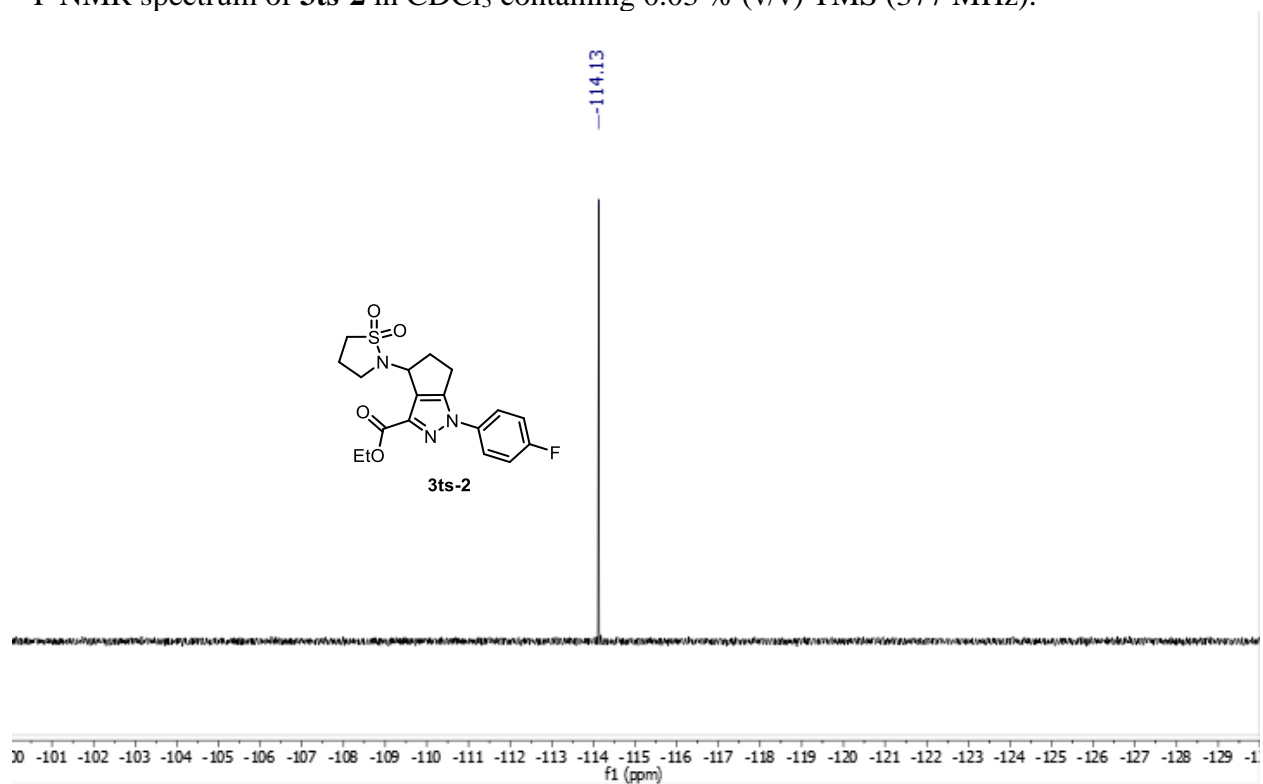
^1H NMR spectrum of **3ts-2** in CDCl_3 containing 0.03 % (v/v) TMS (500 MHz).



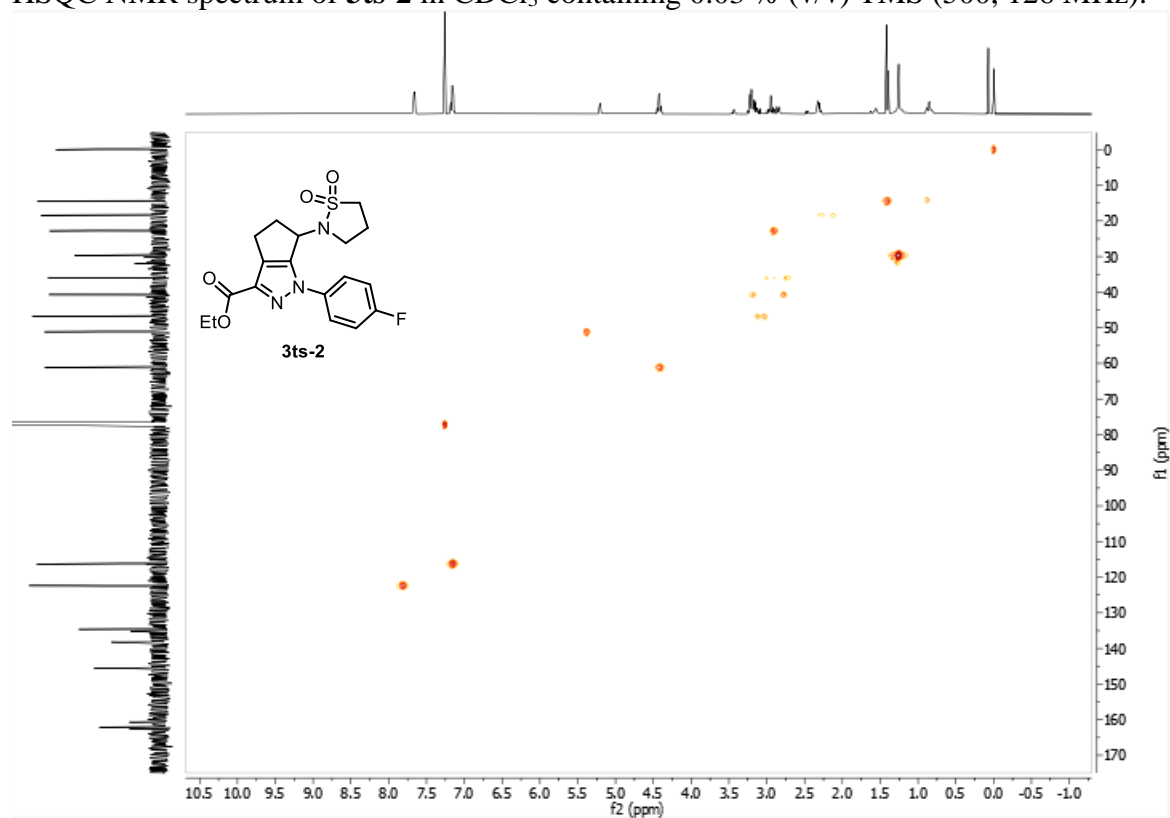
^{13}C NMR spectrum of **3ts-2** in CDCl_3 containing 0.03 % (v/v) TMS (126 MHz).



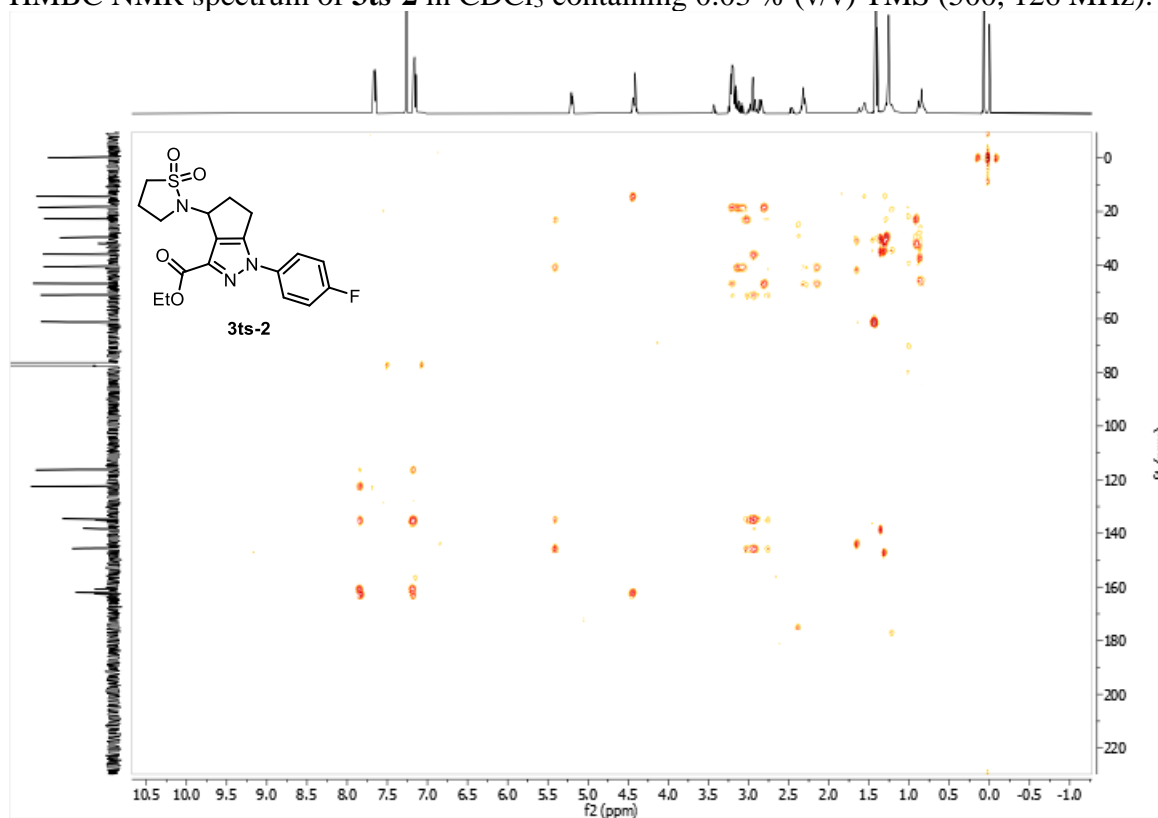
^{19}F NMR spectrum of **3ts-2** in CDCl_3 containing 0.03 % (v/v) TMS (377 MHz).



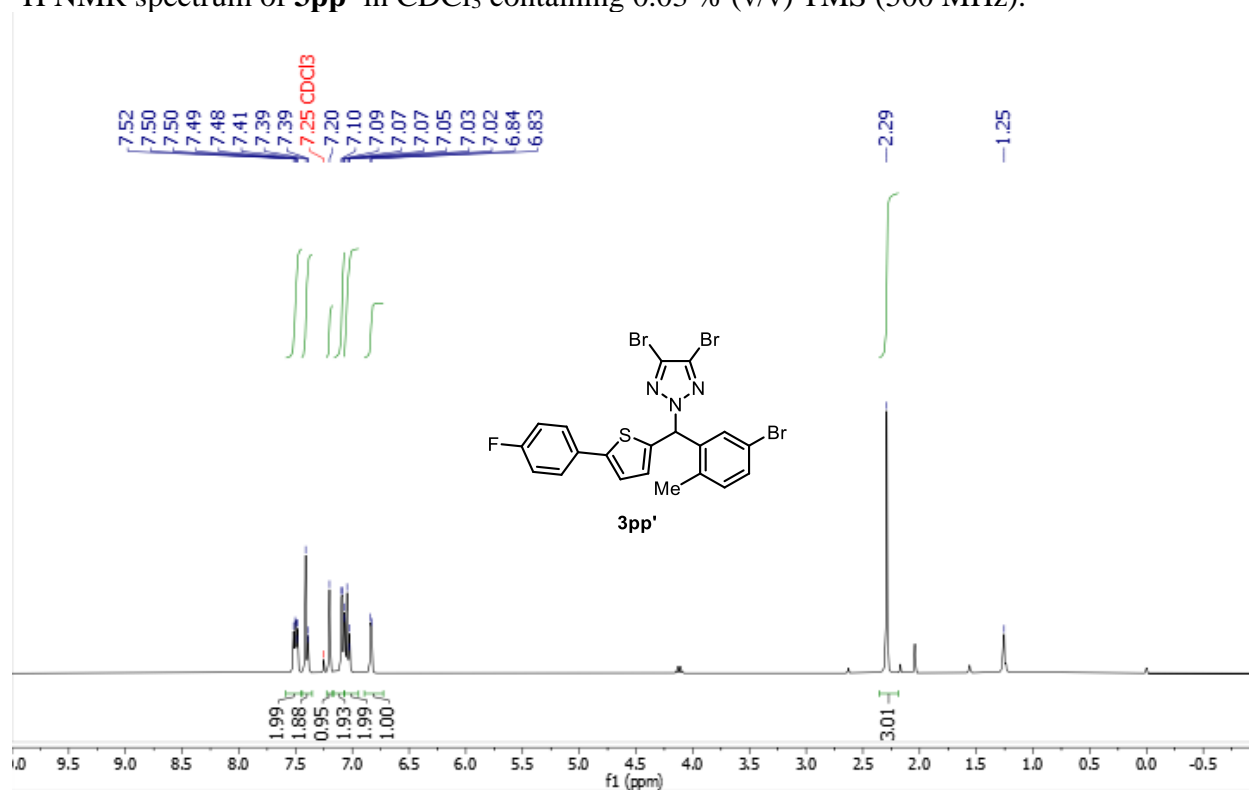
HSQC NMR spectrum of **3ts-2** in CDCl_3 containing 0.03 % (v/v) TMS (500, 126 MHz).



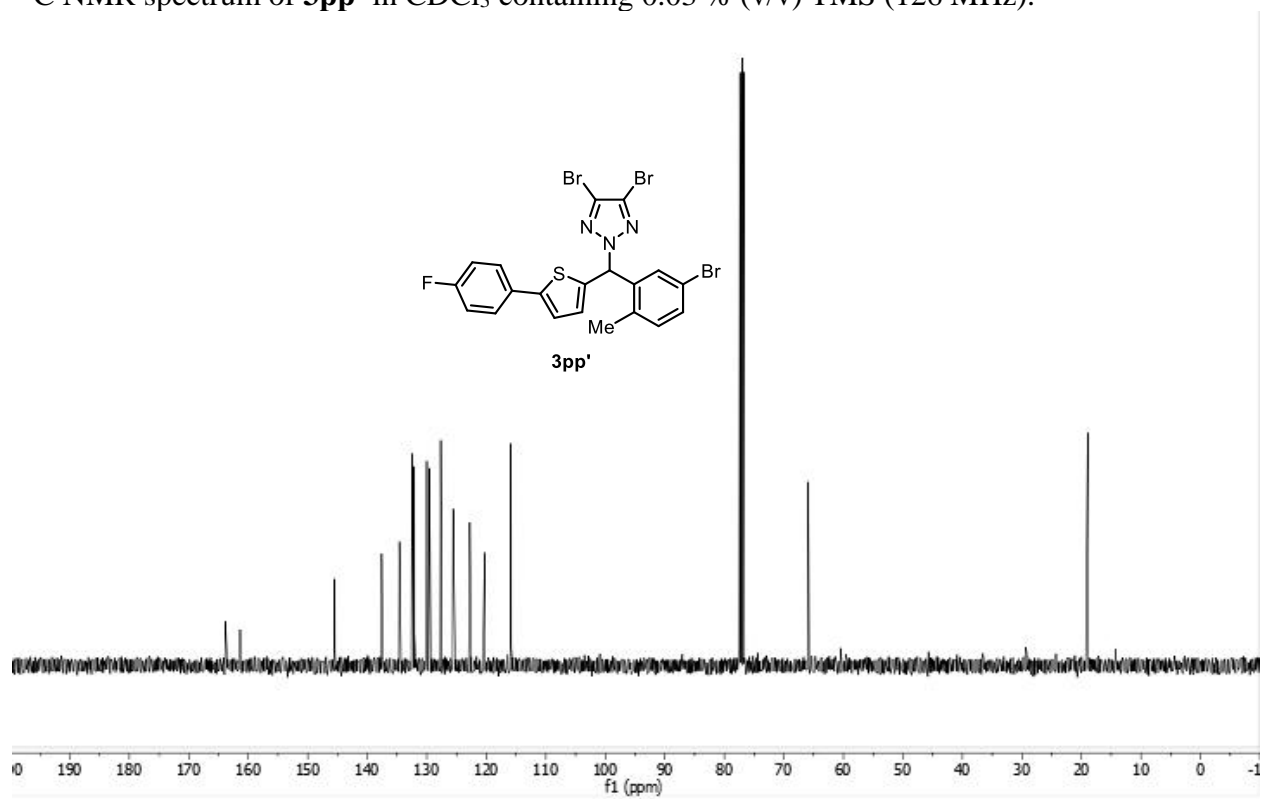
HMBC NMR spectrum of **3ts-2** in CDCl₃ containing 0.03 % (v/v) TMS (500, 126 MHz).



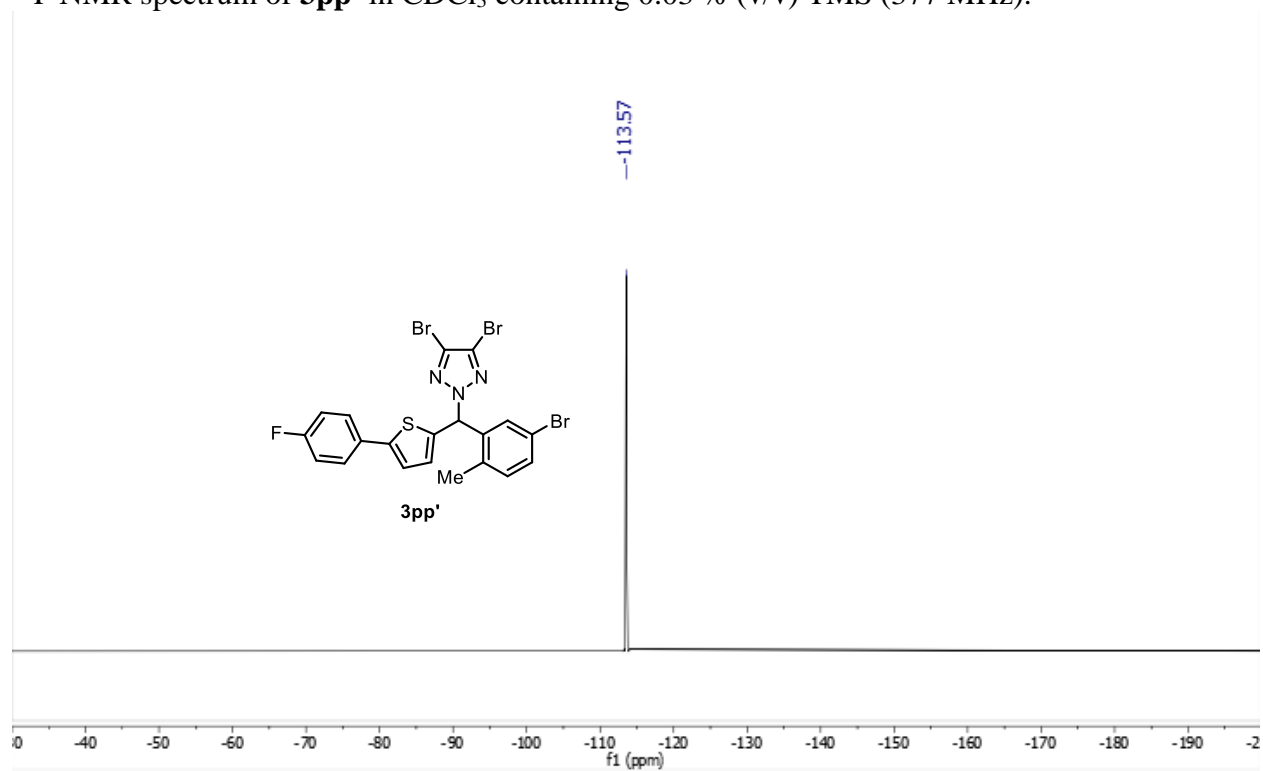
¹H NMR spectrum of **3pp'** in CDCl₃ containing 0.03 % (v/v) TMS (500 MHz).



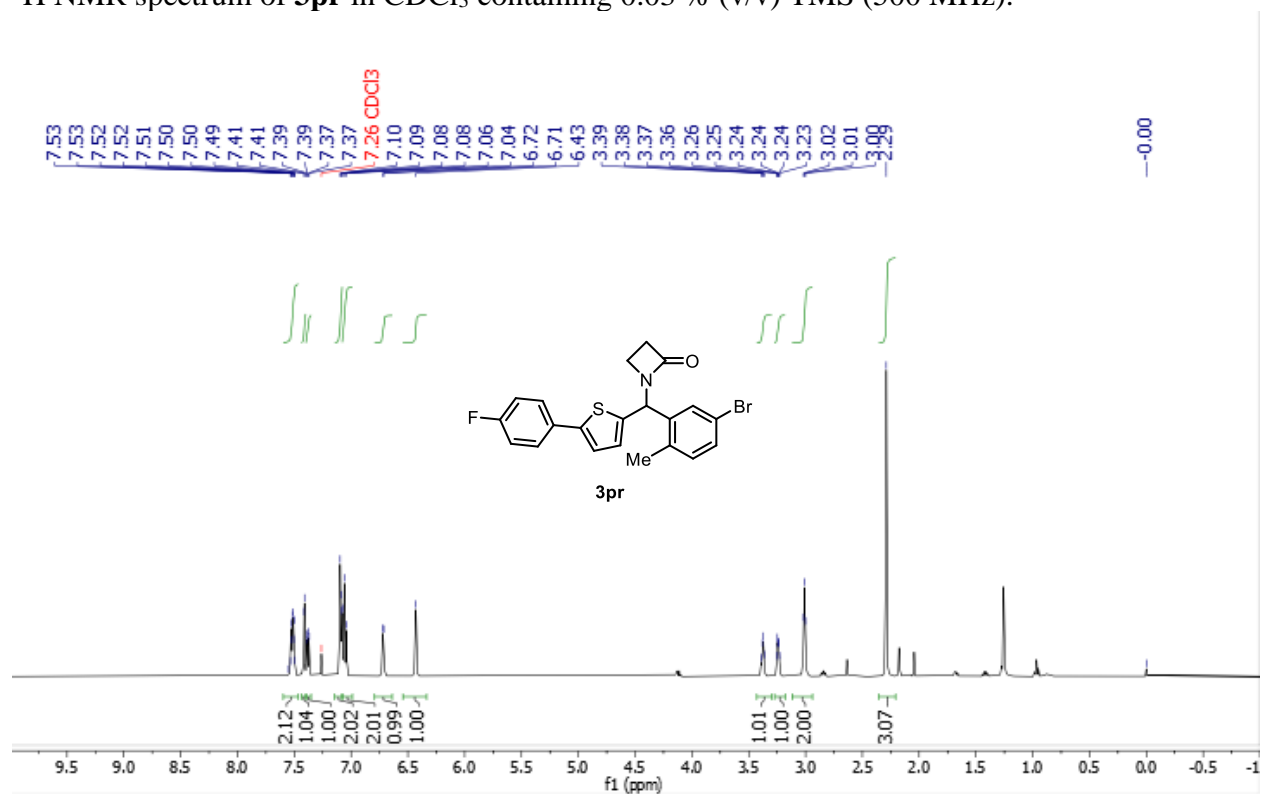
^{13}C NMR spectrum of **3pp'** in CDCl_3 containing 0.03 % (v/v) TMS (126 MHz).



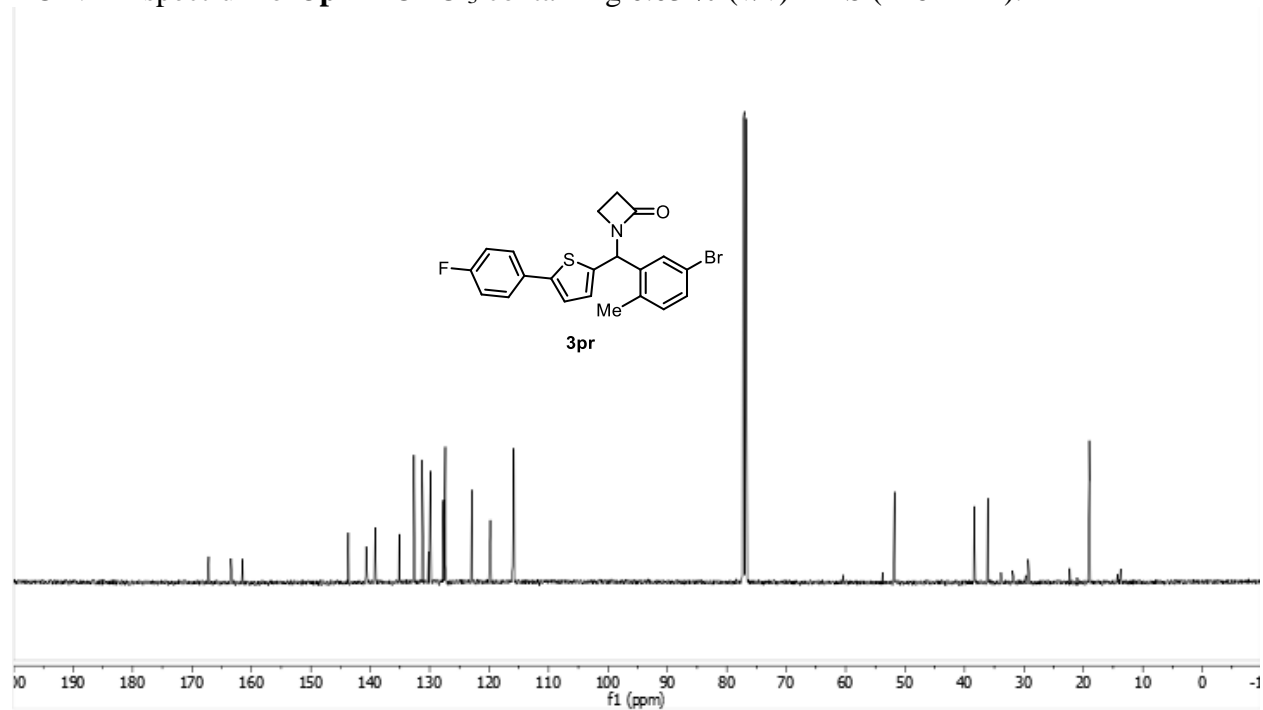
^{19}F NMR spectrum of **3pp'** in CDCl_3 containing 0.03 % (v/v) TMS (377 MHz).



^1H NMR spectrum of **3pr** in CDCl_3 containing 0.03 % (v/v) TMS (500 MHz).



^{13}C NMR spectrum of **3pr** in CDCl_3 containing 0.03 % (v/v) TMS (126 MHz).



^{19}F NMR spectrum of **3pr** in CDCl_3 containing 0.03 % (v/v) TMS (377 MHz).

